Granite-hosted mineral deposits of the New Ross area, South Mountain Batholith, Nova Scotia, Canada

by

Sarah Carruzzo

Submitted in partial fulfillment of the requirements
for the degree of Doctor of Philosophy

at

Dalhousie University
Halifax, Nova Scotia
July 2003

Your file Votre référence
ISBN: 0-612-83698-3
Our file Notre référence
ISBN: 0-612-83698-3

DALHOUSIE UNIVERSITY

DEPARTMENT OF EARTH SCIENCES

The undersigned hereby certify that they have read and recommend to the Faculty of Graduate Studies for acceptance a thesis entitled "Granite-Hosted Mineral Deposits of the New Ross Area, South Mountain Batholith, Nova Scotia, Canada" by Sarah Carruzzo in partial fulfillment for the degree of Doctor of Philosophy.

Dated: August 18, 2003

External Examiner

Research Supervisor

Examining Committee

Departmental Representative

DALHOUSIE UNIVERSITY

DATE: August 18th, 2003

AUTHOR: Sarah Carruzzo

TITLE: Granite-hosted mineral deposits of the New Ross area, South Mountain Batholith, Nova Scotia, Canada

DEPARTMENT OR SCHOOL: Earth Sciences

DEGREE: PhD CONVOCATION: October YEAR: 2003

Permission is herewith granted to Dalhousie University to circulate and to have copied for non-commercial purposes, at its discretion, the above title upon the request of individuals or institutions.

[redacted]
Signature of Author

Table of Contents

List of Figures

List of Tables

Abstract

The most evolved rocks of the South Mountain Batholith host polymetallic (Sn-W-U-Mo-Cu-Mn) mineral deposits in the New Ross area (NRA). This project presents new data (fluid inclusions, stable isotopes, mineral chemistry, and $^{40}Ar/^{39}Ar$ and $^{187}Re/^{187}Os$ dating) to define the hydrothermal fluids related to the mineralisation of the NRA, and to create an integrated model for the origin of the mineral deposits. Single-grain Ar/Ar laserprobe ages for white micas from unmineralised and mineralised samples range from 382 to 320 Ma. Molybdenite Re/Os ages on two pegmatite samples are 377 ± 3 Ma and 371 ± 3 Ma. The main phases of hydrothermal activity leading to polymetallic mineralisation occurred in close temporal relationship to granite crystallisation at ~ 380 Ma, and episodic reheating events occurred at ~371 Ma and ~320 Ma, partially resetting the Ar/Ar system. Three distinct fluids in the mineral deposits of the NRA are: (i) a Na/K-rich magmatic fluid; (ii) a Ca-rich metamorphic fluid; and (iii) a meteoric fluid. Mixing of these fluids occurred, implying that the three fluids were contemporaneous. The isotopic compositions ($\delta^{18}O$, δD) of white mica from unmineralised and mineralised samples of the NRA, and δD values for fluid inclusion extracts from coexisting quartz, record a transition from a magma-dominated, low water/rock ratio system to a fluid-dominated, higher water/rock ratio system, into which meteoric water infiltrated at the time of SMB crystallisation and greisen/vein formation. Fluctuating pH conditions of hydrothermal fluids at the contact with host granitoid rocks and variations in redox conditions, triggered by incursion of increasing amounts of meteoric fluid along deep-penetrating faults as the system evolved from magmatic to hydrothermal, caused metal deposition. Over ~10 My, the concurrence of highly evolved granitic melts rich in incompatible elements in the late-stage of granite emplacement with intense fluid circulation, particularly those of meteoric origin, formed the NRA mineral deposits.

Acknowledgements

M

To Barrie Clarke, my supervisor, for sharing with me his passion for granites, in particular for the South Mountain Batholith, and for welcoming me so warmly to Canada. He certainly believed in me more than I ever did...;

To all the other members of my committee, Dan Kontak, George O'Reilly, Peter Reynolds, and Alan Anderson for helping and encouraging me throughout the meanders of my degree;

To Gordon Brown for his wonderful thin and thick sections and, most importantly, for always being so accommodating;

E

To Robert Creaser and David Selby for their help in getting and interpreting the Re-Os ages;

To Keith Taylor for the Ar/Ar dating work;

To Sandy Grist for guiding me through the mineral separation lab;

To Kurt Kyser and Kerry Klassen for performing the isotopic measurements;

To Bob MacKay for his endless help with the electron microprobe;

R

To Martin Gibling, Becky Jamieson, Milton Graves, Marcos Zentilli, and Nick Culshaw for sharing their knowledge about various aspects of my thesis;

To Norma, Darlene, Jane, Tom, and Charlie for making the logistic part of my stay at Dalhousie smoother;

To all the wonderful friends I made while I was here, in particular Patricia Corcoran for "giving me the talk when I needed it", Lexie Arnott for "showing me the way out", Sharon Lee for keeping me company during the "night shifts", Joyia Chakungal for helping me in the critical moments, and Jane Sherrard for always being there to share a "fizzy";

C

To Tasha Smith and Sabrina Taylor for welcoming me in their comfortable office in biology and for sharing so many good laughs;

To Catherine Muir, for suffering through the formatting of the longest appendix of this thesis;

To Rachel Speller, my field assistant, with whom I shared so many fun times in New Ross;

I

To Marie Walker for her warm welcoming of Rachel and I in her house in New Ross;

To Kevin, for being so patient and supportive;

A maman, papa, Marie, Paul et Judith pour leur support de toujours. Sans eux, rien n'aurait été possible.

CHAPTER 1

INTRODUCTION

1.1. Granite-related mineral deposits

Mineral deposits are any natural, but locally restricted, concentration of minerals in the Earth's crust (Skinner 1997), and represent geochemical anomalies where the concentration of one or several element(s) is at least two times the background level. **Ore deposits** are any mineral deposit rich enough to allow mining economically (Skinner 1997). Large Mo, Sn, and W deposits, rare metals (Ta, Nb, Li, Be, Zr, Ga, REE), more than half the Cu resources, significant Fe, Au, Zn, Pb, Ag, and U deposits, and many minor metals (Bi, Cd, Sb, Te, Re, In, Sc) occur within, or in close proximity to, granitic plutons (Sillitoe 1996).

Granite-related mineral deposits are generally associated with the late differentiated fractions of a given granitic body. Volatile-rich liquids can accumulate in the roof area of a granitic batholith when crystallisation of the body is already advanced (Hutchison 1982). Therefore, depending on the degree of fracturing of the surrounding country rock (fracturing depending on the location of the brittle-ductile boundary, Fournier 1999), these liquids may have the opportunity to leave the granitic body.

An important question to ponder is why some granitoid rocks remain barren, whereas others are mineralised. Urabe (1985) provided a partial answer to this question based on experimental data, by stressing the difference in solid-melt-fluid partition coefficients between aluminous and alkaline melts in natural acidic rocks. Urabe (1985) concluded that granite of slightly peraluminous composition is more likely to produce metal-rich hydrothermal fluids, whereas alkaline-rich melt would preferentially retain the metals instead of releasing them into a fluid phase. Urabe (1985) proposed a chemical compositional continuum from a more alkaline to more

aluminous magma where the more alkaline fraction stores metals as the magma slowly rises to the surface, and releases them whenever it becomes aluminous and water-saturated. Of course, Urabe's interpretation presents one control, among many potential physical and chemical conditions, for metal concentration, transportation, and deposition. However, of crucial importance in the development of economic ore deposits is the evolution of hot fluid phases (hydrothermal solutions) from a magmatic body. The understanding of the sources, pathways, compositions, and temperature/pressure conditions of hydrothermal fluids provides clues to the origin, transport, and deposition of metals.

Other factors are also important in deciding what type of mineral deposit will be hosted in a certain variety of granite. For example, the association of more oxidised magma with Cu deposits and of more reduced magma with Sn deposits, underlines the importance of oxidation state (Candela 1989; Blevin and Chappell 1991). Candela (1997) emphasised the following factors present at the magmatic stage as being crucial for the formation of granite-related deposit: 1) original composition of the magma (concentration of ore metals, Cl and H_2O content); 2) magma oxidation state; 3) depth of emplacement; and 4) relative timing of crystallisation, magma ascent, and exsolution of a magmatic volatile phase. The magmatic volatile phase and the crystallising minerals compete for ore metals, such as Cu and Mo, and the outcome depends on the initial metal concentration, depth of emplacement (both influencing the timing of a magmatic volatile phase exsolution), and composition of the volatile phase (Candela and Holland 1984, 1986). Another example is the influence of oxygen fugacity on W, Sn, and Mo partitioning between the melt and magmatic mineral phases: at high fO_2, W partitions into magmatic minerals, whereas Mo preferentially remains in the melt; at low fO_2, the reverse is true (Candela and Bouton 1990). In summary, the large number of variables involved in the mineralisation process heightens the complexity of any model attempting to explain all observations.

The South Mountain Batholith (SMB) of Nova Scotia, and more precisely its most evolved phases, represents a large natural laboratory in which to investigate granite-related mineral deposits, mainly because of its great diversity of metals concentrated

in a relatively restricted area. Furthermore, the SMB was sporadically explored for metals, and an important increase in exploration happened in the mid- to late 1970's leading to the discovery of the East Kemptville tin (southern Nova Scotia) and Millet Brook uranium (central Nova Scotia) deposits. Similarities between the SMB and world tin and uranium producers (for example the Cornwall district in England and the Massif Central in France) suggest that a higher ore mineral potential still has to be considered in the SMB (MacDonald 2001). Therefore, a detailed investigation of mineral occurrences hosted in the SMB has the potential to significantly increase the general understanding of mineral deposits related to peraluminous granites.

1.2. Geology of the Meguma Zone

The Meguma Lithotectonic Terrane (MLT) (Fig. 1.1) is the easternmost terrane of the northern Appalachians and is separated from the Avalon Terrane by the transcurrent Cobequid-Chedabucto Fault System (Williams 1979; Williams and Hatcher 1982, 1983), also called the Minas Fault System (Keppie 1985, 1989). The MLT occurs in mainland Nova Scotia, and is also the foundation of the Scotian Shelf to the south, the continental shelf southeast of Cape Breton Island and south of Newfoundland, and part of the Bay of Fundy to the northwest (Schenk 1983, 1995b). Stratigraphy, paleontology, and geophysics of the MLT suggest that it was a fragment of the continental margin of Gondwana stranded against North America after rifting in the Jurassic (Schenk 1971; Bouyx et al. 1997). Keppie and Dallmeyer (1987, 1995) and Keppie (1989) dated the accretion of the MLT between ~400 and 385 Ma (Devonian) using $^{40}Ar/^{39}Ar$ plateau ages on phyllite that developed during accretion in the Cobequid-Chedabucto fault area. After accretion, movement between the Avalon Terrane and the MLT sporadically occurred at least until 270 ± 8 Ma (Dallmeyer and Keppie 1987; Keppie and Dallmeyer 1995).

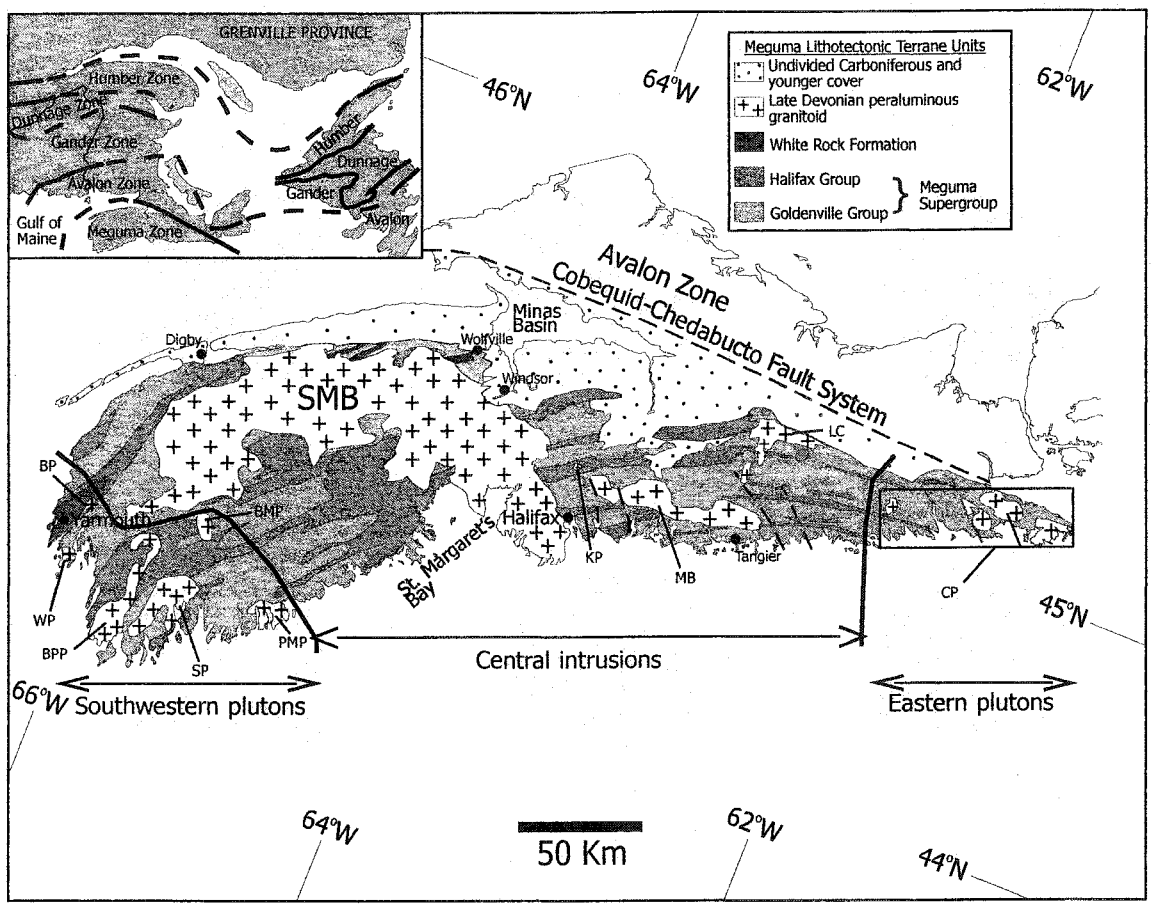

Fig. 1.1: Simplified geological map of the Meguma Lithotectonic Terrane of the Canadian Appalachians. BMP Bald Mountain pluton, BP Brenton pluton, BPP Barrington Passage pluton, CP Canso plutons, KP Kinsac pluton, LC Liscomb Complex, MB Musquodoboit Batholith, SMB South Mountain Batholith, SP Shelburne pluton, WP Wedgeport pluton. Modified after Tate and Clarke (1995).

Period	Epoch	Supergroups	Groups	Formations	Sediment type	Sedimentary rocks depositional environments	Meguma Zone events
Carboniferous (355-300)	Tournaisian		Horton	Coldstream	Conglomerate, sandstone, and shale	fluvial	
	Tournaisian			Cheverie	Sandstone, mudstone	fluvial	
Devonian (418-355)	Late Devonian (Famennian)			Horton Bluff	Sandstone, mudstone	fluvial and lacustrine	
							-Intrusion of granitoid rocks (385-372? Ma) -Intrusion of mafic dykes (380-370 Ma)
							Acadian Orogeny (ca. 395-388 Ma)
							Accretion of the Meguma terrane to North America (405 ± 7 Ma)
	Gedinnian to Siegenian/Emsian	Annapolis	Torbrook	5	Sandstone	High stand deposition on inner shelf	
				4			
				3	Black slate and limestone, grey mudstone and tuff		
				2	Sandstone	Submergence	
				1	Sandstone	Storm-dominated shelf	
Silurian (441-418)	Pridoli?		New Canaan		Tuff and basalt	Nearby subaerial exposure	
	Ludlow to Pridoli		Kentville	Tremont	Dark grey and greenish grey slate	High stand deposition on inner shelf	
	Ashgill or Llandovery			Elderkin	Slate and felsite	Nearby subaerial exposure	
Ordovician (490-441)	Ludlow ?		White Rock	Deep Hollow 2	Dark grey slate	High stand deposition on outer shelf	
				Deep Hollow 1 and 3	Sandstone, quartz arenite	Storm deposits on outer continental shelf	
	Late Arenig to Llanvirn or Llandeilo			Fales River	Quartz arenite, shale, and sandstone	Storm-influenced, muddy inner shelf	
	Ashgill			Nictaux Volcanics	Ash-flow tuffs and basalt	Nearby subaerial exposure	
	Tremadoc	Meguma	Halifax	Rockville Notch	Grey to black laminite and siltstone	Slope	
				Delanceys	Grey slate and siltstone	Shelf	
				Feltzen	Siltstone and black and grey slate		
				Cunard	Black slate, siltstone, and sandstone	Prograding wedge complex	
				Mosher's Island	Grey slate (metalliferous)	Downlap surface	
Cambrian (544-490)	Merioneth or Tremadoc		Goldenville	West Dublin and Tancook	Turbidites and sandstone	Slope fan	
				Risser's Beach	Slate, siltstone, and sandstone		
	Early Cambrian			New Harbour	Metawacke and slate	Basin floor fan	
Precambrian (> 544 Ma)							source rocks for sediments present in Goldenville and Halifax Groups

Table 1.1: Stratigraphy of the Meguma and Annapolis Supergroups of the Meguma Zone and the base of the Carboniferous, after the sequence stratigraphy studies by Schenk (1995a, 1995b, 1997); Martel et al. (1993); and Martel and Gibling (1996). Heavy horizontal lines identify unconformities. Time scale of Okulitch (1999), except for Devonian time scale of Tucker et al. (1998).

1.2.1. The pre-granitic rocks of the MLT

The pre-granitic rocks in the MLT include the Meguma and the Annapolis Supergroups (Table 1.1).

1.2.1.1. The Meguma Supergroup

The Meguma Supergroup (Schenk 1995a) is a thick siliciclastic sequence of Cambrian-Ordovician metasediments. The Meguma Supergroup consists of two Groups: the Goldenville and the Halifax Groups (Schenk 1995a). The Goldenville Group consists mainly of thick strata of grey to greenish-grey sandstones, in which beds thin towards the top and also include more shale and siltstone (Schenk 1975). The transition between the two Groups, the Goldenville-Halifax Transition (GHT) (Graves and Zentilli 1988 for example), is gradational and consists of manganiferous siltstone and shale that locally contain anomalous concentrations of base metals. Also, the GHT contains considerable thickness of calcareous siltstones and wackes (G. A. O'Reilly pers. comm. 2002). Dark grey to grey-green siltstone and slate dominate the conformably overlying Halifax Group (Schenk 1983). The overall model for deposition of the Meguma Supergroup is one of deep-sea fans (Goldenville Group) passing upwards into a continental slope and shelf (Halifax Group) (Schenk 1971, 1981, 1995b). The source area for the Meguma Supergroup sediments is probably Gondwana, and two source areas are proposed:

1) West African craton, based on stratigraphy (Schenk 1971), paleontology, petrology (Richard and Clarke 1989), isotopes (Sm/Nd, Clarke and Halliday 1985), geophysics, and paleomagnetism; and
2) western South America, based on regional syntheses (Keppie 1977; Schenk 1981) and U-Pb ages (Krogh and Keppie 1990).

1.2.1.2. The Annapolis Supergroup

The Annapolis Supergroup (Schenk 1995b) is a thick sequence of fine-grained shallow marine siliciclastic sediments and volcaniclastic rocks of Early Ordovician to Early Devonian age. The Annapolis Supergroup consists of three Groups: White Rock, Kentville, and Torbrook. Each Group comprises a succession of sandstone,

black shale, siltstone and/or sandstone, and volcanics and represents a major transgressive-regressive cycle (Schenk 1991). Igneous activity began each cycle and was subaerial for the most part (Schenk 1995b, 1997). In the same model of an evolving continental margin as the Meguma Supergroup, the Annapolis Supergroup represents the transition from the outer to the inner shelf (Jensen 1975).

1.2.1.3. Deformation style and timing

Regional deformation and metamorphism (regional greenschist facies with amphibolite facies in the southwest and northeast of the Meguma Zone, Raeside et al. 1988) occurred during the Acadian Orogeny (ca. 400-385 Ma based on whole rock and mineral $^{40}Ar/^{39}Ar$ ages, Keppie and Dallmeyer 1987, Muecke et al. 1988, Hicks et al. 1999) and was the first major event affecting both Supergroups, as a consequence of the accretion of the MLT to North America (Williams 1995).

1.2.2. The granitic rocks of the MLT

In the Late Devonian, peraluminous granitoid plutons (Fig. 1.2), as well as small mafic intrusions of the same age (Tate 1995), intruded and truncated both regional folding and cleavage of the Meguma Supergroup. Based on compositional and spatial constraints, Clarke et al. (1997) organized the granitic bodies of the MLT into three main areas (Fig. 1.1): (1) central intrusions (SMB, Musquodoboit Batholith including the Kinsac pluton, and Liscomb Complex); (2) southwestern plutons (Port Mouton, Brenton, Wedgeport, Barrington Passage, Shelburne, and Bald Mountain plutons); and (3) eastern plutons (Canso composite pluton). Clarke et al. (1997) regrouped areas 2 and 3 under the term "peripheral plutons", and mafic intrusions are associated with each of the peripheral plutons (Hill 1991; Tate and Clarke 1995). Mafic intrusions are also associated with the Liscomb Complex and in close proximity to the Musquodoboit Batholith (Clarke et al. 1993a; Kontak and Reynolds 1994).

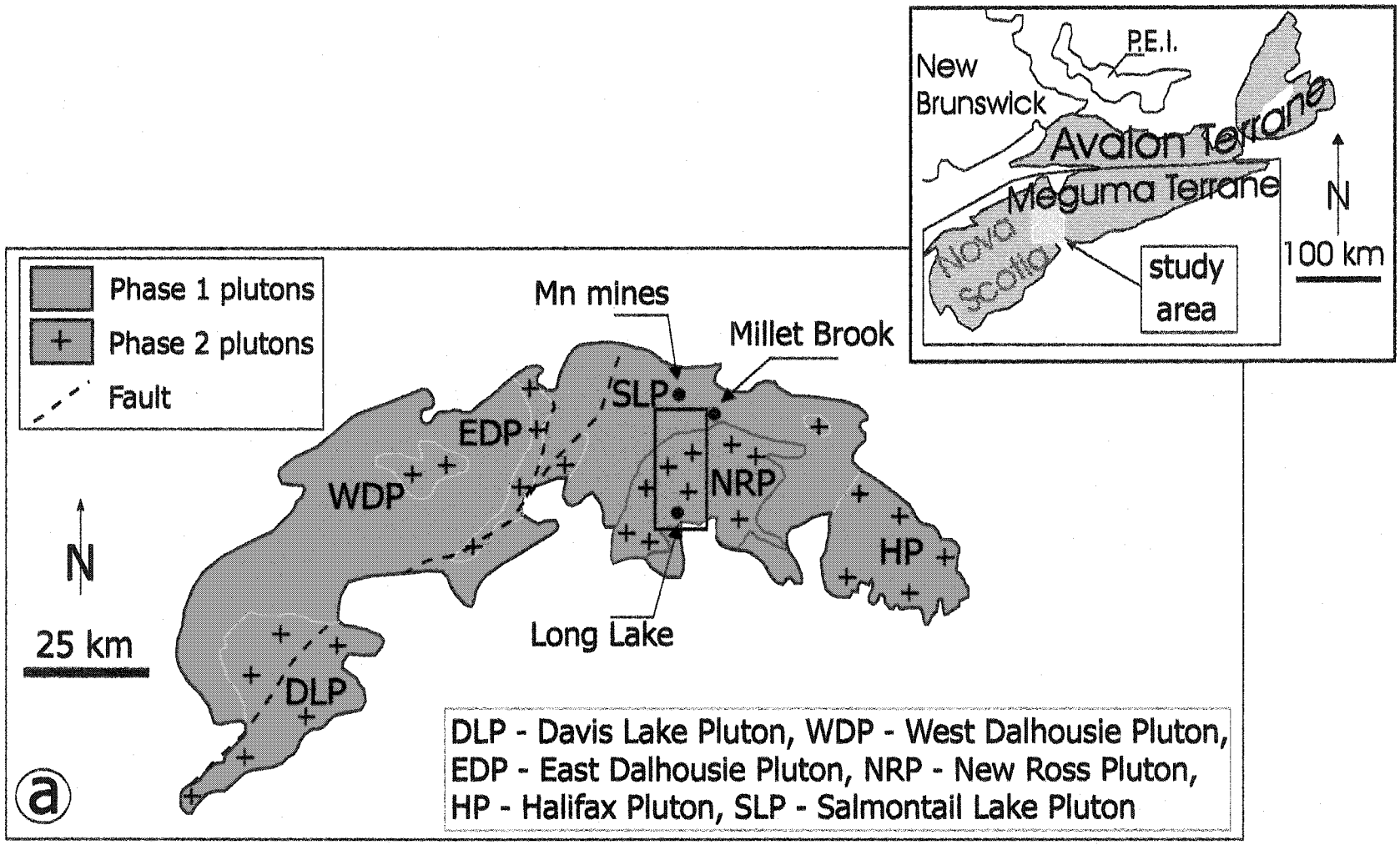

Fig 1.2a: Detailed geological map of the SMB showing the phase 1 and 2 plutons. Black box shows study area detailed on Fig. 1.2b.

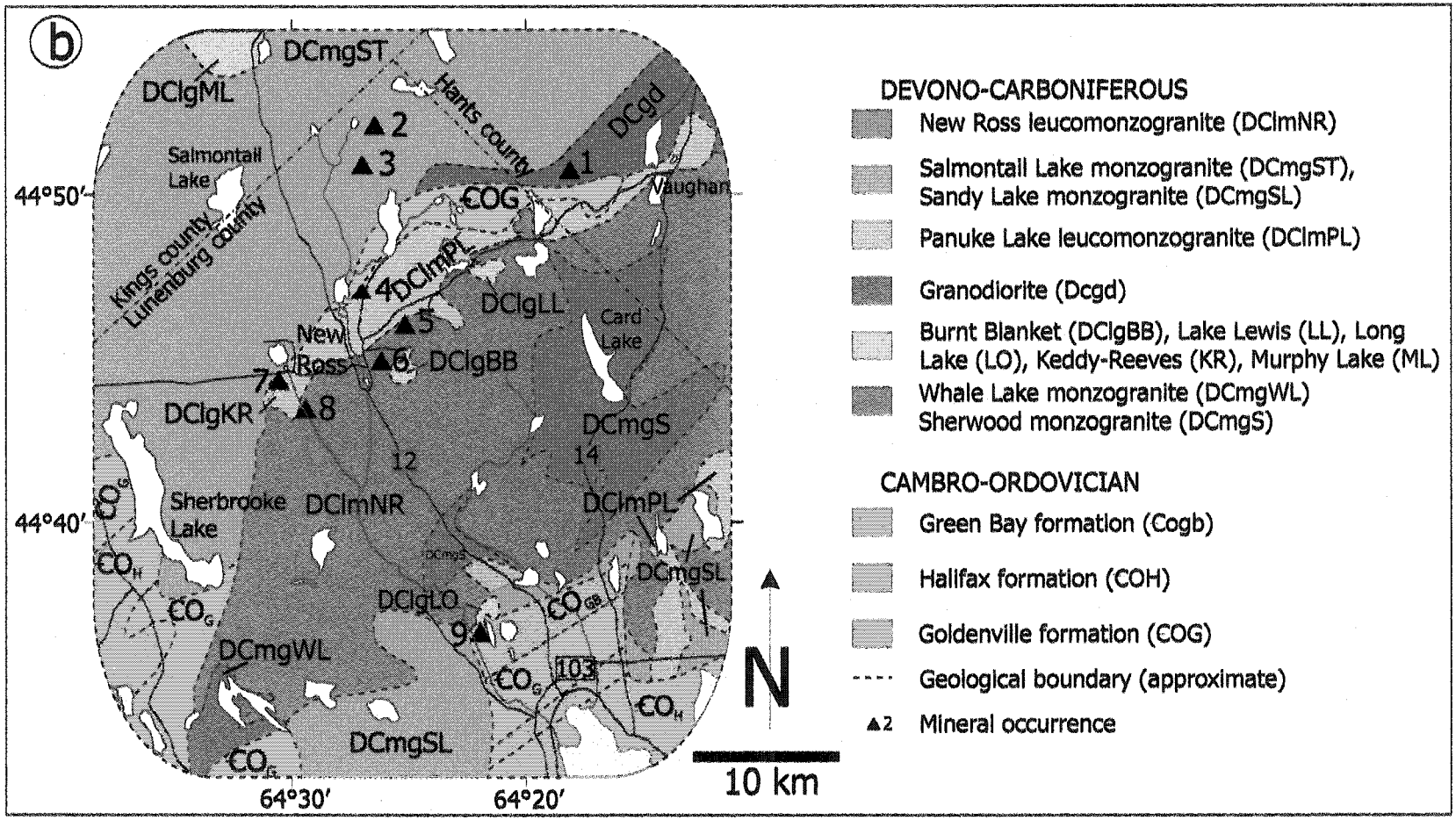

Fig. 1.2: (b) locations of the mineral occurrences of the New Ross area sampled for this study: 1) Millet Brook, 2) Dean and Chapter Mine (part of the Mn mines), 3) Cain and Riddle Mine (part of the Mn mines), 4) Turner, 5) Walker, 6) Morley's, 7) Reeves , 8) Keddy, and 9) Long Lake . Modified after Corey (1991); Ham (1991); Horne (1992).

The SMB (Fig. 1.2) is a large (~ 7,500 km^2) complex of thirteen coalesced plutons (from east to west: Halifax, Big Indian Lake, Five Mile Lake, New Ross, Salmontail Lake, Scrag Lake, East Dalhousie, Cloud Lake, Little Round Lake, West Dalhousie, Kejimkujik, Morse Road, and Davis Lake plutons) and comprises a wide range of granitoid rocks from less evolved granodiorite and monzogranite, to more evolved leucomonzogranite and leucogranite (MacDonald 2001).

1.2.2.1. Petrology

MacDonald et al. (1992) and MacDonald (2001) grouped the thirteen coalesced plutons forming the SMB into two stages:

1) less evolved Stage I plutons consisting mainly of biotite granodiorite and biotite monzogranite; and
2) more evolved Stage II plutons consisting of muscovite-biotite monzogranite, leucomonzogranite, and leucogranite.

Where exposed, the contact between the Stage I and II plutons is intrusive and sharp, with Stage II plutons intruding Stage I bodies (MacDonald 2001). Contrasting with this large granitic body, smaller and more primitive plutons (mainly tonalite and granodiorite) that comprise the peripheral plutons are located in the southwestern and eastern parts of the Meguma Zone (Fig. 1.1). These plutons differ from the central intrusions in several characteristics (Clarke et al. 1997):

1) intruded country rock is of higher metamorphic grade;
2) foliation of the granite is mostly tectonic in origin, with only minor magmatic foliation;
3) granitic rocks commonly contain synplutonic mafic intrusion;
4) peraluminosity is less than in the central intrusions with biotite as the dominant Al-rich mineral;
5) hornblende may be present as a primary phase;
6) origin is not entirely crustal, but rather a mix of Meguma Supergroup source rocks and mantle-derived mafic magma (Tate and Clarke 1997; Clarke et al. 2000).

1.2.2.2. Processes of differentiation in the SMB

As stated previously, several major rock types occur in the SMB, from the least evolved (i.e., most primitive composition) granodiorite to the highly evolved leucogranite/pegmatite/aplite. One and/or several processes contributed to the chemical and mineralogical diversity of major rock types within the SMB. It is, therefore, important to understand how the effect of one or several processes leads to the differentiation level commensurate with the development of granite-related mineral deposits. Clarke and Muecke (1985) proposed three main processes: fractional crystallisation, reaction with the country rock (contamination), and late-stage interaction with fluids (orthomagmatic and hydrothermal alteration). Fractional crystallisation and contamination take place when magma is still present in the system, and hydrothermal alteration happens at a subsolidus stage. Table 1.2 summarises the evidence for all identified processes in the SMB.

1.2.2.3. Granite age

Geological age

Bouyx et al. (1992, 1997) observed benthic faunas from the Lochkovian (418-413.5 Ma), Pragian (413.5-409.5 Ma), and Lower Emsian (<409.5 Ma) Stages in the Torbrook Formation, the youngest Group of the Annapolis Supergroup intruded by the SMB (time scale of Tucker et al. 1998). Also Elias (1986) suggested that the Torbrook Formation might be younger than Emsian, because of the erosion of part of its upper levels, therefore, restricting the SMB maximum age to <394 Ma. The SMB emplacement is late- to post-deformation related to the Acadian orogeny. Hicks et al. (1999) tightly constrained the age of the regional deformation that affected the Meguma Supergroup to between 395 and 388 Ma.

Processes	Type of process	Evidence
fractional crystallisation	physical	♦ field observations of less evolved granitoids being intruded by more evolved granitoids (MacDonald et al. 1992) ♦ layering showing mineral separation (early removal of biotite and plagioclase for example) from a liquid through gravity settling or flowage differentiation (Clarke and Chatterjee 1988)
	chemical	♦ correlation between pairs of chemical elements showing addition or removal of mineral phase(s) (MacDonald and Clarke 1991; Clarke et al. 1997) ♦ decrease in An content of plagioclase, decrease in modal abundance of biotite ♦ lower total of rare-earths for more differentiated fraction (Muecke and Clarke 1981; Kontak et al. 1988) ♦ Rb increases, whereas Sr and Ba decrease. K/Rb decreases (Kontak et al. 1988) ♦ high concentration of incompatible elements in most evolved fraction (Charest 1976; Farley 1978 for example)
contamination	physical	♦ presence of xenoliths, especially in first emplaced granitoid fraction, i.e., least evolved one (McKenzie 1974; Clarke et al. 1998 for example)
	chemical	♦ lower εNd for most differentiated fraction (Clarke et al. 1988) ♦ higher $^{87}Sr/^{86}Sr$ for most differentiated fraction (Clarke and Halliday 1980; Clarke et al. 1988) ♦ close similarity to Meguma Supergroup rocks in S isotopes for more evolved fraction (Poulson et al. 1991)
subsolidus hydrothermal alteration	physical	♦ presence of obvious alteration zones (clays, episyenites, greisens (O'Reilly et al. 1982) ♦ presence of vein-type deposits such as Mn Mines and Millet Brook (Chatterjee et al. 1985; O'Reilly 1992)
	chemical	♦ end-member examples of hydrothermal alteration affecting minerals: • light alteration of one or several rock forming minerals (kaolinisation of alkali feldspar, sericitisation of plagioclase for example) • pervasive alteration leading to greisen, breccia, episyenite, or hematitisation (Logothetis 1985) ♦ preferential partitioning of incompatible elements in a fluid phase, hence presence of mineral deposits (O'Reilly et al. 1982 for example) ♦ mobility of REE in more evolved fraction (Kontak et al. 1988; Kontak 1990) ♦ $\delta^{18}O$ disturbed in alkali feldspar (Kontak et al. 1988) ♦ enrichment in F (Kontak 1990; MacDonald and Clarke 1991) ♦ disturbed element ratio (K/Rb) (MacDonald and Clarke 1991)

Table 1.2: Physical and chemical evidence for the main processes of differentiation in the SMB. Three main processes exist: fractional crystallization, contamination, and hydrothermal alteration.

Clastic sediments and marine carbonates of the Horton and Windsor Groups, respectively, unconformably overlie the SMB. The presence of miospores of Late Devonian age (Late Famennian) in the basal Horton Group indicates a minimum age of ~ 360 Ma (Devonian time scale of Tucker et al. 1998) for exhumation of the NE part of the SMB prior to formation of the Late Devonian/Carboniferous basins (Martel et al. 1993; Martel and Gibling 1995).

Radiometric ages

U-Pb zircon and monazite from the SMB and satellite plutons in the Meguma Zone yield ages ranging between 385 and 368 Ma, with a mean age of ~ 375 Ma (Harper 1988; Hill 1991; Keppie et al. 1993; Currie et al. 1998; Keppie and Krogh 1999; Clarke et al. 2000). A large range of ages exists based on $^{40}Ar/^{39}Ar$ mica dates, but such a range reflects partial resetting of the isotopic system rather than primary magmatic ages. The best magmatic ages for the SMB and satellite plutons obtained using $^{40}Ar/^{39}Ar$ range between 372 and 368 Ma (Reynolds et al. 1987; Kontak et al. 1989; Clarke et al. 1993b; Keppie et al. 1993; Kontak and Reynolds 1994; Keppie and Dallmeyer 1995; Kontak et al. 1999; Fallon et al. 2001). Rb/Sr dating for granite emplacement for the same intrusions ranges between 374 and 361 Ma, whereas several younger ages are certainly the result of resetting of the isotopic system (Clarke and Halliday 1980; Cormier et al. 1988; Harper 1988; Chatterjee and Cormier 1991; Hill 1991). The Wedgeport pluton (western MLT) represents the only apparently younger granitic body within the MLT with an U-Pb age of 316±5 Ma (Cormier et al. 1988) and $^{40}Ar/^{39}Ar$ mica ages of 258±8 Ma (Reynolds et al. 1981; Cormier et al. 1988), although Kontak (pers. comm. 2003) obtained an older U-Pb zircon age of 354 Ma. Table 1.3 summarises the main radiogenic isotope data (U-Pb, $^{40}Ar/^{39}Ar$, or Rb/Sr) available for the granitoid rocks of the MLT. Chapter 4 contains an exhaustive Section about previous age determinations within the MLT, as well as the integration of the new age determinations for this study.

Methods	Central plutons	Southwestern plutons	Eastern plutons	References
Rb-Sr on whole rock	374-361	(WP: 323)	373	Clarke and Halliday (1980) Cormier et al. (1988) Harper (1988) Hill (1991) Chatterjee and Cormier (1991)
$^{40}Ar/^{39}Ar$ on muscovite and biotite	376-366	373-370	377-368	Reynolds et al. (1987) Kontak et al. (1990) Clarke et al. (1993) Keppie et al. (1993) Kontak et Reynolds (1994) Keppie and Dallmeyer (1995) Kontak et al. (1999) Fallon et al. (2001)
U-Pb on monazite or zircon	385-371	378-368 (WP: 316)	378-370	Harper (1988) Cormier et al. (1988) Hill (1991) Keppie et al. (1993) Currie et al. (1998) Keppie and Krogh (1999) Clarke et al. (2000)

Table 1.3: Summary of the main radiogenic isotope data (U-Pb, $^{40}Ar/^{39}Ar$, or Rb/Sr) for the granitoid rocks of the MLT. WP=Wedgeport pluton. Ages in Ma.

1.2.2.4. Petrogenesis

Is the SMB a syn- or post-tectonic body?

Numerous previous studies have concluded that the SMB was mainly unaffected by any regional deformation related to the Acadian Orogeny, and is therefore a post-tectonic body (Cormier and Smith 1973; McKenzie 1974; Clarke and Chatterjee 1988). Other evidence indicates the continuation of transpression of the MLT in a northwest direction during and/or after granite emplacement:

1) general elongation of the SMB parallel to regional fold trends (Horne and Culshaw 2001);
2) presence of syn- to late-intrusion faults and shear zones and of aligned megacrysts and xenoliths parallel to regional structures of the MLT in the granite, as well as the continuation of these structures into the overlying Carboniferous rocks (Horne et al. 1988, 1992; MacDonald et al. 1992);

3) northeast-southwest- to east-west-trending of a magnetic fabric (AMS) in the granite (Benn et al. 1997);
4) presence of structurally controlled tin greisens along extensive fault zones at East Kemptville, within the Davis Lake pluton (Kontak and Cormier 1991; Kontak 1994);
5) weak foliation of cordierite grains (Clarke and Halliday 1980) or other porphyroblasts (MacDonald 1982) in cleavage planes, as well as the truncation of garnet and cordierite grains by flexural-slip structures in the contact aureole (Horne and Culshaw 2001);
6) boudinaged andalusite with sillimanite in boudin necks in the country rock (Culshaw and Bhatnagar 2001);
7) $^{40}Ar/^{39}Ar$ ages recording post-Acadian Orogeny tectono-thermal events in the Meguma rocks (Kontak and Cormier 1991; Keppie and Dallmeyer 1995; Culshaw and Reynolds 1997); and
8) dextral displacement of the Cobequid-Chedabucto Fault System (Mawer and White 1987).

Although the main folding event of the Acadian Orogeny was complete by the time of the SMB emplacement ($^{40}Ar/^{39}Ar$ ages 395-388 Ma, Hicks et al. 1999), there is evidence for brittle flexural-slip deformation ca. 370 Ma ago that may account for the syn-to late-tectonic strain observed within the SMB (Horne and Culshaw 2001). These authors also suggest that the transition from ductile (main folding event) to brittle (flexural slip) may represent unroofing and cooling of the area within the 15-30 My separating both types of deformation.

Pressure constraints

Clarke et al. (1976) report the presence of magmatic andalusite in the SMB, indicating a maximum pressure of 3.3-3.9 kbar and temperature of 650-680 °C for late-stage crystallization of the SMB. Ham and Kontak (1988) proposed a pressure of ~ 2 kbar for magmatic (primary) muscovite crystallisation. Based on a study of the metamorphic aureole of the SMB, Mahoney (1996) reported an average pressure of ca. 3.0-3.5 kbar, corresponding to depths of emplacement of 10-12 km. Halter and

Williams-Jones (1999) and Kontak et al. (2001) used combined geothermometry and fluid inclusion isochors to constrain the pressure of the East Kemptville deposit to 3.5-4 kbar. Keppie and Dallmeyer (1995) suggested rapid exhumation (~ 13 km) in the Meguma Zone between 370 and 360 Ma, and Murphy et al. (1999) proposed that an overridden mantle plume may be the cause of this rapid Late Devonian uplift.

Origin of the granitoid rocks of the MLT

The origin of the SMB is rather controversial. Table 1.4 summarizes the three different protoliths proposed (Meguma Supergroup, Liscomb gneisses, and Tangier granulites) based on diverse sets of evidence. Whereas the Meguma Supergroup seems to be an unlikely protolith for the SMB, both the Liscomb gneisses or/and the Tangier granulites are possible candidates. From a more general point of view, the central intrusions seem to have a crustal origin, whereas the peripheral plutons (represented by the Port Mouton pluton) have physical and chemical evidence of a mixed crustal and mantle origin (Clarke et al., 1997, 2000).

1.3. Purpose, scope, and organisation

1.3.1. Thesis purpose and scope

This project aims to update available field and petrological data, and to gather a new range of data (fluid inclusions, stable isotopes, mineral chemistry, and $^{40}Ar/^{39}Ar$ and $^{75}Re/^{76}Os$ dating), mainly oriented towards a better understanding of the hydrothermal fluids (composition, temperature, pressure, age) related to the mineralisation of the New Ross area. Also, this study furthers the understanding of white mica chemistry, using microprobe analyses, as the starting point for a bivariate and multivariate statistical analysis. This study creates the first integrated model explaining the possible origin and sequence of development of the different mineral deposits of the core of the SMB in a consistent and logical spatial-temporal-thermal and genetic framework.

Proposed protoliths	Evidence	
	Pro	**Con**
Meguma Supergroup	♦ δO^{18} data (Longstaffe et al. 1980)	♦ $^{87}Sr/^{86}Sr$ of granites too low (Clarke and Halliday 1980) ♦ εNd of granites too high (Clarke et al. 1988) ♦ $\delta^{34}S$ ratio too low (Poulson et al. 1991)
Liscomb gneisses	♦ Similarity of the Liscomb Complex granitic rocks with other granitic bodies of the MLT, based on geochemical and isotopic data (Clarke et al. 1993a) ♦ younger crustal residence time than the Meguma Supergroup rocks (Clarke et al. 1988)	
Tangier granulites	♦ Partial fit for range of $^{208}Pb/^{204}Pb$, but contaminated with the Liscomb Complex and Meguma Supergroup (Chatterjee and Ham 1991) ♦ Sr and Nd isotopic composition (Eberz et al. 1991)	♦ Pb isotope evidence for an evolved upper crustal source (and not lower crustal granulite source) (Kontak and Chatterjee 1992)

Table 1.4: Evidence for and against the three proposed protoliths for the granitoid rocks of the SMB: Meguma Supergroup, Liscomb gneisses, and Tangier granulites.

1.3.2. Thesis organisation and relationship to published work

1.3.2.1. Thesis organisation

Chapter 2 provides information about the history, field relations, and petrography of eight mineral deposits in the New Ross area. A detailed optical and chemical study of white mica attempting to discriminate between primary (magmatic) and secondary (hydrothermal) white micas appears in Chapter 3. Chapter 4 presents age data for the mineral deposits obtained using $^{40}Ar/^{39}Ar$ (white micas and alkali feldspars) and $^{187}Re/^{187}Os$ (molybdenite). Chapter 5 provides an insight into the nature of the hydrothermal fluids of the New Ross area based on a detailed fluid inclusion investigation. Stable isotope data (O and H) of both white micas and quartz-hosted fluid inclusions are discussed in Chapter 6. Using the available geochemical dataset for the SMB and applying experimental data from the literature in Chapter 7, I

provide a better constraint on the source(s) of ore metal constituents, their transport by, and precipitation from, hydrothermal solutions. Chapter 7 also attempts to integrate each set of data in a single model explaining the origin of the mineral deposits in the New Ross area. Chapter 8 provides a synthesis of the conclusions reached throughout the thesis and suggestions for future work.

1.3.2.2. Relationship to published work

Two Chapters (5 and 6) of this thesis are independent manuscripts, but complementary in their content. Unavoidably, some repetition of material present in the introductory chapters of this thesis occurs in the papers.

Chapter 5 is published in volume 91 of the Transactions of the Royal Society of Edinburgh as a paper entitled *Granite-hosted mineral deposits of the New Ross area, South Mountain Batholith, Nova Scotia, Canada: P, T, and X constraints of fluids using fluid inclusion thermometry and decrepitate analysis*. Co-authors are Dan Kontak and Barrie Clarke. I did the analytical work myself, under the direction of Dan Kontak, at his fluid inclusion laboratory, located at the Department of Natural Resources. I interpreted the data, with helpful contributions from both co-authors. Other work in this thesis now supersedes some of the material in Chapter 5.

Chapter 6 has been accepted for publication in the Canadian Mineralogist as a paper entitled *An integrated stable isotope and fluid inclusion study of granite-hosted mineral deposits of the New Ross area, South Mountain Batholith, Nova Scotia, Canada: evidence for multiple fluid reservoirs*. Co-authors are Dan Kontak, Barrie Clarke, and Kurt Kyser. Kurt Kyser and his staff conducted the stable isotope analyses at the Isotope Laboratory of the Department of Geological Sciences and Geological Engineering at Queen's University (Kingston, Ontario). I interpreted the data myself, with strong benefit from discussions with the co-authors and members of my Ph.D. supervisory committee. This paper is still subject to modifications as requested by its reviewers.

CHAPTER 2

POLYMETALLIC MINERAL DEPOSITS, NEW ROSS AREA

2.1. Introduction

This chapter contains the location, past exploration history, field description, petrography, and mineralogy of selected samples from eight mineral occurrences in the New Ross and Salmontail Lake Plutons. The descriptions of the mineral occurrences are based on assessment reports in Nova Scotia Department of Natural Resources files, geological maps of the area (particularly the nomenclature of the different map units, see Fig. 1.2b; Corey 1991; Ham 1991; Horne 1992; MacDonald 2001), the earlier work of O'Reilly et al. (1982), the compilation report by MacDonald (2001), and new observations from the present study. With the help of a field assistant, Rachel H. Speller, I carried out field work during the summer of 1998 and investigated seven of the eight mineral occurrences chosen for this study, updating maps from O'Reilly et al. (1982), and sampling. All mineral occurrences are located in Lunenburg County, except for the Millet Brook deposit in Hants County. All samples are listed and described in Tables 2.3 and 2.4.

2.2. The New Ross area

The eight mineral occurrences of this study are part of the New Ross-Vaughan Complex (NRVC) (McKenzie 1974), renamed the Stage II New Ross Pluton (NRP) (MacDonald et al. 1992; MacDonald, 2001) of the SMB, and also the earlier Stage I Salmontail Lake Pluton (SLP). The NRP is an 870 km^2 pluton, roughly circular in shape, displaying muscovite-biotite monzogranite, coarse- and fine-grained leucomonzogranite [rock of monzogranitic composition (Streckeisen 1976) with less than 6% combined mafic minerals (Corey 1991)], and leucogranite [rock of monzogranitic composition (Streckeisen 1976) with less than 2% combined mafic minerals (Corey 1991)]. Granodiorite to the west, and an inlier of metasedimentary

rocks of the Meguma Supergroup to the north, border the NRP. The inlier separates the Stage II NRP from the Stage I SLP (Fig. 1.2a). The SLP is a 650 km^2 pluton, elongated in a northeastern direction, containing biotite granodiorite, biotite monzogranite, and a small proportion of fine-grained leucomonzogranite (Corey 1991; Ham 1991; Horne 1992; MacDonald 2001).

The NRP shows the most pronounced negative gravity anomaly in the SMB (Garland 1953, Williams and Haworth, 1984), and one of the highest average surface concentrations for radioactive elements (Chatterjee and Muecke 1982). The negative Bouguer anomaly suggests a mushroom shape for the SMB with a maximum thickness of 10-20 km near New Ross (O'Reilly 1975). Therefore, the formation of the numerous and varied mineral occurrences in this area may be the logical consequence of the presence of a large volume of highly-evolved granitoid rocks enriched in incompatible metals, and a larger concentration of fluids whose circulation is favoured by a higher heat flow. A more recent interpretation of gravity data shows the SMB as "a tabular body" with a "flat to gently sloping floor" for a thickness of ~ 7 km (Benn et al. 1999).

Most of the New Ross deposits were discovered in the late 1890's-early 1900's, with the notable exception of the Millet Brook uranium deposit, which was discovered in 1976 (Chatterjee et al. 1982; Chatterjee and Strong 1984). The NRP contains aplite-pegmatite deposits (Reeves, Keddy, Morley's, Walker, Long Lake) and greisen-type deposits (Turner, Walker, Long Lake), whereas the SLP hosts vein deposits (Millet Brook, Mn mines). Greisenisation is a process of hydrothermal alteration in which granites are progressively transformed into a mixed assemblage of quartz, white mica (commonly lepidolite), ± topaz, and ± tourmaline. Rocks that underwent only partial greisenisation are referred to as greisenised granite, and total greisenisation (i.e., modal proportion of both feldspars < 10%) forms greisen (definition after Shcherba 1970; Charoy and Ramboz 1981; Bates and Jackson 1987; Foucault and Raoult 1988).

Section 2.3 presents the location, main steps in the discovery and exploration, geology, petrology, and mineralogy of eight selected mineral deposits in the New

Ross area. Table 2.1 presents the metals associated with each deposit and is organised by deposit types.

Deposit Name	Deposit Types	Metal associations
Reeves	aplite/pegmatite	**Sn**, F, W, Li, Nb, Ta, As, P, Mo, Be, B, Mn, Fe, Bi, Pb, Ag, Cu, REE
Morley's	greisen and aplite/pegmatite	**W**, Sn, F, Nb, Ta, Be, Li
Keddy	greisen and aplite/pegmatite	**Mo**, Nb, Ta, W, F, Cu
Long Lake	greisen and aplite/pegmatite	**Mo**, Cu, W, F
Walker	greisen and aplite/pegmatite	**Mo**, Cu, F, Zn, W, Sn
Turner	greisen and vein	**Sn**, Cu, As, Zn, U, W, Fe, F
Millet Brook	vein	**U**, Cu, Pb, Zn, Ag, W
Mn mines	vein	**Mn**, Fe

Table 2.1: Deposit types and their metal associations. Metals are in order of importance within deposit, with those in bold being the most abundant.

2.3. Description of the mineral deposits in the New Ross area

2.3.1. Aplite-Pegmatite Deposits

2.3.1.1. Reeves deposit

Location (Fig. 2.1)

Latitude: 44°43.805' N

Longitude: 64°31.070' W

The Reeves pegmatite lies south of the Forties Road, 4.8 km west of Highway 12. The Morton-Reeves Road leads to the Reeves Farm, and the path leading to the deposit is another 42 m along the road from the farmhouse driveway. A small pit and an overgrown dump area lie 500 m from the road in a southwestern direction. The path is overgrown and a GPS may be necessary to locate the deposit.

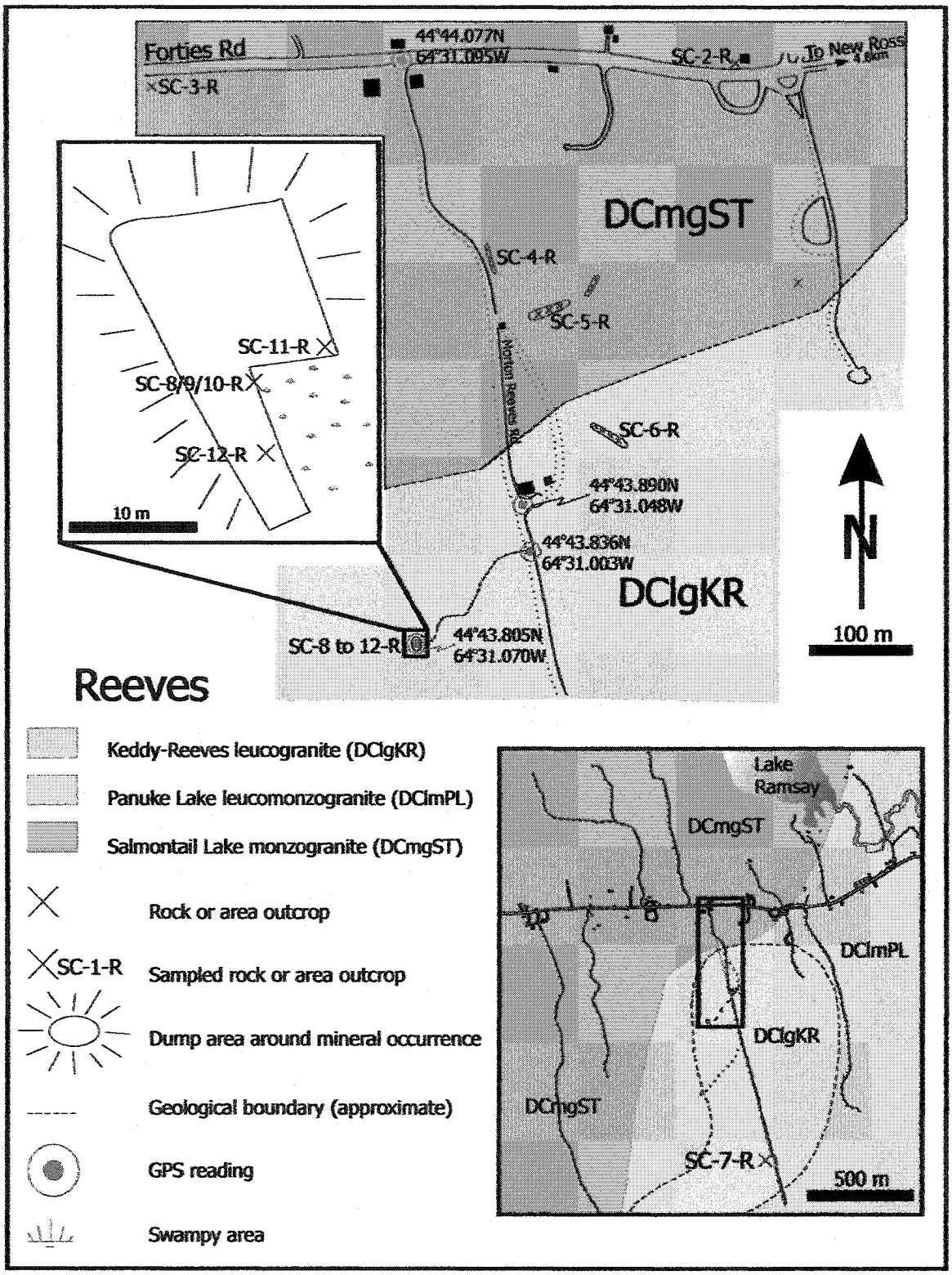

Fig. 2.1: Location map and geology of the Reeves deposit. Geology after O'Reilly et al. (1982) and Horne (1992).

Past exploration

Faribault (1907) first mentioned the Reeves and reported the digging of a pit by the landowner in 1903, uncovering fluorite and cassiterite associated with quartz crystals. Further investigation led to the digging of a shaft (5.4 m deep, 3.6 m long, and 3 m wide), uncovering a pegmatitic segregation within a light grey leucogranite. An impressive diversity of interesting minerals is present in the central part of the pegmatite: cassiterite (Sn); monazite (REE); durangite (As); lepidolite (Li); amblygonite (Li, P, F); wolframite and scheelite (W); molybdenite (Mo); beryl (Be); tourmaline (B); fluorite (F); pyrolusite and manganite (Mn); limonite, hematite, magnetite, siderite, and pyrite (Fe); bismuthinite (Bi); galena (Pb, Ag); and copper (Cu). Faribault (1907) described the pegmatite as having large masses of kaolinised orthoclase enclosing large quartz crystals (more than 30 cm), and some white mica. The pegmatitic dyke has an irregular shape, strikes in 065°, and dips to the northwest. Robinson (1914) reported the absence of radioactive minerals in the Reeves deposit. By then, only the dump around the shaft provided samples, because the shaft had filled with water. Ellsworth (1932) identified amblygonite as the most abundant of the unusual minerals present at Reeves. He also confirmed the presence of topaz (F), zinnwaldite (Li), and manganapatite (Mn). Cameron (1949) also reported no radioactivity for the Reeves deposit. Wallace et al. (1963) led a survey for tin and related minerals in the New Ross area: drill holes proved that the pegmatite pinches out at depth, and chemical analysis of samples from drill holes contained small concentrations of tin (<100 ppm). Charest (1976) recognised tapiolite (Ta, Nb), and listed the following minerals identified by the Nova Scotia Museum staff: columbite (Nb), microlite (Ta), tungstite (W), morinite (F), triploidite (P), triphyllite (Li), and more interestingly U- and Cu-bearing metatorbernite. Felderhof (1978) investigated fluorite potential at the Reeves deposit, but estimated that it was too rare for potential prospect. O'Reilly et al. (1982) observed only few of the minerals (fluorite, lepidolite, fluoroapatite) previously recorded at the Reeves deposit. The landowner has recently reclaimed the site and filled in the small excavation that previously permitted examination of the pegmatite (G. A. O'Reilly pers. comm. 2002).

Geology

The Reeves quartz-feldspar-white mica pegmatite (Figure 2.2) intrudes the medium-grained Keddy-Reeves leucogranite (Figure 2.3), which in turn intrudes the Panuke Lake muscovite-biotite leucomonzogranite (Figure 2.4) and, in its northern part only, the Salmontail Lake biotite monzogranite (Figure 2.5). As stated in the "Past exploration" Section, numerous metallic minerals were reported from the central part of the dyke, but observation of, and access to, the pegmatite is now limited because the excavated pit is filled. The dump area only contains pegmatitic samples, with fluorite and lepidolite, and a small outcrop (~ one metre) borders the edge of a water-filled pit, showing the transitional contact between the Keddy-Reeves leucogranite and the pegmatite.

2.3.1.2. Morley's Pegmatite

Location (Fig. 2.6)

Latitude: 44°44.408' N

Longitude: 64°26.402' W

The Morley's pegmatite prospect lies to the east of the New Russell Road, on the south bank of Mill Brook in New Ross. A wood road parallel to the brook for 400 m leads to the excavated pegmatite site lying 27 m north of the road.

Past exploration

Faribault (1931) reported an elongate pegmatite dyke (1.6 km) on his geological map of the New Ross area. He reported scheelite (W), cassiterite (Sn), beryl (Be), columbite (Nb, Ta), lepidolite (Li), and the presence of radioactive mineral(s). Douglas and Campbell (1941a) reported a strike of 35° and a dip of 60° southeast for the pegmatite, and also described a jasper breccia striking parallel to the pegmatite,

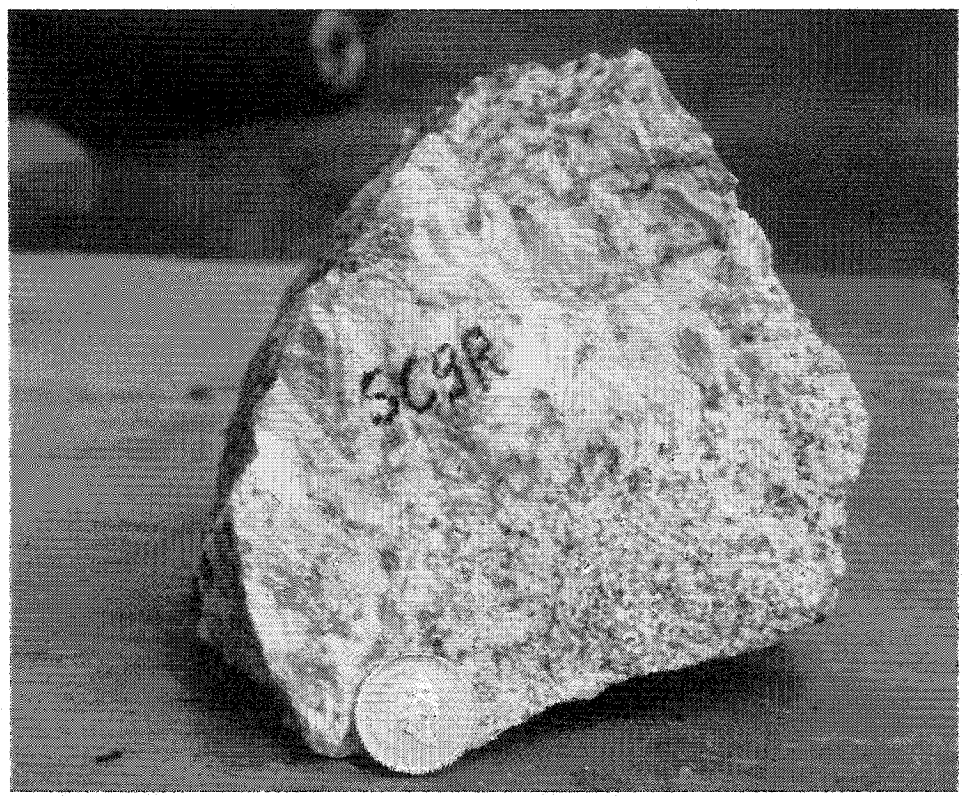

Fig. 2.2: Quartz-feldspar-white mica pegmatite (SC-9-R) from the Reeves deposit, here at the contact with its host rock, the Keddy-Reeves leucogranite. Diameter of coin: 23 mm.

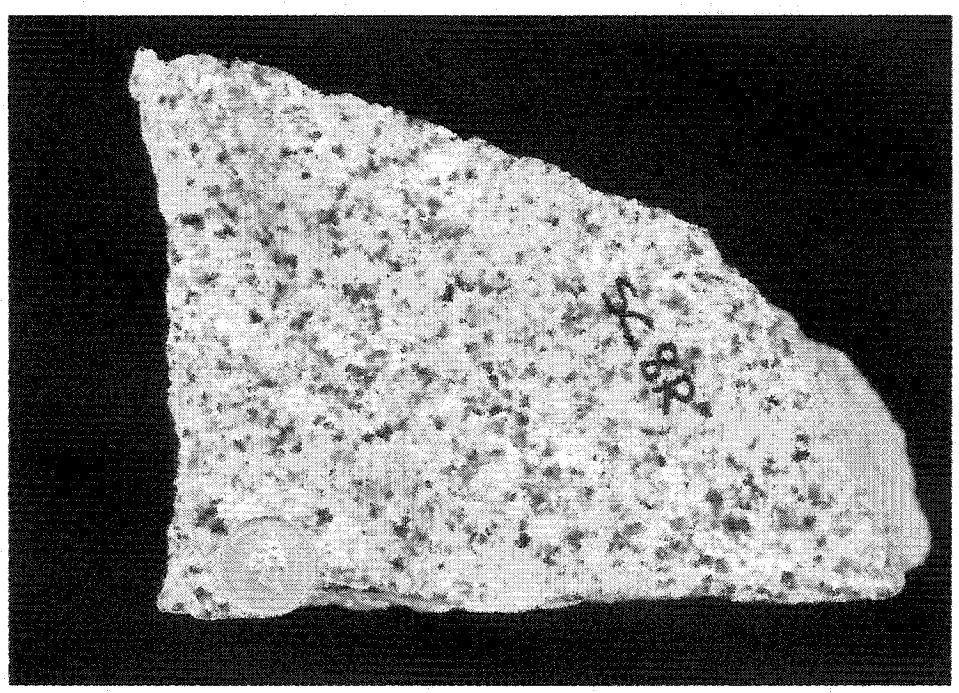

Fig. 2.3: Keddy-Reeves leucogranite (SC-8-R) essentially composed of quartz-two feldspars-white mica. Dark spots represent strongly kaolinised feldspars. Diameter of coin: 23 mm.

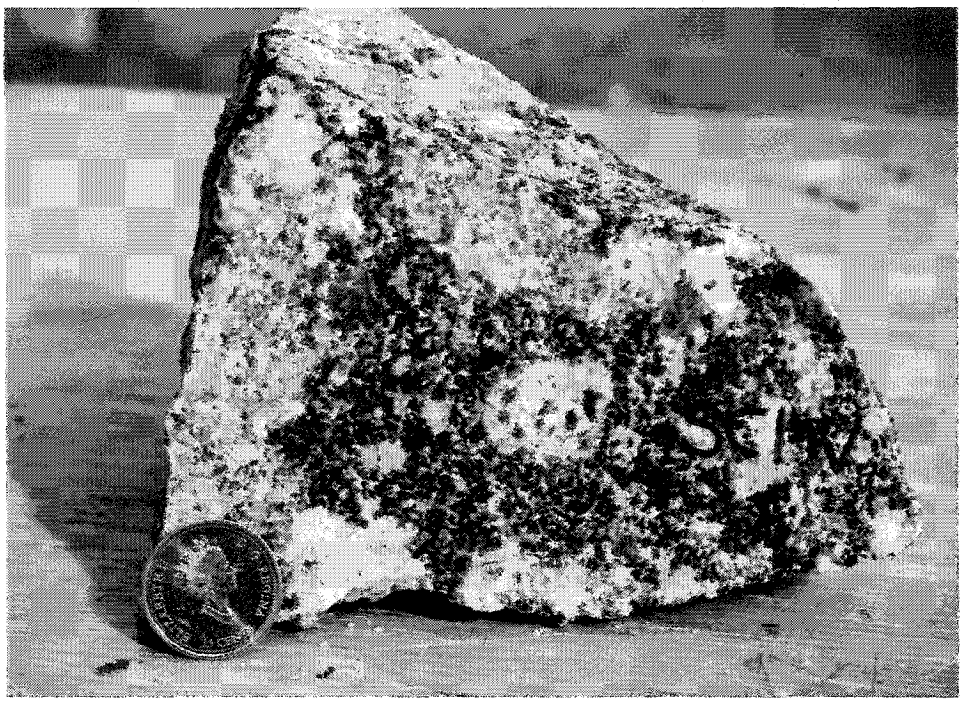

Fig. 2.4: Coarse-grained porphyritic Panuke Lake muscovite-biotite leucomonzogranite (SC-1-W). The sample is slightly hematised. Diameter of coin: 23 mm.

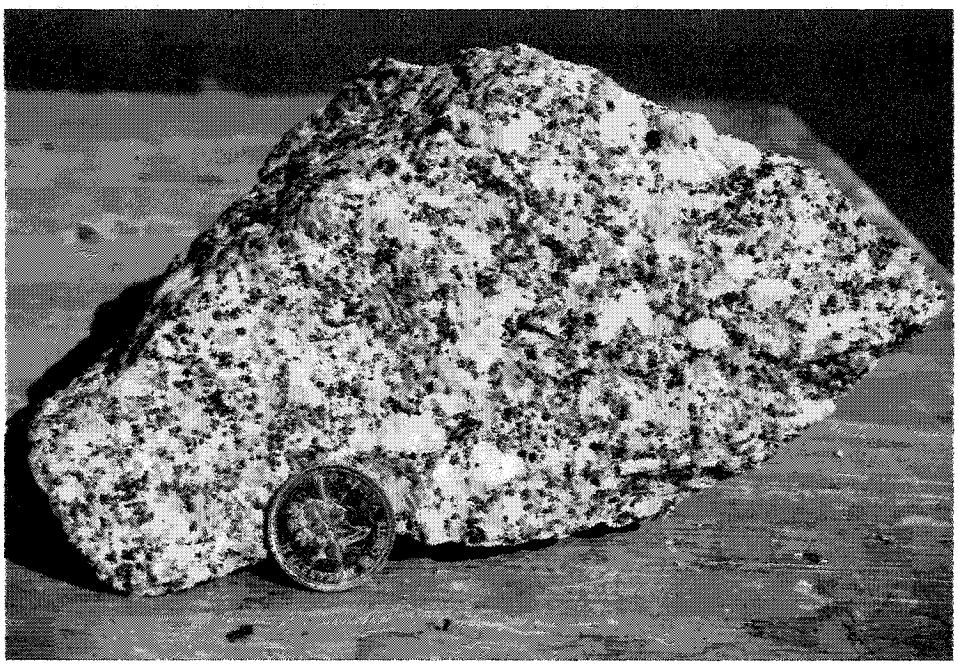

Fig. 2.5: Fresh sample of the Salmontail Lake biotite monzogranite (SC-3-D). Diameter of coin: 23 mm.

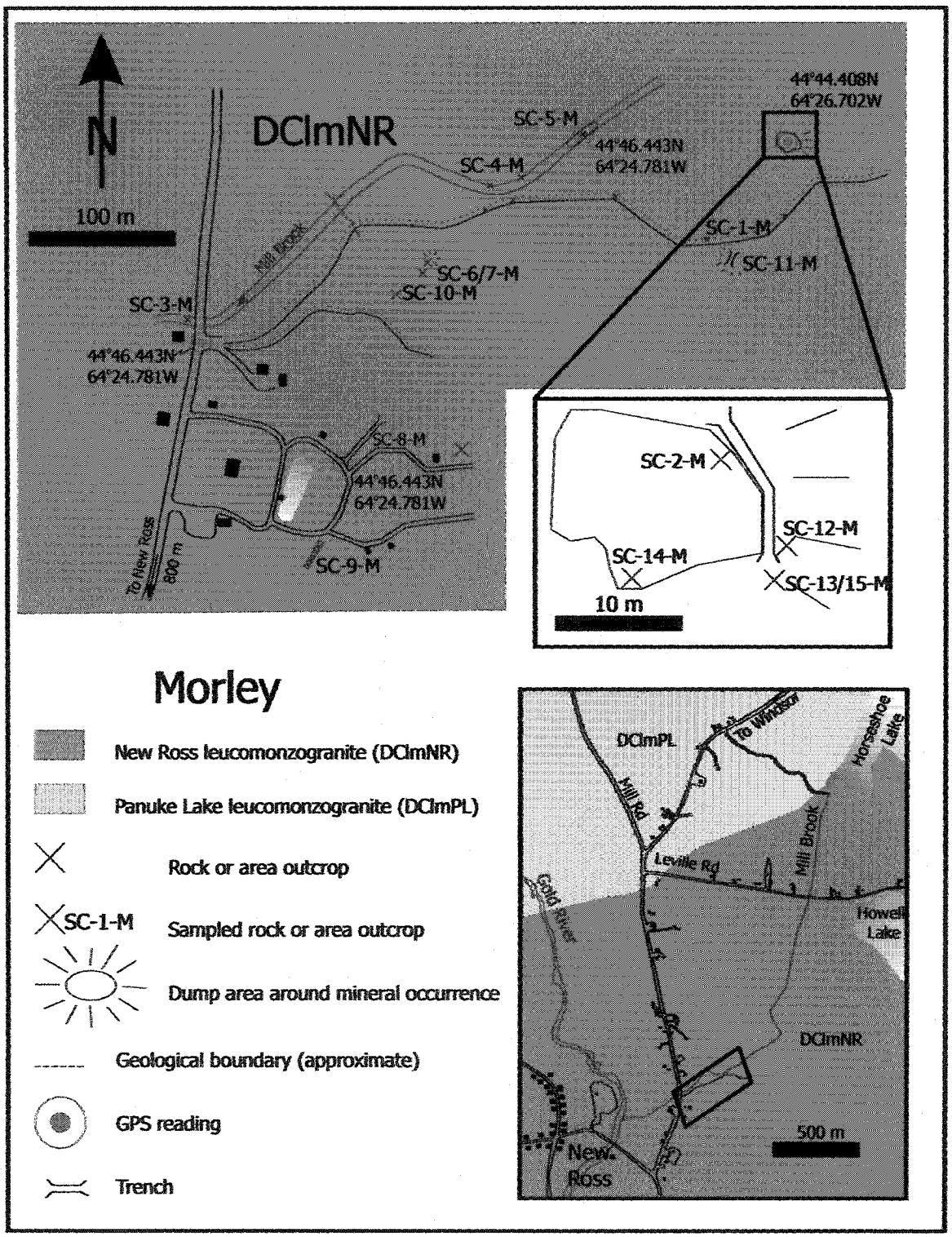

Fig. 2.6: Location map and geology of the Morley's pegmatite. Geology after O'Reilly et al. (1982) and Corey (1991).

but dipping east 55°. Breccia and pegmatite have a gradational contact with each other, and with the surrounding host rock. A 10 m-long trench was dug, but beside pegmatitic quartz, feldspar, and white mica, they found no economically important minerals. A. K. Chatterjee analysed samples from the jasper breccia and obtained higher concentrations of F (~800 ppm), Li (~125 ppm), and W (1000 ppm) than in leucomonzogranite hosting the breccia (cited in O'Reilly et al. 1982). O'Reilly et al. (1982) re-mapped the area, and observed that most of what Faribault mapped as pegmatite might have been a zone of brecciation and hematisation of the host porphyritic monzogranite. O'Reilly et al. (1982) described the Morley's pegmatite as the largest of several exposed in the area. They depicted the pegmatite as being weakly zoned with an outer zone of pink perthitic orthoclase, quartz, and muscovite grading into an inner core of graphic granite and massive white quartz. O'Reilly et al. (1982) noted fluorite as the only mineral of economic significance.

Geology

Morley's pegmatite is hosted by the New Ross biotite-muscovite leucomonzogranite, which strongly resembles the Panuke Lake biotite-muscovite leucomonzogranite (Fig. 2.4). The pegmatite grades into a medium-grained leucogranite suggesting that they are contemporaneous (O'Reilly et al. 1982), and both intrude the host rock. The leucogranite was not observed during field mapping. The pegmatite grades into massive quartz towards the centre of the dyke. Previous investigators reported several pegmatitic pods in the area, but during this study we observed only the one shown on the location map. A pegmatite dump located southwest from the main pegmatite location represents the remains of previous investigations. Only fluorite and minor molybdenite occur, although Campbell (1940) reported other minerals of interest (scheelite, wolframite, cassiterite, columbite). Hematisation (Figure 2.7) and brecciation associated with the intrusion of a brick red jasper breccia dyke overprint the host rock of the pegmatite. The jasper breccia (Figure 2.8) is a fine-grained groundmass of mainly quartz and hematite, with fragments of quartz, feldspar, and granite.

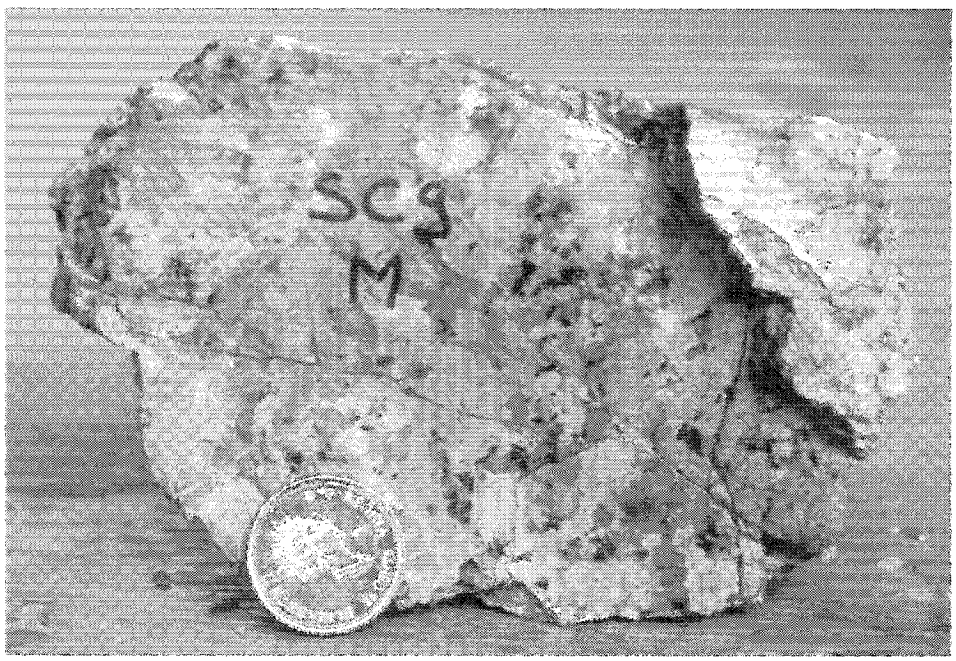

Fig. 2.7: Strongly hematised leucomonzogranite (SC-9-M) in the vicinity of the jasper breccia (Fig. 2.8) near the Morley's pegmatite. Biotite and both feldspars are very altered, making for a crumbly rock. Diameter of coin: 23 mm.

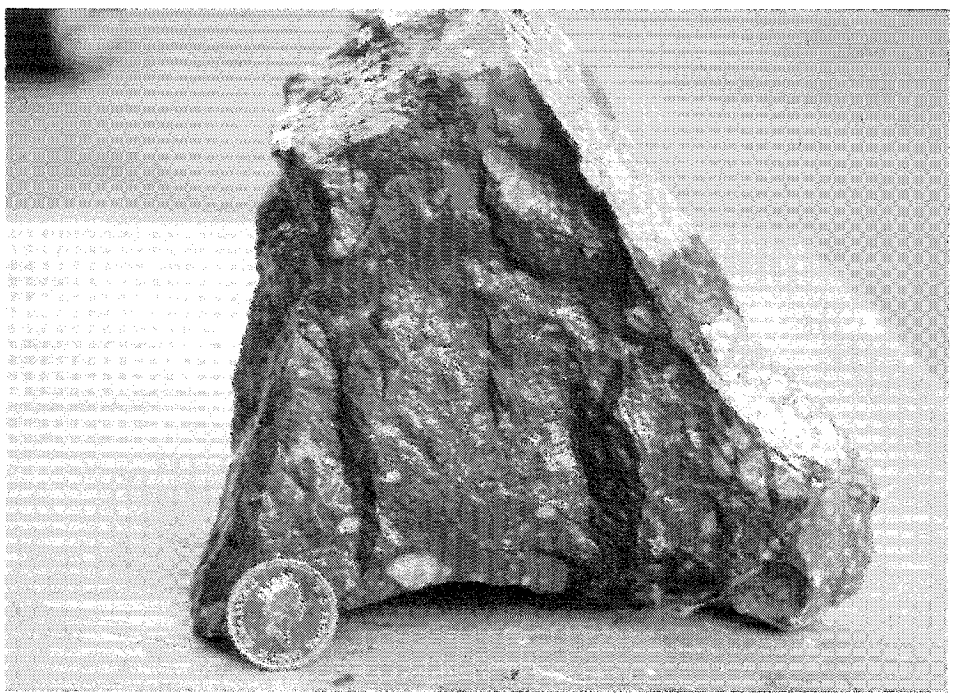

Fig. 2.8: Jasper breccia (SC-8-M) near the Morley's pegmatite. Note the very fine-grained hematised groundmass containing quartz and leucomonzogranite fragments.
Diameter of coin: 23 mm.

2.3.2. Aplite-pegmatite and greisen deposits

2.3.2.1. Keddy Deposit (also Wilcox, Larder River, or Lantz Prospect)

Location (Fig. 2.9)

Latitude: 44°42.983' N

Longitude: 64°29.610' W

The Keddy prospect is located south of the Forties Road, 4.2 km west of Highway 12. A north-south logging road starts off the Forties Road and the prospect lies on the west bank of the Larder River, about 3 km south of the Forties Road. Trails to the prospect have disappeared, and the easiest route to it is along the Larder River until reaching the southernmost part of the pegmatitic outcrop. An access from the other side of the Larder River is possible, but involves a potentially difficult crossing of the river.

Past exploration

After the discovery of the occurrence in the late 19th century, Walker (1911) first reported the presence of a molybdenite-bearing pegmatite near the Larder River in his report of molybdenum ore in Canada. Faribault (1924) mapped two pegmatite dykes bearing molybdenite (Mo) and radioactive minerals in the area. Douglas and Campbell (1941a) described molybdenite flakes scattered in a muscovite-rich granite. Cameron (1949) subdivided the prospect area into three zones: 1) flakes of molybdenite within a "fine aplitic grey granite" (two pits present, 1.8 and 1.2 m deep); 2) small irregular pegmatite dyke striking north and dipping shallowly to the west; and 3) quartz pegmatite with some molybdenite flakes (one pit of 1.8 m deep). Charest (1976) found only two of the three sites described by Cameron (1949), and observed molybdenite as fracture filling, thus concluding a deuteric origin for the mineral. O'Reilly (pers. comm. 2002) recognised columbite (Nb) within the pegmatite.

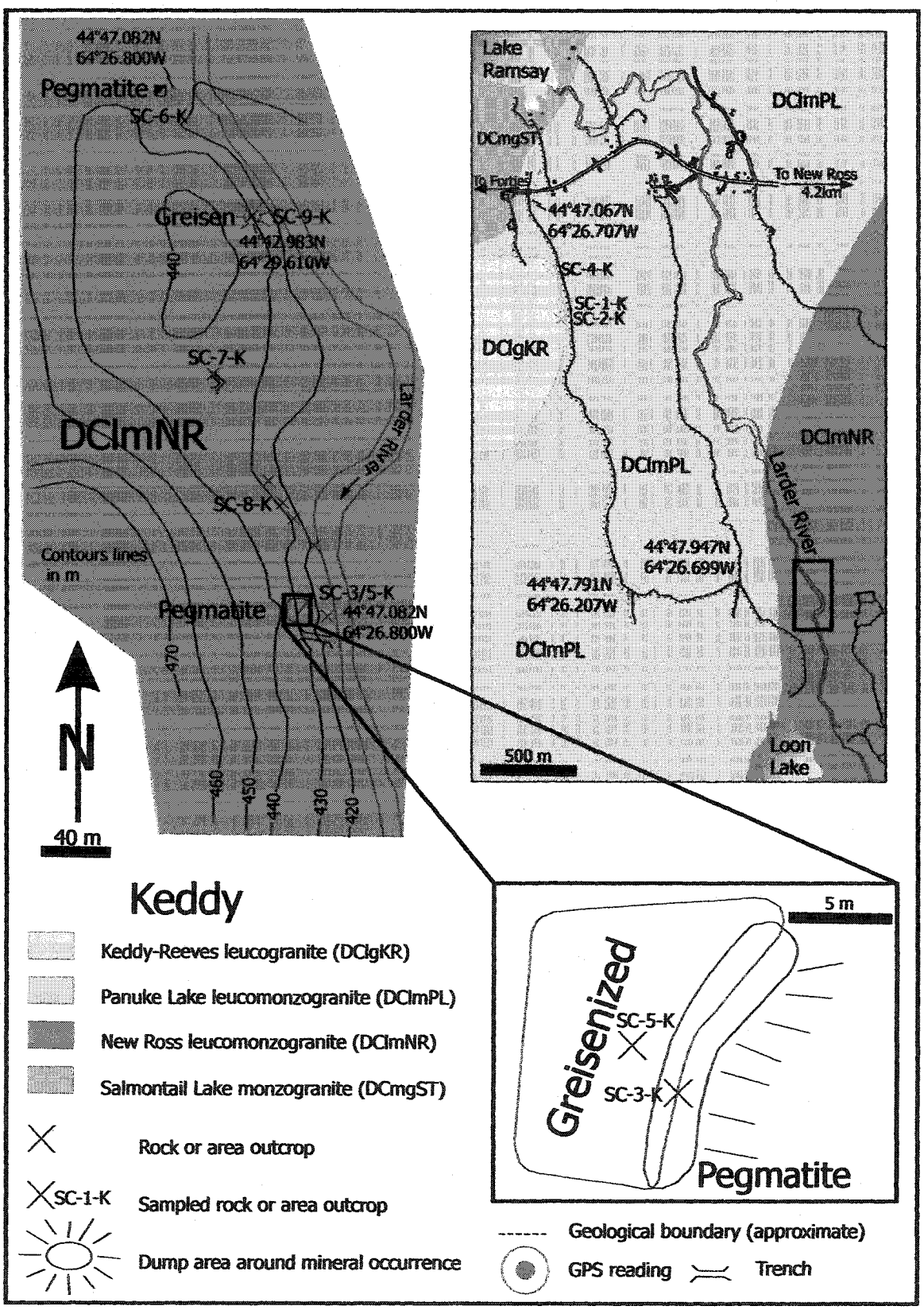

Fig. 2.9: Location map and geology of the Keddy deposit. Geology after O'Reilly et al. (1982) and Corey (1991).

Geology

The host granitoid rock of the prospect is the fine- to medium-grained, muscovite-rich Panuke Lake leucomonzogranite (Fig. 2.4). The prospect is divided into three previously prospected sites:

1) A central site of greisenised leucomonzogranite (Figure 2.10) with rare molybdenite that might be associated with the pegmatite (O'Reilly et al. 1982). A water-filled trench is present and a dump around it contains samples.
2) A southern site exposing a north-trending pegmatite (Figure 2.11) intruding the leucomonzogranite. Greisenised leucomonzogranite locally borders this pegmatite. We observed no mineralisation despite earlier reports citing molybdenite. A few pods of another north-trending pegmatite outcrop north of the southern site, but they are also barren of mineralisation. Numerous quartz veins cut the leucomonzogranite, close to the pegmatite.
3) A site located north of the central area comprises a small pit and dump samples of pegmatite containing molybdenite.

The whole area is heavily overgrown, and no outcrop is visible in the central and northern locations.

2.3.2.2. Long Lake

Location(Fig. 2.12)

Latitude: 44°36.072' N

Longitude: 64°22.469' W

The Long Lake prospect lies at the northwest end of Long Lake, south from New Ross. The site is accessible by a logging road beginning at Wayne Millet's lumberyard in Chester Grant and leading west from highway 12, 5 km north from Highway 103.

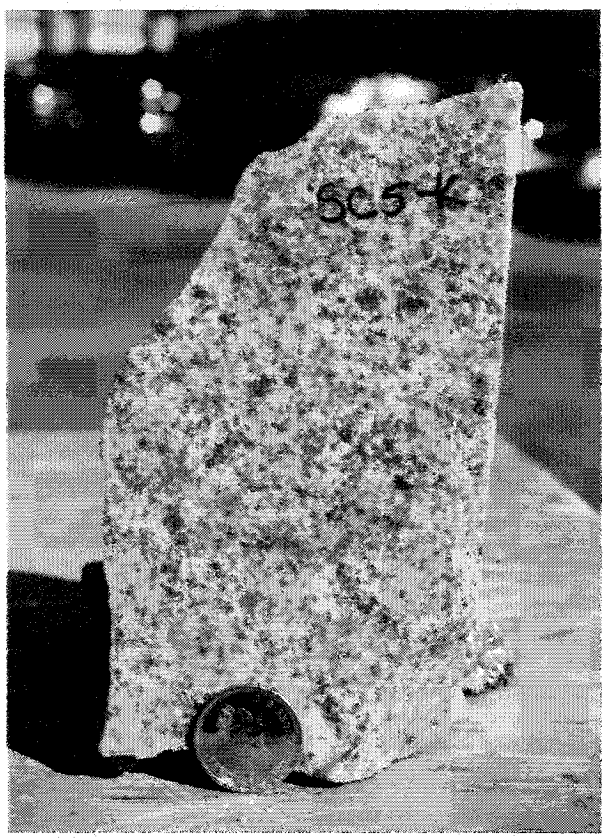

Fig. 2.10: Greisenised leucomonzogranite (SC-5-K) from the Keddy prospect. The rock is fine-grained and contains a high modal proportion of white mica. This sample is slightly hematised. Diameter of coin: 23 mm.

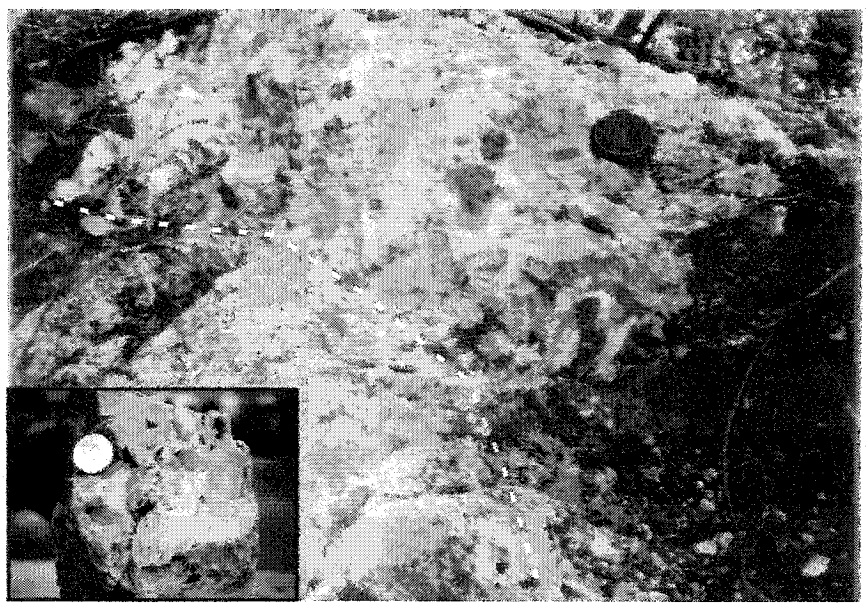

Fig. 2.11: Field exposure of part of the Keddy pegmatite (SC-3-K). Dashed line highlights the contact with the greisenised leucomonzogranite. Diameter of coin: 23 mm.

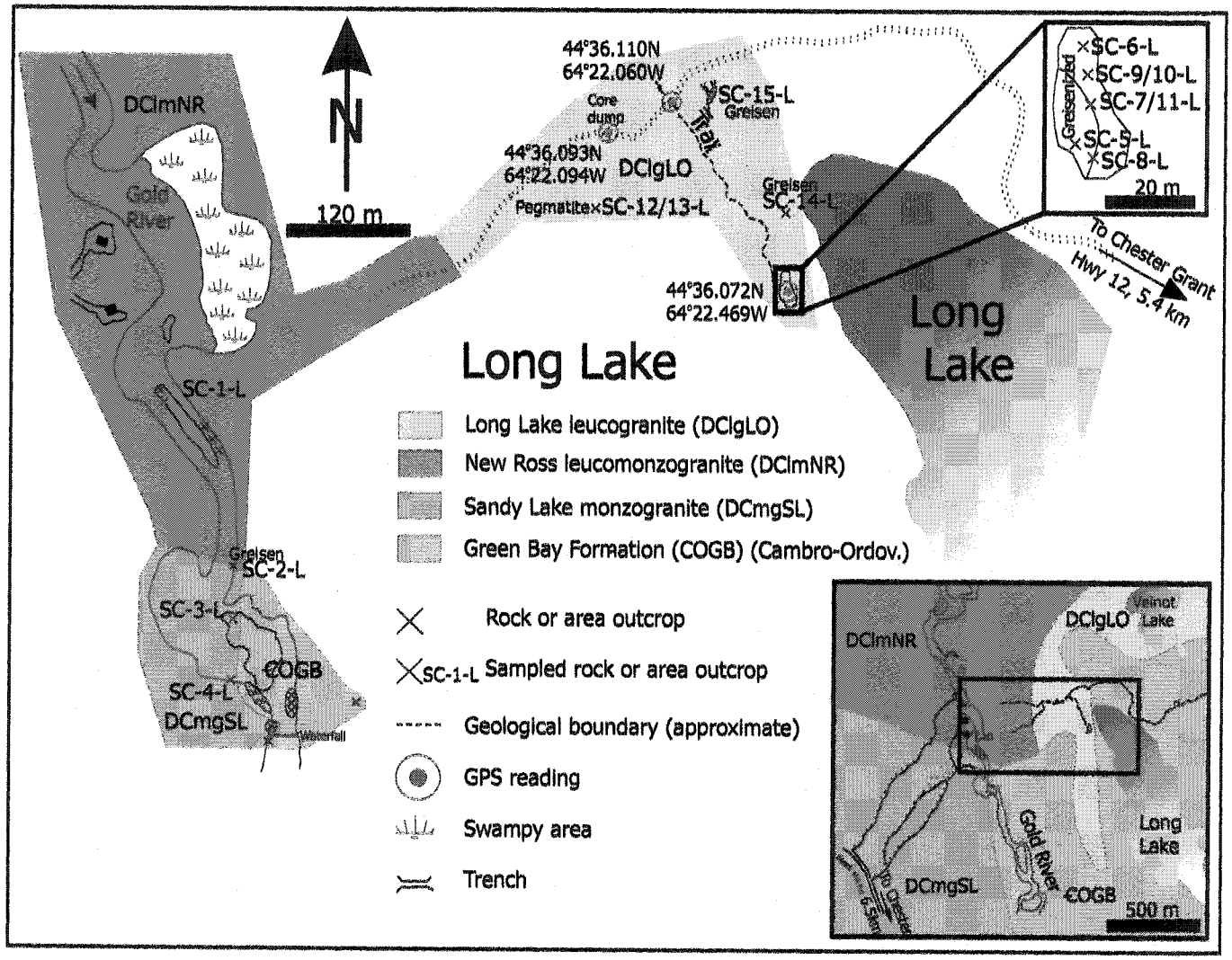

Fig. 2.12: Location map and geology of the Long Lake deposit. Geology after O'Reilly et al. (1982) and Corey (1991).

Past exploration

Faribault (1924) reported the Long Lake mineral deposit as a Mo-bearing locality. Wright (1959) described the first exploration of this deposit, following the discovery of good grade tungsten ore (scheelite) with a fluorescent lamp. Two trenches were dug. Wright (1959) observed scheelite and molybdenite, but in concentrations too low to be of economic interest. Oldale (1966) reported the removal of molybdenite mineralisation located within greisen and advised for further investigation in the area. Johnston (1966) summarised five different styles of molybdenite at Long Lake:

1) as blobs within massive quartz;
2) as blobs within pegmatite;
3) as bands within aplite adjacent to the pegmatite;
4) as fine grains within greisenised granite; and
5) as fine grains within unaltered granite.

Johnston (1966) also advised further trenching and diamond drilling in the Long Lake area. Shewman (1968) carried on a drilling program, but recommended no further work to be done after extensive evaluation for copper at Long Lake. Logothetis (1985) underlined the minor role played by fractures for transporting the greisenising fluids in the Long Lake area, and proposed a model where volatiles accumulated in the roof area of the host leucogranite.

Geology

The Long Lake leucogranite, intruding metasedimentary rocks of the Goldenville Group, hosts the Long Lake Prospect. The main excavated part of the prospect, at the NW end of Long Lake, comprises leucomonzogranite that grades into quartz-muscovite-albite and quartz-muscovite greisen (Figure 2.13). Areas of well-developed greisen contain molybdenite, wolframite, scheelite, fluorite, and copper sulphides either as disseminated grains within the greisen, or within vugs with large quartz crystals (Figure 2.14). West of the greisen zone, molybdenite-bearing boulders from the drilled pegmatite (Figure 2.15) and banded aplite occur. O'Reilly et al. (1982) considered that this pegmatite differs genetically from others in the area (Walker or

Reeves deposits for example). Within the greisen, microcline-coated fractures occur (Figure 2.16). These fractures obviously post-date the greisenisation event, and O'Reilly et al. (1982) stated that they derive from "metasomatic potassic rich fluids permeating outward from a cooling intrusion along fractures and channelways during the later stages of a metasomatic event". No mineralisation is known to be associated with these fractures.

2.3.2.3. Walker Moly

Location (Fig. 2.17)

Latitude: 44°46.350' N

Longitude: 64°24.920' W

The Walker Moly prospect is located in New Russell, a small settlement 6.5 km east of New Ross along the Windsor Road. A private driveway (120 m in a southwestern direction) leads to the beginning of the wood trail, and the deposit lies 230 m west along the trail.

Past exploration

Walker (1911) first noted the presence of "milky white quartz" containing molybdenite and fluorite in the New Russell area. Walker (1911) described the presence of a water-filled pit dug years before his observations. Eardley-Wilmot (1925) mentioned the sinking of a ten metre-deep shaft in 1917. Slipp (1951) reported further sinking of the existing shaft to a depth of nineteen metres, as well as several diamond drill holes and drifting. Slipp (1951) described the greisen as being sporadically distributed along the margins of the pegmatite dyke. One ton of ore was retrieved, but this small prospect closed for economic reasons (Cameron 1950). Charest (1976) reported the presence of gahnite (Zn) and topaz (F), besides the more common metallic minerals present at the Walker deposits (molybdenite, wolframite, cassiterite, bornite, and chalcopyrite). Farley (1978) proposed two scenarios for the origin of mineralisation at the Walker deposit:

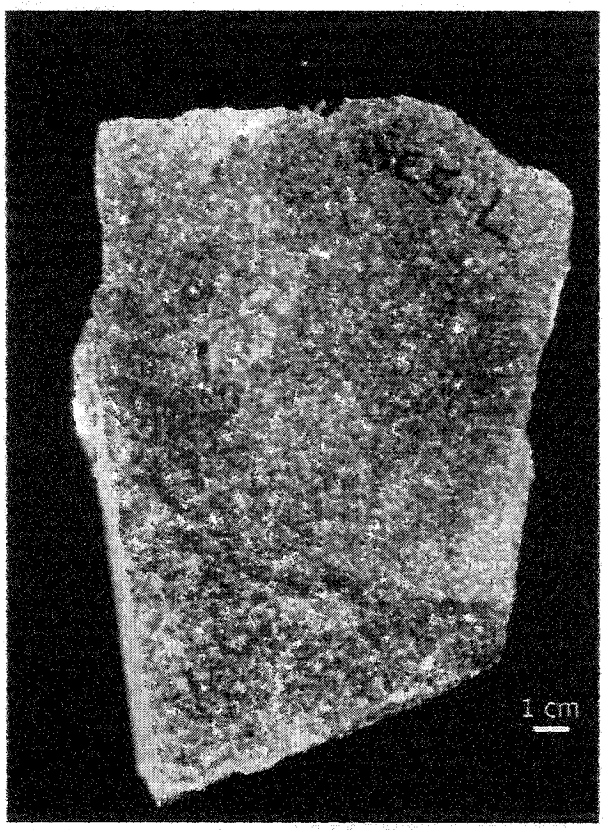

Fig. 2.13: Quartz-muscovite greisen (SC-5-L) from the Long Lake prospect. Note the dark colour of the sample, caused by the presence of black quartz.

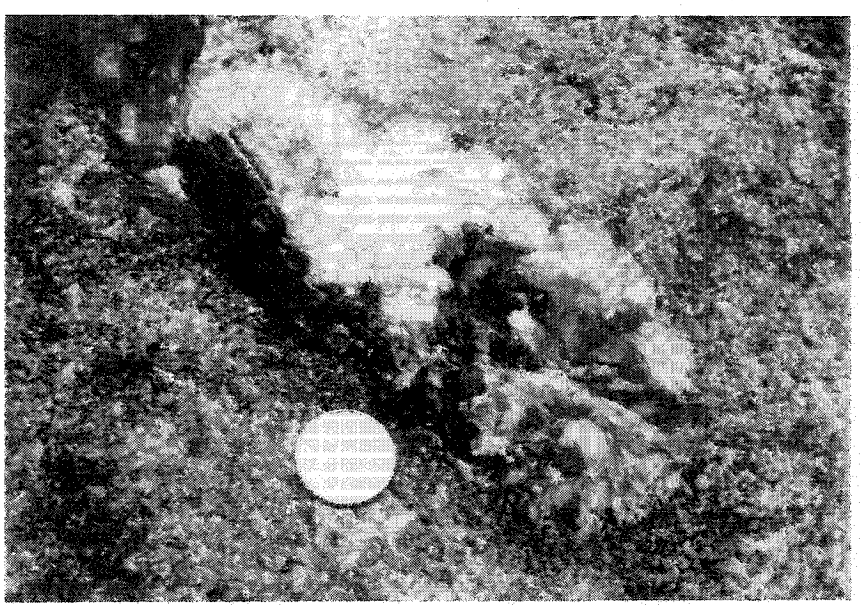

Fig. 2.14: Field exposure of a vug containing quartz and wolframite. The vug occurs in quartz-muscovite greisen. Diameter of coin: 23 mm.

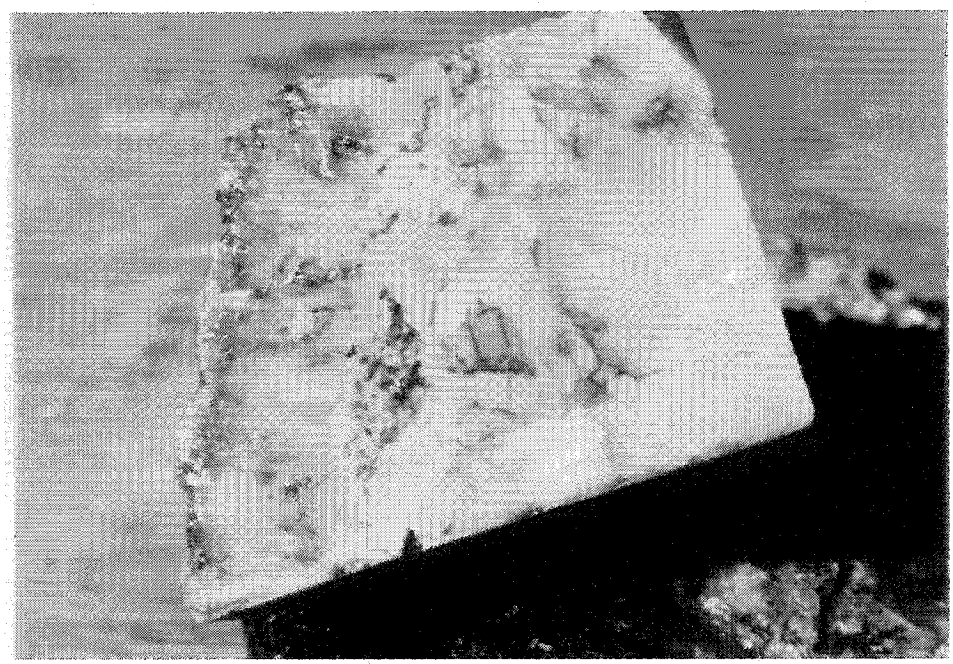

Fig. 2.15: Quartz-alkali feldspar pegmatite (SC-12-L) from the Long Lake prospect containing flakes of molybdenite associated to the quartz-rich zone. The well-developed feldspar crystals suggest that they developed on the wall of the fracture where the fluids were travelling.

Fig. 2.16: Fracture surface displaying large microcline crystals from the Long Lake prospect.

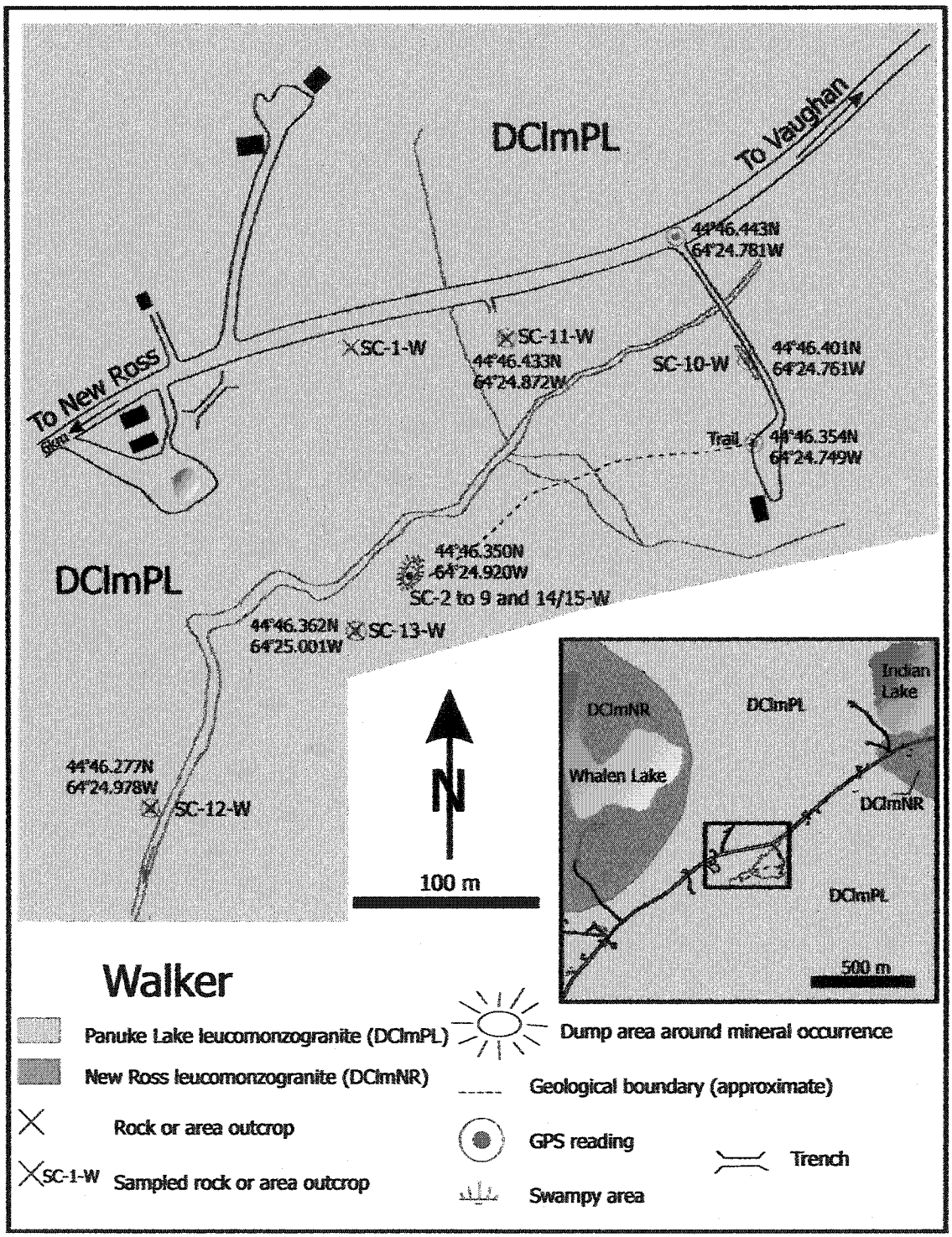

Fig. 2.17: Location map and geology of the Walker prospect. Geology after O'Reilly et al. (1982) and Ham (1991).

1) concentration of incompatible elements by fractional crystallisation, and partitioning into a late fluid phase; and 2) volatile-rich fluid phase leaching elements from the rocks it passes through and depositing them at a higher level within the batholith.

Geology

The coarse-grained Panuke Lake leucomonzogranite (Figure 2.4) hosts the Walker Moly prospect. The deposit site consists of a concrete slab covered shaft, one outcrop of unmineralised leucogranite, and a dump pile containing numerous quartz-K-feldspar pegmatite, aplite (banded or unbanded) (Figure 2.18), and greisen (Figure 2.19) samples. Wolframite, cassiterite, bornite, and chalcopyrite are associated with the greisen, whereas only copper sulphides, malachite, and molybdenite are present in the aplite and pegmatite. Molybdenite forms large crystals in the pegmatite, and appears as flakes parallel to the banding in the aplite. The greisen consists mainly of white mica and quartz, with localised high concentrations of tourmaline.

2.3.3. Greisen and vein deposit

2.3.3.1. Turner deposit

Location (Fig. 2.20)

Latitude: 44°47.155' N

Longitude: 64°27.027' W

An intersection between Mill Road and New Russell Road lies 2.8 km north of New Ross. The Turner Tin Prospect lies 3.7 km along Mill Road. Several veins distributed on both sides of the east branch of the Gold River constitute the Turner deposit. A private woods road leads to the prospect site, however most of the deposit lies on the opposite side of the Gold River.

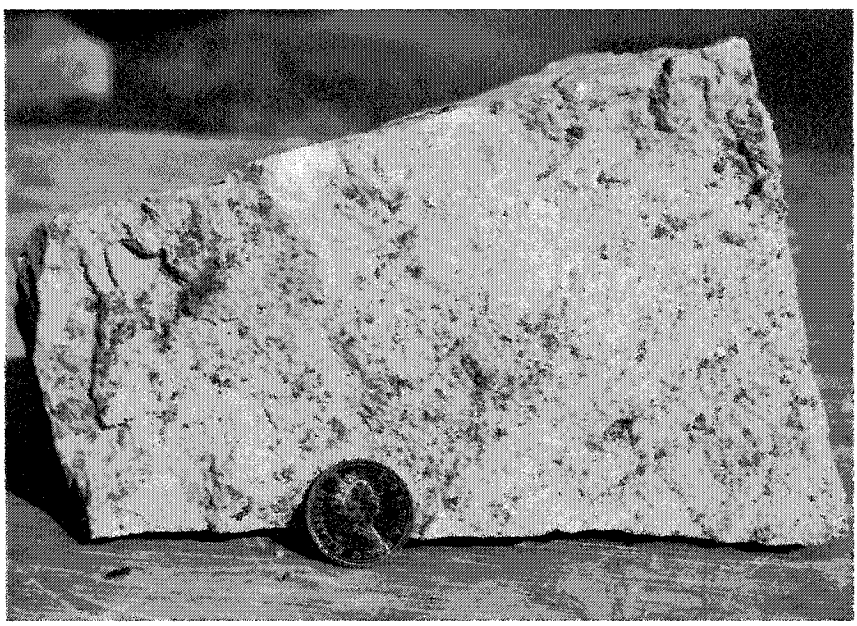

Fig. 2.18: Banded aplite and its contact to coarser pegmatitic material at the Walker deposit. Mineralisation is present in the quartz-rich layers of the aplite. Diameter of coin: 23 mm.

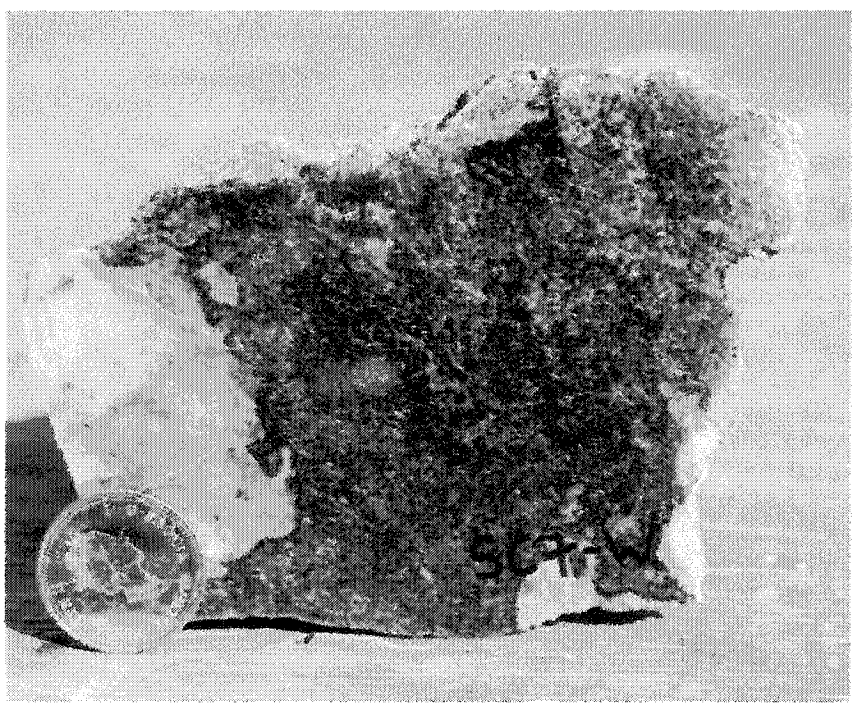

Fig. 2.19: White mica-tourmaline greisen from the Walker deposit. The tourmaline is deep blue, giving the rock its dark colour. Diameter of coin: 23 mm.

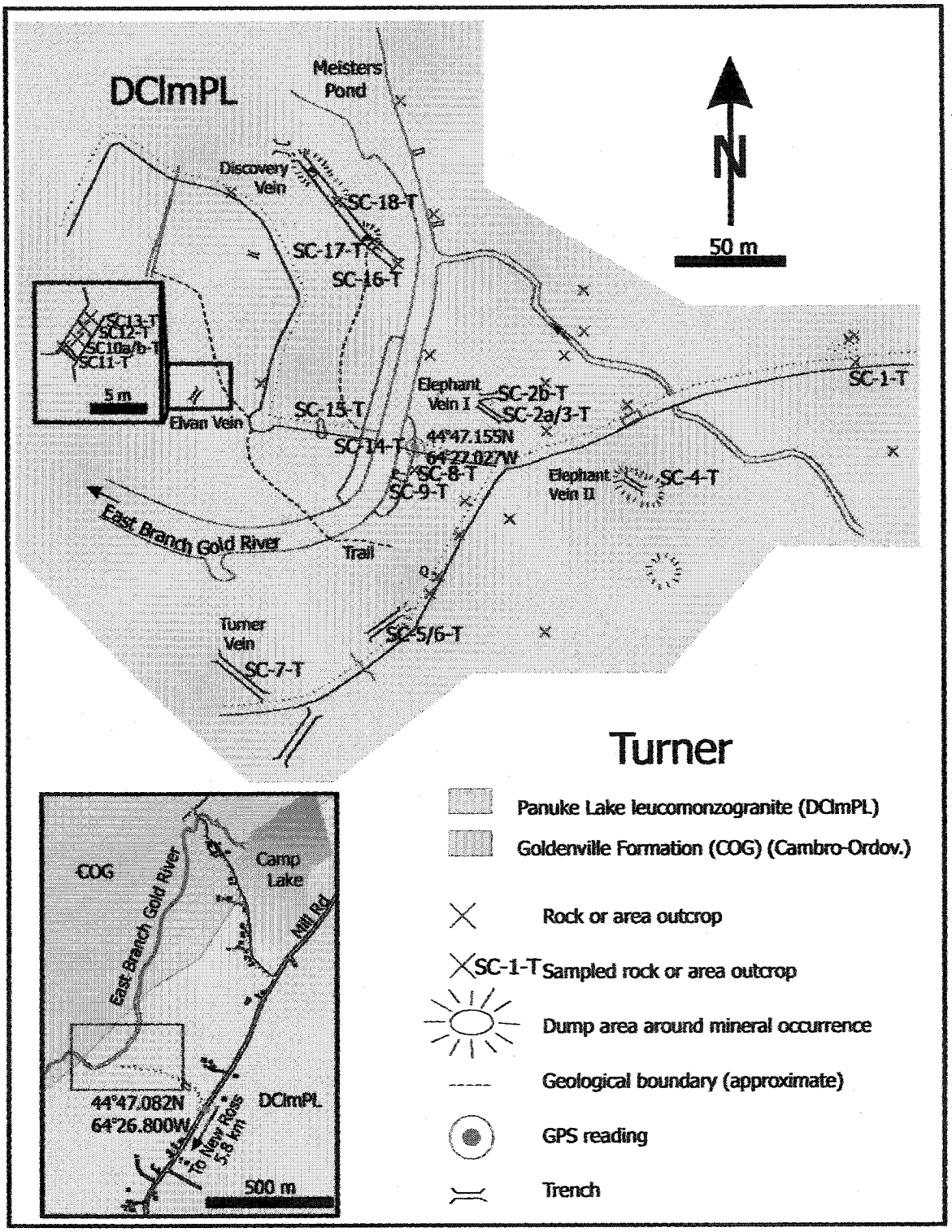

Fig. 2.20: Location map and geology of the Turner deposit. Geology after O'Reilly et al. (1982) and Ham (1991).

Past exploration

Faribault (1910) noted the discovery of a tin-bearing vein at this locality. A six metre-deep trench reveals a quartz-rich vein with tin-rich ore in the centre. Cassiterite, chalcopyrite, W- and Zn-bearing minerals are also present. Work on the Turner deposit proceeded and two shafts (16 m and 7 m deep) were sunk, revealing the pinching out of the vein at depth (Faribault 1911). Other minerals discovered during exploration include: stannite (Cu, Sn), wolframite (W), scheelite (W), tungstite (W), molybdenite (Mo), sphalerite (Zn), and arsenopyrite (As). Douglas and Campbell (1941a) described four main veins from the Turner deposit:

- Discovery vein: the vein is open cut for sixty-four metres, and has two shafts (seventeen and ten metres-deep). The vein consists of greisen and strikes ~190°.
- Elephant vein: the vein is an open cut for 12 m, and has a shaft (seven and a half metres deep). The vein comprises greisen with large amount of quartz and strikes 180°.
- Turner vein: the vein is exposed in a twenty metre-long trench. It consists of greisen and quartz veins striking 190°.
- Elvan dyke: Elvan is a Cornish term for hypabyssal rocks having the composition of granite, such as quartz porphyries (Bates and Jackson 1987). There is no further compositional constraint linked to the word, and elvan mainly describes a specific texture: a fine-grained groundmass containing phenocrysts of granitic minerals. The Elvan dyke is exposed on both banks of the Mill stream (arm of the Gold River) as well as in a pit about seventy-five metres away. Douglas and Campbell (1941a) obtained a Sn content of 800 ppm in the Elvan dyke. Charest (1976) reanalysed samples from this vein, and obtained Sn content values of only 63 and 77 ppm.

Cameron (1949) reported radioactivity from the Turner deposit. Ellsworth (1950) confirmed the presence of radioactive minerals at Turner, but without being able to identify the phase(s) present. Charest (1976) observed bornite, covellite, chalcocite,

and malachite (Cu); pyrite, magnetite, and hematite (Fe); and fluorite (F) in highly fractured quartz veins stained from iron oxide.

Farley (1978) proposed a similar choice of scenarios for the origin of mineralisation at the Turner deposit as described for the Walker deposit (i.e., endogenic origin of both incompatible elements and fluid(s), or exogenic origin of incompatible elements and endogenic origin of fluid(s)). O'Reilly et al. (1982) reported that autunite and metatorbernite occur along fractures in an outcrop located between the two shafts of the Discovery vein; the U-bearing minerals appear to post-date greisenisation (G. A. O'Reilly pers. comm. 2002).

Geology

The Panuke Lake leucomonzogranite hosts the Turner mineral occurrence located south of a roof pendant of Goldenville Group metasedimentary rocks marking the boundary between the New Ross and the Salmontail Lake plutons. The pinkish colour of the host granitoid rock (Figure 2.21) indicates extensive hematisation of feldspars and biotite in the area and its texture is mainly porphyritic with some aplitic and pegmatitic segregations. The prospect consists of 4 m-size, east-dipping veins divided into quartz-greisen zones (Discovery, Elephant I and II, and Turner veins) and a quartz porphyry dyke (Elvan).

1) The Discovery vein consists of a green quartz - white mica - chlorite rich greisen (Figure 2.22). A 66 m-long trench, including two water-filled shafts, provides few outcrops of the vein. Several quartz and feldspar veins cross the greisen throughout the trench (Figure 2.22).
2) The Elephant vein (I and II) is a greisen (Figure 2.23) that outcrops in two different locations (I and II) and has the same mineralogy as the Discovery vein. The Elephant vein I appears in a 5.6 m-long trench with little outcrop exposed. The Elephant vein II consists of a 7 m-long flooded trench surrounded by a dump.
3) The Turner vein is hosted by a finer-grained pink leucomonzogranite. Some pegmatitic segregations are visible along the 24.8 m-long trench. The greisen has a similar mineral assemblage as the Discovery and the Elephant veins.

Two subsequent trenches were dug along the path east from the Turner vein (17 and 25.2 m-long), to trace the vein southwards (Farley 1978). These later trenches do not contain any greisen or quartz vein.

4) The Elvan dyke consists of a pink and a green facies. The pink facies is located on both banks of the river and consists of a very fine-grained groundmass with phenocrysts of quartz, feldspar, and white mica (Figure 2.24 and 2.25). Both Douglas and Campbell (1941a) and Farley (1978) reported a fault running between the two outcrops (eventually through the river), but my observations do not corroborate the presence of a fault. The green facies of the Elvan dyke is displayed in a 6 m-long trench and has the same mineralogy as the red facies. Both facies have a glomeroporphyritic texture. The contact between the vein and the host rock is sharp (Figure 2.24).

Mineralisation is disseminated within the greisen, and the following minerals occur, mainly in the Discovery vein: covellite (Cu), cassiterite (Sn), chalcopyrite (Cu), arsenopyrite (As), and pyrite (Fe). The deposit site presents numerous quartz veins (centimetric to metric in size). O'Reilly et al. (1982) described three preferential orientations of the quartz and greisen veins following joints: 1) strike 128° and dip east (infilled with quartz only, no mineralisation); 2) strike 119° and dip east (few quartz veins, Elvan dyke, and Elephant vein); and 3) strike 150° and dip east (several quartz veins, Turner vein, and Discovery vein).

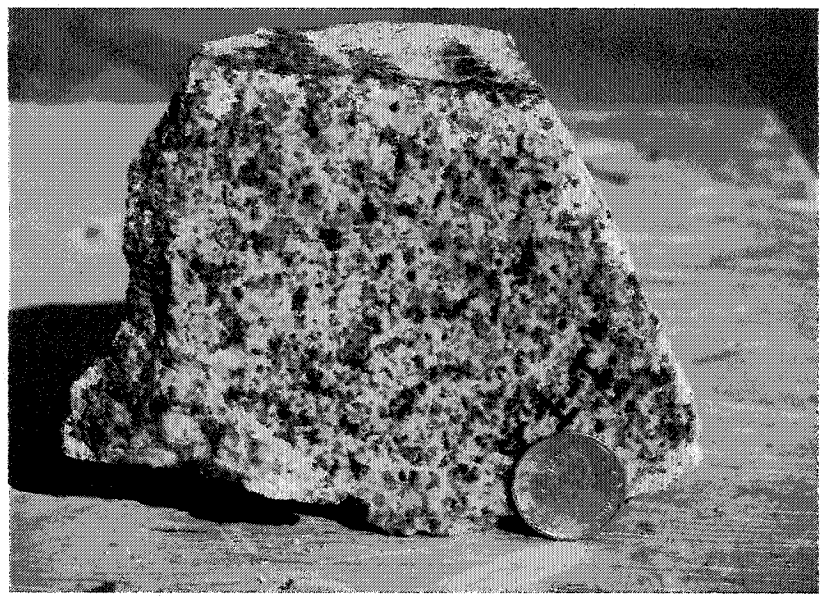

Fig. 2.21: Strongly hematised Panuke Lake leucomonzogranite (SC-1-T) located in the vicinity of the Turner deposit. Diameter of coin: 23 mm.

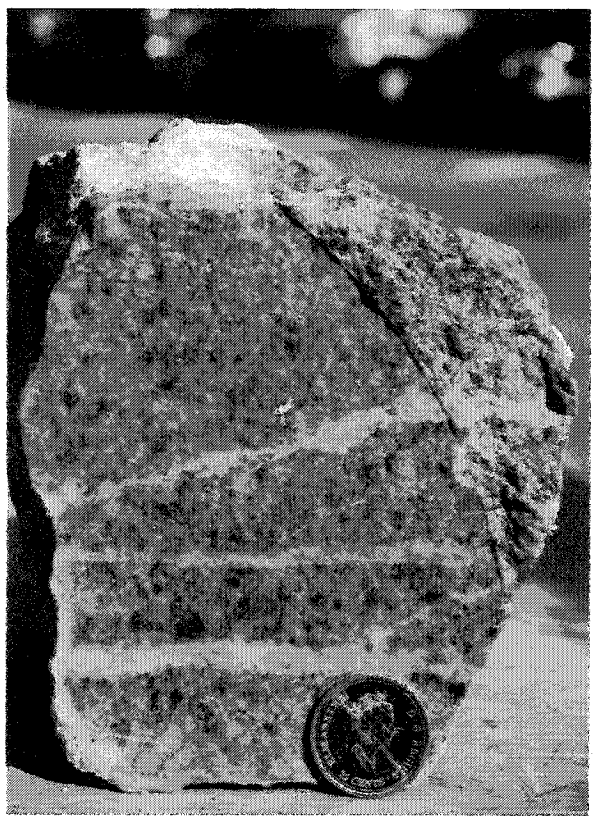

Fig. 2.22: Quartz-white mica-chlorite greisen (SC-18-T) from the Discovery vein at the Turner deposit. Note the quartz vein (white-grey) and two quartz-feldspar vein (orange) cross-cutting the greisen. Diameter of coin: 23 mm.

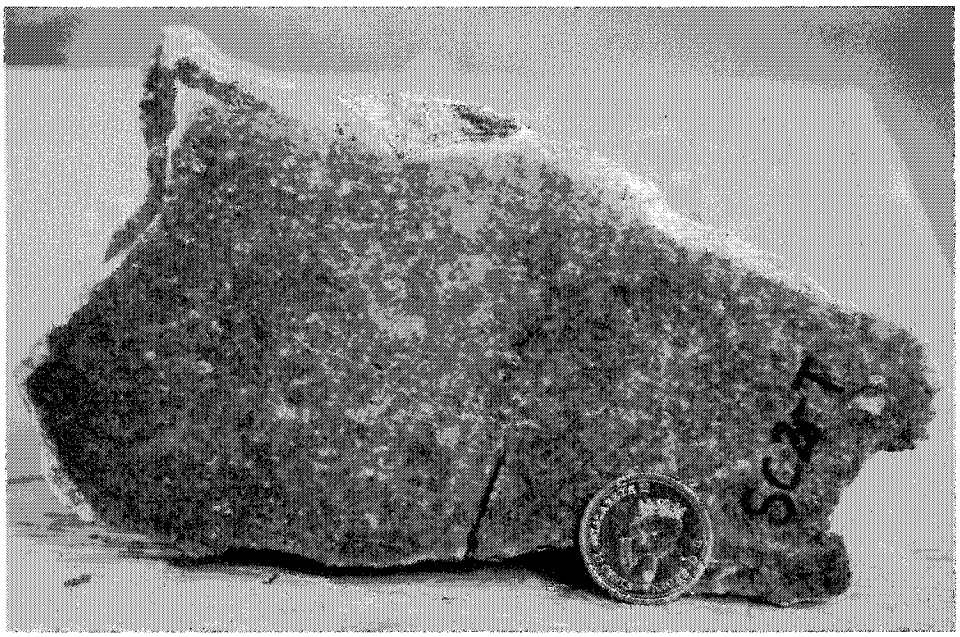

Fig. 2.23: Quartz-white mica-chlorite greisen (SC-2-T) from the Elephant vein at the Turner deposit. The yellowish colour of the feldspar grains is unusual. Diameter of coin: 23 mm.

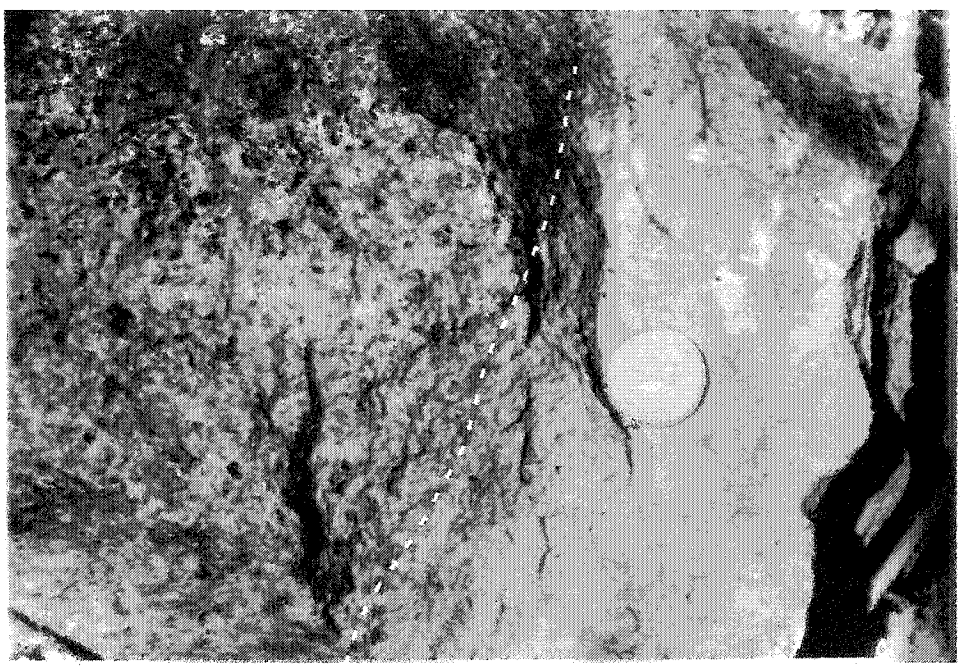

Fig. 2.24: Field exposure of the sharp contact (dashed line) between the Elvan dyke and hematised Panuke Lake leucomonzogranite. Diameter of coin: 26 mm.

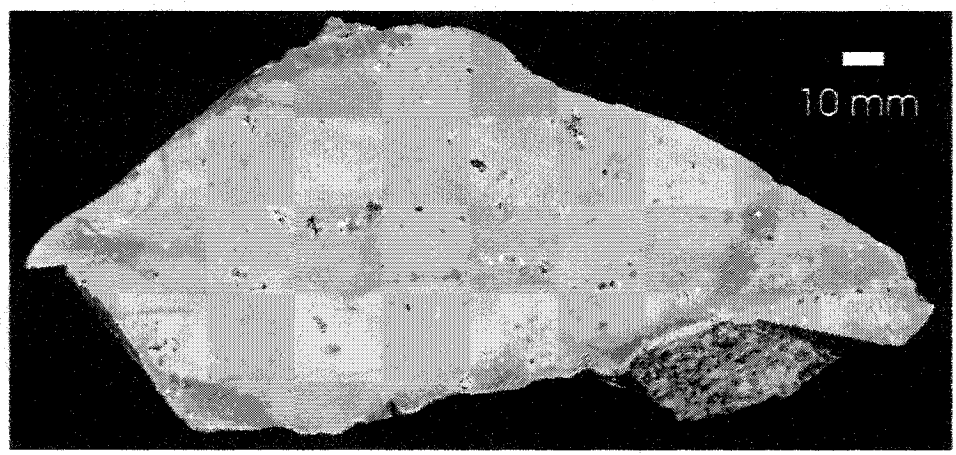

Fig. 2.25: Glomeroporphyritic texture of an elvan (SC-14-T) from the Elvan dyke at the Turner deposit..

2.3.4. Vein deposits

2.3.4.1. Millet Brook

Location (Fig. 2.26)

Latitude: 44°51.000' N

Longitude: 64°16.000' W

The Millet Brook deposit is located 2.8 km west of Highway 14, on the New Russell Road. A 4.1 km logging road leads to the main site of the deposit.

Past exploration

Airborne spectrometer surveys in the New Ross area in 1976 detected a radiometric anomaly in the Millet Brook area (Robertson 1978). Several phases of exploration were undertaken over the following three years, using geological, geochemical, and geophysical methods (Lewis 1980; Wilson 1978; Hendrickson 1979; Palmer 1979; Dvorak and Fraser 1979), and reserves were estimated at about 400 tonnes of U_3O_8. The uranium mineralisation occurred in closely spaced en-echelon pods and lenses, confined to northeast trending shear and fracture zones (Chatterjee et al. 1982). The mineral occurrence is commonly subdivided into four different zones (A, B, C, and F), with zone A9 and C certainly the richest in uranium ore (A. K. Chatterjee pers. comm. 2000; G. A. O'Reilly pers. comm. 2002). The following minerals are present in order of importance: torbernite (U, Cu), autunite (U), uraninite (U), chalcopyrite (Cu), bornite (Cu), covellite (Cu), chalcocite (Cu), proustite (Ag), galena (Pb), sphalerite (Zn), saleeite (U), and wolframite (W). Chatterjee et al. (1982) proposed that the Millet Brook mineralisation resulted from fluids derived from and driven by heat from an underlying leucomonzogranite cupola.

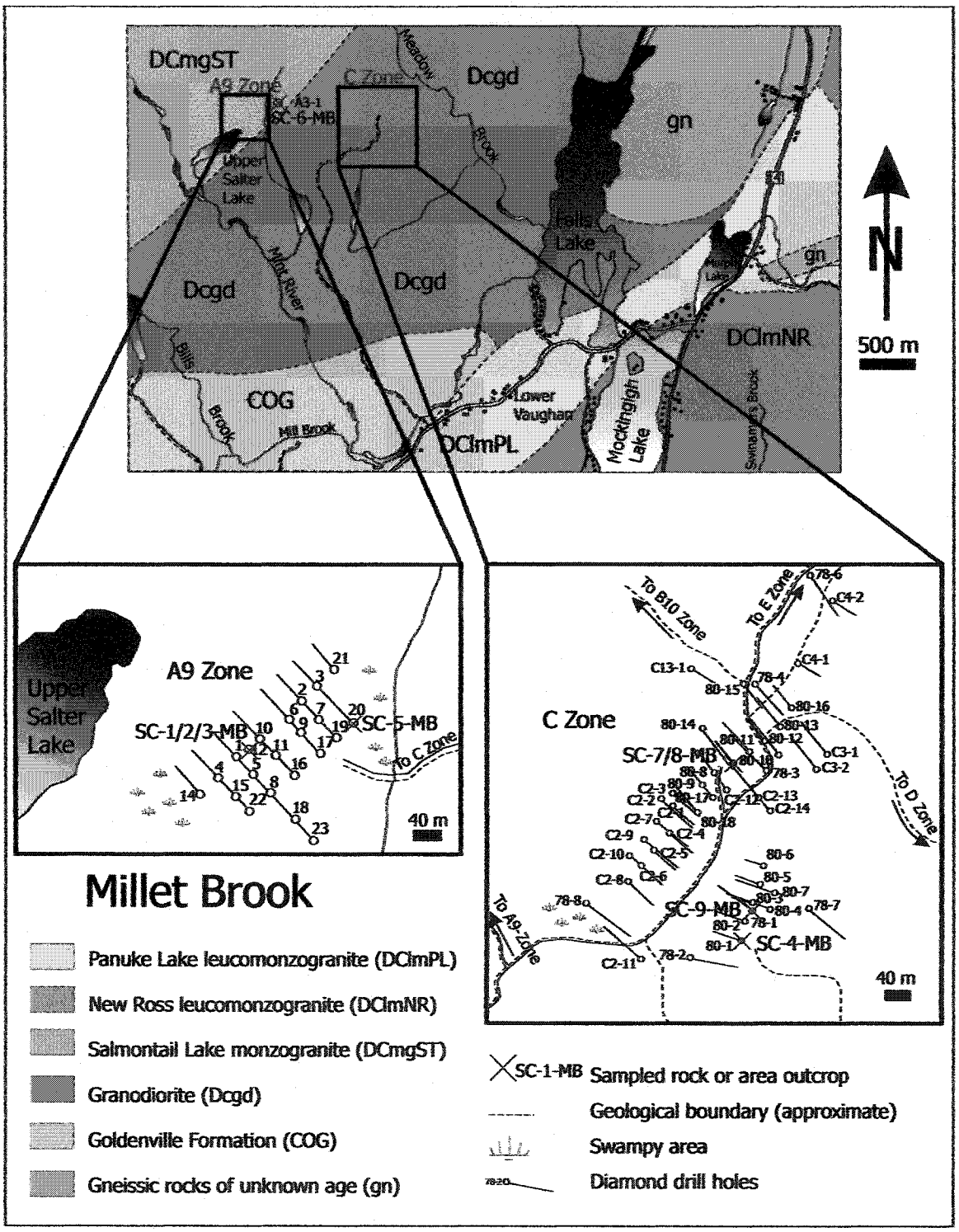

Fig. 2.26: Location map and geology of the Millet Brook deposit. Geology after Chatterjee and Strong (1984), and Ham (1991).

Geology

Biotite granodiorite and biotite monzogranite (Figure 2.5) of the Salmontail Lake pluton host the Millet Brook deposit (Chatterjee et al. 1982; Chatterjee et al. 1985; MacDonald 2001). Similar to the Turner deposit, the Millet Brook deposit is located near a roof pendant of Goldenville Group metasedimentary rocks at the boundary between the New Ross and the Salmontail Lake plutons. Drill cores reveal the presence at depth of leucogranite dykes similar in composition to the Lake Lewis leucogranite (Chatterjee et al. 1985). The uranium mineralisation occurs in en-echelon pods, and lenses are confined to northeast-trending shear and fracture zones in the biotite granodiorite (Chatterjee and Strong 1984). Several types of alteration accompany the mineralised fractures: biotitisation, episyenitisation [a desilication phenomenon usually accompanied by sodic or potassic metasomatic alteration by hydrothermal fluids; definition after Cathelineau (1985)], kaolinisation, chloritisation, and hematisation. Samples used in this study come from drill cores because no outcrop is currently accessible at the deposit site. Mineralised and non-mineralised samples are easy to discriminate: dark grey to black quartz, a higher percentage of modal biotite, altered plagioclase, turbid orange K-feldspar, hematisation, and a general crumbly nature and porous texture characterise the former, whereas the latter shows transparent quartz, lower percentage of modal biotite, less altered plagioclase, white K-feldspar, and a compact texture.

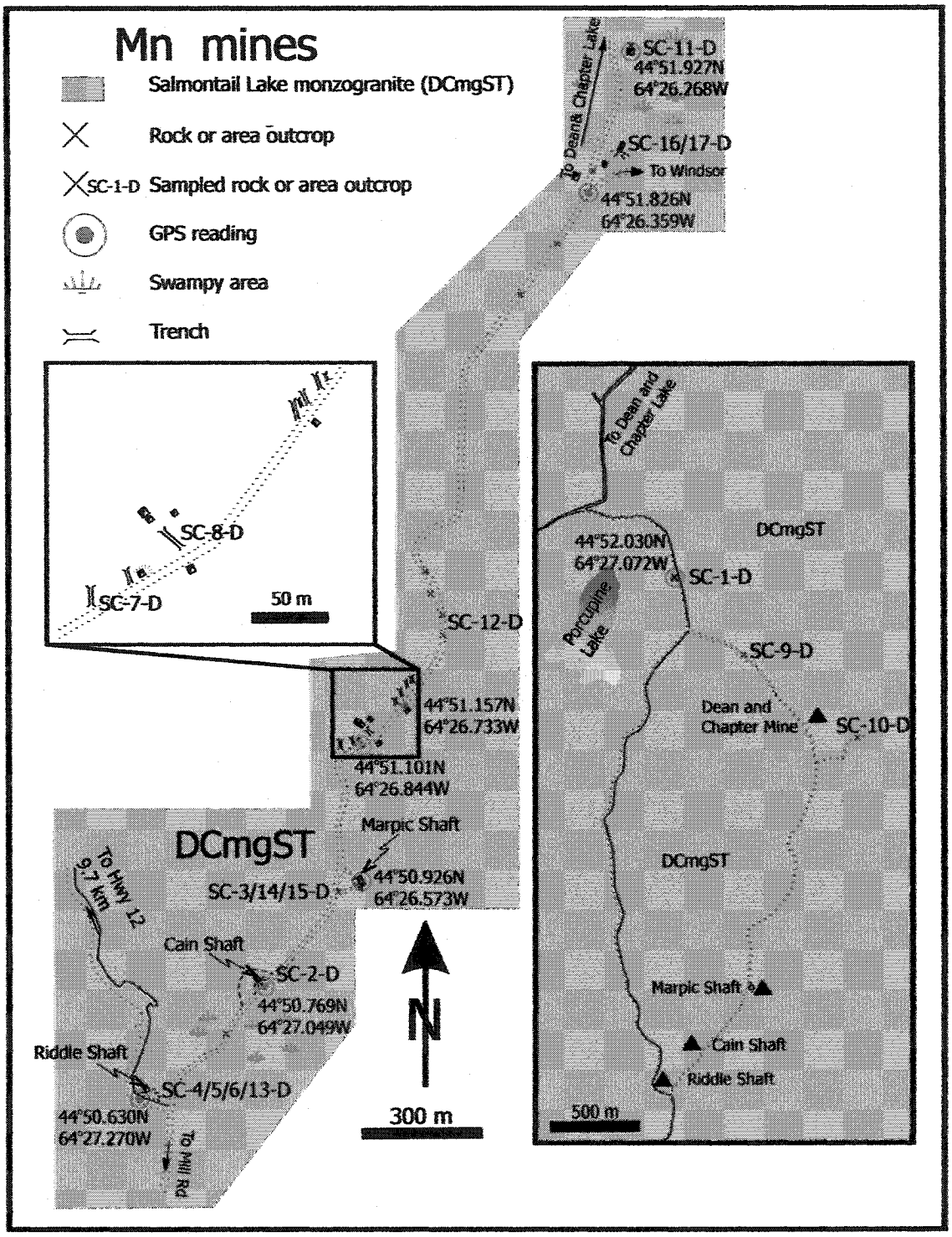

Fig. 2.27: Location map and geology of the Mn Mines deposit. Geology after O'Reilly et al. (1982) and Ham (1991).

2.3.4.2. New Ross Manganese Mines (Cain and Riddle mine or Old mine, and Dean and Chapter mine or New mine)

Location (Fig. 2.27)

Latitude: 44°50.630' N (Cain and Riddle Mines), 44°51.826' N (Dean and Chapter Mines)

Longitude: 64°27.270' W (Cain and Riddle Mines), 64°26.359' W (Dean and Chapter Mines)

The New Ross Mn Mines lie southwest of Dean and Chapter Lake. The old road to the Mines (the continuation of Mill Road) is now passable only by four-wheel drive vehicle, but access from the northwest is provided by a new system of logging roads. A logging road leading to the Mines is located 14.4 km north of New Ross along Highway 12, in Aldersville (Kings County) just before the bridge crossing the Salmontail River. The first exploration site (Cain and Riddle Mines, and Marpic shaft) lies 9.7 km east of this logging road. The second site (Dean and Chapter Mines) lies 2 km northeast from the Cain and Riddle Mines, along the old mines' road.

Past exploration

In the late 19th Century, an occurrence of fault-controlled, vein-type manganese mineralisation, which became the Cain and Riddle mine, was first recognised (Hanson 1932). A shaft was sunk for thirty-four metres, and at twenty-seven metres, drifts were run to the east and west, three and six metres long, respectively. On account of litigation, the mine was closed after three years of production. About a hundred tons of ore were retrieved (Wright 1912).

In 1907, the GSC reported the opening of a second mine, the Dean and Chapter mine, north of the first manganese occurrence. Two pits were sunk (#1 and #2), uncovering a vertical vein containing hematite and manganese ore (pyrolusite, manganite, and psilomelane). The vein runs over thirty metres, strikes northeast, and dips 70 to 90° to the north. Faribault (1910) reported the digging of a forty-three metre-deep shaft on the Dean and Chapter site, revealing high quality manganese ore. Weeks (1945) reported a production of 1850 tons of manganese ore from both mines until 1921. In the early thirties, a new shaft was sunk on the Dean and Chapter site

(#4), and in the early forties, five hundred more tons of ore were mined. After extensive diamond drilling in 1942, Weeks (1945) concluded that both Mn mines could still provide about forty thousands tons of ore. In 1958, a new shaft (the Marpic shaft) was sunk in the hanging wall west of the mineralised zone, a short distance north of the Cain shaft. Exploration work was undertaken in order to assess the potential of the area for other metals (Sn, W) (Graves 1982, 1983). As a result of investigating a "pink felsite" similar to the Elvan dyke from the Turner deposit, Duncan (1983) deduced that both the dyke and the manganese mineralisation are related to a late-stage leucomonzogranite at depth. In 1985, the Nova Scotia Department of Natural Resources drilled three holes under the direction of G. A. O'Reilly, and O'Reilly (1992) provided a description of the cores. Barrett (1985) underlined the excellent potential for manganese mining in the area, but recommended additional work to accurately ascertain the reserves. In 1989, the mining company, Aurion Mineral Limited, determined that exploitation of the Mn mines would be too expensive, and that the reserves were not as large as stated by Weeks (1945). Table 2.2 summarises the depth and orientation of the shafts as well as the depth of the drifts.

Faribault (1917) provided the first genetic model of the Mn mines formation: after manganiferous calcite was deposited in faults and brecciated, surface water percolation induced secondary enrichment and further concentration of the manganiferous ore. Douglas and Campbell (1941b) questioned the supergene or hypogene origin of the manganese ore, but could not form a definite opinion with the available data. Using new geochemical data, Bishop and Wright (1974) concluded that the deposition of hydrothermal solutions in a fault-zone formed the manganese deposits, thus opting for a hypogene origin. Based on a petrographic and geochemical study of drilled material from the area, O'Reilly (1992) confirmed the hypogene origin of the hydrothermal fluids that were certainly derived from leucomonzogranitic rocks located below the faults containing the Mn ore.

Mines	Shafts (orientation)	Shaft depth (m)	Drift depth (m)
Dean and Chapter	#1 (inclined north)	70	67 47 27
	#2 (inclined north)	51	47 27
	#3 (vertical)	7.6	-
	#4 (vertical)	51	27 18
Cain and Riddle	Cain shaft (vertical?)	60	50 29 13.5
	Riddle shaft (vertical)	30.5	
Marpic shaft	Marpic shaft	54	49.5 30

Table 2.2: Orientation and depths of excavations at the Manganese Mines (after Weeks 1945).

Geology

The Mn mines consist of two distinct zones along narrow NE-striking and NW-dipping faults: 1) the Cain and Riddle Mine including the Marpic shaft, and 2) the Dean and Chapter Mine. Both zones are hosted within the Salmontail Lake biotite monzogranite (Figure 2.5), but several small plutons collectively referred to as the Gold River leucomonzogranite (Ham 1991) outcrop in the area and are present at depth (O'Reilly 1992). The presence of a footwall breccia versus unaltered granite in the hanging wall, as well as the textures described in reports, provides evidence for the presence of faults (O'Reilly et al. 1982). The orientation of the faults is similar to that at the Millet Brook deposit, ~15 km east of the Mn mines (Section 2.3.4.1). O'Reilly (1992) also emphasised the northeast elongation of the small Gold River plutons and their brittle deformation along faulted contacts, suggesting that they intruded along NE-trending fractures in the Salmontail Lake monzogranite. The mineralised zones do not outcrop, and only altered dump samples are available at the surface (Figure 2.28).

1) Cain and Riddle Mines and the Marpic shaft: a gossan zone of botryoidal goethite, hematite, and limonite caps the rocks at the Cain shaft from the surface to a depth of 7.5 m. Below the gossan, a vein of hematite-ochre breccia and carbonate (black calcite) with pyrolusite, and further down manganite and psilomelane, occurs. The Riddle shaft does not display a gossan cap, but instead comprises carbonates (mainly black calcite) and broken masses of pyrolusite (O'Reilly et al. 1982).
2) The Dean and Chapter Mine: The Dean and Chapter Mine comprises four shafts on a single mineralised zone trending in a northeastern direction (O'Reilly et al. 1982). O'Reilly (1992) and previous investigators in the area reported a gossan zone of the same composition as the one present in the Cain shaft from surface to a four metres-depth grading into a vein of pyrolusite and hematite-ochre breccia. With increasing depth, pyrolusite decreases whereas manganite alone, followed by manganite and psilomelane occur.

2.4. Petrography and mineralogy of the New Ross area

Following the nomenclature of MacDonald (2001), the New Ross area includes biotite granodiorite (~5%), biotite monzogranite and muscovite-biotite monzogranite (~53%), coarse- and fine-grained leucomonzogranite (~40%), and muscovite leucogranite (~2%). This Section presents the petrography and mineralogy of the granitic rock types hosting the mineral deposits in the New Ross area from less to more evolved types, as well as the petrography of altered and/or mineralised samples and other minor rock types and intrusives associated with the different rock types. The last letter of a sample's name indicates the deposit it belongs to: R for Reeves, W for Walker, L for Long Lake, K for Keddy, M for Morley's, T for Turner, D for the Mn mines, and MB for Millet Brook. G. A. O'Reilly kindly provided the Mn mines samples having names starting with DC and A9. D. J. Kontak kindly provided the Millet Brook samples having names starting with DK. Modal proportions of minerals are estimated from observation of thin sections and hand specimens and figure in

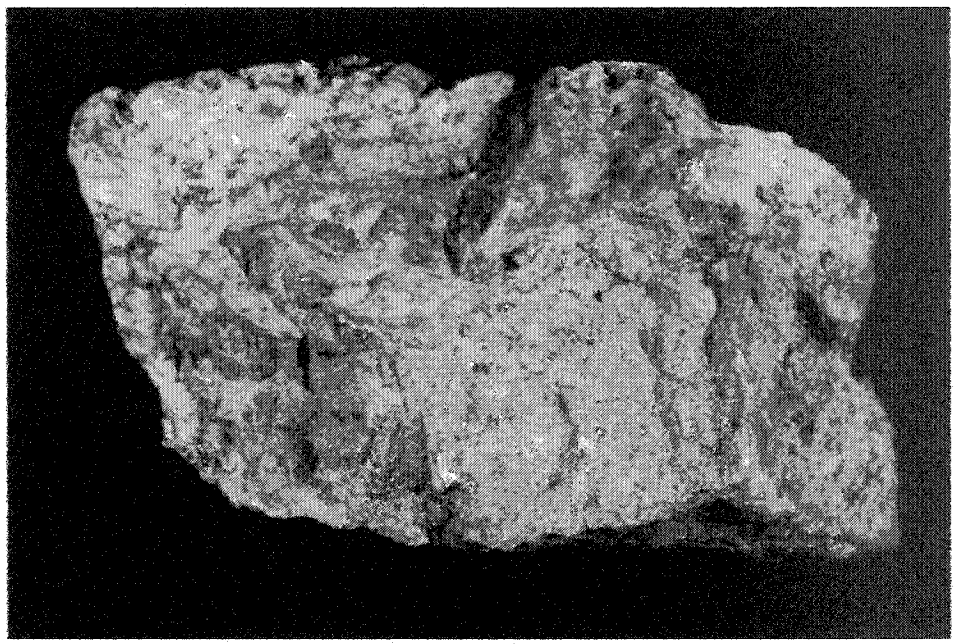

Fig. 2.28: Typical Mn oxides-rich sample (SC-15-D) found in dump area near the Dean and Chapter mine.

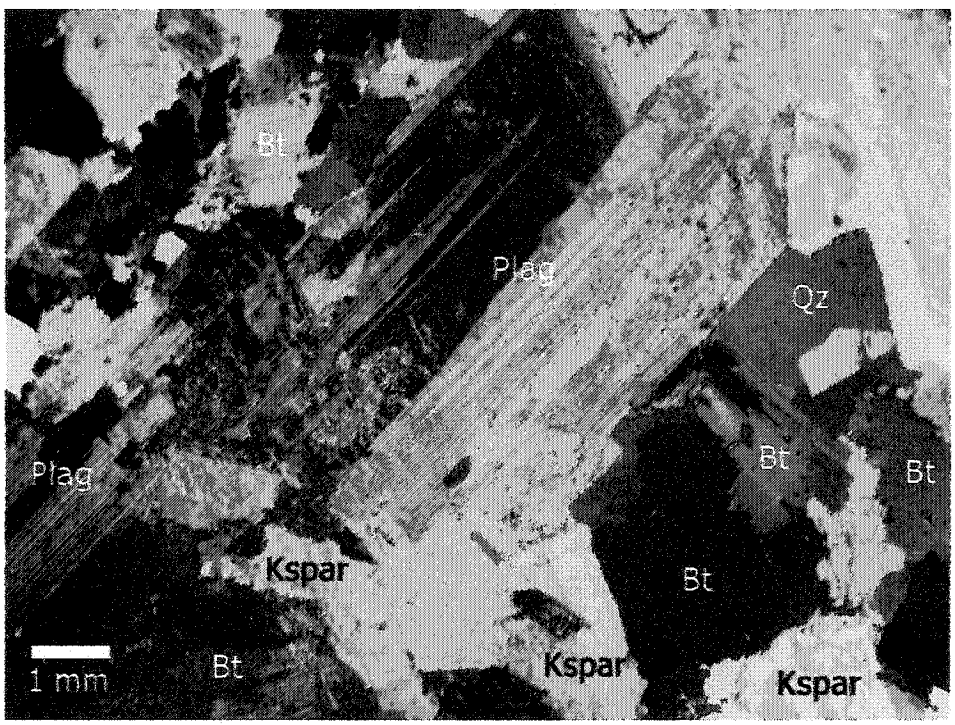

Fig. 2.29: Typical biotite granodiorite appearance in thin section (SC-8-MB): quartz, alkali feldspar, phenocryst of plagioclase, and high concentration of biotite. No white mica present. Crossed polars.

Pluton	Rock type	Name	Modal proportion of minerals (in %)						Alteration	Samples
			Qz	Plag	Kspar	Bt	Musc	Other		
Salmontail Lake	Biotite granodiorite	Unnamed	30	40 (and.) 35 (9-MB)	15 (Or 94)*	15 20 (9-MB)	trace	zircon, apatite, chlorite, opaques, monazite, ilmenite, pyrite, rutile, cordierite (pinitised), garnet?	episyenitisation hematisation	SC-8-MB (non-mineralised) SC-9-MB (mineralised)
	Muscovite-biotite monzogranite	Salmontail Lake	30	30 (and.-olig.)	20 (Or 94)*	15	3		sericitisation chloritisation hematitisation	SC-2/3/4/5-R SC-5-T SC-2/3/4/6/7/8/10-D DC-86-3 847 DC-85-3 217 SC-5-MB and DK-MB-99-05 (non-mineralised) SC-1/3-MB and DK-MB-99-01 (mineralised)
New Ross	Biotite monzogranite	Sandy Lake	32	35 (and.)	20 (Or. 90)	12	1	zircon, apatite, opaques		SC-3/4-L
	Leucomonzogranite	Panuke Lake	35	25 (and.-alb.)	30 (Or 91-98)*	4	6	zircon, apatite, chlorite, rutile, cordierite (pinitised), opaques, fluorite, andalusite		Coarse-grained: SC-1/2/6-K SC-1/8/10-W SC-1/4/9/13/15-T Fine-grained: SC-1-R SC-11/12/13-W SC-3/7/11/12-T
			57	10 (alb.)	10 (Or. 99)	0	15	zircon, apatite, opaques (5%), fluorite, topaz (3%)	greisenisation	SC-14-W (mineralised: bornite, chalcocite, covellite, chalcopyrite) SC-6-T
		New Ross	35	25 (and.-alb.)	30 (Or. 91-98)*	5	5	zircon, apatite, chlorite, rutile, cordierite (pinitised), opaques, fluorite, andalusite	hematisation kaolinisation chloritisation greisenisation	Coarse-grained: SC-1/3/4/5/6/9/10/11/14-M
			45	15 (and. - alb.)	15 (Or. 91-98)*	0	25	topaz, cordierite (pinitised), fluorite, opaque (molybdenite)	greisenisation	SC-5/7/9-K
	Leucogranite	Keddy-Reeves, Long Lake and unnamed	40	30 (alb.)	18 (Or. 98)	trace	10	zircon, apatite, topaz (2%)	sericitisation hematitisation	SC-6/7/8/11-R SC-9-D
			60	12 (alb.)	3 (Or 97)	0	25	apatite, chlorite, opaques (pyrite)	greisenisation hematisation	SC-6/7/14/15-L DC-1406 SC-4-K

Table 2.3: Mineralogy of unaltered samples located in the vicinity of eight mineral deposits of the New Ross area. Alkali feldspar composition with a * from McKenzie (1974).

Pluton	Rock type	Name	Modal proportion of minerals (in %)						Rock type/alteration type		Samples
			Qz	Plag	Kspar	Bt	White mica	Other			
Salmontail Lake	Biotite granodiorite	Unnamed	trace	85 (alb.)	5	0	3	zircon, monazite (2%), chlorite (5%), apatite, rutile	episyenitisation		SC-4b-MB
	Muscovite-biotite monzogranite	Salmontail Lake	0	20 (alb.)	70	3	2	cavities, opaques (5%), chlorite, apatite, rutile	episyenitisation		SC-1-D
			3	0	5	2	trace	calcite hematite 90% chamosite**, apatite	brecciation		SC-5-D DC dump
			30*	40* (olig.)	10*	0*	20*	groundmass (90%)	Elvan		SC-11-D
			0	0	0	0	0	calcite (5%), pyrolusite, hematite, goethite (95%), apatite	Mn mineralisation		SC-13/14/15/16/17-D
New Ross	Leucomonzogranite	Panuke Lake	55	10 (alb.)	20	trace	10	fluorite, topaz, cordierite (pinitised), zircon, epidote, chalcocite, bornite, covellite, chalcopyrite, emplectite, wittichenite	Aplite	greisenisation	SC-2/3/4/5/6-W WAM, WB
			35	3 (alb.)	50	trace	10	rutile, chlorite, molybdenite, chalcocite, bornite, covellite, chalcopyrite, enargite (2 %)	Pegmatite		SC-9/15/20-W
										greisenisation	SC-15-W (mineralised) SC-2-M
			45	5 (alb.)	40 (Or 98)	0	10	opaques, topaz			SC-3/8-K SC-7/12-M
			30*	40* (alb.)	10* (0r 98)	0*	20*	groundmass (90%) groundmass (80%)	Elvan		SC-8/14-T SC-10A-T
		New Ross	62	4 (alb.)	4	0	25	apatite, rutile, zircon, sphalerite, chalcopyrite; hematite (5%)	greisen	quartz-white mica	SC-2-L SC-16-T SC-13/15-M
			65	trace		0	30	chlorite (5%)		quartz-white mica-chlorite	SC-2/18-T
			trace	trace		45	0	tourmaline (50%), topaz (5%)		white mica-tourmaline-topaz	SC-7/20-W
			95	0	0	0	0	chlorite, chalcopyrite (5%)	quartz vein		SC-17-T
			95*	5*		0*	0*	groundmass (75%)	jasper breccia		SC-8-M
	Leucogranite	Keddy-Reeves and Long Lake	40	5(alb.)	40	0	15	topaz, molybdenite	Pegmatite		SC-9/10-R SC-12-L
			40	15	35	trace	10	chlorite, molybdenite, galena, rutile	Aplite		SC-13-L
			40	5		trace	45	chlorite (5%), zircon, apatite, rutile, opaques (5%)	Greisen	quartz-white mica-chlorite	SC-5-L LL2, LL3 A9B-7558

Table 2.4: Mineralogy of altered, mineralized, minor rock types, and/or late intrusives samples located in the New Ross area. Modal proportions with a * sign are reported out of a 100% of phenocrysts. **Chamosite got its name from the little village of Chamoson in the Swiss Alps. I incidentally happen to have been born and raised in that village.

Tables 2.3 (non-pervasively altered samples) and 2.4 (pervasively altered and mineralised samples, and minor rock types and intrusives). Plagioclase composition was determined optically, using either the Michel Levy or the Carlsbad-albite methods when appropriate, and through microprobe analysis. No specific names are used for white micas, because of the range of chemical compositions present in the samples (Chapter 3).

2.4.1. Biotite granodiorite

2.4.1.1. Non-pervasively altered granodiorite (Figure 2.29)

Biotite, as the essential mica and ferromagnesian mineral, and plagioclase, as >65% of the feldspar content, characterise the biotite granodiorite (Streckeisen 1976; McKenzie 1974; MacDonald 2001). An unnamed biotite granodiorite hosts the C-zone of the Millet Brook uranium deposit and belongs to the Stage I Salmontail Lake pluton. Ham (1991) described the fresh granodiorite as a "bluish-grey, medium- to coarse-grained, and megacrystic" rock. The term megacrystic characterizes any crystal or grain in an igneous or metamorphic rock that is significantly larger than the surrounding groundmass or matrix; megacrystic has no genetic connotation. I prefer the term "porphyritic" with the larger crystals being "phenocrysts", the latter implying that the larger crystals grew from the melt (Bates and Jackson 1987). Radiation-damaged samples are easily recognisable by the presence of black quartz and higher modal proportion of biotite. Both plagioclase and alkali feldspar represent phenocrysts that are up to 4 cm in size, and the groundmass around them has a granitic texture with a grain-size of 3-6 mm. A granitic texture is hypidiomorphic (individual mineral crystals are bounded only in part by their own rational faces) granular (mineral grains of approximately the same size) (Bates and Jackson 1987).

Quartz grains are anhedral to subhedral and some of the smaller grains have undulose extinction, suggesting the presence of strain and/or the eventual creation of subgrains. Quartz contains few inclusions of small biotite and plagioclase grains and grain boundaries are sharp and straight, suggesting crystallisation at equilibrium with other minerals present.

Most of the *plagioclase* grains (andesine composition) are subhedral and present normal or oscillatory compositional zoning, commonly overprinted by preferential sericitisation of either the core of the grain or of one or several zone(s), indicating a more calcic composition for those more altered zones. Most of the plagioclase grains have polysynthetic twinning and some also display Carlsbad twinning. Plagioclase contains inclusions of small biotite grains.

Subhedral *alkali feldspars* are both sericitised and kaolinised, and have a perthitic texture. Biotite granodiorite rarely exhibits graphic texture of quartz and alkali feldspar. Alkali feldspars have inclusions of quartz, plagioclase, and biotite grains. Boundaries with biotite and plagioclase can be irregular.

Large, subhedral to euhedral brown *biotite* grains are present. Most of them are slightly altered (hematitisation, chloritisation, and muscovitisation) and can be deformed (displacement of the main cleavage). Both unaltered and altered biotite contain inclusion of a radioactive mineral (zircon?), recognizable by its radioactive halo, apatite, and opaque grains as inclusions.

White mica exists solely as an alteration product of biotite and feldspar (sericite); therefore, no primary white mica is present in the biotite granodiorite. Accessory minerals are zircon, apatite, chlorite, opaques, and monazite.

McKenzie (1974), MacDonald (2001), and Ham (1991), among other authors, reported abundant xenoliths within the granodioritic rocks of the SMB. During this study, the core sampling for the Millet Brook deposit did not allow for the observation of xenoliths in the vicinity of that deposit, but Chatterjee et al. (1985) reported "remnant of Meguma wall rock as well as scattered inclusions of uncertain origin" within the granodiorite of the Millet Brook area.

2.4.1.2. Pervasively altered granodiorite

Episyenite (Figure 2.30)

An episyenite is a rock that underwent alteration by processes such as desilication, albitisation, microclinisation, chloritisation, and/or muscovitisation. Several authors have reported episyenitic alteration associated with uranium deposits throughout the

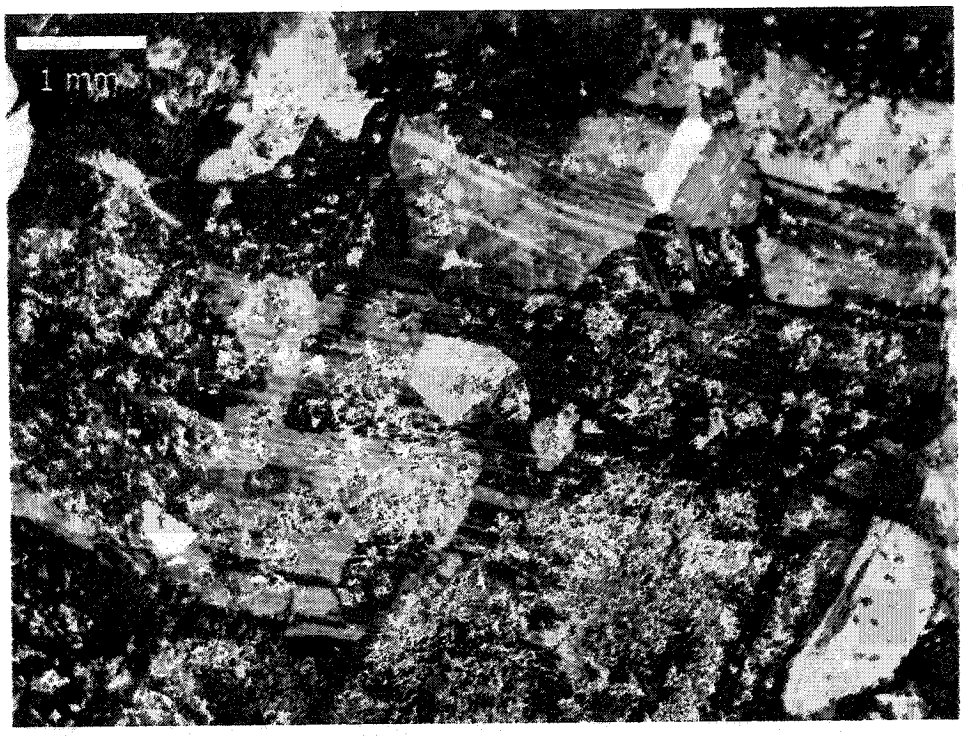

Fig. 2.30: Episyenite sample (SC-4b-MB) mainly composed of plagioclase. Note the overprinting white mica-chlorite alteration. Crossed polars.

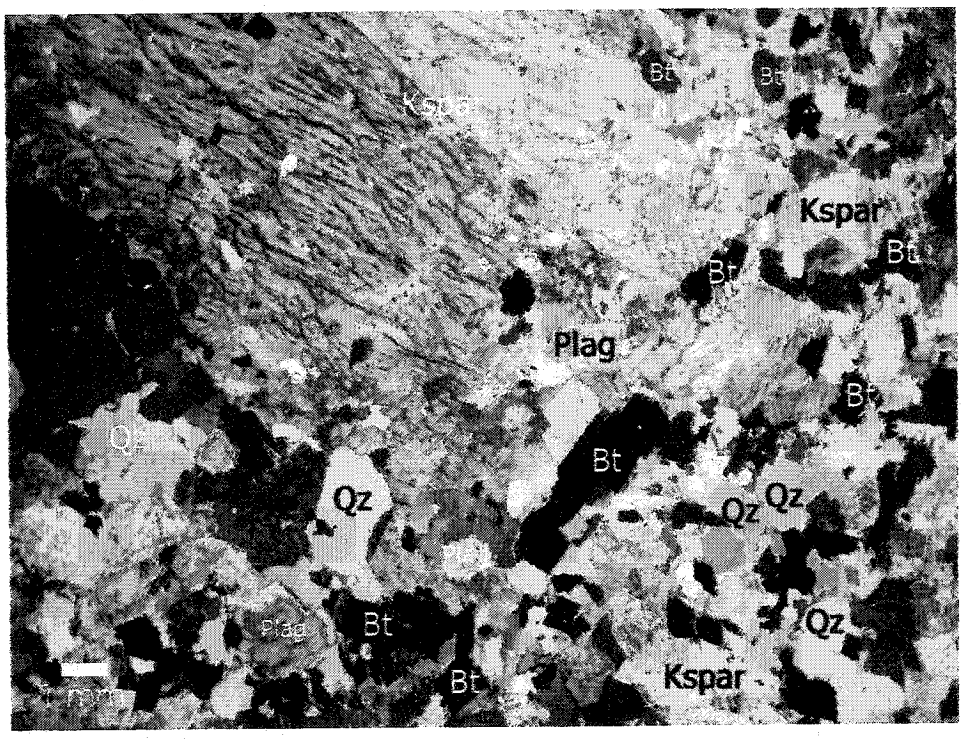

Fig. 2.31: Typical biotite monzogranite (SC-2-R) with a phenocryst of perthitic alkali feldspar containing inclusions of biotite and quartz, and a granular groundmass of biotite, quartz, alkali feldspar, and plagioclase. Crossed polars.

world (Chatterjee et al. 1982; Leroy 1984; Logothetis 1985; Hecht et al. 1991; Leroy et al. 1991; Tornos et al. 1991 among others). Several zones of episyenitised granodiorite occur in the Millet Brook deposit core collection of the NSDNR. In drill hole MB-80-01, the rock has a brownish colour and is porous and crumbly. Contact with non-altered granodiorite is sharp (a few centimetres). In one place, autunite occurs in the episyenitised zone. An abrupt change in texture appears: from being porphyritic, the granodiorite becomes coarse-grained equigranular. Plagioclase and alkali feldspar are the two main minerals present, but are strongly sericitised. Biotite occurs sparsely and white mica is only present as an alteration product. Table 2.5 describes three different stages of episyenitisation similar to stages previously described in the literature (Cathelineau 1985; Logothetis 1985; Leroy et al. 1991). Stage III, potassic metasomatism such as microclinisation (Cathelineau 1985), is not present in the Millet Brook episyenite.

2.4.2. Biotite and muscovite-biotite monzogranite

2.4.2.1. Non-pervasively altered monzogranite (Figure 2.31)

Monzogranites contain biotite as the essential mica and ferromagnesian mineral (although in lower modal proportion than granodiorite), and a plagioclase content between 35 and 65% of the total feldspar content (Streckeisen 1976). The Salmontail Lake monzogranite, hosting both the A-zone of the Millet Brook uranium deposit and the Mn mines, outcrops in the vicinity of the Reeves deposit, and contains 1-3% white mica and 7-12% biotite qualifying it as a muscovite-biotite monzogranite. The Sandy Lake monzogranite outcrops near the Long Lake prospect and contains traces of white mica and ~15% biotite, characteristics of a biotite monzogranite. The Salmontail Lake monzogranite belongs to the Stage I Salmontail Lake pluton, whereas the Sandy Lake monzogranite is part of the Stage II New Ross pluton. Both the Sandy Lake and the Salmontail Lake monzogranites are light grey in colour, medium- to coarse-grained, and have a porphyritic texture. The Salmontail Lake monzogranite may also have an equigranular texture in some places. The phenocrysts are plagioclase and alkali

Episyenitisation stages	Stages (after Cathelineau 1985)	Processes	Observations in Millet Brook samples
dequartzification	I	- magmatic quartz dissolves and leaves empty cavities, or is replaced by albite	- relict quartz crystals, corroded, sinuous grain edges, overgrown by albite - presence of cavities
albitisation	II	- albite crystallises in cavities - alkali feldspars are also partially or totally albitised	- large albite crystals present - partial replacement of alkali feldspars (grains contain abundant inclusions of plagioclase) - total replacement of primary plagioclase by albite
microclinisation	III	- microcline replaces plagioclase, alkali feldspars, and biotite	N/A
phyllitisation	IV	- biotite alters to chlorite and oxides (chloritisation) - albite alters to white mica (muscovitisation)	- no biotite present, only chlorite and plumose white mica assemblage mimicking biotite grain shape - extensive alteration of albite by small white mica flakes

Table 2.5: Different stages of episyenitisation present at the Millet Brook deposit, and comparison with stages previously described in the Massif Central in France (Cathelineau 1985).

feldspar grains (phenocryst size: 3-6 cm) and the groundmass around them has a granitic texture (grain size: 3-6 mm).

Quartz grains are mainly anhedral and show undulose extinction, both in large and small grains. Quartz contains small biotite and plagioclase grains as inclusions. Boundaries among quartz grains are very sinuous, suggesting that the smaller grains are actually subgrains formed from larger quartz crystals. Boundaries with other minerals are sharp and straight.

Plagioclase grains (andesine to oligoclase composition) are subhedral and present normal compositional zoning, commonly underlined by sericitisation of more calcic

zones and/or cores (Figure 2.32). Plagioclase displays both polysynthetic and Carlsbad twinning and contains inclusions of small biotite grains. Boundaries with other minerals are sharp, except with biotite, where it is strongly muscovitised.

Alkali feldspars are subhedral in shape and contain numerous inclusions of quartz, biotite, and plagioclase grains, mostly located in the outer part of the alkali feldspar grains. Alkali feldspars have a perthitic texture and are strongly kaolinised. Alkali feldspars have inclusions of quartz, plagioclase, and biotite grains. Boundaries with other minerals are sharp and straight.

Biotite grains are subhedral to euhedral, and show alteration to hematite, chlorite, and white mica. Biotite grains commonly appear as clusters of several randomly oriented grains. Inclusions of zircons (with a radioactive halo), apatite, and opaque minerals are common.

White mica is an alteration product exclusively, and replaces biotite and plagioclase (sericite). The modal abundance of white mica can vary from a trace to 3%, depending on the alteration state of the biotite. Accessory minerals are zircon, apatite, chlorite, rutile, and opaques. *Cordierite* occurs in some samples and is strongly pinitised. A single *garnet* grain was observed in a sample from the Mn mines.

A sample from the Mn mines contains an enclave. Its mineralogical composition is similar to the monzogranite, but the enclave has an equigranular, fine-grained texture with less modal alkali feldspar. The enclave has a rounded shape, and is easily distinguishable because of its high modal abundance of biotite. Accessory minerals are similar to those present in the monzogranite, with a higher modal proportion of apatite. Origin of this enclave may be twofold: 1) earlier granitic phase (autolith) or 2) assimilation of Meguma Supergroup country rock (xenolith).

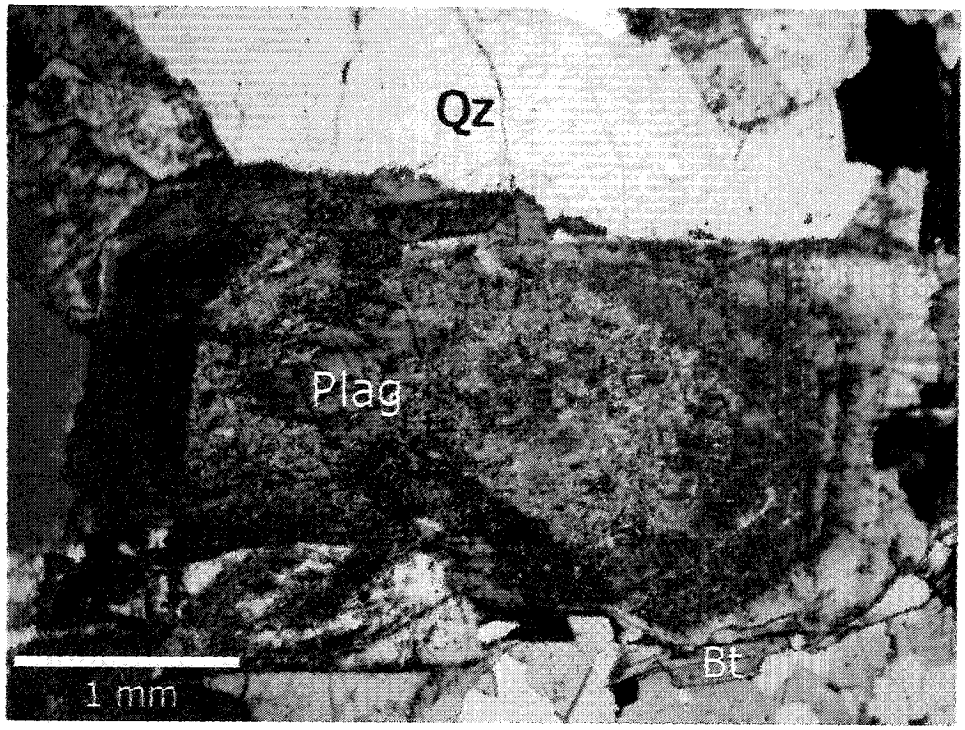

Fig. 2.32: Zoned euhedral plagioclase grain in sample SC-2-D. Note that the most calcic zones are more sericitised than the sodic rims. Crossed polars.

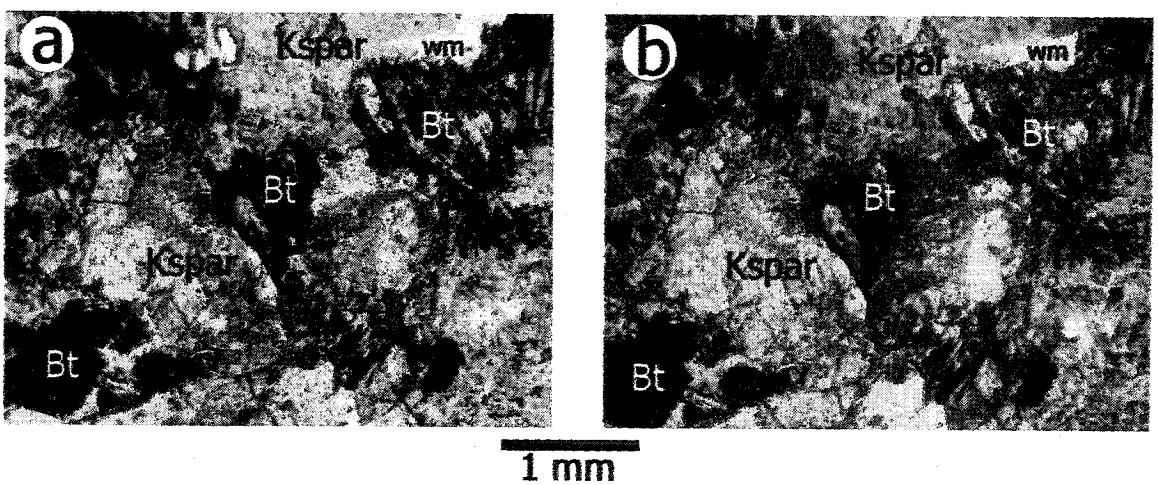

Fig. 2.33: Episyenite from the Mn mines (SC-1-D). Strongly kaolinised alkali feldspar is the main mineral present, biotite is strongly altered to chlorite and hematite, and white mica is an alteration product of both feldspar and biotite; a) plane polarized light, b) crossed polars.

2.4.2.2. Pervasively altered and mineralised monzogranite

Episyenite (Figure 2.33)

An episyenite zone occurs in the area of the Cain and Riddle Mines. The rock is porous and reddish-brown in colour. Its mineralogy differs from the episyenite observed in the vicinity of the Millet Brook deposit:

1. highly kaolinised phenocrysts of alkali feldspar occur as the main minerals, with lesser amount of sericitised and kaolinised albite;
2. biotite is almost entirely replaced by a mix of hematite and chlorite, mimicking the rectangular grain shape of biotite; and
3. white mica is commonly associated with the hematite-chlorite alteration product and with feldspars, suggesting that white mica also replaces biotite and feldspars.

Manganese mineralisation

Manganese mineralisation from the Mn mines contains Mn and Fe oxides (pyrolusite and hematite respectively). A sample from the Marpic shaft contains calcite as an infilling of cavities. Botryoidal goethite occurs within the Mn and Fe oxides, in places as fragments forming a breccia (Figure 2.34). In a sample from the Cain shaft, secondary apatite grows as euhedral grains within cavities left after Mn-Fe mineralisation (Figure 2.35). O'Reilly (1992) provides more detail about the Manganese deposits.

2.4.2.3. Minor rock types and intrusions associated with the monzogranite

Breccia (Figure 2.36)

Two occurrences of brecciated granodiorite occur close to the Riddle shaft and in the vicinity of the Dean and Chapter Mine. The breccia consists of a calcite-hematite matrix (90% of the rock) containing angular granodioritic rock fragments and/or granitic minerals (10% of the rock). O'Reilly et al. (1982) described the brecciated

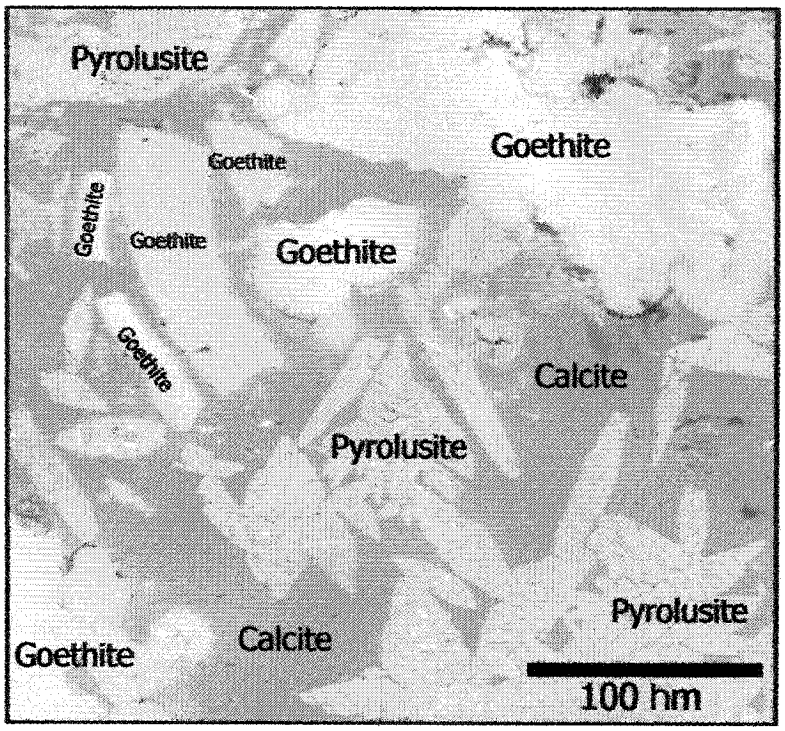

Fig. 2.34: Backscattered image (x 400) of sample SC-14-D displaying botryoidal goethite fragments and pyrolusite in a calcitic groundmass.

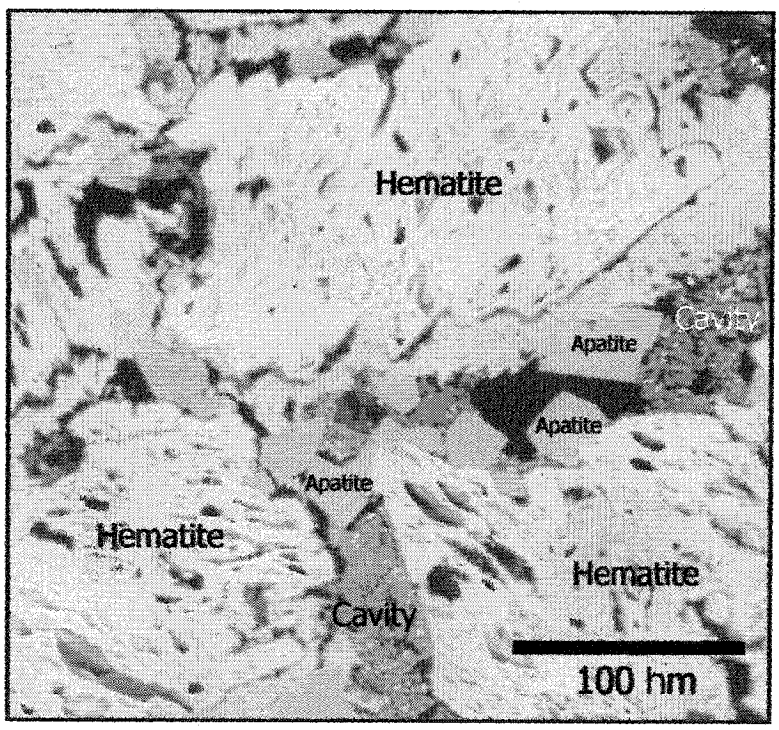

Fig. 2.35: Backscattered image (x 400) of sample SC-15-D showing hematite mineralisation with apatite crystallising within cavities.

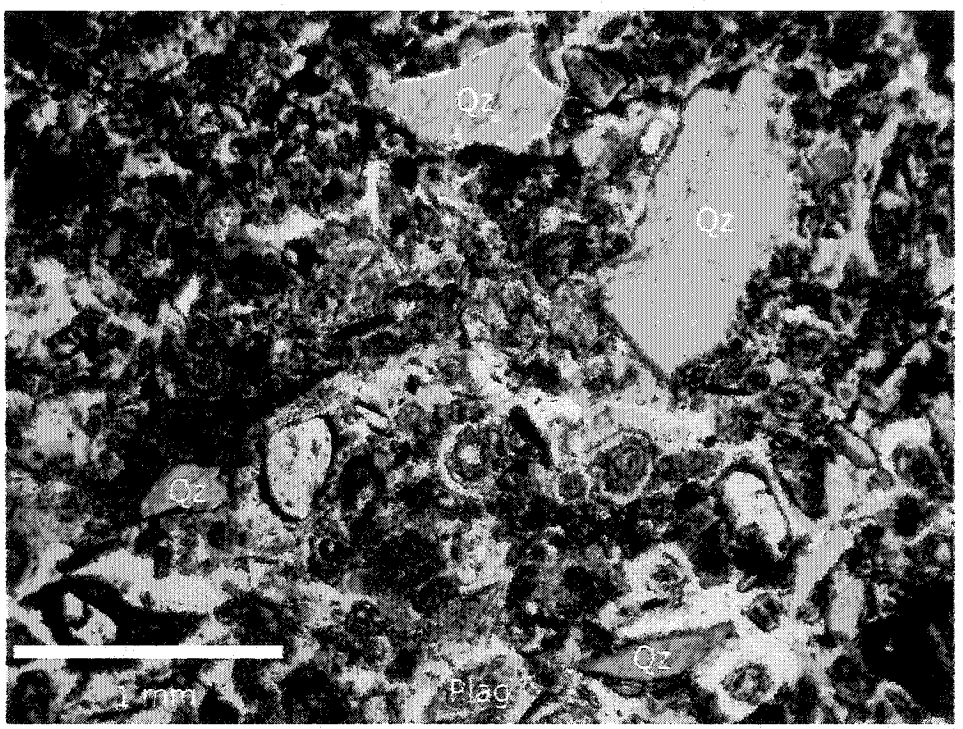

Fig. 2.36: Breccia from the Mn Mines (SC-5-D). Note the angular fragments of quartz, and the zoned plagioclase in a calcite-hematite groundmass. Crossed polars.

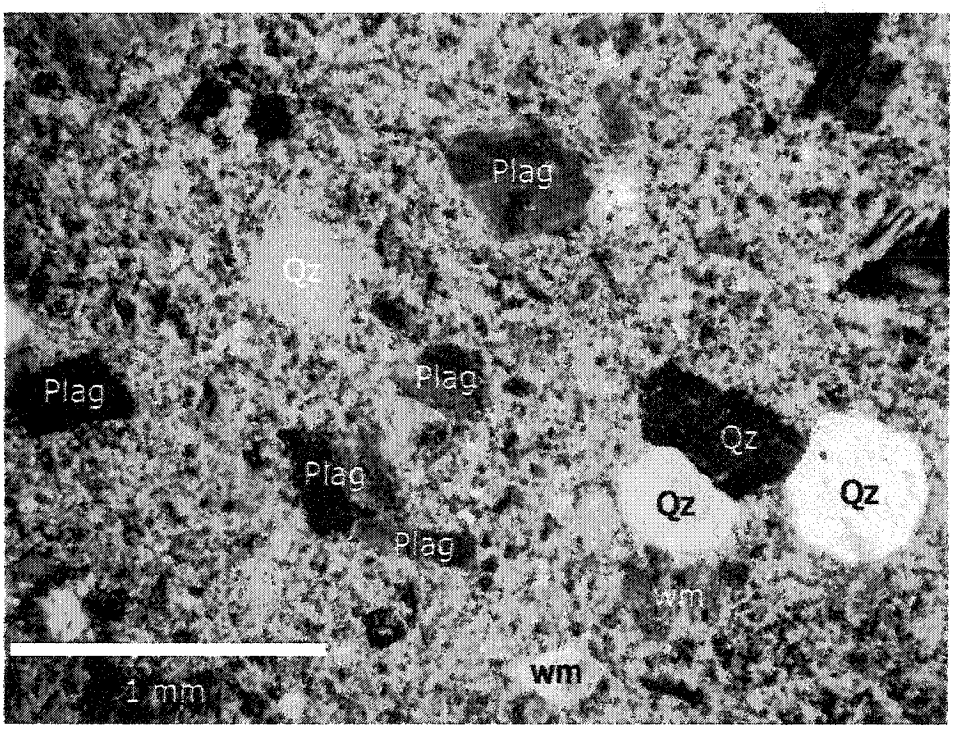

Fig. 2.37: Elvan from the Mn Mines (SC-11-D). The groundmass is difficult to define, but seems to contain white mica, feldspar, and quartz grains. Phenocrysts of quartz and plagioclase are numerous, and there are few white mica and alkali feldspar phenocrysts. Crossed polars.

granodiorite as belonging to the footwall of the fault hosting the manganese mineralisation, a fact also observed in this study.

Elvan (Figure 2.37)

An Elvan dyke occurs close to the Dean and Chapter shaft. The rock has a fine-grained groundmass (90%) of white micas, altered feldspars, and quartz grains (grain size < 0.2 mm) containing subhedral to euhedral phenocrysts (10 %) of quartz, plagioclase, alkali feldspars, and white mica (grain size: 0.5-1.5 mm). The texture is glomeroporphyritic.

Quartz grains are angular and are bordered by a zone of high concentration of fluid inclusions and inclusions of groundmass. Plagioclase also occurs as inclusions in quartz.

Plagioclase grains have an albitic composition and present polysynthetic and/or Carlsbad twinning. Plagioclase is strongly kaolinised and sericitised, and has a diffuse contact with the groundmass.

Alkali feldspar grains have a similar shape to plagioclase, and are distinguishable from them only by their lack of polysynthetic twinning.

White mica grains are large and texturally appear to be primary. In places, they are associated with rutile and have a diffuse contact with the groundmass.

As a whole, this rock can be considered as an extremely fine-grained aplite formed through rapid quenching of the melt. Rapid pressure release through fracturing almost certainly caused the quenching phenomenon.

2.4.3. Leucomonzogranite

2.4.3.1. Non-pervasively altered samples (Figures 2.38 and 2.39)

Leucomonzogranites have a monzogranitic composition with less than 6% combined mafic minerals (Corey 1991; Ham 1991), and the presence of white mica as a main mineral (McKenzie 1974). Adamellite is another name for leucomonzogranite commonly used in the literature (McKenzie 1974 for example). Several units of leucomonzogranite host or/and are in the vicinity of mineral deposits of the New Ross

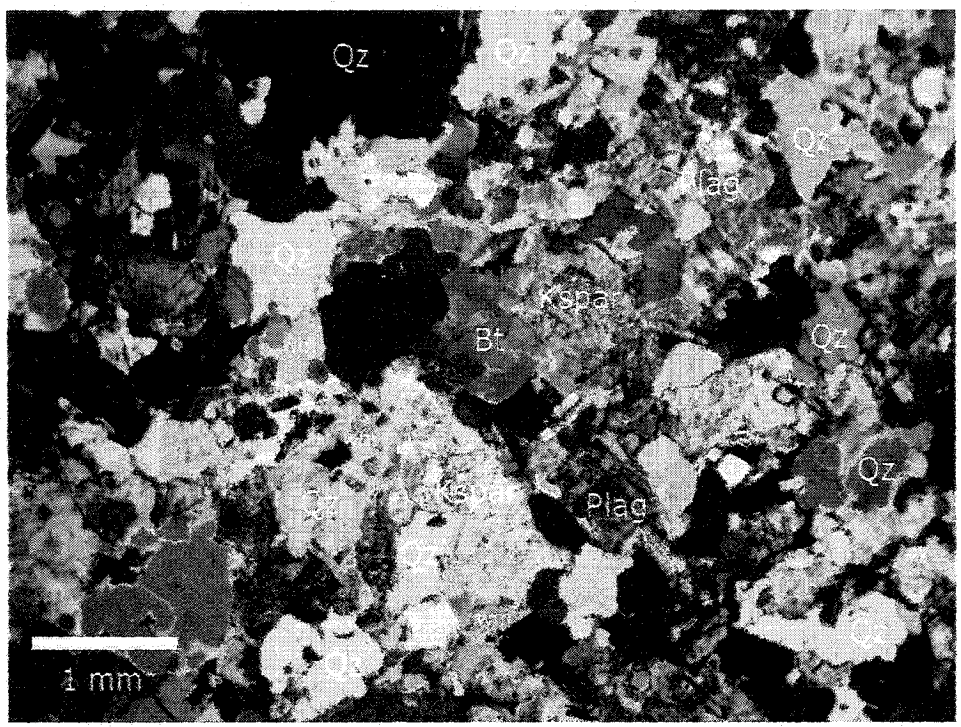

Fig. 2.38: Fine-grained porphyritic leucomonzogranite (SC-1-R) in the vicinity of the Reeves deposit. Crossed polars.

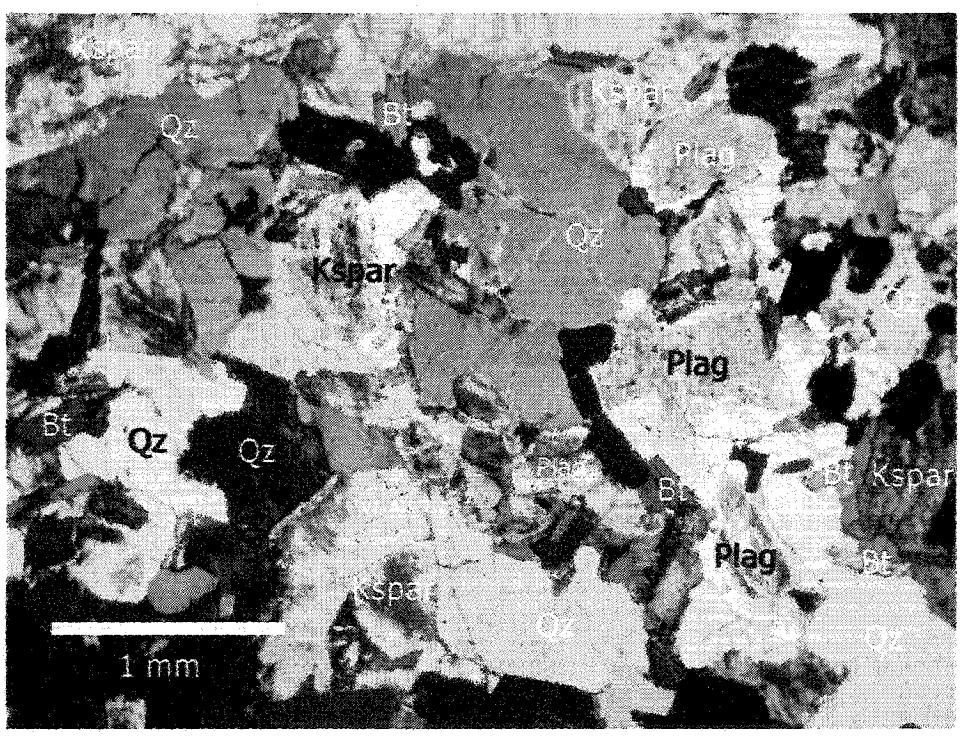

Fig. 2.39: Coarse-grained porphyritic leucomonzogranite (SC-1-W) in the vicinity of the Walker deposit. Crossed polars.

area: the New Ross leucomonzogranite hosts both the Morley's pegmatite and the Keddy prospect, and outcrops in the vicinity of the Long Lake and Walker deposits; the Panuke Lake leucomonzogranite hosts the Walker and Turner deposits and outcrops close to the Keddy prospect, the Reeves deposit, and the Morley's pegmatite. Both leucomonzogranites belong to the Stage II New Ross pluton.
Leucomonzogranites are, in general, more altered than either granodiorite or monzogranite, so in order of increasing hematisation of the alkali feldspars, the Panuke Lake and New Ross leucomonzogranites are light grey, buff, or reddish in colour if hematised. The Panuke Lake leucomonzogranite displays both fine- and coarse-grained textures described in MacDonald (2001) (Figures 2.38 and 2.39, respectively), whereas the New Ross leucomonzogranite only displays a coarse-grained texture (unaltered samples observed mainly in the area of the Morley's pegmatite). The leucomonzogranite is either porphyritic with phenocrysts of plagioclase, alkali feldspar, and occasionally quartz (phenocryst size for fine-grained facies: 1-2 cm and for coarse-grained facies: 4-6 cm) and a granitic groundmass (grain size for fine-grained facies: ~1 mm and for coarse-grained facies: 3-6 mm), or seriate (grain size: 1-4 mm).

Quartz grains are anhedral to subhedral and have undulose extinction. Quartz may contain small biotite and plagioclase grains as inclusions and has sharp and straight boundaries with other minerals.

Plagioclase grains (andesine to albite composition) are subhedral and display both polysynthetic and Carlsbad twinning. Normal compositional zoning is present, especially in smaller grains in inclusions in phenocrysts of alkali feldspars. Plagioclase occurs as a reaction rim around alkali feldspar (rapakivi texture). Plagioclase grains show extensive sericitisation, especially in their cores. Biotite is the only inclusion in plagioclase.

Alkali feldspars are subhedral to euhedral, especially the lath-shaped phenocrysts. Rapakivi texture is common among the phenocrysts. Such a texture, coupled with the observation of very irregular grain boundaries between alkali feldspar and plagioclase, suggests that the alkali feldspar grains have been reacting with the melt in the late stages of crystallisation. Where present as phenocrysts, alkali feldspars

contain numerous inclusions of small rounded quartz and rectangular plagioclase grains that can be distributed within the same zone. Small rounded quartz inclusions (cuniform shape) within a larger alkali feldspar are present in some grains in the matrix. Hematisation affects alkali feldspar the most, and gives a reddish-orange colour to the rock (especially in the vicinity of the Morley's pegmatite).

Biotite grains are small anhedral to subhedral grains, and show different alteration levels of hematitisation, chloritisation, and muscovitisation (Figure 2.40a, b, and c). Biotite has a few zircon grains as inclusions (in most cases, only the radioactive halo is still visible), as well as opaque minerals.

White mica appears both as a primary magmatic mineral and as an alteration product of biotite and feldspar. White micas considered as primary are subhedral to euhedral, have a grain-size comparable to other primary mineral phases present, and have sharp grain boundaries with other minerals (i.e., have no alteration contact with biotite and/or feldspar). Secondary white micas are subhedral, and have fuzzy grain boundaries with minerals they alter (biotite and feldspar), are included in those minerals, and/or have the same mineralogical orientation as the minerals they replace.

Accessory minerals are zircon, apatite, chlorite, rutile, andalusite (altered to white mica), cordierite (pinitised) (Figure 2.41a, b), fluorite, and opaques. In some samples, fluorite is distributed along late fractures.

2.4.3.2. Pervasively altered samples

Greisen

Three types of greisen occur in the New Ross area (Figure 2.42a, b, and c):

1) Quartz-white mica greisen: feldspars, biotite, and primary white mica are replaced by quartz and secondary white mica (Figures 2.42a and 2.43b). Quartz-white mica greisen has a medium-grained seriate texture with quartz and white mica phenocrysts. Quartz grains are anhedral, have undulose extinction, and range from 0.25 to 1 mm in size. White mica flakes are subhedral to euhedral, and/or can display a stellate aggregated texture, and range from 0.1 to 3 mm in size. Quartz and white mica are intimately intergrown (Figure 2.44), indicating that both minerals crystallised

simultaneously (Figure 2.42a). Some small plagioclase and alkali feldspar grains (size: 0.5 mm) are present and have diffuse boundaries with both quartz and white mica. Accessory minerals are apatite, rutile and zircon. Incomplete greisenisation occurs at the Keddy deposit (i.e., there is still ~30% modal feldspar in the rock). Molybdenite flakes in association with topaz and fluorite are present in that greisenised leucomonzogranite. Variable degrees of hematitisation are present in some places, giving the greisen different intensities of red coloration.

2) Quartz-white mica-chlorite greisen: at the Turner deposit, quartz and a mixture of secondary white mica and chlorite replace feldspars, biotite, and primary white mica (Figures 2.42b and 2.43a). The white mica and chlorite are fine-grained (<0.25 mm) and form shapeless aggregates. A few pitted grains of feldspar exist. Numerous quartz veins, some of which are mineralised, cut through the greisen. Some of the quartz veins show deformation (granulation of larger quartz grains). Where opaque minerals are present (arsenopyrite, pyrite, chalcopyrite, and sphalerite), they are in close association with secondary white mica. Farley (1978) proposed the following paragenesis sequence of opaque minerals based on textural observations: arsenopyrite, pyrite, sphalerite, stannite, wittichenite, cassiterite, chalcopyrite, bornite, covellite, and chalcocite.

3) White mica-tourmaline-topaz greisen: at the Walker deposit, secondary white mica replaces feldspar, biotite, and primary white mica (Figure 2.42c). Tourmaline and topaz accompany the white mica. Large stellate aggregated white mica flakes (up to 3mm) have a radial extinction because of their "rosette" pattern. A light brown pleochroic species of white mica also occurs, commonly containing dark alteration patches and fluorite along the cleavages.

   Subhedral tourmaline (1-2 cm in length) is the second most abundant mineral in the greisen. It displays dark-light blue and purple pleochroism. Tourmaline is highly fractured, and fine-grained white mica flakes fill the

cracks. Topaz and opaques are the only accessory minerals. Concentrations of topaz vary from 4 to 8% modal.

2.4.3.3. Minor rock types and intrusives related to the leucomonzogranite

Aplite

Aplites have a fine-grained (grain size: 0.5-1 mm) saccharoidal texture.

Quartz grains are anhedral, can have light undulose extinction, and have sinuous boundaries with other grains. Small anhedral inclusions of plagioclase and white micas, as well as a few euhedral apatite grains, are present in quartz grains. Aplites can contain coarser quartz-rich areas, generally associated with opaque minerals (bornite, covellite, pyrite, chalcopyrite, chalcocite, and wittichenite), as exemplified at the Walker deposit (Figure 2.45).

Farley (1978) also reported the presence of *wolframite* (observed in hand sample, but not in thin section during the present study) and *gahnite*, and she proposed the following opaque minerals paragenesis: 1) molybdenite, wolframite, gahnite, and cassiterite; 2) bornite, mawsonite, wittichenite, and tennantite; and 3) chalcopyrite and native bismuth. Higher modal concentration of quartz grains coupled with the presence of secondary white mica suggests that some aplites show partial greisenisation.

Plagioclase grains (albite composition) are subhedral to euhedral and are strongly kaolinised and sericitised. Grain boundaries are difficult to discern where plagioclase is next to alkali feldspar, because of the similarity in alteration type for both feldspars.

White micas are both primary and secondary. Primary white mica grains have a subhedral to euhedral shape and sharp boundary with feldspar grains. Secondary white micas obviously replace feldspars, have an undefined contour, and are present as both sericitisation and light greisenisation in some cases. White micas, topaz, and fluorite accompany mineralisation. Accessory minerals are topaz, pinitised cordierite, fluorite, rutile, zircon, chlorite, and apatite.

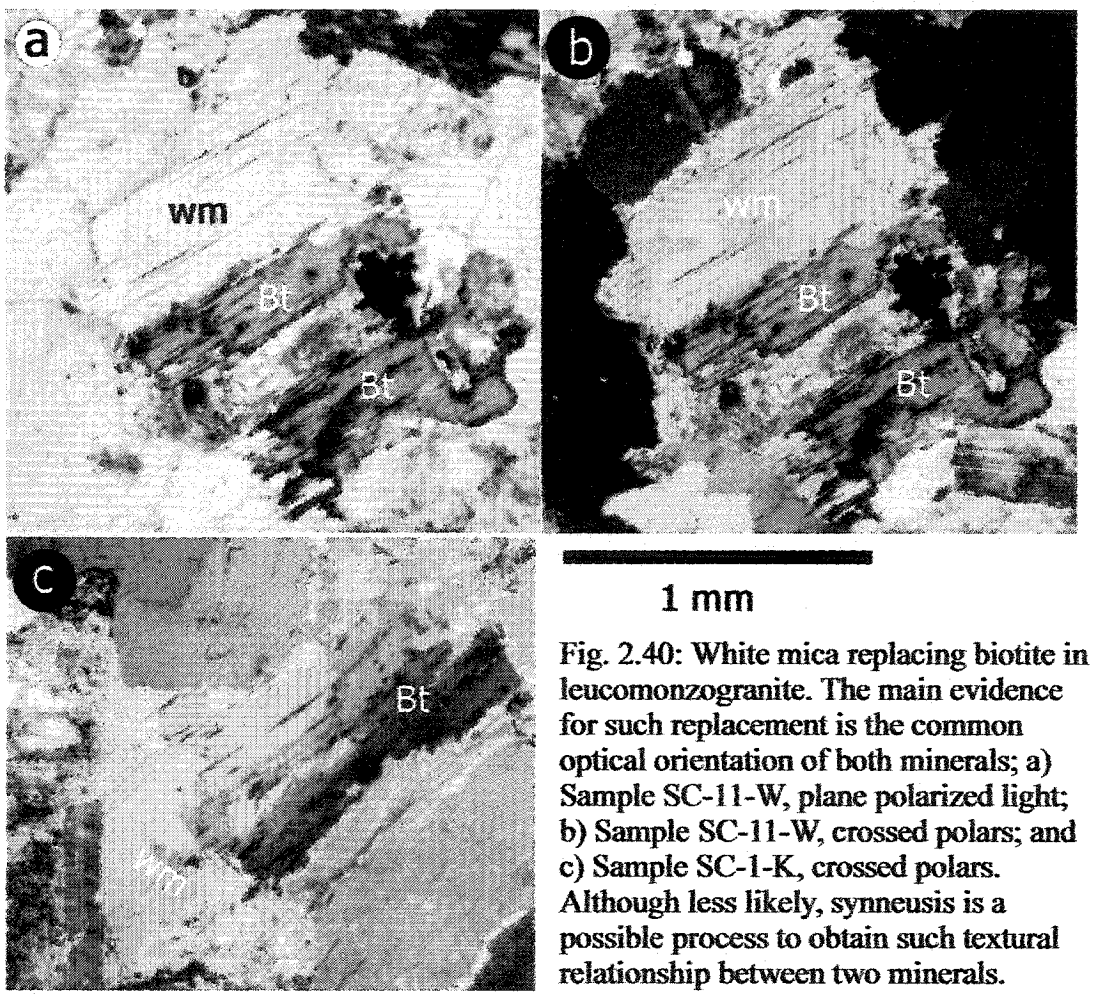

Fig. 2.40: White mica replacing biotite in leucomonzogranite. The main evidence for such replacement is the common optical orientation of both minerals; a) Sample SC-11-W, plane polarized light; b) Sample SC-11-W, crossed polars; and c) Sample SC-1-K, crossed polars. Although less likely, synneusis is a possible process to obtain such textural relationship between two minerals.

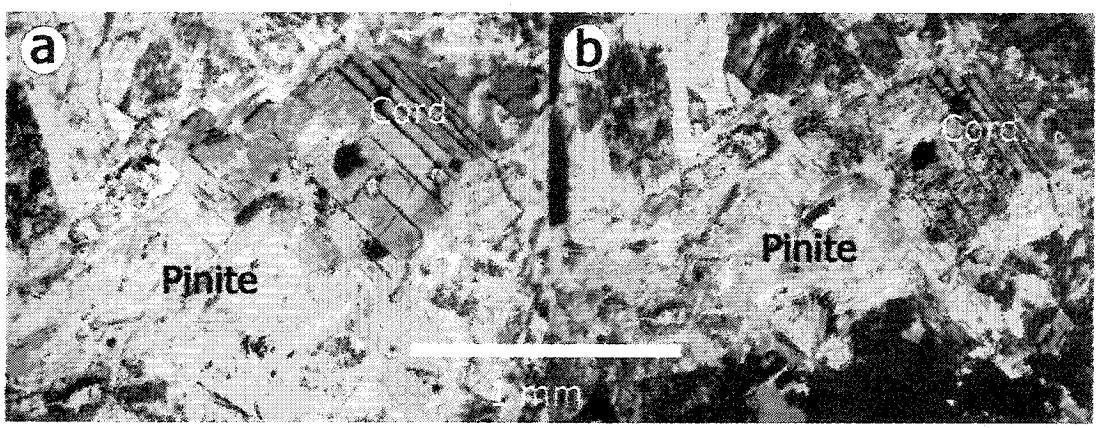

Fig. 2.41: Cordierite mineral altered to a mixture of chlorite and white mica (pinite) in sample SC-1-W; a) Plane polarized light, b) Crossed polars.

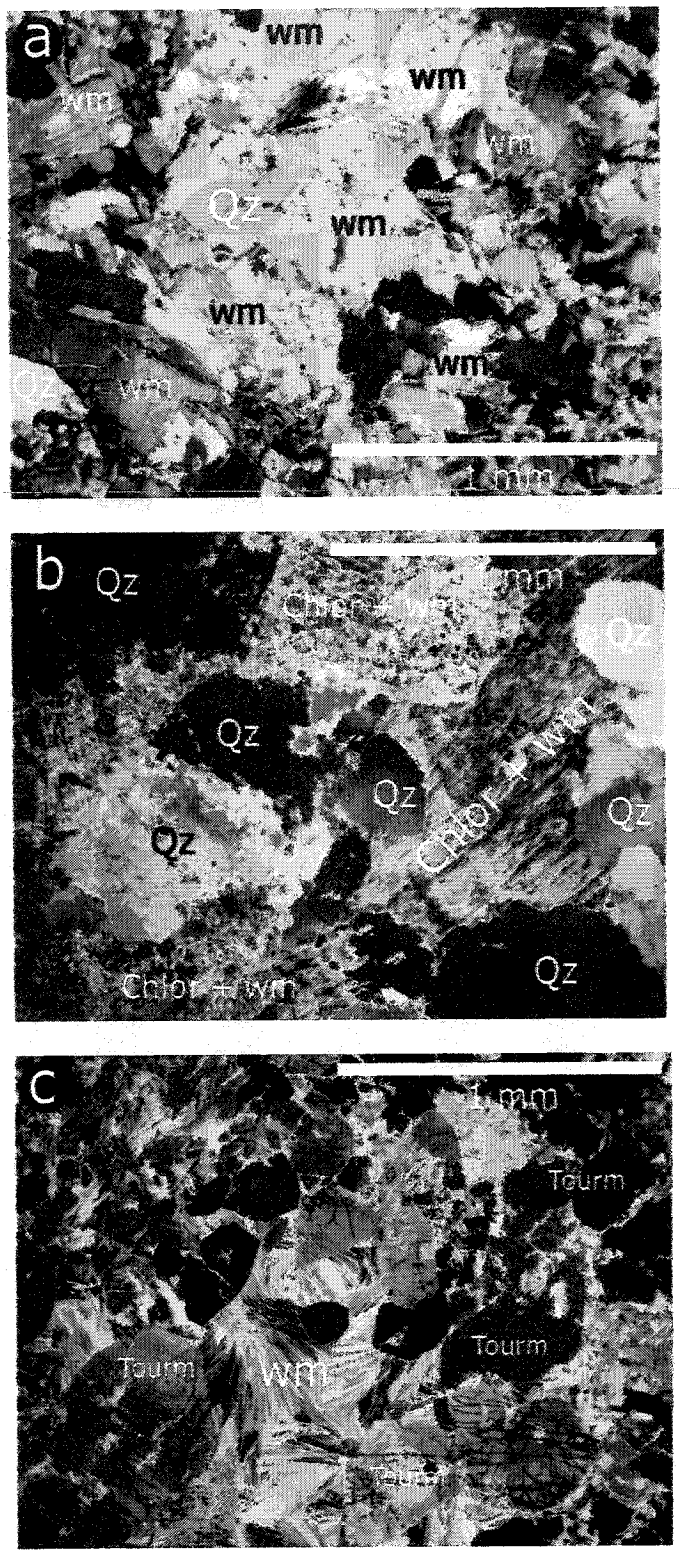

Fig. 2.42: Three different types of greisen observed in the New Ross area: a) Quartz-white mica greisen (SC-2-L); b) Quartz-white mica-chlorite greisen (SC-18-T); and c) white mica-tourmaline-topaz greisen (SC-7-W). All crossed polars.

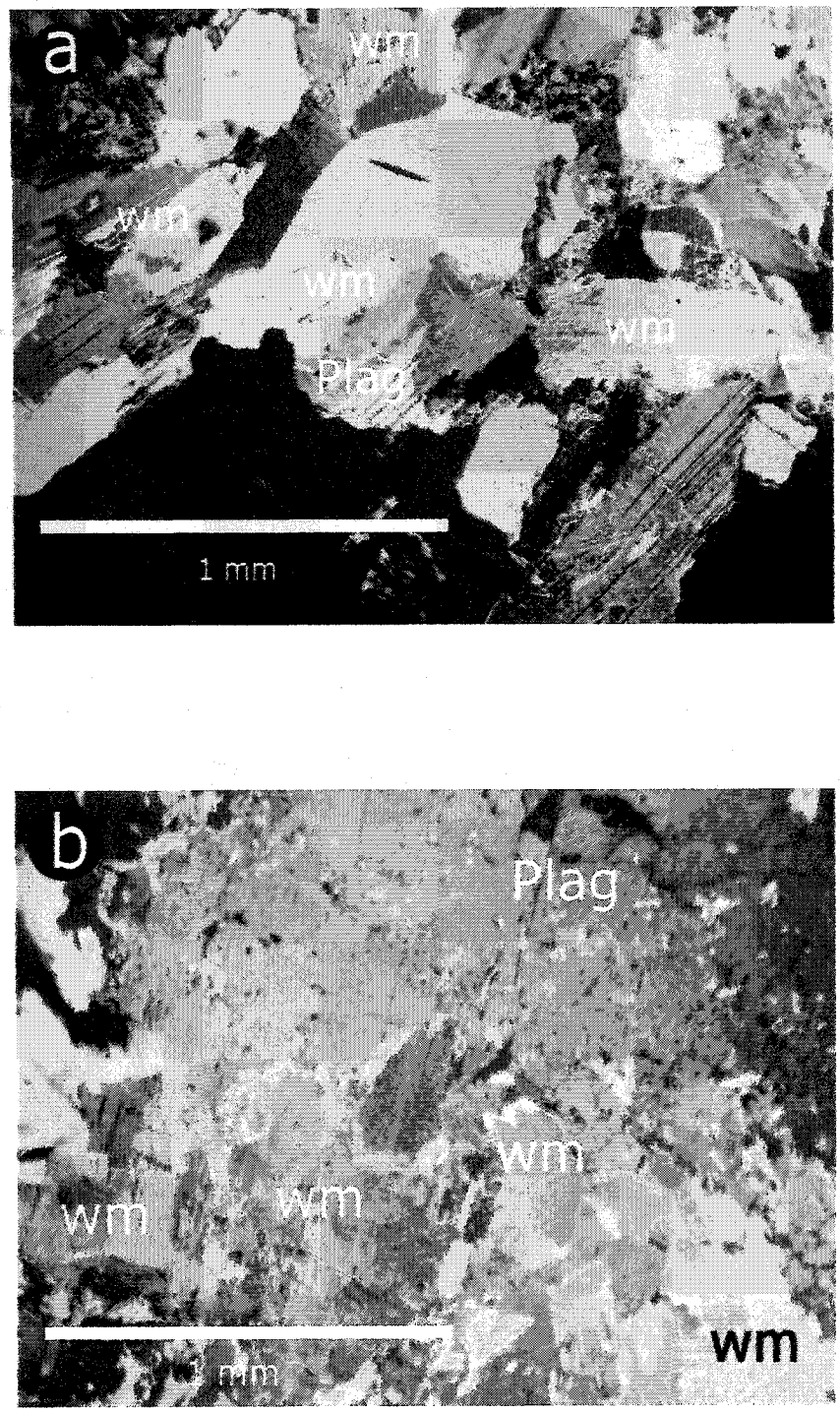

Fig. 2.43: Replacement of plagioclase grains in greisen samples from Long Lake and Morley's; a) a single plagioclase grain is partially replaced by a single white mica grain (SC-5-L), b) a large plagioclase grain is replaced by different size flakes of white mica (SC-13-M). Both crossed polars.

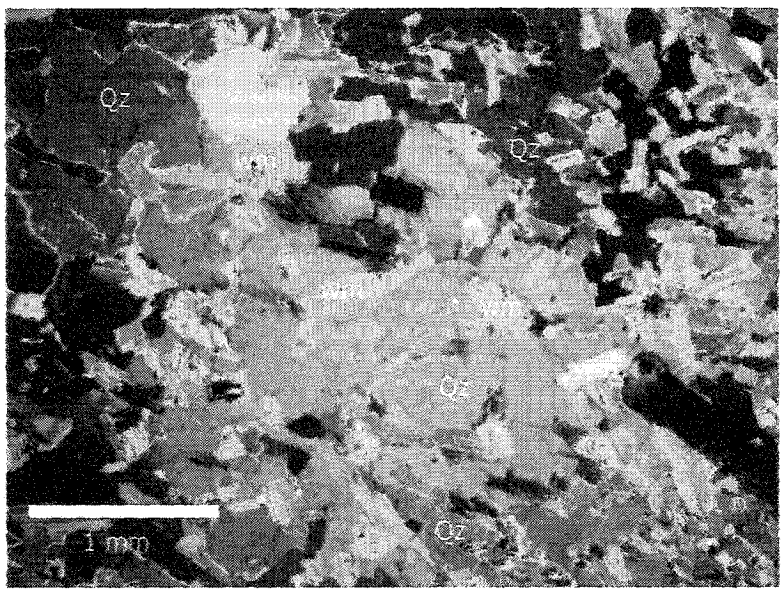

Fig. 2.44: Intergrowth of quartz and white mica in a greisen (SC-13-M) from the Morley's deposit. Crossed polars.

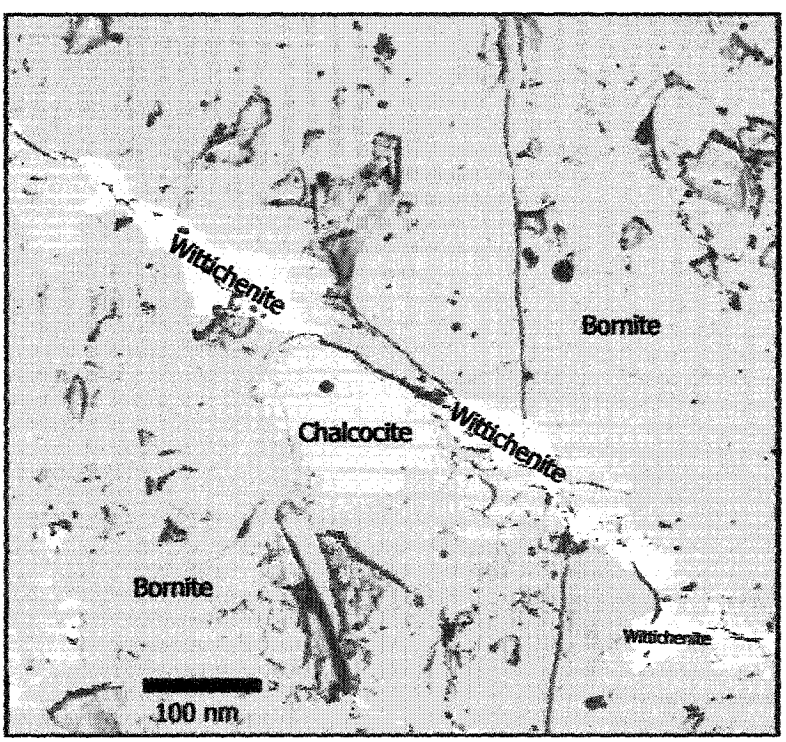

Fig. 2.45: Backscattered image (x 200) of sample SC-5-W showing detailed mineralogy in copper mineralisation: bornite with inclusions of chalcocite, and wittichenite along fractures.

Pegmatite

The pegmatites are exceptionally coarse-grained rocks, mainly containing quartz and alkali feldspars. Lesser amounts of white mica, plagioclase, and opaques are also present. White micas and opaques can occur as large crystals (up to 1 cm), whereas plagioclase only occurs as small (0.5-1 mm) inclusions within large quartz or alkali feldspar grains.

Quartz occurs as large (>1cm) zones in plane polarised light, but under cross-polarised light, subgrains of irregular shape displaying undulose extinction appear.

Alkali feldspars are subhedral to euhedral pink grains (>1cm) with a perthitic texture. Strong kaolinisation and sericitisation alter the alkali feldspar.

White mica is present as an alteration product of alkali feldspar and, although large (certainly primary) white micas (>1cm) are observed in hand specimen, none are observed in thin sections. Green-yellowish white micas also surround sulphide minerals (molybdenite, chalcocite, bornite, covellite, chalcopyrite, and enargite) in veins within the pegmatite (Figure 2.46).

Contacts between the pegmatitic minerals (quartz and alkali feldspar) and the rock hosting the pegmatite are irregular, suggesting that the host rock was not totally solidified at the time of intrusion of the pegmatite (observed at the Keddy deposit). Greisenisation increases the modal proportion of quartz and white micas, and intergrowth of both minerals can be observed in samples from the Walker deposit. At the Walker deposit, molybdenite occurs as small flakes, mostly not associated with other minerals.

Jasper breccia (Figure 2.47)

The intrusion of a jasper breccia dyke in the vicinity of the Morley's pegmatite caused intense hematisation and brecciation of the area (O'Reilly et al. 1982). The breccia is a reddish brown rock with a fine-grained quartz-hematite groundmass containing angular fragments of quartz and host rock leucomonzogranite. The leucomonzogranite is fine- to medium-grained, rarely porphyritic.

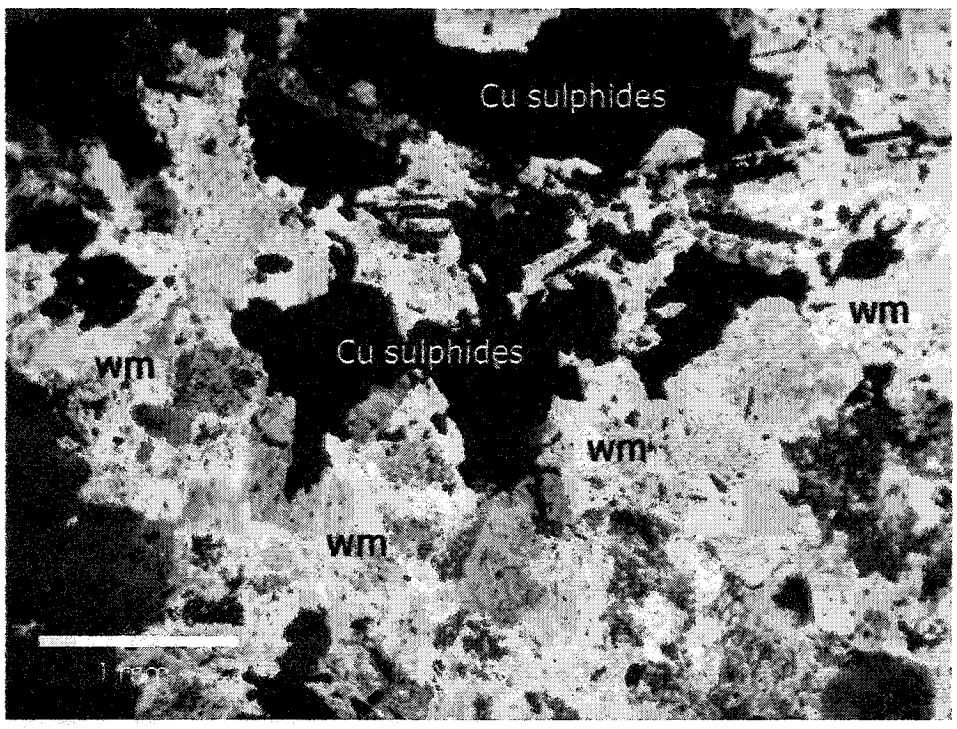

Fig. 2.46: White mica associated with copper mineralisation (SC-6-W) at the Walker deposit. Crossed polars.

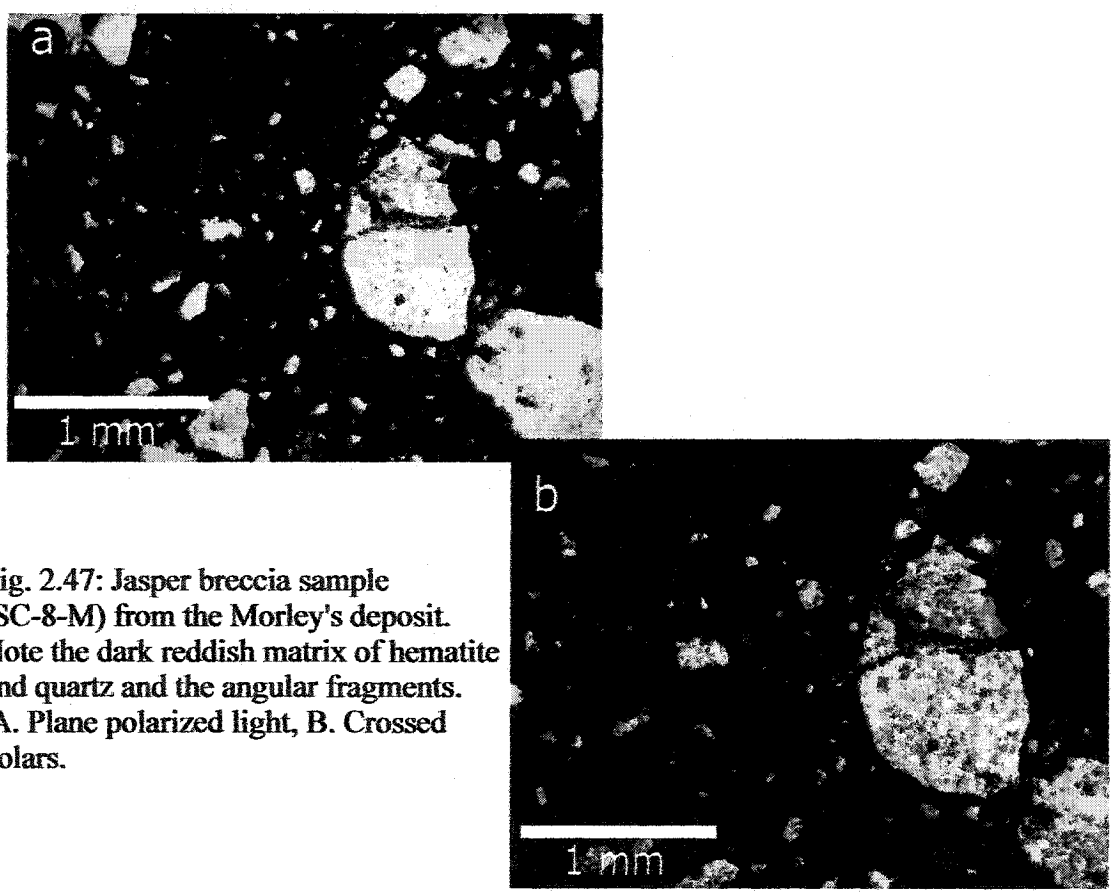

Fig. 2.47: Jasper breccia sample (SC-8-M) from the Morley's deposit. Note the dark reddish matrix of hematite and quartz and the angular fragments. A. Plane polarized light, B. Crossed polars.

Elvan (Figure 2.48)

An elvan dyke intrudes the leucomonzogranite at the Turner deposit. The rock strongly resembles the Elvan at the Mn mines (Section 2.4.2.3). At the Turner deposit (Fig. 2.20), the Elvan dyke is either pink (the southerly outcrop, located on both sides of the river, Fig 2.25) or greenish-beige (northerly outcrop in a trench, Fig. 2.22), but no obvious mineralogical difference accounts for this colour variation. The host rock for the southerly outcrop is a coarse-grained leucomonzogranite, whereas the northerly outcrop is hosted by a fine-grained, porphyritic, and slightly greisenised leucomonzogranite. Table 2.6 summarises the textural and modal changes from within to both sides of the Elvan dyke: quartz is euhedral to subhedral, white mica is euhedral to subhedral, and biotite is totally absent from the dyke, but present in the host rock. A finer-grained facies, with fewer phenocrysts and clusters occurs at the contact with the leucomonzogranite, suggesting chilling of the dyke against cooler host rock. This northerly outcrop is
similar to the Elvan dyke observed at the Mn mines and to the southerly outcrop, with the exception of its greenish-beige colour and a higher concentration of clusters of granitic minerals. The concentration of phenocrysts increases to ~10% towards the centre of the dyke. Farley (1978) suggested that these clusters are xenoliths of the host rock, but alternatively, it is possible that the clusters are pieces of already crystallised magma (autolith). Quartz grains are nearly euhedral, within the clusters and as phenocrysts within the groundmass, whereas it is mainly anhedral within the leucomonzogranite. In addition, the texture of the other minerals forming the clusters is identical to the corresponding isolated phenocryst within the groundmass. Contact with the host rock is sharp, although it involves a change of colour from the usual pink (hematised) to yellow-light green for the feldspars of the fine-grained leucomonzogranite. The change of colour may reflect less hematisation in the green facies or weathering of the greenish facies.

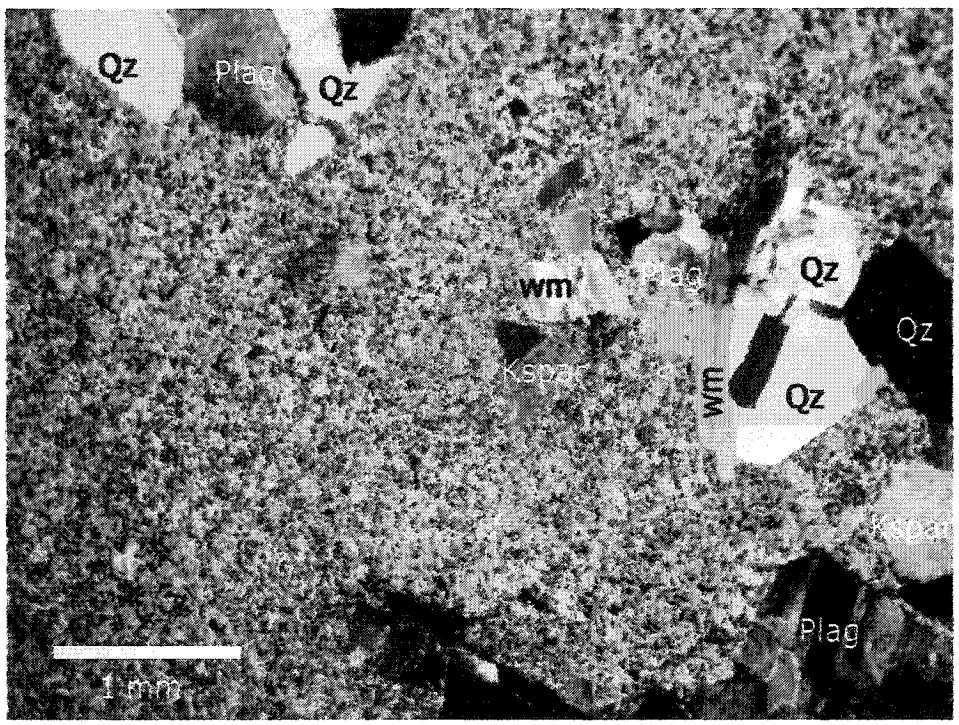

Fig. 2.48: Elvan from the Turner deposit (SC-14-T). Note the finer-grained groundmass compared to the elvan at the Mn mines (Fig. 2.37). Crossed polars.

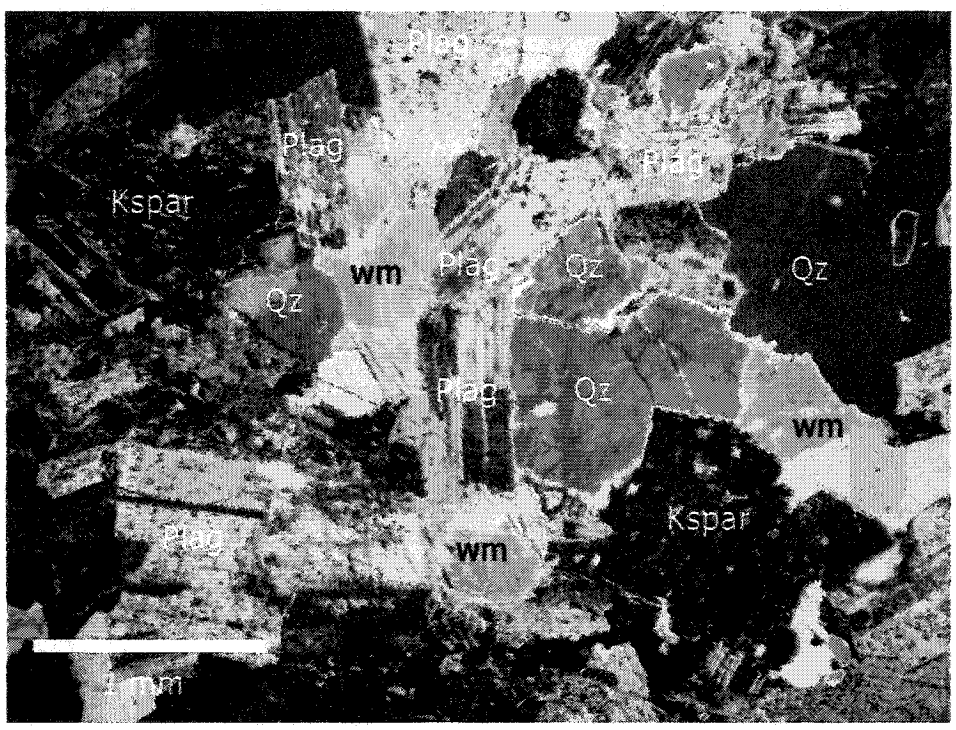

Fig. 2.49: Typical leucogranite (SC-6-R) from the Keddy-Reeves leucogranite hosting the Reeves pegmatite. Note the absence of biotite and the large modal proportion of plagioclase. Crossed polars.

Samples from SW to NE	Modal proportions						Texture
	Qz	Plag	Kspar	Bt	Musc	Groundmass proportion	
SC-11-T	35 anhedral	25	30	5	5 subhedral	0	fine-grained porphyritic
SC-10B-T	3 subhedral	4	1	0	2 euhedral	80	glomeroporphyritic
SC-10A-T	3 subhedral	4	1	0	2 euhedral	85	glomeroporphyritic
SC-12-T	35 anhedral	25	30	4	6 subhedral	0	fine-grained porphyritic
SC-13-T	30 anhedral	30	30	4	6 subhedral	0	fine-grained porphyritic and contact with coarse-grained leucomonzogranite

Table 2.6: Textural observations and modal proportions for the Elvan dyke at the Turner deposit and its immediately adjacent host-rock. Only sections 10A and 10B belong to the dyke.

2.4.4. Muscovite leucogranite

2.4.4.1. Non-pervasively altered samples (Figure 2.49)

Muscovite leucogranites have a monzogranitic composition with less than 2% combined mafic minerals (Corey 1991; Ham 1991), and contain muscovite as the main mica. Other terms used for leucogranite in the literature are leucoadamellite or alaskite (McKenzie 1974 for example). Alaskite is a granitic rock containing only a few percent of dark minerals. The term has mainly been used to designate granitoid rocks in which quartz comprises 20-60% of the felsic minerals and in which the ratio of alkali feldspar to total feldspar is greater than 90% (Bates and Jackson 1987). No such concentration of alkali feldspar was observed in the rocks from the New Ross area, hence the inappropriateness of the term. Two different units of muscovite leucogranite host two mineral deposits: the Keddy-Reeves leucogranite hosts the Reeves deposit and outcrops close to the Keddy prospect, and the Long Lake leucogranite hosts the Long Lake prospect. Both units belong to the Stage II New Ross pluton. The leucogranite has a white to beige colour, and is fine- to medium-grained. Pinkish and reddish colours characterise hematised samples. The texture is usually equigranular (grain size: 1-3 mm), but can be porphyritic (MacDonald 2001). Each sample from the Long Lake leucogranite is altered to a certain extent (greisenisation, K-feldspathisation) (O'Reilly et al. 1982; Corey 1991), and the following description is based solely on samples from the Keddy-Reeves leucogranite.

Quartz grains are anhedral and rarely display undulose extinction. Quartz contains small grains of plagioclase as inclusions, and grain boundaries with other minerals are sharp and sinuous.

Plagioclase grains (albite composition) are subhedral to euhedral and have polysynthetic twinning with or without Carlsbad twinning. Minor zoning is present. Plagioclase laths are strongly kaolinised and sericitised. Different stages in the sericitisation of plagioclase grains are: 1) "dusty"-looking alteration with high birefringence distributed throughout the plagioclase; 2) small white mica flakes

(~0.05 mm) either randomly dispersed in plagioclase or oriented along cleavages; and 3) white mica grains (~0.5 mm) with the same optical orientation as plagioclase, and obviously replacing feldspar. Grains in the third sericitisation stage have a fuzzy and sinuous contact with the plagioclase being altered. Plagioclase grain boundaries with alkali feldspar and with other plagioclase are diffuse, because of extensive sericitic alteration. Plagioclase contains no inclusions of other minerals.

Alkali feldspar grains are anhedral (interstitial), perthitic, and strongly sericitised and kaolinised. Alkali feldspar contains small euhedral plagioclase grains.

Biotite is rare to non-existent. If present, it occurs only as inclusions in quartz grains, which protects biotite from alteration (e.g., muscovitisation).

White mica occurs as a secondary alteration product of plagioclase or alkali feldspar, or as a primary mineral crystallising from the melt. Primary white micas in leucogranites fit the description given in the leucomonzogranite section: subhedral to euhedral, grain-size comparable to other primary mineral phases present, and sharp grain boundaries with other minerals, especially those that white mica is likely to replace (biotite, feldspar).

Topaz appears as an abundant accessory mineral in leucogranites and is commonly associated with white mica (Figure 2.50). Topaz grains are anhedral to euhedral and strongly fractured with sericitic alteration. Grain-size is comparable to other main mineral phases in the rock.

2.4.4.2. Pervasively altered samples

Greisen

A quartz-white mica-chlorite greisen occurs in the Long Lake and Keddy prospect areas. The greisen is similar to that described in Section 2.4.3.2 under quartz-white mica-chlorite greisen.

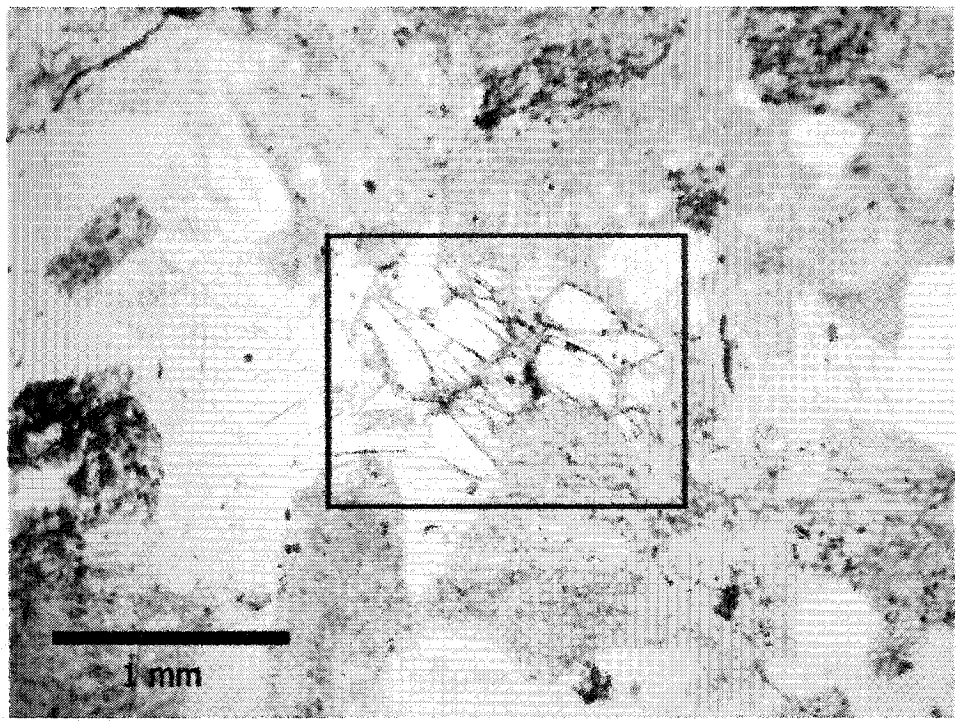

Fig. 2.50: Topaz grains (in box) in the Keddy-Reeves leucogranite (SC-6-R). Plane polarised light.

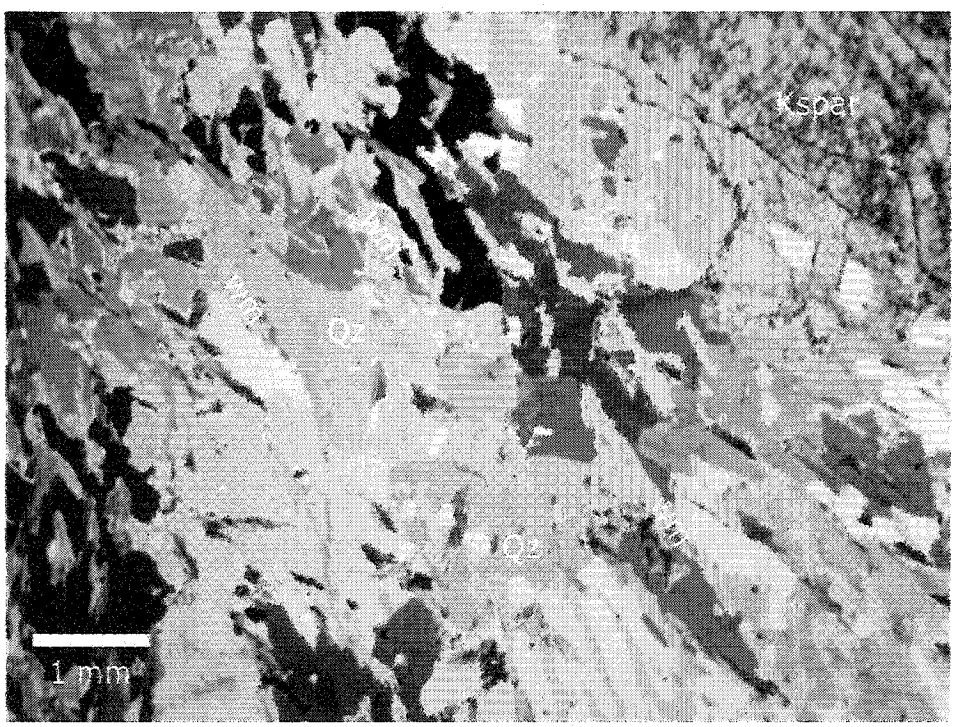

Fig. 2.51: Intergrowth of quartz and white mica in the Reeves pegmatite (SC-9-R). Crossed polars.

2.4.4.3. Minor rock types and intrusives related to the leucomonzogranite

Pegmatite

Two localities with pegmatite hosted in leucogranite exist at the Reeves and Long Lake mineral occurrences, within the New Ross pluton. The Reeves pegmatite contains quartz, perthitic alkali feldspar, and both stellate aggregated and euhedral white mica as very coarse grains (grain size > 2 cm). Some plagioclase grains (albite composition) are present as inclusions along fractures of large alkali feldspars. Accessory topaz is restricted to large white mica rosettes. All mineral boundaries are sharp except for the large alkali feldspar grains, which display small quartz subgrains at the boundary with large quartz grains or irregular, fuzzy contact with white mica grains. A greisenised area exists at the contact with the Keddy-Reeves leucogranite, and remarkable intergrowths of quartz and white mica textures occur (Figure 2.51). Therefore, contact with the leucogranite is gradual, from a "true" pegmatite to a greisenised pegmatite, to a greisenised leucogranite, to a non-altered leucogranite.

The pegmatite occurring at Long Lake contains the same minerals as the Reeves pegmatite; however, a few textural differences exist:

1) The white mica flakes are euhedral and no stellate aggregated white mica is present.
2) Molybdenite flakes occur within quartz and alkali feldspar grains.
3) Contact with the greisenised leucogranite is sharp, and there is no greisenised pegmatite.
4) The pegmatite is associated with a banded greisenised aplite. Poor outcrop means that observation of the contact is only in loose boulders. Within the aplite, molybdenite occurs as flakes in quartz-rich horizons.

Rock type	Grain size	Texture	Modal proportion		Plagioclase	Presence of		
			Biotite (%)	White mica (%)	An content (%)	Cordierite	Andalusite	Topaz
biotite granodiorite	medium- to coarse-grained	**porphyritic**	15	trace-3	andesine-oligoclase	yes	no	no
monzogranite	medium- to coarse-grained	**porphyritic**, equigranular	10-15	trace-3	andesine-oligoclase	yes	no	no
leucomonzogranite	fine- and coarse-grained	**porphyritic,** seriate	5-10	5	andesine-oligoclase-albite	yes	yes	yes
leucogranite	fine- to medium-grained	**equigranular**, porphyritic	0-3	10-25	albite	no	no	yes

Table 2.7: Summary of textural and modal proportion variations within the main rock types present in the New Ross area (after MacDonald 2001).

2.4.5. Summary

Major mineralogical changes in the host granitoid rocks of the New Ross area are: 1) modal proportion of biotite, 2) modal proportion of white mica, 3) anorthite (An) content of plagioclase, and 4) modal proportion of topaz. Also, textural differences exist among members of the rock suite, with porphyritic and equigranular textures as the two dominant ones. Table 2.7 summarises the variation in texture, modal proportion of minerals, and An content of plagioclase for the different host granitoid rocks of the New Ross area. From least evolved granodiorite to more evolved leucogranite, the rock suite generally reflects fractional crystallisation at work within the SMB. Also, the sporadic presence of cordierite and/or andalusite illustrates the peraluminous character of the SMB.

Variable types and intensities of alteration overprinting each type of rocks, allowing for the development of new rock types (episyenite or greisen for example), and the presence of different late intrusives (aplite, pegmatite, elvan, and jasper breccia) indicate that large amount of fluids circulated within the New Ross area. Also, during cooling of the granite, thermal contraction and fracturing created large-scale faults channelling the circulating fluids and allowing for the emplacement of vein deposits. Other processes leading to fracturing may be the reactivation of large-scale tectonic faults within the MLT or fluid overpressure. Further evaluation of these processes is needed to better understand the generation of faults in the New Ross area.

In the New Ross area, therefore, the process of fractional crystallisation led to the development of contrasting host granitoid rocks, whereas fluid-rock interaction promoted formation of altered granites.

CHAPTER 3

TEXTURAL AND CHEMICAL CHARACTERISATION OF WHITE MICAS

3.1. Introduction

A longstanding petrogenetic problem with peraluminous granitoids is the discrimination between primary (magmatic) and secondary (non-magmatic) white micas (Zen 1988). Many scientists (e.g., Miller et al. 1981; Speer 1984; Ham and Kontak 1988; Zen 1988; Roycroft 1991, Zane and Rizzo 1999) have attempted to discriminate between primary and secondary white micas by defining textural and/or chemical criteria possibly applicable to white micas in all peraluminous granitic rocks. One outcome from clearly defining the origin of white micas would be an accurate determination of the white mica stability field in pressure and temperature (Miller et al. 1981; Zen 1988).

The objectives of my detailed petrographic and chemical study of a single mineral are two-fold: (1) to provide useful textural and chemical criteria specific to the SMB to permit distinction between primary (magmatic) and secondary (non-magmatic) white micas; and (2) to apply this knowledge to better interpret the $^{40}Ar/^{39}Ar$ white mica age data (Chapter 4). In this chapter, I first present a general literature review and discussion of textural and chemical criteria for primary and secondary white micas. Subsequently, I present textural criteria specifically defined for the SMB prior to chemical analysis, and use them to assess the origin of white micas for samples from eight mineral occurrences in the New Ross area. As a third step, I establish a chemical classification of the white micas, based on understanding of the substitution(s) taking place within the mineral during alteration and use the results to assess the origin of dated white micas grains. Finally, I use multivariate statistics allowing an investigation of the variability of all chemical elements present in the white micas simultaneously.

3.2. White mica generalities

3.2.1. Principal chemical substitutions in white micas

The general formula for micas is $X_2Y_{4-6}\square Z_8O_{20}(OH, F, Cl, S)_4$, with X being the twelve-fold coordination interlayer site (K, Na, Ca, Cs, Rb, Ba), Y the octahedral site (Al^{vi}, Mg, Fe^{2+}, Fe^{3+}, Mn, Ti, Li, Zn, Cr, V), $\square$ the two vacant octahedral sites, and Z the tetrahedral site (Si, Al^{iv}, Fe^{3+}, Be, B). Depending on the number of octahedral cations, micas are subdivided into dioctahedral (Y<5) and trioctahedral (Y>5) (Monier and Robert 1986, Rieder et al. 1999, Guidotti and Sassi 2002). In the ideal system $KAlO_2$-$NaAlO_2$-$CaAl_2O_4$-Al_2O_3-SiO_2-H_2O, the dioctahedral white micas consist of three end-members:

1. $K_2Al_4\square(Al_2Si_6O_{20})(OH)_4$: muscovite
2. $Na_2Al_4\square(Al_2Si_6O_{20})(OH)_4$: paragonite
3. $Ca_2Al_4\square(Al_4Si_4O_{20})(OH)_4$: margarite

Guidotti and Sassi (1998b) provided a summary of the deviations from the above-mentioned ideal formula through different substitutions. The main interest for this study resides in the substitutions involving significant deviation from ideal muscovite composition. Figure 3.1 shows the ideal paragonite substitution in a binary diagram. Figure 3.2 illustrates the ideal biotite and Tschermak substitutions in a three-dimensional diagram with Fe+Mg+Mn vs. Al_{total} vs. Si.

1. <u>Paragonite substitution:</u>

   $K \leftrightarrow Na$ (Muscovite $\leftrightarrow$Paragonite)

with $Na_2Al_4\square(Al_2Si_6O_{20})(OH)_4$ (paragonite) as end-member. A large miscibility gap exists between the two end-members, mainly because of the size difference of the K^+ and Na^+ cations (Guidotti and Sassi 1998b).

2. <u>Tschermak exchange (also called the phengite or celadonite substitution):</u>

   $Al^{VI}, Al^{IV} \leftrightarrow (Mg, Fe^{2+})^{VI}, Si^{IV}$ (Muscovite $\leftrightarrow$Celadonite)

with $K_2Fe_2^{3+}(Mg, Fe^{2+})_2\square(Si_8O_{20})(OH)_4$ (celadonite) as end-member. Compositions between muscovite and celadonite represent the phengite solid solution (Rieder et al. 1999).

One of the main factors controlling the amount of Fe^{3+} entering the muscovite is the bulk composition of the mineral assemblage, particularly whether the assemblage is Al-

saturated (Guidotti and Sassi 1998b). Furthermore, an increase in water pressure (P_{H2O}) increases the extent of Tschermak substitution (Monier and Robert 1986).

3. Deficiency in the XII (interlayer) site:

Total cation content in the interlayer site should be 2 atoms per formula unit (apfu), but a deficiency in the alkali site exists in all naturally occurring muscovite. No entirely satisfactory explanation exists for the cause of such deficiency, other than the failure to analyse some elements (such as Sr or Rb in the SMB micas), the real existence of a vacancy in the XII site, or an exchange such as $H_3O^+ \rightarrow K^+$.

4. Deviation towards trioctahedral mica (biotite substitution):

Usually, the total for the octahedral site in "muscovite" exceeds the ideal 4, indicating some solid solution of dioctahedral white micas towards trioctahedral micas (Guidotti and Sassi 1998b). Monier and Robert (1986) proposed that the following substitution occurs:

$$4Al^{VI}, 2\square^{VI} \leftrightarrow 6(Mg^{2+}, Fe^{2+})^{VI}$$

Trioctahedral micas have the general formula $K_2(Mg, Fe)_6(Si_6Al_2O_{20})(OH)_4$, with phlogopite as the Mg end-member, and annite as the Fe end-member. The biotite substitution appears in most natural muscovite accompanied by the Tschermak substitution (Monier and Robert 1986).

3.2.2. White mica stability field in granitic rocks

The presence of white micas as coarse euhedral phase in volcanic and dyke rocks establishes it as a magmatic mineral (Zen 1988). The presence of coarse-grained white micas in plutonic rocks may be ambiguous, because white mica can crystallise over a range of temperature and pressure from the magmatic (primary), fluido-magmatic (primary), and subsolidus (secondary) stages. In this study, the term "primary" encompasses any white mica that crystallised in the presence of melt (i.e., suprasolidus stage melt + crystals ± fluid). The term "secondary" covers white micas that crystallised in the absence of melt (i.e., subsolidus hydrothermal stage crystals + fluid). Figure 3.3 is a schematic representation of the possible phase assemblages for primary and secondary white mica formation.

The main interest in recognising white mica as an unequivocal magmatic mineral involves the reconsideration of previously determined temperature and pressure ranges for

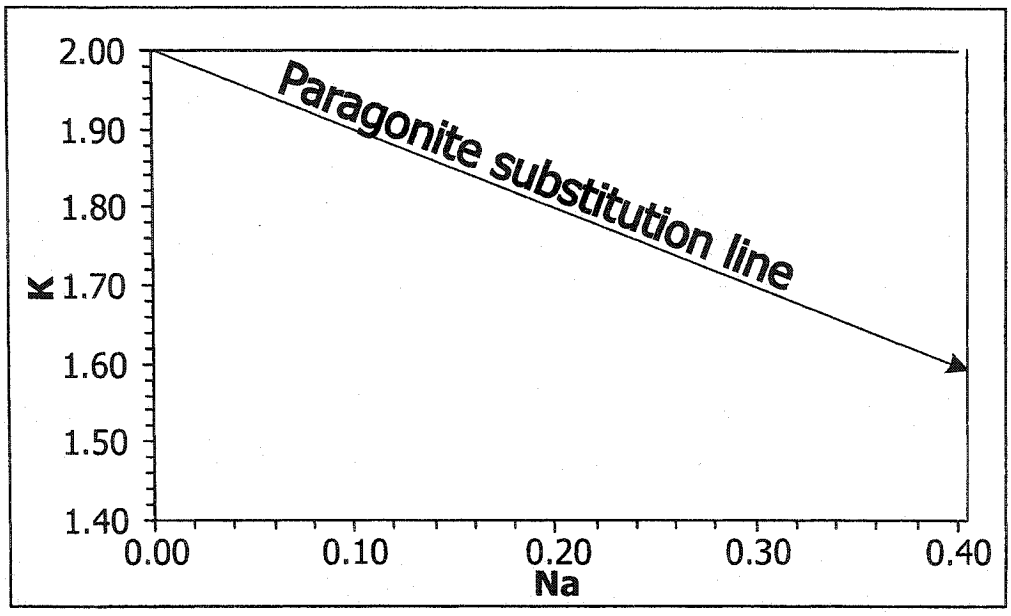

Figure 3.1: Na vs. K diagram showing the ideal paragonite substitution.

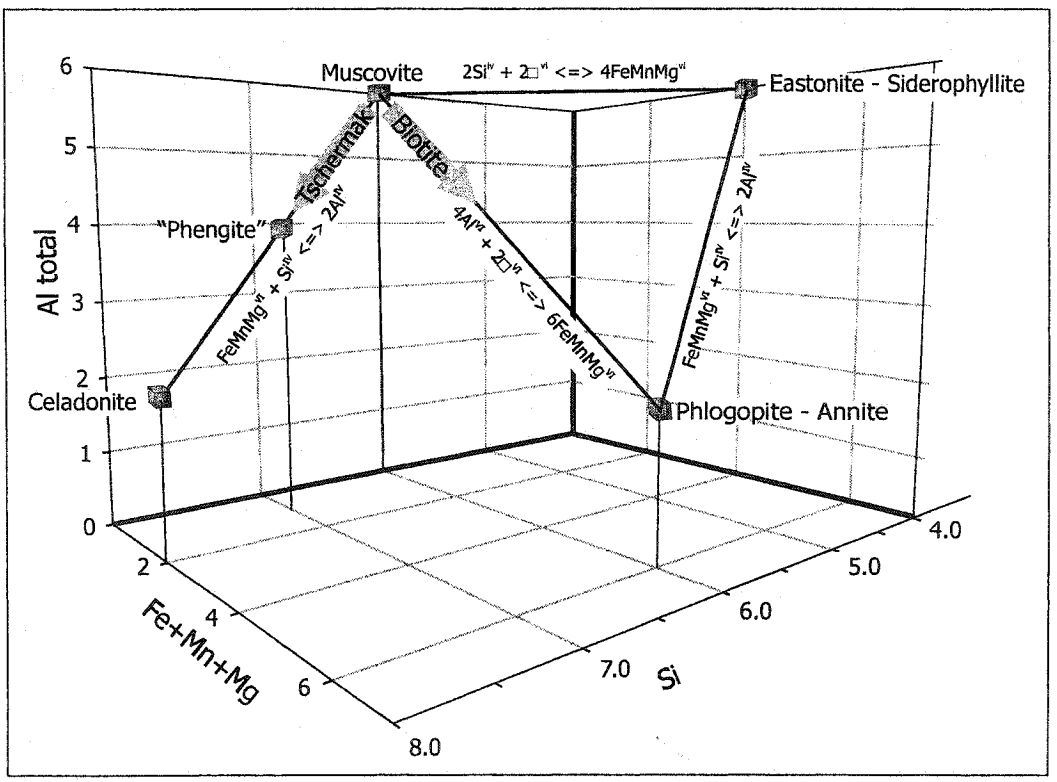

Figure 3.2: Three-D diagram Si vs. Al+Mg+Mn vs. Al_{total} showing the ideal Tschermak and biotite substitutions.

the stability field of white mica (Miller et al. 1981; Zen 1988). Figure 3.4 presents the stability field of white mica on a P-T diagram with white mica equilibrium and peraluminous wet granite solidus curves. Addition of F, B, and/or Li decreases the temperature of the granite solidus. The combined effect of all three is not well understood (P. Candela pers. comm. 2000) but, in the SMB, F is the most likely to affect the granite solidus, because it is the most abundant element of the three. In the literature, the position of the andalusite-sillimanite boundary varies from one author to another (Clarke et al. 2003), and the one used in this thesis is the andalusite-sillimanite equilibrium curve of Pattison (1992). The equilibrium curve of the dehydration reaction muscovite + quartz = alkali feldspar + Al_2SiO_5 + H_2O is discussed by Chatterjee and Johannes (1974). Addition of F and/or Fe expands the stability field of muscovite. For the peraluminous granites of the SMB, magmatic muscovite crystallisation is possible at temperatures above 625°C and pressures above 2.8 kbar. A narrow window of pressure and temperature (T = 635-625°C and P ~ 3 kbars) allows for crystallisation of magmatic andalusite and magmatic muscovite, using the triple point of Pattison (1992). Zen (1988) emphasised that the granite solidus is lowered with the addition of chemical components such as B, F, or Li and will, therefore, allow for muscovite crystallisation at lower P-T conditions.

3.3. Sample selection

The sample set for the characterisation of white micas from the New Ross area contains magmatic host granitoid rocks (granodiorite, monzogranite, leucomonzogranite, and leucogranite), and mineralised and/or altered samples from three mineral deposit types (aplite/pegmatite, greisen, and vein) (Table 3.1). I also used samples from other locations within the SMB to further assess the textural/chemical characteristics of primary white micas and to better understand the textural/chemical variability of white micas at a scale larger than the studied area (Table 3.2). The rationale for including samples from other parts of the SMB is the clear textural evidence for a magmatic (or fluido-magmatic) origin of aplite dykes in those parts and, therefore, the higher probability that those rocks contain primary magmatic white micas.

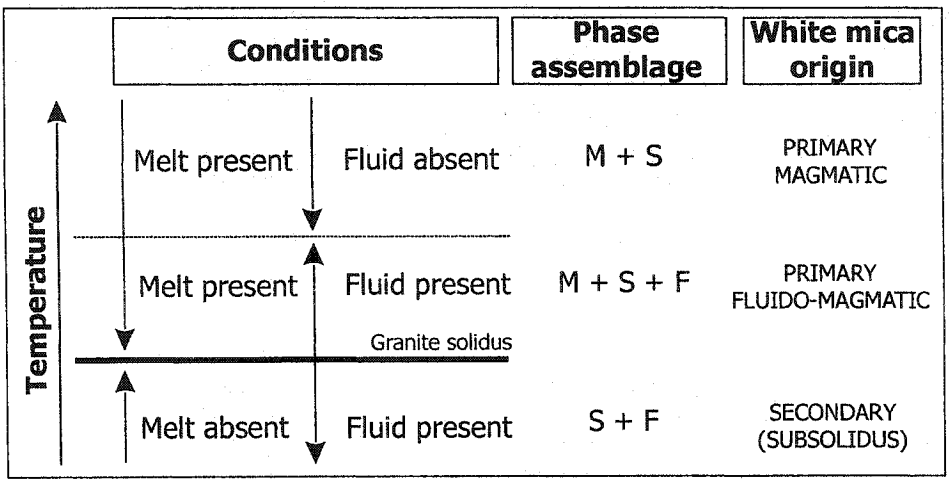

Figure 3.3: Schematic representation of the conditions, phase assemblage, and white mica origin according to the definitions in the text. M = melt, S = solids, and F = fluid.

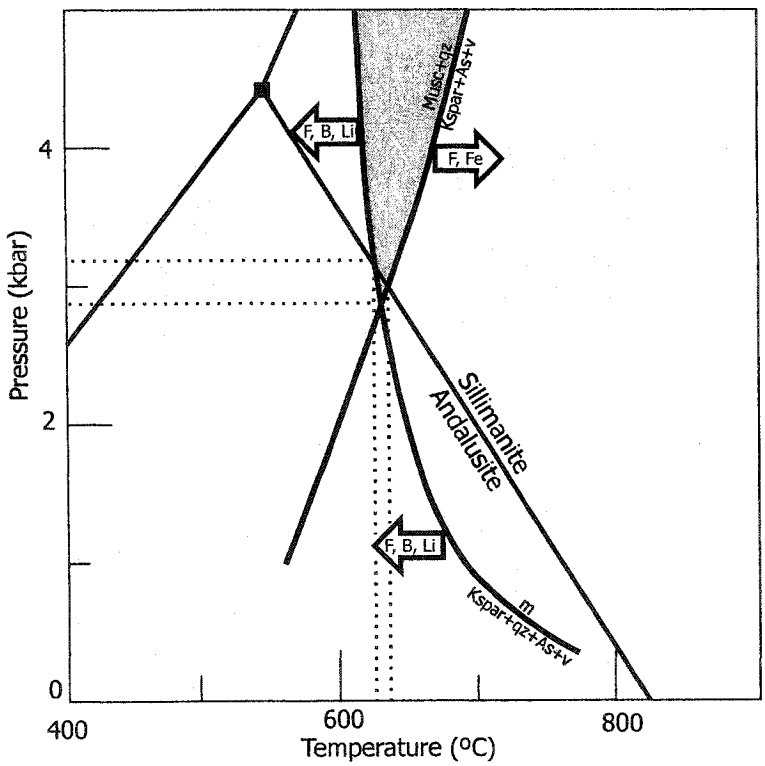

Figure 3.4: Experimental phase equilibrium data bearing on the stability of magmatic muscovite. Arrows show how addition of chemicals such as F, B, and Li affect the temperature of the wet granite solidus. Triple point and aluminosilicate fields (Pattison 1992, 2001); solidus of water-saturated peraluminous granite (Johannes and Holtz 1996); dehydration reaction curve (Chatterjee and Johannes 1974). Position of all three curves subject to other compositional parameters (F, B, Li, Fe) and experimental uncertainty. Shaded area = magmatic muscovite field. Minimum T and P for crystallisation of magmatic muscovite: 625°C and ~ 3 kbars; T and P for crystallisation of magmatic muscovite and andalusite: 635-625°C and ~ 3 kbars.

3.4. Primary versus secondary white micas

3.4.1. Textural criteria for distinguishing primary from secondary white micas

The individual pieces of textural evidence for determining the primary origin of a white mica are rather weak if taken separately, but more convincing if taken collectively, particularly if restricted to a single granitic body. Speer (1984) compiled the following textural criteria for identifying primary muscovite: sharp grain boundaries (i.e., in textural equilibrium with other magmatic minerals), subhedral to euhedral shape, grain size comparable to other magmatic phases (large interstitial grains are more likely to have formed in equilibrium with other mineral phases than small flakes located in feldspar grains for example), absence of reaction relations with other phases (no inclusion of minerals from which it could have been derived, no common twinning with biotite when intergrown, (also used by Saavedra 1978; Miller et al. 1981; Ham and Kontak 1988), and absence of alteration in the host rock (to avoid white mica as a secondary alteration product).

Speer (1984), however, emphasized the uncertainty of the textural evidence catalogued above, and recommended the use of other types of evidence, such as chemical composition or mineral assemblages, to strengthen any choice made about the origin of white micas. Indeed, secondary white mica may have a grain size comparable to the indisputable magmatic phases, and may also have a euhedral shape. Therefore, only the combination of as many criteria as possible can provide sufficiently convincing evidence for a primary origin of the white mica grains. Mineral assemblages can only ensure the peraluminous character of a granitic rock, because excess of alumina is the principal condition for crystallisation of magmatic white mica. The presence of minerals such as biotite, cordierite, tourmaline, topaz, or garnet is a strong indicator of high peraluminosity (Speer 1984).

Roycroft (1991) described zoning textures in granitic rocks from the Leinster granite as a convincing criterion for the magmatic origin of white micas. Ding (1995) found a single zoned grain of white mica in a leucomonzogranite of the Halifax Pluton in the SMB. The composition of the zoned grain in the SMB showed a decrease in Ti and Fe, and an

Mineral deposits	Sample #	Rock type	Rock unit	Textural and chemical investigation	$^{40}Ar/^{39}Ar$ geochronology
Reeves	SC-1-R	host granitoid rock leucomonzogranite	Panuke Lake	√	
	SC-6/7/8/11-R	host granitoid rock leucogranite	Keddy-Reeves	√	
	SC-9/10-R	pegmatite		√	
Morley's	SC-1/3/5-M	host granitoid rock leucomonzogranite	New Ross	√	
	SC-2-M	pegmatite (greisenised)		√	
	SC-7/12-M	pegmatite		√	
	SC-13-M	greisen		√	
Keddy	SC-2/6-K	host granitoid rock leucomonzogranite	Panuke Lake	√	
	SC-3/8-K	pegmatite		√	
	SC-5/7-K	host granitoid rock leucomonzogranite (greisenised)	New Ross	√	
Long Lake	SC-1-L	host granitoid rock leucomonzogranite	New Ross		
	SC-2-L	greisen		√	
	SC-5-L	greisen	Long Lake	√	√
	SC-7/14-L	host granitoid rock leucogranite (greisenised)		√	
	SC-12-L	pegmatite		√	√
	SC-13-L	aplite		√	√
Walker	SC-2/3-W	aplite	Panuke Lake	√	√
	SC-7-W	greisen		√	√
	SC-8/13-W	host granitoid rock leucomonzogranite		√	
	SC-9/15-W	pegmatite		√	√
	SC-14-W	host granitoid rock leucomonzogranite (greisenised)		√	
Turner	SC-2/18-T	greisen	Panuke Lake	√	√
	SC-4/7/9-T	host granitoid rock leucomonzogranite		√	
	SC-10/14-T	elvan		√	√
	SC-16-T	greisen		√	
	SC-17-T	quartz vein		√	
Millet Brook	SC-1/5/6-MB	host granitoid rock monzogranite	Salmontail Lake	√	
	SC-3-MB	mineralized monzogranite		√	√
	SC-4-MB	episyenite		√	
	SC-8-MB	host granitoid rock biotite granodiorite	unnamed	√	
	SC-9-MB and DK MB-99-01	mineralized		√	√
Mn Mines	DC 86-3 847	hematized monzogranite	Salmontail Lake		√
	SC-1-D	episyenite		√	√
	SC-2/3/6-D	host granitoid rock monzogranite		√	
	SC-5-D	breccia		√	

Table 3.1: Sample selection for the white mica textural and chemical investigation. Also listed are the samples used for geochronology.

Sample number	Location	Description
FC-1/2	Ferguson's Cove	aplite within the Tantallon leucomonzogranite. Fine-grained porphyritic texture with quartz phenocrysts. Main minerals: quartz, plagioclase (An_5), alkali feldspar, white mica. Accessories: biotite, chlorite, apatite, zircon
FT-2	Card Lake	aplite within Panuke Lake leucomonzogranite. Fine-grained texture. Main minerals: quartz, plagioclase (An_{10}), alkali feldspar, white mica, biotite. Accessories: chlorite, apatite, zircon, rutile
M72-119*	New Ross	leucomonzogranite within the New Ross leucomonzogranite. Medium-grained texture. Main minerals: quartz, plagioclase (An_{28}), alkali feldspar, white mica, biotite. Accessories: apatite, zircon
M72-182*	West Dalhousie	aplite within the West Dalhousie monzogranite. Fine-grained texture. Main minerals: quartz, plagioclase (An_{10}), alkali feldspar, white mica, biotite. Accessories: chlorite, apatite
M72-43*	Greywood	aplite within the East Dalhousie leucomonzogranite. Fine-grained texture. Main minerals: quartz, plagioclase (An_5), alkali feldspar, white mica, biotite. Accessories: chlorite, apatite, zircon, opaques
PC-1/2	Peggy's Cove	aplite within the Peggy's Cove monzogranite. Fine-grained texture. Main minerals: quartz, plagioclase (An_8), alkali feldspar, white mica. Accessories: biotite, chlorite, apatite, zircon
LL-2**	Lewis Lake	leucogranite from the Lewis Lake leucogranite. Fine-grained texture. Main minerals: quartz, plagioclase (An<5), alkali feldspar, white mica. Accessories: biotite, fluorite, topaz, zircon

Table 3.2: Location and description of granitoid samples from other areas within the SMB. These samples were chosen for comparison with those from the New Ross area on the basis of the primary texture of the white micas they contain. * Samples from McKenzie (1974); ** Sample from Bogutyn (2001).

increase in Mg from core to rim. Ding (1995) concluded that the observed zoning resulted from "an abrupt change in the composition of local magma". Bogutyn (2001) documented epitaxial zoning textures of alternating colorless muscovite and light brown iron-rich zones (intermediate mica phase, Clarke and Bogutyn 2003) in white micas hosted by the Lake Lewis leucogranite located in the vicinity of the New Ross area. Bogutyn (2001) concluded that an oscillating fluid pressure (higher water pressure favouring biotite substitution; Green 1981; Velde 1980) might account for the zoning texture. However, finding zoning involves a fastidious grain-by-grain observation of handpicked white mica flakes of a restricted range of thickness (~0.30 mm). Even so, such zoned grains may be the exception and the majority of unzoned grains may also be primary.

3.4.2. Chemical criteria for distinguishing primary from secondary white micas

Miller et al. (1981) used textural criteria (similar to those later also reported in Speer 1984) to classify white mica grains as primary or secondary, and then correlated their observations to chemical analysis of the grains: most texturally primary white micas are richer in Ti, Al, and Na, and poorer in Mg and Si than secondary white micas. Miller et al. (1981) stated that primary white micas generally have compositions closer to ideal end-member muscovite than do secondary ones. Miller et al. (1981) also stressed the difficulty of basing the origin of white micas solely on textural criteria. Using the textural criteria of Speer (1984) to discriminate between primary and secondary white micas, Monier et al. (1984) then used Na/(Na+K) to distinguish between primary (Na/(Na+K) > 0.06) and secondary (Na/(Na+K) < 0.06) grains of a leucogranite from the Massif Central in France. These authors used the Na/(Na+K) ratio to illustrate the extent of the paragonite substitution among three types of white micas discriminated based on their texture. The Na/(Na+K) ratio is controlled by the composition of coexisting phases (e.g., feldspar and biotite; Monier et al. 1984), pressure, temperature, and presence of a fluid phase. Zen (1988) proposed a minimum content of 0.6 weight percent (wt%) TiO_2 for a white mica to be of magmatic origin. Titanium is a good candidate for indicating a primary magmatic origin for white micas because of its chemical immobility (Zen 1988). Villa et al. (1997) obtained a clear distinction between two generations of white micas (magmatic and

hydrothermal) using their Ti content from a granite in Travale, Italy. They also reported a higher F and Cl contents for the hydrothermal white micas.

Ham and Kontak (1988) analysed primary and secondary white micas (distinction based on textural criteria) from different rock types present in the SMB and found no clear relationship between Ti, Al, or Na content and white mica origin. Ham and Kontak (1988) emphasised that primary white micas are more easily recognizable in less evolved phases (monzogranite and leucomonzogranite) rather than in more evolved phases (leucogranite). Similarly to Ham and Kontak (1988), Zane and Rizzo (1999) observed none of the compositional differences listed by Miller et al. (1981) between primary and secondary white micas using published geochemical data for peraluminous granites worldwide.

Using backscattered electron imaging and electron microprobe analysis, Dempster et al. (1994) discovered chemical zoning in white micas from the Caledonian Oughterard granite in Connemara, Ireland. These samples show variable degrees of alteration of biotite to muscovite. Magmatic white micas have a lower Si content and a lower Mg/(Mg+Fe) ratio. Also, the Fe content appears to decrease with increasing alteration (Dempster et al. 1994). These authors documented three stages of crystallisation and alteration of white micas, among which the third, and maybe even the second, stages are post-magmatic. Gomes and Neiva (2000) studied hydrothermally altered tin-bearing muscovite granites from Ervedosa in northern Portugal. They reported chemical zoning of white micas in the most altered samples (rims richer in celadonite than cores); the thickness of the rims increases with increasing degree of alteration. Chemically, the altered rims are generally richer in Si, Fe+Mg, and Rb, and poorer in Al_{total} and Na than the cores (Gomes and Neiva 2000). Also, the cores have the composition of primary white micas located in unaltered granite, whereas the rims have a similar composition to that of hydrothermal white micas clearly replacing other minerals (Gomes and Neiva 2000). Table 3.3 summarises the textural criteria (grain size, shape, inclusions, abundance, zoning, intergrowth, and contact) utilised for discriminating primary from secondary white micas.

	Primary magmatic white mica	Secondary non-magmatic white mica	How does the criterion apply to the samples used for this investigation?
TEXTURAL CRITERIA			
size	coarse-grained, comparable to other magmatic phases (especially biotite)	variable (including size comparable to other magmatic phases)	• size highly variable in most samples: greisenisation involving appearance of large euhedral secondary white mica
shape	subhedral or euhedral	euhedral to anhedral	• shape highly variable within each sample • presence of anhedral plumose texture in pegmatite (primary) and greisen (secondary)
inclusions	not enclosed by, or enclosing a mineral from which it may have formed (feldspar for example)	usually enclosed by a mineral (feldspar, cordierite, andalusite, or biotite) that the white mica is replacing	• if presence of relict of replaced mineral (or shape of relict mineral preserved), facilitated diagnostic for secondary white mica
abundance	trace to ~25%, depending on granitoid rock type	may be abundant (> 25%)	• minimum modal abundance: trace in biotite granodiorite • maximum modal abundance: 25% in leucogranite • high abundance (>25%) of secondary white mica in episyenite, greisens, and greisenised samples
zoning	may be optically zoned (as in plagioclase)	not known to be optically zoned	• after cursory survey of hand-picked white micas, no optically zoned white mica present, but does not mean none is present
contacts	in contact with mineral white mica replaces, well-defined, euhedral contact and different cleavage orientations (with biotite)	in contact with mineral white mica replaces, fuzzy and irregular contact: • where altering feldspar, fine-grained white mica (sericite) located along cleavages; with increase of alteration, sericite slowly taking over feldspar • where replacing biotite, fine-grained white mica, subhedral along edges of biotite grain or within it; white mica also replacing laths restricted by two cleavages in biotite grains	• different cleavages and/or crystallographic orientation = good criteria to find primary white mica where in contact with biotite, • good criterion to uncover disequilibrium between two mineral phases
CHEMICAL CRITERIA			
TiO_2	TiO_2 > 1 wt % (Miller et al. 1981) TiO_2 > 0.6 wt % (Zen 1988)	TiO_2 < 1 wt % (Miller et al. 1981) TiO_2 < 0.6 wt % (Zen 1988)	• all grains are below 1wt %; criterion may not be applicable to low-TiO_2 late-stage rocks of the SMB
Al_2O_3, Na_2O, SiO_2 ,and MgO, FeO	richer in Al_2O_3 and Na_2O; poorer in SiO_2 and MgO	richer in SiO_2, FeO, and MgO; poorer in in Al_2O_3 and Na_2O	• large overlap of primary and secondary chemistry for all oxides
Na/(Na+K)	Na/(Na+K) > 0.06	Na/(Na+K) < 0.06	• 90% of primary grains are > 0.06, whereas only 60% of secondary grains are > 0.06 • large overlap of the two groups

Table 3.3: Textural and chemical criteria characterising primary and secondary white micas found in the literature.

3.4.3. Chemical compositions of primary white micas

3.4.3.1. Introduction

The first step in defining a field for primary white mica chemical composition is to select samples with the most convincing textural criteria. In the study area, few samples provide unequivocal primary textures, but the following samples contain the most convincingly primary-looking white micas based on textural criteria listed in Section 3.4.1 and more specifically for each sample in Table 3.4:

1. Elvan dyke from the Turner deposit (detailed petrographic description and mineralogy in Section 2.4.3.2);
2. Large hand-picked euhedral to subhedral white mica flakes from pegmatitic samples of the New Ross area (Long Lake, Keddy, and Morley's mineral occurrences; texture determined by examination of thin sections); and
3. Epitaxially zoned white micas from the nearby Lake Lewis leucogranite (LLL) (detailed description in Bogutyn 2001 and Clarke and Bogutyn 2003).

Leucogranites, pegmatites, and elvan have undergone various degrees of subsolidus alteration, as indicated by kaolinisation of alkali feldspar, sericitisation of plagioclase, and, for the elvan, by strong alteration of the groundmass. Also, many fluid inclusions are trapped in quartz crystals and provide further support for extensive fluid circulation within both leucogranites and pegmatites; therefore, primary white micas may have been affected by late fluid circulation, even though they preserve a primary texture. To circumvent the possible modification of the chemical composition of white micas by late fluids, I used published white mica compositions from volcanic and sub-volcanic rocks (rhyolites), as well as chemical analyses from rhyolitic samples from SW Germany. The selected samples show textural evidence of (pressure) quenching (i.e., the magmatic white mica did not have time to react), to avoid the effects of resorption of magmatic white micas back into the melt. Also, each of the chosen samples has fresh sanidine as the alkali feldspar, indicating that no (or little) subsolidus alteration took place. I used the following rhyolitic/sub-volcanic samples (Table 3.5):

4. Macusani (Peru): Noble et al. (1984) presented a preliminary study of the petrology and setting of the peraluminous silicic volcanic rocks from the

Macusani area. Noble et al. (1984) emphasised that the composition of the euhedral white mica grains of the Macusani volcanics strongly resembles those occurring in two-mica granites. In addition, Pichavant et al. (1988a) showed that euhedral white micas in the volcanics from the Macusani area exhibit minor biotite and extensive phengite substitution.

5. Morococala (Bolivia): Morgan et al. (1998) described the petrochemistry of peraluminous volcanics from Morococala in the Bolivian tin belt. Rhyolite tuffs contain few euhedral muscovite grains showing a rather homogeneous chemistry with the exception of increasing F from core to rim (Morgan et al. 1998).
6. Richemont dyke (France): Raimbault and Burnol (1998) described the Richemont rhyolite dyke in the Massif Central in France as a "subvolcanic counterpart of rare-metal-bearing granites and pegmatites". Raimbault and Burnol (1998) described the muscovite phenocrysts as euhedral grains having compositions with phengite substitution.
7. Rhyolite (SW Germany): Schleicher and Lippolt (1981) described white micas of magmatic origin in the Haigerach rhyolite in the Schwarzwald area of Germany. They provided thin sections of rhyolites containing white micas, and I analysed them under the same operating conditions as the SMB samples (Appendix A).

I used these seven groups to evaluate previously defined chemical criteria for magmatic white micas (Section 3.4.3.2) and to define the primary magmatic fields (Fig. 3.7; Section 3.4.3.3). For all chemical analyses in this chapter, I used the molecular proportions method of Deer et al. (1992), based on 24 oxygens, to recalculate the raw microprobe data (Appendix B). In subsequent Sections, I will refer to the samples listed above from 1 to 7 as "texturally primary samples".

3.4.3.2. Evaluation of chemical criteria previously defined for magmatic white micas

I first evaluate the previously defined chemical criteria for magmatic white micas listed in Table 3.3 and Section 3.4.1, using the texturally primary samples described in Section 3.4.3.1. As secondary samples, I use white micas from granitoid rocks from the New Ross area showing clear replacement of feldspar, biotite, cordierite, and andalusite.

Samples	Sample number	Grain			Textural relationship with			Inclusions	Included in other minerals	Comments
		shape	size (mm)	boundary	feldspar	biotite	quartz			
1. Elvan	SC-10/14-T E1/2/3	euhedral to subhedral	≤ 1	sharp (may be diffuse in contact with matrix)	generally sharp and straight contact; reaction rims around some grains	no biotite present	sharp and straight contact	absent	-sericite in inclusion in feldspar suggests a secondary origin -small euhedral white mica grains included in quartz suggests a primary origin	-grains are either isolated in matrix or belong to a cluster - narrow reaction rims between some isolated grains and matrix (measurements were taken on both core and rim of larger grains)
2. Pegmatite	SC-7/12-M	euhedral to subhedral	1-8 ≤ quartz and feldspar grains	sharp	sharp and straight contact	no biotite present	sharp and straight contact	absent		No comment
	SC-12-L		3-6 ≈ quartz < plagioclase							
	SC-3-K		2-7 <than quartz and plagioclase grains							
3. Lake Lewis leucogranite	LL99-6, LL99-8, LL99-11	euhedral to subhedral	3-4	N/A (hand-picked zoned grains)	N/A	no biotite present	N/A	absent	N/A	-description and illustrations in Bogutyn (2001)

Table 3.4: Textural description of primary white micas from the Turner Elvan dyke, three pegmatites from Morley's, Long Lake, and Keddy, and the Lake Lewis leucogranite. N/A means not available.

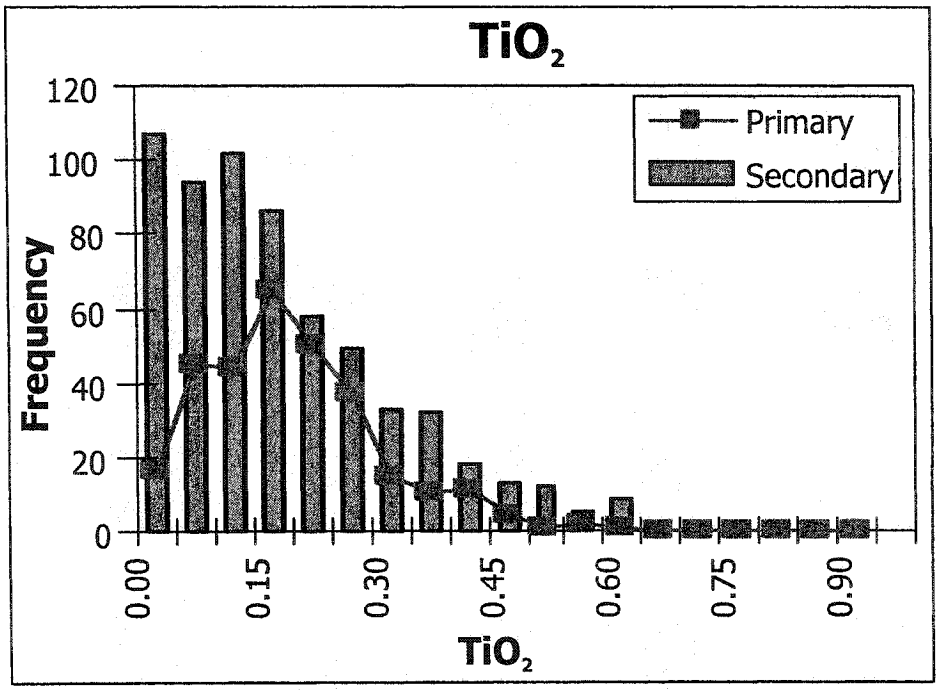

Figure 3.5: Histogram of TiO_2 content of texturally primary and secondary white micas from samples of the New Ross area.

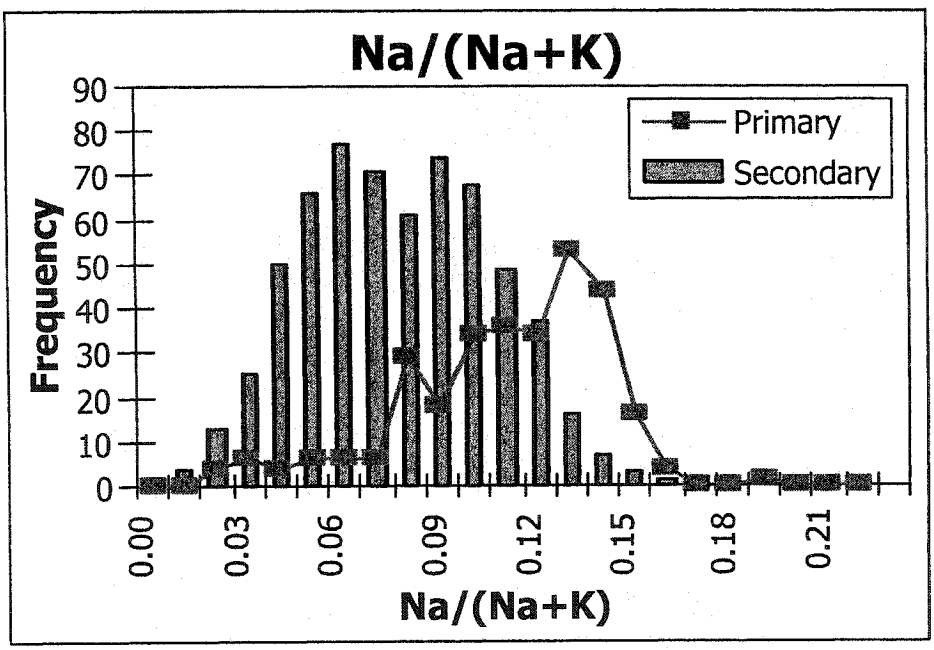

Figure 3.6: Histogram of Na/(Na+K) ratio of texturally primary and secondary white micas from samples of the New Ross area.

Samples	Sample number	Grain			Textural relationship with			Inclusions	Included in other minerals	Comments
		shape	size (mm)	boundary	feldspar	biotite	quartz			
4. Macusani volcanics	MH3, MH7, MH8	euhedral	≤ 1	sharp	sharp and fairly straight	sharp	sharp	biotite, sillimanite, quartz, sanidine	N/A	-description from Pichavant et al. (1988)
5. Morococala volcanics	85-1, 85-7, 85-18, 85-22	subhedral to euhedral	≤ 1	sharp	altered to biotite + plagioclase		N/A	N/A	N/A	-description from Morgan et al. (1998)
6. Richemont subvolcanics	L14d, L14e1, L14a	euhedral (perfect diamond shape)	≤ 1	sharp	sharp	N/A	N/A	feldspar	euhedral in quartz	-description from Raimbault and Burnol (1998)
7. Southwest Germany volcanics	Haigerach porphyry	euhedral	≤ 2	sharp	sharp	N/A	sharp	absent	quartz and feldspar	-description from Schleicher and Lippolt (1981)

Table 3.5: Textural description of primary white micas from volcanic and subvolcanic samples. N/A means not available.

Although higher contents of TiO_2 occur for the Morococala and Macusani white micas, the TiO_2 content of all other analysed white mica grains from the texturally primary samples is less than 1 wt.%. Also, there is no difference in the distribution of the TiO_2 values on a histogram for primary and secondary white micas (Fig. 3.5). Therefore, TiO_2 does not appear as a valid chemical discriminant between primary and secondary white micas from peraluminous rocks of either volcanic or plutonic origin.

The ratio Na/(Na+K) is for the most part higher than 0.06 for the texturally primary samples, and only 5% of the data fall below this limit. A frequency histogram of the Na/(Na+K) ratio for primary and secondary white micas shows a slightly skewed distribution for primary white micas (mean: 0.11) and a normal distribution for secondary white micas (mean: 0.07) with an overlap between both populations. Thus, the ratio Na/(Na+K) appears as an equivocal criterion to chemically identify primary white micas (Fig. 3.6).

3.4.3.3. Substitutions in primary white micas

As stated previously, white micas from the Elvan dyke, the LLL, and pegmatites from the New Ross area texturally appear to be primary. Figure 3.7 compares the chemical composition of white micas from those samples to the chemical composition of white micas from volcanic and subvolcanic samples in three diagrams: (1) Al_{total} vs. Fe+Mg+Mn (information about biotite substitution), (2) Fe+Mg+Mn vs. Si (information about Tschermak substitution), and (3) K vs. Na (information about paragonite substitution), representing the Tschermak, biotite, and paragonite substitutions, respectively, to verify that the primary chemical characteristics are similar for the known primary magmatic volcanic white micas and the texturally magmatic white micas from the SMB.

Samples from rhyolites and from the primary selection of the SMB (Section 3.4.3.1) appear on two parallel sets of diagrams (Fig. 3.7a to f). In diagrams of Fe+Mg+Mn vs. Al_{total} and Si vs. Fe+Mg+Mn, both Tschermak and biotite substitutions occur with a lesser amount of Fe+Mg+Mn replacement in white micas from rhyolites, possibly because of the restricted number of analyses in the literature. Also, ignoring the chemical composition of the brown iron-rich zones of the white micas from LLL, suggested to have been formed by water pressure build-up during the magmatic stage (Bogutyn 2001), the range of

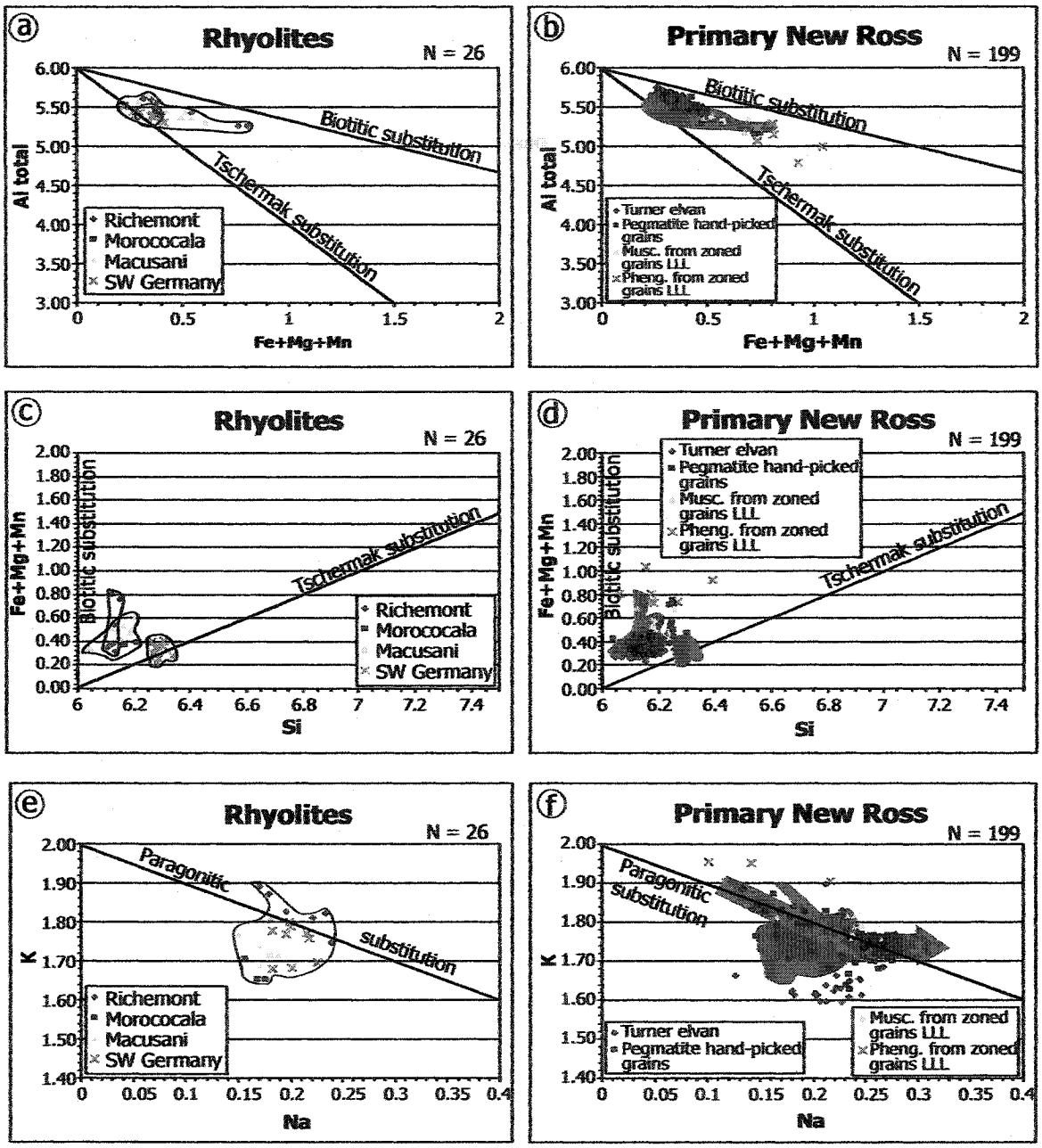

Figure 3.7: Comparison of the chemical composition of white micas from Turner Elvan dyke, pegmatites, and Lake Lewis leucogranite (LLL) samples to the chemical composition of white micas from volcanic and subvolcanic samples in three diagrams: (a and b) Al_{total} vs. Fe+Mg+Mn, (c and d) Fe+Mg+Mn vs. Si, and (e and f) K vs. Na, representing the Tschermak, biotitic, and paragonitic substitutions, respectively. The shaded area on diagrams b, d, and f is the reported field of volcanic and subvolcanic samples from diagrams a, c, and e. The red field in Fig 3.7a is the primary white mica field of Gomes and Neiva (2000). The orange arrow in diagram f highlights the substitution towards paragonite in the primary white micas from the SMB.

Fe+Mg+Mn is 0.2-0.8 apfu and is in close agreement for both sets of data (Fig. 3.7a, b). This range is within the field of primary white mica belonging to strongly peraluminous granites defined by Zane and Rizzo (1999). Also, the primary white mica field of Gomes and Neiva (2000) is included in the primary field of white micas from volcanic and subvolcanic samples (Fig. 3.7a). Close agreement also exists for the Al_{total} content of both rhyolites and primary white mica samples of the SMB (Fig. 3.7a, b). The Fe+Mg+Mn vs. Si diagram also shows both biotite and Tschermak substitutions. Among the white mica analyses in rhyolitic/sub-volcanic rocks, different trends exist according to the location of the samples (Fig. 3.7c):

1. White micas from the Richemont dyke show more biotite substitution than Tschermak substitution;
2. White micas from Macusani show more Tschermak substitution than biotite substitution; and
3. White micas from SW Germany exclusively display Tschermak substitution.

White micas from pegmatites from the New Ross area exhibit a similar substitution trend as the Macusani samples, and white micas from the elvan dyke display a larger extent of Tschermak than biotite substitution (Fig. 3.7d). No trend emerges from the Si vs. Fe+Mg+Mn diagram of white micas analyses from the intermediate mica phase zones of white micas grains from the LLL, but analyses of the muscovitic zones fall within the trend defined by the Macusani data. The field of white micas from the Elvan dyke overlap the low Fe+Mg+Mn area of the Macusani and Richemont fields, and partially overlap the SW Germany field.

Good agreement exists between both sets of data on the type of substitution taking place in a magmatic to fluido-magmatic stage. Ignoring the iron-rich zones of white micas from the LLL, white mica chemical data from the SMB do not significantly expand the primary field defined by white mica data from rhyolitic/sub-volcanic rocks. Therefore, both sets of data allow for the delineation of a primary Al vs. Fe+Mg+Mn and Si vs. Fe+Mg+Mn composition field for reference in subsequent diagrams.

The K vs. Na diagrams (Fig. 3.7e, f) show some substitution towards paragonite, especially in the primary white micas from the SMB (orange arrow on Fig 3.7f). The ranges of Na and K values are similar to those of Zane and Rizzo (1999) for white micas in

peraluminous granitic rocks. However, the white micas from rhyolites (with the exception of the data from the Richemont dyke), and some data from the Elvan dyke and pegmatite samples, have lower K and/or Na content relative to the paragonite substitution line (Na+K = 2). The sum of Na+K reveals a deficit in the interlayer site for ~25% of the data. For the data with a deficit in the interlayer site, the same dilemma as Guidotti and Sassi (1998b) is faced, namely an unknown exchange of non-analysed element(s) with K, or the real existence of a deficiency in the interlayer site. Guidotti and Sassi (1998a and b) invoked structural differences between muscovite and paragonite, with several IV and VI substitutions affecting the XII charge balance. Also, burn-off (volatilisation) of Na, because of the use of a focused microprobe beam, may result in low total in the interlayer site and variable Na concentrations.

For both the rhyolite and SMB sets of data, the Na vs. K diagrams show a trend along the paragonite substitution, to a larger extent in the white micas from the New Ross area (i.e., higher Na content, and lower K content). On the other hand, both sets of data exhibit outliers with lower K and/or Na content, with data from the SMB definitely expanding the K-Na compositional field for white micas from rhyolites towards lower K and Na contents.

3.4.4. Chemical composition of white micas from the New Ross area

This section contains the description of the chemical composition of white micas from host rocks and mineral deposits of the New Ross area, including comments about the substitutions taking place. The high degree of chemical variability of white micas from the studied area requires some kind of subdivision of the data set. I plotted diagrams similar to those presented in Section 3.4.3.3 (Al_{total} vs. Fe+Mg+Mn, Fe+Mg+Mn vs. Si, and K vs. Na). Each diagram presents a shaded primary field delimited by the white mica analyses from sub-volcanic and volcanic rocks, Turner elvan, pegmatites, and the LLL. For each sample, the white micas were first defined as primary or secondary based on their textural criteria (Table 3.3). The primary white micas in this section (+ symbols in diagrams to follow) satisfy the textural conditions for being primary grains in the different rock types of the New Ross area. Several textural subdivisions exist among primary and secondary white micas, and Table 3.6 includes a short description of each subdivision used in the following Sections. Figures 3.8 to 3.15 illustrate the textural subdivisions listed in Table 3.6.

Illustrations	Names of textural types	Description	Chemical reaction involved in creation of secondary white micas
			PRIMARY WHITE MICAS
Fig. 3.8	primary on hand-picked grain (core or rim)	hand-picked white mica from pegmatitic samples (Section 4.3)	
Fig. 3.9	primary	mica fitting most or all textural conditions (Section 4.1 and Table 3.3)	
			SECONDARY WHITE MICAS
Fig. 3.10	stellate aggregates	mica growing as radial/stellate aggregates	
Fig. 3.11	intergrown with mineralisation	white mica intimately intergrown with mineralisation (mostly molybdenite).	
Fig. 3.12	greisen	white mica replacing feldspar and/or biotite in a rock that underwent extensive greisenisation	$3KAlSi_3O_8 + 2H^+ = KAl_3Si_3O_{10}(OH)_2 + 6SiO_2 + 2K^+$ K-feldspar sericite quartz (Guilbert and Park 1986) $3\{K(Mg, Fe)_3[Si_3AlO_{10}(OH, F)_2]\} = KAl_3Si_3O_{10}(OH)_2 + 6SiO_2 + 12(H_2O) + 9(Fe, Mg)^{2+} + 2K^+$ biotite muscovite quartz
Fig. 3.13	fracture filling	white mica growing from fluid circulation along fractures within quartz grain	
Fig. 3.14	replacement of andalusite, cordierite, biotite, or feldspar	white mica visibly replacing either of the listed minerals; part of the replaced mineral still present.	$6Al_2SiO_5 + 2K^+ + 4H^+ = 2[KAl_3Si_3O_{10}(OH)_2] + 2(Al_2O_3) + 2H^+$ andalusite muscovite corundum (Cerny and Burt 1984) $3\{K(Mg, Fe)_3[Si_3AlO_{10}(OH, F)_2]\} = KAl_3Si_3O_{10}(OH)_2 + 6SiO_2 + 12(H_2O) + 9(Fe, Mg)^{2+} + 2K^+$ biotite muscovite quartz $3\{Al_3(Mg, Fe)_2[Si_5AlO_{18}]\} + 4K^+ + 8OH^- = 4[KAl_3Si_3O_{10}(OH)_2] + 2SiO_2 + 6(Fe, Mg)O + 2O^{2-}$ cordierite muscovite quartz
Fig. 3.15	sericite	fine-grained white mica occurring as flakes within feldspar grains	$3KAlSi_3O_8 + 2H^+ = KAl_3Si_3O_{10}(OH)_2 + 6SiO_2 + 2K^+$ K-feldspar sericite quartz (Guilbert and Park 1986) $CaAl_2Si_3O_8 + NaAlSi_3O_8 + 2H^+ + K^+ = KAl_3Si_3O_{10}(OH)_2 + 3SiO_2 + Ca^{2+} + Na^+$ Plagioclase sericite quartz (Burnham 1979)

Table 3.6: Description of the different textural subdivisions among primary and secondary white micas from the New Ross area. Also shown are the chemical reactions creating secondary white micas from other minerals.

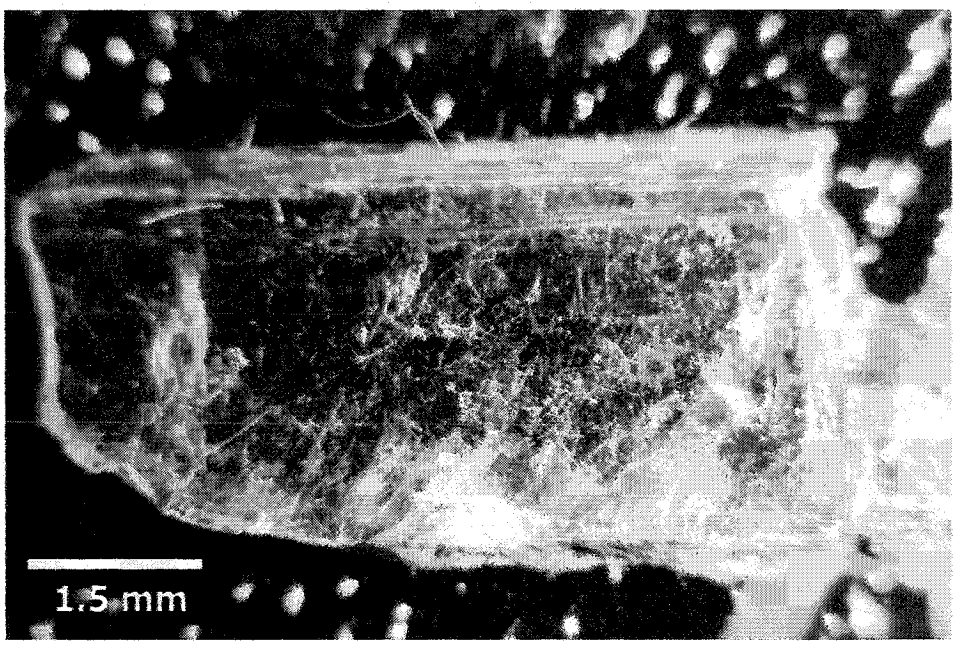

Figure 3.8: Hand-picked primary euhedral white mica in a pegmatite sample (SC-7-M) from the Morley's deposit.

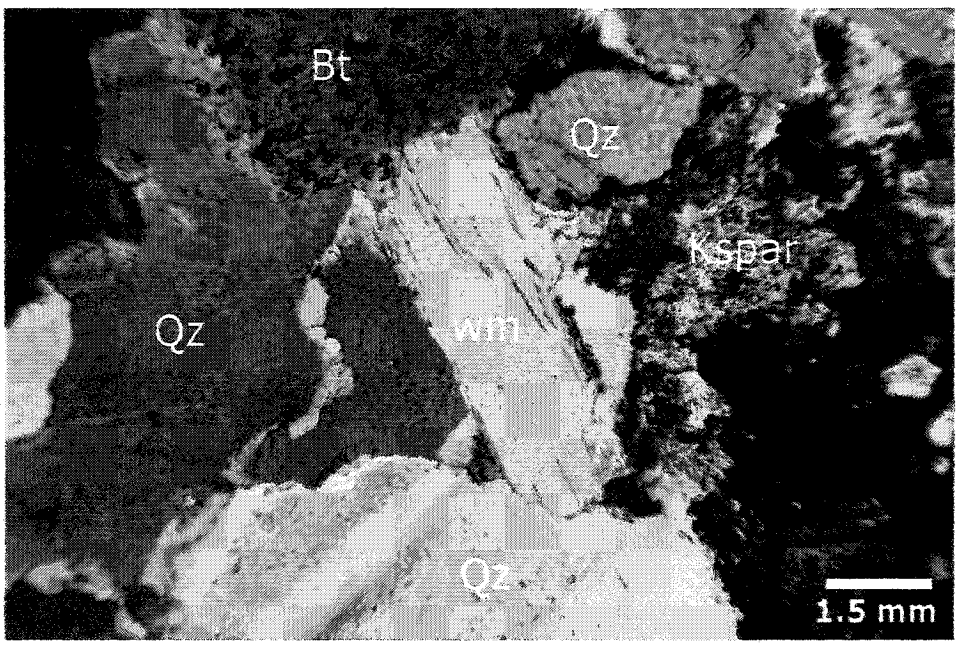

Figure 3.9: Euhedral, texturally primary white mica (size comparable to other magmatic phases in the sample, well-defined contact with biotite, and different cleavage orientation than biotite) in an aplite sample (SC-3-W) from the Walker deposit.

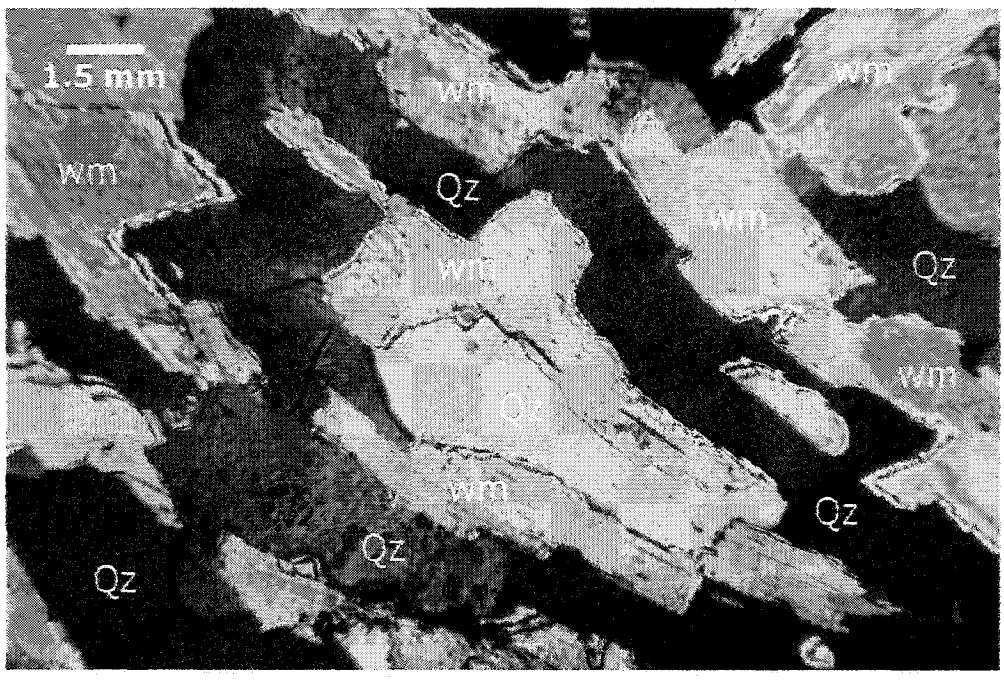

Figure 3.10: Secondary subhedral stellate aggregated white micas in a pegmatite sample (SC-10-R) from the Reeves deposit. This pegmatite shows large areas of white mica and quartz intergrowth.

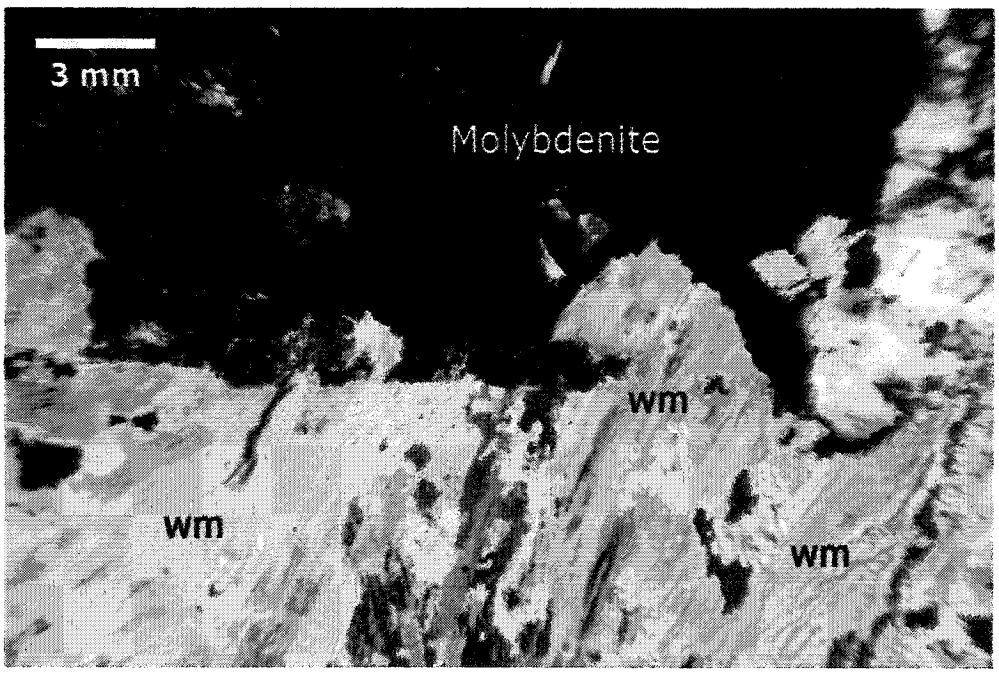

Figure 3.11: Intergrowth of anhedral, "patchy-looking" white mica and molybdenite in a pegmatite sample (SC-15-W) from the Walker deposit.

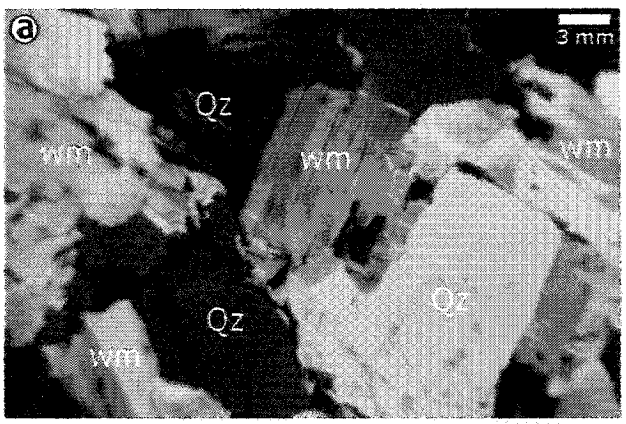

Figure 3.12: (a) Subhedral to euhedral white micas in a quartz-white mica greisen sample (SC-5-L) from the Long Lake deposit.

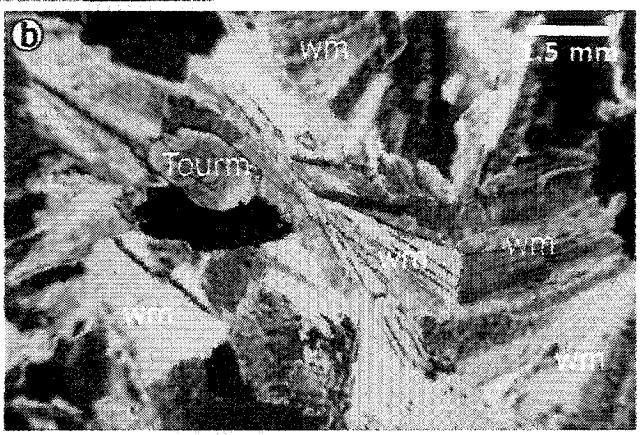

(b) Radial/stellate aggregates of white micas in a white mica-tourmaline-topaz greisen sample (SC-20-W) from the Walker deposit.

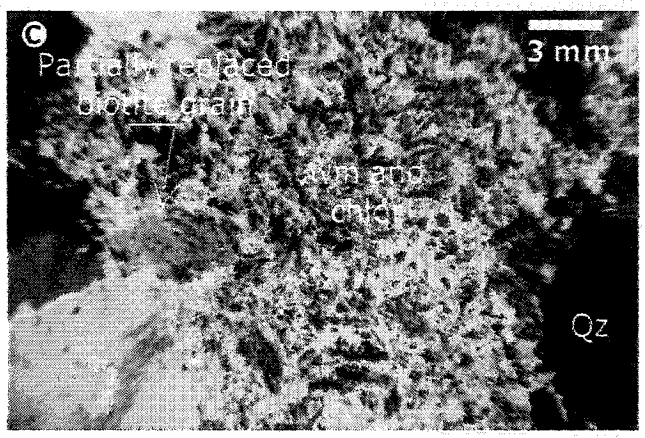

(c) Mixture of fine-grained white mica and chlorite in a quartz-white mica-chlorite greisen sample (SC-18-T) from the Turner deposit. Note the presence of a partially replaced grain of biotite.

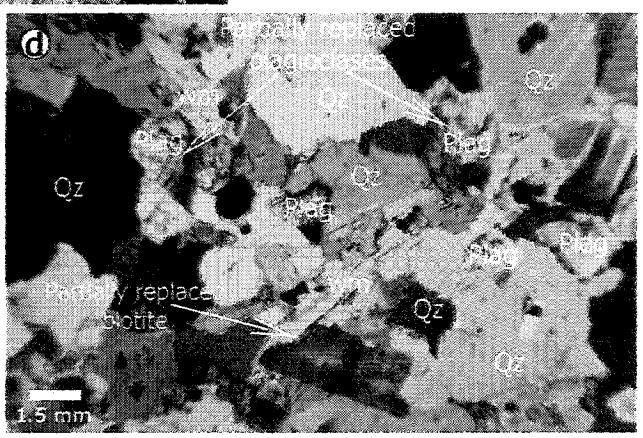

(d) Anhedral white mica aggregate in a greisenised leucomonzogranite (SC-5-K) from the Keddy deposit. Note the presence of partially replaced biotite and plagioclase grains.

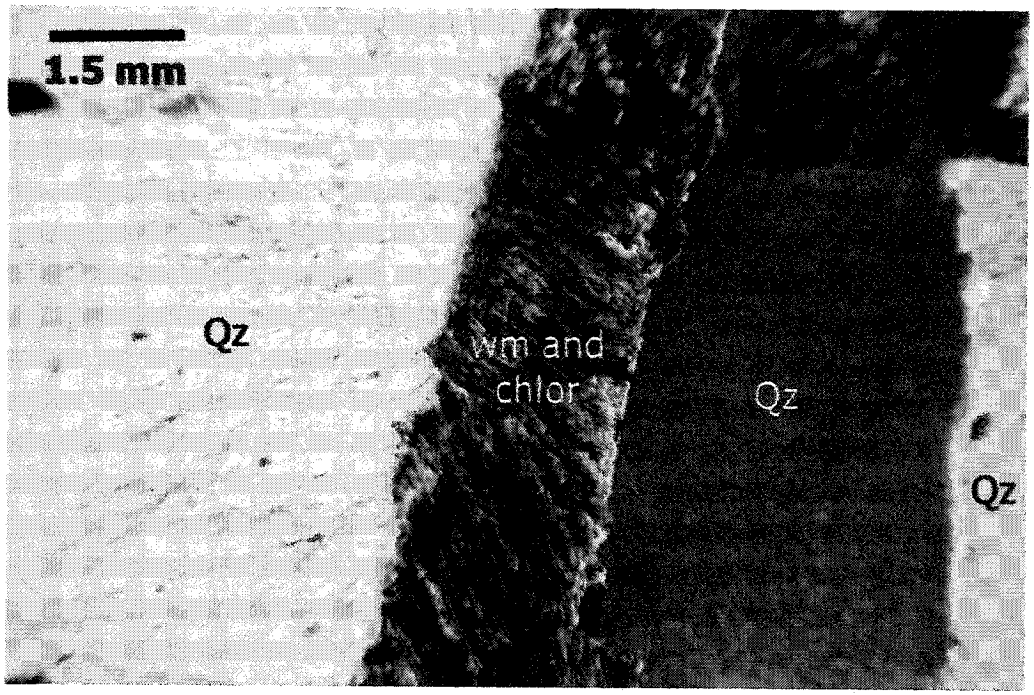

Figure 3.13: Mixture of white mica and chlorite along a fracture in a large quartz grain in a pegmatite sample (SC-9-W) from the Walker deposit.

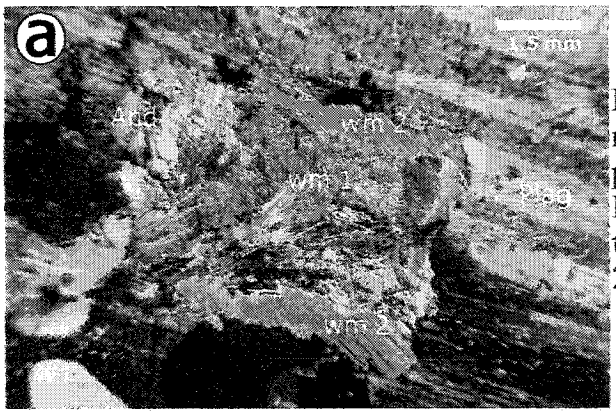

Figure 3.14: (a) Two generations of white mica replacing andalusite in a greisenised pegmatite sample (SC-2-M) from the Morley's deposit. White mica 1 replaces the core of the grain, whereas white mica 2 replaces the rim.

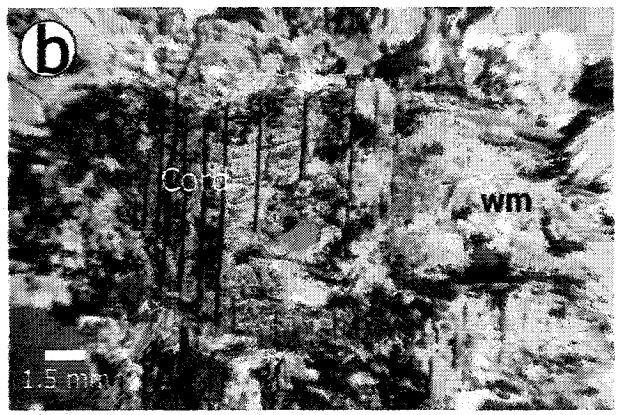

(b) White mica (pinite) replacing cordierite in a coarse-grained leucomonzogranite (SC-1-W) from the Walker deposit.

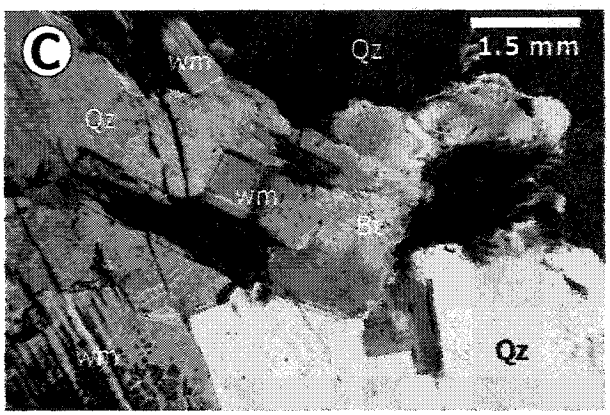

c) In the centre of the picture: white mica replacing biotite in a quartz-white mica greisen sample (SC-5-L) from the Long Lake deposit. The white mica grain has the same optical orientation as the biotite grain it is replacing.

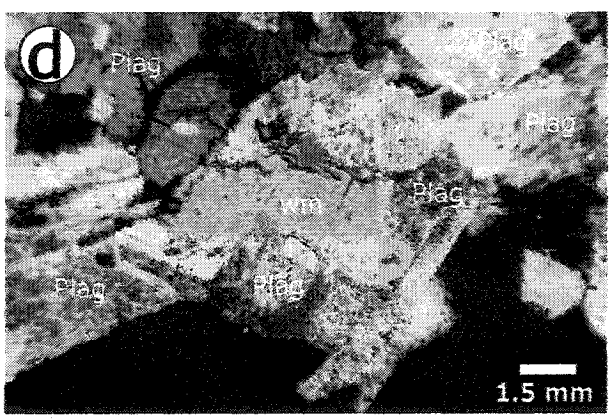

(d) White mica replacing kaolinised plagioclase grains in a pegmatite sample (SC-3-K) from the Keddy deposit. The white mica grain has the same optical orientation as the plagioclase grain it is replacing. Also, the white mica present a pitted surface mimicking the kaolinisation of the plagioclase.

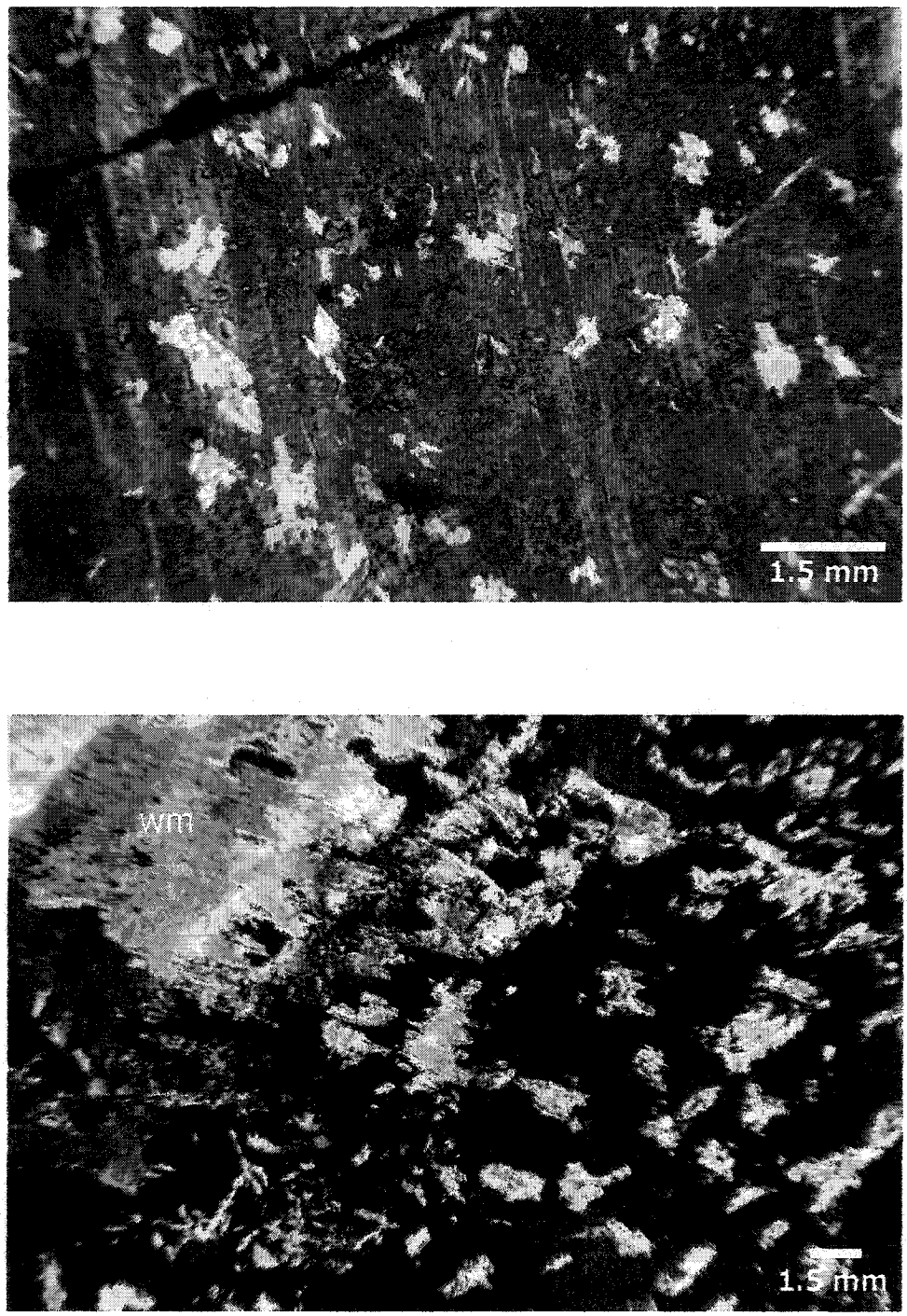

Figure 3.15 (a) Small white mica flakes replacing a large plagioclase grain in a greisenised pegmatite sample (SC-2-M) from the Morley's deposit. (b) Partial sericitisation and greisenisation of a plagioclase in a quartz-white mica greisenised leucomonzogranite (Sc-13-M) from the Morley's deposit. Plagioclase is the mineral at the extinction position.

3.4.4.1. Fe+Mg+Mn vs. Al_{total}

In a diagram of Fe+Mg+Mn vs. Al_{total} for all analyses classified by texture (Fig. 3.16), most data fall between the biotite and Tschermak substitution lines, indicating that both substitutions take place. About 5% of analyses fall below the ideal Tschermak substitution line and are for the most part measurements of secondary white micas replacing feldspar (including sericite), suggesting that the microprobe beam may have partially included the feldspar grain, thereby lowering the alumina content. Another general observation emerging from Figure 3.16 is that there is no systematic chemical discrimination (based on Al_{total} and Fe+Mg+Mn) between texturally primary and secondary white micas. The data (primary and secondary white micas included) define a trend mainly overlapping the shaded areas of the texturally primary samples. Falling outside the shaded area are data closer to the muscovite end-member composition and data showing a larger extent of biotite and Tschermak substitutions. Data closer to the muscovite end-member composition commonly are analyses of sericite. As sericite replaces feldspar, no Fe, Mg, or Mn is available, explaining the generally low Fe+Mg+Mn contents. Data showing a larger extent of biotite and Tschermak substitutions generally belong to white micas from greisens and greisenised samples. Breakdown of both feldspar and biotite results in white mica + quartz; therefore, variable amounts of remaining biotite in the sample may explain the high variability of the Fe+Mg+Mn content.

Host granitoid samples

Primary and secondary white micas from the least altered granitoid host rocks generally show a smaller range of compositions than white micas from altered or mineralised samples. This observation is valid for white micas from the following granitoid host rocks (Fig. 3.17a to d): a granodiorite from Millet Brook (SC-8-MB); monzogranites from Millet Brook (SC-1/5-MB) and the Mn mines (SC-2/6-D); leucomonzogranites from Reeves (SC-1-R), Morley (SC-5-M), Walker (SC-8/14-W), Turner (SC-4/7-T), a leucomonzogranite (M72-119) from the New Ross area, and a leucogranite (LL-2) from Lake Lewis.

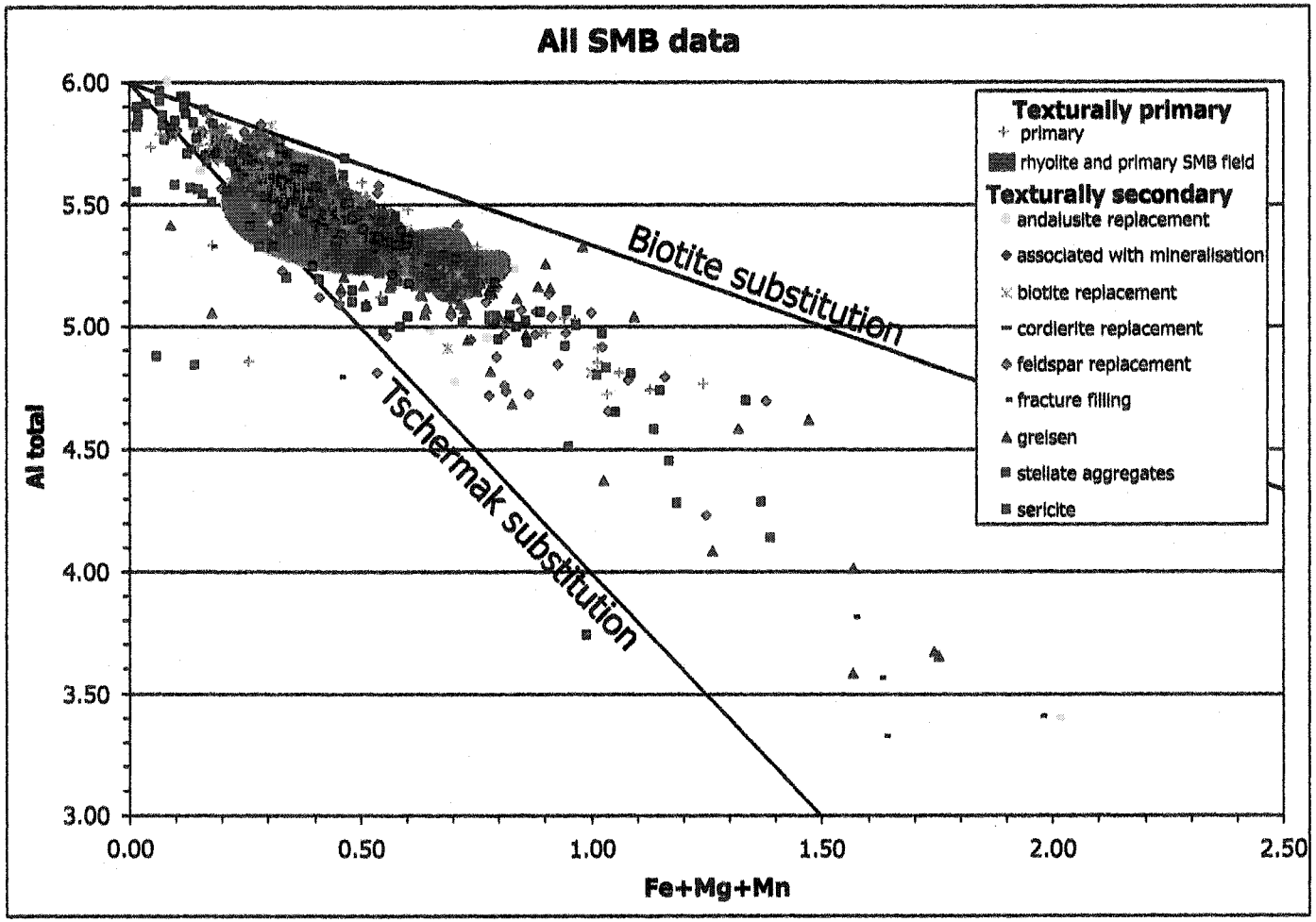

Figure 3.16: Diagram of Fe+Mg+Mn vs. Al_{total} for all analyses of white micas from the New Ross area classified by texture. The shaded area is the reported field of volcanic and subvolcanic samples, and primary samples from the New Ross area.

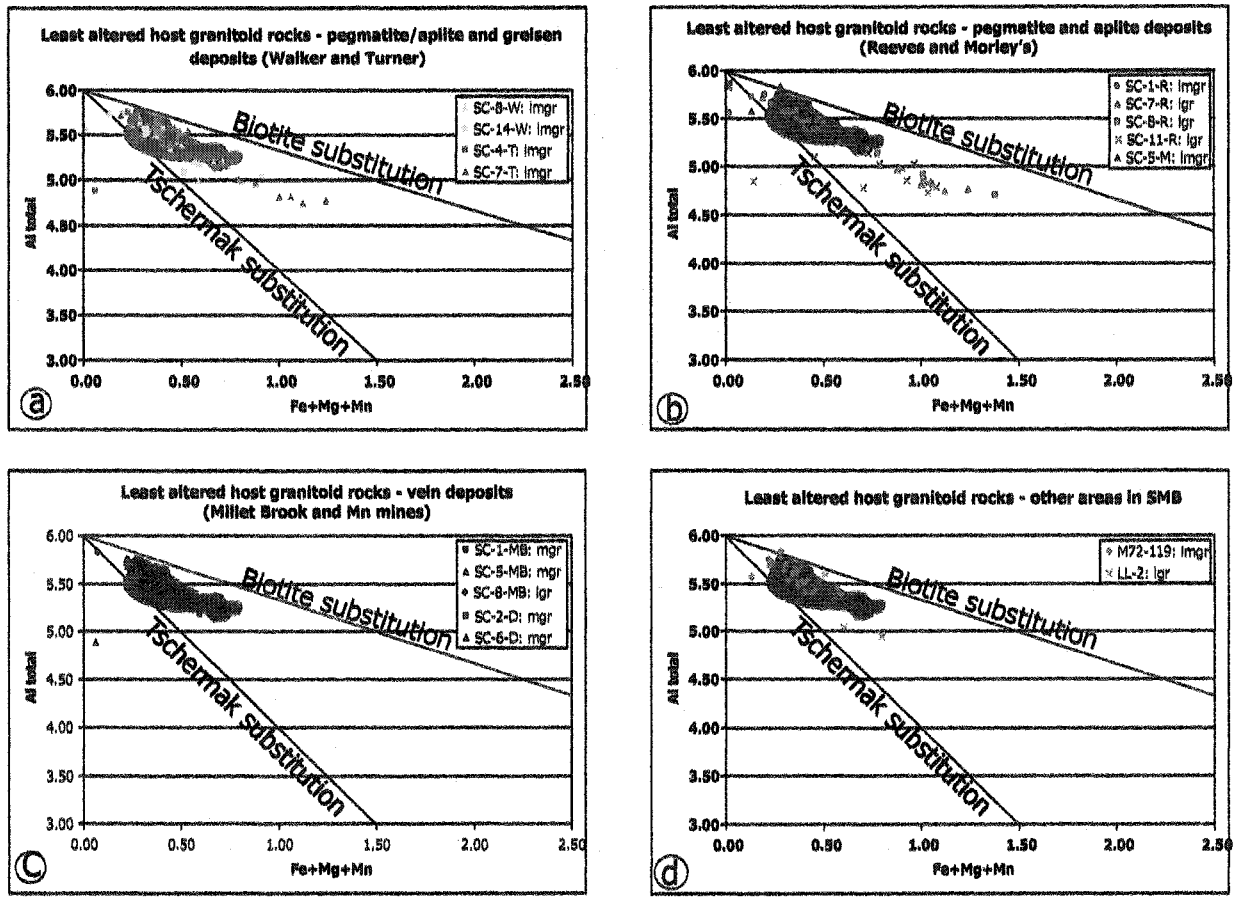

Figure 3.17: Diagrams of Fe+Mg+Mn vs. Al_{total} for primary and secondary white micas from least altered granitoid host rocks from the New Ross area. (a) host granitoid rocks of pegmatite/aplite and greisen deposits, (b) host granitoid rocks of pegmatite/aplite deposits, (c) host granitoid rocks of vein deposits, and (d) host granitoid rocks from other area in the SMB. mgr = monzogranite, lmgr = leucomonzogranite, lgr = leucogranite, W = Walker, T = Turner, R = Reeves, M = Morley's, MB = Millet Brook, D = Mn Mines. The shaded area is the reported field of volcanic and subvolcanic samples, and primary samples from the New Ross area.

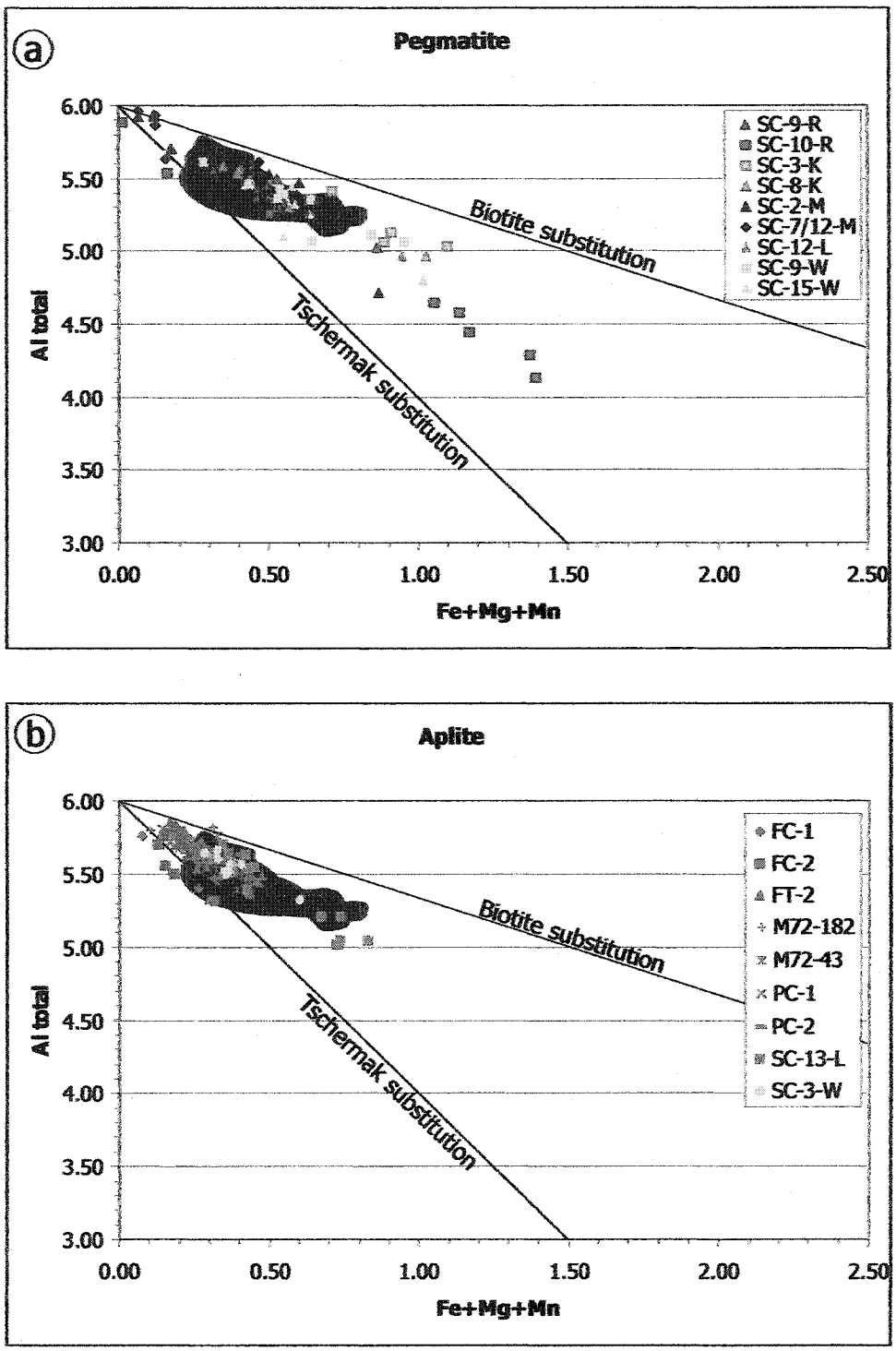

Figure 3.18: Diagrams of Fe+Mg+Mn vs. Al_{total} for primary and secondary white micas from (a) pegmatite and (b) aplite from the New Ross area and other area in the SMB. R = Reeves, K = Keddy, M = Morley's, L = Long Lake, W = Walker. The shaded area is the reported field of volcanic and subvolcanic samples, and primary samples from the New Ross area.

On the other hand, white micas from leucogranitic host rocks of the Reeves deposit (SC-7/8/11-R) (Fig. 3.17c) show large extent of substitutions, similar to white micas from the pegmatite they host (SC-9/10-R) (Fig. 3.18a). Also note the strong enrichment in ferromagnesian components at the expense of alumina of the texturally stellate aggregated grains from sample SC-10-R, suggesting more chemical affinities with secondary white micas than primary ones.

Aplite and pegmatite samples

White micas from pegmatites and aplites (SC-2/12-M from Morley's, SC-3-K from Keddy, SC-12/13-L from Long Lake, and SC-3/9/15/W from Walker) show a similar range of substitutions as those in leucogranite and pegmatite samples from Reeves (Fig. 3.18a and b). In contrast, white micas from aplitic samples of other areas of the SMB (FC-1/2, PC-1/2, FT-2, M72-182, and M72-43) display a small range of substitutions (Fig. 3.18b), in a similar way to white micas of least altered granitoid rocks of the New Ross area. The sampling of white micas in pegmatite is somewhat biased by the difficulty in obtaining a thin section through a large flake of white mica similar in size to other magmatic minerals. Therefore, white micas from pegmatite samples analysed in thin sections are mostly alteration products, and do not reflect the possible (fluido)-magmatic composition of white micas. White micas from samples SC-7/12-M and SC-12-L (Fig. 3.18a) show that the compositions of large hand-picked grains belong to a much narrower range than data obtained from thin sections, and all data points fall within the shaded primary field; therefore, data from hand-picked white micas provide a better picture of the composition of white micas that crystallised in a fluido-magmatic environment.

Greisen and greisenised samples

White mica data from greisenised samples from Morley (SC-3/13/M), Keddy (SC-2/5/6/7-K), Long Lake (SC-2/5/7/14-L), and Walker (SC-7/13-W) (Fig. 3.19a and b) show trends comparable to the pegmatite samples from the corresponding deposit. White micas from samples of the Turner deposit are unusual, because the extent of the biotite and Tschermak substitutions in greisens and greisenised samples (SC-2/16/18-T) are larger than for any other greisenised sample analysed (Fig. 3.19b). Also, the white mica composition

for the samples from the Turner deposit is closer to the ideal Tschermak substitution than other samples in the data set. Similarly, fracture-filling white micas from sample SC-17-T from the Turner deposit also indicate preferential Tschermak substitution.

Vein samples

White micas from mineralised samples from Millet Brook (SC-3/4/9-MB) and the Mn mines (SC1/5-D) show very little compositional variation compared with white micas from unmineralised samples from the same deposits (Fig. 3.20). The composition of white micas from an Elvan dyke at the Mn mines (SC-11-D) falls below the Tschermak substitution line, and probably represents the strongly altered character of that sample.

Summary

In summary, Fe+Mg+Mn vs. Al_{total} diagrams reveal the following (Fig. 3.21):

1) with the exception of a few sericite grains close to the muscovite end-member composition, the compositions of white micas from mineral deposits and their granitoid host rocks in the New Ross area show both biotite and Tschermak substitution.
2) with the exception of white micas from the leucogranite hosting the Reeves deposit, most white micas from host granitoid rocks have a smaller range of substitutions than their corresponding altered rocks.
3) white micas from aplites from other locations in the SMB chemically behave in a similar way as white micas from host granitoid rocks.
4) secondary white micas from aplites and pegmatites from the New Ross area show a larger range of substitutions than their corresponding host rocks, but handpicked white micas from pegmatite samples have a very narrow range of composition.
5) most white micas from greisens and greisenised samples show similar extent of substitutions as white micas from pegmatites from the corresponding deposit, and white micas from greisens from the Turner deposit show the largest substitution range of all white micas analysed.
6) white micas from samples from the vein deposits (Millet Brook and Mn mines) show similar compositions for both mineralised and non-mineralised rock types.

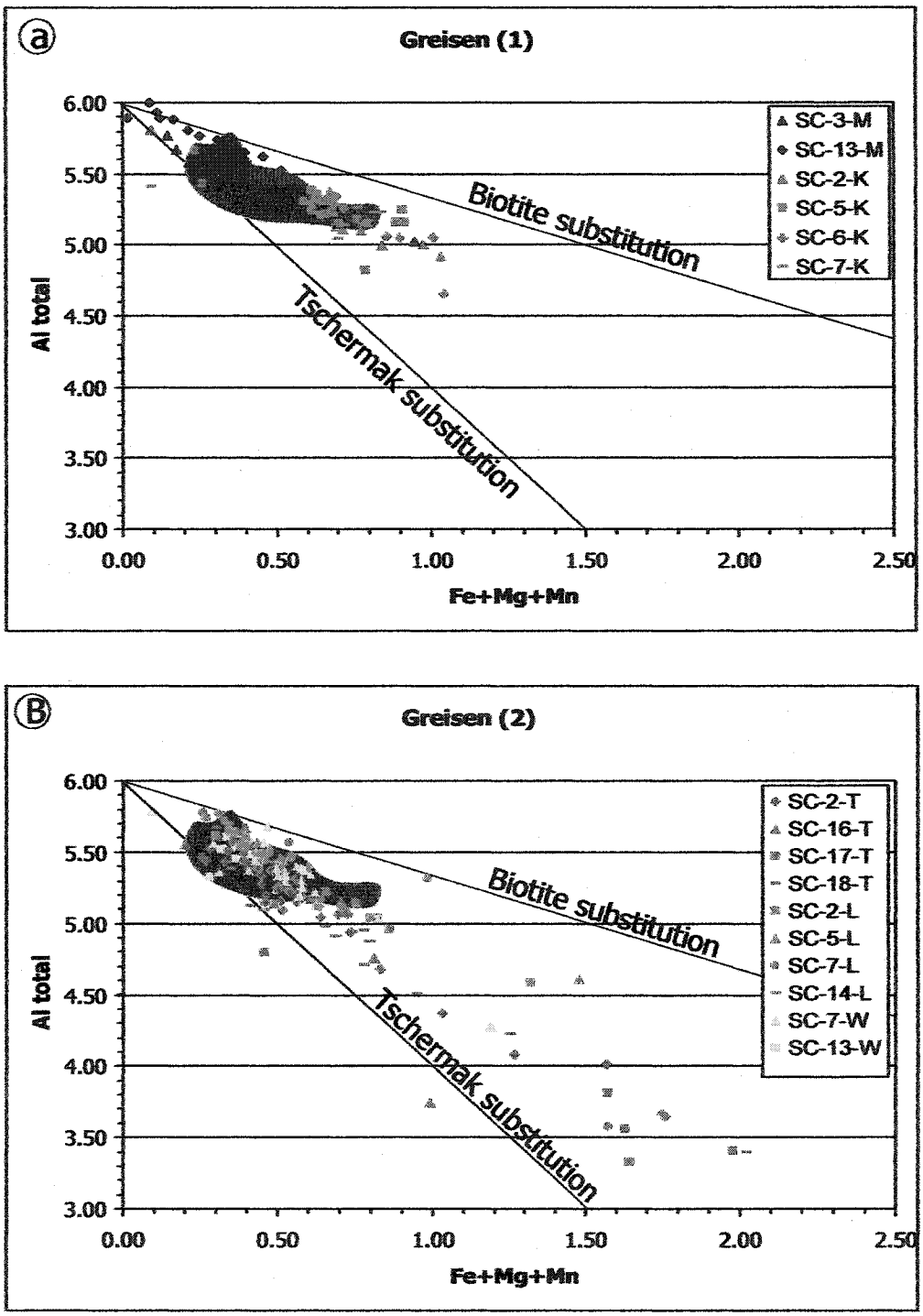

Figure 3.19: Diagrams of Fe+Mg+Mn vs. Al_{total} for primary and secondary white micas from (a) greisen and greisenised samples at the Morley's (M) and Keddy (K) deposits and (b) greisen and greisenised samples at the Turner (T), Long Lake (L), and Walker (W) deposits. The shaded area is the reported field of volcanic and subvolcanic samples, and primary samples from the New Ross area.

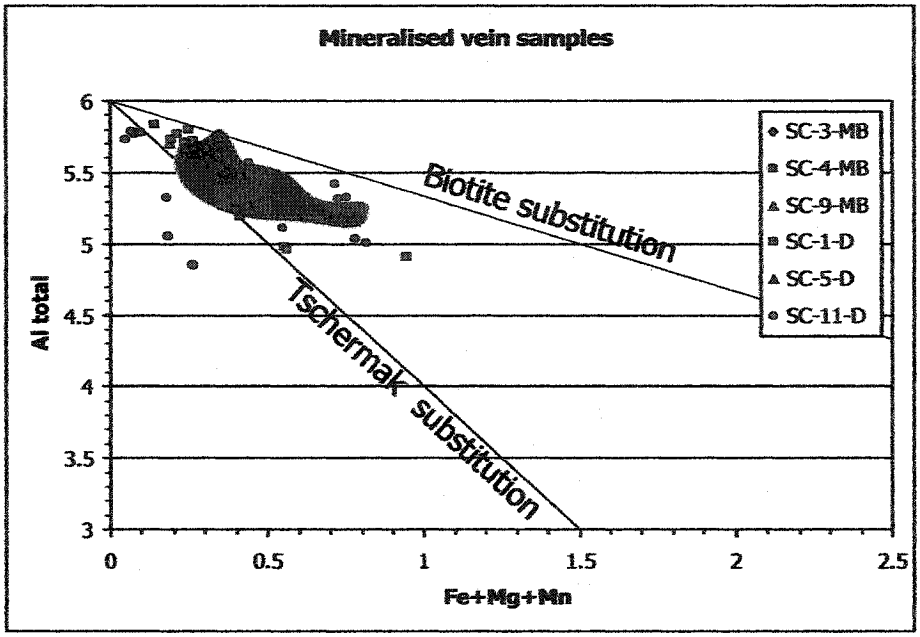

Figure 3.20: Diagram of Fe+Mg+Mn vs. Al_{total} for primary and secondary white micas from mineralised vein samples from the New Ross area. MB = Millet Brook, D = Mn Mines. The shaded area is the reported field of volcanic and subvolcanic samples, and primary samples from the New Ross area.

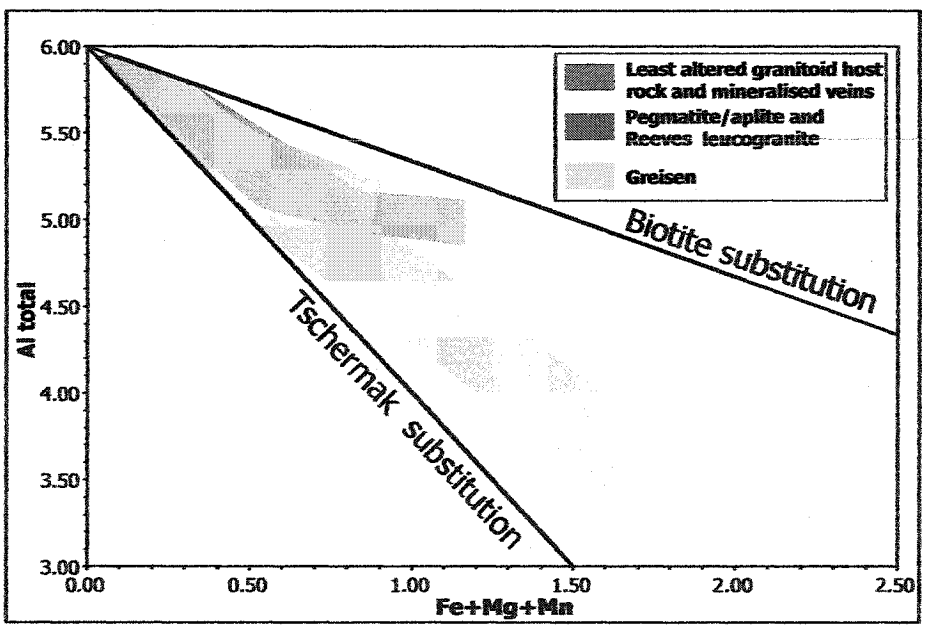

Figure 3.21: Diagram of Fe+Mg+Mn vs. Al_{total} showing the general trends for the composition of white micas from least altered granitoid host rock, mineralised vein, pegmatite/aplite and greisen from the New Ross area.

3.4.4.2. Si vs. Fe+Mg+Mn

In a diagram of Si vs. Fe+Mg+Mn for all analyses classified by texture (Fig. 3.22), most data fall between the biotite and Tschermak substitution lines, indicating that both substitutions take place, as previously observed in Section 3.4.4.1. Again, ~5% of analyses fall below the ideal Tschermak substitution line and are for the most part measurements of secondary white micas replacing feldspar (including sericite), suggesting that the microprobe beam partially included the feldspar grain, thereby increasing the apparent silica content. Most data (texturally primary and secondary white micas included) mainly overlap the shaded areas of the texturally primary samples, therefore appearing to be chemically primary. White micas following the Tschermak substitution line generally have a stellate aggregate texture or belong to greisen samples from the Turner deposit and are, therefore, secondary. Texturally primary white micas show a dominant Tschermak substitution (higher Si content) with increasing exchange of iron for silicon and aluminium simultaneously, therefore bending the trend towards the biotite substitution ("primary magmatic" trend of Bogutyn 2001).

Host granitoid samples

White micas from the least altered granitoid host rocks show dominant Tschermak substitution at the beginning of the trend (falling within the primary field area) and then increasing biotite substitution towards the end of the trend (Fig. 3.23). This tendency is more strongly marked in white micas from granitoid host rocks of pegmatite/aplite and greisen deposits (Fig. 3.23b) than for white micas from granitoid host rocks of vein deposits or located in other area of the SMB (Fig. 3.23c and d). This trend is similar to the chemical composition of primary magmatic white micas from the LLL (Bogutyn 2001).

Aplite and pegmatite samples

Two different trends characterise the substitutions taking place in white micas from pegmatite and aplite (Fig. 3.24a and b): (i) a similar trend as described in the previous paragraph for white micas from least altered granitoid rocks, with lesser biotite substitution, and (2) a dominantly Tschermak substitution. Only white micas with a stellate aggregated

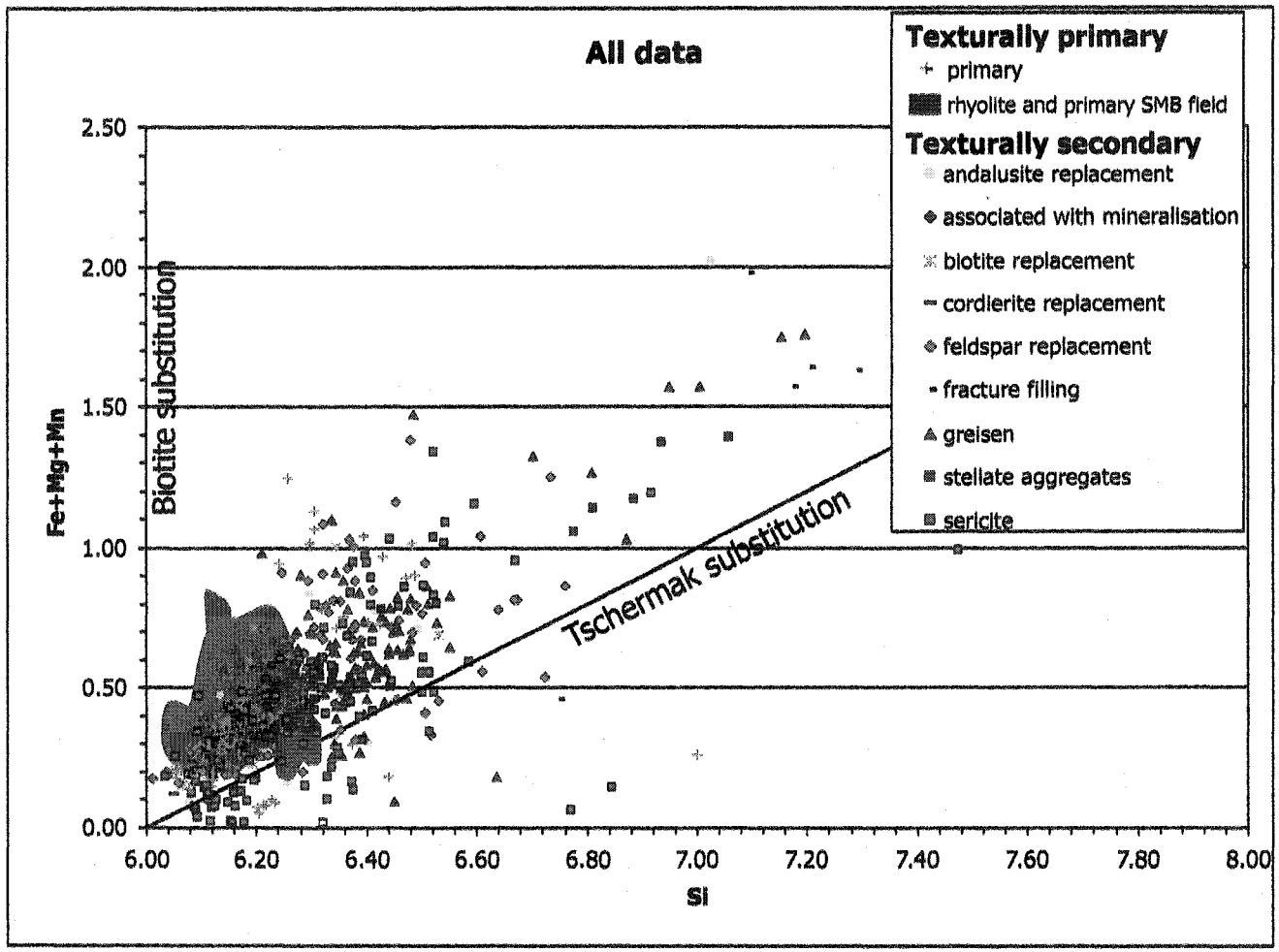

Figure 3.22: Diagram of Si vs. Fe+Mg+Mn for all analyses of white micas from the New Ross area classified by texture. The shaded area is the reported field of volcanic and subvolcanic samples, and primary samples from the New Ross area.

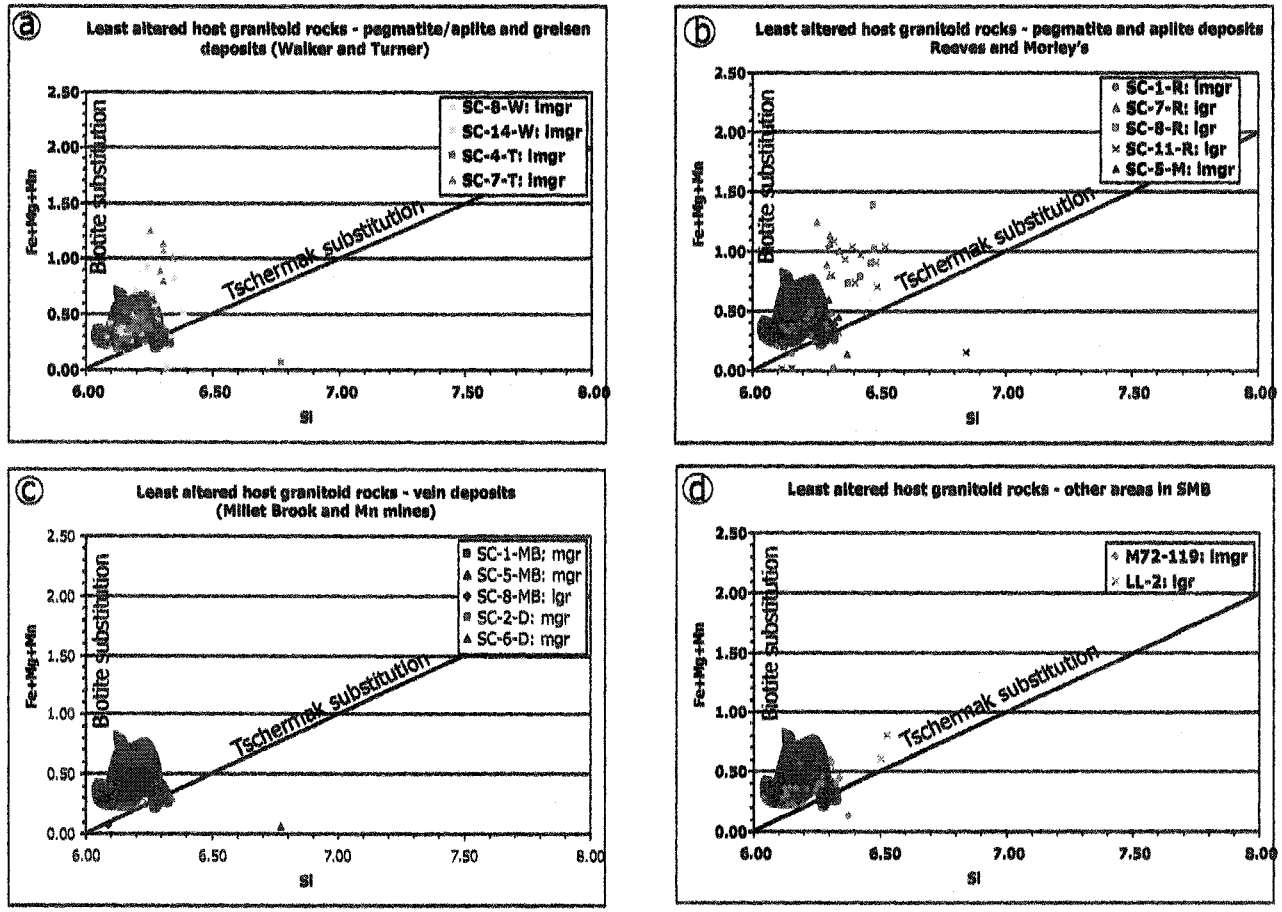

Figure 3.23: Diagrams of Si vs. Fe+Mg+Mn for primary and secondary white micas from least altered granitoid host rocks from the New Ross area. (a) host granitoid rocks of pegmatite/aplite and greisen deposits, (b) host granitoid rocks of pegmatite/aplite deposits, (c) host granitoid rocks of vein deposits, and (d) host granitoid rocks from other area in the SMB. mgr = monzogranite, lmgr = leucomonzogranite, lgr = leucogranite, W = Walker, T = Turner, R = Reeves, M = Morley's, MB = Millet Brook, D = Mn Mines. The shaded area is the reported field of volcanic and subvolcanic samples, and primary samples from the New Ross area.

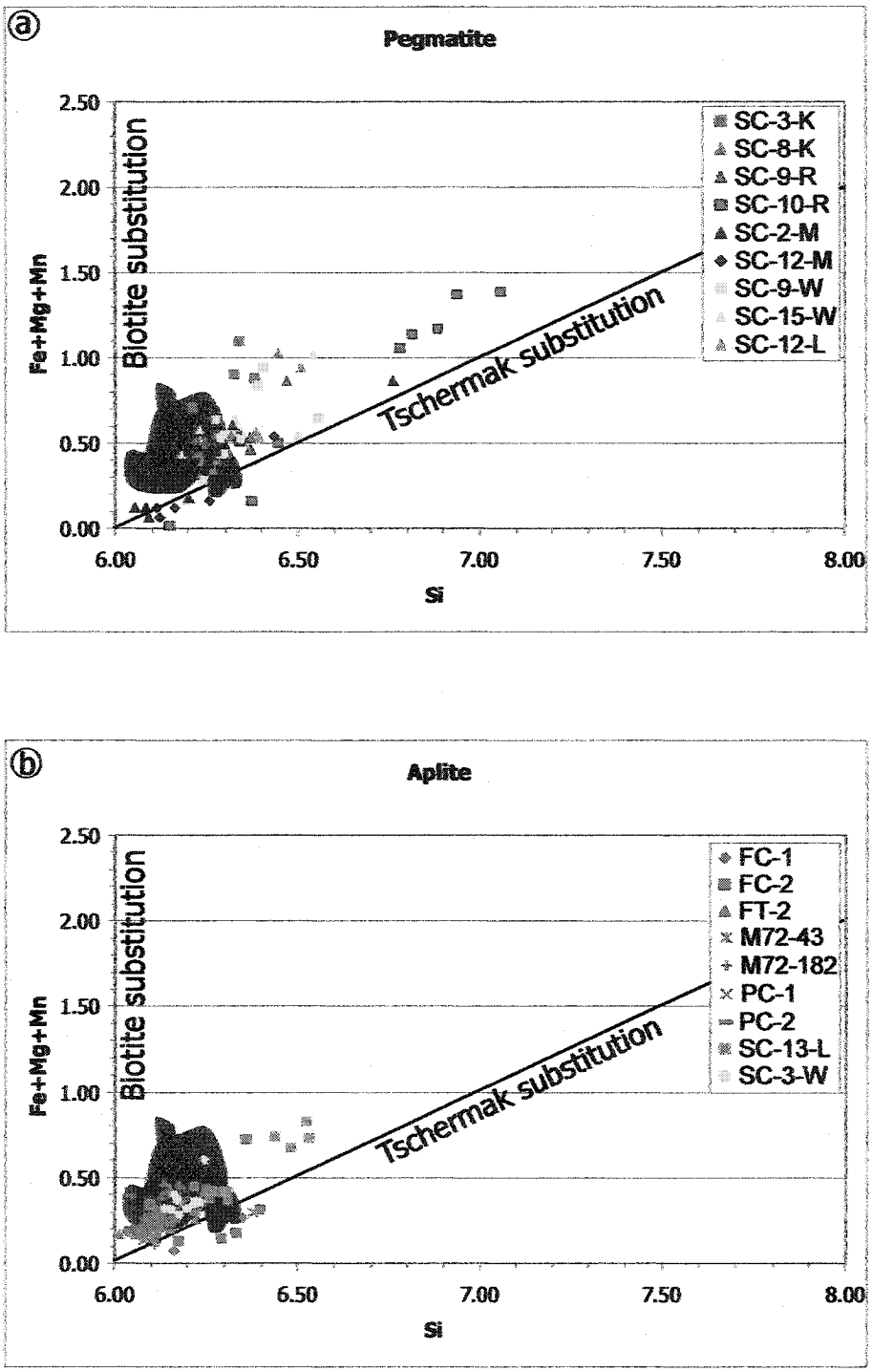

Figure 3.24: Diagrams of Si vs. Fe+Mg+Mn for primary and secondary white micas from (a) pegmatite and (b) aplite from the New Ross area and other area in the SMB. R = Reeves, K = Keddy, M = Morley's, L = Long Lake, W = Walker. The shaded area is the reported field of volcanic and subvolcanic samples, and primary samples from the New Ross area.

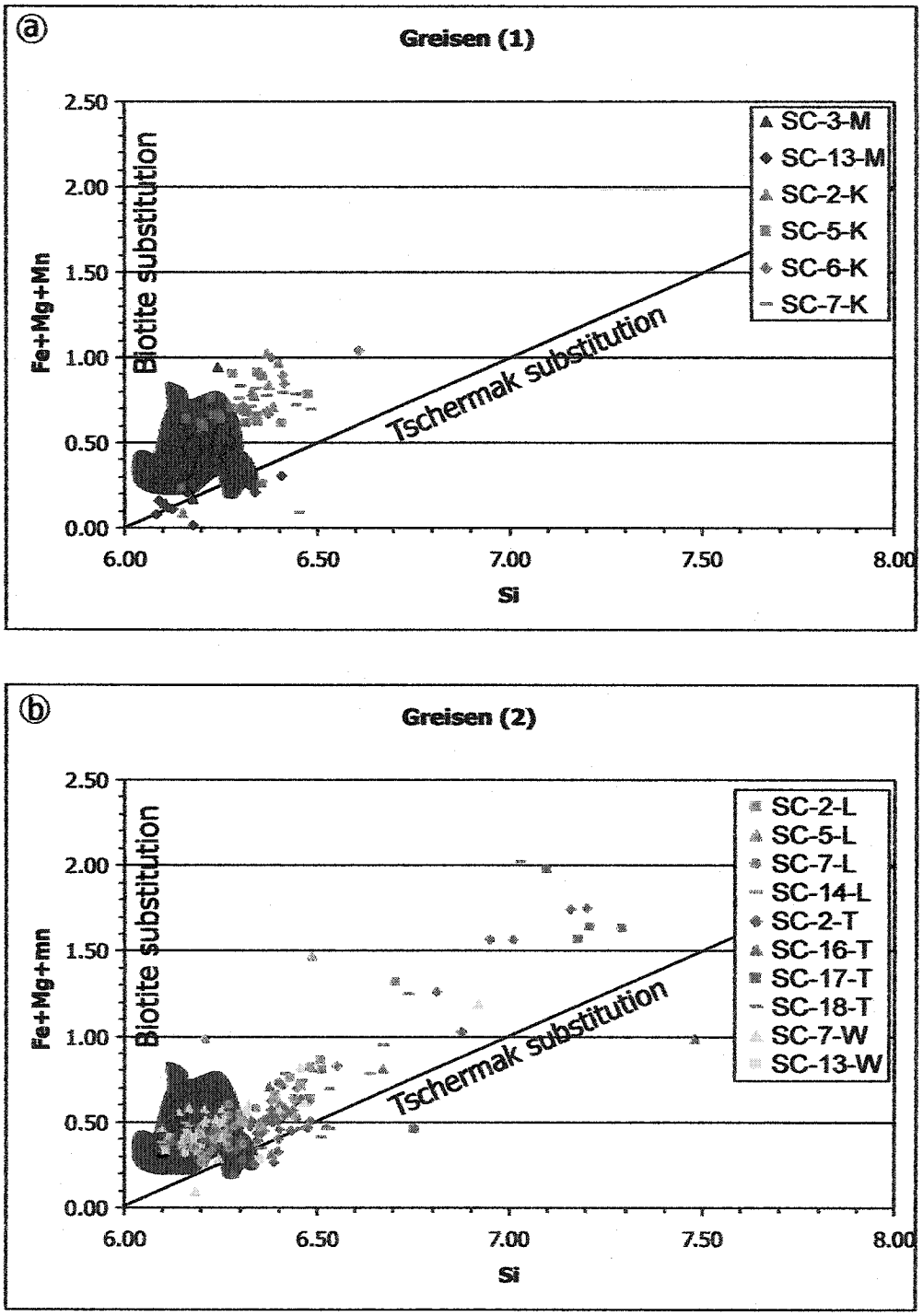

Figure 3.25: Diagrams of Si vs. Fe+Mg+Mn for primary and secondary white micas from (a) greisen and greisenised samples at the Morley's (M) and Keddy (K) deposits and (b) greisen and greisenised samples at the Turner (T), Long Lake (L), and Walker (W) deposits. The shaded area is the reported field of volcanic and subvolcanic samples, and primary samples from the New Ross area.

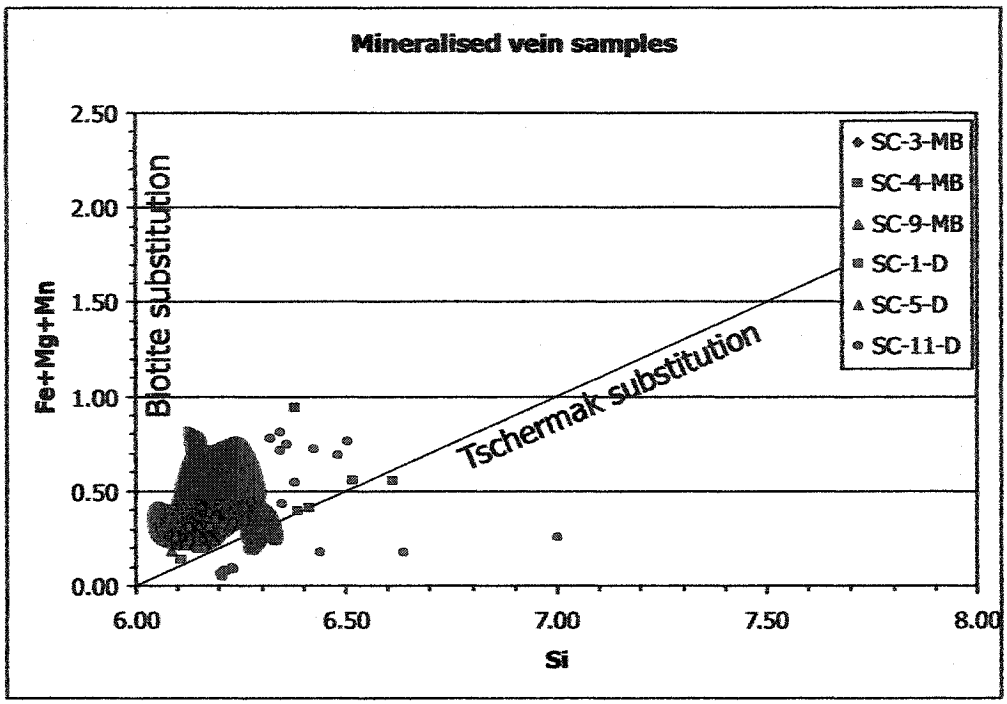

Figure 3.26: Diagram of Si vs. Fe+Mg+Mn for primary and secondary white micas from mineralised vein samples from the New Ross area. MB = Millet Brook, D = Mn Mines. The shaded area is the reported field of volcanic and subvolcanic samples, and primary samples from the New Ross area.

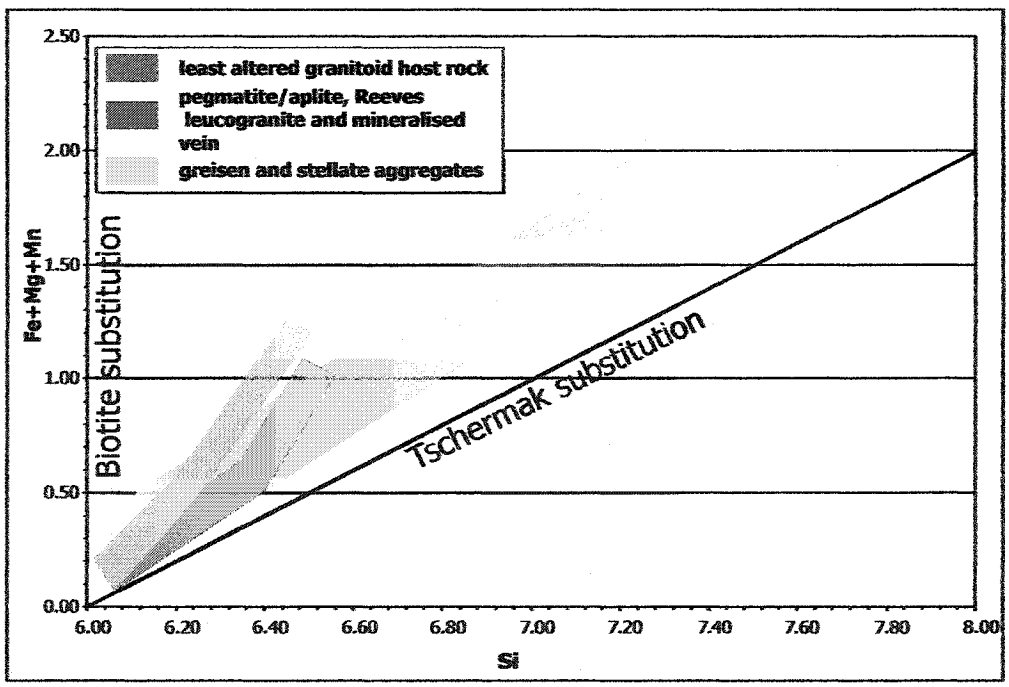

Figure 3.27: Diagram of Si vs. Fe+Mg+Mn showing the general trends for the composition of white micas from least altered granitoid host rock, mineralised vein, pegmatite/aplite and greisen from the New Ross area.

texture from the Reeves and Morley's deposits and, to a lesser extent, white micas from an aplite at Long Lake follow the latter trend. The compositions of white micas from aplites of other areas in the SMB have a small amount of Tschermak and biotite substitutions and fall within the primary white mica field (Fig. 3.24b).

Greisen and greisenised samples

White micas from greisen and greisenised samples show a dominant Tschermak substitution (Fig. 3.25a and b). Similar to diagrams of Fe+Mg+Mn vs. Al_{total}, white micas from samples from the Turner deposit show the largest extent of Tschermak and biotite substitutions of all greisen and greisenised samples, and possibly define a hydrothermal alteration trend (i.e., secondary) (Fig. 3.25b).

Vein samples

Most white mica compositions for mineralised samples from vein deposits lie within the primary composition field, therefore showing little biotite and Tschermak substitutions (Fig. 3.26). The composition of white micas from an altered Elvan dyke at the Mn mines (SC-11-D) follows a similar trend as white micas from pegmatites (i.e., dominant Tschermak substitution at the beginning of the trend and then increasing biotite substitution towards the end of the trend).

Summary

In summary, Si vs. Fe+Mg+Mn diagrams reveal the following (Fig. 3.27):

1. About 70% of the data fall within the Si composition range of 6.04 and 6.24 apfu and Fe+Mg+Mn composition range of 0.2 to 0.6 apfu, belonging to the field previously outlined by white micas from the primary samples. Data obtained from white micas from any rock type (especially most white micas from mineralised samples from vein deposits), both primary or secondary, fall within this category.
2. White micas from least altered granitoid host rocks, aplites, and pegmatites show dominant Tschermak substitution at the beginning of the trend (falling within the primary field area as described above) and then increasing biotite substitution towards the end of the trend. White micas from least altered granitoid host rocks

show a stronger biotite substitution than white micas from aplites and pegmatites. This trend is consistent with the primary magmatic trend for white micas from the SMB.

3. White micas from greisen samples show dominant Tschermak substitution, possibly representing the secondary hydrothermal trend for white micas from the SMB.
4. Although texturally primary and secondary white micas overlap in the Si compositional range < 6.5 apfu, only texturally secondary white micas show Si content > 6.5 apfu (Fig. 3.28).

3.4.4.3. Na vs. K

In an Na vs. K diagram for all analyses classified by texture (Fig. 3.29a), two crude groups of data emerge:

1. data generally following the paragonite substitution line (I); and
2. weak concentration of data below the paragonite substitution line (II).

In a histogram of K distribution, Group I ranges from 1.70 to 1.98 apfu, whereas Group II ranges between 1.4 and 1.70 apfu (Fig. 3.30). Unfortunately, there is no systematic distribution of the data between Groups I and II, with data organised either by textures (Fig. 3.29a) or by rock types (Fig. 3.29b and 3.31a to f). Neither do Groups I and II depend on calibration discrepancies, because (1) white mica analyses from different microprobe sessions belong to both Groups, and (2) white mica analyses from a single session belong to both groups. Also, burn-off of Na may have resulted in variable Na concentrations.

Host granitoid samples

The compositions of white mica from least altered host granitoid rocks belong to Groups I and II (Fig. 3.32a to d). Some samples have white mica compositions falling exclusively in Group I (SC-1, SC-5, SC-8-MB; SC-2-D; SC-8-, SC-14-W; SC-1-, and SC-7-R), exclusively in Group II (SC-6-D; SC-4-T; SC-5-M; and LL-2), and the remaining samples have white mica compositions falling within both Groups (SC-7-T; SC-8-, SC-11-R; and M72-119) (Fig. 3.32a to d). The extent of the paragonite exchange is larger for

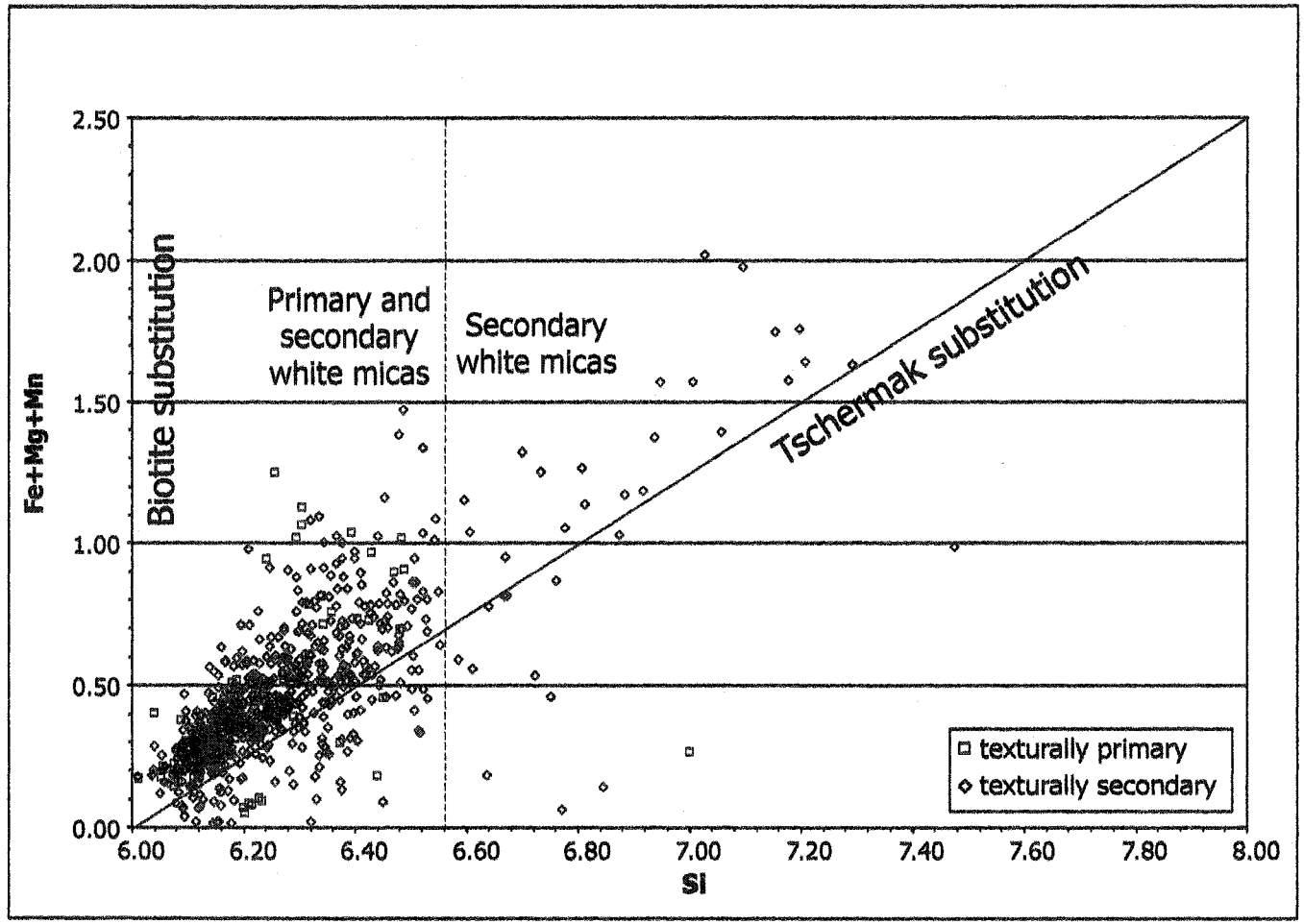

Figure 3.28: Diagram of Si vs. Fe+Mg+Mn for all analyses of white micas from the New Ross area texturally classified as primary or secondary.

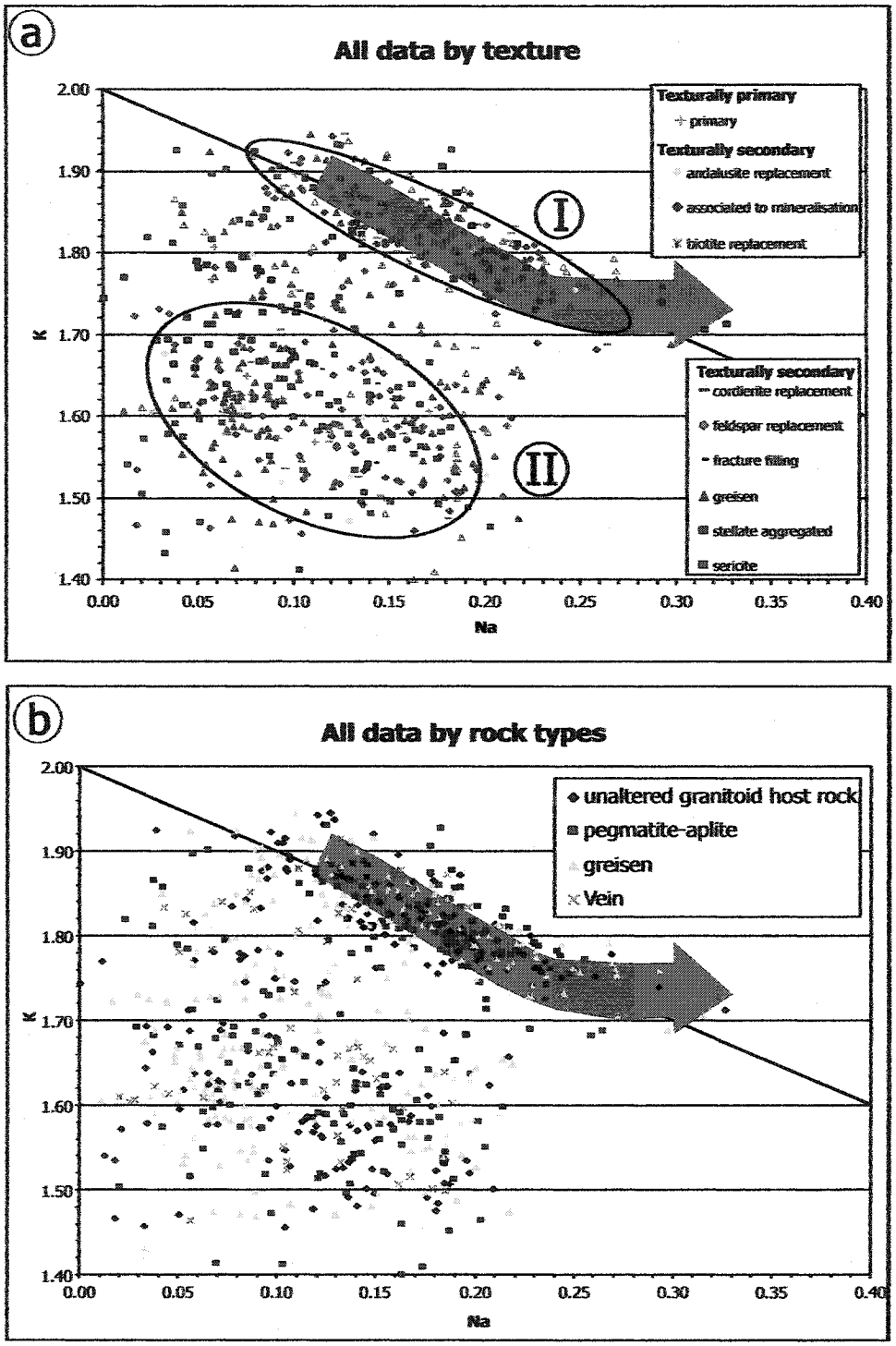

Figure 3.29: Diagrams of Na vs. K for all analyses of white micas from the New Ross area classified (a) by texture, and (b) by rock type. Two groups emerge from (a): data following the paragonitic substitution line (I), and data below the paragonitic substitution line (II). Arrow is the reported paragonite trend of most primary samples from the New Ross area (Fig. 3.7f).

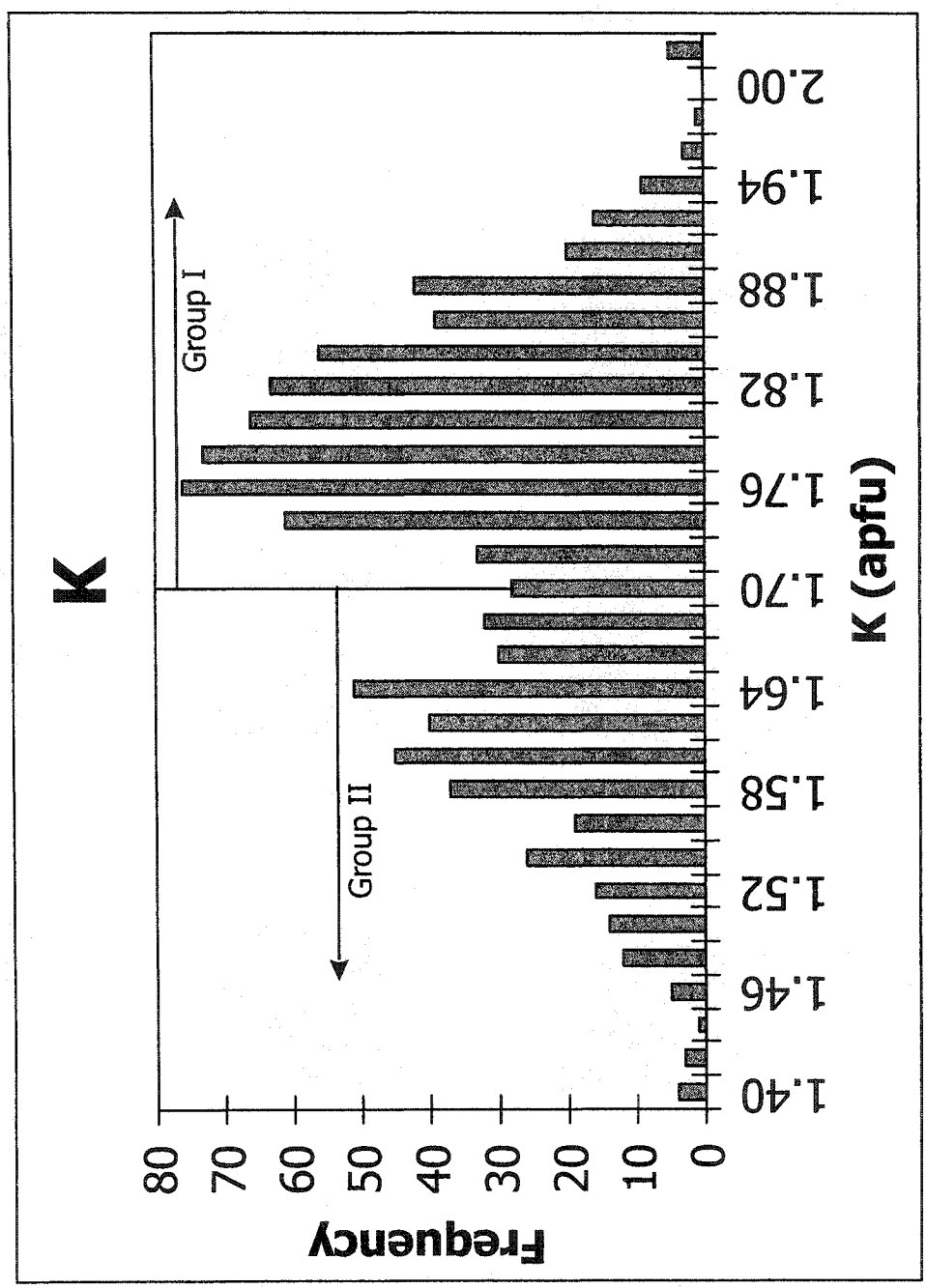

Figure 3.30: Histogram of the K distribution (in apfu) for all white micas from the New Ross area.

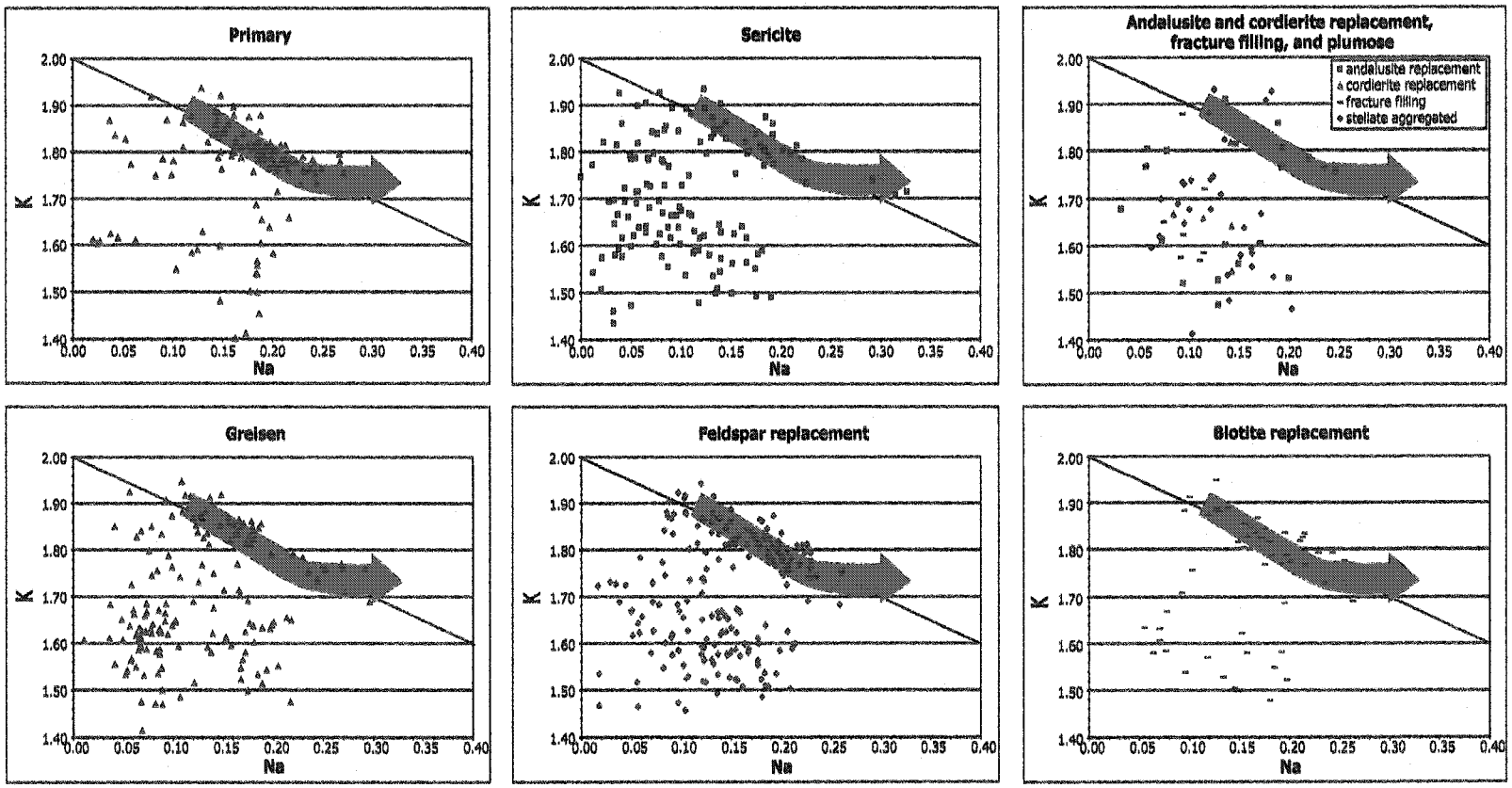

Figure 3.31: Diagrams of Na vs. K for all analyses of white micas from the New Ross area organised by texture: (a) primary, (b) sericite, (c) andalusite and cordierite replacement, fracture filling, and plumose, (d) greisen, (e) feldspar replacement, and (f) biotitereplacement. Arrow is the reported paragonite trend of most primary samples from the New Ross area.

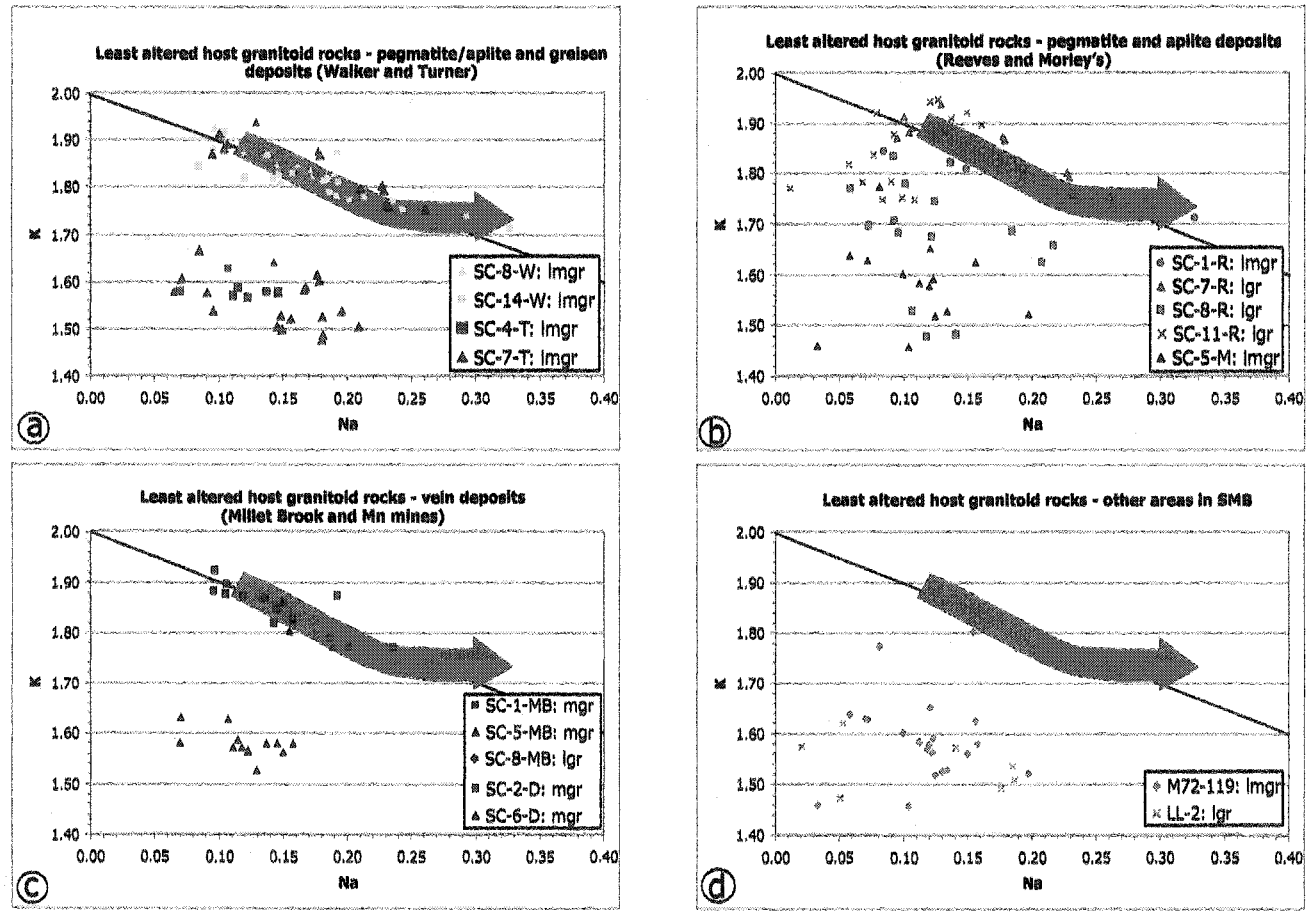

Figure 3.32: Diagrams of Na vs. K for primary and secondary white micas from least altered granitoid host rocks from the New Ross area. (a) host granitoid rocks of pegmatite/aplite and greisen deposits, (b) host granitoid rocks of pegmatite/aplite deposits, (c) host granitoid rocks of vein deposits, and (d) host granitoid rocks from other area in the SMB. mgr = monzogranite, lmgr = leucomonzogranite, lgr = leucogranite, W = Walker, T = Turner, R = Reeves, M = Morley's, MB = Millet Brook, D = Mn Mines. Arrow is the reported paragonite trend of most primary samples from the New Ross area.

white micas of host granitoid rocks from pegmatite/aplite and greisen deposits than from vein deposits (Fig. 3.32a, b, and c).

Aplite and pegmatite samples

Very few white micas from pegmatite samples follow the paragonite substitution line (Fig. 3.33a). White mica from aplite samples from the New Ross area (SC-13-L and SC-3-W) also does not follow the paragonite substitution line, whereas white micas from aplite samples of other areas of the SMB do (Fig. 3.33b). These observations suggest that K and Na are more mobilised in the New Ross area than they are in other areas of the SMB. Intense fluid circulation in the area could be responsible for the redistribution of easily mobile elements such as K and Na.

Greisen and greisenised samples

Similar to white mica from host granitoid rocks, texturally secondary white mica from greisen and greisenised samples either exclusively belongs to Group I (SC-3-M; SC-5-, SC-6-K; SC-13-W; and SC-14-L), or exclusively belongs to Group II (SC-13-M; SC-2-K; SC-18-T; SC-2-, SC-5-, and SC-7-L), or indifferently belongs to both Groups (SC-7-K; SC-2-, SC-16-, SC-17-T; and SC-7-W) (Fig. 3.34a and b). Again, no systematics regarding white mica texture can explain such a distribution of the data. Intensity of greisenisation may be a factor in mobilising alkalies: for example, white mica from a greisenised leucomonzogranite from Morley's (SC-3-M) shows data following the paragonite substitution line, whereas white micas from a more strongly greisenised sample (SC-13-M) show departure from the line (Fig. 3.34a). Also, strong alteration level (hematisation, sericitisation) may facilitate the mobilisation of alkalies (SC-13-W) (Fig. 3.34b), compared with the white mica composition of less altered samples (SC-8-, SC-14-W) (Fig. 3.32b).

Vein samples

Most white mica from mineralised samples from Millet Brook (SC-3- and SC-9-MB) follows the paragonite substitution line, showing that the mineralising event did not mobilise K and Na (Fig. 3.35). On the other hand, white mica from an episyenite (SC-4-MB) displays strong K and Na loss (Fig. 3.35). Therefore, the mineralising event and

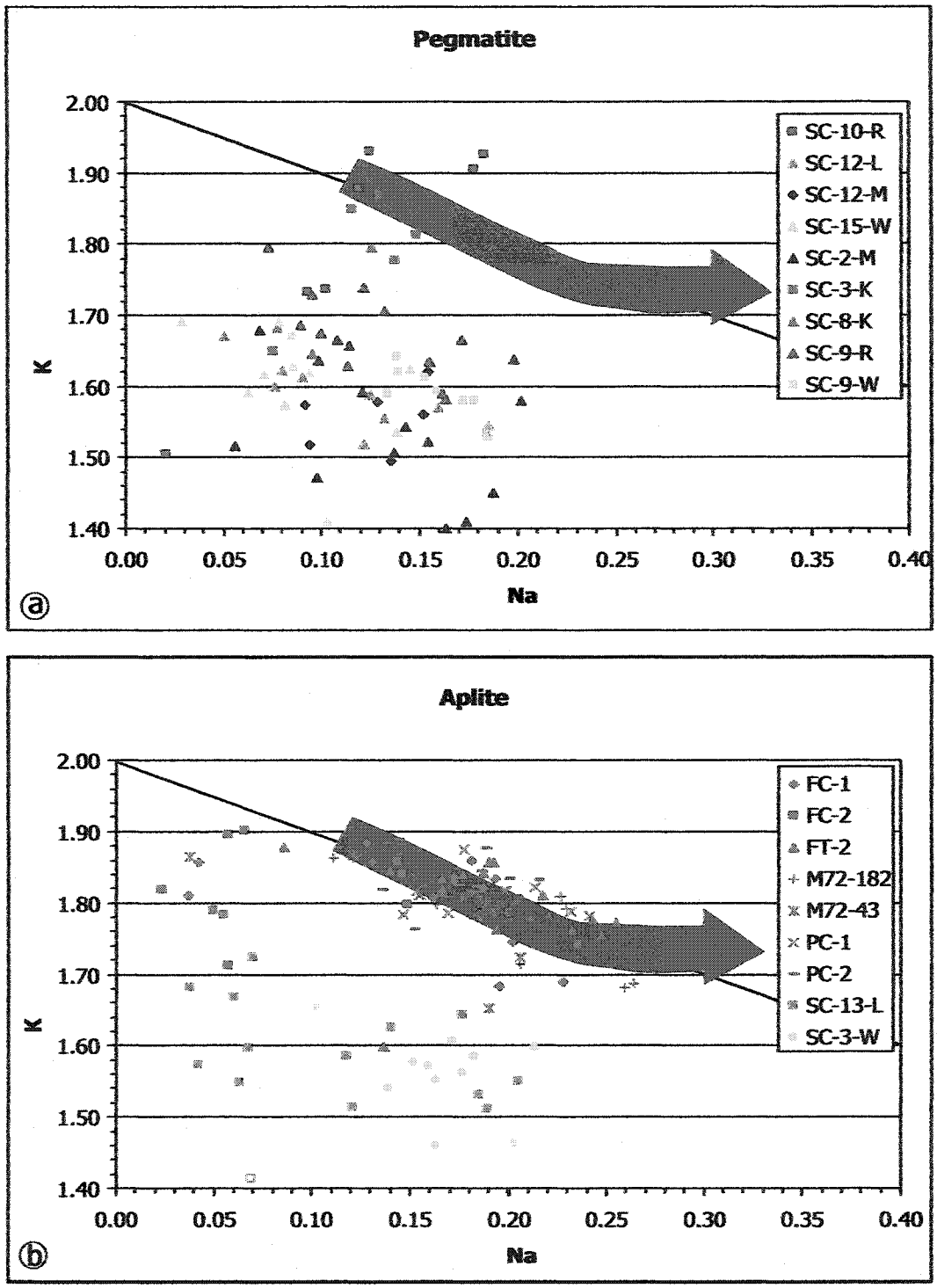

Figure 3.33: Diagrams of Na vs. K for primary and secondary white micas from (a) pegmatite and (b) aplite from the New Ross area and other area in the SMB. R = Reeves, K = Keddy, M = Morley's, L = Long Lake, W = Walker. Arrow is the reported paragonite trend of most primary samples from the New Ross area.

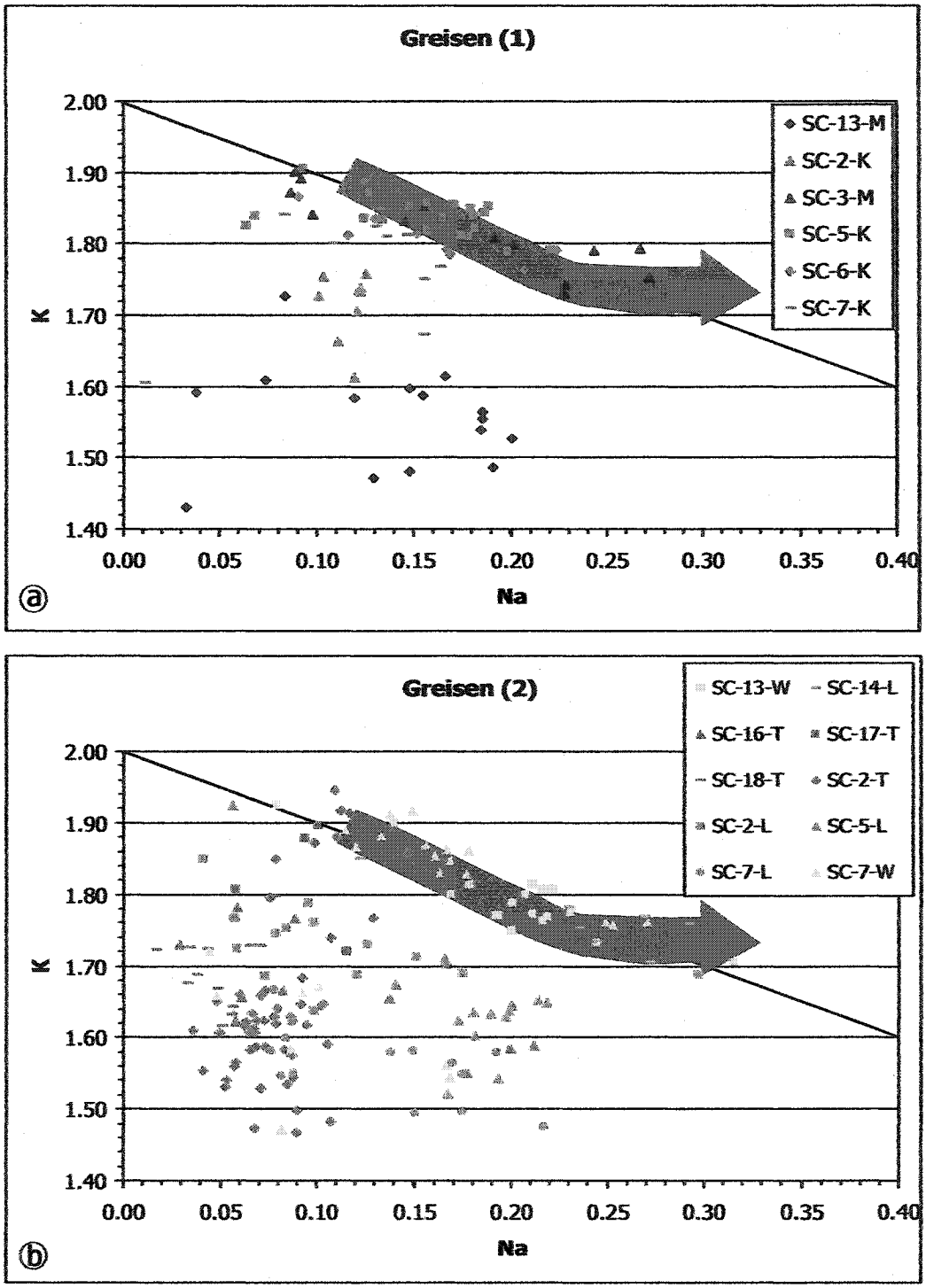

Figure 3.34: Diagrams of Na vs. K for primary and secondary white micas from (a) greisen and greisenised samples at the Morley's (M) and Keddy (K) deposits and (b) greisen and greisenised samples at the Turner (T), Long Lake (L), and Walker (W) deposits. Arrow is the reported paragonitetrend of most primary samples from the New Ross area.

episyenitisation event may not be related to the same fluid circulation event, the second more strongly affecting K and Na mobility than the first. White micas from episyenite, breccia, and Elvan dyke from the Mn mines (SC-1-, SC-5-, and SC-11-D) all show data below the paragonite substitution line (Fig. 3.35). Therefore, the white mica composition in the mineralised facies at the Mn mines may also have undergone fluid circulation affecting K and Na mobility.

Summary

In summary, the K vs. Na diagrams show several features:

1. There is no systematic substitution of Na for K according to white mica texture.
2. In general, white mica from host granitoid rocks follows the paragonite substitution line. The reason for the "departure" from the trend at K ~ 1.75 is unknown.
3. In general, white mica from pegmatites falls below the paragonite substitution line, whereas white mica from aplites follows the paragonite substitution line.
4. In general, white mica from greisens and greisenised samples falls below the paragonite substitution line.
5. In general, white mica from mineralised vein samples falls below the paragonite substitution line.

But most of these statements are undermined by numerous exceptions. Preferential mobility of K and Na seems to be random, maybe related to their mobility potential. Alternatively, analytical problems linked to volatilisation of Na during microprobe analysis may result in the scatter observed in the data.

3.4.4.4. Composition of white micas from dated samples

Figures 3.36a to c show the composition of hand-picked white micas texturally comparable to those dated in Chapter 4. In a Fe+Mg+Mn vs. Al_{total} diagram (Fig. 3.36a), data for white mica at Turner (elvan), the Mn mines (episyenite), and Long Lake (pegmatite) show a small extent of biotite and Tschermak substitutions and fall within the primary field defined earlier (Section 3.4.4.1). Compositions of white mica from greisens (Long Lake and Keddy) spread over a larger area of the diagram, with higher Fe+Mg+Mn

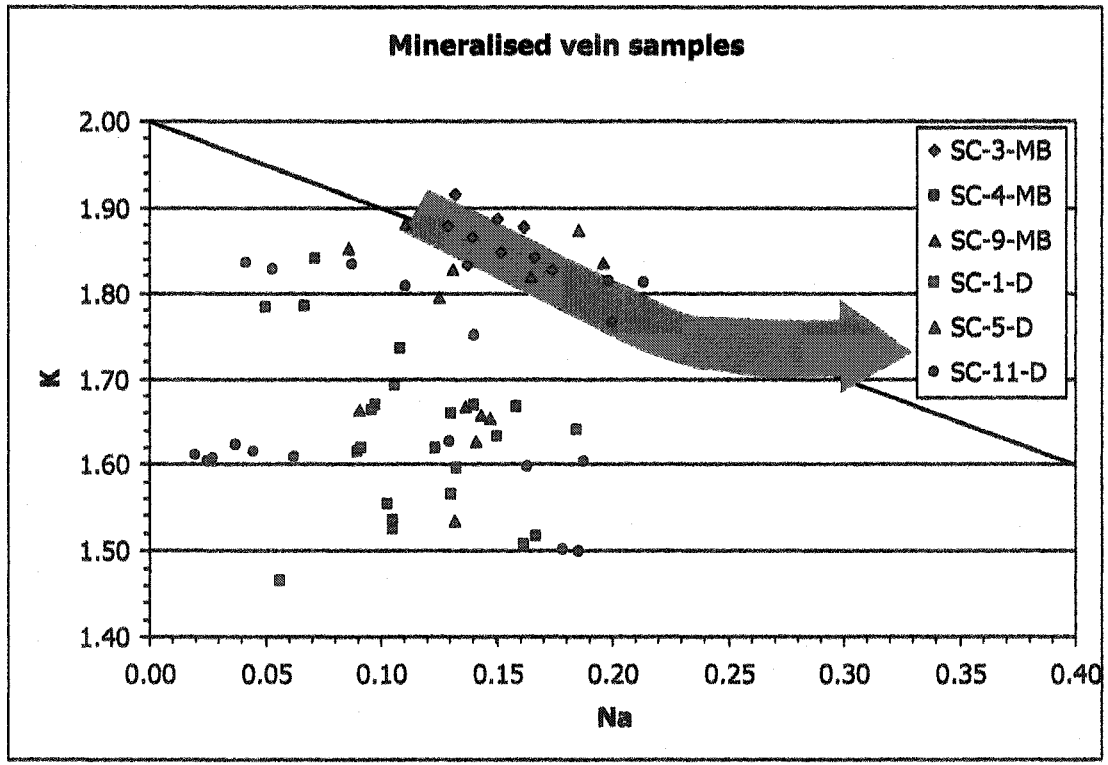

Figure 3.35: Diagram of Na vs. K for primary and secondary white micas from mineralised vein samples from the New Ross area. MB = Millet Brook, D = Mn Mines. Arrow is the reported paragonite trend of most primary samples from the New Ross area.

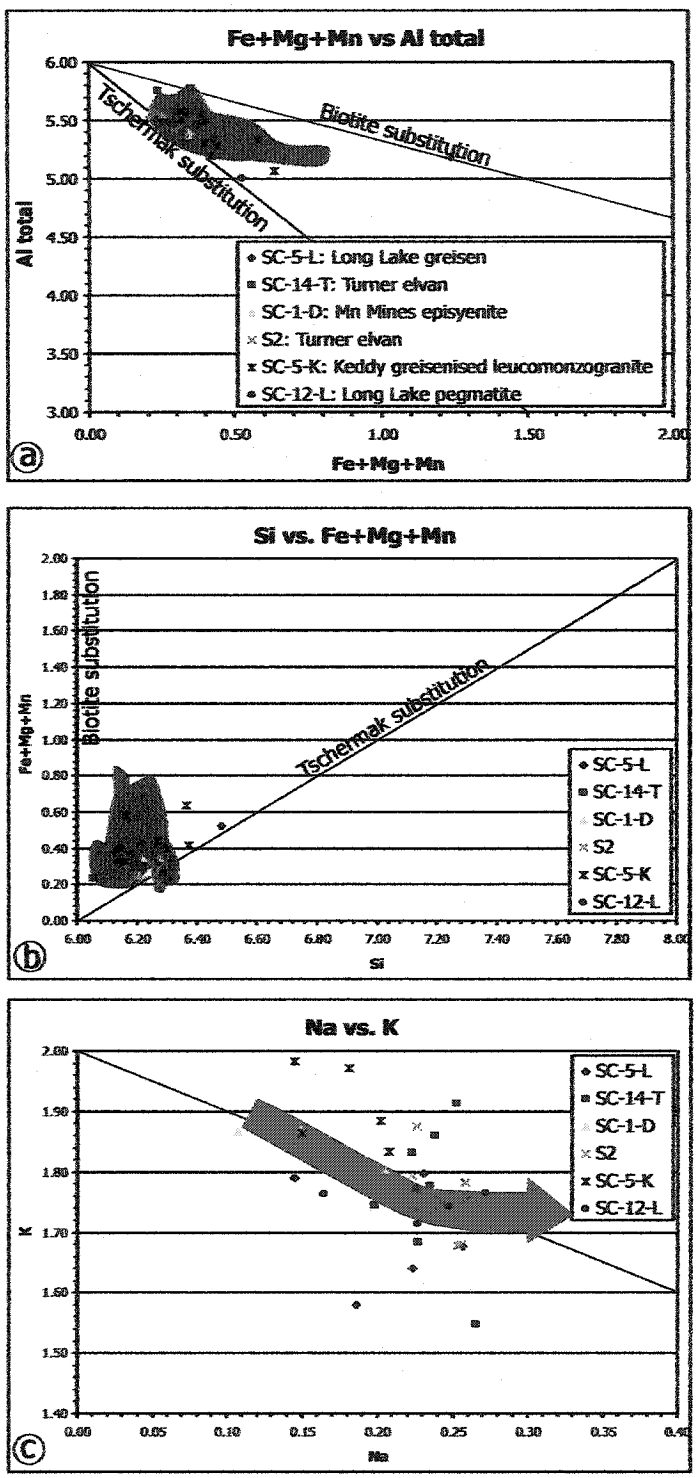

Figure 3.36: Diagrams showing the composition of hand-picked white micas texturally comparable to those dated in Chapter 4. (a) Fe+Mg+Mn vs. Al_{total}, (b) Si vs. Fe+Mg+Mn, and (c) Na vs. K. The shaded area is the reported field of volcanic and subvolcanic samples, and primary samples from the New Ross area. Arrow is the reported paragonite trend of most primary samples from the New Ross area.

content and lesser Al (Fig. 3.36a). In the Si vs. Fe+Mg+Mn diagram (Fig. 3.36b), white mica from greisens underwent more biotite and Tschermak exchange than white mica from pegmatite, episyenite, and elvan. In the Na vs. K diagram (Fig. 3.36c), white mica compositions from all dated samples scatter across the paragonite substitution trend.

Following these observations, the compositions of white micas from samples from Turner (SC-14-T and S2), Long Lake (SC-12-L) and the Mn mines (SC-1-D) appear to be primary, whereas the compositions of white micas from greisens (Long Lake: SC-5-L; and Keddy: SC-5-K) appear to be secondary and reflect a subsolidus exchange.

3.4.4.5. Conclusions

The binary diagrams illustrating the common substitutions in white micas reveal that white micas from the New Ross area show biotite, Tschermak, and paragonite substitutions. Also, most white micas from host granitoid samples have a smaller range of biotite and Tschermak substitutions than white micas from altered samples. Enrichment in Fe+Mn+Mg and Si in aplite/pegmatite and greisen samples suggests that Al is immobile in a fluid environment, thus promoting a rapid increase in deviation from the primary field. The Tschermak substitution is more significant in white mica of presumed secondary origin, whereas the biotite substitution is larger for white micas of presumed primary origin. Alkalis (K and Na) appear to be extremely mobile, therefore, resulting in departures of the composition of most white micas of presumed primary and secondary origin from the paragonite substitution line. As a whole, the bivariate plotting procedure fails to chemically discriminate clearly between primary and secondary white mica compositions for granitoid samples from the New Ross area.

3.5. Statistical analysis of geochemical data

3.5.1. Introduction

Binary diagrams, although useful for illustrating common substitutions in white mica (Fig. 3.1 and 3.2), may lose valuable information contained by other variables in the system. To overcome this loss of information and fully investigate the variability of the

data set, I undertook multivariate analysis of the data as a tool to chemically decipher between primary and secondary white micas.

In this section, I use multivariate statistical methods allowing for the simultaneous analysis of a large number of variables (Swan and Sandilands 1995), to test if the populations of primary and secondary white micas are chemically different. Note that this treatment is critically dependent on being able to assign a primary or secondary origin accurately to white micas based on texture. In the following, I refer to the different chemical elements as "variables" and, based on petrographic evidence (Table 3.3), I assign each analysed grain of white mica to one of the two groups "texturally primary" or "texturally secondary". The chemical elements considered here are Si, Al^{vi}, Ti, Fe, Mg, Na, K, and F. I removed Al^{iv} from the statistical treatment, because of its perfect correlation with the element Si ($Al^{iv} = 8 - Si^{iv}$).

I apply a t-test and a T^2 test to the variables to understand how different (or similar) the means of each group are. In the first case, I test the difference between the means for each group (texturally primary and texturally secondary) separately for each variable. In the second case, I test the difference between the means for each group, but with all variables taken into account. To obtain indisputably independent variables, I perform a principal component analysis. I then complete a discriminant function analysis to verify if both groups of data are distinguishable using as variables: (i) untransformed variables (prior to both log ratio transformation and principal component analysis), (ii) transformed variables (prior to principal component analysis), and (iii) the principal components. To circumvent the effect a non-normal distribution of the variables could have on the statistical results, I finally perform a logistic regression analysis using similar variables (i-ii-iii), as described for the discriminant function analysis. Also, I perform both discriminant function analysis and logistic regression: (i) using all variables simultaneously, and (ii) in a forward stepwise manner. All of the different models are compared to one another to assess which one(s) is (are) the best. Figure 3.37 is a tree diagram describing the statistical treatment of the data to obtain twenty-four possible models.

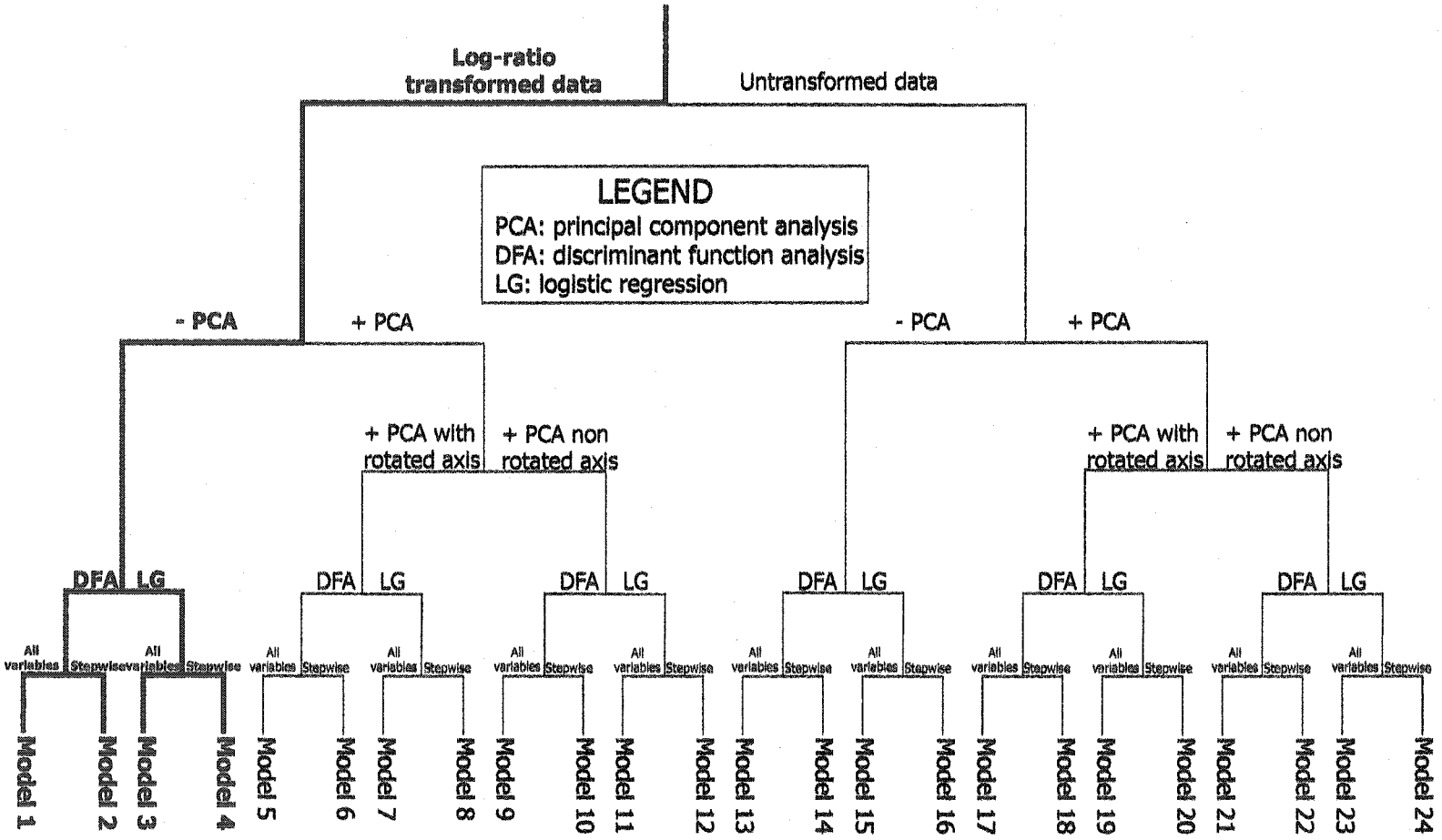

Figure 3.37: Tree diagram summarising the statistical treatment of the data to obtain twenty-four possible models. Models described in details in the text are in red and bold.

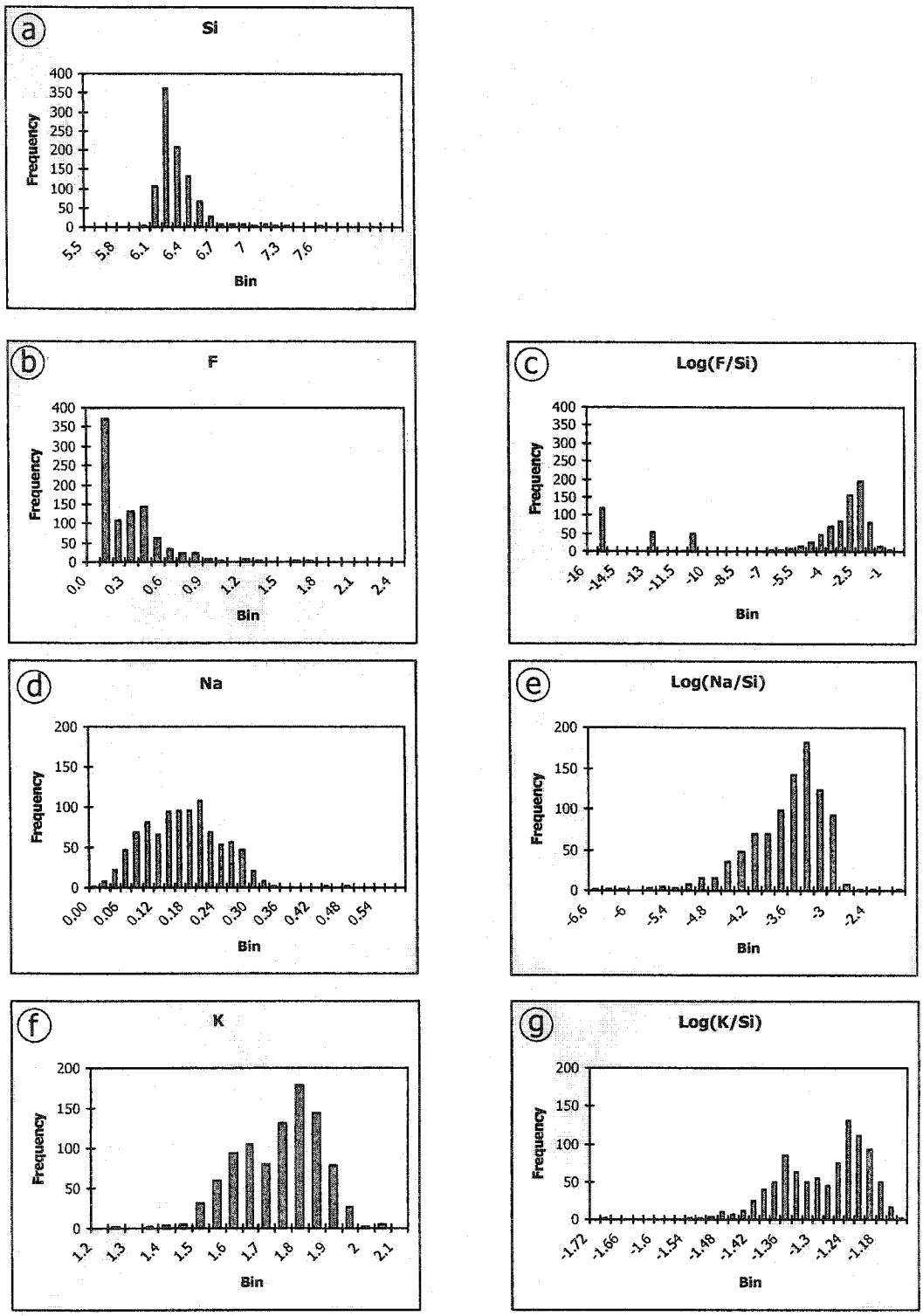

Figure 3.38: Histogram of the distribution of all the variables (a) Si, (b) F, (c) log-transformed F, (d) Na, (e) log-transformed Na, (f) K, (g) log-transformed K.

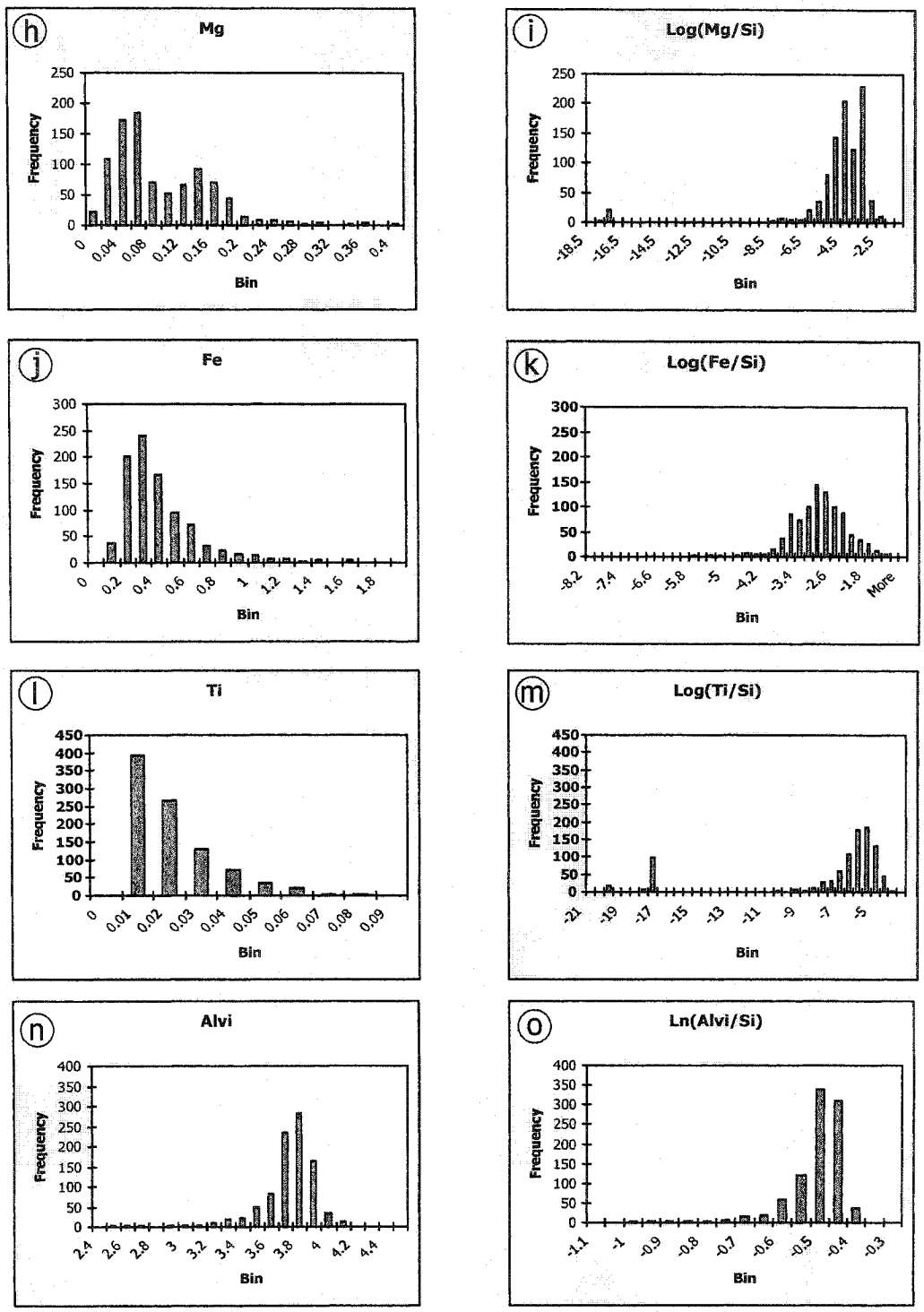

Figure 3.38continued: Histogram of the distribution of all the variables (h) Mg, (i) log-transformed Mg, (j) Fe, (k) log-transformed Fe, (l) Ti, (m) log-transformed Ti, (n) Al^{vi}, and (o) log-transformed Al^{vi}.

3.5.2. Methodology

3.5.2.1. Data transformation

Frequency distribution histograms for each variable show that they all have a skewed distribution. The distributions of Si, Ti, Fe, Mg, Na, and F are positively skewed (skewed to the right), whereas the distributions of K and Al^{vi} are negatively skewed (skewed to the left) (Fig. 3.38a to n). To obtain distributions of variables that are closer to normal distributions, transformation is necessary. Also, chemical analyses of minerals have a constant-sum type of closure, this is, an element cannot increase without one or several of the others decreasing because each analysis sums to a maximum of 100 % (LeMaitre 1982). Therefore, to circumvent both the non-normal distribution of the data and the closure problems, I apply a log-ratio transformation to the data (Fig. 3.38c, e, g, I, k, m, and o):

$$Y_i=\log(X_i/X_j)$$

with i= 1, 2,..., D

where Y_i is the log-ratio transformed value of variable Y, X_i the original value of variable Y in apfu, X_j the corresponding silica value in apfu, and D the finite number of data (LeMaitre 1982)

I refer to the new set of data obtained using this equation as "transformed data". The transformed data are still not normally distributed, and attempts at using other data transformations were similarly unsuccessful. Although not solving the problem of non-normal distribution of the data, the log-ratio transformation allows for the circumventing of the closure problem, and the transformed data will therefore be used for further statistical treatment. The effect of a non-normal distribution problem is addressed by using two different statistical techniques for classification (Section 3.5.2.4).

3.5.2.2. Descriptive statistics, t, and T^2 statistical tests

The descriptive statistics include mean, standard deviation (variation around the mean), and standard error of the mean (standard deviation of the sample mean) for each group, to help understand the structure of the set of data.

The t-test compares the means for each variable between the texturally primary and texturally secondary groups. The t-value is positive if the first mean is larger than the second and negative if it is smaller. To check if the difference between the groups is not only based on chance, a test of significance is needed at the 5% significance level. If the significance values are low (i.e., < 0.05), then the t-test indicates a significant difference between the means of each group.

Hotelling's T^2 test investigates the hypothesis that the means of all variables are the same for two multivariate populations (Manly 1994). This test provides values for the distance between the variable means and is a generalization of the univariate t-test (Stevens 1986, Swan and Sandilands 1995). Again, I perform a test of significance, and significance values < 0.05 indicate that a statistically significant difference between the two groups considered exists and, therefore, a way to discriminate them may be found.

3.5.2.3. Principal component analysis

Principal component analysis is designed to explain the variability in data (Fisher and Van Belle 1993). This technique produces two important results: (i) transformation of the original set of variables into a new set of variables (the principal components) having the most possible variance and being uncorrelated with each other; and (ii) reduction of the number of variables to be considered if the first few sets of principal components account for most of the variance (LeMaitre 1982). The principal components are ordered so that the first one displays the largest amount of variation, the second displays the second largest amount of variation, etc. (Manly 1994), and each principal component represents a linear combination of the original variables (Fisher and Van Belle 1993). I chose to take into consideration as many principal components as necessary to explain at least 80% of the variance.

The principal components may be difficult to interpret, i.e., the same variable may appear in the composition of more than one component. To solve this problem, it is possible to determine "rotated components", specifically determined so that a given variable has a high loading on only one component (Afifi and Clark 1990). The rotation type used here is the varimax rotation. The idea is to rotate the axes representing the component so that they cross through subgroups more efficiently; the new axes must be

perpendicular to each other (Afifi and Clark 1990). Although facilitating the determination of which variable is most important for which component, rotation involves redistribution of variance for each component compared to non-rotated components.

3.5.2.4. Discrimination and classification

Discriminant function analysis

Multiple discriminant analysis classifies individual measurements into one of two or more groups, based on a set of variables (Afifi and Clark 1990) and describe how well the groups are separated given all the variables measured (Manly 1994). Such analyses have to fulfil two basic assumptions: (i) variables have to be normally distributed within groups; and (ii) the within-group covariance matrix should be the same for each group (Manly 1994). I tested two different variable selection methods to assess the importance of some or all of the variables: (i) all variables are introduced in the discriminant function analysis simultaneously, and (ii) variables are introduced one by one in a forward stepwise manner. The latter variable selection method uses values of the general linear hypothesis test (F-test) obtained for each variable. The variable with the highest F-to-enter value (i.e., highest discriminating power) enters the discriminant function analysis first, and so forth until F-to-enter value is lower than 4.

Logistic regression

As stated in Section 3.5.2.1, most variables are not normally distributed; therefore, to assess the effect of the non-normal distribution of the variables, I use another discriminating method, logistic regression, that does not need the two assumptions required by multiple discriminant analysis.

Logistic regression models the logarithm of the odds of belonging to one population (i.e., probability (texturally secondary)/probability (texturally primary), often called logit) as a linear function of the variables used for classification (Afifi and Clark 1990). To use this statistical method, the following assumptions are made: (i) independent observations, (ii) only two possible outcomes (groups), (iii) natural logarithm of the odds linearly related to the independent variables, and (iv) group membership binomially distributed. No assumptions are made about the distributions of the variables (Afifi and Clark 1990),

thereby circumventing the problem of non-normality of the distributions of the variables. Similarly to the discriminant function analysis, the variables can enter the logistic regression all together or in a forward stepwise manner.

Model number	Overall percentage	Model number	Overall percentage
1	69.7	13	76.4
2	71.1	14	75.5
3	74.1	15	75.9
4	73.2	16	75.5
5	69.4	17	75.4
6	69.4	18	74.6
7	69.7	19	75.9
8	69.7	20	75.4
9	69.4	21	75.4
10	68.5	22	75.5
11	69.7	23	75.9
12	68.8	24	75.7

Table 3.7: Overall percentages of success in classifying white micas into the proper group (primary and secondary) using the different models as described in the text.

3.5.3. Results and Models presentation

After completion of the statistical treatment, twenty-four models were created (Fig. 3.37). Only considering models using log-ratio transformed data for the reasons stated in Section 3.5.2.1, the overall percentages of success in classifying the white micas into the proper group (texturally primary and texturally secondary) range from 68.5% (Model 10) to 74.1% (Model 3) (Table 3.7). Based on the overall percentage of success, the following observations emerge:

1. Although providing completely independent variables, principal component analysis generates enough loss of information to produce models with lower overall percentages of success;
2. Logistic regression has higher classification percentages than discriminant function analysis, therefore the non-normal distribution of the data does affect the statistical results of the classification; and

3. Discriminant function analysis generally has higher overall percentage of success for models including the variables in a forward stepwise manner, whereas logistic regression obtains higher or equal overall percentage of success for models including all variables at once.

In the light of these observations, Sections 3.5.3.1, 3.5.3.2, and 3.5.3.3 contain comments on the descriptive statistics for transformed data, as well as a detailed description of Models 1,2, 3, and 4. In the following, texturally primary white micas are represented by 0 (n = 332) and texturally secondary white micas by 1 (n = 591). Every statistical treatment was performed using the computer program SPSS version 10.1.

3.5.3.1. Descriptive statistics, t, and T^2 tests

Table 3.8 contains the descriptive statistics for the white mica dataset. Because the chemical analyses are constrained by the mineral structure, there are no large differences between the means of each variable for the two groups considered. Nonetheless, the small differences in the standard deviation values are statistically significant, because of the large amount of data (n = 923) used in the statistical analysis.

FACTOR		N	Mean	Std. Deviation	Std. Error Mean
Al^{vi}	0	332	-.521	.072	.004
	1	591	-.539	.085	.004
Ti	0	332	-7.037	3.322	.182
	1	591	-8.296	4.554	.187
Fe	0	332	-3.031	.586	.032
	1	591	-3.079	.718	.030
Mg	0	332	-5.401	2.279	.125
	1	591	-4.791	2.191	.090
K	0	332	-1.276	.067	.004
	1	591	-1.307	.084	.003
Na	0	332	-3.506	.453	.025
	1	591	-3.987	.741	.030
F	0	332	-5.362	4.348	.239
	1	591	-6.294	4.917	.202

Table 3.8: Descriptive statistics (mean, standard deviation, and standard error on the mean) for each transformed variable.

Table 3.9 presents the value of a t-test for each variable when equal variances are assumed. The significance values for the t-test indicate a significant difference between the two group means for all variables (significance value < 0.05) except Fe. Table 3.10 shows the multivariate equivalent to the t-test. The significance value for Hotelling's T^2 test shows that there is a difference between the two group means considering all variables at the same time (< 0.05). Therefore, finding a way to separate/discriminate the two groups based on the variables at hand is strongly anticipated and two different statistical methods for classification (discriminant function analysis and logistic regression) are applied in the following two Sections.

	t-test for Equality of Means						
	t	Degree of freedom	Significance of t test	Mean difference	Std. Error Difference	95% Confidence Interval of the Difference	
						Lower	Upper
Al^{vi}	3.347	921	.001	.019	.006	.008	.029
Ti	4.421	921	.000	1.259	.285	.700	1.819
Fe	1.038	921	.300	.048	.046	-.043	.139
Mg	-4.000	921	.000	-.610	.152	-.909	-.311
K	5.872	921	.000	.031	.005	.021	.042
Na	10.739	921	.000	.480	.045	.393	.568
F	2.878	921	.004	.932	.324	.296	1.567

Table 3.9: Value of a t-test for each variable with assumed equal variances. The test shows a significant difference in the means when the significance of the t-test is < 0.05.

	Value	F	Hypothesis df	Error df	Significance
Hotelling's T^2	.207	27.025	7.0	915.0	.00

Table 3.10: Value of a multivariate Hotelling's T^2 test for all variables taken into account in the statistical study. The test shows a significant difference in the means of all variables when taken into account together if the significance of the T^2-test is < 0.05.

3.5.3.2. Models 1 and 2

Tables 3.11 and 3.12 contain the classification function coefficients for each group and the classification results for Model 1, respectively. To obtain a classification score for each case for each group, each coefficient is multiplied by the value of the corresponding

variable, the products are summed, and the constant added to obtain the score. A case is predicted as being a member of the group in which the value of its classification function is the largest (SPSS manual). The classification matrix indicates that 69.7% of all cases are

	FACTOR	
	0	1
Al^{vi}	-269.902	-272.713
Ti	-9.978E-02	-.185
Fe	-32.559	-32.751
Mg	-.789	-.611
K	-239.813	-243.726
Na	7.278	6.323
F	1.713E-02	-2.213E-02
Constant	-262.982	-273.663

Fisher's linear discriminant functions

Table 3.11: Classification function coefficients for primary (0) and secondary (1) white micas, using a straightforward discriminant function analysis.

		Predicted Group Membership		
	FACTOR	0	1	Total
Count	0	271	61	332
	1	219	372	591
%	0	81.6	18.4	100.0
	1	37.1	62.9	100.0

69.7% of original grouped cases correctly classified.

Table 3.12: Classification results for primary (0) and secondary (1) white micas using a straightforward discriminant function analysis. The count gives the amount of data correctly or incorrectly classified. The percent gives the percentage of data correctly or incorrectly classified.

correctly classified during this statistical analysis, indicating chemical differences between texturally primary and texturally secondary white micas. Texturally primary white micas are better classified (81.6 %) than texturally secondary white micas (62.9 %). The alteration of texturally primary white micas to secondary white micas may occur with small chemical variations; therefore, texturally secondary white micas may not be correctly classified based on their chemistry only. Also, it is clear from the standard deviation values on the mean of each group that, although statistically significantly different, both groups overlap considerably, again impeding correct classification based on chemical composition alone.

The structure matrix (Table 3.13) shows which variables are the most useful in the discriminant analysis. The magnitude of the absolute values of the coefficients represents the discriminating power of the concerned variable. Variables with values greater than 0.4 are considered to be important discriminators (SPSS manual), which is the case for Na and K. Sodium and potassium are correlated, because they both enter in the same site in the white mica structure, therefore, it is not surprising that if Na has high discriminating power, so does K (or *vice versa*).

	Function 1
Na	.778
K	.426
Ti	.320
Mg	-.290
Al^{vi}	.243
F	.209
Fe	.075

Table 3.13: Structure matrix showing which variables are the most useful in the straightforward discriminant function analysis. Variables with a coefficient > 0.4 are important discriminators.

To understand better what chemical elements are the most important in the discrimination process, I carry out a discriminant function analysis in a forward stepwise manner. The variables are added to the discriminant functions one by one until the addition of extra variables does not give a significantly better discrimination. The variables enter the model based on their F-to-enter value (i.e., discriminating power; the variable with the largest F-to-enter value at a given step enters the model first). F-to-enter represents the ratio between the mean square between groups and the mean square within group. Under a null hypothesis (a hypothesis hoped to be rejected, for example, that all of the variable means are equal), there is an underlying "model" F-distribution. The calculated F-value is then compared to the F-value from the "model" distribution; and if the two F-values are significantly different, the null hypothesis is rejected and a statistically significant difference among the variable means exists (Le Maitre 1982; Manly 1994). The tolerance is the proportion of a variable's variance not accounted for by other independent variables.

The order of variables entering the model is Na, Mg, Ti, K, and F (Table 3.14). Two variables (Al^{vi} and Fe) are not useful to the stepwise discrimination. Table 3.15 provides the classification function coefficients for each group, and Table 3.16 shows the

		Tolerance	F-to-Enter
Step 0	Al^{VI}	1.000	11.201
	Ti	1.000	19.546
	Fe	1.000	1.077
	Mg	1.000	16.002
	K	1.000	34.476
	Na	1.000	115.330
	F	1.000	8.282
Step 1	Al^{VI}	.941	.526
	Ti	.998	13.803
	Fe	1.000	.777
	Mg	.994	20.778
	K	.943	10.256
	F	1.000	7.569
Step 2	Al^{VI}	.936	.131
	Ti	.956	22.112
	Fe	.997	1.283
	K	.942	10.989
	F	.998	6.242
Step 3	Al^{VI}	.905	1.473
	Fe	.942	.001
	K	.940	11.911
	F	.986	3.927
Step 4	Al^{VI}	.905	1.417
	Fe	.926	.219
	F	.970	5.879
Step 5	Al^{VI}	.866	2.980
	Fe	.807	.182

Table 3.14: Order of the variables entered in the model using a forward stepwise determinant function analysis. The variable with the highest F-to-enter is used first.

classification matrix for Model 2. The classification matrix reveals that 71.1% of all cases are correctly classified during this statistical analysis, a percentage in agreement with Model 1. In this case, the most discriminating variables are Na and Mg. Because Na and K are correlated, K does not have a strong discriminating power when data enter the

discriminant function in a forward stepwise manner. Classification success for texturally secondary white mica is higher using a stepwise introduction of the variables (65.8%), whereas the classification success for texturally primary white mica is slightly lower (80.4%).

	FACTOR	
	0	1
Ti	-.324	-.407
Mg	-.623	-.441
K	-210.623	-214.336
Na	-1.978	-3.026
F	-.679	-.718
Constant	-143.176	-151.837

Fisher's linear discriminant functions

Table 3.15: Classification function coefficients for primary (0) and secondary (1) white micas using a forward stepwise discriminant function analysis.

		Predicted Group Membership		Total
	FACTOR	0	1	
Count	0	267	65	332
	1	202	389	591
%	0	80.4	19.6	100.0
	1	34.2	65.8	100.0

71.1% of original grouped cases correctly classified.

Table 3.16: Classification matrix for primary (0) and secondary (1) white micas using a forward stepwise discriminant function analysis. The count gives the amount of data correctly or incorrectly classified. The percent gives the percentage of data correctly or incorrectly classified.

3.5.3.3. Models 3 and 4

Tables 3.17 and 3.18 show the variables in the equation after performing a logistic regression and the classification table for Model 3, respectively. If the Wald statistic (tests the significance of individual logistic regression coefficients for each independent variable) is significant (i.e., <0.05), then the parameter is useful to the model (SPSS manual). Therefore, similarly to Model 2, two variables (Al^{vi} and Fe) are not useful to Model 3. The

exponential of the logistic regression coefficient [Exp(LRC)] predicts the change in odds for a unit increase in the predictor variable. Therefore, when Exp(LRC) is less than 1, increasing values of the variable correspond to decreasing odds of the event's occurrence. On the other hand, when Exp(LRC) is greater than 1, increasing values of the variable correspond to increasing odds of the event's occurrence (SPSS manual). The classification

	Logistic regression coefficient (LRC)	Std. error on LRC	Wald's test	Degree of freedom	Significance of Wald's test	Exp(LRC)
Al^{vi}	-1.334	1.914	.486	1	.486	.263
Ti	-.087	.022	15.308	1	.000	.917
Fe	-.247	.222	1.231	1	.267	.781
Mg	.196	.040	23.647	1	.000	1.217
K	-3.143	1.097	8.206	1	.004	.043
Na	-2.031	.225	81.783	1	.000	.131
F	-.047	.019	5.804	1	.016	.955
Constant	-12.377	2.165	32.685	1	.000	.000

Table 3.17: Variables included in the model equation after performing a logistic regression.

		Predicted		
		FACTOR		Percentage Correct
Observed		0	1	
FACTOR	0	246	86	74.1
	1	153	438	74.1
Overall percentage				74.1

The cut-off value is 0.6

Table 3.18: Classification table for primary (0) and secondary (1) white micas using a logistic regression technique.

table indicates that 74.1% of all cases are correctly classified using the logistic regression method. The cut-off value (0.6) is defined by the ratio between the number of texturally secondary white micas (n = 521) and the total number of measurements (n = 923). This procedure allows to avoid the introduction of a bias because of the larger amount of measurements for texturally secondary white micas compared to the texturally primary ones. It is important that the "success" scores for discriminating data between the two groups are also close to the overall percentage, because it indicates that the cut-off value is

valid. In this case, there is perfect agreement between the overall percentage and the percentage of successfully discriminated samples in each group, showing that the percentage of error is the same for both groups.

Tables 3.19 and 20 show the variables present in the equation at each step and the classification table at each step again, respectively, when entering the data in the model in a stepwise manner. Based on their F-value, the variables enter the model in the following order: Na, Mg, Ti, F, and K. Each of the variables entered is significant at the 0.05 significance level, according to Wald's test. After completion of the fifth step, the overall percentage is 73.2 %, in good agreement with the percentage of correctly discriminated samples (74.1 and 72.8% for texturally primary and texturally secondary white micas, respectively).

		Logistic regression coefficient (LRC)	Std. error on LRC	Wald's test	Degree of freedom	Significance of Wald's test	Exp(LRC)
Step 1	Na	-2.091	.193	117.782	1	.000	.124
	Constant	-7.162	.701	104.402	1	.000	.001
Step 2	Mg	.168	.037	20.569	1	.000	1.183
	Na	-2.178	.198	121.505	1	.000	.113
	Constant	-6.634	.714	86.406	1	.000	.001
Step 3	Ti	-.092	.022	18.042	1	.000	.912
	Mg	.201	.040	25.596	1	.000	1.223
	Na	-2.138	.198	116.695	1	.000	.118
	Constant	-7.023	.729	92.860	1	.000	.001
Step 4	Ti	-.087	.022	15.927	1	.000	.917
	Mg	.194	.040	23.997	1	.000	1.214
	Na	-2.177	.199	119.128	1	.000	.113
	F	-.045	.017	6.764	1	.009	.956
	Constant	-7.423	.751	97.601	1	.000	.001
Step 5	Ti	-.090	.022	16.773	1	.000	.914
	Mg	.200	.040	25.186	1	.000	1.222
	K	-2.990	1.068	7.834	1	.005	.050
	Na	-2.065	.203	103.242	1	.000	.127
	F	-.054	.018	9.127	1	.003	.947
	Constant	-10.898	1.473	54.742	1	.000	.000

Table 3.19: Variables included in the model equation after performing a stepwise logistic regression.

3.5.4. Conclusions of statistical investigation

The most important conclusion of this statistical section is that the chemical composition of texturally primary and texturally secondary white micas from late-stage facies from the SMB can be discriminated at a multivariate level. Evidently, the overall rate of success is far from perfect (68.5-74.1%), and multivariate statistical treatment is by no means infallible. Nonetheless, the two different classification techniques show similar results:

1. The Al^{vi} and Fe components are not important in classifying white micas as primary or secondary. Both elements are dismissed from the stepwise discriminant function analysis and logistic regression and have low values in the structure matrix.
2. The order of variables used in both stepwise classifications is similar for the first three variables (Na, Mg, Ti) and inverts the two last variables taken into account (K and F).

The elimination of Al^{vi} and Fe from classifying white micas may be a consequence of the good correlation existing between those two elements (i.e., biotite and Tschermak substitutions). Both classifying statistical methods prefer non-correlated variables, so that the discriminating power of the variables is higher.

The five chemical elements of importance in classifying correctly the white micas are similar to those used in the literature: Ti, Na, and Mg (Miller et al. 1981, Monier et al. 1984); Ti (Zen 1988); and F (Villa et al. 1997). The classifications do not put forward which elements are higher or lower in texturally primary or texturally secondary white mica, but it is the combination of all five chemical elements that allow for discrimination. Also, the chemical classification probably suffers from the uncertainty surrounding the textural criteria for primary and secondary white micas. The misclassified samples may be ambiguous grains wrongly classified according to their texture.

To test the coefficients obtained with both discriminant function analysis and logistic regression, I used the chemical composition of white micas from the texturally primary samples (Section 3.4.3.1). All data are classified as texturally primary white micas.

In conclusion, the multivariate statistical tool does not offer perfect results in correctly classifying primary and secondary white micas based on their texture, but produces better results than simple bivariate plots.

Observed			Predicted		
			FACTOR		Percentage Correct
			0	1	
Step 1	FACTOR	0	236	96	71.1
		1	188	403	68.2
	Overall Percentage				69.2
Step 2	FACTOR	0	243	89	73.2
		1	170	421	71.2
	Overall Percentage				71.9
Step 3	FACTOR	0	247	85	74.4
		1	164	427	72.3
	Overall Percentage				73.0
Step 4	FACTOR	0	238	94	71.7
		1	171	420	71.1
	Overall Percentage				71.3
Step 5	FACTOR	0	246	86	74.1
		1	161	430	72.8
	Overall Percentage				73.2

The cut-off value is 0.6

Table 3.20: Classification table for primary (0) and secondary (1) white micas using a stepwise logistic regression technique.

3.6. Conclusions

Previously developed chemical criteria for distinguishing between texturally primary and texturally secondary white micas do not conclusively discriminate the white micas from the New Ross area, driving the search for new criteria particular to the SMB.

Among the usual substitutions taking place in white micas, three substitutions are present in texturally primary and texturally secondary white micas from granitoid rocks of the New Ross area: biotite, Tschermak, and paragonite substitutions. Chemical differences among white micas are linked to the bulk composition of the granitoid rock in which the white mica is present. White micas from host granitoid rocks show narrower ranges of biotite and Tschermak substitutions than their corresponding mineralised (aplite, pegmatite) and altered (greisen) rocks. Highly variable contents of K and Na illustrate the

strong mobility of the two alkali elements. Although better preserved in white micas from host granitoid rocks, even micas from those samples show evidence of alkali mobility and, with increasing alteration, alkali mobility also increases.

Unfortunately, most of what precedes is undermined by several exceptions not explicable using classical substitutions in white mica. Therefore, multivariate statistics were used in order to keep a maximum amount of information by including all chemical elements instead of the incomplete picture of binary plots. Five elements seem consistently important in chemically classifying texturally primary and texturally secondary white micas of the SMB: Na, Mg, Ti, K, and F. Still the highest discriminating percentage is ~ 75 %, which leaves a quarter of the data erroneously classified. A difficult to evaluate fraction of the wrongly classified data may probably be caused by incorrect textural determination. According to personal experience (and statistical results confirm this point), it seems easier to wrongly classify a texturally secondary white mica as primary than the other way around. Also, a secondary white mica replacing a primary white mica might not have changed its composition significantly.

In granites, although the texture of some white mica grains may appear primary, the chemistry of a white mica may significantly change with post-magmatic event (fluid circulation, alteration) without altering the "primary" textural appearance of the grain. Therefore, attempts to link texture to chemical composition are for the most unsuccessful. The problem may reside in the fact that, when going from a primary to a secondary white mica the three following cases are possible: 1) texture may change, but not chemical composition; 2) chemical composition may change, but not texture; and 3) both texture and chemical composition change. Using comparison with volcanic rocks helps distinguish the magmatic imprint recorded by the white mica grains from the late- to post-magmatic chemical disturbances.

For future studies on primary and texturally secondary white mica chemistry, trace element composition may provide more information and allow for easier and more accurate discrimination between different generations of white micas. Also, microprobe imaging techniques, not utilised for this study, would definitely be an asset in recognising the internal complexity of the chemistry of white micas.

The difficulty, indeed even unfeasibility, of definitely defining chemical criteria for primary and texturally secondary white micas, lies in the transitional character of the chemistry of that mineral: micas may be texturally black or white, but their chemistry encompasses many shades of grey.

CHAPTER 4

GEOCHRONOLOGY

4.1. Introduction

Numerous age determinations, using different isotopic systems such as U/Pb, $^{207}Pb/^{206}Pb$, $^{87}Rb/^{87}Sr$, and ^{40}K (or $^{40}Ar)/^{39}Ar$, already exist for the SMB and satellite plutons (Table 4.1; Fig. 4.1 and 4.2).

To assess the temporal relationship between the mineral deposits of the New Ross area and the SMB emplacement, as well as among mineral deposits, this study uses $^{40}Ar/^{39}Ar$ age spectrum and laserprobe studies on white micas and alkali feldspars, as well as the first age determination on mineralisation itself using $^{187}Re/^{187}Os$ on molybdenite. The $^{40}Ar/^{39}Ar$ age determinations constrain the cooling history through ~350°C ± 50°C for the white micas, and <200-250°C for the alkali feldspars, whereas the Re-Os age data give the time of crystallisation of molybdenite, i.e., the mineralisation event.

This chapter provides a summary of the different methodologies used for age determination. A compilation of previous geochronological studies within the MLT follows, as well as information about the dated samples. Presentation and interpretation of the ages obtained in this investigation end this chapter.

4.2. Methodology

4.2.1. $^{187}Re/^{187}Os$ dating method

4.2.1.1. Systematics

Rhenium belongs to Group VIIB of the Periodic Table with Mn and Tc, but chemically is more similar to Tc's neighbour, Mo, than to Tc (Attendorn and Bowen 1997). Osmium belongs to Group VIII of the Periodic Table with Fe and Ru. Crustal rocks have a high Re/Os ratio, not because of high Re contents, but because of the low concentration of Os (Attendorn and Bowen 1997).

The radioactive parent ^{187}Re decays to the daughter isotope ^{187}Os by β^- emission, with a decay constant of 1.666×10^{-11}/yr (Smoliar et al. 1996). The $^{187}Re/^{187}Os$ dating method is unique compared to other conventional dating methods, because both elements are siderophile and chalcophile and they preferentially partition into metal, sulfide, and oxide phases rather than into silicates (Geyh and Schleicher 1990). There are only small amounts of non-radiogenic Os in molybdenite, whereas that mineral is Re-enriched (Markey et al. 1998; Stein et al. 2001). Therefore, essentially all the ^{187}Os comes from the *in situ* decay of ^{187}Re (Geyh and Schleicher 1990; Stein et al. 2001). Both features (i.e., high Re/Os ratio and low amount of initial Os in molybdenite) allow for a simplified age equation:

$t = 1/\lambda \ln [1 + (^{187}Os^*/^{187}Re)]$,

where t is the age of the sample and λ the decay constant.

Rhenium and Osmium are quantitatively separated from one another using solvent extraction and anion chromatography techniques, respectively (Selby and Creaser, 2001b). Both element contents are separately measured using negative thermal ionisation mass spectrometry (Creaser et al. 1991).

Usually, Re-Os ages are older than U-Pb ages but within quoted uncertainty, and almost always older than Ar-Ar ages, usually outside of quoted uncertainty (R. Creaser, pers. comm. 2001). Nonetheless, Suzuki et al. (1996) suggested ~500°C as a rough estimation of the closure temperature of the Re-Os system for molybdenite. These authors stressed the inaccuracy of this temperature estimation as it was based on Re-Os ages with large errors. In the magmatic environment, in which the dated molybdenite samples used for this study crystallised, temperatures of crystallisation are of the order of 650°C (Carruzzo et al. 2000).

Grain size and the amount of molybdenite sample are the main criteria affecting the reproducibility and accuracy of Re-Os ages: finer-grained samples are more homogeneous and overcome the possible spatial decoupling of ^{187}Re and ^{187}Os within a molybdenite grain (Stein et al. 2001). The problem of spatial decoupling of ^{187}Re and ^{187}Os within a molybdenite grain rules out the analysis of parts of grains to provide a representative age, therefore, also precluding the use of laser ablation ICP-MS microanalysis (e.g., Suzuki et al. 2001). McCandless et al. (1993) proposed that infrared microscopy of molybdenite grains should be performed prior to any Re-Os dating, in order to detect increase of mineral

transparency following loss of Re during hydrothermal alteration. Selby and Creaser (2001b) showed that molybdenites from the Endako porphyry Mo deposit in British Columbia, Canada having variable transparencies yield comparable Re-Os ages, and concluded that no relationship exists between transparency and Re-Os ages, a result in agreement with Suzuki et al. (2000). Suzuki et al. (2000) experimentally demonstrated that Re-Os ages are not reproducible for molybdenite in hydrothermally altered samples, because of Re-Os fractionation induced by low salinity and low temperature (~ 180°C) alteration processes. On the other hand, Selby and Creaser (2001b) presented reproducible Re-Os ages for molybdenites that were in contact with low salinity hydrothermal fluids (1-5 wt % NaCl equiv.; Selby et al. 2000). Frei et al. (1998), Stein et al. (1998), Raith and Stein (2000), Torrealday et al. (2000), Selby and Creaser (2001a), Selby and Creaser (2001b), and Stein et al. (2001) have shown that the Re-Os chronometer remains undisturbed by high pressure-high temperature metamorphic events and/or intense deformation, even within Proterozoic and Archaean terranes with complex tectonic histories.

The Re-Os geochronometer applied to carefully sampled and prepared molybdenite samples seems robust and geologically reliable, and represents the only method to directly date sulphide mineralisation in a system in which the parent isotope substitutes directly for a major element of the sulphide structure (Stein et al. 2001). However, care should be taken when analysing hydrothermally altered samples (Suzuki et al. 2000).

4.2.1.2. Analytical method

Selby and Creaser (2001b) described the procedures for molybdenite sampling and measurement of Re and Os. The SMB samples were analysed in the Department of Earth and Atmospheric Sciences of the University of Alberta in Edmonton.

4.2.2. $^{40}Ar/^{39}Ar$ dating method

4.2.2.1. Systematics

McDougall and Harrison (1999) described the principles and method of $^{40}Ar/^{39}Ar$ dating in great detail and, except when otherwise mentioned, this Section is based on their work.

The $^{40}Ar/^{39}Ar$ method is based on the potassium-argon (K/Ar) dating method. The radioactive parent ^{40}K occurs in nature and decays to the daughter isotopes ^{40}Ca and ^{40}Ar. The decay of interest for $^{40}Ar/^{39}Ar$ dating is ^{40}K to ^{40}Ar with a decay constant of 4.962 x 10^{-10}/yr (Steiger and Jager 1977). Argon is a noble gas and is not structurally bound within the crystal structure of minerals, thus ^{40}Ar present in a mineral results either from the decay of ^{40}K or is externally derived (excess argon). Measurement of parent ^{40}K and daughter $^{40}Ar^*$ (radiogenic argon), coupled with the rate of decay from parent to daughter, permits the calculation of an age, representing the time since cooling through the blocking temperature of a given mineral.

For $^{40}Ar/^{39}Ar$ dating, the sample is first irradiated in a nuclear reactor (a 2 MW swimming pool type reactor located at McMaster University in Hamilton, Ontario) to transform some ^{39}K atoms into ^{39}Ar. It is then heated in an ultrahigh vacuum system, and the gas produced is analysed by a mass spectrometer (VG 3600) to obtain the $^{40}Ar^*/^{39}Ar$ ratio (both done at the Earth Sciences Department of Dalhousie University in Halifax). Knowing that the amount of ^{39}Ar is proportional to the amount of ^{39}K in the sample and that the ratio $^{39}K/^{40}K$ is a constant in nature, the amount of ^{39}Ar is proportional to the abundance of ^{40}K in the sample. The $^{40}Ar^*/^{39}Ar_K$ ($^{39}Ar_K$ is the ^{39}Ar produced from ^{39}K during irradiation) is thus proportional to the $^{40}Ar^*/^{40}K$ ratio in the sample, and is therefore proportional to the age.

The age equation is:

$$t = 1/\lambda \ln [1 + (J) * (^{40}Ar^*/^{39}Ar)],$$

where t is the age of the sample, λ the decay constant, and J a dimensionless irradiation parameter measuring the efficiency of conversion of ^{39}K to ^{39}Ar.

A standard sample of determined K-Ar age (MMHb-1 called McClure Mountain Hornblende having an age of 520 ± 2 Ma; Samson and Alexander 1987) is irradiated with the unknown sample in the reactor, and J is calculated using the following equation:

$$J = (\exp \lambda t) - 1/(^{40}Ar^*/^{39}Ar_K),$$

where t is the assumed age of the standard and the $^{40}Ar^*/^{39}Ar_K$ is the ratio measured in the gas extracted from the standard sample after irradiation.

4.2.2.2. $^{40}Ar/^{39}Ar$ step-heating method

One of the main advantages of $^{40}Ar/^{39}Ar$ dating compared to the conventional K-Ar method is that the argon can be extracted in a stepwise fashion by heating the sample to successively higher temperatures (Hanes 1991). For each step, an apparent age can be calculated, the result being an age spectrum (a diagram plotting the apparent $^{40}Ar/^{39}Ar$ age against the fraction of ^{39}Ar gas evolved), offering information on the thermal history of the sample (Hanes 1991; Reynolds 1992).

During cooling, there is a small temperature range (the closure temperature range) over which each mineral changes from being completely open, to being completely closed, to argon loss by diffusion (Hanes 1991). The closure temperature depends on factors such as cooling rate, mineral composition, effective radii of diffusion, and other diffusion parameters (e.g., activation energy for diffusion) (Dodson 1973; Hanes 1991). Therefore, for a slowly cooled rock, apparent ages from a variety of minerals may be different, providing clues about the cooling history of the rock (i.e., providing cooling ages). The two minerals of interest for this study are white mica and alkali feldspar. White mica has a closure temperature of ~350°C ± 50°C for moderate cooling rates (McDougall and Harrison 1999 and references therein). Alkali feldspar has a wider range of closure temperature (from 350°C to 125°C; Hanes 1991). Low closure temperatures may be a result of unmixing or exsolution in alkali feldspars equilibrating in the subsolidus region of the stability field, therefore making the mineral rather inhomogeneous and facilitating loss of argon (McDougall and Harrison 1999).

In an ideal closed system, the mineral containing ^{40}Ar is not reheated or thermally disturbed after cooling below its closure temperature. Therefore, the step heating analysis should yield a flat age spectrum (plateau age) (McDougall and Harrison 1999). Several workers have recommended a set of criteria for the identification of a plateau: e.g., minimum number of concordant age steps, minimum proportion of ^{39}Ar released, and/or whether the chosen steps need to be contiguous (McDougall and Harrison 1999 and references therein). The plateau definition used in this thesis follows the criteria of Fleck et al. (1977), i.e., contiguous gas fractions together representing more than 50% of the total ^{39}Ar released from the sample and no differences in age detected between any two fractions

belonging to the plateau at the 95% confidence level (i.e., 2σ). Prior to interpreting a spectrum, the following errors have to be assessed: uncertainty in J value (including the error in the age of the standard), error in the decay constant, and measuring error (step error). The error in the decay constant affects all ages similarly and can be ignored when making comparisons among argon data. Special care has to be taken when comparing ages from different isotopic systems, in which case all errors have to be included. In the present study, a plateau age is calculated as the ^{39}Ar-weighted mean of the steps comprising the plateau (McDougall and Harrison 1999).

With argon loss because of thermal event(s) or natural diffusion processes (especially in feldspars), spectra are not flat. Lovera et al. (1989, 1991) developed a multi-domain diffusion model for alkali feldspars. In their model, diffusion of argon is not controlled by the whole grain, but rather by microdomains having variable sizes. Domain size matters, because the closure temperature differs between large domains (higher temperature) and small domains (low temperature), thus explaining the large range of closure temperature for alkali feldspar (McDougall and Harrison 1999). Following this model, the low temperature part of a step heating analysis should show a disturbed pattern, because the argon measured at lower temperature comes from domains in the grains most susceptible to argon loss (i.e., small domains). With increasing temperature, progressively higher ^{40}Ar/^{39}Ar ratios represent the removal of argon from more and more retentive locations in the grain (i.e., larger domains) (Attendorn and Bowen 1997). The ^{40}Ar/^{39}Ar ratios may approach or even reach a plateau representing locations in the grain without any gas loss and, therefore, represent the time of closure of the largest domains (Attendorn and Bowen 1997).

Parsons et al. (1999) described microtextural features that might provide pathways for gas loss at temperatures as low as 70°C. They emphasised the role of fluids in changing the texture of alkali feldspars at any time during their cooling history and concluded that step-heating analysis of alkali feldspars cannot provide usable information on cooling history. Other workers do not share such negative views (Foland 1974, 1994; Lovera et al. 1989, 1991, 1997; Wartho et al. 1999). Here it is assumed that ^{40}Ar/^{39}Ar age spectra on alkali feldspars may provide useful constraints on the thermal history at temperatures below 350°C (McDougall and Harrison 1999).

4.2.2.3. Laserprobe $^{40}Ar/^{39}Ar$ method

Laserprobe $^{40}Ar/^{39}Ar$ analysis allows for the acquisition of age data from single small grains or parts of a grain. The laboratory at Dalhousie University is equipped with a Quantronix 117 Nd-YAG laser, operated in TEM_{00} mode (Fallon 1998). This laser can be used in either pulsed or continuous wave modes; the pulsed mode is preferred for melting parts of grains, whereas the continuous mode is more favourable for total fusion of a grain. The laser has a wavelength of 1064 nm (in the near infrared) and can be focused to a minimum diameter spot size of ~20 μm (McDougall and Harrison 1999). Important considerations in the use of laserprobes are: (1) the absorbance characteristics of a mineral (i.e., a transparent mineral does not couple as well as coloured or opaque minerals); and (2) the incident power density and stability of the laser beam (McDougall and Harrison 1999). Fallon (1998) described the detailed procedures used in the laboratory at Dalhousie University.

4.3. Previous geochronological work in the MLT

4.3.1. Introduction

Table 4.1 summarises the geochronological data available for the MLT by date of analysis, and Figures 4.1 and 4.2 display all data for the SMB and northeastern / southwestern plutons, respectively.

For the past forty years, numerous geochronological studies on granitic rocks from the MLT have appeared in the literature. Fairbairn et al. (1960), Lowdon (1960), Lowdon et al. (1963), Fairbairn et al. (1964), Reynolds et al. (1973), and Cormier and Smith (1973) provided the first ages for undifferentiated granitic phases of the MLT, using Rb-Sr or K-Ar methods on either whole rock and/or mineral separates. Ages obtained in these early studies range from ~240 to 420 Ma after recalculation of the ages by Keppie and Smith (1978) using revised half-life values (Steiger and Jager 1977). Cormier and Smith (1973) concluded that there were two different granitic sequences with different ages present: (i) monzogranite and leucomonzogranite 395 ± 15 and 373 ± 21 Ma, and (ii) leucogranite 336 ± 9, 338 ± 10, and 340 ± 23 Ma. However, ages below 360 Ma are not consistent with the

presence of Late Devonian-Carboniferous basins at this time, as previously discussed in Section 1.2.2.3. Cormier ran these samples again and obtained ages of ~ 375 Ma for both suites (D. J. Kontak pers. comm. 2002). Reynolds et al. (1981) provided K-Ar and $^{40}Ar/^{39}Ar$ ages for several granitic rocks of the MLT. Ages are better constrained and range from 351 to 380 Ma, but no systematic age variation emerged according to rock types.

4.3.2. Satellite plutons

4.3.2.1. Canso plutons, Liscomb Complex, and Musquodoboit Batholith

Hill (1991) reported U-Pb ages from monazite and zircon and Rb-Sr whole rock ages for granitic rocks of the Canso plutons. The U-Pb ages are 371 ± 2 Ma, 372 ± 1 Ma, and 370 ± 3 (monazite), and 378.5 ± 2 Ma (zircon), whereas the Rb-Sr isochron defined an age of 373 ± 24 Ma. Keppie and Krogh (1999) dated monazite and zircon from granitoid samples of the Canso plutons, using U-Pb isotopic analyses. They obtained monazite ages ranging between 371 ± 2 and 376 ± 2 Ma for four different granitic bodies in the area and interpreted those ages as being close to the intrusion age, using a closure temperature of ~650°C for monazite (blocking temperature of Parrish 1990).

Using $^{40}Ar/^{39}Ar$ dating of micas, Kontak et al. (1990a) obtained ages of 368 to 372 Ma for granitic lithologies from the Liscomb Complex. This result is in concordance with the generally accepted emplacement age of the SMB. Kontak and Reynolds (1994) conducted an $^{40}Ar/^{39}Ar$ study on micas from granodiorite and monzogranite from the Liscomb Complex and obtained plateau ages between 369 ± 3 Ma and 373 ± 3 Ma for white mica and between 367 ± 4 Ma and 368 ± 3 Ma for biotite. These authors noted the apparent rapid cooling of the Liscomb Complex (comprising gneisses, gabbros, and granites) through the 350-300°C-temperature interval.

Kontak et al. (1999) reported a $^{40}Ar/^{39}Ar$ plateau age of 368 ± 2 Ma for white micas from a mineralised vein of the Dunbrack deposit in the Musquodoboit Batholith. They also reported laserprobe analysis on white mica at ~370 Ma. They interpreted the ~ 370 Ma ages as the time of emplacement and associated hydrothermal activity of the mineralised dyke at the Dunbrack deposit, an age essentially identical to the age of the Musquodoboit Batholith determined by Keppie and Dallmeyer (1987).

Kontak et al. (1993) dated a monzogranite from the River Lake intrusion (north of the Musquodoboit Batholith) and obtained Ar/Ar plateau ages of 379 ± 2 Ma on biotite and 371.0 ± 2 on muscovite.

4.3.2.2. Wedgeport, Barrington Passage, Shelburne, and Port Mouton plutons

Cormier et al. (1988) dated monzogranite from the Wedgeport pluton using U-Pb isotopic analyses on zircon and Rb-Sr on whole rock and mineral separates (alkali feldspar, biotite, and quartz + plagioclase). U-Pb ages are concordant at 316 ± 5 Ma. The whole rock Rb-Sr age is 323 ± 12 Ma, whereas isochrons for individual minerals yield ages of 257 ± 8 Ma. These authors interpreted the older age as representing the intrusion time, whereas they believed the younger age to be evidence of a reheating event related to additional plutonism around 257 ± 8 Ma. The Wedgeport pluton was recently dated at 354 Ma, using U/Pb on zircon (D. Kontak, pers. comm. 2003).

Reynolds et al. (1987) dated rocks from two distinct areas (southwestern and eastern Nova Scotia) of the MLT using the $^{40}Ar/^{39}Ar$ method on micas, alkali feldspars, and hornblendes and fission tracks on apatites. They identified five different stages in the cooling history of the MLT: (i) minimum intrusive age for the Barrington Passage pluton based on $^{40}Ar/^{39}Ar$ on hornblende: 385 Ma; (ii) intrusive age for the Shelburne pluton based on $^{40}Ar/^{39}Ar$ on micas: ~370 Ma (SMB intrusive age); (iii) resetting of $^{40}Ar/^{39}Ar$ system in feldspars and some micas in southwestern Nova Scotia by a late thermal event: 300-320 Ma; (iv) record of a thermal event in $^{40}Ar/^{39}Ar$ system of feldspars from southwestern Nova Scotia: 220-230 Ma; and (v) final cooling of the MLT under 100°C using fission track age determination: ~180 Ma. Reynolds et al. (1987) emphasised that the northeastern area (New Ross and Halifax plutons) did not undergo the systematic resetting of $^{40}Ar/^{39}Ar$ system observed in the southwestern area at 300-320 Ma.

Keppie and Dallmeyer (1995) dated granitic rocks from the Barrington Passage pluton using the $^{40}Ar/^{39}Ar$ method on muscovite and obtained plateau ages ~320 ± 1.5 Ma. Integrating those ages with others from southwestern Nova Scotia, Keppie and Dallmeyer (1995) interpreted older ages (368-360 Ma) as cooling times through ~300°C and younger ages (350-260 Ma), such as those obtained for the Barrington Passage pluton, as a result of

Location (pluton when available)	Dated rock type	Dating method	Age (Ma)	Interpretation by author	References
SMB	undifferentiated granitic phases	Rb-Sr and K-Ar	240-420	age of granite emplacement	Fairbairn et al. 1964; Fairbairn et al. 1960; Lowdon 1960; Lowdon et al. 1963; Reynolds et al. 1973*
Halifax pluton	mgr, lmgr, lgr, gr	Rb-Sr	395±15 (mgr), 373±21 (lmgr), 336±9 (lgr)	significant age difference between early and late stage granitic rocks	Cormier and Smith 1973*
New Ross pluton			338±10 (lgr)		
Port Mouton pluton			340±23 (gr)		
New Ross pluton	gdr, lmgr, lgr	Rb-Sr	371-372±3 (gdr), 364-365±2 (lgr)		Clarke and Halliday 1980
West Dalhousie pluton			364±2 (lgr)		
New Ross pluton	greisen	$^{40}Ar/^{39}Ar$	376±10, 375±10 (Turner deposit)	greisenisation age	Farley 1978
Halifax pluton	gdr, mgr, lmgr, lgr	K-Ar, $^{40}Ar/^{39}Ar$	364-368 (gdr), 358-369 (lmgr)	-all ages ±8 Ma -no significant age difference between early and late stage granitic rocks (~ 367 Ma). -southwestern plutons yield younger apparent Ar ages (~300-320 Ma), that might reflect a thermotectonic event in the Late Carboniferous.	Reynolds et al. 1981
New Ross pluton			366-374 (lmgr), 361-376 (lgr)		
Davis Lake pluton			317-372 (gdr)		
Undifferentiated Stage I plutons			362-380 (gdr)		
Kinsac pluton			363-373 (lmgr)		
Musquodoboit batholith			362 (lmgr)		
Canso pluton			368 (lgr)		
Brenton pluton			314-328 (foliated gdr)		
Shelburne pluton			302-353 (gdr)		
Barrington Passage pluton			306-308 (gdr)		
Port Mouton pluton			297-300 (mgr)		
Wedgeport pluton			258 (gdr)		
Davis Lake pluton (EK)	greisenised mgr	$^{40}Ar/^{39}Ar$	295±5	age of the greisenisation process accompanying mineralisation (i.e., tectonothermal event)	Zentilli and Reynolds 1985

Table 4.1: Chronological summary of all geochronological data available for the MLT. gdr = granodiorite, mgr = monzogranite, lmgr = leucomonzogranite, lgr = leucogranite, gr = granite. * Ages recalculated by Keppie and Smith (1978) using revised half-life values.

Location (pluton when available)	Dated rock type	Dating method	Age (Ma)	Interpretation by author	References
New Ross pluton	lmgr, lgr	Rb-Sr	332±10 (Long Lake deposit), 270±14 (Westfield deposit), 281±5 (Lake Darling deposit)	evidence for Carboniferous magmatism and mineralisation	O'Reilly et al. 1985
Barrington Passage pluton	tonalite	$^{40}Ar/^{39}Ar$	350-372±3	resetting of the Ar isotopic system in the southwestern part of the MLT	Reynolds et al. 1987
Bald Mountain pluton	mgr		365 to 370±2		
Port Mouton pluton	tonalite, mgr		318 to 343±2		
Shelburne pluton	mgr		337 to 361±2		
Wedgeport pluton	mgr	U-Pb, Rb-Sr	316±5 (U-Pb), 323±12 (w.r. Rb-Sr), 257±8(m.s. Rb-Sr)	-older age = intrusion age -younger age = resetting because of reheating event	Cormier et al. 1988
New Ross and West Dalhousie plutons	mgr, lmgr	U-Pb, Rb-Sr	374±2, 371±2 (U-Pb), 371±5, 370±6 (Rb-Sr)	crystallisation ages	Harper 1988
Liscomb Complex	gdr, mgr	$^{40}Ar/^{39}Ar$	368-372	crystallisation ages	Kontak et al. 1990
Davis Lake pluton	lgr	Rb-Sr, $^{40}Ar/^{39}Ar$	344±5 (Rb-Sr), 338±2 ($^{40}Ar/^{39}Ar$)	-minimum age of mineralisation -wide range and discordance in $^{40}Ar/^{39}Ar$ spectra = reheating event	Kontak and Cormier 1991
Canso plutons	tonalite	U-Pb, Rb-Sr	371±2, 372±1, and 370±3 (U-Pb monazite), 378.5±2 (U-Pb zircon), 373±24 (Rb-Sr)	crystallisation ages	Hill 1991
SMB	gdr, lgr	Pb-Pb	373±3.5, 365±5.5	crystallisation age	Chatterjee and Ham 1991
Davis Lake pluton	greisen, lgr	Pb-Pb	366±3 (greisen), 366±6 (greisen, lgr)	mineralisation and crystallisation age	Chatterjee and MacDonald 1991
Davis Lake pluton	lgr, greisen	$^{207}Pb/^{206}Pb$, U-Pb	366±4 ($^{207}Pb/^{206}Pb$), 367±10 (U-Pb)	crystallisation and mineralisation age	Kontak and Chatterjee 1992

Table 4.1: continued.

Location (pluton when available)	Dated rock type	Dating method	Age (Ma)	Interpretation by author	References
Halifax pluton	lgr	$^{40}Ar/^{39}Ar$	369±2 to 375±4	crystallisation age	Clarke et al. 1993
New Ross pluton					
Scrag Lake pluton					
East Dalhousie pluton					
Salmontail Lake pluton (Millet Brook deposit)	gdr, lmgr	$^{40}Ar/^{39}Ar$, U-Pb	377±4 (U-Pb gdr), 366 to 376±6 ($^{40}Ar/^{39}Ar$ lmgr)	-crystallisation age	Keppie et al. 1993
Little Round Lake pluton (Westfield deposit)	lmgr		381 to 385±2 (U-Pb), 368±6 ($^{40}Ar/^{39}Ar$)	-older age = crystallisation age -younger age = time at closure temperature of white mica	
Liscomb Complex	gdr, mgr	$^{40}Ar/^{39}Ar$	369±3 to 373±4	cooling age at temperature 300-350°C	Kontak and Reynolds 1994
Barrington Passage pluton	undetermined	$^{40}Ar/^{39}Ar$	320±1	-~360 Ma = cooling age at temperature 300-350°C -~350-260 Ma = resetting of isotopic system	Keppie and Dallmeyer 1995
SMB (undifferentiated plutons)			338-361±1		
Port Mouton pluton			340±1		
Davis Lake pluton	lgr	Pb-Pb	367±3.5	crystallisation age	Dostal and Chatterjee 1995
Port Mouton pluton Shelburne pluton	tonalite, gdr	U-Pb	368±1 (gdr), 378±3 (ton) 373±1 (gdr)	crystallisation age	Currie et al. 1998
Canso plutons	gdr, mgr	U-Pb	370±3	intrusion ages	Keppie and Krogh 1999
Shelburne pluton			372±3		
Barrington Passage pluton			373±2		
Musquodoboit Batholith (Dunbrack deposit)	qz-musc vein	$^{40}Ar/^{39}Ar$	368±3 (plateau), 361-372 (laser)		Kontak et al. 1999
Port Mouton	tonalite, mgr	U-Pb	373±1	crystallisation age	Clarke et al. 2000
Port Mouton	tonalite, mgr	$^{40}Ar/^{39}Ar$	359±2, 349±2 (spectra) 373-310 range (laser)	373 = crystallisation age, younger ages = resetting	Fallon et al. 2001

Table 4.1: continued.

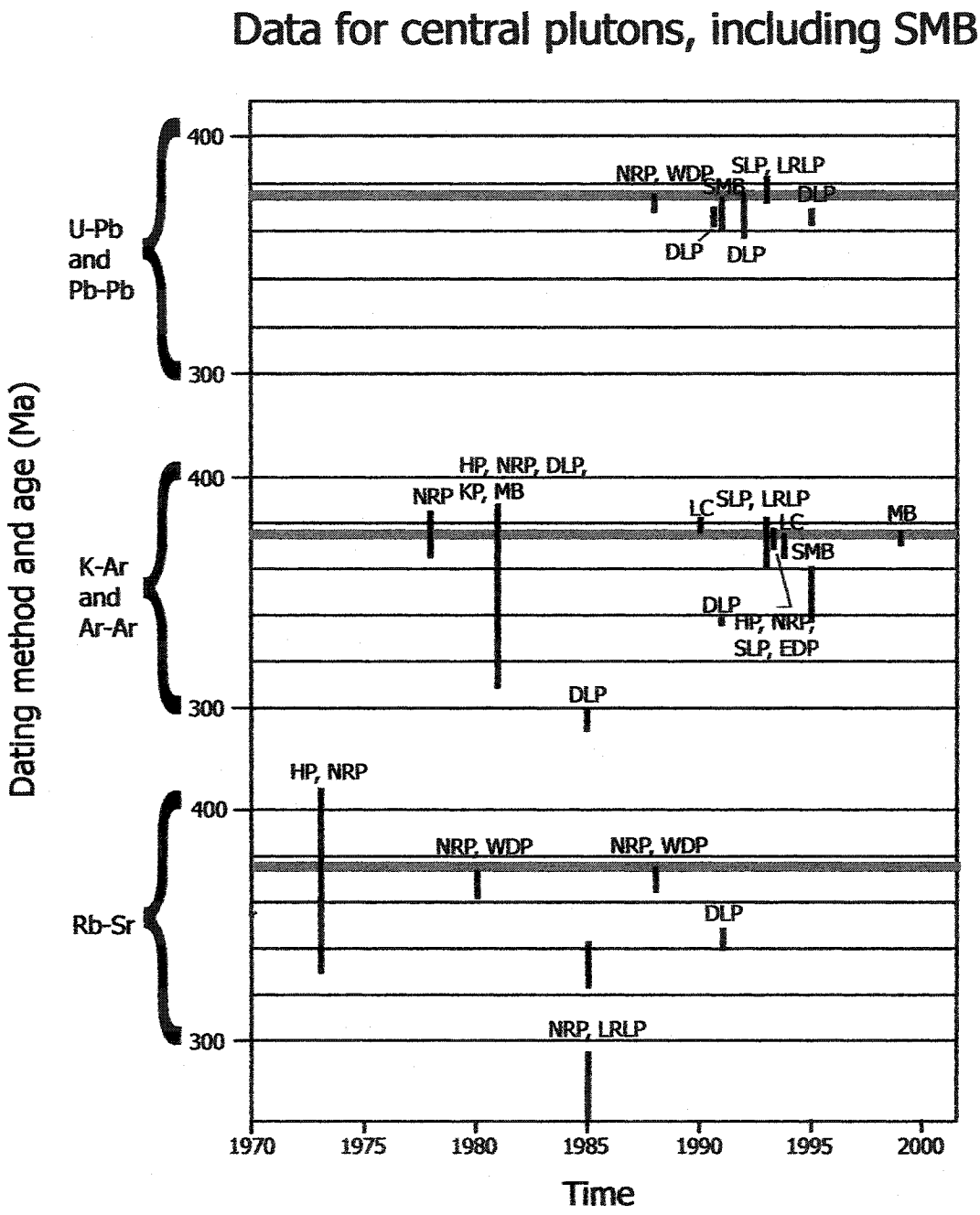

Figure 4.1: Geochronological data for the SMB using U-Pb, Pb-Pb, K-Ar, Ar-Ar, and Rb-Sr methodologies. NRP = New Ross pluton; WDP = West Dalhousie pluton; DLP = Davis Lake pluton; SLP = Salmontail Lake pluton; LRLP = Little Round Lake pluton; HP = Halifax pluton; KP = Kejimkujik pluton; MB = Musquodoboit Batholith; LC = Liscomb Complex; EDP = East Dalhousie pluton. Red line represents the best estimate of the SMB age (375 Ma). Data include error.

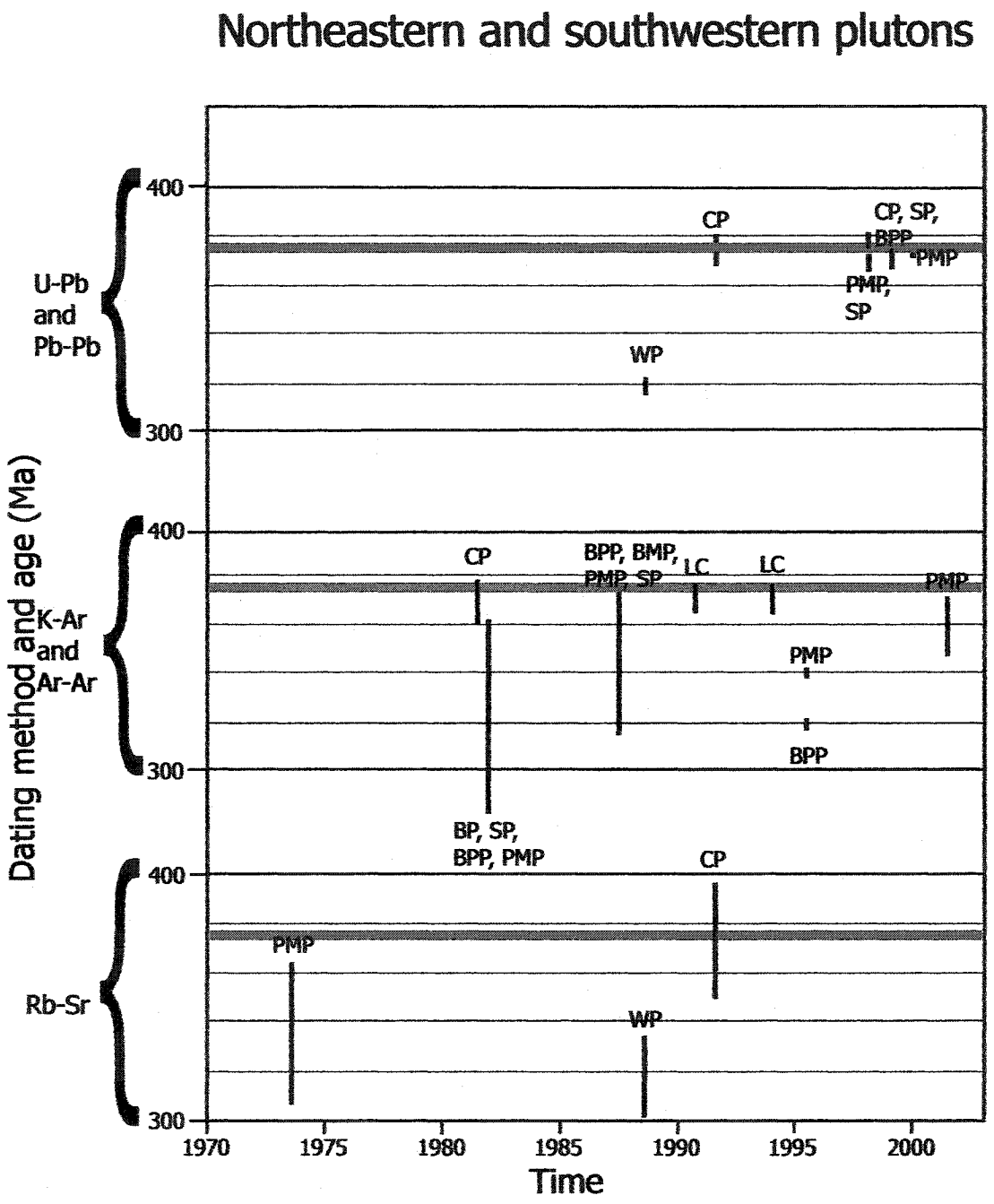

Figure 4.2: Geochronological data for satellite plutons of the MLT using U-Pb, Pb-Pb, K-Ar, Ar-Ar, and Rb-Sr methodologies. WP = Wedgport pluton; CP = Canso pluton; SP = Shelburne pluton; PMP = Port Mouton pluton; BMP = Bold Mountain pluton; BPP = Barrington Passage pluton. Red line represents the best estimate of the SMB age (375 Ma). Data include error.

partial or total resetting of isotopic systems as a consequence of burial under Carboniferous sediments and possibly fluid circulation. Currie et al. (1998) reported U-Pb monazite ages of 373 ± 1 Ma for a granodiorite from the Shelburne pluton. Keppie and Krogh (1999) dated monazite and zircon from the same plutons, using U-Pb isotopic analyses. They obtained a similar age of 372 ± 2 Ma for both plutons. Currie et al. (1998) and Keppie and Krogh (1999) interpreted these ages as the crystallisation times for both southwestern plutons. Dallmeyer and Keppie (1988) proposed a thermal event ~290-315 Ma in southwestern Nova Scotia using $^{40}Ar/^{39}Ar$ age data for micas from the contact aureole around the Shelburne and Barrington Passage plutons.

Keppie and Dallmeyer (1995) dated a granitic sample from the Port Mouton pluton using the $^{40}Ar/^{39}Ar$ method on muscovite and obtained a plateau age of 340 ± 1 Ma. These authors interpreted that age as being the result of resetting of the isotopic system. Currie et al. (1998) reported U-Pb monazite ages of 378 ± 3 Ma for a tonalite and 368 ± 1 Ma for a granodiorite from the Port Mouton pluton. They interpreted these ages as showing a crystallisation age difference between older mafic and younger felsic parts of the pluton. Clarke et al. (2000) used the U-Pb method on monazite from tonalite and monzogranite from the Port Mouton pluton. They obtained a well constrained age of 373 ± 1 Ma and interpreted it as the crystallisation age of the Port Mouton pluton. Fallon et al. (2001) used $^{40}Ar/^{39}Ar$ age spectrum and laserprobe data on white micas from tonalite and monzogranite from the Port Mouton pluton. They obtained spectrum ages between 349 and 359 ± 2 Ma, whereas laserprobe data ranged from ~310 Ma to ~373 Ma with grain cores consistently older than rims. Fallon et al. (2001) concluded that the oldest laserprobe data represent cooling ages, whereas younger ages appearing in age spectra are an average of age variation within a single grain and therefore have no geochronological meaning.

4.3.3. SMB

4.3.3.1. SMB eastern area

Farley (1978) dated two greisen samples from the Turner deposit using $^{40}Ar/^{39}Ar$ stepwise heating on white mica separates. She obtained plateau ages of 376 ± 10 and 375 ± 10 Ma and interpreted them as dating the greisenisation event.

Clarke and Halliday (1980) constructed Rb-Sr isochrons from whole rocks and mineral separates of granodiorite (372 ± 2 Ma), leucomonzogranite (364 ± 1 Ma), and porphyry (361 ± 1 Ma). Their dates show similar variations, from least to most evolved phases of the SMB, as those described by Cormier and Smith (1973). This is the first time a 372 Ma age was obtained and this age is still currently considered as representing the age of emplacement of the SMB.

O'Reilly et al. (1985) used the Rb-Sr method to date leucomonzogranite and leucogranite associated to three mineral occurrences in the New Ross area. They obtained younger ages (332 ± 10 for Long Lake, 270 ± 14 for Westfield, and 281 ± 5 for Lake Darling) than the ages determined by Reynolds et al. (1981) and interpreted them as evidence for a Carboniferous magmatism and mineralisation.

Harper (1988) used U-Pb on monazite and Rb-Sr on whole rock and mineral separates for monzogranites and leucomonzogranites of the New Ross area. He obtained a U-Pb age of 374 ± 2 Ma and a Rb-Sr age of 371 ± 5 Ma for monzogranites, and a U-Pb age of 373 ± 2 Ma and a Rb-Sr age of 370 ± 6 Ma for leucomonzogranites. Harper (1988) interpreted these ages as crystallisation times of the granite.

Chatterjee and Ham (1991) obtained whole rock Pb-Pb isochron ages of 373 ± 3.5 Ma and 365 ± 5.5 Ma for a granodiorite and a leucogranite from the SMB, respectively.

Clarke et al. (1993b) determined $^{40}Ar/^{39}Ar$ ages on white micas for several leucogranitic bodies from the eastern part of the SMB and obtained plateau values between 369 ± 2 Ma and 375 ± 4 Ma. Such ages are concordant with those of less evolved phases of the SMB and thus suggest rapid crystallisation and cooling of the batholith.

Keppie et al. (1993) obtained ages for granodiorite and leucomonzogranite hosting the Millet Brook uranium deposit and leucomonzogranite from the Westfield tungsten deposit using U-Pb for monazite and zircon and $^{40}Ar/^{39}Ar$ for white mica. The granodiorite from Millet Brook yielded a 377 ± 4 Ma U-Pb monazite age, whereas $^{40}Ar/^{39}Ar$ plateau ages for white micas from leucomonzogranites ranged between 366 ± 5 Ma and 376 ± 6 Ma. The leucomonzogranite from Westfield generated a 385 ± 2 Ma U-Pb zircon age and a 368 ± 6 Ma $^{40}Ar/^{39}Ar$ age. Keppie et al. (1993) interpreted the U-Pb ages as crystallization ages, and the $^{40}Ar/^{39}Ar$ ages as cooling times through temperature ~375-400°C (note that

the closure temperature of white micas has since been re-evaluated at ~300-350°C; McDougall and Harrison 1999).

Chatterjee and Dostal (1995) constructed whole rock and mineral Pb-Pb isochrons for granodiorite and leucogranite from the SMB and obtained ages ranging between 367 ± 4 Ma and 385 ± 17 Ma. These authors interpreted these ages as essentially similar to those obtained throughout the SMB using other radiogenic systems.

4.3.3.2. SMB western area

Using the $^{40}Ar/^{39}Ar$ method, Zentilli and Reynolds (1985) obtained an alteration (greisenisation) age of 295 ± 5 Ma for the East Kemptville tin deposit (belonging to the Davis Lake pluton in southwestern Nova Scotia), contrasting with the 317-372 Ma age determined by Reynolds et al. (1981) for other parts of the Davis Lake pluton. Richardson et al. (1988, 1989) published two errorchrons at 330 ± 7 Ma for whole rock samples from the Davis Lake pluton reflecting resetting of the Rb-Sr isotopic system. Chatterjee and MacDonald (1991) obtained a Pb/Pb age of 367 ± 4 Ma for whole rock samples from the Davis Lake pluton and concluded that that age represents the time of crystallisation of the pluton. Chatterjee and Cormier (1991) obtained a Rb/Sr age of 375 ± 3 Ma on whole rock from the Davis Lake pluton and interpreted that age as being the crystallisation age for the pluton. Kontak and Cormier (1991) obtained Rb-Sr data from both whole rock and mineral separates (white mica, plagioclase, and alkali feldspar) and $^{40}Ar/^{39}Ar$ spectra on white mica from leucogranites of the East Kemptville tin deposit. They deduced a minimum mineralisation age of 344 ± 5 Ma (Rb-Sr isochron) supported by $^{40}Ar/^{39}Ar$ ages for white micas of 338 ± 2 Ma. Kontak and Cormier (1991) attributed the wide range of ages (361-311 Ma obtained using both of the above methods), as representing re-equilibration of Sr isotopes, and discordant $^{40}Ar/^{39}Ar$ spectra as evidence of reheating events in southwestern Nova Scotia. Using Pb isotopic data for whole rocks and mineral separates from leucogranite and mineralised greisen, Kontak and Chatterjee (1992) estimated the time of magmatic and hydrothermal events at the East Kemptville tin deposit to be 366 ± 4 Ma. Kontak et al. (1995) emphasised the difference in $^{40}Ar/^{39}Ar$ age spectra for muscovite of the East Kemptville Sn deposit, and suggested that this phenomenon reflects argon diffusivity within muscovite grains, because of the concentration of hot fluids in the fault

zone hosting the deposit. Keppie et al. (1993) obtained an U/Pb age of 385 ± 2 Ma for zircon from the Westfield area in the Little Round Lake pluton.

4.3.4. Discussion of previous age data in the MLT

The Lower Devonian Torbrook Formation [Lochkovian to Lower Emsian, i.e., 418 to ~409 Ma or slightly younger, using time scale of Tucker et al. (1998)] is the youngest exposed formation intruded by the SMB, and provides its maximum age. Also, the SMB emplacement is late- to post-deformation (Section 1.2.2.4) relative to the Acadian orogeny [main phase of deformation (isoclinal folding) of Meguma Supergroup between 410 and 385 Ma; Keppie and Dallmeyer 1987; Muecke et al. 1988; Hicks et al. 1999]. Clastic sediments and marine carbonates of the Horton and Windsor Groups, respectively, unconformably overlie the SMB. Miospores of Late Devonian age (Late Famennian) in the basal part of the Horton Group provide a minimum age of ca. 360 Ma [time scale of Tucker et al. (1998)] for exhumation of the NE part of the SMB (Martel et al. 1993; Martel and Gibling 1996).

Rb-Sr ages are scattered between ~250 and >400 Ma, with two clusters of data, one around 290 Ma and the other around 370 Ma (Fig. 4.3a). Several younger ages (i.e., younger than ~ 370 Ma) may be the result of fluid-rock interaction (Kontak and Cormier 1991) or resetting of the isotopic system as a consequence of a reheating event (Cormier et al. 1988) and, therefore, do not represent either a significant difference in age between early and late stage granitic rocks (Cormier and Smith 1973; Clarke and Halliday 1980) or a Carboniferous magmatism (O'Reilly et al. 1985).

Most of the ages obtained using the U-Pb method on monazite or zircon (or Pb-Pb on whole rocks) cluster narrowly around 375 Ma for both the SMB (Fig. 4.3c) (Keppie et al. 1993; Harper 1988) and satellite plutons (Hill 1991; Currie et al. 1998; Keppie and Krogh 1999; Clarke et al. 2000). Based on available data and with the exception of a young age for the Wedgeport pluton reported by Cormier et al. (1988), the U-Pb isotopic system, unlike the Rb-Sr and K-Ar systems, was not affected by ca. 300 Ma tectonothermal or fluid interaction events in the southwestern part of the MLT.

Age determinations using K-Ar or $^{40}Ar/^{39}Ar$ methods yield a large cluster around 370 Ma and a smaller group of data around 300-325 Ma (Fig. 4.3b). All rock types (from

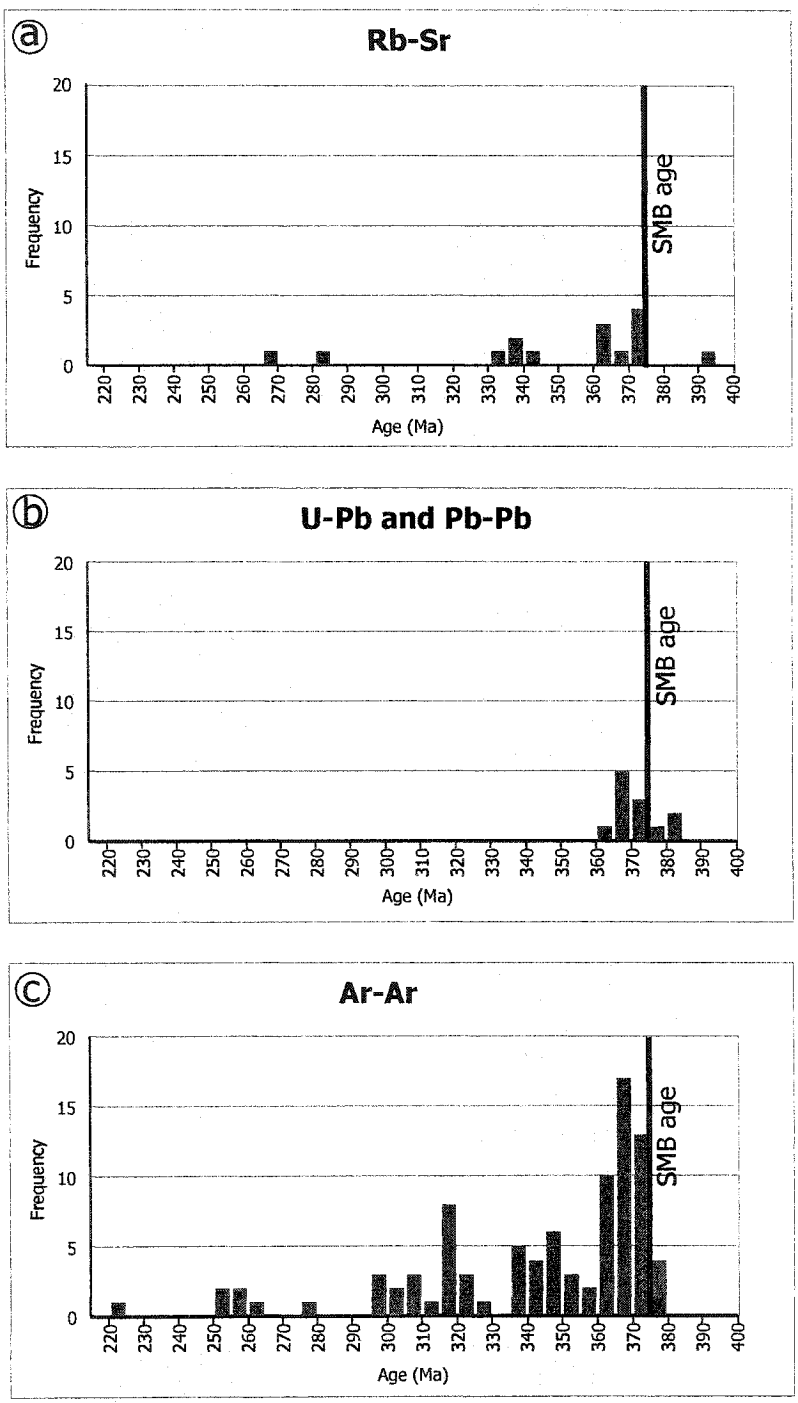

Figure 4.3: Histograms of all available ages for granitoid rocks of the MLT, classified by age determination method: (a) Rb-Sr, (b) U-Pb and Pb-Pb, and (c) Ar-Ar. In black, best estimate of the SMB age (375 Ma).

granodiorite to leucogranite) composing the SMB cooled through temperatures of ~300-350°C at about 370 Ma (Reynolds et al. 1981; Clarke et al. 1993b; Keppie et al. 1993). Undisturbed K-Ar or $^{40}Ar/^{39}Ar$ ages are systematically younger than those obtained using U-Pb, reflecting the lower closure temperature of the former isotopic system. Younger K-Ar or $^{40}Ar/^{39}Ar$ ages appear mainly in the southwestern part of the MLT and appear to be the consequence of the resetting of ages following a reheating event associated with the Alleghanian deformation in that part of the terrane around 320 Ma (Reynolds et al. 1981; Zentilli and Reynolds 1985; Reynolds et al. 1987; Kontak and Cormier 1991; Keppie and Dallmeyer 1995; Fallon et al. 2001).

4.4. Sampling

4.4.1. Sample selection

I dated samples from six mineral deposits of the New Ross area (Table 4.2). For aplite/pegmatite and greisen mineralisation, I chose samples of white micas for $^{40}Ar/^{39}Ar$ work on white micas based on their potential to yield either fluido-magmatic event ages (pegmatite and aplite) or alteration ages (greisen). Chemically, white micas from greisen samples at Long Lake and Keddy show a larger extent of biotitic and Tschermak substitution than white micas from least altered host granitoid rocks, pegmatite, and elvan; therefore, the greisen samples may record a later hydrothermal history than least altered host granitoid rocks, pegmatite, and elvan (Section 3.4.4.4). I chose to date mineralised and/or altered and barren and/or unaltered samples from the vein deposits to verify if an age discrepancy exists among them. Because of the scarcity of white micas in the vein deposits, and to gather further information about lower temperature events, I also dated alkali feldspars. To compare ages, I decided to date alkali feldspars from aplite/pegmatite deposits. I also dated a reference sample from the Halifax pluton (i.e., away from the New Ross area), with which to compare our alkali feldspar data. Appendix C contains tables presenting all Ar/Ar data illustrated graphically in the following Sections.

I dated two molybdenite-bearing pegmatites (from the Walker and Long Lake deposits) using $^{187}Re/^{187}Os$ to obtain direct information on the age of the mineralising event that accompanied the formation of each pegmatite. A molybdenite-bearing pegmatite

Deposits	Sample #	Rock type	Dating methods		
			$^{40}Ar/^{39}Ar$ spectrum	$^{40}Ar/^{39}Ar$ laserprobe	$^{187}Re/^{187}Os$
Walker	WAM, WB	aplite	Y (wm)	Y (wm)	N
	SC-9, 15, 20-W	pegmatite	Y (Kspar)	Y (wm and Kspar)	Y (SC-15/21-W)
Long Lake	SC-13-L	aplite	N	N	Y
	SC-12-L	pegmatite	Y (Kspar)	Y (wm and Kspar)	Y
	SC-5-L, LL2, LL3, A9B-7558	greisen	Y (wm)	Y (wm)	N
	SW-LL01, A9b-7504	microcline along fracture in greisen	Y (Kspar in A9B-7504)	Y (Kspar in both)	N
Keddy	SC-5-K	greisen	N	Y (wm)	N
Turner	SC-2-T	greisen	N	Y (wm)	N
	SC-14-T, S1	elvan (pink facies)	N	Y (wm)	N
	S2	elvan (green facies)	N	Y (wm)	N
Millet Brook	SC-3-MB	mineralised mgr	N	Y (wm)	N
	DK-MB-99-01	mineralised mgr	Y (Kspar)	Y (wm and Kspar)	N
	DK-MB-99-05	barren mgr	Y (Kspar)	N	N
Mn mines	DC-86-3 847	hematised mgr	Y (Kspar)	N	N
	SC-1-D	episyenite	N	Y (wm)	N
	DC-85-3 217	barren mgr	Y (Kspar)	N	N
	DC-1406	hematised lgr	Y (Kspar)	N	N
	DC dump	breccia with altered mgr pieces	Y (Kspar)	N	N
	SC-11-D	elvan	N	Y (wm)	N
Halifax pluton	NS-86-3	gdr	Y (Kspar)	N	N

Table 4.2: Samples used for geochronological investigation. Y = dated samples, N = undated samples, wm = white mica, Kspar = K-feldspar, gdr = granodiorite, mgr = monzogranite, lgr = leucogranite.

Sample No.	Sample wt. (mg)	Total Re (ppm)	^{187}Re (ppm)	^{187}Os (ppb)	Re-Os Date (Ma)	Relative error	Absolute error
SC-13-L-1	10.0	6.709 ± 0.034	4.217 ± 0.021	26.46 ± 0.12	375.40	± 1.54	± 2.78
SC-13-L-2	10.5	6.741 ± 0.033	4.237 ± 0.021	26.08 ± 0.12	368.27	± 1.51	± 2.74
SC-13-L-3	21.1	6.703 ± 0.024	4.213 ± 0.015	26.11 ± 0.07	370.84	± 1.41	± 2.7
SC-13-L-4	20.2	6.593 ± 0.023	4.144 ± 0.014	25.69 ± 0.07	371.09	± 1.42	± 2.7
SC-13-L-5	20.2	6.775 ± 0.024	4.258 ± 0.015	26.39 ± 0.07	370.84	± 1.44	± 2.71
SC-13-L-6	29.8	6.380 ± 0.022	4.276 ± 0.014	26.50 ± 0.06	370.85	± 1.39	± 2.69
SC-13-L-7	30.1	6.731 ± 0.022	4.230 ± 0.014	26.33 ± 0.06	372.44	± 1.40	± 2.7
SC-12-L-1	10	6.300 ± 0.038	3.960 ± 0.019	25.07 ± 0.11	378.79	±1.58	±2.8
SC-12-L-2	30	6.339 ± 0.019	3.985 ± 0.012	25.15 ± 0.06	377.61	±1.38	±2.72
SC-15-W-1	100.1	2.383 ± 0.008	1.498 ± 0.005	9.297 ± 0.02	371.49	± 1.56	± 2.78
SC-15-W-2	49.6	2.382 ± 0.009	1.497 ± 0.006	9.284 ± 0.03	370.99	± 1.93	± 3
SC-15-W-3	21.5	2.355 ± 0.010	1.480 ± 0.006	9.144 ± 0.03	369.66	± 1.82	± 2.93
SC-20-W-1	10.9	0.712 ± 0.004	0.447 ± 0.003	2.811 ± 0.02	375.78	± 2.39	± 3.3
SC-20-W-2	10.7	0.786 ± 0.006	0.494 ± 0.004	2.962 ± 0.02	358.55	± 3.49	± 4.15
SC-20-W-3	21.4	0.743 ± 0.005	0.467 ± 0.003	3.469 ± 0.02	444.30	± 4.15	± 4.99
SC-20-W-4	20.1	0.739 ± 0.005	0.465 ± 0.003	2.969 ± 0.02	381.24	± 3.59	± 4.32
SC-20-W-5	29.4	0.791 ± 0.004	0.497 ± 0.002	3.194 ± 0.02	383.60	± 2.61	± 3.54
SC-20-W-6	21.4	0.830 ± 0.004	0.521 ± 0.003	3.169 ± 0.02	363.48	± 2.51	± 3.38
SC-20-W-7	49.10	0.536 ± 0.003	0.337 ± 0.002	1.861 ± 0.01	330.83	± 2.12	± 2.95
SC-20-W-8	52.18	0.698 ± 0.003	0.439 ± 0.002	1.932 ± 0.01	263.46	± 1.69	± 2.35
SC-20-W-X-A	5.0	0.607 ± 0.010	0.382 ± 0.006	2.806 ± 0.05	439.80	± 9.28	± 9.71
SC20-W-X-B1	29.2	0.581 ± 0.003	0.645 ± 0.002	2.345 ± 0.01	384.41	± 2.63	± 3.56
SC-20-W-X-B2	20.9	0.555 ± 0.005	0.349 ± 0.003	2.229 ± 0.02	382.01	± 4.47	± 5.07
SC-20-W-X-B3	17.8	0.413 ± 0.004	0.259 ± 0.003	1.752 ± 0.02	403.93	± 5.38	± 5.95
SC-20-W-X-B4	24.1	0.624 ± 0.004	0.392 ± 0.003	2.513 ± 0.02	383.47	± 3.60	± 4.33
SC-20-W-X-C*	~32	0.657 ± 0.005	0.413 ± 0.003	3.380 ± 0.02	489.08	± 4.70	± 5.61

Table 4.3: Summary of Re-Os age determinations for four samples from Long Lake and Walker. Relative error includes all causes of analytical uncertainties, and absolute error also includes error on the decay constant, allowing for comparison between Re-Os ages and ages obtained using other isotopic systems. Standard deviation is 2σ. Age calculated using the decay constant $\lambda^{187}Re = 1.666 \times 10^{-11} y^{-1}$ (Smoliar et al. 1996). SC-20-W-X-A, B, and C are analysed single grains and B1-4 are one grain cut into four.

sample from the East Kemptville area was also dated (D. J. Kontak, pers. comm. 2002), to provide a regional $^{187}Re/^{187}Os$ age comparison.

Table 4.2 provides a list of samples used for age determination and of the methods utilized. For detailed descriptions of the samples, refer to Chapter 2.

4.4.2. Sample preparation for Ar-Ar work

All samples were crushed for a few seconds in a rock crusher and a disk mill, with the exception of coarse-grained pegmatites that were crushed with a rock hammer. I removed the finest fraction (i.e., dust) by suspension in water and air-dried the remainder. I sieved the crushed rock to remove the fraction <0.5 mm. Using a binocular microscope, I handpicked both white micas and alkali feldspars. The size of all picked minerals ranged between 0.5 and 2 mm, with the exception of grains from pegmatites (SC-12-L and A9B-7558) ranging between 0.5 and 6 mm. White mica grains were for the most part subhedral to euhedral, but in some cases, only grain fragments were available. Dated alkali feldspars were fragments of larger grains for pegmatite samples, whereas subhedral to euhedral grains could be obtained for finer-grained samples. I then cleaned all picked minerals in an ultrasonic bath of distilled water and rinsed them in acetone. Finally, I verified the quality of picked minerals under a binocular microscope before sending the samples to be irradiated.

Alkali feldspar grains for laserprobe analysis were carefully removed from each sample and broken into 0.5-1 mm fragments. Core and rim fragments were kept separate to detect potential age variation between them (Warren 2001).

4.5. $^{187}Re/^{187}Os$ results

4.5.1. Data description

We dated four molybdenite-bearing samples from the Long Lake and Walker deposits, using $^{187}Re/^{187}Os$ methodology. Table 4.3 contains sample weight, total Re, ^{187}Re and ^{187}Os concentrations, and Re-Os dates for molybdenite. Two types of errors are given: (a) the relative error includes all known causes of analytical uncertainty (such as in mass

spectrometer, spike calibration, and standard Re and Os isotope composition) and is appropriate for the relative comparison of various $^{187}Re/^{187}Os$ age data; and (b) the absolute error includes in addition the uncertainty in decay constant, and is appropriate for the comparison of $^{187}Re/^{187}Os$ ages to those from other isotopic systems.

4.5.1.1. Long Lake

The Re-Os ages for molybdenite (grain size 0.5 cm) from an aplite at the Long Lake (SC-13-L) deposit range between 375±1.5 Ma and 368±1.5 Ma. The mean age is 371 ± 4.3 Ma. From seven age determinations for this sample, the five that were completed with more than 20 mg of molybdenite show a mean age of 371±1.4 Ma, whereas the two runs completed with ~10 mg of molybdenite give distinctly different ages far from the mean. Heterogeneity of Re and Os distribution within the molybdenite sample appears to explain such discrepancy in the ages (D. Selby, pers. comm. 2002). The reproducibility of the ages for samples larger than ~20 mg suggests that the heterogeneity disappears with a larger size grain of ~20 mg for molybdenite grains of ~0.5 cm in size. On the other hand, true age variations within a sample may be eliminated by analysing larger samples; therefore the mean value calculated here would be of limited significance.

Two Re-Os age determinations for a pegmatite (SC-12-L) associated with the aplite (SC-13-L) provide older ages: 379±1.5 Ma and 378±1.5 Ma, values in close agreement with each other, although different amounts of molybdenite (10 and 30 mg, respectively) were used. Therefore, molybdenite from SC-12-L does not appear to have a heterogeneous distribution of Re and Os throughout the grains, as sample SC-13-L does.

4.5.1.2. Walker deposit

Three Re-Os ages on molybdenite from a pegmatite at the Walker deposit (SC-15-W) are narrowly distributed between 369.6±2 Ma and 371.5±1.5 Ma, with a mean age of 370.7±2 Ma. Different amounts of sample (between ~20 and 100 mg) do not appear to affect the ages, as previously noted for an aplite samples at Long Lake.

Selby et al. (in press) reported an experiment to investigate the role of sample size and Re content on age variation using molybdenite from a pegmatite sample from the Walker deposit (SC-21-W). Apparent ages range between 489±5 Ma and 263±2 Ma. Both

heterogeneity of Re and Os distribution in the molybdenite and the large size of the grain (~1.5 cm, which would require much more than ~50 mg of sample for the heterogeneity to be sufficiently reduced so that the age would be reproducible) explain the poor reproducibility of the ages (Selby et al. in press). Also, low total rhenium concentration may be a factor for non-reproducible ages in this sample: small variation of Re content for this sample equates to a larger deviation from the mean age of sample SC-15-W than if the Re content was higher (Selby et al in press).

Although SC-15-W and SC-21-W are both pegmatitic samples from the same deposit, a significant difference in grain size coupled with a low Re content allows for important decoupling of Re and Os in SC-21-W, therefore, data for sample SC-21-W will not be further considered.

4.5.1.3. East Kemptville

A molybdenite-bearing pegmatite sample from the Baby Zone of the East Kemptville deposit in the southwestern part of the SMB yields a Re-Os age of 376±3.3 Ma (D. J. Kontak, pers. comm. 2002). This sample is characterised by low total rhenium concentrations.

4.5.2. Summary of $^{187}Re/^{187}Os$ results

The Re-Os mean ages for three samples from Long Lake and Walker are: (1) 371±1.5 Ma (SC-15-W), (2) 378±2 Ma (SC-12-L), and (3) 375 ± 1.5 Ma to 368 ± 1.5 Ma (SC-13-L). The variability of ages for associated pegmatite and aplite at the Long Lake deposit is striking. Furthermore, there is a significant time range obtained for sample SC-13-L. The younger ages (~371 Ma) definitely fit into the classical time frame defined from Ar-Ar and some U-Pb studies in the SMB (Reynolds et al. 1981; Reynolds et al. 1987; Harper 1988; Clarke et al. 1993b) and satellite plutons (Kontak et al. 1990a; Keppie et al. 1993; Kontak and Reynolds 1994; Keppie and Krogh 1999; Clarke et al. 2000; Fallon et al. 2001), whereas the older ages (~378 Ma) are in close agreement with previously published U-Pb data for the SMB (Harper 1988; Keppie et al. 1993) and satellite plutons (Hill 1991; Currie et al. 1998), as well as laserprobe analyses on white micas in the present study (discussed below). Also, low Re concentration in molybdenite appears as an obstacle to the Re-Os

dating method, as illustrated by the scattered ages obtained with sample SC-21-W. In light of these results, two important questions emerge from Re-Os ages when integrating them with Ar-Ar and U-Pb ages: (1) are Re-Os ages in close agreement with U-Pb ages on zircon for samples from the SMB as described in other working areas (e.g., Stein et al. 1998)?; and (2) does the Re-Os chronometer definitely retain the crystallisation age even for rocks that underwent metamorphism and/or metasomatism (as is the case in the New Ross area), as postulated by Frei et al. (1998), Stein et al. (1998), and Selby and Creaser (2001)?

4.6. $^{40}Ar/^{39}Ar$ results

4.6.1. White micas

The dataset for white micas includes incremental heating spectra and laserprobe intra-grain and single grain total ages. We first performed both incremental heating and laserprobe experiments on samples from the Long Lake and Walker deposits to: (1) compare the consistency of ages obtained from a single deposit (LL2, LL3, A9B-7558); (2) compare ages obtained by incremental heating to ages obtained by laserprobe analysis of single white mica grains; (3) compare the ages obtained with other $^{40}Ar/^{39}Ar$ ages within the SMB. Table 4.4 summarises the data in terms of the maximum, minimum, and plateau ages obtained using $^{40}Ar/^{39}Ar$ on white mica.

Most of the laserprobe data represent total fusion of either full grains or grain fragments. When grain size permitted, we tested for possible intra-grain age variations by performing spot analysis on core and rim areas (see diagrams for distinction between mode of analysis). The aim of laserprobe dating is the detection of intra- and inter-grain age differences and the interpretation of these differences in terms of events (for example, primary magmatic versus hydrothermal resetting). I report data as follows: (1) only a range (maximum and minimum ages) for samples with heterogeneous ages; and (2) both a range and a weighted mean age for samples with homogeneous ages.

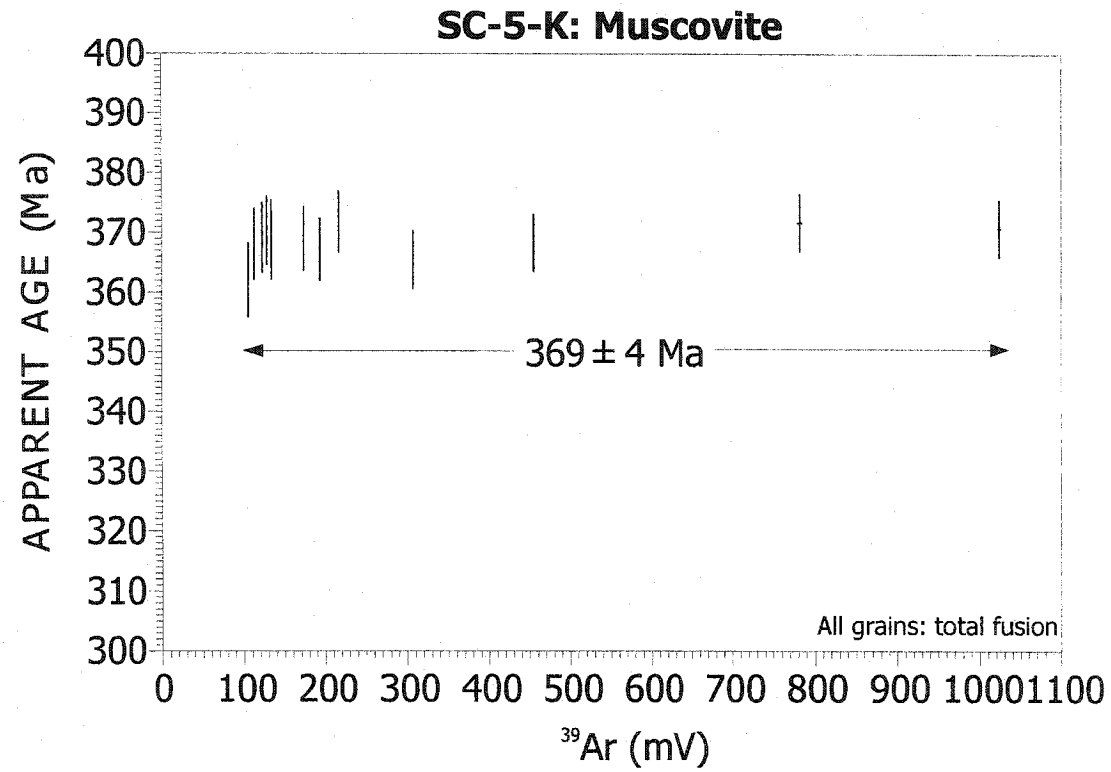

Figure 4.4: Total fusion data for white micas grains from a greisen sample (SC-5-K) at the Keddy deposit.

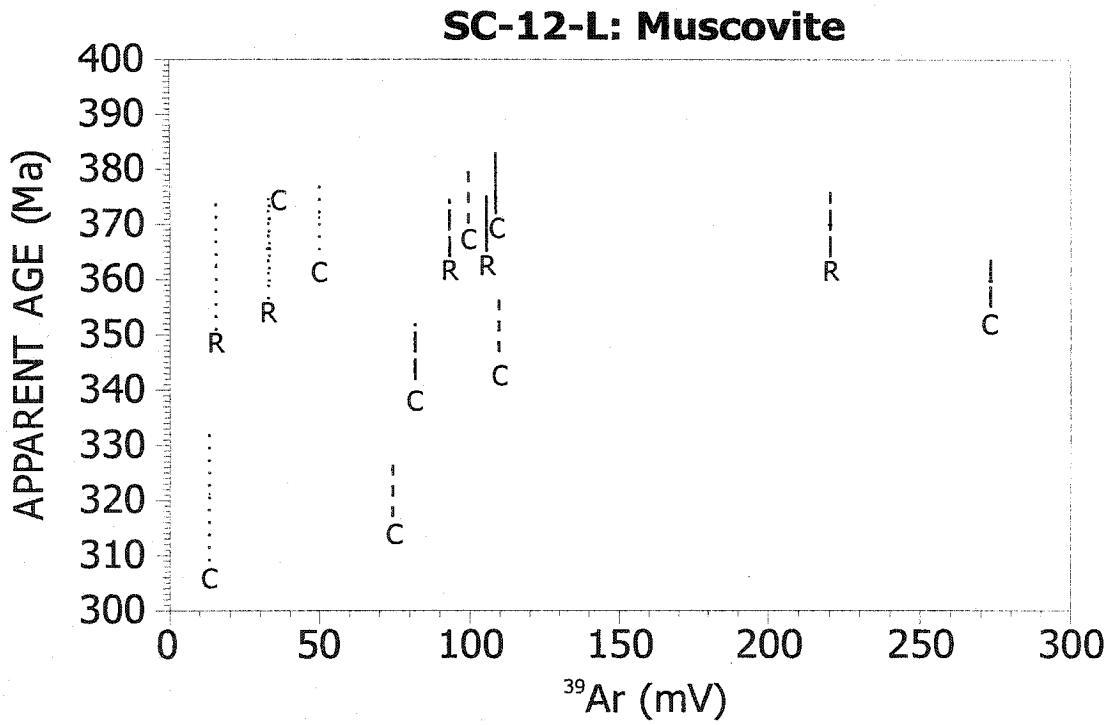

Figure 4.5: Spot data for white micas grains from a pegmatite sample (SC-12-L) at the Long Lake deposit. R = rim, C = core.

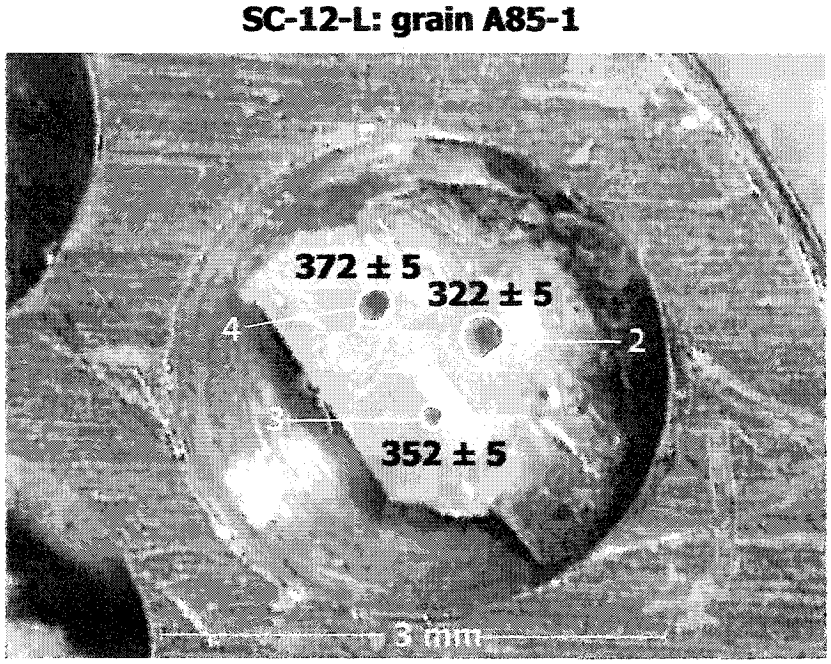

Figure 4.6: Spot data for a white mica grain from a pegmatite sample (SC-12-L) at the Long Lake deposit.

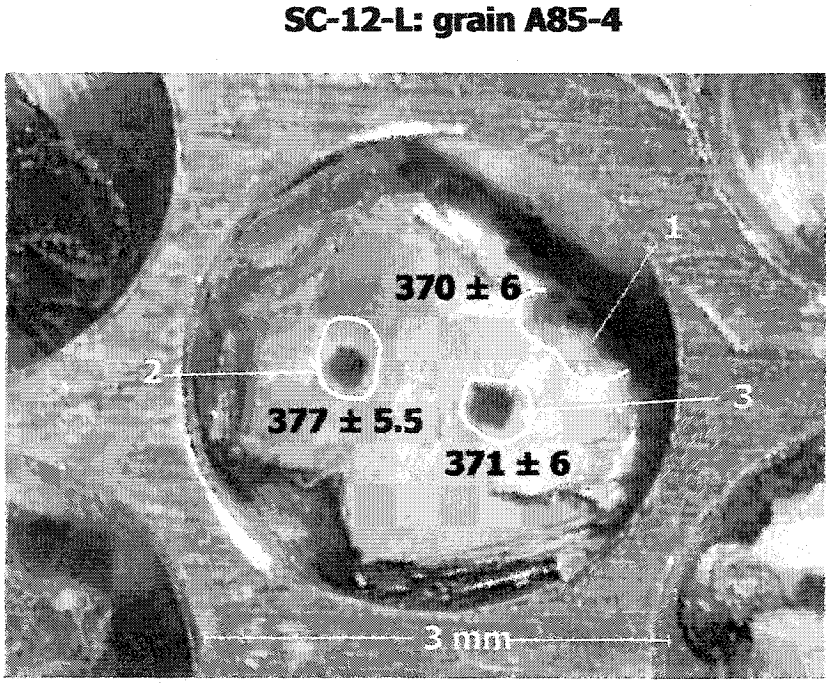

Figure 4.7: Spot data for a white mica grain from a pegmatite sample (SC-12-L) at the Long Lake deposit.

4.6.1.1. Data description

Keddy mineral deposit

A greisen sample from the Keddy mineral occurrence (SC-5-K) yields data that display no significant inter-grain age differences (ages range from 372 ± 5 Ma (grain B59-7) to 362 ± 6 Ma (grain B59-13)(Fig. 4.4). The mean weighted age of thirteen total fusion laserprobe analyses is 369 ± 4 Ma. All ages were obtained on 1-2 mm fragments of white mica.

Deposits	Sample	Incremental heating			Laserprobe	
		Maximum age	Minimum age	Plateau age	Maximum age	Minimum age
Walker	WAM				367±5	365±5
	WB	368±2	364±2	365±2	369±5	363±6
	SC-9-W				369±6	327±5
Long Lake	SC-12-L				377±6	321±12
	LL2	366±2	360±3	364±2		
	LL3	371±12	354±5	364±2		
	A9B-7558	370±2	365±3	367±2	377±5	357±16
Keddy	SC-5-K				372±5	362±6
Turner	SC-2-T				377±5	322±6
	SC-14-T				374±5	352±6
	S1				378±5	361±5
	S2				382±5	372±5
Millet Brook	SC-3-MB				374±5	321±12
	DK-MB-99-01				374±7	339±8
Mn mines	SC-1-D				379±5	354±5
	SC-11-D				375±5	369±5

Table 4.4: Summary of all $^{40}Ar/^{39}Ar$ age data on white micas in terms of maximum, minimum, and plateau ages using both incremental heating and laser spot techniques.

Long Lake deposit

Four large (3 mm) white mica flakes from a pegmatite at the Long Lake deposit (SC-12-L) permit multiple age measurements within a single grain using laserprobe methodology (Fig. 4.5). Large ranges of age exist within the single grains (Table 4.5). The oldest age measured is 377.5 ± 5.5 Ma (grain A85-4), whereas the youngest age is 321 ± 12 Ma (grain A85-2). The spatially random distribution of ages (i.e., no core/rim correlation)

within each grain suggests that post-crystallisation Ar loss occurred from parts of the grains without regard to grain boundaries (Fig.4.6 and 4.7). The oldest age measured probably represents the minimum crystallisation age of the white mica grain, whereas the youngest age might correspond to a maximum age for a resetting event.

A flat spectrum characterizes a greisen from Long Lake (A9B-7558) (Fig. 4.8), and fourteen increments (750-1450°C) record a plateau age of 367 ± 2 Ma. Six laserprobed grains (2-6 mm) from sample A9B-7558 yield no significant intra-grain age differences. The weighted mean age is 368 ± 4 Ma with individual spot ages ranging from 357 ± 16 to 377 ± 5 Ma (Fig. 4.9). Table 4.6 shows the range of ages obtained for several measurements within a single grain. Figures 4.10 and 4.11 show the laser spots produced in two different grains of this sample.

Grain	Laser spot age	Range	Location of measurement
1	322±5	375±5 to 322±5	core
	352±5.5		core
	375±5		core
2	362.5±12	371±6 to 321±12	rim
	365.5±9		rim
	366.5±7		core
	321±12		core
	371±6		core
4	370±6	377±5.5 to 370±6	rim
	377±5.5		core
	371±6		core
8	369±5	370±5 to 347±5	rim
	370±5		rim
	360±4.5		core
	347±5		core

Table 4.5: Summary of laser spot ages (age, range, and location in the grain) obtained for four grains from a pegmatite sample from Long Lake (SC-12-L).

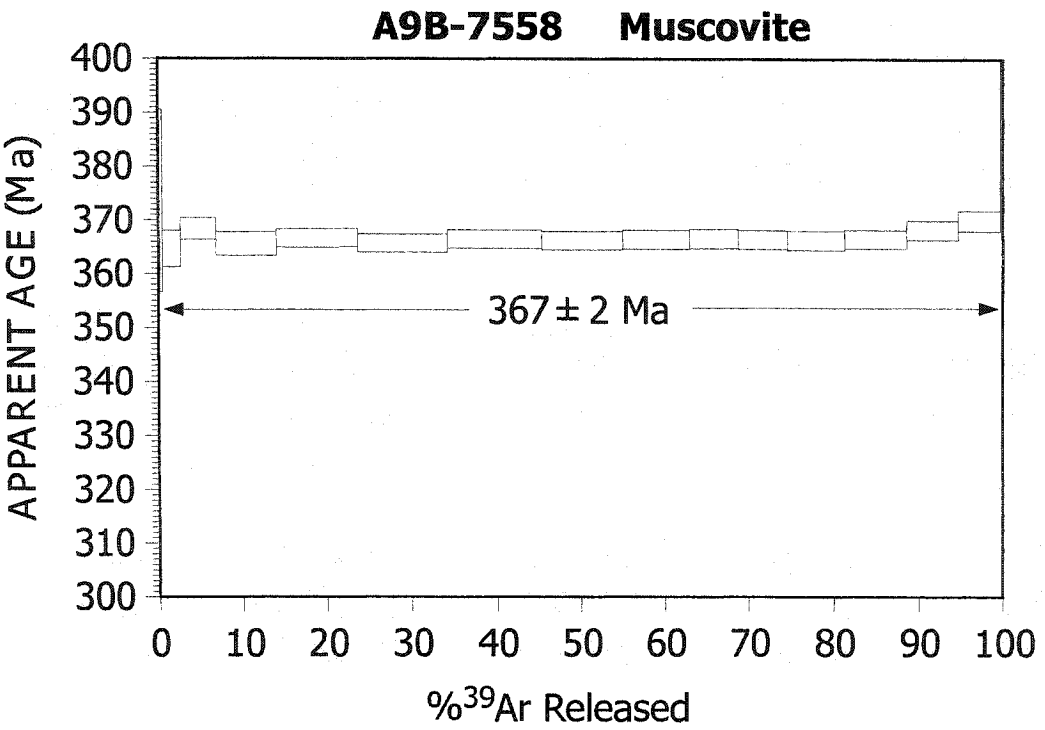

Figure 4.8: Incremental heating spectrum for white micas from a greisen sample (A9B-7558) at the Long Lake deposit. Mean ages are shown for the number of increments indicated.

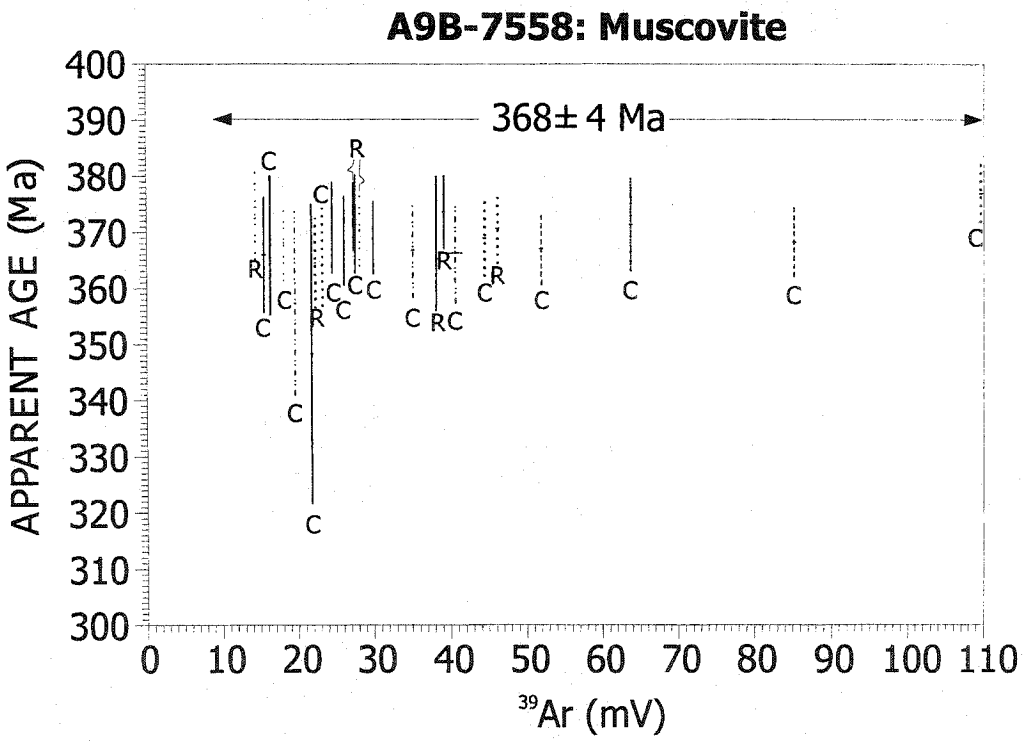

Figure 4.9: Spot data for a white mica grain from a greisen sample (A9B-7558) at the Long Lake deposit.

A9B-7558: grain Y80-1

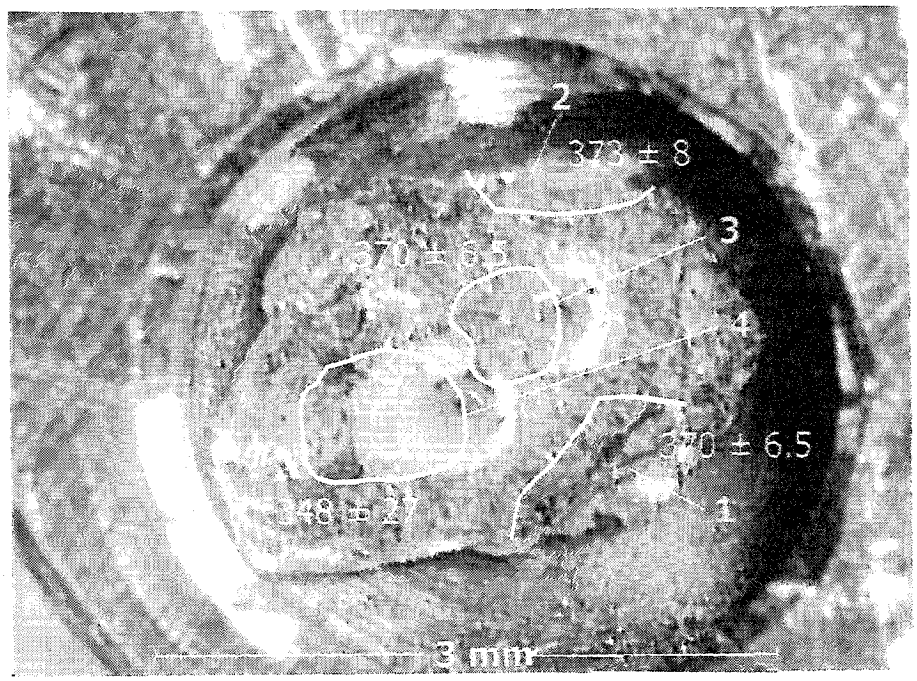

Figure 4.10: Spot data for a white mica grain from a greisen sample (A9B-7558) at the Long Lake deposit.

A9B-7558: grain Y80-2

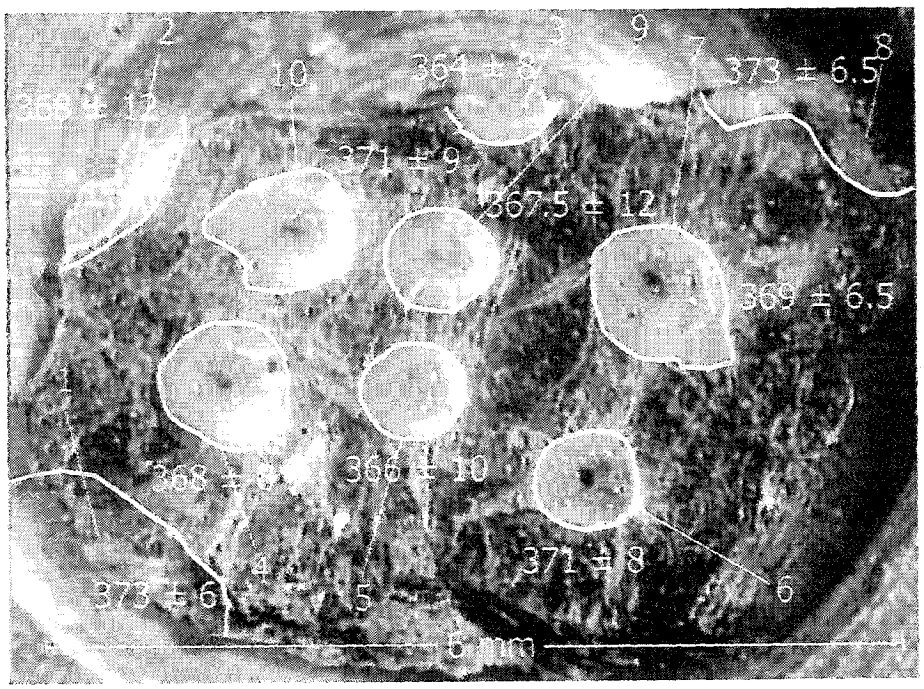

Figure 4.11: Spot data for a white mica grain from a greisen sample (A9B-7558) at the Long Lake deposit.

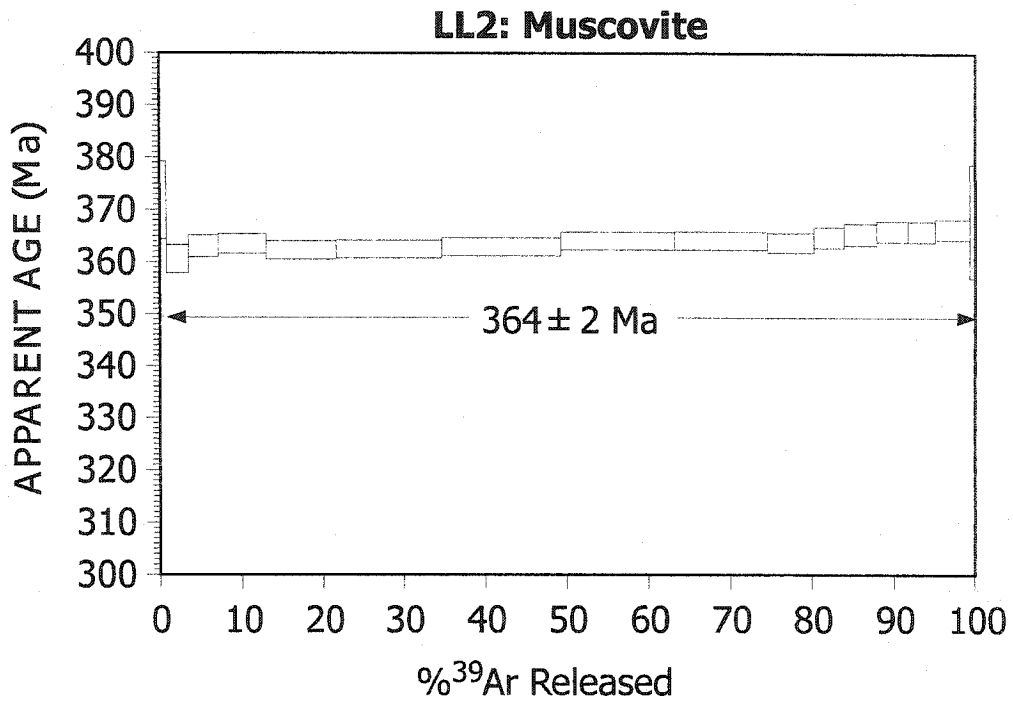

Figure 4.12: Incremental heating spectrum for white micas from a greisen sample (LL2) at the Long Lake deposit. Mean ages are shown for the number of increments indicated.

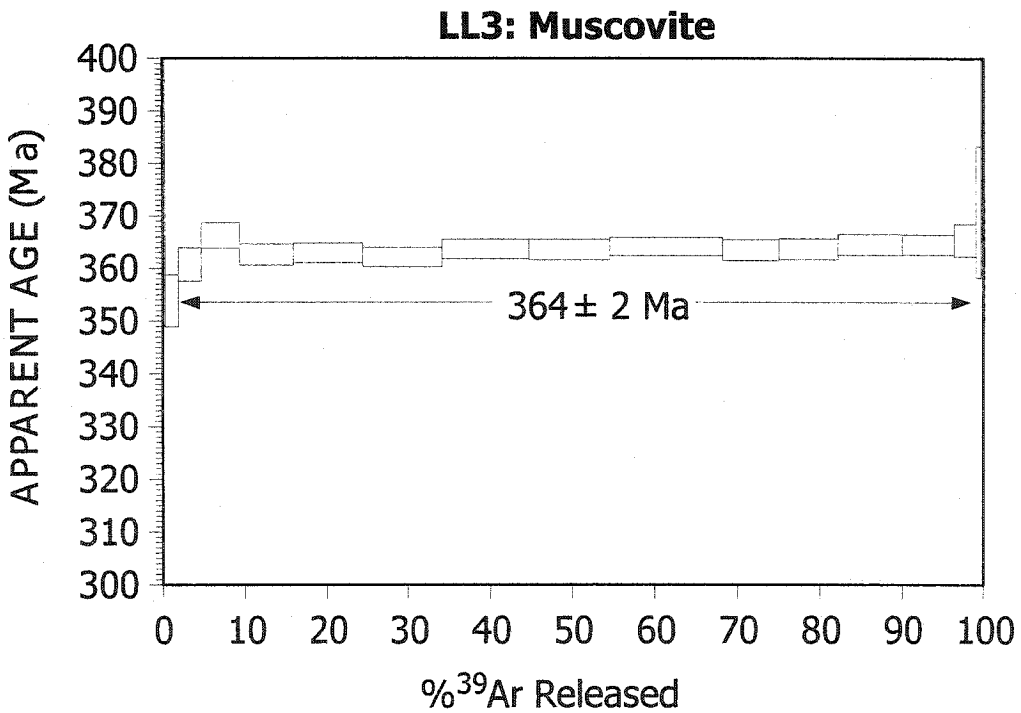

Figure 4.13: Incremental heating spectrum for white micas from a greisen sample (LL3) at the Long Lake deposit. Mean ages are shown for the number of increments indicated.

Two greisen samples from Long Lake (LL2 and LL3) have identical plateau ages of 364 ± 2 Ma for thirteen and fourteen increments (700-1150°C), respectively (Fig. 4.12 and 4.13).

Walker deposit

The oldest total fusion age is 368 ± 5 Ma (grain A84-7 and A84-15), and the youngest is 327 ± 5.5 (grain A84-8) for euhedral white mica grains (0.5-1.5 mm) from a pegmatite from the Walker deposit (SC-9-W) (Fig. 4.14).

Grain	Laser spot age	Range	Location of measurement
1	370±6	373±8 to 368±7	rim
	373±8		rim
	368±7		core
2	373±6	373±6 to 364±8	rim
	368±12		rim
	364±8		rim
	368±8		core
	366±10		core
	371±8		core
	369±6		core
	373±6		rim
	367±12		core
	371±9		core
3	371±8	371±8 to 363±11	core
	363±11		core
4	357±16	367±8 to 357±16	core
	366±9		core
	367±8		core
5	368±6	368±6 to 367±6	core
	367±6		core
7	365±9	377±5 to 362±14	core
	362±14		core
	369±7		core
	371±6		rim
	377±5		core

Table 4.6: Summary of laser spot ages (age, range, and location in the grain) obtained for six grains from a greisen sample from Long Lake (A9B-7558).

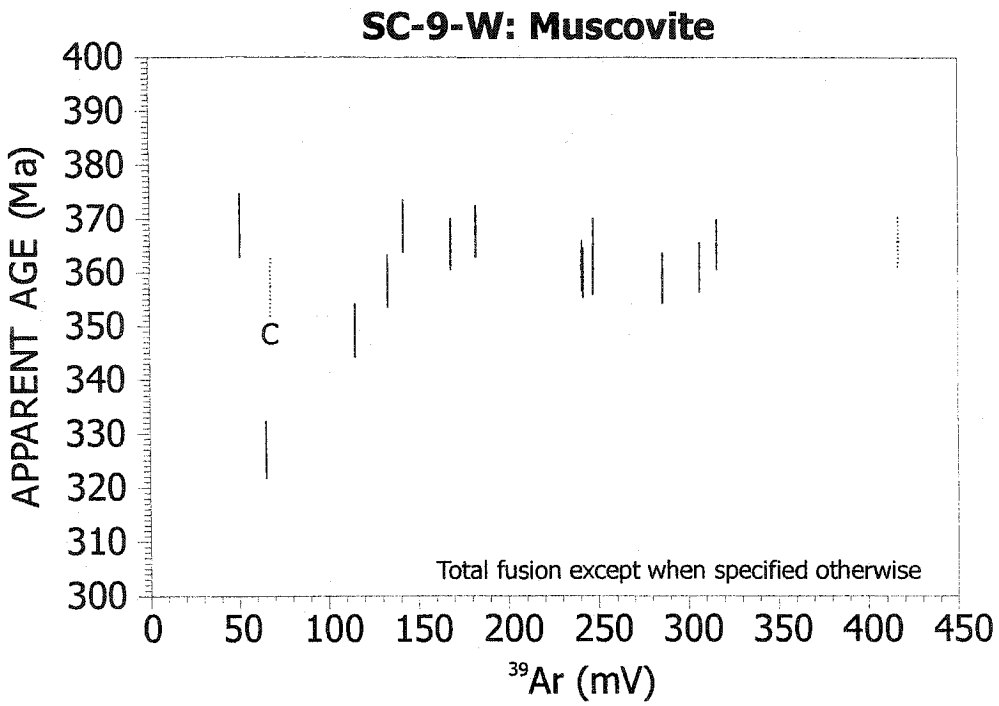

Figure 4.14: Spot and total fusion data for white micas grains from a pegmatite sample (SC-9-W) at the Walker deposit. C = core.

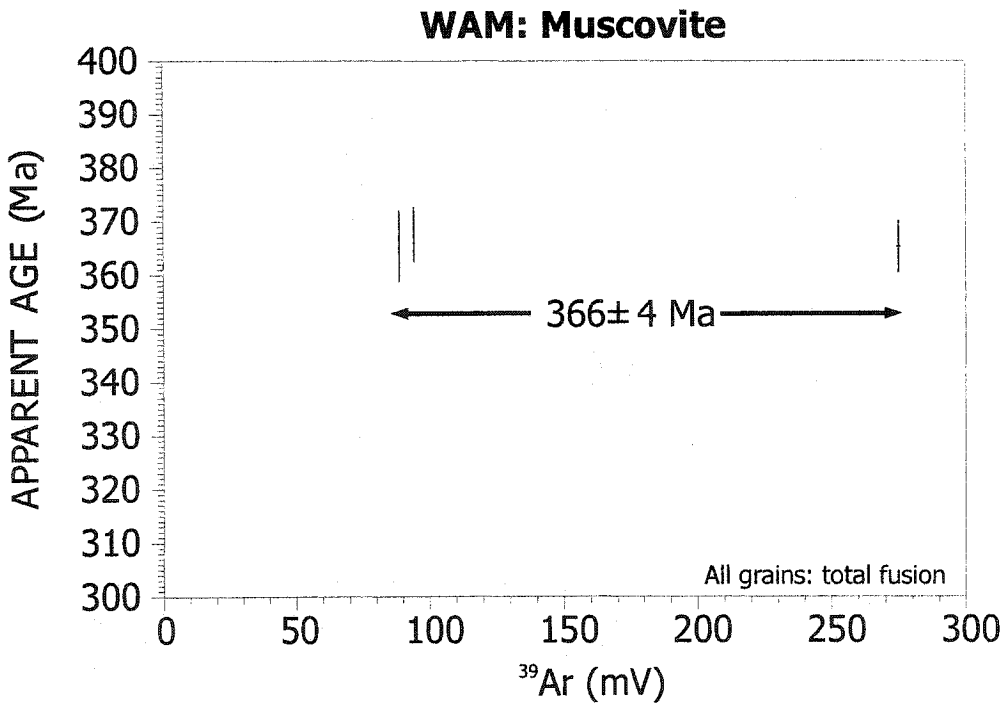

Figure 4.15: Total fusion data for white micas grains from an aplite sample (WAM) at the Walker deposit.

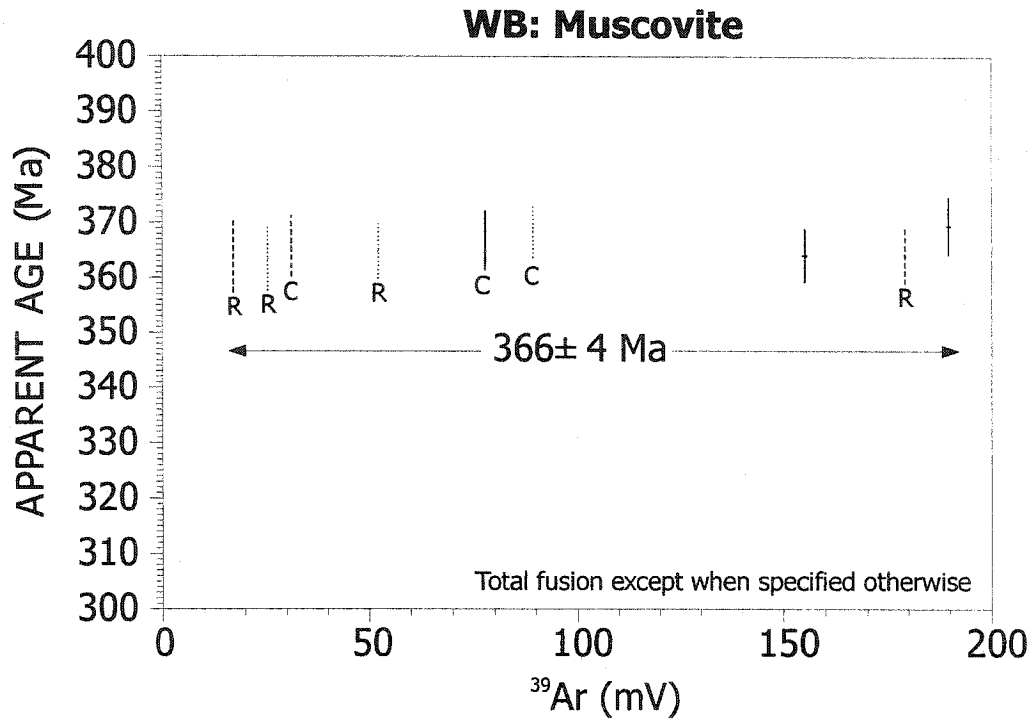

Figure 4.16: Spot and total fusion data for white micas grains from an aplite sample (WB) at the Walker deposit. R = rim, C = core.

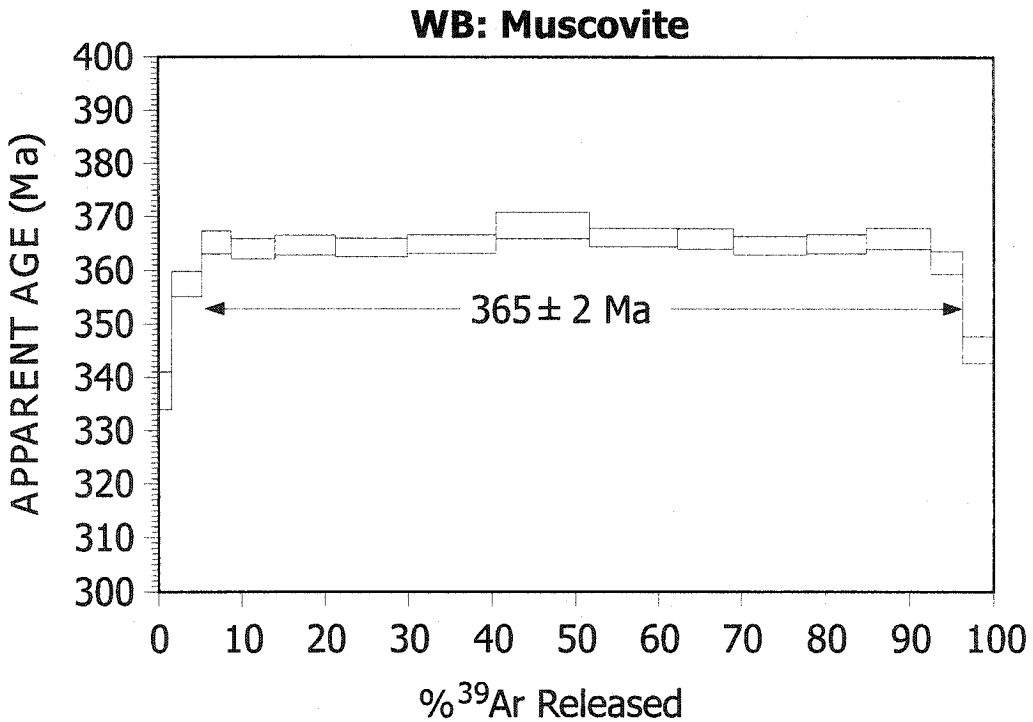

Figure 4.17: Incremental heating spectrum for white micas from an aplite sample (WB) at the Walker deposit. Mean ages are shown for the number of increments indicated.

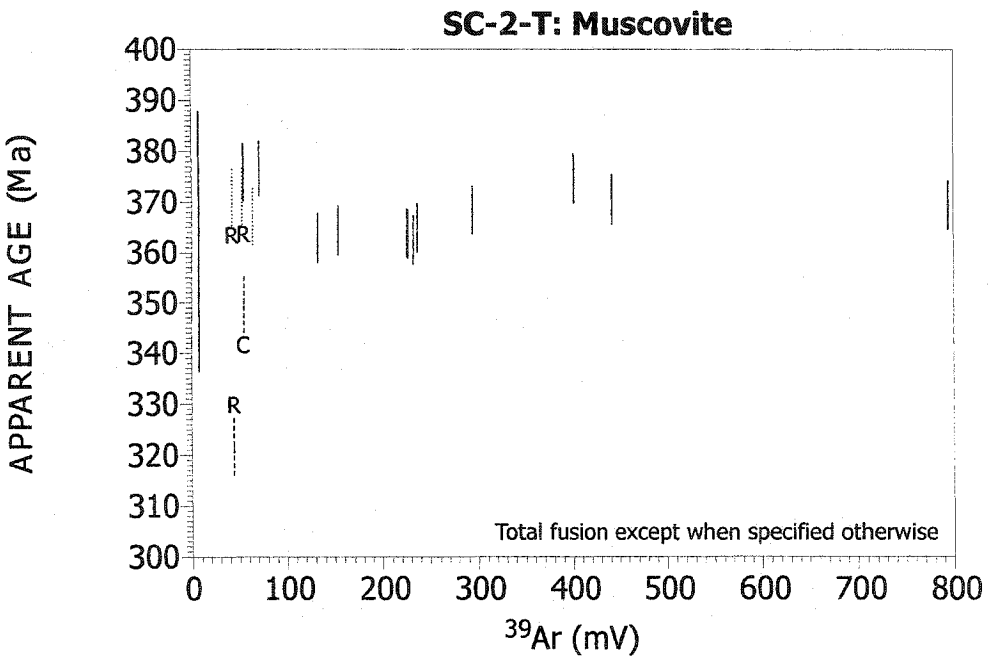

Figure 4.18: Spot and total fusion data for white micas grains from a greisen sample (SC-2-T) at the Turner deposit. R = rim, C = core.

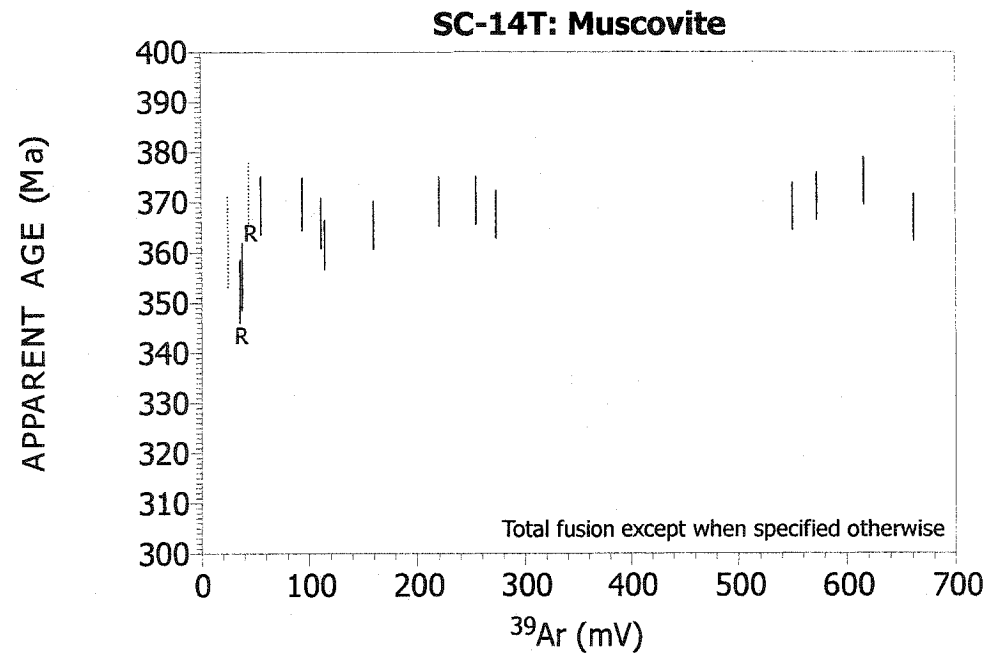

Figure 4.19: Spot and total fusion data for white micas grains from an elvan sample (SC-14-T) at the Turner deposit. R = rim.

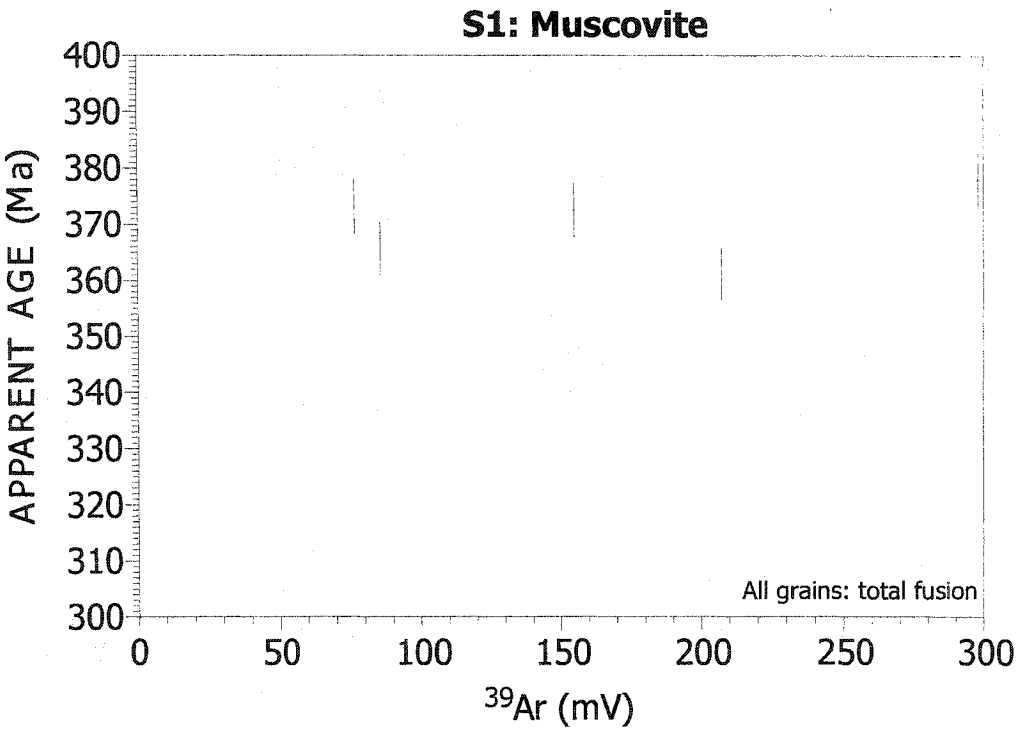

Figure 4.20: Total fusion data for white micas grains from an elvan sample (S1) at the Turner deposit.

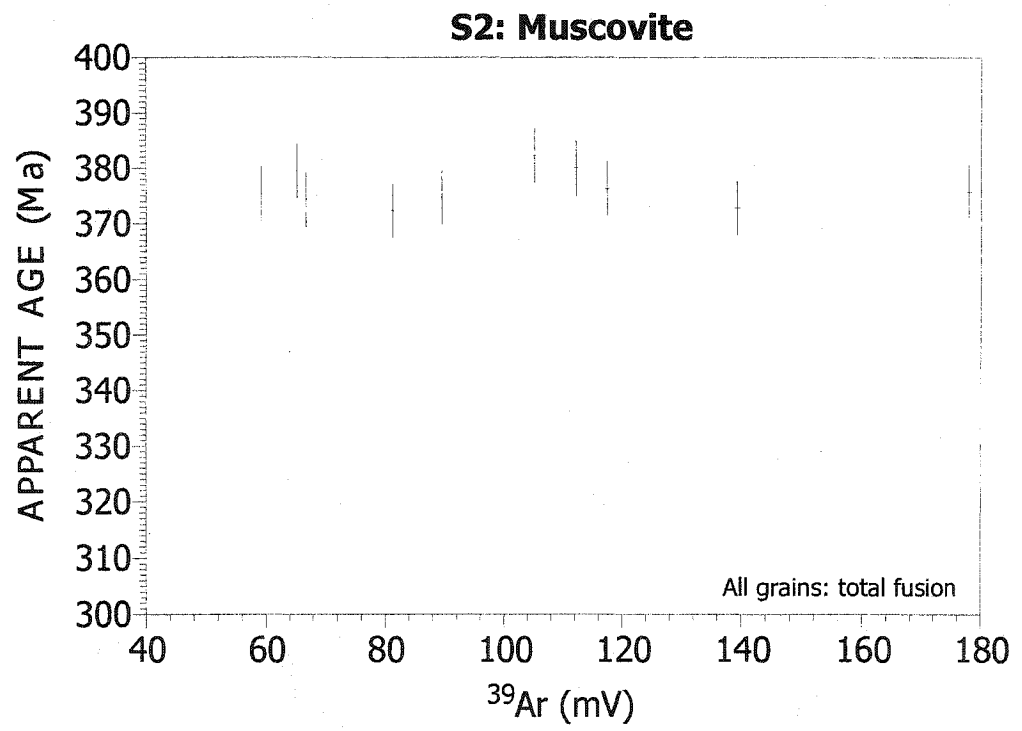

Figure 4.21: Total fusion data for white micas grains from an elvan sample (S2) at the Turner deposit.

Two aplites from the Walker deposit (WAM and WB) present a narrow range of both total fusion and laser spot ages on euhedral single grains (0.5-1 mm), with the oldest being 370 ± 5 Ma (grain Y75-8) and the youngest being 363 ± 6 Ma (grain Y75-3) (Fig. 4.15 and 4.16). The weighted mean of both samples is similar at 366 ± 4 Ma. Sample WB yields an age spectrum with small and variable initial and final steps, but over 90% of the gas released yields a plateau age of 365 ± 2 Ma (Fig. 4.17).

Turner deposit

A muscovite-chlorite greisen from the Turner deposit (SC-2-T) yields ages ranging from 377 ± 5 Ma (grain A82-21) to 322 ± 6 Ma (grain A82-5) (Fig. 4.18). These data include both single grain total fusion and laser spot analyses. Some grains are highly homogeneous (grain A82-3 has ages ranging from 371 ± 6 Ma to 367 ± 5.5 Ma), whereas others exhibit a heterogeneous distribution of Ar (grain A82-5 yields ages ranging from 350 ± 6 Ma to 321 ± 6 Ma), suggesting a variable resetting of Ar within the second grain. All grains analysed were fragments of 1.5-2 mm in size, with a powdery texture.

All white mica grains from three samples of an elvan dyke at the Turner deposit (SC-14-T, S1, S2) are euhedral single grains (0.5-1 mm). Samples SC-14-T, S1, and S2 yield ages ranging from 352 ± 6 Ma (grain A81-11) to 372 ± 6 Ma (grain A81-6), 361 ± 5 Ma (grain C58-2) to 378 ± 5 Ma (grain C58-10), and 372 ± 5 Ma (grain C59-4) to 382 ± 5 Ma (grain C59-13), respectively (Fig. 4.19, 4.20, and 4.21). All ages for sample S2 are within error, allowing for the calculation of a meaningful mean age of 376 ± 4 Ma. For sample SC-14-T, two measurements were taken on grain A81-6: (1) a rim age (372 ± 6 Ma) and a total fusion age (362 ± 9 Ma). That a range of ages exists, and that the rim age is the oldest, suggests that resetting was variable without regard for grain boundaries.

Millet Brook deposit

Age data were obtained from samples of two mineralised monzogranites from the Millet Brook deposit (SC-3-MB and DK-MB-99-1) for euhedral grains (1-2 mm) and grain fragments (0.5-1 mm). Both euhedral grains and grain fragments yield low and high ages, excluding the possibility of lower ages as a consequence of grain fragmentation. The ages range from 374 ± 6 Ma (grain A79-4) to 322 ± 13 Ma (grain A79-12) for SC-3-MB and

from 374 ± 7 Ma (grain A83-6) to 339 ± 8 Ma (grain A83-10) for DK-MB-0-99-1 (Fig. 4.22 and 4.23). White micas from Millet Brook do not appear to have been chemically affected by the mineralising fluid that circulated in the area (Sections 3.4.4.1 and 3.4.4.2), therefore, high ages for white micas grains from Millet Brook are not unexpected.

Mn mines

Small and large fragments (0.5-1.5 mm) as well as large euhedral grains (1.5 mm) for an episyenite from the Mn mines (SC-1-D) yield a range of total fusion ages; the oldest age is 379 ± 6 Ma (grains A80-18 and A80-15), with the youngest 354 ± 5 Ma (grainA80-4) (Fig. 4.24). As for the mineralised monzogranites from Millet Brook, grain fragments do not systematically yield younger ages. Also, white micas from the episyenite at the Mn mines have a primary chemical composition (Section 3.4.4.4), hence the high ages obtained for samples SC-1-D.

Grains from an elvan dyke from the Mn mines (SC-11-D) are subhedral to euhedral and less than 1 mm in size The sample yields laser total fusion ages ranging from 375 ± 5 Ma (grain C60-3) to 370 ± 5 Ma (grain C60-2) (Fig. 4.25).

4.6.1.2. Summary of laserprobe age data on white micas

All age data obtained using $^{40}Ar/^{39}Ar$ laserprobe analysis range between 382 ± 5 Ma and 321 ± 12 Ma (Table 4.4). An elvan dyke from the Turner deposit (3 samples) and an episyenite from the Mn mines yield the oldest age (382-378 Ma) and are also samples containing white micas showing convincing textural and chemical primary features (Section 3.4.4.4). Other samples from the Long Lake deposit, Turner deposit, and Mn mines yield slightly younger ages (377-374 Ma), whereas samples from the Walker and Keddy deposits show the youngest maximum ages (372-367 Ma). A minimum age of ~ 320 Ma appears in several mineral deposits (Walker, Long Lake, Turner, and Millet Brook), whereas higher minimum ages exist for the Keddy deposit and the Mn mines (362-354 Ma).

On a diagram showing a frequency distribution of all ages (Fig. 4.26), most of the laser total fusion and laser spot ages are distributed approximately symmetrically between 360 and 375 Ma, with two secondary peaks around 320 and 340 Ma. Also, the distribution

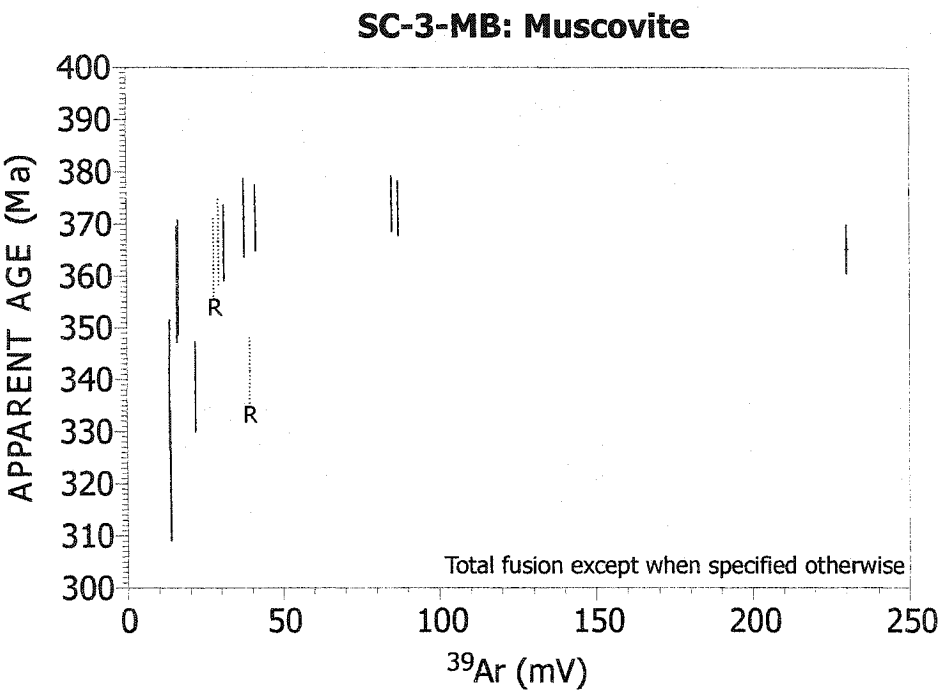

Figure 4.22: Spot and total fusion data for white micas grains from a mineralised monzogranite sample (SC-3-MB) at the Millet Brook deposit. R = rim.

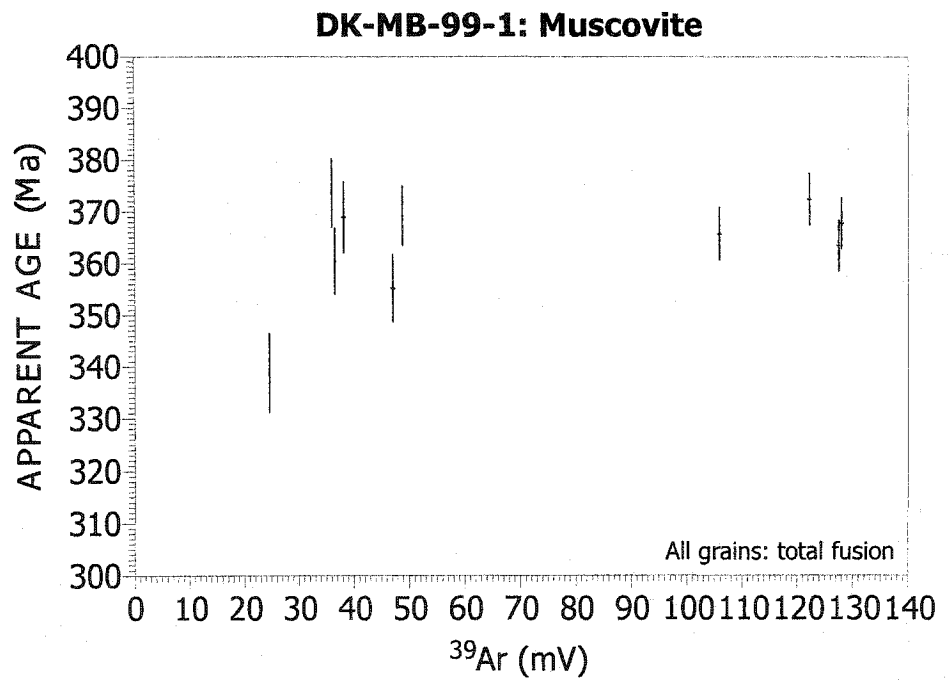

Figure 4.23: Total fusion data for white micas grains from a mineralised monzogranite sample (DK-MB-99-1) at the Millet Brook deposit.

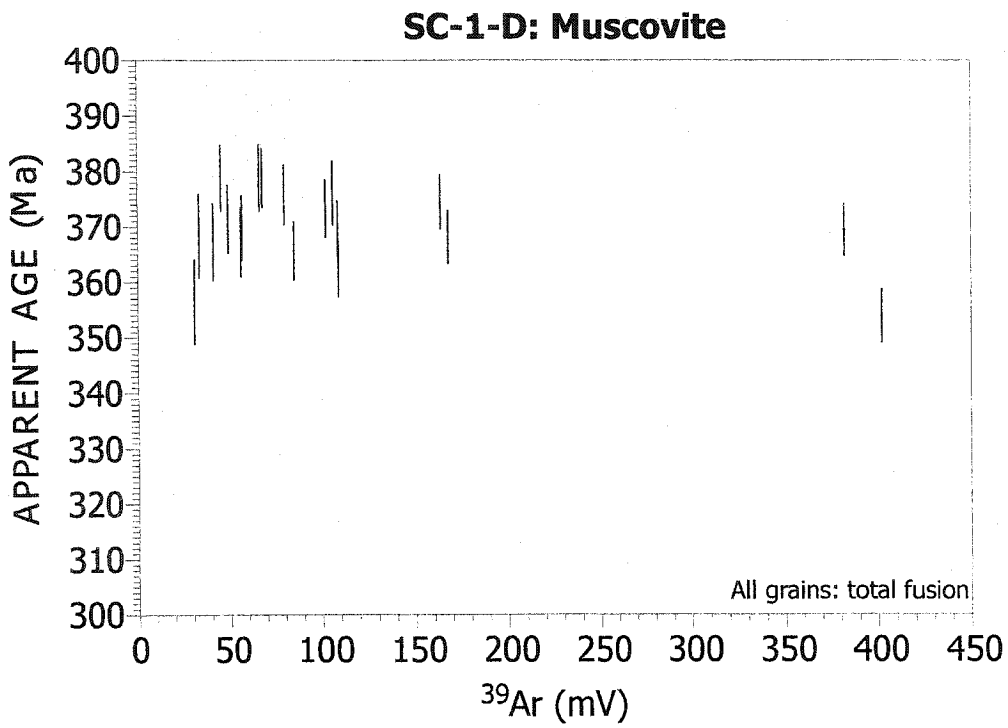

Figure 4.24: Total fusion data for white micas grains from an episyenite sample (SC-1-D) at the Mn Mines.

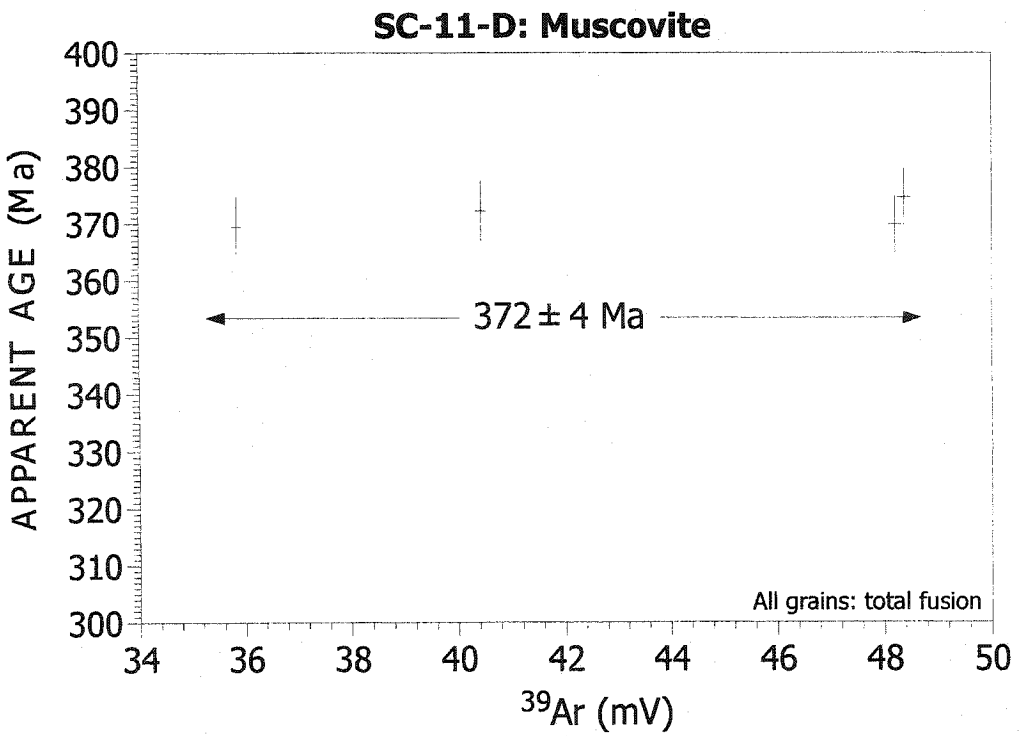

Figure 4.25: Total fusion data for white micas grains from an elvan sample (SC-11-D) at the Mn Mines.

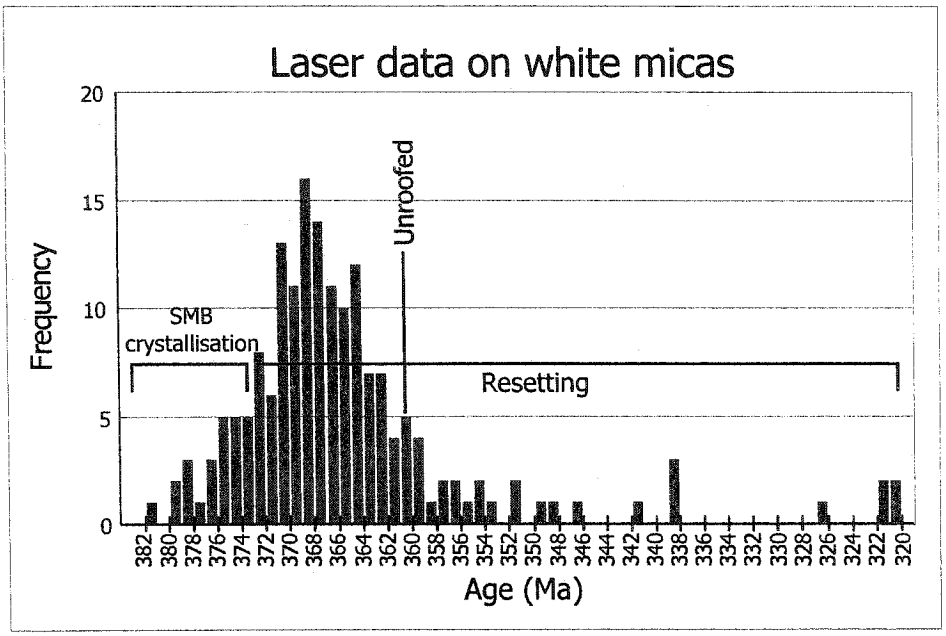

Figure 4.26: Frequency distribution of ages obtained by laserprobe analysis on white micas for mineral occurrences of the New Ross area.

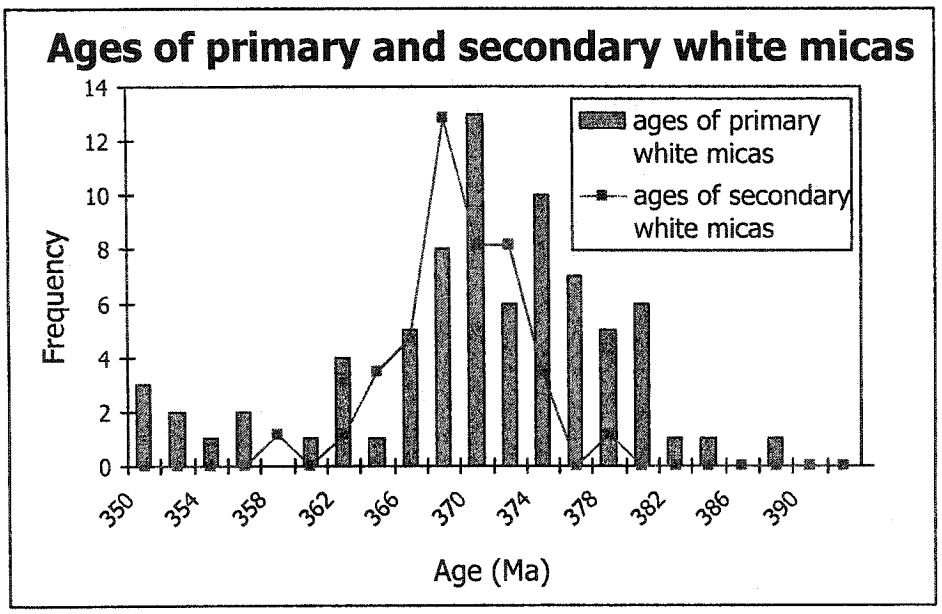

Figure 4.27: Frequency distribution of ages obtained for white mica texturally primary or secondary according to Section 3.4.4.4. Both sets of data are within error of each other.

of data is skewed towards younger ages, indicating resetting of the isotopic system. The possible mechanisms causing argon resetting are discussed in the next Section.

On a diagram showing a frequency distribution of ages obtained for chemically and texturally primary and secondary white micas (Section 3.4.4.4), primary grains display most ages between 382 and 367 Ma, whereas ages of secondary grains range between 378 and 365 Ma (Fig. 4.27). Each age has an error of ± 5 Ma, therefore both sets of data are within error of each other and no age discrimination is possible between chemically primary and secondary white micas.

4.6.1.3. Discussion of data

Discussion of incremental heating data and comparison with laserprobe analyses

Three greisen samples from the Long Lake mineral occurrence yield ages in good agreement with each other. Although McDougall and Harrison (1999) emphasised that a slowly cooled mineral is likely to undergo argon loss during cooling, each spectrum presents a good plateau and there is no indication of argon loss.

Samples	Incremental heating spectra ages	Range of laserprobe ages
WB	365±2 Ma	364±5 and 369±5 Ma
LL2	364±2 Ma	
LL3	364±2 Ma	357±16 to 377±5 Ma
A9B-7558	367±2 Ma	

Table 4.7: Summary of the ages obtained by incremental heating and laserprobe techniques for four samples from the Long Lake and Walker deposits.

Table 4.7 summarises the ages obtained by incremental heating and laserprobe techniques for samples from the Long Lake and Walker deposits. For both samples (WB and A9B-7558), no significant age difference exists between the two methods used for dating. For both samples, plateaus are well constrained, which can either mean that the laser data are also well constrained at the same age as the plateau age (i.e., no intergrain age differences), or that the plateau age is an average age of higher and lower laserprobe ages. In the case of the second alternative, laserprobe analysis are more likely to provide better

information in terms of an age gradient within a single grain, as is the case for alkali feldspars.

The plateau ages obtained for the samples from the Long Lake and Walker deposits are slightly lower, but still within error of previously determined ages using the same method within the SMB. Also, previous dating in the New Ross area revealed ages between 376 and 361 Ma (Farley 1978; Reynolds et al. 1981; Reynolds et al. 1987; Keppie et al. 1993; Clarke et al. 1993b), a range in which the ages determined for the present study fall.

Discussion of laserprobe data

Different mechanisms can cause ^{40}Ar loss that may result in age gradients within single analysed grains. Slow cooling promotes volume diffusion of Ar gas (Hodges et al. 1994); also, later reheating events may reset the isotopic clock (e.g., Fallon et al. 2001). Both deformation and recrystallisation promote ^{40}Ar loss from minerals, as exemplified in several $^{40}Ar/^{39}Ar$ studies in metamorphic rocks (e.g., Kirschner et al. 1996; Hames and Cheney 1997). The regional geology of the New Ross area does not support the possibility of ^{40}Ar loss enhanced by a deformational event, but other mechanisms have to be considered, especially recrystallisation promoted by intense fluid circulation within the area.

Figure 4.26 includes age data from the following samples: pegmatites from Walker and Long Lake, mineralised monzogranites from the Millet Brook deposit, an episyenite from the Mn mines, and a white mica-chlorite greisen from the Turner deposit. How do these samples rank in the crystallisation sequence of granitoid rocks? From older to younger, the following succession has been inferred:

1. The monzogranite samples from Millet Brook are the initial magmatic host rocks (only melt present); a late-circulating fluid subsequently caused mineralisation.
2. The pegmatite samples from Walker and Long Lake are fluido-magmatic rocks (i.e., they crystallised in the presence of both melt and fluid) and, therefore, are the result of the same protracted magmatic event.
3. The episyenite from the Mn mines and the greisen from the Turner deposit are the product of subsolidus (no melt present) hydrothermal alteration.

The maximum age obtained for each of these samples does not reflect the order of crystallisation above, with a pegmatite from Walker displaying the youngest maximum age (369 Ma), and both episyenite from the Mn mines (379 Ma) and greisen from the Turner deposit (378-382 Ma) yielding highest maximum ages comparable to those of the pegmatite at Long Lake (377 Ma) and the monzogranites at Millet Brook (374 Ma).

The pegmatite samples from Walker and Long Lake contain large white mica grains, with higher volume to surface ratio than smaller grains. Large grains might be more susceptible to diffusion of argon gas within the grain itself, therefore presenting areas of different ages within a grain (McDougall and Harrison 1999). The process of diffusion involves relocation of atoms from high concentration to low concentration areas within a grain. Whole-grain volume diffusion is unlikely though, because there was no correlation between younger ages and grain rims. The samples from the New Ross area having a bimodal distribution of ages may have inhomogeneously recorded a reheating event associated with the Alleghanian deformation and that has previously been documented at ca. 330-300 Ma in granitoid rocks from the southwestern part of the MLT (Reynolds et al. 1981; Zentilli and Reynolds 1985; Dallmeyer and Keppie 1987, Reynolds et al. 1987; Kontak and Cormier 1991; Keppie and Dallmeyer 1995; Kontak et al. 1995, Fallon et al. 2001). Although the granitoid rocks of the SMB do not show textural or physical evidence of the mid-Carboniferous Alleghanian deformation, Culshaw and Reynolds (1997) obtained ages of 320 ± 5 Ma for white micas from pressure shadows of pyrite grains aligned parallel to the schistosity in rocks of southwestern Nova Scotia. This age is in agreement with the time of dextral shearing and reactivation in southwestern Nova Scotia (Muecke et al. 1988; Keppie and Dallmeyer 1995), as well as with the emplacement age of the Wedgeport pluton (Cormier et al. 1988) in that area. Culshaw and Liesa (1997) suggested that the Alleghanian deformation corresponds to the deformation of Carboniferous sediments in the northern part of the MLT.

The mineralised monzogranites from Millet Brook, the episyenite from the Mn mines, and the white mica-chlorite greisen from Turner all belong to vein deposit types (vein-greisen type for the Turner deposit). Such deposits facilitate fluid circulation throughout the rock along the fracture areas where the mineralisation occurs. Heat and/or high fluid pressure is a triggering agent increasing circulation of hot fluids along these

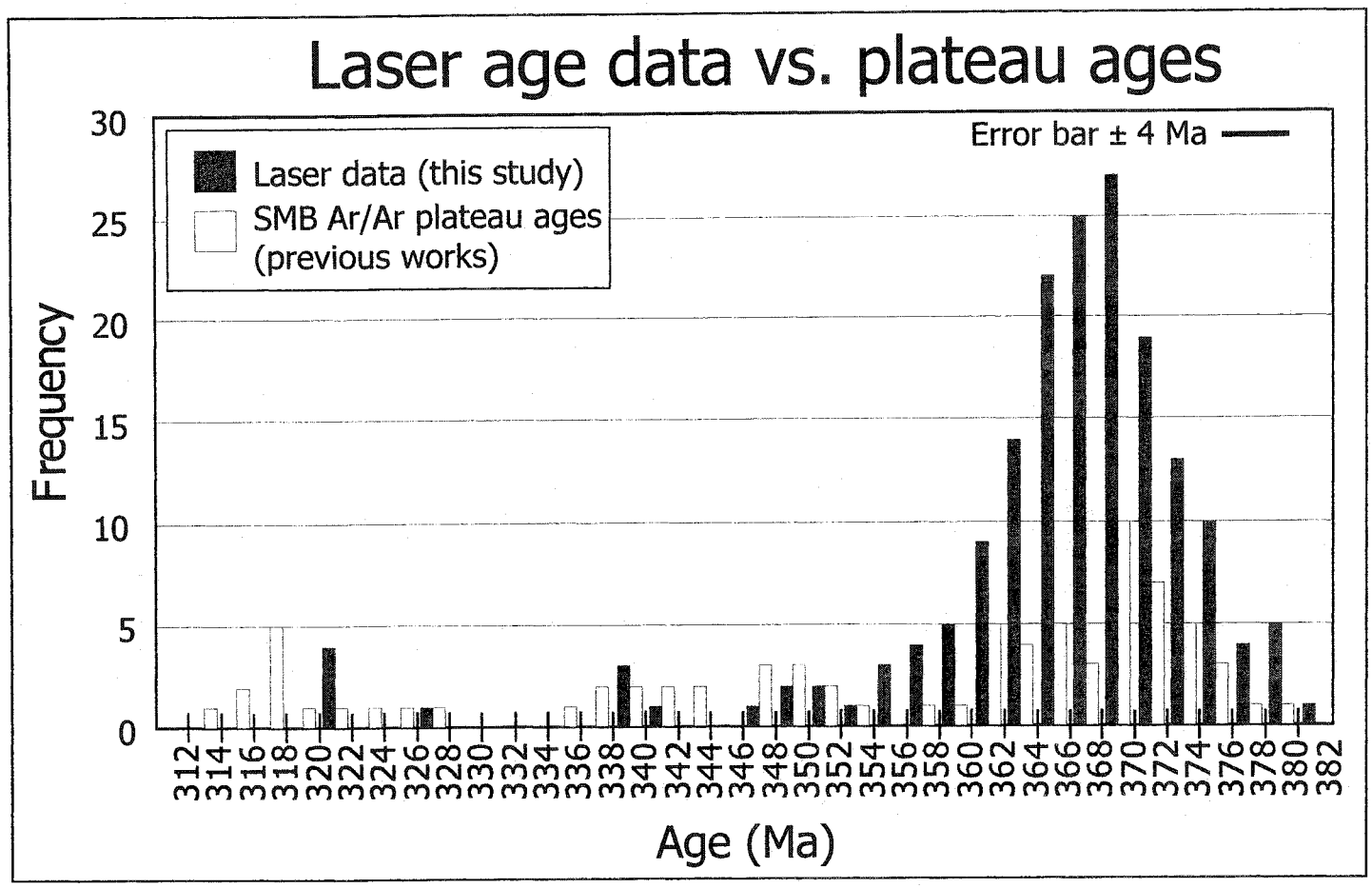

Figure 4.28: Frequency distribution of ages comparing ages obtained by laserprobe analysis for mineral occurrences of the New Ross area to those determined by incremental heating for the SMB in previous works (Farley 1978; Reynolds et al. 1981; Reynolds et al. 1987; Kontak and Cormier 1991; Clarke et al. 1993; Keppie et al. 1993; Dostal and Chatterjee 1995; Keppie and Dallmeyer 1995).

fractures. Argon diffusion may occur on a large scale during intense fluid circulation caused by a reheating event. Here again, reheating associated with the tectono-thermal Alleghanian event appears to be the latest event which affected the isotopic system. Also, sample SC-2-T shows incomplete recrystallisation of white mica grains, implying imperfections in the mineral lattices allowing for Ar diffusion along defects.

A comparison of the spectra ages available for the SMB with the laserprobe data obtained in the present study (Fig. 4.28) reveals a new trend in the evolution of dating within the SMB, i.e., a relatively larger number of laserprobe data are above the previously widely accepted age for the SMB crystallisation (372 Ma). Previously, the histogram was mainly skewed towards ages younger than 372 Ma, therefore, generally recording a history of post-crystallisation resetting of ages and giving some hints about possible older ages; laserprobe data not only record post-crystallisation resetting ages, but also substantiate the existence of ages older than 372 Ma.

4.6.2. Alkali feldspars

The dataset for alkali feldspars includes incremental heating spectra, and in addition, laserprobe total fusion of grain fragments for four samples. Most of the laserprobe work is from an Honours thesis done at Dalhousie University on samples from the Walker, Long Lake, and Millet Brook deposits (Warren 2001).

For spectra ages, all samples were heated over a temperature range of 500-550°C to 1450-1500°C.

4.6.2.1. Description of data

Long Lake deposit

Two samples (SW-LL01 and A9B-7504) containing microcline located on a fracture within the greisenised Long Lake leucogranite (Fig. 2.17) provide distinct ages. Fragments of microcline in sample A9B-7504 define a discordant spectrum with an age gradient; the maximum age is 346±2 Ma and the minimum 298±5 Ma (Fig. 4.29). Laserprobe data on microcline fragments extend the spectral age range, i.e., laser ages range between 360±5 Ma and 281±4 Ma (Fig. 4.30).

Sample SW-LL01 provides consistent laserprobe ages from microcline fragments (Fig. 4.31). These ages define a narrow range between 257±4 Ma and 265±4 Ma. O'Reilly et al. (1982) stated that the alkali feldspars formed from the circulation of K-rich fluids along the fracture; if so, the age of the microcline grains appears to be considerably younger than the age of the greisen.

A pegmatite sample from Long Lake (SC-12-L) has an age spectrum that is particularly discordant (Fig. 4.32). For the first 30% of ^{39}Ar released, the steps are generally small and the ages variable. Between 30 and 100% of ^{39}Ar released, there is a regular increase of age in parallel with an increase in step size. The maximum and minimum ages recorded are 346 ± 6 Ma and 294 ± 6 Ma, respectively. Similarly, the laserprobe data are widely scattered and indicate ages ranging between 353 ± 6 Ma and 284 ± 4 Ma (Fig. 4.33), again extending slightly the spectral age range.

Walker deposit

A pegmatite sample (SC-9-W) from the Walker mineral occurrence presents a spectrum with a shape similar to the above, but over a smaller range, i.e., 336±5 Ma to 359±3 Ma (Fig. 4.34). The two last steps have large errors and are not considered here. Laserprobe total fusion data of grain fragments for sample SC-9-W (Fig. 4.35) show ages ranging between 351±5 Ma (grain fragment B80-13) and 335±5 Ma (grain fragment B80-4), mirroring the spectral age range. Warren (2001) attempted to use laserprobe dating to detect core-rim variations, but obtained no systematic age variation.

Millet Brook deposit

I analysed a barren (DK-MB-99-05) and a mineralised (DK-MB-99-01) monzogranite from the Millet Brook deposit. Both samples present similarly shaped spectra as above. Sample DK-MB-99-05 shows ages ranging between 372±3 Ma and 344±5 Ma (Fig. 4.36). Sample DK-MB-99-01 shows incremental heating ages ranging between 365±4 Ma and 356±7 Ma (Fig. 4.37). Laserprobe total fusion data for grain fragments from sample DK-MB-99-01 define ages ranging between 363±5 Ma (grain fragment B82-18) and 346±5 Ma (grain fragment B82-22) (Fig. 4.38). The laserprobe data slightly extend the spectral age range.

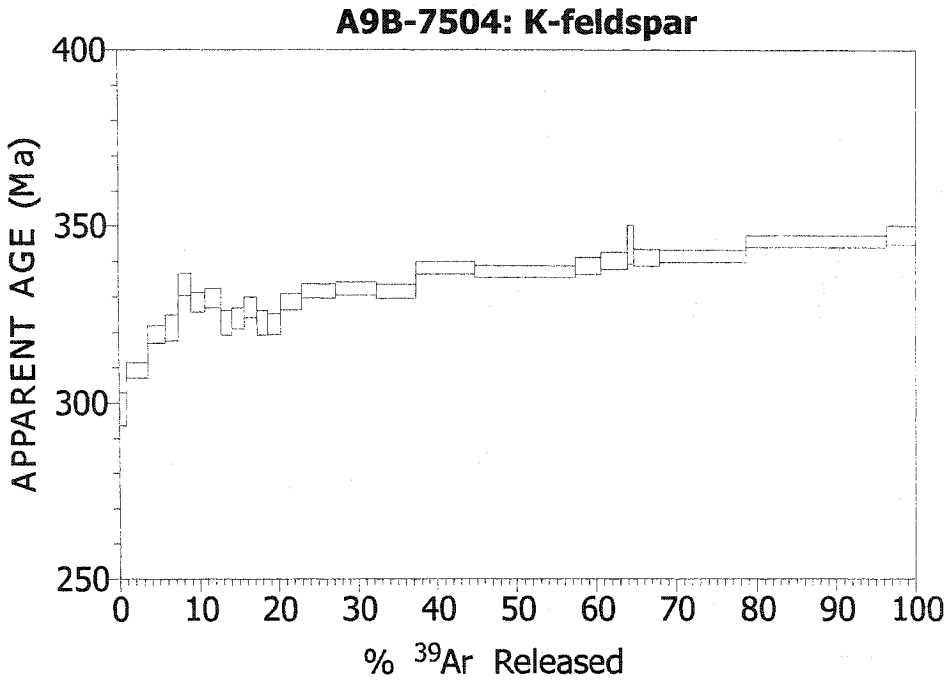

Figure 4.29: Incremental heating spectrum for alkali feldspars from a fracture (A9B-7504) at the Long Lake deposit.

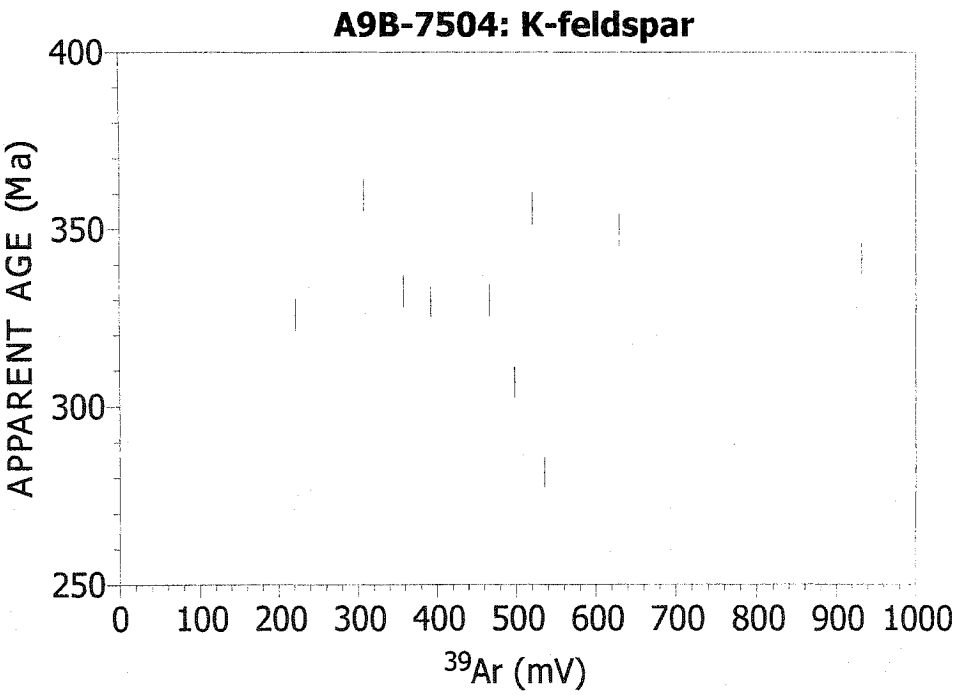

Figure 4.30: Total fusion data for alkali feldspar grains from a fracture (A9B-7504) at the Long Lake deposit.

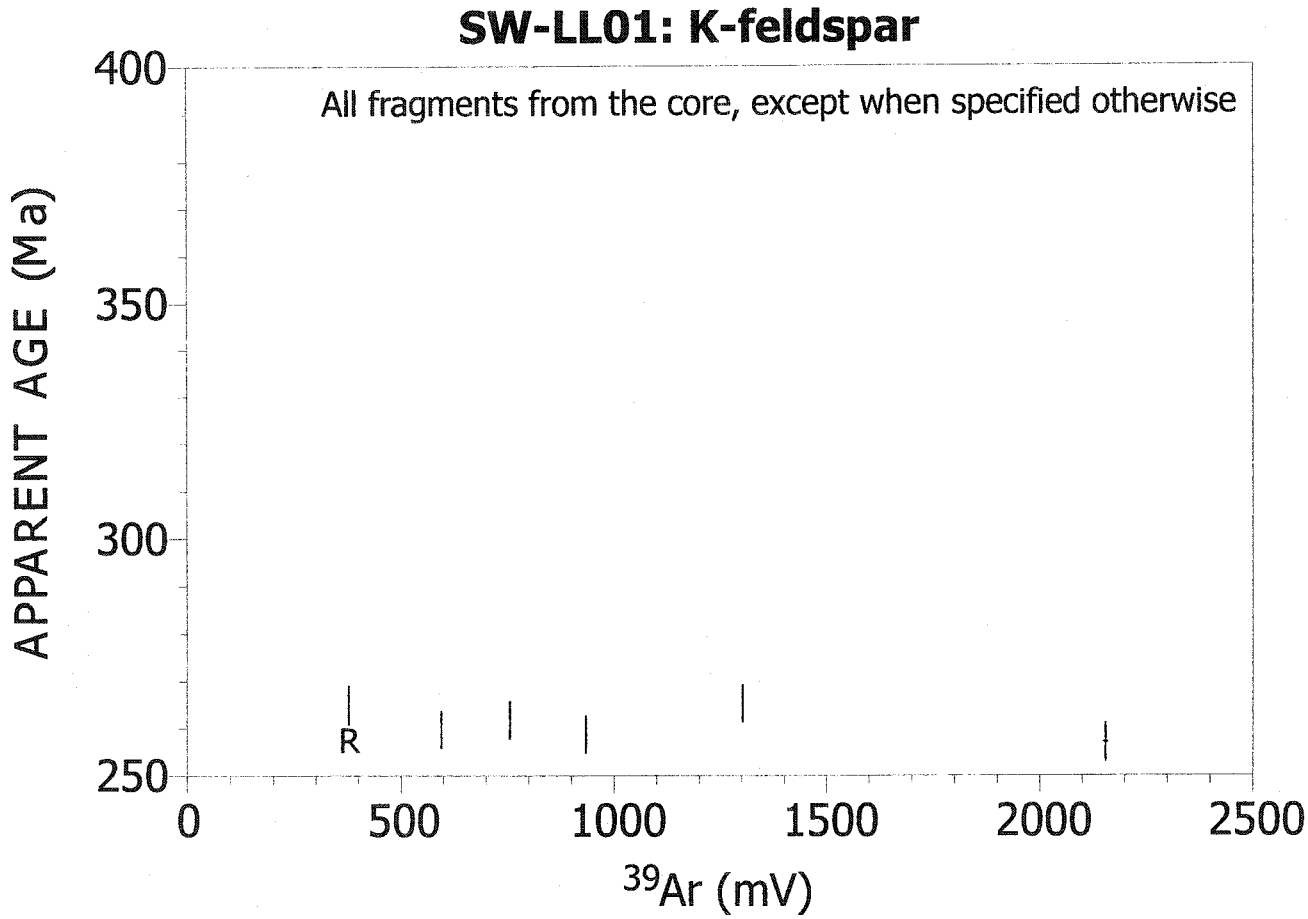

Figure 4.31: Total fusion data for alkali feldspar grains from a fracture (SW-LL01) at the Long Lake deposit. R = rim.

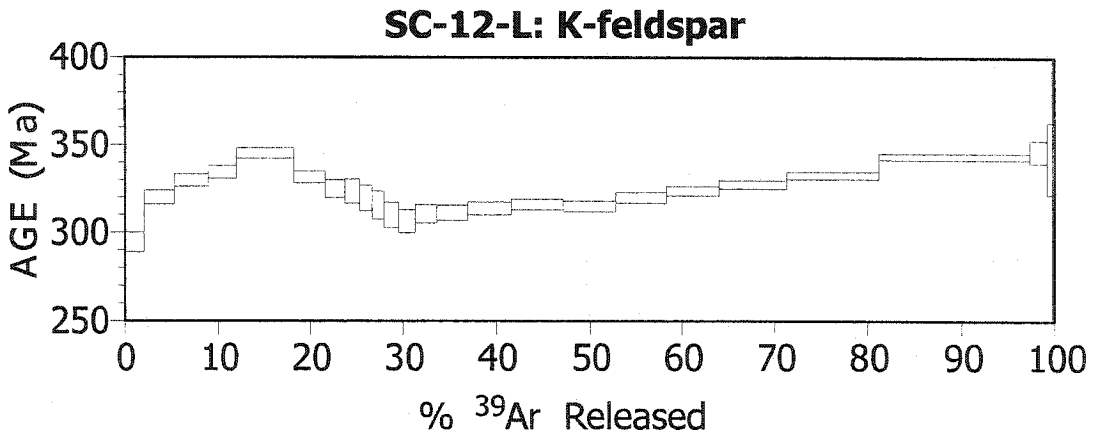

Figure 4.32: Incremental heating spectrum for alkali feldspars from a pegmatite sample (SC-12-L) at the Long Lake deposit.

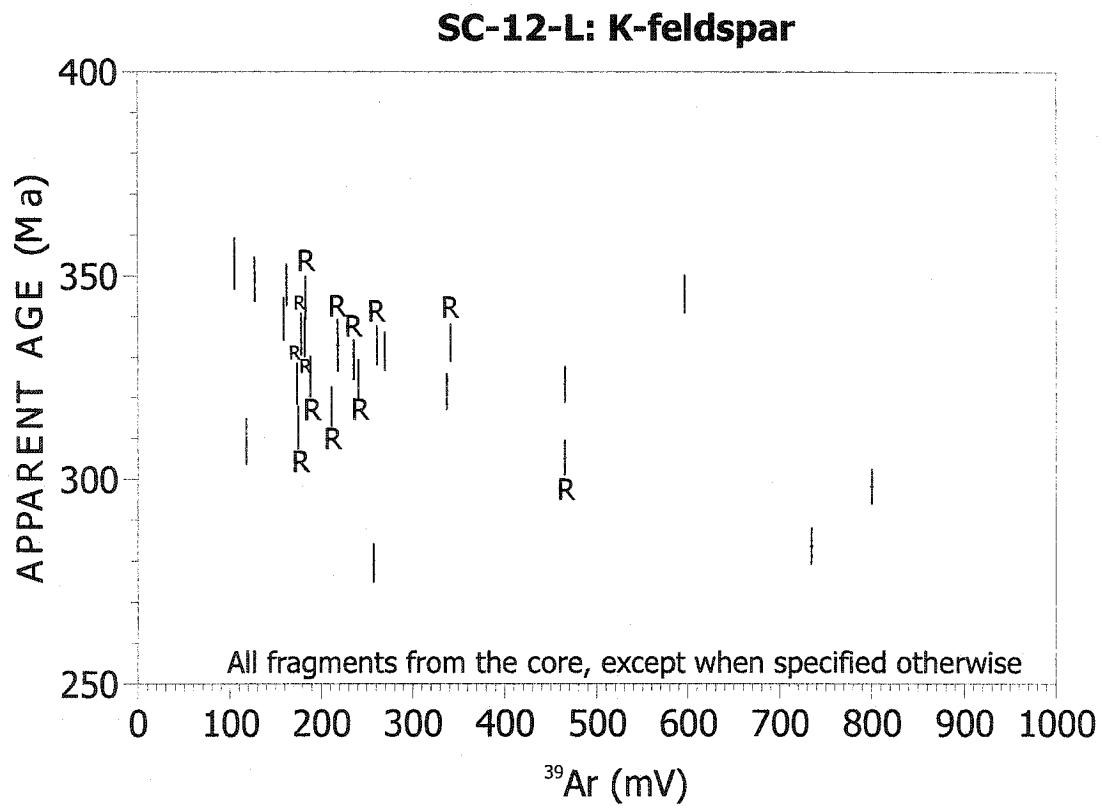

Figure 4.33: Total fusion data for alkali feldspar grains a pegmatite sample (SC-12-L) at the Long Lake deposit. R = rim.

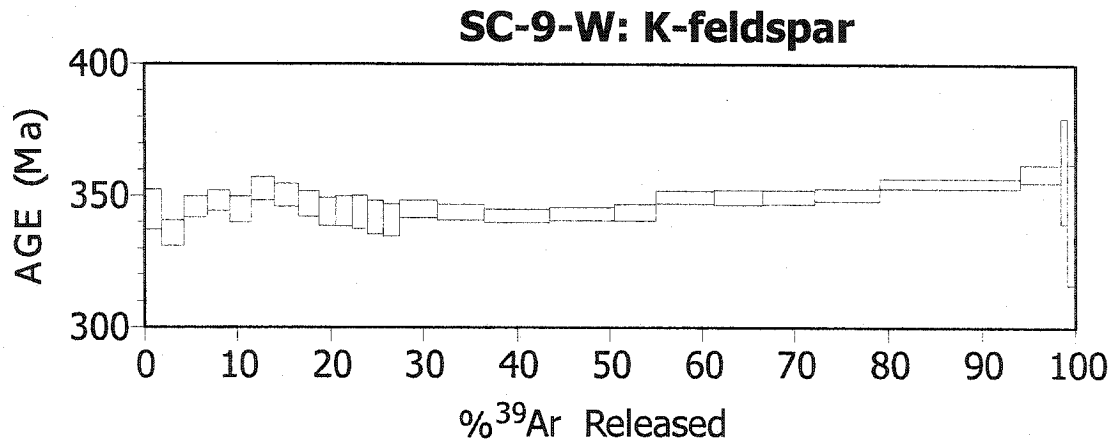

Figure 4.34: Incremental heating spectrum for alkali feldspars from a pegmatite sample (SC-9-W) at the Walker deposit.

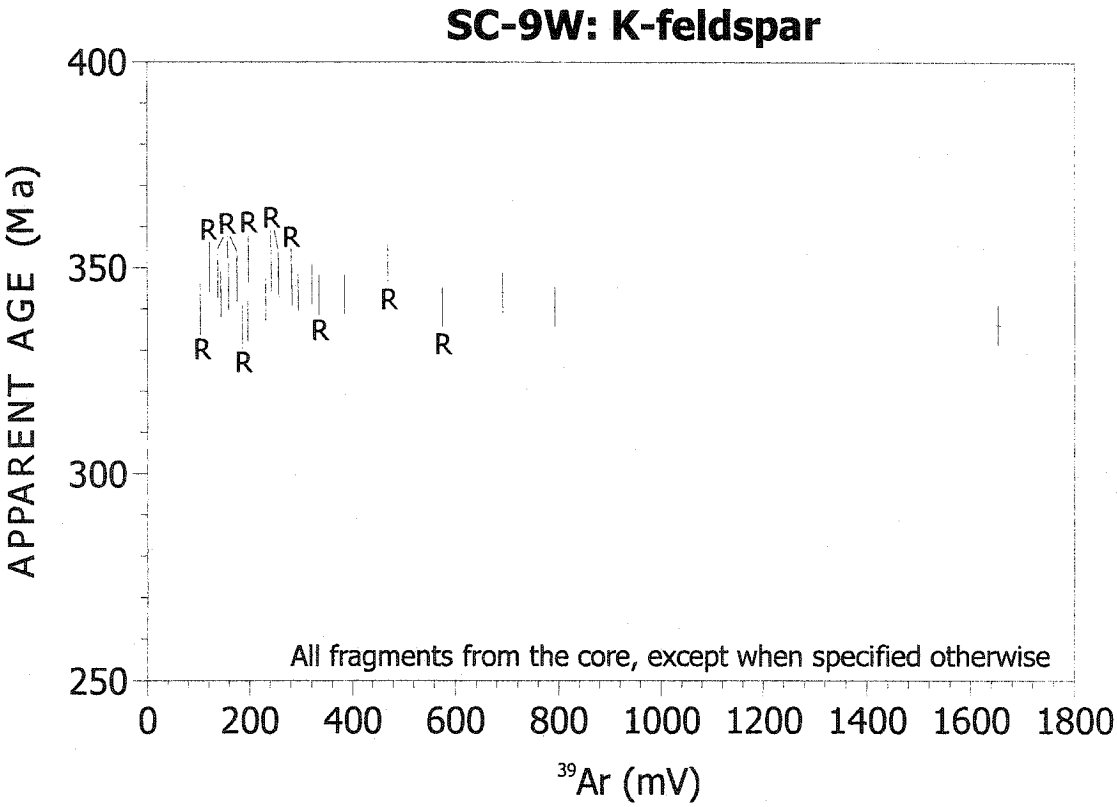

Figure 4.35: Total fusion data for alkali feldspar grains from a pegmatite sample (SC-9-W) at the Walker deposit. R = rim.

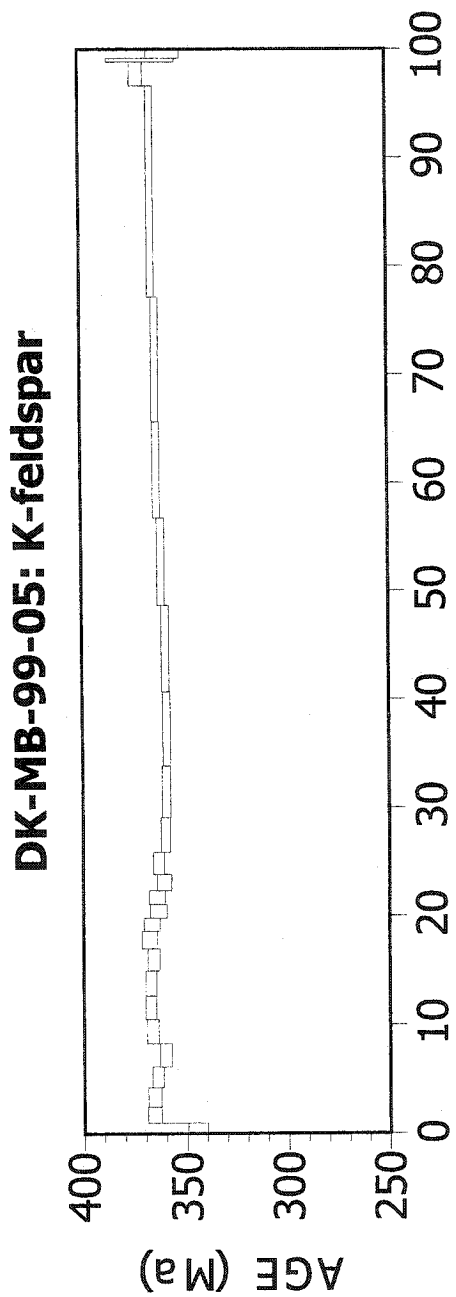

Figure 4.36: Incremental heating spectrum for alkali feldspars from barren monzogranite sample (DK-MB-99-05) at the Millet Brook deposit.

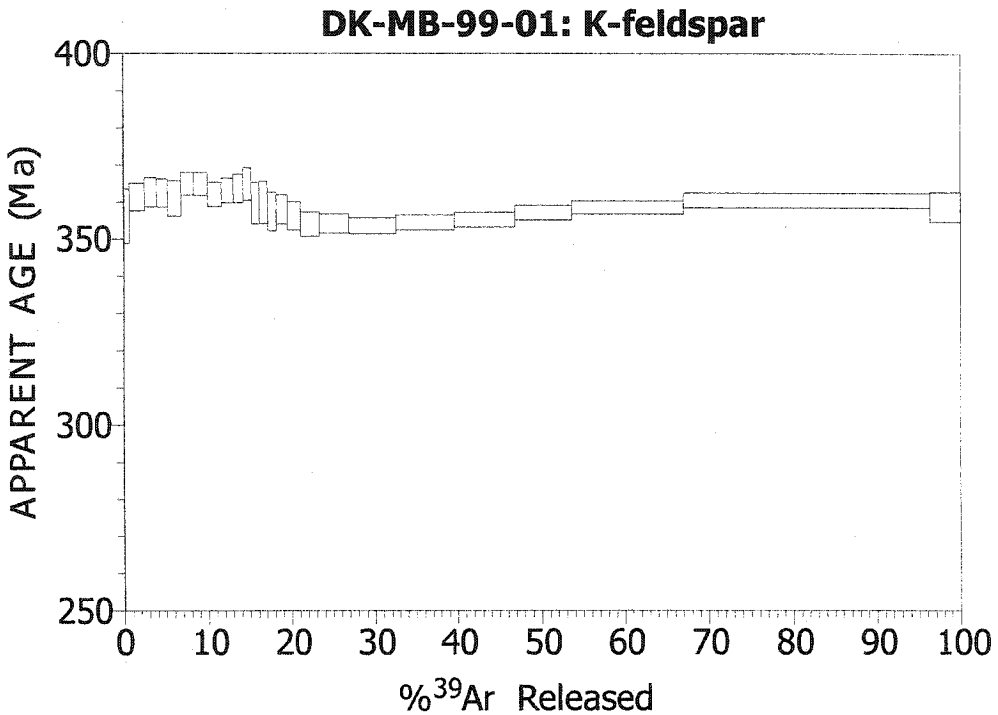

Figure 4.37: Incremental heating spectrum for alkali feldspars from mineralised monzogranite sample (DK-MB-99-01) at the Millet Brook deposit.

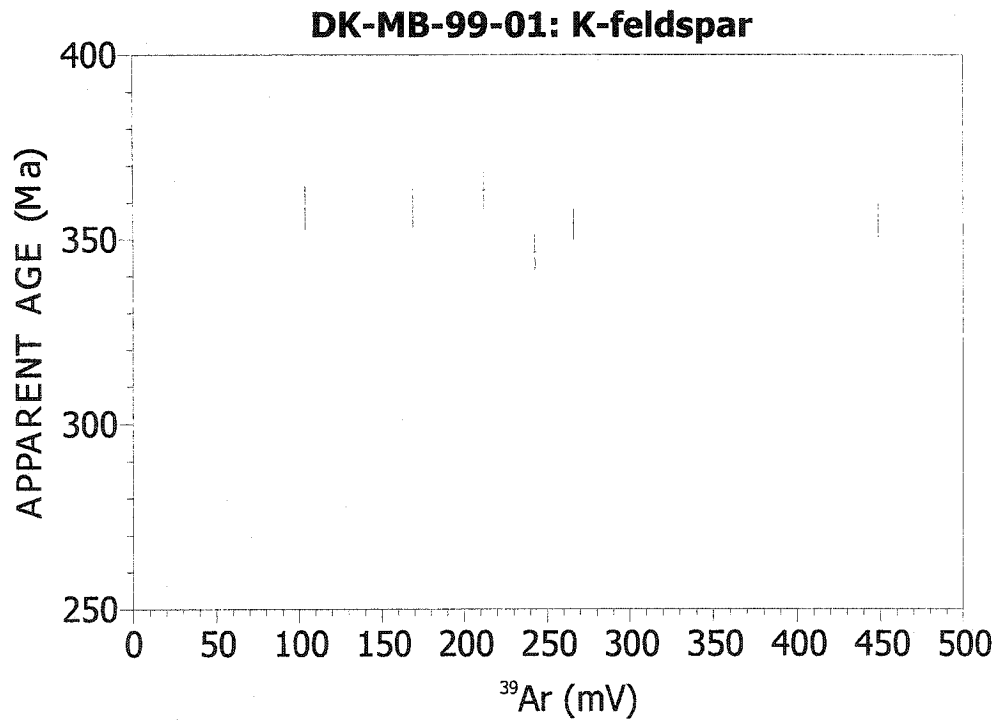

Figure 4.38: Total fusion data for alkali feldspar grains from a mineralised monzogranite sample (DK-MB-99-01) at the Millet Brook deposit.

Mn mines deposit

The age spectrum obtained for alkali feldspar from a breccia sample (DC-dump) from the Mn mines has gradually increasing ages from 276±2 Ma to 343±3 Ma over the first half of the gas release, followed by a plateau over the last eleven steps at 349±2 Ma (Fig. 4.39).

The spectrum for alkali feldspar from a hematised leucogranite (DC-1406) has gradually increasing ages for the first four steps (from 294±3 Ma to 333±2 Ma) followed by a plateau over the last steps (~80% of the ^{39}Ar released) at 343±3 Ma (Fig. 4.40).

Alkali feldspar from a hematised monzogranite (DC-86-3-847) at the Mn mines has a noisy spectrum with no plateau and an age range between 297±6 Ma and 344±4 Ma (Fig. 4.41). The alkali feldspar grains tend to contain many secondary white micas as alteration; therefore, hand-picked alkali feldspar grains may contain a considerable and variable amount of white micas that may have affected the overall spectrum for the alkali feldspar.

A barren monzogranite (DC-85-3-217) yields a spectrum similar to DK-MB-99-05 and DK-MB-99-01 in shape (Fig. 4.42). The spectrum shows increasing ages from 361±2 Ma to 365±4 Ma and then decreasing ages to 357±5 Ma in the first 15 % of gas released. The following steps show ages gradually increasing to 364±2 Ma. Ten successive steps representing about 65% of the ^{39}Ar released define a mean age at 362±2 Ma. Technical problems occurred at the end of the incremental heating experiment, resulting in loss of the final step(s). Hence, the maximum age might not have been reached.

Halifax Pluton

Sample NS-86-3, representing a typical monzogranite from the Halifax pluton, was analysed as a reference from outside of the current study area (Fig. 4.43). The spectrum for this sample first shows an increase in age from 285 ± 2 Ma to 345 ± 3 Ma within the first 20% of ^{39}Ar released. The ages then drop slightly before increasing in a regular fashion to a maximum value of 357 ± 2 Ma.

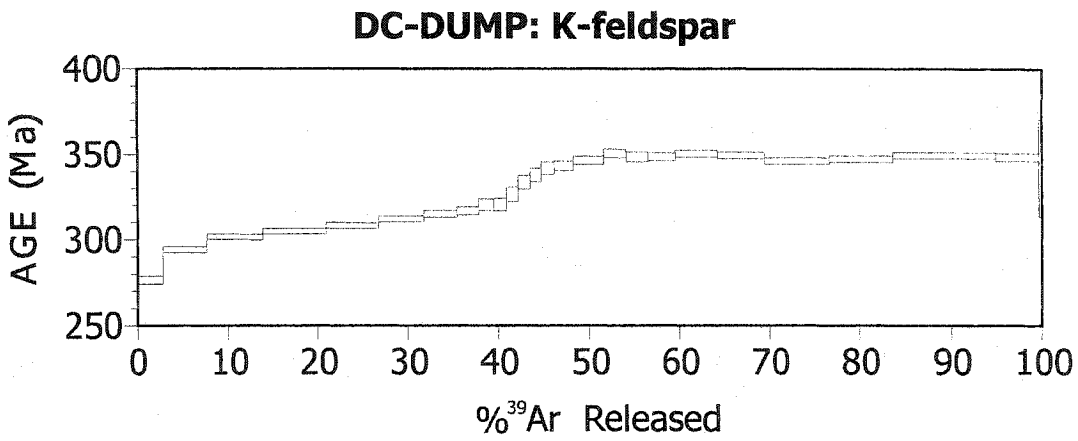

Figure 4.39: Incremental heating spectrum for alkali feldspars from a breccia sample (DC-dump) at the Mn Mines.

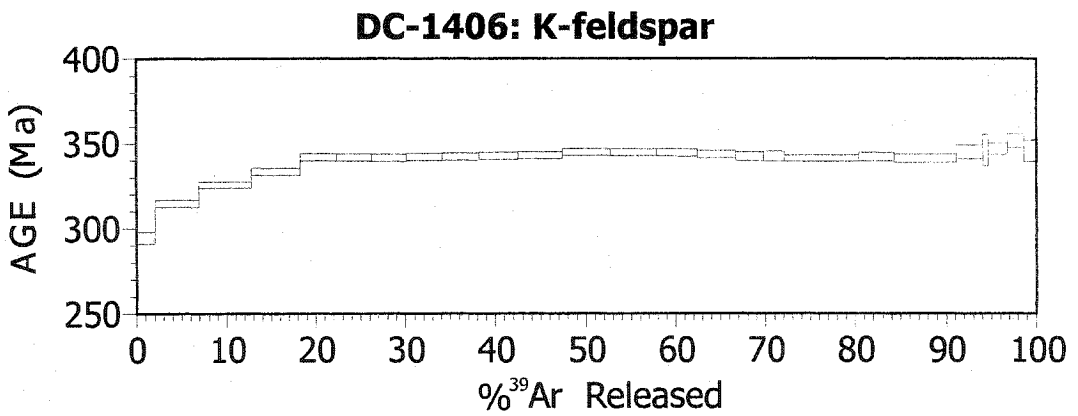

Figure 4.40: Incremental heating spectrum for alkali feldspars from a breccia sample (DC-dump) at the Mn Mines.

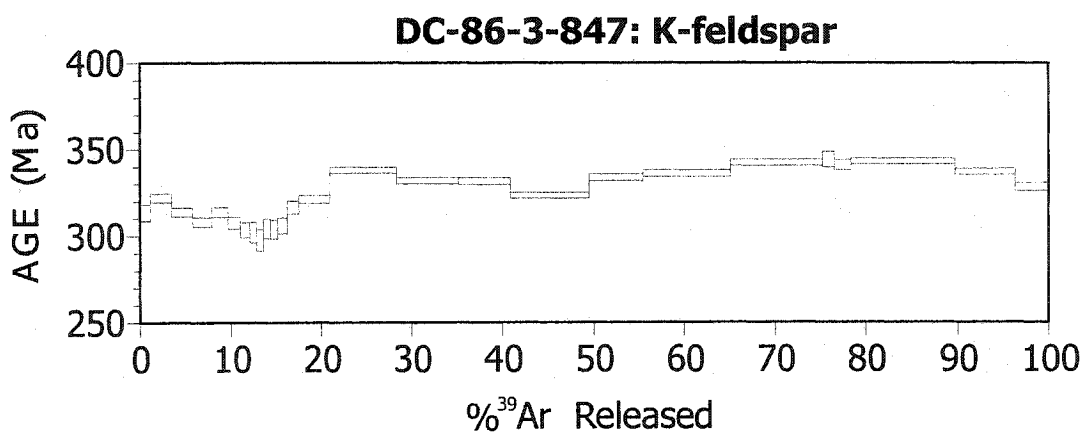

Figure 4.41: Incremental heating spectrum for alkali feldspars from a hematised monzogranite (DC-86-3-847) at the Mn Mines.

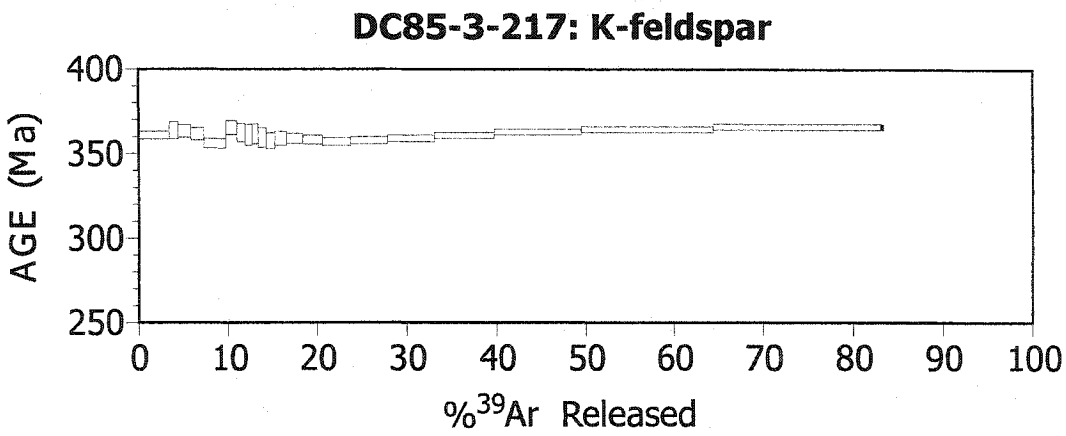

Figure 4.42: Incremental heating spectrum for alkali feldspars from a barren monzogranite (DC-85-3-217) at the Mn Mines.

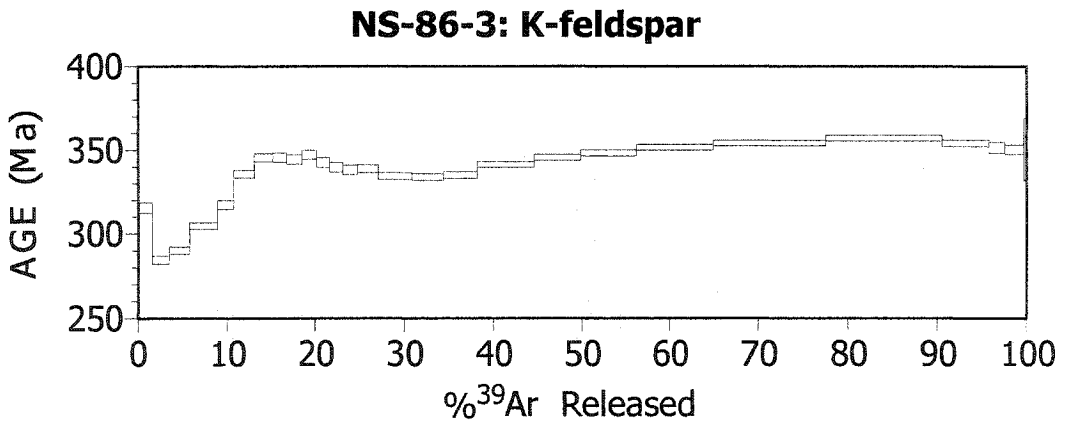

Figure 4.43: Incremental heating spectrum for alkali feldspars from a granodiorite (NS-86-3) of the Halifax pluton.

Deposits	Sample	Incremental heating			Laserprobe	
		Maximum age	Minimum age	Plateau age	Maximum age	Minimum age
Walker	SC-9-W	359±3	336±5		352±6	335±5
Long Lake	SC-12-L	346±6	294±6		349±6	280±5
	SW-LL01				265±4	257±4
	A9b-7504	348±3	298±5		360±5	281±4
Millet Brook	DK-MB-99-01	365±3	354±2		363±5	347±5
	DK-MB-99-05	372±3	345±5	363±2 (mean age)		
Mn Mines	DC-86-3 847	344±4	298±6			
	DC-85-3 217	366±2	356±3	362±2 (mean age)		
	DC-1406	352±4	294±3	343±3		
	DC dump	351±3	276±2	349±2		
Halifax pluton	NS-86-3	357±2	285±2			

Table 4.8: Summary of all $^{40}Ar/^{39}Ar$ age data on alkali feldspars in terms of maximum, minimum, and plateau ages using both incremental heating and laser spot techniques.

4.6.2.2. Summary of $^{40}Ar/^{39}Ar$ data on alkali feldspars

All age data obtained using $^{40}Ar/^{39}Ar$ incremental heating and laserprobe analysis on alkali feldspars range between 372 ± 3 Ma and 276 ± 2 Ma and between 363 ± 5 Ma and 257 ± 4 Ma, respectively (Table 4.8). Two plateau ages were defined at 363 ± 2 Ma (Millet Brook) and 362 ± 2 Ma (Mn mines).

On a histogram of laserprobe ages for alkali feldspars (Fig. 4.44), a weak peak of ages appears around 346 Ma. The histogram of laserprobe data for alkali feldspars shows the data skewed towards younger ages, indicating either slow cooling of the area or resetting of the isotopic system. In the latter case, even the maximum age obtained probably represents partial resetting.

Relative to Ar-Ar ages obtained for white micas, both maximum and minimum ages for alkali feldspars are lower indicating, therefore, that the latter mineral is more susceptible to resetting.

4.6.2.3. Discussion of $^{40}Ar/^{39}Ar$ data from alkali feldspars

Comparison of incremental heating spectra and laserprobe data

Warren (2001) obtained laserprobe data for alkali feldspar fragments from four samples belonging to this study. Two of those samples (SC-12-L and A9B-7504) have irregular incremental heating spectra with a 50 Ma range between maximum and minimum step ages. Laser total fusion of alkali feldspar fragments yields even larger differences between extremes (70-80 Ma). On the other hand, the age spectra for samples DK-MB-99-01 and SC-9-W show a narrower range of ages (~10-25 Ma), which translates into narrower ranges than the corresponding laserprobe data (~15 Ma). These observations suggest that the less disturbed the age spectrum, the smaller the range in the laserprobe data, and the spectra tend to average over some of the age variation detected using the laserprobe method. Fragments of alkali feldspar grains have domains of differing age. Age spectra definitely illustrate the difference in size of each of these regions with the first small steps (i.e., smallest amount of ^{39}Ar released) representing small volumes with low retention of gas, whereas the larger steps at higher ^{39}Ar released correspond to larger areas with higher retention of gas. The variable resetting of ^{39}Ar

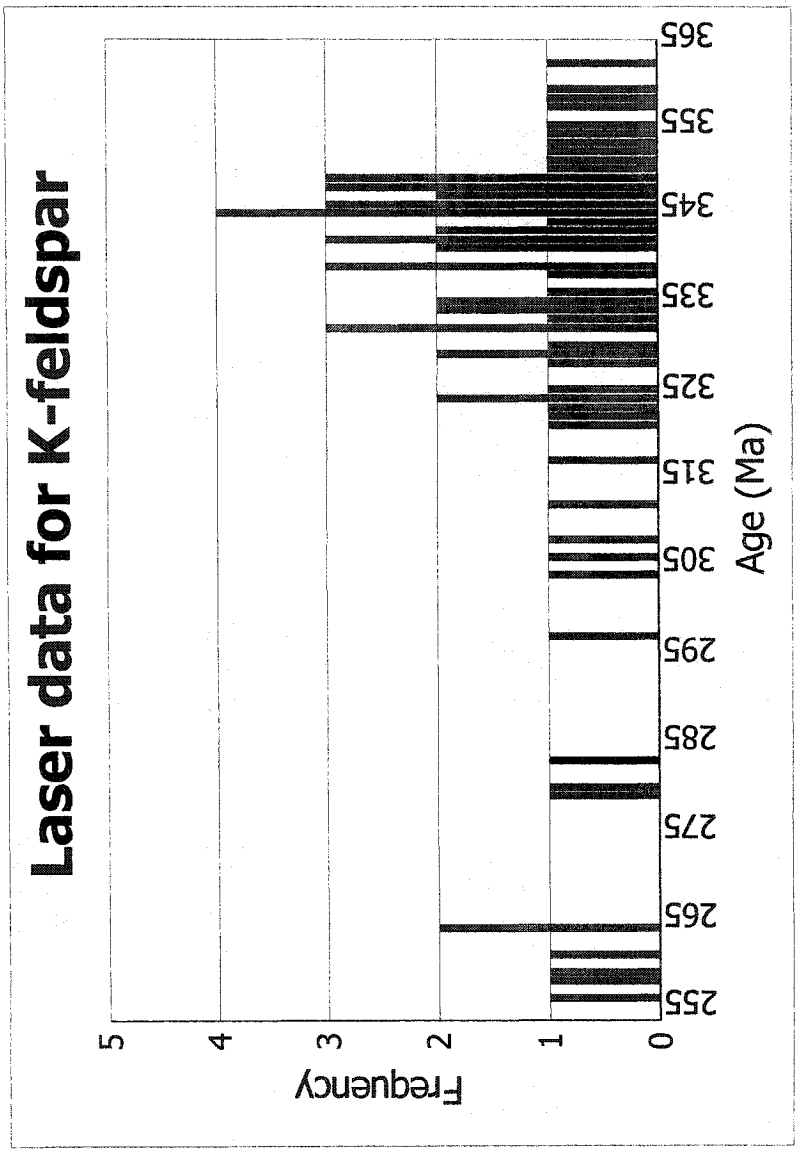

Figure 4.44: Frequency distribution of ages obtained by laserprobe analysis on alkali feldspars for mineral occurrences of the New Ross area.

throughout an alkali feldspar grain may be the consequence of imperfections (dislocation for example) within the grain that provide an escape route for the gas (e.g., Parsons et al. 1999).

In conclusion, laserprobe data seem to be consistent with data obtained by incremental heating. Conventional ages tend to average some of the within-grain age variations. Laserprobe total fusion data on grain fragments is more able to resolve such variations. Also, it is possible that higher ages would have been obtained if smaller fragments of alkali feldspars had been used, because averaging of ages from several domains would have been avoided.

Geological significance of $^{40}Ar/^{39}Ar$ data on alkali feldspars

The reference sample from the Halifax pluton provided spectral information (e.g., ages) comparable to data obtained for samples from the New Ross area.

The oldest ages (365-372 Ma) obtained for alkali feldspars from monzogranite from the Millet Brook deposit, and another from the Mn mines, are close to 372 Ma, but lower than the ~378 Ma recorded from white micas. These oldest ages may represent cooling ages through the closure temperature for alkali feldspars, possibly <350°C (McDougall and Harrison 1999). These three samples are the least altered of the entire data set and, therefore, the least susceptible to argon loss. Also, the higher Ar-Ar feldspar ages (least disturbed) belong to mineral occurrences located furthest to the east (Millet Brook, Mn mines), suggesting that the Alleghanian deformation more strongly affected southwestern Nova Scotia and waned towards the east. Maximum ages for the Long Lake and Walker deposits are lower than 360 Ma, the exhumation age of the NE part of the SMB. If no argon was lost after initial closure of the feldspars, ages lower than 360 Ma may represent the time of closure following cooling, which would be slower in these areas. Exhumation of the terrane and/or erosion of the country rocks above the batholith might not have happened at the same time in all parts of the SMB. Although the SMB intruded the Meguma Supergroup at ~10-12 km (Mahoney 1996), the New Ross area is located above the root zone of the SMB and might have undergone continued influx of magma that kept the area at a higher temperature for a longer time than outer margins of the batholith. Therefore, the cooling rate in the New Ross area depends mainly on the rate of

exhumation by any mechanism above the batholith, the level of heat flow, and fluid circulation. These three factors together may allow for a slower cooling rate in the New Ross area than in more peripheral zones of the SMB. Also, Ford and O'Reilly (1985) documented enrichment in uranium for late-stage leucomonzogranite and/or leucogranite in the New Ross area with, as a consequence, high heat-flow beneath the granitic intrusions (Hyndman et al. 1979). Consequently, minerals with low argon closure temperatures (such as alkali feldspar) may record ages younger than ~360 Ma in the New Ross area. If argon loss occurred, none of the ages obtained using $^{40}Ar/^{39}Ar$ on alkali feldspar has any geological significance, and they only illustrate post-crystallisation resetting of the isotopic system in that mineral.

Minimum ages are definitely too young to be solely explained by slow cooling in the New Ross area; therefore, the isotopic system appears to have been reset. As for the low argon ages in white micas, fluid circulation may favour periodic argon loss in the New Ross area, explaining ages between ~350-330 Ma. Feldspar dating at the Mn mines, Long Lake, and Walker deposit also recorded a reheating event between ~298-275 Ma, corresponding to white mica ages ~300 Ma. This event also partially reset the isotopic system of the sample from the Halifax pluton. Dating of microclines from a fracture within greisen at the Long Lake deposit yields the youngest ages for alkali feldspars in this study (265-257 Ma) and may represent a late-stage fluid circulation event that reset the argon system only locally.

4.7. Integration of Re-Os and Ar-Ar ages into the MLT time frame

4.7.1. Geological time constraints of SMB emplacement within the MLT

The maximum age of the SMB is constrained because it intrudes the ~410 Ma Torbrook Formation. The SMB is also a late- to post-deformation intrusion related to the Acadian Orogeny in the MLT (410-385 Ma, Keppie and Dallmeyer 1987; Muecke et al. 1988; Hicks et al. 1999). The granitic body definitely truncates both the regional folds and the cleavage present in the Meguma Supergroup (Horne and Culshaw 2001), but Horne et

al. (1992) documented formation of a pattern infilled with pegmatitic or quartzitic material that is oriented according to a NW-directed transpression. Also, Benn et al. (1997) reported NE-trending alignment of the magnetic lineations in the granite and foliation patterns of AMS in early Stage I plutons. This NW-oriented transpression is also recorded by dextral displacement along the Cobequid-Chedabucto Fault System (Mawer and White 1987). Horne and Culshaw (2001) subdivided the deformation attributed to the Acadian Orogeny into two events, the second being late relative to the first, maybe even totally separate: 1) a ductile flexural-flow deformation (~395-388 Ma, Hicks et al. 1999), and 2) a brittle flexural-slip deformation (~376 Ma white mica in pressure shadows around arsenopyrite present in the hinge of the Ovens anticline (Hicks et al. 1999; Horne and Culshaw 2001). Horne and Culshaw (2001) suggested a flexural-slip origin for Meguma gold deposits dated at ~ 370 Ma (Kontak et al. 1990b; Kontak and Smith 1993).

The basal part of the Horton Group directly overlying the SMB contains miospores of Late Devonian age (~ 360 Ma) and, therefore, provides a minimum age of exhumation for the NE part of the SMB (Martel et al. 1993; Martel and Gibling 1996). As presented in Section 4.6.2.3, exhumation and/or erosion rates of country rock may not be similar everywhere above the SMB; furthermore, the location of the New Ross area above the root zone of the SMB (i.e., last gasp of magma, higher heat-flow as a consequence of higher concentration of radioactive elements) may have delayed the closure of the isotopic clocks compared to more marginal areas of the SMB.

4.7.2. Discussion

A large number of ages obtained using different isotopic systems since the early 1980's support a ~372 Ma "emplacement" time for the SMB (Clarke and Halliday 1980, Reynolds et al. 1981; Reynolds et al. 1987; Harper 1988; Clarke et al. 1993b), but older ages have sporadically been reported within the MLT, especially when using U-Pb dating on zircon (Hill 1991, Keppie et al. 1993) or monazite (Keppie et al. 1993) (Fig. 4.45).

The Rb-Sr whole rock system is commonly disturbed in granitoid rocks because of the isotopically heterogeneous character of the sources of the magma (Romer 1994 and references herein) and because of disturbance caused by alteration. Therefore, the range of

ages obtained within the MLT using Rb-Sr isotopic dating may be the result of a heterogeneous magma, the consequence of resetting of the isotopic system, or both.

The problem of zircon inheritance for the U-Pb ages mentioned above appears to have been avoided by careful sample preparation by T. E. Krogh (i.e., selection of flat zircon grains without a core) (T. E. Krogh, pers. comm. 2002).

Fallon et al. (2001) reported $^{40}Ar/^{39}Ar$ ages obtained from both step heating and laserprobe analysis for the Port Mouton Pluton in Nova Scotia. They observed an averaging of intra-grain variation by conventional age spectra, whereas laserprobe analysis recorded both older ages, probably related to emplacement, and younger reset ones. In this case, the technological evolution of $^{40}Ar/^{39}Ar$ dating revealed a weakness in conventional age spectrum studies. Similar observations are documented in the present study.

An important point to keep in mind while interpreting the present set of age data is the late character of the dated rocks in the emplacement history of the SMB. The mineral deposits of the New Ross area intruded into a late-stage II pluton and are, for the most part, hosted by highly evolved leucogranites (such as the Keddy-Reeves leucogranite 373 ± 4 Ma to 370 ± 2 Ma Ar-Ar age; Clarke et al. 1993b). The pegmatites represent the last episode of fluido-magmatic crystallisation, i.e., all host granitoid rocks are older. The elvan dykes were magmatic, perhaps preceding the pegmatites. Greisen and vein deposits represent subsolidus alteration of the host granitoid rocks. Therefore, Stage II plutons may be older and ages using similar techniques as those used in this thesis are needed to further assess the duration of SMB emplacement.

Two pegmatite samples dated for this study (SC-12-L and SC-9/15-W) are particularly important because they yield ages from both Re-Os on molybdenite and Ar-Ar on white mica (Fig. 4.46), therefore providing information on the cooling history of each pegmatite. The pegmatite from the Long Lake mineral deposit yields older ages of ~378-376 Ma for both dating methods, suggesting that (1) ~378-377±3 Ma is a close estimate of both crystallisation and mineralisation ages, and (2) the cooling rate between ~500°C and ~350°C was fast, allowing for closing of both isotopic systems within error of the techniques. The pegmatite from the Walker mineral deposit shows the same pattern, but instead with younger ages of ~371-369 Ma. Similar comments about crystallisation age and cooling rate to those for sample SC-12-L are valid for this sample.

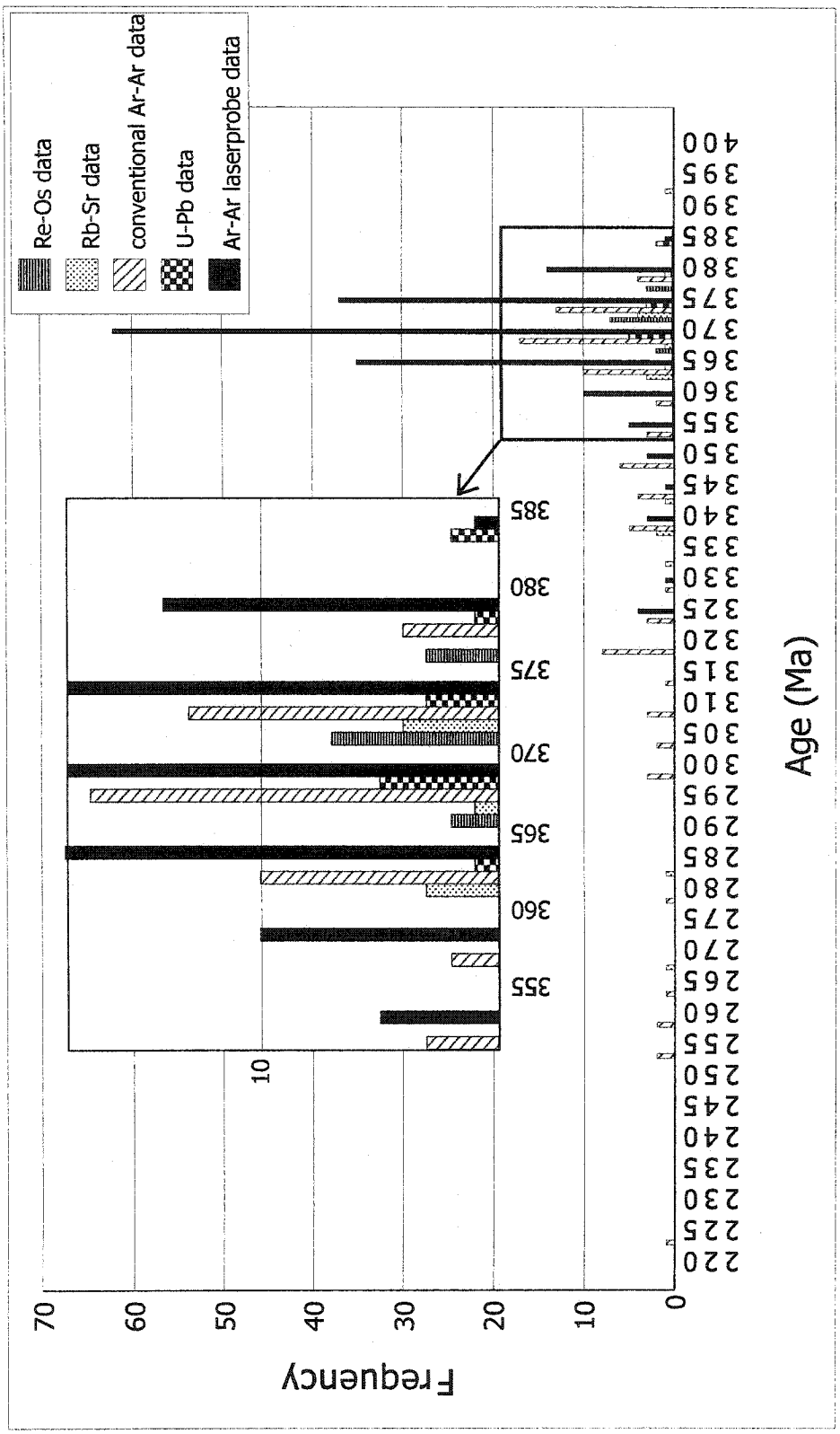

Figure 4.45: Frequency distribution of ages obtained by Ar-Ar incremental heating and laserprobe analysis, U-Pb, Rb-Sr, and Re-Os within the MLT.

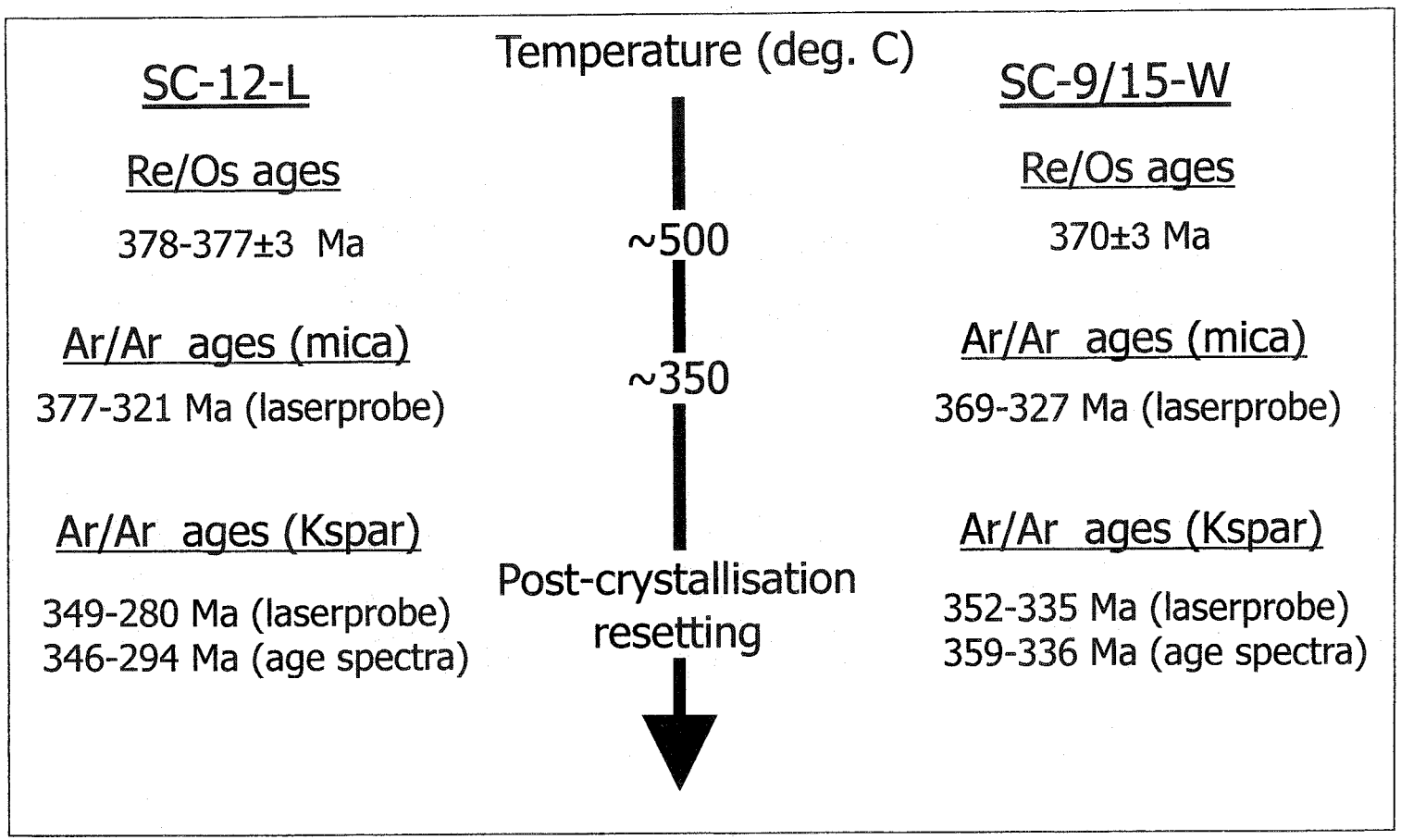

Figure 4.46: Cooling history of two pegmatite samples (SC-12-L and SC-9/15-W) dated for this study using Re-Os on molybdenite and Ar-Ar on white mica.

These new older ages (~378 Ma) for the crystallisation of at least some late-stage mineralisation of the New Ross area define a minimum crystallisation age for the host granitoid rocks to these mineral deposits and require a reinterpretation of the accumulated geochronological dataset.

To account for all observations, the following model involves a monotonic cooling history from crystallisation at ~378 Ma to ~371 Ma for the SMB. Molybdenite from pegmatites at Long Lake and Walker crystallised at, or before, ~378 Ma. The Long Lake area, located closer to the margin of the New Ross pluton cooled below the ~500°C isotherm at ~378 Ma. Because of its more central location within the New Ross pluton, the Walker area cooled more slowly below the ~500°C isotherm, therefore, molybdenite from the Walker deposit indicates a younger ~371 Ma age. In addition, an aplite associated with the pegmatite at Long Lake yields a younger ~371 Ma age, suggesting that post-molybdenite crystallisation resetting may actually occur in the Re-Os isotopic system. For both deposits, the Ar-Ar isotopic clocks in white micas are almost totally reset, because of a regional reheating event at ~371 Ma. This reheating event is either also recorded by satellite plutons around the SMB [the Port Mouton and the Shelburne plutons to the southeast of the MLT (Currie et al. 1998; Keppie and Krogh 1999; Clarke et al. 2000; Fallon et al. 2001) and the Liscomb Complex and Musquodoboit Batholith (with the mineralisation of the Dunbrack deposit) to the northeast (Kontak et al. 1990a; Kontak and Reynolds 1994; Kontak et al. 1999)], or those satellite plutons truly crystallised at that time and caused the reheating event. The ~ 371 Ma reheating event involved intense fluid circulation within the SMB

Other dated mineral deposits in the New Ross area have similar emplacement histories as the Long Lake and Walker deposits: the Turner deposit and the Mn mines yield ages similar to the ~378 Ma obtained at Long Lake. Both of these are vein deposits for which episyenitisation and greisenisation apparently occurred in the same time frame as granite emplacement. Also, the elvan dyke from the Turner deposit retained its crystallisation age better than any other rock type in the New Ross area. An elvan dyke from the Mn mines yields an age in agreement with emplacement at ~378 Ma, although this sample presents a more altered facies than the elvan at the Turner deposit. The Millet Brook deposit has a maximum age of ~375 Ma, an age in agreement within error with

either ~378 Ma or ~371 Ma. A monazite U-Pb age for an unaltered sample from this deposit yield a 377 ± 4 Ma age (Keppie et al. 1993) suggesting, therefore, a similar time frame as presented for the Long Lake deposit. Greisenisation at the Keddy mineral deposit occurred at ~371 Ma, but crystallisation of the granitoid host rock probably took place within the same time frame as other analysed mineral deposits of the New Ross area. Further Re-Os dating is required to better establish the relationship between molybdenite and host rock crystallisation at the Keddy deposit.

A model involving a different time frame for the Long Lake and the Walker deposit with two separate molybdenite mineralisation events (the first one at Long Lake, and the second at Walker) is also possible. In this model, the Walker pegmatite crystallised at ~371 Ma and cooled quickly through the ~350°C isotherm. The Long Lake pegmatite crystallised at ~378 Ma and quickly cooled to ~350°C. Then, the rate of cooling declined, perhaps because of the event of a second pulse of magma in the SMB and provided the energy necessary for generating the fluid circulation leading to the formation of other mineral deposits (such as the Walker deposit). This ~371 Ma event partially reset the Ar-Ar clock of older granitoid rocks of the area, as shown at the Long Lake deposit and previously discussed. This model does not accommodate a younger age for the aplite associated with the pegmatite at the Long Lake deposit.

The implications following the data reported in this study are: (1) the oldest cooling ages obtained using both Re-Os and Ar-Ar laserprobe analysis (~378 Ma) are similar to U-Pb crystallisation ages. They represent the closest estimation to the emplacement time of the SMB and imply a rapid cooling of the New Ross area to the white mica closure temperature, a phenomenon previously observed by Fallon et al. (2001) in the Port Mouton Pluton in the southeastern part of the MLT; (2) the time between deformation of the Meguma Supergroup and granite emplacement is shorter than previously believed (~ 10-15 Ma); and (3) the time gap between granite emplacement and its maximal time of exhumation (360 Ma, Martel et al. 1993; Martel and Gibling 1996) is longer, allowing more time for the exhumation process.

CHAPTER 5

FLUID INCLUSIONS

5.1. Introduction

Chapter 5 is a slightly modified version of a published paper entitled "Granite-hosted mineral deposits of the New Ross area, South Mountain Batholith, Nova Scotia, Canada: P, T, and X constraints of fluids using fluid inclusion thermometry and decrepitate analysis" (Carruzzo et al. 2000; Section 1.3.2.2). The paper is reproduced with permission of the Transactions of the Royal Society of London, which owns the copyrights.

The 370 Ma South Mountain Batholith (SMB) of southwestern Nova Scotia is the largest (~7300 km^2) peraluminous granitoid complex in the Appalachian Orogen of eastern North America (Fig. 1.1). Located above the negative gravity anomaly of the SMB (Clarke and Chatterjee 1988), the New Ross area is unique within this granitic intrusion in its concentration of polymetallic (Sn, U, Mo, Cu, Mn, W) mineral occurrences, which are directly or indirectly associated with highly-evolved fractions of the SMB (Clarke et al. 1985; O'Reilly 1992). O'Reilly et al. (1982) presented the most recent summary of the mineral occurrences of the New Ross area. The intent of the present study is to develop an integrated model clarifying the origin of this diverse suite of mineralization by employing geochemistry, stable isotopes, fluid inclusions, and geochronology. Herein we present the results of the fluid inclusion study.

This investigation employs a set of fluid inclusion data (fluid inclusion petrography, thermometry, and decrepitate analysis) from eight mineralized centers of the New Ross area, distributed over an area of ~ 500 km^2. The objectives of the study are to provide compositional constraints on the fluids present (both in terms of salinity and cation content), to constrain the temperature of fluid entrapment, and to determine the origin of the fluids involved in mineralization and alteration. The data presented here reveal the presence of fluids of inferred magmatic, metamorphic, and meteoric origin. For pegmatite-

and greisen-type mineralization, fluids were entrapped under isobaric (the pressure applicable to the emplacement depth of the SMB at 370 Ma) conditions of decreasing temperature (500° to 200 °C). For vein-type deposits, which are dominated by low-salinity (<2-3 wt. % equiv. NaCl) fluids, the pressure-corrected homogenisation temperatures are excessively high, implying a lower pressure than that of the batholith emplacement at 370 Ma. These data suggest that the vein deposits were either connected to the surface through fractures, or that they did not form at the same depth as pegmatite and greisen deposits, suggesting rapid uplift or exhumation of the area and a temporal gap in hydrothermal activity. Future dating of the mineral deposits should provide a better understanding of the temporal evolution of the New Ross mineral occurrences.

5.2. Regional geology

The Meguma Zone is the outermost lithotectonic terrane of the Canadian Appalachians, and two distinct lithologies dominate its bedrock geology (Fig. 1.1): (i) the Meguma Supergroup (Schenk 1995a), composed of Cambrian-Ordovician metasedimentary rocks (Halifax and Goldenville groups), which underwent regional deformation and metamorphism related to the ca. 400 ± 10 Ma Acadian Orogeny (Keppie and Dallmeyer 1987; Muecke et al. 1988; Hicks et al. 1999); and (ii) thirteen coalesced peraluminous granitoid plutons [comprising the South Mountain Batholith (SMB)] intruding the Meguma Supergroup. The SMB is generally subdivided into early Stage I plutons (granodiorite, biotite monzogranite) and more evolved Stage II plutons (leucomonzogranite) (Fig. 1.2a).

The eight mineral occurrences of this study are part of the New Ross-Vaughan Complex (NRVC) (McKenzie 1974), renamed the New Ross pluton (NRP) (MacDonald et al. 1992; MacDonald, 2001; Fig. 1.2a) of the SMB, and also an earlier pluton (i.e., Stage I pluton) called the Salmontail Lake Pluton (SLP) (Fig. 1.2a). The NRP contains pegmatite deposits (Reeves, Keddy, Morley's, Walker, Long Lake) and greisen-type deposits (Turner, Walker, Long Lake), whereas the SLP hosts vein deposits (Millet Brook, Mn Mines), (nomenclature of deposits after MacDonald, 2001; see Fig. 1.2a, b for locations).

The NRP shows the most pronounced negative gravity anomaly in the SMB (Garland 1953, Clarke and Chatterjee 1988). This negative Bouguer anomaly indicates a mushroom

shape for the SMB with a maximum thickness of 10-20 km near New Ross (O'Reilly 1975). Therefore, the formation of the numerous and varied mineral occurrences in this area (Fig. 1.2b) is a logical consequence of a higher heat flow favoring intensive fluid circulation, and the presence of highly-evolved granitoid rocks enriched in incompatible metals.

Radiogenic isotope data (U-Pb, $^{40}Ar/^{39}Ar$, or Rb/Sr) available for the SMB give remarkably similar ages: U-Pb zircon and monazite ages for the SMB and six satellite plutons in the Meguma Zone yield similar ages of 373 ± 2 Ma (Harper 1988; Tate et al. 1997; Keppie and Krogh 1999), essentially the same as $^{40}Ar/^{39}Ar$ mica ages for the same intrusions (Reynolds et al. 1981; Reynolds et al. 1987; Clarke et al. 1993b; Fallon 1998) and Rb/Sr dating of granodiorite and monzogranite phases of the SMB (Clarke and Halliday 1980; Harper 1988). Clastic sediments and marine carbonates of the Horton and Windsor Groups, respectively, unconformably overlie the SMB. The presence of miospores of Late Devonian age (Late Famennian) in the basal Horton Group indicates a minimum age of ~ 360 Ma (time scale of Tucker et al. 1998) for exhumation of the NE part of the SMB prior to formation of the Late Devonian/Carboniferous basins (Martel et al. 1993; Martel and Gibling 1995). Keppie and Dallmeyer (1995) suggest rapid exhumation (~ 13 km) in the Meguma Zone between 370 and 360 Ma. Murphy et al. (1999) propose that an overridden plume is the cause of the rapid Late Devonian uplift and exhumation of the Meguma Zone. Clarke et al. (1976) observed magmatic andalusite in the SMB, which indicates a pressure of 3.3-3.9 kbars and temperature of 650-680 °C for late-stage crystallization of the SMB. Ham and Kontak (1988) propose a pressure of ~ 2 kbars for magmatic (primary) muscovite crystallization. Based on a study of the metamorphic aureole of the SMB, Mahoney and Raeside (1995) report an average pressure of ca. 3-3.5 kbars, corresponding to depths of emplacement of 10-12 km.

Deposits (type)	Host granitoid	Metal association, mineralization	Alteration types	Fluid inclusion samples	References
Reeves (pegmatite)	Keddy-Reeves lgr (which intrudes the Salmontail Lake mgr to the north)	**Sn**: cassiterite; F: fluorite; W: wolframite, scheelite, tungstite; Li: lepidolite; Nb, Ta: columbite		▪ Salmontail Lake mgr ▪ Keddy-Reeves lgr ▪ quartz vein ▪ pegmatite	1, 2, 3
Morley's (pegmatite)	New Ross lgr	**W**: scheelite, wolframite; Sn: cassiterite; F: fluorite; Na, Ta: columbite	▪ hematisation ▪ brecciation	▪ pegmatite	1, 2, 3
Keddy (pegmatite, greisen)	New Ross lmgr	**Mo**: molybdenite; W: wolframite, scheelite; F: fluorite; Nb, Ta: columbite	▪ greisenisation (qz, wm, topaz)	▪ New Ross lmgr ▪ pegmatite	1, 2, 3
Long Lake (pegmatite, aplite, greisen)	Long Lake lgr	**Mo**: molybdenite; Cu: chalcopyrite; W: wolframite, scheelite; F: fluorite	▪ greisenisation (qz, wm, chl)	▪ Long Lake lgr ▪ pegmatite ▪ banded aplite ▪ greisen	2, 3
Walker (pegmatite, aplite, greisen)	Panuke Lake lmgr	**Mo**: molybdenite; Cu: chalcopyrite, bornite; F: fluorite; Zn: gahnite; W: wolframite; Sn: cassiterite	▪ greisenisation (qz, wm, chl, tourmaline)	▪ Panuke Lake lmgr ▪ Pegmatite ▪ aplite	1, 2, 3
Turner (greisen)	Panuke Lake lmgr	**Sn**: cassiterite; Cu: chalcopyrite, chalcocite, covellite; As: arsenopyrite; Zn: sphalerite; U: autunite	▪ greisenisation (qz, wm, chl) ▪ chloritisation ▪ hematisation	▪ greisen	1, 2, 3, 4
Millet Brook (vein)	Salmontail Lake mgr and biotite gdr	**U**: pitchblende, autunite, torbernite; Cu: chalcopyrite, bornite, covellite, chalcocite; Pb: galena; Zn: sphalerite W: wolframite	▪ hematisation ▪ carbonitisation ▪ albitisation ▪ biotitisation	▪ Salmontail Lake mgr ▪ U-irradiated samples (smoky quartz)	3, 5, 6
Mn mines (vein)	Salmontail Lake mgr	**Mn**: pyrolusite, manganite, psilomelane, rhodochrosite; Fe: hematite, goethite, limonite	▪ episyenitisation ▪ hematitisation	▪ Salmontail Lake mgr ▪ breccia ▪ Gold River lmgr	2, 3, 7

Table 5.1: Description of host granitoid rock, mineralisation (main metal in bold), alteration, samples, and references for eight mineral deposits of the New Ross area. References: 1) Charest 1976, 2) O'Reilly et al. 1982, 3) Logothetis 1985, 4) Farley 1978, 5) Chatterjee et al. 1982, 6) Chatterjee and Strong 1984, 7) O'Reilly 1992. gdr = granodiorite, mgr = monzogranite, lmgr = leucomonzogranite, lgr = leucogranite.

5.3. Mineral deposits and sampling

MacDonald (2001) provides an exhaustive history of base-metal and lithophile-element exploration in the SMB, including the New Ross area, from the initial discovery of mineral occurrences in the 1900's to the present. Apart from the past-producing (1985-1992) East Kemptville Sn-Zn-Cu-Ag deposit located in the southwestern part of the SMB, the only past-producing mine of the SMB was the Mn-Fe mines, exclusive of the environmental moratorium placed on the Millet Brook U-Cu deposit of the New Ross area. The Mn mines and the Millet Brook deposit still contain possible reserves of 15,000 tons of Mn oxides (Weeks 1945) and 500 tons of U_3O_8 (Chatterjee and Strong 1984), respectively. The following description of the mineral occurrences is based on assessment reports in NSDNR files, geological maps of the area (Corey 1991; Ham 1991; Horne 1992), the earlier work of O'Reilly et al. (1982), and new observations of the present study. Summarized in Table 5.1 is information concerning the host granitoid rock, mineralisation, alteration, fluid inclusion samples, and references for each mineral deposit. Figure 5.1 provides the general paragenetic sequence of the host granitoid rocks, pegmatite/greisen/vein type deposits, and observed alteration in the deposit sites. Detailed mineral parageneses for each deposit are beyond the scope of this paper, but are found in the references cited in Table 5.1.

Reeves Sn Pit: The Reeves quartz-feldspar-white mica pegmatite intrudes the medium-grained Keddy-Reeves leucogranite, which in turn intrudes the Panuke Lake muscovite-biotite leucomonzogranite, and, to its northern part only, the Salmontail Lake biotite monzogranite. Numerous metallic minerals (cassiterite, wolframite, scheelite, tungstite, columbite) were reported from the central part of the dyke, but observation of and access to the pegmatite is limited after the excavated pit was filled up. The dump area contains pegmatitic samples, with fluorite and lepidolite.

Morley's pegmatite: The Morley's pegmatite is hosted by the Panuke Lake biotite-muscovite leucomonzogranite. The pegmatite grades into a medium-grained leucogranite suggesting that they are contemporaneous, and both intrude the host rock. The pegmatite grades into massive quartz towards the center of the dyke. Fluorite and minor molybdenite occur, although other minerals of interest (scheelite, wolframite, cassiterite, columbite)

have been reported (Campbell 1940). Hematisation and brecciation associated with the intrusion of a brick red jasper breccia dyke overprint both the host rock and the leucogranite.

Keddy Prospect: The host granitoid rock of the prospect is the fine- to medium-grained, muscovite-rich Panuke Lake leucomonzogranite. The prospect is divided into three sites previously prospected for molybdenite: (1) a central site of greisenised leucomonzogranite with rare molybdenite; and (2) a southern site exposing a north-trending pegmatite intruding the leucomonzogranite. Greisenised leucomonzogranite locally borders this pegmatite. Minor molybdenite occurs and significant amount of columbite is present. A few pods of another north-trending pegmatite outcrop north of the southern site, but this was barren of mineralization. (3) A site located north from the central area comprises a small pit and dump samples of pegmatite contain molybdenite.

Long Lake Prospect: This prospect is hosted by the Long Lake leucogranite that intrudes metasedimentary rocks of the Goldenville Group. The main location for the prospect, at the NW end of Long Lake, comprises leucomonzogranite that grades into quartz-muscovite-albite and quartz-muscovite greisen. Areas of well-developed greisen contain molybdenite, wolframite, fluorite, and copper sulphides. West from the greisen zone, a molybdenite-bearing pegmatite and banded aplite are found.

Walker Moly: The Walker Moly occurrence is hosted by the coarse-grained Panuke Lake leucomonzogranite. The deposit site lacks outcrop, but a dump pile contains numerous pegmatite, aplite, and greisen samples. Slipp (1946) reported the greisen as being distributed sporadically along the margins of the pegmatite dyke. Molybdenite, wolframite, cassiterite, bornite, and chalcopyrite are associated with the greisen, whereas only copper sulphides and molybdenite are present in the aplite and pegmatite.

Turner Tin Prospect: The Turner prospect is hosted by the Panuke Lake leucomonzogranite, and is located south of a roof pendant of Goldenville Group metasedimentary rocks marking the boundary between the New Ross and Salmontail Lake plutons. The prospect consists of four metre-size east-dipping veins divided into quartz-greisen zones (Discovery, Elephant, and Turner veins) and a quartz porphyry dyke (Elvan vein). Most of the quartz and greisen veins are steeply-dipping to the east. Mineralization is

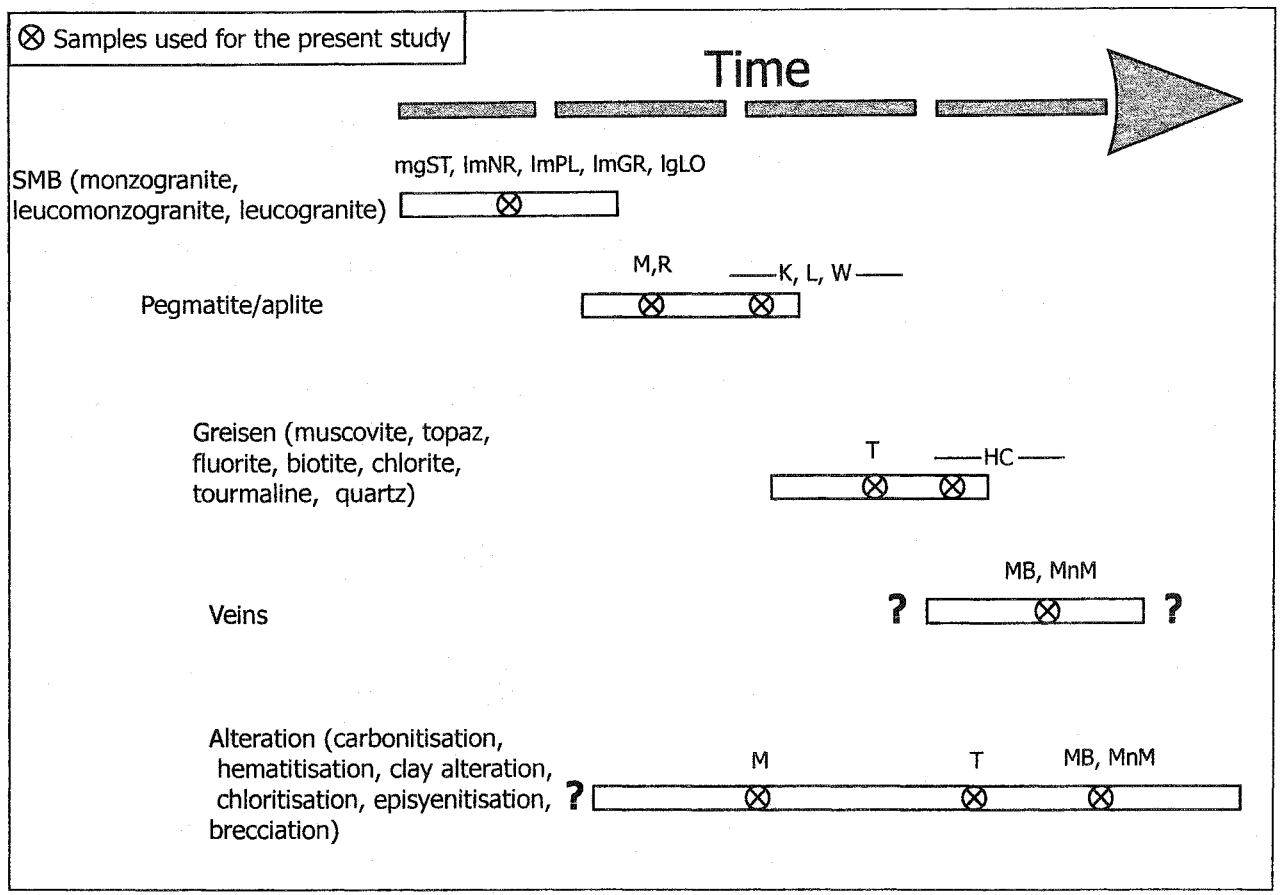

Fig. 5.1: General paragenetic sequence in the New Ross area. Abbreviations: mgST = Salmontail Lake monzogranite, lmNR = New Ross leucomonzogranite, lmPL = Panuke Lake leucomonzogranite, lmGR = Gold River leucomonzogranite, lgLO = Long Lake leucogranite, M = Morley's, R = Reeves deposit, K = Keddy deposit, L = Long Lake deposit, W = Walker deposit, T = Turner deposit, HC = Herring Cove vein system, MB = Millet Brook deposit, MnM = Mn mines.

scattered within the greisen, and the following minerals occur: cassiterite, chalcopyrite, arsenopyrite, and pyrite. The deposit site presents numerous quartz veins (centimetric to metric in size).

Millet Brook Deposit: Biotite granodiorite and the Salmontail Lake biotite monzogranite host the Millet Brook deposit (MacDonald 2001). Similar to the Turner prospect, the Millet Brook deposit is located near a roof pendant of Goldenville Group metasedimentary rocks at the boundary between the New Ross and the Salmontail Lake plutons. A cupola and late-stage dykes of leucomonzogranite underlie the deposit site (Chatterjee and Strong 1984). The uranium mineralization occurs in en-echelon pods and lenses confined to NE trending fault zones in the biotite granodiorite (Chatterjee and Strong 1984). Several types of alteration accompany the mineralized fractures: biotitisation, episyenitisation, kaolinisation, chloritisation, and hematisation. A variety of minerals are reported in previous studies (pitchblende, autunite, tobernite, chalcopyrite, bornite, covellite, chalcocite, galena, sphalerite, wolframite). Samples used in the present study come from drill cores since the site has been reclaimed and no outcrops are presently accessible. Mineralized and non-mineralized samples are easy to discriminate: the former are characterized by dark gray to black quartz, a higher percentage of modal biotite, altered plagioclase, turbid orange K-feldspar, hematisation, and a general crumbly nature and porous texture.

New Ross Mn mines: The Mn mines consist of two separate zones: the Cain and Riddle Mine and the Dean and Chapter Mine. The manganese deposits, found along northeast faults zones that dip steeply to the NW and are hosted by the Salmontail Lake biotite monzogranite. Several bodies of Gold River leucomonzogranite outcrop in the area and intrude the fault zone at depth (O'Reilly 1992). O'Reilly et al. (1982) suggest that the mineralized zones are within steeply-dipping faults. The presence of a footwall breccia versus unaltered granite in the hanging wall provides further evidence for the presence of faults. Using mineralogical, textural and geochemical data, O'Reilly (1992) suggested a hypogene origin for the Mn mineralization with the fluids and heat derived from the Gold River leucomonzogranite. The mineralized zones do not outcrop, therefore samples were collected from drill core and dump material.

5.4. Fluid Inclusions

5.4.1. Petrography and classification of fluid inclusions

Because of the regional scope of the present study, fluid inclusion material was collected from host granitoid rocks, pegmatite/aplite, greisen, and vein material. Thick (100-150 μm) polished sections of all samples (n = 90) were examined at room temperature (ca. +25°C) using a petrographic microscope and, based on phases present (Roedder 1984; Goldstein and Reynolds 1994), the following types of fluid inclusions (Fig. 5.2a, b, c) hosted in quartz are: (1) monophase liquid (L); (2) monophase vapour (V); (3) aqueous, L-V; (4) aqueous, L-rich ± solids (carbonates, silicates); and (5) aqueous, L-rich + Halite. Types 3, 4, and 5 are dominant, with type 3 clearly the most abundant. It was not possible to recognize primary inclusions based on the conventional criteria (e.g., growth zones), hence all inclusions are interpreted as secondary or pseudo-secondary (Goldstein and Reynolds 1994). A variant of the inclusion types based on texture is a group of decrepitates or imploded inclusions, discussed in more detail below. Post-entrapment necking occurred in samples from each deposit, as evidenced by the presence of highly variable L:V ratios in the same assemblages and the general highly-irregular shapes of these fluid inclusions. Table 5.2 gives detailed descriptions of fluid inclusion characteristics for each deposit.

Accidental trapping of minerals (carbonates, white mica, and undetermined phases) occurs in fluid inclusions from several deposits. Rare cases of aqueous fluid inclusions containing CO_2 in solution, as indicated from clathrate formation, exist in pegmatitic samples from the Long Lake and Walker deposits. Complex fluid inclusions (e.g., Sterner and Bodnar 1989) (Fig. 5.2d) occur in several mineralised samples from Long Lake, Reeves, and Walker, as well as in samples from the host granitoid rock at Reeves. These complex fluid inclusions (Fig. 5.2d) appear as an annulus of small dark inclusions surrounding a much larger ovoid/rounded central area; the small outer inclusions are also arranged in a star-like pattern. A preferred orientation of the small inclusions occurs in the sample from Walker. At Reeves, the central part of the clusters is enriched in birefringent phases (silicates?). Similar complex fluid inclusions occur in quartz and scheelite crystals

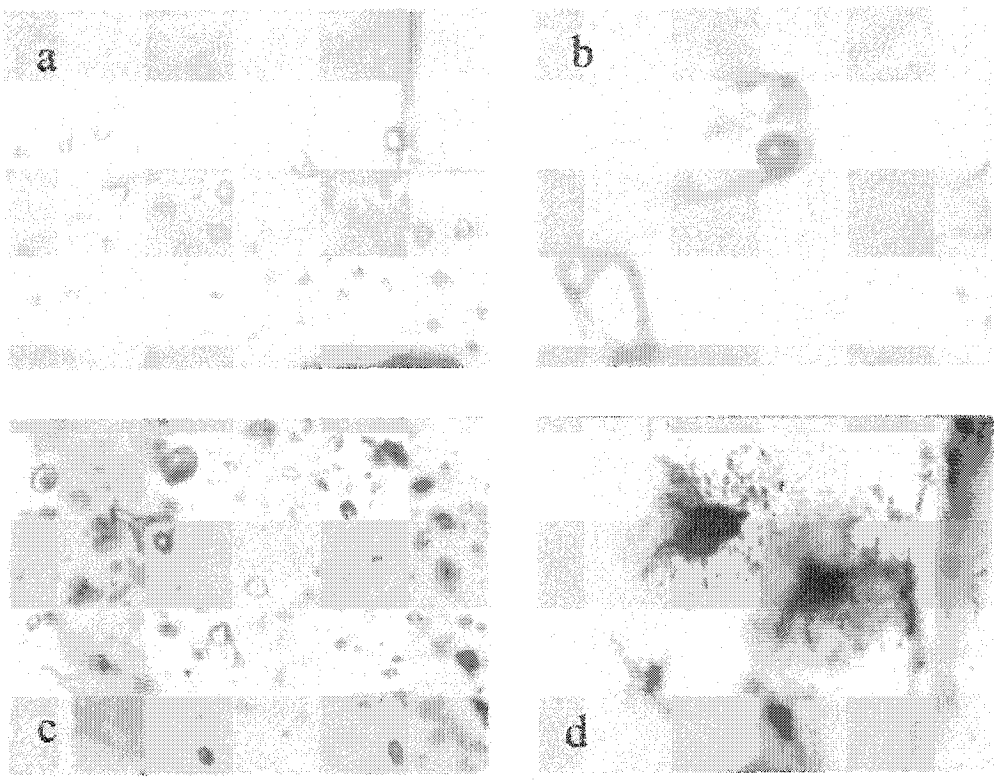

Fig. 5.2: Photomicrographs of fluid inclusions hosted by quartz from mineral deposits of the New Ross area. (a) sericitised leucomonzogranite at the Mn mines: two-phase (L-V), negative-shaped/equant, ~ 30 m in size, low salinity (0 wt. % NaCl equiv.). (b) quartz vein at the Reeves deposit: three-phase (L-V-H), irregular in shape, 60 m in length, high salinity (26 wt. % NaCl equiv.). (c) pegmatite at the Long Lake deposit: monophase V-rich and L-rich, and two-phase (L-V), irregular in shape, between 15 and 20 m in size; variable L/V ratios indicate necking. (d) complex fluid inclusions from a pegmatite at the Long Lake deposit; the lower left inclusion shows a large ovoid centre area surrounded by small outer inclusions arranged in a star-like pattern. Larger complex inclusion is 30 m in size.

from vein gold deposits hosted in the Meguma metasediments (Baker 1996; Kontak et al. 2002).

5.4.2. Methods/Analytical Techniques

Fluid inclusion thermometric measurements were made using a modified U.S.G.S-type gas-flow heating-freezing stage. The instrument was calibrated with a variety of standards, and then tested by using synthetic fluid inclusions and an ice bath. Through repetition of measurements on inclusions, the precision is ±0.2 °C. Larger uncertainties apply to small fluid inclusions (<3-4 μm). Accuracy for the equipment is ±0.2 °C for low-temperature runs and ±1 °C for high temperatures (Kontak 1998a). Low-temperature phase changes were measured first to avoid potential stretching of inclusions and decrepitation. In addition, quartz chips having a range of T_h were observed at gradually increasing temperatures to avoid stretching or decrepitation of inclusions with lower T_h values. Polished plates of quartz previously studied for microthermometry were rapidly heated to 400-420°C to facilitate decrepitation of fluid inclusions. After adhering the quartz chips to double-sided carbon tape attached to a glass slide, the decrepitate mounds were analysed on a JEOL 733 electron microprobe (SEM-EDS analytical system) at Dalhousie University, Halifax, Nova Scotia. The operating conditions of the probe were: beam diameter 1 to 10 μm, counting time 20 s, sample current 15 nA, and accelerating voltage 15 kV. Raw data were corrected using Link's ZAF matrix correction program. Detection limits on measurements made with a counting time of 40 s on a smooth surface would be 0.1 to 0.3 wt. % for elemental concentrations ≥ ca. 1 wt %. The shorter counting time and an irregular topography raise the detection level by a few tenths of percent. Both raster measurements (overlapping most of the decrepitate) and point analyses were made, with similar results being obtained for a given mound. Furthermore, several point measurements were taken on different parts of a single decrepitate to test both homogeneity and consistency of results, following the method of Savard and Chi (1998); no significant variation in proportions of cations was detected. The mounds were analysed for Ti, Al, Fe, Mn, Mg, Ca, Na, K, Cr, Ni, P, Cl, Ba, Sr, and S. The analyses are considered semiquantitative and reflect the

			Fluid inclusion types				
Deposit	**Rock type**		**Aqueous L-V**	**Aqueous, L-rich + solid(s)**	**Aqueous, L-rich + halite**	**V-rich**	**Monophase liquid**
Morley's	Pegmatite with molybdenite mineralization	Frequency	Dominant			Rare	
		L:V ratio	Variable				
		Shape	Equant/regular to irregular			As aqueous L-V	
		Size	□5μm-20μm			As aqueous L-V	
		Comment	Mostly located along fracture planes			Along fracture planes or isolated	
Reeves	Quartz vein and pegmatite	Frequency	Dominant	Minor	Rare	Minor	
		L:V ratio	Regular to irregular				
		Shape	Equant negative or irregular to equant	Equant negative	Equant negative	Equant negative	
		Size	□10μm-100μm	□10μm-100μm	10μm-60μm	10μm-60μm	
		Comment	Chips indented with fluid inclusions. Sometimes trails of inclusions emplaced during deformation	Solid (white mica)			
	Host granitoid (Keddy-Reeves lgr and Salmontail Lake mgr)	Frequency	Dominant		Rare		
		L:V ratio	Variable				
		Shape	Regular/equant		Regular/equant		
		Size	□10μm		□10μm		
		Comment	Inclusions along trails or en echelon fractures in deformed quartz		Inclusions appear along trails in deformed quartz		
Walker	Aplite and pegmatite with molybdenite; greisen with chalcopyrite, fluorite, and bornite.	Frequency	Dominant	Rare	Rare	Minor	
		L:V ratio	Variable				
		Shape	Regular/equant, sometimes elongated	As for aqueous L-V inclusions	Regular/equant	Equant	
		Size	□10μm	As for aqueous L-V inclusions	□10μm	As for aqueous L-V inclusions	
		Comment	Inclusions along trails in deformed quartz	Solid (white micas)	Location as for aqueous L-V inclusions	Localised in planes with V-rich inclusions only	
	Host granitoid (Panuke Lake leucomonzogranite)	Frequency	Dominant	minor		Minor	
		L:V ratio	Variable				
		Shape	Equant sometimes elongated, irregular in some planes			Irregular	
		Size	Size □5μm-12μm	□5μm		□10μm	
		Comment	Inclusions along planes in undeformed quartz Rare presence of decrepitated fluid inclusions.	Inclusions along planes		Inclusions grouped into isolated planes	

Table 5.2: detailed descriptions of fluid inclusion characteristics for each deposit as observed during thermometric study.

			Fluid inclusion types				
Deposit	**Rock type**		**Aqueous L-V**	**Aqueous, L-rich + solid(s)**	**Aqueous, L-rich + halite**	**V-rich**	**Monophase liquid**
Keddy	Pegmatite with molybdenite mineralization	Frequency	Dominant	Rare			
		L:V ratio	Highly variable				
		Shape	Equant, rounded, regular				
		Size	10-15μm				
		Comment	Concentration of inclusions around mineralised areas, or along healed planes.	Solid(s) undetermined but birefringent.			
	Host granitoid (Panuke Lake lmgr)	Frequency	Abundant	Abundant	Rare		
		L:V ratio	Variable				
		Shape	Irregular	Irregular	Irregular		
		Size	Generally smaller in size than inclusion containing solid	10μm	10μm		
		Comment	Located along fractures	Located along fractures. Solid(s) undetermined but birefringent	Part of aqueous L-V planes		
Long Lake	Aplite/pegmatite with molybdenite mineralization; greisen with wolframite and chalcopyrite mineralization	Frequency	Dominant	Rare	Rare	Rare	
		L:V ratio	Variable to good				
		Shape	Equant/rounded to irregular, some elongated	As for aqueous L-V	As for aqueous L-V	Equant/rounded to irregular	
		Size	5μm-50μm	50μm-70μm	15μm	5μm-50μm	
		Comment	Mostly located along healed fractures	Randomly localised in chip	Location as for aqueous L-V	Located in both independent planes or planes containing aqueous L:V	
	Host granitoid (Long Lake lgr)	Frequency	Dominant		Rare		
		L:V ratio	Variable				
		Shape	Irregular		As for aqueous L-V		
		Size	5μm-10μm		Size 10μm		
		Comment	Mostly located along healed fractures		As for aqueous L-V		

Table 5.2: continued.

			Fluid inclusion types				
Deposit	**Rock type**		**Aqueous L-V**	**Aqueous, L-rich + solid(s)**	**Aqueous, L-rich + halite**	**V-rich**	**Monophase liquid**
Turner	Greisen from the Discovery Vein with chalcopyrite and cassiterite.	Frequency	Dominant	Rare		Rare	Rare
		L:V ratio	Highly variable				
		Shape	Equant to irregular	As for aqueous L-V inclusions		Equant negative	As for aqueous L-V
		Size	□5μm-15μm	As for aqueous L-V inclusions		Size □5μm-10μm	As for aqueous L-V
		Comment	Mostly located along fracture planes, with some shear fabric.	Solid (carbonates)		Located in planes with aqueous L-V	
Millet Brook	Irradiated and non-irradiated host granitoid (Salmontail Lake mgr)	Frequency	Dominant		Rare	Abundant	Abundant
		L:V ratio	Highly variable				
		Shape	Mainly irregular, few equant or negative		Equant/regular to irregular	Irregular	irregular
		Size	5μm-10μm		5μm-12μm	As for aqueous L-V	As for aqueous L-V
		Comment	Located along healed fractures		As for aqueous L-V	Located in planes with aqueous L-V	
Mn mines	Sericitized and silicified lmgr (Dean and Chapter Mine); breccia (Cain and Riddle Mine).	Frequency	Very abundant				
		L:V ratio	Very regular				
		Shape	Equant/regular negative				
		Size	10μm-100μm				
		Comment	Located in large planes				
	Host granitoid (Salmontail Lake mgr)	Frequency	Dominant	Rare		Rare	
		L:V ratio	Variable (necking)				
		Shape	Equant negative to irregular	As for aqueous L-V		As for aqueous L-V	
		Size	□5μm-10μm	As for aqueous L-V		As for aqueous L-V	
		Comment	Mostly located along planes	Solid undetermined, but birefringent. Location as for aqueous L-V		As for aqueous L-V	

Table 5.2: continued.

composition of the fluid present in the inclusions as element ratios (Haynes and Kesler 1987; Savard and Chi 1998).

5.5. Results

The results obtained from freezing and heating runs described in the following three subsections are tabulated for the individual deposits in Figure 5.3. Also, Appendix D contains the details of measurements compiled throughout the fluid inclusion study. This figure presents results for approximately a thousand inclusions obtained from thirty fluid inclusion sections.

5.5.1. Low-temperature observations

Fluid inclusions were cooled to about -120°C, and rarely to -160°C. Freezing normally occured between –35°C and -60°C, but highly-saline inclusions froze near -80°C. Freezing behavior was very consistent, with low-salinity inclusions consistently freezing at higher temperatures than highly-saline inclusions, hence the importance of carefully recording and reporting these data. In some cases, freezing was not observed, but other low-temperature phase transition(s) could subsequently be seen, thus indicating that freezing had occurred. During warming, the first phase change observed was recorded as first melting (T_{fm}), equivalent to the eutectic (T_e) temperature. The T_{fm} data covered a large range of values between –75°C to -15°C, with values above -21°C relating to metastability and/or difficulty in observing the phase change. During melting of the frozen inclusions, the presence of hydrohalite (HH) + ice + liquid or just ice + liquid was observed. When present, hydrohalite melted before ice, with the exception of a few fluid inclusions from the Reeves deposit, where metastable hydrohalite crystals melted above 0°C. Clathrates formed in a few fluid inclusions in single samples from Long Lake, Reeves, and Walker. These clathrates appeared before final melting of ice crystals, and persisted to temperatures above 0°C, melting by ~ 20°C. Melting behaviour was variable within a chip, but consistent within a given population of fluid inclusions.

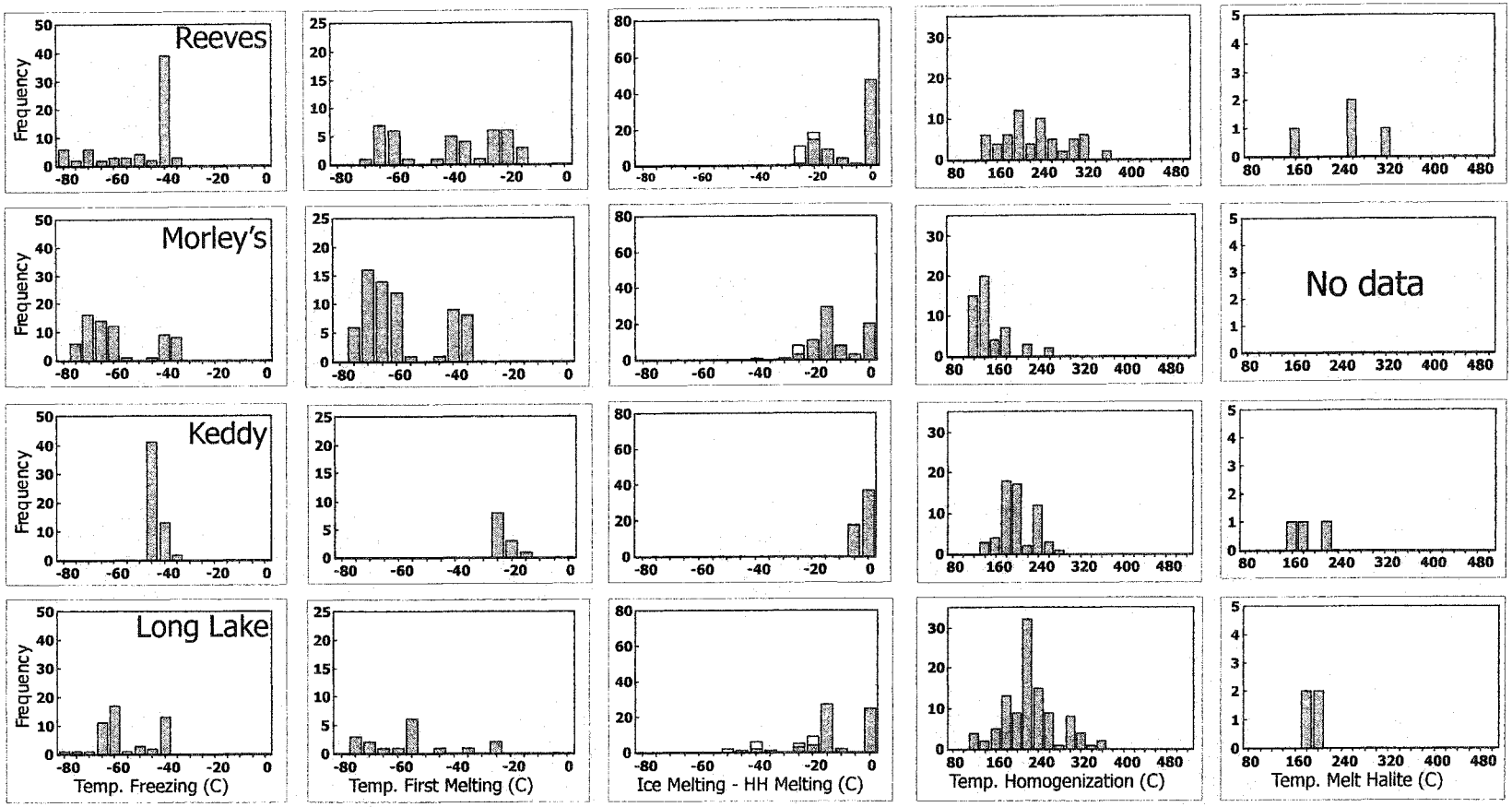

Fig. 5.3: Thermometric data [Freezing temperature (T_f), first melting temperature (T_{fm}), hydrohalite melting temperature (T_{mHH}), ice melting temperature (T_{mice}), homogenisation temperature (T_h), and halite melting temperature ($T_{mHalite}$)] for two-phase (L-V) and three-phase (L-V-H) inclusions in quartz from eight mineral deposits of the New Ross area.

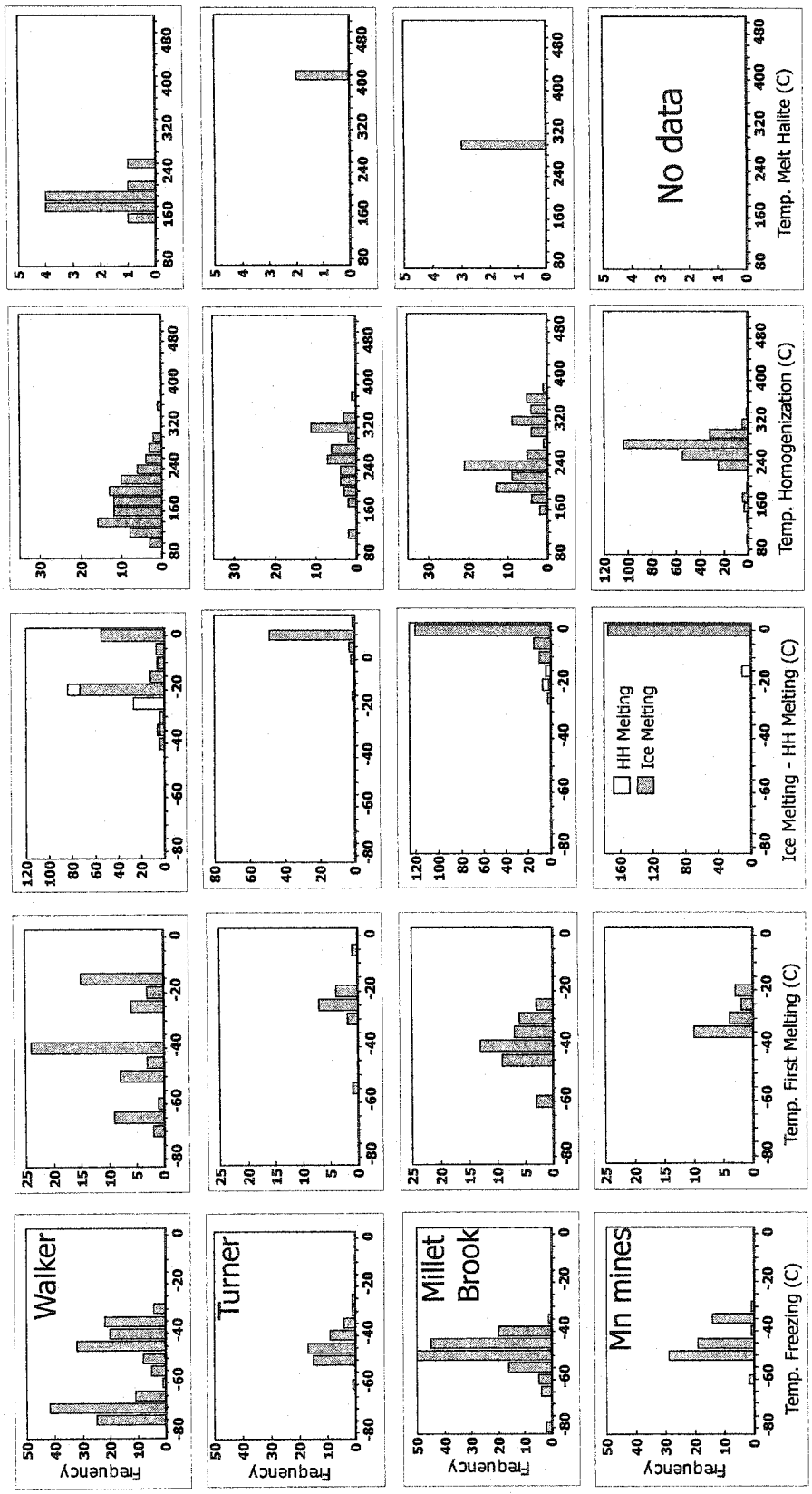

Fig. 5.3: continued.

5.5.2. Composition and salinity of inclusions

Melting behavior for fluid inclusions indicated three compositional groups based on salinity. (1) For inclusions having T_e indicating the binary system H_2O-NaCl (T_e = -21.2°C; Davis et al. 1990) or the ternary system H_2O-NaCl-KCl (T_e = -22.9°C; Sterner et al. 1988), salinity (wt. % equiv. NaCl) was interpreted from the T_m ice data, using Bodnar's (1993) equation. (2) For inclusions containing halite as a daughter mineral at room temperature, the temperature of dissolution of halite was used to determine salinity (Sterner et al. 1988). The equation used is theoretically valid only for inclusions where halite and vapour bubble disappear simultaneously. An error of a few wt. % is expected when this condition is not fulfilled (Bodnar and Vityk 1994). Halite systematically melted after L-V homogenisation. (3) For inclusions with T_e indicating the ternary system H_2O-NaCl-$CaCl_2$ (T_e=-52°C, Davis et al. 1990; Oakes et al. 1990) and with hydrohalite melting before ice, the ternary diagram and salinity table developed by Oakes et al. (1990) were used. Salinities are expressed in wt. % equiv. NaCl and range from 0 to 48 wt. % equiv. NaCl. Observation of melting of both hydrohalite and ice permitted estimation of the NaCl/(NaCl + $CaCl_2$) of the fluid inclusions (ratios between 0-1) (Fig. 5.4). These results are not unexpected, as large ranges in the NaCl/(NaCl + $CaCl_2$) ratio of fluid inclusions are commonly reported (e.g., Boullier et al. 1998).

5.5.3. Homogenisation Temperatures

Homogenisation data (T_h) collectively range from ca. 80°C to 370°C for all the deposits, but within individual deposits, the range of T_h values is 100° to 240°C. However, much narrower Th ranges (<25°C) occur within single fluid inclusion populations. For example, in a chip from the Mn mines, a maximum variability of 20°C occurs for T_h for nine different populations, with an overall range of 265° to 323°C (Fig. 5.5). The narrow T_h range for fluid inclusion populations indicates that post-entrapment modification of the inclusions is minimal, hence, the data provide a reliable estimate of a minimum temperature of entrapment (Goldstein and Reynolds 1994).

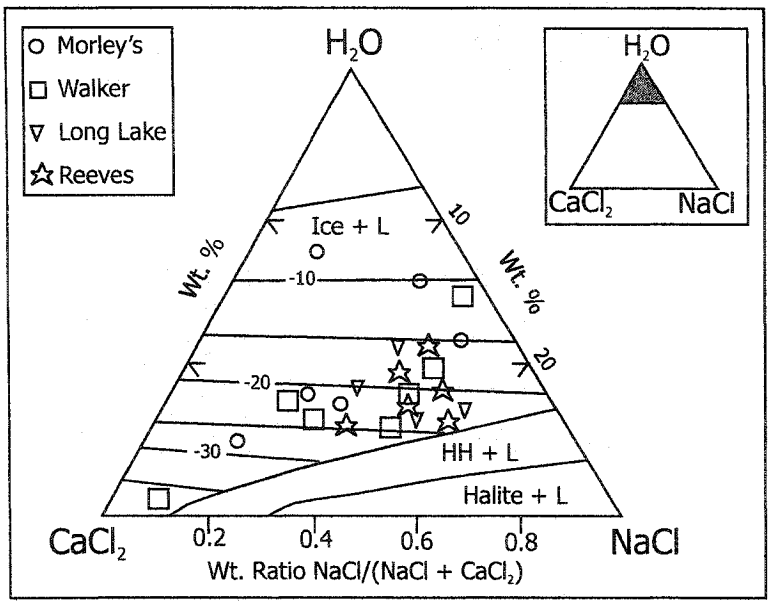

Fig.5.4: Plot of liquidus relations in part of the ternary system NaCl-$CaCl_2$-H_2O (Oakes et al. 1990) with inferred bulk compositions of fluid inclusions for the Morley's, Walker, Long Lake, and Reeves deposits. HH = hydrohalite, L = liquid.

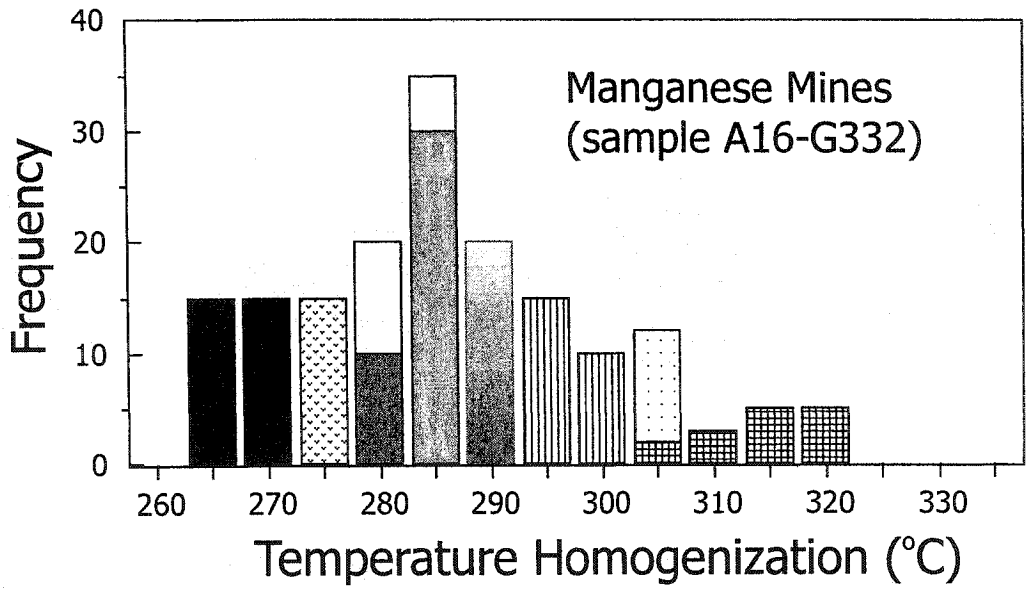

Fig. 5.5: Homogenisation temperature for fluid inclusions of a single sample from the Mn mines. Each shading represents a narrow range of data for the same inclusion group.

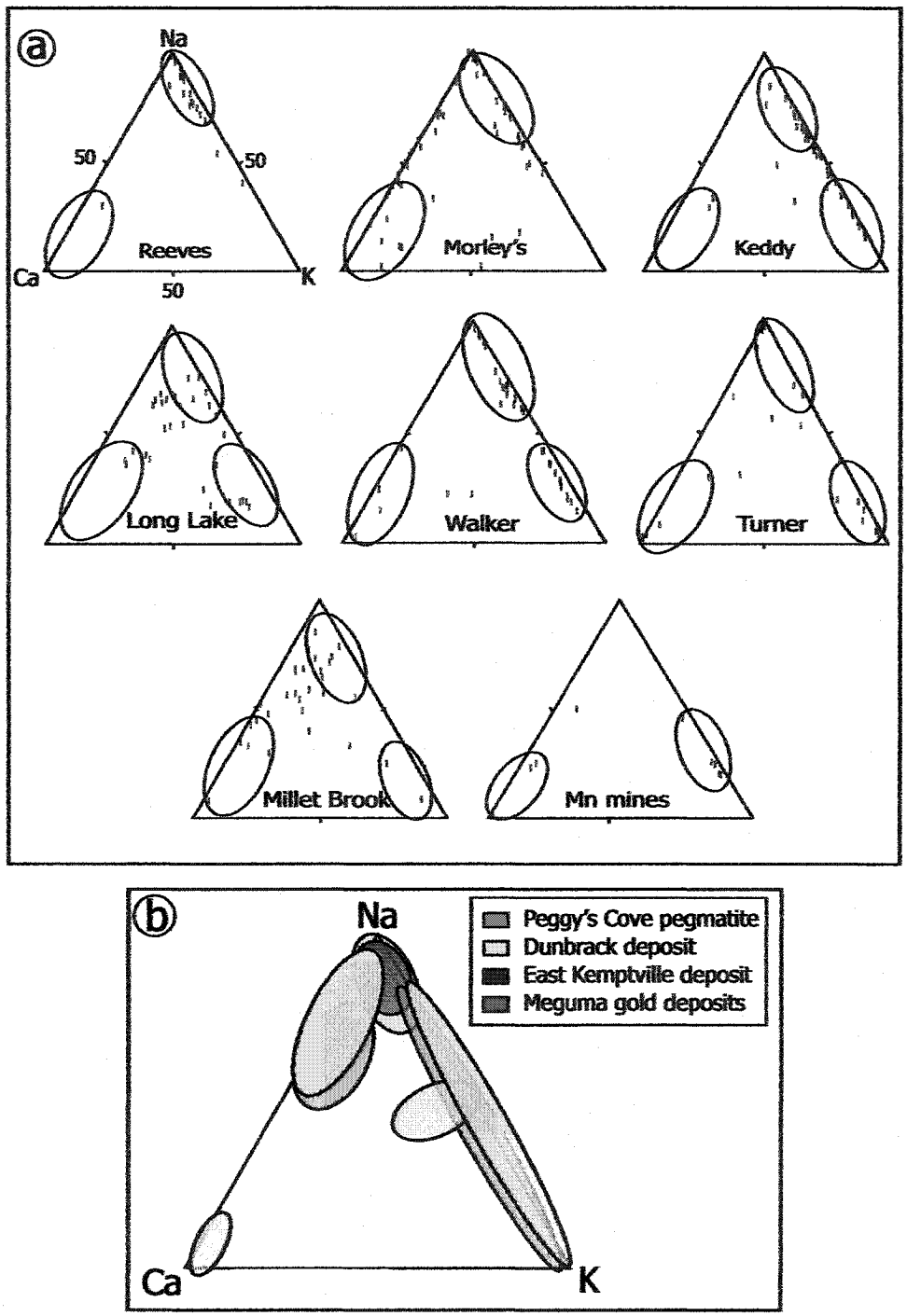

Fig. 5.6: (a) Compositional data for decrepitate mounds hosted by quartz from eight deposits of the New Ross area. (b) Diagram containing available data for other mineralised districts in the Meguma Zone (the Dunbrack and East Kemptville deposits hosted by granitoid rocks, Peggy's Cove pegmatite, and the gold deposits hosted by Meguma rocks).

5.5.4. Decrepitate analysis

Decrepitate mounds in samples from each deposit were analysed in order to qualitatively determine the major solutes present in the brine (e.g., NaCl, $CaCl_2$, and KCl). As described and illustrated by Haynes et al. (1988), size and shape of mounds prove that they originate from the decrepitation of a single inclusion. A mound size depends on salinity, with a low-salinity inclusion producing a relatively small mound during decrepitation. Low-salinity fluids characterise both the Mn mines and Millet Brook, and in these samples mounds are relatively small and rare, hence, only a small amount of data could be obtained for these deposits. In addition, the observation of evacuated inclusions without adjacent mounds is consistent with the presence of low-salinity inclusions at these deposits (e.g., Morley's pegmatite or Millet Brook).

Major solutes identified in the decrepitates are Na, K, and Ca. In general, there is a good correlation between the T_{fm} data and the composition of decrepitate mounds.

Potassium-dominated fluid inclusions occur in all deposits, but such inclusions were classified as Na-bearing during low-temperature thermometric analyses given the small difference in T_e between the NaCl-H_2O (-21.2°C) and NaCl-KCl-H_2O (-22.9°C) systems. Furthermore, complex brines containing any combination of two and three cations occur (Fig. 5.6a). The dominant anion is Cl, but detectable S occurs in some mounds. Other detectable solute components are also identified in decrepitate mounds at the Turner (Fe), Walker (Fe, Ba), and Millet Brook (Ba) deposits. A variety of metals of unknown speciation occur at the Morley's (Cu, Zn) and Walker (Fe, Ni, Cu) pegmatites, as well as at the Millet Brook deposit (Cu, Zn).

5.6. Discussion

5.6.1. Constraints and limitations of the fluid inclusion data

The inundated nature of the fluid inclusions present in quartz samples of the mineral occurrences in the New Ross area does not permit establishing a relative chronology among

fluid inclusion assemblages. Thus, the following discussion focuses on the general groupings of fluid inclusion populations that are recognized from thermometric data.

5.6.2. Composition and origin of the fluids

In a T_h vs. salinity diagram (Fig. 5.7), the data are clearly distributed into three populations: 1) 19-25 wt. % equiv. NaCl (rarely 14-28 wt. % equiv. NaCl; 2) 30-48 wt. % equiv. NaCl; and 3) 0-10 wt % equiv. NaCl. Several potential origins for fluids circulating in the New Ross area are considered in order of importance: (i) magmatic (derived from the SMB), (ii) metamorphic (originating from the Meguma Supergroup), (iii) meteoric, (iv) basinal (derived from the overlying Late Devonian/Carboniferous basins), or (v) deep crustal/upper mantle origin. Firstly, we dismiss a basinal origin for some of the fluids for geological reasons: the trapping temperatures obtained in the present study are inconsistent with an already unroofed batholith, a prerequisite condition to allow formation of the Late Devonian/Carboniferous basins. A deep crustal/upper mantle origin is not rejected, but such fluids would be indistinguishable from magmatic or metamorphic fluids based on thermometric analyses alone.

As shown by T_e and decrepitate analyses, at least three different cations (Na, K, and Ca) are present in the fluids at each deposit, with the exception of the Mn mines. Mixing among these three end-members (mainly NaCl-$CaCl_2$ and NaCl-KCl, but not $CaCl_2$-KCl) also occurs in most of the deposits (Fig. 5.6a).

Other mineralised districts in the Meguma Zone, for which fluid inclusion data are available for comparison, include; (i) the 370 Ma Dunbrack Zn-Pb-Cu-Au-Ag vein system hosted by granitoid rocks of the nearby Musquodoboit Batholith (Fig. 1.1); (ii) the ca. 370 Ma East Kemptville greisen deposit (Sn-Zn-Cu-Ag) hosted by granitoid rocks of the Davis Lake pluton (western part of the SMB) (Fig. 1.1); and (iii) the 370 Ma Meguma gold deposits hosted by the Goldenville Group (Fig. 1.1). Comparison of the fluid inclusion data from these mineral deposits with those of the NRP reveals the following similarities: (i) presence of a (Na, Ca)-rich solute for samples from the Meguma gold deposits (particularly for the Caribou and Beaver Dam gold deposits) (Kontak and Kerrich 1995; Kontak et al. 1988a; Kontak and Smith 1989; Kontak et al. 1996); and (ii) presence of a (Na, K)-rich solute for samples from the Dunbrack and the East Kemptville deposits (Kontak et al. in

press, Kontak et al. 1999; Halter et al. 1995). Evidence for mixing of solute between end-members also exists for fluid inclusions of these deposits (Fig. 5.6b).

5.6.2.1. Magmatic fluids

A (Na, K)-rich fluid of similar salinity and composition to group I fluids is generally reported in the literature for granite-related mineralization (e.g., Roedder 1984; Hollister and Crawford 1981). A similar fluid is present in granite-related mineral deposits at the East Kemptville (Sn-Zn-Cu-Ag) greisen and Dunbrack (Zn-Pb-Cu-Ag) vein deposits. Based on isotopic data, Kontak et al. (1999) propose a dominantly magmatic origin for the fluids at Dunbrack, with fluids originating from a nearby leucomonzogranite. Halter et al. (1995) also suggest a late-stage magmatic origin for the (Na, K)-bearing fluid at East Kemptville, a conclusion supported by more recent isotopic data (Halter et al. 1996).

The bulk composition of the SMB falls largely in the system $NaAlSiO_4$-$KAlSiO_4$-SiO_2, obviously providing the sodium and potassium needed for the (Na, K)-rich fluids. At the East Kemptville and Dunbrack deposits, Kontak et al. (1999, 2001) interpret (Na, K)-rich fluids as also being of magmatic origin. According to Orville (1963), fractionation of alkalis between a fluid phase and a crystalline phase (i.e., feldspars) mainly depends on temperature: lowering of temperature results in Na enrichment relative to K in the fluid. Lagache and Weisbrod (1977) offer another model in which an isothermal decompression enriches the fluid in Na relative to K. Both explanations may account for the variable Na/K ratios within fluids of the New Ross area. Further constraints of the P-T conditions are needed to permit a better understanding of such alkali exchanges (Section 5.8.3).

5.6.2.2. Metamorphic fluids

Isotopic data for the Meguma gold deposits favour a genetic model involving fluid derivation from lower crustal levels, with subsequent contamination during interaction with the Meguma Supergroup (i.e., Ca-enrichment) (Kontak and Kerrich 1995; Kontak et al. 1990b). In addition, Ca-rich fluid inclusions in vein barite-fluorite hosted by the 370 Ma Kinsac Pluton (Fig. 1.1) originated from Carboniferous basinal fluids interacting with the Meguma Group or its detrital equivalent, the Horton Group (Kontak et al. 1999). Therefore, in the New Ross area, the Na-Ca trends in Fig. 5.6a are plausibly related to interaction of magmatic fluids with contact metamorphic generated fluids originating from

metasedimentary rocks of the Meguma Supergroup, particularly from metawackes of the Goldenville Group located in close proximity to several mineral deposits near New Ross (Turner, Walker, Morley's, Millet Brook, Long Lake). Linnen (1998) reports Ca-rich fluids in pegmatitic quartz veins enveloped by metasedimentary rocks in several Sn-W provinces (i.e., western Thailand; Cornwall, England; Spanish-Portugese Hercynian). A fluid inclusion thermometric study of quartz veins and host monzogranite samples from an arsenopyrite-tourmaline-greisen vein system near Herring Cove (~ 75 km from New Ross) (Fig. 1.1), spatially located at the contact between the SMB and the Meguma Supergroup, was studied in order to evaluate this possibility. As expected, given the proximity of the Meguma metasedimentary rocks and stable isotope data indicating incursion of extraneous fluids (Kontak et al. 1988b), thermometric measurements indicate the presence of Ca-rich fluids (through T_f and T_{fm}) in both quartz vein and host granitoid rock (Fig. 5.8).

5.6.2.3. Meteoric fluids

Numerous inclusions from all the deposits of the New Ross area contain a very low-salinity fluid, with a predominance of 0 wt. % equiv. NaCl values (Fig. 5.7). We emphasize here the lack of petrographic and thermometric evidence supporting fluid unmixing (i.e. coexisting V-rich and L-rich inclusions with similar T_h data), which could have generated such a low-salinity fluid via complementary vapour condensation. Also relevant is the fact that a V-rich condensate will not have a 0 wt. % equiv. NaCl salinity, as documented for the inclusions here (Bodnar et al. 1985; Hedenquist et al. 1998). Therefore, this very low-salinity fluid is tentatively interpreted to be of meteoric origin, considered as a major source of fluid in epithermal mineral deposits (Roedder 1984).

5.6.2.4. Origin and evolution of the fluids

Three populations of fluids with varying salinity emerge from the salinity versus T_h diagram (Fig. 5.7).

Fluid I shows moderately saline compositions, with Na (±K?) as the dominant cation(s). Fluid I is dominantly of magmatic origin, corresponding in general to a fluid generated late in the evolution of a felsic magma (Burnham 1979, Cline and Bodnar 1991).

Fluid II is a highly-saline fluid characterised by either high Ca or high Na (±K?) content. We interpret the Ca-rich component of the fluid to be dominantly of metamorphic

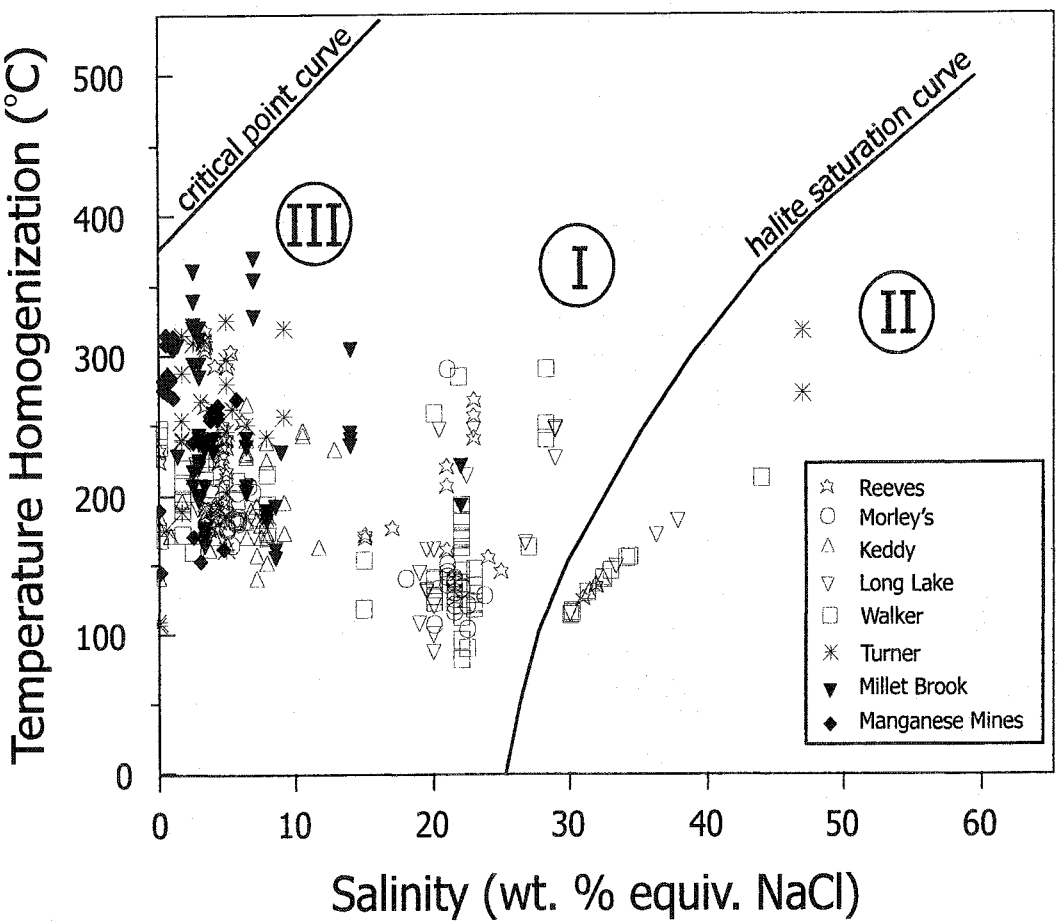

Fig. 5.7: T_h-salinity diagram showing three compositionally distinct fluids (Fluids I, II, and III) hosted by inclusions in quartz from eight mineral deposits of the New Ross area. Fluid I has a dominant magmatic origin, fluid II has a dominant metamorphic origin, and Fluid III has a dominant meteoric origin.

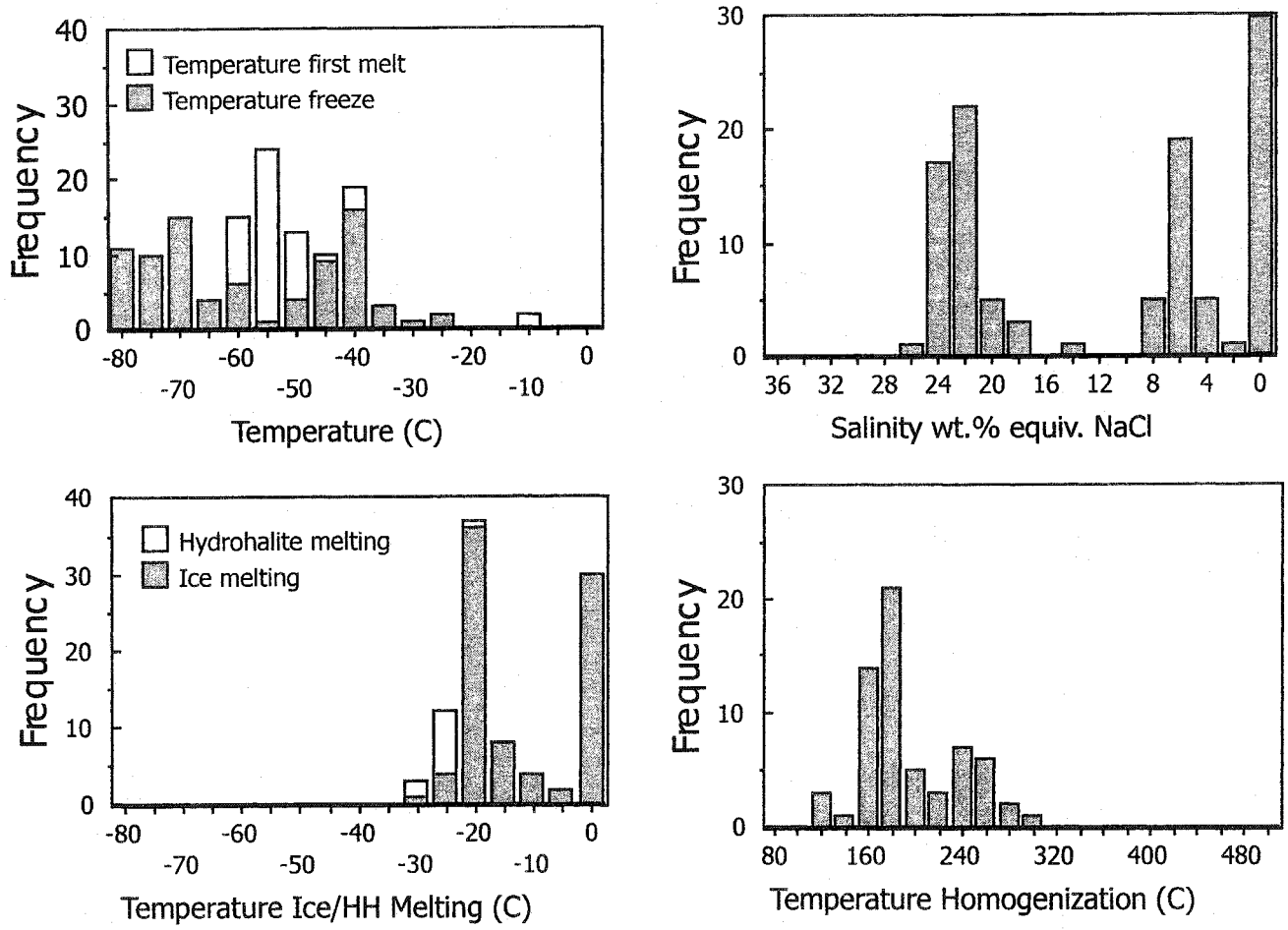

Fig. 5.8: Thermometric measurements for the arsenopyrite-tourmaline-greisen vein near Herring Cove (~ 75 km from New Ross): (a) temperature of first melting and freezing temperature as stacked histogram, (b) HH melting and ice melting as stacked histogram, (c) salinity in wt. % equiv. NaCl, and (d) temperature of homogenisation.

origin, reflecting incursion of a contact metamorphic-generated fluid derived form the Meguma Supergroup, whereas the Na-rich component of the fluid is dominantly of magmatic origin.

Fluid III is a low-salinity fluid, with a large proportion of fluid inclusions containing 0 wt. % equiv. NaCl values, as well as values between 1 and 10 wt. % equiv. NaCl. After excluding the possibility of fluid unmixing, as noted above, the non-saline part of Fluid III is interpreted to be of meteoric origin. For the saline part of Fluid III, two possible scenarios are considered. Firstly, the saline part of this fluid reflects mixing of a meteoric fluid with the moderately-saline Fluid I. Simple mass balance suggests a larger contribution of the meteoric fluid than of the magmatic fluid given the lack of inclusions with 10-18 wt. % equiv. NaCl composition. Alternatively, a fluid exsolved from the melt may have *evolved* to lower salinities (e.g., Cline and Bodnar 1991), however, the paucity of data in the ca 10-18 wt. % equiv. NaCl range suggests that this scenario is unlikely to have occurred.

In summary, the following scenario is proposed for the generation of the three populations of fluid inclusions I, II, and III in Fig. 5.7: during the late-stage evolution of the granitic magma a moderately-saline fluid is released (Fluid I), and interaction of Fluid I with other fluid reservoirs (i.e. metamorphic and meteoric) is responsible for generating Fluids II and III.

Author(s)	**Methods**	**Pressure (in kbars)**
McKenzie (1974)	normative An-Ab-Or for representative compositions of the SMB	1-4
Clarke et al. (1976)	andalusite crystallisation as a primary magmatic phase	3.3-3.9
Ham and Kontak (1988)	muscovite present as a primary magmatic mineral	ca. 2
Mahoney (1996)	thermal metamorphic aureole associated with the SMB intrusion	2.5-4

Table 5.3: Summary of methods used to obtain pressure constraints for the emplacement of the SMB.

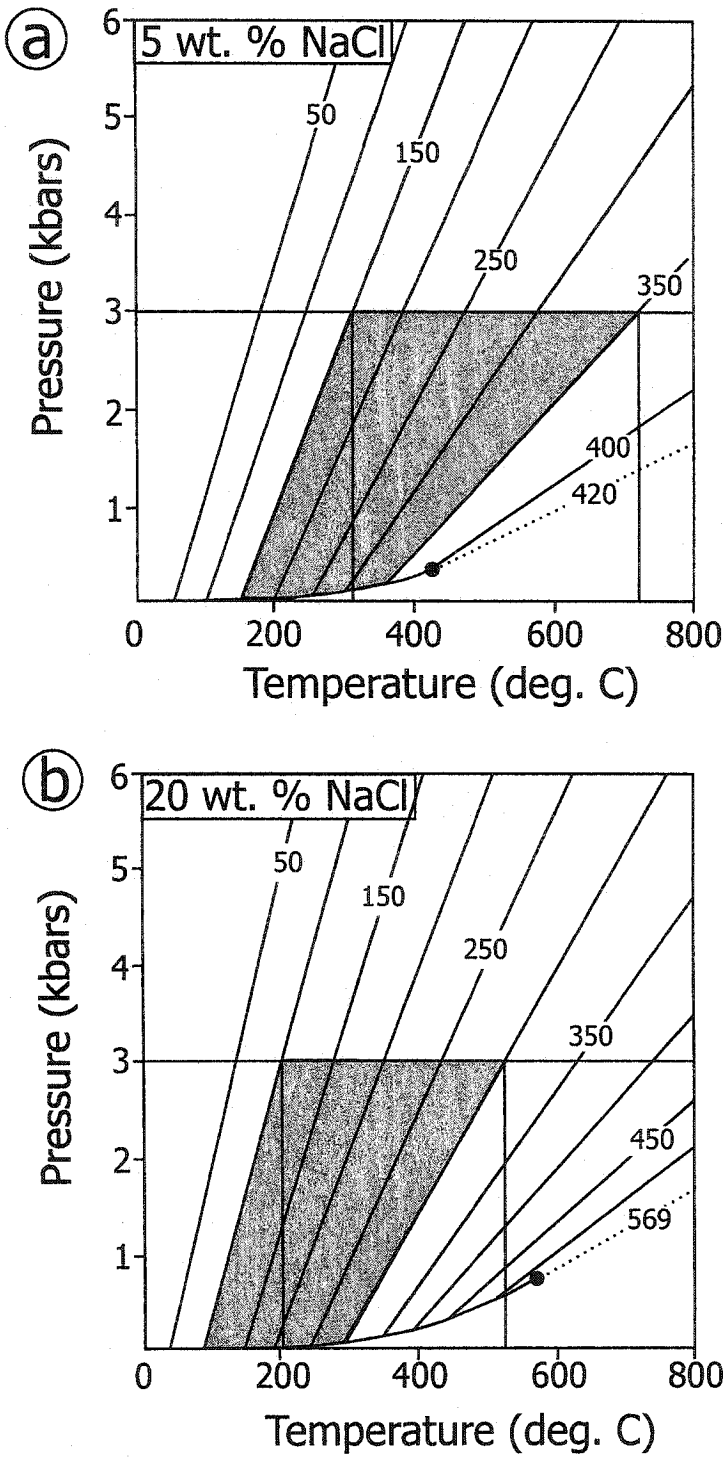

Fig. 5.9: Pressure-temperature diagrams showing the entrapment temperatures for fluids with (a) 5 wt. % NaCl equiv. and (b) 20 wt. % NaCl equiv. Iso-T_h lines from Bodnar and Vityk (1994).

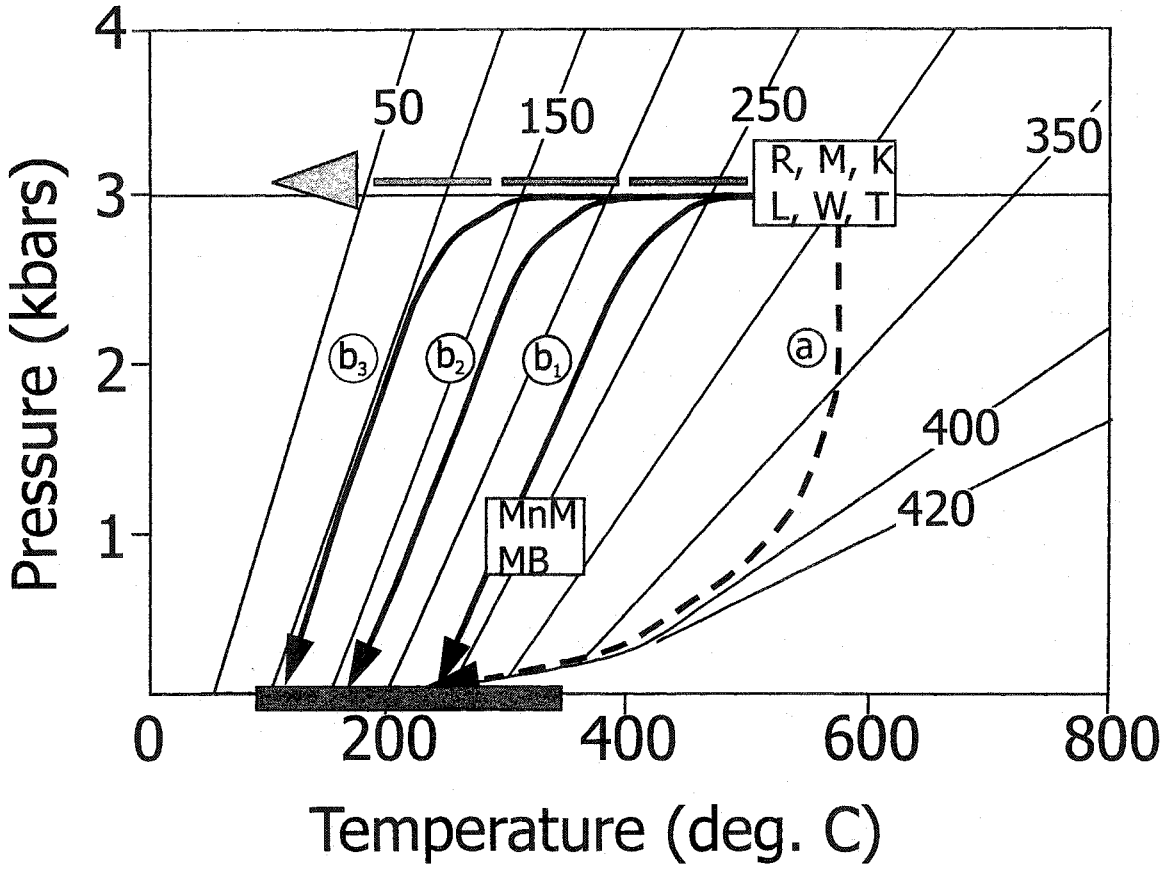

Fig. 5.10: Summary diagram showing the possible P-T paths undergone by the fluids present in the mineral occurrences of the New Ross area. Isothermal decompression is unlikely given the lack of high T_h values recorded (a). The observed T_h range (dark area) is more consistent with trends b_1, b_2, and b_3 resulting from fluid entrapment during isobaric cooling with some accompanying exhumation.

5.6.3. P-T conditions

The separate ranges in T_h for fluid inclusion populations reflect trapping of fluids at different temperatures, however, these T_h data still require pressure correcting (Roedder 1984). Several methods have been used in order to obtain pressure constraints for emplacement of the SMB (Table 5.3). In general, the various estimates constrain the P to ca. 3 kbars. The minimum pressure for fluid entrapment based on the T_h of inclusions and dissolution of halite is ~ 1 kbar (Bodnar and Vityk 1994). Using the composition and homogenisation temperatures of inclusions, isochore diagrams have been constructed for representative fluids of 5 and 20 wt. % equiv. NaCl (Bodnar and Vityk 1994) for a pressure of 3 kbars (Fig. 5.9a, b). These diagrams should be used for the H_2O-NaCl system only, but they were also used to interpret the microthermometric data for inclusions of other compositions because the errors introduced by changes in the isochore slopes and in vapour pressures are generally small compared to those associated with temperature and pressure of mineralisation (Roedder and Bodnar 1997).

Entrapment temperatures for the fluids at 3 kbars range from 300° to 700°C and 200° to 500°C for Fluids III and I, respectively. These trapping temperatures are consistent with the suggested secondary or pseudosecondary origin for the fluid inclusions, based on petrography. The large range in homogenisation temperatures for each deposit is consistent with isobaric trapping. Assuming fluid entrapment at 3 kbars, initial trapping for fluids related to pegmatite and greisen mineralization commenced at about 550°C with continued trapping to 200°C (Fig. 5.10). However, we note that the entrapment temperatures obtained for the vein deposits (Mn mines and Millet Brook), assuming this occurred at 3 kbars, are too high (maximum T=600-700°C) for the mineral assemblages (O'Reilly 1992; O'Reilly et al. 1982). A lower pressure, and hence trapping temperature, is the most likely explanation for the T_h values at the Mn mines and at Millet Brook (Fig. 5.10). Assuming that the ambient pressure at the time of entrapment of the vein fluids was 1 kbar, we now consider the implications of this in terms of the other mineral deposits and uplift of the SMB. For example, if the pressure is entirely lithostatic, there must have been rapid uplift and exhumation post-370 Ma, and consequently vein-type deposits must be younger than the pegmatite- and greisen-type. This model requires an exceptional geothermal gradient (i.e.,

125-150°C), which we consider to be a limitation for this scenario. However, if hydrostatic conditions dominated during this style of mineralization, then the vein deposits may have formed at a depth of ca. 10-12 km, which would require less post-SMB crystallization uplift and a much lower geothermal gradient. This model also allows us to integrate this mineralization with the pegmatite/greisen type in the New Ross area. Observation of complex inclusions is consistent with rapid post-SMB uplift; therefore, we interpret them as being implosions rather than decrepitates, although further investigation to clarify this point is needed. Further evaluation of this model is currently being tested via age dating of the mineralization, and preliminary $^{40}Ar/^{39}Ar$ age data on K-feldspars from the New Ross area mineral deposits confirm the rapid post-SMB uplift.

5.7. Conclusions

A detailed study of the chemistry and thermometry of fluid inclusions from pegmatite, greisen, and vein types deposits from the New Ross area results in several new findings.

1) Freezing temperatures, which are not often reported, proved to be important in confirming the presence of a divalent cation (Ca) in some fluid inclusions.

2) Three different fluids are present in most of the deposits: (i) a magmatic fluid evolved from the late-stage granitoid rocks in the area; (ii) a Ca-rich metamorphic fluid originating from the Meguma Supergroup metasedimentary rocks; and (iii) a meteoric fluid that interacted with the two previous fluids in variable proportions.

3) The range of T_h values for pegmatite and greisen type deposits reflects an isobaric (3 kbars) decrease in entrapment temperatures between 550° and 200°C. For vein type deposits, the inferred trapping temperatures require a lower pressure than ambient pressure at the time of emplacement of the SMB, suggesting either deeply penetrating fractures to generate hydrostatic pressures or rapid post-370 Ma exhumation of the area or both. If the second process is valid, time of formation of deposits in the New Ross area is not the same for all deposit types.

CHAPTER 6

STABLE ISOTOPES

6.1. Introduction

Chapter 6 is a slightly modified version of a manuscript entitled "An integrated stable isotope and fluid inclusion study of granite-hosted mineral deposits of the New Ross area, South Mountain Batholith, Nova Scotia, Canada: evidence for multiple fluid reservoirs" (Carruzzo et al. 2003; Section 1.3.2.2). The manuscript is accepted for publication in Canadian Mineralogist with minor revisions.

In an effort to investigate the nature and origin of the fluids involved in the granite-hosted mineralization of the New Ross area of the South Mountain Batholith (SMB) in Nova Scotia (Fig. 1.1), we have coupled stable isotopic analyses with results of our earlier fluid inclusion study (Carruzzo et al. 2000). The granite-hosted polymetallic (Cu, Mo, Mn, Sn, U, W) mineral deposits of the study area show a large variety of silicate, phosphate, oxide, and sulphide minerals, and each deposit has a unique assemblage (O'Reilly et al 1982). Our previous fluid inclusion study demonstrated that at least three different fluid reservoirs (magmatic, metamorphic, meteoric) were involved in the mineralized environments (Carruzzo et al. 2000). Also, mineralization and crystallization of the SMB are penecontemporaneous, based on $^{40}Ar/^{39}Ar$ laserprobe dating of white mica and Re/Os dating of molybdenite (Chapter 4). In this paper, we present stable isotopic data from white mica (δD, $\delta^{18}O$) and quartz-hosted fluid inclusion extracts (δD) from eight mineral occurrences in the New Ross area (~500km^2) of the SMB.

The objectives are to examine possible isotopic equilibrium of different minerals (white mica, quartz, and alkali feldspar) and to characterize the isotopic composition of fluids involved in the environments of mineralization. Integration of the fluid inclusion and isotopic data indicates that varying proportions of both magmatic and non-magmatic fluid reservoirs were involved in the mineralising systems, but the non-magmatic

component is masked by the intrinsically low fluid:rock ratios that characterize the systems.

6.1.1. Regional geological setting

The Meguma Lithotectonic Terrane (MLT) is the easternmost terrane of the northern Appalachians and is separated from the Avalon Terrane by the Cobequid-Chedabucto Fault (Fig. 1.1; Williams and Hatcher 1983). Two distinct lithologies dominate the bedrock geology of the MLT: (1) Cambrian-Ordovician metawackes and metapelites of the Goldenville and Halifax groups, respectively, of the Meguma Supergroup (Schenk 1995a), which underwent regional deformation and greenschist-amphibolite grade metamorphism during the Acadian Orogeny (ca. 400 ± 10 Ma; Keppie and Dallmeyer 1987; Muecke et al. 1988; Hicks et al. 1999) and (2) ~25 Late Devonian peraluminous granitoid plutons, including the large SMB, which intruded the Meguma Supergroup (Clarke et al. 1997). MacDonald et al. (1992) subdivided the SMB into early Phase I plutons (granodiorite, biotite monzogranite), and more evolved Phase II plutons (leucomonzogranite, leucogranite) (Fig. 1.2a).

There are several mineral occurrences in the SMB, and those central to this study include six locations in a Phase II pluton (New Ross pluton, NRP) and two locations in a Phase I pluton (Salmontail Lake pluton, SLP) (Fig. 1.2b). The NRP contains aplite/pegmatite-type deposits (Reeves, Keddy, Morley's, Walker, Long Lake) and greisen-type deposits (Turner, Walker, Long Lake), whereas the SLP includes vein-type deposits (Millet Brook, Mn Mines) (Fig. 1.2b). MacDonald (2001) gave a detailed history of base-metal and lithophile-element exploration in the SMB, including the New Ross area. Past-producing mineral deposits include East Kemptville (Sn-Zn-Cu-Ag), located in the southwestern part of the SMB (Kontak 1994), and the Mn Mines in the New Ross area (O'Reilly 1992), whereas U occurs in the undeveloped Millet Brook deposit (Chatterjee and Strong 1984). Table 5.1 contains information about the host granitoid rock, mineralisation, alteration, and samples used in this investigation. Carruzzo et al. (2000) described the geology and mineralogy for each mineral occurrence.

Radiogenic age determinations (U-Pb, $^{40}Ar/^{39}Ar$, Rb/Sr) available for the SMB provide a narrow range of well-constrained magmatic ages around ca. 373 Ma. (Clarke

and Halliday 1980, Reynolds et al. 1981, 1987, Harper 1988, Clarke et al. 1993b, 1997, Keppie and Krogh 1999). Younger ages reported for the granites are the consequence of post-crystallisation tectono-thermal activity (e.g., Alleghanian deformation at ~320 Ma; Kontak and Cormier 1991; MacDonald 2001).

The Lower Devonian (Lochkovian to Lower Emsian) Torbrook Formation is the youngest formation intruded by the SMB. Clastic sediments and marine carbonates of the Horton and Windsor Groups, respectively, unconformably overlie the SMB. Miospores of Late Devonian age (Late Famennian) in the basal part of the Horton Group provide a minimum age of ca. 360 Ma [time scale of Tucker et al. (1998)] for exhumation of the northeastern part of the SMB (Martel et al. 1993). Thus, emplacement, crystallization, uplift, and erosion of at least part of the SMB occurred after the Lower Emsian and before the Late Famennian. Keppie and Dallmeyer (1995) proposed an exhumation of ca. 13 km in the MLT between 370 and 360 Ma.

Based on a study of the contact metamorphic aureole of the SMB, Raeside and Mahoney (1996) obtained pressures of 3.2 to 3.8 kbars for batholith emplacement, corresponding to a depth of emplacement of 10-12 km. This pressure is in agreement with those inferred from other mineral equilibria (Clarke et al. 1976, Ham and Kontak 1988, Halter and Williams-Jones 1999).

6.2. Methodology

6.2.1. Sampling, preparation of material, and analytical techniques

Samples were collected during detailed mapping of eight mineral deposits in the New Ross area in 1998, whereas samples for the Millet Brook and Mn mines deposits (except SC-1/3-D) come from drill core stored by the Nova Scotia Department of Natural Resources. In all cases, we selected samples of mineralised zones and their host granitoid rock.

Quartz and white mica grains (1-3 mm diameter) were handpicked from crushed and sieved material using a binocular microscope. For finer-grained samples (e.g., aplite), conventional magnetic and heavy liquid techniques were used to prepare separates.

White mica grains from host granitoid rocks and pegmatite/aplite (with the exception of a pegmatite at the Reeves deposit) have chemical and textural evidence of crystallisation at the magmatic stage of the SMB evolution, whereas white mica grains from greisen represent either a chemically modified version of grains that crystallise during the magmatic stage, or newly crystallised grains formed during a subsequent hydrothermal stage (Chapter 3.). White mica grains from a pegmatite at the Reeves deposit are stellate aggregates, and have a chemical enrichment in Fe+Mg+Mn similar to white mica grains from greisens. The origin of white mica grains from vein deposits is ambiguous, because these altered rocks contain white mica with a chemical composition similar to typically magmatic white micas (i.e., limited biotite and Tschermak substitutions).

Twenty-six samples of white mica were analysed for their δ^{18}Oand δD values at the Isotope Laboratory of the Department of Geological Sciences and Geological Engineering at Queen's University (Kingston, Ontario). Twenty-two samples of fluid-inclusion extracts from quartz grains were also analysed for their δD values at the same laboratory. Table 6.1 summarizes the δD and δ^{18}O data for white mica and δD data for fluid inclusion extracts from quartz grains. The data include analyses for all three deposit types (aplite/pegmatite, greisen, and vein) from the New Ross area and their various host rocks (i.e., granodiorite, monzogranite, leucomonzogranite, leucogranite). Analytical procedures appear in Kyser et al. (1998).

We use the standard δ^{18}O and δD notation in per mil (‰) relative to the reference V-SMOW. Reproducibility of the data is ± 0.2‰ for δ^{18}O on silicates and ± 5‰ for δD values for fluid inclusion extracts.

6.3. Results of isotopic analysis

6.3.1. δD data for fluid inclusion extracts

The δD values for fluid inclusion extracts from quartz grains in the deposits range from –42 to –97‰ (mean: -62‰) with 19 of 22 values between -42 and -75‰ (Fig. 6.1a). This range is consistent with previous studies in the MLT (Kontak et al. 1999, 2001, Kontak and Kyser 2002). The isotopic compositions of fluid inclusions in mineralised

Sample no.	Location (deposit)	Rock type	$\delta D_{fluid\ inclusions}$	$\delta^{18}O_{mica}$	$\delta^{18}O_{fluid}$ at 600°C	$\delta^{18}O_{fluid}$ at 400°C	δD_{mica}	δD_{fluid} at 600°C	δD_{fluid} at 400°C
SC-2-W	Walker	aplite	-58	9.9	10.67	8.54	-52	-42.11	-22.33
SC-9-W		pegmatite	-48	7.8	8.57	6.44	N/D	N/D	N/D
SC-7-W		greisen	N/D	9.5	10.27	8.14	-47	-37.11	-17.33
SC-13-W		Panuke Lake mgr (host)	-76	9.4	10.17	8.04	-56	-46.11	-26.33
SC-14-W		greisen	-55	9.2	9.97	7.84	-52	-42.11	-22.33
SC-3-MB	Millet Brook	U-irradiated sample	-71	9	9.77	7.64	-69	-59.11	-39.33
SC-5-MB		host granitoid rock	-68	9.4	10.17	8.04	-57	-47.11	-27.33
SC-6-MB		host granitoid rock	-72	8.9	9.67	7.54	-68	-58.11	-38.33
SC-2a-T	Turner	greisen	-46	4	4.77	2.64	-45	-35.11	-15.33
SC-9-T		Panuke Lake mgr (host)	-55	7.9	8.67	6.54	-50	-40.11	-20.33
SC-14-T		Elvan	-83	7.2	7.97	5.84	-56	-46.11	-26.33
SC-13-L	Long Lake	aplite	N/D	9.4	10.17	8.04	-60	-50.11	-30.33
SC-12-L		pegmatite	-42	10	10.77	8.64	-57	-47.11	-27.33
SC-5-L		greisen	-49	9.2	9.97	7.84	-42	-32.11	-12.33
SC-1-L		New Ross lmgr (host)	-97	9.8	10.57	8.44	-75	-65.11	-45.33
DC 86-3 847	Mn Mines	hematized mgr	-53	9	9.77	7.64	-54	-44.11	-24.33
SC-1-D		episyenite	N/D	9.3	10.07	7.94	-53	-43.11	-23.33
SC-3-D		Salmontail Lake mgr (host)	-61	9.8	10.57	8.44	-59	-49.11	-29.33
SC-7-M	Morley's	pegmatite	-48	8.5	9.27	7.14	-57	-47.11	-27.33
SC-1-M		New Ross lmgr (host)	-57	9.3	10.07	7.94	-61	-51.11	-31.33
SC-3-K	Keddy	pegmatite	-46	9.5	10.27	8.14	-82	-72.11	-52.33
SC-5-K		greisen	-91	9.5	10.27	8.14	-63	-53.11	-33.33
SC-2-K		Panuke Lake mgr (host)	-68	9.3	10.07	7.94	-85	-75.11	-55.33
SC-10-R	Reeves	pegmatite	-60	9.5	10.27	8.14	-108	-98.11	-78.33
U2		pegmatite	-40	N/D	N/D	N/D	N/D	N/D	N/D
SC-6-R		Keddy-Reeves lgr (host)	-72	9.7	10.47	8.34	-48	-38.11	-18.33

Table 6.1: Hydrogen and oxygen isotope data (‰) for the mineral deposits and their host rock in the New Ross area, Nova Scotia, as well as calculated fluid compositions for muscovite-H_2O oxygen and hydrogen isotopic equilibria at temperatures of 600° and 400°C.

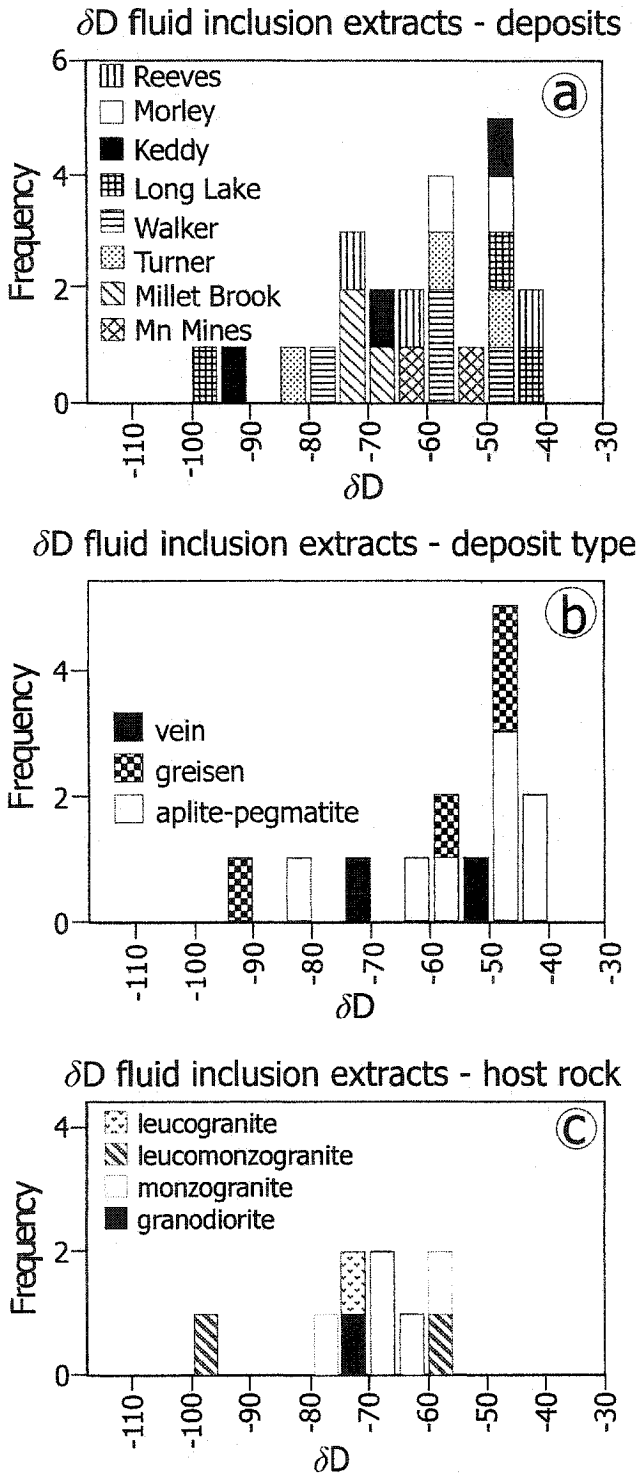

Figure 6.1: δD values for fluid inclusion extracts from quartz grains organised by a) deposit (location), b) deposit type (vein, greisen, and aplite/pegmatite), and c) host rock type (granodiorite, monzogranite, leucomonzogranite, and leucogranite).

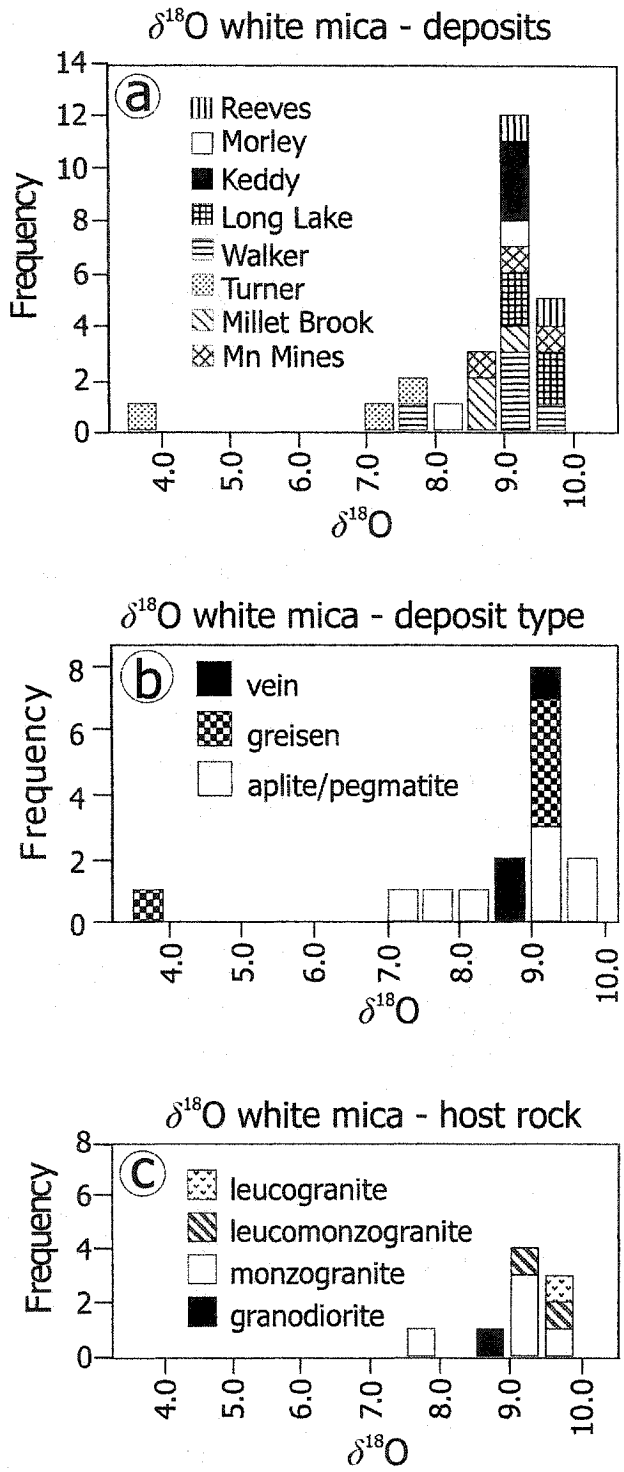

Figure 6.2: $\delta^{18}O$ values for white mica separates organised by a) deposit, b) deposit type, and c) host rock type.

and unmineralised samples show considerable overlap, regardless of deposit style or host-rock types (Fig. 6.1b,c).

6.3.2. $\delta^{18}O$ data for white mica separates

The values for white mica separates range from +4 to +10‰ (mean: +9‰), with all but one (a greisen from the Turner deposit) within a range of +7.2 to +10‰ (Fig. 6.2a). No trend is apparent in the data arranged by deposit, deposit types, or host rock (Fig. 6.2b, c). These values compare well with other $\delta^{18}O$ values for white mica from granitoid rocks of the MLT (Longstaffe et al. 1980, Kontak et al. 1988b, 1991, 1999, 2001, 2002, Poulson et al. 1991, Dinnett 1995). The $\delta^{18}O$ values of whole-rock samples from the SMB range from +7.7 to+15‰ (Longstaffe et al. 1980, Chatterjee et al. 1985, Kontak 1988, Clarke et al. 1993b, Kontak et al. 1988b, 1991, 2002), and are typical of peraluminous crustal-derived granites worldwide (Sheppard 1986).

We calculated the $\delta^{18}O$ composition of water in equilibrium with white micas using the equations of O'Neil and Taylor (1969) at temperatures of 600°C and 400°C (Table 6.1), with the former representing a magmatic temperature close to the granite solidus (host rock, pegmatite/aplite) and the latter a minimum temperature for hydrothermal alteration (greisen, vein). Calculated $\delta^{18}O_{water}$ values for white micas from host granitoid rocks and pegmatite/aplite range between +8.0 and +10.8‰, whereas calculated $\delta^{18}O_{water}$ values for white micas from greisen and vein deposits range between +7.6 and +8.1‰ except for a greisen sample from the Turner deposit at +2.6 ‰.

6.3.3. δD data for white mica separates

The δD values for white mica separates range from -42 to -108‰ (mean: -61‰), with 20 of 24 values between -42 and -69‰ (Fig. 6.3a). No systematic pattern emerges from arranging the data by deposit or host rock type (Fig. 6.3b, c). Few δD data exist for white mica in the SMB (-30 to-59‰; Kontak et al. 2001, 2002, Dinnett 1995), but they are close to the main range of values obtained in the present study.

We calculated the δD composition of water in equilibrium with white micas using the equations of Suzuoki and Epstein (1976) at temperatures of 600°C and 400°C (Table 6.1). Calculated δD_{water} values for the host granitoid and pegmatite/aplite white micas

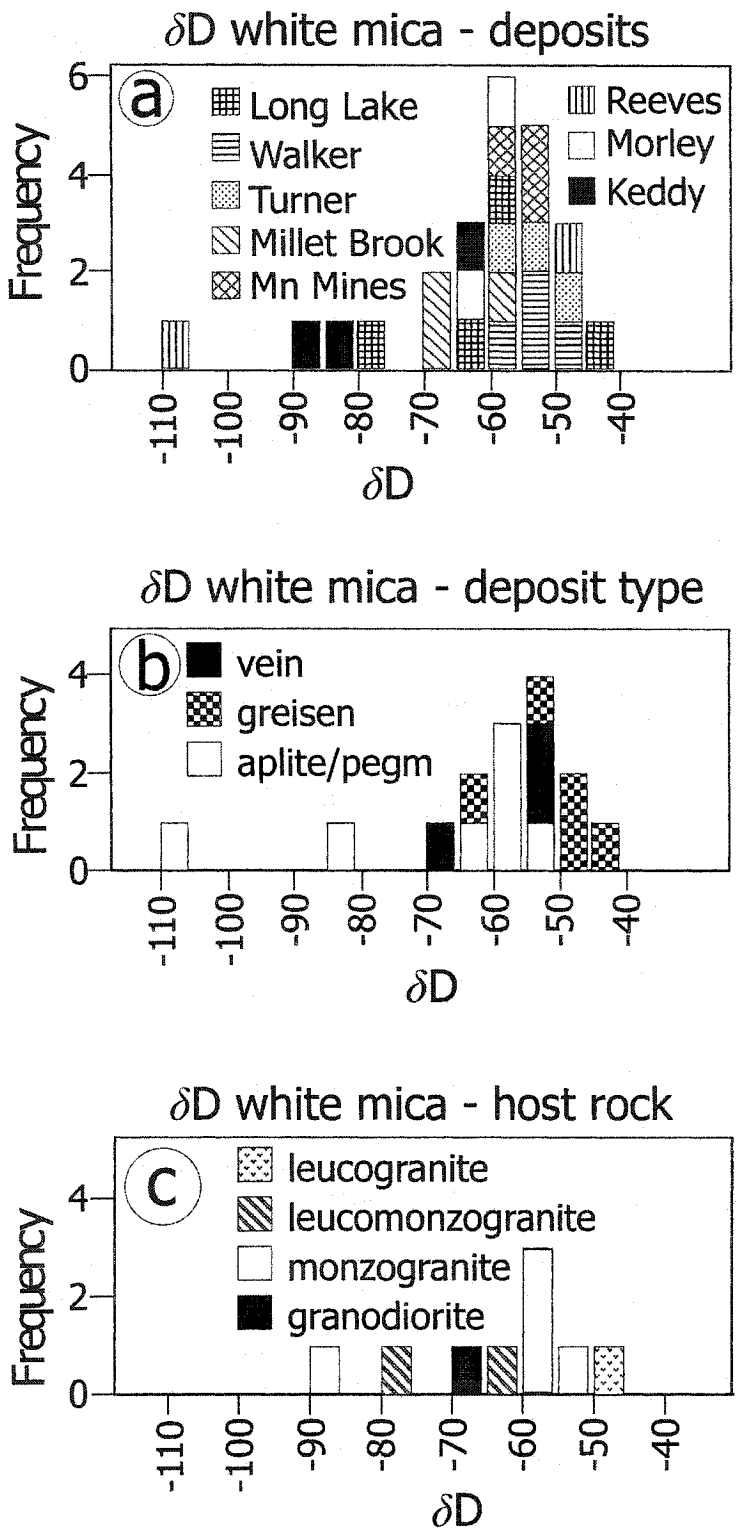

Figure 6.3: δD values for white mica separates organised by a) deposit, b) deposit type, and c) host rock type.

range between -38 and -58‰, whereas calculated δD_{water} values for greisen and vein white micas range between -12 and -39‰. The four white micas with anomalously low δD values are for host rock and pegmatite/aplite and these have calculated δD_{water} values of -65 to -98‰ at 600°C.

6.4. Discussion

6.4.1. Integration with previous data

Sample origin	Rock type	$\delta^{18}O$ Quartz	$\delta^{18}O$ White mica	$\delta^{18}O$ K-feldspar
Keddy	Pegmatite	17.2		10.6
		11.9		11.0
Reeves		11.4		11.4
		15.5		9.9
Morley's		11.6		
		10.9	9.1	10.0
		8.9		
Walker		8.9	8.2	9.8
Long Lake		10.6		
		10.8		11.0
		11.6		11.0
		12.5		

Table 6.2: Isotopic values for minerals other than white mica from Kontak et al. (1988, 1991). These data permit the determination of isotopic equilibrium among coexisting minerals for five locations in the New Ross area.

Two previous papers presented results of stable isotopic investigations of the mineral deposits of the New Ross area (Kontak et al. 1988b, 1991). Isotopic values for minerals other than white mica are available (Table 6.2), permitting determination of isotopic equilibrium among coexisting minerals. The three main criteria used to test for isotopic equilibrium are: (1) no isotopic reversals; (2) no unusually large fractionation values between coexisting phases; and (3) concordance of temperature using different mineral pairs (O'Neil 1986). The order of $\delta^{18}O$ values in granite minerals, assuming isotopic equilibrium, should be quartz > feldspar > white mica (O'Neil 1986). Figure 6.4 shows all available isotopic data for mineral separates from the mineral deposits of the New Ross area. Although $\delta^{18}O$ values are not in the expected order for quartz and feldspar in a few

cases, most white micas have lower $\delta^{18}O$ values than coexisting quartz and alkali feldspar.

Kontak et al. (1991) calculated temperatures of 600 ± 65°C using fractionation factors for quartz-white mica data ($\delta^{18}O_{q\text{-}m}$) from Longstaffe et al. (1980), whereas $\delta^{18}O_{q\text{-}m}$ data from pegmatites in the New Ross area provide a large range of apparent temperatures (1200° to 230°C), indicating post-crystallisation isotopic exchange. Using the values obtained for this study, $\delta^{18}O_{q\text{-}m}$ ($\delta^{18}O_{quartz}$ - $\delta^{18}O_{muscovite}$) ranges from 0.4 to 8.1. The expected $\delta^{18}O_{q\text{-}m}$ values for magmatic conditions within granitoids is 3.8±0.3‰ (Longstaffe 1982), and with the exception of two samples, the calculated $\delta^{18}O_{q\text{-}m}$ values for samples from the New Ross area are below this range and represent isotopic disequilibrium (Fig. 6.5). The $\delta^{18}O_{q\text{-}f}$ ($\delta^{18}O_{quartz}$ - $\delta^{18}O_{alkali\ feldspar}$) range from 0 to 7. Longstaffe (1982) provided a $\delta^{18}O_{q\text{-}f}$ range of 1.6 to 2.4‰ for granitoids equilibrated under magmatic conditions. Pegmatites from Reeves and Morley's show an appropriate $\delta^{18}O_{q\text{-}f}$ and temperatures calculated for these samples are between 480° and 520°C. This temperature range is in close agreement with pressure-corrected entrapment temperature from fluid inclusion thermometry of pegmatites. Disequilibrium values are expected within the SMB, as slowly cooling magmas (plutonic environment) are more susceptible to isotopic exchange with an orthomagmatic or deuteric fluid both at high and low temperature (Giletti 1986).

6.4.2. Isotopic signature of fluid types

Carruzzo et al. (2000) used salinity and decrepitate analysis of fluid inclusions in quartz from each of the eight mineral deposits of the New Ross area to identify three different fluid reservoirs (magmatic, metamorphic, meteoric). Such fluids are normally isotopically distinct (Sheppard 1986) and their signature within the SMB should, therefore, be discernable. Other sources of fluids at the time of fluid circulation (i.e., 373 Ma), such as evaporated brines or seawater, are not considered because of their absence from the stratigraphic record at the time of SMB emplacement. The isotopic signature of magmatic and metamorphic fluids depends mainly on the isotopic composition of the source rock, whereas the isotopic signature of the meteoric fluid depends on terrane-

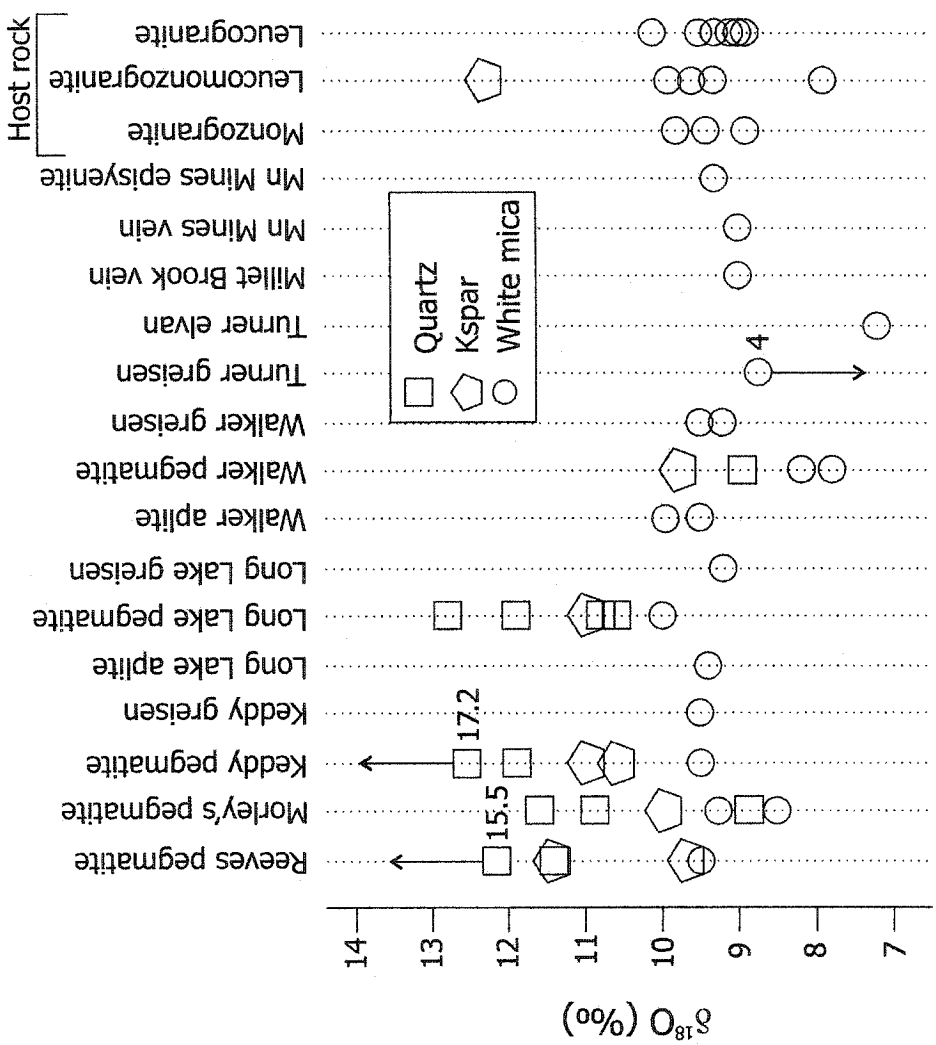

Figure 6.4: Integrated isotopic data for mineral separates from the mineral deposits of the New Ross area using data from Kontak et al. (1988, 1991) and this study.

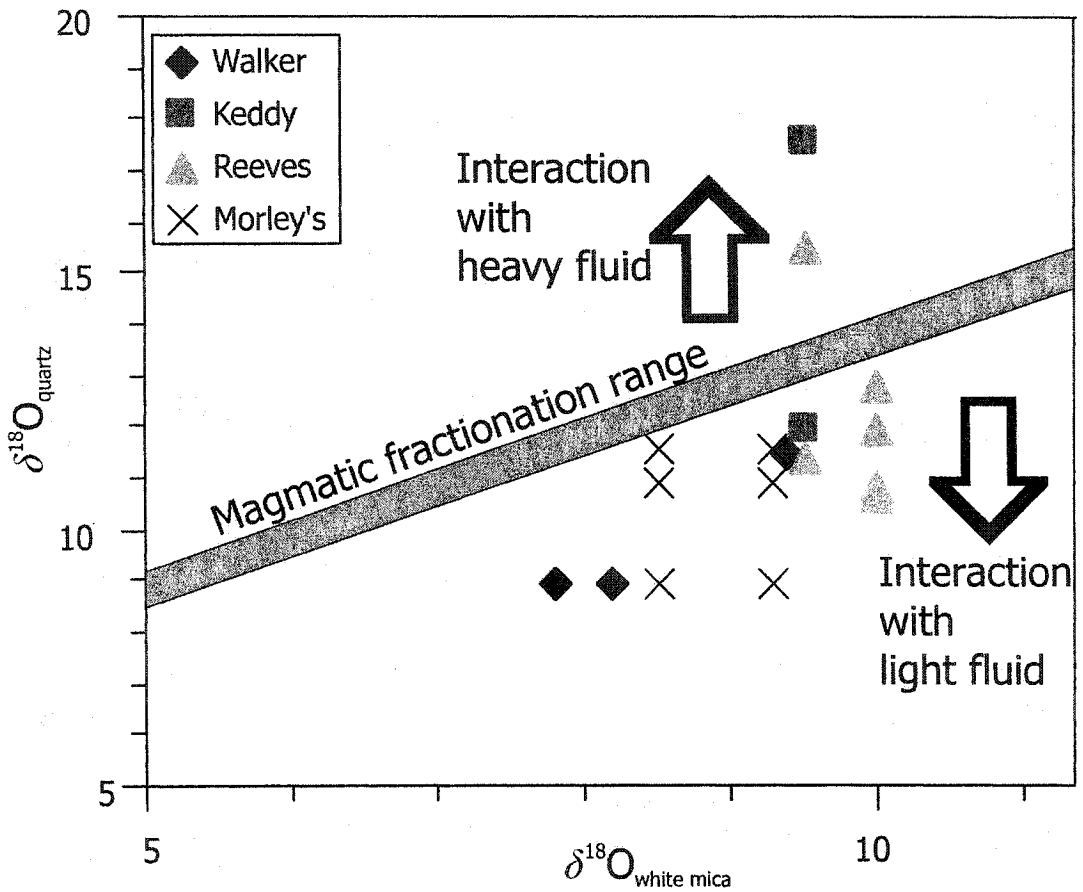

Figure 6.5: $\delta^{18}O_{white\ mica}$ versus $\delta^{18}O_{quartz}$ diagram for mineral pairs from mineral deposits of the New Ross area. The magmatic fractionation field (Longstaffe 1982) represents the area where data plot if equilibrium between both minerals exists. $\delta^{18}O_{quartz}$ values from Kontak et al. (1988, 1991) and $\delta^{18}O_{white\ mica}$ values from this study.

specific parameters such as latitude and altitude. The following presents the isotopic signature of the three fluids previously recognised in the New Ross area.

Magmatic: Sheppard et al. (1969) defined the isotopic composition of magmatic fluid as having δD values from –40 to –80‰ and $\delta^{18}O$ values from +5.5 to +9.5‰. However, a magmatic fluid in equilibrium with high-$\delta^{18}O$ peraluminous granites might plot outside this range [i.e., shows enrichment of a few ‰ of $\delta^{18}O$, Sheppard (1986)], similar to the peraluminous granites of the Cornubian Batholith of SW England (Sheppard 1977). Using $\delta^{18}O$ data (n = 24) from unaltered granitoid rocks (Longstaffe et al. 1980, Dinnett 1995), we defined $\delta^{18}O_{magmatic\ water}$ for the SMB to be +10 ± 2‰ at 600°C. Using $\delta D_{mineral}$ data (n = 2) from Dinnett (1995) (the only available δD values for unaltered granitoid rocks of the SMB), we approximated the δD range for the SMB to be -40 ± 10‰ again at 600°C. However, note that the SMB magmatic field is probably artificially shortened because of the limited amount of $\delta D_{mineral}$ data available. Nonetheless, the δD values used here are within the range proposed by Taylor (1987) for water exsolved from felsic melts.

Metamorphic: Sheppard (1986) gave values of δD from 0 to –70‰ and $\delta^{18}O$ from +3 to +20‰ for a metamorphic fluid in equilibrium with minerals of its host rock. To narrow this large range, which reflects the diversity of possible protoliths, we calculated a hypothetical metamorphic fluid composition specific to the Meguma Supergroup [psammite and pelite, average compositions in Kontak and Dostal (1992)]. The only isotopic data existing for the Meguma Supergroup are $\delta^{18}O_{whole\ rock}$ (Longstaffe et al. 1980). Assuming a certain $\delta^{18}O_{metamorphic\ water}$ at 600° and 400°C and knowing the fractionation factor between each mineral of the sample (quartz, chlorite, albite, white mica, and biotite) and water, we obtain the $\delta^{18}O$ for each mineral (using the equations of Bottinga and Javoy (1973) for quartz/albite/muscovite/biotite-water fractionation and Savin and Lee (1988) for chlorite-water fractionation). We then assign a weighted $\delta^{18}O$ value to each mineral according to the amount of oxygen it contains; the sum of weighted $\delta^{18}O$ value for each mineral represents $\delta^{18}O_{whole\ rock}$. By comparing the $\delta^{18}O_{whole\ rock}$ calculated to the measured values from Longstaffe et al. (1980), we vary the $\delta^{18}O_{metamorphic\ water}$ to obtain matching values (Table 6.3). Between 600° and 400°C, $\delta^{18}O_{metamorphic\ water}$ ranges from +7.5 to +10.8‰; this range overlaps the $\delta^{18}O_{magmatic\ water}$.

Sandstone	Mineral modal proportion (%)	proportion of O in each mineral	proportion of O in whole sample	1000lnα at 600°C	1000lnα at 400°C	$\delta^{18}O_{mineral}$ at 600°C with $\delta^{18}O_{fluid}$=10.8	$\delta^{18}O_{mineral}$ at 400°C with $\delta^{18}O_{fluid}$=8.8	Weighted $\delta^{18}O_{mineral}$ at 600°C	Weighted $\delta^{18}O_{mineral}$ at 400°C
quartz	30	0.53	15.9	1.59	3.42	12.39	12.27	4.29	4.25
feldspar	20	0.49	9.8	0.99	2.41	11.79	11.26	2.52	2.40
chlorite	30	0.39	11.7	-5.32	-2.35	5.48	6.5	1.40	1.66
biotite	10	0.39	3.9	-2.54	-2.08	8.26	6.77	0.70	0.58
muscovite	10	0.46	4.6	-0.77	1.36	10.03	10.21	1.01	1.02
		Total oxygen in sample:	45.9				$\delta^{18}O_{whole\ rock}$:	9.91	9.91
								corresponding to mean $\delta^{18}O$ of sandstone samples of Meguma (9.9)[1]	

Siltstone	Mineral modal proportion (%)	proportion of O in each mineral	proportion of O in whole sample	1000lnα at 600°C	1000lnα at 400°C	$\delta^{18}O_{mineral}$ at 600°C with $\delta^{18}O_{fluid}$=9.3	$\delta^{18}O_{mineral}$ at 400°C with $\delta^{18}O_{fluid}$=7.5	Weighted $\delta^{18}O_{mineral}$ at 600°C	Weighted $\delta^{18}O_{mineral}$ at 400°C
quartz	48	0.53	25.44	1.59	3.42	10.89	10.92	5.68	5.69
feldspar	28	0.49	13.72	0.99	2.41	10.29	9.91	2.89	2.79
chlorite	15	0.39	5.85	-5.32	-2.35	3.98	5.15	0.48	0.62
biotite	5	0.39	1.95	-2.54	-2.08	6.76	5.42	0.27	0.22
muscovite	4	0.46	1.84	-0.77	1.36	8.53	8.86	0.32	0.33
		Total oxygen in sample:	48.8				$\delta^{18}O_{whole\ rock}$:	9.64	9.65
								corresponding to mean $\delta^{18}O$ of siltstone samples of Meguma (9.6)[1]	

Table 6.3: Calculations of $\delta^{18}O_{metamorphic\ water}$ in equilibrium with a sandstone and siltstone from the Meguma Supergroup from $\delta^{18}O_{whole\ rock}$ values of Longstaffe et al. (1980). [1] Longstaffe et al. (1980).

Meteoric: The meteoric water line (MWL) shows the systematic variation of present-day meteoric water isotopic composition, and ancient meteoric water may present a similar relationship (Sheppard 1986). Paleoreconstructions of the position of Laurentia (Kent and Van der Voo 1990, Scotese and McKerrow 1990) reveal that the Meguma Terrane was located ~20° South latitude during the Late Devonian (Famennian) and show the closure of the Theic Ocean between Laurentia and Gondwana by Late Carboniferous - Early Permian (Scotese and McKerrow 1990), leaving the MLT close to open sea water until ~300 Ma. Using isostatic calculations (Airy Model), assuming that the present crustal thickness is similar to the crust thickness in the Late Devonian minus erosional effect (estimated from geobarometry to be ~12 km, the depth of emplacement of the SMB, Raeside and Mahoney 1996), a compensation depth of ~ 100 km, and using densities of 2.8 g/cm^3 for the crust and 3.3 g/cm^3 for the mantle, we obtained a paleo-altitude of ~1700 m for 370 My ago.

A possible model for the paleo-isotopic composition of the MLT, considering both latitude (20° S) and altitude (~1700 m) restrictions, is the Andes in South America, where a $\delta^{18}O$ value of –6 ± 2‰ exists for a meteoric fluid (Taylor 1997). We obtained a δD_{water} value for that range of $\delta^{18}O$ by applying the equation for the meteoric water line ($\delta D = -38‰ \pm 16$). Recent measured isotopic values from precipitation in South America (Los Molinos station in Argentina, latitude of ~ 24° and altitude of 1300 m) are $\delta^{18}O$ = -8 to 0‰ and δD = -40 to -5‰.

6.4.3. Nature and origin of fluids based on white mica data

The mineral deposits of the New Ross area represent a variety of mineralization styles and, as shown by Carruzzo et al. (2000), their formation involved three roughly coeval fluid reservoirs. In the conventional $\delta^{18}O$ - δD diagram (Fig. 6.6), the standard fields for different types of water (Sheppard 1986 and references therein, Ohmoto 1986) are outlined and compared to (i) fields for meteoric and magmatic fluids within the Meguma Supergroup; (ii) the calculated $\delta^{18}O$ range for a metamorphic fluid in equilibrium with the Meguma metasediments; and (iii) the data, calculated at 600°and 400°C for mineral deposit environments of the New Ross area. From this diagram, we note the following points: (1) most mineral deposit data fall within the metamorphic

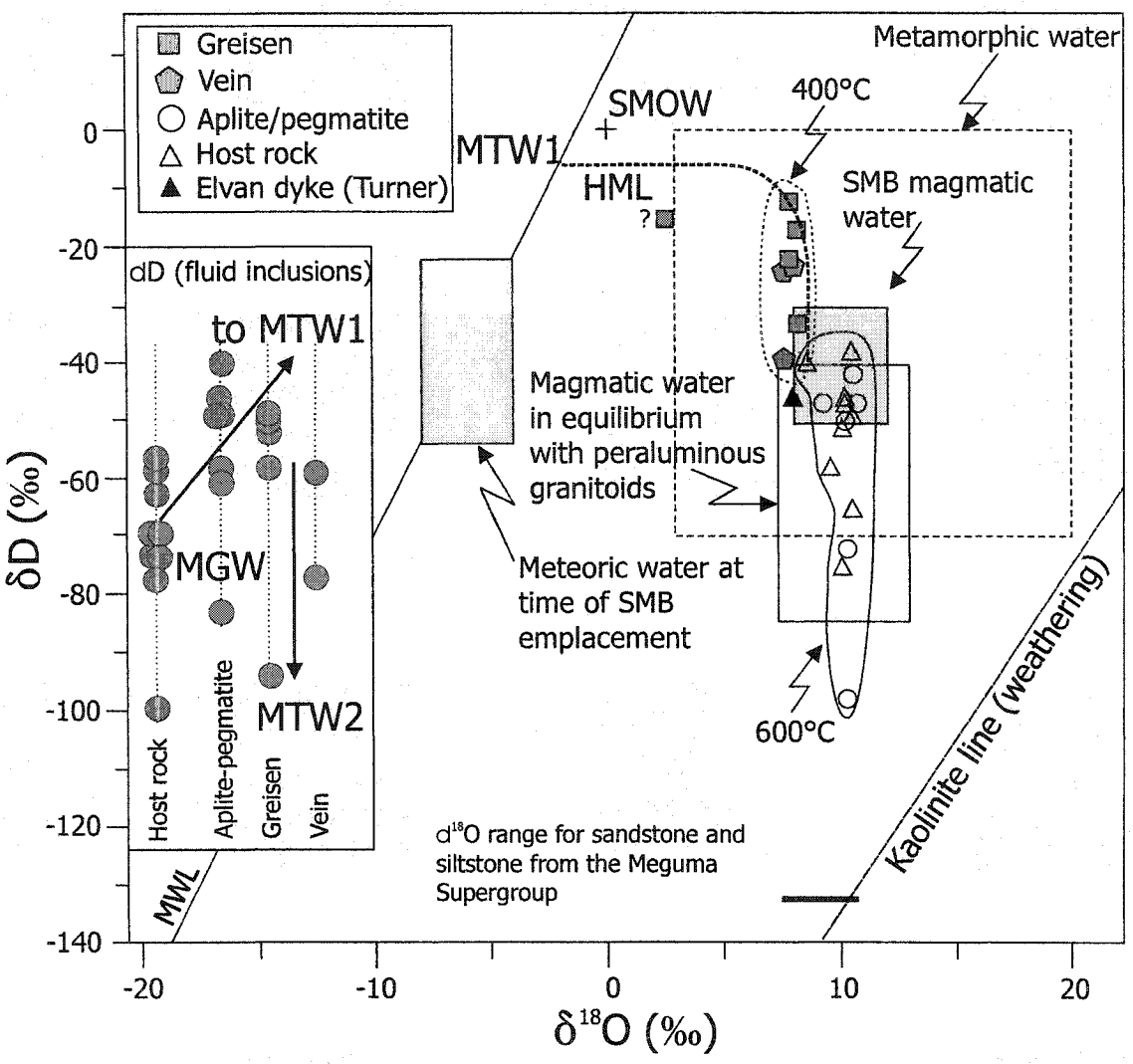

Figure 6.6: Plot of δD versus $\delta^{18}O$ showing fluid reservoirs (Sheppard 1986 and references therein); magmatic field for water in equilibrium with peraluminous granitoids from Ohmoto (1986). Meteoric water line of Craig (1961). Meteoric water field at time of SMB emplacement, SMB magmatic water, and $\delta^{18}O$ range for water in equilibrium with Meguma metasediments as defined in the text. Circles = δD values for fluid inclusion extracts; unfilled symbols = δD values for a fluid in equilibrium with white mica at 600°C (host granitoid rocks and pegmatite/aplite samples); filled symbols = δD values for a fluid in equilibrium with white mica at 400°C (greisen and vein samples). MGW = magmatic water; MTW1 = first generation of meteoric water (contemporaneous to SMB emplacement); MTW2 = later generation of meteoric water. HML = hypothetic mixing line.

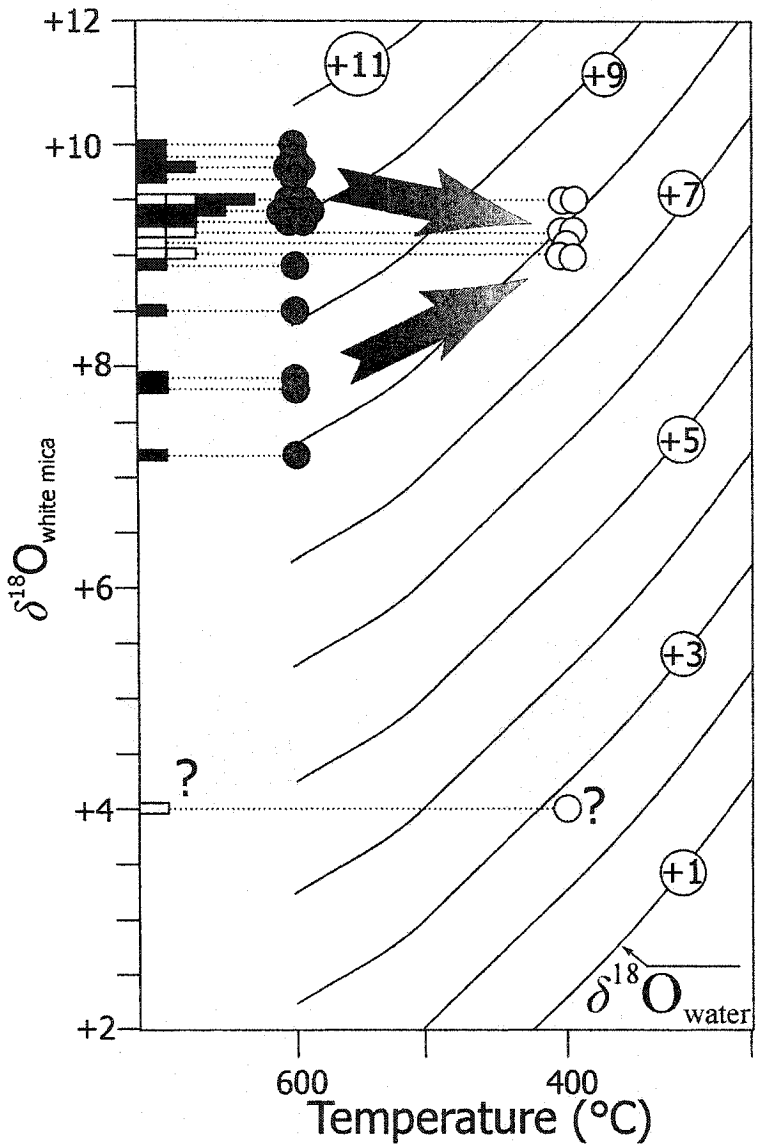

Figure 6.7: Diagrams of $\delta^{18}O_{white\ mica}$ versus temperature (in °C) with isopleths for δD_{water} calculated using the muscovite-water fractionation equation of O'Neil & Taylor (1969). Filled rectangles = $\delta^{18}O_{white\ mica}$ for host granitoid rocks and aplite/pegmatite samples, open rectangles = $\delta^{18}O_{white\ mica}$ for greisen and vein samples, filled circles = calculated $\delta^{18}O$ values of the fluid in equilibrium with white micas from host granitoid rocks and aplite/pegmatite samples, and open circles = $\delta^{18}O$ values of the fluid in equilibrium with white micas from greisen and vein samples.

water field and in the $\delta^{18}O$ range defined for water equilibrated with metasedimentary rocks of the Meguma Supergroup; (2) most granite host rock and pegmatite/aplite data fall in the field for magmatic water equilibrated with peraluminous granitoid rocks at 600°C (except for a single point with an anomalously low δD value), and in the low δD end of the SMB magmatic water field (except for five points with lower δD values); and (3) the greisen and vein data fall at the low end of the $\delta^{18}O$ field for magmatic water and have generally higher δD values compared with the peraluminous magmatic range for δD. Thus, there appears to be a shift towards lower $\delta^{18}O$ and higher δD values in the isotopic signature of the fluids equilibrated with the white micas from the magmatic through to the hydrothermal regime.

An erroneous estimation of temperature alone cannot account for the range in isotopic composition of the fluids shown in Figure 6.6, therefore, we explore other reasons for such variations below. A progressive lowering of $\delta^{18}O$ values from ~ + 10.0 to ~ +8.0 can result from interaction with a low $\delta^{18}O$ fluid. We suggest that the low $\delta^{18}O$ fluid is of meteoric origin and the proportion of this meteoric fluid increased with time concomitant with a change from a magmatic regime to a greisen-vein regime. First, the observation of low-salinity fluids dominating the fluid inclusions from greisen-vein deposits whereas high-salinity fluids dominate the fluid inclusions from host granitoid rocks and pegmatite/aplite (Carruzzo et al. 2000) is consistent with the lowering of $\delta^{18}O$ values related to incursion of a meteoric fluid (Fig. 6.7). Secondly, with decreasing temperatures, the isotopic composition of a hydrothermal fluid in equilibrium with white mica evolves towards lower δD values (see isopleths in Fig. 6.8). However, instead of following this expected closed-system tendency (i.e., dominantly magmatic), we observe higher δD values for the greisen and vein samples (Fig. 6.6) and, therefore, mixing with a fluid of higher δD composition appears as the most likely explanation. This shift to higher δD values may also reflect the presence of meteoric water in the system.

Therefore, based on the isotopic data for the white micas, we suggest that an evolution of increasing fluid to rock ratio through time as the system changed from a magmatic to a hydrothermal regime may explain the distribution of the data in Figure 6.6. Simultaneous with this evolution, the nature of the fluid changed from early magmatic to later meteoric. A hypothetical mixing line (HML) between the presumed end member

fluids illustrates this evolution of the isotopic signature in $\delta^{18}O$-δD space (Fig. 6.6). The composition of the end-member meteoric fluid (MTW 1) has a significantly higher δD value (~-6‰) than the range calculated for the MLT at ca. 373 Ma. Although the incursion of a metamorphic fluid may also explain the distribution of the data, we again note that our fluid inclusion thermometric study indicates the dominance of a meteoric fluid rather than a metamorphic fluid in the system. Kontak and Kyser (2002) also reported the presence of low $\delta^{18}O$ fluids in a vein-hosted silica-clay mineralised zone at the Flintstone Rock area in the southwestern part of the SMB and, in addition, the fluid inclusions in the quartz record the dominance of a low-salinity (<1 wt.% equiv. NaCl) fluid, similar to that in the greisen and vein deposits of the New Ross area.

6.4.4. Nature and origin of fluids based on fluid inclusion extracts

The δD_{water} values for fluid inclusion extracts arranged according to host rock are shown inset in Figure 6.6. We note that there is a progressive trend towards higher δD_{water} values from host granitoid rocks to greisen, with some anomalously low values. We interpret the data to reflect two stages of incursion of meteoric water: the first (MTW1) mixing with magmatic water (MGW) during orthomagmatic-hydrothermal stage of the SMB, and the second (MTW2) appearing during a post-crystallisation stage of the SMB. Before discussing the reason for this interpretation, we compare the δD_{water} values from the fluid inclusion extract with those inferred from white micas in the same samples.

Figure 6.8 consists of four diagrams of $\delta D_{white\ mica}$ versus temperature (in °C) with isopleths for δD_{water} calculated using the muscovite-water fractionation equation of Suzuoki and Epstein (1976). These diagrams also show the δD data from fluid inclusion extracts (closed circles) and the calculated δD data for fluids in equilibrium with white micas (open circles). A temperature of 600°C is used for isotopic data from white micas in host granitoid rocks and aplite/pegmatite, versus 400°C for white micas in veins and greisens. Pressure-corrected entrapment temperatures of 500°C are used for fluid inclusions in host granitoid rock and aplite/pegmatite samples, versus 400 °C for vein and greisen samples. With decreasing temperature, trapped fluids in equilibrium with white micas evolve towards lower δD values. If fluid inclusions in quartz contained the same water as bound in the white micas, then both δD_{water} compositions should lie on the same

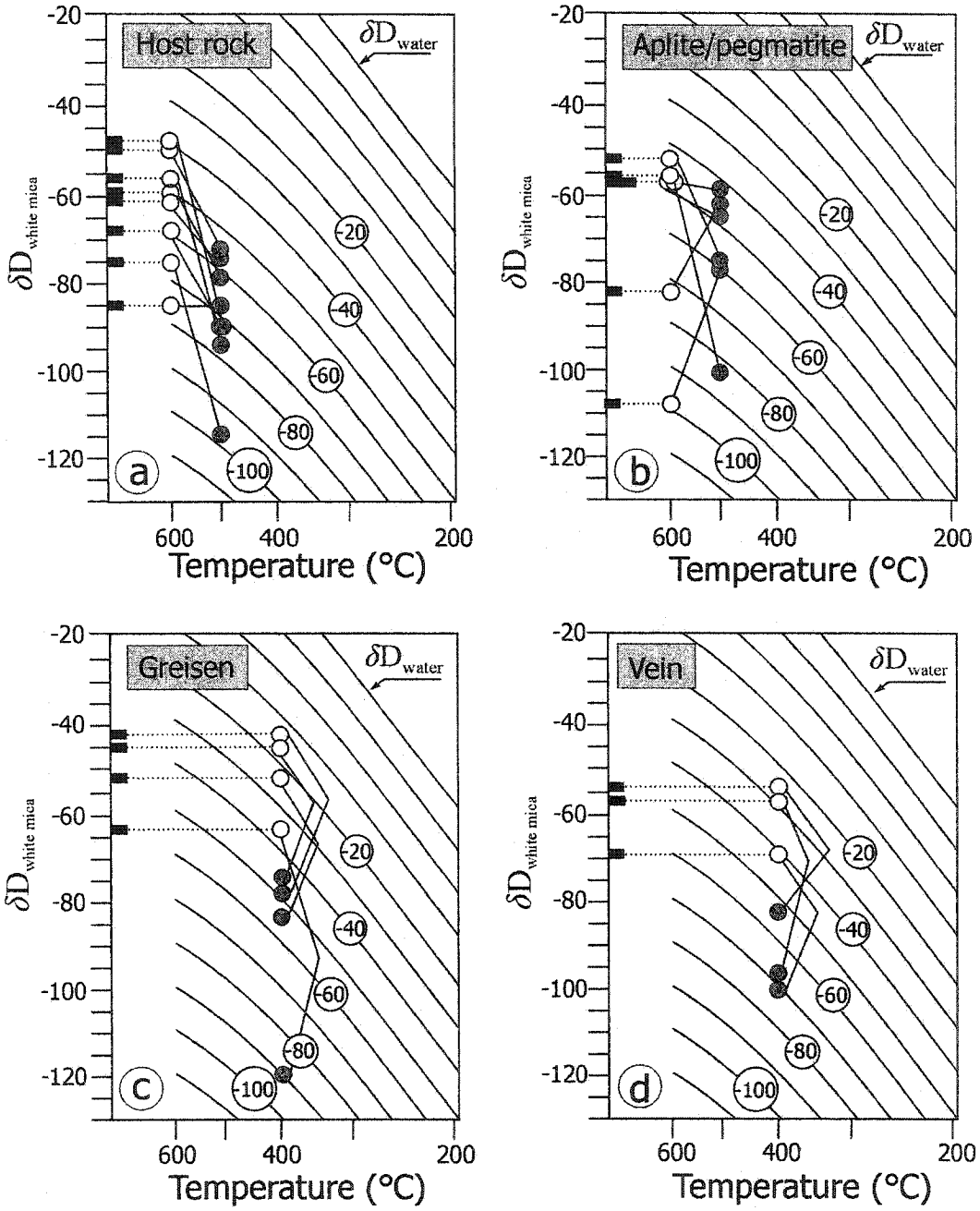

Figure 6.8: Diagrams of $\delta D_{white\ mica}$ versus temperature (in °C) with isopleths for δD_{water} calculated using the muscovite-water fractionation equation of Suzuoki and Epstein (1976); a) host granitoid rock samples; b) aplite/pegmatite samples; c) greisen samples; d) vein samples. Rectangles = $\delta D_{white\ mica}$, open circles = calculated δD values of the fluid in equilibrium with white micas, closed circles = δD values from fluid inclusion extracts, and solid lines link the δD datum from white mica to the δD datum from fluid inclusion extracts for the same sample. A temperature of 600°C is used for isotopic data from white micas in host granitoid rocks and aplite/pegmatite and of 400°C for white micas in greisens and veins.

isopleth. Instead, the fluid inclusion extracts generally have lower δD values than the δD_{water} in equilibrium with the white mica and do not fall on the same isopleth as the fluid in equilibrium with white micas. Several possible explanations exist for such a difference:

1. An analytical-related phenomenon: This possibility relates to release of molecular water or H-balanced defects in quartz during in vacuo thermal decrepitation of the sample (Gleeson et al. 2002). In their study, Gleeson et al (2002) found that samples with anomalously low δD values are characterized by a low abundance of fluid inclusions. Given that the samples used in the present study are inundated with fluid inclusions and that the above mechanism remains poorly studied to date, we reject this possibility as a viable explanation.
2. Incursion of a low δD fluid after white mica formation and before entrapment of the fluid, still during the hydrothermal stage: this process requires involvement of a low δD fluid during hydrothermal activity. Given that a much higher δD value characterises the signature of meteoric water during hydrothermal activity, we exclude such a fluid reservoir. An alternative fluid is that of organic origin, as originally suggested by Sheppard and Charef (1986) and used by Linnen (1995) to explain low δD fluids in Sn-mineralized pegmatites of Thailand. This explanation is difficult to assess given the lack of documentation of such fluids in organic-rich sedimentary basins, therefore we also reject this possibility.
3. Incursion of a low δD fluid during a fluid event subsequent to SMB emplacement: in this case, we appeal to trapping of fluid of probably meteoric origin much later in time than emplacement of the SMB (MTW2). Relevant to this case are the following: (i) the presence of low-temperature (i.e., 100-150°C), low-salinity fluid inclusions and the presence of monophase liquid inclusions in most samples (Carruzzo et al. 2000); and (ii) the documentation of low δD_{water} by other investigators and attributed to trapping of later, younger meteoric water (e.g., Sun and Eadington 1987 in tin-mineralised granite from New South Wales in Australia; Criss and Taylor 1983 in the Idaho Batholith, US).

The δD values for a fluid in equilibrium with white micas of two samples hosted by the Keddy-Reeves leucogranite (pegmatites from Keddy and Reeves deposits) are lower

than the corresponding δD from fluid inclusion extracts, suggesting strong interaction between MTW2 and the area where both pegmatites are located during white mica crystallisation.

6.4.5. Isotopic evolution of fluids with cooling temperatures

In an integrated model for fluid circulation within the New Ross area (Fig.6.9), we recognize the following succession of fluids involvement: a magmatic fluid characterised by salinities of 19-25 wt. % equiv. NaCl, Na-K chlorides as major solutes, a $\delta^{18}O$ isotopic composition of +8 to +12‰, and δD of -20 to -40‰ exsolves from the magma at temperature of ~650°C (Stage 1). As the system slowly cools to subsolidus temperature of 400-500°C and the fluids react with feldspars, the K/Na ratio of the fluid decreases. A low-salinity water with a $\delta^{18}O$ of ~-2‰ and a δD of ~-6‰ enters the system, as recorded by the fluid in equilibrium with white micas and the progressive increase in δD of fluid inclusion extracts (Stage 2). We suggest that this fluid is dominantly of meteoric origin (MTW1 in Figure 6.6). Fluid inclusions from meteoric water-dominated mineral deposits (mainly vein deposits) record a temperature of ~400°C. Meteoric fluid can reach such elevated temperature by travelling to a depth of ~10-12 km (emplacement depth for the SMB) through fractures created either by thermal contraction of the cooling batholith, by overpressure release by potential explosive unroofing of the batholith (Clarke and Bogutyn in press), or by active faulting related to regional tectonics at the time of SMB emplacement (Horne et al. 1992). Also, convection cells driven by heat in the batholith allow for some mixing of magmatic fluid with a Ca-rich, high-salinity (29-43 wt. % equiv. NaCl) metamorphic fluid originating within the Meguma metasediments (Stage 3). Such mixing is recorded by the cation content of fluid inclusion decrepitates (Carruzzo et al. 2000). In addition, the δD composition of the fluid in equilibrium with white mica from two samples (pegmatites from Keddy and Reeves deposits) hosted by the Keddy-Reeves leucogranite may have been affected by MTW1, therefore explaining the secondary chemical character of the white micas from both pegmatites.

After crystallisation and cooling of the SMB, a second generation of meteoric fluid (MTW2) with a lower δD signature than MTW1 enters the system and is trapped

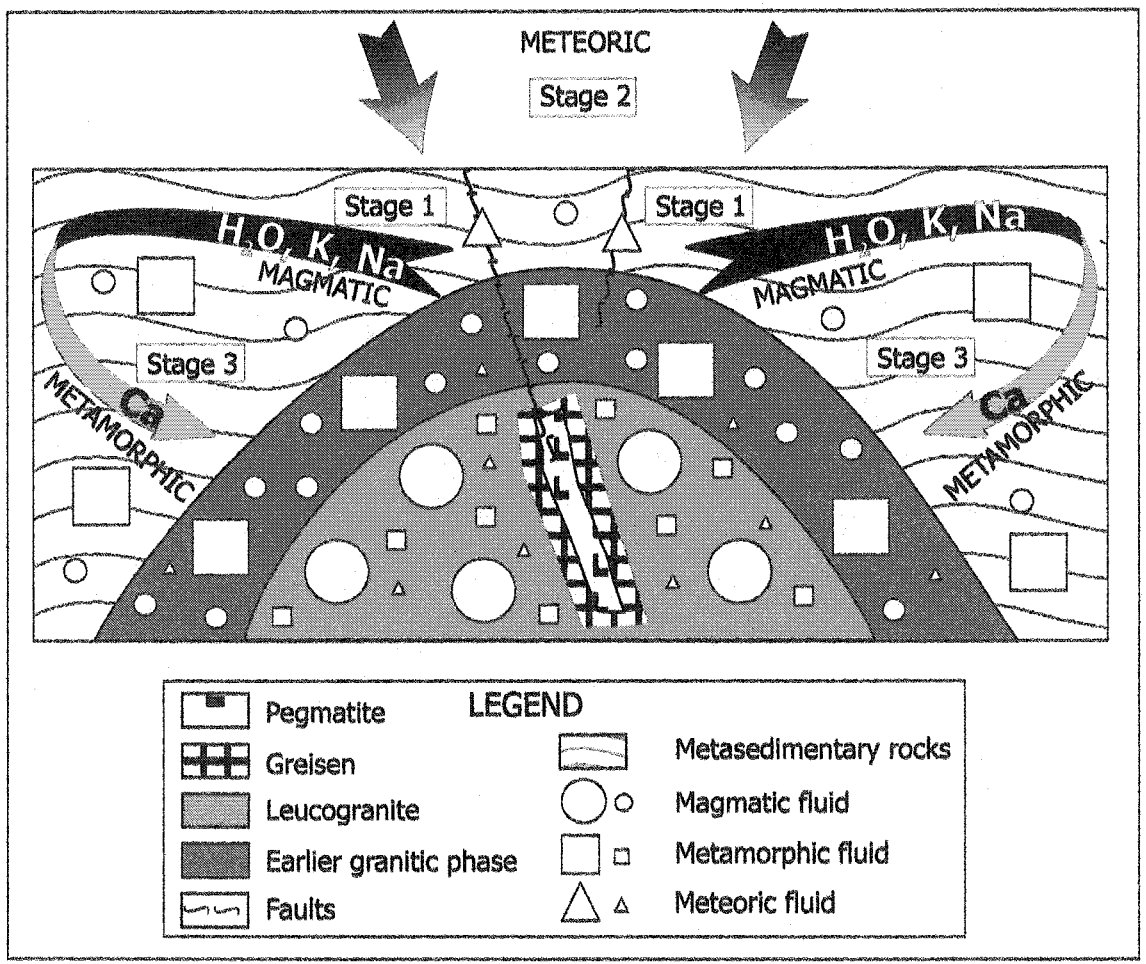

Figure 6.9: Integrated model for fluid circulation within the New Ross area with the different fluids involved. Stages are as described in the text. Large and small squares, circles, and triangles schematically represent the amount of fluid interacting with the granitic samples and the Meguma metasediments.

along healing fractures in quartz grains. This second generation of meteoric water accounts for the difference between the calculated δD_{water} values of white mica and the δD values of fluid inclusion extracts in coexisting quartz.

6.5. Conclusions

Isotopic data for white micas and fluid inclusion extracts from eight mineral deposits of the New Ross area of the South Mountain Batholith, Nova Scotia, permit the following conclusions:

1. As noted by previous studies (Kontak et al. 1988b, 1991), coexisting minerals have not preserved isotopic equilibrium, impeding further determination of formation temperature using isotopic fractionation. Variable degrees of mineral-fluid re-equilibration during subsolidus stage are probably the reason for the isotopic disequilibrium and relate to the protracted thermal history of the SMB.
2. The isotopic compositions ($\delta^{18}O$, δD) of white mica from host granitoid rocks, pegmatite/aplite, greisen, and vein samples along with δD values for fluid inclusion extracts from quartz in the same samples record a transition from a magmatic-dominated, melt-orthomagmatic, low water : rock ratio system to a hydrothermal-dominated, higher water : rock ratio system into which meteoric water infiltrated at the time of SMB emplacement, crystallisation, and greisen/vein formation. We propose a hypothetical mixing line between magmatic and meteoric waters for the SMB during its emplacement and subsequent crystallisation at 373 Ma.
3. Fluid inclusion extracts from quartz record lower δD_{water} values than calculated for coexisting white mica samples using appropriate fractionation factors and temperatures of crystallisation. We attribute these differences to post-crystallisation entrapment of later meteoric water and emphasize the importance of integrating δD values obtained from minerals with those from fluid inclusion extracts. Anomalous depleted δD values for white micas from two pegmatite samples also reflect fluid-mediated recrystallisation of these phases at the same time as the infiltration of the low δD water.
4. Integration of a previous detailed fluid inclusion study of the same samples with the isotopic data provides corroborating support for incursion of meteoric water

during crystallisation and subsequent hydrothermal alteration of the SMB. A set of low temperature, low-salinity fluid inclusions plausibly records the incursion of a second meteoric fluid, as suggested from the isotope data.

5. Although we identified the participation of a metamorphic fluid reservoir in the hydrothermal fluid history of the New Ross area through the fluid inclusion study, our isotopic data do not allow the discrimination of this fluid, given the lack of δD data for the Meguma metasediments.

In summary, the evolution of fluids from a magmatic to hydrothermal regime within the New Ross area is as follows: (i) exsolution of a magmatic fluid at ~ 650°C; (ii) before cooling to ~400-500°C, incursion of a meteoric fluid via fractures with subsequent mixing with magmatic and metamorphic fluids through fluid circulation by convection; and (iii) incursion of a late, low δD meteoric fluid some time after cooling of the area. Finally, this paper clearly identifies the need to define more precisely the isotopic composition of all potential fluids interacting within the MLT, if complete understanding of fluid reservoirs involved in mineralising processes is expected.

CHAPTER 7

DISCUSSION

7.1. Differentiation processes

7.1.1. Introduction

Three main processes of chemical differentiation (fractional crystallisation, contamination, and hydrothermal alteration) occur within the SMB (Clarke and Chatterjee 1988), and physical and chemical evidence for them exist throughout this large granitic body (Table 1.2). To what extent are all of these processes also at work within the New Ross pluton, and how do they lead to the production of mineral occurrences?

7.1.2. Major and trace elements

Ham et al. (1989) published an extensive geochemical database for the SMB, including chemical analyses for all rock types from the New Ross pluton (Appendix E). Using the data from Ham et al. (1989), Figure 7.1 consists of several bivariate diagrams showing major and trace element variation from least to most evolved fractions of the New Ross pluton. In these diagrams, major and trace elements vary mostly because of fractional crystallisation and hydrothermal alteration; therefore, both processes will be the main focus of Section 7.1.2.

All samples from the New Ross pluton present similar trends of evolution to the rest of the SMB (MacDonald and Clarke 1991; Clarke et al. 1993b; Tate and Clarke 1997) in the following cases:

1. biotite and zircon fractionation appears to control the Ti-Zr variation (Fig.7.1a) and fractionation of both cordierite and biotite probably controls the MgO variation (Fig. 7.1b);
2. plagioclase fractionation controls the CaO-Sr variation (Fig. 7.1c), with decreasing An content of plagioclase from least to most evolved fractions;

3. plagioclase and K-feldspar control the Ba-Sr variation (Fig. 7.1d); and
4. MgO and Ba decrease with decreasing of modal abundance of biotite and K-feldspar, respectively, whereas Rb behaves as an incompatible element up to the latest stages of the evolution (Fig. 7.1e, f).

Granodiorite and monzogranite samples from the New Ross pluton show similar evolutionary trends to the rest of the SMB, whereas more evolved fractions of the New Ross pluton do not. This geochemical behaviour probably reflects fluid involvement in the process:

1. Both Ta and Nb are enriched in leucomonzogranite and leucogranite of the New Ross pluton and similarly, to leucogranites from various locations within the SMB (Clarke et al. 1993b) (Fig. 7.1g);
2. Li behaves as an incompatible element with strong enrichment in the latest phases of the New Ross pluton and may relate to concentration by late-stage fluids (Fig. 7.1h); and
3. The K/Rb ratio decreases from least to most evolved fraction of the New Ross pluton, apparently showing increasing involvement of fluids (Shaw 1968) (Fig. 7.1i).

Samples showing evidence of hydrothermal overprint have a K/Rb ratio less than 150, thus most leucomonzogranite and all leucogranite samples of the NRP fall within that category. Such involvement of hydrothermal processes allows for the two trends observed in the Rb-MgO and Rb-Ba diagrams (Fig. 7.1e, f).

7.1.3. Rare earth elements

The REE are also good monitors of the chemical evolutionary processes and demonstrate the existence of fractional crystallisation and subsolidus hydrothermal alteration in the SMB (Table 1.2). Chatterjee et al. (1985), Kontak et al. (1988), and Clarke et al. (1993) presented REE data for different granitoid types in the New Ross area. Figure 7.2a compiles the REE profiles from Kontak et al. (1988) and Clarke et al. (1993) for the NRP and the following points emerge:

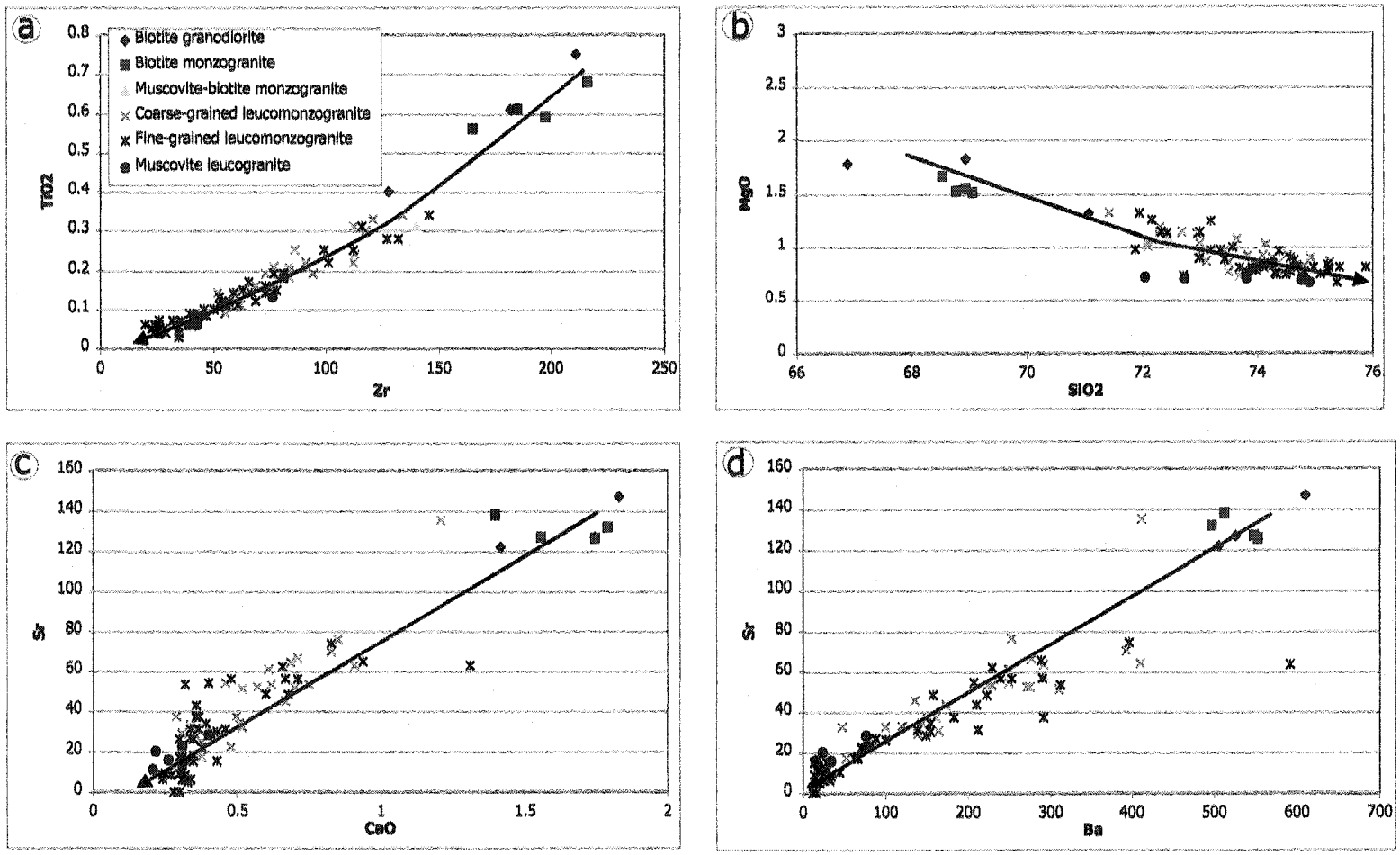

Figure 7.1: Binary diagrams showing chemical element variation from least to most evolved fractions of the New Ross pluton. Arrows represent fractionation trend. Geochemical data from Ham et al. (1989).

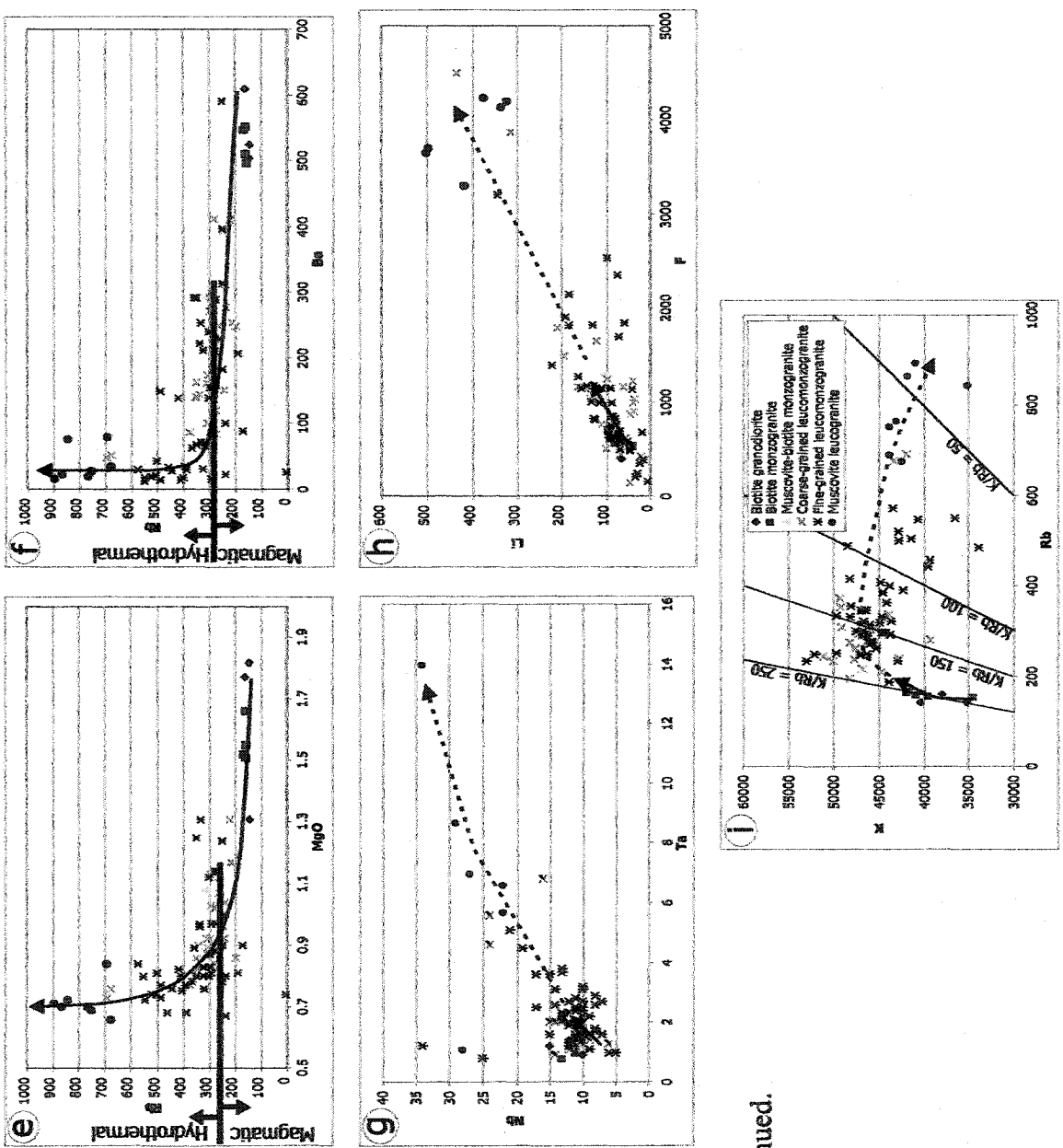

Fig. 7.1: continued.

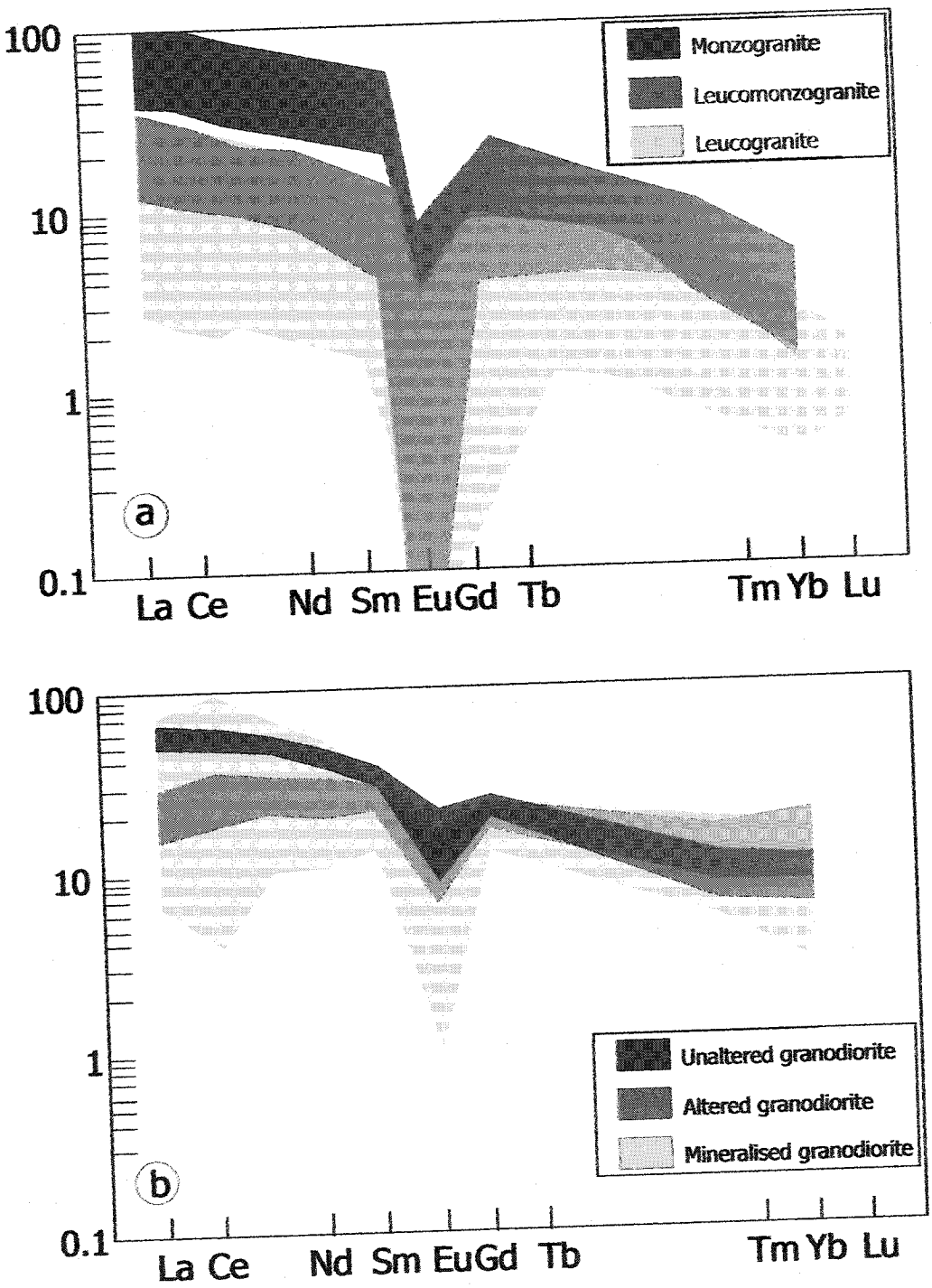

Figure. 7.2: REE profiles for a) least to most fractionated fraction of the SMB and b) least to most altered granodiorite from the Millet Brook deposit.

1. La/Yb ratio for monzogranites between 13 and 37 (mean = 28), for leucomonzogranites between 8 and 37 (mean = 17), and for leucogranites between 1 and 28 (mean = 10);
2. decrease of ΣREE for leucogranites and leucomonzogranites compared to monzogranites; and
3. increase of the magnitude of the negative Eu anomaly for leucomonzogranites and leucogranites compared to monzogranites.

All three points above suggest progressive removal of plagioclase and REE-bearing accessory phases (monazite, xenotime, titanite, apatite) from least to most evolved fractions of the New Ross pluton, indicating fractional crystallisation. However, several authors (Muecke and Clarke 1981; Chatterjee et al. 1985; Kontak et al. 1988b; Corey and Chatterjee 1990) emphasised that the amount of REE depletion (especially in the most evolved fraction of granitoids) is too great to be solely explained by fractional crystallisation and, therefore, may require the presence of a fluid phase for REE removal. Figure 7.2b shows the REE profiles for unaltered, altered, and mineralised granodiorite in the vicinity of the Millet Brook uranium deposit (Chatterjee et al. 1985). The general pattern of the unaltered granodiorite is consistent with that of other granodiorites from the SMB. The altered granodiorite pattern is flat compared to the unaltered one, showing an increase in the heavy REE and a loss of the light REE. Flynn and Burnham (1978) determined that chlorine may complex the light REE. The depletion of the light REE in the most evolved fractions of the NRP probably records such complexing and transport of the light REE. The mineralised granodiorites have variable patterns depending on alteration type accompanying the mineralisation, coupled with a more pronounced Eu anomaly than unaltered and altered granodiorite. Such patterns reveal a more intense effect of fluids from unaltered, to altered, to mineralised granodiorite (Chatterjee et al. 1985).

7.1.4. Stable isotopes

Kontak et al. (1988) and Clarke et al. (1993) presented whole-rock $\delta^{18}O$ for monzogranitic, leucomonzogranitic, leucogranitic, pegmatitic, and greisenised samples from the New Ross area (Table 7.1). The $\delta^{18}O$ values are similar to those reported for the

Sample #	Rock type	Source	Whole rock $\delta^{18}O$
9	monzogranite	Kontak et al. (1988, 1991)	11.1
14			9.5
53			11.0
17-1	leucomonzogranite		10.8
17-2			10.4
39			9.9
20	mineralised leucomonzogranite		10.7
21			11.4
26-1			10.9
26-2			10.0
11-2			10.0
33			10.4
37A			11.3
39			9.9
13	elvan dyke		3.6
KR3028	leucogranite	Clarke et al. (1993)	11.8
KR3028-3			11.5
KRLU-1M			11.4
LL1216-4			10.2
LL1256			11.1
LL1265			11.3
LLLU-7C			11.5
LLLU-8			12.7
BB1260-1			11.1
BB2146-2			11.7
BB2152-1			11.6
BB2152-2			11.5
BBLU-6			11.6
CL-LU-9			15.0
CL20-9-3			11.0
CL20-9-4			11.3

Table 7.1: whole rock $\delta^{18}O$ for monzogranitic, leucomonzogranitic, leucogranitic, pegmatitic, and greisenised samples from the New Ross area. Data from Kontak et al. (1988) and Clarke et al. (1993).

SMB (+10 to +12‰, Longstaffe et al. 1980) regardless of the granitoid rock type, and are typical of peraluminous, crustal-derived granitoids (Sheppard 1986). A single low value (elvan dyke at the Turner deposit) betrays the participation of a low-^{18}O fluid, probably of meteoric origin (Kontak et al. 1988b and Chapter 6).

Sample #	Rock type and location	$\delta^{18}O$ quartz	$\delta^{18}O$ K-feldspar	$\delta^{18}O$ muscovite
9	monzogranite		11.0	
11-1	monzogranite	11.5	12.3	
11	pegmatite Walker	8.9	9.8	8.2
18	pegmatite Keddy	17.6	10.6	
19		11.9	11.0	
22B	pegmatite Reeves	15.5	9.7	
22C		11.4	11.4	
24	pegmatite Grassy Brook	10.3	10.1	
25		11.4	8.9	
34-1	pegmatite Long Lake	10.6	11.0	
34A		10.8	11.0	
34B		12.8		
36	pegmatite Morley's	8.9		9.3
36A		10.9		
38		11.6	10.0	

Table 7.2: $\delta^{18}O$ data for mineral separates (quartz, K-feldspar, muscovite) from monzogranite, leucomonzogranite, and pegmatite samples from the New Ross area. Data from Kontak et al. (1988, 1991).

Kontak et al. (1988, 1991) presented $\delta^{18}O$ data for mineral separates (quartz, K-feldspar, muscovite) from monzogranite, leucomonzogranite, and pegmatite samples from the New Ross area (Table 7.2). Also, Chapter 6 contains $\delta^{18}O$ and δD data for white mica from similar samples to those used by Kontak et al. (1988, 1991). The $\delta^{18}O_{mineral}$ values spread over larger ranges (8.9-17.6‰ for quartz, 8.9-12.3‰ for K-feldspar, 4-9.9‰ for muscovite) than $\delta^{18}O_{whole\ rock}$ values. Furthermore, isotopic disequilibria among coexisting minerals are present, especially for pegmatite samples, therefore suggesting the incursion of fluid(s) in the late-stage of evolution of the area (Kontak et al. 1991, Chapter 6).

Poulson et al. (1991) provided $\delta^{34}S$ isotopic data for a few monzogranitic samples from the New Ross pluton. They obtained a wide range of values (+1.6 to +15.0‰; average = +9.1). Samples from the New Ross pluton do not contain a large amount of sulphur; therefore, assimilation of various quantities of country rock ($\delta^{34}S$ from –3.7 to +24.2‰;

average = +13.0‰) may allow for the considerable variation in $\delta^{34}S$ values (Poulson et al. 1991).

7.1.5. Radiogenic isotopes

Clarke et al. (1988) provided $\varepsilon\ ^{t}_{Nd}$ values (-5.2, -5.2, -4.9) at t = 376 Ma for three porphyritic monzogranites from the New Ross pluton. In an $\varepsilon\ ^{t}_{Nd}$ vs. $^{87}Sr/^{86}Sr$ diagram (Fig.7.3), all data fall at the edge of the data field for the SMB, towards the field for Meguma metasedimentary $\varepsilon\ ^{t}_{Nd}$ values, indicative of some degree of assimilation of country rock in the area (Clarke et al. 1988; Tate and Clarke 1997), consistent with the $\delta^{34}S$ data discussed above.

7.1.6. Summary

The mineralogical and geochemical diversity of the New Ross pluton is the result of the three main processes at work within the SMB: fractional crystallisation, contamination, and subsolidus hydrothermal alteration. Major, trace, REE elements, and oxygen isotopes attest to the existence of fractional crystallisation and fluid alteration, whereas sulphur and neodymium isotopes indicate the presence of contamination of Meguma Supergroup metasediments within the New Ross pluton.

7.2. Concentration of incompatible elements

7.2.1. Introduction

Metals of interest in granite-related ore deposits are incompatible trace elements, because they do not "fit" in the crystalline structure of common rock-forming silicate minerals (e.g., Rollinson 1993). This section deals with the classification, distribution, and concentration of metals present in the mineral occurrences of the New Ross area.

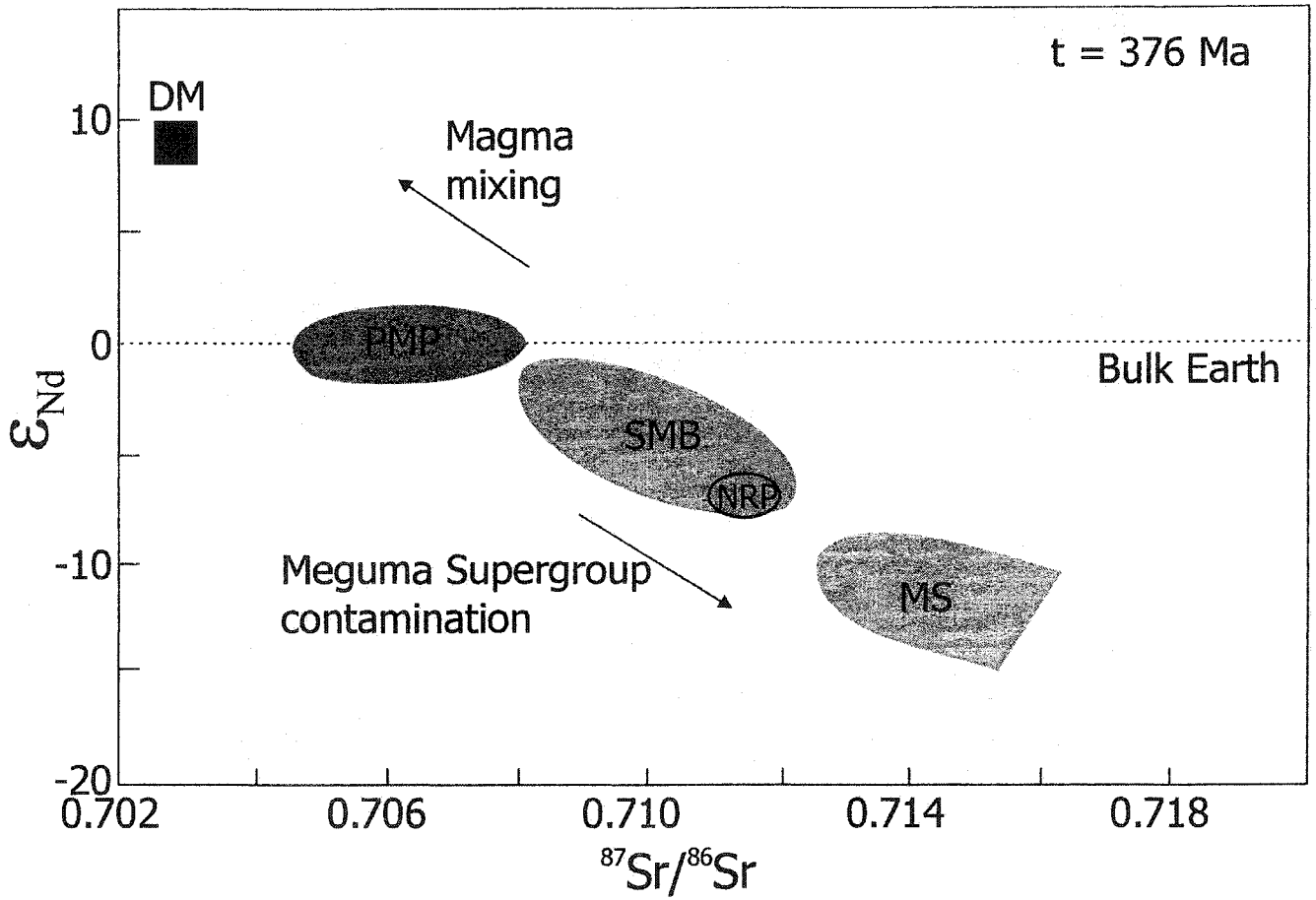

Figure 7.3: Plot of ε^{t}_{Nd} vs. $^{87}Sr/^{86}Sr$ for the SMB. MS Meguma Supergroup, SMB South Mountain Batholith, PMP Port Mouton Pluton, DM depleted mantle. Data recalculated to t = 376 Ma. Note the location of data from the New Ross pluton (NRP). From Tate and Clarke (1997).

7.2.2. Classification of metals

Most metals of interest in this study belong to the transition metals group (atomic numbers 22 to 29 and 40 to 47). The transition elements (e.g., Mn, Fe, Cu, Zn, Mo, W) have in common their incompletely filled d-orbital, becoming more filled from left to right in the Periodic Table (e.g., Faure 1991), and generally have variable valences. Elements present in granite-related mineral deposits range from **chalcophile** (strong affinity for sulphur and forming covalent bonds; e.g., Cu, Pb, Zn, As, Bi) to **lithophile** (strong affinity for oxygen and forming ionic bonds, e.g., Li, Be, F, Mn, Nb, Ta, Ba, W, U) elements, with **siderophile** elements having a weak affinity for both sulphur and oxygen (e.g., Fe, Mo, Sn) (Strong 1988). Also, some metals change their geochemical character or behaviour depending on the chemical environment (Strong 1988).

Incompatible elements are commonly subdivided on the basis of their ionic potential (ratio of the valence to the ionic radius of the element): small and highly charged elements are the high field strength cations (**HFS**) with an ionic potential greater than 2, and large cations of small charge are the low field strength cations (or large ion lithophile elements **LILE**) with an ionic potential less than 2 (e.g., Rollinson 1993; Strong 1988) (Fig. 7.4).

7.2.3. Distribution of metals

The distribution, or partition, coefficient describes the distribution of metals or any trace element between a solid and a liquid phase as follows:

K_{Di} = C_i in mineral/C_i in liquid, where K_{Di} is the partition coefficient for an element i and C is the concentration of i in ppm or wt. % (e.g., Barnes 1979). A similar partition coefficient exists between the melt and a fluid or solid phase (minerals) (Barnes 1979). Most authors use the abbreviation D instead of K_D, and I will use this notation for the following part of this chapter. In general, partition coefficients vary according to temperature, pressure, composition, pH, and oxygen activity ($a_{O2} = \gamma c$ where γ is the **activity** coefficient and c is the concentration of O_2 in solution; also, activity of a solute $a = f/f^0$ where f is the fugacity of the solute in the solution and f^0 is its fugacity when the vapor is in equilibrium with the pure substance in the standard state. The fugacity represents the

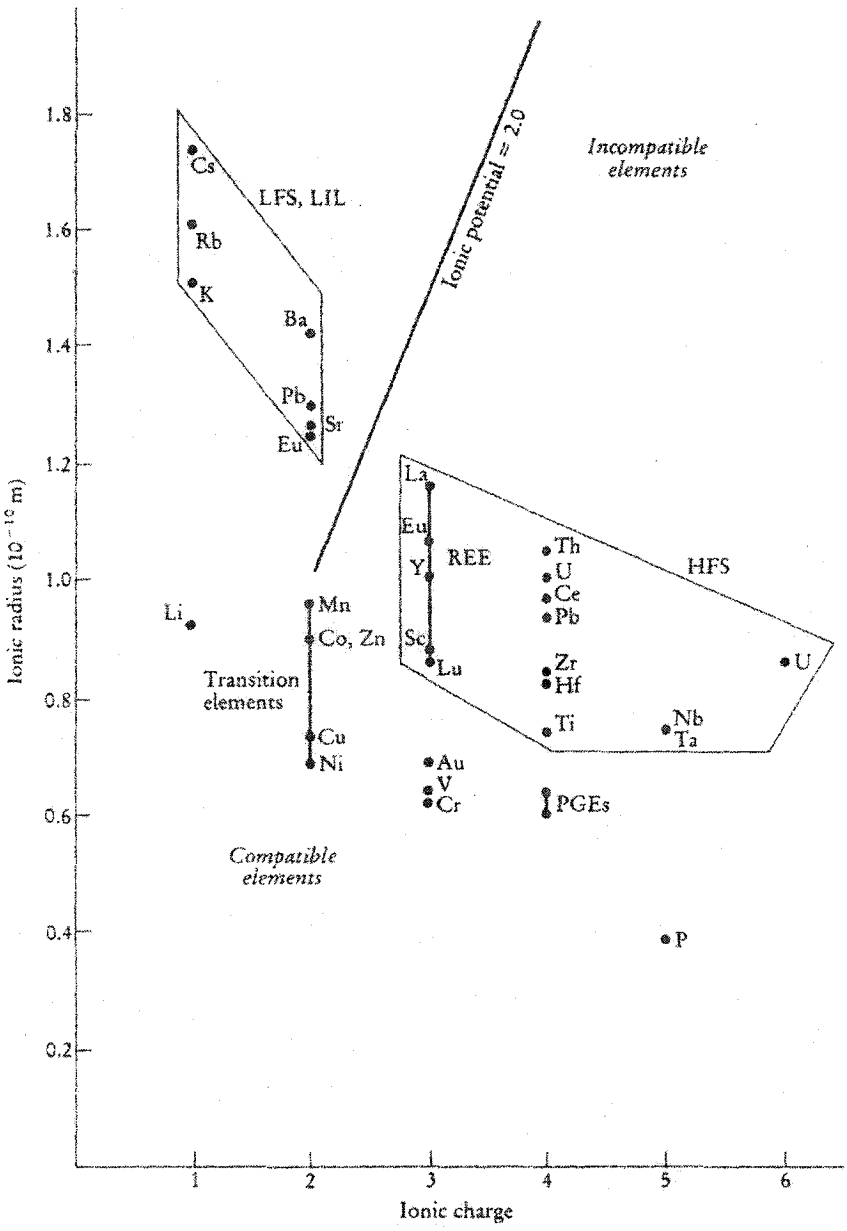

Figure 7.4: Plot of ionic radius vs ionic charge for trace elements. Ionic potential (charge /size ratio) of 2.0 subdivides the incompatible elements into LFS elements (or LIL) and HFS elements. From Rollinson (1993).

partial pressure a real gas would have if it were ideal; Faure 1991) conditions. With pressures higher than 3-4 kbar, the melt/vapour partition coefficients for many incompatibles decrease (e.g., Urabe 1987).

7.2.4. Concentration of metals

Clarke (1992) reviewed the processes of concentration of incompatible elements leading to mineral deposits in granitoid rocks and the following succinctly retraces the main steps.

A. Melt present

1. Incompatible elements are enriched in the silicate melt phase during partial melting.
2. Assimilation of country rock may provide the silicate melt phase with some incompatible elements.
3. Thermogravitational diffusion (a process balancing the chemical potential of every component throughout the magma) concentrates incompatible elements near the roof of the pluton (Hildreth 1981).
4. Fractional crystallisation further concentrates the incompatible elements in the melt. As described in Section 7.2.3, the partition coefficients for incompatible elements between rock-forming minerals and melt range between 0 and 1, therefore, a fraction of incompatibles leaves the melt.
5. Water saturation allows for the separation of an aqueous fluid phase (magmatic fluid) from the melt. For many incompatible elements, the partition coefficient between such fluid phase and the melt is greater than 1. Factors such as temperature, pressure, fluid composition, pH, and fO_2 dictate the value of partition coefficients. Section 7.3.3 details the important factors for the main metals present in the New Ross area.

B. Melt absent

6. The fluid transporting incompatible elements can extend below solidus temperatures by fluid egress from the melt region into cooler parts of the pluton or country rock or, if remaining in the melt region, by complete crystallisation of the melt. The fluid continues to react with the minerals from

the surrounding rocks, producing secondary minerals and taking some materials into solution (i.e., alteration process). Interaction of the magmatic fluid with fluids of other origin (e.g., metamorphic, meteoric, connate, seawater) is also possible, further promoting cooling of the fluid phase.

7. Through decreasing temperatures and pressures, the aqueous fluid phase reaches the liquid-vapour divariant boundary, resulting in retrograde boiling. Volatile constituents enter the vapour phase and leave the system; as a consequence of the vapour phase leaving the system, the solubility of incompatible elements drops and precipitation occurs.
8. Further concentration of incompatible elements occasionally occurs in the weathering environment with percolating surface water dissolving incompatible-bearing minerals and transporting and concentrating the incompatible elements to another favourable deposition location.

7.3. Partitioning, transport, and deposition of incompatibles

7.3.1. Hydrothermal solutions: generalities

Hydrothermal solutions are hot, aqueous solutions from which ore minerals may precipitate (Skinner 1997). From fluid inclusion and stable isotope (O and H) studies, we know that hydrothermal solutions have highly variable compositions (e.g., Roedder 1984; Sheppard 1986; Roedder and Bodnar 1997), providing clues about their source(s) and/or travel path(s). Possible sources of solutions are magmatic, meteoric, metamorphic, connate, and ocean water (Barnes 1979), and input from these different reservoirs may be traceable using stable isotopes (Chapter 6).

Besides being hot and H_2O-dominated, hydrothermal solutions contain variable concentrations of dissolved solids, with Na, K, Ca, and Cl as major components (present as alkali chlorides), whereas ore metals such as Cu, Pb, Zn, Sn, Mo, W, Ag, etc. (present as complex ions) are rarely, if ever, present as major constituents (Pirajno 1992; Skinner 1997). The source of both major and minor constituents (cooling magma and/or fluids and/or rocks travelled through) is rarely determined with certainty (Pirajno 1992).

Solubility of a solute in water depends on the bonding of the solute to water (H_2O); therefore, it is important to understand the structure and characteristics of water. Water is a polar molecule (i.e., has unequal charge distribution), allowing the positive ends of the water molecule to be attracted to anions and the negative ends of the water molecule to cations (i.e., hydration). Water molecules link to each other through a bond (hydrogen bond) between the oxygen of one molecule and the hydrogen of another, forming tetrahedrally coordinated clusters (Liu et al. 1996). Variations of temperature and/or pressure prompt changes in water structure (Seward and Barnes 1997). An increase of temperature (i) weakens hydrogen bonding, and liquid water expands; (ii) decreases the dielectric constant [expression of the extent to which a material concentrates electric flux, Atkins (1994)], therefore enhancing ion-pairing and metal complexing; and (iii) lowers the value for neutral pH (i.e., increases K_w, the ion product constant), allowing for the formation of hydroxide complexes at higher temperatures. An increase in pressure (i) decreases water density (enhanced by higher temperature); (ii) has no effect on the dielectric constant; and (iii) increases ionisation of water.

At higher temperatures and lower pressures, most solutes tend to form ion pairs (single cation and single anion held together by electrostatic attraction only), thereby leading to a decrease in the activity of potential ligands for metals, and in turn limiting the concentration of metal complexes (Brimhall and Crerar 1987; Seward and Barnes 1997).

7.3.2. Transport of metals

7.3.2.1. Introduction

To better understand metal transport processes, it is important to recognise the role of ligands in the complexing process. Several papers and chapters in specialised publications (Barnes 1979; Seward 1981; Crerar et al. 1985; Eugster 1986; Pirajno 1992; Seward and Barnes 1997; Wood and Samson 1998) review metal complexing and its chemical controls. The following is a compilation from these sources.

In solution, metals associate with ligands to form complex ions, allowing for transport of metals in a hydrothermal fluid. The interaction between metals and ligands is comparable to acid-base reactions, with the metal accepting, and the ligand giving, an electron. Based on charge and size, hard and soft metals and ligands exist with, given

competition between several ligands and metals, soft metals binding more easily with soft ligands, whereas hard metals bind preferentially with hard ligands. The main characteristics for each class are:

1) **hard**: high charge, small radius, slightly polarisable, preferring ionic or electrostatic bonding (i.e., involves transfer of electrons); and
2) **soft**: low charge, large radius, highly polarisable, preferring covalent bonding (i.e., involves sharing of electrons).

Table 7.3 contains a classification of metals (~ bases) and ligands (~acids) according to their hardness. Important to note in this Table is that, within a category, hardness decreases to the right. As stated in Section 7.3.1, changes in water structure with increasing temperature decrease the dielectric constant of the water, consequently "hardening" the interaction between metal and ligand (Brimhall and Crerar 1987; Seward and Barnes 1997).

7.3.2.2. Stability of complexes

At hydrothermal temperatures (<400˚C), only the following few ligands are present in sufficient quantities to allow metal complexing: Cl^-, F^-, HS^- or H_2S, PO_4^{3-}, and OH^- (Barnes 1979).

The activity of the ligands controls the metal-carrying capacity of the fluids, rather than the abundance of the metals (Barnes 1979). Temperature and pressure are the main controls of metal complexing; in general, higher temperatures enhance complex formation, whereas higher pressures cause dissociation of metal complexes (Seward and Barnes 1997). Temperature and pressure affect the stability of various ligands differently, for example, chloride complexes are more stable at high temperature (> 400ºC) than sulphide complexes (Barnes 1979).

Bases		
Hard	**Borderline**	**Soft**
H^+	Fe^{2+}, $Mn^{2+}Co^{2+}$, Ni^{2+}	Au^+, Ag^+, Cu^+
Li^+, Na^+, K^+, Rb^+, Cs^+	Cu^{2+}, Zn^{2+}, Pb^{2+}, Sn^{2+}	Hg^{2+}, Cd^{2+}
Be^{2+}, Mg^{2+}, Ca^{2+}	As^{3+}, Sb^{3+}, Bi^{3+}	
Sr^{2+}, Ba^{2+}		
Al^{3+}, Ga^{3+}		
Ce^{4+}, Sn^{4+}		
Ti^{4+}, Ti^{3+}, Zr^{4+}		
Mo^{6+}, Mo^{5+}, Mo^{4+}		
W^{6+}, W^{4+}, Nb^{5+}, Ta^{5+}		
Mn^{4+}, Fe^{3+}, Co^{3+}		
U^{6+}, U^{4+}		
Acids		
Hard	**Borderline**	**Soft**
NH_3, H_2O, OH^-	**Br^-**	**CN^-, CO**
CO_3^{2-}, NO_3^-		S^{2+}, HS^-, H_2S, SO_3^{2+}
PO_4^{3-}, SO_4^{2-}		I^-
F^-, Cl^-		

Table 7.3: Classification of ligands and metals according to their hardness. After Seward and Barnes (1997), Brimhall and Crerar (1987), and Pirajno (1992). In bold, most important ligands in natural hydrothermal fluids.

7.3.2.3. Solubility

If simple aqueous ions dominate in a solution, the ore mineral solubilities are too low for the transport of significant quantities of ore metals; however, formation of complexes increases solubility so that ore deposit formation becomes possible (Barnes 1979; Wood and Samson 1998). High metal solubilities require either large solubility constants (K_{SP} = activity *a*) and/or large stability constants (K_n; degree to which a metal and a ligand tend to form a complex) for the predominant complex(es) (Wood and Samson 1998). Also, solubility increases with higher temperature for most solids in water; several variables (i.e., pH, fO_2, fS_2, a_{Cl} for the most important) change with increasing temperature, therefore, influencing the solubility of minerals (Brimhall and Crerar 1987).

7.3.3. Partitioning of metals and ligands from melts into fluids

As described in Section 7.2.4, metals concentrate in one phase or another, depending on the value of the partition coefficient between two phases. This Section details the

different factors affecting the partition coefficients of both ligands and metals between different phases (mainly fluid-melt, fluid-mineral).

7.3.3.1. Ligands

Chlorine

Although not always the most ideal ligand for the available metal (according to the hard-soft classification of ligands in Section 7.3.2.1), both its ubiquitous presence and abundance make chlorine the most significant ligand in the majority of hydrothermal ore-forming fluids (Seward and Barnes 1997; Wood and Samson 1998). At temperature between 725° and 950°C and pressure ranging from 0.5 to 5 kbar, Cl partitions in favour of the fluid rather than the melt with the fluid phase being H_2O alone or $H_2O + CO_2$ (Webster and Holloway 1988). Factors enhancing the partitioning of Cl towards the fluid phase are higher concentrations of Cl in the melt (Fig.7.5), decrease of fluorine content, increase of pressure and temperature, and increase of the melt peraluminosity (Kilinc and Burnham 1972; Webster and Holloway 1988; Webster 1990, 1992). Higher chlorine concentrations in the melt trigger the exsolution of that fluid from the melt earlier (i.e., at lower H_2O concentration in the melt) than if there were no Cl; consequently, a Cl-rich brine can evolve from a felsic magma prior to extensive crystallisation and, more importantly, prior to boiling of a volatile phase (Webster 1992; 1997a; 1997b).

Fluorine

Fluorine preferentially partitions towards the silicate melt in a fluid-melt system (e.g., $D_F^{f/m} < 1$) (Koster Van Groos and Wyllie 1968; Dingwell and Scarfe 1983; Webster and Holloway 1987; London 1987; London et al. 1988). At temperatures close to 800°C and pressures of ~ 2 kbar, the presence of fluorine in a haplogranitic melt-fluid system increases the solubility of some high field strength-bearing minerals in the melt (e.g., manganocolumbite, manganotantalite, zircon, rutile), therefore, favouring the enrichment

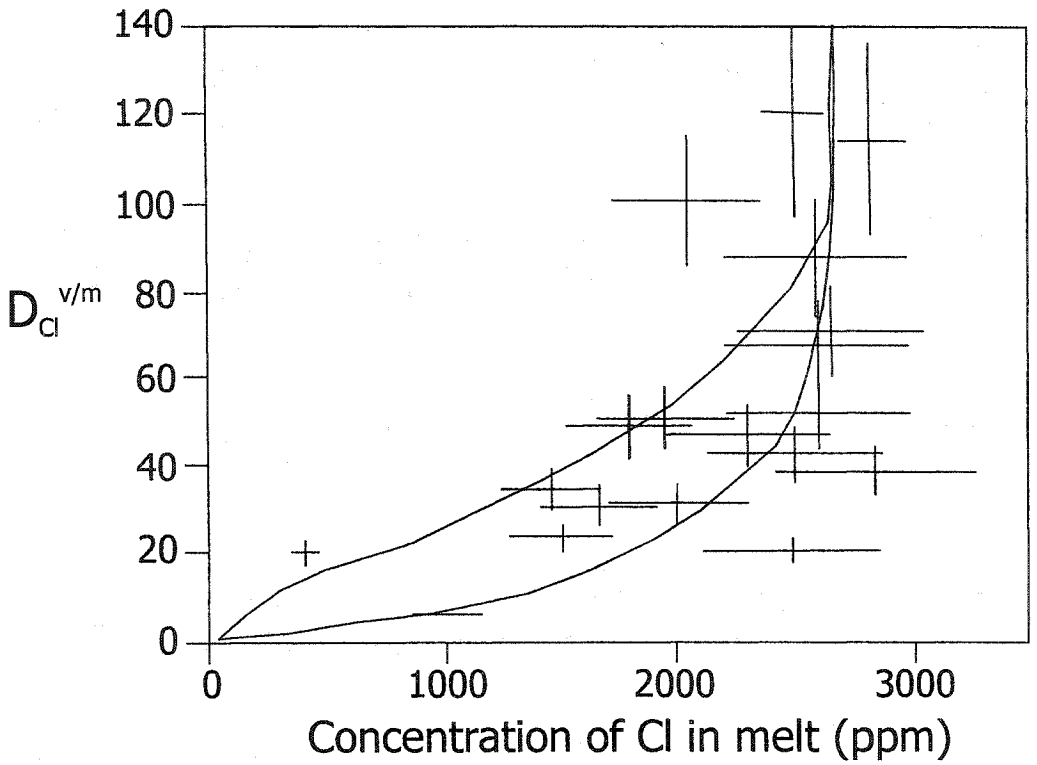

Figure 7.5: Plot of the $D_{Cl}^{v/m}$ as a function of the ppm Cl in the melt for an 800°C and 2 kbar experiment. From Webster and Holloway (1988).

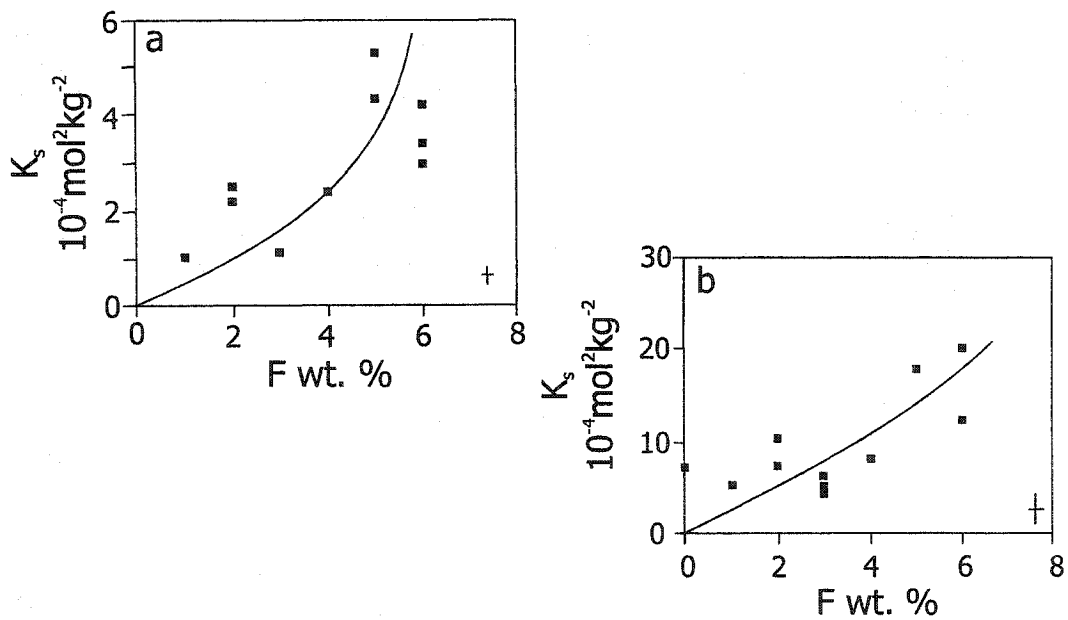

Figure 7.6: Solubility of (a) manganocolumbite $MnNb_2O_6$ and (b) manganotantalite $MnTa_2O_6$ in water-saturated haplogranitic melt at 2 kbar and 800°C.
K_s = [MnO][Nb_2O_6] or [MnO][Ta_2O_6]. From Keppler (1993).

of those elements (Ti, Nb, Ta, Zr, Hf, Th, U, REE) in the melt (Fig. 7.6) (Keppler and Wyllie 1991; Keppler 1993). With increasing amount of F in the system, the solubility of peraluminous melts increases; therefore, $D_F^{f/m}$ increases to values >1 with concentration of more than 8 wt % of F in melt (London 1987; Webster 1990). Other effects of increasing the amount of F in the melt are larger $D^{f/m}$ for Sn, W, Mo, Cu, and REE (Dingwell 1985).

Sulphur

Sulphur dissolves as HS^- in hydrous melts and strongly partitions towards the fluid phase if sulphide minerals (e.g., pyrrhotite) are not stable (Burnham 1979; Brimhall and Crerar 1987). The $D_S^{f/m}$ does not vary with temperature, but is highly sensitive to pressure variations (Burnham and Ohmoto 1980): sulphur exists as H_2S and SO_2 in the fluid phase and, HS^- being mostly present in the melt phase, its partition coefficient is sensitive to f_{H2O} and fO_2 (Fig 7.7) (Burnham and Ohmoto 1980; Carroll and Webster 1994 and references therein). An increase in f_{H2O} decreases $D_S^{f/m}$, because the H_2S/SO_2 ratio increases in the fluid phase; an increase in fO_2 decreases the H_2S/SO_2 ratio, thereby increasing $D_S^{f/m}$ (Burnham and Ohmoto 1980). The fO_2 of peraluminous granites is generally below the QFM buffer (Fig. 7.7), hence H_2S dominates in the system compared to SO_2, indicating a more reducing environment (Burnham and Ohmoto 1980). The ionisation reactions of H_2S are:

$H_2S_{(aq)} = H^+ + HS^-$

and $HS^- = H^+ + S^{2-}$

The equilibrium constant of the second reaction is small (10^{-16} to 10^{-18}), therefore, a_S^{2-} is negligible and metal sulphide solubility equilibrium is:

$MS_{n/2}(s) + n/2\ H^+ = M^{n+} + n/2HS^-$ where M is metal and n = 1, 2, … (Seward and Barnes 1997).

Phosphorus

High phosphorus concentrations are systematically associated with late-stage peraluminous granitic rocks and P may be considered as a ligand in ore mineralisation processes (London 1992). The dominant phosphate complexes in peraluminous melts are $AlPO_4$ and P_2O_7 (Mysen et al. 1999), the first one accounting for the increasing solubility

cases, most white micas have lower $\delta^{18}O$ values than coexisting quartz and alkali feldspar.

Kontak et al. (1991) calculated temperatures of 600 ± 65°C using fractionation factors for quartz-white mica data ($\delta^{18}O_{q-m}$) from Longstaffe et al. (1980), whereas $\delta^{18}O_{q-m}$ data from pegmatites in the New Ross area provide a large range of apparent temperatures (1200° to 230°C), indicating post-crystallisation isotopic exchange. Using the values obtained for this study, $\delta^{18}O_{q-m}$ ($\delta^{18}O_{quartz}$ - $\delta^{18}O_{muscovite}$) ranges from 0.4 to 8.1. The expected $\delta^{18}O_{q-m}$ values for magmatic conditions within granitoids is 3.8±0.3‰ (Longstaffe 1982), and with the exception of two samples, the calculated $\delta^{18}O_{q-m}$ values for samples from the New Ross area are below this range and represent isotopic disequilibrium (Fig. 6.5). The $\delta^{18}O_{q-f}$ ($\delta^{18}O_{quartz}$ - $\delta^{18}O_{alkali\ feldspar}$) range from 0 to 7. Longstaffe (1982) provided a $\delta^{18}O_{q-f}$ range of 1.6 to 2.4‰ for granitoids equilibrated under magmatic conditions. Pegmatites from Reeves and Morley's show an appropriate $\delta^{18}O_{q-f}$ and temperatures calculated for these samples are between 480° and 520°C. This temperature range is in close agreement with pressure-corrected entrapment temperature from fluid inclusion thermometry of pegmatites. Disequilibrium values are expected within the SMB, as slowly cooling magmas (plutonic environment) are more susceptible to isotopic exchange with an orthomagmatic or deuteric fluid both at high and low temperature (Giletti 1986).

6.4.2. Isotopic signature of fluid types

Carruzzo et al. (2000) used salinity and decrepitate analysis of fluid inclusions in quartz from each of the eight mineral deposits of the New Ross area to identify three different fluid reservoirs (magmatic, metamorphic, meteoric). Such fluids are normally isotopically distinct (Sheppard 1986) and their signature within the SMB should, therefore, be discernable. Other sources of fluids at the time of fluid circulation (i.e., 373 Ma), such as evaporated brines or seawater, are not considered because of their absence from the stratigraphic record at the time of SMB emplacement. The isotopic signature of magmatic and metamorphic fluids depends mainly on the isotopic composition of the source rock, whereas the isotopic signature of the meteoric fluid depends on terrane-

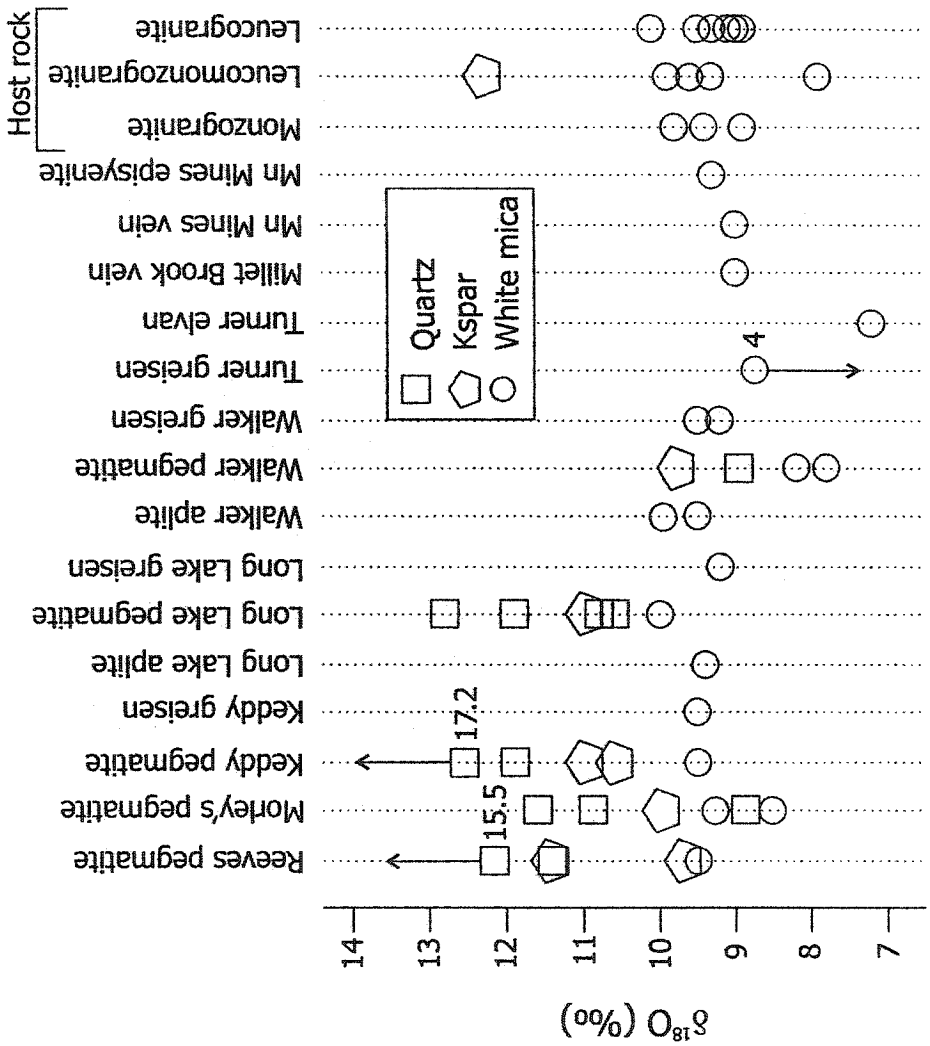

Figure 6.4: Integrated isotopic data for mineral separates from the mineral deposits of the New Ross area using data from Kontak et al. (1988, 1991) and this study.

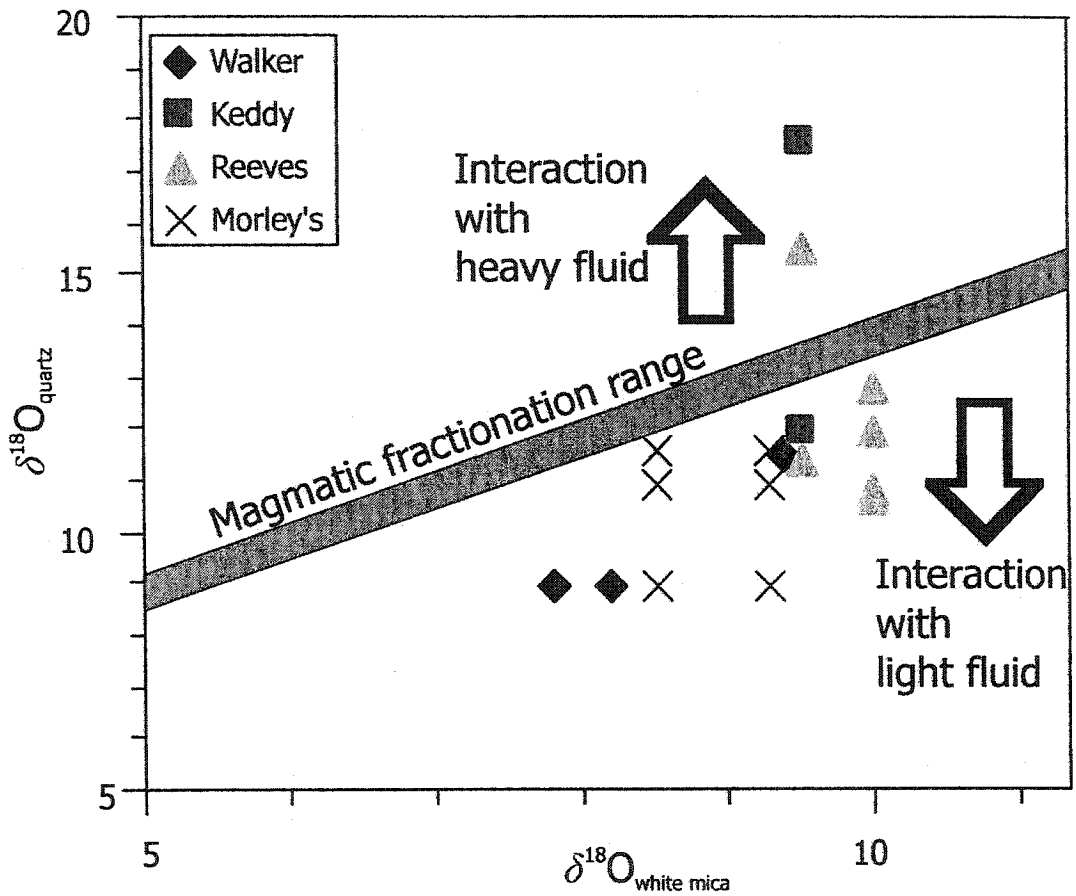

Figure 6.5: $\delta^{18}O_{white\ mica}$ versus $\delta^{18}O_{quartz}$ diagram for mineral pairs from mineral deposits of the New Ross area. The magmatic fractionation field (Longstaffe 1982) represents the area where data plot if equilibrium between both minerals exists. $\delta^{18}O_{quartz}$ values from Kontak et al. (1988, 1991) and $\delta^{18}O_{white\ mica}$ values from this study.

specific parameters such as latitude and altitude. The following presents the isotopic signature of the three fluids previously recognised in the New Ross area.

Magmatic: Sheppard et al. (1969) defined the isotopic composition of magmatic fluid as having δD values from –40 to –80‰ and $\delta^{18}O$ values from +5.5 to +9.5‰. However, a magmatic fluid in equilibrium with high-$\delta^{18}O$ peraluminous granites might plot outside this range [i.e., shows enrichment of a few ‰ of $\delta^{18}O$, Sheppard (1986)], similar to the peraluminous granites of the Cornubian Batholith of SW England (Sheppard 1977). Using $\delta^{18}O$ data (n = 24) from unaltered granitoid rocks (Longstaffe et al. 1980, Dinnett 1995), we defined $\delta^{18}O_{magmatic\ water}$ for the SMB to be +10 ± 2‰ at 600°C. Using $\delta D_{mineral}$ data (n = 2) from Dinnett (1995) (the only available δD values for unaltered granitoid rocks of the SMB), we approximated the δD range for the SMB to be -40 ± 10‰ again at 600°C. However, note that the SMB magmatic field is probably artificially shortened because of the limited amount of $\delta D_{mineral}$ data available. Nonetheless, the δD values used here are within the range proposed by Taylor (1987) for water exsolved from felsic melts.

Metamorphic: Sheppard (1986) gave values of δD from 0 to –70‰ and $\delta^{18}O$ from +3 to +20‰ for a metamorphic fluid in equilibrium with minerals of its host rock. To narrow this large range, which reflects the diversity of possible protoliths, we calculated a hypothetical metamorphic fluid composition specific to the Meguma Supergroup [psammite and pelite, average compositions in Kontak and Dostal (1992)]. The only isotopic data existing for the Meguma Supergroup are $\delta^{18}O_{whole\ rock}$ (Longstaffe et al. 1980). Assuming a certain $\delta^{18}O_{metamorphic\ water}$ at 600° and 400°C and knowing the fractionation factor between each mineral of the sample (quartz, chlorite, albite, white mica, and biotite) and water, we obtain the $\delta^{18}O$ for each mineral (using the equations of Bottinga and Javoy (1973) for quartz/albite/muscovite/biotite-water fractionation and Savin and Lee (1988) for chlorite-water fractionation). We then assign a weighted $\delta^{18}O$ value to each mineral according to the amount of oxygen it contains; the sum of weighted $\delta^{18}O$ value for each mineral represents $\delta^{18}O_{whole\ rock}$. By comparing the $\delta^{18}O_{whole\ rock}$ calculated to the measured values from Longstaffe et al. (1980), we vary the $\delta^{18}O_{metamorphic\ water}$ to obtain matching values (Table 6.3). Between 600° and 400°C, $\delta^{18}O_{metamorphic\ water}$ ranges from +7.5 to +10.8‰; this range overlaps the $\delta^{18}O_{magmatic\ water}$.

Sandstone	Mineral modal proportion (%)	proportion of O in each mineral	proportion of O in whole sample	1000lnα at 600°C	1000lnα at 400°C	$\delta^{18}O_{mineral}$ at 600°C with $\delta^{18}O_{fluid}$=10.8	$\delta^{18}O_{mineral}$ at 400°C with $\delta^{18}O_{fluid}$=8.8	Weighted $\delta^{18}O_{mineral}$ at 600°C	Weighted $\delta^{18}O_{mineral}$ at 400°C
quartz	30	0.53	15.9	1.59	3.42	12.39	12.27	4.29	4.25
feldspar	20	0.49	9.8	0.99	2.41	11.79	11.26	2.52	2.40
chlorite	30	0.39	11.7	-5.32	-2.35	5.48	6.5	1.40	1.66
biotite	10	0.39	3.9	-2.54	-2.08	8.26	6.77	0.70	0.58
muscovite	10	0.46	4.6	-0.77	1.36	10.03	10.21	1.01	1.02
		Total oxygen in sample:	45.9				$\delta^{18}O_{whole\ rock}$:	9.91 corresponding to mean $\delta^{18}O$ of sandstone samples of Meguma (9.9)[1]	9.91

Siltstone	Mineral modal proportion (%)	proportion of O in each mineral	proportion of O in whole sample	1000lnα at 600°C	1000lnα at 400°C	$\delta^{18}O_{mineral}$ at 600°C with $\delta^{18}O_{fluid}$=9.3	$\delta^{18}O_{mineral}$ at 400°C with $\delta^{18}O_{fluid}$=7.5	Weighted $\delta^{18}O_{mineral}$ at 600°C	Weighted $\delta^{18}O_{mineral}$ at 400°C
quartz	48	0.53	25.44	1.59	3.42	10.89	10.92	5.68	5.69
feldspar	28	0.49	13.72	0.99	2.41	10.29	9.91	2.89	2.79
chlorite	15	0.39	5.85	-5.32	-2.35	3.98	5.15	0.48	0.62
biotite	5	0.39	1.95	-2.54	-2.08	6.76	5.42	0.27	0.22
muscovite	4	0.46	1.84	-0.77	1.36	8.53	8.86	0.32	0.33
		Total oxygen in sample:	48.8				$\delta^{18}O_{whole\ rock}$:	9.64 corresponding to mean $\delta^{18}O$ of siltstone samples of Meguma (9.6)[1]	9.65

Table 6.3: Calculations of $\delta^{18}O_{metamorphic\ water}$ in equilibrium with a sandstone and siltstone from the Meguma Supergroup from $\delta^{18}O_{whole\ rock}$ values of Longstaffe et al. (1980). [1] Longstaffe et al. (1980).

Meteoric: The meteoric water line (MWL) shows the systematic variation of present-day meteoric water isotopic composition, and ancient meteoric water may present a similar relationship (Sheppard 1986). Paleoreconstructions of the position of Laurentia (Kent and Van der Voo 1990, Scotese and McKerrow 1990) reveal that the Meguma Terrane was located ~20° South latitude during the Late Devonian (Famennian) and show the closure of the Theic Ocean between Laurentia and Gondwana by Late Carboniferous - Early Permian (Scotese and McKerrow 1990), leaving the MLT close to open sea water until ~300 Ma. Using isostatic calculations (Airy Model), assuming that the present crustal thickness is similar to the crust thickness in the Late Devonian minus erosional effect (estimated from geobarometry to be ~12 km, the depth of emplacement of the SMB, Raeside and Mahoney 1996), a compensation depth of ~ 100 km, and using densities of 2.8 g/cm^3 for the crust and 3.3 g/cm^3 for the mantle, we obtained a paleo-altitude of ~1700 m for 370 My ago.

A possible model for the paleo-isotopic composition of the MLT, considering both latitude (20° S) and altitude (~1700 m) restrictions, is the Andes in South America, where a $\delta^{18}O$ value of $-6 \pm 2‰$ exists for a meteoric fluid (Taylor 1997). We obtained a δD_{water} value for that range of $\delta^{18}O$ by applying the equation for the meteoric water line ($\delta D = -38‰ \pm 16$). Recent measured isotopic values from precipitation in South America (Los Molinos station in Argentina, latitude of ~ 24° and altitude of 1300 m) are $\delta^{18}O = -8$ to 0‰ and $\delta D = -40$ to -5‰.

6.4.3. Nature and origin of fluids based on white mica data

The mineral deposits of the New Ross area represent a variety of mineralization styles and, as shown by Carruzzo et al. (2000), their formation involved three roughly coeval fluid reservoirs. In the conventional $\delta^{18}O$ - δD diagram (Fig. 6.6), the standard fields for different types of water (Sheppard 1986 and references therein, Ohmoto 1986) are outlined and compared to (i) fields for meteoric and magmatic fluids within the Meguma Supergroup; (ii) the calculated $\delta^{18}O$ range for a metamorphic fluid in equilibrium with the Meguma metasediments; and (iii) the data, calculated at 600°and 400°C for mineral deposit environments of the New Ross area. From this diagram, we note the following points: (1) most mineral deposit data fall within the metamorphic

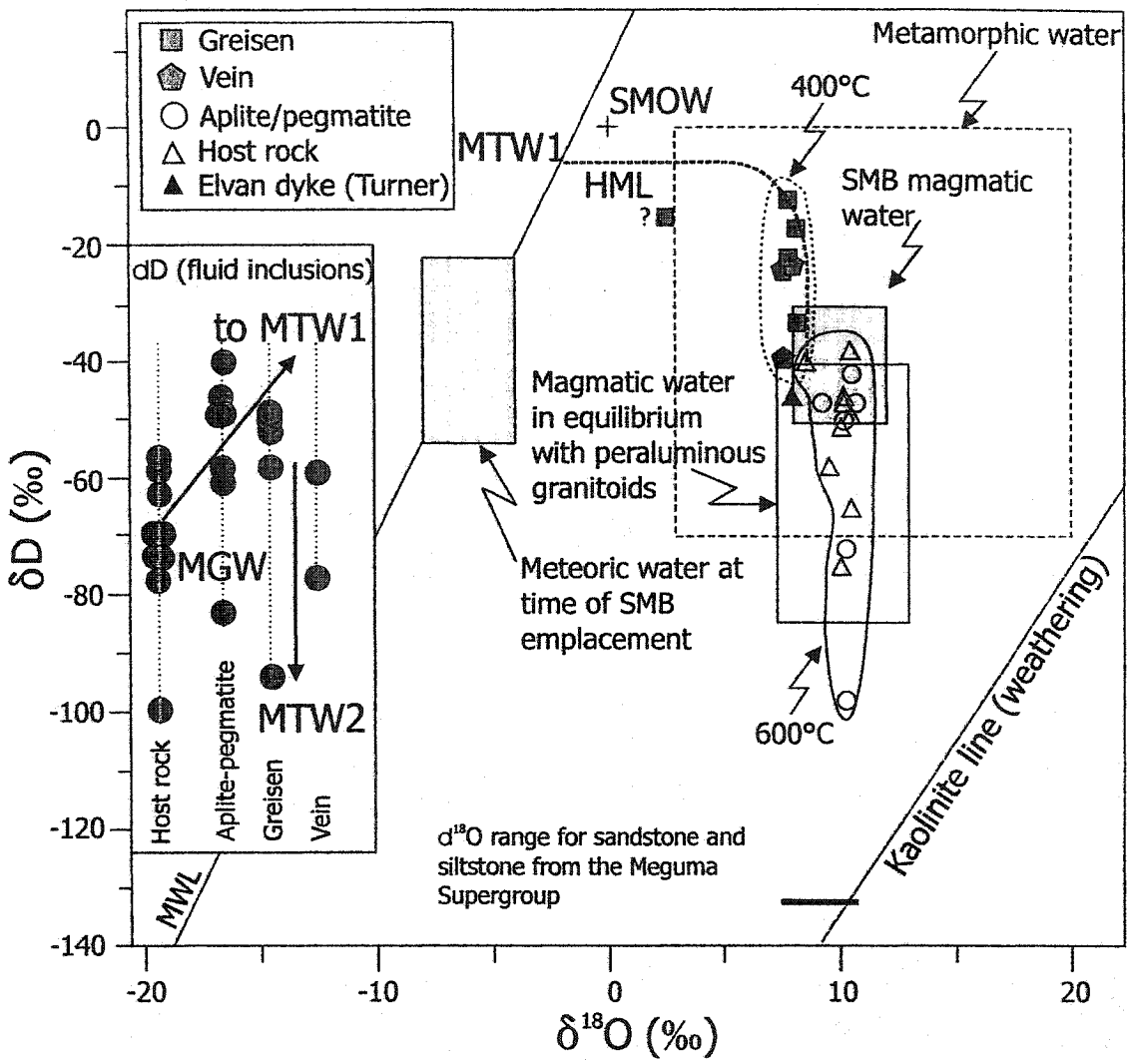

Figure 6.6: Plot of δD versus $\delta^{18}O$ showing fluid reservoirs (Sheppard 1986 and references therein); magmatic field for water in equilibrium with peraluminous granitoids from Ohmoto (1986). Meteoric water line of Craig (1961). Meteoric water field at time of SMB emplacement, SMB magmatic water, and $\delta^{18}O$ range for water in equilibrium with Meguma metasediments as defined in the text. Circles = δD values for fluid inclusion extracts; unfilled symbols = δD values for a fluid in equilibrium with white mica at 600°C (host granitoid rocks and pegmatite/aplite samples); filled symbols = δD values for a fluid in equilibrium with white mica at 400°C (greisen and vein samples). MGW = magmatic water; MTW1 = first generation of meteoric water (contemporaneous to SMB emplacement); MTW2 = later generation of meteoric water. HML = hypothetic mixing line.

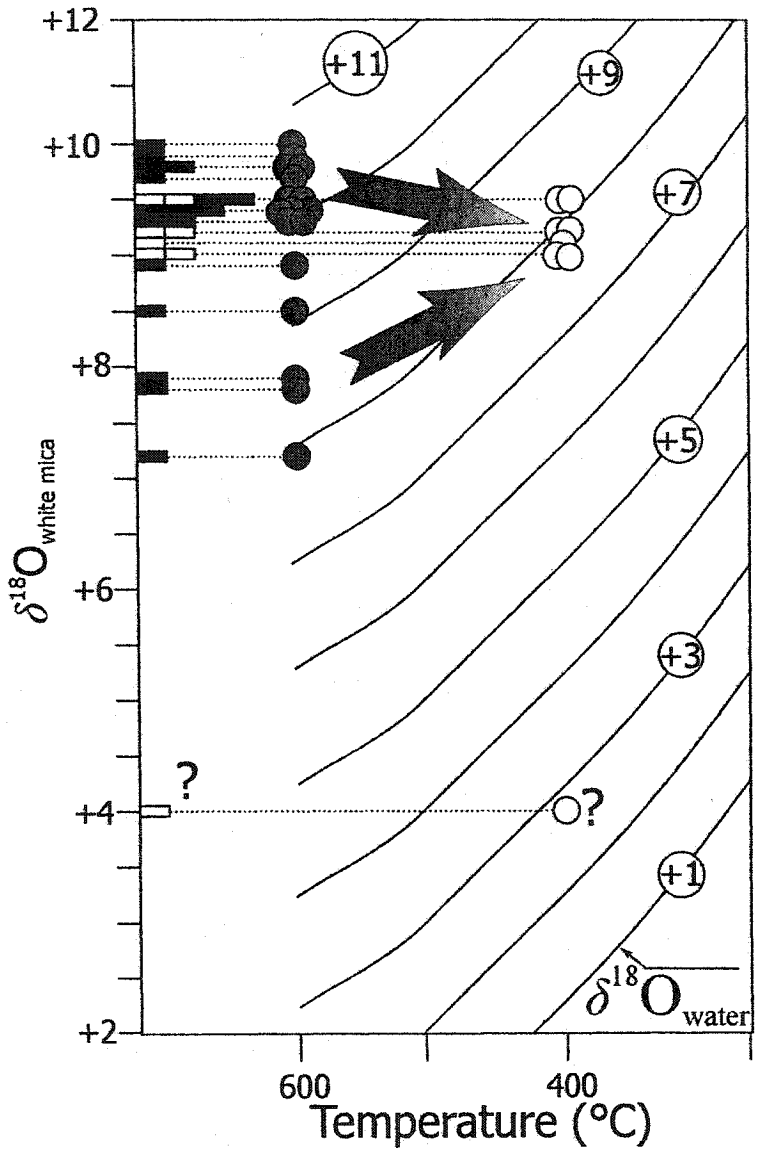

Figure 6.7: Diagrams of $\delta^{18}O_{white\ mica}$ versus temperature (in °C) with isopleths for δD_{water} calculated using the muscovite-water fractionation equation of O'Neil & Taylor (1969). Filled rectangles = $\delta^{18}O_{white\ mica}$ for host granitoid rocks and aplite/pegmatite samples, open rectangles = $\delta^{18}O_{white\ mica}$ for greisen and vein samples, filled circles = calculated $\delta^{18}O$ values of the fluid in equilibrium with white micas from host granitoid rocks and aplite/pegmatite samples, and open circles = $\delta^{18}O$ values of the fluid in equilibrium with white micas from greisen and vein samples.

water field and in the $\delta^{18}O$ range defined for water equilibrated with metasedimentary rocks of the Meguma Supergroup; (2) most granite host rock and pegmatite/aplite data fall in the field for magmatic water equilibrated with peraluminous granitoid rocks at 600°C (except for a single point with an anomalously low δD value), and in the low δD end of the SMB magmatic water field (except for five points with lower δD values); and (3) the greisen and vein data fall at the low end of the $\delta^{18}O$ field for magmatic water and have generally higher δD values compared with the peraluminous magmatic range for δD. Thus, there appears to be a shift towards lower $\delta^{18}O$ and higher δD values in the isotopic signature of the fluids equilibrated with the white micas from the magmatic through to the hydrothermal regime.

An erroneous estimation of temperature alone cannot account for the range in isotopic composition of the fluids shown in Figure 6.6, therefore, we explore other reasons for such variations below. A progressive lowering of $\delta^{18}O$ values from ~ + 10.0 to ~ +8.0 can result from interaction with a low $\delta^{18}O$ fluid. We suggest that the low $\delta^{18}O$ fluid is of meteoric origin and the proportion of this meteoric fluid increased with time concomitant with a change from a magmatic regime to a greisen-vein regime. First, the observation of low-salinity fluids dominating the fluid inclusions from greisen-vein deposits whereas high-salinity fluids dominate the fluid inclusions from host granitoid rocks and pegmatite/aplite (Carruzzo et al. 2000) is consistent with the lowering of $\delta^{18}O$ values related to incursion of a meteoric fluid (Fig. 6.7). Secondly, with decreasing temperatures, the isotopic composition of a hydrothermal fluid in equilibrium with white mica evolves towards lower δD values (see isopleths in Fig. 6.8). However, instead of following this expected closed-system tendency (i.e., dominantly magmatic), we observe higher δD values for the greisen and vein samples (Fig. 6.6) and, therefore, mixing with a fluid of higher δD composition appears as the most likely explanation. This shift to higher δD values may also reflect the presence of meteoric water in the system.

Therefore, based on the isotopic data for the white micas, we suggest that an evolution of increasing fluid to rock ratio through time as the system changed from a magmatic to a hydrothermal regime may explain the distribution of the data in Figure 6.6. Simultaneous with this evolution, the nature of the fluid changed from early magmatic to later meteoric. A hypothetical mixing line (HML) between the presumed end member

fluids illustrates this evolution of the isotopic signature in $\delta^{18}O$-δD space (Fig. 6.6). The composition of the end-member meteoric fluid (MTW 1) has a significantly higher δD value (~-6‰) than the range calculated for the MLT at ca. 373 Ma. Although the incursion of a metamorphic fluid may also explain the distribution of the data, we again note that our fluid inclusion thermometric study indicates the dominance of a meteoric fluid rather than a metamorphic fluid in the system. Kontak and Kyser (2002) also reported the presence of low $\delta^{18}O$ fluids in a vein-hosted silica-clay mineralised zone at the Flintstone Rock area in the southwestern part of the SMB and, in addition, the fluid inclusions in the quartz record the dominance of a low-salinity (<1 wt.% equiv. NaCl) fluid, similar to that in the greisen and vein deposits of the New Ross area.

6.4.4. Nature and origin of fluids based on fluid inclusion extracts

The δD_{water} values for fluid inclusion extracts arranged according to host rock are shown inset in Figure 6.6. We note that there is a progressive trend towards higher δD_{water} values from host granitoid rocks to greisen, with some anomalously low values. We interpret the data to reflect two stages of incursion of meteoric water: the first (MTW1) mixing with magmatic water (MGW) during orthomagmatic-hydrothermal stage of the SMB, and the second (MTW2) appearing during a post-crystallisation stage of the SMB. Before discussing the reason for this interpretation, we compare the δD_{water} values from the fluid inclusion extract with those inferred from white micas in the same samples.

Figure 6.8 consists of four diagrams of $\delta D_{white\ mica}$ versus temperature (in °C) with isopleths for δD_{water} calculated using the muscovite-water fractionation equation of Suzuoki and Epstein (1976). These diagrams also show the δD data from fluid inclusion extracts (closed circles) and the calculated δD data for fluids in equilibrium with white micas (open circles). A temperature of 600°C is used for isotopic data from white micas in host granitoid rocks and aplite/pegmatite, versus 400°C for white micas in veins and greisens. Pressure-corrected entrapment temperatures of 500°C are used for fluid inclusions in host granitoid rock and aplite/pegmatite samples, versus 400 °C for vein and greisen samples. With decreasing temperature, trapped fluids in equilibrium with white micas evolve towards lower δD values. If fluid inclusions in quartz contained the same water as bound in the white micas, then both δD_{water} compositions should lie on the same

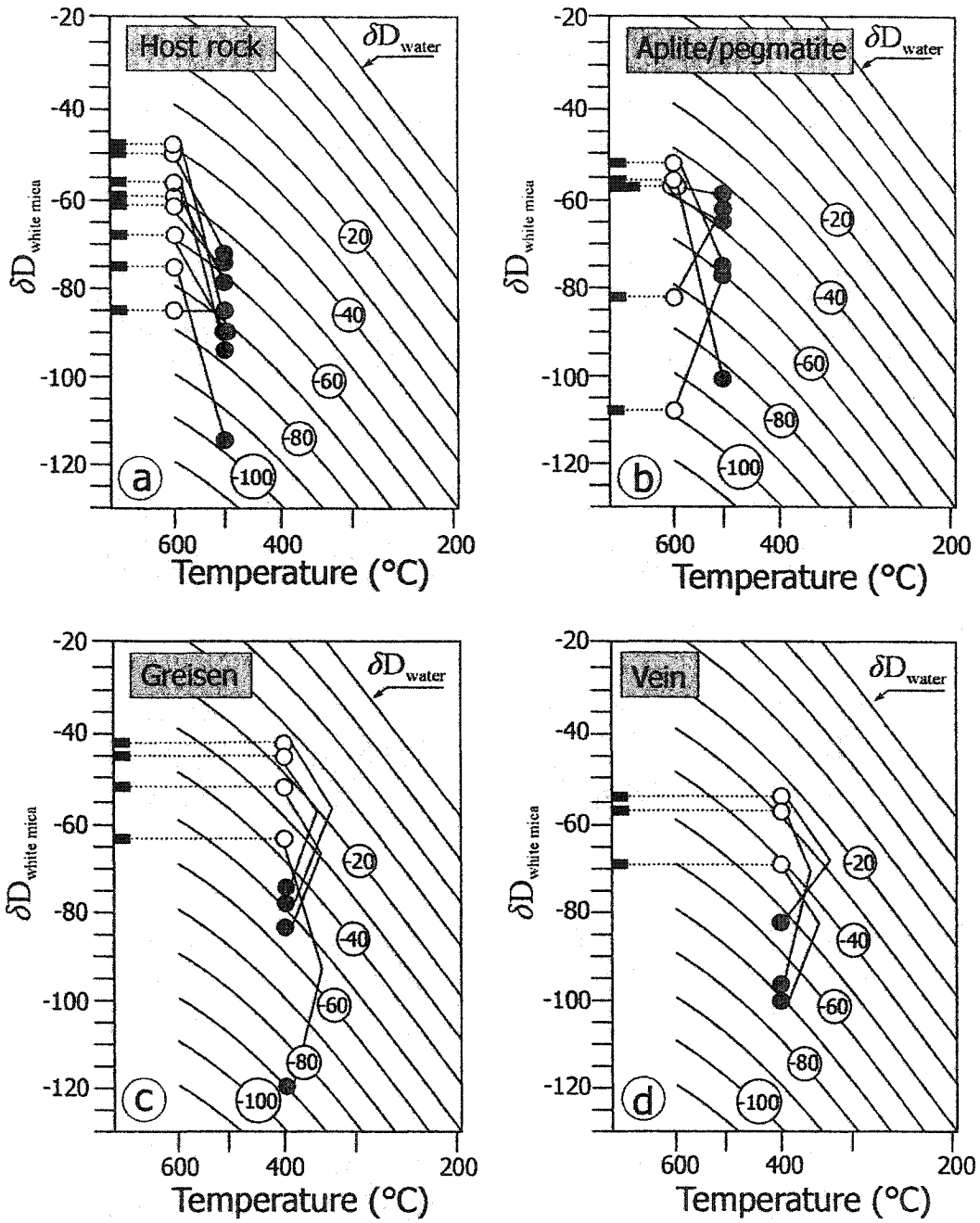

Figure 6.8: Diagrams of $\delta D_{white\ mica}$ versus temperature (in °C) with isopleths for δD_{water} calculated using the muscovite-water fractionation equation of Suzuoki and Epstein (1976); a) host granitoid rock samples; b) aplite/pegmatite samples; c) greisen samples; d) vein samples. Rectangles = $\delta D_{white\ mica}$, open circles = calculated δD values of the fluid in equilibrium with white micas, closed circles = δD values from fluid inclusion extracts, and solid lines link the δD datum from white mica to the δD datum from fluid inclusion extracts for the same sample. A temperature of 600°C is used for isotopic data from white micas in host granitoid rocks and aplite/pegmatite and of 400°C for white micas in greisens and veins.

isopleth. Instead, the fluid inclusion extracts generally have lower δD values than the δD_{water} in equilibrium with the white mica and do not fall on the same isopleth as the fluid in equilibrium with white micas. Several possible explanations exist for such a difference:

1. An analytical-related phenomenon: This possibility relates to release of molecular water or H-balanced defects in quartz during in vacuo thermal decrepitation of the sample (Gleeson et al. 2002). In their study, Gleeson et al (2002) found that samples with anomalously low δD values are characterized by a low abundance of fluid inclusions. Given that the samples used in the present study are inundated with fluid inclusions and that the above mechanism remains poorly studied to date, we reject this possibility as a viable explanation.
2. Incursion of a low δD fluid after white mica formation and before entrapment of the fluid, still during the hydrothermal stage: this process requires involvement of a low δD fluid during hydrothermal activity. Given that a much higher δD value characterises the signature of meteoric water during hydrothermal activity, we exclude such a fluid reservoir. An alternative fluid is that of organic origin, as originally suggested by Sheppard and Charef (1986) and used by Linnen (1995) to explain low δD fluids in Sn-mineralized pegmatites of Thailand. This explanation is difficult to assess given the lack of documentation of such fluids in organic-rich sedimentary basins, therefore we also reject this possibility.
3. Incursion of a low δD fluid during a fluid event subsequent to SMB emplacement: in this case, we appeal to trapping of fluid of probably meteoric origin much later in time than emplacement of the SMB (MTW2). Relevant to this case are the following: (i) the presence of low-temperature (i.e., 100-150°C), low-salinity fluid inclusions and the presence of monophase liquid inclusions in most samples (Carruzzo et al. 2000); and (ii) the documentation of low δD_{water} by other investigators and attributed to trapping of later, younger meteoric water (e.g., Sun and Eadington 1987 in tin-mineralised granite from New South Wales in Australia; Criss and Taylor 1983 in the Idaho Batholith, US).

The δD values for a fluid in equilibrium with white micas of two samples hosted by the Keddy-Reeves leucogranite (pegmatites from Keddy and Reeves deposits) are lower

than the corresponding δD from fluid inclusion extracts, suggesting strong interaction between MTW2 and the area where both pegmatites are located during white mica crystallisation.

6.4.5. Isotopic evolution of fluids with cooling temperatures

In an integrated model for fluid circulation within the New Ross area (Fig.6.9), we recognize the following succession of fluids involvement: a magmatic fluid characterised by salinities of 19-25 wt. % equiv. NaCl, Na-K chlorides as major solutes, a $\delta^{18}O$ isotopic composition of +8 to +12‰, and δD of -20 to -40‰ exsolves from the magma at temperature of ~650°C (Stage 1). As the system slowly cools to subsolidus temperature of 400-500°C and the fluids react with feldspars, the K/Na ratio of the fluid decreases. A low-salinity water with a $\delta^{18}O$ of ~-2‰ and a δD of ~-6‰ enters the system, as recorded by the fluid in equilibrium with white micas and the progressive increase in δD of fluid inclusion extracts (Stage 2). We suggest that this fluid is dominantly of meteoric origin (MTW1 in Figure 6.6). Fluid inclusions from meteoric water-dominated mineral deposits (mainly vein deposits) record a temperature of ~400°C. Meteoric fluid can reach such elevated temperature by travelling to a depth of ~10-12 km (emplacement depth for the SMB) through fractures created either by thermal contraction of the cooling batholith, by overpressure release by potential explosive unroofing of the batholith (Clarke and Bogutyn in press), or by active faulting related to regional tectonics at the time of SMB emplacement (Horne et al. 1992). Also, convection cells driven by heat in the batholith allow for some mixing of magmatic fluid with a Ca-rich, high-salinity (29-43 wt. % equiv. NaCl) metamorphic fluid originating within the Meguma metasediments (Stage 3). Such mixing is recorded by the cation content of fluid inclusion decrepitates (Carruzzo et al. 2000). In addition, the δD composition of the fluid in equilibrium with white mica from two samples (pegmatites from Keddy and Reeves deposits) hosted by the Keddy-Reeves leucogranite may have been affected by MTW1, therefore explaining the secondary chemical character of the white micas from both pegmatites.

After crystallisation and cooling of the SMB, a second generation of meteoric fluid (MTW2) with a lower δD signature than MTW1 enters the system and is trapped

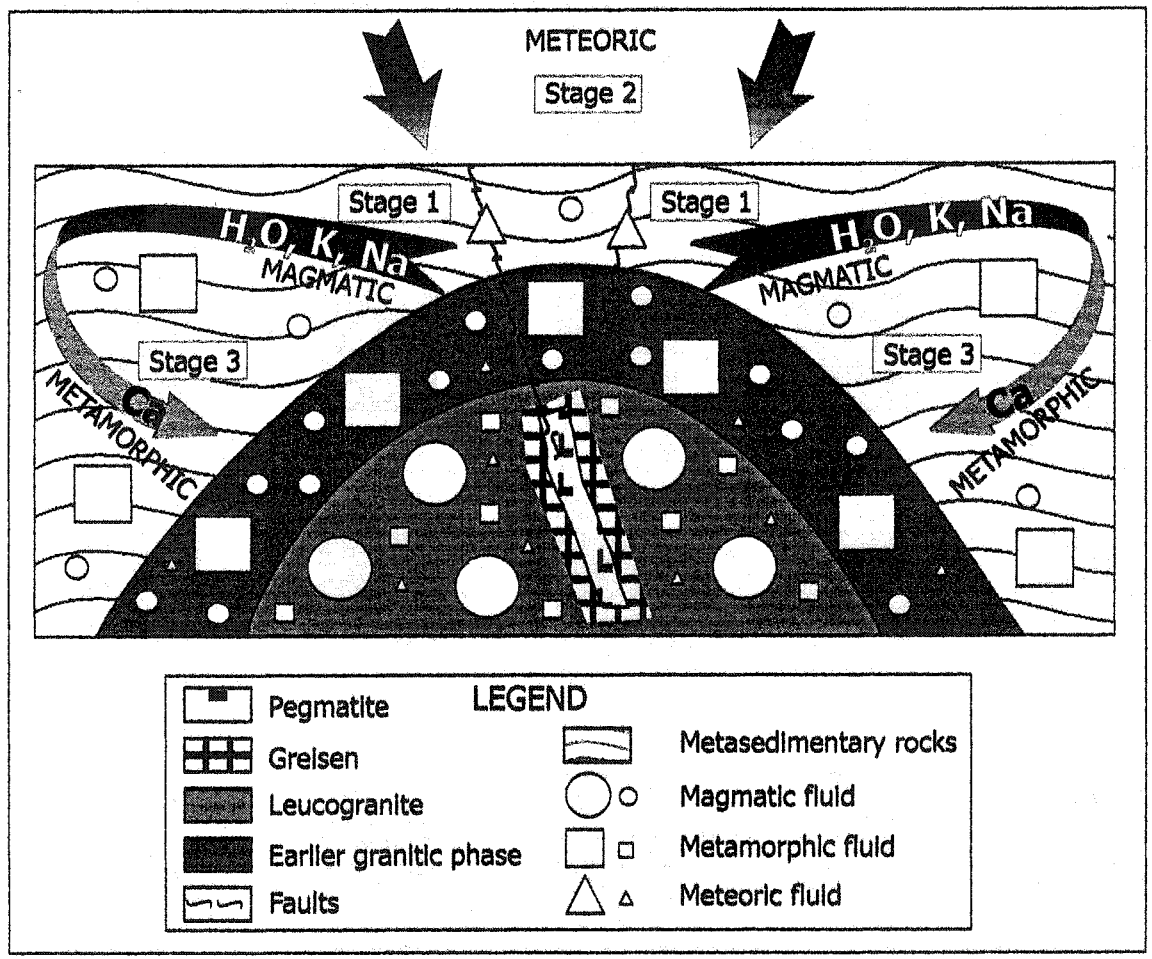

Figure 6.9: Integrated model for fluid circulation within the New Ross area with the different fluids involved. Stages are as described in the text. Large and small squares, circles, and triangles schematically represent the amount of fluid interacting with the granitic samples and the Meguma metasediments.

along healing fractures in quartz grains. This second generation of meteoric water accounts for the difference between the calculated δD_{water} values of white mica and the δD values of fluid inclusion extracts in coexisting quartz.

6.5. Conclusions

Isotopic data for white micas and fluid inclusion extracts from eight mineral deposits of the New Ross area of the South Mountain Batholith, Nova Scotia, permit the following conclusions:

1. As noted by previous studies (Kontak et al. 1988b, 1991), coexisting minerals have not preserved isotopic equilibrium, impeding further determination of formation temperature using isotopic fractionation. Variable degrees of mineral-fluid re-equilibration during subsolidus stage are probably the reason for the isotopic disequilibrium and relate to the protracted thermal history of the SMB.
2. The isotopic compositions ($\delta^{18}O$, δD) of white mica from host granitoid rocks, pegmatite/aplite, greisen, and vein samples along with δD values for fluid inclusion extracts from quartz in the same samples record a transition from a magmatic-dominated, melt-orthomagmatic, low water : rock ratio system to a hydrothermal-dominated, higher water : rock ratio system into which meteoric water infiltrated at the time of SMB emplacement, crystallisation, and greisen/vein formation. We propose a hypothetical mixing line between magmatic and meteoric waters for the SMB during its emplacement and subsequent crystallisation at 373 Ma.
3. Fluid inclusion extracts from quartz record lower δD_{water} values than calculated for coexisting white mica samples using appropriate fractionation factors and temperatures of crystallisation. We attribute these differences to post-crystallisation entrapment of later meteoric water and emphasize the importance of integrating δD values obtained from minerals with those from fluid inclusion extracts. Anomalous depleted δD values for white micas from two pegmatite samples also reflect fluid-mediated recrystallisation of these phases at the same time as the infiltration of the low δD water.
4. Integration of a previous detailed fluid inclusion study of the same samples with the isotopic data provides corroborating support for incursion of meteoric water

during crystallisation and subsequent hydrothermal alteration of the SMB. A set of low temperature, low-salinity fluid inclusions plausibly records the incursion of a second meteoric fluid, as suggested from the isotope data.

5. Although we identified the participation of a metamorphic fluid reservoir in the hydrothermal fluid history of the New Ross area through the fluid inclusion study, our isotopic data do not allow the discrimination of this fluid, given the lack of δD data for the Meguma metasediments.

In summary, the evolution of fluids from a magmatic to hydrothermal regime within the New Ross area is as follows: (i) exsolution of a magmatic fluid at ~ 650°C; (ii) before cooling to ~400-500°C, incursion of a meteoric fluid via fractures with subsequent mixing with magmatic and metamorphic fluids through fluid circulation by convection; and (iii) incursion of a late, low δD meteoric fluid some time after cooling of the area. Finally, this paper clearly identifies the need to define more precisely the isotopic composition of all potential fluids interacting within the MLT, if complete understanding of fluid reservoirs involved in mineralising processes is expected.

CHAPTER 7

DISCUSSION

7.1. Differentiation processes

7.1.1. Introduction

Three main processes of chemical differentiation (fractional crystallisation, contamination, and hydrothermal alteration) occur within the SMB (Clarke and Chatterjee 1988), and physical and chemical evidence for them exist throughout this large granitic body (Table 1.2). To what extent are all of these processes also at work within the New Ross pluton, and how do they lead to the production of mineral occurrences?

7.1.2. Major and trace elements

Ham et al. (1989) published an extensive geochemical database for the SMB, including chemical analyses for all rock types from the New Ross pluton (Appendix E). Using the data from Ham et al. (1989), Figure 7.1 consists of several bivariate diagrams showing major and trace element variation from least to most evolved fractions of the New Ross pluton. In these diagrams, major and trace elements vary mostly because of fractional crystallisation and hydrothermal alteration; therefore, both processes will be the main focus of Section 7.1.2.

All samples from the New Ross pluton present similar trends of evolution to the rest of the SMB (MacDonald and Clarke 1991; Clarke et al. 1993b; Tate and Clarke 1997) in the following cases:

1. biotite and zircon fractionation appears to control the Ti-Zr variation (Fig.7.1a) and fractionation of both cordierite and biotite probably controls the MgO variation (Fig. 7.1b);
2. plagioclase fractionation controls the CaO-Sr variation (Fig. 7.1c), with decreasing An content of plagioclase from least to most evolved fractions;

3. plagioclase and K-feldspar control the Ba-Sr variation (Fig. 7.1d); and
4. MgO and Ba decrease with decreasing of modal abundance of biotite and K-feldspar, respectively, whereas Rb behaves as an incompatible element up to the latest stages of the evolution (Fig. 7.1e, f).

Granodiorite and monzogranite samples from the New Ross pluton show similar evolutionary trends to the rest of the SMB, whereas more evolved fractions of the New Ross pluton do not. This geochemical behaviour probably reflects fluid involvement in the process:

1. Both Ta and Nb are enriched in leucomonzogranite and leucogranite of the New Ross pluton and similarly, to leucogranites from various locations within the SMB (Clarke et al. 1993b) (Fig. 7.1g);
2. Li behaves as an incompatible element with strong enrichment in the latest phases of the New Ross pluton and may relate to concentration by late-stage fluids (Fig. 7.1h); and
3. The K/Rb ratio decreases from least to most evolved fraction of the New Ross pluton, apparently showing increasing involvement of fluids (Shaw 1968) (Fig. 7.1i).

Samples showing evidence of hydrothermal overprint have a K/Rb ratio less than 150, thus most leucomonzogranite and all leucogranite samples of the NRP fall within that category. Such involvement of hydrothermal processes allows for the two trends observed in the Rb-MgO and Rb-Ba diagrams (Fig. 7.1e, f).

7.1.3. Rare earth elements

The REE are also good monitors of the chemical evolutionary processes and demonstrate the existence of fractional crystallisation and subsolidus hydrothermal alteration in the SMB (Table 1.2). Chatterjee et al. (1985), Kontak et al. (1988), and Clarke et al. (1993) presented REE data for different granitoid types in the New Ross area. Figure 7.2a compiles the REE profiles from Kontak et al. (1988) and Clarke et al. (1993) for the NRP and the following points emerge:

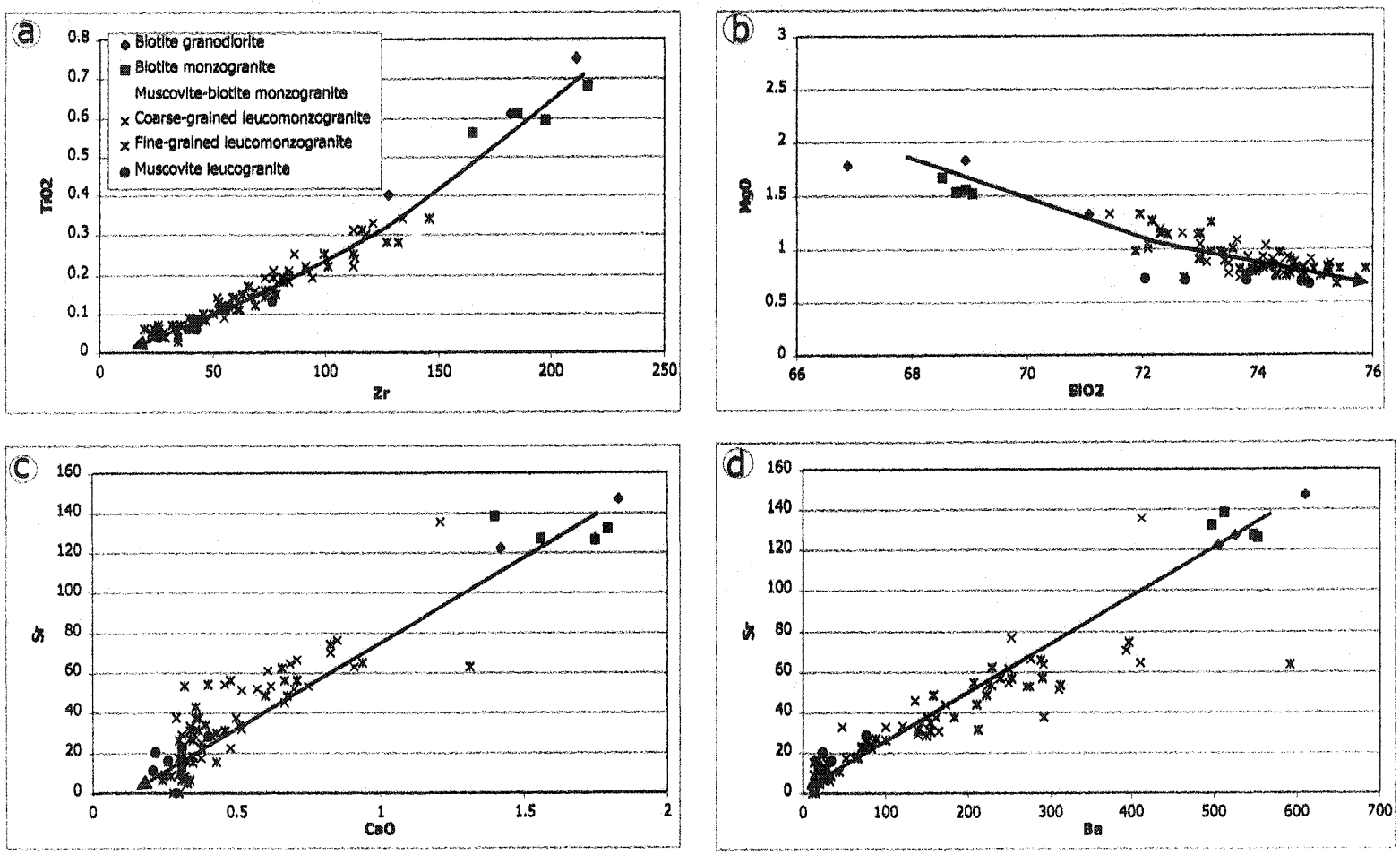

Figure 7.1: Binary diagrams showing chemical element variation from least to most evolved fractions of the New Ross pluton. Arrows represent fractionation trend. Geochemical data from Ham et al. (1989).

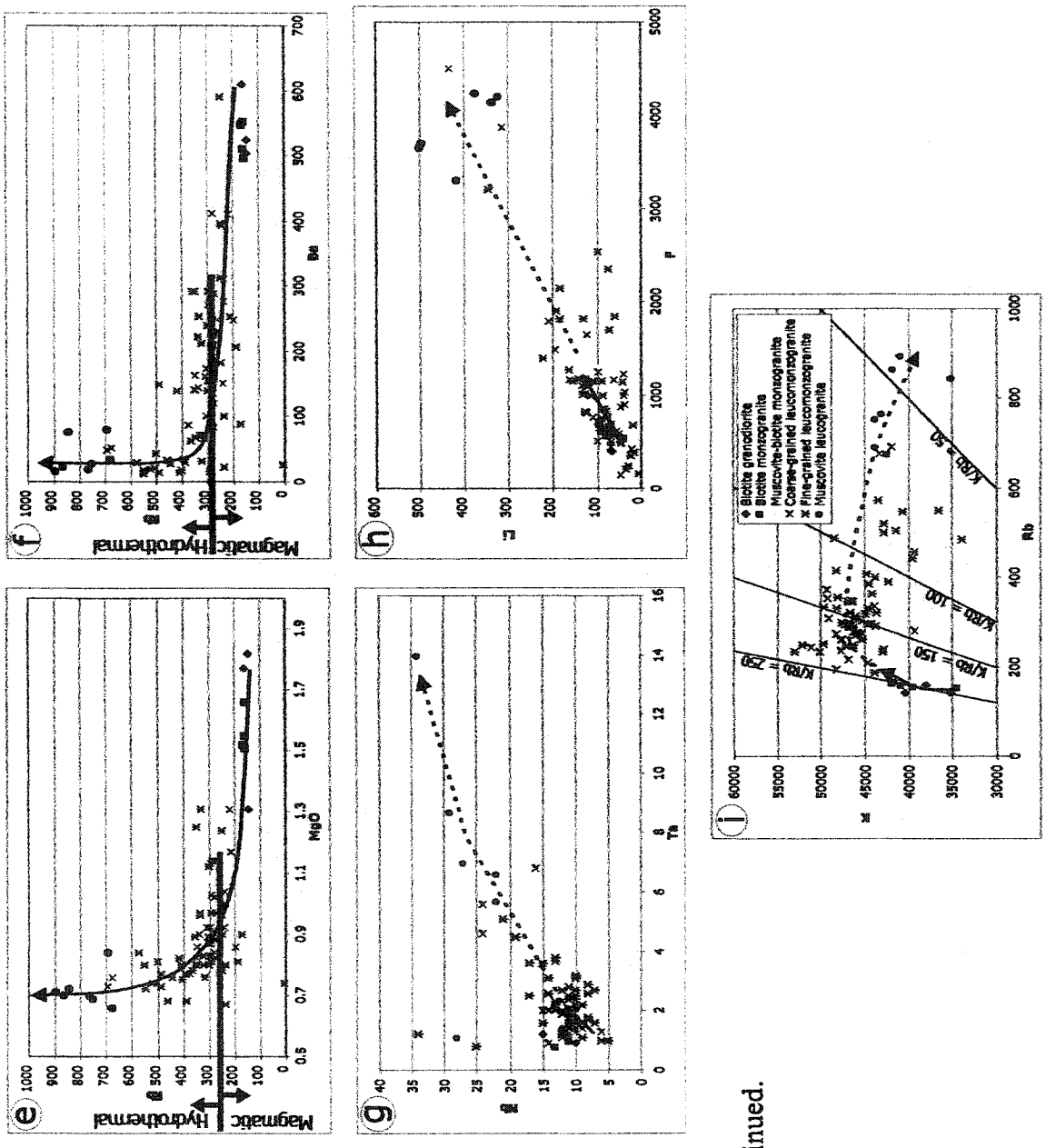

Fig. 7.1: continued.

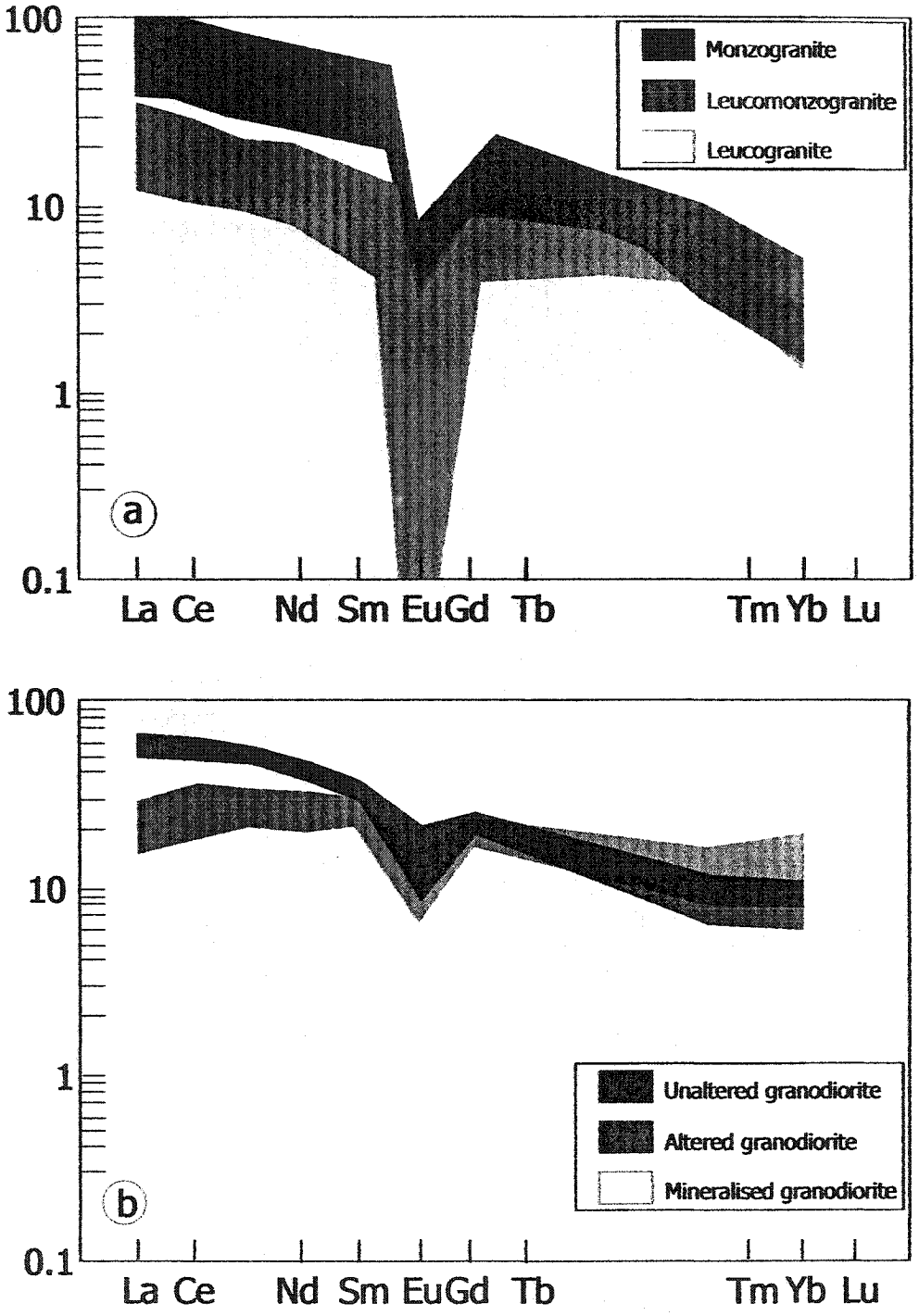

Figure. 7.2: REE profiles for a) least to most fractionated fraction of the SMB and b) least to most altered granodiorite from the Millet Brook deposit.

1. La/Yb ratio for monzogranites between 13 and 37 (mean = 28), for leucomonzogranites between 8 and 37 (mean = 17), and for leucogranites between 1 and 28 (mean = 10);
2. decrease of ΣREE for leucogranites and leucomonzogranites compared to monzogranites; and
3. increase of the magnitude of the negative Eu anomaly for leucomonzogranites and leucogranites compared to monzogranites.

All three points above suggest progressive removal of plagioclase and REE-bearing accessory phases (monazite, xenotime, titanite, apatite) from least to most evolved fractions of the New Ross pluton, indicating fractional crystallisation. However, several authors (Muecke and Clarke 1981; Chatterjee et al. 1985; Kontak et al. 1988b; Corey and Chatterjee 1990) emphasised that the amount of REE depletion (especially in the most evolved fraction of granitoids) is too great to be solely explained by fractional crystallisation and, therefore, may require the presence of a fluid phase for REE removal. Figure 7.2b shows the REE profiles for unaltered, altered, and mineralised granodiorite in the vicinity of the Millet Brook uranium deposit (Chatterjee et al. 1985). The general pattern of the unaltered granodiorite is consistent with that of other granodiorites from the SMB. The altered granodiorite pattern is flat compared to the unaltered one, showing an increase in the heavy REE and a loss of the light REE. Flynn and Burnham (1978) determined that chlorine may complex the light REE. The depletion of the light REE in the most evolved fractions of the NRP probably records such complexing and transport of the light REE. The mineralised granodiorites have variable patterns depending on alteration type accompanying the mineralisation, coupled with a more pronounced Eu anomaly than unaltered and altered granodiorite. Such patterns reveal a more intense effect of fluids from unaltered, to altered, to mineralised granodiorite (Chatterjee et al. 1985).

7.1.4. Stable isotopes

Kontak et al. (1988) and Clarke et al. (1993) presented whole-rock $\delta^{18}O$ for monzogranitic, leucomonzogranitic, leucogranitic, pegmatitic, and greisenised samples from the New Ross area (Table 7.1). The $\delta^{18}O$ values are similar to those reported for the

Sample #	Rock type	Source	Whole rock $\delta^{18}O$
9	monzogranite	Kontak et al. (1988, 1991)	11.1
14			9.5
53			11.0
17-1	leucomonzogranite		10.8
17-2			10.4
39			9.9
20	mineralised leucomonzogranite		10.7
21			11.4
26-1			10.9
26-2			10.0
11-2			10.0
33			10.4
37A			11.3
39			9.9
13	elvan dyke		3.6
KR3028	leucogranite	Clarke et al. (1993)	11.8
KR3028-3			11.5
KRLU-1M			11.4
LL1216-4			10.2
LL1256			11.1
LL1265			11.3
LLLU-7C			11.5
LLLU-8			12.7
BB1260-1			11.1
BB2146-2			11.7
BB2152-1			11.6
BB2152-2			11.5
BBLU-6			11.6
CL-LU-9			15.0
CL20-9-3			11.0
CL20-9-4			11.3

Table 7.1: whole rock $\delta^{18}O$ for monzogranitic, leucomonzogranitic, leucogranitic, pegmatitic, and greisenised samples from the New Ross area. Data from Kontak et al. (1988) and Clarke et al. (1993).

SMB (+10 to +12‰, Longstaffe et al. 1980) regardless of the granitoid rock type, and are typical of peraluminous, crustal-derived granitoids (Sheppard 1986). A single low value (elvan dyke at the Turner deposit) betrays the participation of a low-^{18}O fluid, probably of meteoric origin (Kontak et al. 1988b and Chapter 6).

Sample #	Rock type and location	$\delta^{18}O$ quartz	$\delta^{18}O$ K-feldspar	$\delta^{18}O$ muscovite
9	monzogranite		11.0	
11-1	monzogranite	11.5	12.3	
11	pegmatite Walker	8.9	9.8	8.2
18	pegmatite Keddy	17.6	10.6	
19		11.9	11.0	
22B	pegmatite Reeves	15.5	9.7	
22C		11.4	11.4	
24	pegmatite Grassy Brook	10.3	10.1	
25		11.4	8.9	
34-1	pegmatite Long Lake	10.6	11.0	
34A		10.8	11.0	
34B		12.8		
36	pegmatite Morley's	8.9		9.3
36A		10.9		
38		11.6	10.0	

Table 7.2: $\delta^{18}O$ data for mineral separates (quartz, K-feldspar, muscovite) from monzogranite, leucomonzogranite, and pegmatite samples from the New Ross area. Data from Kontak et al. (1988, 1991).

Kontak et al. (1988, 1991) presented $\delta^{18}O$ data for mineral separates (quartz, K-feldspar, muscovite) from monzogranite, leucomonzogranite, and pegmatite samples from the New Ross area (Table 7.2). Also, Chapter 6 contains $\delta^{18}O$ and δD data for white mica from similar samples to those used by Kontak et al. (1988, 1991). The $\delta^{18}O_{mineral}$ values spread over larger ranges (8.9-17.6‰ for quartz, 8.9-12.3‰ for K-feldspar, 4-9.9‰ for muscovite) than $\delta^{18}O_{whole\ rock}$ values. Furthermore, isotopic disequilibria among coexisting minerals are present, especially for pegmatite samples, therefore suggesting the incursion of fluid(s) in the late-stage of evolution of the area (Kontak et al. 1991, Chapter 6).

Poulson et al. (1991) provided $\delta^{34}S$ isotopic data for a few monzogranitic samples from the New Ross pluton. They obtained a wide range of values (+1.6 to +15.0‰; average = +9.1). Samples from the New Ross pluton do not contain a large amount of sulphur; therefore, assimilation of various quantities of country rock ($\delta^{34}S$ from –3.7 to +24.2‰;

average = +13.0‰) may allow for the considerable variation in $\delta^{34}S$ values (Poulson et al. 1991).

7.1.5. Radiogenic isotopes

Clarke et al. (1988) provided $\varepsilon\ ^{t}_{Nd}$ values (-5.2, -5.2, -4.9) at t = 376 Ma for three porphyritic monzogranites from the New Ross pluton. In an $\varepsilon\ ^{t}_{Nd}$ vs. $^{87}Sr/^{86}Sr$ diagram (Fig.7.3), all data fall at the edge of the data field for the SMB, towards the field for Meguma metasedimentary $\varepsilon\ ^{t}_{Nd}$ values, indicative of some degree of assimilation of country rock in the area (Clarke et al. 1988; Tate and Clarke 1997), consistent with the $\delta^{34}S$ data discussed above.

7.1.6. Summary

The mineralogical and geochemical diversity of the New Ross pluton is the result of the three main processes at work within the SMB: fractional crystallisation, contamination, and subsolidus hydrothermal alteration. Major, trace, REE elements, and oxygen isotopes attest to the existence of fractional crystallisation and fluid alteration, whereas sulphur and neodymium isotopes indicate the presence of contamination of Meguma Supergroup metasediments within the New Ross pluton.

7.2. Concentration of incompatible elements

7.2.1. Introduction

Metals of interest in granite-related ore deposits are incompatible trace elements, because they do not "fit" in the crystalline structure of common rock-forming silicate minerals (e.g., Rollinson 1993). This section deals with the classification, distribution, and concentration of metals present in the mineral occurrences of the New Ross area.

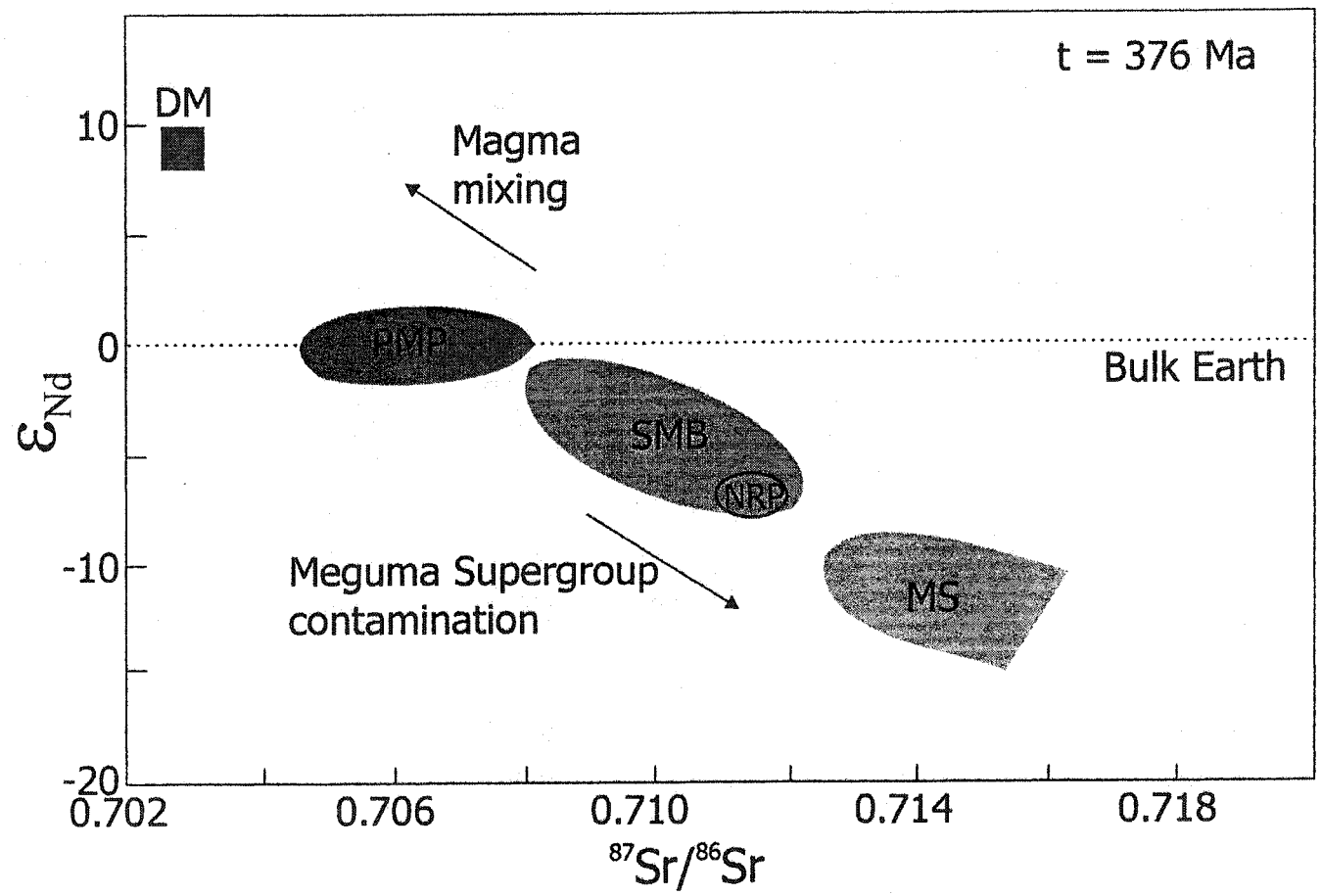

Figure 7.3: Plot of ε^{i}_{Nd} vs. $^{87}Sr/^{86}Sr$ for the SMB. MS Meguma Supergroup, SMB South Mountain Batholith, PMP Port Mouton Pluton, DM depleted mantle. Data recalculated to t = 376 Ma. Note the location of data from the New Ross pluton (NRP). From Tate and Clarke (1997).

7.2.2. Classification of metals

Most metals of interest in this study belong to the transition metals group (atomic numbers 22 to 29 and 40 to 47). The transition elements (e.g., Mn, Fe, Cu, Zn, Mo, W) have in common their incompletely filled d-orbital, becoming more filled from left to right in the Periodic Table (e.g., Faure 1991), and generally have variable valences. Elements present in granite-related mineral deposits range from **chalcophile** (strong affinity for sulphur and forming covalent bonds; e.g., Cu, Pb, Zn, As, Bi) to **lithophile** (strong affinity for oxygen and forming ionic bonds, e.g., Li, Be, F, Mn, Nb, Ta, Ba, W, U) elements, with **siderophile** elements having a weak affinity for both sulphur and oxygen (e.g., Fe, Mo, Sn) (Strong 1988). Also, some metals change their geochemical character or behaviour depending on the chemical environment (Strong 1988).

Incompatible elements are commonly subdivided on the basis of their ionic potential (ratio of the valence to the ionic radius of the element): small and highly charged elements are the high field strength cations (**HFS**) with an ionic potential greater than 2, and large cations of small charge are the low field strength cations (or large ion lithophile elements **LILE**) with an ionic potential less than 2 (e.g., Rollinson 1993; Strong 1988) (Fig. 7.4).

7.2.3. Distribution of metals

The distribution, or partition, coefficient describes the distribution of metals or any trace element between a solid and a liquid phase as follows:

K_{Di} = C_i in mineral/C_i in liquid, where K_{Di} is the partition coefficient for an element i and C is the concentration of i in ppm or wt. % (e.g., Barnes 1979). A similar partition coefficient exists between the melt and a fluid or solid phase (minerals) (Barnes 1979). Most authors use the abbreviation D instead of K_D, and I will use this notation for the following part of this chapter. In general, partition coefficients vary according to temperature, pressure, composition, pH, and oxygen activity ($a_{O2} = \gamma c$ where γ is the **activity** coefficient and c is the concentration of O_2 in solution; also, activity of a solute $a = f/f^0$ where f is the fugacity of the solute in the solution and f^0 is its fugacity when the vapor is in equilibrium with the pure substance in the standard state. The fugacity represents the

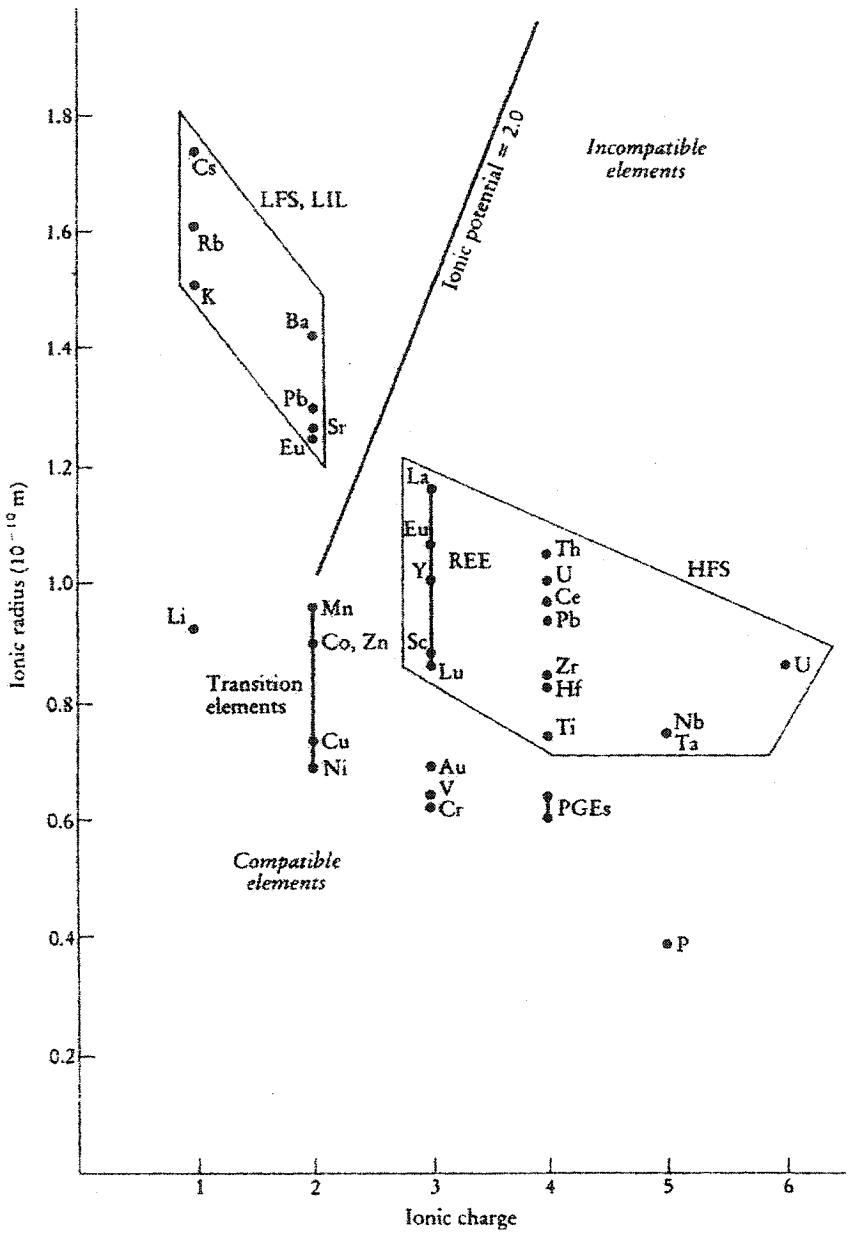

Figure 7.4: Plot of ionic radius vs ionic charge for trace elements. Ionic potential (charge /size ratio) of 2.0 subdivides the incompatible elements into LFS elements (or LIL) and HFS elements. From Rollinson (1993).

partial pressure a real gas would have if it were ideal; Faure 1991) conditions. With pressures higher than 3-4 kbar, the melt/vapour partition coefficients for many incompatibles decrease (e.g., Urabe 1987).

7.2.4. Concentration of metals

Clarke (1992) reviewed the processes of concentration of incompatible elements leading to mineral deposits in granitoid rocks and the following succinctly retraces the main steps.

A. Melt present

1. Incompatible elements are enriched in the silicate melt phase during partial melting.
2. Assimilation of country rock may provide the silicate melt phase with some incompatible elements.
3. Thermogravitational diffusion (a process balancing the chemical potential of every component throughout the magma) concentrates incompatible elements near the roof of the pluton (Hildreth 1981).
4. Fractional crystallisation further concentrates the incompatible elements in the melt. As described in Section 7.2.3, the partition coefficients for incompatible elements between rock-forming minerals and melt range between 0 and 1, therefore, a fraction of incompatibles leaves the melt.
5. Water saturation allows for the separation of an aqueous fluid phase (magmatic fluid) from the melt. For many incompatible elements, the partition coefficient between such fluid phase and the melt is greater than 1. Factors such as temperature, pressure, fluid composition, pH, and fO_2 dictate the value of partition coefficients. Section 7.3.3 details the important factors for the main metals present in the New Ross area.

B. Melt absent

6. The fluid transporting incompatible elements can extend below solidus temperatures by fluid egress from the melt region into cooler parts of the pluton or country rock or, if remaining in the melt region, by complete crystallisation of the melt. The fluid continues to react with the minerals from

the surrounding rocks, producing secondary minerals and taking some materials into solution (i.e., alteration process). Interaction of the magmatic fluid with fluids of other origin (e.g., metamorphic, meteoric, connate, seawater) is also possible, further promoting cooling of the fluid phase.

7. Through decreasing temperatures and pressures, the aqueous fluid phase reaches the liquid-vapour divariant boundary, resulting in retrograde boiling. Volatile constituents enter the vapour phase and leave the system; as a consequence of the vapour phase leaving the system, the solubility of incompatible elements drops and precipitation occurs.
8. Further concentration of incompatible elements occasionally occurs in the weathering environment with percolating surface water dissolving incompatible-bearing minerals and transporting and concentrating the incompatible elements to another favourable deposition location.

7.3. Partitioning, transport, and deposition of incompatibles

7.3.1. Hydrothermal solutions: generalities

Hydrothermal solutions are hot, aqueous solutions from which ore minerals may precipitate (Skinner 1997). From fluid inclusion and stable isotope (O and H) studies, we know that hydrothermal solutions have highly variable compositions (e.g., Roedder 1984; Sheppard 1986; Roedder and Bodnar 1997), providing clues about their source(s) and/or travel path(s). Possible sources of solutions are magmatic, meteoric, metamorphic, connate, and ocean water (Barnes 1979), and input from these different reservoirs may be traceable using stable isotopes (Chapter 6).

Besides being hot and H_2O-dominated, hydrothermal solutions contain variable concentrations of dissolved solids, with Na, K, Ca, and Cl as major components (present as alkali chlorides), whereas ore metals such as Cu, Pb, Zn, Sn, Mo, W, Ag, etc. (present as complex ions) are rarely, if ever, present as major constituents (Pirajno 1992; Skinner 1997). The source of both major and minor constituents (cooling magma and/or fluids and/or rocks travelled through) is rarely determined with certainty (Pirajno 1992).

Solubility of a solute in water depends on the bonding of the solute to water (H_2O); therefore, it is important to understand the structure and characteristics of water. Water is a polar molecule (i.e., has unequal charge distribution), allowing the positive ends of the water molecule to be attracted to anions and the negative ends of the water molecule to cations (i.e., hydration). Water molecules link to each other through a bond (hydrogen bond) between the oxygen of one molecule and the hydrogen of another, forming tetrahedrally coordinated clusters (Liu et al. 1996). Variations of temperature and/or pressure prompt changes in water structure (Seward and Barnes 1997). An increase of temperature (i) weakens hydrogen bonding, and liquid water expands; (ii) decreases the dielectric constant [expression of the extent to which a material concentrates electric flux, Atkins (1994)], therefore enhancing ion-pairing and metal complexing; and (iii) lowers the value for neutral pH (i.e., increases K_w, the ion product constant), allowing for the formation of hydroxide complexes at higher temperatures. An increase in pressure (i) decreases water density (enhanced by higher temperature); (ii) has no effect on the dielectric constant; and (iii) increases ionisation of water.

At higher temperatures and lower pressures, most solutes tend to form ion pairs (single cation and single anion held together by electrostatic attraction only), thereby leading to a decrease in the activity of potential ligands for metals, and in turn limiting the concentration of metal complexes (Brimhall and Crerar 1987; Seward and Barnes 1997).

7.3.2. Transport of metals

7.3.2.1. Introduction

To better understand metal transport processes, it is important to recognise the role of ligands in the complexing process. Several papers and chapters in specialised publications (Barnes 1979; Seward 1981; Crerar et al. 1985; Eugster 1986; Pirajno 1992; Seward and Barnes 1997; Wood and Samson 1998) review metal complexing and its chemical controls. The following is a compilation from these sources.

In solution, metals associate with ligands to form complex ions, allowing for transport of metals in a hydrothermal fluid. The interaction between metals and ligands is comparable to acid-base reactions, with the metal accepting, and the ligand giving, an electron. Based on charge and size, hard and soft metals and ligands exist with, given

competition between several ligands and metals, soft metals binding more easily with soft ligands, whereas hard metals bind preferentially with hard ligands. The main characteristics for each class are:

1) **hard**: high charge, small radius, slightly polarisable, preferring ionic or electrostatic bonding (i.e., involves transfer of electrons); and
2) **soft**: low charge, large radius, highly polarisable, preferring covalent bonding (i.e., involves sharing of electrons).

Table 7.3 contains a classification of metals (~ bases) and ligands (~acids) according to their hardness. Important to note in this Table is that, within a category, hardness decreases to the right. As stated in Section 7.3.1, changes in water structure with increasing temperature decrease the dielectric constant of the water, consequently "hardening" the interaction between metal and ligand (Brimhall and Crerar 1987; Seward and Barnes 1997).

7.3.2.2. Stability of complexes

At hydrothermal temperatures (<400°C), only the following few ligands are present in sufficient quantities to allow metal complexing: Cl^-, F^-, HS^- or H_2S, PO_4^{3-}, and OH^- (Barnes 1979).

The activity of the ligands controls the metal-carrying capacity of the fluids, rather than the abundance of the metals (Barnes 1979). Temperature and pressure are the main controls of metal complexing; in general, higher temperatures enhance complex formation, whereas higher pressures cause dissociation of metal complexes (Seward and Barnes 1997). Temperature and pressure affect the stability of various ligands differently, for example, chloride complexes are more stable at high temperature (> 400°C) than sulphide complexes (Barnes 1979).

Bases		
Hard	**Borderline**	**Soft**
H^+	Fe^{2+}, $Mn^{2+}Co^{2+}$, Ni^{2+}	Au^+, Ag^+, Cu^+
Li^+, Na^+, K^+, Rb^+, Cs^+	Cu^{2+}, Zn^{2+}, Pb^{2+}, Sn^{2+}	Hg^{2+}, Cd^{2+}
Be^{2+}, Mg^{2+}, Ca^{2+}	As^{3+}, Sb^{3+}, Bi^{3+}	
Sr^{2+}, Ba^{2+}		
Al^{3+}, Ga^{3+}		
Ce^{4+}, Sn^{4+}		
Ti^{4+}, Ti^{3+}, Zr^{4+}		
Mo^{6+}, Mo^{5+}, Mo^{4+}		
W^{6+}, W^{4+}, Nb^{5+}, Ta^{5+}		
Mn^{4+}, Fe^{3+}, Co^{3+}		
U^{6+}, U^{4+}		
Acids		
Hard	**Borderline**	**Soft**
NH_3, H_2O, OH^-	Br^-	CN^-, CO
CO_3^{2-}, NO_3^-		S^{2+}, HS^-, H_2S, SO_3^{2+}
PO_4^{3-}, SO_4^{2-}		I^-
F^-, Cl^-		

Table 7.3: Classification of ligands and metals according to their hardness. After Seward and Barnes (1997), Brimhall and Crerar (1987), and Pirajno (1992). In bold, most important ligands in natural hydrothermal fluids.

7.3.2.3. Solubility

If simple aqueous ions dominate in a solution, the ore mineral solubilities are too low for the transport of significant quantities of ore metals; however, formation of complexes increases solubility so that ore deposit formation becomes possible (Barnes 1979; Wood and Samson 1998). High metal solubilities require either large solubility constants (K_{SP} = activity a) and/or large stability constants (K_n; degree to which a metal and a ligand tend to form a complex) for the predominant complex(es) (Wood and Samson 1998). Also, solubility increases with higher temperature for most solids in water; several variables (i.e., pH, fO_2, fS_2, a_{Cl} for the most important) change with increasing temperature, therefore, influencing the solubility of minerals (Brimhall and Crerar 1987).

7.3.3. Partitioning of metals and ligands from melts into fluids

As described in Section 7.2.4, metals concentrate in one phase or another, depending on the value of the partition coefficient between two phases. This Section details the

different factors affecting the partition coefficients of both ligands and metals between different phases (mainly fluid-melt, fluid-mineral).

7.3.3.1. Ligands

Chlorine

Although not always the most ideal ligand for the available metal (according to the hard-soft classification of ligands in Section 7.3.2.1), both its ubiquitous presence and abundance make chlorine the most significant ligand in the majority of hydrothermal ore-forming fluids (Seward and Barnes 1997; Wood and Samson 1998). At temperature between 725° and 950°C and pressure ranging from 0.5 to 5 kbar, Cl partitions in favour of the fluid rather than the melt with the fluid phase being H_2O alone or $H_2O + CO_2$ (Webster and Holloway 1988). Factors enhancing the partitioning of Cl towards the fluid phase are higher concentrations of Cl in the melt (Fig.7.5), decrease of fluorine content, increase of pressure and temperature, and increase of the melt peraluminosity (Kilinc and Burnham 1972; Webster and Holloway 1988; Webster 1990, 1992). Higher chlorine concentrations in the melt trigger the exsolution of that fluid from the melt earlier (i.e., at lower H_2O concentration in the melt) than if there were no Cl; consequently, a Cl-rich brine can evolve from a felsic magma prior to extensive crystallisation and, more importantly, prior to boiling of a volatile phase (Webster 1992; 1997a; 1997b).

Fluorine

Fluorine preferentially partitions towards the silicate melt in a fluid-melt system (e.g., $D_F^{f/m} < 1$) (Koster Van Groos and Wyllie 1968; Dingwell and Scarfe 1983; Webster and Holloway 1987; London 1987; London et al. 1988). At temperatures close to 800°C and pressures of ~ 2 kbar, the presence of fluorine in a haplogranitic melt-fluid system increases the solubility of some high field strength-bearing minerals in the melt (e.g., manganocolumbite, manganotantalite, zircon, rutile), therefore, favouring the enrichment

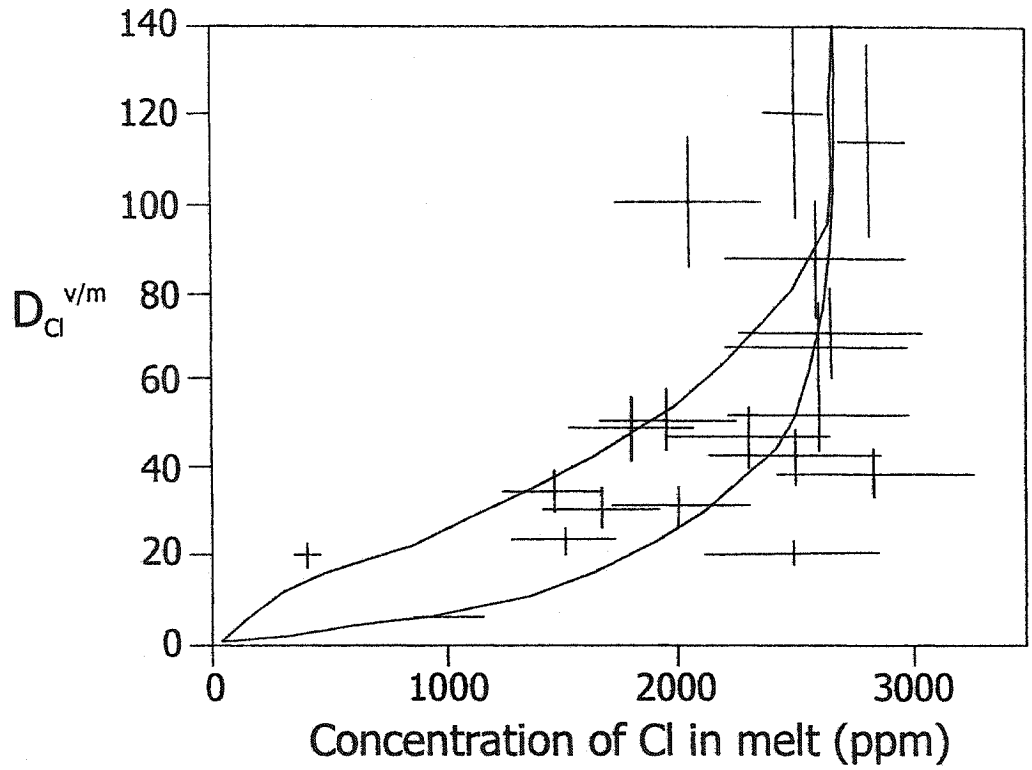

Figure 7.5: Plot of the $D_{Cl}^{v/m}$ as a function of the ppm Cl in the melt for an 800°C and 2 kbar experiment. From Webster and Holloway (1988).

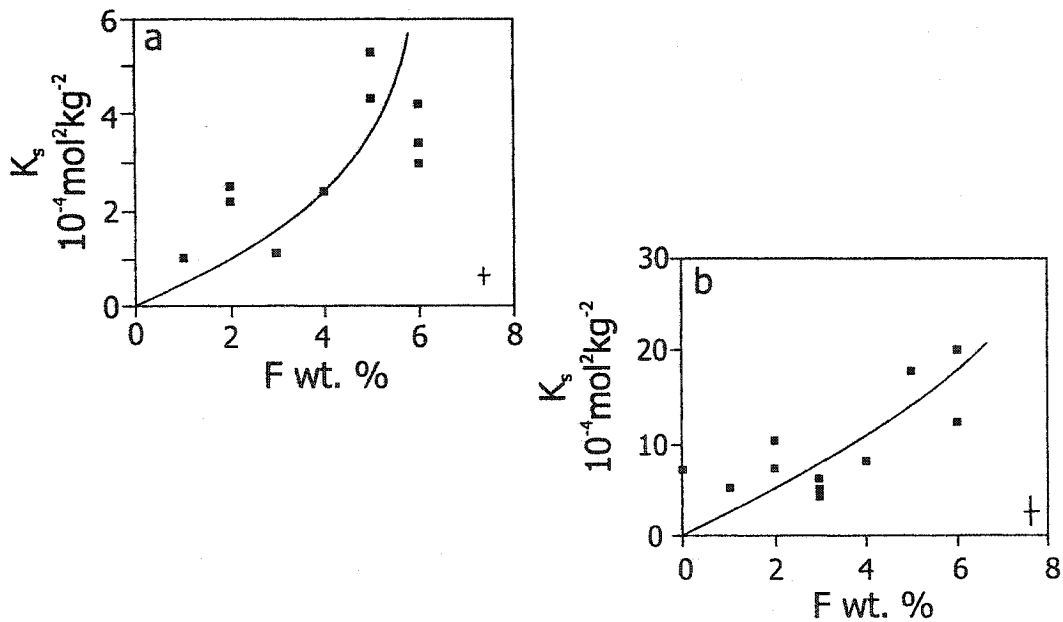

Figure 7.6: Solubility of (a) manganocolumbite $MnNb_2O_6$ and (b) manganotantalite $MnTa_2O_6$ in water-saturated haplogranitic melt at 2 kbar and 800°C.
$K_s = [MnO][Nb_2O_6]$ or $[MnO][Ta_2O_6]$. From Keppler (1993).

of those elements (Ti, Nb, Ta, Zr, Hf, Th, U, REE) in the melt (Fig. 7.6) (Keppler and Wyllie 1991; Keppler 1993). With increasing amount of F in the system, the solubility of peraluminous melts increases; therefore, $D_F^{f/m}$ increases to values >1 with concentration of more than 8 wt % of F in melt (London 1987; Webster 1990). Other effects of increasing the amount of F in the melt are larger $D^{f/m}$ for Sn, W, Mo, Cu, and REE (Dingwell 1985).

Sulphur

Sulphur dissolves as HS^- in hydrous melts and strongly partitions towards the fluid phase if sulphide minerals (e.g., pyrrhotite) are not stable (Burnham 1979; Brimhall and Crerar 1987). The $D_S^{f/m}$ does not vary with temperature, but is highly sensitive to pressure variations (Burnham and Ohmoto 1980): sulphur exists as H_2S and SO_2 in the fluid phase and, HS^- being mostly present in the melt phase, its partition coefficient is sensitive to f_{H2O} and fO_2 (Fig 7.7) (Burnham and Ohmoto 1980; Carroll and Webster 1994 and references therein). An increase in f_{H2O} decreases $D_S^{f/m}$, because the H_2S/SO_2 ratio increases in the fluid phase; an increase in fO_2 decreases the H_2S/SO_2 ratio, thereby increasing $D_S^{f/m}$ (Burnham and Ohmoto 1980). The fO_2 of peraluminous granites is generally below the QFM buffer (Fig. 7.7), hence H_2S dominates in the system compared to SO_2, indicating a more reducing environment (Burnham and Ohmoto 1980). The ionisation reactions of H_2S are:

$H_2S_{(aq)} = H^+ + HS^-$

and $HS^- = H^+ + S^{2-}$

The equilibrium constant of the second reaction is small (10^{-16} to 10^{-18}), therefore, a_S^{2-} is negligible and metal sulphide solubility equilibrium is:

$MS_{n/2}(s) + n/2\ H^+ = M^{n+} + n/2HS^-$ where M is metal and n = 1, 2, … (Seward and Barnes 1997).

Phosphorus

High phosphorus concentrations are systematically associated with late-stage peraluminous granitic rocks and P may be considered as a ligand in ore mineralisation processes (London 1992). The dominant phosphate complexes in peraluminous melts are $AlPO_4$ and P_2O_7 (Mysen et al. 1999), the first one accounting for the increasing solubility

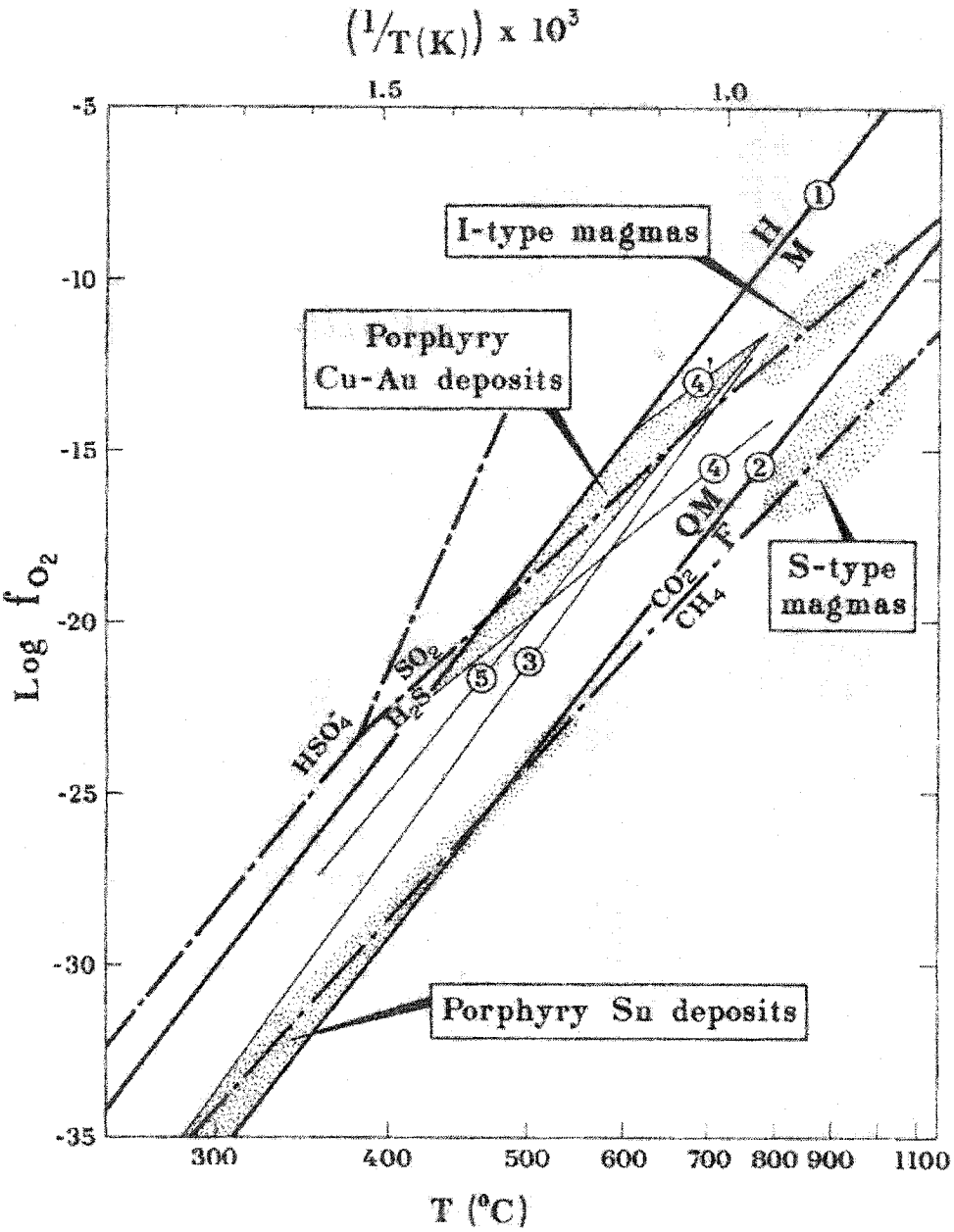

Figure 7.7: Oxygen fugacity vs temperature relations for the predominant sulfur species (and carbon species) in broken lines in aqueous fluids, and the fO_2 buffers (solid lines) at 1 kbar. The SO_2/HSO_4^- and HSO_4^-/H_2S boundaries are for unit activity ratios at pH=4. Mineral equilibria represented are: (1) magnetite + hematite, (2) fayalite + magnetite + quartz, (3) pyrrhotite + pyrite + magnetite, (4) biotite + K-feldspar + magnetite, (5) anorthite + K-feldspar + pyrite + muscovite + quartz + anhydrite. From Burnham and Ohmoto (1980).

of apatite with increasing A/CNK ratio (Pichavant et al. 1992; Wolf et al. 1994). Because of the formation of aluminophosphate complexes, the solubility of P in peraluminous melts is higher than in metaluminous to peralkaline melts (Mysen et al. 1981) and the $D_P^{f/m}$ is between 0.2 and 0.5 (but still <1) for the peraluminous composition (London et al. 1988, 1993). The solubility of phosphates (monazite, apatite) increases with peraluminosity, mainly because of the strong stability of aluminum phosphate complexes (London 1992). In experiments carried out in the system haplogranite-H_2O-P_2O_5 at 1-5 kbar and 700°-1100°C, Keppler (1994) observed that the depth of emplacement of the granitic pluton controls the behaviour of P: $D_P^{f/m}$ increases with increasing pressure (> 1 above 3 kbar) (Fig 7.8), therefore, at such pressure P is a potential ligand for metal transportation in the fluid phase.

Hydroxide

The pH of pure water at 25°C is 7, because the concentration of H^+ is 1 x 10^{-7} mol/L and the definition of pH is $-\log_{10}[H^+]$ (Faure 1991). Water is amphiprotic (can act as both an acid and a base), therefore, a molecule of H_2O can act as an acid by donating a proton to another H_2O molecule acting as a base:

$$H_2O + H_2O = H_3O^+ + OH^-$$

Acid Base

The dissociation constant of this reaction is $a(H_3O^+)$ x $a(OH^-)$, where a is the activity of the ion, which is equal to 1 x 10^{-14} at 25°C; the constant increases with temperature (Clark and Hawley 1966). The concentration of OH^- produced this way (i.e., with pure H_2O only) is small, but will increase as a base enters the solution, for example by adding ammonium hydroxide:

$$H_2O + NH_3 \tau NH_4^+ + OH^-$$

Acid Base

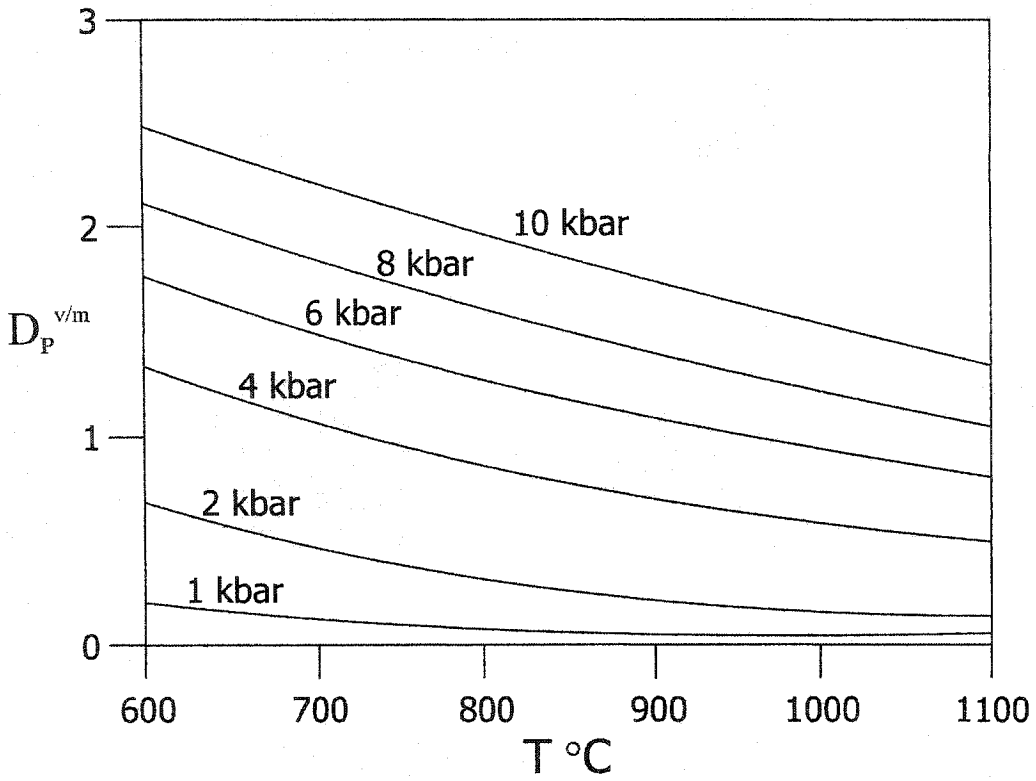

Figure 7.8: Calculated $D_P^{v/m}$ in the system haplogranite-H_2O-P_2O_5 at the indicated pressures. From Keppler (1994).

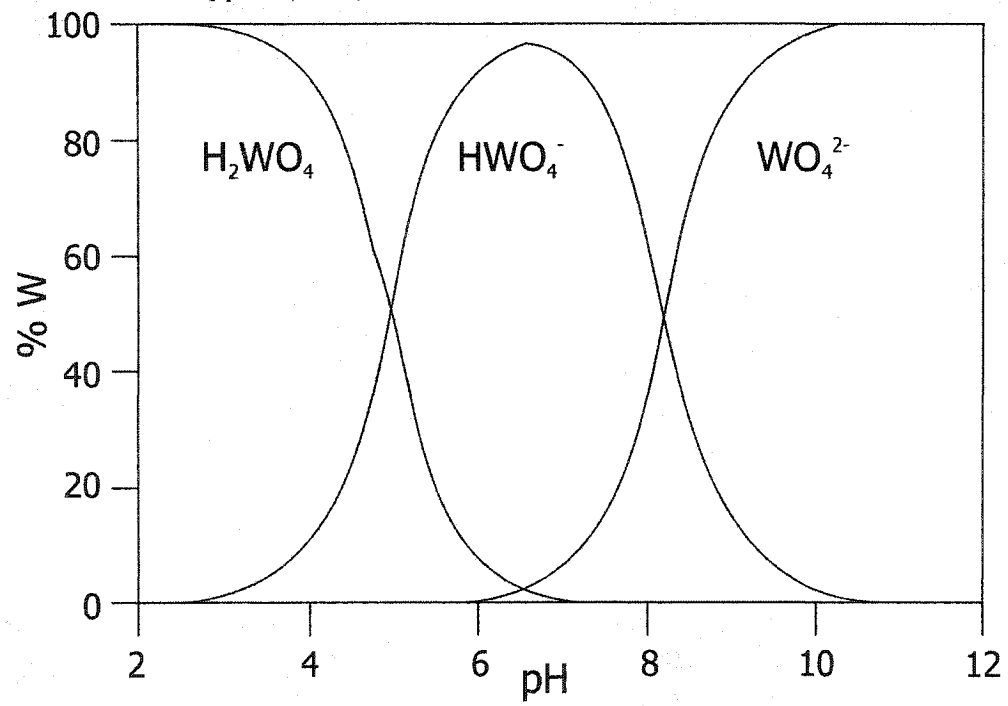

Figure 7.9: Diagram showing fields of predominance of tungstate species as a function of pH at 400°C and 0.5 kbar. From Wood and Samson (1998).

7.3.3.2. Metals

Molybdenum

Molybdenum is a hard metal with several oxidation states; under oxidising conditions Mo^{6+} is predominant, whereas under more reducing conditions Mo^{5+}, Mo^{4+}, and Mo^{3+} can be present (Wood and Samson 1998). Molybdenum forms strong complexes with O^{2-} and OH^- (especially for higher oxidation states), whereas chloride and sulphide complexes are unimportant (Smith et al. 1980; Candela and Holland 1984; Wood et al. 1987; Keppler and Wyllie 1991). The predominant species for transport of Mo under hydrothermal conditions are $MoO_2(OH)_2$ (Candela and Holland 1984), H_2MoO_4, and $HMoO_4^-$ (Wood et al. 1987). Although Candela and Holland (1981b), Candela and Holland (1984), and Tingle and Fenn (1984) concluded that fluorine did not affect Mo concentration in the fluid phase, Bai and Koster Van Groos (1999) reported an increase of Mo solubility in the melt with increasing fluorine present.

Oxygen fugacity is the main control for Mo partitioning between a melt and a mineral phase: increasing fO_2 favours the partitioning of Mo in the melt phase, therefore, Mo is available for partitioning into the fluid phase when it forms (Tacker and Candela 1985; Candela and Holland 1986; Bouton et al. 1987; Tacker and Candela 1987; Candela 1992). The partition coefficient of Mo is fairly high in pure H_2O fluid and decreases with an increasing amount of F or Cl in the fluid phase (Candela and Holland 1984; Keppler and Wyllie 1991). As the melt evolves from granodioritic to leucogranitic compositions, the partition coefficient of Mo between a Cl- or F-bearing fluid and a melt increases, favouring the partitioning of Mo into the fluid phase (Chevychelov 1996).

Tungsten

The main oxidation state of tungsten in hydrothermal fluid is W^{6+}, but under highly reducing conditions W^{5+} may occur, although no experimental data exist for the +5 oxidation state (Wood and Samson 1998). Similarly to Mo, W is a strong base, hence forming strong complexes with $O^{2-} > F^- > CO_3^{2-} > PO_4^{3-} > Cl^-$. The predominant species for transport of W under hydrothermal conditions are WO_4^{2-} (in more alkaline fluids), HWO_4^-,

H_2WO_4 (in more acidic fluids) (Wood 1992) and references therein. The reactions involved for the dissociation of these species are:

$HWO_4^- = WO_4^{2-} + H^+$ more alkaline fluids

$H_2WO_4 = HWO_4^- + H^+$ more acidic fluids (Fig 7.9)

Also, Manning and Pichavant (1985) reported $H_6[H_2W_{12}O_{40}]$ and $H_3[PW_{12}O_{40}]$ as stable complexes, depending on the pH (increasing at low pH, because at pH > 7, WO_4 is stable). Manning and Henderson (1984) and Keppler and Wyllie (1991) reported that, in melt-vapour partitioning experiments, W partitions preferentially into the melt if the fluid phase is H_2O alone or F-, CO_2, or B-bearing. Because W partitions preferentially towards the melt in F-bearing systems, W-fluoride complexes do not increase the solubility of minerals containing W in ore-forming fluids (Manning and Henderson 1984; Keppler and Wyllie 1991). Also, the partition coefficient of W between fluid and melt and between WO_3 and fluid is independent of Cl concentration in the system (Wood and Vlassopoulos 1989; Keppler and Wyllie 1991). Contrary to the behaviour of Mo, increasing fO_2 favours the partitioning of W into the solid phase (Candela and Bouton 1990).

Tin

Under oxidising conditions, tin is present as Sn^{4+}, whereas under reducing conditions Sn^{2+} exists in hydrothermal solutions (Wood and Samson 1998). Tin is a moderately hard metal ("borderline ion") and mainly forms complexes with Cl^- and OH^- (Fig. 7.10). Depending on redox conditions, the predominant species for transport of Sn under hydrothermal conditions are $Sn(OH)_2Cl_2$ (highly oxidising conditions; low cassiterite solubility) and $SnCl_2$ (highly reducing conditions; high cassiterite solubility) (Dubessy et al. 1987; Wilson and Eugster 1990; Linnen et al. 1995). Nonetheless, chloride complexes of Sn^{2+} dominate in moderately acidic or reducing solutions, therefore $D_{Sn}^{f/m}$ increases with increased Cl concentration in the system (Heinrich 1990; Keppler and Wyllie 1991; Taylor and Wall 1993) whereas fluoride complexes are unimportant (Jackson and Helgeson 1985; Eugster and Wilson 1985; Eugster 1986; Eadington 1988; Keppler and Wyllie 1991). No experiments deal with the influence of fO_2 on $D^{s/m}$, but Candela (1992) suggests similarities with W behaviour (i.e., with increasing fO_2, Sn will partition preferentially into a solid phase). Tin solubility in melt inversely depends on fO_2: in late-stage crystallisation of

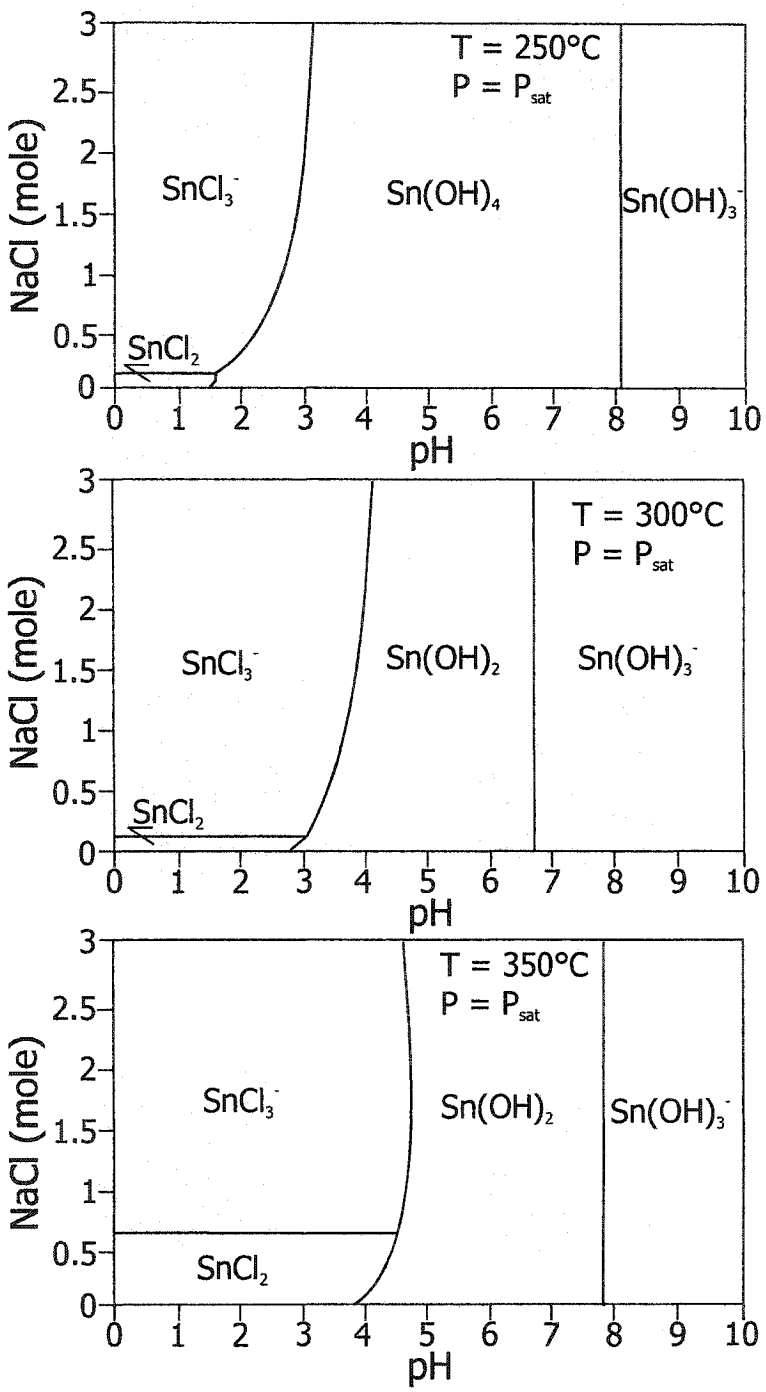

Figure 7.10: Relative stability fields of the hydroxide and chloride complexes of Sn in NaCl solutions with fO_2 buffered by Ni-Ni oxide as a function of solution pH at 250°, 300°, and 350°C along the liquid-vapour equilibrium curve for H_2O. The curves represent equal activities of the aqueous species shown in adjacent stability fields. From Jackson and Helgeson (1985).

granitic melts, the increase in fO_2 is an effective mechanism for cassiterite crystallisation (Cuney et al. 1992; Linnen and Williams-Jones 1994; Linnen et al. 1995). Therefore, granite-related tin deposits are commonly considered to have had a redox state between FMQ and NNO buffers (Dubessy et al. 1987). The granitic melt composition also controls cassiterite solubility: the solubility is minimal if the composition is subaluminous, increases strongly with alkali content in peralkaline composition, and increases weakly with Al content in peraluminous compositions (Linnen et al. 1996).

Uranium

Uranium is a hard metal and is present as U^{6+} in hydrothermal solutions (Keppler and Wyllie 1991). Depending on redox conditions, the predominant species for transport of U under hydrothermal conditions are UCl_{1-2} (reducing conditions) and UO_2Cl_{1-5} (oxidizing conditions) (Grenthe et al. 1992; Kojima et al. 1994). Other possible complexes are UO_2F_2 and $UO_2Cl_3^-$ (Keppler and Wyllie 1991), UO_2CO_3, $UO_2(CO_3)_2^{2-}$, and $UO_2(CO_3)_3^{4-}$ (Kojima et al. 1994), and UF_2^{2+}, UF_3^+, UF_4 (Sassani et al. 1993). Polymerisation state of the melt becomes important when no fluid phase is present: if the melt is depolymerised (not organised as chains), then uranium bonds with free oxygen in the melt and remains in the melt phase. Silicate melt becomes more polymerised towards the end of crystallisation; therefore, because of a shortage of free oxygen, uranium partitions into minerals (U oxides) and is more compatible (Farges et al. 1992). Peraluminous melts show low U solubilities, therefore, uraninite saturation can be reached easily. Fluorine enhances U solubility in the melt, whereas U partitions strongly into an exsolving Cl-bearing fluid phase if a small amount of fluorine is present, thereby decreasing the U content of melt (Peiffert et al. 1996). The solubility of UO_2 also varies as a function of pH for a fixed temperature and fO_2: higher fO_2 enhances solubility in acidic to neutral solutions. With increasing temperatures, the stability of U complexes decreases, because of higher values of fO_2 (Fig. 7.11) (Dubessy et al. 1987). Low temperature fluids are more efficient for U transport than high temperature ones, because fO_2 is controlled at levels higher than the Ni-NiO buffer (Dubessy et al. 1987).

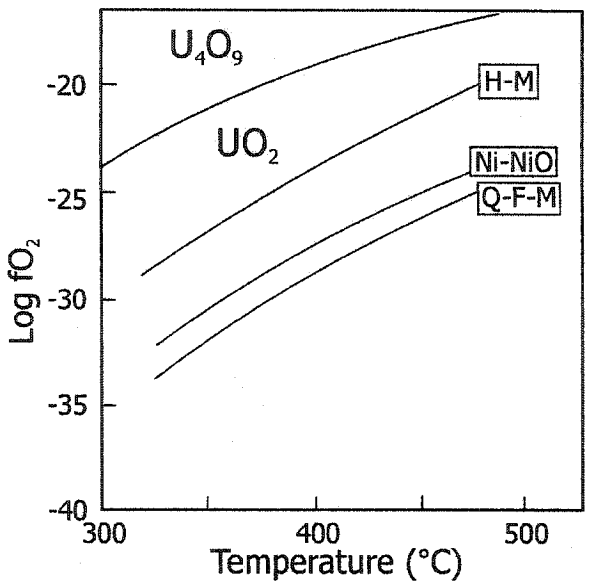

Figure 7.11: Uranium oxide stability fields and fluid compositions associated with U, Sn, and W deposits in an log fO_2-temperature diagram at 1 kbar.
From Dubessy et al. (1987).

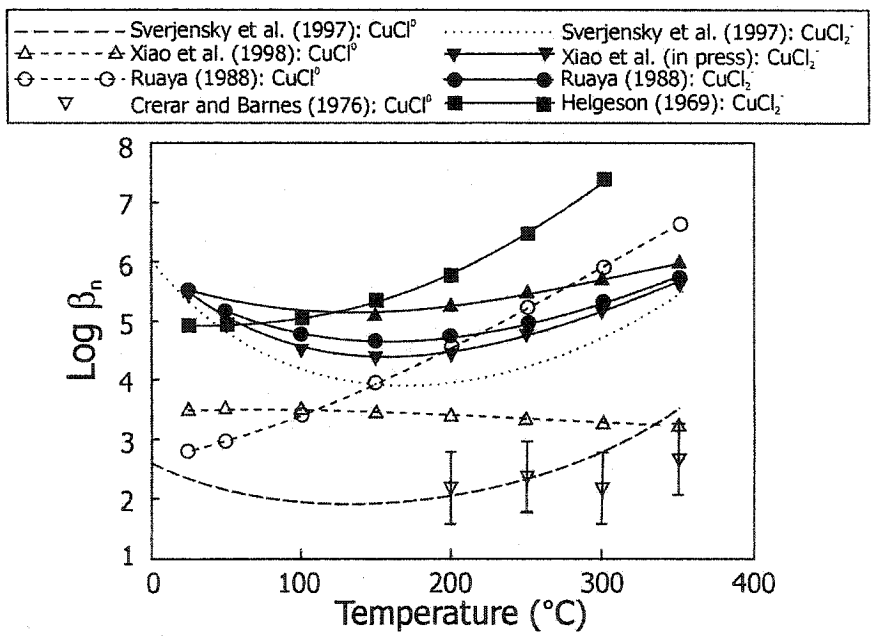

Figure 7.12: Plot of cumulative stability constant (degree to which a metal and a ligand tend to form a complex $\hat{O}_n=K_1K_2K_3\ldots K_n$) of CuCl from the literature vs temperature. The U-shape in function of temperature is consistent with the "soft" character of Cu+ and "borderline" character of Cl-. At low temperature, the soft-soft interaction between Cu+ and Cl- is driven by an exothermic process, whereas at higher temperature the interaction switches to hard-hard and the interaction is driven by an endothermic process. From Wood and Samson (1998).

Copper

The oxidation state Cu^{+} is predominant at hydrothermal conditions (Crerar and Barnes 1976; Candela and Holland 1984; Hemley et al. 1992; Xiao et al. 1998). Although copper is a relatively soft ion, it still forms stable chloride and bisulphide complexes (Wood and Samson 1998). The predominant species for transport of Cu under hydrothermal conditions are $CuCl_{(aqueous)}$ (Crerar and Barnes 1976; Candela and Holland 1984; Keppler and Wyllie 1991; Bai and Koster Van Groos 1999) and $CuCl_2^-$ (Var'yash and Rekharskiy 1981; Gammons et al. 1996; Xiao et al. 1998). The stability of the complex CuCl varies as a function of temperature, with a stability constant value minimum between 150° and 200°C and increasing as temperature rises beyond 200°C (because the interaction between Cu and Cl becomes hard-hard instead of soft-borderline at lower temperature) (Wood and Samson 1998) (Fig. 7.12). With little or no fluid present, Cu behaves as a compatible element during fractional crystallisation (Candela and Holland 1986) and sulphides are the most likely candidates to host Cu (e.g., pyrrhotite in volcanic rocks) (Blevin and Chappell 1992). At fO_2 higher than NNO, Cu behaves incompatibly, because sulphides are destabilised (Candela 1987). When an aqueous phase is present, Cu partitions preferentially towards a saline aqueous phase rather than the melt (Khitarov et al. 1982); therefore, the presence of a fluid phase is imperative early in the crystallisation of an intrusion, otherwise the copper will be locked in mineral phases (Candela and Holland 1981b; Jugo et al. 1999). Changes in fO_2 (higher) and fS_2 (lower) may result in the decomposition of pyrrhotite to magnetite allowing the trace amount of Cu in pyrrhotite to return into the melt (Jugo et al. 1999). As a result, the maximum Cu enrichment of a magmatic volatile phase will occur in highly oxidised magmas with low fS_2 (Jugo et al. 1999).

Manganese

Manganese exists under two oxidation states: oxidising conditions (Mn^{3+}) and reducing conditions (Mn^{2+}) (Wood and Samson 1998). Manganese is a borderline cation, therefore, not showing preferences between hard or soft ligand (Cl^-, OH^-). The predominant species for transport of Mn under hydrothermal conditions are $MnCl_2$ (Boctor 1985;

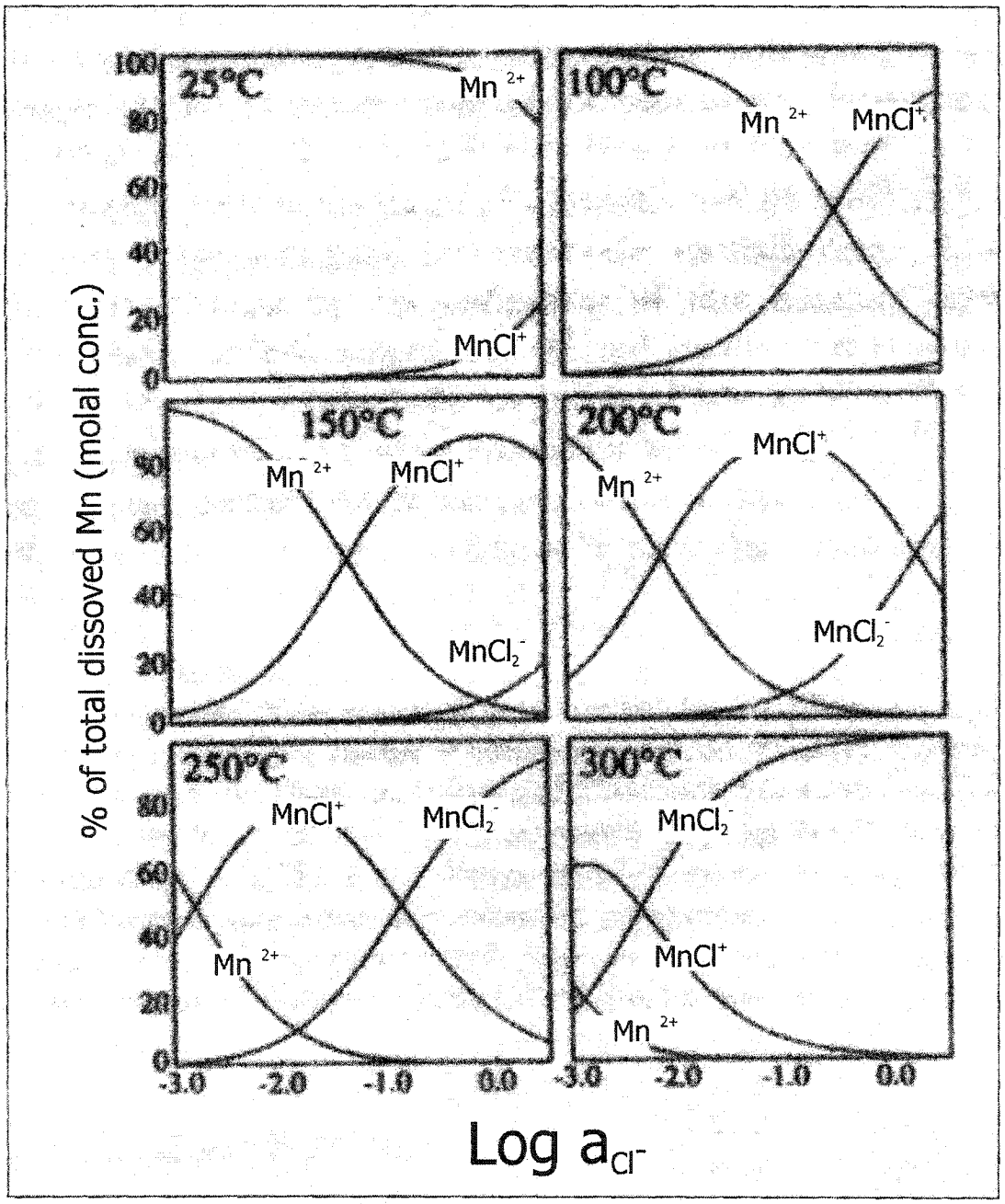

Figure 7.13: Speciation diagrams summarising the distribution of Mn^{2+}, $MnCl^{+}$, and $MnCl_2$ as a function of chloride activity between 25° and 300°C. The curve shows the percent of total dissolved Mn (in molal concentration units) present as each complex. From Gammons and Seward (1996).

Element name		Geochemical characteristics					Possible source of metal			Ligand(s)				
Symbol	Name	Atomic number	Atomic weight	Size (10^3 kg/m^3)	Charge	Classification	Melt	Meguma Supergroup	SMB alteration	Cl^-	F^-	OH^-	CO_3^{2-}	HS^-
F	Fluorine	9	18.998	1.696	**-1**	Lithophile, ligand								
Cl	Chlorine	17	35.453	3.214	1, 3, 5, 7, **-1**	Ligand								
Mn	Manganese	25	54.938	7.2	**2**, 3, 4, 6, 7	Lithophile, TM	Y	Y (GHT)	Y (biotite, ilmenite)	Y				
Cu	Copper	29	63.546	8.92	1, **2**	Chalcophile, TM	Y		Y (biotite)	Y				Y
Mo	Molybdenum	42	95.94	10.2	2, 3, 4, 5, **6**	Siderophile	Y					Y		
Sn	Tin	50	118.69	7.28	2, **4**	Siderophile	Y		Y (biotite)	Y		Y		
W	Tungsten	74	183.85	19.35	2, 3, 4, 5, **6**	Lithophile	Y					Y		
U	Uranium	92	238.03	19.0	3, 4, 5, **6**	Lithophile, HFS	Y			Y	Y		Y	

Table 7.4: Geochemical characteristics, metal source(s), and possible ligands for the metals present in the mineral occurrences of the New Ross area.

Gammons and Seward 1996) and $MnCl^+$ (Wolfram and Krupp 1996) (Fig 7.13). Very few studies provide thermodynamic data for aqueous Mn complexes. What follows is from a paper by Gammons and Seward (1996), who did experiments at temperature between 25° and 300°C. Rhodonite and rhodocrosite are highly soluble in mildly acidic brines, but may precipitate in response to sudden changes in pH, P_{CO2}, or a_{Cl}. Rhodonite has retrograde solubility with respect to temperature, whereas rhodocrosite solubility is either prograde (ore fluid is saline) or retrograde (ore fluid is dilute). Manganese is easily transported in hydrothermal fluids and will precipitate as Mn oxides or hydroxides upon reaching an oxidation front.

7.3.3.3. Summary

Table 7.4 summarises the data presented in Section 7.3.3.2. Chlorine is a prime ligand for most metals present in the mineral deposits of the New Ross area; only Mo and W complex strongly with OH^- and show no affinity for Cl^-. There is little mineralogical evidence for the presence of chlorine, but fluid inclusions contain Cl^- as the main anion (Section 5.4.4). Although ubiquitous in the mineral occurrences of the New Ross area, according to experimental studies, F^- is a possible ligand for U only, and may only be an "accompanying" anion. Several sulphide minerals occur in the New Ross area (mostly Cu and Mo sulphides), but only Cu shows possible complexing with HS^-. Small concentrations of S occurred in the fluid inclusion decrepitates (Section 5.4.4).

Oxygen fugacity is the main control of metal partitioning between the melt and a solid phase, whereas ligand concentration largely controls the partitioning between the melt and a fluid phase.

7.3.4. Deposition of metals from hydrothermal fluids

The following variations in temperature, pressure, and composition can lead to deposition of metals:

Temperature changes affect the solubility of sulphides and oxides and the stability of complex ions (Skinner 1997). Decrease of temperature is the main factor for lowering metal solubility and triggering metal deposition if saturation is reached. Mixing with cooler fluids and/or adiabatic decompression (change from lithostatic to hydrostatic pressure) may

cause such temperature decreases (e.g., Candela 1987). Two other consequences of mixing with meteoric fluid are: (i) dilution, consequently decreasing temperature; and (ii) oxidation, because meteoric fluids contain dissolved O^{2-} (Faure 1991). During retrograde boiling, the most volatile constituents of the aqueous fluid phase (H_2, CH_4, CO_2, H_2S, SO_2) partition into the vapour phase. The remaining liquid phase has a much higher pH than before, thereby lowering the solubility and initiating metal precipitation (Drummond and Ohmoto 1985). In the absence of boiling, decreasing temperature causes oxidation (fO_2 increase) and ionisation of acid and neutral complexes (Burt 1981). In the fluid inclusions of the New Ross area, no evidence for boiling exists.

Chemical reactions with the country rock also affect the solubility of sulphides and oxides and the stability of complex ions. In acidic solutions, the extraction of H^+ occurs because of hydrolysis of feldspars and other silicates (argillic alteration). The H^+ loss from solution increases the pH and reduces the stability of chloride complexes, and may cause the precipitation of sulphides if S is present in the system (Pirajno 1992) according to the following reaction:

$MCl_{2(aqueous)} + H_2S_{(aqueous)} \rightarrow MS + 2H^+ + 2Cl^-$ (M = metal) (Barnes 1979).

Deposition from sulphide complexes is most efficient with increasing fO_2, because it decreases both the pH and the total sulphide concentration:

$M(HS)_3^- \rightarrow MS + HS^- + H_2S_{(aqueous)}$ (Barnes 1979).

The change of oxidation state of some metals may cause precipitation (e.g., change from Fe^{2+} to Fe^{3+} causes the precipitation of Fe_2O_3). If fluids transporting UO_2^{2+} enter a reducing environment, precipitation occurs with a change of valence of U from +6 to +4 (Pirajno 1992).

7.3.5. Deposition of metals present in the New Ross area

7.3.5.1. Introduction

Alteration and mineralisation of granitic rocks result from the reaction of hydrothermal fluids with solid rocks, and the partitioning of metal complexes, respectively. Both fluids and metals may derive from within or from outside of the granitic body, therefore, four end-member situations are possible (Table 7.3 in Clarke 1992; Clarke 2003, Fig. 7.14):

1. **Fluids and metals are internally derived.** The fluid is the result of water-saturation in the magma and metals present in the melt partition preferentially into that fluid phase, or may originate from the alteration of solid phases in the granitic body as the fluid travels through it.
2. **Fluids are internally derived and metals are externally derived.** The fluid results from water-saturation in the magma and alters the country rock, leaching metals from it.
3. **Fluids are externally derived and metals are internally derived.** Heat produced by the magmatic body triggers convection cells, circulating an external fluid or fluids of diverse origins (meteoric, metamorphic, connate, seawater). Metals originate either directly from the melt or from the alteration of solid phases in the granitic body.
4. **Fluids and metals are externally derived.** The fluid originates outside of the granitic body (heat driven) and alters the country rock, leaching metals from it.

In each case, deposition of the metals may be either internal or external to the granitic body.

7.3.5.2. Fluid origin(s) in the New Ross area

Natural systems never are as simple as the models that attempt to describe them, and the source of fluids in the New Ross area is no exception. Fluid inclusion analysis and stable isotope data on fluid inclusions and fluid in equilibrium with white micas (Chapters 5 and 6) provide some insight in the fluid reservoirs involved in the metals transport in the New Ross area. We recognised three fluids, based on salinity and cation content: (i) a K-Na-bearing magmatic fluid with a salinity range of 19 to 25 wt. % equiv. NaCl; (ii) a low salinity (0-9 wt. % equiv. NaCl) meteoric-dominated fluid; and (iii) a Ca-bearing fluid with a salinity range of 29 to 43 wt. % equiv. NaCl, likely of metamorphic origin, although a magmatic contribution is not excluded. Mixing among those different fluids occurs in pegmatite/aplite and greisen deposits, whereas vein deposits are strongly dominated by

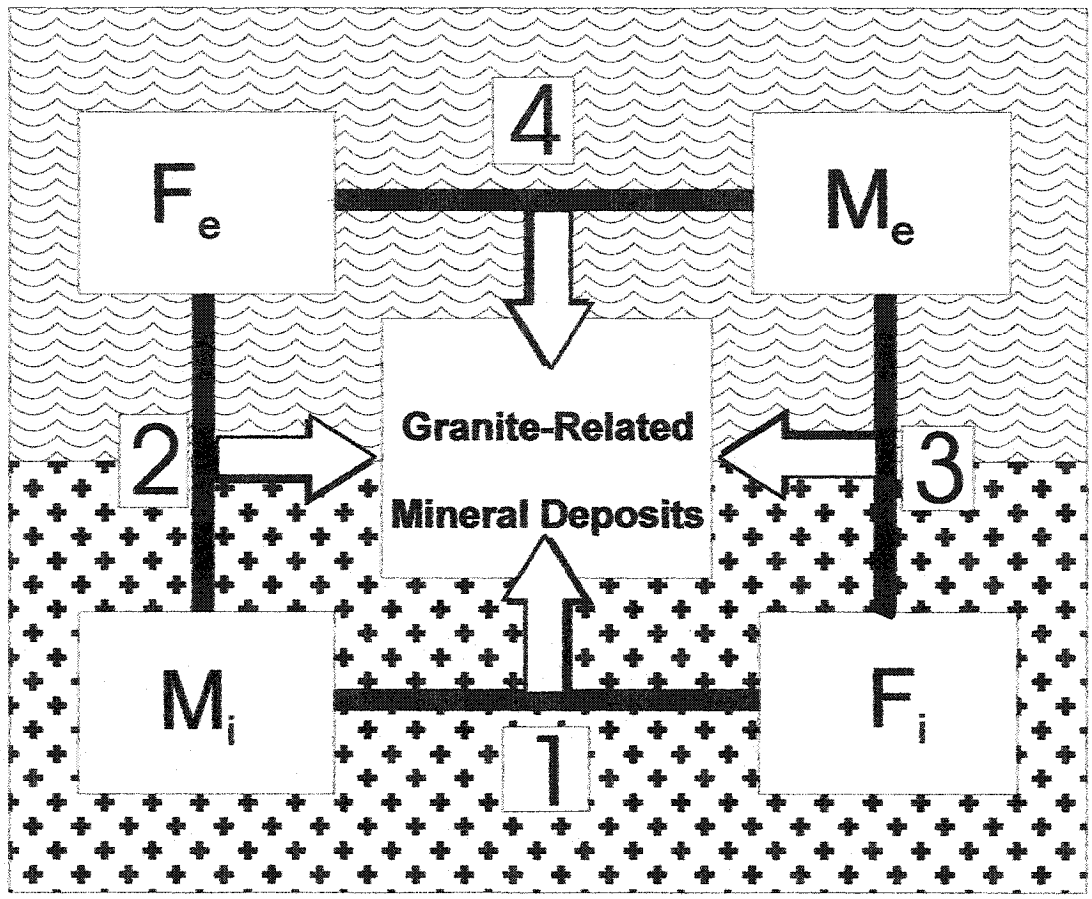

Figure 7.14: Model illustrating the possible fluxes of metals and fluids through the granite and its country rock. F_i (M_i)=fluids (metals) originating from an internal source in the granite, F_e (M_e)=fluids (metals) originating from an external source to the granite. Model 1: both fluids and metals originate from the granite; Model 2: metals originate from the granite, fluids come from outside of the granite; Model 3: fluids originate from the granite, metals come from outside of the granite; and Model 4: both fluids and metals originate from outside of the granite.

meteoric fluids. Such mixing is only possible if fluids are contemporaneous. Furthermore, a progressive lowering of $\delta^{18}O$ and increase in δD values for fluid in equilibrium with white micas from greisen and vein deposits may also show the influence of increasing amounts of meteoric fluid incursion as the system passes from a magmatic to a hydrothermal regime. Also, the comparison of δD values from fluid inclusion extracts with that of a fluid in equilibrium with white micas suggests the introduction of a later generation of meteoric fluid into the system. The timing of the different fluid incursions in the system is difficult to establish, because samples are inundated with fluid inclusions; nonetheless, to allow for fluid mixing in the fluid inclusions, fluids have to be contemporaneous, therefore, magmatic, meteoric, and possibly metamorphic fluids were probably present at the same time. Also, geochronological data (Chapter 4) show that the ages of granite emplacement and mineralisation event are coeval, within error; therefore, mineral deposit formation occurred in close temporal relationship with batholith crystallisation.

In conclusion, both internally- and externally-derived fluids are present in the New Ross area at the time of granite emplacement, with mixing between fluids originating from at least two reservoirs (possibly three) and with increasing amount of meteoric water flushing through the system as it evolves from a magmatic to a hydrothermal regime.

7.3.5.3. Metal origin(s) in the New Ross area

Similarly to fluids, and as stated in Section 7.3.5.1, metals may be internally and/or externally derived. Internally derived metals originate directly from the melt (concentration as incompatibles) and/or originate from the breakdown of magmatic minerals because of alteration. Externally derived metals derive from the country rock (in this case, probably from the Meguma Supergroup) by leaching (either *in situ*, or from xenocrystic minerals in the granite). The following lists the possible sources for the metals present in the New Ross mineral occurrences, keeping in mind the geological context of the South Mountain Batholith, and more widely of the Meguma Terrane. In the following, I have sorted the metals in increasing order of probability of being externally derived. In other words, the first metal(s) dealt with is/are the most likely to be entirely magmatic in origin.

Molybdenum and tungsten

Because of size and charge considerations, both molybdenum and tungsten are highly incompatible chemical elements, thereby becoming concentrated in late melts by fractional crystallisation.

Molybdenite solubility in the fluid phase is poorly constrained, and experimental studies are contradictory, with the main point of dissension being the dependence of molybdenite solubility on temperature variation. Westrich (1974) and Smith et al. (1980) showed positive temperature dependence for experiments between 300° and 650°C, whereas Wood et al. (1987) and Cao et al. (1988) found that molybdenite solubility is independent of temperature between 200° and 400°C. Also Wood et al. (1987) demonstrated the lack of dependence of molybdenite solubility on chloride concentration, whereas Cao et al. (1988) found that molybdenite solubility increases with NaCl concentration. Differences between results of these studies may occur because neither pH nor fO_2 were well constrained.

Wood and Samson (2000) provided a thorough review of granite-related W deposits and of solubilities of the main W-bearing minerals (wolframite, with its Fe end-member ferberite and Mn end-member hübnerite, as well as scheelite). The main conclusions of their paper are: (1) scheelite and ferberite (Fe-bearing wolframite) are deposited by fluids at temperatures between 200° and 500°C, pressures between 0.2 and 1.5 kbars, salinities generally < 15 wt. % equiv. NaCl (but can reach values of 55 wt. % equiv. NaCl), either very little or no CO_2, moderately acidic pH, and fO_2 between QFM and HM buffers; (2) scheelite and ferberite solubilities increase with increasing temperature, increasing chloride concentration, and decreasing pH; and (3) ferberite is stable over a large range of oxygen fugacities (as high as the CuO/Cu_2O and Mn_3O_4/Mn_2O_3 buffers and as low as the FeO/Fe_3O_4 buffer) (Hsu 1976; Trumm and Schroecke 1979). Also, ferberite crystallises from more acidic solutions, whereas hübnerite requires neutral to slightly alkaline conditions (Horner 1979).

Trapping temperatures and salinities obtained from fluid inclusions present in quartz from mineralised samples from the New Ross area belong to the range provided by Wood and Samson (2000). Pressure at the time of emplacement of the SMB was probably higher than the range postulated by Wood and Samson (2000), but these authors emphasise that

scheelite and ferberite solubilities are weak functions of pressure; therefore, higher pressures utilised for this study should not affect the solubility of W-bearing minerals. Farley (1978) reported wolframite compositions of $Fe_{0.8}Mn_{0.2}WO_4$ at the Walker deposit, suggesting that transporting fluids are more acidic and would be consistent with the pH range (4-6) compiled by Wood and Samson (2000) for the pH composition of W-mineralising fluids.

Uranium

Some U may replace Zr in zircon; because zircon forms early in the crystallisation history (hence at high temperature), U is initially compatible. Later in the crystallisation history, U behaves as an incompatible element and will concentrate in the melt. Also, a fluid phase must evolve prior to a shortage of O^{2-} in the melt (i.e., melt becoming more polymerised). If no fluid phase is present before the polymerisation level is too high, then U becomes saturated in the melt, and it will form U-bearing minerals (e.g., U oxides, apatite, titanite) (Farges et al. 1992) and will not be readily available for ore deposit formation.

An experiment controlling pH, a_{CO2}, and a_{SO4} for torbernite and autunite, the main U-bearing phases in the New Ross area, reveals that both minerals have a solubility minimum in neutral to weakly acidic conditions, depending on a_{CO2} and a_{SO4} (Fig 7.15) (Pakul'nis et al. 1986). The main physico-chemical factors controlling uraninite solubility are oxygen activity (a_{O2}) and pH at temperatures up to 200°C; decrease of a_{O2} and pH decrease uraninite solubility and deposition occurs (Kojima et al. 1994). Also, Pohl and Parks (1984) found that uraninite is not soluble at redox below the Ni-Ni oxide buffer and Yudintsev (1996) constrained the fO_2 of granitic magmas to values close to the QFM-NNO buffers, therefore, fO_2 is important. Parks and Pohl (1988) conducted experiments on uraninite solubility at hydrothermal temperatures (100-350°C). They noted that uraninite solubility in alkaline solutions is lower than previously stated and maximum solubility occurs at pH = 3 (Fig. 7.16). Most importantly, Parks and Pohl (1988) documented that uraninite solubility is independent of temperature. For uraninite to precipitate from a solution, the decrease in

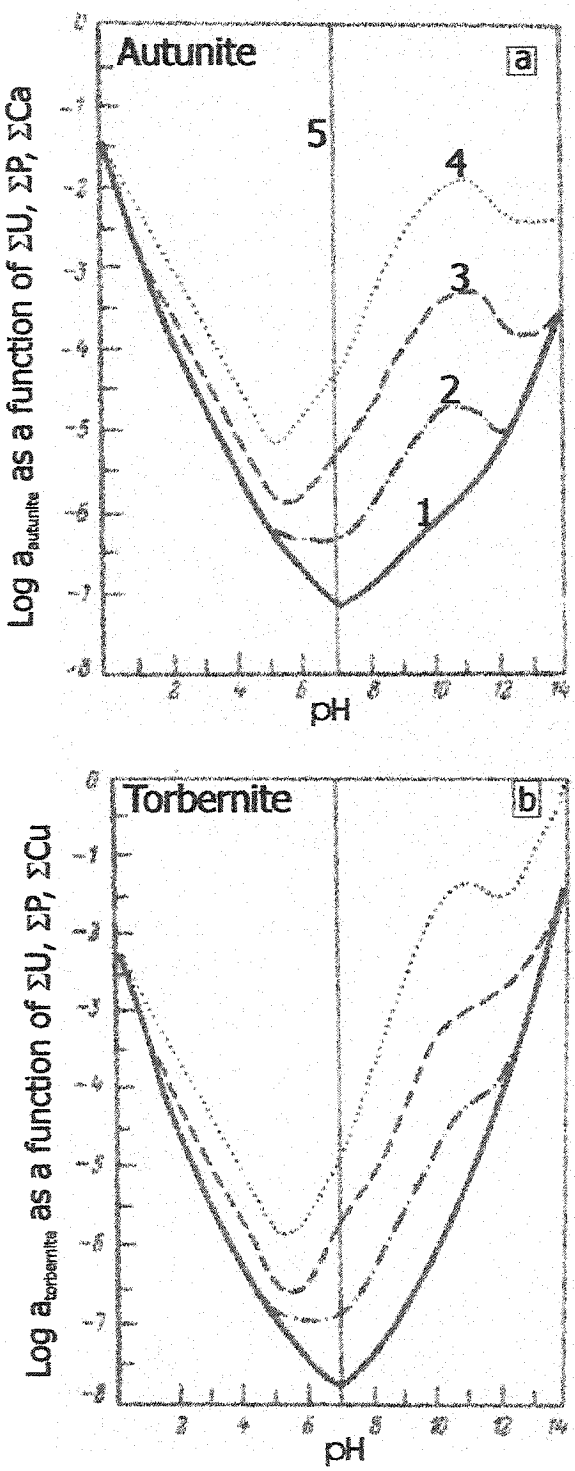

Figure 7.15: Solubility curves relating the solubility to the pH for autunite and torbernite for various possible cases of sulfate and carbonate solutions..
1) $a_{CO2} = a_{SO4} = 0$; 2) $a_{CO2} = a_{SO4} = 0.001$; 3) $a_{CO2} = a_{SO4} = 0.01$;
4) $a_{CO2} = a_{SO4} = 0.1$ mol/kg H_2O; 5) neutral line for water. From Pakul'nis et al. (1986).

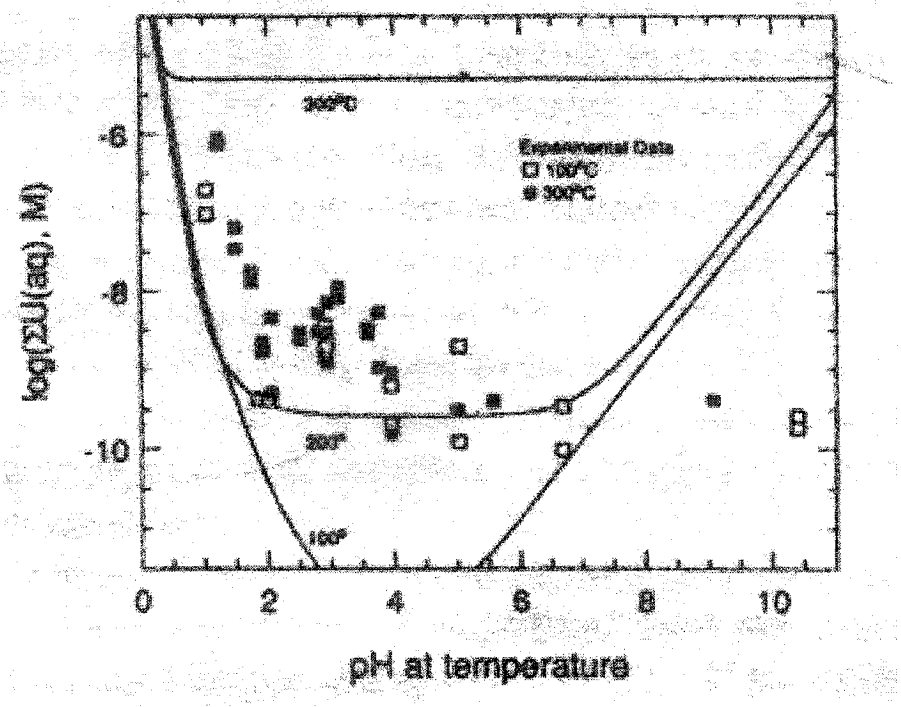

Figure 7.16: Computed (solid curve) and experimental (points) solubilities of UO_2 as a function of pH. The temperature dependence is lower than expected. Maximum solubility occurs at pH near 3. From Parks and Pohl (1988).

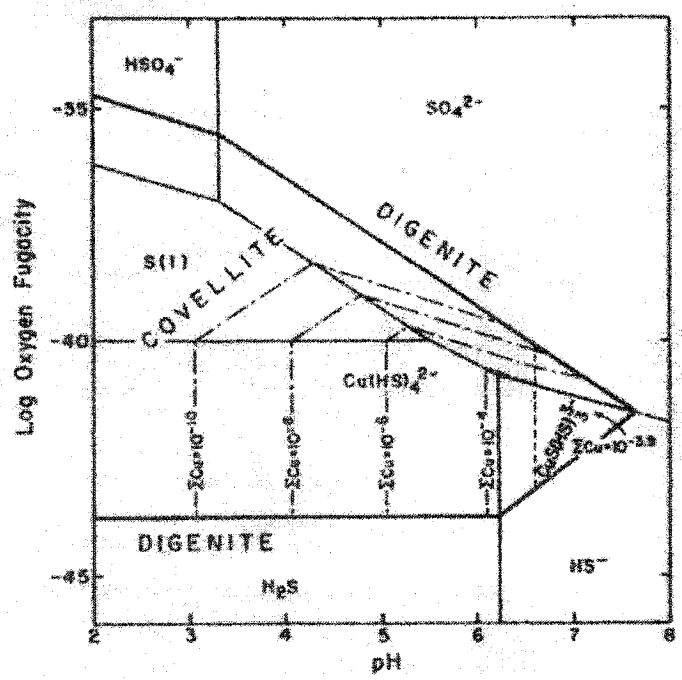

Figure 7.17: Equilibrium relations between covellite and digenite in aqueous solutions at 200°C and 0.25 *m* total S, as a function of pH and fO2. From Romberger and Barnes (1970).

activity of a ligand associated with the uranium (Cl^-, F^-, CO_2) is an obvious process. But a reaction such as

$$2U^{+5}O_2 + H_2O = 2U^{+4}O_2 + \frac{1}{2}O_2 + 2H^+$$

where H^+ and O_2 are consumed, increases UO_2 crystallisation (Dubessy et al. 1987). Mixing with a fluid having a low fO_2 may possibly explain the reduction process.

Copper and tin

As stated in Section 7.3.3.2, Cu may behave compatibly if no saline fluid phase is present. In the New Ross area, fluids exsolved early enough in the crystallisation history of the Walker and Turner deposit, because Cu-bearing sulphides at both locations crystallised late compared to other metal-bearing minerals (Farley 1978). Another possibility is that Cu was present as a trace element in biotite (substitution of Cu^{2+} for Fe^{2+}); alteration of biotite through fluid circulation in the New Ross pluton may have released the Cu into the fluid phase and redeposited it when favourable conditions occurred. Strong hematisation and muscovitisation in the vicinity of the mineral occurrences of the New Ross area illustrates the breakdown of biotite and remobilisation of the iron content of that mineral is evident (rusty colour of granitic rocks). Copper may well be mobilised similarly to Fe^{2+}, as Fe^{2+} is the element Cu substitutes for in biotite. Charest (1976) observed that the degree of alteration or abundance of biotite does not correlate with the copper content of whole rock samples; therefore, concentration of Cu directly in the melt appears as the most likely process for Cu concentration.

Sinclair (1972) did experiments to measure the solubility of chalcocite in aqueous chloride, sulphur-free solutions from 25° to 250°C. He noticed that solubility decreases with an increase in pH and also mentioned the possibility of dilution of the ore fluid (dilution will decrease a_{Cl}, therefore reducing complex formation) as a means for mineral deposition. Crerar and Barnes (1976) ran experiments at temperatures between 200° and 350°C and obtained results similar to those of Sinclair (1972) and added that an increase in S concentration, decrease in fO_2, and/or decrease in temperature allow for deposition of Cu-bearing sulphides when Cu is transported as chloride complexes. Xiao et al. (1998) and Liu et al. (2002) concluded from experiments between 40° and 350°C that decrease of temperature, a_{Cl}, and fO_2, and pH increase are the main mechanisms for chalcopyrite

deposition, and this especially in the temperature range 200° to 350°C. The solubility of covellite (Fig. 7.17) increases with increasing temperature, fO_2, and/or pH (Romberger and Barnes 1970).

Similarly to Cu, Sn may be present as a trace element in both white and black micas, replacing Fe^{3+} and/or Mg^{2+}. Again, it is difficult to evaluate what amount of the Sn concentration the alteration of biotite may have contributed. Biotite mainly alters to white mica and chlorite and both minerals could easily reintegrate the Sn present in biotite. Whole-rock geochemical analyses from least to most evolved fractions of the New Ross pluton show an increase in Sn content [geochemical analyses from Charest (1976) and MacDonald (2001)]. Such distribution of Sn throughout the pluton follows the increase of white mica modal proportion and decrease of biotite modal proportion, but both phenomena may only reflect the increase of differentiation of the melt and the incompatible character of Sn in the melt. Chemical analyses of rock types representing the melt composition, such as quenched glasses [e.g., ongonites, Antipin et al. (1981) or Macusani glasses, Pichavant et al. (1988b)] contain high concentrations of Sn (~50 ppm), as do melt inclusions in quartz from a peraluminous pegmatite (Webster et al. 1997).

Cassiterite solubility in hydrothermal fluids is temperature dependent up to 350°C (as temperature decreases, solubility decreases too) and not in the range 500°-750°C, but concurrent increase of pH and fO_2 strongly reduce cassiterite solubility (Fig. 7.18) (Jackson and Helgeson 1985; Eadington 1988; Wilson and Eugster 1990; Taylor and Wall 1993). Maximum cassiterite solubility will occur at redox conditions below the QFM buffer (Eadington 1988). Most pH-related solubility changes are linked to tin speciation: chloride complexes of tin dominate in acid solutions, whereas hydroxide complexes of tin dominate at intermediate to high pH (Jackson and Helgeson 1985). By quantifying the chemical changes in fluid composition during interaction with the leucogranitic host rock at the East Kemptville deposit, Halter et al. (1998) concluded that acid neutralisation (i.e., pH increase) because of fluid mixing is an efficient way to precipitate cassiterite.

Cassiterite mineralisation, and the New Ross area is no exception, occurs associated with acidic conditions, shown by acid-alteration assemblages such as greisenisation, alteration of feldspars to muscovite, and alteration of biotite to muscovite (Wilson and Eugster 1990). These types of alteration set the maximum pH of the ore-forming fluids at

below neutral (i.e., 4-5.5) where deposition occurs (Patterson et al. 1981; Jackson and Helgeson 1985; Wilson and Eugster 1990). Oxygen fugacities of the ore-forming fluids generally lie close to the QFM buffer (e.g., Patterson et al. 1981).

Manganese

Manganese is definitely the most difficult metal when considering its origin in mineral occurrences of the SMB. Several origins that may involve different fluid reservoirs for transportation are possible:

1) **External to the SMB**: The Meguma Supergroup consist of two major units (Goldenville and Halifax Groups) (Section 2.2.1.1). The transition between these units (called the Goldenville-Halifax transition or GHT) contains a finely laminated, manganiferous unit rich in calcareous nodules, quartzites, and sulphides in places (Graves and Zentilli 1988). These authors described the formation of the GHT as "the product of manganese carbonate precipitation from pore fluids near the sediment-water interface during early diagenesis by oxidation of organic matter". Spessartine garnets developed later at the expense of the carbonate, because of regional metamorphism (Graves and Zentilli 1988). Manganese oxide in garnet decreases significantly in the contact aureole surrounding the SMB (from 30 wt. % to 3.5 wt. %); similarly, the Mn content of biotite decreases with increasing metamorphic grade in the contact aureole, reflecting "dispersion" of Mn instead of concentration prior to garnet crystallisation (Cameron and Zentilli 1997). The presence of a fluid during such dispersion (e.g., a metamorphic fluid with high salinity, or a circulating magmatic fluid with intermediate salinity as discussed in Chapter 5) may have complexed the available Mn and transported it along fractures (i.e., Mn mines).
2) **Internal to the SMB**: Destruction of Mn-bearing magmatic minerals (biotite, ilmenite) during hydrothermal alteration may be a source for the metal. Pelrine (2003) reported high concentrations of Mn in ilmenite (pyrophanite) from the SMB. She showed the replacement of Mn for Fe in ilmenite (increase of Mn/(Mn+Fe)) accompanying increasing fractionation of the batholith. Alteration of pyrophanite may be a source of Mn in the New Ross area mineral deposits. Inherited ilmenite from assimilation of stoped blocks of Meguma metasedimentary rocks could also provide Mn if digestion of

those blocks occurs. Manganese from such xenocrystic ilmenite would then technically be external to the SMB, although when Mn is leached the ilmenite already belongs to the SMB. Similarly to Cu and Sn, Mn can replace Fe in biotite and hydrothermal alteration of such Mn-enriched biotite will release the Mn in the fluid phase. Again, hematisation, muscovitisation, and/or episyenitisation are different types of alteration present in the vicinity of the Mn mines in the New Ross area. O'Reilly (1992) noted the decrease of Mn and Fe concentration from unaltered to altered (hematised) samples in the Salmontail Lake monzogranite, host granitoid rock for the Mn mines.

In summary, manganese in the New Ross area may have a mixed origin, with some of the metal originating from leaching of minerals in the GHT, and some from alteration of ilmenite and/or biotite in the granite (origin of the ilmenite also possibly mixed from inherited ilmenite from the Meguma or from magmatic ilmenite).

Virtually no solubility data exist for Mn-bearing minerals (pyrolusite, manganite, psilomelane) present in the mineral deposits of the SMB. Crerar et al. (1980), cited in Gammons and Seward (1996), stated that Mn oxides are stable only at very high oxidation state, suggesting that an increase in fO_2 will reduce their solubility (Fig. 7.19).

7.3.5.4. Summary and conclusions

Table 7.5 summarises the information of Sections 7.3.3.2 and 7.3.5.2. The following generalisations are possible:

1. Two variables generally decrease the solubility of minerals: a decrease in temperature and a decrease in the ligand concentration (by dilution for example) in the fluid phase;
2. Oxidation allows for precipitation of Mn and Sn oxides, whereas reduction allows for precipitation of Cu sulphides and uraninite;
3. Increasing pH of the fluid phase allows for precipitation of Cu sulphides (except covellite), cassiterite, and tungstates, whereas decreasing pH of the fluid phase allows for precipitation of uraninite; and
4. Near neutral to slightly acidic conditions allow for precipitation of the U-phosphates, autunite and torbernite.

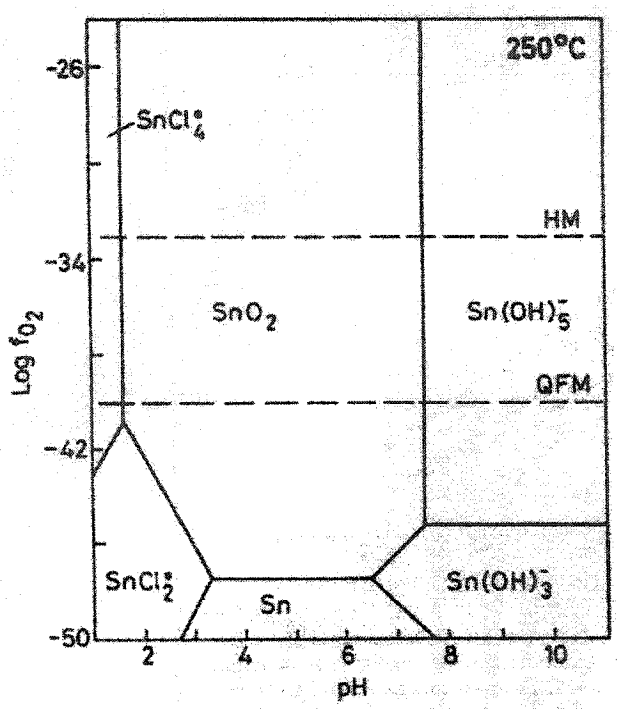

Figure 7.18: Equilibrium phase diagram for cassiterite and some chloro- and hydroxy-complexes of Sn at 250°C. Boundaries of the complexes are drawn at an activity of 10^{-3}, $a_{Cl^-} = 1$. From Eadington (1988).

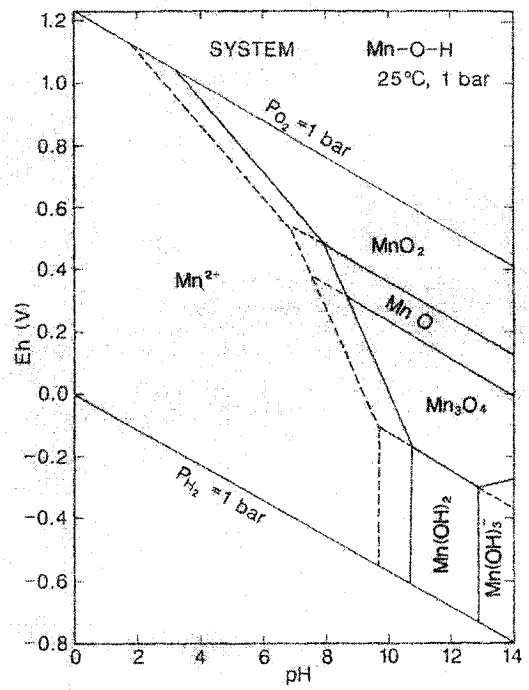

Figure 7.19: Example of an Eh-pH diagram for part of the system Mn-O-H at 25°C and 1 bar. Most of the field is occupied by Mn^{2+}, and the oxides and oxyhydroxides of Mn become important under basic pH except at high Eh. From Brookins (1988).

Element names	Main control(s) of partitioning between melt and solid phase prior to fluid phase evolution	Main control(s) of partitioning between melt and fluid phase	Main mineral(s)	Main control(s) for mineral precipitation
Symbol				
F	N/A	N/A	N/A	N/A
Cl	N/A	N/A	N/A	N/A
Mn	N/A	N/A	pyrolusite MnO_2	- fO_2 (increase)
Cu	fO_2 (increase favours partitioning in melt)	simple presence of a fluid phase favours partitioning in fluid)	chalcocite Cu_2S chalcopyrite $CuFeS_2$ covellite CuS	- pH (increase except decrease for covellite) - S^- concentration (increase) - Cl^- concentration (decrease) - fO_2 (decrease) - temperature (decrease)
Mo	fO_2 (increase favours partitioning in melt)	Cl, F (absence favours partitioning in fluid)	molybdenite MoS_2	- temperature, Cl^- concentration (contradictory experimental results)
Sn	fO_2 (increase favours partitioning in solid phase)	Cl^- concentration (increase favours partitioning in melt)	cassiterite SnO_2	- fO_2 (increase) - pH (increase) -temperature (decrease) - peraluminosity (decrease)
W	fO_2 (increase favours partitioning in solid phase)	N/A	wolframite $(Fe, Mn)WO_4$ scheelite $CaWO_4$	- temperature (decrease) - Cl^- concentration (decrease) - pH (increase)
U	Polymerisation level, F^- (increase favours partitioning in melt)	Cl^- concentration (increase favours partitioning in fluid)	uraninite UO_2	- fO_2 (decrease in acidic to neutral solutions) - a_{O2} (decrease) - pH (decrease in alkaline solutions) - Cl^-, F^-, CO_3^{2-} concentration (decrease)

Table 7.5: Main controls of metals and ligand partitioning from the melt into solid or fluid phase, and main control of mineral deposition.

7.3.6. Formation of mineral deposits in the New Ross area

The formation of hydrothermal mineral deposits involves the uptake of metals in a fluid, their transport, and their release from the transporting fluid. Each of these stages depends on a set of variables including temperature, pressure, composition of fluid, composition of host rock, redox conditions, and pH. The way these variables evolve through time, as the magmatic body cools, dictates the solubility of metal-bearing minerals. The mineral occurrences of the New Ross area each have a unique assemblage of metal-bearing minerals, providing clues to decipher the conditions at the time of deposition. Section 7.3.5 provided a framework narrowing down the possible origin of both fluids and metals. The following two Sections attempt to integrate the information provided above into a comprehensive mineralisation model for the main mineral occurrences of the New Ross area. The locations chosen for this model are: (i) Walker (aplite/pegmatite with some greisenisation around) illustrating the beginning of the magmatic to hydrothermal transition, (ii) Long Lake (mostly greisen) exemplifying a more mature hydrothermal system, (iii) Turner (greisen within veins) showing the link between a greisen and vein mineralised system, and (iv) Mn mines and Millet Brook (veins) illustrating "pure" end-member vein deposits.

Before dealing with the main mineral occurrences of the New Ross area in more detail, I note the following points:

1. All deposits have a host rock with fO_2 slightly reducing, as calculated using Mössbauer spectroscopy of biotite from the SMB (Shabani 1999). This fO_2 condition represents the conditions prevailing at temperature above the solidus and may vary at the temperature of mineralisation;
2. Fluid inclusions from all deposits contain at least some low salinity fluid (0 wt. % NaCl) characteristic of a meteoric fluid with stable isotope data showing the influence of increasing amounts of meteoric water as the system evolved from magmatic to hydrothermal. Also, fluid inclusions from vein deposits are dominated by the meteoric fluid;

3. All vein deposits (Mn mines, Millet Brook, and Turner) have a host rock that was strongly hematised in the vicinity of the mineralised areas, indicating an increase in fO_2 (i.e., fluid inducing hematisation was oxidising);
4. The main phase(s) of hydrothermal activity leading to polymetallic mineralization occurred in close temporal relationship to granite emplacement for all mineral occurrences.

Considering the New Ross area deposits arranged by deposit style (aplite/pegmatite, greisen, and vein), the following suite of metals occurs from most to least abundant (this order may vary slightly when considering a single mineral occurrence):

- aplite/pegmatite: Mo, W, Cu, Sn, U
- greisen: Cu, Sn, W, Mo
- vein: Mn, U, Cu, Sn, W

Greisen is generally associated with aplite/pegmatite deposit types; consequently Section 7.3.6.1 deals with both deposit types for the Walker, Long Lake, and Turner deposits, whereas Section 7.3.6.2 examines the Mn mines and Millet Brook deposits for the vein type.

7.3.6.1. Aplite/pegmatite and greisen deposits

Walker

As described in Section 7.3.2.3, Cu sulphides are present in both aplite/pegmatite and greisen, whereas molybdenite is predominantly associated with aplite/pegmatite and wolframite and cassiterite occur principally in greisen. Also, the presence of abundant tourmaline and topaz within the greisen suggests strong concentrations of volatiles (B, F). The greisen occurs as pods around the aplite/pegmatite, but greisenisation of aplitic and pegmatitic samples, as well as geochronological results (Chapter 4), suggest that the greisenisation process occurs simultaneously with aplite/pegmatite emplacement. Molybdenite and Cu sulphides are the metal-bearing minerals present in the aplite/pegmatite. Oxygen fugacity of the crystallising magma is the main factor controlling the "separation" of Mo and Cu from W and Sn: if a fluid phase is already present, a decrease in fO_2 during magmatic crystallisation favours the partitioning of Mo and Cu towards the fluid phase, whereas W and Sn will partition towards the melt phase (Candela

1992). This process may account for the dominant (but not exclusive) presence of Mo and Cu in aplite/pegmatite and of W and Sn in the greisen. The molybdenum and copper partition towards the fluid phase earlier than the tungsten and tin as fO_2 decreases and, as fO_2 stabilises (or increases) in the melt, the tungsten and tin commence to partition towards the fluid phase as well.

With careful petrographic observations of the greisen, Farley (1978) noted that molybdenite, wolframite, and cassiterite crystallised earlier than covellite. A common precipitating factor for the three first minerals is an increase of pH, whereas covellite precipitates with a decreasing pH. Episodically (i.e., when H_2O saturation is reached) a fluid evolves from the crystallising magma; it is typically HCl-rich and contains the metals that are favourably partitioned into the fluid phase (depending on the conditions listed in Section 7.3.3). Interaction of such acidic fluid with minerals already crystallised in the granite (i) neutralises the HCl (i.e., increases the pH of the fluid), (ii) produces a fluid rich in NaCl, KCl, $CaCl_2$, and other metal chlorides (Eugster 1985), (iii) alters the crystallised granite (i.e., acidic alteration such as greisenisation), and (iv) enhances the deposition of cassiterite and wolframite. An increase in pH will also favour the dissociation of H_2S, which in turn increases the concentration of aqueous sulphide, making it available for precipitation of molybdenite. Finally, precipitation of sulphide minerals eventually decreases the pH of the fluid (Reed 1997), allowing for precipitation of covellite. The temperature decrease accompanying the cooling of the area impedes dissolution of already precipitated oxides and sulphides. Strongly hematised zones in the vicinity of the Walker deposit show that fO_2 was elevated, another variable favouring cassiterite precipitation. The progressive infiltration of a meteoric fluid, marking the transition between the magmatic and the hydrothermal stages of the system, had the dual effect of being oxidising and of decreasing chlorine concentration, both processes that most likely added to the pH effect in favouring precipitation of the metal-bearing minerals.

Long Lake

The Long Lake prospect is a larger, more extensively greisenised, area than the Walker prospect and, as suggested by O'Reilly et al. (1982) and Logothetis (1985), because of the vicinity of Long Lake to the Meguma Supergroup, probably represents a cupola of

greisenised leucogranite where volatiles accumulated and incompatible elements concentrated. Molybdenite is the dominant metal-bearing mineral in the aplite/pegmatite at Long Lake. Other oxides and sulphides (including molybdenite) are disseminated within the greisen, in places within quartz-rich vugs. The disseminated character of the mineralisation impedes the determination of a clear paragenesis, but the fact that pyrite, chalcopyrite, and molybdenite are disseminated within the greisen, whereas wolframite and scheelite occur along fractures and within pods suggests that Fe-, Cu-, and Mo-sulphides crystallised earlier than the tungstates. As previously explained for the Walker deposit, decreasing fO_2 of the crystallising magma may have kept W in the melt, whereas Cu and Mo were able to partition towards the fluid phase. Deposition occurred in the greisen as the pH of the fluid phase increased because of greisenisation of the granitic host rock. Stabilisation and/or increase of fO_2 may then have allowed for W partitioning, transport, and deposition as greisenisation still occurred so that the pH continued to increase. Table 7.6 confirms that the controls for pyrite precipitation do not contradict those stated above: Rafal'skiy (1985) proposed that pH increase is a factor favouring pyrite precipitation, whereas fO_2 of the fluid phase does not influence pyrite solubility. As at Walker, the presence of meteoric fluid in fluid inclusions from mineralised samples from Long Lake probably facilitated precipitation of the metal-bearing minerals.

Turner

The Turner occurrence (with the exception of the Elvan dyke, discussed below) comprises quartz veins along which a greisenising fluid circulated and deposited metal-bearing minerals. Farley (1978) provided the following order of crystallisation for sulphides and oxides: pyrite, sphalerite, chalcopyrite and cassiterite, and covellite. A model of alternation of acidity-basicity involving vein deposition similar to that proposed by Shcherba (1970) in Kazakhstan appears as a possible process for ore-bearing mineral deposition at Turner: (i) pyrite precipitates from a fluid phase because of a pH increase (caused by greisenisation when acidic fluid interacts with host rock) (Table 7.6); (ii) sphalerite precipitates in response to pH decrease (caused by the precipitation of pyrite) (Table 7.6); (iii) both chalcopyrite and cassiterite precipitate because of a pH increase

Element names	Preferred complex in H_2O	Main mineral(s)	Main control(s) for mineral precipitation	References
Fe	$FeCl^+$, $FeCl_2$, $FeCl_3^-$	magnetite pyrite	-T (decrease) -Cl^- concentration (decrease) -pH (increase) -independent from fO_2	Chou and Eugster (1977), Helz and Barnes (1970), Wang et al. (1984), Rafal'skiy (1985)
Zn	$ZnCl^+$, $ZnCl_2$, $ZnCl_3^-$, $ZnCl_4^{2-}$, $Zn(HS)_2$, $Zn(HS)_3$, $Zn(HS)_4^{2-}$, $ZnS(OH)(HS)_2^-$, $Zn(OH)(HS)_3^{2-}$	sphalerite	-S concentration at lower temperature for S complexes (decrease) -Cl concentration at higher temperature for Cl complexes (decrease) -temperature (decrease) -pH (decrease)	Hayashi et al. (1990)

Table 7.6 Main controls for Fe- and Zn-bearing mineral deposition.

(caused by further greisenisation), and (iv) covellite precipitates in response to a pH decrease (caused by the precipitation of chalcopyrite). Fluid inclusions at the Turner deposit (Chapter 5) revealed the presence of a dominantly meteoric fluid, which decreased Cl concentration by dilution.

The Elvan dyke, containing a low concentration of Sn (Charest 1976), has a finer-grained aplitic texture and strikes in the same direction as the quartz-greisen veins at Turner. Similar dykes occur in the Cornwall Sn domain (e.g., Henley 1972; Henley 1974; Hawkes et al. 1975; Thorne and Edwards 1985) and in the Massif Central of France (Raimbault and Burnol 1998) and Clarke and Bogutyn (2003) suggested that they represent a possible extrusive event caused by release of overpressured water, as recorded by epitactically zoned micas in the nearby Lake Lewis leucogranite.

7.3.6.2. Vein deposits

Mn mines

The Mn mineralisation is located along northeast-trending faults and occurs as a vein-type deposit. O'Reilly (1992) provided a detailed description of the main Mn oxides present in the deposit: both manganite and pyrolusite occur with some pyrolusite (not all) obviously replacing the manganite. Replacement of manganite by pyrolusite involves oxidation of Mn^{3+} to Mn^{4+} and, therefore, an increase in fO_2. Also, hematite is present, indicating oxidising conditions of mineral precipitation at the Mn mines. O'Reilly (1992) dealt with the supergene (meteoric)-hypogene (magmatic) origin of the fluid phase that

deposited the Mn oxides. He made a case for the fluid being of hypogene origin based on the high-temperature alteration (greisenisation, silicification, K-feldspathisation, albitisation, episyenitisation) assemblages within the Mn mines, on the presence of other granophile elements (e.g., Sn, U, Cu, W), and the association of the veins with the Gold River leucomonzogranite. A fluid inclusion study (Chapter 5) revealed that a meteoric fluid of fairly high temperature (i.e., 300°C) dominates the Mn mines. Such a fluid might have travelled at depth along deep-penetrating faults. Therefore, the deep-penetrating meteoric fluid may reach higher temperatures than expected (in contact with the granite), allowing for the alteration types encountered. Also, meteoric fluids would be oxidising, therefore, providing the necessary environment for the deposition of Mn oxides. Such a scenario favours either an origin for the Mn external to the SMB or an origin from the alteration of ilmenite and/or biotite in the granite, or both, rather than being directly partitioned from the melt into the fluid phase (Section 7.3.5.3).

Millet Brook

Similarly to the Mn mines, the Millet Brook deposit is located along northeast-trending faults and occurs as a vein-type deposit. The U^{4+} chloride appears as the most stable complex at temperatures above 200°C in acidic solution (Dubessy et al. 1987). We observed no CO_2 in the fluid inclusions in the Millet Brook samples (Carruzzo et al. 2000, Chapter 5), therefore, monocarbonate complexing may be ruled out. Phosphate complexes of U are stable, even with low concentration of P [Nguyen-Trung (1985) cited in Dubessy et al. (1987)]. Other metal-bearing minerals (chalcopyrite, covellite, chalcocite, wolframite) present at the Millet Brook deposit precipitated as pH increased, a process contrary to the conditions necessary for uraninite precipitation (Dubessy et al. 1987). Also, no evidence for a decrease of fO_2 exists at the Millet Brook deposit. The presence of U phosphates (torbernite and autunite) at the Millet Brook deposit suggests that phosphate complexes are a viable possibility for U transport in acidic fluids. A decrease in the P activity would therefore involve precipitation of U-bearing minerals (Fig 7.20). As shown by fluid inclusion data (Chapter 5), a meteoric fluid dominates the fluid phase at the Millet Brook deposit, therefore, a process of strong dilution of P-bearing magmatic fluid at a pressure ~ 3 kbar (Section 7.3.3.1) is possible. Uranium may have originated in the nearby Lake Lewis

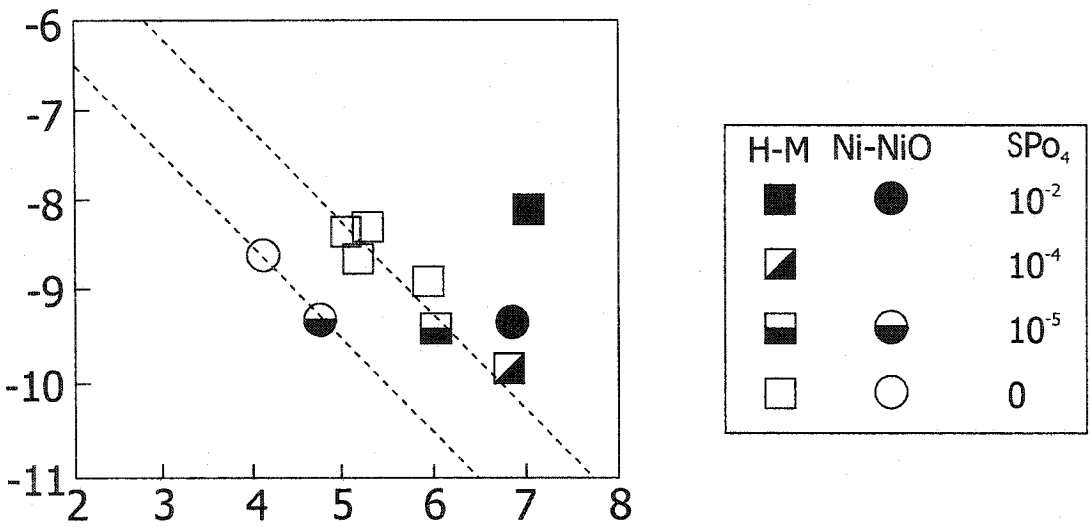

Figure 7.20: UO_2 solubility at 400°C as a function of room temperature pH with hematite-magnetite (H-M) and Nickel-nickel oxide (Ni-NiO) buffers: (1) in the pure water system: continuous and dashed lines established for different pH using boric acid, and (2) in the H_2O-PO_4 system, the numbers give the bulk phosphate concentration in log molal unit. From Dubessy et al. (1987).

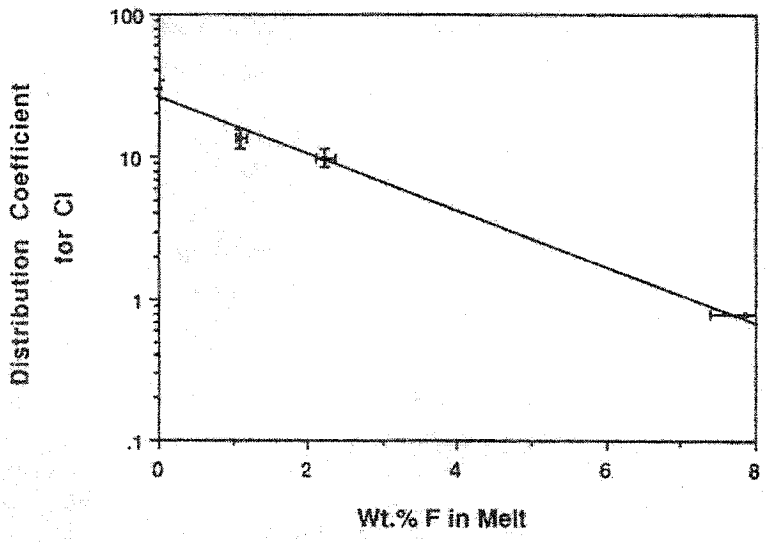

Figure 7.21: Graph of the decrease in D_{Cl} with increasing F concentration of the melt for experiments conducted on haplogranite glass at 2 kbar. From Webster and Holloway (1988).

leucogranite, as proposed by Chatterjee et al. (1982): circulation of meteoric fluids along fractures (similar to the Mn mines) would allow for such uranium stripping to happen.

7.3.6.3. Fluorine, an ubiquitous element

Fluorine is a common element crystallising its own minerals (e.g., fluorite, topaz) at each studied location and is also present in large concentrations in micas from the New Ross area (Carruzzo et al. 1998; Clarke and Bogutyn in press), although, at first sight, it is not strongly involved with metal transport or metal-bearing mineral precipitation. Most experimental petrologists agree that the increase of F in the melt favours the partitioning of metals towards the melt (Section 7.3.3.1). Also, F impedes the partitioning of Cl towards the fluid phase (e.g., Webster and Holloway 1988, 1990 and Fig. 7.21), therefore retaining the most important ligand in the melt (hence retaining incompatible metals that would complex with Cl). This process has the consequence of concentrating F, Cl, and incompatibles in the melt until the F concentration reaches saturation and topaz and other F-bearing minerals start crystallising. At that point, Cl will partition towards the fluid phase, complexed with incompatibles.

7.3.6.4. Relationship between mineral occurrences in the New Ross area

The aplite/pegmatite and greisen type deposits of the New Ross area are spatially and temporally (Chapter 4) related. This chapter demonstrates that the principal factor for mineral deposition (i.e., pH variation) is common to both types of deposits. Other factors (fO_2, temperature decrease) also play an important role for ore mineral precipitation. A transition to vein deposits seems possible with the Turner deposit where, again, pH appears as the main control for mineral precipitation. The main difference to favour such transition is the intense channelling of meteoric fluids within the faults hosting the vein deposits. As suggested by MacDonald (2001), the Mn mines and Millet Brook may represent the upper part of buried greisenised cupolas similar to that now exposed at the Long Lake deposit and in other areas within the SMB (e.g., Kempt Snare Lake). If this is the case, a genetic link between vein deposits and aplite/pegmatite and greisen deposit may well exist. In such a

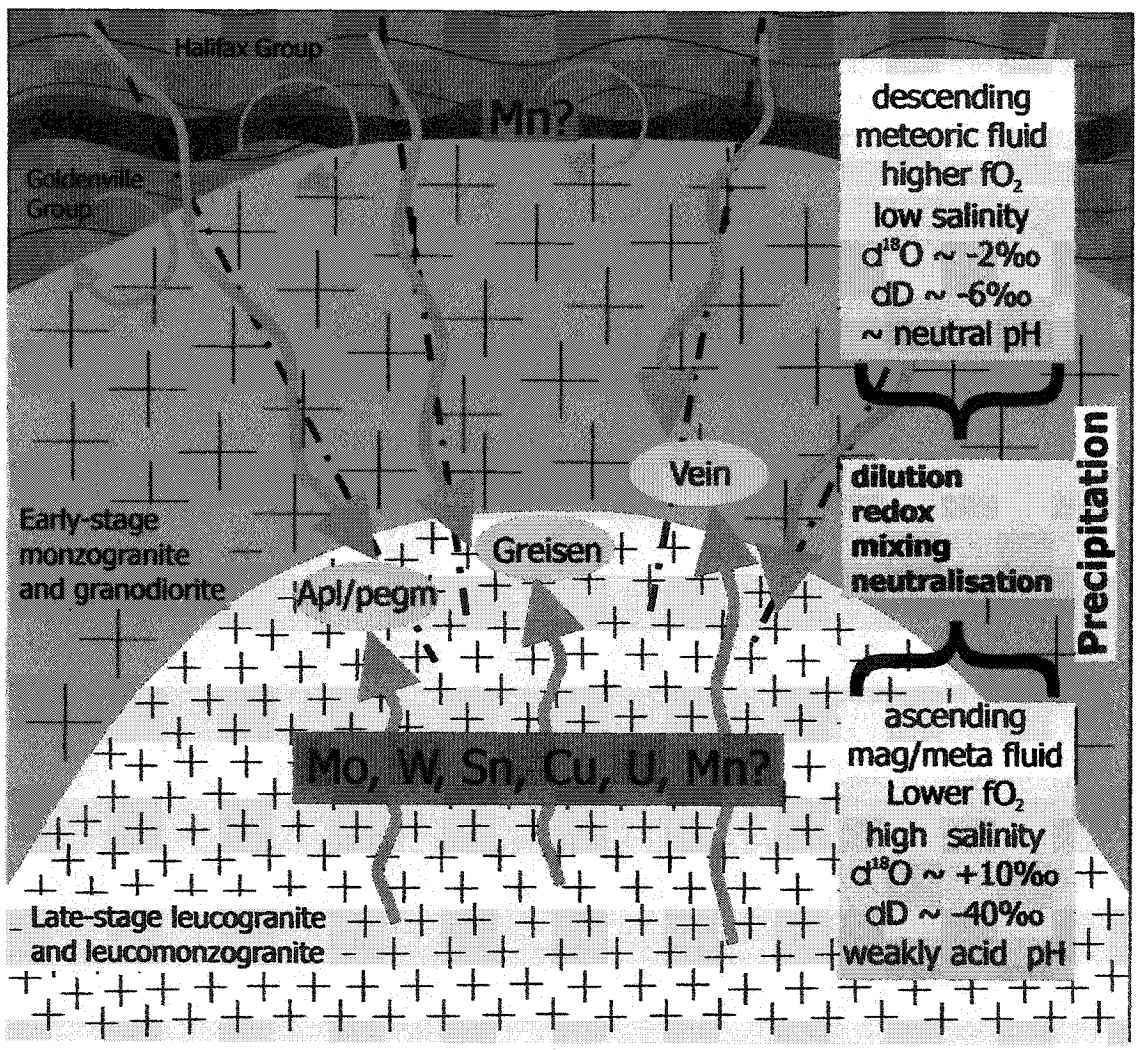

Figure 7.22: "Fluid interaction" model described above for the different mineral deposit types of the New Ross area, with pH variations and dilution (creating a cooler and more oxidising environment) by meteoric fluids as the main controls on mineralisation processes. Cooler, more oxidising descending fluids penetrate at depth along deep-penetrating faults, while hotter ascending fluids of magmatic origin collide with the meteoric fluids, allowing for mineralisation to occur. Type of mineralisation mainly depends on the amount of meteoric fluid present.

model, the upper part of the granitic body, more fractured, would facilitate the circulation of meteoric fluids downwards, therefore explaining the dominance of such a fluid within the vein deposits that they would reach first. At depth, the meteoric fluid would be increasingly mixed with hot, upwards-driven magmatic (and eventually of metamorphic) fluids, therefore, explaining the difference of metal concentration from bottom to top of the system. Both fluid inclusions and stable isotopes show that such fluid mixing is present in samples from the New Ross area. No evidence supporting fluid unmixing was found in the fluid inclusion study (Chapter 5), therefore, second boiling is not considered in this model as a possible process for pH variation. Figure 7.22 illustrates the "fluid interaction" model described above for the different mineral deposit types of the New Ross area, with pH variations and dilution (creating a cooler and more oxidising environment) by meteoric fluids as the main controls on mineralisation processes.

7.4. Conclusions

As evidenced by major, trace, REE elements, and stable and radiogenic isotopes, the mineralogical and geochemical diversity in the New Ross area results from fractional crystallisation, contamination, and hydrothermal alteration.

Metal concentration, transport, and deposition depend on numerous physico-chemical factors affecting their behaviour from their origin to their final destination, with hydrothermal fluids as the transporting agent. Chlorine and hydroxide appear as the main ligands for metal transportation in the New Ross area. Deposition strongly depends on pH conditions at the contact between hydrothermal fluids and host granitoid rocks. Also, variations in redox conditions, triggered by incursion of increasing amounts of meteoric fluid along deep-penetrating faults as the system evolves from magmatic to hydrothermal, play an important part in metal precipitation. Over ~10 My, the concurrence of highly evolved granitic melts rich in incompatible elements in the late-stage of granite emplacement with intense fluids circulation, particularly those of meteoric origin, allowed for the formation of the New Ross mineralised aplite/pegmatite, greisen, and vein deposits.

CHAPTER 8

CONCLUSIONS AND RECOMMENDATIONS

8.1. Conclusions

The main conclusions of this thesis are as follows:

1) Chemical differences among white micas from differently evolved fractions of the New Ross pluton do not correlate well to the textural characteristics of the white mica, but rather to the bulk composition of the granitoid rock in which the white mica is present: white micas from granitoid rocks have narrower range of biotitic and Tschermak substitutions than their hosted mineralised and altered rocks.
2) Single-grain Ar/Ar laserprobe ages of white micas from samples from the mineral occurrences of the New Ross area range between 382 and 320 Ma. Molybdenite Re/Os ages on two pegmatite samples are 377 ± 3 Ma and 371 ± 3 Ma. The age of crystallisation of the SMB is older than previously determined, because the dated samples correspond to the latest pulse of magma emplaced. The main phases of hydrothermal activity leading to polymetallic mineralisation occurred in close temporal relationship to granite crystallisation, and episodic tectonic-thermal-hydrothermal events took place ~371 Ma and ~320 Ma, partially resetting the Ar/Ar system. K-feldspar Ar/Ar ages reveal that the isotopic system was reset in most cases, because of the low closure temperature of that mineral.
3) Three different fluids are present in most mineral deposits of the New Ross area: (i) a magmatic fluid evolved from the late-stage granitoid rocks; (ii) a Ca-rich metamorphic fluid originating from the Meguma Supergroup metasedimentary rocks during granite intrusion; and (iii) a meteoric fluid that interacted with the two previous fluids in variable proportions. Fluid mixing occurred, implying that the three fluids were contemporaneous, therefore, all were present at the time of SMB emplacement. The range of homogenisation temperature values for pegmatite and greisen type deposits reflects an isobaric (3 kbar, the pressure at the time of SMB

emplacement) decrease in entrapment temperatures between 550° and 200°C. For vein type deposits, the inferred trapping temperatures require a pressure lower than 3 kbar, suggesting the presence of deeply penetrating fractures to generate hydrostatic pressures only.

4) The isotopic compositions ($\delta^{18}O$, δD) of white mica from host granitoid rocks, pegmatite/aplite, greisen, and vein samples along with δD values for fluid inclusion extracts from quartz in the same samples, record a transition from a magmatic-dominated, low water : rock ratio system to a hydrothermal-dominated, higher water : rock ratio system into which meteoric water infiltrated at the time of SMB emplacement, crystallisation, and greisen/vein formation. The evolution of fluids from a magmatic to hydrothermal regime within the New Ross area is as follows: (i) exsolution of a magmatic fluid at ~ 650°C; (ii) before cooling to ~400-500°C, incursion of a meteoric fluid via faults with subsequent mixing with magmatic and metamorphic fluids through fluid circulation by convection; and (iii) incursion of a late, low δD meteoric fluid some time after cooling of the area
5) Metal concentration, transport, and deposition depend on numerous physico-chemical factors affecting their behaviour from their origin to their final destination, with hydrothermal fluids acting as the transporting agent. Chlorine and hydroxide appear as the main ligands for metal transportation in the New Ross area. Deposition depends strongly on pH conditions of the hydrothermal fluids at the contact with host granitoid rocks. Also, variations in redox conditions, triggered by incursion of increasing amounts of meteoric fluid along deep-penetrating faults as the system evolves from magmatic to hydrothermal, play an important part in metal precipitation. In summary, ascending magmatic fluids mix with descending meteoric fluids, with the potential presence of a metamorphic fluid originating in the metasediments of the Meguma Supergroup. Over ~10 Ma, the concurrence of highly evolved granitic melts rich in incompatible elements in the late-stage of granite emplacement with intense fluid circulation, and more particularly the increasing amount of fluids of meteoric origin, allowed for the formation of the New Ross mineralised aplite/pegmatite, greisen, and vein deposits.

8.2. Recommendations for future work

Throughout this investigation, the following points calling for further work arose:

1) A trace element study of texturally primary and secondary white mica might help to identify a characteristically primary chemical composition, which would be different (hence slightly or not at all overlapping) from a secondary chemical composition. The ideal would be to base the discrimination between both groups more on their chemical composition and less on equivocal textural criteria.
2) White mica single-grain Ar/Ar laserprobe dating should be done in other areas of the SMB, in order to relate the ages obtained in the New Ross area to the entire batholith. Also, further Re/Os on mineralised samples from the SMB is on the way and will provide a basis of comparison with this study. Dating of the mineralisation at the vein deposits would be an asset (using U/Pb on tantalite for example).
3) More careful (or rather more successful) sampling of quartz grains may allow for better quality study of fluid inclusions and, therefore, for establishment of a relative chronology among fluid inclusion assemblages. Using ICP-MS on fluid inclusions may allow for the geochemical characterisation of the different fluids present in the New Ross area.
4) A clear determination of the isotopic composition of all potential fluids interacting within the MLT is needed to reach a better understanding of fluid reservoirs involved in mineralising processes. In particular, the knowledge of δD values for the Meguma Supergroup is important.

REFERENCES

Afifi, A.A. and Clark, V. (1990): Computer-aided multivariate analysis **1**, Van Nostrand Reinhold Company, London, 480 pp.

Antipin, V.S., Kovalenko, V.I., Kuznetsova, A.I. and Persikova, L.A. (1981): Distribution coefficients for tin and tungsten in ore-bearing acid igneous rocks. Geochemistry International **18**, 92-106.

Atkins, P. (1994): Physical chemistry **1**, W. H. Freeman and Company, Oxford, 1031 pp.

Attendorn, H.-G. and Bowen, R.N.C. (1997): Radioactive and stable isotope geology **1**, Chapman & Hall, New York, 522 pp.

Bai, T.B. and Koster van Groos, A.F. (1999): The distributions of Na, K, Rb, Sr, Al, Ge, Cu, W, Mo, La, and Ce between granitic melts and coexisting aqueous fluids. Geochimica et Cosmochimica Acta **63**, 1117-1131.

Baker, D.E.L. (1996): Fluid inclusions and microstructure of flexural-slip bedding-concordant veins within the Ovens Anticline, Lunenburg, Nova Scotia, Honours Thesis, Dalhousie University, Halifax.

Barnes, H.L. (1979): Solubilities of ore minerals. *In* H.L. Barnes (ed) *Geochemistry of hydrothermal ore deposits*, Wiley-Interscience, New York, 404-460.

Barrett, A.M. (1985): Report on exploration and development histories. AR 85-086, NSDNR, Halifax.

Bates, R.L. and Jackson, J.A. (1987): Glossary of geology **1**, American Geological Institute, Alexandria, Virginia, 788 pp.

Benn, K., Horne, R.J., Kontak, D.J., Pignotta, G.S. and Evans, N.G. (1997): Syn-Acadian emplacement model for the South Mountain Batholith, Meguma terrane, Nova Scotia: magnetic fabric and structural analyses. GSA Bulletin **109**, 1279-1293.

Benn, K., Roest, W.R., Rochette, P., Evans, N.G. and Pignotta, G.S. (1999): Geophysical and structural signatures of syntectonic batholith construction: the South Mountain Batholith, Meguma Terrane, Nova Scotia. Geophysical Journal International **136**, 144-158.

Bishop, D.G. and Wright, J.D. (1974): Geology and trace element studies of manganese occurrences in Nova Scotia, NSDNR, Halifax.

Blevin, P.L. and Chappell, B.W. (1992): The role of magma sources, oxidation states and fractionation in determining the granite metallogeny of eastern Australia. Geological Society of America Special Paper **272**, 305-316.

Boctor, N.Z. (1985): Rhodonite solubility and thermodynamic properties of aqueous $MnCl_2$ in the system MnO-SiO_2-HCl-H_2O. Geochimica and Cosmochimica Acta **49**, 565-575.

Bodnar, R.J. (1993): Revised equation and table for determining the freezing point depression of H_2O-NaCl solutions. Geochimica et Cosmochimica Acta **57**, 683-684.

Bodnar, R.J. and Vityk, M.O. (1994): Interpretation of microthermometric data for H_2O-NaCl fluid inclusions. *In* Short Course of the working group (IMA) Pontignano, Siena, 117-131.

Bodnar, R.J., Reynolds, T.J. and Kuehn, C.A. (1985): Fluid-inclusion systematics in epithermal systems. Reviews in Economic Geology **2**, 73-97.

Bogutyn, P.A. (2001): White micas in the Lake Lewis leucogranite, Nova Scotia, Honours Thesis, Dalhousie University, Halifax.

Bottinga, Y. and Javoy, M. (1973): Comments on oxygen isotope geothermometry. Earth and Planetary Science Letters **20**, 250-265.

Boullier, A.-M., Firdaous, K. and Robert, F. (1998): On the significance of aqueous fluid inclusion in gold-bearing quartz vein deposits from the southeastern Abitibi Subprovince (Quebec, Canada). Economic Geology **93**, 216-223.

Bouton, S.L., Candela, P.A., Weidner, J.R. and Joseph, J. (1987): Experimental determination of the partitioning of tungsten and molybdenum between a high silica melt and Ti-bearing minerals. Abstracts with programs **19**, 596.

Bouyx, E., Blaise, J., Brice, D., Gourvennec, R., Lardeux, H. LeMenn, J. (1992): Implications paleogeographiques des affinites nord-gondwaniennes et rhenanes des faunes devoniennes de la zone de Meguma (Appalaches septentrionales). Comptes-Rendus de l'Academie des Sciences de Paris **315**, 337-343.

Bouyx, E., Blaise J., Brice, D., Degardin, D. M., Goujet, D., Gourvennec, R., Le Menn, J., Lardeux, H., Morzadec, P., Paris, F. (1997): Biostratigraphie et paleobiogeographie du Siluro-Devonien de la zone de Meguma (Nouvelle-Ecosse, Canada). Canadian Journal of Earth Sciences **34**, 1295-1309.

Brimhall, G.H. and Crerar, D.A. (1987): Ore fluids: magmatic to supergene. *In* I.S.E. Carmichael and H.P. Eugster (eds) *Thermodynamic modeling of geological materials: minerals, fluids and melts*, Reviews in Mineralogy. Mineralogical Society of America, 235-321.

Burnham, C.W. (1979): Magmas and hydrothermal fluids. *In* H.L. Barnes (ed) *Geochemistry of hydrothermal ore deposits*, John Wiley and Sons, New York, 71-136.

Burnham, C.W. and Ohmoto, H. (1980): Late-stage processes of felsic magmatism. Mining Geology Special Issue **8**, 1-11.

Burt, D.M. (1981): Acidity-salinity diagrams-Application to greisen and porphyry deposits. Economic Geology **76**, 832-843.

Cameron, B.I. and Zentilli, M. (1997): Geochemical characterization of the mineralized transition between the Goldenville and Halifax Formations and the interaction with adjacent granitoid intrusions of the Liscomb Complex, Nova Scotia. Maritime Sediments and Atlantic Geology **33**, 143-155.

Cameron, J.R. (1949): The New Ross area. NSDME Annual report, 119-127.

Cameron, J.R. (1950): The New Ross area. 119-127, NSDME, Halifax.

Campbell, C.O. (1940): New Ross pegmatite. 21A/16B 51-L-19(00), NSDME, Halifax.

Candela, P.A. (1989a): Felsic magmas, volatiles, and metallogenesis. *In* J.A. Whitney and A.J. Naldrett (eds) *Ore deposition associated with magmas*, Reviews in Economic Geology. Society of Economic Geologists, 223-233.

Candela, P.A. (1989b): Magmatic ore-forming fluids: thermodynamic and mass transfer calculations of metal concentrations. *In* J.A. Whitney and A.J. Naldrett (eds) *Ore deposition associated with magmas*, Reviews in Economic Geology. Society of Economic Geologists, 203-221.

Candela, P.A. (1992): Controls on ore metal ratios in granite-related ore systems: an experimental and computational approach. Geological Society of America Special Paper **272**, 317-326.

Candela, P.A. (1997): A review of shallow, ore-related granites: textures, volatiles, and ore metals. Journal of Petrology **38**, 1619-1633.

Candela, P.A. and Bouton, S.L. (1990): The influence of oxygen fugacity on tungsten and molybdenum partitioning between silicate melts and ilmenite. Economic Geology **85**, 633-640.

Candela, P.A. and Holland, H.D. (1981a): Cu and Mo in silicate melt - aqueous fluid systems. EOS **62**, 413.

Candela, P.A. and Holland, H.D. (1981b): The effect of fluorine on the partitioning of molybdenum between a magma and a hydrothermal fluid. Abstracts with Programs **13**, 422.

Candela, P.A. and Holland, H.D. (1982): The partitioning of copper and molybdenum between magmas and hydrothermal fluids. Abstracts with Programs **14**, 458.

Candela, P.A. and Holland, H.D. (1984): The partitioning of copper and molybdenum between silicate melts and aqueous fluids. Geochimica and Cosmochimica Acta **48**, 373-380.

Candela, P.A. and Holland, H.D. (1986): A mass transfer model for copper and molybdenum in magmatic hydrothermal systems: the origin of porphyry-type ore deposits. Economic Geology **81**, 1-19.

Cao, X., Richardson, S.M. and Richardson, C.K. (1988): Solubility of molybdenite (MoS_2) in hydrothermal solutions. Abstracts with Programs **20**, 43.

Carroll, M.R. and Webster, J.D. (1994): Solubilities of sulfur, noble gases, nitrogen, chlorine, and fluorine in magmas. *In* M.R. Carroll and J.R. Holloway (eds) *Volatiles in magmas*, Reviews in Mineralogy. Mineralogical Society of America, Washington, 231-279.

Carruzzo, S., Reynolds, P.H., Clarke, D.B., O'Reilly, G.R., Speller, R.H. (1998): Granite-hosted mineral deposits of the New Ross area, South Mountain Batholith (SMB), Nova Scotia: field observations and preliminary white mica dating. 1998-2, NSDNR, Halifax.

Carruzzo, S., Kontak, D.J., Clarke, D.B. (2000): Granite-hosted mineral deposits of the New Ross area, South Mountain Batholith, Nova Scotia, Canada: P, T, and X constraints of fluids using fluid inclusion thermometry and decrepitate analysis. Transactions of the Royal Society of Edinburgh, Earth Sciences **91**, 303-319.

Carruzzo, S., Kontak, D.J., Kyser, K., Clarke, D.B. (2003): An integrated stable isotope and fluid inclusion study of granite-hosted mineral deposits of the New Ross area, South Mountain Batholith, Nova Scotia, Canada: evidence for multiple fluid reservoirs. Canadian Mineralogist. **In press.**

Cathelineau, M. (1985): Episyenitisation ou dequartzification hydrothermal: une typologie basee sur les successions minerales et sur le comportement differentiel de Si, Na et K. Comptes-Rendus de l'Academie des Sciences Paris **300**, 677-680.

Cerny, P. and Burt, D.M. (1984): Paragenesis, crystallochemical characteristics, and geochemical evolution of micas in granite pegmatites. *In* P.H. Ribbe (ed) *Micas* . Mineralogical Society of America, 257-297.

Charest, M.H. (1976): Petrology, geochemistry, and mineralization of the New Ross area, Lunenburg County, Nova Scotia, MSc Thesis, Dalhousie University, Halifax.

Charoy, B. and Ramboz, C. (1981): A model for the geochemical balance in greisenisation processes. Terra Cognita Special Issue, 94.

Chatterjee, A.K. and Cormier, R.F. (1991): A Rb-Sr geochronological study of the Davis Lake pluton, South Mountain Batholith, southern Nova Scotia: evidence for a 374 Ma time of emplacement. 91-A, NSDNR, Halifax.

Chatterjee, A.K. and Dostal, J. (1995): Lead isotope evidence for a short-lived hydrothermal system in an epizonal granite batholith, Meguma Terrane, Nova Scotia. Program with Abstracts **20**, 16.

Chatterjee, A.K. and Ham, L.J. (1991): U-Th-Pb systematics of the South Mountain Batholith, Nova Scotia. Atlantic Geology **27**, 149.

Chatterjee, A.K. and MacDonald, M.A. (1991): Contrasting greisens and associated granitoid rocks of the Davis Lake pluton: implications for the origin of the East Kemptville tin deposit, Nova Scotia. Atlantic Geology **27**, 150.

Chatterjee, A.K. and Muecke, G.K. (1982).:Geochemistry and the distribution of uranium and thorium in the granitoid rocks of the South Mountain Batholith, Nova Scotia: some genetic and exploration implications. 81-1, NSDNR, Halifax.

Chatterjee, A.K. and Strong, D.F. (1984): Discriminant and factor analysis of geochemical data from granitoid rocks hosting the Millet Brook uranium mineralization, South Mountain Batholith, Nova Scotia. Uranium **1**, 289-305.

Chatterjee, A.K., Robertson, J. and Pollock, D. (1982): A summary on the petrometallogenesis of the uranium mineralization at Millet Brook, South Mountain Batholith, Nova Scotia. 82-1, NSDME report, Halifax.

Chatterjee, A.K., Strong, D. F., Clarke, D. B., Robertson, J., Pollock, D., Muecke G. K., (1985): Geochemistry of the granodiorite hosting uranium mineralization at Millet Brook. 85-3, NSDNR, Halifax.

Chatterjee, N.D. and Johannes, W. (1974): Thermal stability and standard thermodynamic properties of synthetic 2M1-muscovite, $KAl_2[AlSi_3O_{10}(OH)_2]$. Contributions to Mineralogy and Petrology **48**, 89-114.

Chevychelov, V. (1996): The influence of the granitoid melt composition on the partitioning of W, Mo in the systems melt-chloride fluid and melt-fluoride fluid. Terra Nova **1**, 12.

Clark, G.L. and Hawley, G.G. (1966): The encyclopaedia of chemistry **1**, Van Nostrand Reinhold Company, New York, 1144 pp.

Clarke, D.B. (1992): Granitoid rocks. Topics in Earth Sciences **7**, Chapman & Hall, New York, 283 pp.

Clarke, D. B. (2003): Exploded xenoliths, layered granodiorites, and chaotic schlieren associated with the eastern contact of the South Mountain Batholith. Geological Society of America - Atlantic Geoscience Society Field Trip Guidebook 403, Halifax '03, 26 pp.

Clarke, D.B. and Bogutyn, P.A. (2003): Oscillatory epitactic zoning in biotite and muscovite from the Lake Lewis leucogranite, South Mountain Batholith, Nova Scotia. Canadian Mineralogist **in press**.

Clarke, D.B. and Chatterjee, A.K. (1988): Physical and chemical processes in the South Mountain Batholith. *In* R. P. Taylor, D. F. Strong (eds) *Recent advances in the geology of granite-related mineral deposits*. Canadian Institute of Mining and Metallurgy **39**, 223-233.

Clarke, D.B. and Halliday, A.N. (1980): Strontium isotope geology of the South Mountain Batholith, Nova Scotia. Geochimica et Cosmochimica Acta **44**, 1045-1058.

Clarke, D.B. and Halliday, A.N. (1985): Sm/Nd isotopic investigation of the age and origin of the Meguma Zone metasedimentary rocks. Canadian Journal of Earth Sciences **22**, 102-107.

Clarke, D.B. and Muecke, G.K. (1985): Review of the petrochemistry and origin of the South Mountain Batholith and associated plutons, Nova Scotia, Canada. *In* High heat production (HHP) granites, hydrothermal circulation and ore genesis. Institution of Mining and Metallurgy, St. Austell, Cornwall, England, 41-54.

Clarke, D.B., McKenzie, C.B., Muecke, G.K. and Richardson, S.W. (1976): Magmatic andalusite from the South Mountain Batholith, Nova Scotia. Contributions to Mineralogy and Petrology **56**, 279-287.

Clarke, D.B., Muecke, G.K. and Chatterjee, A.K. (1985): The South Mountain Batholith: geology, petrology, geochemistry. 650, NSDNR, Halifax.

Clarke, D.B., Halliday, A.N. and Hamilton, P.J. (1988): Neodymium and strontium isotopic constraints on the origin of the peraluminous granitoids of the South Mountain Batholith, Nova Scotia, Canada. Chemical Geology **73**, 15-24.

Clarke, D.B., Chatterjee, A.K. and Giles, P.S. (1993a): Petrochemistry, tectonic history, and Sr-Nd systematics of the Liscomb Complex, Meguma Lithotectonic Zone, Nova Scotia. Canadian Journal of Earth Sciences **30**, 449-464.

Clarke, D.B., MacDonald, M.A., Reynolds, P.H. and Longstaffe, F.J. (1993b): Leucogranites from the Eastern part of the South Mountain Batholith, Nova Scotia. Journal of Petrology **34**, 653-679.

Clarke, D.B., MacDonald, M.A. and Tate, M.C. (1997): Late Devonian mafic-felsic magmatism in the Meguma Zone, Nova Scotia. Geological Society of America Memoir **191**, 107-127.

Clarke, D.B., Henry, A.S. and White, M.A. (1998): Exploding xenoliths and the absence of "elephants' graveyards" in granite batholiths. *In* K. Benn, A.R. Cruden, E.W. Sawyer and J.P. Evans (eds) *Extraction, transport and emplacement of granitic magmas*, Journal of Structural Geology. Pergamon, Oxford-New York, 1325-1343.

Clarke, D.B., Fallon, R. and Heaman, L.M. (2000): Interaction among upper crustal, lower crustal, and mantle materials in the Port Mouton pluton, Meguma Lithotectonic Zone, southwest Nova Scotia. Canadian Journal of Earth Sciences **37**, 579-600.

Clarke, D. B. et al. (2003): Occurrence and origin of andalusite in peraluminous felsic igneous rocks. Journal of Petrology. **In press.**

Cline, J.S. and Bodnar, R.J. (1991): Can economic porphyry copper mineralization be generated by a typical calc-alkaline melt? Journal of Geophysical Research **96**, 8113-8126.

Corey, M.C. (1991): Chester, sheet 21A/09. NSDNR, Halifax.

Corey, M.C. and Chatterjee, A.K. (1990): Characteristics of REE and other trace elements in response to successive and superimposed metasomatism within a portion of the South Mountain Batholith, Nova Scotia, Canada. Chemical Geology **85**, 265-285.

Cormier, R.F. and Smith, T.E. (1973): Radiometric ages of granitic rocks , Southwestern Nova Scotia. Canadian Journal of Earth Sciences **10**, 12011210.

Cormier, R.F., Keppie, J.D. and Odom, A.L. (1988): U-Pb and Rb-Sr geochronology of the Wedgeport granitoid pluton, soutwestern Nova Scotia. Canadian Journal of Earth Sciences **25**, 255-261.

Craig, H. (1961): Isotopic variations in meteoric waters. Science **133**, 1702-1703.

Creaser, R.A., Papanastassiou, D.A. and Wasserburg, G.J. (1991): Negative thermal ion mass spectrometry of osmium, rhenium and iridium. Geochimica and Cosmochimica Acta **55**, 397-401.

Crerar, D.A. and Barnes, H.L. (1976): Ore solution chemistry V: solubilities of chalcopyrite and chalcocite assemblages in hydrothermal solution at 200 to 350 C. Economic Geology **71**, 772-794.

Crerar, D.A., Cormick, R.K. and Barnes, H.L. (1980): Geochemistry of manganese; an overview. Schweizerbart'sche Verlagsbuchhandlung, 293-334.

Crerar, D.A., Wood, S., Brantley, S. and Bocarsly, A. (1985): Chemical controls on solubility of ore-forming minerals in hydrothermal solutions. Canadian Mineralogist **23**, 333-352.

Criss, R. E. and Taylor, H. P. Jr (1983): An $^{18}O/^{16}O$ and D/H study of Tertiary hydrothermal systems in the southern half of the Idaho Batholith. Geological Society of America Bulletin **94**, 640-663.

Culshaw, N. and Bhatnagar, P. (2001): The interplay of regional structure and emplacement mechanisms at the contact of the South Mountain Batholith, Nova Scotia: floor-down or wall-up? Canadian Journal of Earth Sciences **38**, 1285-1299.

Culshaw, N. and Liesa, M. (1997): Alleghanian reactivation of the Acadian fold belt, Meguma Zone, southwest Nova Scotia. Canadian Journal of Earth Sciences **34**, 833-847.

Culshaw, N. and Reynolds, P.H. (1997): $^{40}Ar/^{39}Ar$ age of shear zones in the southwest Meguma Zone between Yarmouth and Meteghan, Nova Scotia. Canadian Journal of Earth Sciences **34**, 848-853.

Cuney, M., Marignac, C. and Weisbrod, A. (1992): The Beauvoir topaz-lepidolite albite granite (Massif Central, France): the disseminated magmatic Sn-Li-Ta-Nb-be mineralization. Economic Geology **87**, 1766-1794.

Currie, K.L., Whalen, J.B., Davis, W.J., Longstaffe, F.J. and Cousens, B.L. (1998): Geochemical evolution of peraluminous plutons in southern Nova Scotia, Canada - a pegmatite-poor suite. Lithos **44**, 117-140.

Dallmeyer, R.D. and Keppie, J.D. (1987): Polyphase late Paleozoic tectonothermal evolution of the southwestern Meguma terrane, Nova Scotia: evidence from $^{40}Ar/^{39}Ar$ mineral ages. Canadian Journal of Earth Sciences **24**, 1242-1254.

Dallmeyer, R.D. and Keppie, J.D. (1988): Superposed Late Paleozoic thermal events in the southwestern Meguma Terrane, Nova Scotia. Maritime Sediments and Atlantic Geology **24**, 157-169.

Davis, D.W., Lowenstein, T.K. and Spencer, R.J. (1990): Melting behavior of fluid inclusions in laboratory-grown halite crystals in the systems NaCl-H_2O, NaCl-KCl-H_2O, NaCl-$MgCl_2$-H_2O, and NaCl-$CaCl_2$-H_2O. Geochimica and Cosmochimica Acta **54**, 591-601.

Deer, W.A., Howie, R.A. and Zussman, J. (1992): An introduction to the rock-forming minerals 1, Longmans, London, 515 pp.

Dempster, T.J., Tanner, P.W.G. and Ainsworth, P. (1994): Chemical zoning of white micas: a record of fluid infiltration in the Oughterard granite western Ireland. American Mineralogist **79**, 536-544.

Ding, Y. (1995): AFM minerals in the Halifax Pluton, MSc Thesis, Dalhousie University, Halifax.

Dingwell, D.B. (1985): The structures and properties of fluorine-rich magmas: a review of experimental studies. *In* R.P. Taylor and D.F. Strong (eds) *Recent advances in the geology of granite-related mineral deposits*, Canadian institute of Mining and Metallurgy, Halifax, 1-12.

Dingwell, D.B. and Scarfe, C.M. (1983): Major element partitioning in the system haplogranite-HF-H_2O - implications for leucogranites and high-silica rhyolites. EOS **64**, 342.

Dinnett, L. (1995): Stable isotope (O, H, S, and C) and geochemical study of the Kempt Snare Lake mineral prospect, southwestern Nova Scotia., MSc Thesis, Dalhousie University, Halifax.

Dodson M. H. (1973): Closure temperature in cooling geochronological and petrological systems . Contributions to Mineralogy and Petrology **40**, 259-274.

Dostal, J. and Chatterjee, A.K. (1995): origin of topaz-bearing and related peraluminous granites of the Late Devonian Davis Lake pluton, Nova Scotia, Canada: crystal versus fluid fractionation. Chemical Geology **123**, 67-88.

Douglas, G.V. and Campbell, C.O. (1941a): New Ross area. NSDME Annual Report, 101-112.

Douglas, G.V. and Campbell, C.O. (1941b): New Ross manganese deposits. NSDNR Annual Report, 93-100.

Drummond, S.E. and Ohmoto, H. (1985): Chemical evolution and mineral deposition in boiling hydrothermal systems. Economic Geology **80**, 126-147.

Dubessy, J., Ramboz, C., Nguyen-Trung, C., Cathelineau, M., Charoy, B., Cuney, M., Leroy, J., Poty, B., Weisbrod, A. (1987): Physical and chemical controls (fO_2, T, pH) of the opposite behaviour of U and Sn-W as exemplified by hydrothermal deposits in France and Great Britain, and solubility data. Bulletin de Mineralogie **110**, 261-281.

Duncan, D.R. (1983): Manganese, New Ross, Lunenburg County, Nova Scotia. 21A/16B 31-L-19 (23), Kidd Creek Mines Limited, Halifax.

Dvorak, Z. and Fraser, D.C. (1979): Uranium, Millet Brook, Hants and Lunenburg County, Nova Scotia. AR 21A/16B 54-I-64(04), NSDNR, Halifax.

Eadington, P.J. (1988): The solubility of cassiterite in hydrothermal solutions in relation to some lithological and mineral associations of tin ores. *In* R.P. Taylor and D.F. Strong (eds) *Recent advances in the geology of granite-related mineral deposits*, Canadian Institute of Mining and Metallurgy, Halifax, 25-32.

Eardley-Wilmot, V.L. (1925): Molybdenum. 592, Canada Mines branch.

Eberz, G.W., Clarke, D.B., Chatterjee, A.K. and Giles, P.S. (1991): Chemical and isotopic composition of the lower crust beneath the Meguma Lithotectonic Zone, Nova Scotia: evidence from granulite facies xenoliths. Contributions to Mineralogy and Petrology **109**, 69-88.

Elias, P. (1986): Thermal history of the Meguma Terrane: a study based on $^{40}Ar/^{39}Ar$ and fission track dating, PhD Thesis, Dalhousie University, Halifax.

Ellsworth, H.V. (1932): Rare element minerals of Canada. Economic Geology series **11**, 255-256.

Ellsworth, H.V. (1950): Uranium, New Ross, Lunenburg County. 21A/16B 54-L-19 (00), NSDME, Halifax.

Eugster, H.P. (1985): Granite and hydrothermal ore deposits: a geochemical framework. Mineralogical Magazine **49**, 7-23.

Eugster, H.P. (1986): Minerals in hot water. American Mineralogist **71**, 655-673.

Eugster, H.P. and Wilson, G.A. (1985): Transport and deposition of ore-forming elements in hydrothermal systems associated with granites. *In* High heat production (HHP) granites, hydrothermal circulation and ore genesis. Institution of Mining and Metallurgy, St. Austell, Cornwall, England, 87-98.

Fairbairn, H.W., Hurley, P.M., Pinson, W.H. and Cormier, R.F. (1960): Age of the granitic rocks of Nova Scotia. Geological Society of America Bulletin **71**, 399-414.

Fairbairn, H.W., Hurley, P.M. and Pinson, W.H. (1964): Preliminary age study and initial $^{87}Sr/^{86}Sr$ of Nova Scotia granitic rocks by the Rb-Sr whole-rock method. Geological Society of America Bulletin **75**, 253-258.

Fallon, R.P. (1998): Age and thermal history of the Port Mouton Pluton, Southwest Nova Scotia: a combined U-Pb, $^{40}Ar/^{39}Ar$ age spectrum, and $^{40}Ar/^{39}Ar$ laserprobe study, MSc Thesis, Dalhousie University, Halifax.

Fallon, R.P., Reynolds, P.H. and Clarke, D.B. (2001): A comparative $^{40}Ar/^{39}Ar$ conventional and laserprobe study of muscovite from the Port Mouton pluton, southwest Nova Scotia. Canadian Journal of Earth Sciences **38**, 347-357.

Farges, F., Ponader, C.W., Calas, G. and Brown, G.E. (1992): Structural environments of incompatible elements in silicate glass / melt systems: II. UIV, UV, and UVI. Geochimica and Cosmochimica Acta **56**, 4205-4220.

Faribault, E.R. (1907): New Ross tin deposits, GSC.

Faribault, E.R. (1910): Tin and Manganese at New Ross, GSC, Halifax.

Faribault, E.R. (1911): New Ross. GSC Summary Report, 339-340.

Faribault, E.W. (1917): New Ross, Lunenburg. GSC Summary Report, 27-28.

Faribault, E.R. (1924): Chester Basin sheet. GSC, Halifax.

Faribault, E.R. (1931): New Ross sheet, map # 86. GSC Publication, Halifax.

Farley, E. (1978): Mineralization at the Turner and Walker deposits, South Mountain Batholith, MSc Thesis, Dalhousie University, Halifax.

Faure, G. (1991): Principles and applications of inorganic geochemistry **1**, MacMillan, New York, 626 pp.

Felderhof (1978): Forties Settlement (Reeves tin Prospect). Bulletin NSDME, 349-358.

Fisher, L.D. and Van Belle, G.V. (1993): Biostatistics: a methodology for the health sciences **1**, Wiley and Sons, New York, 991 pp.

Fleck, R.J., Sutter, J.F. and Elliot, D.H. (1977): Interpretation of discordant $^{40}Ar/^{39}Ar$ age-spectra of Mesozoic tholeiites from Antarctica. Geochimica and Cosmochimica Acta **41**, 15-32.

Flynn, R.T. and Burnham, C.W. (1978): An experimental determination of rare earth partition coefficients between a chloride containing vapour phase and silicate melts. Geochimica and Cosmochimica Acta **42**, 685-701.

Foland, K.A. (1974): Alkali diffusion in orthoclase. Carnegie Institution of Washington Publication **634**, 77-98.

Foland, K.A. (1994): Argon diffusion in feldspars. NATO ASI Series. Series C: Mathematical and Physical Sciences **421**, 415-447.

Ford, K.L. and O'Reilly, G.A. (1985): Airborne gamma-ray spectrometric surveys as an indicator of granophile element specialization and associated mineral deposits in the granitic rocks of the Meguma Zone of Nova Scotia, Canada. *In* High heat

production (HHP) granites, hydrothermal circulation and ore genesis. Institution of Mining and Metallurgy, St. Austell, Cornwall, England, 113-133.

Foucault, A. and Raoult, J.-F. (1988): Dictionnaire de geologie **1**, Masson, Paris, 352 pp.

Fournier, R.O. (1999): Hydrothermal processes related to movement of fluid from plastic into brittle rock in the magmatic-epithermal environment. Economic Geology **94**, 1193-1211.

Frei, R., Nagler, T.F., Schonberg, R. and Kramers, J.D. (1998): Re-Os, Sm-Nd, U-Pb, and stepwise lead leaching isotope systematics in shear-zone hosted gold mineralization: genetic tracing and age constraints of crustal hydrothermal activity. Geochimica and Cosmochimica Acta **62**, 1925-1936.

Gammons, C.H. and Seward, T.M. (1996): Stability of manganese (II) chloride complexes from 25 to 300°C. Geochimica and Cosmochimica Acta **60**, 4295-4311.

Gammons, C.H., Xiao, Z. and Williams-Jones, A.E. (1996): Solubility of copper and gold in magmatic -epithermal systems. Abstracts with Programs **28**, A402.

Garland, G.D. (1953): Gravity measurements in the Maritime provinces. Dominion Observatory of Canada Publications **16**, 185-275.

Geyh, M.A. and Schleicher, H. (1990): Absolute age determination : physical and chemical dating methods and their application **1**, Springer-Verlag, Berlin, 503 pp.

Gibling, M.R. (1995): Upper Paleozoic rocks, Nova Scotia. *In* H. Williams (ed) *Geology of the Appalachian-Caledonian orogen in Canada and Greenland*, Geological Survey of Canada, 493-523.

Giletti, B.J. (1986): Diffusion effects on oxygen isotope temperatures of slowly cooled igneous and metamorphic rocks. Earth and Planetary Science Letters **77**, 218-228.

Gleeson, S. A., Roberts, S., Grant, K., Fallick, A. E., Boyce A. J. (2002): The origin of anomalously low fluid inclusion δD values in hydrothermal quartz veins. Program with Abstracts PACROFI, 28-29.

Goldstein, R.H. and Reynolds, T.J. (1994): Systematics of fluid inclusions in diagenetic minerals. SEPM Short Course **31**, Tulsa, Oklahoma, 199 pp.

Gomes, M.E.P. and Neiva, A.M.R. (2000): Chemical zoning of muscovite from the Ervedosa granite, northern Portugal. Mineralogical Magazine **64**, 347-358.

Graves, M.C. and Zentilli, M. (1988): The lithochemistry of metal-enriched coticules in the Goldenville-Halifax transition zone of the Meguma Group, Nova Scotia. Current research, Part B, 251-261.

Graves, R.M. (1982): Manganese, New Ross, Lunenburg County, Nova Scotia. 21A/16B 31-L-19 (21), Kidd Creek Mines Limited, Halifax.

Graves, R.M. (1983): Manganese, New Ross, Lunenburg County, Nova Scotia. 21A/16B 31-L-19 (22), Kidd Creek Mines Limited, Halifax.

Green, T.H. (1981): Synthetic high-pressure micas compositionally intermediate between the dioctahedral and trioctahedral mica series. Contributions to Mineralogy and Petrology **78**, 452-458.

Grenthe, I., Fuger, J., Konings, J. M., Muller, A. B., Nguyen-Trung, C., Wanner, H. (1992): Chemical thermodynamics of uranium, Chemical Thermodynamics Series **1**, North Holland, 734 pp.

Guidotti, C.V. and Sassi, F.P. (1998a): Miscellaneous isomorphous substitutions in Na-K white micas: a review, with special emphasis to metamorphic micas. Atti della Accademia Nazionale dei Lincei. Rendiconti Lincei. Scienze Fisiche e Naturali **9**, 57-78.

Guidotti, C.V. and Sassi, F.P. (1998b): Petrogenetic significance of Na-K white mica mineralogy: recent advances for metamorphic rocks. European Journal of Mineralogy **10**, 815-854.

Guidotti, C.V. and Sassi, F.P. (2002): Constraints on studies of metamorphic K-Na white micas. *In* A. Mottana, F.P. Sassi, J.B. Thompson and S. Guggenheim (eds) *Micas: crystal chemistry & Metamorphic petrology*, Reviews in Mineralogy & Geochemistry. Mineralogical Society of America, Washington, 413-462.

Guilbert, J.M. and Park, C.F. (1986): The geology of ore deposits **1**, Freeman and Cie, New York, 985 pp .

Halter, W.E. and Williams-Jones, A.E. (1999): Application of topaz-muscovite F-OH exchange as a geothermometer. Economic Geology **94**, 1249-1258.

Halter, W.E., Williams-Jones, A.E. and Kontak, D.J. (1995): Origin and evolution of the greisenizing fluid at the East Kemptville tin deposit, Nova Scotia, Canada. Economic Geology **93**, 1026-1051.

Halter, W.E., Williams-Jones, A.E. and Kontak, D.J. (1996): The role of greisenization in cassiterite precipitation at the East Kemptville tin deposit, Nova Scotia. Economic Geology **91**, 368-385.

Halter, W.E., Williams-Jones, A.E. and Kontak, D.J. (1998): Modeling fluid-rock interaction during greisenization at the East Kemptville tin deposit: implications for mineralization. Chemical Geology **150**, 1-17.

Ham, L.J. (1991): Windsor (west half), 21A/16. NSDNR, Halifax.

Ham, L.J. and Kontak, D.J. (1988): A textural and chemical study of white mica in the South Mountain Batholith, Nova Scotia: primary versus secondary origin. Maritime sediments and Atlantic Geology **24**, 111-121.

Ham, L.J., Marsh, S.W., Corey, M.C., Horne, R.J. and MacDonald, M.A. (1989): Lithogeochemistry of the eastern portion of the South Mountain Batholith, Nova Scotia. 89-001, NSDNR, Halifax.

Hames, W.E. and Cheney, J.T. (1997): On the loss of $^{40}Ar^{*}$ from muscovite during polymetamorphism. Geochimica and Cosmochimica Acta **61**, 3863-3872.

Hanes, J.A. (1991): K-Ar and $^{40}Ar/^{39}Ar$ geochronology: methods and applications. *In* L. Heaman and J.N. Ludden (eds) *Short course handbook on applications of radiogenic isotope systems to problems in geology*, Mineralogical Association of Canada, 27-57.

Hanson, G. (1932): Manganese deposits of Canada. Canada Geological Survey Economic Geology Serie **12**, 53-61.

Harper, C.L. (1988): On the nature of time in the cosmological perspective, PhD Thesis, Oxford University, London.

Hawkes, J.R., Harding, R.R. and Darbyshire, D.P.F. (1975): Petrology and Rb/Sr age of the Brannel, South Crofty and Wherry elvan dykes, Cornwall. Bulletin of the Geological Survey of Great Britain **52**, 27-42.

Haynes, F.M. and Kesler, S.E. (1987): Chemical evolution of brines during Mississippi Valley-Type mineralization: evidence form East Tennessee and Pine Point. Economic Geology **82**, 53-71.

Haynes, F.M., Sterner, S.M. and Bodnar, R.J. (1988): Synthetic fluid inclusions in natural quartz. IV. Chemical analyses of fluid inclusions by SEM/EDA: evaluation of method. Geochimica et Cosmochimica Acta **52**, 969-977.

Hecht, L., Spiegel, W. and Morteani, G. (1991): Multiphase alteration including disseminated uranium mineralization in quartz-depleted granites (episyenites) of the Fichtelgebirge (Northeastern Bavaria, Germany). *In* M. Pagel, J. L. Leroy (eds) *Source, transport and deposition of metals*, Balkema, Rotterdam, 53-56.

Hedenquist, J.W., Arribas, A. and Reynolds, T.J. (1998): Evolution of an intrusion-centered hydrothermal system; Far Southeast-Lepanto porphyry and epithermal Cu-Au deposits, Philippines. Economic Geology **93**, 373-404.

Heinrich, C.A. (1990): The chemistry of hydrothermal tin (-tungsten) ore deposition. Economic Geology **85**, 457-482.

Hemley, J.J., Cygan, G.L., Fein, J.B., Robinson, G.R., D'Angelo, W. M. (1992): Hydrothermal ore-forming processes in the light of studies in rock-buffered

systems; I, Iron-copper-zinc-lead sulfide solubility relations. Economic Geology **87**, 1-22.

Hendrickson, G.A. (1979): Millet Brook project report on geophysical work. AR 21A/16B 54-I-64(03), Aquitaine, Halifax.

Henley, S. (1972): Petrogenesis of quartz porphyry dykes in south-west England. Nature **235**, 95-97.

Henley, S. (1974): Geochemistry and petrogenesis of elvan dykes n the Perranporth area, Cornwall. Proceedings of the Ussher Society **3**, 136-145.

Hicks, R.J., Jamieson, R.A. and Reynolds, P.H. (1999): Detrital and metamorphic $^{40}Ar/^{39}Ar$ ages from muscovite and whole-rock samples, Meguma Supergroup, southern Nova Scotia. Canadian Journal of Earth Sciences **36**, 23-32.

Hildreth, W. (1981): Gradients in silicic magma chambers: implications for lithospheric magmatism. Journal of Geophysical Research **86**, 10153-10192.

Hill, J.D. (1991): Petrology, tectonic setting , and economic potential of Devonian peraluminous granitoid plutons in the Canso and Forest Hill areas, eastern Meguma terrane, Nova Scotia. Geological Survey of Canada Bulletin **383**, 96.

Hodges, K.V., Hames, W.E. and Bowring, S.A. (1994): $^{40}Ar/^{39}Ar$ age gradients in micas from a high-temperature-low-pressure metamorphic terrain: evidence for very slow cooling and implications for the interpretation of age spectra. Geology **22**, 55-58.

Hollister, L.S. and Crawford, M.L. (1981): Short course in fluid inclusions: applications to petrology, Mineralogical Association of Canada **6**, 304 pp.

Horne, R.J. (1992): New Germany, Sheet 21A/10. NSDNR, Halifax.

Horne, R. and Culshaw, N. (2001): Flexural-slip folding in the Meguma Group, Nova Scotia, Canada. Journal of Structural Geology **23**, 1631-1652.

Horne, R.J., Corey, M.C., Ham, L.J. and MacDonald, M.A. (1988): Primary and secondary structural features in the eastern portion of the South Mountain Batholith, Southwestern Nova Scotia: implications for regional stress orientations during intrusion. Atlantic Geology **24**, 71-82.

Horne, R.J., MacDonald, M.A., Corey, M.C. and Ham, L.J. (1992): Structure and emplacement of the South Mountain Batholith, southwestern Nova Scotia. Atlantic Geology **28**, 29-50.

Horner, C. (1979): Solubility and hydrolysis of $FeWO_4$ and $MnWO_4$ in the 25 - 300°C range, and the zonation of wolframite. Chemical Geology **27**, 85-97.

Hsu, L.C. (1976): The stability relations of the wolframite series. American Mineralogist **61**, 944-955.

Hutchison, C.S. (1982): Batholith-associated mineralization. *In* Economic deposits and their tectonic setting, John Wiley & Sons, New York, 130-167.

Hyndman, R.D., Jessop, A.M., Judge, A.S. and Rankin, D.S. (1979): Heat flow in the Maritime provinces of Canada. Canadian Journal of Earth Sciences **16**, 1154-1165.

Jackson, K.J. and Helgeson, H.C. (1985): Chemical and thermodynamic constraints on the hydrothermal transport and deposition of tin: I. Calculation of the solubility of cassiterite at high pressures and temperatures. Geochimica and Cosmochimica Acta **49**, 1-22.

Jensen, L. R. (1975): The Torbrook Formation. Maritime Sediments **11**, 107-118.

Johannes, W. and Holtz, F. (1996): Petrogenesis and experimental petrology of granitic rocks. Minerals and Rocks **22**, Springer, Berlin, 335pp.

Johnston (1966): Report on the Long Lake molybdenite property. 21A/09B 35-L-09 (01), NSDNR, Halifax.

Jugo, P.J., Candela, P.A. and Piccoli, P.M. (1999): Magmatic sulfides and Au-Cu ratios in porphyry deposits: an experimental study of copper and gold partitioning at 850°C, 100 MPa in haplogranitic melt-pyrrhotite-intermediate solid solution-gold metal assemblage, at gas saturation. Lithos **46**, 573-589.

Kent, D.V. and Van der Voo, R.V.D. (1990): Palaeozoic palaeogeography from palaeomagnetism of the Atlantic-bordering continents. *In* W.S. McKerrow and C.R. Scotese (eds) *Palaeozoic Palaeogeography and Biogeography*, Geological Society of America Memoir **12**, 49-56.

Keppie, J.D. (1977): Tectonics of Southern Nova Scotia. 77-1, NSDNR, Halifax.

Keppie, J.D. (1985): The Appalachian collage. *In* D.G. Gee and B.A. Sturt (eds) *The Caledonide orogen: Scandinavia and related areas*, Wiley & Sons, Chichester, 1217-1226.

Keppie, J.D. (1989): Northern Appalachian terranes and their accretionary history. Geological Society of America Special Paper **230**, 159-185.

Keppie, J.D. and Dallmeyer, R.D. (1987): Dating transcurrent terrane accretion: an example from the Meguma and Avalon composite terranes in the northern Appalachians. Tectonics **6**, 831-847.

Keppie, J.K. and Dallmeyer, R.D. (1995): Late Paleozoic collision, delamination, short-lived magmatism, and rapid denudation in the Meguma terrane (Nova Scotia, Canada): constraints from $^{40}Ar/^{39}Ar$ isotopic data. Canadian Journal of Earth Sciences **32**, 644-659.

Keppie, J.D. and Krogh, T.E. (1999): U-Pb geochronology of Devonian granites in the Meguma Terrane of Nova Scotia, Canada: evidence for hotspot melting of a neoproterozoic source. Journal of Geology **107**, 555-568.

Keppie, J.D. and Smith, P.K. (1978): Compilation of isotopic age data of Nova Scotia. 78-4, NSDME, Halifax.

Keppie, J.D., Dallmeyer, R.D., Krogh, T.E., Cormier, R.F. and Halliday, A.N. (1985): Geochronological constraints for mineralization in the easternmost Meguma Terrane, Nova Scotia. Information Series NSDME, 39-40.

Keppie, J.K., Dallmeyer, R.D., Krogh, T.E. and Aftalion, M. (1993): Dating mineralization using several isotopic methods: an example from the South Mountain Batholith, Nova Scotia, Canada. Chemical Geology **103**, 251-270.

Keppler, H. (1993): Influence of fluorine on the enrichment of high field strength trace elements in granitic rocks. Contributions to Mineralogy and Petrology **114**, 479-488.

Keppler, H. (1994): Partitioning of phosphorus between melt and fluid in the system haplogranite-H2O-P2O5. Chemical Geology **117**, 345-353.

Keppler, H. and Wyllie, P.J. (1991): Partitioning of Cu, Sn, Mo, W, U, and Th between melt and aqueous fluid in the systems haplogranite-H_2O-HCl and haplogranite-H_2O-HF. Contributions to Mineralogy and Petrology **109**, 139-150.

Khitarov, H.I., Malinin, S.P., Lebedev, Y.B. and Shibayeva, N.P. (1982): The distribution of Zn, Cu, Pb, and Mo between a fluid phase and a silicate melt of granitic composition at high temperatures and pressures. Transactions from Geokhimiya **8**, 1094-1107.

Kilinc, A.I. and Burnham, C.W. (1972): Partitioning of chlorine between a silicate melt and coexisting aqueous phase from 2 to 8 kbar. Economic Geology **67**, 231-235.

Kirschner, D.L., Cosca, M.A., Masson, H. and Hunziker, J.C. (1996): Staircase $^{40}Ar/^{39}Ar$ spectra of fine-grained white mica: timing and duration of deformation and empirical constraints on argon diffusion. Geology **24**, 747-750.

Kojima, S., Takeda, S. and Kogita, S. (1994): Chemical factors controlling the solubility of uraninite and their significance in the genesis of unconformity-related uranium deposits. Mineralium Deposita **29**, 353-360.

Kontak, D.J. (1990): The East Kemptville topaz-muscovite leucogranite, Nova Scotia I. Geological setting and whole-rock geochemistry. Canadian Mineralogist **28**, 787-825.

Kontak, D.J. (1994): Geological and geochemical studies of alteration processes in a fluorine-rich environment: the East Kemptville Sn-(Zn-Cu-Ag) deposit, Yarmouth County, Nova Scotia, Canada. *In* D.R. Lentz (ed) *Alteration and alteration processes associated with ore-forming systems*, Short Course Notes. Geological Association of Canada, mineral deposits division, 261-314.

Kontak, D.J. (1998a): Aqueous an liquid petroleum inclusions in barite from the Walton deposit, Nova Scotia, Canada: a Carboniferous, carbonate-hosted Ba-Pb-Zn-Cu-Ag deposit. Economic Geology **93**, 845-868.

Kontak, D.J. (1998b): A study of fluid inclusions in sulfide and nonsulfide mineral phases from a carbonate-hosted Zn-Pb deposit, Gays River, Nova Scotia, Canada. Economic Geology **93**, 793-817.

Kontak, D.J. and Chatterjee, A.K. (1992): The East Kemptville tin deposit, Yarmouth County, Nova Scotia: a Pb-isotope study of the leucogranite and mineralized greisens - evidence for a 366 Ma metallogenic event. Canadian Journal of Earth Sciences **29**, 1180-1196.

Kontak, D.J. and Cormier, R.F. (1991): Geochronological evidence for multiple tectono-thermal overprinting events in the East Kemptville muscovite-topaz leucogranite, Yarmouth County, Nova Scotia, Canada. Canadian Journal of Earth Sciences **28**, 209-224.

Kontak, D. J. and Dostal, J. (1992): The East Kemptville tin deposit, Yarmouth County, southwestern Nova Scotia; a lithogeochemical study of wallrock metasedimentary rocks. Atlantic Geology **28**, 63-83.

Kontak, D.J. and Kerrich, R. (1995): Geological and geochemical studies of a metaturbidite-hosted Lode gold deposit: the Beaver Dam deposit, Nova Scotia: II. Isotopic studies. Economic Geology **90**, 885-901.

Kontak, D. J. and Kyser, K. (2002): Preliminary fluid inclusion and oxygen isotope studies of silica-clay mineralization, Yarmouth County, Nova Scotia. **In press.**

Kontak, D.J. and Reynolds, P.H. (1994): $^{40}Ar/^{39}Ar$ dating of metamorphic and igneous rocks of the Liscomb Complex, Meguma Terrane, southern Nova Scotia, Canada. Canadian Journal of Earth Sciences **31**, 1643-1653.

Kontak, D.J. and Smith, P.K. (1989): Fluid inclusion studies of quartz vein polytypes from the Beaver Dam and Caribou gold deposits, Meguma Zone, Nova Scotia: evidence for a single vein-forming event. 89-1, NSDNR, Halifax.

Kontak, D.J. and Smith, P.K. (1993): An overview of Meguma gold deposits in the Meguma Terrane of southern Nova Scotia. Exploration and Mining Geology **2**, 418-421.

Kontak, D.J., MacDonald, D. and Smith, P.K. (1988a): Fluid inclusion study of the Beaver Dam gold deposit, Meguma terrane, Nova Scotia. 88-3, NSDNR, Halifax.

Kontak, D.J., Strong, D.F. and Kerrich, R. (1988b): Crystal-melt-fluid phase equilibria versus late-stage fluid-rock interaction in granitoid rocks of the South Mountain Batholith, Nova Scotia: whole rock geochemistry and oxygen isotope evidence. Maritime Sediments and Atlantic Geology **24**, 97-110.

Kontak, D.J., Smith, P.K., Chatterjee, A.K., Giles, P.S. and Reynolds, P.H. (1989): $^{40}Ar/^{39}Ar$ geochronological studies in the Beaver Dam-Liscomb area, southern Nova Scotia; recognition of a major 370 Ma magmatic-metallogenetic event. Program with Abstracts **14**, 11.

Kontak, D.J., Chatterjee, A.K., Reynolds, P.H. and Taylor, K. (1990a): A $^{40}Ar/^{39}Ar$ geochronological study of metamorphic and igneous rocks of the Liscomb Complex, southern Nova Scotia. 90-1, NSDNR, Halifax.

Kontak, D.J., Smith, P.K., Kerrich, R. and Williams, P.F. (1990b): Integrated model for Meguma Group iode gold deposits, Nova Scotia, Canada. Geology **18**, 238-242.

Kontak, D. J., Kerrich, R., Strong, D. F. (1991): The role of fluids in the late-stage evolution of the South Mountain Batholith, Nova Scotia: further geochemical and oxygen isotopic studies. Atlantic Geology **27**, 29-47.

Kontak, D.J., Smith, P.K. and Reynolds, P.H. (1993): Geology and $^{40}Ar/^{39}Ar$ geochronology of the Beaver Dam gold deposit, Meguma Terrane, Nova Scotia, Canada: evidence for mineralization at 370 Ma. Economic Geology **88**, 139-170.

Kontak, D.J., Farrar, E., McBride, S. and Martin, R.F. (1995): Mineral chemistry and $^{40}Ar/^{39}Ar$ dating of muscovite from the East Kemptville leucogranite, southern Nova Scotia: evidence for localized resetting of $^{40}Ar/^{39}Ar$ systematics in a shear zone. Canadian Mineralogist **33**, 1237-1253.

Kontak, D.J., Horne, R.J. and Smith, P.K. (1996): Hydrothermal characterization of the West Gore Sb-Au deposit, Meguma Terrane, Nova Scotia, Canada. Economic Geology **91**, 1239-1262.

Kontak, D.J., Ansdell, K. and Archibald, D. (1999): New constraints on the age and origin of the Dunbrack Pb-Cu-Zn-Ag deposit, Musquodoboit Batholith, southern Nova Scotia. Atlantic Geology **35**, 19-42.

Kontak, D.J., Ansdell, K., Dostal, J., Halter, W., Martin, R., Williams-Jones, A.E. (2001): The nature and origin of pegmatite in a fluorine-rich leucogranite, East Kemptville, Nova Scotia, Canada. Transactions of the Royal Society of Edinburgh **92**, 173-200.

Kontak, D. J., Dostal, J., Kyser, T. K., Archibald, D. A. (2002): A petrological, geochemical, isotopic and fluid inclusion study of 370 Ma pegmatite-aplite sheets, Peggy's Cove, Nova Scotia, Canada. Canadian Mineralogist **40**, 1249-1286.

Koster van Groos, A.F. and Wyllie, P.J. (1968): Melting relationships in the system $NaAlSi_3O_8$-NaF-H_2O to 4 kilobars pressure. Journal of Geology **76**, 50-70.

Krogh, T.E. and Keppie, J.D. (1990): Age of detrital zircon and titanite in the Meguma Group, southern Nova Scotia, Canada; clues to the origin of the Meguma Terrane. *In* P. Matte (ed) *Terranes in the Variscan Belt of Europe and Circum-Atlantic Paleozoic orogens*, Elsevier, Amsterdam, 307-323.

Kyser, T.K., Lesher, C.E. and Walker, D. (1998): The effects of liquid immiscibility and thermal diffusion on oxygen isotopes in silicate liquids. Contributions to Mineralogy and Petrology **133**, 373-381.

Lagache, M. and Weisbrod, A. (1977): The system: two alkalo feldspars-KCl-NaCl-H_2O at moderate to high temperatures and low pressures. Contributions to Mineralogy and Petrology **62**, 77-101.

LeMaitre, R.W. (1982): Numerical petrology: statistical interpretation of geochemical data **8**, Elsevier, Amsterdam, 281 pp.

Leroy, J. (1984): Episyenitisation dans le gisement d'uranium du Bernardan (Marche): comparaison avec des gisements similaires du Nord-Ouest du massif Central Francais. Mineralium Deposita **19**, 26-35.

Leroy, J.L., Fritz, B., Cathelineau, M. and Lespinasse, M. (1991): Geochemical modelling of two-mica granite alterations: subsolidus changes related to dequartzification and clay alteration. *In* M. Pagel, J. L. Leroy (eds) *Source, transport and deposition of metals*, Balkema, Rotterdam, 69-72.

Lewis, D.W.T. (1980): Uranium, New Ross, Lunenburg County, Nova Scotia. 21A/09C 54-L-19 (04), Shell Canada Resources Limited, Halifax.

Linnen, R.L. (1998): Depth of emplacement , fluid provenance and metallogeny in granitic terranes: a comparison of western Thailand with other tin belts. Mineralium Deposita **33**, 461-476.

Linnen, R.L. and Williams-Jones, A.E. (1994): The evolution of pegmatite-hosted Sn-W mineralization at Nong sua, Thailand: evidence from fluid inclusions and stable isotopes. Geochimica et Cosmochimica Acta **58**, 735-747.

Linnen, R.L., Pichavant, M., Holtz, F. and Burgess, S. (1995): The effect of fO_2 on the solubility, diffusion, and speciation of tin in haplogranitic melt at 850°C and 2 kbar. Geochimica and Cosmochimica Acta **59**, 1579-1588.

Linnen, R.L., Pichavant, M. and Holtz, F. (1996): The combined effects of fO_2 and melt composition on SnO_2 solubility and tin diffusivity in haplogranitic melts. Geochimica and Cosmochimica Acta **60**, 4965-4976.

Liu, K., Cruzan, J.D. and Saykally, R.J. (1996): Water clusters. Science **271**, 929-933.

Liu, W., Brugger, J., McPhail, D.C. and Spiccia, L. (2002): A spectrophotometric study of aqueous copper(I)-chloride complexes in LiCl solutions between 100°C and 250°C. Geochimica and Cosmochimica Acta **66**, 3615-3633.

Logothetis, J. (1985): The mineralogy and geochemistry of metasomatized granitoid rocks from occurrences in the South Mountain: New Ross area, Southwestern Nova Scotia, MSc Thesis, Dalhousie University, Halifax.

London, D. (1987): Internal differentiation of rare-element pegmatites: effects of boron, phosphorus, and fluorine. Geochimica and Cosmochimica Acta **51**, 403-420.

London, D. (1992): Phosphorus in S-type magmas: the P_2O_5 content of feldspars from peraluminous granites, pegmatites, and rhyolites. American Mineralogist **77**, 126-145.

London, D., Hervig, R.L. and Morgan, G.B. (1988): Melt-vapor solubilities and elemental partitioning in peraluminous granite-pegmatite systems: experimental results with Macusani glass at 200 MPa. Contributions to Mineralogy and Petrology **99**, 360-373.

London, D., Morgan, G.B., Babb, H.A. and Loomis, J.L. (1993): Behavior and effects of phosphorus in the system Na_2O-K_2O-Al_2O_3-SiO_2-P_2O_5-H_2O at 200 MPa (H_2O). Contributions to Mineralogy and Petrology **113**, 450-465.

Longstaffe, F.J. (1982): Stable isotopes in the study of granitic pegmatites and related rocks. *In* P. Cerny (ed) *Short course in granitic pegmatites in science and industry*, Mineralogical Association of Canada, Winnipeg, 373-404.

Longstaffe, F.J., Smith, T.E. and Muehlenbachs, K. (1980): Oxygen isotope evidence for the genesis of Upper Paleozoic granitoids from southwestern Nova Scotia. Canadian Journal of Earth Sciences **17**, 132-141.

Lovera, O.M., Richter, F.M. and Harrison, T.M. (1989): The $^{40}Ar/^{39}Ar$ thermochronometry for slowly cooled samples having a distribution of diffusion domain sizes. Journal of Geophysical Research, B, Solid Earth and Planets **94**, 17917-17935.

Lovera, O.M., Richter, F.M. and Harrison, T.M. (1991): Diffusion domains determined by ^{39}Ar released during step heating. Journal of Geophysical Research, B, Solid Earth and Planets **96**, 2057-2069.

Lovera, O.M., Grove, M., Harrison, T.M. and Mahon, K.I. (1997): Systematic analysis of K-feldspar $^{40}Ar/^{39}Ar$ step heating results; I, Significance of activation energy determinations. Geochimica et Cosmochimica Acta **61**, 3171-3192.

Lowdon, J.A. (1960): Age determinations by the Geological Survey of Canada, report I-isotopic ages. 60-17, GSC.

Lowdon, J.A., Stockwell, C.H., Tipper, H.W. and Wanless, R.K. (1963): Age determinations and geological studies; part I. Isotopic ages. Report 3. 62-17, GSC.

MacDonald, M.A. (1982): The mineralogy, petrography and geochemistry of the Musquodoboit Batholith, MSc Thesis, Dalhousie, Halifax.

MacDonald, M.A. (2001): Geology of the South Mountain Batholith, southwestern Nova Scotia. ME 2001-2, NSDNR, Halifax.

MacDonald, M.A. and Clarke, D.B. (1991): Use of nonparametric ranking statistics to characterize magmatic and post-magmatic processes in the eastern South Mountain Batholith, Nova Scotia, Canada. Chemical Geology **92**, 1-20.

MacDonald, M.A., Horne, R.J., Corey, M.C. and Ham, L.J. (1992): An overview of recent bedrock mapping and follow-up petrological studies of the South Mountain Batholith, Southwestern Nova Scotia, Canada. Atlantic Geology **28**, 7-28.

Mahoney, K.L. (1996): The contact metamorphic aureole of the South Mountain Batholith, Nova Scotia, MSc Thesis, Acadia University, Wolfville.

Mahoney, K.L. and Raeside, R.P. (1995): The contact aureole of the South Mountain Batholith, southern Nova Scotia. 95-2, NSDNR, Halifax.

Manly, B.F.J. (1994): Multivariate statistical methods: a primer **1**, Chapman & Hall, New York, 215 pp.

Manning, D.A.C. and Henderson, P. (1984): The behaviour of tungsten in granitic melt-vapour systems. Contributions to Mineralogy and Petrology **86**, 286-293.

Manning, D.A.C. and Pichavant, M. (1985): Volatiles and their bearing on the behaviour of metals in granitic systems. *In* R.P. Taylor and D.F. Strong (eds) *Recent advances in the geology of granite-related mineral deposits*, Canadian institute of Mining and Metallurgy, Halifax, 13-24.

Markey, R., Stein, H. and Morgan, J.W. (1998): Highly precise Re-Os dating for molybdenite using alkaline fusion and NTIMS. Talanta **45**, 935-946.

Martel, A.T. and Gibling, M.R. (1996): Stratigraphy and tectonic history of the Upper Devonian to Lower Carboniferous Horton Bluff Formation, Nova Scotia. Atlantic Geology **32**, 13-38.

Martel, A.T., Gregor, D.C.M. and Utting, J. (1993): Stratigraphic significance of Upper Devonian and Lower Carboniferous miospores from the type area of the Horton Group, Nova Scotia. Canadian Journal of Earth Sciences **30**, 1091-1098.

Mawer, C.K. and White, J.C. (1987): Sense of displacement on the Cobequid-Chedabucto Fault System, Nova Scotia, Canada. Canadian Journal of Earth Sciences **24**, 217-223.

McCandless, T.E., Ruiz, J. and Campbell, A.R. (1993): Rhenium behavior in molybdenite in hypogene and near-surface environments: implications for Re-Os geochronometry. Geochimica et Cosmochimica Acta **57**, 889-905.

McDougall, I. and Harrison, T.M. (1999): Geochronology and thermochronology by the $^{40}Ar/^{39}Ar$ method, Oxford University Press, New York, 269 pp.

McKenzie, C.B. (1974): Petrology of the South Mountain Batholith, western Nova Scotia, MSc Thesis, Dalhousie University, Halifax.

Miller, C.F., Stoddard, E.F., Bradfish, L.J. and Dollase, W.A. (1981): Composition of plutonic muscovite: genetic implications. Canadian Mineralogist **19**, 25-34.

Monier, G. and Robert, J.-L. (1986): Muscovite solid solutions in the system K_2O-MgO-FeO-Al_2O_3-SiO_2-H_2O: an experimental study at 2 kbar P_{H2O} and comparison with natural Li-free white micas. Mineralogical Magazine **50**, 257-266.

Monier, G., Mergoil-Daniel, J. and Labernardiere, H. (1984): Generations successives de muscovites et feldspaths potassiques dans les leucogranites du massif de Millevaches (Massif Central francais). Bulletin de Mineralogie **107**, 55-68.

Morgan, G.B., London, D. and Luedke, R.G. (1998): Petrochemistry of Late Miocene Peraluminous silicic volcanic rocks from the Morococala Field, Bolivia. Journal of Petrology **39**, 601-632.

Muecke, G.K. and Clarke, D.B. (1981): Geochemical evolution of the South Mountain Batholith, Nova Scotia: rare-earth element evidence. Canadian Mineralogist **19**, 133-145.

Muecke, G.K., Elias, P. and Reynolds, P.H. (1988): Hercynian/Alleghanian overprinting of an Acadian terrane: $^{40}Ar/^{39}Ar$ studies in the Meguma Zone, Nova Scotia, Canada. Chemical Geology **73**, 153-167.

Murphy, J.B., Van Stall, C.R. and Keppie, J.D. (1999): Middle to late Paleozoic Acadian orogeny in the northern Appalachians: a Laramide-style plume-modified orogeny? Geology **27**, 653-656.

Mysen, B.O., Ryerson, F.J. and Virgo, D. (1981): The structural role of phosphorus in silicate melts. American Mineralogist **66**, 106-117.

Mysen, B.O., Holtz, F., Pichavant, M., Beny, J.-M. and Montel, J.-M. (1999): The effect of temperature and bulk composition on the solution mechanism of phosphorus in peraluminous haplogranitic magma. American Mineralogist **84**, 1336-1345.

Nguyen-Trung, C. (1985): Geochimie theorique et experimentale des oxydes d'uranium dans les solutions aqueuses de 25 a 700°C sous une pression de 1 a 6000 bars. Synthese hydrothermale de certains mineraux d'uranium VI et IV., PhD thesis, Universite de Nancy, Nancy.

Noble, D.C., Vogel, T. A., Peterson, P. S., Landis, G. P., Grant, N. K., Jezek, P. A., McKee, E. H. (1984): Rare-element-enriched S-type ash-flow tuffs containing phenocrysts of muscovite, andalusite, and sillimanite, Southeastern Peru. Geology **12**, 35-39.

Oakes, C.S., Bodnar, R.J. and Simonson, J.M. (1990): The system NaCl-$CaCl_2$-H_2O: I. The ice liquidus at 1 atm total pressure. Geochimica and Cosmochimica Acta **54**, 603-610.

Okulitch, A.V. (1999): Geological time chart. Geology (supplement) **29**, 1-2.

Oldale, H.R. (1966): Report on the Long Lake molybdenum property Gold River district, Lunenburg County, Nova Scotia. 21A/9B 35-L-09 (06), NSDME, Halifax.

O'Neil, J.R. (1986): Theoretical and experimental aspects of isotopic fractionation. *In* J.W. Valley, H.P. Taylor and J.R. O'Neil (eds) *Stable isotopes in high temperature geological processes,* Mineralogical Society of America, 1-40.

O'Neil, J.R. and Taylor, H.P. (1969): Oxygen isotope equilibrium between muscovite and water. Journal of Geophysical Research **74**, 6012-6022.

O'Reilly, C.T. (1975): Gravitational interpretation and modelling of the South mountain Batholith utilizing 2 and 3 dimensional computer programming, BSc Thesis, Dalhousie University, Halifax.

O'Reilly, G.A. (1992): Petrographic and geochemical evidence for a hypogene origin of granite-hosted, vein-type Mn mineralization at the New Ross Mn deposits, Lunenburg County, Nova Scotia, Canada. Economic Geology **87**, 1275-1300.

O'Reilly, G.A., Farley, E.J. and Charest, M.H. (1982): Metasomatic-hydrothermal mineral deposits of the New Ross-Mahone Bay area, Nova Scotia. 82-2, NSDME, Halifax..

O'Reilly, G.A., Gauthier, G. and Brooks, C. (1985): Three Permo-Carboniferous Rb/Sr age determinations from the South Mountain Batholith, southwestern Nova Scotia. 85-1, NSDNR, Halifax.

Ohmoto, H. (1986): Stable isotope geochemistry of ore deposits. *In* J.W. Valley, H.P. Taylor and J.R. O'Neil (eds) *Stable isotopes in high temperature geological processes,* Mineralogical Society of America, 491-559.

Orville, P.M. (1963): Alkali ion exchange between vapor and feldspar phases. American Journal of Science **261**, 201-237.

Pakul'nis, G.V., Shmariovich, Y.M., Zhil'tsova, I.G., Polupanova, L.I. and Shugina, G.A. (1986): Mineral assemblages and physicochemical conditions for carnotite-autunite-torbernite mineralization in carbonaceous phyllites. International Geology Review **28**, 100-113.

Palmer, M.G.B. (1979): Uranium, New Ross area, Lunenburg County, Nova Scotia. 21A/09C 54-L-19 (02), Can-Lake Explorations limited, Halifax.

Parrish, R. R. (1990): U-Pb dating of monazite and its application to geological problems. Canadian Journal of Earth Sciences **27**, 1431-1450.

Parks, G.A. and Pohl, D.C. (1988): Hydrothermal solubility of uraninite. Geochimica and Cosmochimica Acta **52**, 863-875.

Parsons, I., Brown, W.L. and Smith, J.V. (1999): $^{40}Ar/^{39}Ar$ thermochronology using alkali feldspars: real thermal history or mathematical mirage of microtexture? Contributions to Mineralogy and Petrology **136**, 92-110.

Patterson, D.J., Ohmoto, H. and Solomon, M. (1981): Geologic setting and genesis of cassiterite-sulfide mineralization at Renison Bell, western Tasmania. Economic Geology **76**, 393-438.

Pattison, D.R.M. (1992): Stability of andalusite and sillimanite and the Al_2SiO_5 triple point: constraints from the Ballachulish aureole, Scotland. Journal of Geology **100**, 423-446.

Peiffert, C., Nguyen-Trung, C. and Cuney, M. (1996): Uranium in granitic magmas: Part 2. Experimental determination of uranium solubility and fluid-melt partition coefficients in the uranium oxide-haplogranite-H_2O-NaX (X=C., F) system at 770°C, 2 kbar. Geochimica et Cosmochimica Acta **60**, 1515-1529.

Pelrine, K.M. (2003): Ilmenite-pyrophanite and niobian rutile in the South Mountain Batholith, Nova Scotia, BSc Thesis, Dalhousie University, Halifax.

Pichavant, M., Kontak, D.J., Briqueu, L., Herrera, J.V. and Clark, A.H. (1988a): The Miocene-Pliocene Macusani volcanics, SE Peru II. Geochemistry and origin of a felsic peraluminous magma. Contributions to Mineralogy and Petrology **100**, 325-338.

Pichavant, M., Kontak, D.J., Herrera, J.V. and Clark, A.H. (1988b): The Miocene-Pliocene Macusani volcanics, SE Peru I. Mineralogy and magmatic evolution of a two-mica aluminosilicate-bearing ignimbrite suite. Contributions to Mineralogy and Petrology **100**, 300-324.

Pichavant, M., Montel, J.-M. and Richard, L.R. (1992): Apatite solubility in peraluminous liquids; experimental data and an extension of the Harrison-Watson model. Geochimica et Cosmochimica Acta **56**, 3858-3861.

Pirajno, F. (1992): Hydrothermal mineral deposits: principles and fundamental concepts for the exploration geologist, Springer-Verlag, Berlin, 709 pp.

Pohl, D.C. and Parks, G.A. (1984): Solubility of uraninite under reducing conditions at elevated temperatures and pressures. Abstracts with Programs **6**, 625.

Poulson, S.R., Kubilius, W.P. and Ohmoto, H. (1991): Geochemical behavior of sulfur in granitoids during intrusion of the South Mountain Batholith, Nova Scotia, Canada. Geochimica and Cosmochimica Acta **55**, 3809-3830.

Raeside, R.P., Hill, J.D. and Eddy, B.G. (1988): metamorphism of Meguma Group metasedimentary rocks, Whitehead Harbour area, Guysborough County, Nova Scotia. Maritime Sediments and Atlantic Geology **24**, 1-9.

Rafal'skiy, R.P. (1985): The solubility of pyrite in hydrothermal solutions. Geochemistry International **22**, 130-144.

Raimbault, L. and Burnol, L. (1998): The Richemont rhyolite dyke, massif central, France: a subvolcanic equivalent of rare-metal granites. The Canadian Mineralogist **36**, 265-282.

Raith, J.G. and Stein, H.J. (2000): Re-Os dating and sulfur isotope composition of molybdenite from tungsten deposits in western Namaqualand, South Africa: implications for ore genesis and the timing of metamorphism. Mineralium Deposita **35**, 741-753.

Reed, M.H. (1997): Hydrothermal alteration and its relationship to ore fluid composition. *In* H.L. Barnes *Geochemistry of hydrothermal ore deposits*, John Wiley and Sons, Toronto, 303-365.

Reynolds, P.H. (1992): Low temperature thermochronology by the $^{40}Ar/^{39}Ar$ method. In M. Zentilli, P. H. Reynolds (eds) *Low temperature thermochronology short course handbook* **20**, 3-19.

Reynolds, P.H., Zentilli, M. and Muecke, G.K. (1981): K-Ar and Ar/Ar geochronology of granitoid rocks from Southern Nova Scotia: its bearing on the geological evolution of the Meguma Zone of the Appalachians. Canadian Journal of Earth Sciences **18**, 386-394.

Reynolds, P.H., Elias, P., Muecke, G.K. and Grist, A.M. (1987): Thermal history of the southwestern Meguma Zone, Nova Scotia, from an $^{40}Ar/^{39}Ar$ and fission track dating study of intrusive rocks. Canadian Journal of Earth Sciences **24**, 1952-1965.

Reynolds, P.H., Kublick, E.E. and Muecke, G.K. (1973): Potassium-argon dating of slates from the Meguma Group, Nova Scotia. Canadian Journal of Earth Sciences **10**, 1059-1067.

Richard, L.R. and Clarke, D.B. (1989): Multivariate statistical models for granites in terrane analysis: Nova Scotia, Morocco, and Iberia. Geological Society of America Bulletin **101**, 1157-1162.

Richardson, J.M., Bell, K., Blenkinsop, J. and Watkinson, D.H. (1988): Fluid saturation textures and Rb-Sr isochron data from the East Kemptville tin deposit, Southwestern Nova Scotia. Geological Survey of Canada Paper **88-1B**, 163-171.

Richardson, J.M., Bell, K., Blenkinsop, J. and Watkinson, D.H. (1989): Rb-Sr age and geochemical distinctions between the Carboniferous tin-bearing Davis Lake

complex and the Devonian South Mountain batholith, Meguma terrane, Nova Scotia. Canadian Journal of Earth Sciences **26**, 2044-2061.

Rieder, M., Cavazzini, G., Yakonov, Y. S. D., Frank-Kamenetskii, V. A., Gottardi, G. Guggenheim, S., Koval P. V., Muller, G., Neiva, A. M. R., Radoslovich, E. W., Robert, J.-L., Sassi, F. P., Takeda, H., Weiss, Z., Wones, D. R. (1999): Nomenclature of the micas. Mineralogical Magazine **63**, 267-279.

Robertson, D.J. (1978): Report of work on Millet Brook uranium property, Nova Scotia. AR 21A/16B 54-I-64 (02), Aquitaine, Calgary.

Robinson, C.W. (1914): An investigation of radio-active minerals in eastern Canada, GSC.

Roedder, E. (1984): Fluid inclusions, Reviews in Mineralogy **12**, Mineralogical Society of America, 644 pp.

Roedder, E. and Bodnar, R.J. (1997): Fluid inclusion studies of hydrothermal ore deposits. *In* H.L. Barnes (ed) *Geochemistry of hydrothermal ore deposits*, John Wiley & Sons, New York, 657-697.

Rollinson, H. (1993): Using geochemical data: evaluation, presentation, interpretation. Geochemistry, Longman scientific & technical, Wiley & Sons, New York, 352 pp.

Romberger, S.B. and Barnes, H.L. (1970): Ore solubility chemistry III. Solubility of CuS in sulfide solutions. Economic Geology **65**, 901-919.

Romer, R.L. (1994): Rb-Sr data structure - a possible cause for differences in Rb-Sr whole-rock and U-Pb zircon ages. Geologiska Foereningen i Stockholm Foerhandlingar **116**, 93-103.

Roycroft, P. (1991): Magmatically zoned muscovite from the peraluminous two-mica granites of the Leinster batholith, southeast Ireland. Geology **19**, 437-440.

Saavedra, J. (1978): Geochemical and petrological characteristics of mineralised granites of the west centre of Spain. *In* M. Stemprok, L. Burnol and G. Tischendorf (eds) *Metallization associated with acid magmatism*, Geological Survey of Czechoslovakia, 279-291.

Samson, S.D. and Alexander, E.C. (1987): Calibration of the interlaboratory $^{40}Ar/^{39}Ar$ dating standard, MMhb-1. Chemical Geology **66**, 27-34.

Sassani, D.C., Betz, H. and Shock, E.L. (1993): Predicted effects of temperature, oxygen fugacity, pH, and solution composition on the speciation of aqueous uranium and the solubility of uraninite. Abstracts with Programs **25**, A438.

Savard, M.M. and Chi, G. (1998): Cation study of fluid inclusion decrepitates in the Jubilee and gays River (Canada) Zn-Pb deposits-Characterization of ore-forming brines. Economic Geology **93**, 920-931.

Savin, S.M. and Lee, M. (1988): Isotopic studies of phyllosilicates, *In* S. W. Bailey (ed) *Hydrous phyllosilicates*, Reviews in Mineralogy **19**, 189-223.

Schenk, P.E. (1971): Southeastern Atlantic Canada, Northwestern Africa, and continental drift. Canadian Journal of Earth Sciences **8**, 1218-1248.

Schenk, P.E. (1975): A regional Synthesis. Maritime Sediments **11**, 17-24.

Schenk, P.E. (1981): The Meguma Zone of Nova Scotia-a remnant of Western Europe, South America, or Africa? Canadian Society of Petroleum Geology Memoir **7**, 119-148.

Schenk, P.E. (1983): The Meguma Terrane of Nova Scotia, Canada - an aid in trans-Atlantic correlation. *In* P.E. Schenk (ed) *Regional trends in the geology of the Appalachian-Caledonian-Hercynian-Mauritanide orogen*, D. Reidel, 121-130.

Schenk, P. E. (1991): Events and sea-level changes on Gondwana's margin; the Meguma Zone (Cambrian to Devonian) of Nova Scotia, Canada. Geological Society of America Bulletin **103**, 512-521.

Schenk, P.E. (1995a): Meguma Zone. *In* H. Williams (ed) *Geology of the Appalachian-Caledonian orogen in Canada and Greenland*, Geological Survey of Canada, 261-277.

Schenk, P.E. (1995b): Annapolis Belt. *In* H. Williams (ed) *Geology of the Appalachian-Caledonian orogen in Canada and Greenland*, Geological Survey of Canada, 367-383.

Schenk, P.E. (1997): Sequence stratigraphy and provenance on Gondwana's margin: the Meguma zone (Cambrian to Devonian) of Nova Scotia. Geological Society of America Bulletin **109**, 395-409.

Sheppard, S.M.F. (1977): The Cornubian batholith, SW England: D/H and 18O/16O studies of kaolinite and other alteration minerals. Journal of the Geological Society of London **133**, 573-591.

Sheppard, S.M.F. (1986): Characterization and isotopic variations in natural waters. *In* J.W. Valley, H.P.T. Jr. and J.R. O'Neil (eds) *Stable isotopes in high temperature geological processes,* Mineralogical Society of America, Blacksburg, 165-183.

Sheppard, S.M.F. and Charef, A. (1986): Eau organique: caracterisation isotopique et evidence de son role dans le gisement Pb-Zn de Fedj-el-Adoum, Tunisie. Comptes-Rendus de l'Academie des Sciences, Serie II **19**, 1189-1192.

Sheppard, S.M.F., Nielsen, R.L. and Jr., H.P.T. (1969): Oxygen and hydrogen isotope ratios of clay minerals from porphyry copper deposits. Economic Geology **64**, 755-777.

Schleicher, H. and Lippolt, J.J. (1981): Magmatic muscovite in felsitic parts of rhyolites from southwest Germany. Contributions to Mineralogy and Petrology **78**, 220-224.

Scotese, C. R. and McKerrow, W. S. (1990): Revised world maps and introduction. In Palaeozoic Palaeogeography and Biogeography (W. S. McKerrow and C. R. Scotese). Geological Society of America Memoir **12**, 1-21.

Selby, D. and Creaser, R.A. (2001a): Late and Mid-Cretaceous mineralization in the northern Canadian Cordillera: constraints from Re-Os molybdenite dates. Economic Geology **96**, 1461-1467.

Selby, D. and Creaser, R.A. (2001b): Re-Os geochronology and systematics in molybdenite from the Endako Porphyry molybdenum deposit, British Columbia, Canada. Economic Geology **96**, 197-204.

Selby, D., Nesbitt, B.E., Muehlenbachs, K. and Prochaska, W. (2000): Hydrothermal alteration and fluid chemistry of the Endako porphyry molybdenum deposit, British Columbia. Economic Geology **95**, 183-202.

Seward, T.M. (1981): Metal complex formation in aqueous solutions at elevated temperatures and pressures. Physics and Chemistry of the Earth **13/14**, 113-132.

Seward, T.M. and Barnes, H.L. (1997): Metal transport by hydrothermal ore fluids. *In* H.L. Barnes (ed) *Geochemistry of Hydrothermal ore deposits*, Wiley and Sons, New York, 435-486.

Shabani, A.A.T. (1999): Mineral chemistry and Mossbauer spectroscopy of micas from granitic rocks of the Canadian Appalachians, PhD Thesis, University of Ottawa, Ottawa.

Shaw, D.M. (1968): A review of K-Rb fractionation trend by covariance analysis. Geochimica and Cosmochimica Acta **32**, 573-601.

Shcherba, G.N. (1970): Greisens. International Geology Reviews **12**, 114-150 and 238-255.

Shewman (1968): Long Lake. 21A/9B 35-L-09 (04), NSDME, Halifax.

Sillitoe, R.H. (1996): Granites and metal deposits. Episodes **19**, 126-133.

Sinclair, W.D. (1972): The solubility of copper and chalcocite in aqueous chloride solutions from 25 to 250°C. Abstracts with programs **4**, 667.

Skinner, B.J. (1997): Hydrothermal mineral deposits: what we do and don't know. *In* H.L. Barnes (ed) *Geochemistry of Hydrothermal ore deposits*, Wiley and Sons, New York, 1-29.

Slipp, R.M. (1951): Molybdenite at New Russell, NSDME, Halifax.

Smith, R.W., Norman, D.I. and Popp, C.J. (1980): Calculated solubility of molybdenite in hydrothermal solutions. Geological Society of America Abstracts with Programs **12**, 525.

Smoliar, M.I., Walker, R.J. and Morgan, J.W. (1996): Re-Os isotope constraints on the age of Group IIA, IIIA, IVA, and IVB iron meteorites. Science **271**, 1099-1102.

Speer, J.A. (1984): Micas in igneous rocks. In S.W. Bakley (ed) *Micas*, Reviews in Mineralogy. Mineralogical Society of America, Chelsea, 299-356.

Steiger, R.H. and Jager, E. (1977): Subcommission on geochronology: convention on the use of decay constants in geo- and cosmochronology. Earth and Planetary Science Letters **36**, 359-362.

Stein, H.J., Sundblad, K., Markey, R.J., Morgan, J.W. and Motuza, G. (1998): Re-Os ages for Archean molybdenite and pyrite, Kuittila-Kivisuo, Finland and Proterozoic molybdenite, Kabeliai, Lithuania: testing the chronometer in a metamorphic and metasomatic setting. Mineralium Deposita **33**, 329-345.

Stein, H.J., Markey, R.J., Morgan, J.W., Hannah, J.L. and Schersten, A. (2001): The remarkable Re-Os chronometer in molybdenite: how and why it works. Terra Nova **13**, 479-486.

Sterner, S.M. and Bodnar, R.J. (1989): Synthetic fluid inclusions - VII. Re-equilibration of fluid inclusions in quartz during laboratory-simulated metamorphic burial and uplift. Journal of metamorphic Geology **7**, 243-260.

Sterner, S.M., Hall, D.L. and Bodnar, R.J. (1988): Synthetic fluid inclusions. V. Solubility relations in the system NaCl-KCl-H_2O under vapor-saturated conditions. Geochimica and Cosmochimica Acta **52**, 989-1005.

Stevens, J. (1986): Applied multivariate statistics for the social sciences, Lawrence Erlbaum Associates, 515 pp.

Streckeisen, A. (1976): To each plutonic rock its proper name. Earth-Science Reviews **12**, 1-33.

Strong, D.F. (1988): A review and model for granite-related mineral deposits. *In* R.P. Taylor and D.F. Strong (eds) *Recent advances in the geology of granite-related mineral deposits*, Canadian institute of Mining and Metallurgy, Halifax, 424-445.

Sun, S.-S. and Eadington, P.J. (1987): Oxygen isotope evidence for the mixing of magmatic and meteoric waters during tin mineralization in the Mole granite, New South Wales, Australia. Economic Geology **83**, 43-52.

Suzuki, K., Shimizu, H. and Masuda, A. (1996): Re-Os dating of molybdenites from ore deposits in Japan: implication for the closure temperature of the Re-Os system for molybdenite and the cooling history of molybdenum ore deposits. Geochimica et Cosmochimica Acta **60**, 3151-3159.

Suzuki, K., Kagi, H., Nara, M., Takano, B. and Nozaki, Y. (2000): Experimental alteration of molybdenite of the Re-Os system, infrared spectroscopic profile and polytype. Geochimica and Cosmochimica Acta **60**, 223-232.

Suzuki, K., Feely, M. and O-Reilly, C. (2001): Disturbance of the Re-Os chronometer of molybdenites from the late-Caledonian Galway granite, Ireland, by hydrothermal fluid circulation. Geochemical Journal **35**, 29-35.

Suzuoki, T. and Epstein, S. (1976): Hydrogen isotope fractionation between OH-bearing minerals and water. Geochimica and Cosmochimica Acta **40**, 1229-1240.

Swan, A.R.H. and Sandilands, M. (1995): Introduction to geological data analysis, Blackwell Scientific, Oxford, 446 pp.

Tacker, R.C. and Candela, P.A. (1985): Experimental determination of crystal-melt partitioning of molybdenum in high-silica systems. Abstracts with programs **17**, 732.

Tacker, R.C. and Candela, P.A. (1987): partitioning of molybdenum between magnetite and melt: a preliminary experimental study of partitioning of ore metals between silicic magmas and crystalline phases. Economic Geology **82**, 1827-1838.

Tate, M.C. (1995): The relationship between late Devonian mafic intrusions and peraluminous granitoid generation in the Meguma lithotectonic Zone, Nova Scotia, Canada, PhD Thesis, Dalhousie University, Halifax.

Tate, M.C. and Clarke, D.B. (1995): Petrogenesis and regional tectonic significance of late Devonian mafic intrusions in the Meguma Zone, Nova Scotia. Canadian Journal of Earth Sciences **32**, 1883-1898.

Tate, M.C. and Clarke, D.B. (1997): Compositional diversity among Late Devonian peraluminous granitoid intrusions in the Meguma Zone of Nova Scotia, Canada. Lithos **39**, 179-194.

Tate, M.J.C., Clarke, D.B. and Heaman, L.M. (1997): Progressive hybridisation between Late Devonian mafic-intermediate and felsic magmas in the Meguma Zone of Nova Scotia, Canada. Contributions to Mineralogy and Petrology **126**, 401-415.

Taylor, B.E. (1987): Stable isotope geochemistry of ore-forming fluids. *In* T.K. Kyser (ed) *Short Course in stable isotope geochemistry of low temperature fluids,* Mineralogical Association of Canada, Saskatoon, 337-445.

Taylor, H.P. (1997): Oxygen and hydrogen isotope relationships in hydrothermal mineral deposits. *In* H.L. Barnes (ed) *Geochemistry of hydrothermal mineral deposits,* Wiley & Sons, 229-302.

Taylor, J.R. and Wall, V.J. (1993): Cassiterite solubility, tin speciation, and transport in a magmatic aqueous phase. Economic Geology **88**, 437-460.

Thorne, M.G. and Edwards, R.P. (1985): Recent advances in concepts of ore genesis in south west England. Transactions of the Royal Geological Society of Cornwall **21**, 113-152.

Tingle, T.N. and Fenn, P.M. (1984): Transport and concentration of molybdenum in granite and molybdenite systems: effect of fluorine and sulfur. Geology **12**, 156-158.

Tornos, F., Casquet, C., Caballero, J.M. and Galindo, C. (1991): A chemical model for the genesis of episyenites and superimposed ores linked with phyllic alteration. *In* M. Pagel, J. L. Leroy (eds) *Source, Transport, and deposition of metals*, Balkema, Rotterdam, 143-146.

Torrealday, H.I., Hitzman, M. W., Stein, H. J., Markley, R. J., Armstrong, R., Broughton, D. (2000): Re-Os and U-Pb dating of the vein-hosted mineralization at the Kansanshi copper deposit, Northern Zambia. Economic Geology **95**, 1165-1170.

Trumm, A. and Schroecke, H. (1979): Bestimmung thermodynamischer Parameter mittels elektrochemischer Messungen im System Fe-W-O. Determination of thermodynamic parameters by electrochemical measurements in the system of Fe-W-O. Neues Jahrbuch fuer Mineralogie Abhandlungen **134**, 157-166.

Tucker, R.D., Bradley, D. C., Ver Straeten, C. A., Harris, A. G., Ebert, J. R., McCutcheon, S. R. (1998): New U-Pb zircon ages and the duration and division of Devonian time. Earth and Planetary Science Letters **158**, 175-186.

Urabe, T. (1985): Aluminous granite as a source magma of hydrothermal ore deposits. An experimental study. Economic Geology **80**, 148-157.

Urabe, T. (1987): The effect of pressure on the partitioning ratios of lead and zinc between vapor and rhyolite melts. Economic Geology **82**, 1049-1052.

Var'yash, L.N. and Rekharskiy, V.I. (1981): Behaviour of Cu(I) in chloride solutions. Geochemistry International **7**, 1003-1008.

Velde, B. (1980): Cell dimensions, polymorph type, and infrared spectra of synthetic white micas: the importance of ordering. American Mineralogist **65**, 1277-1282.

Villa, I.M., Ruggieri, G. and Puxeddu, M. (1997): Petrological and geochronological discrimination of two white-mica generations in a granite cored from the

Larderello-Travale geothermal field (Italy). European Journal of Mineralogy 9, 563-568.

Walker, T.L. (1911): Report of the molybdenum ores of Canada. 93, Canada Department of Mines, Mines Branch.

Wallace, J.D., Bingley, J.M. and Shea, F.S. (1963): Geological and geochemical investigation of tin bearing area of New Ross, Lunenburg County. 48, NSDME, Halifax.

Warren, S.N. (2001): $^{40}Ar/^{39}Ar$ laser-probe study of K-feldspars from the New Ross area of the South Mountain Batholith, Nova Scotia, BSc Thesis, Dalhousie University, Halifax.

Wartho, J.-A., Kelley, S. P., Brooker, R. A., Carroll, M. R., Villa, I. M. Lee, M. R. (1999): Direct measurement of Ar diffusion profiles in a gem-quality Madagascar K-feldspar using the ultra-violet laser ablation microprobe (UVLAMP). Earth and Planetary Science Letters **170**, 141-153.

Webster, J.D. (1990): Partitioning of F between H_2O and CO_2 fluids and topaz rhyolite melt. Contributions to Mineralogy and Petrology **104**, 424-438.

Webster, J.D. (1992): Fluid-melt interactions involving Cl-rich granites: experimental study from 2 to 8 kbar. Geochimica and Cosmochimica Acta **56**, 659-678.

Webster, J.D. (1997a): Chloride solubility in felsic melts and the role of chloride in magmatic degassing. Journal of Petrology **38**, 1793-1807.

Webster, J.D. (1997b): Exsolution of magmatic volatile phases from Cl-enriched mineralizing granitic magmas and implications for ore metal transport. Geochimica et Cosmochimica Acta **61**, 1017-1029.

Webster, J.D. and Holloway, J.R. (1987): Partitioning of halogens between topaz rhyolite melt and aqueous and aqueous-carbonic fluids. Abstracts with Programs **19**, 884.

Webster, J.D. and Holloway, J.R. (1988): Experimental constraints on the partitioning of Cl between topaz rhyolite melt and H2O and H2O+CO2 fluids: new implications for granitic differentiation and ore deposition. Geochimica and Cosmochimica Acta **52**, 2091-2105.

Webster, J.D. and Holloway, J.R. (1990): Partitioning of F and Cl between magmatic hydrothermal fluids and highly evolved granitic magmas. *In* H.J. Stein and J.L. Hannah (eds) *Ore-bearing granite systems: Petrogenesis and Mineralising processes*, Geological Society of America Special Paper, 21-34.

Webster, J.D., Thomas, R. D., Forster, H.-J. and Seltmann, R. (1997): Melt inclusions in quartz from an evolved peraluminous pegmatite: geochemical evidence for strong tin enrichment in fluorine-rich and phosphorus-rich residual liquids. Geochimica et Cosmochimica Acta **61**, 2589-2604.

Weeks, L.J. (1945): Manganese, New Ross. NSDME Annual report, 135-166.

Westrich, H.R. (1974): The solubility of molybdenite in pH buffered KCl-HCl fluids. EOS **55**, 1200.

Williams, H. (1979): Appalachian Orogen in Canada. Canadian Journal of Earth Sciences **16**, 792-807.

Williams, H. (1995): Summary and overview. *In* H. Williams (ed) *Geology of the Appalachian-Caledonian orogen in Canada and Greenland*, 843-890.

Williams, H. and Hatcher, R.D. (1982): Suspect terranes and accretionary history of the Appalachian orogen. Geology **10**, 530-536.

Williams, H. and Hatcher, R.D. (1983): Appalachian suspect terranes. Geological Society of America Memoir **158**, 33-53.

Williams, H. and Haworth, R.T. (1984): Bouguer gravity anomaly map of Atlantic Canada. Memorial University of Newfoundland.

Wilson, A.F. (1978): Results of geological, geophysical and geochemical investigations at Millet Brook. 21A/16B 54-I-64(01), NSDNR, Halifax.

Wilson, G.A. and Eugster, H.P. (1990): Cassiterite solubility and tin speciation in supercritical chloride solutions. *In* R.J. Spencer and I.M. Chou (eds) *Fluid-mineral interactions - A tribute to H. P. Eugster*, The Geochemical Society Special Publication, 179-195.

Wolf, M.B., London, D. and Morgan, G.B. (1994): Effects of boron on the solubility of cassiterite and tantalite in granitic liquids. Abstracts with Programs **26**, A-450.

Wolfram, O. and Krupp, R.E. (1996): Hydrothermal solubility of rhodochrosite, Mn(II) speciation, and equilibrium constants. Geochimica et Cosmochimica Acta **60**, 3983-3994.

Wood, S.A. (1992): Experimental determination of the solubility of WO3 (s) and the thermodynamic properties of $H_2WO_{4(aq)}$ in the range 300-600°C at 1 kbar: calculation of scheelite solubility. Geochimica and Cosmochimica Acta **56**, 1827-1836.

Wood, S.A. and Samson, I.M. (1998): Solubility of ore minerals and complexation of ore minerals in hydrothermal solutions. *In* J.P. Richards and P.B. Larson (eds) *Techniques in hydrothermal ore deposits geology*, Society of Economic Geologists, Littletown, 33-80.

Wood, S.A. and Samson, I.M. (2000): The hydrothermal geochemistry of tungsten in granitoid environments: I. relative solubilities of ferberite and scheelite as a function of T, P, pH, and mNaCl. Economic Geology **95**, 143-182.

Wood, S.A. and Vlassopoulos, D. (1989): Experimental determination of the hydrothermal solubility and speciation of tungsten at 500°C and 1 kbar. Geochimica and Cosmochimica Acta **53**, 303-312.

Wood, S.A., Crerar, D.A. and Borcsik, M.P. (1987): Solubility of the assemblage pyrite-pyrrhotite-magnetite-sphalerite-galena-Au-stibnite-bismuthinite-argentite-molybdenite in H_2O-CO_2-NaCl solutions from 200 to 350°C. Economic Geology **82**, 1864-1887.

Wright, W.G. (1959): Memorandum. 21A/9B 35-L-09 (02), NSDME, Halifax.

Wright, W.J. (1912): Geology of the neighbourhood of New Ross, Lunenburg county, Nova Scotia. GSC Summary Report, 384-389.

Xiao, Z., Gammons, C.H. and Williams-Jones, A.E. (1998): Experimental study of copper(I) chloride complexing in hydrothermal solutions at 40 to 300°C and saturated water vapor pressure. Geochimica et Cosmochimica Acta **62**, 2949-2964.

Yudintsev, S. (1996): Solubility and valency of uranium in model granitic melts. Terra Nova **1**, 69.

Zane, A. and Rizzo, G. (1999): The compositional space of muscovite in granitic rocks. The Canadian Mineralogist **37**, 1229-1238.

Zen, E.-a. (1988): Phases relations of peraluminous granitic rocks and their petrogenetic implications. Annual Review of Earth and Planetary Sciences **16**, 21-51.

Zentilli, M. and Reynolds, P.H. (1985): 40Ar/39Ar dating of micas from the East Kemptville tin deposit, Yarmouth County, Nova Scotia. Canadian Journal of Earth Sciences **22**, 1546-1548.

Appendix A: Electron microprobe setting for white mica chemistry analyses

Analyses were carried out on a JEOL 733 electron microprobe equipped with four wavelength dispersive spectrometers and an Oxford Link eXL energy dispersive system. The energy dispersive system was used for all elements. Resolution of the energy dispersive detector was 137 ev at 5.9 Kev. Each spectrum was acquired for 40 seconds with an accelerating voltage of 15 Kv and a beam current of 15 nA. Probe spot size was approximately 1 micron. The raw data was corrected using Link's ZAF matrix correction program. Instrument calibration was performed on cobalt metal. Instrument precision on cobalt metal (n=10) was ± 0.5% at 1 standard deviation. Accuracy for major elements was ± 1.5 to 2% relative. Geological standards were used as controls. Detection limits for most elements using the energy dispersive system range from ~0.1 to 0.3%.

Appendix B: Geochemical data for white micas from the New Ross area

Abbreviations in the following Table are as follow:

P: primary

RB: biotite replacement

RF: feldspar replacement

S: sericite

SA: stellate aggregate

HP: hand-picked

G: greisen

FF: fracture filling

RA: andalusite replacement

RC: cordierite replacement

Sample	SC-1-R	SC-1-R	SC-1-R	SC-1-R	SC-1-R	SC-1-R	SC-1-R	SC-1-R
Point	5	7	7	5	8	6	2	1
Description	P	P	P	P	RB	RB	RF	RF
SiO2	46.08	45.83	46.48	46.20	46.11	45.97	46.21	45.90
TiO2	0.18	0.17	0.13	0.12	0.00	0.16	0.21	0.15
Al2O3	35.10	35.23	35.74	35.66	36.81	35.07	34.87	34.89
FeO	1.70	1.88	1.87	1.77	1.36	2.00	2.10	2.08
MnO	0.06	0.12	0.08	0.07	0.11	0.06	0.07	0.11
MgO	0.58	0.43	0.63	0.64	0.20	0.51	0.61	0.65
CaO	0.05	0.07	0.00	0.03	0.00	0.00	0.00	0.01
Na2O	0.74	0.70	0.72	0.75	0.63	0.66	0.57	0.66
K2O	10.41	10.59	10.77	10.68	10.94	10.65	10.61	10.72
Cr2O3	0.00	0.02	0.01	0.00	0.00	0.00	0.11	0.02
Cl	N/D	N/D	N/D	N/D	N/D	N/D	N/D	N/D
P2O5	N/D	N/D	N/D	N/D	N/D	N/D	N/D	N/D
BaO	0.06	0.00	N/D	N/D	0.23	0.03	0.00	0.00
F	N/D	N/D	0.60	0.82	N/D	N/D	N/D	N/D
Total	94.95	95.05	97.03	96.73	96.39	95.11	95.35	95.19
Si	6.40	6.30	6.22	6.15	6.14	6.20	6.15	6.26
Ti	0.02	0.04	0.00	0.02	0.03	0.02	0.02	0.02
Al Total	4.72	4.85	5.48	5.63	5.62	5.55	5.65	5.48
Al IV	1.60	1.70	1.78	1.85	1.86	1.80	1.85	1.74
Al VI	3.11	3.15	3.70	3.78	3.77	3.74	3.81	3.73
Fe	0.94	0.92	0.39	0.25	0.25	0.32	0.19	0.37
Mn	0.03	0.04	0.02	0.01	0.01	0.00	0.01	0.00
Mg	0.06	0.06	0.00	0.05	0.02	0.02	0.03	0.03
Ca	0.01	0.01	0.00	0.00	0.00	0.00	0.00	0.00
Na	0.15	0.16	0.13	0.18	0.20	0.20	0.22	0.22
K	1.92	1.90	1.66	1.62	1.61	1.62	1.63	1.57
Cr	0.00	0.00	0.01	0.00	0.00	0.00	0.00	0.01
Cl			0.01	0.00	0.00	0.01	0.01	0.01
P			0.00	0.00	0.01	0.01	0.00	0.01
Ba		0.00	0.01	0.00	0.01	0.00	0.00	0.00
F	0.77	0.71	0.00	0.00	0.00	0.04	0.00	0.22
OH	3.23	3.29	3.99	4.00	4.00	3.95	4.00	3.78
Tetrahedral	8.00	8.00	8.00	8.00	8.00	8.00	8.00	8.00
Octahedral	4.19	4.21	4.11	4.11	4.08	4.10	4.06	4.16
Dodecahedral	2.07	2.06	1.82	1.80	1.83	1.83	1.86	1.81

Sample	SC-1-R	SC-1-R	SC-1-R	SC-1-R	SC-7-R	SC-7-R	SC-7-R	SC-7-R
Point	2	1	10	10	1	6	1	6
Description	RF	RF	S	S	P	P	P	P
SiO2	46.46	45.88	48.96	47.41	44.30	46.06	44.56	45.49
TiO2	0.13	0.06	0.01	0.01	0.58	0.07	0.36	0.53
Al2O3	34.99	35.45	36.44	37.34	28.23	33.69	28.75	29.42
FeO	2.18	2.15	0.16	1.14	8.62	3.07	9.89	8.43
MnO	0.09	0.01	0.00	0.04	0.25	0.12	0.26	0.14
MgO	0.65	0.64	0.00	0.04	0.33	0.27	0.25	0.33
CaO	0.01	0.07	0.00	0.05	0.00	0.00	0.00	0.07
Na2O	0.71	0.73	1.30	0.33	0.47	0.89	0.65	0.35
K2O	10.76	10.72	10.39	11.12	10.66	10.16	10.46	10.56
Cr2O3	0.06	0.00	0.00	0.00	0.00	0.00	0.00	0.08
Cl	N/D	N/D	N/D	N/D	N/D	N/D	N/D	N/D
P2O5	N/D	N/D	N/D	N/D	N/D	N/D	N/D	N/D
BaO	0.01	0.00	N/D	0.01	0.08	0.00	N/D	0.00
F	0.79	1.02	0.14	0.21	N/D	N/D	3.22	2.61
Total	96.85	96.73	97.41	97.70	93.52	94.33	98.39	98.02
Si	6.25	6.18	6.17	6.21	6.25	6.38	6.21	6.32
Ti	0.01	0.02	0.03	0.03	0.00	0.03	0.00	0.01
Al Total	5.47	5.62	5.63	5.55	5.37	5.06	5.41	5.13
Al IV	1.75	1.82	1.83	1.79	1.75	1.62	1.79	1.68
Al VI	3.72	3.80	3.81	3.76	3.62	3.44	3.62	3.45
Fe	0.41	0.27	0.25	0.33	0.53	0.77	0.56	0.71
Mn	0.00	0.00	0.01	0.00	0.02	0.01	0.01	0.02
Mg	0.03	0.02	0.03	0.03	0.12	0.10	0.15	0.18
Ca	0.00	0.00	0.01	0.00	0.01	0.00	0.00	0.00
Na	0.21	0.20	0.18	0.18	0.13	0.12	0.14	0.15
K	1.60	1.53	1.61	1.63	1.76	1.85	1.78	1.81
Cr	0.00	0.00	0.00	0.00	0.00	0.00	0.00	0.01
Cl	0.00	0.01	0.00	0.01	0.01	0.00	0.01	0.00
P	0.01	0.00	0.00	0.00	0.00	0.02	0.00	0.01
Ba	0.00	0.00	0.00	0.00	0.01	0.00	0.01	0.01
F	0.17	0.00	0.11	0.12	0.38	0.62	0.46	0.61
OH	3.83	4.00	3.89	3.87	3.61	3.38	3.53	3.39
Tetrahedral	8.00	8.00	8.00	8.00	8.00	8.00	8.00	8.00
Octahedral	4.17	4.12	4.14	4.15	4.30	4.35	4.34	4.37
Dodecahedral	1.81	1.73	1.80	1.81	1.90	1.98	1.93	1.99

Sample	SC-7-R	SC-7-R	SC-7-R	SC-7-R	SC-7-R	SC-7-R	SC-7-R	SC-7-R
Point	4	7	2	5	5	2	2	8
Description	RB	RB	RF	RF	RF	RF	RF	S
SiO2	45.31	44.92	46.40	45.60	46.21	46.69	45.52	46.15
TiO2	0.30	0.43	0.10	0.14	0.13	0.14	0.36	0.38
Al2O3	32.55	28.86	34.17	34.17	34.09	34.25	30.46	31.09
FeO	4.41	7.73	2.86	2.96	3.48	3.38	7.05	6.24
MnO	0.14	0.12	0.00	0.06	0.11	0.00	0.16	0.11
MgO	0.30	0.36	0.40	0.29	0.21	0.33	0.23	0.33
CaO	0.01	0.00	0.00	0.00	0.00	0.02	0.04	0.04
Na2O	0.86	0.37	1.00	0.87	0.87	0.69	0.39	0.40
K2O	10.23	10.60	10.23	10.18	10.50	10.98	10.65	10.84
Cr2O3	0.00	0.03	0.09	0.00	0.00	0.02	0.06	0.00
Cl	N/D	N/D	N/D	N/D	N/D	N/D	N/D	N/D
P2O5	N/D	N/D	N/D	N/D	N/D	N/D	N/D	N/D
BaO	0.00	0.00	0.17	0.00	N/D	N/D	0.00	N/D
F	N/D	N/D	N/D	N/D	1.60	1.87	2.33	2.21
Total	94.11	93.42	95.43	94.26	97.21	98.35	97.23	97.79
Si	6.11	6.14	6.12	6.12	6.15	6.15	6.16	6.13
Ti	0.03	0.05	0.05	0.05	0.04	0.04	0.01	0.02
Al Total	5.63	5.53	5.54	5.56	5.48	5.50	5.67	5.68
Al IV	1.89	1.86	1.88	1.88	1.85	1.85	1.84	1.87
Al VI	3.74	3.66	3.66	3.68	3.63	3.65	3.82	3.81
Fe	0.12	0.18	0.16	0.18	0.21	0.18	0.14	0.15
Mn	0.00	0.00	0.00	0.00	0.01	0.01	0.00	0.00
Mg	0.13	0.15	0.16	0.15	0.19	0.17	0.12	0.11
Ca	0.00	0.01	0.01	0.00	0.01	0.00	0.01	0.01
Na	0.15	0.14	0.13	0.17	0.14	0.17	0.15	0.14
K	1.89	1.87	1.91	1.84	1.83	1.83	1.65	1.62
Cr	0.01	0.00	0.01	0.00	0.01	0.00	0.00	0.01
Cl							0.02	0.00
P							0.00	0.00
Ba	0.02	0.00	0.01	0.02	0.00	0.01	0.00	0.00
F	0.02	0.02	0.02	0.04	0.03	0.06	0.00	0.00
OH	3.98	3.98	3.98	3.96	3.97	3.94	3.99	4.00
Tetrahedral	8.00	8.00	8.00	8.00	8.00	8.00	8.00	8.00
Octahedral	4.02	4.05	4.03	4.05	4.08	4.06	4.09	4.11
Dodecahedral	2.06	2.01	2.06	2.02	1.97	2.01	1.80	1.78

Sample	SC-7-R	SC-8-R	SC-8-R	SC-8-R	SC-8-R	SC-8-R	SC-8-R	SC-8-R
Point	9	12	33	36	43	52	15	17
Description	S	SA	SA	SA	SA	SA	P	P
SiO2	44.59	46.60	46.13	46.27	46.35	46.02	46.84	45.89
TiO2	0.01	0.09	0.04	0.08	0.06	0.00	0.21	0.40
Al2O3	35.26	31.51	34.52	34.70	34.54	34.19	34.46	29.47
FeO	1.67	6.39	3.97	2.90	3.50	4.14	2.95	7.85
MnO	0.00	0.13	0.12	0.14	0.18	0.16	0.01	0.32
MgO	0.00	0.14	0.08	0.03	0.07	0.06	0.28	0.23
CaO	0.00	0.00	0.00	0.00	0.00	0.00	0.00	0.00
Na2O	0.79	0.27	0.46	0.53	0.52	0.47	0.83	0.37
K2O	10.24	9.64	9.72	8.53	10.64	10.09	9.67	9.87
Cr2O3	0.00	0.00	0.06	0.00	0.00	0.00	0.00	0.00
Cl	N/D	0.00	0.00	0.17	0.00	0.00	0.01	0.00
P2O5	N/D	0.12	0.17	0.13	0.21	0.14	0.00	0.08
BaO	0.00	0.00	0.00	0.00	0.00	0.11	0.00	0.00
F	1.14	2.40	1.25	1.35	1.06	1.41	1.23	3.49
Total	93.69	97.29	96.53	94.83	97.13	96.80	96.47	97.96
Si	6.18	6.08	6.33	6.09	6.22	6.37	6.52	6.85
Ti	0.02	0.00	0.00	0.00	0.04	0.00	0.05	0.00
Al Total	5.62	5.75	5.57	5.74	5.44	5.53	4.82	4.83
Al IV	1.82	1.92	1.67	1.91	1.78	1.63	1.48	1.15
Al VI	3.80	3.83	3.90	3.82	3.66	3.91	3.35	3.68
Fe	0.13	0.14	0.04	0.13	0.17	0.07	0.95	0.10
Mn	0.00	0.01	0.02	0.00	0.00	0.00	0.02	0.01
Mg	0.13	0.05	0.04	0.09	0.15	0.08	0.06	0.04
Ca	0.01	0.00	0.01	0.01	0.01	0.01	0.00	0.00
Na	0.14	0.18	0.00	0.18	0.18	0.02	0.11	0.01
K	1.66	1.84	1.74	1.77	1.80	1.50	1.75	1.77
Cr	0.00	0.01	0.00	0.00	0.00	0.00	0.00	0.00
Cl	0.00					0.00	0.00	0.00
P	0.00					0.00	0.02	0.01
Ba	0.00	0.00	0.00	0.01		0.00	0.00	0.00
F	0.00	0.06	0.01	0.08	0.06	0.00	0.75	0.00
OH	4.00	3.94	3.99	3.92	3.94	4.00	3.25	4.00
Tetrahedral	8.00	8.00	8.00	8.00	8.00	8.00	8.00	8.00
Octahedral	4.10	4.02	4.01	4.06	4.02	4.08	4.43	3.83
Dodecahedral	1.80	2.02	1.74	1.96	1.99	1.54	1.87	1.79

Sample	SC-8-R	SC-8-R	SC-8-R	SC-8-R	SC-8-R	SC-8-R	SC-8-R	SC-8-R
Point	17edge	48	7	23	26	26b	42	25
Description	P	P	RB	RF	RF	RF	RF	S
SiO2	46.19	46.49	46.84	44.67	46.63	46.56	46.75	46.86
TiO2	0.31	0.14	0.07	0.30	0.08	0.04	0.03	0.00
Al2O3	30.13	35.49	33.93	27.43	35.36	34.65	32.21	35.92
FeO	7.03	3.18	3.99	10.78	2.31	3.63	5.72	1.93
MnO	0.11	0.06	0.10	0.22	0.00	0.13	0.32	0.03
MgO	0.27	0.01	0.07	0.22	0.16	0.23	0.17	0.07
CaO	0.00	0.00	0.00	0.00	0.00	0.00	0.06	0.02
Na2O	0.21	0.71	0.36	0.33	0.80	0.41	0.36	0.46
K2O	9.90	9.89	9.92	9.91	9.52	8.95	9.67	8.68
Cr2O3	0.06	0.01	0.08	0.02	0.00	0.09	0.00	0.00
Cl	0.00	0.00	0.00	0.02	0.04	0.00	0.00	0.02
P2O5	0.05	0.02	0.13	0.02	0.11	0.21	0.11	0.04
BaO	0.00	0.00	0.00	0.10	0.00	0.00	0.10	0.06
F	2.76	1.30	1.41	3.63	0.66	0.31	1.78	0.09
Total	97.02	97.30	96.88	97.64	95.70	95.21	97.26	94.21
Si	6.12	6.15	6.16	6.35	6.39	6.12	6.11	6.16
Ti	0.00	0.00	0.00	0.03	0.01	0.00	0.01	0.01
Al Total	5.86	5.83	5.81	5.39	5.35	5.96	5.93	5.87
Al IV	1.88	1.85	1.84	1.65	1.61	1.88	1.89	1.84
Al VI	3.98	3.98	3.97	3.74	3.75	4.08	4.05	4.03
Fe	0.01	0.02	0.01	0.36	0.36	0.05	0.10	0.11
Mn	0.00	0.00	0.00	0.00	0.01	0.01	0.00	0.00
Mg	0.01	0.00	0.00	0.15	0.17	0.01	0.02	0.02
Ca	0.00	0.00	0.01	0.00	0.00	0.00	0.01	0.01
Na	0.08	0.07	0.06	0.08	0.08	0.13	0.15	0.14
K	1.84	1.78	1.82	1.60	1.62	1.58	1.62	1.50
Cr	0.00	0.00	0.01	0.00	0.00	0.00	0.01	0.00
Cl				0.00	0.00	0.00	0.02	0.01
P				0.01	0.00	0.00	0.00	0.00
Ba				0.00	0.00	0.00	0.00	0.00
F	0.09	0.10	0.10	0.43	0.48	0.22	0.34	0.18
OH	3.91	3.90	3.90	3.56	3.52	3.78	3.65	3.82
Tetrahedral	8.00	8.00	8.00	8.00	8.00	8.00	8.00	8.00
Octahedral	4.00	4.01	3.99	4.28	4.30	4.15	4.18	4.16
Dodecahedral	1.91	1.85	1.88	1.68	1.70	1.71	1.79	1.63

Sample	SC-9-R	SC-9-R	SC-9-R	SC-9-R	SC-9-R	SC-9-R	SC-9-R	SC-9-R
Point	3b	14	15	28	35	40	42	43
Description	SA	SA	SA	SA	SA	SA	SA	SA
SiO2	47.47	46.61	46.29	46.95	47.02	46.88	47.05	47.23
TiO2	0.02	0.15	0.06	0.01	0.04	0.00	0.18	0.00
Al2O3	33.59	34.51	33.96	33.81	35.59	33.46	33.78	34.50
FeO	4.63	4.20	4.65	4.38	2.61	4.58	4.25	3.80
MnO	0.12	0.14	0.12	0.19	0.00	0.10	0.09	0.12
MgO	0.00	0.05	0.03	0.11	0.13	0.11	0.16	0.11
CaO	0.06	0.00	0.00	0.00	0.04	0.00	0.00	0.00
Na2O	0.37	0.47	0.34	0.37	0.67	0.38	0.63	0.63
K2O	9.61	10.18	9.76	10.08	9.85	9.71	9.21	9.34
Cr2O3	0.01	0.00	0.00	0.00	0.02	0.00	0.03	0.07
Cl	0.00	0.00	0.00	0.02	0.01	0.02	0.00	0.01
P2O5	0.14	0.12	0.11	0.06	0.06	0.13	0.05	0.11
BaO	0.07	0.01	0.00	0.00	0.12	0.06	0.00	0.17
F	1.64	1.33	1.39	1.28	0.68	1.46	1.57	1.35
Total	97.74	97.76	96.72	97.24	96.84	96.89	97.00	97.42
Si	7.48	6.40	6.52	6.67	6.50	6.11	6.26	6.21
Ti	0.00	0.02	0.00	0.01	0.00	0.01	0.00	0.00
Al Total	3.74	5.17	5.14	4.50	5.09	5.83	5.54	5.57
Al IV	0.52	1.60	1.48	1.33	1.50	1.89	1.74	1.79
Al VI	3.21	3.57	3.66	3.17	3.60	3.94	3.80	3.77
Fe	0.86	0.47	0.26	0.78	0.30	0.10	0.16	0.18
Mn	0.06	0.02	0.03	0.04	0.03	0.00	0.00	0.01
Mg	0.08	0.11	0.19	0.13	0.16	0.04	0.17	0.14
Ca	0.00	0.00	0.00	0.01	0.01	0.00	0.00	0.02
Na	0.15	0.09	0.08	0.07	0.04	0.12	0.11	0.10
K	1.86	1.77	1.67	1.73	1.61	1.62	1.53	1.66
Cr	0.00	0.00	0.00	0.00	0.01	0.00	0.00	0.00
Cl	0.00	0.01	0.00	0.00	0.00	0.02	0.00	0.00
P	0.00	0.00	0.00	0.01	0.00	0.00	0.00	0.00
Ba	0.00	0.00	0.00	0.00	0.01	0.01	0.00	0.01
F	1.11	0.27	0.26	0.00	0.00	0.00	0.00	0.00
OH	2.89	3.73	3.74	4.00	4.00	3.99	4.00	4.00
Tetrahedral	8.00	8.00	8.00	8.00	8.00	8.00	8.00	8.00
Octahedral	4.20	4.20	4.15	4.14	4.09	4.09	4.14	4.12
Dodecahedral	2.01	1.86	1.75	1.81	1.67	1.75	1.64	1.77

Sample	SC-9-R	SC-9-R	SC-9-R	SC-9-R	SC-10-R	SC-10-R	SC-10-R	SC-10-R
Point	47	57	9	12	15	2	3	4
Description	SA	SA	S	S	FF	SA	SA	SA
SiO2	46.31	46.00	47.47	46.47	47.28	47.12	47.26	46.64
TiO2	0.00	0.01	0.08	0.08	0.00	0.04	0.11	0.17
Al2O3	34.71	33.80	33.97	30.57	38.38	23.42	32.69	25.54
FeO	4.41	3.72	3.78	7.00	0.02	10.22	4.09	8.53
MnO	0.10	0.11	0.30	0.31	0.00	0.86	0.30	0.93
MgO	0.09	0.03	0.02	0.03	0.06	0.00	0.00	0.00
CaO	0.00	0.01	0.00	0.00	0.00	0.00	0.00	0.00
Na2O	0.51	0.58	0.44	0.27	0.30	0.61	0.35	0.44
K2O	9.97	9.36	9.51	10.10	9.95	9.97	9.96	10.25
Cr2O3	0.05	0.00	0.00	0.00	0.00	0.04	0.00	0.00
Cl	0.00	0.00	0.00	0.04	0.02	0.04	0.00	0.00
P2O5	0.10	0.18	0.07	0.08	0.02	0.15	0.10	0.04
BaO	0.28	0.11	0.04	0.00	0.19	0.00	0.00	0.07
F	1.60	1.65	1.51	2.68	0.00	6.84	2.14	5.91
Total	98.12	95.56	97.19	97.64	96.20	99.31	97.00	98.52
Si	6.32	6.16	6.15	6.37	6.38	6.43	6.38	6.45
Ti	0.00	0.00	0.00	0.06	0.03	0.01	0.01	0.02
Al Total	5.55	5.72	5.80	4.99	5.35	5.31	5.21	5.07
Al IV	1.68	1.84	1.85	1.63	1.62	1.57	1.62	1.55
Al VI	3.87	3.87	3.95	3.36	3.73	3.74	3.59	3.52
Fe	0.02	0.12	0.06	0.70	0.43	0.50	0.48	0.63
Mn	0.00	0.00	0.01	0.01	0.03	0.01	0.01	0.03
Mg	0.00	0.01	0.03	0.12	0.04	0.04	0.04	0.07
Ca	0.00	0.01	0.00	0.00	0.00	0.01	0.00	0.00
Na	0.33	0.08	0.11	0.10	0.05	0.05	0.09	0.07
K	1.71	1.84	1.66	1.73	1.65	1.54	1.62	1.63
Cr	0.00	0.00	0.01	0.00	0.00	0.00	0.01	0.00
Cl			0.00	0.03	0.00	0.02	0.00	0.00
P			0.00	0.01	0.00	0.01	0.02	0.00
Ba		0.00	0.01	0.00	0.00	0.00	0.00	0.00
F	0.03	0.04	0.01	0.24	0.38	0.43	0.11	0.26
OH	3.97	3.96	3.99	3.74	3.62	3.56	3.89	3.74
Tetrahedral	8.00	8.00	8.00	8.00	8.00	8.00	8.00	8.00
Octahedral	3.89	4.02	4.04	4.26	4.26	4.31	4.14	4.27
Dodecahedral	2.04	1.93	1.79	1.84	1.70	1.60	1.74	1.70

Sample	SC-10-R	SC-10-R	SC-10-R	SC-10-R	SC-11-R	SC-11-R	SC-11-R	SC-11-R
Point	11	12	13	17	8	8	8	24
Description	SA	SA	SA	S	P	P	P	P
SiO2	46.73	46.14	46.85	49.23	46.86	45.26	44.57	46.29
TiO2	0.14	0.11	0.12	0.00	0.01	0.23	0.37	0.09
Al2O3	26.62	24.17	27.21	36.27	31.38	28.33	29.11	30.08
FeO	8.36	9.87	7.74	0.67	3.57	7.94	7.76	6.86
MnO	0.82	1.01	0.91	0.01	0.15	0.28	0.35	0.34
MgO	0.08	0.01	0.02	0.44	0.12	0.30	0.27	0.28
CaO	0.04	0.00	0.06	0.06	0.03	0.09	0.07	0.00
Na2O	0.36	0.63	0.43	0.08	0.29	0.54	0.59	0.33
K2O	9.33	10.05	10.18	9.10	10.92	10.66	10.52	9.97
Cr2O3	0.00	0.07	0.00	0.04	0.02	0.00	0.00	0.01
Cl	0.00	0.02	0.00	0.00	N/D	N/D	N/D	0.00
P2O5	0.13	0.05	0.00	0.04	N/D	N/D	N/D	0.12
BaO	0.00	0.12	0.00	0.07	0.08	N/D	0.00	0.08
F	5.35	6.57	5.30	0.00	N/D	3.44	3.18	2.99
Total	97.95	98.81	98.82	96.01	93.43	97.08	96.79	97.44
Si	6.40	6.36	6.41	7.16	6.24	6.20	6.15	6.18
Ti	0.01	0.00	0.02	0.03	0.02	0.02	0.00	0.00
Al Total	5.38	5.29	5.09	3.66	5.18	5.30	5.51	5.48
Al IV	1.60	1.64	1.59	0.84	1.76	1.80	1.85	1.82
Al VI	3.78	3.65	3.50	2.82	3.42	3.51	3.66	3.65
Fe	0.35	0.46	0.62	1.54	0.68	0.55	0.28	0.31
Mn	0.02	0.03	0.04	0.09	0.02	0.01	0.02	0.00
Mg	0.03	0.03	0.06	0.11	0.02	0.03	0.11	0.12
Ca	0.00	0.01	0.00	0.00	0.00	0.00	0.00	0.00
Na	0.11	0.07	0.09	0.13	0.15	0.19	0.26	0.26
K	1.59	1.67	1.62	1.77	1.84	1.83	1.77	1.72
Cr	0.00	0.00	0.00	0.00	0.00	0.00	0.00	0.01
Cl	0.00	0.00	0.00	0.00				
P	0.00	0.00	0.01	0.00				
Ba	0.00	0.01	0.00	0.00	0.00	0.00	0.00	0.01
F	0.28	0.13	0.19	1.11	0.42	0.36	0.34	0.39
OH	3.72	3.87	3.81	2.89	3.58	3.64	3.66	3.61
Tetrahedral	8.00	8.00	8.00	8.00	8.00	8.00	8.00	8.00
Octahedral	4.19	4.18	4.24	4.59	4.16	4.12	4.08	4.09
Dodecahedral	1.70	1.75	1.72	1.89	1.99	2.02	2.03	1.99

Sample	SC-11-R	SC-11-R	SC-11-R	SC-11-R	SC-11-R	SC-11-R	SC-11-R	SC-11-R
Point	24b	24c	5	6	7	2	3	3
Description	P	P	RA	RA	RB	RF	RF	RF
SiO2	45.67	46.71	45.87	46.86	46.21	44.53	45.78	45.45
TiO2	0.45	0.24	0.00	0.51	0.00	0.38	0.33	0.27
Al2O3	30.26	31.72	36.00	29.19	32.84	28.54	29.55	30.64
FeO	7.51	5.75	1.29	5.54	2.53	8.03	7.25	6.09
MnO	0.24	0.15	0.04	0.15	0.09	0.35	0.30	0.19
MgO	0.25	0.27	0.68	0.22	0.05	0.40	0.24	0.29
CaO	0.00	0.04	0.00	0.08	0.00	0.01	0.00	0.00
Na2O	0.31	0.37	0.75	0.51	0.48	0.44	0.49	0.34
K2O	9.72	10.00	10.60	10.80	11.11	10.73	10.59	10.59
Cr2O3	0.00	0.00	0.00	0.09	0.00	0.00	0.00	0.09
Cl	0.06	0.01	N/D	N/D	N/D	N/D	N/D	N/D
P2O5	0.01	0.10	N/D	N/D	N/D	N/D	N/D	N/D
BaO	0.00	0.03	0.24	0.00	0.05	0.17	N/D	0.00
F	3.28	2.22	N/D	N/D	N/D	N/D	3.09	2.17
Total	97.75	97.61	95.46	93.95	93.37	93.57	97.61	96.14
Si	6.10	6.13	6.16	6.11	6.09	6.10	6.14	6.16
Ti	0.02	0.02	0.00	0.01	0.02	0.03	0.01	0.02
Al Total	5.60	5.52	5.52	5.63	5.58	5.56	5.58	5.60
Al IV	1.90	1.87	1.84	1.89	1.91	1.90	1.86	1.84
Al VI	3.70	3.64	3.68	3.74	3.67	3.66	3.72	3.77
Fe	0.23	0.29	0.25	0.33	0.37	0.34	0.31	0.25
Mn	0.00	0.01	0.00	0.01	0.01	0.00	0.01	0.00
Mg	0.10	0.13	0.13	0.03	0.03	0.05	0.02	0.03
Ca	0.01	0.00	0.00	0.00	0.00	0.00	0.00	0.00
Na	0.28	0.28	0.31	0.23	0.25	0.16	0.26	0.23
K	1.72	1.70	1.74	1.64	1.77	1.87	1.74	1.67
Cr	0.01	0.01	0.00	0.00	0.00	0.00	0.00	0.00
Cl								
P								
Ba	0.00	0.00	0.01	0.00	0.00	0.00	0.00	0.00
F	0.30	0.39	0.36	0.24	0.28	0.35	0.31	0.26
OH	3.70	3.61	3.64	3.76	3.72	3.65	3.69	3.74
Tetrahedral	8.00	8.00	8.00	8.00	8.00	8.00	8.00	8.00
Octahedral	4.06	4.10	4.06	4.13	4.09	4.07	4.07	4.07
Dodecahedral	2.01	1.98	2.05	1.87	2.01	2.04	2.00	1.90

Sample	SC-11-R	SC-11-R	SC-11-R	SC-11-R	SC-11-R	SC-2-M	SC-2-M	SC-2-M
Point	63	64	11	9	10	1	12	12b
Description	S	S	S	S	S	P	P	P
SiO2	46.16	52.73	46.01	45.63	46.71	46.86	45.88	46.23
TiO2	0.44	0.05	0.00	0.00	0.00	0.21	0.11	0.12
Al2O3	28.95	31.59	37.40	36.69	37.42	34.76	33.70	34.86
FeO	8.03	0.88	0.09	0.15	0.12	3.16	4.55	3.26
MnO	0.20	0.10	0.00	0.01	0.00	0.05	0.09	0.02
MgO	0.30	0.18	0.04	0.00	0.02	0.45	0.33	0.42
CaO	0.00	0.00	0.01	0.02	0.04	0.00	0.02	0.03
Na2O	0.40	0.04	0.30	0.26	0.22	0.76	0.61	0.71
K2O	9.69	10.68	10.82	10.35	10.80	9.57	7.97	8.37
Cr2O3	0.00	0.00	0.00	0.00	0.06	0.09	0.00	0.03
Cl	0.00	0.00	N/D	N/D	N/D	0.00	0.00	0.01
P2O5	0.14	0.05	N/D	N/D	N/D	0.00	0.11	0.04
BaO	0.00	0.00	N/D	N/D	N/D	0.01	0.05	0.00
F	3.38	0.00	0.43	0.45	0.47	2.22	2.68	2.46
Total	97.67	96.31	95.11	93.56	95.87	98.14	96.10	96.56
Si	6.17	6.13	6.12	6.15	6.14	6.07	6.05	6.34
Ti	0.02	0.01	0.01	0.01	0.05	0.01	0.00	0.00
Al Total	5.48	5.59	5.54	5.58	5.49	5.79	5.78	5.31
Al IV	1.83	1.87	1.88	1.85	1.86	1.93	1.95	1.66
Al VI	3.65	3.73	3.65	3.74	3.64	3.86	3.83	3.65
Fe	0.34	0.29	0.37	0.29	0.25	0.13	0.15	0.29
Mn	0.00	0.00	0.01	0.00	0.00	0.00	0.01	0.01
Mg	0.03	0.04	0.02	0.04	0.15	0.03	0.05	0.01
Ca	0.00	0.01	0.01	0.01	0.00	0.00	0.00	0.00
Na	0.21	0.16	0.27	0.23	0.23	0.20	0.22	0.13
K	1.83	1.79	1.76	1.63	1.71	1.79	1.83	1.95
Cr	0.01	0.01	0.01	0.01	0.00	0.01	0.00	0.00
Cl								
P								
Ba	0.00	0.00	0.00	0.00	0.00	0.00	0.00	0.00
F	0.28	0.40	0.27	0.17	0.19	0.00	0.00	
OH	3.72	3.60	3.73	3.83	3.81	4.00	4.00	4.00
Tetrahedral	8.00	8.00	8.00	8.00	8.00	8.00	8.00	8.00
Octahedral	4.04	4.07	4.07	4.10	4.09	4.02	4.03	3.97
Dodecahedral	2.06	1.97	2.04	1.87	1.94	1.99	2.05	2.07

Sample	SC-2-M	SC-2-M	SC-2-M	SC-2-M	SC-2-M	SC-2-M	SC-2-M	SC-2-M
Point	12c	13	8	8b	2	2b	11	15
Description	P	P	RC	RC	RF	RF	RF	RF
SiO2	45.71	46.62	46.20	47.70	46.36	46.38	46.80	49.18
TiO2	0.15	0.16	0.09	0.17	0.02	0.00	0.33	0.07
Al2O3	34.58	34.77	38.40	35.86	35.55	36.97	33.90	29.11
FeO	3.13	3.76	0.91	3.09	3.27	2.10	3.88	7.00
MnO	0.04	0.24	0.01	0.18	0.01	0.00	0.00	0.00
MgO	0.31	0.24	0.09	0.34	0.07	0.22	0.35	0.29
CaO	0.02	0.00	0.02	0.12	0.08	0.07	0.01	0.07
Na2O	0.65	0.77	0.45	0.56	0.59	0.38	0.46	0.21
K2O	8.02	9.19	9.92	9.21	8.85	8.73	9.21	8.64
Cr2O3	0.00	0.02	0.12	0.00	0.06	0.12	0.00	0.01
Cl	0.03	0.00	0.02	0.02	0.00	0.00	0.00	0.01
P2O5	0.00	0.00	0.00	0.00	0.09	0.25	0.04	0.00
BaO	0.02	0.00	0.00	0.00	0.09	0.11	0.02	0.18
F	2.44	2.66	0.37	1.69	2.28	0.67	2.25	2.60
Total	95.10	98.43	96.60	98.94	97.32	96.00	97.25	97.37
Si	6.23	6.20	6.10	6.16	6.09	6.15	6.26	6.22
Ti	0.00	0.03	0.00	0.02	0.00	0.01	0.02	0.03
Al Total	5.43	5.45	5.74	5.54	5.70	5.40	5.22	5.27
Al IV	1.77	1.80	1.90	1.84	1.91	1.85	1.74	1.78
Al VI	3.66	3.64	3.83	3.70	3.78	3.55	3.48	3.49
Fe	0.28	0.25	0.15	0.22	0.13	0.46	0.54	0.51
Mn	0.01	0.01	0.01	0.01	0.01	0.01	0.01	0.02
Mg	0.11	0.10	0.04	0.10	0.14	0.08	0.06	0.06
Ca	0.00	0.00	0.00	0.00	0.00	0.00	0.00	0.00
Na	0.22	0.21	0.16	0.17	0.20	0.24	0.16	0.23
K	1.76	1.81	1.85	1.82	1.77	1.79	1.85	1.79
Cr	0.00	0.00	0.00	0.00	0.01	0.01	0.00	0.00
Cl								
P								
Ba	0.01	0.00	0.01	0.00	0.00	0.00	0.00	0.00
F					0.00	0.23	0.26	
OH	4.00	4.00	4.00	4.00	4.00	3.77	3.74	4.00
Tetrahedral	8.00	8.00	8.00	8.00	8.00	8.00	8.00	8.00
Octahedral	4.06	4.04	4.03	4.05	4.07	4.11	4.11	4.10
Dodecahedral	1.98	2.02	2.02	1.99	1.98	2.04	2.01	2.02

Sample	SC-2-M	SC-2-M	SC-2-M	SC-2-M	SC-3-M	SC-3-M	SC-3-M	SC-3-M
Point	4	5	6	16	3	1	5	3
Description	S	S	S	S	P	P	P	P
SiO2	46.79	46.03	47.17	46.73	45.85	46.18	44.85	45.82
TiO2	0.00	0.17	0.01	0.06	0.14	0.15	0.22	0.15
Al2O3	38.57	35.19	36.78	38.61	33.69	34.41	30.64	33.45
FeO	0.54	2.91	1.48	0.94	3.76	3.39	7.52	3.77
MnO	0.06	0.02	0.00	0.00	0.05	0.01	0.14	0.00
MgO	0.00	0.23	0.06	0.09	0.43	0.39	0.25	0.36
CaO	0.06	0.06	0.00	0.02	0.05	0.00	0.00	0.00
Na2O	0.43	0.52	0.27	0.39	1.02	1.05	0.54	0.77
K2O	10.03	8.69	10.01	9.85	10.41	10.27	10.32	10.40
Cr2O3	0.08	0.00	0.00	0.02	0.01	0.06	0.00	0.09
Cl	0.02	0.02	0.02	0.01	N/D	N/D	N/D	N/D
P2O5	0.16	0.01	0.28	0.07	N/D	N/D	N/D	N/D
BaO	0.02	0.02	0.02	0.00	N/D	N/D	0.00	0.03
F	0.74	1.95	0.67	0.74	1.26	1.62	1.78	1.22
Total	97.50	95.82	96.77	97.53	96.66	97.51	96.25	96.07
Si	6.34	6.21	6.19	6.17	6.28	6.19	6.19	6.14
Ti	0.05	0.01	0.02	0.03	0.05	0.01	0.05	0.06
Al Total	4.80	5.50	5.57	5.67	5.18	5.41	5.28	5.47
Al IV	1.66	1.79	1.81	1.83	1.72	1.81	1.81	1.86
Al VI	3.15	3.71	3.76	3.84	3.46	3.61	3.47	3.61
Fe	0.91	0.32	0.27	0.22	0.29	0.22	0.31	0.19
Mn	0.01	0.00	0.01	0.01	0.00	0.00	0.00	0.02
Mg	0.07	0.17	0.15	0.14	0.30	0.25	0.28	0.16
Ca	0.00	0.01	0.00	0.00	0.00	0.00	0.01	0.02
Na	0.10	0.06	0.15	0.15	0.10	0.12	0.13	0.16
K	1.91	1.58	1.50	1.50	1.88	1.87	1.88	1.82
Cr	0.00	0.01	0.00	0.00	0.00	0.00	0.00	0.01
Cl		0.00	0.00	0.00				
P		0.01	0.00	0.01				
Ba	0.00	0.00	0.00	0.00	0.00	0.01	0.01	0.03
F		0.10	0.07	0.27	0.07	0.04	0.03	0.02
OH	4.00	3.90	3.93	3.73	3.93	3.96	3.97	3.98
Tetrahedral	8.00	8.00	8.00	8.00	8.00	8.00	8.00	8.00
Octahedral	4.20	4.23	4.21	4.25	4.10	4.09	4.12	4.06
Dodecahedral	2.01	1.66	1.65	1.66	1.98	2.00	2.02	2.02

Sample	SC-3-M	SC-3-M	SC-3-M	SC-3-M	SC-3-M	SC-3-M	SC-3-M	SC-3-M
Point	1	4	7	2	8	6	8	6
Description	P	P	RB	RB	RF	RF	RF	RF
SiO2	45.66	46.17	45.22	45.88	45.98	46.60	45.79	45.89
TiO2	0.14	0.14	0.10	0.21	0.11	0.22	0.13	0.16
Al2O3	34.64	34.34	33.71	32.47	33.40	32.56	34.11	31.96
FeO	3.31	3.40	4.06	4.76	4.06	5.16	3.50	5.51
MnO	0.08	0.05	0.09	0.05	0.06	0.00	0.06	0.05
MgO	0.37	0.36	0.39	0.27	0.36	0.22	0.30	0.27
CaO	0.03	0.02	0.02	0.00	0.04	0.00	0.00	0.04
Na2O	0.87	1.05	0.92	0.59	0.73	0.33	0.87	0.33
K2O	10.07	10.26	10.32	10.64	10.48	10.88	10.11	10.90
Cr2O3	0.00	0.00	0.05	0.00	0.00	0.06	0.00	0.05
Cl	N/D	N/D	N/D	N/D	N/D	N/D	N/D	N/D
P2O5	N/D	N/D	N/D	N/D	N/D	N/D	N/D	N/D
BaO	0.00	N/D	0.01	0.01	N/D	N/D	0.03	0.00
F	1.17	1.20	1.05	1.20	1.25	0.87	1.12	0.93
Total	96.35	96.99	95.94	96.08	96.48	96.89	96.03	96.10
Si	6.13	6.27	6.35	6.24	6.08	6.53	6.38	6.14
Ti	0.00	0.04	0.00	0.04	0.00	0.02	0.01	0.00
Al Total	5.64	5.39	5.51	5.61	5.69	4.91	5.11	5.75
Al IV	1.87	1.73	1.65	1.76	1.92	1.47	1.62	1.86
Al VI	3.77	3.66	3.87	3.84	3.77	3.44	3.49	3.88
Fe	0.14	0.45	0.41	0.31	0.15	0.56	0.67	0.13
Mn	0.00	0.01	0.01	0.02	0.00	0.02	0.01	0.00
Mg	0.15	0.15	0.05	0.07	0.13	0.11	0.03	0.09
Ca	0.00	0.01	0.01	0.00	0.00	0.01	0.00	0.00
Na	0.15	0.19	0.08	0.08	0.20	0.06	0.10	0.16
K	1.80	1.58	1.58	1.67	1.83	1.63	1.75	1.58
Cr	0.00	0.00	0.00	0.00	0.01	0.00	0.00	0.00
Cl		0.00	0.00	0.00		0.00	0.00	0.00
P		0.01	0.00	0.00		0.00	0.01	0.00
Ba	0.00	0.00	0.00	0.00	0.01	0.01	0.00	0.01
F	0.00	0.45	0.60	0.46	0.00	0.00	0.26	0.00
OH	4.00	3.55	3.40	3.54	4.00	4.00	3.74	4.00
Tetrahedral	8.00	8.00	8.00	8.00	8.00	8.00	8.00	8.00
Octahedral	4.07	4.31	4.35	4.28	4.05	4.15	4.22	4.11
Dodecahedral	1.96	1.78	1.66	1.75	2.05	1.69	1.87	1.75

Sample	SC-3-M	SC-3-M	SC-3-M	SC-5-M	SC-5-M	SC-5-M	SC-5-M	SC-5-M
Point	9	4	9	1	1b	2	2b	2c
Description	S	S	S	RB	RB	RF	RF	RF
SiO2	45.69	45.61	46.45	46.76	47.25	47.12	46.26	45.80
TiO2	0.00	0.16	0.00	0.60	0.32	0.23	0.13	0.17
Al2O3	36.62	34.04	36.17	36.22	35.25	35.40	35.47	34.31
FeO	1.13	3.76	1.47	1.91	2.45	2.83	2.52	4.20
MnO	0.06	0.01	0.00	0.00	0.08	0.09	0.10	0.06
MgO	0.06	0.29	0.03	0.78	0.64	0.45	0.31	0.43
CaO	0.00	0.06	0.00	0.03	0.11	0.04	0.10	0.00
Na2O	0.35	0.86	0.38	0.77	0.52	0.28	0.46	0.31
K2O	11.10	10.01	10.86	9.03	9.02	9.59	9.20	10.29
Cr2O3	0.00	0.00	0.03	0.00	0.00	0.00	0.00	0.00
Cl	N/D	N/D	N/D	0.04	0.02	0.00	0.01	0.03
P2O5	N/D	N/D	N/D	0.02	0.12	0.12	0.20	0.23
BaO	N/D	0.00	0.03	0.10	0.09	0.00	0.00	0.12
F	0.38	1.13	0.48	1.34	1.38	1.80	1.35	1.44
Total	95.40	95.92	95.88	97.60	97.25	97.95	96.11	97.39
Si	6.19	6.27	6.23	6.22	6.30	6.38	6.24	6.38
Ti	0.01	0.00	0.07	0.01	0.04	0.01	0.02	0.03
Al Total	5.68	5.42	5.52	5.38	4.96	5.36	5.48	5.15
Al IV	1.81	1.73	1.77	1.78	1.70	1.62	1.76	1.62
Al VI	3.88	3.70	3.75	3.60	3.26	3.74	3.72	3.52
Fe	0.13	0.21	0.28	0.38	0.82	0.23	0.28	0.50
Mn	0.00	0.02	0.00	0.00	0.02	0.02	0.01	0.02
Mg	0.10	0.23	0.16	0.07	0.05	0.06	0.15	0.19
Ca	0.01	0.00	0.00	0.00	0.01	0.01	0.00	0.01
Na	0.12	0.07	0.18	0.18	0.10	0.03	0.14	0.06
K	1.57	1.63	1.54	1.86	1.88	1.73	1.65	1.66
Cr	0.00	0.00	0.00	0.00	0.01	0.00	0.00	0.00
Cl	0.01	0.00	0.00			0.00	0.01	0.02
P	0.00	0.00	0.01			0.01	0.00	0.01
Ba	0.00	0.00	0.00		0.00	0.00	0.00	0.00
F	0.00	0.00	0.38	0.39	0.51	0.08	0.13	0.24
OH	3.99	4.00	3.62	3.61	3.49	3.92	3.86	3.75
Tetrahedral	8.00	8.00	8.00	8.00	8.00	8.00	8.00	8.00
Octahedral	4.12	4.16	4.25	4.05	4.18	4.07	4.18	4.27
Dodecahedral	1.69	1.70	1.74	2.05	1.99	1.77	1.79	1.73

Sample	SC-5-M	SC-5-M	SC-5-M	SC-5-M	SC-5-M	SC-5-M	SC-5-M	SC-5-M
Point	3	5	10	11	12	6	7	8
Description	RF	RF	RF	RF	RF	S	S	S
SiO2	46.57	47.48	47.43	46.41	45.48	48.37	49.17	47.90
TiO2	0.07	0.31	0.26	0.00	0.03	0.07	0.00	0.15
Al2O3	35.48	34.31	35.35	37.12	37.21	35.07	36.39	34.73
FeO	2.25	2.52	2.23	1.97	2.22	3.12	0.87	3.23
MnO	0.00	0.10	0.16	0.05	0.00	0.17	0.00	0.12
MgO	0.46	0.75	0.67	0.31	0.19	0.23	0.20	1.13
CaO	0.06	0.17	0.03	0.08	0.00	0.00	0.02	0.03
Na2O	0.40	0.48	0.48	0.61	0.47	0.23	0.13	0.39
K2O	8.51	8.90	9.42	9.65	9.74	9.81	8.81	9.53
Cr2O3	0.00	0.01	0.03	0.03	0.00	0.04	0.10	0.00
Cl	0.03	0.03	0.00	0.00	0.00	0.00	0.01	0.04
P2O5	0.22	0.00	0.06	0.27	0.50	0.00	0.00	0.04
BaO	0.09	0.00	0.00	0.00	0.00	0.03	0.16	0.11
F	1.12	1.26	1.38	1.34	1.29	0.34	0.00	1.60
Total	95.26	96.32	97.50	97.84	97.13	97.48	95.86	99.00
Si	6.21	6.67	6.19	6.28	6.12	6.15	6.26	6.62
Ti	0.02	0.01	0.02	0.02	0.01	0.03	0.00	0.01
Al Total	5.49	4.75	5.53	5.56	5.61	5.63	5.65	5.04
Al IV	1.79	1.33	1.81	1.72	1.88	1.85	1.74	1.38
Al VI	3.71	3.42	3.72	3.84	3.74	3.78	3.90	3.66
Fe	0.24	0.49	0.26	0.16	0.26	0.30	0.22	0.58
Mn	0.01	0.03	0.01	0.00	0.01	0.02	0.00	0.00
Mg	0.15	0.29	0.15	0.03	0.13	0.00	0.10	0.16
Ca	0.00	0.00	0.01	0.00	0.00	0.00	0.00	0.01
Na	0.21	0.06	0.20	0.06	0.18	0.16	0.10	0.06
K	1.59	1.78	1.58	1.62	1.55	1.57	1.58	1.45
Cr	0.01	0.00	0.00	0.00	0.00	0.00	0.01	0.00
Cl	0.02	0.00	0.02	0.00	0.01	0.01	0.00	0.00
P	0.02	0.00	0.02	0.00	0.03	0.01	0.00	0.00
Ba	0.00	0.00	0.00	0.00	0.00	0.00	0.00	0.00
F	0.14	0.46	0.18	0.00	0.08	0.00	0.33	0.66
OH	3.85	3.54	3.81	4.00	3.92	4.00	3.67	3.34
Tetrahedral	8.00	8.00	8.00	8.00	8.00	8.00	8.00	8.00
Octahedral	4.13	4.25	4.17	4.07	4.15	4.12	4.23	4.42
Dodecahedral	1.83	1.84	1.80	1.68	1.76	1.74	1.69	1.52

Sample	SC-5-M	SC-7-M	SC-7-M	SC-7-M	SC-7-M	SC-7-M	SC-7-M	SC-7-M
Point	9	1	1b	2	3	5	6	7
Description	S	HP	HP	HP	HP	HP	HP	HP
SiO2	47.33	44.96	44.59	42.91	45.53	44.35	44.27	44.96
TiO2	0.09	0.12	0.16	0.26	0.06	0.14	0.14	0.10
Al2O3	35.56	35.13	34.67	33.21	35.12	34.22	33.36	34.78
FeO	2.04	2.92	3.22	2.86	2.75	2.18	2.91	2.51
MnO	0.17	0.12	0.05	0.04	0.12	0.00	0.03	0.02
MgO	0.72	0.15	0.13	0.22	0.08	0.16	0.16	0.18
CaO	0.10	0.03	0.02	0.00	0.00	0.00	0.00	0.06
Na2O	0.44	0.88	0.93	0.59	0.99	0.87	0.78	0.62
K2O	9.38	9.45	10.15	10.33	10.12	9.40	10.28	10.30
Cr2O3	0.06	0.00	0.00	0.04	0.00	0.00	0.12	0.08
Cl	0.03	0.01	0.03	0.02	0.00	0.00	0.00	0.00
P2O5	0.00	0.14	0.03	0.06	0.10	0.11	0.07	0.07
BaO	0.00	0.00	0.01	0.00	0.09	0.01	0.09	0.00
F	0.83	1.10	1.30	1.55	1.45	1.18	1.26	1.87
Total	96.75	94.99	95.29	92.09	96.43	92.64	93.47	95.54
Si	6.24	6.18	6.14	6.22	6.10	6.61	6.13	6.19
Ti	0.01	0.01	0.00	0.00	0.00	0.00	0.01	0.00
Al Total	5.65	5.66	5.73	5.59	5.79	4.96	5.66	5.53
Al IV	1.76	1.82	1.86	1.78	1.90	1.39	1.87	1.81
Al VI	3.89	3.84	3.88	3.82	3.89	3.57	3.79	3.72
Fe	0.32	0.17	0.10	0.13	0.13	0.21	0.15	0.17
Mn	0.01	0.00	0.00	0.01	0.00	0.01	0.01	0.01
Mg	0.06	0.14	0.09	0.17	0.11	0.34	0.14	0.17
Ca	0.00	0.00	0.00	0.00	0.00	0.00	0.00	0.00
Na	0.15	0.10	0.18	0.16	0.13	0.06	0.13	0.11
K	1.59	1.55	1.64	1.51	1.56	1.46	1.66	1.73
Cr	0.00	0.00	0.00	0.01	0.00	0.01	0.01	0.00
Cl	0.00	0.00	0.00	0.01	0.00	0.01	0.01	0.00
P	0.00	0.00	0.00	0.00	0.00	0.00	0.01	0.01
Ba	0.01	0.00	0.01	0.00	0.01	0.01	0.00	0.01
F	0.50	0.00	0.00	0.00	0.00	0.01	0.00	0.00
OH	3.50	4.00	4.00	3.99	4.00	3.98	4.00	4.00
Tetrahedral	8.00	8.00	8.00	8.00	8.00	8.00	8.00	8.00
Octahedral	4.29	4.15	4.07	4.13	4.14	4.13	4.11	4.07
Dodecahedral	1.75	1.66	1.83	1.68	1.71	1.54	1.80	1.87

Sample	SC-7-M	SC-7-M	SC-7-M	SC-7-M	SC-7-M	SC-7-M	SC-7-M	SC-7-M
Point	8	9	1c	3b	3c	5b	6b	7b
Description	HP	HP	HP	HP	HP	HP	HP	HP
SiO2	45.36	47.07	44.91	43.95	45.17	44.00	43.48	48.20
TiO2	0.13	0.11	0.20	0.02	0.14	0.13	0.19	0.07
Al2O3	34.83	36.24	34.43	33.34	34.30	34.04	34.37	32.87
FeO	3.28	2.67	3.58	3.00	2.93	2.65	3.16	2.61
MnO	0.07	0.03	0.06	0.02	0.03	0.01	0.02	0.00
MgO	0.11	0.22	0.13	0.11	0.12	0.07	0.27	0.94
CaO	0.03	0.06	0.05	0.05	0.00	0.02	0.18	0.04
Na2O	1.02	0.93	0.96	0.62	0.58	0.97	0.78	0.42
K2O	10.22	9.76	9.78	10.24	10.48	9.44	10.03	9.73
Cr2O3	0.09	0.09	0.01	0.00	0.05	0.00	0.00	0.02
Cl	0.07	0.01	0.02	0.01	0.03	0.01	0.00	0.01
P2O5	0.13	0.14	0.00	0.15	0.11	0.17	0.20	0.02
BaO	0.00	0.00	0.04	0.13	0.01	0.00	0.00	0.03
F	1.25	0.81	1.45	1.52	1.29	1.58	1.16	0.47
Total	96.60	98.14	95.62	93.17	95.24	93.09	93.83	95.43
Si	6.15	6.16	6.15	6.14	6.18	6.33	6.32	6.37
Ti	0.01	0.05	0.07	0.03	0.03	0.08	0.00	0.06
Al Total	5.67	5.51	5.49	5.54	5.38	5.10	5.23	4.91
Al IV	1.85	1.84	1.85	1.86	1.82	1.67	1.68	1.63
Al VI	3.81	3.66	3.64	3.68	3.57	3.43	3.55	3.28
Fe	0.12	0.19	0.15	0.17	0.27	0.72	0.52	0.92
Mn	0.00	0.00	0.00	0.00	0.01	0.01	0.02	0.01
Mg	0.12	0.14	0.16	0.17	0.23	0.04	0.15	0.10
Ca	0.01	0.00	0.01	0.01	0.00	0.00	0.00	0.01
Na	0.14	0.14	0.15	0.10	0.11	0.12	0.12	0.12
K	1.67	1.87	1.85	1.92	1.88	1.74	1.73	1.71
Cr	0.01	0.00	0.00	0.00	0.00	0.00	0.01	0.00
Cl	0.01					0.00	0.01	0.00
P	0.01					0.01	0.00	0.01
Ba	0.00	0.00	0.00	0.01	0.02	0.00	0.00	0.00
F	0.00	0.03	0.05	0.02	0.01	0.40	0.22	0.40
OH	4.00	3.97	3.95	3.98	3.99	3.60	3.78	3.60
Tetrahedral	8.00	8.00	8.00	8.00	8.00	8.00	8.00	8.00
Octahedral	4.07	4.04	4.04	4.05	4.10	4.28	4.24	4.38
Dodecahedral	1.83	2.00	1.99	2.03	2.01	1.87	1.86	1.83

Sample	SC-7-M	SC-12-M	SC-12-M	SC-12-M	SC-12-M	SC-12-M	SC-12-M	SC-12-M
Point	9b	5	1	2	3a	4	6a	7
Description	HP	FF	HP	HP	HP	HP	HP	HP
SiO2	46.77	47.45	44.94	45.34	45.90	43.47	44.95	44.37
TiO2	0.05	0.15	0.15	0.14	0.00	0.22	0.06	0.04
Al2O3	35.68	33.32	32.53	33.26	32.04	32.30	32.73	31.85
FeO	3.45	4.52	4.14	4.55	6.15	3.72	4.46	4.52
MnO	0.11	0.06	0.00	0.08	0.11	0.12	0.15	0.10
MgO	0.06	0.10	0.11	0.12	0.05	0.06	0.15	0.12
CaO	0.01	0.06	0.00	0.10	0.05	0.00	0.01	0.00
Na2O	1.03	0.35	0.79	0.89	0.87	0.67	0.91	0.84
K2O	10.39	9.10	9.46	10.07	10.42	9.89	10.01	9.90
Cr2O3	0.01	0.03	0.07	0.04	0.10	0.07	0.13	0.00
Cl	0.00	0.03	0.02	0.02	0.03	0.02	0.03	0.01
P2O5	0.10	0.00	0.10	0.00	0.09	0.13	0.02	0.06
BaO	0.11	0.14	0.00	0.12	0.15	0.00	0.00	0.06
F	1.28	2.51	1.84	1.51	2.05	1.62	1.67	1.87
Total	99.04	97.82	94.17	96.22	98.02	92.31	95.27	93.75
Si	6.33	6.44	6.38	6.21	6.34	6.35	6.05	6.09
Ti	0.02	0.00	0.00	0.00	0.01	0.00	0.03	0.02
Al Total	5.16	5.33	5.12	5.73	5.01	5.27	5.71	5.65
Al IV	1.67	1.56	1.62	1.79	1.66	1.65	1.95	1.91
Al VI	3.49	3.77	3.49	3.94	3.35	3.61	3.76	3.74
Fe	0.64	0.14	0.51	0.03	0.78	0.40	0.24	0.25
Mn	0.00	0.02	0.04	0.02	0.03	0.03	0.00	0.01
Mg	0.16	0.02	0.00	0.00	0.00	0.00	0.03	0.03
Ca	0.01	0.01	0.00	0.00	0.00	0.01	0.00	0.00
Na	0.12	0.04	0.20	0.05	0.20	0.11	0.29	0.28
K	1.74	1.83	1.81	1.83	1.76	1.81	1.75	1.75
Cr	0.00	0.00	0.01	0.00	0.00	0.00	0.00	0.00
Cl	0.00							
P	0.00							
Ba	0.00						0.00	0.00
F	0.34	0.17	0.42	0.09	0.48	0.37	0.15	0.13
OH	3.66	3.83	3.58	3.91	3.52	3.63	3.85	3.87
Tetrahedral	8.00	8.00	8.00	8.00	8.00	8.00	8.00	8.00
Octahedral	4.31	3.96	4.04	3.98	4.17	4.06	4.05	4.05
Dodecahedral	1.86	1.88	2.02	1.88	1.97	1.92	2.04	2.03

Sample	SC-12-M	SC-12-M	SC-12-M	SC-12-M	SC-12-M	SC-12-M	SC-12-M
Point	9	10	12	13	3b	6b	4
Description	HP	HP	HP	HP	HP	HP	RA
SiO2	44.03	46.40	45.26	45.11	44.65	46.37	47.68
TiO2	0.10	0.14	0.18	0.15	0.06	0.14	0.00
Al2O3	31.86	33.06	31.88	32.72	31.29	34.50	36.42
FeO	4.13	3.71	5.88	4.78	5.75	4.18	0.89
MnO	0.06	0.17	0.15	0.04	0.20	0.02	0.15
MgO	0.16	0.14	0.10	0.17	0.24	0.15	0.22
CaO	0.02	0.08	0.00	0.02	0.00	0.01	0.04
Na2O	0.87	0.55	0.55	0.71	0.73	0.89	0.37
K2O	9.37	10.18	10.49	10.40	10.03	10.02	9.07
Cr2O3	0.00	0.00	0.00	0.02	0.00	0.01	0.06
Cl	0.00	0.00	0.00	0.00	0.00	0.00	0.02
P2O5	0.03	0.06	0.17	0.10	0.09	0.00	0.20
BaO	0.00	0.00	0.00	0.00	0.02	0.00	0.06
F	2.06	1.12	1.93	1.66	1.94	1.63	0.00
Total	92.70	95.64	96.58	95.89	95.00	97.92	95.18
Si	6.08	6.15	6.04	6.12	6.11	6.10	6.15
Ti	0.01	0.02	0.01	0.01	0.01	0.02	0.02
Al Total	5.65	5.51	5.72	5.54	5.63	5.66	5.47
Al IV	1.92	1.85	1.96	1.88	1.89	1.90	1.85
Al VI	3.74	3.66	3.76	3.66	3.74	3.76	3.62
Fe	0.29	0.31	0.25	0.38	0.26	0.22	0.37
Mn	0.01	0.01	0.00	0.02	0.01	0.00	0.01
Mg	0.01	0.05	0.03	0.02	0.03	0.03	0.07
Ca	0.00	0.00	0.00	0.01	0.00	0.00	0.01
Na	0.28	0.27	0.29	0.12	0.27	0.27	0.26
K	1.73	1.75	1.75	1.90	1.75	1.74	1.76
Cr	0.01	0.01	0.00	0.00	0.00	0.00	0.00
Cl							
P							
Ba	0.00	0.00	0.00	0.00	0.00	0.00	0.00
F	0.32	0.22	0.30	0.06	0.15	0.07	0.32
OH	3.68	3.78	3.70	3.94	3.85	3.93	3.68
Tetrahedral	8.00	8.00	8.00	8.00	8.00	8.00	8.00
Octahedral	4.06	4.05	4.06	4.09	4.05	4.04	4.09
Dodecahedral	2.02	2.03	2.04	2.02	2.02	2.01	2.02

Sample	SC-12-M	SC-12-M	SC-12-M	SC-12-M	SC-13-M	SC-13-M	SC-13-M
Point	1	2	3	6	6	6b	6c
Description	S	S	S	S	P	P	P
SiO2	47.01	46.18	47.77	46.83	46.89	47.38	47.06
TiO2	0.00	0.10	0.07	0.16	0.13	0.17	0.07
Al2O3	38.83	38.03	38.60	35.85	35.05	36.15	37.64
FeO	0.44	0.92	0.99	3.56	3.86	2.86	1.69
MnO	0.11	0.00	0.00	0.15	0.10	0.20	0.00
MgO	0.03	0.10	0.08	0.27	0.35	0.26	0.12
CaO	0.01	0.04	0.04	0.02	0.02	0.02	0.05
Na2O	0.51	0.60	0.54	0.59	0.71	0.58	0.73
K2O	9.50	9.60	9.09	9.21	9.02	9.52	9.37
Cr2O3	0.00	0.08	0.00	0.00	0.00	0.00	0.00
Cl	0.01	0.05	0.02	0.02	0.00	0.08	0.00
P2O5	0.03	0.00	0.04	0.00	0.00	0.12	0.00
BaO	0.00	0.04	0.00	0.12	0.04	0.06	0.00
F	1.05	1.64	0.86	2.03	2.30	1.77	1.38
Total	97.53	97.38	98.10	98.81	98.47	99.17	98.11
Si	6.14	6.09	6.15	6.19	6.10	6.10	6.12
Ti	0.01	0.02	0.02	0.04	0.02	0.02	0.01
Al Total	5.50	5.68	5.56	5.43	5.66	5.58	5.57
Al IV	1.86	1.91	1.85	1.81	1.90	1.90	1.88
Al VI	3.64	3.77	3.71	3.62	3.76	3.69	3.69
Fe	0.39	0.23	0.27	0.33	0.24	0.27	0.32
Mn	0.02	0.01	0.01	0.01	0.00	0.01	0.01
Mg	0.03	0.02	0.04	0.06	0.03	0.06	0.04
Ca	0.01	0.00	0.01	0.00	0.00	0.00	0.01
Na	0.15	0.24	0.28	0.25	0.27	0.32	0.26
K	1.85	1.74	1.71	1.76	1.71	1.74	1.75
Cr	0.00	0.00	0.00	0.00	0.00	0.00	0.00
Cl							
P							
Ba	0.00	0.01	0.00	0.00			
F	0.09				0.13	0.21	0.30
OH	3.91	4.00	4.00	4.00	3.87	3.79	3.70
Tetrahedral	8.00	8.00	8.00	8.00	8.00	8.00	8.00
Octahedral	4.10	4.06	4.06	4.06	4.06	4.05	4.08
Dodecahedral	2.00	1.99	1.99	2.00	1.98	2.06	2.01

Sample	SC-13-M	SC-13-M	SC-13-M	SC-13-M	SC-13-M	SC-13-M	SC-13-M
Point	7	8	8b	3	3b	10	1
Description	P	P	P	RA	RA	RA	RF
SiO2	46.51	46.84	46.90	46.45	49.09	46.88	47.10
TiO2	0.06	0.04	0.18	0.00	0.08	0.15	0.13
Al2O3	36.74	35.75	35.03	38.90	35.23	37.40	36.17
FeO	2.57	3.43	3.59	0.73	1.77	2.04	2.91
MnO	0.00	0.11	0.16	0.00	0.00	0.00	0.09
MgO	0.11	0.29	0.45	0.02	0.57	0.14	0.30
CaO	0.05	0.07	0.07	0.01	0.02	0.00	0.00
Na2O	0.72	0.46	0.57	0.51	0.29	0.79	0.60
K2O	9.20	9.30	8.68	8.81	9.67	9.15	9.39
Cr2O3	0.00	0.01	0.06	0.00	0.04	0.06	0.00
Cl	0.01	0.00	0.00	0.00	0.00	0.02	0.00
P2O5	0.00	0.04	0.08	0.00	0.00	0.21	0.00
BaO	0.14	0.00	0.14	0.09	0.00	0.00	0.15
F	1.15	2.60	2.28	0.52	1.03	1.20	2.37
Total	97.26	98.94	98.19	96.04	97.79	98.04	99.21
Si	6.14	6.10	6.09	6.11	6.08	6.09	6.16
Ti	0.00	0.02	0.02	0.02	0.02	0.02	0.01
Al Total	5.57	5.61	5.67	5.61	5.66	5.63	5.49
Al IV	1.86	1.90	1.91	1.89	1.92	1.91	1.84
Al VI	3.71	3.71	3.76	3.72	3.74	3.71	3.65
Fe	0.32	0.29	0.25	0.26	0.25	0.30	0.36
Mn	0.01	0.02	0.01	0.01	0.00	0.00	0.01
Mg	0.04	0.04	0.03	0.05	0.04	0.04	0.05
Ca	0.00	0.00	0.00	0.00	0.00	0.00	0.00
Na	0.25	0.26	0.27	0.26	0.27	0.26	0.23
K	1.74	1.75	1.71	1.73	1.76	1.75	1.75
Cr	0.00	0.00	0.00	0.01	0.00	0.00	0.01
Cl							
P							
Ba					0.00	0.00	0.00
F	0.32	0.32	0.23	0.30	0.31	0.33	0.32
OH	3.68	3.68	3.77	3.70	3.69	3.67	3.68
Tetrahedral	8.00	8.00	8.00	8.00	8.00	8.00	8.00
Octahedral	4.08	4.08	4.07	4.06	4.06	4.07	4.08
Dodecahedral	1.98	2.00	1.98	2.00	2.03	2.02	1.99

Sample	SC-13-M	SC-13-M	SC-13-M	SC-13-M	SC-13-M	SC-2-K	SC-2-K	SC-2-K
Point	2	4	9	11	12	14	3	28
Description	S	S	S	S	S	RB	RF	RF
SiO2	46.92	47.76	49.29	46.68	46.71	46.53	46.19	46.75
TiO2	0.00	0.02	0.11	0.00	0.00	0.14	0.77	0.01
Al2O3	38.46	38.65	36.62	38.39	38.22	31.61	31.56	32.88
FeO	1.21	0.08	1.23	1.02	0.84	5.86	6.30	4.58
MnO	0.08	0.07	0.00	0.00	0.01	0.12	0.06	0.13
MgO	0.11	0.00	0.42	0.00	0.14	0.13	0.21	0.76
CaO	0.00	0.00	0.07	0.02	0.00	0.00	0.00	0.01
Na2O	0.66	0.15	0.13	0.75	0.33	0.39	0.46	0.47
K2O	9.75	9.64	8.73	8.89	10.34	10.02	9.94	10.05
Cr2O3	0.03	0.10	0.05	0.00	0.03	0.00	0.00	0.07
Cl	0.03	0.03	0.04	0.02	0.00	0.00	0.01	0.02
P2O5	0.14	0.00	0.32	0.08	0.11	0.08	0.07	0.00
BaO	0.00	0.00	0.00	0.07	0.05	0.05	0.00	0.00
F	0.94	0.40	0.63	1.22	1.28	1.21	1.83	1.02
Total	98.33	96.90	97.64	97.14	98.06	96.13	97.40	96.74
Si	6.07	6.06	6.07	6.15	6.11	6.13	6.12	6.48
Ti	0.00	0.02	0.03	0.01	0.01	0.01	0.02	0.01
Al Total	5.64	5.60	5.69	5.56	5.58	5.77	5.58	4.98
Al IV	1.93	1.94	1.93	1.85	1.89	1.87	1.88	1.52
Al VI	3.71	3.66	3.76	3.71	3.68	3.90	3.70	3.46
Fe	0.33	0.26	0.24	0.32	0.31	0.22	0.28	0.54
Mn	0.01	0.02	0.00	0.01	0.01	0.00	0.02	0.02
Mg	0.04	0.12	0.03	0.02	0.05	0.03	0.04	0.10
Ca	0.00	0.00	0.01	0.00	0.00	0.00	0.01	0.00
Na	0.27	0.21	0.26	0.24	0.26	0.20	0.27	0.03
K	1.75	1.90	1.74	1.73	1.76	1.53	1.71	1.68
Cr	0.00	0.00	0.00	0.00	0.00	0.01	0.01	0.01
Cl						0.01		0.00
P						0.02		0.02
Ba	0.00	0.00				0.00	0.01	0.00
F	0.29	0.06	0.27	0.36	0.33	0.25		0.00
OH	3.71	3.94	3.73	3.64	3.67	3.75	4.00	4.00
Tetrahedral	8.00	8.00	8.00	8.00	8.00	8.00	8.00	8.00
Octahedral	4.10	4.07	4.06	4.07	4.08	4.16	4.07	4.12
Dodecahedral	2.02	2.11	2.00	1.98	2.03	1.76	2.00	1.74

Sample	SC-2-K	SC-2-K	SC-2-K	SC-2-K	SC-2-K	SC-2-K	SC-3-K	SC-3-K	SC-3-K
Point	30	32	42	10	16	20	5	1	2
Description	RF	RF	RF	S	S	S	G	HP	HP
SiO2	45.70	46.08	45.91	46.53	47.21	46.55	45.19	45.58	44.35
TiO2	0.59	0.20	0.04	0.00	0.57	0.21	0.33	0.00	0.00
Al2O3	29.92	31.87	33.45	37.27	31.39	30.85	30.44	34.62	33.38
FeO	7.90	5.55	4.69	0.50	6.23	7.02	7.71	2.52	2.66
MnO	0.07	0.00	0.18	0.05	0.09	0.27	0.03	0.17	0.00
MgO	0.47	0.77	0.57	0.14	0.62	0.63	0.89	0.55	0.60
CaO	0.08	0.05	0.05	0.00	0.00	0.04	0.01	0.02	0.01
Na2O	0.45	0.46	0.48	0.43	0.39	0.45	0.48	0.98	0.95
K2O	9.59	9.91	10.13	9.86	10.03	9.20	10.45	10.26	9.67
Cr2O3	0.02	0.02	0.04	0.07	0.00	0.00	0.00	0.00	0.05
Cl	0.00	0.00	0.03	0.01	0.07	0.00	0.02	0.00	0.00
P2O5	0.04	0.00	0.01	0.00	0.12	0.00	0.03	0.05	0.04
BaO	0.00	0.00	0.15	0.22	0.00	0.00	0.16	0.06	0.14
F	1.80	1.57	1.77	0.03	1.15	1.68	3.64	1.57	1.78
Total	96.63	96.47	97.49	95.12	97.84	96.89	99.37	96.38	93.64
Si	7.03	6.42	6.13	6.15	6.30	6.23	6.19	6.20	6.25
Ti	0.02	0.02	0.00	0.01	0.02	0.00	0.06	0.04	0.03
Al Total	3.39	4.95	5.70	5.71	5.22	5.49	5.52	5.53	5.51
Al IV	0.97	1.58	1.87	1.85	1.70	1.77	1.81	1.80	1.75
Al VI	2.42	3.37	3.84	3.86	3.52	3.72	3.72	3.73	3.76
Fe	1.61	0.66	0.16	0.13	0.69	0.19	0.26	0.23	0.25
Mn	0.12	0.02	0.00	0.00	0.02	0.00	0.00	0.00	0.00
Mg	0.28	0.10	0.15	0.11	0.12	0.15	0.14	0.15	0.16
Ca	0.00	0.00	0.00	0.00	0.00	0.01	0.00	0.00	0.00
Na	0.08	0.06	0.15	0.13	0.15	0.19	0.10	0.18	0.15
K	1.80	1.76	1.56	1.52	1.81	1.68	1.54	1.47	1.50
Cr	0.01	0.01	0.01	0.00	0.00	0.01	0.00	0.00	0.00
Cl	0.00	0.01	0.00	0.00	0.00		0.00	0.00	0.03
P	0.00	0.00	0.00	0.01	0.01		0.02	0.02	0.02
Ba	0.00	0.00	0.00	0.00	0.00	0.01	0.00	0.01	0.01
F	0.30	0.00	0.00	0.00	0.64		0.13	0.07	0.18
OH	3.70	4.00	4.00	4.00	3.36	4.00	3.86	3.93	3.80
Tetrahedral	8.00	8.00	8.00	8.00	8.00	8.00	8.00	8.00	8.00
Octahedral	4.46	4.16	4.14	4.12	4.38	4.07	4.18	4.15	4.19
Dodecahedral	1.88	1.84	1.72	1.67	1.97	1.90	1.66	1.68	1.67

Sample	SC-3-K	SC-3-K	SC-3-K	SC-3-K	SC-3-K	SC-3-K	SC-5-K	SC-5-K	SC-5-K
Point	3	5	1	1	21	25	4	5	6
Description	HP	HP	HP	RF	RF	RF	G	G	G
SiO2	45.62	42.70	46.03	46.43	45.59	46.25	45.88	45.92	45.42
TiO2	0.23	0.18	0.00	0.28	0.03	0.14	0.03	0.12	0.12
Al2O3	35.54	32.61	34.97	31.23	33.66	31.84	32.61	31.64	31.26
FeO	2.02	2.45	2.24	6.74	4.89	6.22	4.94	5.78	5.83
MnO	0.01	0.07	0.02	0.08	0.05	0.14	0.05	0.09	0.12
MgO	0.52	0.61	0.65	0.48	0.73	0.88	0.23	1.13	0.90
CaO	0.05	0.00	0.00	0.00	0.03	0.00	0.00	0.02	0.00
Na2O	1.08	0.99	1.18	0.44	0.52	0.56	0.61	0.50	0.47
K2O	10.06	9.29	10.17	10.55	10.23	10.40	10.40	10.40	10.49
Cr2O3	0.10	0.06	0.00	0.00	0.00	0.07	0.00	0.00	0.00
Cl	0.03	0.00	0.02	0.00	0.02	0.00	0.00	0.02	0.00
P2O5	0.12	0.06	0.03	0.15	0.04	0.10	0.07	0.00	0.03
BaO	0.03	0.00	0.19	0.00	0.11	0.10	0.09	0.00	0.00
F	1.42	1.72	1.68	2.86	2.15	2.81	2.91	3.11	3.35
Total	96.83	90.73	97.19	99.24	98.05	99.52	97.81	98.73	97.99
Si	6.26	6.17	6.27	6.29	6.31	6.20	6.12	6.12	6.15
Ti	0.00	0.06	0.03	0.02	0.01	0.04	0.02	0.00	0.00
Al Total	5.56	5.63	5.51	5.42	5.39	5.21	5.67	5.70	5.68
Al IV	1.74	1.83	1.73	1.71	1.69	1.80	1.88	1.88	1.85
Al VI	3.82	3.80	3.77	3.70	3.70	3.41	3.79	3.82	3.83
Fe	0.23	0.21	0.27	0.38	0.45	0.39	0.13	0.15	0.14
Mn	0.00	0.00	0.01	0.01	0.01	0.00	0.00	0.00	0.00
Mg	0.14	0.15	0.13	0.17	0.01	0.32	0.09	0.06	0.05
Ca	0.00	0.00	0.02	0.00	0.00	0.00	0.01	0.00	0.00
Na	0.07	0.20	0.13	0.15	0.09	0.11	0.18	0.19	0.17
K	1.60	1.52	1.53	1.62	1.71	1.90	1.82	1.84	1.81
Cr	0.00	0.00	0.00	0.00	0.01	0.00	0.00	0.00	0.00
Cl	0.00	0.02	0.01	0.00	0.00				
P	0.01	0.00	0.01	0.00	0.01				
Ba	0.00	0.01	0.00	0.01	0.00	0.01			
F	0.20	0.28	0.29	0.39	0.30	0.04	0.00	0.00	0.00
OH	3.80	3.71	3.71	3.60	3.70	3.96	4.00	4.00	4.00
Tetrahedral	8.00	8.00	8.00	8.00	8.00	8.00	8.00	8.00	8.00
Octahedral	4.19	4.23	4.23	4.29	4.19	4.16	4.03	4.02	4.02
Dodecahedral	1.69	1.72	1.68	1.78	1.82	2.01	2.01	2.03	1.98

Sample	SC-5-K	SC-5-K	SC-5-K	SC-5-K	SC-5-K	SC-5-K	SC-5-K	SC-5-K	SC-5-K
Point	21	25	41	58	61	62	64	68	11
Description	G	G	G	G	G	G	G	G	G
SiO2	46.74	44.90	46.05	45.93	47.49	46.04	46.25	45.71	45.19
TiO2	0.00	0.03	0.17	0.16	0.01	0.00	0.05	0.12	0.17
Al2O3	36.53	31.84	32.72	32.54	34.44	32.98	32.05	33.05	31.95
FeO	0.65	6.29	5.62	5.16	2.26	5.25	5.29	5.13	5.28
MnO	0.02	0.18	0.03	0.10	0.02	0.08	0.00	0.07	0.15
MgO	0.82	0.69	0.00	0.23	0.01	0.07	0.00	0.05	0.05
CaO	0.02	0.00	0.00	0.00	0.11	0.08	0.00	0.02	0.00
Na2O	0.25	0.64	0.68	0.59	0.26	0.47	0.55	0.74	0.67
K2O	10.89	10.16	10.38	10.31	10.77	10.45	10.49	10.16	10.48
Cr2O3	0.09	0.06	0.03	0.00	0.06	0.00	0.13	0.00	0.04
Cl	0.00	0.05	0.00	0.00	0.00	0.00	0.00	0.06	N/D
P2O5	0.31	0.03	0.10	0.04	0.29	0.05	0.07	0.16	N/D
BaO	0.01	0.22	0.02	0.00	0.00	0.24	0.10	0.00	N/D
F	0.63	3.28	3.21	2.98	1.70	3.27	3.04	3.32	2.17
Total	96.95	98.38	99.01	98.04	97.41	98.96	98.01	98.57	96.16
Si	6.04	6.11	6.32	6.37	6.31	6.18	6.16	6.16	6.16
Ti	0.00	0.01	0.04	0.03	0.03	0.04	0.01	0.03	0.01
Al Total	5.80	5.70	4.78	4.84	5.02	5.44	5.47	5.45	5.50
Al IV	1.96	1.89	1.68	1.63	1.69	1.82	1.84	1.84	1.84
Al VI	3.84	3.81	3.10	3.21	3.33	3.63	3.64	3.61	3.65
Fe	0.17	0.13	0.95	0.84	0.71	0.26	0.29	0.28	0.25
Mn	0.00	0.00	0.04	0.03	0.02	0.01	0.01	0.01	0.01
Mg	0.03	0.07	0.08	0.05	0.06	0.13	0.13	0.14	0.14
Ca	0.00	0.00	0.00	0.00	0.00	0.01	0.01	0.00	0.00
Na	0.20	0.17	0.12	0.13	0.09	0.19	0.22	0.23	0.22
K	1.83	1.82	1.94	1.88	1.88	1.77	1.81	1.77	1.81
Cr	0.00	0.00	0.00	0.00	0.01	0.00	0.01	0.00	0.01
Cl									
P									
Ba	0.00	0.00	0.01		0.00	0.01	0.00	0.01	
F	0.00	0.00		0.68	0.48				0.12
OH	4.00	4.00	4.00	3.32	3.52	4.00	4.00	4.00	3.88
Tetrahedral	8.00	8.00	8.00	8.00	8.00	8.00	8.00	8.00	8.00
Octahedral	4.04	4.03	4.22	4.17	4.15	4.07	4.07	4.08	4.06
Dodecahedral	2.04	2.00	2.07	2.01	1.98	1.97	2.03	2.01	2.04

Sample	SC-5-K	SC-5-K	SC-5-K	SC-5-K	SC-5-K	SC-5-K	SC-5-K	SC-5-K	SC-6-K
Point	12	13	2	3	6	7	9	15	2
Description	G	G	G	G	G	G	G	G	RF
SiO2	44.91	44.93	45.53	46.22	44.54	47.19	44.96	45.40	45.13
TiO2	0.14	0.14	0.10	0.08	0.08	0.20	0.10	0.11	0.15
Al2O3	32.56	31.68	32.33	31.86	30.98	29.77	32.52	33.35	32.47
FeO	4.91	6.42	5.23	5.74	5.73	6.33	5.24	5.17	4.84
MnO	0.01	0.02	0.19	0.13	0.05	0.05	0.00	0.05	0.04
MgO	0.08	0.07	0.20	0.12	0.10	0.25	0.06	0.20	0.58
CaO	0.00	0.02	0.06	0.00	0.01	0.00	0.01	0.02	0.04
Na2O	0.64	0.66	0.68	0.83	0.68	0.35	0.70	0.59	0.76
K2O	10.52	10.24	10.54	10.30	10.26	10.89	10.53	10.72	9.90
Cr2O3	0.00	0.00	0.09	0.03	0.00	0.03	0.07	0.04	0.04
Cl	N/D	N/D	N/D	N/D	N/D	N/D	N/D	N/D	0.00
P2O5	N/D	N/D	N/D	N/D	N/D	N/D	N/D	N/D	0.00
BaO	N/D	N/D	N/D	N/D	N/D	N/D	0.01	0.00	0.00
F	2.07	2.61	2.28	2.43	2.14	2.42	2.29	2.18	2.98
Total	95.84	96.78	97.24	97.73	94.57	97.48	96.50	97.85	96.94
Si	6.20	6.22	6.12	6.22	6.11	6.18	6.16	6.18	6.26
Ti	0.02	0.01	0.01	0.02	0.02	0.02	0.02	0.01	0.02
Al Total	5.40	5.44	5.56	5.36	5.60	5.49	5.51	5.48	5.54
Al IV	1.80	1.78	1.88	1.78	1.89	1.82	1.84	1.82	1.74
Al VI	3.59	3.66	3.68	3.58	3.71	3.67	3.67	3.66	3.81
Fe	0.28	0.25	0.25	0.33	0.22	0.23	0.23	0.24	0.31
Mn	0.01	0.01	0.02	0.01	0.01	0.01	0.01	0.01	0.01
Mg	0.15	0.13	0.14	0.15	0.10	0.12	0.13	0.13	0.09
Ca	0.00	0.00	0.00	0.00	0.00	0.00	0.00	0.00	0.01
Na	0.20	0.18	0.22	0.20	0.21	0.15	0.17	0.18	0.07
K	1.79	1.81	1.77	1.75	1.80	1.81	1.83	1.83	1.63
Cr	0.02	0.00	0.00	0.01	0.00	0.01	0.00	0.01	0.00
Cl									0.00
P									0.01
Ba			0.00	0.00	0.00	0.00	0.00	0.00	0.00
F	0.13	0.13	0.11	0.12	0.11			0.17	0.38
OH	3.87	3.87	3.89	3.88	3.89	4.00	4.00	3.83	3.62
Tetrahedral	8.00	8.00	8.00	8.00	8.00	8.00	8.00	8.00	8.00
Octahedral	4.06	4.06	4.10	4.09	4.07	4.06	4.06	4.05	4.25
Dodecahedral	2.00	1.99	1.99	1.96	2.01	1.97	2.01	2.02	1.71

Sample	SC-6-K	SC-6-K	SC-6-K	SC-6-K	SC-6-K	SC-6-K	SC-6-K	SC-6-K
Point	18	21	23	29	35	38	14	19
Description	RF	RF	RF	RF	RF	RF	S	S
SiO2	46.20	46.30	46.09	46.21	47.57	45.59	46.20	45.78
TiO2	0.00	0.10	0.20	0.13	0.73	0.26	0.08	0.21
Al2O3	32.94	31.00	32.59	32.22	28.41	30.66	32.52	30.60
FeO	4.90	5.84	4.87	4.83	7.86	7.41	5.65	6.82
MnO	0.02	0.00	0.10	0.09	0.03	0.01	0.04	0.08
MgO	0.55	0.84	0.72	0.51	0.59	0.64	0.14	0.41
CaO	0.04	0.00	0.01	0.02	0.01	0.00	0.00	0.00
Na2O	0.84	0.56	0.44	0.63	0.33	0.48	0.62	0.46
K2O	10.26	10.27	10.39	10.14	10.54	10.29	10.20	10.59
Cr2O3	0.09	0.03	0.01	0.00	0.00	0.07	0.00	0.07
Cl	0.04	0.00	0.00	0.00	0.02	0.03	0.02	0.00
P2O5	0.11	0.11	0.11	0.04	0.00	0.06	0.12	0.00
BaO	0.05	0.21	0.10	0.00	0.00	0.00	0.08	0.15
F	3.22	2.90	2.38	2.67	3.28	3.62	3.47	3.25
Total	99.25	98.16	98.01	97.48	99.36	99.11	99.15	98.42
Si	6.21	6.18	6.25	6.34	6.27	6.11	6.04	6.48
Ti	0.01	0.02	0.01	0.03	0.03	0.00	0.00	0.03
Al Total	5.61	5.46	5.61	5.40	5.51	5.76	5.82	4.69
Al IV	1.79	1.82	1.75	1.66	1.73	1.89	1.96	1.52
Al VI	3.82	3.64	3.86	3.74	3.78	3.88	3.87	3.17
Fe	0.28	0.47	0.25	0.28	0.25	0.22	0.25	1.31
Mn	0.01	0.01	0.00	0.01	0.02	0.01	0.00	0.03
Mg	0.06	0.09	0.09	0.15	0.13	0.06	0.04	0.05
Ca	0.01	0.00	0.01	0.02	0.00	0.01	0.00	0.00
Na	0.12	0.08	0.10	0.12	0.12	0.16	0.12	0.09
K	1.58	1.77	1.46	1.52	1.59	1.62	1.65	1.83
Cr	0.00	0.00	0.00	0.00	0.00	0.00	0.00	0.00
Cl	0.00	0.01	0.01	0.01	0.00	0.00	0.00	0.01
P	0.02	0.03	0.02	0.00	0.01	0.03	0.06	0.00
Ba	0.00	0.01	0.00	0.00	0.00	0.00	0.00	0.01
F	0.29	0.31	0.24	0.27	0.29	0.28	0.27	0.83
OH	3.71	3.69	3.76	3.73	3.71	3.72	3.73	3.16
Tetrahedral	8.00	8.00	8.00	8.00	8.00	8.00	8.00	8.00
Octahedral	4.21	4.23	4.22	4.24	4.21	4.17	4.15	4.58
Dodecahedral	1.72	1.89	1.59	1.64	1.72	1.81	1.83	1.94

Sample	SC-7-K	SC-7-K	SC-7-K	SC-7-K	SC-7-K	SC-7-K	SC-7-K	SC-7-K
Point	16	40	40b	44	9	2	24	29
Description	G	G	G	G	RA	RF	RF	RF
SiO2	45.90	45.81	46.46	49.80	45.57	47.59	45.68	47.40
TiO2	0.07	0.12	0.00	0.11	0.18	0.13	0.24	0.00
Al2O3	32.54	31.41	31.40	35.43	32.07	31.38	31.95	32.07
FeO	5.34	6.49	6.21	0.79	6.01	5.04	5.50	4.98
MnO	0.25	0.02	0.22	0.00	0.13	0.00	0.16	0.23
MgO	0.57	0.10	0.19	0.03	0.60	0.60	0.76	0.62
CaO	0.00	0.00	0.00	0.08	0.03	0.00	0.00	0.00
Na2O	0.49	0.61	0.51	0.04	0.55	0.32	0.58	0.41
K2O	10.43	9.97	10.23	9.71	10.28	10.59	9.45	10.37
Cr2O3	0.09	0.08	0.00	0.00	0.01	0.07	0.02	0.00
Cl	0.01	0.01	0.00	0.00	0.00	0.03	0.00	0.00
P2O5	0.07	0.22	0.00	0.17	0.09	0.08	0.13	0.01
BaO	0.18	0.00	0.05	0.00	0.00	0.00	0.00	0.19
F	2.52	2.75	3.19	0.00	2.91	2.25	3.10	2.64
Total	98.45	97.60	98.47	96.16	98.45	98.07	97.56	98.91
Si	6.23	6.23	6.38	6.50	6.51	6.27	6.39	6.27
Ti	0.01	0.00	0.00	0.01	0.03	0.03	0.06	0.02
Al Total	5.57	5.47	5.18	5.20	4.97	5.59	5.30	5.56
Al IV	1.77	1.77	1.62	1.50	1.49	1.73	1.61	1.73
Al VI	3.80	3.70	3.56	3.70	3.48	3.85	3.69	3.83
Fe	0.26	0.41	0.65	0.67	0.79	0.22	0.35	0.27
Mn	0.00	0.02	0.04	0.06	0.01	0.01	0.00	0.01
Mg	0.03	0.05	0.03	0.03	0.15	0.12	0.18	0.13
Ca	0.00	0.00	0.01	0.00	0.01	0.01	0.00	0.00
Na	0.21	0.11	0.10	0.16	0.05	0.13	0.09	0.12
K	1.62	1.53	1.68	1.60	1.67	1.56	1.61	1.52
Cr	0.00	0.01	0.00	0.00	0.00	0.00	0.00	0.00
Cl	0.02	0.00	0.00	0.00	0.00	0.01	0.00	0.02
P	0.01	0.02	0.01	0.00	0.00	0.00	0.00	0.00
Ba	0.00	0.00	0.01	0.00	0.00	0.00	0.00	0.00
F	0.14	0.06	0.38	0.95	0.68	0.34	0.47	0.31
OH	3.85	3.93	3.62	3.05	3.32	3.66	3.53	3.68
Tetrahedral	8.00	8.00	8.00	8.00	8.00	8.00	8.00	8.00
Octahedral	4.10	4.17	4.29	4.48	4.46	4.24	4.28	4.26
Dodecahedral	1.84	1.67	1.80	1.77	1.72	1.69	1.70	1.64

Sample	SC-7-K	SC-7-K	SC-8-K	SC-2-L	SC-2-L	SC-2-L	SC-2-L	SC-2-L
Point	12	36	3	1.00	2.00	3.00	4.00	5.00
Description	S	S	S	G	G	G	G	G
SiO2	45.93	45.58	45.20	47.12	47.71	48.01	47.85	48.03
TiO2	0.18	0.11	0.23	0.55	0.59	0.32	0.27	0.41
Al2O3	32.47	31.19	29.54	32.09	33.06	32.62	31.54	31.06
FeO	5.12	6.51	7.51	2.98	2.47	2.63	3.98	4.06
MnO	0.00	0.02	0.07	0.10	0.11	0.00	0.13	0.09
MgO	0.59	0.12	0.58	1.39	1.84	1.72	1.75	1.93
CaO	0.00	0.00	0.03	0.04	0.04	0.00	0.00	0.03
Na2O	0.58	0.49	0.46	1.13	0.38	0.38	0.28	0.32
K2O	9.96	10.30	9.87	9.76	9.58	10.29	9.75	10.14
Cr2O3	0.00	0.00	0.06	0.00	0.00	0.11	0.01	0.00
Cl	0.00	0.00	0.00	0.01	0.01	0.00	0.00	0.00
P2O5	0.06	0.00	0.12	0.00	0.06	0.00	0.04	0.03
BaO	0.00	0.00	0.07	0.10	0.04	0.15	0.21	0.15
F	2.51	3.40	3.71	1.90	2.59	2.63	2.74	3.21
Total	97.40	97.72	97.44	97.17	98.48	98.86	98.55	99.46
Si	6.24	6.25	6.14	6.09	6.09	6.15	6.11	6.22
Ti	0.07	0.05	0.00	0.03	0.00	0.05	0.01	0.01
Al Total	5.53	5.49	5.67	5.66	5.69	5.50	5.60	5.36
Al IV	1.76	1.75	1.86	1.91	1.91	1.85	1.89	1.78
Al VI	3.77	3.73	3.81	3.75	3.78	3.65	3.71	3.58
Fe	0.25	0.31	0.18	0.16	0.24	0.25	0.29	0.44
Mn	0.00	0.01	0.01	0.00	0.00	0.00	0.00	0.02
Mg	0.14	0.18	0.03	0.09	0.05	0.07	0.05	0.01
Ca	0.01	0.00	0.00	0.01	0.00	0.01	0.00	0.00
Na	0.18	0.16	0.14	0.13	0.17	0.18	0.25	0.17
K	1.54	1.57	1.85	1.88	1.83	1.84	1.77	1.86
Cr	0.01	0.00	0.00	0.00	0.00	0.00	0.00	0.00
Cl	0.00	0.00						
P	0.00	0.00						
Ba	0.00	0.00		0.01	0.00	0.00	0.00	0.01
F	0.41	0.43	0.09			0.13	0.10	
OH	3.59	3.57	3.91	4.00	4.00	3.87	3.90	4.00
Tetrahedral	8.00	8.00	8.00	8.00	8.00	8.00	8.00	8.00
Octahedral	4.24	4.30	4.03	4.04	4.06	4.03	4.07	4.06
Dodecahedral	1.74	1.73	1.99	2.02	2.00	2.02	2.03	2.04

Sample	SC-2-L	SC-2-L	SC-2-L	SC-2-L	SC-2-L	SC-2-L	SC-2-L	SC-2-L	SC-2-L
Point	6.00	6b	6c	7	8	9	10	13	14
Description	G	G	G	G	G	G	G	G	G
SiO2	47.36	47.49	47.09	47.30	47.00	47.36	47.94	47.03	46.56
TiO2	0.03	0.04	0.23	0.16	0.20	0.44	0.35	0.06	0.00
Al2O3	35.57	35.63	31.95	35.21	36.02	31.09	32.19	27.25	36.34
FeO	1.59	1.69	4.20	1.97	1.29	3.93	3.07	7.19	1.57
MnO	0.00	0.09	0.05	0.08	0.00	0.11	0.11	0.20	0.09
MgO	1.05	1.02	1.32	1.19	0.80	1.64	1.72	2.06	0.80
CaO	0.02	0.00	0.01	0.00	0.00	0.00	0.00	0.08	0.00
Na2O	0.47	0.59	0.36	0.49	0.65	0.22	0.30	0.15	0.68
K2O	10.01	10.17	10.26	10.25	10.09	9.83	10.15	10.17	9.98
Cr2O3	0.00	0.00	0.00	0.04	0.05	0.00	0.00	0.00	0.00
Cl	0.00	0.00	0.01	0.01	0.05	0.00	0.00	0.00	0.00
P2O5	0.00	0.00	0.00	0.00	0.00	0.00	0.05	0.01	0.00
BaO	0.14	0.12	0.02	0.23	0.08	0.03	0.08	0.08	0.15
F	1.27	1.84	2.90	1.84	1.21	3.37	2.77	5.03	1.57
Total	97.51	98.68	98.40	98.77	97.44	98.02	98.73	99.31	97.74
Si	6.15	6.21	6.11	6.18	5.98	6.20	6.06	6.12	6.08
Ti	0.04	0.04	0.05	0.02	0.01	0.01	0.00	0.00	0.00
Al Total	5.54	5.49	5.59	5.49	5.82	5.47	5.76	5.68	5.78
Al IV	1.85	1.79	1.89	1.82	2.02	1.80	1.94	1.88	1.92
Al VI	3.69	3.71	3.70	3.67	3.80	3.68	3.82	3.80	3.85
Fe	0.21	0.15	0.17	0.23	0.19	0.22	0.16	0.21	0.17
Mn	0.01	0.00	0.01	0.01	0.00	0.01	0.00	0.00	0.00
Mg	0.12	0.12	0.14	0.11	0.11	0.15	0.05	0.04	0.02
Ca	0.00	0.00	0.01	0.00	0.01	0.01	0.00	0.01	0.00
Na	0.19	0.15	0.18	0.14	0.26	0.24	0.21	0.18	0.18
K	1.77	1.81	1.76	1.88	1.69	1.72	1.82	1.78	1.81
Cr	0.00	0.00	0.00	0.00	0.00	0.00	0.00	0.00	0.00
Cl									
P									
Ba	0.01	0.00	0.00	0.00	0.01	0.00	0.01	0.00	0.00
F			0.10					0.01	0.00
OH	4.00	4.00	3.90	4.00	4.00	4.00	4.00	3.99	4.00
Tetrahedral	8.00	8.00	8.00	8.00	8.00	8.00	8.00	8.00	8.00
Octahedral	4.06	4.02	4.07	4.04	4.12	4.08	4.04	4.06	4.04
Dodecahedral	1.97	1.97	1.94	2.03	1.96	1.96	2.04	1.97	2.00

Sample	SC-5-L	SC-5-L	SC-5-L	SC-5-L	SC-5-L	SC-5-L	SC-5-L	SC-5-L	SC-5-L
Point	1	1b	1c	2	3	3b	4	5	6
Description	G	G	G	G	G	G	G	G	G
SiO2	47.35	47.20	46.61	47.14	46.20	44.77	46.39	47.30	47.19
TiO2	0.15	0.37	0.12	0.53	0.50	0.29	0.46	0.47	0.60
Al2O3	34.73	34.15	35.57	34.82	34.96	27.02	34.60	35.27	35.05
FeO	3.05	3.30	3.57	2.87	2.80	10.86	3.44	2.56	2.80
MnO	0.18	0.04	0.07	0.05	0.09	0.22	0.12	0.00	0.02
MgO	0.80	0.77	0.16	0.62	0.75	0.60	0.70	0.76	0.69
CaO	0.00	0.03	0.00	0.00	0.00	0.00	0.00	0.02	0.02
Na2O	0.75	0.70	0.83	0.67	0.84	0.20	0.54	0.77	0.65
K2O	9.09	9.40	9.76	9.58	9.64	10.41	9.79	9.68	8.98
Cr2O3	0.09	0.05	0.00	0.00	0.00	0.00	0.00	0.03	0.01
Cl	0.04	0.00	0.02	0.00	0.01	0.00	0.01	0.00	0.01
P2O5	0.01	0.08	0.14	0.11	0.02	0.08	0.13	0.00	0.07
BaO	0.17	0.00	0.00	0.00	0.00	0.00	0.00	0.15	0.00
F	1.87	1.89	1.57	1.75	1.75	3.88	1.96	1.63	1.96
Total	98.28	97.98	98.42	98.14	97.56	98.33	98.14	98.64	98.05
Si	6.12	6.10	6.18	6.16	6.22	6.29	6.19	6.27	6.35
Ti	0.01	0.00	0.00	0.02	0.01	0.02	0.01	0.02	0.02
Al Total	5.57	5.56	5.60	5.55	5.33	5.18	5.43	5.15	4.96
Al IV	1.88	1.90	1.82	1.84	1.78	1.71	1.81	1.73	1.65
Al VI	3.70	3.66	3.78	3.71	3.55	3.46	3.62	3.42	3.32
Fe	0.24	0.26	0.12	0.18	0.46	0.58	0.40	0.63	0.72
Mn	0.00	0.00	0.00	0.00	0.01	0.00	0.01	0.01	0.04
Mg	0.13	0.15	0.13	0.14	0.07	0.04	0.06	0.06	0.05
Ca	0.01	0.00	0.00	0.01	0.01	0.00	0.00	0.01	0.00
Na	0.19	0.19	0.19	0.16	0.19	0.09	0.23	0.09	0.14
K	1.82	1.87	1.79	1.83	1.81	1.87	1.74	1.90	1.87
Cr	0.00	0.01	0.00	0.00	0.00	0.01	0.00	0.00	0.00
Cl									
P									
Ba	0.00	0.01		0.00			0.00	0.00	0.00
F	0.22		0.00	0.01	0.27	0.19	0.24	0.20	
OH	3.78	4.00	4.00	3.99	3.73	3.81	3.76	3.80	4.00
Tetrahedral	8.00	8.00	8.00	8.00	8.00	8.00	8.00	8.00	8.00
Octahedral	4.08	4.07	4.03	4.05	4.10	4.11	4.10	4.13	4.15
Dodecahedral	2.01	2.08	1.97	1.99	2.00	1.97	1.97	1.99	2.00

Sample	SC-5-L	SC-5-L	SC-5-L	SC-5-L	SC-5-L	SC-7-L	SC-7-L	SC-7-L	SC-7-L
Point	6b	6c	7	8	8b	2	7	7b	7c
Description	G	G	G	G	G	G	G	G	G
SiO2	46.51	46.46	46.55	47.01	47.14	46.21	44.94	46.99	46.77
TiO2	0.00	0.61	0.73	0.26	0.31	0.00	0.37	0.10	0.34
Al2O3	36.30	34.47	34.43	34.81	34.27	36.50	32.66	36.87	34.46
FeO	3.20	2.66	2.85	3.01	3.01	1.98	7.46	1.97	3.47
MnO	0.00	0.14	0.09	0.14	0.01	0.04	0.10	0.02	0.09
MgO	0.22	0.73	0.86	0.82	0.85	0.15	0.52	0.25	0.74
CaO	0.00	0.00	0.01	0.04	0.03	0.01	0.41	0.05	0.05
Na2O	0.78	0.69	0.73	0.77	0.64	0.53	0.63	0.34	0.67
K2O	9.73	9.54	9.57	9.66	10.04	9.22	7.67	9.63	8.71
Cr2O3	0.00	0.00	0.00	0.00	0.01	0.00	0.00	0.00	0.00
Cl	0.05	0.00	0.01	0.00	0.00	0.03	0.00	0.00	0.01
P2O5	0.01	0.01	0.10	0.06	0.06	0.12	0.11	0.00	0.10
BaO	0.18	0.00	0.04	0.37	0.08	0.14	0.03	0.00	0.00
F	1.45	1.69	1.73	1.96	2.17	2.21	2.83	1.46	2.74
Total	98.43	97.00	97.70	98.91	98.62	97.14	97.73	97.68	98.15
Si	6.26	6.25	6.23	6.19	6.21	6.39	6.51	6.64	6.74
Ti	0.01	0.02	0.01	0.01	0.01	0.02	0.02	0.01	0.01
Al Total	5.19	5.03	5.40	5.46	5.40	5.30	5.12	4.71	4.23
Al IV	1.74	1.75	1.77	1.81	1.79	1.61	1.49	1.36	1.26
Al VI	3.45	3.28	3.63	3.65	3.61	3.69	3.63	3.35	2.96
Fe	0.45	0.64	0.32	0.34	0.39	0.39	0.34	0.65	1.07
Mn	0.01	0.01	0.00	0.01	0.01	0.00	0.02	0.03	0.05
Mg	0.22	0.26	0.08	0.06	0.04	0.17	0.05	0.10	0.12
Ca	0.00	0.00	0.00	0.00	0.00	0.01	0.00	0.00	0.00
Na	0.10	0.10	0.26	0.23	0.23	0.08	0.04	0.06	0.07
K	1.92	1.91	1.75	1.76	1.80	1.68	1.69	1.64	1.73
Cr	0.00	0.00	0.01	0.00	0.00	0.00	0.00	0.00	0.00
Cl						0.00	0.00	0.00	0.02
P						0.00	0.00	0.00	0.01
Ba		0.00	0.01	0.00		0.00	0.00	0.01	0.01
F	0.20	0.18			0.34	0.46	0.00	0.00	0.00
OH	3.80	3.82	4.00	4.00	3.66	3.54	4.00	4.00	3.99
Tetrahedral	8.00	8.00	8.00	8.00	8.00	8.00	8.00	8.00	8.00
Octahedral	4.13	4.21	4.04	4.07	4.07	4.29	4.05	4.14	4.22
Dodecahedral	2.02	2.01	2.03	1.99	2.03	1.76	1.73	1.71	1.81

Sample	SC-7-L	SC-7-L	SC-7-L	SC-7-L	SC-7-L	SC-7-L	SC-7-L	SC-7-L	SC-7-L
Point	10	12	13	13b	13c	6	6b	8	3
Description	G	G	RB	RB	RB	RF	RF	RF	S
SiO2	47.56	46.90	46.76	46.78	46.76	47.10	46.51	46.41	47.36
TiO2	0.41	0.01	0.40	0.03	0.35	0.15	0.00	0.00	0.35
Al2O3	34.26	37.01	34.08	34.45	35.67	35.96	35.05	35.23	35.14
FeO	3.61	2.48	3.97	3.63	2.80	2.60	4.18	2.86	3.04
MnO	0.06	0.00	0.07	0.12	0.14	0.00	0.24	0.09	0.00
MgO	0.84	0.19	0.73	0.25	0.34	0.27	0.20	0.15	0.71
CaO	0.04	0.00	0.04	0.04	0.00	0.05	0.07	0.00	0.00
Na2O	0.84	0.66	0.74	0.29	0.30	0.58	0.32	0.31	0.68
K2O	8.67	9.27	9.23	9.13	9.79	9.31	9.30	8.92	9.14
Cr2O3	0.00	0.10	0.02	0.00	0.04	0.03	0.00	0.00	0.00
Cl	0.00	0.03	0.00	0.00	0.01	0.03	0.05	0.01	0.00
P2O5	0.00	0.02	0.07	0.03	0.00	0.00	0.00	0.00	0.04
BaO	0.00	0.00	0.00	0.00	0.00	0.00	0.00	0.22	0.04
F	2.53	2.34	2.11	2.80	2.16	2.44	2.63	2.54	2.33
Total	98.82	99.01	98.22	97.55	98.36	98.52	98.55	96.74	98.83
Si	6.53	6.49	6.35	6.46	6.13	6.16	6.22	6.26	6.18
Ti	0.00	0.01	0.00	0.02	0.01	0.00	0.01	0.00	0.02
Al Total	5.09	4.87	5.38	5.13	5.71	5.73	5.55	5.47	5.65
Al IV	1.47	1.51	1.65	1.54	1.87	1.84	1.78	1.74	1.82
Al VI	3.62	3.36	3.74	3.59	3.85	3.89	3.76	3.73	3.83
Fe	0.38	0.66	0.28	0.38	0.12	0.11	0.16	0.19	0.14
Mn	0.02	0.03	0.02	0.02	0.00	0.00	0.00	0.00	0.00
Mg	0.06	0.11	0.05	0.06	0.11	0.08	0.16	0.22	0.12
Ca	0.00	0.00	0.00	0.00	0.01	0.00	0.01	0.00	0.00
Na	0.05	0.04	0.05	0.02	0.15	0.10	0.11	0.13	0.09
K	1.62	1.72	1.67	1.72	1.63	1.67	1.69	1.60	1.62
Cr	0.01	0.00	0.00	0.00	0.00	0.01	0.00	0.00	0.00
Cl	0.00	0.01	0.00	0.03	0.00	0.00	0.00	0.00	0.00
P	0.00	0.00	0.00	0.01	0.00	0.00	0.00	0.00	0.01
Ba	0.00	0.00	0.00	0.00	0.00	0.00	0.00	0.00	0.00
F	0.00	0.00	0.00	0.00	0.00	0.00	0.00	0.00	0.00
OH	4.00	4.00	4.00	3.99	4.00	4.00	4.00	4.00	4.00
Tetrahedral	8.00	8.00	8.00	8.00	8.00	8.00	8.00	8.00	8.00
Octahedral	4.08	4.17	4.09	4.07	4.10	4.08	4.10	4.14	4.10
Dodecahedral	1.68	1.77	1.72	1.75	1.78	1.77	1.80	1.73	1.72

Sample	SC-7-L	SC-7-L	SC-12-L	SC-12-L	SC-12-L	SC-12-L	SC-12-L	SC-12-L
Point	5	9	1	3	5	6	11	2b
Description	S	S	HP	HP	HP	HP	HP	HP
SiO2	46.48	47.13	44.86	44.61	43.95	43.99	44.40	43.14
TiO2	0.12	0.06	0.12	0.13	0.24	0.21	0.15	0.48
Al2O3	36.25	33.22	34.48	34.29	30.45	31.42	34.19	32.73
FeO	2.15	4.11	2.88	2.28	3.28	3.42	2.38	2.13
MnO	0.14	0.06	0.04	0.06	0.04	0.10	0.00	0.00
MgO	0.36	0.21	0.26	0.26	0.59	0.69	0.26	0.69
CaO	0.00	0.09	0.00	0.03	0.03	0.01	0.05	0.00
Na2O	0.58	0.33	1.02	0.61	0.30	0.37	0.92	0.82
K2O	8.75	8.89	10.14	10.01	9.79	10.87	9.88	9.43
Cr2O3	0.00	0.11	0.00	0.00	0.00	0.04	0.03	0.00
Cl	0.00	0.00	0.02	0.00	0.00	0.02	0.00	0.01
P2O5	0.14	0.00	0.05	0.07	0.10	0.07	0.05	0.08
BaO	0.06	0.00	0.15	0.08	0.00	0.05	0.08	0.00
F	2.40	2.86	1.05	0.82	1.28	0.98	0.76	0.86
Total	97.43	97.07	95.07	93.24	90.04	92.22	93.16	90.35
Si	6.13	6.15	6.25	6.18	6.12	6.17	6.17	6.14
Ti	0.01	0.01	0.01	0.01	0.02	0.00	0.01	0.01
Al Total	5.71	5.72	5.16	5.42	5.53	5.51	5.52	5.60
Al IV	1.87	1.85	1.75	1.82	1.88	1.83	1.83	1.86
Al VI	3.84	3.87	3.41	3.61	3.65	3.68	3.68	3.74
Fe	0.11	0.14	0.67	0.47	0.41	0.35	0.33	0.31
Mn	0.00	0.00	0.02	0.00	0.01	0.00	0.00	0.00
Mg	0.12	0.11	0.05	0.03	0.03	0.02	0.02	0.01
Ca	0.00	0.00	0.00	0.00	0.01	0.01	0.00	0.00
Na	0.16	0.10	0.20	0.23	0.25	0.17	0.15	0.26
K	1.67	1.52	1.79	1.70	1.70	1.83	1.83	1.68
Cr	0.00	0.01	0.00	0.00	0.00	0.00	0.01	0.00
Cl	0.00	0.00						
P	0.00	0.00						
Ba	0.01	0.00	0.00	0.00	0.00	0.01	0.00	0.00
F	0.00	0.00	0.43	0.34	0.31	0.34	0.28	0.35
OH	4.00	4.00	3.57	3.66	3.69	3.66	3.72	3.65
Tetrahedral	8.00	8.00	8.00	8.00	8.00	8.00	8.00	8.00
Octahedral	4.08	4.14	4.17	4.12	4.12	4.07	4.06	4.08
Dodecahedral	1.84	1.64	1.99	1.94	1.96	2.01	1.99	1.94

Sample	SC-12-L	SC-12-L	SC-12-L	SC-12-L	SC-12-L	SC-12-L	SC-12-L	SC-12-L
Point	14	1	2	2b	8	9	10	11
Description	P	RB	RF	RF	RF	RF	RF	RF
SiO2	47.66	47.01	47.65	48.53	47.65	47.74	48.21	47.84
TiO2	0.34	0.66	0.04	0.12	0.25	0.31	0.58	0.21
Al2O3	35.81	35.35	36.48	31.33	30.86	36.11	33.93	35.97
FeO	2.59	2.50	2.01	5.07	6.88	2.03	3.14	2.43
MnO	0.12	0.03	0.00	0.02	0.08	0.05	0.00	0.11
MgO	0.68	0.82	0.51	0.80	0.74	0.60	0.91	0.65
CaO	0.03	0.00	0.00	0.05	0.07	0.04	0.00	0.00
Na2O	0.49	0.72	0.38	0.23	0.19	0.52	0.35	0.48
K2O	9.47	9.14	9.45	8.36	9.59	9.29	9.53	9.08
Cr2O3	0.07	0.02	0.08	0.00	0.00	0.00	0.02	0.03
Cl	0.00	0.01	0.00	0.01	0.00	0.03	0.01	0.04
P2O5	0.00	0.05	0.00	0.00	0.00	0.00	0.00	0.00
BaO	0.00	0.00	0.01	0.00	0.06	0.00	0.00	0.00
F	2.21	1.80	1.59	3.06	3.15	1.62	2.24	1.49
Total	99.47	98.11	98.20	97.58	99.52	98.34	98.92	98.33
Si	6.04	6.43	6.15	6.11	6.10	6.14	6.16	6.12
Ti	0.02	0.01	0.00	0.01	0.02	0.01	0.01	0.01
Al Total	5.63	5.17	5.53	5.62	5.65	5.57	5.56	5.62
Al IV	1.96	1.57	1.85	1.89	1.90	1.86	1.84	1.88
Al VI	3.66	3.60	3.67	3.73	3.75	3.70	3.72	3.75
Fe	0.37	0.29	0.38	0.28	0.24	0.29	0.27	0.25
Mn	0.00	0.00	0.01	0.01	0.01	0.01	0.00	0.01
Mg	0.06	0.19	0.01	0.04	0.04	0.04	0.04	0.02
Ca	0.03	0.01	0.00	0.00	0.00	0.00	0.00	0.00
Na	0.21	0.11	0.26	0.27	0.24	0.29	0.25	0.27
K	1.78	1.66	1.74	1.72	1.73	1.73	1.73	1.73
Cr	0.00	0.00	0.00	0.00	0.00	0.00	0.00	0.01
Cl								
P								
Ba	0.00	0.00	0.01	0.00	0.00			
F	0.26	0.10	0.27	0.27	0.25	0.32	0.32	0.28
OH	3.74	3.90	3.73	3.73	3.75	3.68	3.68	3.72
Tetrahedral	8.00	8.00	8.00	8.00	8.00	8.00	8.00	8.00
Octahedral	4.14	4.09	4.08	4.07	4.07	4.06	4.05	4.04
Dodecahedral	1.99	1.77	2.01	2.00	1.97	2.02	1.98	2.01

Sample	SC-12-L	SC-12-L	SC-12-L	SC-12-L	SC-12-L	SC-13-L	SC-13-L	SC-13-L
Point	12	13	13b	3	7	3	5	12.00
Description	RF	RF	RF	S	S	S	S	S
SiO2	47.33	47.16	47.90	47.10	48.16	46.39	47.28	46.90
TiO2	0.73	0.53	0.24	0.33	0.13	0.36	0.06	0.48
Al2O3	35.62	35.17	33.75	33.90	34.23	36.81	34.32	36.13
FeO	2.25	2.84	3.50	3.17	3.25	2.10	3.38	2.21
MnO	0.02	0.13	0.04	0.00	0.10	0.00	0.05	0.10
MgO	0.73	0.91	0.87	0.75	0.85	0.57	0.19	0.54
CaO	0.04	0.03	0.04	0.00	0.00	0.00	0.04	0.00
Na2O	0.72	0.62	0.30	0.29	0.31	0.55	0.27	0.46
K2O	9.14	9.30	9.89	9.30	9.58	9.70	10.13	9.38
Cr2O3	0.10	0.00	0.00	0.00	0.03	0.04	0.00	0.00
Cl	0.01	0.00	0.00	0.01	0.00	0.02	0.05	0.00
P2O5	0.04	0.03	0.00	0.07	0.00	0.38	0.09	0.05
BaO	0.00	0.00	0.00	0.00	0.00	0.00	0.04	0.00
F	1.96	2.07	2.16	2.04	2.27	1.36	0.61	2.06
Total	98.69	98.79	98.69	96.96	98.91	98.28	96.51	98.31
Si	6.13	6.11	6.07	6.13	6.32	6.08	6.14	6.14
Ti	0.01	0.02	0.02	0.01	0.01	0.01	0.00	0.02
Al Total	5.59	5.65	5.70	5.61	5.03	5.65	5.61	5.58
Al IV	1.87	1.89	1.93	1.87	1.68	1.92	1.86	1.86
Al VI	3.71	3.76	3.77	3.74	3.35	3.74	3.76	3.73
Fe	0.30	0.24	0.24	0.24	0.72	0.26	0.28	0.31
Mn	0.00	0.01	0.01	0.00	0.05	0.02	0.01	0.02
Mg	0.02	0.02	0.02	0.06	0.01	0.05	0.01	0.04
Ca	0.00	0.00	0.00	0.00	0.00	0.00	0.00	0.00
Na	0.28	0.24	0.26	0.28	0.21	0.29	0.15	0.23
K	1.77	1.73	1.71	1.73	1.81	1.74	1.83	1.63
Cr	0.00	0.00	0.01	0.00	0.00	0.00	0.00	0.00
Cl								
P								
Ba						0.00	0.00	0.00
F	0.26	0.26	0.24	0.29	0.59			
OH	3.74	3.74	3.76	3.71	3.41	4.00	4.00	4.00
Tetrahedral	8.00	8.00	8.00	8.00	8.00	8.00	8.00	8.00
Octahedral	4.04	4.06	4.06	4.05	4.14	4.07	4.06	4.12
Dodecahedral	2.05	1.97	1.98	2.01	2.03	2.03	1.98	1.86

Sample	SC-13-L	SC-14-L	SC-14-L	SC-14-L	SC-14-L	SC-14-L	SC-14-L	SC-14-L
Point	14.00	1	2	3	5	6	4	9
Description	S	G	G	G	G	G	G	G
SiO2	48.52	46.25	45.92	45.45	45.70	45.66	46.46	45.82
TiO2	0.35	0.00	0.00	0.19	0.00	0.00	0.22	0.00
Al2O3	31.81	36.46	35.52	34.00	35.64	35.66	34.72	35.20
FeO	5.00	2.59	3.43	3.23	2.98	3.03	2.92	3.06
MnO	0.14	0.00	0.00	0.11	0.12	0.00	0.15	0.09
MgO	1.24	0.07	0.06	0.56	0.15	0.06	0.69	0.00
CaO	0.04	0.00	0.02	0.07	0.01	0.00	0.04	0.00
Na2O	0.16	0.48	0.89	0.93	1.13	1.04	1.06	0.90
K2O	9.18	10.99	10.49	10.03	10.34	10.37	10.07	10.24
Cr2O3	0.00	0.06	0.00	0.08	0.00	0.00	0.00	0.01
Cl	0.00	N/D	N/D	N/D	N/D	N/D	N/D	N/D
P2O5	0.11	N/D	N/D	N/D	N/D	N/D	N/D	N/D
BaO	0.00	N/D	N/D	N/D	N/D	N/D	0.00	0.00
F	3.30	1.22	1.28	1.24	1.16	1.16	1.48	1.24
Total	99.85	98.12	97.62	95.89	97.23	96.98	97.80	96.57
Si	6.22	6.10	6.05	6.11	6.15	6.10	6.06	6.13
Ti	0.01	0.02	0.03	0.02	0.00	0.01	0.02	0.01
Al Total	5.45	5.59	5.65	5.62	5.49	5.59	5.68	5.58
Al IV	1.78	1.90	1.95	1.89	1.85	1.90	1.94	1.87
Al VI	3.66	3.69	3.70	3.73	3.64	3.70	3.74	3.71
Fe	0.41	0.31	0.27	0.29	0.39	0.31	0.27	0.28
Mn	0.00	0.01	0.01	0.00	0.01	0.00	0.01	0.00
Mg	0.02	0.04	0.05	0.05	0.04	0.05	0.05	0.05
Ca	0.01	0.00	0.01	0.00	0.02	0.01	0.01	0.01
Na	0.15	0.26	0.31	0.24	0.26	0.26	0.27	0.26
K	1.73	1.75	1.75	1.71	1.75	1.74	1.68	1.75
Cr	0.00	0.01	0.00	0.00	0.00	0.00	0.00	0.01
Cl								
P								
Ba		0.00	0.00	0.00	0.00	0.00	0.00	0.00
F	0.05	0.34	0.29	0.39	0.39	0.35	0.33	0.34
OH	3.95	3.66	3.71	3.61	3.61	3.65	3.67	3.66
Tetrahedral	8.00	8.00	8.00	8.00	8.00	8.00	8.00	8.00
Octahedral	4.11	4.06	4.07	4.08	4.10	4.09	4.09	4.06
Dodecahedral	1.88	2.02	2.05	1.96	2.02	2.00	1.96	2.01

Sample	SC-3-W	SC-3-W	SC-3-W	SC-3-W	SC-3-W	SC-3-W	SC-3-W	SC-3-W
Point	7	5	4a	4b	4c	9	2	2b
Description	FF	IM	SA	SA	SA	RF	RF	RF
SiO2	47.32	47.18	47.26	47.21	47.46	47.24	47.12	47.21
TiO2	0.00	0.24	0.27	0.14	0.30	0.30	0.09	0.34
Al2O3	37.07	36.23	36.64	36.16	35.54	36.66	36.03	35.49
FeO	2.67	2.49	2.24	3.55	2.84	2.71	2.83	3.02
MnO	0.00	0.11	0.00	0.00	0.07	0.17	0.13	0.10
MgO	0.17	0.19	0.19	0.09	0.16	0.00	0.22	0.08
CaO	0.00	0.06	0.04	0.00	0.00	0.00	0.01	0.00
Na2O	0.68	0.64	0.80	0.60	0.64	0.63	0.84	0.69
K2O	9.71	8.71	8.78	9.47	9.27	9.46	9.56	9.29
Cr2O3	0.09	0.06	0.02	0.08	0.04	0.00	0.07	0.00
Cl	0.00	0.02	0.02	0.00	0.00	0.02	0.00	0.00
P2O5	0.00	0.00	0.03	0.07	0.00	0.06	0.00	0.00
BaO	0.16	0.00	0.01	0.00	0.17	0.00	0.08	0.00
F	0.00	0.00	0.10	0.00	0.03	0.00	0.02	0.00
Total	97.87	95.93	96.40	97.37	96.52	97.25	97.00	96.22
Si	6.11	6.10	6.16	6.23	6.13	6.08	6.25	6.09
Ti	0.01	0.00	0.02	0.00	0.03	0.00	0.01	0.04
Al Total	5.63	5.56	5.60	5.47	5.63	5.71	5.36	5.64
Al IV	1.89	1.90	1.84	1.77	1.87	1.92	1.75	1.91
Al VI	3.75	3.66	3.76	3.69	3.76	3.79	3.61	3.73
Fe	0.17	0.18	0.15	0.17	0.15	0.16	0.34	0.16
Mn	0.01	0.01	0.00	0.01	0.00	0.00	0.01	0.01
Mg	0.13	0.12	0.12	0.14	0.10	0.10	0.08	0.12
Ca	0.00	0.01	0.00	0.01	0.00	0.01	0.02	0.00
Na	0.21	0.47	0.23	0.18	0.20	0.17	0.20	0.24
K	1.78	1.82	1.69	1.86	1.74	1.83	1.80	1.74
Cr	0.00	0.00	0.00	0.01	0.01	0.00	0.00	0.00
Cl								
P								
Ba	0.00	0.01				0.00	0.01	0.00
F			0.05	0.04	0.08	0.04		0.03
OH	4.00	4.00	3.95	3.96	3.92	3.96	4.00	3.97
Tetrahedral	8.00	8.00	8.00	8.00	8.00	8.00	8.00	8.00
Octahedral	4.06	3.97	4.05	4.01	4.05	4.06	4.06	4.06
Dodecahedral	1.99	2.30	1.92	2.05	1.96	2.00	2.00	1.98

Sample	SC-3-W	SC-3-W	SC-3-W	SC-7-W	SC-7-W	SC-7-W	SC-7-W	SC-7-W
Point	2c	6	8	1	5	6	8	9
Description	RF	S	S	G	G	G	G	G
SiO2	47.06	46.66	46.96	46.78	48.20	47.52	47.69	35.40
TiO2	0.30	0.25	0.40	0.00	0.00	0.00	0.09	0.14
Al2O3	35.44	35.68	33.98	35.44	33.55	31.42	36.09	22.62
FeO	2.78	3.11	4.82	3.73	4.93	6.87	2.45	26.79
MnO	0.03	0.11	0.16	0.11	0.13	0.12	0.21	0.56
MgO	0.19	0.06	0.24	0.13	0.09	0.14	0.00	0.19
CaO	0.06	0.08	0.08	0.00	0.04	0.02	0.08	0.06
Na2O	0.40	0.71	0.54	0.65	0.22	0.35	0.34	0.35
K2O	9.82	9.40	9.09	9.10	9.66	9.60	9.49	9.39
Cr2O3	0.00	0.05	0.01	0.00	0.06	0.05	0.00	0.04
Cl	0.03	0.00	0.01	0.00	0.02	0.01	0.00	0.05
P2O5	0.02	0.00	0.00	0.02	0.00	0.08	0.20	0.11
BaO	0.00	0.00	0.00	0.16	0.13	0.00	0.00	0.00
F	0.00	0.00	0.07	1.17	1.17	1.78	0.53	2.98
Total	96.13	96.11	96.36	97.29	98.20	97.96	97.17	98.68
Si	6.12	6.22	6.15	6.13	6.16	6.46	7.59	6.22
Ti	0.00	0.00	0.02	0.02	0.03	0.02	0.01	0.00
Al Total	5.67	5.54	5.54	5.65	5.65	4.94	3.80	5.72
Al IV	1.88	1.78	1.85	1.87	1.84	1.54	0.41	1.78
Al VI	3.79	3.76	3.69	3.78	3.81	3.40	3.39	3.94
Fe	0.16	0.22	0.27	0.25	0.25	0.61	1.09	0.15
Mn	0.00	0.00	0.02	0.01	0.00	0.03	0.05	0.01
Mg	0.10	0.03	0.08	0.13	0.12	0.10	0.07	0.00
Ca	0.00	0.01	0.00	0.00	0.00	0.00	0.00	0.00
Na	0.18	0.09	0.19	0.21	0.19	0.03	0.09	0.07
K	1.81	1.88	1.78	1.50	1.51	1.73	1.89	1.75
Cr	0.00	0.00	0.00	0.01	0.00	0.00	0.00	0.01
Cl				0.02	0.00	0.00	0.02	0.01
P				0.02	0.01	0.00	0.01	0.00
Ba	0.00	0.00		0.01	0.00	0.00	0.00	0.01
F	0.04	0.10	0.19	0.18	0.22	0.00	2.23	0.18
OH	3.96	3.90	3.81	3.81	3.78	4.00	1.76	3.82
Tetrahedral	8.00	8.00	8.00	8.00	8.00	8.00	8.00	8.00
Octahedral	4.05	4.03	4.07	4.20	4.22	4.16	4.61	4.09
Dodecahedral	1.99	1.96	1.98	1.75	1.70	1.76	1.98	1.83

Sample	SC-7-W	SC-7-W	SC-7-W	SC-7-W	SC-7-W	SC-7-W	SC-7-W	SC-7-W
Point	10	6	7	8	1	2	4	7
Description	G	G	G	G	G	G	G	G
SiO2	47.57	45.50	45.44	45.57	46.24	45.20	45.96	45.96
TiO2	0.00	0.01	0.00	0.04	0.00	0.04	0.09	0.00
Al2O3	32.57	34.33	33.48	32.99	32.22	32.79	33.51	32.07
FeO	5.09	3.58	4.15	4.23	4.67	4.51	3.20	4.90
MnO	0.18	0.00	0.05	0.12	0.14	0.22	0.10	0.05
MgO	0.10	0.02	0.09	0.02	0.09	0.17	0.15	0.03
CaO	0.00	0.00	0.00	0.02	0.00	0.06	0.00	0.00
Na2O	0.31	0.95	0.67	0.61	0.63	0.52	0.96	0.50
K2O	8.48	10.17	10.49	10.47	10.61	10.92	10.13	10.74
Cr2O3	0.00	0.00	0.03	0.00	0.12	0.03	0.08	0.00
Cl	0.02	N/D	N/D	N/D	N/D	N/D	N/D	N/D
P2O5	0.08	N/D	N/D	N/D	N/D	N/D	N/D	N/D
BaO	0.03	0.11	0.08	0.00	0.14	0.00	0.00	0.20
F	1.69	N/D	N/D	N/D	N/D	N/D	N/D	N/D
Total	96.12	94.67	94.48	94.06	94.84	94.45	94.18	94.44
Si	6.46	6.25	6.09	6.31	6.21	6.52	6.35	6.16
Ti	0.00	0.02	0.04	0.01	0.05	0.04	0.00	0.01
Al Total	5.23	5.61	5.70	5.40	5.64	5.04	5.40	5.76
Al IV	1.54	1.75	1.91	1.69	1.79	1.48	1.65	1.84
Al VI	3.70	3.85	3.79	3.70	3.86	3.56	3.75	3.92
Fe	0.46	0.26	0.23	0.38	0.24	0.56	0.19	0.06
Mn	0.01	0.00	0.00	0.01	0.01	0.02	0.00	0.01
Mg	0.00	0.03	0.11	0.04	0.11	0.25	0.07	0.01
Ca	0.00	0.00	0.00	0.01	0.00	0.01	0.00	0.00
Na	0.07	0.22	0.14	0.07	0.12	0.04	0.04	0.04
K	1.69	1.58	1.63	1.72	1.59	1.57	1.81	1.86
Cr	0.00	0.01	0.00	0.00	0.00	0.00	0.00	0.00
Cl	0.00	0.00	0.01	0.02	0.00	0.00		
P	0.03	0.01	0.04	0.01	0.01	0.01		
Ba	0.01	0.00	0.00	0.00	0.00	0.00		
F	0.42	0.32	0.28	0.13	0.43	0.70	0.03	0.00
OH	3.58	3.68	3.71	3.86	3.57	3.30	3.97	4.00
Tetrahedral	8.00	8.00	8.00	8.00	8.00	8.00	8.00	8.00
Octahedral	4.18	4.17	4.17	4.13	4.27	4.43	4.02	4.00
Dodecahedral	1.79	1.82	1.81	1.81	1.71	1.63	1.85	1.90

Sample	SC-7-W	SC-7-W	SC-7-W	SC-7-W	SC-7-W	SC-7-W	SC-7-W	SC-7-W
Point	1	2	3	4	5	6	7	7
Description	G	G	G	G	G	G	G	G
SiO2	45.48	45.98	46.87	46.65	45.07	45.83	46.06	46.04
TiO2	0.07	0.00	0.00	0.00	0.00	0.02	0.04	0.00
Al2O3	33.95	34.01	33.51	33.51	33.32	33.50	34.39	33.40
FeO	4.59	4.82	4.70	4.46	4.73	4.37	3.36	4.48
MnO	0.16	0.05	0.05	0.00	0.17	0.05	0.07	0.07
MgO	0.13	0.16	0.23	0.11	0.12	0.13	0.21	0.04
CaO	0.03	0.00	0.13	0.04	0.00	0.07	0.09	0.05
Na2O	0.57	0.68	0.44	0.62	0.59	0.63	1.04	0.46
K2O	11.13	10.87	11.11	10.83	10.71	10.78	10.28	10.80
Cr2O3	0.00	0.00	0.00	0.06	0.00	0.00	0.05	0.04
Cl	N/D	N/D	N/D	N/D	N/D	N/D	N/D	N/D
P2O5	N/D	N/D	N/D	N/D	N/D	N/D	N/D	N/D
BaO	N/D	N/D	N/D	N/D	N/D	N/D	N/D	0.00
F	1.43	1.64	1.72	1.73	1.73	1.88	1.71	1.71
Total	97.53	98.21	98.75	98.01	96.43	97.25	97.30	97.10
Si	6.13	6.09	6.04	6.39	6.29	6.36	6.11	6.11
Ti	0.00	0.00	0.00	0.00	0.00	0.02	0.00	0.00
Al Total	5.62	5.74	5.83	5.32	5.55	5.01	5.67	5.76
Al IV	1.87	1.91	1.96	1.61	1.71	1.64	1.89	1.89
Al VI	3.75	3.84	3.86	3.71	3.85	3.37	3.78	3.87
Fe	0.17	0.15	0.12	0.16	0.09	0.52	0.16	0.12
Mn	0.01	0.00	0.00	0.00	0.01	0.01	0.01	0.01
Mg	0.12	0.05	0.06	0.15	0.05	0.19	0.09	0.01
Ca	0.00	0.00	0.00	0.00	0.01	0.00	0.00	0.00
Na	0.19	0.19	0.18	0.02	0.05	0.06	0.18	0.06
K	1.83	1.79	1.81	1.82	1.78	1.90	1.80	1.90
Cr	0.00	0.00	0.00	0.00	0.00	0.01	0.01	0.00
Cl								
P								
Ba			0.00				0.00	0.00
F	0.07	0.05	0.03	0.07	0.04	0.06	0.05	0.02
OH	3.93	3.95	3.97	3.93	3.96	3.94	3.95	3.98
Tetrahedral	8.00	8.00	8.00	8.00	8.00	8.00	8.00	8.00
Octahedral	4.05	4.04	4.05	4.03	4.01	4.12	4.04	4.02
Dodecahedral	2.03	1.98	2.00	1.84	1.84	1.96	2.00	1.97

Sample	SC-7-W	SC-7-W	SC-7-W	SC-7-W	SC-8-W	SC-8-W	SC-8-W	SC-8-W
Point	2	2b	3	4	11	6	9	10
Description	S	S	S	S	RB	RF	S	S
SiO2	48.84	47.51	45.47	47.34	47.24	47.65	47.27	48.13
TiO2	0.28	0.00	0.08	0.00	0.21	0.14	0.08	0.00
Al2O3	25.59	34.10	35.97	37.56	34.53	34.95	38.37	35.71
FeO	9.75	5.11	3.96	0.61	3.45	3.17	0.55	2.92
MnO	0.00	0.07	0.21	0.04	0.11	0.00	0.07	0.08
MgO	0.15	0.14	0.00	0.11	0.85	0.84	0.03	0.18
CaO	0.03	0.02	0.14	0.05	0.00	0.00	0.04	0.01
Na2O	0.16	0.39	0.64	0.19	0.59	0.72	0.22	0.22
K2O	9.52	9.85	9.14	9.95	9.54	8.94	10.36	10.12
Cr2O3	0.06	0.04	0.00	0.00	0.00	0.01	0.00	0.00
Cl	0.01	0.03	0.00	0.02	0.01	0.00	0.00	0.01
P2O5	0.00	0.00	0.08	0.00	0.00	0.06	0.00	0.00
BaO	0.00	0.10	0.00	0.15	0.11	0.00	0.00	0.10
F	3.46	1.56	1.00	0.00	1.87	1.68	0.14	0.78
Total	97.85	98.92	96.69	96.02	98.51	98.16	97.13	98.26
Si	6.33	6.17	6.13	6.12	6.22	6.09	6.18	6.34
Ti	0.00	0.03	0.01	0.00	0.02	0.00	0.00	0.01
Al Total	5.50	5.70	5.59	5.61	5.61	5.88	5.89	5.55
Al IV	1.67	1.83	1.87	1.88	1.78	1.91	1.82	1.66
Al VI	3.83	3.87	3.72	3.73	3.83	3.97	4.07	3.89
Fe	0.12	0.07	0.27	0.26	0.40	0.13	0.01	0.13
Mn	0.00	0.01	0.01	0.00	0.02	0.01	0.01	0.00
Mg	0.06	0.04	0.05	0.04	0.05	0.02	0.00	0.08
Ca	0.01	0.00	0.00	0.00	0.00	0.00	0.00	0.01
Na	0.06	0.05	0.22	0.20	0.15	0.17	0.04	0.03
K	1.71	1.79	1.81	1.80	1.56	1.61	1.59	1.43
Cr	0.01	0.00	0.00	0.01	0.00	0.00	0.01	0.01
Cl					0.01	0.01	0.01	0.02
P					0.00	0.02	0.00	0.03
Ba	0.00	0.00			0.01	0.00	0.00	0.00
F	0.03	0.04	0.08	0.09	0.43	0.19	0.08	0.13
OH	3.97	3.96	3.92	3.91	3.57	3.80	3.91	3.86
Tetrahedral	8.00	8.00	8.00	8.00	8.00	8.00	8.00	8.00
Octahedral	4.02	4.03	4.06	4.04	4.31	4.13	4.09	4.12
Dodecahedral	1.78	1.84	2.03	2.02	1.72	1.80	1.64	1.50

Sample	SC-8-W	SC-8-W	SC-8-W	SC-8-W	SC-9-W	SC-9-W	SC-9-W	SC-9-W
Point	15	1	3	4	3	4	7	7b
Description	S	S	S	S	G	G	G	G
SiO2	47.41	46.95	47.07	45.81	46.26	46.51	47.41	49.00
TiO2	0.02	0.49	0.30	0.25	0.35	0.41	0.02	0.07
Al2O3	38.99	29.21	28.63	27.93	33.45	31.56	36.13	32.17
FeO	0.21	7.83	8.65	9.80	5.01	6.45	2.14	5.15
MnO	0.00	0.10	0.04	0.30	0.10	0.13	0.00	0.16
MgO	0.07	0.78	0.63	0.62	0.29	0.41	0.24	0.24
CaO	0.00	0.00	0.01	0.02	0.01	0.01	0.08	0.03
Na2O	0.65	0.30	0.24	0.30	0.53	0.32	0.62	0.33
K2O	9.99	10.01	9.09	9.78	9.36	9.53	9.49	9.53
Cr2O3	0.04	0.05	0.06	0.00	0.00	0.01	0.10	0.00
Cl	0.01	0.00	0.01	0.00	0.00	0.00	0.02	0.00
P2O5	0.00	0.00	0.08	0.08	0.07	0.03	0.08	0.01
BaO	0.14	0.00	0.00	0.11	0.07	0.03	0.00	0.01
F	0.00	3.80	3.44	3.82	1.80	2.38	1.03	2.21
Total	97.53	99.52	98.25	98.82	97.30	97.78	97.36	98.91
Si	6.12	6.11	6.32	6.19	6.40	6.09	6.25	6.20
Ti	0.00	0.00	0.01	0.01	0.02	0.00	0.02	0.00
Al Total	5.93	5.90	5.23	5.52	5.00	5.92	5.64	5.70
Al IV	1.88	1.89	1.68	1.81	1.60	1.91	1.75	1.80
Al VI	4.06	4.01	3.55	3.71	3.40	4.01	3.89	3.90
Fe	0.11	0.09	0.28	0.23	0.81	0.06	0.33	0.16
Mn	0.00	0.00	0.01	0.00	0.03	0.01	0.00	0.00
Mg	0.00	0.03	0.21	0.09	0.13	0.00	0.05	0.01
Ca	0.00	0.00	0.00	0.01	0.01	0.01	0.01	0.00
Na	0.19	0.08	0.08	0.19	0.12	0.11	0.14	0.07
K	1.49	1.73	1.92	1.77	1.61	1.67	1.51	1.68
Cr	0.00	0.00	0.00	0.01	0.00	0.01	0.00	0.00
Cl	0.01	0.00			0.00	0.01	0.01	0.01
P	0.01	0.01			0.00	0.02	0.00	0.03
Ba	0.00	0.00			0.00	0.00	0.00	0.00
F	0.25	0.26	0.14	0.09	0.36	0.15	0.42	0.14
OH	3.74	3.74	3.86	3.91	3.64	3.84	3.58	3.86
Tetrahedral	8.00	8.00	8.00	8.00	8.00	8.00	8.00	8.00
Octahedral	4.17	4.13	4.06	4.05	4.39	4.08	4.30	4.07
Dodecahedral	1.69	1.83	2.00	1.97	1.73	1.80	1.65	1.78

Sample	SC-9-W	SC-9-W	SC-9-W	SC-9-W	SC-9-W	SC-13-W	SC-13-W	SC-13-W
Point	8	9	10	1	6	7	7	3
Description	G	G	G	S	S	P	P	RB
SiO2	47.30	47.55	47.41	46.54	47.50	45.70	45.76	45.61
TiO2	0.31	0.15	0.31	0.41	0.28	0.05	0.06	0.05
Al2O3	34.34	34.10	34.75	31.19	34.93	34.53	34.08	33.74
FeO	4.34	4.18	4.12	7.51	3.44	2.49	2.24	2.41
MnO	0.23	0.14	0.22	0.19	0.07	0.13	0.09	0.06
MgO	0.21	0.22	0.27	0.30	0.23	0.70	0.81	0.54
CaO	0.00	0.00	0.00	0.04	0.00	0.00	0.00	0.00
Na2O	0.52	0.59	0.67	0.52	0.69	0.94	0.80	0.82
K2O	9.36	9.48	9.34	9.36	9.34	10.06	10.26	10.12
Cr2O3	0.00	0.08	0.03	0.02	0.00	0.01	0.05	0.00
Cl	0.01	0.05	0.00	0.01	0.01	N/D	N/D	N/D
P2O5	0.06	0.00	0.01	0.03	0.00	N/D	N/D	N/D
BaO	0.00	0.06	0.04	0.00	0.11	0.01	0.24	0.11
F	1.54	1.62	1.86	3.01	1.48	0.57	N/D	N/D
Total	98.22	98.22	99.03	99.13	98.08	95.20	94.42	93.46
Si	6.08	6.11	6.18	6.18	6.17	6.09	6.15	6.16
Ti	0.01	0.00	0.02	0.00	0.02	0.03	0.01	0.01
Al Total	5.92	5.77	5.43	5.67	5.56	5.63	5.49	5.56
Al IV	1.92	1.89	1.82	1.82	1.83	1.91	1.85	1.84
Al VI	4.01	3.87	3.61	3.85	3.73	3.72	3.64	3.72
Fe	0.10	0.13	0.43	0.16	0.34	0.26	0.41	0.26
Mn	0.00	0.01	0.00	0.00	0.01	0.01	0.01	0.00
Mg	0.02	0.01	0.06	0.01	0.01	0.05	0.02	0.05
Ca	0.00	0.00	0.01	0.00	0.01	0.00	0.01	0.00
Na	0.10	0.09	0.23	0.10	0.18	0.29	0.26	0.28
K	1.64	1.89	1.73	1.84	1.59	1.72	1.74	1.74
Cr	0.00	0.00	0.00	0.00	0.01	0.00	0.00	0.00
Cl	0.00				0.00			
P	0.01				0.00			
Ba	0.00		0.00	0.00	0.00			
F	0.15	0.08	0.24	0.10	0.00	0.30	0.38	0.33
OH	3.85	3.92	3.76	3.90	4.00	3.70	3.62	3.67
Tetrahedral	8.00	8.00	8.00	8.00	8.00	8.00	8.00	8.00
Octahedral	4.14	4.02	4.12	4.02	4.13	4.07	4.10	4.04
Dodecahedral	1.74	1.98	1.96	1.94	1.77	2.01	2.00	2.02

Sample	SC-13-W	SC-13-W	SC-13-W	SC-13-W	SC-13-W	SC-13-W	SC-13-W
Point	4	5	6	1	5	6	1
Description	RB	RF	RF	RF	RF	RF	RF
SiO2	45.97	45.98	45.76	45.61	45.87	46.40	46.19
TiO2	0.30	0.44	0.07	0.33	0.07	0.25	0.06
Al2O3	34.27	34.37	34.48	34.25	34.75	34.27	34.29
FeO	2.26	2.30	2.57	2.46	2.21	2.52	2.24
MnO	0.06	0.06	0.07	0.12	0.09	0.07	0.13
MgO	0.50	0.65	0.62	0.70	0.72	0.76	0.63
CaO	0.00	0.04	0.04	0.00	0.00	0.00	0.02
Na2O	0.80	0.74	0.83	0.88	0.85	0.77	0.68
K2O	10.55	10.33	10.52	10.30	10.56	10.49	10.56
Cr2O3	0.00	0.01	0.05	0.00	0.08	0.15	0.03
Cl	N/D	N/D	N/D	N/D	N/D	N/D	N/D
P2O5	N/D	N/D	N/D	N/D	N/D	N/D	N/D
BaO	0.00	0.12	0.07	0.17	N/D	N/D	N/D
F	N/D	N/D	N/D	N/D	0.57	0.62	0.62
Total	94.71	95.03	95.06	94.82	95.78	96.30	95.45
Si	6.12	6.14	6.11	6.16	6.19	6.16	6.15
Ti	0.01	0.01	0.02	0.00	0.02	0.00	0.01
Al Total	5.58	5.48	5.56	5.48	5.48	5.49	5.55
Al IV	1.88	1.86	1.89	1.84	1.81	1.84	1.85
Al VI	3.70	3.62	3.68	3.64	3.67	3.65	3.70
Fe	0.35	0.44	0.25	0.42	0.30	0.36	0.33
Mn	0.00	0.03	0.00	0.00	0.01	0.01	0.00
Mg	0.03	0.03	0.12	0.03	0.05	0.06	0.02
Ca	0.01	0.00	0.00	0.00	0.01	0.00	0.00
Na	0.24	0.22	0.18	0.25	0.25	0.23	0.28
K	1.74	1.74	1.84	1.77	1.74	1.76	1.73
Cr	0.00	0.00	0.00	0.00	0.00	0.00	0.00
Cl							
P							
Ba	0.00	0.00	0.00	0.00	0.00	0.00	0.00
F	0.31	0.34					
OH	3.69	3.66	4.00	4.00	4.00	4.00	4.00
Tetrahedral	8.00	8.00	8.00	8.00	8.00	8.00	8.00
Octahedral	4.09	4.12	4.07	4.09	4.06	4.09	4.06
Dodecahedral	1.98	1.96	2.03	2.02	1.98	2.00	2.01

Sample	SC-13-W	SC-13-W	SC-13-W	SC-13-W	SC-13-W	SC-13-W	SC-13-W
Point	5	6	1	9	10	9	8
Description	RF	RF	RF	S	S	S	S
SiO2	46.04	46.99	46.14	46.75	46.16	48.17	46.46
TiO2	0.09	0.16	0.22	0.07	0.06	0.04	0.22
Al2O3	35.52	34.37	35.90	32.83	34.89	34.27	35.43
FeO	2.22	3.00	2.01	2.44	2.08	1.76	1.81
MnO	0.16	0.09	0.08	0.10	0.00	0.00	0.12
MgO	0.72	0.76	0.51	1.05	0.47	0.45	0.76
CaO	0.03	0.03	0.00	0.03	0.04	0.02	0.03
Na2O	0.85	0.78	0.80	0.30	0.74	1.23	0.66
K2O	10.44	10.36	10.66	11.16	10.35	10.14	10.66
Cr2O3	0.00	0.09	0.00	0.01	0.07	0.10	0.05
Cl	N/D	N/D	N/D	N/D	N/D	N/D	N/D
P2O5	N/D	N/D	N/D	N/D	N/D	N/D	N/D
BaO	0.01	0.00	0.00	N/D	N/D	0.13	0.00
F	0.51	0.55	0.54	0.63	0.44	0.17	0.63
Total	96.58	97.16	96.86	95.36	95.29	96.49	96.82
Si	7.52	7.06	7.15	7.28	6.08	6.08	6.04
Ti	0.01	0.01	0.01	0.01	0.03	0.03	0.03
Al Total	3.23	3.61	3.49	3.44	5.61	5.65	5.69
Al IV	0.48	0.94	0.85	0.72	1.92	1.92	1.96
Al VI	2.75	2.67	2.64	2.72	3.70	3.72	3.73
Fe	0.93	1.13	1.14	1.01	0.30	0.25	0.25
Mn	0.06	0.08	0.07	0.06	0.02	0.02	0.01
Mg	0.07	0.18	0.17	0.15	0.03	0.03	0.05
Ca	0.00	0.00	0.00	0.00	0.00	0.00	0.02
Na	0.06	0.07	0.10	0.05	0.26	0.27	0.25
K	2.01	2.01	2.01	2.02	1.74	1.74	1.74
Cr	0.00	0.00	0.00	0.01	0.00	0.00	0.00
Cl							
P							
Ba				0.00	0.00	0.00	0.01
F	1.57	1.49	1.52	1.58	0.30	0.32	0.25
OH	2.43	2.51	2.48	2.42	3.70	3.68	3.75
Tetrahedral	8.00	8.00	8.00	8.00	8.00	8.00	8.00
Octahedral	3.81	4.08	4.03	3.95	4.08	4.06	4.09
Dodecahedral	2.07	2.08	2.12	2.07	2.00	2.02	2.00

Sample	SC-13-W	SC-14-W	SC-14-W	SC-14-W	SC-14-W	SC-14-W	SC-14-W
Point	10	12	3	3b	6	6b	9
Description	S	P	RF	RF	RF	RF	RF
SiO2	46.41	47.10	51.53	46.35	47.89	47.33	46.86
TiO2	0.34	0.00	0.05	0.08	0.07	0.02	0.08
Al2O3	35.31	34.36	31.24	29.17	33.65	32.70	33.89
FeO	1.68	4.37	3.29	9.64	5.03	5.58	4.95
MnO	0.00	0.22	0.00	0.08	0.11	0.18	0.00
MgO	0.65	0.00	0.91	0.13	0.15	0.11	0.07
CaO	0.00	0.02	0.09	0.06	0.00	0.00	0.03
Na2O	0.54	0.40	0.07	0.31	0.53	0.37	0.48
K2O	11.22	9.05	9.22	9.82	9.03	9.20	9.39
Cr2O3	0.00	0.01	0.03	0.00	0.00	0.11	0.05
Cl	N/D	0.00	0.00	0.00	0.00	0.00	0.01
P2O5	N/D	0.00	0.00	0.00	0.09	0.00	0.03
BaO	0.05	0.09	0.08	0.08	0.00	0.12	0.03
F	0.42	1.09	0.00	1.76	1.32	1.16	1.01
Total	96.63	96.71	96.51	97.48	97.87	96.88	96.88
Si	6.08	6.13	6.15	6.14	6.13	6.12	6.17
Ti	0.03	0.01	0.03	0.03	0.01	0.00	0.00
Al Total	5.62	5.64	5.56	5.61	5.63	5.65	5.60
Al IV	1.92	1.87	1.85	1.86	1.87	1.88	1.83
Al VI	3.70	3.77	3.71	3.75	3.77	3.77	3.77
Fe	0.27	0.17	0.16	0.15	0.17	0.17	0.15
Mn	0.00	0.00	0.00	0.01	0.00	0.00	0.01
Mg	0.06	0.11	0.12	0.11	0.10	0.11	0.12
Ca	0.02	0.00	0.00	0.00	0.00	0.00	0.00
Na	0.27	0.16	0.19	0.15	0.14	0.20	0.15
K	1.75	1.81	1.82	1.80	1.86	1.79	1.84
Cr	0.00	0.00	0.00	0.00	0.00	0.01	0.00
Cl							
P							
Ba	0.00	0.00		0.01	0.00	0.00	0.00
F	0.34		0.04				
OH	3.66	4.00	3.96	4.00	4.00	4.00	4.00
Tetrahedral	8.00	8.00	8.00	8.00	8.00	8.00	8.00
Octahedral	4.07	4.06	4.03	4.05	4.04	4.05	4.04
Dodecahedral	2.02	1.97	2.01	1.95	2.00	1.99	1.99

Sample	SC-14-W	SC-14-W	SC-14-W	SC-14-W	SC-14-W	SC-14-W	SC-14-W
Point	10	13	15	16	11	17	18
Description	RF	RF	RF	RF	S	S	S
SiO2	46.42	46.85	49.77	49.01	46.63	47.43	47.73
TiO2	0.08	0.09	0.07	0.10	0.03	0.00	0.00
Al2O3	34.55	34.22	33.83	29.51	33.67	38.34	35.59
FeO	3.90	4.86	1.48	7.08	5.00	0.69	2.65
MnO	0.11	0.10	0.00	0.02	0.16	0.12	0.01
MgO	0.03	0.17	0.87	0.04	0.10	0.06	0.01
CaO	0.05	0.03	0.08	0.04	0.06	0.00	0.00
Na2O	0.52	0.54	0.07	0.27	0.38	0.46	0.13
K2O	8.66	9.49	8.78	9.73	9.78	9.63	9.78
Cr2O3	0.00	0.02	0.00	0.05	0.12	0.06	0.00
Cl	0.00	0.02	0.00	0.00	0.00	0.02	0.00
P2O5	0.05	0.07	0.12	0.00	0.02	0.07	0.00
BaO	0.00	0.06	0.06	0.00	0.06	0.28	0.00
F	0.84	1.07	0.00	1.53	0.99	0.00	0.00
Total	95.21	97.59	95.13	97.38	97.00	97.16	95.90
Si	6.11	6.14	6.13	6.11	6.18	6.17	6.01
Ti	0.00	0.00	0.00	0.00	0.00	0.00	0.00
Al Total	5.63	5.61	5.65	5.65	5.45	5.48	5.86
Al IV	1.89	1.86	1.87	1.89	1.82	1.83	1.99
Al VI	3.74	3.75	3.78	3.77	3.63	3.65	3.87
Fe	0.17	0.16	0.17	0.17	0.39	0.34	0.14
Mn	0.00	0.00	0.00	0.01	0.00	0.02	0.01
Mg	0.13	0.13	0.10	0.12	0.06	0.07	0.03
Ca	0.00	0.01	0.00	0.00	0.00	0.00	0.00
Na	0.20	0.19	0.19	0.19	0.24	0.23	0.19
K	1.81	1.79	1.78	1.80	1.78	1.76	1.84
Cr	0.01	0.00	0.00	0.00	0.00	0.00	0.00
Cl							
P							
Ba				0.00		0.00	0.00
F	0.06	0.06	0.04	0.06	0.10		0.01
OH	3.94	3.94	3.96	3.94	3.90	4.00	3.99
Tetrahedral	8.00	8.00	8.00	8.00	8.00	8.00	8.00
Octahedral	4.05	4.06	4.06	4.06	4.09	4.09	4.04
Dodecahedral	2.02	1.98	1.97	1.99	2.02	1.99	2.03

Sample	SC-14-W	SC-14-W	SC-15-W	SC-15-W	SC-15-W	SC-15-W	SC-15-W
Point	1	14	5	3	10	8a	8b
Description	S	S	FF	SA	SA	SA	SA
SiO2	50.40	48.84	47.02	47.14	46.98	46.28	46.31
TiO2	0.12	0.00	0.00	0.15	0.02	0.00	0.12
Al2O3	34.09	31.40	33.09	33.67	33.60	35.53	34.34
FeO	1.60	5.02	5.42	4.85	5.06	3.65	4.92
MnO	0.03	0.00	0.06	0.14	0.00	0.18	0.19
MgO	0.85	0.11	0.11	0.01	0.09	0.04	0.01
CaO	0.02	0.08	0.02	0.00	0.02	0.00	0.04
Na2O	0.05	0.17	0.36	0.53	0.27	0.71	0.24
K2O	9.34	9.84	9.44	8.95	9.43	8.99	9.28
Cr2O3	0.05	0.00	0.00	0.00	0.09	0.00	0.00
Cl	0.01	0.00	0.02	0.01	0.00	0.00	0.00
P2O5	0.12	0.00	0.04	0.05	0.08	0.17	0.03
BaO	0.00	0.02	0.06	0.00	0.09	0.15	0.00
F	0.00	1.19	0.43	1.34	0.94	1.02	0.64
Total	96.68	96.67	96.07	96.84	96.67	96.72	96.12
Si	6.15	6.10	6.21	6.14	6.38	6.16	6.19
Ti	0.02	0.04	0.01	0.04	0.00	0.02	0.00
Al Total	5.58	5.62	5.48	5.51	5.33	5.62	5.45
Al IV	1.85	1.90	1.79	1.86	1.62	1.84	1.81
Al VI	3.73	3.72	3.69	3.65	3.70	3.78	3.64
Fe	0.24	0.16	0.19	0.19	0.19	0.17	0.29
Mn	0.00	0.01	0.01	0.00	0.00	0.00	0.00
Mg	0.06	0.12	0.15	0.15	0.11	0.12	0.14
Ca	0.00	0.00	0.00	0.02	0.00	0.00	0.00
Na	0.20	0.21	0.21	0.22	0.04	0.19	0.20
K	1.79	1.78	1.76	1.78	1.87	1.65	1.79
Cr	0.00	0.00	0.00	0.02	0.01	0.01	0.01
Cl							
P							
Ba		0.00	0.00	0.01			0.01
F	0.15	0.08			0.03	0.04	
OH	3.85	3.92	4.00	4.00	3.97	3.96	4.00
Tetrahedral	8.00	8.00	8.00	8.00	8.00	8.00	8.00
Octahedral	4.05	4.06	4.06	4.04	4.00	4.08	4.08
Dodecahedral	1.99	1.99	1.97	2.02	1.91	1.85	2.00

Sample	SC-15-W	SC-15-W	SC-15-W	SC-15-W	SC-15-W	SC-2a-T	SC-2a-T	SC-2a-T
Point	8c	12	1	6	9	7	8	1
Description	SA	RF	S	S	S	G	G	G
SiO2	47.44	46.64	47.64	46.80	49.00	47.98	47.36	47.50
TiO2	0.13	0.12	0.00	0.12	0.02	0.11	0.07	0.16
Al2O3	34.97	34.46	37.16	29.11	32.61	32.77	31.94	28.79
FeO	3.49	4.27	1.46	8.30	4.50	3.70	3.99	6.13
MnO	0.08	0.13	0.07	0.03	0.10	0.30	0.09	0.36
MgO	0.15	0.12	0.00	0.19	0.21	0.06	0.27	0.40
CaO	0.02	0.03	0.00	0.00	0.00	0.00	0.05	0.11
Na2O	0.40	0.56	0.31	0.30	0.11	0.38	0.45	0.41
K2O	8.36	9.53	10.20	8.83	10.00	11.00	11.10	10.68
Cr2O3	0.00	0.07	0.00	0.00	0.00	0.00	0.09	0.02
Cl	0.00	0.03	0.00	0.07	0.00	N/D	N/D	N/D
P2O5	0.14	0.07	0.03	0.10	0.03	N/D	N/D	N/D
BaO	0.00	0.00	0.16	0.00	0.07	N/D	N/D	N/D
F	0.00	0.53	0.04	1.51	0.77	0.50	0.68	0.76
Total	95.18	96.56	97.07	95.36	97.42	96.80	96.08	95.32
Si	6.15	6.15	6.10	6.12	6.05	6.16	6.16	6.31
Ti	0.00	0.00	0.01	0.00	0.02	0.02	0.02	0.00
Al Total	5.59	5.67	5.67	5.72	5.79	5.58	5.64	5.43
Al IV	1.85	1.85	1.90	1.88	1.95	1.84	1.84	1.69
Al VI	3.74	3.82	3.77	3.84	3.85	3.74	3.80	3.74
Fe	0.22	0.15	0.19	0.15	0.13	0.28	0.25	0.49
Mn	0.00	0.00	0.00	0.00	0.01	0.01	0.01	0.02
Mg	0.07	0.03	0.05	0.02	0.04	0.04	0.04	0.00
Ca	0.00	0.00	0.00	0.00	0.00	0.00	0.00	0.00
Na	0.19	0.20	0.24	0.12	0.19	0.23	0.20	0.10
K	1.79	1.76	1.78	1.88	1.80	1.61	1.61	1.55
Cr	0.01	0.01	0.01	0.00	0.00	0.01	0.01	0.00
Cl						0.00	0.01	0.00
P						0.00	0.01	0.00
Ba	0.00	0.02	0.00		0.00	0.00	0.00	0.00
F				0.00	0.00	0.00	0.16	0.23
OH	4.00	4.00	4.00	4.00	4.00	4.00	3.83	3.77
Tetrahedral	8.00	8.00	8.00	8.00	8.00	8.00	8.00	8.00
Octahedral	4.05	4.02	4.03	4.01	4.04	4.09	4.13	4.26
Dodecahedral	1.99	1.99	2.03	2.00	1.99	1.85	1.84	1.66

Sample	SC-2a-T	SC-2a-T	SC-2a-T	SC-2a-T	SC-2a-T	SC-2a-T	SC-2a-T	SC-2a-T
Point	2	1	5	1	2	3	4	5
Description	G	G	G	G	G	G	G	G
SiO2	47.14	47.97	48.44	47.44	46.91	47.00	47.90	46.93
TiO2	0.19	0.08	0.12	0.07	0.10	0.05	0.03	0.05
Al2O3	30.89	20.78	24.63	33.01	32.84	32.23	31.65	33.80
FeO	5.45	11.32	9.47	3.96	4.17	4.45	4.89	3.73
MnO	0.31	0.67	0.48	0.20	0.01	0.07	0.13	0.14
MgO	0.40	0.47	0.45	0.32	0.18	0.33	0.35	0.20
CaO	0.04	0.04	0.04	0.02	0.09	0.01	0.01	0.03
Na2O	0.43	0.38	0.29	0.33	0.39	0.35	0.39	0.28
K2O	11.07	10.44	10.31	9.44	9.50	9.67	9.53	9.23
Cr2O3	0.01	0.00	0.00	0.13	0.17	0.12	0.00	0.00
Cl	N/D	N/D	N/D	0.00	0.00	0.00	0.00	0.03
P2O5	N/D	N/D	N/D	0.06	0.02	0.03	0.11	0.00
BaO	N/D	0.00	0.01	0.00	0.11	0.07	0.00	0.00
F	1.06	4.21	1.63	1.69	0.94	1.12	0.73	0.17
Total	96.98	96.38	95.87	96.67	95.43	95.50	95.72	94.59
Si	6.17	6.15	6.14	6.14	6.28	6.32	6.28	6.30
Ti	0.02	0.02	0.01	0.01	0.02	0.01	0.01	0.02
Al Total	5.54	5.57	5.57	5.58	5.49	5.47	5.58	5.61
Al IV	1.83	1.85	1.86	1.86	1.72	1.68	1.72	1.70
Al VI	3.72	3.71	3.71	3.72	3.78	3.79	3.87	3.91
Fe	0.19	0.21	0.21	0.20	0.35	0.52	0.37	0.36
Mn	0.01	0.01	0.01	0.01	0.01	0.01	0.00	0.00
Mg	0.12	0.09	0.12	0.13	0.09	0.07	0.09	0.06
Ca	0.01	0.01	0.00	0.00	0.00	0.00	0.00	0.00
Na	0.19	0.18	0.18	0.19	0.20	0.16	0.19	0.17
K	1.78	1.81	1.81	1.81	1.64	1.40	1.45	1.41
Cr	0.00	0.00	0.00	0.00	0.01	0.00	0.00	0.00
Cl					0.00	0.00	0.00	0.01
P					0.00	0.01	0.00	0.00
Ba	0.00	0.00			0.00	0.00	0.00	0.00
F			0.12	0.17	0.47	0.58	0.53	0.53
OH	4.00	4.00	3.88	3.83	3.53	3.42	3.47	3.46
Tetrahedral	8.00	8.00	8.00	8.00	8.00	8.00	8.00	8.00
Octahedral	4.05	4.05	4.06	4.06	4.25	4.41	4.34	4.36
Dodecahedral	1.97	2.00	2.00	2.00	1.84	1.58	1.65	1.58

Sample	SC-2a-T	SC-2a-T	SC-2a-T	SC-2a-T	SC-2a-T	SC-2a-T	SC-2a-T	SC-2a-T
Point	6	7	8	9	9b	10	11	12
Description	G	G	G	G	G	G	G	G
SiO2	47.39	47.15	47.59	47.21	47.02	47.59	48.00	46.29
TiO2	0.08	0.12	0.10	0.20	0.02	0.17	0.15	0.17
Al2O3	32.91	33.49	33.11	32.15	34.49	33.03	35.13	33.90
FeO	4.37	3.79	3.29	4.23	3.04	3.94	1.97	3.08
MnO	0.20	0.21	0.13	0.16	0.06	0.19	0.09	0.08
MgO	0.27	0.24	0.30	0.32	0.20	0.36	0.14	0.15
CaO	0.00	0.02	0.05	0.01	0.02	0.08	0.01	0.08
Na2O	0.25	0.30	0.27	0.27	0.34	0.32	0.14	0.26
K2O	9.36	9.43	8.87	9.56	8.53	9.24	9.56	9.14
Cr2O3	0.10	0.00	0.06	0.04	0.00	0.00	0.00	0.03
Cl	0.02	0.00	0.04	0.00	0.09	0.03	0.00	0.00
P2O5	0.01	0.09	0.05	0.00	0.00	0.02	0.07	0.00
BaO	0.03	0.13	0.04	0.00	0.04	0.00	0.00	0.00
F	0.29	0.86	0.68	0.51	0.80	0.39	0.00	0.29
Total	95.28	95.83	94.58	94.66	94.65	95.36	95.26	93.47
Si	6.29	6.19	6.18	6.24	6.22	6.15	6.15	6.14
Ti	0.02	0.01	0.01	0.02	0.02	0.01	0.01	0.01
Al Total	5.52	5.36	5.42	5.03	5.35	5.50	5.53	5.54
Al IV	1.71	1.81	1.82	1.76	1.78	1.85	1.85	1.86
Al VI	3.81	3.55	3.60	3.27	3.56	3.64	3.68	3.68
Fe	0.42	0.42	0.38	0.87	0.43	0.37	0.22	0.22
Mn	0.03	0.01	0.00	0.02	0.00	0.01	0.01	0.01
Mg	0.05	0.09	0.08	0.05	0.07	0.07	0.15	0.15
Ca	0.00	0.01	0.00	0.00	0.00	0.01	0.00	0.01
Na	0.20	0.27	0.27	0.15	0.20	0.23	0.21	0.24
K	1.58	1.79	1.75	1.83	1.80	1.73	1.78	1.75
Cr	0.00	0.00	0.01	0.00	0.01	0.00	0.00	0.00
Cl	0.00							
P	0.00							
Ba	0.00			0.00	0.00	0.00		0.00
F	0.57	0.27	0.34	0.39	0.26	0.25	0.11	0.13
OH	3.43	3.73	3.66	3.61	3.74	3.75	3.89	3.87
Tetrahedral	8.00	8.00	8.00	8.00	8.00	8.00	8.00	8.00
Octahedral	4.33	4.09	4.07	4.23	4.08	4.11	4.08	4.08
Dodecahedral	1.78	2.06	2.03	1.98	2.01	1.96	1.99	2.00

Sample	SC-2a-T	SC-2a-T	SC-2a-T	SC-2a-T	SC-2a-T	SC-2a-T	SC-2a-T	SC-2a-T
Point	12b	12c	13	14	15	16	17	18
Description	G	G	G	G	G	G	G	G
SiO2	47.83	46.07	47.97	48.22	47.09	47.10	47.28	45.72
TiO2	0.23	0.03	0.25	0.07	0.15	0.17	0.09	0.16
Al2O3	32.59	34.94	23.49	20.74	33.87	32.08	33.83	31.97
FeO	3.67	2.58	10.91	12.23	3.74	4.15	3.80	3.63
MnO	0.11	0.18	0.75	0.84	0.05	0.21	0.13	0.14
MgO	0.18	0.19	0.71	0.55	0.33	0.34	0.32	0.28
CaO	0.00	0.00	0.00	0.00	0.00	0.00	0.00	0.00
Na2O	0.20	0.24	0.33	0.37	0.35	0.24	0.30	0.28
K2O	8.87	9.36	9.11	9.14	9.56	9.30	9.54	10.11
Cr2O3	0.00	0.00	0.00	0.00	0.14	0.00	0.00	0.00
Cl	0.03	0.01	0.05	0.01	0.00	0.02	0.01	0.05
P2O5	0.00	0.00	0.00	0.12	0.01	0.00	0.03	0.05
BaO	0.00	0.27	0.00	0.00	0.02	0.00	0.02	0.08
F	0.42	0.37	3.64	5.08	2.06	0.58	0.45	0.69
Total	94.13	94.24	97.21	97.37	97.37	94.19	95.80	93.16
Si	6.31	6.25	6.26	6.31	6.18	6.49	6.43	6.41
Ti	0.06	0.01	0.04	0.05	0.00	0.01	0.05	0.02
Al Total	4.74	5.38	4.76	4.81	5.58	4.97	5.02	5.13
Al IV	1.69	1.75	1.74	1.69	1.82	1.51	1.57	1.59
Al VI	3.04	3.63	3.02	3.11	3.76	3.46	3.45	3.53
Fe	1.03	0.35	1.16	0.98	0.32	0.80	0.88	0.66
Mn	0.03	0.01	0.03	0.02	0.01	0.04	0.03	0.02
Mg	0.07	0.06	0.05	0.07	0.18	0.06	0.05	0.06
Ca	0.00	0.00	0.00	0.01	0.00	0.00	0.00	0.01
Na	0.13	0.23	0.18	0.09	0.18	0.09	0.08	0.10
K	1.94	1.76	1.87	1.87	1.54	1.78	1.75	1.75
Cr	0.00	0.00	0.00	0.01	0.00	0.00	0.00	0.00
Cl					0.00	0.00	0.03	0.01
P					0.01	0.01	0.00	0.01
Ba	0.00	0.00		0.00	0.00	0.00	0.00	0.00
F			0.72	0.57	0.27	0.66	0.73	0.48
OH	4.00	4.00	3.28	3.43	3.73	3.34	3.26	3.52
Tetrahedral	8.00	8.00	8.00	8.00	8.00	8.00	8.00	8.00
Octahedral	4.23	4.06	4.30	4.24	4.27	4.37	4.46	4.29
Dodecahedral	2.07	1.99	2.05	1.97	1.74	1.89	1.83	1.86

Sample	SC-2a-T	SC-2a-T	SC-2a-T	SC-2a-T	SC-2a-T	SC-2a-T	SC-2a-T	SC-2a-T
Point	18b	18c	19	20	21	22	23	26
Description	G	G	G	G	G	G	G	G
SiO2	46.85	47.08	47.17	47.58	46.90	47.69	48.81	47.29
TiO2	0.00	0.22	0.03	0.21	0.20	0.16	0.30	0.18
Al2O3	34.84	32.51	31.86	33.88	33.83	34.02	26.30	31.76
FeO	2.11	4.81	3.69	3.44	3.33	3.44	7.42	4.67
MnO	0.22	0.18	0.11	0.16	0.13	0.18	0.45	0.39
MgO	0.09	0.30	0.35	0.22	0.21	0.21	0.48	0.24
CaO	0.00	0.00	0.06	0.00	0.01	0.03	0.00	0.03
Na2O	0.19	0.26	0.40	0.34	0.34	0.28	0.21	0.32
K2O	9.35	9.29	8.46	9.06	8.68	9.55	8.69	8.78
Cr2O3	0.01	0.00	0.04	0.03	0.01	0.04	0.00	0.00
Cl	0.01	0.00	0.06	0.02	0.00	0.00	0.03	0.02
P2O5	0.03	0.00	0.14	0.00	0.06	0.00	0.00	0.00
BaO	0.00	0.19	0.22	0.00	0.00	0.00	0.00	0.00
F	0.20	0.58	0.73	0.35	0.66	0.63	1.72	1.17
Total	93.90	95.42	93.32	95.29	94.36	96.23	94.41	94.85
Si	6.27	6.27	6.23	6.16	6.16	6.25	6.27	6.18
Ti	0.03	0.01	0.02	0.01	0.01	0.00	0.02	0.01
Al Total	5.55	5.53	5.60	5.81	5.73	5.62	5.52	5.42
Al IV	1.73	1.73	1.77	1.84	1.84	1.75	1.73	1.82
Al VI	3.82	3.80	3.83	3.97	3.89	3.88	3.80	3.60
Fe	0.28	0.43	0.31	0.19	0.28	0.38	0.40	0.38
Mn	0.01	0.01	0.02	0.00	0.00	0.01	0.02	0.01
Mg	0.13	0.07	0.05	0.02	0.02	0.06	0.09	0.07
Ca	0.00	0.00	0.00	0.01	0.01	0.01	0.01	0.00
Na	0.12	0.18	0.15	0.19	0.18	0.12	0.15	0.27
K	1.59	1.54	1.60	1.57	1.55	1.58	1.48	1.75
Cr	0.01	0.00	0.00	0.00	0.00	0.00	0.01	0.00
Cl	0.00	0.00	0.04	0.00	0.00	0.00	0.00	
P	0.00	0.00	0.01	0.00	0.00	0.00	0.01	
Ba	0.00	0.00	0.00	0.00	0.01	0.00	0.01	
F	0.46	0.49	0.37	0.29	0.24	0.55	0.48	0.25
OH	3.54	3.51	3.61	3.71	3.76	3.45	3.52	3.75
Tetrahedral	8.00	8.00	8.00	8.00	8.00	8.00	8.00	8.00
Octahedral	4.29	4.33	4.24	4.19	4.21	4.34	4.33	4.08
Dodecahedral	1.72	1.73	1.76	1.75	1.75	1.71	1.65	2.02

Sample	SC-2a-T	SC-2a-T	SC-2a-T	SC-2a-T	SC-2a-T	SC-2a-T	SC-2a-T	SC-2a-T
Point	27	28	29	30	31	33	34	34b
Description	G	G	G	G	G	G	G	G
SiO2	47.10	47.86	48.06	46.69	47.27	46.81	47.67	46.99
TiO2	0.22	0.02	0.20	0.00	0.24	0.14	0.12	0.00
Al2O3	32.73	34.49	32.67	34.69	31.80	33.67	34.43	32.53
FeO	3.96	2.22	4.80	2.52	4.82	3.27	2.11	4.18
MnO	0.25	0.15	0.10	0.15	0.23	0.14	0.14	0.17
MgO	0.12	0.32	0.36	0.18	0.27	0.22	0.08	0.21
CaO	0.00	0.05	0.06	0.00	0.07	0.00	0.00	0.00
Na2O	0.23	0.26	0.26	0.25	0.22	0.33	0.16	0.30
K2O	9.59	9.46	8.62	9.21	8.99	9.10	9.09	9.42
Cr2O3	0.00	0.06	0.01	0.10	0.00	0.04	0.00	0.05
Cl	0.01	0.02	0.03	0.06	0.03	0.00	0.02	0.01
P2O5	0.00	0.00	0.10	0.02	0.00	0.01	0.00	0.07
BaO	0.12	0.04	0.02	0.14	0.00	0.00	0.11	0.00
F	0.60	1.27	0.89	0.29	0.89	0.86	0.21	1.04
Total	94.93	96.22	96.18	94.30	94.83	94.59	94.14	94.97
Si	6.17	6.15	6.14	6.29	6.48	6.47	6.21	6.14
Ti	0.06	0.04	0.04	0.02	0.04	0.03	0.01	0.00
Al Total	5.46	5.48	5.54	5.46	4.91	4.98	5.59	5.52
Al IV	1.83	1.85	1.86	1.71	1.52	1.53	1.79	1.86
Al VI	3.63	3.63	3.68	3.75	3.39	3.45	3.80	3.66
Fe	0.18	0.19	0.18	0.33	0.93	0.82	0.35	0.37
Mn	0.00	0.00	0.00	0.00	0.04	0.01	0.01	0.01
Mg	0.17	0.17	0.14	0.06	0.05	0.06	0.00	0.04
Ca	0.00	0.00	0.01	0.00	0.00	0.00	0.00	0.00
Na	0.15	0.16	0.15	0.22	0.10	0.06	0.18	0.27
K	1.85	1.88	1.84	1.66	1.78	1.77	1.69	1.76
Cr	0.00	0.01	0.00	0.00	0.00	0.01	0.00	0.00
Cl				0.00	0.00	0.00	0.00	
P				0.00	0.01	0.01	0.00	
Ba	0.01	0.01	0.00	0.00	0.00	0.00	0.00	0.00
F	0.03	0.06	0.03	0.26	0.78	0.61	0.27	0.35
OH	3.97	3.94	3.97	3.74	3.22	3.39	3.73	3.65
Tetrahedral	8.00	8.00	8.00	8.00	8.00	8.00	8.00	8.00
Octahedral	4.04	4.04	4.05	4.15	4.45	4.37	4.18	4.08
Dodecahedral	2.01	2.05	2.00	1.87	1.89	1.84	1.87	2.03

Sample	SC-2a-T	SC-2a-T	SC-2a-T	SC-2a-T	SC-2a-T	SC-2a-T	SC-2a-T	SC-2a-T
Point	34c	35	38	40	42	44	45	46
Description	G	G	G	G	G	G	G	G
SiO2	47.36	46.25	46.42	47.11	47.14	47.12	47.27	47.06
TiO2	0.13	0.25	0.08	0.12	0.21	0.05	0.00	0.24
Al2O3	31.57	32.92	32.54	32.67	31.41	33.64	33.33	31.70
FeO	5.25	3.72	4.34	4.26	5.50	3.08	4.05	5.41
MnO	0.31	0.22	0.11	0.11	0.26	0.17	0.24	0.31
MgO	0.31	0.21	0.20	0.22	0.33	0.17	0.17	0.31
CaO	0.04	0.00	0.07	0.00	0.01	0.00	0.06	0.00
Na2O	0.26	0.18	0.20	0.36	0.25	0.40	0.28	0.33
K2O	9.35	9.38	8.72	9.37	9.35	9.19	9.70	9.34
Cr2O3	0.00	0.00	0.00	0.06	0.00	0.00	0.01	0.00
Cl	0.02	0.00	0.04	0.01	0.01	0.00	0.00	0.00
P2O5	0.04	0.00	0.06	0.15	0.00	0.02	0.00	0.06
BaO	0.05	0.00	0.00	0.09	0.00	0.04	0.14	0.04
F	0.76	1.76	1.95	0.52	1.18	1.29	0.61	0.87
Total	95.45	94.89	94.73	95.05	95.65	95.17	95.86	95.67
Si	6.12	6.17	6.09	6.14	6.14	6.09	6.13	6.18
Ti	0.00	0.01	0.02	0.01	0.02	0.03	0.03	0.01
Al Total	5.60	5.51	5.64	5.58	5.55	5.68	5.53	5.44
Al IV	1.88	1.83	1.91	1.86	1.86	1.91	1.87	1.82
Al VI	3.72	3.68	3.73	3.72	3.69	3.77	3.66	3.62
Fe	0.31	0.34	0.26	0.28	0.29	0.16	0.34	0.38
Mn	0.02	0.01	0.01	0.00	0.01	0.00	0.02	0.01
Mg	0.02	0.05	0.05	0.04	0.06	0.10	0.04	0.06
Ca	0.01	0.00	0.00	0.01	0.00	0.00	0.01	0.00
Na	0.26	0.20	0.25	0.23	0.22	0.19	0.25	0.22
K	1.75	1.73	1.74	1.74	1.77	1.76	1.75	1.78
Cr	0.00	0.01	0.00	0.00	0.00	0.00	0.00	0.00
Cl								
P								
Ba	0.00	0.00	0.00	0.01	0.00	0.00	0.00	0.00
F	0.24	0.33	0.34	0.21	0.00			
OH	3.76	3.67	3.66	3.79	4.00	4.00	4.00	4.00
Tetrahedral	8.00	8.00	8.00	8.00	8.00	8.00	8.00	8.00
Octahedral	4.07	4.09	4.07	4.07	4.07	4.06	4.08	4.09
Dodecahedral	2.01	1.93	1.99	1.99	1.99	1.96	2.00	2.00

Sample	SC-2a-T	SC-4-T	SC-4-T	SC-4-T	SC-4-T	SC-4-T	SC-4-T	SC-4-T	SC-4-T
Point	48	3	3	6	6	6	10	9	10
Description	G	P	P	RF	RF	RF	S	S	S
SiO2	47.40	45.89	46.36	45.57	45.80	45.73	45.52	46.38	48.01
TiO2	0.24	0.11	0.13	0.16	0.05	0.17	0.30	0.07	0.32
Al2O3	20.60	35.02	35.45	30.21	32.17	31.27	32.05	33.32	32.37
FeO	12.18	2.00	2.00	6.19	3.91	5.57	3.02	3.13	2.89
MnO	0.74	0.06	0.08	0.31	0.07	0.12	0.14	0.02	0.06
MgO	0.50	0.76	0.76	0.25	1.07	1.30	1.00	0.44	0.94
CaO	0.00	0.00	0.04	0.00	0.01	0.00	0.17	0.03	0.09
Na2O	0.44	0.82	0.95	0.51	0.39	0.39	0.55	0.46	1.13
K2O	9.17	10.39	10.36	10.49	10.98	10.96	10.39	10.52	10.25
Cr2O3	0.00	0.00	0.00	0.00	0.00	0.00	0.05	0.06	0.06
Cl	0.00	N/D	N/D	N/D	N/D	N/D	N/D	N/D	N/D
P2O5	0.00	N/D	N/D	N/D	N/D	N/D	N/D	N/D	N/D
BaO	0.00	N/D	0.02	0.00	N/D	0.00	N/D	N/D	0.00
F	4.65	0.53	0.60	N/D	0.92	0.82	0.67	0.29	0.58
Total	95.92	95.58	96.76	93.69	95.36	96.32	93.85	94.71	96.70
Si	6.12	6.17	6.10	6.13	6.16	6.12	6.11	6.18	6.14
Ti	0.01	0.01	0.00	0.01	0.02	0.03	0.03	0.03	0.02
Al Total	5.73	5.46	5.71	5.54	5.59	5.63	5.62	5.54	5.62
Al IV	1.88	1.83	1.90	1.87	1.84	1.88	1.89	1.82	1.86
Al VI	3.85	3.64	3.81	3.67	3.75	3.74	3.73	3.71	3.77
Fe	0.22	0.23	0.16	0.23	0.16	0.15	0.15	0.16	0.14
Mn	0.00	0.01	0.01	0.01	0.00	0.00	0.00	0.00	0.00
Mg	0.06	0.17	0.07	0.17	0.09	0.13	0.12	0.13	0.10
Ca	0.00	0.01	0.00	0.00	0.00	0.01	0.00	0.00	0.00
Na	0.14	0.23	0.16	0.23	0.12	0.19	0.20	0.12	0.15
K	1.60	1.81	1.82	1.79	1.87	1.80	1.80	1.86	1.82
Cr	0.00	0.01	0.00	0.00	0.00	0.00	0.00	0.00	0.00
Cl									
P									
Ba	0.00		0.00	0.00				0.00	0.01
F	0.08	0.10	0.07	0.11	0.06	0.04	0.04	0.05	
OH	3.92	3.90	3.93	3.89	3.94	3.96	3.96	3.95	4.00
Tetrahedral	8.00	8.00	8.00	8.00	8.00	8.00	8.00	8.00	8.00
Octahedral	4.13	4.06	4.06	4.08	4.03	4.05	4.04	4.03	4.04
Dodecahedral	1.74	2.04	1.98	2.02	1.99	1.99	2.01	1.99	1.98

Sample	SC-7-T	SC-7-T	SC-7-T	SC-7-T	SC-7-T	SC-7-T	SC-7-T	SC-7-T	SC-7-T
Point	4	16	16b	17	17b	17b2	17c	27	10
Description	P	RB	RB	RB	RB	RB	RB	RB	RC
SiO2	44.71	46.47	46.45	46.56	46.48	46.03	46.65	46.28	46.86
TiO2	0.00	0.14	0.16	0.31	0.56	0.40	0.30	0.00	0.00
Al2O3	34.26	34.98	35.50	36.26	35.16	34.80	34.92	34.90	34.83
FeO	2.77	2.87	2.39	1.99	2.33	2.02	2.22	2.01	2.16
MnO	0.08	0.04	0.12	0.08	0.02	0.03	0.00	0.01	0.00
MgO	0.85	0.84	0.78	0.72	0.70	0.73	0.78	0.71	1.23
CaO	0.01	0.08	0.01	0.01	0.03	0.00	0.00	0.00	0.01
Na2O	0.69	0.25	0.58	0.58	0.37	0.69	0.56	0.27	0.33
K2O	8.71	9.26	8.80	8.84	9.03	8.58	8.79	9.29	9.82
Cr2O3	0.00	0.05	0.00	0.04	0.02	0.00	0.01	0.00	0.03
Cl	0.00	0.00	0.00	0.00	0.01	0.01	0.06	0.00	0.00
P2O5	0.11	0.07	0.02	0.07	0.20	0.18	0.16	0.09	0.13
BaO	0.04	0.00	0.00	0.04	0.06	0.11	0.15	0.05	0.07
F	1.24	0.45	0.31	1.28	0.64	0.34	0.87	0.95	0.35
Total	93.47	95.50	95.12	96.78	95.61	93.92	95.47	94.56	95.82
Si	6.15	6.15	6.13	6.12	6.17	6.34	6.14	6.20	6.17
Ti	0.01	0.02	0.06	0.05	0.01	0.01	0.00	0.00	0.01
Al Total	5.57	5.64	5.54	5.51	5.72	5.44	5.72	5.58	5.69
Al IV	1.85	1.85	1.87	1.88	1.83	1.66	1.86	1.80	1.83
Al VI	3.72	3.79	3.67	3.63	3.88	3.79	3.86	3.78	3.86
Fe	0.16	0.15	0.18	0.19	0.10	0.13	0.15	0.19	0.12
Mn	0.01	0.01	0.00	0.00	0.02	0.00	0.00	0.02	0.00
Mg	0.15	0.12	0.14	0.17	0.10	0.16	0.12	0.15	0.12
Ca	0.01	0.00	0.01	0.01	0.00	0.00	0.00	0.01	0.00
Na	0.12	0.14	0.19	0.15	0.12	0.07	0.15	0.14	0.12
K	1.79	1.67	1.77	1.86	1.56	1.58	1.58	1.58	1.56
Cr	0.01	0.00	0.00	0.01	0.00	0.01	0.00	0.00	0.01
Cl	0.01	0.00			0.00	0.00	0.02	0.00	0.01
P	0.01	0.01			0.00	0.00	0.00	0.00	0.00
Ba	0.01	0.00	0.03	0.00	0.00	0.00	0.01	0.01	0.01
F	0.00	0.00	0.03	0.02	0.00	0.00	0.00	0.00	0.00
OH	4.00	4.00	3.97	3.98	4.00	4.00	3.99	4.00	4.00
Tetrahedral	8.00	8.00	8.00	8.00	8.00	8.00	8.00	8.00	8.00
Octahedral	4.06	4.09	4.06	4.05	4.12	4.09	4.13	4.14	4.12
Dodecahedral	1.94	1.82	1.99	2.02	1.69	1.65	1.73	1.73	1.70

Sample	SC-7-T	SC-7-T	SC-7-T	SC-7-T	SC-7-T	SC-7-T	SC-7-T	SC-7-T	SC-7-T
Point	10b	1	5	21	21b	21b2	28	29	29b
Description	RC	RF	RF	RF	RF	RF	RF	RF	RF
SiO2	46.22	45.57	45.12	45.94	46.39	46.35	45.92	46.12	46.85
TiO2	0.08	0.08	0.05	0.26	0.36	0.19	0.00	0.01	0.00
Al2O3	34.29	34.66	34.47	35.23	35.32	35.15	34.64	34.49	34.31
FeO	2.87	2.53	3.00	2.01	1.99	2.03	2.63	2.86	3.01
MnO	0.13	0.07	0.04	0.08	0.06	0.08	0.12	0.07	0.16
MgO	1.18	0.82	0.93	0.73	0.65	0.61	0.89	0.94	0.84
CaO	0.03	0.01	0.02	0.05	0.00	0.02	0.10	0.00	0.00
Na2O	0.55	0.56	0.59	0.56	0.68	0.64	0.69	0.64	0.35
K2O	9.58	8.76	8.73	9.16	9.44	9.22	8.59	9.20	9.20
Cr2O3	0.00	0.00	0.11	0.00	0.01	0.05	0.03	0.00	0.07
Cl	0.00	0.00	0.01	0.00	0.03	0.03	0.03	0.00	0.00
P2O5	0.14	0.00	0.09	0.17	0.04	0.05	0.09	0.14	0.03
BaO	0.00	0.00	0.00	0.00	0.00	0.00	0.00	0.07	0.30
F	0.53	1.12	0.50	1.17	0.93	1.01	0.93	1.59	0.81
Total	95.60	94.18	93.66	95.36	95.90	95.43	94.66	96.13	95.93
Si	6.13	6.30	6.32	6.41	6.31	6.37	6.61	6.38	6.48
Ti	0.00	0.02	0.00	0.01	0.02	0.01	0.08	0.03	0.01
Al Total	5.74	5.34	5.31	5.06	5.25	5.24	4.65	5.05	5.04
Al IV	1.87	1.70	1.68	1.59	1.69	1.63	1.39	1.62	1.52
Al VI	3.87	3.64	3.64	3.47	3.56	3.61	3.26	3.43	3.52
Fe	0.12	0.56	0.56	0.68	0.56	0.56	0.91	0.87	0.57
Mn	0.00	0.01	0.00	0.00	0.01	0.01	0.00	0.00	0.00
Mg	0.11	0.12	0.11	0.17	0.15	0.10	0.12	0.13	0.12
Ca	0.00	0.01	0.01	0.00	0.00	0.00	0.00	0.00	0.00
Na	0.11	0.21	0.22	0.15	0.12	0.17	0.09	0.13	0.08
K	1.63	1.76	1.79	1.81	1.81	1.78	1.87	1.84	1.84
Cr	0.02	0.00	0.01	0.00	0.00	0.00	0.00	0.01	0.01
Cl	0.00	0.00	0.02	0.00	0.00	0.00	0.01	0.01	0.02
P	0.00	0.00	0.01	0.01	0.01	0.00	0.00	0.01	0.01
Ba	0.00	0.00	0.00	0.01	0.01	0.00	0.00	0.00	0.00
F	0.00	0.66	0.70	0.63	0.51	0.58	0.72	0.80	0.48
OH	4.00	3.34	3.29	3.37	3.49	3.42	3.28	3.19	3.51
Tetrahedral	8.00	8.00	8.00	8.00	8.00	8.00	8.00	8.00	8.00
Octahedral	4.10	4.35	4.32	4.33	4.30	4.30	4.37	4.46	4.23
Dodecahedral	1.75	1.97	2.04	1.99	1.95	1.96	1.96	1.98	1.94

Sample	SC-7-T	SC-7-T	SC-7-T	SC-7-T	SC-7-T	SC-7-T	SC-7-T	SC-7-T	SC-7-T
Point	7	7b	7c	8	8b	3	9	12	13
Description	RF	RF	RF	RF	RF	S	S	S	S
SiO2	45.25	45.71	45.77	45.49	45.36	46.81	46.03	48.11	47.46
TiO2	0.24	0.29	0.18	0.17	0.33	0.10	0.39	0.21	0.07
Al2O3	35.16	35.07	35.13	35.63	35.33	35.01	35.26	31.59	30.46
FeO	2.16	2.05	2.04	2.25	2.23	2.74	1.88	3.38	4.62
MnO	0.00	0.04	0.04	0.11	0.01	0.01	0.00	0.09	0.18
MgO	0.64	0.60	0.66	0.65	0.59	0.82	0.67	1.05	1.21
CaO	0.00	0.00	0.00	0.02	0.02	0.02	0.00	0.04	0.10
Na2O	0.74	0.69	0.68	0.80	0.71	0.68	0.54	0.08	0.19
K2O	8.83	8.85	9.29	8.74	8.70	8.77	9.17	9.11	8.38
Cr2O3	0.00	0.07	0.00	0.10	0.00	0.00	0.06	0.06	0.03
Cl	0.00	0.02	0.01	0.05	0.00	0.00	0.02	0.03	0.00
P2O5	0.05	0.21	0.10	0.17	0.09	0.00	0.05	0.16	0.03
BaO	0.14	0.06	0.05	0.16	0.00	0.00	0.09	0.02	0.11
F	1.04	0.23	0.44	0.84	1.02	0.44	0.20	0.61	0.71
Total	94.25	93.89	94.39	95.18	94.39	95.40	94.36	94.54	93.55
Si	6.34	6.45	6.27	6.27	6.31	6.22	6.16	6.19	6.21
Ti	0.03	0.00	0.02	0.00	0.00	0.01	0.01	0.03	0.04
Al Total	5.23	5.14	5.64	5.57	5.64	5.58	5.54	5.59	5.57
Al IV	1.66	1.55	1.73	1.73	1.69	1.78	1.84	1.81	1.79
Al VI	3.57	3.58	3.92	3.84	3.95	3.80	3.70	3.79	3.77
Fe	0.64	0.57	0.29	0.47	0.33	0.29	0.34	0.23	0.22
Mn	0.02	0.03	0.00	0.03	0.01	0.01	0.00	0.01	0.01
Mg	0.16	0.13	0.05	0.04	0.03	0.17	0.19	0.15	0.13
Ca	0.00	0.00	0.01	0.01	0.00	0.00	0.00	0.01	0.00
Na	0.16	0.11	0.15	0.08	0.08	0.15	0.16	0.15	0.18
K	1.67	1.80	1.58	1.60	1.55	1.53	1.52	1.57	1.61
Cr	0.00	0.00	0.00	0.00	0.00	0.00	0.01	0.00	0.00
Cl	0.00	0.00	0.01	0.02	0.00	0.00	0.00	0.00	0.01
P	0.01	0.00	0.00	0.00	0.00	0.00	0.01	0.02	0.00
Ba	0.00	0.01	0.00	0.00	0.01	0.00	0.00	0.00	0.00
F	0.68	0.57	0.51	0.56	0.55	0.24	0.11	0.25	0.20
OH	3.32	3.43	3.48	3.43	3.45	3.76	3.89	3.75	3.80
Tetrahedral	8.00	8.00	8.00	8.00	8.00	8.00	8.00	8.00	8.00
Octahedral	4.41	4.30	4.28	4.39	4.32	4.27	4.24	4.20	4.17
Dodecahedral	1.84	1.92	1.73	1.68	1.64	1.67	1.70	1.74	1.79

Sample	SC-7-T	SC-7-T	SC-7-T	SC-7-T	SC-7-T	SC-7-T	SC-7-T	SC-10-T	SC-10-T
Point	14	15	24	25	26	30	19	3	4
Description	S	S	S	S	S	S	S	P	P
SiO2	46.48	47.27	47.12	47.00	46.60	47.84	47.54	44.67	44.42
TiO2	0.15	0.07	0.04	0.16	0.00	0.13	0.09	0.25	0.19
Al2O3	33.38	32.34	34.80	30.97	33.21	30.75	33.82	35.32	35.18
FeO	3.84	3.76	2.34	4.39	3.29	5.14	3.20	2.35	2.43
MnO	0.20	0.11	0.21	0.25	0.04	0.27	0.03	0.12	0.00
MgO	0.46	1.10	0.25	1.24	0.98	1.22	0.44	0.24	0.25
CaO	0.00	0.07	0.00	0.03	0.04	0.00	0.05	0.05	0.08
Na2O	0.20	0.13	0.13	0.19	0.33	0.14	0.25	1.17	1.13
K2O	9.35	9.12	9.91	9.10	9.43	9.59	9.58	9.95	9.82
Cr2O3	0.00	0.05	0.03	0.00	0.00	0.00	0.00	0.00	0.00
Cl	0.00	0.01	0.00	0.00	0.02	0.01	0.00	0.02	0.04
P2O5	0.04	0.00	0.00	0.10	0.00	0.01	0.00	0.06	0.02
BaO	0.00	0.00	0.04	0.22	0.00	0.00	0.01	0.00	0.04
F	0.43	0.75	0.74	1.20	0.97	1.31	0.82	1.54	1.55
Total	94.53	94.78	95.61	94.85	94.91	96.41	95.83	95.75	95.12
Si	6.23	6.22	6.24	6.28	6.17	6.16	6.17	7.06	6.44
Ti	0.02	0.00	0.00	0.00	0.02	0.03	0.02	0.00	0.01
Al Total	5.57	5.53	5.50	5.42	5.65	5.57	5.58	4.14	5.25
Al IV	1.77	1.78	1.76	1.72	1.83	1.84	1.83	0.94	1.56
Al VI	3.80	3.75	3.74	3.70	3.81	3.74	3.76	3.19	3.70
Fe	0.23	0.30	0.32	0.34	0.25	0.23	0.23	1.28	0.47
Mn	0.01	0.01	0.01	0.02	0.00	0.00	0.00	0.11	0.03
Mg	0.12	0.18	0.19	0.17	0.13	0.12	0.13	0.00	0.00
Ca	0.00	0.01	0.00	0.00	0.00	0.00	0.00	0.00	0.00
Na	0.17	0.18	0.17	0.09	0.20	0.18	0.18	0.18	0.09
K	1.58	1.48	1.59	1.57	1.53	1.52	1.60	1.91	1.73
Cr	0.01	0.00	0.00	0.01	0.00	0.01	0.00	0.01	0.00
Cl	0.01	0.01	0.00	0.00	0.00	0.01	0.00	0.02	0.00
P	0.01	0.01	0.02	0.00	0.01	0.02	0.01	0.02	0.01
Ba	0.00	0.00	0.00	0.02	0.01	0.00	0.00	0.00	0.00
F	0.21	0.20	0.34	0.17	0.22	0.05	0.09	1.62	0.46
OH	3.78	3.79	3.66	3.83	3.78	3.95	3.90	2.37	3.54
Tetrahedral	8.00	8.00	8.00	8.00	8.00	8.00	8.00	8.00	8.00
Octahedral	4.18	4.26	4.26	4.23	4.21	4.12	4.14	4.59	4.21
Dodecahedral	1.76	1.68	1.78	1.69	1.74	1.74	1.79	2.11	1.84

Sample	SC-10-T	SC-10-T	SC-10-T	SC-10-T	SC-10-T	SC-10-T	SC-10-T	SC-10-T
Point	7	20	21	29	30	3	8	7
Description	P	P	P	P	P	P	P	P
SiO2	45.18	45.24	44.67	44.62	45.64	45.86	45.61	45.96
TiO2	0.17	0.22	0.26	0.37	0.06	0.14	0.20	0.14
Al2O3	35.73	36.09	35.30	35.65	35.42	35.80	35.85	35.37
FeO	2.29	2.32	2.37	2.23	2.72	2.51	2.17	2.57
MnO	0.03	0.11	0.08	0.00	0.15	0.09	0.06	0.12
MgO	0.22	0.25	0.22	0.24	0.12	0.18	0.19	0.18
CaO	0.05	0.05	0.04	0.02	0.00	0.01	0.02	0.03
Na2O	1.02	1.14	1.03	1.08	0.96	1.06	0.93	1.11
K2O	10.07	10.36	9.96	10.13	10.18	10.13	10.13	10.18
Cr2O3	0.00	0.05	0.00	0.00	0.07	0.00	0.00	0.01
Cl	0.00	0.00	0.03	0.00	0.05	N/D	N/D	N/D
P2O5	0.07	0.07	0.16	0.03	0.01	N/D	N/D	N/D
BaO	0.04	0.00	0.02	0.00	0.14	0.03	0.02	N/D
F	1.45	1.81	1.39	1.59	1.38	1.29	1.18	1.50
Total	96.33	97.74	95.51	95.96	96.91	97.09	96.37	97.14
Si	6.89	6.81	6.94	6.78	6.34	6.32	6.18	6.16
Ti	0.02	0.01	0.01	0.01	0.02	0.00	0.03	0.01
Al Total	4.44	4.57	4.28	4.64	5.34	5.32	5.65	5.56
Al IV	1.11	1.19	1.06	1.22	1.66	1.68	1.82	1.84
Al VI	3.33	3.39	3.22	3.42	3.68	3.64	3.82	3.73
Fe	1.05	1.02	1.24	0.94	0.55	0.57	0.24	0.39
Mn	0.12	0.10	0.13	0.11	0.02	0.00	0.00	0.00
Mg	0.00	0.02	0.00	0.01	0.00	0.02	0.04	0.02
Ca	0.00	0.01	0.00	0.01	0.00	0.00	0.01	0.00
Na	0.12	0.10	0.18	0.12	0.14	0.07	0.20	0.15
K	1.93	1.74	1.93	1.88	1.54	1.62	1.46	1.58
Cr	0.00	0.00	0.01	0.00	0.00	0.01	0.00	0.01
Cl	0.00	0.00	0.01	0.00	0.00	0.00	0.01	0.00
P	0.01	0.02	0.01	0.00	0.01	0.01	0.00	0.01
Ba	0.00	0.00	0.01	0.00	0.00	0.00	0.00	0.00
F	1.38	1.23	1.56	1.21	0.29	0.20	0.02	0.00
OH	2.62	2.77	2.43	2.79	3.71	3.80	3.97	4.00
Tetrahedral	8.00	8.00	8.00	8.00	8.00	8.00	8.00	8.00
Octahedral	4.52	4.54	4.60	4.50	4.26	4.23	4.14	4.15
Dodecahedral	2.06	1.85	2.13	2.00	1.68	1.71	1.67	1.74

Sample	SC-10-T	SC-10-T	SC-10-T	SC-10-T	SC-10-T	SC-10-T	SC-10-T	SC-10-T
Point	8	6	5	1	2	3	2	5
Description	P	P	P	P	P	P	P	P
SiO2	46.13	45.31	45.47	45.58	45.25	46.10	44.84	45.41
TiO2	0.14	0.09	0.13	0.22	0.23	0.11	0.31	0.32
Al2O3	35.36	35.29	35.19	35.75	36.10	35.80	35.13	35.78
FeO	2.42	2.24	2.63	2.15	2.15	2.18	2.68	2.21
MnO	0.00	0.13	0.01	0.10	0.09	0.00	0.15	0.14
MgO	0.21	0.09	0.10	0.11	0.09	0.28	0.12	0.17
CaO	0.00	0.03	0.00	0.00	0.00	0.00	0.02	0.02
Na2O	0.95	1.04	1.07	0.94	1.02	1.10	0.99	1.06
K2O	10.18	10.02	10.30	10.09	10.01	10.17	10.08	10.18
Cr2O3	0.03	0.06	0.00	0.00	0.09	0.00	0.00	0.03
Cl	N/D	N/D	N/D	N/D	N/D	N/D	0.01	0.01
P2O5	N/D	N/D	N/D	N/D	N/D	N/D	0.00	0.00
BaO	N/D	N/D	N/D	N/D	N/D	N/D	0.00	0.00
F	1.53	1.33	1.24	1.24	1.15	1.38	1.41	1.53
Total	96.96	95.64	96.13	96.18	96.18	97.13	95.74	96.85
Si	6.23	6.43	6.23	6.30	6.22	6.24	6.37	6.24
Ti	0.03	0.01	0.00	0.01	0.01	0.00	0.00	0.02
Al Total	5.50	5.12	5.49	5.57	5.46	5.46	5.31	5.44
Al IV	1.77	1.57	1.77	1.70	1.78	1.76	1.63	1.76
Al VI	3.74	3.55	3.72	3.87	3.68	3.70	3.68	3.69
Fe	0.31	0.74	0.45	0.33	0.39	0.47	0.52	0.47
Mn	0.01	0.02	0.01	0.02	0.02	0.02	0.01	0.02
Mg	0.03	0.03	0.02	0.01	0.01	0.01	0.00	0.01
Ca	0.00	0.00	0.00	0.00	0.00	0.00	0.01	0.00
Na	0.16	0.07	0.12	0.14	0.14	0.12	0.10	0.12
K	1.55	1.70	1.67	1.48	1.82	1.75	1.65	1.74
Cr	0.00	0.00	0.01	0.00	0.00	0.00	0.00	0.00
Cl	0.00	0.00	0.00	0.08	0.00	0.00	0.00	0.00
P	0.00	0.01	0.02	0.01	0.02	0.02	0.02	0.01
Ba	0.01	0.00	0.00	0.00	0.00	0.01	0.00	0.00
F	0.01	0.52	0.27	0.29	0.22	0.30	0.35	0.28
OH	3.99	3.48	3.73	3.67	3.78	3.70	3.65	3.72
Tetrahedral	8.00	8.00	8.00	8.00	8.00	8.00	8.00	8.00
Octahedral	4.12	4.34	4.20	4.23	4.12	4.20	4.23	4.20
Dodecahedral	1.73	1.78	1.82	1.64	1.98	1.89	1.76	1.88

Sample	SC-10-T	SC-10-T	SC-10-T	SC-10-T	SC-10-T	SC-10-T	SC-10-T	SC-10-T
Point	6	9	10	11	12	15	16	17
Description	P	P	P	P	P	P	P	P
SiO2	45.49	44.27	44.86	44.82	44.88	45.44	45.74	45.39
TiO2	0.30	0.25	0.20	0.31	0.18	0.01	0.13	0.25
Al2O3	36.36	34.71	34.85	35.52	35.08	34.43	35.55	36.08
FeO	2.28	2.31	2.68	2.36	2.51	3.45	2.82	2.42
MnO	0.11	0.03	0.05	0.09	0.00	0.09	0.02	0.05
MgO	0.27	0.29	0.19	0.27	0.24	0.20	0.28	0.24
CaO	0.12	0.11	0.01	0.08	0.00	0.13	0.05	0.04
Na2O	0.98	1.02	0.98	1.18	0.92	0.98	0.99	1.03
K2O	10.30	9.99	10.08	10.14	9.87	10.16	10.20	9.89
Cr2O3	0.00	0.00	0.08	0.00	0.00	0.04	0.01	0.05
Cl	0.00	0.05	0.02	0.02	0.00	0.05	0.00	0.02
P2O5	0.10	0.10	0.04	0.08	0.00	0.00	0.09	0.00
BaO	0.13	0.00	0.00	0.00	0.00	0.06	0.00	0.00
F	1.18	1.58	1.60	1.34	1.79	1.81	1.66	1.58
Total	97.61	94.72	95.63	96.21	95.49	96.84	97.55	97.02
Si	6.27	6.32	6.23	6.34	6.34	6.31	6.22	6.30
Ti	0.01	0.00	0.00	0.00	0.02	0.00	0.00	0.00
Al Total	5.42	5.36	5.56	5.33	5.36	5.43	5.49	5.45
Al IV	1.73	1.68	1.77	1.66	1.66	1.69	1.78	1.70
Al VI	3.69	3.68	3.79	3.67	3.70	3.74	3.71	3.75
Fe	0.53	0.49	0.29	0.52	0.48	0.42	0.50	0.43
Mn	0.01	0.02	0.00	0.01	0.01	0.01	0.01	0.01
Mg	0.01	0.02	0.03	0.02	0.03	0.02	0.02	0.01
Ca	0.00	0.00	0.01	0.00	0.00	0.00	0.00	0.00
Na	0.09	0.10	0.17	0.10	0.16	0.16	0.13	0.15
K	1.69	1.73	1.67	1.67	1.58	1.59	1.71	1.63
Cr	0.00	0.00	0.00	0.00	0.00	0.01	0.00	0.00
Cl	0.00	0.01	0.00	0.01	0.00	0.00	0.00	0.00
P	0.01	0.01	0.01	0.01	0.01	0.01	0.01	0.02
Ba	0.00	0.00	0.01	0.00	0.00	0.01	0.01	0.01
F	0.30	0.27	0.14	0.31	0.33	0.28	0.34	0.36
OH	3.70	3.72	3.86	3.68	3.67	3.71	3.66	3.64
Tetrahedral	8.00	8.00	8.00	8.00	8.00	8.00	8.00	8.00
Octahedral	4.24	4.21	4.11	4.22	4.24	4.20	4.24	4.20
Dodecahedral	1.79	1.83	1.85	1.79	1.75	1.78	1.87	1.82

Sample	SC-10-T	SC-10-T	SC-10-T	SC-10-T	SC-10-T	SC-10-T	SC-10-T	SC-10-T
Point	18	23	24	26	27	32	33	34
Description	P	P	P	P	P	P	P	P
SiO2	45.40	44.71	44.65	44.89	44.74	44.81	44.86	46.01
TiO2	0.10	0.29	0.16	0.24	0.13	0.15	0.25	0.20
Al2O3	35.04	34.80	35.02	35.97	34.27	35.33	35.51	35.69
FeO	2.49	2.31	2.02	1.99	3.49	2.68	2.28	2.23
MnO	0.00	0.00	0.03	0.00	0.13	0.14	0.18	0.11
MgO	0.27	0.28	0.15	0.36	0.27	0.29	0.35	0.31
CaO	0.04	0.34	0.00	0.00	0.04	0.00	0.00	0.00
Na2O	0.98	1.15	0.67	1.13	0.91	0.91	1.11	0.99
K2O	10.14	10.14	10.38	9.95	10.17	9.84	10.10	10.29
Cr2O3	0.08	0.12	0.05	0.02	0.03	0.06	0.00	0.03
Cl	0.00	0.03	0.00	0.02	0.02	0.01	0.02	0.01
P2O5	0.02	0.07	0.01	0.04	0.00	0.00	0.03	0.04
BaO	0.05	0.12	0.17	0.14	0.09	0.03	0.00	0.00
F	1.62	1.10	1.09	1.59	1.90	1.51	1.44	1.30
Total	96.23	95.46	94.40	96.34	96.19	95.75	96.13	97.20
Si	6.18	6.23	6.28	6.06	6.06	6.15	6.10	6.13
Ti	0.00	0.01	0.01	0.03	0.02	0.00	0.02	0.00
Al Total	5.59	5.44	5.46	5.65	5.66	5.46	5.63	5.54
Al IV	1.82	1.77	1.72	1.94	1.94	1.85	1.90	1.87
Al VI	3.78	3.67	3.74	3.71	3.72	3.61	3.72	3.67
Fe	0.41	0.55	0.39	0.27	0.28	0.43	0.25	0.35
Mn	0.02	0.02	0.01	0.01	0.00	0.01	0.01	0.00
Mg	0.01	0.00	0.03	0.05	0.05	0.05	0.05	0.06
Ca	0.00	0.01	0.00	0.01	0.01	0.00	0.00	0.00
Na	0.18	0.06	0.10	0.31	0.30	0.24	0.27	0.27
K	1.53	1.59	1.41	1.72	1.71	1.77	1.75	1.75
Cr	0.00	0.00	0.00	0.00	0.00	0.00	0.00	0.01
Cl	0.00	0.00	0.00					
P	0.02	0.00	0.02					
Ba	0.01	0.00	0.00	0.00	0.00	0.00	0.00	0.00
F	0.22	0.14	0.00	0.33	0.33	0.37	0.32	0.33
OH	3.78	3.86	4.00	3.67	3.67	3.63	3.68	3.67
Tetrahedral	8.00	8.00	8.00	8.00	8.00	8.00	8.00	8.00
Octahedral	4.21	4.27	4.18	4.07	4.08	4.11	4.06	4.07
Dodecahedral	1.74	1.66	1.53	2.03	2.01	2.01	2.01	2.03

Sample	SC-10-T	SC-10-T	SC-10-T	SC-10-T	SC-10-T	SC-10-T	SC-10a-T	SC-10a-T
Point	8	22	1	10real	13	19	2	2light
Description	P	P	P	P	P	P	G	G
SiO2	45.62	45.30	45.91	45.17	45.65	45.30	47.68	48.56
TiO2	0.18	0.18	0.04	0.05	0.10	0.22	0.14	0.09
Al2O3	34.54	34.75	35.03	35.09	34.55	35.60	21.07	22.77
FeO	2.70	3.36	3.27	2.73	2.98	2.29	9.64	9.09
MnO	0.18	0.00	0.05	0.13	0.06	0.10	0.62	0.44
MgO	0.26	0.36	0.22	0.09	0.25	0.26	0.22	0.29
CaO	0.06	0.07	0.00	0.06	0.00	0.00	0.09	0.00
Na2O	0.83	0.97	1.06	0.98	0.75	0.95	0.29	0.26
K2O	10.39	10.21	10.29	10.14	10.00	10.15	10.26	9.82
Cr2O3	0.00	0.09	0.00	0.00	0.09	0.04	0.00	0.06
Cl	0.00	0.01	0.01	0.00	0.02	0.03	0.04	0.02
P2O5	0.00	0.08	0.00	0.00	0.10	0.00	0.09	0.01
BaO	0.03	0.00	0.09	0.06	0.00	0.00	0.06	0.09
F	1.19	1.63	1.64	1.13	1.56	1.61	6.89	7.10
Total	95.97	97.00	97.58	95.63	96.12	96.55	97.08	98.60
Si	6.15	6.14	6.14	6.08	6.04	6.07	6.95	7.20
Ti	0.00	0.00	0.01	0.02	0.02	0.03	0.03	0.01
Al Total	5.54	5.53	5.54	5.66	5.68	5.65	4.01	3.65
Al IV	1.85	1.86	1.86	1.92	1.96	1.93	1.05	0.80
Al VI	3.68	3.67	3.68	3.74	3.71	3.72	2.96	2.85
Fe	0.33	0.36	0.35	0.26	0.26	0.27	1.32	1.53
Mn	0.02	0.00	0.01	0.00	0.01	0.01	0.09	0.11
Mg	0.05	0.04	0.03	0.04	0.05	0.05	0.15	0.12
Ca	0.01	0.00	0.01	0.01	0.01	0.01	0.00	0.00
Na	0.22	0.26	0.19	0.27	0.30	0.27	0.09	0.11
K	1.74	1.75	1.79	1.73	1.76	1.73	1.68	1.74
Cr	0.01	0.01	0.00	0.00	0.01	0.00	0.00	0.00
Cl							0.02	0.01
P							0.00	0.02
Ba	0.01	0.01	0.01	0.00	0.00	0.00	0.00	0.00
F	0.30	0.00	0.00	0.31	0.38	0.30	0.83	1.20
OH	3.70	4.00	4.00	3.69	3.62	3.70	3.15	2.80
Tetrahedral	8.00	8.00	8.00	8.00	8.00	8.00	8.00	8.00
Octahedral	4.10	4.08	4.08	4.07	4.07	4.08	4.55	4.61
Dodecahedral	1.97	2.03	2.00	2.00	2.06	2.00	1.78	1.86

Sample	SC-10a-T	SC-10a-T	SC-10a-T	SC-10a-T	SC-10a-T	SC-10a-T	SC-10a-T
Point	3	4	5	7	7	10	13
Description	G	G	G	G	G	G	G
SiO2	45.97	45.44	45.62	45.84	47.34	46.08	46.61
TiO2	0.08	0.31	0.27	0.10	0.14	0.13	0.22
Al2O3	35.26	36.00	35.63	35.29	31.69	35.71	35.79
FeO	3.76	2.49	2.29	2.79	4.67	2.48	2.81
MnO	0.14	0.15	0.04	0.00	0.23	0.03	0.13
MgO	0.14	0.11	0.13	0.14	0.15	0.07	0.22
CaO	0.05	0.00	0.00	0.00	0.00	0.00	0.00
Na2O	0.73	0.81	0.84	0.88	0.57	0.99	0.95
K2O	8.82	8.67	9.44	9.94	9.75	9.91	9.72
Cr2O3	0.00	0.00	0.03	0.00	0.03	0.00	0.00
Cl	0.00	0.00	0.00	0.00	0.01	0.00	0.01
P2O5	0.04	0.02	0.08	0.01	0.08	0.04	0.00
BaO	0.16	0.00	0.00	0.08	0.05	0.00	0.00
F	2.58	2.12	2.01	1.45	3.51	1.80	1.96
Total	97.73	96.12	96.38	96.51	98.21	97.25	98.43
Si	6.36	6.44	6.33	6.36	6.31	6.38	6.48
Ti	0.02	0.02	0.01	0.02	0.00	0.02	0.00
Al Total	5.39	5.17	5.34	5.24	5.53	5.19	5.16
Al IV	1.64	1.56	1.67	1.64	1.69	1.62	1.52
Al VI	3.75	3.60	3.67	3.61	3.83	3.57	3.64
Fe	0.42	0.47	0.43	0.42	0.24	0.54	0.42
Mn	0.01	0.02	0.01	0.02	0.03	0.02	0.01
Mg	0.07	0.07	0.06	0.06	0.02	0.06	0.07
Ca	0.00	0.00	0.00	0.00	0.00	0.00	0.01
Na	0.09	0.06	0.08	0.08	0.05	0.07	0.11
K	1.65	1.62	1.63	1.80	1.61	1.61	1.48
Cr	0.01	0.00	0.00	0.00	0.00	0.00	0.00
Cl	0.00	0.01	0.00	0.02	0.00	0.00	0.03
P	0.00	0.00	0.00	0.01	0.00	0.00	0.02
Ba	0.00	0.00	0.00	0.00	0.00	0.01	0.01
F	0.44	0.13	0.10	0.15	0.04	0.12	0.16
OH	3.56	3.87	3.90	3.84	3.96	3.88	3.83
Tetrahedral	8.00	8.00	8.00	8.00	8.00	8.00	8.00
Octahedral	4.26	4.19	4.18	4.12	4.11	4.22	4.17
Dodecahedral	1.76	1.68	1.71	1.88	1.66	1.68	1.62

Sample	SC-10a-T	SC-10a-T	SC-10a-T	SC-10a-T	SC-10a-T	SC-10a-T	SC-10a-T
Point	16	20	20b	22	24	26	29
Description	G	G	G	G	G	G	G
SiO2	46.72	46.67	46.76	46.84	46.42	46.34	46.33
TiO2	0.33	0.12	0.12	0.00	0.11	0.10	0.05
Al2O3	36.10	36.07	35.65	34.97	35.93	35.66	35.28
FeO	2.37	2.38	2.51	2.94	2.77	2.25	3.03
MnO	0.16	0.01	0.00	0.00	0.02	0.06	0.21
MgO	0.22	0.17	0.02	0.12	0.08	0.30	0.12
CaO	0.02	0.05	0.00	0.00	0.07	0.03	0.05
Na2O	0.69	0.88	0.75	0.67	0.59	0.91	0.81
K2O	9.37	9.40	9.08	9.98	7.78	9.67	9.55
Cr2O3	0.01	0.13	0.02	0.08	0.06	0.01	0.00
Cl	0.00	0.03	0.02	0.00	0.00	0.00	0.05
P2O5	0.06	0.06	0.07	0.00	0.26	0.00	0.00
BaO	0.00	0.23	0.12	0.16	0.00	0.22	0.01
F	1.76	1.76	1.60	1.63	1.39	1.34	1.90
Total	97.80	97.96	96.71	97.37	95.48	96.87	97.39
Si	6.36	6.35	6.36	6.87	6.48	6.40	6.40
Ti	0.02	0.02	0.02	0.03	0.02	0.02	0.00
Al Total	5.34	5.39	5.34	4.36	5.13	5.24	5.43
Al IV	1.64	1.65	1.64	1.13	1.52	1.60	1.60
Al VI	3.70	3.74	3.70	3.24	3.61	3.63	3.83
Fe	0.38	0.38	0.38	0.87	0.53	0.45	0.25
Mn	0.02	0.01	0.02	0.05	0.05	0.03	0.02
Mg	0.04	0.04	0.04	0.10	0.05	0.02	0.06
Ca	0.00	0.00	0.00	0.00	0.00	0.00	0.01
Na	0.09	0.09	0.07	0.06	0.08	0.06	0.07
K	1.55	1.50	1.62	1.56	1.53	1.66	1.61
Cr	0.00	0.00	0.00	0.00	0.00	0.00	0.01
Cl	0.01	0.00	0.00	0.01	0.01	0.00	0.01
P	0.00	0.01	0.00	0.00	0.00	0.00	0.00
Ba	0.00	0.00	0.00	0.00	0.00	0.01	0.00
F	0.07	0.14	0.13	0.38	0.25	0.13	0.27
OH	3.92	3.86	3.87	3.61	3.74	3.87	3.73
Tetrahedral	8.00	8.00	8.00	8.00	8.00	8.00	8.00
Octahedral	4.17	4.20	4.17	4.30	4.26	4.16	4.17
Dodecahedral	1.64	1.60	1.70	1.62	1.62	1.73	1.69

Sample	SC-10a-T	SC-10a-T	SC-10a-T	SC-10a-T	SC-10a-T	SC-10a-T	SC-10a-T
Point	32	40	41	2	21	23	31
Description	G	G	G	S	S	S	S
SiO2	46.20	46.07	46.58	49.81	47.02	47.56	47.15
TiO2	0.00	0.18	0.17	0.08	0.00	0.02	0.17
Al2O3	34.69	35.77	35.50	21.17	36.68	32.69	35.91
FeO	3.62	2.32	2.71	8.55	1.33	4.08	2.39
MnO	0.15	0.07	0.02	0.41	0.05	0.13	0.04
MgO	0.13	0.21	0.13	0.29	0.00	0.01	0.16
CaO	0.00	0.00	0.00	0.00	0.00	0.00	0.00
Na2O	0.84	0.93	0.81	0.29	0.28	0.25	0.87
K2O	9.64	9.66	9.32	9.71	10.35	9.74	9.35
Cr2O3	0.05	0.00	0.04	0.00	0.07	0.00	0.05
Cl	0.04	0.02	0.04	0.03	0.02	0.01	0.00
P2O5	0.06	0.11	0.01	0.05	0.00	0.23	0.06
BaO	0.09	0.00	0.00	0.06	0.14	0.12	0.08
F	2.14	1.73	2.04	9.25	0.86	1.97	1.55
Total	97.66	97.08	97.37	99.70	96.80	96.82	97.78
Si	6.44	6.29	6.46	6.36	6.39	6.42	6.45
Ti	0.02	0.00	0.02	0.01	0.01	0.00	0.01
Al Total	5.16	5.51	5.12	5.39	5.44	5.23	5.07
Al IV	1.56	1.71	1.54	1.64	1.61	1.58	1.55
Al VI	3.60	3.80	3.58	3.74	3.82	3.65	3.51
Fe	0.54	0.28	0.55	0.37	0.24	0.48	0.60
Mn	0.01	0.02	0.03	0.02	0.02	0.02	0.04
Mg	0.07	0.04	0.05	0.04	0.02	0.04	0.06
Ca	0.01	0.00	0.01	0.00	0.00	0.00	0.01
Na	0.07	0.07	0.06	0.09	0.04	0.08	0.07
K	1.47	1.58	1.57	1.58	1.55	1.64	1.62
Cr	0.00	0.01	0.00	0.00	0.00	0.01	0.00
Cl	0.01	0.03	0.01	0.00	0.01	0.00	0.01
P	0.01	0.00	0.00	0.00	0.00	0.01	0.00
Ba	0.00	0.01	0.00	0.00	0.01	0.00	0.00
F	0.19	0.06	0.19	0.18	0.04	0.22	0.16
OH	3.80	3.92	3.80	3.82	3.95	3.77	3.83
Tetrahedral	8.00	8.00	8.00	8.00	8.00	8.00	8.00
Octahedral	4.25	4.14	4.24	4.19	4.10	4.19	4.23
Dodecahedral	1.55	1.67	1.62	1.67	1.60	1.73	1.70

Sample	SC-14-T	SC-14-T	SC-14-T	SC-14-T	SC-14-T	SC-14-T	SC-14-T	SC-14-T
Point	2	3	4	5	6	7	8	9
Description	P	P	P	P	P	P	P	P
SiO2	45.51	45.49	45.65	46.19	45.52	45.27	45.79	45.95
TiO2	0.27	0.18	0.13	0.23	0.15	0.06	0.14	0.18
Al2O3	36.46	35.79	36.02	35.09	36.57	34.75	35.82	36.18
FeO	2.12	2.25	2.59	2.79	2.27	3.33	2.33	2.01
MnO	0.03	0.07	0.06	0.05	0.01	0.20	0.10	0.00
MgO	0.14	0.15	0.06	0.24	0.17	0.08	0.16	0.16
CaO	0.00	0.00	0.00	0.01	0.02	0.04	0.01	0.01
Na2O	1.14	1.08	1.08	1.05	1.11	0.46	1.04	1.04
K2O	10.32	10.23	10.18	10.31	10.36	11.04	10.31	10.26
Cr2O3	0.00	0.00	0.11	0.06	0.04	0.00	0.00	0.04
Cl	N/D	N/D	N/D	N/D	N/D	N/D	N/D	N/D
P2O5	N/D	N/D	N/D	N/D	N/D	N/D	N/D	N/D
BaO	0.02	0.01	0.05	0.01	0.00	0.00	0.00	0.00
F	0.74	0.63	1.52	1.02	1.43	0.27	0.72	0.32
Total	96.74	95.89	97.46	97.06	97.64	95.51	96.41	96.16
Si	6.08	6.11	6.04	6.11	6.07	6.06	6.12	6.09
Ti	0.03	0.02	0.02	0.01	0.01	0.03	0.02	0.01
Al Total	5.58	5.65	5.71	5.51	5.64	5.65	5.59	5.64
Al IV	1.92	1.89	1.96	1.89	1.93	1.94	1.88	1.91
Al VI	3.65	3.76	3.75	3.62	3.72	3.71	3.71	3.73
Fe	0.26	0.23	0.22	0.40	0.30	0.26	0.25	0.29
Mn	0.00	0.00	0.00	0.02	0.02	0.02	0.01	0.01
Mg	0.06	0.03	0.07	0.06	0.06	0.07	0.06	0.05
Ca	0.05	0.00	0.00	0.01	0.00	0.00	0.00	0.00
Na	0.30	0.18	0.29	0.24	0.24	0.29	0.25	0.26
K	1.76	1.81	1.71	1.77	1.70	1.74	1.75	1.73
Cr	0.01	0.01	0.00	0.00	0.01	0.00	0.00	0.00
Cl								
P								
Ba	0.01	0.01	0.01	0.00	0.00	0.00	0.00	0.01
F	0.24	0.24	0.34	0.41	0.32	0.31	0.27	0.31
OH	3.76	3.76	3.66	3.59	3.68	3.69	3.73	3.69
Tetrahedral	8.00	8.00	8.00	8.00	8.00	8.00	8.00	8.00
Octahedral	4.05	4.04	4.07	4.11	4.11	4.08	4.06	4.09
Dodecahedral	2.08	2.00	2.01	2.02	1.95	2.03	2.00	2.00

Sample	SC-14-T	SC-14-T	SC-14-T	SC-14-T	SC-14-T	SC-14-T	SC-14-T	SC-14-T
Point	10	11	3	5	6	?	9	11
Description	P	P	P	P	P	P	P	P
SiO2	45.99	45.80	45.31	46.17	46.38	45.39	45.69	45.64
TiO2	0.17	0.10	0.21	0.19	0.36	0.09	0.02	0.15
Al2O3	34.67	34.83	35.84	35.45	34.52	35.79	35.41	35.22
FeO	3.29	3.44	2.05	2.41	2.93	2.31	2.49	2.79
MnO	0.08	0.19	0.10	0.10	0.10	0.15	0.10	0.16
MgO	0.33	0.14	0.09	0.20	0.29	0.23	0.05	0.21
CaO	0.04	0.10	0.00	0.07	0.00	0.00	0.00	0.01
Na2O	1.00	0.59	0.93	1.07	0.95	1.13	0.58	0.86
K2O	10.30	10.80	10.13	10.07	10.31	10.17	10.65	9.49
Cr2O3	0.00	0.00	0.00	0.00	0.00	0.00	0.00	0.04
Cl	N/D	N/D	N/D	N/D	N/D	N/D	N/D	N/D
P2O5	N/D	N/D	N/D	N/D	N/D	N/D	N/D	N/D
BaO	0.02	0.00	0.18	0.00	0.00	0.00	0.08	0.01
F	1.53	0.42	N/D	N/D	N/D	N/D	N/D	N/D
Total	97.41	96.41	94.85	95.72	95.84	95.26	95.07	94.57
Si	6.07	6.11	6.07	6.11	6.07	6.06	6.10	6.13
Ti	0.02	0.02	0.01	0.02	0.02	0.02	0.02	0.01
Al Total	5.76	5.59	5.62	5.58	5.65	5.67	5.60	5.54
Al IV	1.93	1.89	1.93	1.89	1.93	1.94	1.90	1.87
Al VI	3.82	3.70	3.69	3.69	3.72	3.73	3.71	3.68
Fe	0.23	0.31	0.30	0.30	0.29	0.28	0.29	0.34
Mn	0.00	0.02	0.01	0.01	0.01	0.01	0.01	0.01
Mg	0.03	0.05	0.05	0.08	0.03	0.02	0.03	0.04
Ca	0.00	0.01	0.01	0.01	0.00	0.00	0.01	0.00
Na	0.25	0.24	0.30	0.25	0.27	0.26	0.27	0.17
K	1.61	1.70	1.78	1.71	1.77	1.76	1.75	1.82
Cr	0.00	0.00	0.00	0.00	0.00	0.00	0.00	0.00
Cl								
P								
Ba	0.00	0.00	0.00	0.00	0.00	0.00	0.00	0.00
F	0.27	0.30	0.34	0.26	0.20	0.07	0.00	0.00
OH	3.73	3.70	3.66	3.74	3.80	3.93	4.00	4.00
Tetrahedral	8.00	8.00	8.00	8.00	8.00	8.00	8.00	8.00
Octahedral	4.11	4.10	4.07	4.10	4.07	4.07	4.06	4.08
Dodecahedral	1.86	1.95	2.08	1.96	2.04	2.02	2.02	1.99

Sample	SC-14-T	SC-14-T	SC-14-T	SC-14-T	SC-14-T	SC-14-T	SC-14-T	SC-14-T
Point	1	3	4	1	2	3	5	8
Description	P	P	P	P	P	P	P	P
SiO2	46.12	46.25	45.67	46.71	46.48	46.39	47.01	46.41
TiO2	0.06	0.24	0.20	0.01	0.23	0.32	0.23	0.22
Al2O3	34.29	36.46	35.46	34.97	36.16	36.03	35.71	36.19
FeO	3.65	2.17	2.45	3.51	2.28	2.25	2.87	1.69
MnO	0.02	0.00	0.08	0.13	0.04	0.08	0.00	0.09
MgO	0.08	0.15	0.29	0.00	0.24	0.12	0.09	0.17
CaO	0.05	0.00	0.00	0.00	0.00	0.00	0.00	0.00
Na2O	0.57	1.06	1.23	0.49	0.70	0.79	0.79	0.85
K2O	10.07	10.16	10.22	9.80	9.61	9.55	9.61	9.62
Cr2O3	0.04	0.00	0.02	0.09	0.00	0.00	0.02	0.02
Cl	N/D	N/D	N/D	0.03	0.01	0.00	0.01	0.01
P2O5	N/D	N/D	N/D	0.04	0.03	0.07	0.05	0.04
BaO	N/D	N/D	N/D	0.26	0.00	0.10	0.00	0.08
F	0.22	0.61	1.00	0.00	0.00	0.00	0.21	0.00
Total	95.16	97.11	96.61	96.03	95.79	95.71	96.62	95.38
Si	6.19	6.07	6.21	6.12	6.09	6.11	6.12	6.04
Ti	0.01	0.03	0.00	0.01	0.02	0.01	0.02	0.03
Al Total	5.43	5.64	5.42	5.57	5.61	5.59	5.56	5.66
Al IV	1.81	1.93	1.79	1.88	1.91	1.89	1.88	1.96
Al VI	3.62	3.71	3.63	3.69	3.70	3.70	3.68	3.70
Fe	0.41	0.26	0.40	0.27	0.27	0.34	0.28	0.26
Mn	0.02	0.01	0.01	0.01	0.02	0.00	0.00	0.01
Mg	0.01	0.04	0.02	0.03	0.04	0.06	0.08	0.07
Ca	0.00	0.00	0.01	0.00	0.01	0.01	0.02	0.01
Na	0.23	0.28	0.15	0.31	0.23	0.22	0.29	0.29
K	1.79	1.76	1.84	1.80	1.83	1.73	1.74	1.75
Cr	0.00	0.00	0.01	0.01	0.00	0.00	0.00	0.00
Cl								
P								
Ba	0.00	0.00	0.00	0.00	0.00	0.00	0.00	0.00
F	0.00	0.00	0.00	0.00	0.00	0.00	0.00	0.00
OH	4.00	4.00	4.00	4.00	4.00	4.00	4.00	4.00
Tetrahedral	8.00	8.00	8.00	8.00	8.00	8.00	8.00	8.00
Octahedral	4.07	4.06	4.06	4.01	4.06	4.11	4.07	4.08
Dodecahedral	2.02	2.04	2.01	2.13	2.06	1.95	2.02	2.04

Sample	SC-14-T	SC-14-T	SC-14-T	SC-14-T	SC-14-T	SC-14-T	SC-14-T	SC-16-T
Point	9	9b	9c	11	11b	12	14	2
Description	P	P	P	P	P	P	P	RF
SiO2	46.90	46.98	46.97	46.49	46.15	46.78	46.60	48.08
TiO2	0.20	0.13	0.22	0.28	0.27	0.20	0.20	0.08
Al2O3	34.83	34.87	36.24	36.00	34.98	35.92	36.19	34.29
FeO	3.29	3.65	2.49	2.29	2.93	2.52	2.29	2.08
MnO	0.03	0.04	0.02	0.05	0.03	0.11	0.12	0.15
MgO	0.17	0.14	0.12	0.17	0.16	0.22	0.22	0.32
CaO	0.00	0.02	0.03	0.06	0.00	0.00	0.00	0.06
Na2O	0.84	0.80	0.79	0.70	0.69	0.91	0.79	0.11
K2O	9.23	9.41	9.13	9.53	9.47	9.58	9.57	10.22
Cr2O3	0.10	0.00	0.02	0.00	0.00	0.08	0.08	0.04
Cl	0.02	0.00	0.02	0.00	0.03	0.00	0.01	0.00
P2O5	0.10	0.07	0.00	0.00	0.00	0.02	0.10	0.05
BaO	0.00	0.00	0.00	0.00	0.00	0.02	0.00	0.00
F	1.03	0.82	0.00	0.53	0.57	0.00	0.79	0.36
Total	96.74	96.92	96.05	96.12	95.25	96.36	96.97	95.84
Si	6.12	6.12	6.17	6.16	6.10	6.15	6.16	6.08
Ti	0.02	0.00	0.02	0.02	0.02	0.01	0.00	0.00
Al Total	5.60	5.56	5.52	5.50	5.52	5.54	5.55	5.81
Al IV	1.88	1.88	1.83	1.84	1.90	1.85	1.84	1.92
Al VI	3.72	3.68	3.69	3.66	3.62	3.69	3.71	3.88
Fe	0.28	0.36	0.26	0.30	0.38	0.21	0.32	0.12
Mn	0.00	0.01	0.01	0.02	0.00	0.01	0.01	0.00
Mg	0.04	0.04	0.06	0.05	0.07	0.13	0.03	0.02
Ca	0.00	0.01	0.00	0.01	0.01	0.00	0.00	0.00
Na	0.26	0.24	0.13	0.22	0.25	0.29	0.25	0.19
K	1.75	1.76	1.89	1.79	1.75	1.75	1.75	1.79
Cr	0.00	0.00	0.00	0.00	0.01	0.00	0.00	0.00
Cl								
P								
Ba	0.00	0.00	0.01	0.00	0.00	0.00	0.00	0.00
F	0.00	0.29	0.00	0.25	0.35	0.34	0.28	0.00
OH	4.00	3.71	4.00	3.75	3.65	3.66	3.72	4.00
Tetrahedral	8.00	8.00	8.00	8.00	8.00	8.00	8.00	8.00
Octahedral	4.06	4.10	4.04	4.07	4.10	4.05	4.07	4.03
Dodecahedral	2.01	2.00	2.03	2.01	2.02	2.04	2.00	1.98

Sample	SC-16-T	SC-16-T	SC-16-T	SC-16-T	SC-16-T	SC-16-T	SC-16-T	SC-16-T
Point	9	11	14	26	33	42	55	17
Description	RF	RF	RF	RF	RF	RF	RF	S
SiO2	46.83	47.32	46.27	49.40	46.85	48.12	46.60	51.36
TiO2	0.16	0.30	0.22	0.08	0.24	0.25	0.14	0.00
Al2O3	34.91	32.41	34.73	29.85	35.49	36.11	36.25	21.79
FeO	2.52	4.44	2.17	4.36	2.33	1.47	2.34	7.03
MnO	0.12	0.14	0.08	0.28	0.08	0.03	0.07	0.46
MgO	0.73	0.95	0.73	1.43	0.74	0.18	0.65	0.36
CaO	0.02	0.05	0.02	0.01	0.05	0.00	0.03	0.00
Na2O	0.53	0.23	0.81	0.23	0.78	0.23	0.69	0.52
K2O	9.74	9.64	9.28	10.34	9.39	9.73	9.25	10.02
Cr2O3	0.00	0.00	0.06	0.04	0.00	0.00	0.05	0.00
Cl	0.02	0.03	0.05	0.00	0.05	0.00	0.01	0.00
P2O5	0.00	0.06	0.19	0.00	0.19	0.03	0.29	0.00
BaO	0.02	0.00	0.00	0.00	0.00	0.00	0.00	0.01
F	0.63	1.12	0.68	2.16	0.84	0.00	0.38	4.80
Total	96.25	96.71	95.27	98.17	97.03	96.15	96.77	96.35
Si	6.09	6.10	6.08	6.15	6.11	6.06	6.16	6.20
Ti	0.01	0.01	0.00	0.04	0.02	0.02	0.01	0.01
Al Total	5.76	5.73	5.75	5.60	5.68	5.76	5.49	5.44
Al IV	1.91	1.90	1.92	1.85	1.89	1.94	1.84	1.80
Al VI	3.85	3.83	3.82	3.75	3.79	3.81	3.65	3.64
Fe	0.14	0.16	0.18	0.12	0.15	0.11	0.28	0.25
Mn	0.00	0.00	0.01	0.01	0.00	0.01	0.02	0.01
Mg	0.04	0.05	0.03	0.09	0.08	0.10	0.14	0.16
Ca	0.00	0.00	0.00	0.00	0.00	0.00	0.00	0.00
Na	0.17	0.18	0.19	0.14	0.17	0.18	0.24	0.21
K	1.79	1.80	1.80	1.82	1.81	1.81	1.73	1.77
Cr	0.00	0.00	0.00	0.01	0.00	0.00	0.00	0.01
Cl								
P								
Ba	0.00	0.00	0.00	0.01	0.00	0.00	0.00	0.01
F	0.00					0.00	0.12	
OH	4.00	4.00	4.00	4.00	4.00	4.00	3.88	4.00
Tetrahedral	8.00	8.00	8.00	8.00	8.00	8.00	8.00	8.00
Octahedral	4.05	4.04	4.05	4.02	4.04	4.05	4.10	4.07
Dodecahedral	1.96	1.98	2.00	1.97	1.98	2.00	1.98	2.00

Sample	SC-16-T	SC-16-T	SC-17-T	SC-17-T	SC-17-T	SC-17-T	SC-17-T	SC-18-T
Point	36	47	1	01b	2	6	7	30
Description	S	S	FF	FF	FF	FF	FF	RA
SiO2	47.49	49.33	48.02	47.59	50.68	47.38	49.91	48.45
TiO2	0.18	0.04	0.09	0.00	0.02	0.06	0.02	0.07
Al2O3	32.51	32.99	19.53	19.71	30.51	21.35	19.52	31.57
FeO	4.18	2.38	15.14	11.80	3.81	11.29	13.02	4.80
MnO	0.21	0.26	0.58	0.50	0.12	0.40	0.36	0.18
MgO	0.56	0.98	0.15	0.22	0.10	0.40	0.11	0.48
CaO	0.02	0.00	0.00	0.00	0.04	0.00	0.00	0.00
Na2O	0.34	0.32	0.33	0.34	0.22	0.39	0.21	0.13
K2O	10.27	9.88	9.96	9.70	10.40	8.90	9.81	9.82
Cr2O3	0.00	0.00	0.08	0.06	0.00	0.02	0.00	0.08
Cl	0.01	0.00	0.03	0.05	0.05	0.00	0.01	0.01
P2O5	0.03	0.00	0.04	0.08	0.06	0.03	0.08	0.14
BaO	0.00	0.04	0.00	0.06	0.01	0.03	0.00	0.06
F	1.27	1.22	2.57	4.83	0.76	4.91	0.00	0.00
Total	97.07	97.45	96.52	94.94	96.78	95.16	93.06	95.79
Si	6.09	6.17	6.15	6.18	6.12	6.10	6.19	6.16
Ti	0.04	0.01	0.00	0.01	0.01	0.04	0.04	0.01
Al Total	5.66	5.46	5.53	5.54	5.57	5.64	5.48	5.53
Al IV	1.91	1.83	1.85	1.82	1.88	1.90	1.81	1.84
Al VI	3.75	3.63	3.68	3.72	3.69	3.73	3.67	3.69
Fe	0.15	0.31	0.28	0.25	0.25	0.16	0.17	0.18
Mn	0.00	0.00	0.01	0.01	0.01	0.00	0.01	0.01
Mg	0.10	0.13	0.09	0.08	0.09	0.13	0.13	0.14
Ca	0.00	0.00	0.01	0.00	0.00	0.00	0.00	0.00
Na	0.19	0.16	0.14	0.15	0.25	0.16	0.19	0.27
K	1.79	1.86	1.84	1.76	1.76	1.79	1.81	1.78
Cr	0.01	0.00	0.01	0.00	0.01	0.00	0.01	0.00
Cl								
P								
Ba					0.00	0.01	0.00	0.01
F	0.03	0.21	0.20	0.21	0.21			
OH	3.97	3.79	3.80	3.79	3.79	4.00	4.00	4.00
Tetrahedral	8.00	8.00	8.00	8.00	8.00	8.00	8.00	8.00
Octahedral	4.04	4.09	4.07	4.08	4.06	4.07	4.02	4.03
Dodecahedral	1.98	2.02	1.99	1.91	2.02	1.95	2.00	2.06

Sample	SC-18-T	SC-18-T	SC-18-T	SC-18-T	SC-18-T	SC-18-T	SC-18-T	SC-18-T
Point	32	33	2	1	2	7	15	23
Description	RA	RA	RB	RF	RF	RF	RF	RF
SiO2	48.43	47.34	48.16	49.42	49.01	47.93	48.82	48.05
TiO2	0.20	0.17	0.16	0.17	0.09	0.06	0.02	0.14
Al2O3	19.83	30.96	30.70	32.99	29.50	25.52	32.27	30.61
FeO	13.28	5.83	4.92	3.12	5.73	9.11	3.39	5.80
MnO	1.02	0.15	0.19	0.15	0.24	0.45	0.18	0.27
MgO	1.31	0.48	0.54	0.26	0.50	0.60	0.28	0.55
CaO	0.02	0.00	0.03	0.01	0.01	0.03	0.00	0.00
Na2O	0.28	0.22	0.21	0.15	0.21	0.26	0.20	0.17
K2O	9.71	10.20	9.43	10.05	9.50	9.64	9.47	10.00
Cr2O3	0.04	0.13	0.00	0.00	0.00	0.00	0.06	0.01
Cl	0.00	0.01	0.00	0.00	0.01	0.05	0.01	0.02
P2O5	0.00	0.00	0.00	0.00	0.00	0.07	0.00	0.00
BaO	0.00	0.05	0.11	0.00	0.22	0.13	0.08	0.06
F	1.31	0.00	0.00	0.00	0.00	0.00	0.00	0.00
Total	95.44	95.55	94.47	96.32	95.01	93.85	94.77	95.68
Si	6.13	6.16	6.12	6.16	6.15	6.11	6.12	6.06
Ti	0.01	0.03	0.02	0.02	0.02	0.04	0.02	0.01
Al Total	5.61	5.55	5.68	5.57	5.58	5.61	5.74	5.77
Al IV	1.87	1.84	1.88	1.84	1.85	1.89	1.88	1.94
Al VI	3.74	3.71	3.81	3.73	3.72	3.72	3.86	3.83
Fe	0.19	0.18	0.14	0.18	0.18	0.18	0.12	0.17
Mn	0.00	0.00	0.00	0.00	0.00	0.00	0.00	0.00
Mg	0.11	0.11	0.03	0.10	0.14	0.11	0.03	0.03
Ca	0.00	0.00	0.00	0.00	0.00	0.01	0.00	0.00
Na	0.16	0.19	0.21	0.20	0.22	0.20	0.18	0.21
K	1.82	1.80	1.81	1.80	1.76	1.77	1.76	1.78
Cr	0.00	0.00	0.00	0.00	0.00	0.00	0.00	0.00
Cl								
P								
Ba	0.00				0.00	0.00	0.00	0.00
F		0.12	0.10	0.08	0.11	0.12	0.08	
OH	4.00	3.88	3.90	3.92	3.89	3.88	3.92	4.00
Tetrahedral	8.00	8.00	8.00	8.00	8.00	8.00	8.00	8.00
Octahedral	4.05	4.04	4.00	4.04	4.06	4.06	4.02	4.04
Dodecahedral	1.99	1.99	2.02	1.99	1.98	1.98	1.94	2.00

Sample	SC-18-T	SC-18-T	SC-18-T	SC-18-T	SC-18-T	SC-E1	SC-E1	SC-E1	SC-E1
Point	26	37	3	25	34	1	2	4	5
Description	RF	RF	RF	S	S	P	P	P	P
SiO2	48.10	48.72	47.78	49.11	48.95	45.58	46.10	45.73	46.37
TiO2	0.00	0.21	0.23	0.07	0.02	0.13	0.05	0.19	0.19
Al2O3	34.60	32.87	31.01	28.11	32.54	35.25	35.52	35.73	36.65
FeO	2.52	3.42	5.36	6.88	2.66	2.87	2.91	2.62	2.26
MnO	0.15	0.19	0.30	0.32	0.23	0.11	0.06	0.14	0.11
MgO	0.27	0.29	0.50	0.66	0.82	0.19	0.18	0.21	0.16
CaO	0.03	0.02	0.00	0.03	0.08	0.04	0.01	0.01	0.00
Na2O	0.19	0.06	0.13	0.25	0.16	1.00	0.96	0.99	1.06
K2O	9.90	10.19	10.01	9.97	9.52	10.22	10.22	10.27	10.20
Cr2O3	0.03	0.00	0.04	0.00	0.11	0.00	0.00	0.00	0.00
Cl	0.00	0.06	0.00	0.01	0.00	N/D	N/D	N/D	N/D
P2O5	0.00	0.08	0.00	0.12	0.02	N/D	N/D	N/D	N/D
BaO	0.02	0.00	0.00	0.07	0.14	N/D	N/D	N/D	N/D
F	0.00	0.00	0.00	0.00	0.00	1.44	1.52	1.53	1.11
Total	95.82	96.12	95.34	95.60	95.24	96.84	97.52	97.43	98.11
Si	6.15	6.15	6.17	6.18	6.17	6.24	6.39	6.41	6.52
Ti	0.00	0.01	0.00	0.01	0.02	0.04	0.02	0.01	0.01
Al Total	5.64	5.54	5.57	5.51	5.55	5.32	5.24	5.19	4.98
Al IV	1.85	1.85	1.83	1.82	1.83	1.76	1.61	1.59	1.48
Al VI	3.79	3.69	3.74	3.69	3.71	3.57	3.62	3.60	3.49
Fe	0.16	0.22	0.19	0.24	0.22	0.54	0.18	0.19	0.20
Mn	0.01	0.00	0.01	0.00	0.00	0.02	0.01	0.00	0.00
Mg	0.06	0.12	0.10	0.13	0.10	0.05	0.20	0.22	0.35
Ca	0.00	0.01	0.00	0.01	0.00	0.01	0.01	0.00	0.01
Na	0.17	0.15	0.15	0.21	0.11	0.14	0.07	0.07	0.05
K	1.84	1.87	1.88	1.71	1.86	1.54	1.78	1.84	1.78
Cr	0.00	0.00	0.00	0.00	0.01	0.00	0.00	0.00	0.00
Cl						0.00			
P						0.00			
Ba	0.01				0.00	0.00	0.00	0.01	0.01
F		0.07	0.08	0.09	0.06	0.01	0.03	0.05	0.11
OH	4.00	3.93	3.92	3.91	3.94	3.98	3.97	3.95	3.89
Tetrahedral	8.00	8.00	8.00	8.00	8.00	8.00	8.00	8.00	8.00
Octahedral	4.02	4.06	4.03	4.09	4.05	4.22	4.05	4.02	4.07
Dodecahedral	2.01	2.01	2.03	1.92	1.98	1.68	1.86	1.93	1.85

Sample	SC-E1	SC-E1	SC-E1	SC-E1	SC-E1	SC-E1	SC-E1	SC-E2	SC-E2	SC-E2
Point	6	6	4	5	1	7	5	1	11	15
Description	P	P	P	P	P	P	RA	P	P	P
SiO2	46.43	45.67	45.20	45.90	45.52	44.32	45.48	46.09	45.15	45.52
TiO2	0.16	0.19	0.17	0.14	0.03	0.17	0.15	0.04	0.25	0.01
Al2O3	36.23	36.07	35.46	34.73	35.88	34.75	35.22	34.67	35.37	34.88
FeO	2.36	2.28	2.64	3.20	2.99	2.26	2.45	3.82	2.18	3.07
MnO	0.10	0.00	0.00	0.09	0.12	0.17	0.14	0.13	0.08	0.00
MgO	0.25	0.21	0.21	0.23	0.19	0.58	0.22	0.25	0.26	0.29
CaO	0.03	0.00	0.01	0.00	0.00	0.00	0.10	0.01	0.00	0.01
Na2O	1.02	1.03	1.01	0.88	1.03	0.80	1.04	0.94	1.02	1.03
K2O	10.29	10.34	10.20	10.23	10.29	10.88	9.99	10.37	10.14	10.18
Cr2O3	0.12	0.03	0.04	0.09	0.00	0.00	0.09	0.00	0.00	0.12
Cl	N/D	N/D	N/D	N/D	N/D	N/D	N/D	0.00	0.02	0.00
P2O5	N/D	N/D	N/D	N/D	N/D	N/D	N/D	0.09	0.02	0.01
BaO	N/D	0.02	0.00	0.00	0.02	0.00	0.10	0.00	0.00	0.00
F	1.46	1.49	1.53	1.50	1.40	0.28	N/D	1.77	1.50	1.55
Total	98.45	97.33	96.48	96.99	97.46	94.20	94.98	98.19	95.98	96.67
Si	6.38	6.27	6.29	6.39	6.23	6.19	6.33	6.38	6.30	6.25
Ti	0.03	0.03	0.01	0.03	0.01	0.01	0.01	0.00	0.01	0.01
Al Total	4.91	5.20	5.32	5.07	5.55	5.67	5.41	5.56	5.38	5.54
Al IV	1.62	1.73	1.71	1.61	1.77	1.81	1.67	1.62	1.70	1.75
Al VI	3.29	3.48	3.61	3.46	3.78	3.86	3.73	3.94	3.69	3.79
Fe	0.55	0.35	0.36	0.32	0.16	0.12	0.34	0.09	0.36	0.23
Mn	0.01	0.02	0.00	0.01	0.01	0.00	0.02	0.00	0.01	0.02
Mg	0.39	0.21	0.09	0.19	0.16	0.12	0.04	0.04	0.22	0.14
Ca	0.02	0.02	0.00	0.01	0.00	0.01	0.00	0.00	0.00	0.01
Na	0.09	0.15	0.12	0.29	0.09	0.13	0.06	0.03	0.10	0.11
K	1.61	1.83	1.82	1.74	1.66	1.53	1.64	1.46	1.60	1.58
Cr	0.01	0.01	0.01	0.01	0.00	0.01	0.00	0.01	0.00	0.01
Cl					0.01	0.00	0.00	0.00	0.02	0.01
P					0.00	0.00	0.00	0.00	0.00	0.00
Ba	0.01			0.00	0.00	0.00	0.00	0.01	0.01	0.00
F	0.11	0.15	0.06	0.12	0.00	0.00	0.07	0.00	0.33	0.17
OH	3.89	3.85	3.94	3.88	4.00	4.00	3.93	4.00	3.66	3.82
Tetrahedral	8.00	8.00	8.00	8.00	8.00	8.00	8.00	8.00	8.00	8.00
Octahedral	4.28	4.10	4.07	4.02	4.11	4.12	4.14	4.07	4.30	4.20
Dodecahedral	1.72	1.98	1.94	2.04	1.76	1.67	1.70	1.51	1.71	1.70

Sample	SC-E2	SC-E2	SC-E2	SC-E2	SC-E2	SC-E2	SC-E2	SC-E2	SC-E2	SC-E2
Point	16	29	31	2	3	8	13	14	2	3
Description	P	P	P	P	P	P	P	P	P	P
SiO2	45.34	44.86	45.21	44.91	45.19	45.78	45.39	45.50	45.62	45.85
TiO2	0.00	0.00	0.11	0.29	0.04	0.09	0.14	0.04	0.26	0.13
Al2O3	34.68	34.31	34.59	35.64	35.85	35.65	35.13	34.46	36.33	35.17
FeO	2.91	3.19	3.05	2.17	2.01	2.56	2.59	2.60	2.14	2.83
MnO	0.18	0.01	0.05	0.00	0.02	0.10	0.04	0.00	0.01	0.08
MgO	0.24	0.22	0.14	0.10	0.15	0.20	0.27	0.21	0.15	0.10
CaO	0.08	0.00	0.06	0.00	0.06	0.03	0.00	0.03	0.05	0.02
Na2O	0.83	0.99	0.72	1.08	0.63	0.95	0.90	0.54	1.00	0.93
K2O	10.05	10.03	10.35	10.22	7.94	10.31	10.32	10.58	10.27	10.14
Cr2O3	0.07	0.06	0.04	0.06	0.05	0.00	0.00	0.10	0.03	0.00
Cl	0.01	0.00	0.00	0.00	0.02	0.02	0.00	0.00	N/D	N/D
P2O5	0.00	0.06	0.00	0.07	0.00	0.08	0.10	0.08	N/D	N/D
BaO	0.21	0.15	0.17	0.00	0.17	0.08	0.00	0.00	N/D	N/D
F	1.39	0.00	0.00	1.49	1.10	1.48	1.16	1.01	1.29	1.68
Total	96.00	93.87	94.50	96.04	93.23	97.33	96.04	95.13	97.14	96.94
Si	6.37	6.41	6.32	6.41	6.29	6.23	6.45	6.31	6.12	6.24
Ti	0.01	0.02	0.02	0.01	0.03	0.01	0.01	0.04	0.00	0.01
Al Total	5.28	5.05	5.27	5.17	5.50	5.72	5.36	5.01	5.71	5.50
Al IV	1.63	1.59	1.68	1.59	1.71	1.77	1.55	1.69	1.88	1.76
Al VI	3.65	3.46	3.60	3.58	3.79	3.95	3.80	3.31	3.83	3.73
Fe	0.65	0.80	0.59	0.76	0.34	0.24	0.47	0.71	0.19	0.31
Mn	0.00	0.01	0.00	0.00	0.00	0.02	0.01	0.01	0.00	0.00
Mg	0.03	0.09	0.12	0.03	0.14	0.07	0.04	0.07	0.00	0.16
Ca	0.00	0.00	0.00	0.00	0.00	0.00	0.01	0.01	0.00	0.00
Na	0.17	0.12	0.16	0.13	0.18	0.15	0.09	0.11	0.21	0.18
K	1.79	1.89	1.75	1.85	1.55	1.50	1.55	1.89	1.79	1.49
Cr	0.00	0.01	0.00	0.00	0.00	0.00	0.01	0.00	0.00	0.00
Cl	0.01	0.00	0.00	0.00	0.00	0.00	0.00			0.00
P	0.01	0.00	0.01	0.00	0.00	0.02	0.00			0.00
Ba	0.00	0.01	0.00	0.00	0.00	0.00	0.00		0.00	0.00
F	0.76	0.72	0.55	0.76	0.49	0.51	0.62	0.48	0.25	0.09
OH	3.24	3.28	3.45	3.24	3.51	3.49	3.38	3.52	3.75	3.91
Tetrahedral	8.00	8.00	8.00	8.00	8.00	8.00	8.00	8.00	8.00	8.00
Octahedral	4.34	4.38	4.32	4.38	4.30	4.29	4.34	4.15	4.02	4.22
Dodecahedral	1.98	2.03	1.91	1.98	1.73	1.66	1.65	2.00	2.00	1.67

Sample	SC-E2	SC-E2	SC-E2	SC-E2	SC-E2	SC-E2	SC-E2	SC-E2	SC-E2	SC-E2
Point	4	5	6	7	6	4	1	2	3	4
Description	P	P	P	P	P	P	P	P	P	P
SiO2	45.75	45.92	45.95	46.19	45.70	45.60	44.77	44.60	45.80	45.66
TiO2	0.11	0.30	0.06	0.13	0.08	0.12	0.18	0.04	0.22	0.03
Al2O3	35.44	36.06	34.78	35.35	35.36	34.51	34.57	33.68	34.38	34.51
FeO	2.82	2.31	3.68	2.34	3.16	3.91	2.15	3.62	2.65	3.20
MnO	0.13	0.12	0.12	0.00	0.00	0.25	0.04	0.01	0.05	0.12
MgO	0.26	0.25	0.12	0.23	0.13	0.14	0.59	0.16	0.24	0.28
CaO	0.03	0.00	0.05	0.00	0.05	0.00	0.00	0.00	0.09	0.00
Na2O	1.02	1.13	1.00	1.08	0.91	0.82	0.68	0.94	0.94	0.89
K2O	10.36	10.16	10.17	10.22	10.18	10.15	10.58	10.03	10.07	10.20
Cr2O3	0.02	0.00	0.03	0.03	0.02	0.05	0.04	0.00	0.00	0.04
Cl	N/D	N/D	N/D	N/D	N/D	N/D	N/D	N/D	N/D	N/D
P2O5	N/D	N/D	N/D	N/D	N/D	N/D	N/D	N/D	N/D	N/D
BaO	N/D	N/D	N/D	N/D	0.00	0.00	0.00	0.04	0.00	0.00
F	1.57	1.45	1.78	1.55	1.47	1.60	N/D	N/D	N/D	N/D
Total	97.50	97.71	97.74	97.12	97.07	97.14	93.61	93.12	94.43	94.94
Si	6.18	6.51	6.53	6.31	6.41	6.31	6.46	6.34	6.50	6.92
Ti	0.04	0.02	0.01	0.02	0.01	0.00	0.02	0.00	0.01	0.03
Al Total	5.58	5.03	4.94	5.34	5.17	5.49	5.02	5.32	4.93	4.27
Al IV	1.82	1.49	1.47	1.69	1.59	1.69	1.54	1.66	1.50	1.08
Al VI	3.75	3.54	3.47	3.64	3.58	3.81	3.47	3.66	3.43	3.19
Fe	0.21	0.38	0.53	0.44	0.43	0.26	0.50	0.37	0.58	1.15
Mn	0.00	0.01	0.02	0.02	0.01	0.02	0.03	0.00	0.03	0.00
Mg	0.13	0.21	0.25	0.09	0.22	0.05	0.25	0.20	0.25	0.03
Ca	0.00	0.01	0.01	0.00	0.01	0.00	0.00	0.01	0.00	0.00
Na	0.14	0.02	0.05	0.05	0.03	0.03	0.05	0.09	0.04	0.04
K	1.57	1.57	1.47	1.62	1.58	1.69	1.60	1.64	1.66	1.72
Cr	0.01	0.01	0.00	0.00	0.01	0.00	0.00	0.00	0.00	0.01
Cl	0.01	0.01	0.00	0.00	0.00	0.00	0.00	0.01	0.00	0.00
P	0.01	0.02	0.00	0.00	0.00	0.00	0.01	0.00	0.00	0.00
Ba	0.00	0.00	0.01	0.00	0.00	0.00	0.01	0.00	0.00	0.00
F	0.04	0.13	0.15	0.09	0.16	0.16	0.26	0.21	0.28	0.77
OH	3.95	3.86	3.85	3.91	3.84	3.84	3.74	3.79	3.72	3.22
Tetrahedral	8.00	8.00	8.00	8.00	8.00	8.00	8.00	8.00	8.00	8.00
Octahedral	4.14	4.17	4.29	4.21	4.26	4.15	4.28	4.25	4.31	4.41
Dodecahedral	1.73	1.62	1.53	1.68	1.62	1.73	1.67	1.72	1.70	1.77

Sample	SC-E2	SC-E2	SC-E2	SC-E2	SC-E2	SC-E2	SC-E2	SC-E2	SC-E2	SC-E2
Point	6	4	5	9	12	19	21	22	23	25
Description	P	P	P	P	P	P	P	P	P	P
SiO2	45.82	44.92	44.97	45.09	44.84	45.57	45.49	45.04	45.19	45.36
TiO2	0.10	0.06	0.18	0.17	0.08	0.18	0.16	0.22	0.19	0.13
Al2O3	35.08	35.29	36.23	34.99	35.19	35.28	35.95	35.76	35.20	34.76
FeO	2.96	2.59	2.03	2.72	2.66	2.72	2.59	2.52	2.54	2.96
MnO	0.04	0.09	0.04	0.13	0.12	0.05	0.06	0.12	0.10	0.13
MgO	0.10	0.23	0.16	0.23	0.24	0.41	0.17	0.11	0.14	0.21
CaO	0.00	0.00	0.00	0.06	0.04	0.04	0.02	0.02	0.07	0.02
Na2O	1.06	1.00	0.94	0.90	1.15	0.96	1.06	1.00	1.02	0.65
K2O	10.10	10.01	9.39	9.84	10.29	9.99	10.37	10.26	10.15	10.58
Cr2O3	0.00	0.00	0.00	0.03	0.01	0.00	0.00	0.00	0.02	0.00
Cl	N/D	0.01	0.02	0.00	0.00	0.04	0.00	0.00	0.00	0.00
P2O5	N/D	0.06	0.22	0.03	0.00	0.00	0.00	0.10	0.07	0.03
BaO	0.00	0.13	0.00	0.08	0.03	0.00	0.00	0.00	0.00	0.00
F	N/D	1.42	1.28	1.42	1.58	1.25	0.94	0.31	0.00	0.00
Total	95.27	95.80	95.46	95.69	96.22	96.47	96.81	95.46	94.68	94.82
Si	6.32	6.10	6.18	6.44	6.18	6.09	6.05	6.25	6.12	6.29
Ti	0.00	0.01	0.00	0.02	0.04	0.00	0.02	0.00	0.01	0.00
Al Total	5.35	5.68	5.78	4.96	5.40	5.82	5.72	5.64	5.86	5.50
Al IV	1.68	1.90	1.82	1.56	1.82	1.91	1.95	1.75	1.88	1.71
Al VI	3.67	3.78	3.97	3.41	3.58	3.91	3.77	3.89	3.98	3.80
Fe	0.57	0.44	0.07	0.89	0.19	0.02	0.13	0.22	0.06	0.32
Mn	0.01	0.02	0.00	0.01	0.00	0.00	0.00	0.00	0.01	0.01
Mg	0.03	0.00	0.02	0.12	0.23	0.05	0.12	0.01	0.01	0.04
Ca	0.00	0.02	0.01	0.01	0.02	0.02	0.02	0.00	0.01	0.00
Na	0.10	0.17	0.05	0.13	0.12	0.04	0.13	0.12	0.06	0.06
K	1.67	1.56	1.66	1.79	1.93	1.92	1.87	1.48	1.71	1.69
Cr	0.00	0.00	0.00	0.01	0.00	0.01	0.00	0.00	0.00	0.00
Cl	0.01	0.00	0.01	0.00				0.01	0.00	0.00
P	0.00	0.01	0.00	0.01				0.01	0.00	0.00
Ba	0.01	0.00	0.01	0.00	0.00	0.01	0.00	0.00	0.00	0.01
F	0.33	0.21	0.00	0.84	0.03	0.00	0.00	0.02	0.03	0.16
OH	3.67	3.79	4.00	3.16	3.97	4.00	4.00	3.98	3.97	3.84
Tetrahedral	8.00	8.00	8.00	8.00	8.00	8.00	8.00	8.00	8.00	8.00
Octahedral	4.28	4.27	4.07	4.46	4.05	4.00	4.06	4.13	4.07	4.16
Dodecahedral	1.78	1.74	1.71	1.95	2.06	1.98	2.00	1.60	1.77	1.75

Sample	SC-E2	SC-E2	SC-E2	SC-E2	SC-E2	SC-E2	SC-E2	SC-E2	SC-E2	SC-E2
Point	26	27	28	30	33	37	38	39	44	18
Description	P	P	P	P	P	P	P	P	P	P
SiO2	45.70	44.79	45.90	44.81	43.91	45.63	46.14	45.16	45.73	45.88
TiO2	0.07	0.27	0.04	0.15	0.18	0.06	0.18	0.33	0.17	0.00
Al2O3	33.96	35.28	33.97	34.62	34.35	35.44	35.59	35.90	35.49	35.34
FeO	3.64	2.34	3.53	2.40	2.31	3.01	2.54	2.30	2.53	3.22
MnO	0.15	0.08	0.05	0.06	0.14	0.00	0.00	0.09	0.02	0.06
MgO	0.07	0.22	0.11	0.16	0.22	0.28	0.41	0.37	0.18	0.18
CaO	0.00	0.02	0.05	0.00	0.05	0.06	0.11	0.07	0.01	0.10
Na2O	0.86	1.07	0.57	1.18	0.84	0.83	1.11	1.11	0.99	0.92
K2O	10.36	10.15	10.69	10.34	10.34	10.11	10.27	10.25	10.28	10.35
Cr2O3	0.03	0.00	0.11	0.08	0.00	0.02	0.00	0.00	0.00	0.00
Cl	0.03	0.00	0.00	0.09	0.00	0.00	0.00	0.01	0.00	0.02
P2O5	0.15	0.04	0.05	0.08	0.06	0.02	0.07	0.00	0.05	0.05
BaO	0.03	0.00	0.00	0.06	0.00	0.06	0.00	0.00	0.00	0.09
F	0.00	0.00	0.00	0.00	0.00	0.00	0.00	0.00	0.00	1.37
Total	95.04	94.25	95.06	94.03	92.41	95.52	96.41	95.59	95.46	97.58
Si	6.09	6.18	6.19	6.16	6.09	6.11	6.37	6.47	6.40	6.30
Ti	0.00	0.00	0.03	0.05	0.04	0.03	0.01	0.01	0.04	0.03
Al Total	5.91	5.50	5.46	5.45	5.70	5.58	5.37	5.02	5.06	5.46
Al IV	1.91	1.82	1.81	1.84	1.91	1.89	1.63	1.53	1.60	1.70
Al VI	4.00	3.68	3.65	3.60	3.78	3.69	3.74	3.49	3.46	3.76
Fe	0.02	0.21	0.22	0.22	0.11	0.16	0.42	0.82	0.86	0.38
Mn	0.00	0.00	0.00	0.00	0.00	0.00	0.03	0.04	0.02	0.01
Mg	0.01	0.18	0.16	0.20	0.07	0.15	0.00	0.01	0.06	0.05
Ca	0.00	0.00	0.00	0.01	0.01	0.01	0.00	0.00	0.01	0.00
Na	0.16	0.11	0.09	0.13	0.17	0.19	0.11	0.07	0.14	0.18
K	1.64	1.88	1.85	1.83	1.82	1.87	1.63	1.79	1.64	1.58
Cr	0.00	0.01	0.01	0.00	0.01	0.00	0.00	0.00	0.00	0.00
Cl	0.00						0.00	0.02	0.00	0.00
P	0.00						0.01	0.01	0.00	0.00
Ba	0.01	0.02	0.00	0.01	0.00	0.00	0.00	0.00	0.00	0.01
F	0.00	0.02	0.02	0.02	0.02	0.01	0.32	0.59	0.65	0.31
OH	4.00	3.98	3.98	3.98	3.98	3.99	3.68	3.40	3.34	3.69
Tetrahedral	8.00	8.00	8.00	8.00	8.00	8.00	8.00	8.00	8.00	8.00
Octahedral	4.04	4.07	4.06	4.09	4.02	4.04	4.21	4.35	4.45	4.22
Dodecahedral	1.81	2.01	1.95	1.97	1.99	2.06	1.75	1.88	1.79	1.76

Sample	SC-E2	SC-E2	SC-E2	SC-E2	SC-E2	SC-E3	SC-E3	SC-E3	SC-E3
Point	45	6	10	20	40	1	3	1	3
Description	P	P	P	P	P	P	P	P	P
SiO2	45.81	45.43	45.59	45.84	45.95	52.67	49.01	49.06	49.75
TiO2	0.18	0.12	0.00	0.09	0.19	0.07	0.10	0.11	0.06
Al2O3	34.76	34.73	34.81	35.37	35.28	19.17	21.25	20.31	19.91
FeO	2.34	1.83	2.81	2.54	2.60	7.77	9.37	9.31	8.22
MnO	0.08	0.05	0.06	0.00	0.05	0.46	0.67	0.55	0.49
MgO	0.28	0.66	0.16	0.21	0.30	0.34	0.85	0.79	0.68
CaO	0.00	0.03	0.00	0.05	0.02	0.00	0.00	0.03	0.02
Na2O	0.51	1.09	0.94	0.90	0.85	0.22	0.24	0.36	0.18
K2O	10.97	10.12	10.15	10.18	10.40	11.02	10.94	10.81	10.79
Cr2O3	0.00	0.00	0.00	0.04	0.02	0.04	0.03	0.03	0.06
Cl	0.00	0.04	0.00	0.01	0.00	N/D	N/D	N/D	N/D
P2O5	0.02	0.10	0.00	0.08	0.01	N/D	N/D	N/D	N/D
BaO	0.16	0.05	0.02	0.16	0.00	N/D	N/D	N/D	0.00
F	0.00	1.61	1.31	0.98	0.00	6.95	6.52	6.61	6.84
Total	95.12	95.85	95.86	96.46	95.66	98.69	98.98	97.97	97.00
Si	6.51	6.59	6.20	6.54	6.50	6.37	6.55	6.60	6.52
Ti	0.01	0.00	0.00	0.01	0.00	0.01	0.05	0.03	0.03
Al Total	5.19	4.99	5.70	4.80	5.10	5.34	4.80	4.73	4.69
Al IV	1.49	1.41	1.80	1.46	1.50	1.63	1.45	1.40	1.48
Al VI	3.71	3.58	3.89	3.34	3.60	3.72	3.35	3.33	3.21
Fe	0.17	0.57	0.16	0.97	0.50	0.36	0.91	1.01	1.17
Mn	0.00	0.00	0.01	0.00	0.01	0.00	0.01	0.00	0.04
Mg	0.16	0.02	0.00	0.04	0.04	0.09	0.16	0.13	0.13
Ca	0.00	0.01	0.00	0.00	0.00	0.01	0.00	0.00	0.00
Na	0.01	0.04	0.08	0.08	0.03	0.06	0.08	0.07	0.08
K	1.54	1.69	1.69	1.57	1.69	1.64	1.78	1.63	1.78
Cr	0.01	0.00	0.00	0.00	0.00	0.00	0.01	0.01	0.00
Cl	0.00	0.00	0.00	0.03	0.00	0.00	0.00	0.00	0.00
P	0.01	0.00	0.00	0.01	0.00	0.00	0.00	0.01	0.01
Ba	0.00	0.00	0.01	0.00	0.00	0.00	0.00	0.00	0.01
F	0.00	0.25	0.01	0.33	0.16	0.17	0.84	0.76	0.86
OH	4.00	3.75	3.99	3.65	3.84	3.83	3.16	3.24	3.14
Tetrahedral	8.00	8.00	8.00	8.00	8.00	8.00	8.00	8.00	8.00
Octahedral	4.06	4.18	4.06	4.36	4.15	4.18	4.48	4.51	4.58
Dodecahedral	1.57	1.74	1.78	1.67	1.73	1.70	1.87	1.71	1.88

Sample	SC-1-MB	SC-1-MB	SC-1-MB	SC-1-MB	SC-1-MB	SC-1-MB	SC-1-MB
Point	5	7	8	1	2	3	4
Description	RB	RB	RB	RF	RF	RF	RF
SiO2	45.31	45.14	46.02	44.94	44.04	45.62	45.20
TiO2	0.36	0.45	0.10	0.47	0.68	0.27	0.28
Al2O3	32.34	31.57	34.14	34.11	33.37	34.92	33.38
FeO	3.41	2.50	1.96	1.64	1.30	1.49	2.33
MnO	0.01	0.02	0.02	0.00	0.00	0.00	0.08
MgO	1.58	1.45	1.26	0.66	0.77	0.84	1.10
CaO	0.02	0.00	0.01	0.02	0.08	0.04	0.01
Na2O	0.40	0.35	0.46	0.51	0.54	0.37	0.40
K2O	10.86	10.60	10.91	10.69	10.36	11.20	10.75
Cr2O3	0.00	0.00	0.00	0.00	0.01	0.04	0.03
Cl	0.01	0.10	0.01	0.06	0.14	0.00	0.04
P2O5	0.10	0.00	0.00	0.00	0.02	0.08	0.00
BaO	0.15	0.00	0.21	0.02	0.00	0.13	0.44
F	0.20	0.31	0.20	0.12	0.21	0.10	0.04
Total	94.74	92.50	95.30	93.24	91.52	95.08	94.08
Si	6.22	6.36	7.00	6.23	6.48	6.20	6.45
Ti	0.00	0.01	0.00	0.00	0.01	0.01	0.00
Al Total	5.77	5.32	4.85	5.78	5.19	5.78	5.09
Al IV	1.78	1.64	1.00	1.77	1.52	1.80	1.55
Al VI	3.99	3.68	3.86	4.01	3.68	3.98	3.54
Fe	0.06	0.71	0.18	0.06	0.64	0.03	0.41
Mn	0.01	0.02	0.04	0.02	0.04	0.01	0.02
Mg	0.00	0.02	0.04	0.01	0.01	0.03	0.03
Ca	0.01	0.01	0.02	0.01	0.00	0.00	0.00
Na	0.03	0.19	0.06	0.02	0.13	0.04	0.08
K	1.61	1.60	1.61	1.61	1.63	1.62	1.92
Cr	0.01	0.01	0.00	0.00	0.01	0.00	0.00
Cl	0.01	0.00	0.00	0.00	0.00	0.00	
P	0.00	0.01	0.00	0.01	0.00	0.00	
Ba	0.01	0.00	0.00	0.01	0.00	0.00	0.00
F	0.05	0.80	0.83	0.15	0.75	0.01	
OH	3.95	3.20	3.17	3.85	3.25	3.99	4.00
Tetrahedral	8.00	8.00	8.00	8.00	8.00	8.00	8.00
Octahedral	4.08	4.45	4.14	4.11	4.38	4.06	4.00
Dodecahedral	1.66	1.81	1.68	1.64	1.77	1.66	2.00

Sample	SC-3-MB	SC-3-MB	SC-3-MB	SC-3-MB	SC-3-MB	SC-3-MB	SC-3-MB
Point	1	1b	3	2	7	8	11
Description	P	P	RB	RF	RF	RF	RF
SiO2	46.09	45.10	44.89	45.56	45.29	45.65	42.89
TiO2	0.55	0.39	0.46	0.30	0.47	0.48	0.44
Al2O3	34.60	34.11	32.47	35.66	34.60	35.06	33.07
FeO	1.65	1.69	2.71	1.10	1.63	1.41	1.49
MnO	0.02	0.03	0.00	0.00	0.00	0.00	0.00
MgO	0.86	0.83	1.38	0.66	0.72	0.80	0.70
CaO	0.01	0.00	0.08	0.01	0.05	0.06	0.00
Na2O	0.59	0.61	0.48	0.58	0.53	0.51	0.60
K2O	10.82	10.79	10.68	11.03	10.79	11.20	10.13
Cr2O3	0.01	0.06	0.00	0.05	0.00	0.06	0.00
Cl	0.04	0.06	0.03	0.01	0.02	0.00	0.22
P2O5	0.08	0.04	0.00	0.00	0.02	0.00	0.02
BaO	0.13	0.11	0.14	0.33	0.00	0.16	0.28
F	0.14	0.26	0.12	0.10	0.08	0.10	0.18
Total	95.57	94.08	93.44	95.36	94.20	95.49	90.01
Si	6.22	6.14	6.23	6.20	6.05	6.27	6.30
Ti	0.02	0.00	0.00	0.01	0.01	0.02	0.01
Al Total	5.47	5.61	5.45	5.42	5.93	5.55	5.45
Al IV	1.78	1.86	1.77	1.80	1.95	1.73	1.70
Al VI	3.70	3.75	3.68	3.62	3.98	3.82	3.74
Fe	0.17	0.16	0.24	0.32	0.10	0.34	0.35
Mn	0.00	0.00	0.00	0.01	0.00	0.02	0.00
Mg	0.15	0.13	0.24	0.24	0.02	0.07	0.17
Ca	0.00	0.00	0.00	0.00	0.00	0.02	0.00
Na	0.14	0.23	0.09	0.14	0.11	0.14	0.18
K	1.82	1.77	1.66	1.64	1.66	1.54	1.51
Cr	0.00	0.01	0.00	0.00	0.01	0.00	0.00
Cl			0.00	0.00	0.01	0.01	0.00
P			0.01	0.02	0.00	0.00	0.01
Ba	0.00	0.00	0.00	0.00	0.00	0.00	0.00
F			0.07	0.11	0.08	0.35	0.35
OH	4.00	4.00	3.93	3.89	3.92	3.64	3.65
Tetrahedral	8.00	8.00	8.00	8.00	8.00	8.00	8.00
Octahedral	4.04	4.04	4.16	4.21	4.11	4.28	4.27
Dodecahedral	1.96	2.01	1.77	1.80	1.78	1.69	1.70

Sample	SC-3-MB	SC-3-MB	SC-4-MB	SC-4-MB	SC-4-MB	SC-4-MB	SC-5-MB
Point	12	13	1	3	6	8	4
Description	RF	RF	S	S	S	S	RB
SiO2	44.87	44.96	47.30	47.20	47.71	46.52	44.79
TiO2	0.38	0.38	0.21	0.09	0.09	0.26	0.57
Al2O3	33.90	34.12	32.90	32.39	30.92	30.38	33.85
FeO	1.83	1.57	1.57	1.67	1.75	4.77	1.68
MnO	0.07	0.09	0.13	0.00	0.00	0.08	0.13
MgO	0.94	0.85	1.01	1.10	1.73	1.90	0.80
CaO	0.05	0.02	0.05	0.03	0.09	0.13	0.12
Na2O	0.52	0.66	0.26	0.27	0.19	0.34	0.59
K2O	10.48	10.46	10.36	10.62	10.23	9.23	10.43
Cr2O3	0.05	0.00	0.00	0.04	0.04	0.06	0.06
Cl	0.05	0.08	0.01	0.00	0.03	0.03	0.09
P2O5	0.02	0.01	0.00	0.00	0.00	0.00	0.02
BaO	0.00	0.15	0.09	0.20	0.20	0.15	0.61
F	0.13	0.28	0.12	0.22	0.49	0.49	0.11
Total	93.27	93.64	94.01	93.82	93.47	94.33	93.86
Si	6.12	6.13	6.19	6.01	6.21	6.11	6.72
Ti	0.00	0.00	0.01	0.03	0.01	0.00	0.00
Al Total	5.72	5.67	5.48	5.84	5.49	5.80	4.80
Al IV	1.88	1.87	1.81	1.99	1.79	1.89	1.28
Al VI	3.83	3.80	3.67	3.85	3.70	3.91	3.53
Fe	0.16	0.14	0.26	0.14	0.19	0.10	0.36
Mn	0.00	0.00	0.00	0.00	0.00	0.00	0.00
Mg	0.02	0.09	0.12	0.04	0.13	0.01	0.18
Ca	0.00	0.00	0.01	0.00	0.00	0.00	0.01
Na	0.17	0.13	0.14	0.19	0.20	0.26	0.02
K	1.84	1.86	1.81	1.77	1.78	1.68	1.53
Cr	0.00	0.00	0.00	0.00	0.00	0.00	0.00
Cl							0.00
P							0.00
Ba	0.00	0.00	0.00	0.00		0.00	0.00
F			0.19		0.11		0.00
OH	4.00	4.00	3.81	4.00	3.89	4.00	4.00
Tetrahedral	8.00	8.00	8.00	8.00	8.00	8.00	8.00
Octahedral	4.02	4.03	4.08	4.06	4.03	4.02	4.08
Dodecahedral	2.01	1.99	1.96	1.97	1.99	1.94	1.56

Sample	SC-5-MB	SC-5-MB	SC-5-MB	SC-8-MB	SC-8-MB	SC-8-MB	SC-8-MB
Point	6	2	8	5	3	6	7
Description	RB	RF	RF	P	S	S	S
SiO2	46.31	45.07	45.33	45.41	45.70	45.99	45.75
TiO2	0.00	0.60	0.47	0.35	0.39	0.03	0.21
Al2O3	36.11	34.53	34.63	34.75	33.85	37.30	36.68
FeO	1.31	1.57	1.67	1.55	1.66	0.22	1.19
MnO	0.03	0.00	0.04	0.00	0.01	0.00	0.00
MgO	0.75	0.69	0.85	0.72	1.13	0.25	0.61
CaO	0.00	0.09	0.05	0.09	0.16	0.12	0.11
Na2O	0.60	0.71	0.57	0.58	0.47	0.15	0.52
K2O	10.66	10.20	10.80	10.66	11.20	11.40	11.08
Cr2O3	0.00	0.00	0.10	0.02	0.00	0.09	0.00
Cl	0.02	0.06	0.02	0.01	0.00	0.02	0.04
P2O5	0.04	0.00	0.00	0.00	0.00	0.05	0.00
BaO	0.09	0.55	0.02	0.05	0.04	0.18	0.00
F	0.00	0.16	0.10	0.13	0.13	0.00	0.00
Total	95.92	94.24	94.64	94.31	94.73	95.80	96.18
Si	6.45	6.37	6.39	6.15	6.11	6.13	6.17
Ti	0.01	0.01	0.00	0.01	0.00	0.00	0.02
Al Total	4.79	5.28	5.20	5.48	5.70	5.66	5.56
Al IV	1.55	1.63	1.61	1.85	1.89	1.87	1.83
Al VI	3.24	3.65	3.59	3.63	3.80	3.79	3.74
Fe	1.12	0.56	0.63	0.35	0.20	0.17	0.18
Mn	0.01	0.01	0.02	0.01	0.00	0.00	0.00
Mg	0.03	0.03	0.02	0.07	0.04	0.07	0.11
Ca	0.01	0.00	0.00	0.00	0.00	0.00	0.00
Na	0.08	0.14	0.10	0.19	0.17	0.22	0.13
K	1.74	1.53	1.58	1.86	1.82	1.78	1.84
Cr	0.00	0.00	0.01	0.00	0.00	0.00	0.00
Cl	0.00	0.00	0.00				
P	0.00	0.01	0.00				
Ba	0.00	0.00	0.01	0.00	0.00		
F	0.39	0.28	0.25	0.13	0.08	0.10	0.10
OH	3.61	3.72	3.75	3.87	3.92	3.90	3.90
Tetrahedral	8.00	8.00	8.00	8.00	8.00	8.00	8.00
Octahedral	4.42	4.26	4.27	4.07	4.05	4.03	4.04
Dodecahedral	1.83	1.68	1.70	2.05	1.98	2.00	1.97

Sample	SC-9-MB	SC-9-MB	SC-9-MB	SC-9-MB	SC-9-MB	SC-9-MB	SC-1-D	SC-1-D
Point	4	1	5	6	7	8	5	3
Description	RB	S	S	S	S	S	IM	RF
SiO2	45.20	45.26	45.51	45.43	44.89	44.86	47.59	47.44
TiO2	0.00	0.00	0.30	0.50	0.40	0.30	0.23	0.15
Al2O3	35.89	34.18	34.03	34.11	35.66	34.72	38.05	37.49
FeO	1.32	1.82	1.92	1.95	0.98	1.37	0.98	1.15
MnO	0.00	0.00	0.00	0.01	0.00	0.00	0.07	0.04
MgO	0.62	0.91	0.79	1.01	0.37	0.73	0.51	0.55
CaO	0.03	0.00	0.00	0.09	0.09	0.09	0.01	0.04
Na2O	0.75	0.42	0.33	0.50	0.63	0.70	0.67	0.60
K2O	10.68	10.80	10.67	10.57	10.52	10.77	9.24	9.89
Cr2O3	0.07	0.07	0.08	0.00	0.05	0.00	0.00	0.01
Cl	0.00	0.00	0.01	0.03	0.00	0.00	0.02	0.00
P2O5	0.01	0.00	0.08	0.00	0.00	0.00	0.04	0.00
BaO	0.17	0.29	0.01	0.20	0.07	0.08	0.18	0.00
F	0.00	0.09	0.11	0.09	0.11	0.06	0.00	0.00
Total	94.75	93.82	93.83	94.47	93.78	93.68	97.59	97.36
Si	6.35	6.15	6.16	6.28	6.13	6.29	6.10	6.20
Ti	0.00	0.02	0.03	0.00	0.00	0.00	0.00	0.01
Al Total	5.32	5.53	5.52	5.34	5.84	5.53	5.69	5.50
Al IV	1.65	1.85	1.84	1.72	1.87	1.71	1.90	1.80
Al VI	3.67	3.68	3.68	3.62	3.96	3.81	3.79	3.69
Fe	0.19	0.20	0.19	0.56	0.07	0.29	0.18	0.19
Mn	0.00	0.01	0.00	0.02	0.01	0.00	0.01	0.02
Mg	0.09	0.15	0.13	0.02	0.01	0.00	0.11	0.14
Ca	0.00	0.00	0.00	0.01	0.00	0.00	0.00	0.01
Na	0.32	0.17	0.14	0.10	0.12	0.03	0.16	0.18
K	1.70	1.80	1.90	1.68	1.59	1.64	1.80	1.79
Cr	0.01	0.01	0.00	0.01	0.01	0.00	0.00	0.00
Cl				0.00	0.01	0.00		
P				0.00	0.01	0.00		
Ba	0.01	0.00	0.00	0.00	0.01	0.00	0.00	0.00
F	0.04	0.13	0.09	0.21	0.00	0.00	0.07	0.10
OH	3.96	3.87	3.91	3.79	4.00	4.00	3.93	3.90
Tetrahedral	8.00	8.00	8.00	8.00	8.00	8.00	8.00	8.00
Octahedral	3.96	4.07	4.03	4.23	4.06	4.11	4.08	4.06
Dodecahedral	2.04	1.97	2.04	1.80	1.73	1.68	1.96	1.98

Sample	SC-1-D	SC-1-D	SC-1-D	SC-1-D	SC-1-D	SC-1-D	SC-1-D	SC-1-D	SC-1-D
Point	3b	3c	6	7	8	9	10	11	12
Description	RF	RF	RF	RF	RF	RF	RF	RF	RF
SiO2	47.54	47.59	48.35	47.20	47.19	46.59	47.73	47.16	47.74
TiO2	0.00	0.06	0.02	0.16	0.07	0.08	0.10	0.00	0.02
Al2O3	37.47	36.04	35.82	36.67	37.32	36.75	37.11	37.33	36.42
FeO	1.02	1.47	1.76	1.24	0.99	1.28	1.56	0.91	1.15
MnO	0.00	0.03	0.01	0.01	0.01	0.04	0.00	0.00	0.09
MgO	0.41	0.84	1.13	0.59	0.64	0.58	0.70	0.48	0.89
CaO	0.02	0.05	0.00	0.03	0.02	0.00	0.03	0.00	0.01
Na2O	0.39	0.42	0.53	0.36	0.63	0.41	0.41	0.73	0.64
K2O	10.09	10.15	9.66	9.69	10.06	9.04	9.40	9.86	9.06
Cr2O3	0.06	0.01	0.00	0.00	0.00	0.11	0.00	0.00	0.10
Cl	0.00	0.01	0.00	0.01	0.00	0.00	0.00	0.00	0.03
P2O5	0.00	0.00	0.00	0.09	0.04	0.01	0.00	0.00	0.00
BaO	0.00	0.09	0.00	0.00	0.18	0.01	0.09	0.17	0.08
F	0.00	0.00	0.00	0.00	0.00	0.00	0.00	0.00	0.00
Total	97.00	96.76	97.28	96.05	97.15	94.90	97.13	96.64	96.23
Si	6.15	6.09	6.08	6.08	6.09	6.10	6.11	6.11	6.08
Ti	0.02	0.03	0.00	0.00	0.02	0.01	0.01	0.02	0.00
Al Total	5.40	5.57	5.77	5.77	5.72	5.72	5.74	5.71	5.74
Al IV	1.85	1.91	1.92	1.92	1.91	1.90	1.89	1.89	1.92
Al VI	3.54	3.66	3.86	3.85	3.80	3.82	3.85	3.81	3.82
Fe	0.22	0.25	0.14	0.15	0.17	0.17	0.15	0.16	0.17
Mn	0.00	0.01	0.00	0.01	0.00	0.01	0.00	0.01	0.00
Mg	0.17	0.12	0.02	0.03	0.03	0.03	0.03	0.04	0.05
Ca	0.01	0.01	0.00	0.01	0.01	0.00	0.00	0.00	0.00
Na	0.43	0.18	0.20	0.15	0.23	0.22	0.15	0.18	0.24
K	1.90	1.87	1.82	1.84	1.79	1.78	1.78	1.81	1.76
Cr	0.00	0.00	0.00	0.00	0.00	0.00	0.00	0.00	0.00
Cl									
P									
Ba	0.00	0.00	0.00	0.00			0.00	0.00	0.00
F	0.05				0.00	0.00	0.00	0.02	0.00
OH	3.95	4.00	4.00	4.00	4.00	4.00	4.00	3.98	4.00
Tetrahedral	8.00	8.00	8.00	8.00	8.00	8.00	8.00	8.00	8.00
Octahedral	3.97	4.07	4.02	4.04	4.03	4.04	4.04	4.03	4.05
Dodecahedral	2.33	2.05	2.02	1.99	2.02	2.00	1.93	1.99	2.00

Sample	SC-1-D	SC-1-D	SC-1-D	SC-1-D	SC-1-D	SC-1-D	SC-1-D	SC-1-D	SC-2-D
Point	12b	12c	13	13b	13c	1	2	4	1
Description	RF	RF	RF	RF	RF	S	S	S	RB
SiO2	46.24	50.13	47.32	47.55	47.47	47.04	48.52	47.65	46.66
TiO2	0.00	0.00	0.14	0.05	0.12	0.12	0.03	0.00	0.00
Al2O3	37.29	31.90	37.09	36.01	37.12	38.12	36.46	36.24	37.06
FeO	1.19	1.93	1.41	1.56	1.11	0.88	1.50	1.61	1.18
MnO	0.04	0.08	0.08	0.07	0.00	0.00	0.00	0.08	0.12
MgO	0.57	1.71	0.73	0.88	0.60	0.23	0.90	0.72	0.73
CaO	0.00		0.00	0.00	0.07	0.02	0.02	0.13	0.00
Na2O	0.51	0.22	0.52	0.43	0.56	0.49	0.42	0.38	0.79
K2O	9.30	8.70	10.04	10.44	10.10	9.77	9.32	10.00	10.64
Cr2O3	0.03	0.08	0.10	0.02	0.06	0.00	0.04	0.00	0.08
Cl	0.00	0.03	0.02	0.01	0.02	0.04	0.00	0.00	N/D
P2O5	0.00	0.04	0.05	0.12	0.08	0.00	0.00	0.01	N/D
BaO	0.26	0.19	0.00	0.22	0.04	0.16	0.00	0.17	0.07
F	0.00	0.07	0.00	0.00	0.00	0.00	0.00	0.00	0.02
Total	95.43	95.08	97.50	97.36	97.35	96.87	97.21	96.99	97.34
Si	6.12	6.10	6.04	6.23	6.43	6.28	6.21	6.35	6.14
Ti	0.01	0.02	0.02	0.00	0.01	0.00	0.01	0.01	0.00
Al Total	5.69	5.65	5.63	5.77	5.32	5.56	5.77	5.42	5.48
Al IV	1.88	1.90	1.96	1.77	1.57	1.72	1.79	1.65	1.86
Al VI	3.82	3.75	3.67	4.01	3.74	3.84	3.99	3.76	3.62
Fe	0.12	0.15	0.26	0.05	0.65	0.41	0.04	0.64	0.40
Mn	0.00	0.01	0.00	0.03	0.03	0.02	0.02	0.03	0.00
Mg	0.08	0.09	0.13	0.00	0.05	0.01	0.02	0.04	0.07
Ca	0.00	0.01	0.00	0.01	0.01	0.00	0.00	0.00	0.00
Na	0.17	0.14	0.19	0.02	0.14	0.19	0.04	0.18	0.19
K	1.81	1.89	1.88	1.60	1.37	1.50	1.61	1.50	1.86
Cr	0.00	0.00	0.00	0.00	0.00	0.00	0.00	0.00	0.00
Cl				0.00	0.00	0.00	0.03	0.00	
P				0.01	0.01	0.02	0.01	0.00	
Ba	0.00	0.00	0.00	0.01	0.00	0.01	0.00	0.00	0.00
F		0.01	0.04	0.16	0.72	0.48	0.04	0.79	0.08
OH	4.00	3.99	3.96	3.84	3.28	3.52	3.94	3.21	3.92
Tetrahedral	8.00	8.00	8.00	8.00	8.00	8.00	8.00	8.00	8.00
Octahedral	4.03	4.03	4.09	4.11	4.49	4.28	4.08	4.49	4.10
Dodecahedral	1.98	2.03	2.07	1.65	1.52	1.71	1.67	1.68	2.05

Sample	SC-2-D	SC-2-D	SC-2-D	SC-2-D	SC-2-D	SC-5-D	SC-5-D	SC-5-D	SC-5-D
Point	3	3	4	4	4	2	7	8	9
Description	RC	RC	RF	RF	RF	RF	RF	RF	RF
SiO2	46.66	46.50	44.88	46.71	46.67	47.09	47.19	47.56	46.77
TiO2	0.21	0.00	0.04	0.00	0.18	0.12	0.22	0.17	0.10
Al2O3	34.83	36.06	34.73	35.89	35.67	36.77	37.15	36.71	35.95
FeO	1.51	1.44	2.27	1.13	1.61	1.27	1.42	1.23	1.46
MnO	0.00	0.00	0.00	0.00	0.00	0.00	0.03	0.00	0.12
MgO	0.74	0.66	0.74	0.64	0.69	0.60	0.57	0.69	0.76
CaO	0.02	0.00	0.00	0.01	0.05	0.04	0.05	0.10	0.04
Na2O	0.55	0.92	0.73	0.72	0.61	0.58	0.56	0.57	0.49
K2O	10.68	10.50	10.80	10.59	10.85	9.91	9.81	10.00	10.69
Cr2O3	0.01	0.05	0.06	0.00	0.00	0.00	0.09	0.00	0.06
Cl	N/D	N/D	N/D	N/D	N/D	0.05	0.00	0.01	0.02
P2O5	N/D	N/D	N/D	N/D	N/D	0.03	0.00	0.00	0.08
BaO	0.06	0.09	0.24	N/D	0.10	0.04	0.07	0.00	0.10
F	N/D	N/D	N/D	0.02	0.04	0.00	0.00	0.00	0.00
Total	95.28	96.23	94.50	95.72	96.46	96.50	97.16	97.04	96.64
Si	6.12	6.49	6.26	6.08	6.41	6.19	6.00	6.08	6.08
Ti	0.00	0.05	0.00	0.00	0.01	0.02	0.04	0.01	0.00
Al Total	5.66	4.77	5.63	6.00	5.42	5.48	5.76	5.75	5.73
Al IV	1.88	1.51	1.74	1.92	1.59	1.81	2.00	1.92	1.92
Al VI	3.77	3.26	3.89	4.08	3.82	3.68	3.76	3.84	3.81
Fe	0.14	0.64	0.10	0.08	0.19	0.19	0.17	0.15	0.17
Mn	0.00	0.02	0.02	0.00	0.00	0.01	0.00	0.00	0.01
Mg	0.13	0.05	0.04	0.00	0.11	0.16	0.15	0.05	0.05
Ca	0.00	0.01	0.01	0.00	0.00	0.00	0.00	0.00	0.01
Na	0.19	0.14	0.09	0.13	0.07	0.23	0.21	0.21	0.15
K	1.80	1.91	1.52	1.47	1.61	1.74	1.72	1.76	1.81
Cr	0.00	0.01	0.01	0.00	0.00	0.00	0.00	0.00	0.01
Cl			0.01	0.00	0.00				
P			0.02	0.00	0.00				
Ba	0.01	0.00	0.00	0.00	0.00	0.00	0.00	0.01	
F			0.00	0.11	0.21				0.00
OH	4.00	4.00	4.00	3.89	3.79	4.00	4.00	4.00	4.00
Tetrahedral	8.00	8.00	8.00	8.00	8.00	8.00	8.00	8.00	8.00
Octahedral	4.06	4.03	4.05	4.17	4.14	4.06	4.12	4.05	4.06
Dodecahedral	2.01	2.05	1.64	1.61	1.69	1.97	1.94	1.97	1.97

Sample	SC-5-D	SC-5-D	SC-5-D	SC-6-D	SC-6-D	SC-6-D	SC-6-D	SC-6-D	SC-6-D
Point	10	1	5	1	10	4	8	5	11
Description	RF	S	S	FF	FF	RA	RA	RB	RB
SiO2	47.14	47.93	47.23	47.47	48.45	46.83	46.90	47.53	47.76
TiO2	0.17	0.08	0.10	0.12	0.02	0.00	0.15	0.00	0.06
Al2O3	36.70	36.28	36.73	37.11	37.04	36.94	36.94	37.77	37.17
FeO	1.39	1.46	1.14	1.30	1.18	1.45	1.15	1.22	1.18
MnO	0.10	0.05	0.00	0.05	0.05	0.00	0.00	0.00	0.00
MgO	0.62	0.82	0.59	0.62	0.59	0.76	0.58	0.47	0.51
CaO	0.00	0.00	0.05	0.06	0.01	0.00	0.01	0.02	0.08
Na2O	0.54	0.36	0.52	0.44	0.46	0.59	0.51	0.63	0.47
K2O	10.02	10.03	9.17	9.47	9.65	9.33	9.11	9.58	9.48
Cr2O3	0.00	0.00	0.08	0.00	0.00	0.09	0.00	0.00	0.00
Cl	0.00	0.02	0.00	0.00	0.01	0.00	0.01	0.01	0.03
P2O5	0.10	0.00	0.00	0.08	0.01	0.00	0.11	0.02	0.00
BaO	0.02	0.08	0.00	0.00	0.09	0.05	0.00	0.24	0.00
F	0.00	0.00	0.00	0.00	0.00	0.00	0.00	0.00	0.00
Total	96.80	97.11	95.61	96.72	97.56	96.04	95.47	97.49	96.74
Si	6.06	6.04	6.12	6.29	6.27	6.26	6.52	6.67	6.23
Ti	0.01	0.03	0.01	0.01	0.01	0.01	0.01	0.01	0.01
Al Total	5.80	5.79	5.72	5.36	5.50	5.39	5.22	4.73	5.43
Al IV	1.94	1.96	1.88	1.71	1.73	1.74	1.48	1.33	1.77
Al VI	3.86	3.83	3.83	3.66	3.76	3.65	3.74	3.40	3.66
Fe	0.14	0.13	0.15	0.56	0.44	0.54	0.16	0.81	0.48
Mn	0.00	0.01	0.01	0.00	0.01	0.01	0.00	0.00	0.01
Mg	0.02	0.04	0.05	0.01	0.01	0.03	0.17	0.01	0.02
Ca	0.00	0.00	0.00	0.00	0.01	0.00	0.01	0.01	0.00
Na	0.20	0.20	0.15	0.12	0.14	0.14	0.02	0.07	0.15
K	1.82	1.78	1.76	1.61	1.49	1.62	1.47	1.69	1.62
Cr	0.00	0.00	0.00	0.01	0.00	0.00	0.00	0.01	0.01
Cl				0.00	0.00	0.01	0.00	0.00	0.01
P				0.00	0.01	0.01	0.01	0.00	0.01
Ba	0.00	0.00	0.00	0.00	0.00	0.00	0.00	0.00	0.00
F	0.00			0.21	0.18	0.23	0.00	0.33	0.11
OH	4.00	4.00	4.00	3.78	3.82	3.77	4.00	3.67	3.88
Tetrahedral	8.00	8.00	8.00	8.00	8.00	8.00	8.00	8.00	8.00
Octahedral	4.02	4.05	4.05	4.24	4.24	4.25	4.09	4.23	4.19
Dodecahedral	2.02	1.98	1.92	1.74	1.63	1.77	1.50	1.77	1.78

Sample	SC-6-D	SC-6-D	SC-6-D	SC-6-D	SC-6-D	SC-6-D	SC-6-D	SC-11-D	SC-11-D
Point	11b	2	2b	3	6	7	7b	1	5
Description	RB	RF	RF	RF	RF	RF	RF	G	G
SiO2	48.38	47.75	49.42	47.37	47.38	47.86	47.82	49.62	46.76
TiO2	0.04	0.14	0.11	0.00	0.00	0.12	0.02	0.00	0.02
Al2O3	35.50	37.56	36.00	37.39	36.22	37.43	37.96	32.03	34.97
FeO	1.94	0.97	1.21	1.36	1.73	1.12	1.14	1.19	2.70
MnO	0.16	0.16	0.03	0.00	0.15	0.03	0.00	0.32	0.17
MgO	1.18	0.51	0.84	0.63	0.77	0.64	0.57	0.06	0.07
CaO	0.03	0.00	0.00	0.00	0.04	0.01	0.00	0.02	0.00
Na2O	0.28	0.49	0.28	0.58	0.54	0.49	0.43	0.34	0.54
K2O	9.85	9.48	9.64	9.53	9.45	9.51	9.94	10.73	10.28
Cr2O3	0.00	0.00	0.06	0.02	0.02	0.08	0.18	0.03	0.03
Cl	0.00	0.00	0.00	0.04	0.00	0.02	0.00	N/D	N/D
P2O5	0.00	0.02	0.00	0.01	0.00	0.00	0.00	N/D	N/D
BaO	0.01	0.00	0.02	0.11	0.19	0.12	0.00	0.00	0.00
F	0.00	0.00	0.00	0.00	0.00	0.00	0.00	2.18	1.19
Total	97.37	97.08	97.61	97.04	96.49	97.43	98.06	96.51	96.71
Si	6.25	6.13	6.34	6.76	6.17	6.22	6.21	6.04	6.12
Ti	0.00	0.00	0.03	0.01	0.01	0.03	0.03	0.04	0.01
Al Total	5.65	5.76	5.41	4.72	5.56	5.51	5.52	5.69	5.60
Al IV	1.75	1.87	1.66	1.24	1.83	1.78	1.79	1.96	1.88
Al VI	3.89	3.89	3.75	3.48	3.74	3.73	3.73	3.72	3.72
Fe	0.37	0.23	0.44	0.80	0.31	0.33	0.31	0.25	0.31
Mn	0.00	0.00	0.00	0.00	0.01	0.01	0.00	0.00	0.02
Mg	0.01	0.04	0.07	0.06	0.04	0.02	0.04	0.05	0.02
Ca	0.01	0.01	0.00	0.01	0.00	0.00	0.01	0.00	0.00
Na	0.15	0.10	0.12	0.06	0.21	0.18	0.10	0.28	0.25
K	1.52	1.47	1.59	1.52	1.60	1.56	1.65	1.75	1.74
Cr	0.01	0.01	0.00	0.00	0.01	0.00	0.00	0.00	0.01
Cl	0.00	0.00	0.00	0.00	0.00	0.00	0.01		
P	0.01	0.03	0.00	0.00	0.00	0.00	0.00		
Ba	0.00	0.01	0.00	0.01	0.00	0.00	0.00	0.00	0.01
F	0.49	0.14	0.48	0.57	0.00	0.00	0.00	0.34	0.29
OH	3.51	3.86	3.52	3.43	4.00	4.00	3.99	3.66	3.71
Tetrahedral	8.00	8.00	8.00	8.00	8.00	8.00	8.00	8.00	8.00
Octahedral	4.29	4.18	4.29	4.36	4.12	4.12	4.12	4.07	4.07
Dodecahedral	1.70	1.62	1.72	1.58	1.82	1.74	1.76	2.03	2.01

Sample	SC-11-D	SC-11-D	SC-11-D	SC-11-D	SC-11-D	SC-11-D	SC-11-D	SC-11-D
Point	1	2	6	8	9	11	1	2
Description	P	P	P	P	P	P	P	P
SiO2	45.79	48.57	47.30	46.92	46.19	47.14	48.52	46.62
TiO2	0.08	0.02	0.04	0.00	0.06	0.03	0.00	0.11
Al2O3	30.95	34.07	32.20	36.76	30.92	33.20	38.13	32.74
FeO	6.24	1.30	4.52	0.27	6.78	3.59	0.51	5.65
MnO	0.43	0.16	0.31	0.16	0.23	0.25	0.31	0.22
MgO	0.05	0.09	0.00	0.00	0.02	0.00	0.00	0.23
CaO	0.00	0.07	0.00	0.00	0.01	0.05	0.08	0.05
Na2O	0.80	0.16	0.76	0.21	0.75	0.42	0.10	0.54
K2O	10.29	10.84	10.55	10.82	10.07	10.52	9.78	7.80
Cr2O3	0.00	0.00	0.08	0.04	0.00	0.00	0.03	0.00
Cl	N/D	N/D	N/D	N/D	N/D	N/D	0.00	0.01
P2O5	N/D	N/D	N/D	N/D	N/D	N/D	0.08	0.06
BaO	N/D	N/D	N/D	N/D	N/D	N/D	0.21	0.00
F	2.72	0.83	1.96	0.45	2.20	1.75	0.78	3.29
Total	97.35	96.10	97.72	95.63	97.23	96.95	98.53	97.32
Si	6.07	6.15	6.11	6.12	6.18	6.12	6.16	6.35
Ti	0.03	0.00	0.01	0.01	0.00	0.01	0.01	0.03
Al Total	5.67	5.75	5.61	5.58	5.52	5.55	5.58	5.18
Al IV	1.93	1.85	1.89	1.88	1.82	1.88	1.84	1.65
Al VI	3.74	3.91	3.72	3.70	3.70	3.67	3.74	3.53
Fe	0.25	0.23	0.29	0.29	0.30	0.33	0.26	0.40
Mn	0.00	0.00	0.01	0.00	0.00	0.00	0.01	0.00
Mg	0.02	0.03	0.04	0.05	0.04	0.05	0.05	0.13
Ca	0.00	0.01	0.00	0.00	0.00	0.00	0.00	0.00
Na	0.28	0.17	0.25	0.23	0.14	0.27	0.16	0.08
K	1.76	1.38	1.76	1.78	1.83	1.77	1.76	1.80
Cr	0.01	0.01	0.00	0.00	0.01	0.00	0.00	0.00
Cl								
P								
Ba	0.00	0.01	0.00	0.00	0.00	0.01	0.00	0.00
F	0.32	0.24	0.31	0.25	0.22	0.23	0.18	0.29
OH	3.68	3.76	3.69	3.75	3.78	3.77	3.82	3.71
Tetrahedral	8.00	8.00	8.00	8.00	8.00	8.00	8.00	8.00
Octahedral	4.04	4.18	4.07	4.07	4.05	4.07	4.08	4.09
Dodecahedral	2.05	1.56	2.01	2.01	1.99	2.04	1.93	1.89

Sample	SC-11-D	SC-11-D	SC-11-D	SC-11-D	SC-11-D	SC-11-D	SC-11-D	SC-11-D
Point	3	4	5	6	7	7b	8	10
Description	P	P	P	P	P	P	P	P
SiO2	47.33	48.37	46.23	48.27	46.54	51.97	48.37	47.44
TiO2	0.01	0.07	0.10	0.03	0.06	0.04	0.00	0.12
Al2O3	35.59	38.15	33.48	37.99	33.05	30.58	38.05	32.25
FeO	3.71	0.41	5.57	0.56	6.21	1.60	0.57	5.61
MnO	0.20	0.15	0.30	0.13	0.15	0.33	0.22	0.37
MgO	0.03	0.10	0.19	0.01	0.12	0.21	0.07	0.04
CaO	0.00	0.03	0.00	0.08	0.04	0.14	0.07	0.02
Na2O	0.72	0.18	0.67	0.11	0.71	0.24	0.08	0.49
K2O	8.86	9.85	8.57	9.78	9.19	9.36	9.80	9.33
Cr2O3	0.00	0.00	0.02	0.13	0.08	0.04	0.00	0.12
Cl	0.00	0.06	0.00	0.02	0.00	0.00	0.00	0.01
P2O5	0.18	0.06	0.00	0.00	0.05	0.00	0.08	0.00
BaO	0.11	0.00	0.00	0.16	0.04	0.00	0.10	0.00
F	2.28	0.22	3.62	0.23	3.69	3.89	0.72	3.45
Total	99.02	97.65	98.75	97.50	99.93	98.40	98.13	99.25
Si	6.24	6.14	6.25	6.19	6.26	6.18	6.20	6.25
Ti	0.02	0.02	0.02	0.01	0.00	0.02	0.01	0.00
Al Total	5.25	5.57	5.33	5.35	5.15	5.41	5.33	5.28
Al IV	1.76	1.86	1.75	1.81	1.74	1.82	1.80	1.75
Al VI	3.49	3.71	3.59	3.54	3.40	3.59	3.53	3.53
Fe	0.41	0.27	0.48	0.52	0.70	0.44	0.51	0.53
Mn	0.01	0.00	0.00	0.01	0.01	0.02	0.02	0.01
Mg	0.15	0.05	0.02	0.02	0.01	0.01	0.03	0.03
Ca	0.00	0.01	0.00	0.01	0.01	0.00	0.00	0.00
Na	0.10	0.25	0.21	0.24	0.23	0.19	0.24	0.23
K	1.97	1.74	1.68	1.75	1.81	1.79	1.76	1.78
Cr	0.00	0.00	0.01	0.00	0.01	0.01	0.01	0.00
Cl								
P								
Ba	0.00	0.00	0.00	0.01	0.01	0.00	0.00	0.00
F	0.22	0.17	0.41	0.33	0.44	0.36	0.36	0.42
OH	3.78	3.83	3.59	3.67	3.56	3.64	3.64	3.58
Tetrahedral	8.00	8.00	8.00	8.00	8.00	8.00	8.00	8.00
Octahedral	4.07	4.06	4.11	4.12	4.13	4.09	4.10	4.10
Dodecahedral	2.07	2.00	1.90	2.00	2.06	1.99	2.02	2.01

Sample	SC-11-D	SC-11-D	FC-1	FC-1	FC-1	FC-1	FC-1	FC-1	FC-1	FC-1	FC-1
Point	13	9	6	6	x	2	1	1	7	3	1
Description	P	RF	P	P	RB	RB	RF	RF	RF	RF	RF
SiO2	47.93	46.99	46.32	46.80	45.96	45.86	45.81	46.32	45.72	45.63	46.82
TiO2	0.11	0.05	0.06	0.35	0.00	0.32	0.00	0.00	0.06	0.00	0.23
Al2O3	37.92	31.89	36.15	35.94	34.35	36.19	36.33	36.35	35.75	35.27	36.12
FeO	0.26	5.83	1.51	1.45	1.64	1.46	1.47	1.28	1.56	1.59	1.33
MnO	0.12	0.53	0.00	0.03	0.00	0.04	0.02	0.01	0.05	0.05	0.00
MgO	0.13	0.14	0.57	0.61	0.74	0.45	0.09	0.47	0.63	0.59	0.61
CaO	0.02	0.02	0.01	0.01	0.08	0.06	0.00	0.00	0.00	0.06	0.03
Na2O	0.15	0.61	0.63	0.73	0.74	0.50	0.66	0.51	0.81	1.83	0.89
K2O	9.83	9.05	10.70	10.87	9.73	11.12	10.78	11.00	10.43	10.64	10.07
Cr2O3	0.03	0.02	0.00	0.04	0.07	0.02	0.00	0.04	0.04	0.00	0.02
Cl	0.00	0.01	N/D	N/D	N/D	N/D	N/D	N/D	N/D	N/D	N/D
P2O5	0.00	0.00	N/D	N/D	N/D	N/D	N/D	N/D	N/D	N/D	N/D
BaO	0.00	0.07	0.00	N/D	0.22	0.13	0.00	0.05	0.02	0.20	N/D
F	0.03	4.32	N/D	0.20	N/D	N/D	N/D	N/D	N/D	N/D	0.22
Total	96.53	99.53	95.95	97.04	93.55	96.13	95.17	96.02	95.07	95.85	96.35
Si	6.24	6.30	6.14	7.10	7.29	6.75	7.18	7.21	6.43	6.15	6.16
Ti	0.01	0.01	0.00	0.01	0.00	0.00	0.01	0.00	0.02	0.00	0.01
Al Total	5.33	5.29	5.66	3.40	3.56	4.79	3.81	3.32	5.32	5.88	5.68
Al IV	1.76	1.70	1.86	0.90	0.71	1.25	0.82	0.79	1.57	1.85	1.84
Al VI	3.57	3.59	3.80	2.50	2.85	3.54	2.99	2.53	3.76	4.02	3.84
Fe	0.49	0.42	0.29	1.87	1.51	0.42	1.43	1.57	0.51	0.00	0.14
Mn	0.01	0.02	0.00	0.07	0.06	0.01	0.05	0.04	0.01	0.00	0.01
Mg	0.03	0.03	0.03	0.03	0.05	0.02	0.09	0.02	0.02	0.01	0.12
Ca	0.00	0.01	0.00	0.00	0.00	0.01	0.00	0.00	0.01	0.00	0.01
Na	0.24	0.15	0.17	0.09	0.10	0.06	0.12	0.06	0.09	0.08	0.11
K	1.70	1.76	1.61	1.88	1.90	1.77	1.72	1.81	1.57	1.65	1.57
Cr	0.00	0.00	0.01	0.01	0.01	0.00	0.00	0.00	0.00	0.00	0.00
Cl			0.00	0.01	0.03	0.02	0.00	0.01	0.01	0.01	0.00
P			0.00	0.01	0.01	0.01	0.00	0.01	0.00	0.00	0.01
Ba	0.00	0.00	0.01	0.00	0.00	0.00	0.00	0.00	0.01	0.01	0.00
F	0.46	0.24	0.00	0.60	1.17	0.16	1.18	0.00	0.54	0.00	0.00
OH	3.54	3.76	4.00	3.39	2.82	3.83	2.82	4.00	3.46	4.00	4.00
Tetrahedral	8.00	8.00	8.00	8.00	8.00	8.00	8.00	8.00	8.00	8.00	8.00
Octahedral	4.11	4.09	4.12	4.48	4.48	4.01	4.57	4.17	4.32	4.04	4.13
Dodecahedral	1.94	1.91	1.79	1.99	2.02	1.83	1.84	1.88	1.68	1.74	1.69

Sample	FC-1	FC-1	FC-1	FC-1	FC-1	FC-1	FC-1	FC-1	FC-2	FC-2	FC-2
Point	7	3	7	10	9	9	8	8	6	4	7
Description	RF	RF	RF	S	S	S	S	S	P	P	P
SiO2	45.49	46.47	46.49	48.21	46.65	46.65	46.26	45.53	46.62	46.07	46.02
TiO2	0.00	0.26	0.00	0.01	0.06	0.00	0.02	0.04	0.33	0.07	0.02
Al2O3	33.90	36.24	37.03	34.82	37.01	36.29	36.99	37.28	36.10	35.89	36.04
FeO	1.46	1.39	1.50	1.72	0.55	1.52	1.37	1.11	1.34	1.52	1.54
MnO	0.06	0.04	0.00	0.00	0.08	0.07	0.00	0.01	0.05	0.00	0.00
MgO	0.68	0.53	0.54	0.38	0.03	0.63	0.25	0.29	0.55	0.51	0.57
CaO	0.04	0.01	0.05	0.01	0.00	0.00	0.00	0.00	0.03	0.01	0.00
Na2O	0.68	0.79	0.68	0.14	0.16	0.76	0.74	0.70	0.58	0.56	0.78
K2O	10.65	10.37	10.97	10.78	11.02	10.94	10.64	10.72	10.69	10.94	10.53
Cr2O3	0.05	0.09	0.01	0.01	0.00	0.01	0.02	0.02	0.00	0.00	0.07
Cl	N/D	N/D	N/D	N/D	N/D	N/D	N/D	N/D	N/D	N/D	N/D
P2O5	N/D	N/D	N/D	N/D	N/D	N/D	N/D	N/D	N/D	N/D	N/D
BaO	N/D	N/D	0.00	N/D	N/D	N/D	N/D	0.07	0.13	0.00	0.00
F	0.17	0.36	0.19	0.14	0.00	0.34	0.23	0.12	N/D	N/D	N/D
Total	93.20	96.56	97.46	96.22	95.56	97.20	96.50	95.88	96.42	95.56	95.56
Si	6.23	6.33	6.12	6.20	6.64	6.24	6.10	6.12	6.16	6.10	6.10
Ti	0.00	0.00	0.02	0.02	0.00	0.00	0.00	0.00	0.02	0.00	0.00
Al Total	5.62	5.25	5.77	5.61	5.05	5.50	5.67	5.58	5.43	5.60	5.62
Al IV	1.77	1.67	1.88	1.80	1.36	1.76	1.90	1.88	1.84	1.90	1.90
Al VI	3.85	3.58	3.88	3.80	3.69	3.73	3.77	3.69	3.59	3.70	3.72
Fe	0.13	0.61	0.11	0.27	0.13	0.30	0.29	0.38	0.37	0.33	0.34
Mn	0.01	0.01	0.01	0.01	0.04	0.02	0.00	0.00	0.01	0.01	0.00
Mg	0.11	0.02	0.10	0.04	0.01	0.01	0.01	0.01	0.11	0.03	0.01
Ca	0.00	0.00	0.00	0.01	0.00	0.00	0.00	0.00	0.01	0.00	0.00
Na	0.11	0.09	0.17	0.16	0.09	0.14	0.12	0.23	0.24	0.29	0.27
K	1.58	1.62	1.52	1.46	1.83	1.75	1.85	1.78	1.73	1.76	1.77
Cr	0.00	0.00	0.00	0.01	0.00	0.00	0.01	0.00	0.01	0.00	0.00
Cl	0.00	0.01	0.01	0.01							
P	0.00	0.00	0.00	0.00							
Ba	0.00	0.00	0.01	0.00	0.00	0.00					
F	0.00	0.09	0.00	0.00	0.46	0.25	0.26	0.27	0.26	0.24	0.25
OH	4.00	3.90	4.00	4.00	3.54	3.75	3.74	3.73	3.74	3.76	3.75
Tetrahedral	8.00	8.00	8.00	8.00	8.00	8.00	8.00	8.00	8.00	8.00	8.00
Octahedral	4.10	4.22	4.12	4.16	3.87	4.07	4.07	4.09	4.11	4.08	4.07
Dodecahedral	1.70	1.72	1.70	1.63	1.92	1.89	1.98	2.01	1.99	2.05	2.04

Sample	FC-2	FC-2	FC-2	FC-2	FC-2	FC-2	FC-2	FC-2	FC-2	FC-2	FC-2
Point	5	6	7	4	7	2	1	1	4	8	9
Description	P	P	P	P	P	P	RF	RF	RF	S	S
SiO2	46.25	45.79	46.81	46.55	46.25	46.25	45.60	45.95	46.21	48.59	48.53
TiO2	0.02	0.00	0.04	0.00	0.02	0.41	0.08	0.40	0.00	0.00	0.03
Al2O3	35.63	35.77	36.23	36.39	36.30	36.44	33.19	36.15	36.34	34.30	36.35
FeO	1.32	1.51	1.48	1.59	1.51	1.35	3.00	1.48	1.44	1.49	0.79
MnO	0.05	0.00	0.00	0.00	0.05	0.02	0.07	0.05	0.00	0.03	0.11
MgO	0.58	0.66	0.66	0.52	0.61	0.51	0.39	0.59	0.51	0.74	0.26
CaO	0.02	0.03	0.09	0.00	0.00	0.03	0.11	0.00	0.00	0.01	0.07
Na2O	0.56	0.79	0.74	0.73	0.74	0.76	0.74	0.92	0.69	0.09	0.22
K2O	10.82	10.60	10.69	10.59	10.68	10.63	10.28	10.30	10.70	10.84	10.79
Cr2O3	0.00	0.13	0.00	0.00	0.00	0.05	0.02	0.00	0.00	0.00	0.02
Cl	N/D	N/D	N/D	N/D	N/D	N/D	N/D	N/D	N/D	N/D	N/D
P2O5	N/D	N/D	N/D	N/D	N/D	N/D	N/D	N/D	N/D	N/D	N/D
BaO	0.09	N/D	N/D	N/D	0.01	N/D	0.15	0.04	0.05	N/D	N/D
F	N/D	0.27	0.29	0.18	0.27	0.16	N/D	0.14	0.18	0.36	0.22
Total	95.35	95.55	97.03	96.54	96.44	96.61	93.64	96.02	96.12	96.45	97.38
Si	6.17	6.15	6.40	6.40	6.55	6.40	7.01	6.81	6.39	6.39	6.44
Ti	0.02	0.00	0.01	0.01	0.02	0.02	0.01	0.01	0.06	0.06	0.03
Al Total	5.43	5.57	5.15	5.09	4.68	4.94	3.58	4.08	5.13	5.22	5.16
Al IV	1.83	1.85	1.60	1.60	1.45	1.60	0.99	1.19	1.61	1.61	1.56
Al VI	3.60	3.72	3.55	3.49	3.23	3.34	2.58	2.89	3.51	3.61	3.60
Fe	0.32	0.34	0.41	0.45	0.71	0.62	1.38	1.11	0.34	0.28	0.30
Mn	0.02	0.01	0.03	0.01	0.04	0.04	0.08	0.06	0.01	0.01	0.00
Mg	0.14	0.00	0.01	0.05	0.08	0.08	0.10	0.09	0.28	0.37	0.34
Ca	0.01	0.00	0.00	0.01	0.02	0.01	0.01	0.01	0.01	0.01	0.00
Na	0.27	0.24	0.10	0.12	0.11	0.11	0.11	0.08	0.30	0.10	0.10
K	1.71	1.75	1.87	1.91	1.88	1.92	1.95	1.85	1.69	1.64	1.76
Cr	0.00	0.00	0.00	0.01	0.00	0.00	0.00	0.00	0.00	0.00	0.01
Cl									0.00	0.00	0.00
P									0.00	0.01	0.00
Ba	0.00	0.00					0.00	0.00	0.01	0.00	0.01
F	0.31	0.26	0.10	0.14	0.17	0.23	0.97	0.36	0.41	0.55	0.56
OH	3.69	3.74	3.90	3.86	3.83	3.77	3.03	3.64	3.59	3.45	3.44
Tetrahedral	8.00	8.00	8.00	8.00	8.00	8.00	8.00	8.00	8.00	8.00	8.00
Octahedral	4.10	4.07	4.03	4.02	4.09	4.10	4.17	4.17	4.20	4.33	4.27
Dodecahedral	1.98	1.99	1.97	2.04	1.99	2.03	2.05	1.93	1.99	1.74	1.88

Sample	FC-2	FC-2	FC-2	FC-2	FC-2	FT-2	FT-2	FT-2	FT-2	FT-2	FT-2
Point	10	8	9	11	10	6	6	6	3	4	3
Description	S	S	S	S	S	P	P	P	RA	RA	RA
SiO2	47.36	46.06	45.97	48.26	46.28	47.15	45.57	45.40	45.84	45.70	46.09
TiO2	0.25	0.02	0.03	0.00	0.30	0.01	0.04	0.00	0.28	0.27	0.12
Al2O3	31.67	36.30	36.78	35.58	36.25	35.33	34.30	37.52	36.28	34.99	34.44
FeO	4.59	1.45	1.12	1.12	0.64	3.54	3.04	1.25	1.48	3.01	3.43
MnO	0.13	0.05	0.06	0.00	0.11	0.03	0.14	0.05	0.04	0.14	0.13
MgO	0.97	0.46	0.07	0.29	0.21	0.33	0.33	0.14	0.49	0.19	0.32
CaO	0.03	0.00	0.00	0.07	0.00	0.00	0.02	0.00	0.00	0.05	0.00
Na2O	0.22	0.72	0.25	0.22	0.19	0.96	0.88	0.73	0.75	0.95	0.85
K2O	11.07	10.66	11.21	10.23	10.52	10.63	10.20	10.90	10.41	10.26	10.43
Cr2O3	0.07	0.08	0.00	0.09	0.00	0.00	0.00	0.00	0.04	0.00	0.00
Cl	N/D	N/D	N/D	N/D	N/D	N/D	N/D	N/D	N/D	N/D	N/D
P2O5	N/D	N/D	N/D	N/D	N/D	N/D	N/D	N/D	N/D	N/D	N/D
BaO	N/D	0.01	0.00	0.01	0.08	N/D	0.00	0.01	0.07	0.00	0.00
F	0.29	0.24	0.09	0.15	0.17	0.48	N/D	0.04	N/D	N/D	N/D
Total	96.64	96.05	95.59	96.02	94.75	98.47	94.52	96.04	95.66	95.57	95.81
Si	6.48	6.51	6.26	6.27	6.43	6.26	6.21	6.51	6.46	6.70	6.18
Ti	0.03	0.04	0.00	0.00	0.02	0.02	0.02	0.05	0.04	0.01	0.00
Al Total	5.04	4.96	5.54	5.54	5.14	5.49	5.61	5.04	5.11	4.58	5.68
Al IV	1.52	1.49	1.74	1.73	1.57	1.74	1.79	1.49	1.54	1.30	1.82
Al VI	3.52	3.47	3.80	3.81	3.57	3.75	3.83	3.55	3.57	3.28	3.86
Fe	0.45	0.46	0.18	0.19	0.48	0.22	0.14	0.45	0.35	0.86	0.17
Mn	0.01	0.01	0.00	0.01	0.01	0.01	0.00	0.01	0.01	0.02	0.01
Mg	0.35	0.39	0.21	0.20	0.27	0.23	0.16	0.34	0.35	0.44	0.16
Ca	0.00	0.00	0.00	0.00	0.00	0.00	0.00	0.00	0.00	0.01	0.00
Na	0.07	0.08	0.12	0.15	0.10	0.13	0.17	0.06	0.08	0.04	0.17
K	1.68	1.75	1.69	1.71	1.79	1.73	1.70	1.72	1.74	1.85	1.69
Cr	0.00	0.00	0.00	0.00	0.00	0.00	0.01	0.00	0.00	0.00	0.00
Cl	0.00	0.00	0.00	0.00	0.00	0.00	0.02	0.00	0.00	0.00	0.00
P	0.00	0.00	0.00	0.00	0.00	0.00	0.00	0.00	0.01	0.00	0.00
Ba	0.01	0.01	0.01	0.01	0.00	0.01	0.00	0.00	0.00	0.00	0.01
F	0.59	0.69	0.27	0.38	0.63	0.38	0.25	0.73	0.59	1.13	0.33
OH	3.41	3.31	3.73	3.62	3.37	3.61	3.74	3.27	3.41	2.87	3.67
Tetrahedral	8.00	8.00	8.00	8.00	8.00	8.00	8.00	8.00	8.00	8.00	8.00
Octahedral	4.36	4.38	4.19	4.21	4.35	4.23	4.15	4.40	4.31	4.62	4.20
Dodecahedral	1.78	1.85	1.82	1.87	1.88	1.87	1.88	1.78	1.83	1.90	1.87

Sample	FT-2	FT-2	FT-2	FT-2	FT-2	FT-2	FT-2	FT-2	FT-2	FT-2	FT-2
Point	3	4	2	5	2	1	7	7	8	8	7
Description	RA	RA	RB	RB	RB	RF	S	S	S	S	S
SiO2	45.28	45.56	45.65	46.07	45.38	46.18	46.34	46.05	46.23	45.44	45.92
TiO2	0.10	0.00	0.00	0.54	0.11	0.02	0.05	0.03	0.00	0.06	0.00
Al2O3	36.00	34.55	36.16	34.98	35.31	34.86	35.87	35.80	36.27	34.34	36.33
FeO	1.91	3.55	2.11	2.23	2.59	1.96	2.49	2.31	1.64	3.13	1.82
MnO	0.00	0.03	0.00	0.01	0.03	0.03	0.10	0.03	0.08	0.11	0.00
MgO	0.28	0.35	0.23	0.37	0.25	0.17	0.23	0.22	0.15	0.37	0.21
CaO	0.00	0.00	0.01	0.06	0.00	0.05	0.00	0.00	0.03	0.01	0.03
Na2O	0.52	0.73	0.64	0.68	0.98	0.33	0.85	0.79	0.54	0.73	0.64
K2O	9.28	10.81	10.77	10.81	10.32	10.93	10.73	10.63	10.90	10.76	10.72
Cr2O3	0.02	0.01	0.00	0.03	0.00	0.00	0.02	0.14	0.02	0.04	0.00
Cl	N/D	N/D	N/D	N/D	N/D	N/D	N/D	N/D	N/D	N/D	N/D
P2O5	N/D	N/D	N/D	N/D	N/D	N/D	N/D	N/D	N/D	N/D	N/D
BaO	0.03	0.00	0.00	0.00	0.01	0.00	N/D	N/D	N/D	0.01	0.00
F	0.39	0.40	N/D	0.60	0.46	0.48	0.37	0.41	0.45	0.61	0.39
Total	93.80	95.99	95.56	96.37	95.45	95.03	97.05	96.41	96.31	95.61	96.05
Si	6.34	6.35	6.35	6.36	6.15	6.28	6.33	6.35	6.36	6.34	6.41
Ti	0.03	0.00	0.01	0.01	0.00	0.00	0.02	0.02	0.00	0.00	0.00
Al Total	5.03	5.32	5.15	5.16	5.66	5.25	5.30	5.30	5.43	5.35	5.23
Al IV	1.66	1.65	1.65	1.64	1.85	1.72	1.67	1.65	1.64	1.66	1.59
Al VI	3.37	3.66	3.50	3.51	3.81	3.53	3.64	3.64	3.79	3.69	3.64
Fe	0.90	0.57	0.67	0.68	0.07	0.74	0.65	0.60	0.25	0.60	0.61
Mn	0.00	0.01	0.01	0.01	0.00	0.02	0.00	0.01	0.00	0.01	0.00
Mg	0.19	0.05	0.23	0.19	0.16	0.14	0.00	0.05	0.00	0.01	0.00
Ca	0.00	0.00	0.00	0.00	0.00	0.00	0.00	0.00	0.02	0.01	0.00
Na	0.13	0.16	0.13	0.13	0.06	0.17	0.18	0.16	0.07	0.12	0.15
K	1.87	1.83	1.83	1.87	1.83	1.81	1.82	1.82	1.84	1.84	1.85
Cr	0.00	0.00	0.00	0.00	0.01	0.01	0.00	0.00	0.01	0.00	0.01
Cl	0.01	0.00	0.01	0.00	0.00	0.02	0.00	0.00	0.00	0.00	0.00
P	0.00	0.01	0.00	0.00	0.03	0.00	0.01	0.00	0.03	0.01	0.01
Ba	0.01	0.00	0.00	0.00	0.00	0.01	0.00	0.00	0.00	0.01	0.01
F	0.81	0.64	0.68	0.74	0.13	0.72	0.70	0.65	0.36	0.71	0.67
OH	3.19	3.36	3.32	3.26	3.87	3.26	3.30	3.35	3.64	3.29	3.33
Tetrahedral	8.00	8.00	8.00	8.00	8.00	8.00	8.00	8.00	8.00	8.00	8.00
Octahedral	4.50	4.29	4.42	4.41	4.04	4.43	4.31	4.32	4.06	4.33	4.26
Dodecahedral	2.01	2.01	1.97	2.00	1.93	2.01	2.02	1.98	1.95	1.98	2.03

Sample	LL-2	LL-2	LL-2	LL-2	LL-2	LL-2	LL-2	M72-43	M72-43	M72-43
Point	6	3	4	1	1	5	5	7	6	8
Description	P	P	P	P	P	RF	RF	P	P	P
SiO2	47.10	46.37	46.02	46.87	46.26	46.52	46.58	47.91	46.02	45.10
TiO2	0.21	0.06	0.05	0.13	0.15	0.19	0.10	0.02	0.16	0.22
Al2O3	36.25	34.84	35.11	35.69	35.67	35.51	35.03	33.96	35.63	33.59
FeO	2.19	2.79	2.51	2.30	2.30	2.40	2.36	1.68	1.50	1.90
MnO	0.01	0.03	0.04	0.10	0.08	0.16	0.03	0.00	0.00	0.03
MgO	0.32	0.68	0.43	0.41	0.44	0.39	0.62	0.55	0.60	0.85
CaO	0.00	0.02	0.07	0.00	0.00	0.02	0.06	0.00	0.03	0.05
Na2O	0.79	0.61	0.54	0.59	0.97	0.74	0.56	0.15	0.73	1.64
K2O	10.75	10.96	10.76	10.47	10.43	10.55	10.69	10.99	9.68	10.92
Cr2O3	0.00	0.03	0.11	0.00	0.10	0.04	0.04	0.05	0.07	0.00
Cl	N/D	N/D	N/D	N/D	N/D	N/D	N/D	N/D	N/D	N/D
P2O5	N/D	N/D	N/D	N/D	N/D	N/D	N/D	N/D	N/D	N/D
BaO	N/D	N/D	N/D	N/D	0.00	N/D	0.02	N/D	N/D	0.01
F	0.74	1.00	0.92	1.01	1.00	0.91	0.91	0.15	0.19	0.24
Total	98.35	97.40	96.56	97.58	97.42	97.43	97.01	95.46	94.60	94.54
Si	6.31	6.25	6.21	6.23	6.23	6.30	6.27	6.31	6.14	6.17
Ti	0.01	0.02	0.02	0.01	0.01	0.01	0.01	0.00	0.01	0.00
Al Total	5.38	5.21	5.30	5.17	5.21	5.12	5.14	5.19	5.40	5.38
Al IV	1.69	1.75	1.79	1.77	1.77	1.70	1.73	1.69	1.86	1.83
Al VI	3.69	3.45	3.51	3.40	3.45	3.42	3.42	3.51	3.54	3.55
Fe	0.59	0.61	0.57	0.74	0.60	0.65	0.68	0.56	0.52	0.54
Mn	0.01	0.02	0.00	0.00	0.02	0.01	0.01	0.01	0.02	0.01
Mg	0.01	0.01	0.02	0.01	0.04	0.02	0.02	0.01	0.03	0.03
Ca	0.00	0.00	0.00	0.00	0.01	0.00	0.00	0.00	0.00	0.00
Na	0.20	0.18	0.17	0.18	0.18	0.22	0.19	0.13	0.15	0.18
K	1.79	1.85	1.86	1.81	1.84	1.79	1.84	1.88	1.92	1.86
Cr	0.00	0.00	0.00	0.00	0.01	0.00	0.00	0.00	0.00	0.00
Cl	0.03									
P	0.02									
Ba	0.00							0.01		
F	0.72	0.47	0.45	0.57	0.49	0.52	0.48		0.31	0.35
OH	3.26	3.53	3.55	3.43	3.51	3.48	3.52	4.00	3.69	3.65
Tetrahedral	8.00	8.00	8.00	8.00	8.00	8.00	8.00	8.00	8.00	8.00
Octahedral	4.32	4.11	4.11	4.18	4.13	4.12	4.13	4.08	4.12	4.12
Dodecahedral	2.01	2.03	2.03	1.99	2.03	2.01	2.03	2.03	2.07	2.04

Sample	M72-43	M72-43	M72-43	M72-43	M72-43	M72-43A	M72-43A	M72-43A
Point	1	5	3	3	9	7	5	2
Description	RF	RF	RF	RF	S	P	RF	RF
SiO2	46.06	46.30	45.76	46.25	47.08	46.18	46.14	45.95
TiO2	0.19	0.28	0.34	0.27	0.42	0.00	0.23	0.21
Al2O3	35.42	36.16	35.70	35.21	34.93	34.47	35.81	34.53
FeO	1.43	1.33	1.33	1.46	1.57	2.62	1.28	1.69
MnO	0.00	0.01	0.00	0.00	0.00	0.00	0.01	0.07
MgO	0.47	0.64	0.61	0.65	0.76	0.69	0.53	0.79
CaO	0.02	0.04	0.00	0.00	0.04	0.02	0.00	0.00
Na2O	0.47	0.73	0.77	0.48	0.72	0.75	0.59	0.87
K2O	10.93	10.68	10.58	10.94	10.68	10.48	10.70	10.12
Cr2O3	0.03	0.00	0.04	0.00	0.03	0.09	0.00	0.00
Cl	N/D	N/D	N/D	N/D	N/D	N/D	N/D	N/D
P2O5	N/D	N/D	N/D	N/D	N/D	N/D	N/D	N/D
BaO	N/D	N/D	N/D	0.02	N/D	0.11	0.22	0.03
F	0.27	0.19	0.20	0.25	0.30	N/D	N/D	N/D
Total	95.30	96.36	95.34	95.53	96.52	95.41	95.50	94.26
Si	6.25	6.26	6.17	6.21	6.18	6.24	6.28	6.39
Ti	0.00	0.00	0.00	0.00	0.00	0.00	0.04	0.04
Al Total	5.27	5.30	5.37	5.35	5.44	5.33	5.35	5.11
Al IV	1.75	1.74	1.83	1.79	1.82	1.76	1.72	1.61
Al VI	3.52	3.55	3.54	3.56	3.62	3.57	3.63	3.50
Fe	0.52	0.50	0.54	0.49	0.38	0.51	0.57	0.74
Mn	0.01	0.00	0.02	0.01	0.01	0.01	0.01	0.02
Mg	0.05	0.02	0.02	0.03	0.04	0.01	0.06	0.08
Ca	0.02	0.01	0.00	0.01	0.01	0.01	0.00	0.00
Na	0.11	0.16	0.16	0.17	0.27	0.12	0.14	0.09
K	1.89	1.85	1.87	1.86	1.76	1.87	1.62	1.67
Cr	0.00	0.01	0.00	0.00	0.01	0.00	0.00	0.00
Cl							0.00	0.00
P							0.01	0.00
Ba						0.00	0.00	0.00
F	0.36	0.37	0.37	0.40	0.36	0.37	0.39	0.52
OH	3.64	3.63	3.63	3.60	3.64	3.63	3.61	3.48
Tetrahedral	8.00	8.00	8.00	8.00	8.00	8.00	8.00	8.00
Octahedral	4.11	4.08	4.13	4.10	4.07	4.10	4.30	4.38
Dodecahedral	2.00	2.02	2.03	2.03	2.04	1.99	1.77	1.76

Sample	M72-43A	M72-119	M72-119	M72-119	M72-119	M72-119	M72-119	M72-119
Point	3	7	7	8	5	6	3	6
Description	RF	P	P	P	P	P	P	P
SiO2	46.38	45.69	46.44	44.79	46.55	45.99	45.33	45.46
TiO2	0.36	0.37	0.10	0.38	0.42	0.42	0.14	0.13
Al2O3	37.78	35.76	34.76	34.16	36.52	34.57	34.51	35.26
FeO	1.59	1.48	1.70	1.65	1.50	1.53	1.58	1.67
MnO	0.00	0.11	0.11	0.00	0.00	0.11	0.05	0.02
MgO	0.79	0.61	0.77	0.72	0.67	0.62	0.69	0.54
CaO	0.00	0.00	0.01	0.13	0.01	0.00	0.00	0.00
Na2O	0.82	0.81	0.79	0.84	0.63	0.72	1.02	0.63
K2O	10.45	10.45	10.33	10.17	10.71	10.52	10.25	10.60
Cr2O3	0.01	0.00	0.00	0.14	0.00	0.09	0.00	0.03
Cl	N/D	N/D	N/D	N/D	N/D	N/D	N/D	N/D
P2O5	N/D	N/D	N/D	N/D	N/D	N/D	N/D	N/D
BaO	0.07	0.06	0.05	0.10	0.10	0.01	0.25	0.02
F	N/D	0.39	N/D	N/D	N/D	N/D	N/D	N/D
Total	98.27	95.71	95.05	93.08	97.11	94.59	93.81	94.35
Si	6.24	6.48	6.20	6.16	6.30	6.30	6.19	6.26
Ti	0.00	0.02	0.01	0.01	0.02	0.04	0.01	0.05
Al Total	5.61	4.81	5.29	5.34	5.44	5.38	5.57	5.45
Al IV	1.76	1.52	1.80	1.84	1.70	1.70	1.81	1.74
Al VI	3.85	3.29	3.49	3.50	3.74	3.68	3.76	3.71
Fe	0.24	0.73	0.60	0.59	0.34	0.37	0.40	0.32
Mn	0.00	0.01	0.00	0.01	0.02	0.00	0.01	0.01
Mg	0.05	0.05	0.01	0.04	0.16	0.15	0.03	0.12
Ca	0.01	0.00	0.00	0.00	0.00	0.00	0.00	0.00
Na	0.16	0.09	0.19	0.16	0.19	0.18	0.21	0.17
K	1.59	1.91	1.85	1.86	1.54	1.60	1.65	1.62
Cr	0.01	0.00	0.01	0.00	0.01	0.01	0.00	0.00
Cl	0.01				0.02	0.00	0.01	0.00
P	0.01				0.00	0.01	0.02	0.01
Ba	0.00		0.00	0.00	0.01	0.00	0.00	0.00
F	0.21	0.53	0.50	0.47	0.39	0.40	0.33	0.37
OH	3.78	3.47	3.50	3.53	3.60	3.60	3.67	3.63
Tetrahedral	8.00	8.00	8.00	8.00	8.00	8.00	8.00	8.00
Octahedral	4.15	4.09	4.11	4.15	4.27	4.25	4.21	4.21
Dodecahedral	1.77	2.00	2.05	2.02	1.75	1.80	1.88	1.81

Sample	M72-119	M72-119	M72-119	M72-119	M72-119	M72-119	M72-119	M72-119
Point	5	6	3	3	5	6	4	4
Description	P	P	P	P	P	P	RB	RB
SiO2	45.87	46.09	47.00	46.48	46.12	46.53	45.59	46.06
TiO2	0.29	0.19	0.21	0.20	0.36	0.17	0.13	0.39
Al2O3	35.11	36.31	36.08	35.79	35.88	37.02	33.35	35.16
FeO	1.62	1.30	1.65	1.60	1.66	1.09	3.85	1.84
MnO	0.02	0.00	0.02	0.04	0.00	0.00	0.21	0.08
MgO	0.55	0.16	0.53	0.68	0.55	0.15	0.03	0.59
CaO	0.00	0.00	0.00	0.00	0.06	0.00	0.01	0.00
Na2O	0.71	0.81	0.78	0.84	0.79	0.71	0.64	0.75
K2O	10.54	10.70	10.75	10.44	10.49	10.46	10.71	10.37
Cr2O3	0.02	0.00	0.00	0.00	0.02	0.03	0.04	0.01
Cl	N/D	N/D	N/D	N/D	N/D	N/D	N/D	N/D
P2O5	N/D	N/D	N/D	N/D	N/D	N/D	N/D	N/D
BaO	N/D	N/D	N/D	0.09	0.06	0.02	0.11	0.19
F	0.55	0.47	0.39	0.53	0.56	0.38	N/D	N/D
Total	95.29	96.04	97.40	96.69	96.54	96.55	94.67	95.43
Si	6.19	6.49	6.22	6.24	6.27	6.16	6.25	6.23
Ti	0.05	0.03	0.05	0.05	0.06	0.00	0.06	0.07
Al Total	5.52	4.61	5.47	5.49	5.49	5.67	5.46	5.43
Al IV	1.81	1.51	1.78	1.76	1.73	1.84	1.75	1.77
Al VI	3.72	3.10	3.68	3.73	3.76	3.83	3.71	3.65
Fe	0.31	1.32	0.39	0.28	0.31	0.35	0.30	0.32
Mn	0.01	0.03	0.01	0.00	0.00	0.00	0.02	0.01
Mg	0.15	0.13	0.14	0.15	0.14	0.04	0.15	0.17
Ca	0.00	0.00	0.00	0.00	0.00	0.00	0.00	0.00
Na	0.22	0.06	0.14	0.20	0.17	0.20	0.18	0.19
K	1.65	1.92	1.67	1.63	1.52	1.64	1.64	1.63
Cr	0.00	0.00	0.00	0.00	0.00	0.00	0.00	0.00
Cl	0.00	0.00	0.00	0.00	0.00	0.02	0.00	0.00
P	0.00	0.01	0.01	0.00	0.01	0.00	0.00	0.01
Ba	0.00	0.00	0.00	0.01	0.00	0.01	0.00	0.00
F	0.37	0.89	0.42	0.34	0.41	0.30	0.36	0.37
OH	3.63	3.11	3.58	3.66	3.59	3.69	3.64	3.63
Tetrahedral	8.00	8.00	8.00	8.00	8.00	8.00	8.00	8.00
Octahedral	4.24	4.60	4.27	4.21	4.27	4.23	4.23	4.23
Dodecahedral	1.87	1.99	1.83	1.84	1.70	1.86	1.82	1.84

Sample	M72-119	M72-119	M72-119	M72-119	M72-119	M72-119	M72-119	M72-119
Point	1	4	2	2	11	9	11	10
Description	RB	RB	RF	RF	S	S	S	S
SiO2	46.50	46.33	45.77	46.24	46.17	46.31	46.03	48.31
TiO2	0.37	0.49	0.30	0.15	0.00	0.16	0.02	0.00
Al2O3	34.88	35.97	37.71	34.67	36.18	35.42	36.96	36.08
FeO	1.32	1.52	1.26	1.67	1.55	1.59	1.24	0.35
MnO	0.02	0.07	0.00	0.01	0.00	0.00	0.07	0.15
MgO	0.61	0.71	0.20	0.66	0.34	0.57	0.23	0.23
CaO	0.02	0.04	0.02	0.00	0.00	0.00	0.00	0.06
Na2O	0.57	0.69	0.76	0.78	0.86	0.52	0.69	0.00
K2O	10.63	10.49	10.54	10.40	10.51	10.80	10.90	10.43
Cr2O3	0.02	0.00	0.04	0.04	0.02	0.01	0.10	0.00
Cl	N/D	N/D	N/D	N/D	N/D	N/D	N/D	N/D
P2O5	N/D	N/D	N/D	N/D	N/D	N/D	N/D	N/D
BaO	0.06	0.03	0.08	N/D	N/D	N/D	0.03	0.00
F	N/D	0.46	N/D	0.50	0.47	0.46	0.28	0.06
Total	95.02	96.81	96.68	95.11	96.09	95.83	96.54	95.66
Si	6.25	6.30	6.30	6.37	6.44	6.45	6.21	6.21
Ti	0.03	0.03	0.01	0.01	0.00	0.01	0.00	0.04
Al Total	5.45	5.40	5.26	5.15	5.13	5.41	5.78	5.32
Al IV	1.75	1.70	1.70	1.63	1.56	1.55	1.79	1.79
Al VI	3.70	3.70	3.56	3.51	3.58	3.86	3.98	3.53
Fe	0.33	0.34	0.61	0.75	0.72	0.09	0.22	0.86
Mn	0.02	0.00	0.03	0.00	0.03	0.00	0.00	0.01
Mg	0.16	0.17	0.12	0.02	0.04	0.01	0.03	0.11
Ca	0.01	0.00	0.00	0.00	0.00	0.01	0.00	0.06
Na	0.20	0.17	0.13	0.16	0.14	0.01	0.14	0.17
K	1.64	1.71	1.82	1.77	1.81	1.61	1.58	1.35
Cr	0.00	0.00	0.01	0.01	0.00	0.00	0.00	0.00
Cl	0.00	0.00	0.00	0.00	0.00	0.00	0.01	0.00
P	0.01	0.01	0.01	0.03	0.00	0.02	0.01	0.01
Ba	0.02	0.00	0.01	0.00	0.00	0.00	0.01	0.00
F	0.41	0.46	0.55	0.60	0.70	0.00	0.47	0.62
OH	3.59	3.54	3.45	3.39	3.30	4.00	3.52	3.38
Tetrahedral	8.00	8.00	8.00	8.00	8.00	8.00	8.00	8.00
Octahedral	4.25	4.24	4.32	4.30	4.36	3.98	4.24	4.61
Dodecahedral	1.86	1.89	1.98	1.97	1.95	1.63	1.74	1.54

Sample	M72-119	M72-182	M72-182	M72-182	M72-182	M72-182	M72-182	M72-182
Point	9	5	4	5	7	4	5	7
Description	S	P	P	P	P	P	P	P
SiO2	45.55	45.31	46.02	45.80	46.48	46.17	46.23	46.24
TiO2	0.05	0.05	0.05	0.14	0.03	0.11	0.15	0.03
Al2O3	36.43	36.59	35.84	35.03	35.57	34.93	35.31	36.62
FeO	1.20	1.48	1.44	1.93	1.69	2.18	2.00	1.59
MnO	0.00	0.00	0.07	0.03	0.06	0.03	0.00	0.05
MgO	0.45	0.18	0.29	0.61	0.48	0.67	0.49	0.55
CaO	0.08	0.00	0.00	0.09	0.00	0.10	0.00	0.00
Na2O	0.71	0.82	0.66	0.56	0.57	0.79	0.43	0.64
K2O	10.37	10.43	10.78	10.91	11.12	10.04	10.95	10.69
Cr2O3	0.00	0.05	0.00	0.00	0.01	0.00	0.06	0.00
Cl	N/D	N/D	N/D	N/D	N/D	N/D	N/D	N/D
P2O5	N/D	N/D	N/D	N/D	N/D	N/D	N/D	N/D
BaO	0.12	0.05	0.10	N/D	N/D	N/D	0.00	0.03
F	0.38	N/D	N/D	0.34	0.38	0.43	0.30	0.34
Total	95.34	94.96	95.25	95.44	96.38	95.44	95.92	96.78
Si	6.20	6.30	6.34	6.20	6.23	6.40	6.46	6.24
Ti	0.01	0.03	0.04	0.00	0.00	0.00	0.00	0.01
Al Total	5.73	5.47	5.38	5.77	5.56	5.25	5.03	5.57
Al IV	1.80	1.70	1.66	1.80	1.77	1.60	1.54	1.76
Al VI	3.93	3.77	3.72	3.96	3.79	3.65	3.49	3.81
Fe	0.22	0.39	0.40	0.27	0.42	0.55	0.78	0.27
Mn	0.00	0.01	0.01	0.00	0.01	0.01	0.01	0.02
Mg	0.05	0.15	0.17	0.04	0.03	0.02	0.03	0.00
Ca	0.01	0.01	0.01	0.00	0.00	0.01	0.00	0.01
Na	0.09	0.17	0.22	0.17	0.17	0.06	0.09	0.09
K	1.62	1.50	1.47	1.56	1.55	1.64	1.66	1.59
Cr	0.00	0.00	0.00	0.01	0.00	0.01	0.01	0.00
Cl	0.00	0.00	0.00	0.01	0.00	0.01	0.00	0.00
P	0.00	0.01	0.00	0.00	0.00	0.00	0.01	0.02
Ba	0.00	0.00	0.00	0.00	0.01	0.01	0.00	0.00
F	0.30	0.58	0.53	0.49	0.25	0.25	0.38	0.11
OH	3.70	3.41	3.47	3.50	3.75	3.75	3.62	3.89
Tetrahedral	8.00	8.00	8.00	8.00	8.00	8.00	8.00	8.00
Octahedral	4.22	4.36	4.35	4.28	4.24	4.24	4.31	4.13
Dodecahedral	1.71	1.68	1.69	1.74	1.72	1.71	1.77	1.69

Sample	M72-182	M72-182	M72-182	M72-182	M72-182	M72-182	M72-182	M72-182
Point	4	6	1	3	2	2	3	2
Description	P	RB	RB	RB	RF	RF	RF	RF
SiO2	46.48	45.81	45.97	46.68	45.90	46.88	46.07	46.25
TiO2	0.09	0.21	0.08	0.05	0.00	0.06	0.00	0.05
Al2O3	34.99	34.50	37.96	34.96	36.97	35.21	36.59	35.44
FeO	1.72	2.00	1.76	1.99	0.86	2.08	1.48	2.07
MnO	0.14	0.08	0.04	0.08	0.00	0.08	0.12	0.08
MgO	0.70	0.53	0.58	0.78	0.05	0.86	0.37	0.84
CaO	0.05	0.03	0.04	0.06	0.03	0.04	0.00	0.02
Na2O	0.71	0.53	1.05	0.91	1.00	0.88	0.61	0.89
K2O	10.54	10.95	10.17	10.17	9.91	10.77	10.80	10.60
Cr2O3	0.01	0.02	0.00	0.00	0.00	0.08	0.00	0.00
Cl	N/D	N/D	N/D	N/D	N/D	N/D	N/D	N/D
P2O5	N/D	N/D	N/D	N/D	N/D	N/D	N/D	N/D
BaO	0.04	0.01	0.13	0.06	0.03	N/D	0.00	0.00
F	0.47	N/D	N/D	N/D	N/D	0.48	0.32	0.50
Total	95.94	94.66	97.78	95.75	94.73	97.44	96.36	96.75
Si	5.63	6.47	6.17	6.21	6.25	6.31	6.21	6.25
Ti	0.02	0.00	0.00	0.00	0.00	0.00	0.00	0.01
Al Total	4.24	5.22	5.49	5.39	5.33	5.19	5.31	5.37
Al IV	2.37	1.53	1.83	1.79	1.75	1.69	1.79	1.75
Al VI	1.86	3.69	3.66	3.59	3.58	3.50	3.51	3.62
Fe	3.56	0.58	0.41	0.47	0.48	0.53	0.52	0.36
Mn	0.08	0.02	0.00	0.01	0.01	0.02	0.03	0.01
Mg	0.05	0.02	0.00	0.02	0.00	0.02	0.03	0.03
Ca	0.01	0.00	0.00	0.00	0.00	0.00	0.01	0.00
Na	0.11	0.08	0.25	0.18	0.16	0.17	0.14	0.25
K	1.90	1.47	1.76	1.83	1.83	1.85	1.91	1.76
Cr	0.01	0.00	0.00	0.00	0.00	0.01	0.00	0.01
Cl	0.03	0.01						
P	0.01	0.01						
Ba	0.00	0.00	0.01	0.00	0.00	0.01	0.00	0.00
F	0.75	0.36						
OH	3.24	3.63	4.00	4.00	4.00	4.00	4.00	4.00
Tetrahedral	8.00	8.00	8.00	8.00	8.00	8.00	8.00	8.00
Octahedral	5.57	4.31	4.07	4.09	4.09	4.07	4.10	4.04
Dodecahedral	2.03	1.56	2.02	2.01	1.99	2.04	2.05	2.02

Sample	PC-1	PC-1	PC-1	PC-1	PC-1	PC-1	PC-1	PC-1	PC-1	PC-1	PC-1
Point	9	11	8	8	8	9	11	6	2	2	3
Description	P	P	P	P	P	P	P	P	P	P	P
SiO2	46.10	46.37	45.93	46.59	45.99	45.46	44.91	44.79	45.60	45.69	45.95
TiO2	0.05	0.00	0.15	0.02	0.17	0.03	0.05	0.29	0.04	0.00	0.15
Al2O3	35.59	36.30	36.23	36.93	37.33	36.85	36.01	34.77	36.71	36.76	36.60
FeO	1.98	1.38	1.72	1.37	1.15	1.06	1.28	2.16	1.23	1.31	1.50
MnO	0.04	0.03	0.00	0.03	0.06	0.00	0.03	0.05	0.00	0.09	0.03
MgO	0.37	0.18	0.25	0.09	0.22	0.10	0.21	0.60	0.10	0.15	0.15
CaO	0.00	0.02	0.00	0.00	0.00	0.00	0.01	0.04	0.00	0.04	0.06
Na2O	0.74	0.76	0.94	0.47	0.74	0.72	0.64	0.67	0.77	0.58	0.90
K2O	10.53	10.42	10.52	11.20	10.71	10.52	10.32	10.80	10.67	10.84	10.58
Cr2O3	0.06	0.10	0.05	0.04	0.00	0.00	0.00	0.00	0.00	0.00	0.00
Cl	N/D	N/D	N/D	N/D	N/D	N/D	N/D	N/D	N/D	N/D	N/D
P2O5	N/D	N/D	N/D	N/D	N/D	N/D	N/D	N/D	N/D	N/D	N/D
BaO	0.00	0.29	0.00	N/D	0.05	0.00	0.02	0.00	0.02	0.00	N/D
F	N/D	N/D	N/D	0.00	0.00	0.00	0.00	N/D	N/D	N/D	0.01
Total	95.46	95.86	95.78	96.74	96.39	94.74	93.49	94.18	95.14	95.46	95.93
Si	6.55	6.30	6.34	6.28	7.32	7.27	6.23	6.17	6.19	6.19	6.53
Ti	0.01	0.03	0.02	0.03	0.02	0.01	0.01	0.03	0.03	0.01	0.02
Al Total	5.07	5.39	5.36	5.43	3.81	4.02	5.63	5.76	5.69	5.62	5.15
Al IV	1.45	1.70	1.66	1.72	0.68	0.73	1.77	1.83	1.81	1.81	1.47
Al VI	3.62	3.68	3.70	3.71	3.13	3.29	3.86	3.93	3.88	3.81	3.69
Fe	0.58	0.48	0.47	0.46	1.24	1.14	0.43	0.28	0.26	0.31	0.54
Mn	0.02	0.03	0.02	0.02	0.08	0.06	0.02	0.02	0.00	0.00	0.03
Mg	0.05	0.04	0.04	0.05	0.05	0.06	0.03	0.02	0.03	0.03	0.03
Ca	0.00	0.00	0.00	0.00	0.01	0.00	0.01	0.00	0.00	0.00	0.00
Na	0.09	0.13	0.15	0.17	0.09	0.08	0.19	0.21	0.22	0.23	0.15
K	1.63	1.59	1.61	1.58	2.01	1.88	1.52	1.50	1.63	1.71	1.72
Cr	0.00	0.00	0.01	0.00	0.00	0.01	0.00	0.00	0.00	0.00	0.00
Cl	0.00	0.00	0.02	0.00	0.02	0.01	0.00	0.00	0.00	0.00	0.01
P	0.00	0.01	0.00	0.00	0.01	0.00	0.00	0.00	0.01	0.00	0.01
Ba	0.00	0.00	0.00	0.00	0.00	0.01	0.01	0.00	0.00	0.00	0.00
F	0.47	0.32	0.34	0.39	1.67	1.68	0.55	0.46	0.43	0.31	0.77
OH	3.53	3.67	3.65	3.61	2.32	2.31	3.45	3.54	3.57	3.69	3.23
Tetrahedral	8.00	8.00	8.00	8.00	8.00	8.00	8.00	8.00	8.00	8.00	8.00
Octahedral	4.28	4.26	4.24	4.28	4.52	4.56	4.35	4.28	4.20	4.16	4.30
Dodecahedral	1.71	1.73	1.78	1.76	2.11	1.96	1.73	1.72	1.87	1.95	1.88

Sample	PC-1	PC-1	PC-1	PC-1	PC-1	PC-1	PC-1	PC-1	PC-1	PC-1	PC-2
Point	10	2	3	10	7	7	5	4	4	4	6
Description	P	P	P	P	RB	RB	RB	RF	RF	RF	P
SiO2	46.42	45.84	46.05	46.26	45.67	46.18	45.57	45.50	45.74	44.82	46.24
TiO2	0.05	0.11	0.15	0.03	0.02	0.00	0.01	0.07	0.00	0.08	0.06
Al2O3	36.93	36.52	36.52	37.01	36.84	36.38	36.77	36.51	36.55	36.39	36.86
FeO	1.59	1.32	1.44	1.51	1.44	1.87	1.49	1.36	1.56	1.26	1.41
MnO	0.07	0.00	0.06	0.02	0.00	0.00	0.00	0.03	0.13	0.00	0.00
MgO	0.18	0.14	0.20	0.27	0.27	0.23	0.08	0.27	0.27	0.09	0.24
CaO	0.00	0.00	0.00	0.00	0.01	0.04	0.00	0.00	0.08	0.00	0.00
Na2O	0.85	0.57	0.69	0.93	0.83	0.71	0.70	0.80	0.60	0.75	0.70
K2O	10.61	10.49	10.72	10.50	10.77	10.55	10.66	10.30	10.67	10.53	10.72
Cr2O3	0.01	0.03	0.00	0.00	0.00	0.00	0.00	0.01	0.05	0.02	0.00
Cl	N/D	N/D	N/D	N/D	N/D	N/D	N/D	N/D	N/D	N/D	N/D
P2O5	N/D	N/D	N/D	N/D	N/D	N/D	N/D	N/D	N/D	N/D	N/D
BaO	N/D	0.00	0.00	0.01	0.16	0.00	0.05	0.14	N/D	0.02	0.00
F	0.00	0.00	0.09	0.00	N/D	0.07	0.00	N/D	0.00	0.00	N/D
Total	96.71	95.01	95.91	96.54	95.99	96.02	95.33	94.98	95.65	93.97	96.23
Si	6.19	6.21	6.21	6.21	6.26	6.28	6.22	6.20	6.24	6.25	6.19
Ti	0.01	0.02	0.03	0.01	0.01	0.00	0.01	0.01	0.00	0.00	0.02
Al Total	5.66	5.62	5.65	5.65	5.63	5.53	5.68	5.62	5.60	5.53	5.66
Al IV	1.81	1.79	1.79	1.79	1.74	1.72	1.78	1.80	1.76	1.75	1.81
Al VI	3.85	3.83	3.86	3.86	3.89	3.81	3.90	3.83	3.84	3.79	3.85
Fe	0.28	0.31	0.26	0.26	0.28	0.33	0.31	0.25	0.34	0.41	0.26
Mn	0.00	0.01	0.02	0.00	0.00	0.00	0.00	0.01	0.02	0.02	0.01
Mg	0.01	0.04	0.04	0.03	0.00	0.02	0.02	0.06	0.02	0.03	0.04
Ca	0.00	0.00	0.00	0.01	0.00	0.00	0.01	0.00	0.01	0.00	0.00
Na	0.26	0.24	0.18	0.23	0.20	0.17	0.15	0.23	0.21	0.22	0.24
K	1.70	1.65	1.59	1.59	1.55	1.71	1.33	1.65	1.64	1.66	1.65
Cr	0.00	0.00	0.00	0.01	0.00	0.01	0.01	0.00	0.00	0.01	0.00
Cl	0.00	0.01	0.00	0.01	0.01	0.00	0.00	0.00	0.02	0.02	0.01
P	0.00	0.00	0.01	0.01	0.01	0.00	0.03	0.00	0.00	0.01	0.01
Ba	0.00	0.00	0.00	0.01	0.01	0.01	0.00	0.01	0.00	0.01	0.00
F	0.38	0.41	0.37	0.37	0.34	0.35	0.29	0.28	0.40	0.46	0.37
OH	3.62	3.58	3.63	3.62	3.66	3.65	3.70	3.72	3.59	3.53	3.63
Tetrahedral	8.00	8.00	8.00	8.00	8.00	8.00	8.00	8.00	8.00	8.00	8.00
Octahedral	4.16	4.22	4.22	4.18	4.18	4.16	4.25	4.16	4.24	4.24	4.17
Dodecahedral	1.96	1.90	1.77	1.85	1.76	1.90	1.52	1.90	1.85	1.90	1.91

Sample	PC-2	PC-2	PC-2	PC-2	PC-2	PC-2	PC-2	PC-2	PC-2	PC-2	PC-2
Point	7	4	5	7	2	6	5	2	1	3	1
Description	P	P	P	P	P	P	P	RB	RB	RF	RF
SiO2	45.68	45.32	46.33	45.64	45.92	45.90	44.22	45.62	45.76	46.07	46.45
TiO2	0.03	0.39	0.18	0.20	0.09	0.22	0.17	0.10	0.02	0.29	0.15
Al2O3	36.64	35.00	36.53	36.82	36.23	36.04	34.98	36.98	37.03	37.50	36.84
FeO	1.60	1.04	1.36	0.97	1.12	1.37	2.30	1.14	1.34	1.21	1.37
MnO	0.10	0.12	0.03	0.08	0.04	0.08	0.00	0.01	0.05	0.10	0.06
MgO	0.16	0.45	0.42	0.48	0.38	0.46	0.66	0.13	0.23	0.22	0.24
CaO	0.00	0.02	0.01	0.00	0.00	0.06	0.00	0.00	0.00	0.01	0.00
Na2O	0.75	0.52	0.65	0.72	0.65	0.56	0.71	0.77	0.84	0.79	0.60
K2O	10.62	10.50	10.76	10.72	10.62	11.13	10.77	10.53	10.85	10.63	10.49
Cr2O3	0.00	0.06	0.02	0.00	0.02	0.00	0.03	0.08	0.00	0.00	0.00
Cl	N/D	N/D	N/D	N/D	N/D	N/D	N/D	N/D	N/D	N/D	N/D
P2O5	N/D	N/D	N/D	N/D	N/D	N/D	N/D	N/D	N/D	N/D	N/D
BaO	0.00	0.14	0.08	0.03	0.07	0.00	0.04	0.00	0.01	0.00	0.03
F	N/D	N/D	N/D	0.00	N/D	0.04	0.19	0.00	0.00	N/D	N/D
Total	95.58	93.57	96.36	95.67	95.16	95.86	94.08	95.34	96.13	96.83	96.22
Si	6.26	6.42	6.38	6.41	6.48	6.32	6.38	6.35	6.43	6.42	6.35
Ti	0.02	0.01	0.01	0.01	0.00	0.01	0.01	0.01	0.01	0.02	0.00
Al Total	5.62	5.26	5.26	5.18	5.05	5.37	5.22	5.32	5.27	5.15	5.49
Al IV	1.74	1.58	1.62	1.59	1.52	1.68	1.62	1.65	1.57	1.58	1.65
Al VI	3.88	3.68	3.64	3.60	3.52	3.69	3.60	3.67	3.71	3.58	3.83
Fe	0.30	0.45	0.47	0.51	0.55	0.42	0.49	0.43	0.37	0.48	0.34
Mn	0.00	0.02	0.00	0.01	0.01	0.02	0.02	0.02	0.01	0.02	0.01
Mg	0.03	0.06	0.04	0.07	0.07	0.04	0.05	0.05	0.06	0.06	0.04
Ca	0.00	0.00	0.01	0.00	0.00	0.00	0.00	0.00	0.01	0.00	0.00
Na	0.21	0.09	0.10	0.09	0.10	0.07	0.07	0.08	0.07	0.07	0.09
K	1.60	1.63	1.65	1.68	1.64	1.59	1.61	1.62	1.53	1.66	1.47
Cr	0.00	0.01	0.02	0.01	0.00	0.00	0.01	0.00	0.01	0.00	0.00
Cl	0.02	0.00	0.00	0.00	0.00	0.01	0.01	0.00	0.02	0.00	0.04
P	0.00	0.01	0.00	0.00	0.01	0.00	0.00	0.01	0.01	0.00	0.00
Ba	0.00	0.00	0.01	0.00	0.00	0.00	0.00	0.01	0.00	0.00	0.00
F	0.43	0.36	0.20	0.24	0.16	0.04	0.06	0.18	0.15	0.11	0.17
OH	3.56	3.64	3.80	3.76	3.84	3.96	3.93	3.82	3.85	3.89	3.81
Tetrahedral	8.00	8.00	8.00	8.00	8.00	8.00	8.00	8.00	8.00	8.00	8.00
Octahedral	4.23	4.23	4.17	4.19	4.17	4.18	4.18	4.19	4.17	4.16	4.23
Dodecahedral	1.81	1.74	1.78	1.80	1.76	1.66	1.69	1.72	1.61	1.73	1.56

Sample	PC-2	PC-2	PC-2	PC-2	PC-2
Point	3	4	4	3	4
Description	RF	RF	RF	RF	RF
SiO2	46.12	44.96	45.45	45.44	46.06
TiO2	0.17	0.00	0.00	0.00	0.14
Al2O3	36.25	35.56	35.63	37.06	36.45
FeO	1.19	1.30	1.23	1.51	1.19
MnO	0.02	0.00	0.00	0.00	0.00
MgO	0.44	0.27	0.24	0.16	0.37
CaO	0.04	0.00	0.00	0.00	0.00
Na2O	0.71	0.71	0.63	0.78	0.68
K2O	10.77	10.63	10.49	10.82	10.78
Cr2O3	0.00	0.00	0.01	0.00	0.00
Cl	N/D	N/D	N/D	N/D	N/D
P2O5	N/D	N/D	N/D	N/D	N/D
BaO	N/D	N/D	N/D	0.04	0.01
F	0.00	0.00	0.00	0.02	0.00
Total	95.70	93.44	93.68	95.82	95.68
Si	6.39	6.34	6.30	6.47	6.24
Ti	0.02	0.01	0.02	0.02	0.00
Al Total	5.23	5.47	5.44	5.20	5.57
Al IV	1.61	1.66	1.70	1.53	1.76
Al VI	3.62	3.80	3.74	3.67	3.81
Fe	0.44	0.22	0.35	0.42	0.29
Mn	0.02	0.01	0.01	0.01	0.02
Mg	0.07	0.03	0.03	0.04	0.04
Ca	0.01	0.00	0.01	0.00	0.00
Na	0.08	0.04	0.07	0.05	0.06
K	1.58	1.61	1.59	1.53	1.62
Cr	0.00	0.00	0.00	0.00	0.00
Cl	0.01	0.00	0.00	0.01	0.00
P	0.00	0.01	0.00	0.00	0.00
Ba	0.00	0.00	0.00	0.00	0.01
F	0.08	0.00	0.06	0.09	0.08
OH	3.91	4.00	3.94	3.90	3.92
Tetrahedral	8.00	8.00	8.00	8.00	8.00
Octahedral	4.18	4.07	4.16	4.16	4.16
Dodecahedral	1.67	1.65	1.66	1.58	1.69

SC-5-K MUSCOVITE ARGON SUMMARY

SPOT NO.	CODE NO	mV 39	AGE (Ma)±2σ	% ATM	37/39	36/40	39/40	% IIC
1	B59-1	133.6	367.8 ± 5.6	1.1	0.01	0.000039	0.011348	0
2	B59-2	127.6	370.3 ± 5.8	0.8	0.01	0.000027	0.011304	0
3	B59-3	307.6	365.4 ± 4.9	1.2	0.04	0.000043	0.011419	0
4	B59-4	122	369.1 ± 5.9	0.7	0.01	0.000024	0.011354	0
5	B59-5	112	368 ± 6	0.4	0.01	0.000015	0.011425	0
6	B59-6	193.5	367.1 ± 5.2	0.7	0	0.000026	0.011416	0
7	B59-7	216.4	371.8 ± 5.1	0.7	0	0.000026	0.011258	0
8	B59-8	133.2	369.8 ± 5.7	0.4	0.02	0.000014	0.011368	0
9	B59-9	172.8	369 ± 5.4	0.9	0.01	0.000031	0.011338	0
10	B59-10	781.9	371.6 ± 4.8	2.3	0.01	0.000081	0.011081	0
11	B59-11	1023.9	370.7 ± 4.8	1.1	0	0.000038	0.011254	0
12	B59-12	455	368.3 ± 4.8	1.2	0.02	0.000043	0.01132	0
13	B59-13	105.3	361.9 ± 6.2	3.9	0.17	0.000133	0.011228	0.02

MEAN AGE(SPOTS 1 - 13)= 369.5 ± 3.4 Ma (2σ UNCERTAINTY,INCLUDING ERROR IN J)

J = .002598 ± .000025 (.9 %)

37/39,36/40 AND 39/40 Ar RATIOS ARE CORRECTED FOR MASS SPECTROMETER DISCRIMINATION,INTERFERING ISOTOPES AND SYSTEM BLANKS

% IIC - INTERFERING ISOTOPES CORRECTION

LL2 MUSCOVITE ARGON SUMMARY

T°C	mV 39	39%	AGE (Ma)±1σ	% ATM	37/39	36/40	39/40	% IIC
650	15.7	0.7	371.8 ± 7.3	22.8	0.03	0.000774	0.007411	0
750	57	2.7	360.5 ± 2.6	14.6	0.01	0.000495	0.008492	0
775	74.5	3.6	363 ± 2	4.4	0	0.00015	0.009435	0
800	120.1	5.8	363.5 ± 1.8	1.8	0	0.000062	0.009676	0
825	177.3	8.6	362.2 ± 1.7	0.9	0	0.000031	0.009804	0
850	268.8	13	362.4 ± 1.6	0.6	0	0.000023	0.009824	0
875	300.7	14.6	362.9 ± 1.6	0.5	0	0.000019	0.009821	0
900	285.9	13.8	364 ± 1.6	0.6	0	0.000022	0.009778	0
925	234.9	11.4	364.1 ± 1.7	0.7	0	0.000025	0.009767	0
950	116	5.6	363.7 ± 1.8	0.8	0.01	0.000029	0.009769	0
975	75.1	3.6	364.7 ± 1.9	0.9	0.01	0.000032	0.00973	0
1000	82.1	3.9	365.3 ± 2	0.6	0.01	0.000022	0.009741	0
1025	78.4	3.8	365.9 ± 1.9	0.7	0.01	0.000023	0.00972	0
1050	69.7	3.3	365.8 ± 1.9	0.6	0.01	0.00002	0.00973	0
1150	87.4	4.2	366.3 ± 1.9	1.1	0.02	0.000038	0.009666	0
1450	13.7	0.6	367.8 ± 10.9	51.1	0.41	0.00173	0.004752	0.05

MEAN AGE(750°C-1450°C)= 363.6 ± 2.1 Ma (2σ UNCERTAINTY,INCLUDING ERROR IN J)
J = .002202 ± .000012 (.5 %)
37/39,36/40 AND 39/40 Ar RATIOS ARE CORRECTED FOR MASS SPECTROMETER DISCRIMINATION,INTERFERING ISOTOPES AND SYSTEM BLANKS
% IIC - INTERFERING ISOTOPES CORRECTION

LL3 MUSCOVITE ARGON SUMMARY

T°C	mV 39	39%	AGE (Ma)±1σ	% ATM	37/39	36/40	39/40	% IIC
600	3.4	0.2	444.6 ± 28	8	0.02	0.00027	0.007223	0
700	19.3	1.6	353.8 ± 4.9	12.6	0	0.000428	0.008866	0
750	33	2.7	360.7 ± 3.2	7.8	0	0.000265	0.009161	0
775	55.3	4.6	366.2 ± 2.4	3.3	0	0.000111	0.009455	0
800	77.8	6.5	362.6 ± 2	1.4	0	0.000048	0.009746	0
825	101.9	8.5	362.9 ± 1.8	0.7	0	0.000023	0.009808	0
850	115.8	9.7	362.1 ± 1.8	0.5	0	0.000019	0.009845	0
875	125.3	10.5	363.7 ± 1.8	0.6	0	0.00002	0.009794	0
900	117.7	9.8	363.5 ± 1.9	0.7	0	0.000023	0.009788	0
950	163.1	13.6	364.1 ± 1.7	0.8	0	0.000027	0.009761	0
975	82	6.8	363.4 ± 2	0.9	0	0.000031	0.009769	0
1000	84.4	7	363.6 ± 2	0.7	0	0.000026	0.009777	0
1025	92.6	7.7	364.5 ± 2	0.7	0	0.000024	0.009761	0
1050	76.1	6.3	364.5 ± 1.9	0.6	0	0.000022	0.009764	0
1075	32.4	2.7	365.3 ± 3	1.4	0	0.00005	0.009657	0
1100	7.4	0.6	370.7 ± 12.4	6.7	0	0.000227	0.008983	0
1150	2.5	0.2	415.8 ± 52	52.3	0.01	0.001767	0.004036	0
1450	0.9	0	919 ± 568	87	0.02	0.002944	0.000428	0

MEAN AGE(750°C-1075°C)= 363.6 ± 2.1 Ma (2σ UNCERTAINTY,INCLUDING ERROR IN J)
J = .002202 ± .000012 (.5 %)
37/39,36/40 AND 39/40 Ar RATIOS ARE CORRECTED FOR MASS SPECTROMETER DISCRIMINATION,INTERFERING ISOTOPES AND SYSTEM BLANKS
% IIC - INTERFERING ISOTOPES CORRECTION

SC-12-L MUSCOVITE ARGON SUMMARY

SPOT NO.	CODE NO.	mV 39	AGE (Ma)±2σ	% ATM	37/39	36/40	39/40	% IIC
1	A85-1-2	74.4	322.2 ± 5.3	8.9	0.19	0.000301	0.011347	0.03
2	A85-1-3	109.6	352.2 ± 5.4	1.8	0.11	0.000063	0.011085	0.01
3	A85-1-4	99.4	375.2 ± 5.1	0.4	0	0.000016	0.010486	0
4	A85-2-1	15.3	362.6 ± 11.8	2.1	0.05	0.000072	0.010712	0
5	A85-2-2	32.6	365.5 ± 9.1	1.9	0.03	0.000067	0.010633	0
6	A85-2-3	33	366.5 ± 6.9	1.9	0.03	0.000065	0.010606	0
7	A85-2-4	13.1	321.1 ± 12.1	5.5	0.19	0.000189	0.011811	0.03
8	A85-2-4	49.9	371.2 ± 5.9	4.8	0.03	0.000165	0.010144	0
9	A85-4-1	220.2	369.9 ± 5.9	6.6	0.02	0.000224	0.009994	0
10	A85-4-2	108.5	377.4 ± 5.6	3.5	0	0.000119	0.0101	0
11	A85-4-3	771.8	370.8 ± 5.9	2.8	0.02	0.000096	0.010372	0
12	A85-8-1	93.1	369.3 ± 5.2	4.1	0.01	0.000139	0.010284	0
13	A85-8-2	105.5	370.1 ± 5	2.7	0.02	0.000091	0.01041	0
14	A85-8-3	273.1	359.7 ± 4.6	1	0.02	0.000035	0.010923	0
15	A85-8-4	81.7	346.9 ± 5.1	1.4	0.11	0.000048	0.011325	0.01

MEAN AGE(SPOTS 1 - 15)= 365.6 ± 3.8 Ma (2σ UNCERTAINTY,INCLUDING ERROR IN J)
J = .002437 ± .0000244 (1 %)
37/39,36/40 AND 39/40 Ar RATIOS ARE CORRECTED FOR MASS SPECTROMETER DISCRIMINATION,INTERFERING ISOTOPES AND SYSTEM BLANKS
% IIC - INTERFERING ISOTOPES CORRECTION

A9B-7558 MUSCOVITE ARGON SUMMARY

SPOT NO.	CODE NO.	mV 39	AGE (Ma)±2σ	% ATM	37/39	36/40	39/40	% IIC
1	Y80-1-1	28.1	370.4 ± 6.4	16.2	0	0.000548	0.008176	0
2	Y80-1-2	14.3	373.1 ± 8	10.6	0	0.00036	0.008647	0
3	Y80-1-3	18	368 ± 6.7	9.3	0	0.000315	0.008911	0
4	Y80-2-1	27.3	372.7 ± 6.1	9.1	0	0.000309	0.008804	0
5	Y80-2-2	38.1	367.9 ± 12	46.4	0	0.001571	0.005266	0
6	Y80-2-3	22.2	364.4 ± 8	25.3	0.03	0.000859	0.007412	0
7	Y80-2-4	26	368.4 ± 7.9	26.4	0.01	0.000895	0.00722	0
8	Y80-2-5	15.5	365.9 ± 10.3	23.1	0	0.000784	0.007596	0
9	Y80-2-6	24.5	370.8 ± 8.2	28.5	0	0.000967	0.00696	0
10	Y80-2-7	29.9	369 ± 6.5	14.7	0	0.0005	0.008349	0
11	Y80-2-8	39.1	373.5 ± 6.5	3.6	0	0.000124	0.009309	0
12	Y80-2-9	16.3	367.5 ± 12.4	15	1.09	0.000507	0.008368	0.15
13	Y80-2-10	27.5	371.4 ± 8.8	14.5	0.8	0.000492	0.008316	0.11
14	Y80-3-3	63.7	371.3 ± 8.3	31.4	0	0.001063	0.006673	0
15	Y80-3-4	21.7	362.7 ± 10.7	39.2	0	0.001327	0.006069	0
16	Y80-4-1	19.5	357.2 ± 16.4	42.3	0.83	0.001434	0.005854	0.11
17	Y80-4-2	40.6	366.2 ± 8.9	3.1	0.41	0.000105	0.009574	0.05
18	Y80-4-3	35.1	366.7 ± 8.5	22.4	0.78	0.000759	0.007654	0.1
19	Y80-5-1	85.1	368.1 ± 6.2	15.3	0.18	0.000518	0.008319	0.02
20	Y80-5-2	51.8	367 ± 6.5	8.8	0.44	0.000299	0.008985	0.06
21	Y80-7-1	23.2	366.1 ± 8.8	6.8	1.58	0.000233	0.009205	0.22
22	Y80-7-2	22.2	362.8 ± 13.8	38.7	1.51	0.001312	0.006112	0.21
23	Y80-7-3	44.4	369.5 ± 6.8	11	0.84	0.000373	0.008706	0.11
24	Y80-7-4	46.1	370.7 ± 6.3	5.8	0.66	0.000197	0.009167	0.09
25	Y80-7-5	109.5	376.9 ± 5.2	4.7	0.32	0.00016	0.009102	0.04

MEAN AGE(SPOTS 1 - 26)= 368.5 ± 3.7 Ma (2σ UNCERTAINTY,INCLUDING ERROR IN J)

J = .002221 ± .0000222 (.9 %)

37/39,36/40 AND 39/40 Ar RATIOS ARE CORRECTED FOR MASS SPECTROMETER DISCRIMINATION,INTERFERING ISOTOPES AND SYSTEM BLANKS

% IIC - INTERFERING ISOTOPES CORRECTION

A9B-7558 MUSCOVITE ARGON SUMMARY

T°C	mV 39	39%	AGE (Ma)±1σ	% ATM	37/39	36/40	39/40	% IIC
650	11.8	0.4	373.5 ± 16.9	63.3	0	0.002144	0.003506	0
750	55.1	2.1	364.6 ± 3.3	23.6	0	0.000799	0.007517	0
775	107	4.2	368.4 ± 2	5.4	0	0.000184	0.009202	0
800	182.1	7.1	365.6 ± 2.2	1.6	0	0.000054	0.009659	0
825	245.2	9.6	366.5 ± 1.7	0.6	0	0.000023	0.009719	0
850	266.2	10.5	365.6 ± 1.6	0.3	0	0.000013	0.009777	0
875	280.7	11	366.4 ± 1.6	0.4	0	0.000014	0.009748	0
900	244.3	9.6	366.2 ± 1.7	0.5	0	0.000018	0.009745	0
925	200.6	7.9	366.4 ± 1.7	0.6	0	0.000023	0.009725	0
950	147.1	5.8	366.6 ± 1.7	0.6	0	0.000022	0.009721	0
975	148.1	5.8	366.4 ± 1.7	0.5	0	0.000017	0.00974	0
1000	169.9	6.7	366.3 ± 1.7	0.4	0	0.000013	0.009756	0
1025	184.4	7.2	366.4 ± 1.7	0.3	0	0.000013	0.009752	0
1050	157.5	6.2	368.2 ± 1.7	0.3	0	0.000011	0.009706	0
1250	124.9	4.9	369.9 ± 1.8	1.5	0	0.000053	0.009534	0
1450	7.4	0.2	415.9 ± 21.8	49.5	0	0.001675	0.004285	0

MEAN AGE(750°C-1250°C)= 366.6 ± 2 Ma (2σ UNCERTAINTY,INCLUDING ERROR IN J)
J = .002206 ± .000012 (.5 %)
37/39,36/40 AND 39/40 Ar RATIOS ARE CORRECTED FOR MASS SPECTROMETER DISCRIMINATION,INTERFERING ISOTOPES AND SYSTEM BLANKS
% IIC - INTERFERING ISOTOPES CORRECTION

SC-12-L K-FELDSPAR ARGON SUMMARY

SPOT NO.	CODE NO.	mV 39	AGE (Ma)±2σ	% ATM	37/39	36/40	39/40	% IIC
1	B79-1	236	329.3 ± 4.9	7.1	0.01	0.00024	0.01157	0
2	B79-16	800.1	298.2 ± 4.2	10.3	0.01	0.00035	0.01245	0
3	B79-17	464.9	323.3 ± 4.4	5.9	0.01	0.0002	0.01196	0
4	B79-2	240.7	324.7 ± 4.7	7.6	0.01	0.00026	0.01169	0
5	B79-3	341.2	333.5 ± 4.7	6.7	0	0.00023	0.01146	0
6	B79-18	159.3	339.3 ± 5.3	5	0.01	0.00017	0.01145	0
7	B79-19	596.4	345.5 ± 4.6	5.3	0	0.00018	0.01119	0
8	B79-4	211.3	317.8 ± 4.8	8	0.01	0.00027	0.01191	0
9	B79-5	261.1	332.9 ± 4.9	9.1	0.01	0.00031	0.01119	0
10	B79-6	464.7	305.2 ± 4.3	8.3	0.01	0.00028	0.0124	0
11	B79-20	337	321.5 ± 4.4	5.5	0.01	0.00019	0.01208	0
12	B79-21	734.6	283.6 ± 4.5	17.6	0.01	0.0006	0.01207	0
13	B79-7	173.9	323.5 ± 5.1	9.4	0.01	0.00032	0.0115	0
14	B79-8	178.9	335.6 ± 5.1	6.6	0.01	0.00022	0.0114	0
15	B79-9	218.3	332.9 ± 6.4	6.9	0.01	0.00024	0.01145	0
16	B79-10	183.6	344.5 ± 5.3	6.4	0.01	0.00022	0.0111	0
17	B79-22	127.8	349.1 ± 5.6	3.8	0.02	0.00013	0.01124	0
18	B79-23	162.8	347.6 ± 5.2	2.6	0.01	8.9E-05	0.01143	0
19	B79-26	257.4	279.5 ± 4.7	17.8	0.02	0.0006	0.01224	0
20	B79-11	175.4	312.6 ± 5.3	10.7	0.02	0.00036	0.01177	0
21	B79-12	188.1	325.2 ± 5	6.5	0.01	0.00022	0.01181	0
22	B79-13	182.8	334.9 ± 5	5.4	0.01	0.00019	0.01156	0
23	B79-24	105.4	353 ± 6.3	3.3	0	0.00011	0.01116	0
24	B79-25	118.1	309.2 ± 5.7	12.6	0.01	0.00043	0.01165	0
25	B79-29	269.7	331.4 ± 4.7	6.6	0	0.00022	0.01156	0

MEAN AGE(SPOTS 1 - 25)= 319.6 ± 3 Ma (2σ UNCERTAINTY,INCLUDING ERROR IN J) J = .002496 ± .000025 (1 %)
37/39,36/40 AND 39/40 Ar RATIOS ARE CORRECTED FOR MASS SPECTRO-METER DISCRIMINATION,INTERFERING ISOTOPES AND SYSTEM BLANKS
% IIC - INTERFERING ISOTOPES CORRECTION

SC-12-L K-FELDSPAR ARGON SUMMARY

T°C	mV 39	39%	AGE (Ma)±1σ	% ATM	37/39	36/40	39/40	% IIC
550	49.8	2	294.4 ± 5.6	3.7	0.01	0.000127	0.012276	0
580	78.2	3.2	320 ± 3.9	4.2	0	0.000143	0.011144	0
610	88.1	3.6	329.6 ± 3.5	2.7	0	0.000094	0.010952	0
640	74.8	3	334.3 ± 3.6	1.1	0	0.000037	0.010969	0
700	153.2	6.3	345.2 ± 2.9	9.8	0	0.000332	0.00965	0
730	80.7	3.3	331.5 ± 3.3	0.9	0	0.000033	0.011085	0
760	51.5	2.1	324.9 ± 4.9	0.6	0.01	0.000022	0.011377	0
790	37.8	1.5	323.5 ± 6.8	0.2	0	0.000009	0.011492	0
820	33.8	1.3	319.6 ± 7.3	0.3	0	0.000011	0.011644	0
850	31.7	1.3	315.5 ± 7.9	1.1	0.01	0.00004	0.011711	0
880	37.1	1.5	309.9 ± 7.1	4.9	0.01	0.000167	0.011481	0
910	42.2	1.7	306.4 ± 6.4	4.8	0.01	0.000164	0.011627	0
940	57.3	2.3	310.6 ± 5.2	7.3	0.01	0.000249	0.011143	0
970	80.5	3.3	311.1 ± 4.2	8.7	0.01	0.000295	0.010949	0
1000	113.2	4.6	313.6 ± 3.6	9.2	0.01	0.000313	0.010785	0
1025	133.8	5.5	315.9 ± 2.9	9.5	0	0.000322	0.010667	0
1050	137.3	5.6	314.8 ± 2.9	9.3	0.01	0.000317	0.010726	0
1075	135.3	5.5	319.7 ± 3	7.2	0.01	0.000246	0.010789	0
1100	138.6	5.7	323.7 ± 2.7	4.9	0	0.000167	0.010914	0
1125	176.5	7.2	327.4 ± 2.3	3.7	0	0.000125	0.010918	0
1150	238.8	9.8	332.5 ± 2	3.1	0	0.000106	0.010791	0
1200	393.2	16.1	343.5 ± 1.8	2.4	0	0.000081	0.010493	0
1250	44.7	1.8	346.3 ± 6.4	6.6	0	0.000225	0.009974	0
1350	14.7	0.6	342.3 ± 20.6	31.6	0	0.001079	0.007416	0
1450	5.7	0.2	329 ± 79.6	77	0.04	0.002623	0.002599	0

TOTAL GAS AGE = 327 ± 2.1 Ma

J = .002255 ± 1.1275E-05 (.5 %)

37/39,36/40 AND 39/40 Ar RATIOS ARE CORRECTED FOR MASS SPECTROMETER DISCRIMINATION,INTERFERING ISOTOPES AND SYSTEM BLANKS

% IIC - INTERFERING ISOTOPES CORRECTION

A9B-7504 K-FELDSPAR ARGON SUMMARY

SPOT NO.	CODE NO.	mV 39	AGE (Ma)±2σ	% ATM	37/39	36/40	39/40	% IIC
1	B81-6	629.1	349.8 ± 4.6	1.4	0	0.00005	0.011744	0
2	B81-7	534.9	281.3 ± 4.3	14.2	0.01	0.000482	0.01296	0
3	B81-12	520	355.8 ± 4.7	1.6	0	0.000056	0.011503	0
4	B81-13	931.9	341.5 ± 4.5	3.8	0	0.000129	0.011771	0
5	B81-2	497.5	306.8 ± 4.3	7.1	0	0.00024	0.012786	0
6	B81-5	466.3	329.8 ± 4.5	4.4	0	0.000151	0.012145	0
7	B81-11	357.6	332.5 ± 4.6	5.1	0	0.000175	0.011948	0
8	B81-10	392.2	329.7 ± 4.5	4.2	0	0.000144	0.012177	0
9	B81-4	307.2	359.5 ± 4.8	1	0	0.000034	0.011452	0
10	B81-1	221.3	325.7 ± 4.5	1.3	0	0.000044	0.012725	0

MEAN AGE(SPOTS 1 - 10)= 331.8 ± 3.1 Ma (2σ UNCERTAINTY,INCLUDING ERROR IN J)

J = .002552 ± .000025 (.9 %)

37/39,36/40 AND 39/40 Ar RATIOS ARE CORRECTED FOR MASS SPECTROMETER DISCRIMINATION,INTERFERING ISOTOPES AND SYSTEM BLANKS

% IIC - INTERFERING ISOTOPES CORRECTION

A9B-7504 K-FELDSPAR ARGON SUMMARY

T°C	mV 39	39%	AGE (Ma)±1σ	% ATM	37/39	36/40	39/40	% IIC
550	33.8	0.8	298.2 ± 4.6	0.3	0	0.000013	0.01246	0
600	103.6	2.7	309.2 ± 2.1	1	0	0.000034	0.011878	0
640	82.5	2.1	319.3 ± 2.4	1.1	0	0.00004	0.011453	0
680	61.2	1.6	321.2 ± 3.6	6.8	0	0.000233	0.010726	0
720	59.4	1.5	333.4 ± 3.1	1	0	0.000035	0.010943	0
760	66.2	1.7	328.4 ± 2.7	0.8	0	0.000028	0.011148	0
800	76.4	2	329.5 ± 2.7	1	0	0.000035	0.011082	0
825	54.1	1.4	322.6 ± 3.5	1	0	0.000036	0.011343	0
850	59	1.5	323.9 ± 2.9	0.7	0	0.000025	0.011329	0
875	61.7	1.6	327 ± 2.9	0.5	0	0.000019	0.011231	0
900	51.6	1.3	322.7 ± 3.4	0.2	0	0.000008	0.011436	0
920	61.6	1.6	322.2 ± 2.9	1	0	0.000037	0.011353	0
940	99.9	2.6	328.6 ± 2.2	1.9	0	0.000065	0.011014	0
960	163.4	4.3	331.6 ± 1.9	2.6	0	0.000088	0.010825	0
980	195.5	5.1	332.3 ± 1.8	3.2	0	0.00011	0.010726	0
1000	187.3	4.9	331.5 ± 1.9	3.9	0	0.000134	0.010676	0
1025	283.1	7.4	338.2 ± 1.7	2.7	0	0.000094	0.010576	0
1050	479.2	12.6	337.2 ± 1.6	3.8	0	0.00013	0.010491	0
1075	124.6	3.2	338.8 ± 2.3	5.7	0	0.000194	0.010238	0
1100	122.4	3.2	340.2 ± 2.3	6.1	0	0.000209	0.010143	0
1100	31.7	0.8	344.7 ± 5.5	5	0	0.000172	0.01013	0
1150	124.4	3.2	341.1 ± 2.3	4.1	0	0.000141	0.010328	0
1200	405.8	10.6	341.6 ± 1.7	3.5	0	0.00012	0.010377	0
1300	667.8	17.5	345.7 ± 1.6	3.4	0	0.000116	0.010251	0
1450	138.4	3.6	347.6 ± 2.6	16.9	0	0.000573	0.008771	0

TOTAL GAS AGE = 335.8 ± 1.8 Ma

J = .002243 ± 1.1215E-05 (.5 %)

37/39,36/40 AND 39/40 Ar RATIOS ARE CORRECTED FOR MASS SPECTROMETER DISCRIMINATION,INTERFERING ISOTOPES AND SYSTEM BLANKS

% IIC - INTERFERING ISOTOPES CORRECTION

SW-LL-01 K-FELDSPAR ARGON SUMMARY

SPOT NO.	CODE NO.	mV 39	AGE (Ma)±2σ	% ATM	37/39	36/40	39/40	% IIC
1	B78-21	934.1	258.7 ± 4	15.4	0.06	0.000523	0.013882	0.01
2	B78-17	755.7	261.7 ± 4	15.4	0.01	0.000521	0.013718	0
3	B78-13	376.3	265 ± 4.1	13.7	0	0.000465	0.013804	0
4	B78-20	2154.9	257 ± 4.1	17.3	0.01	0.000588	0.013657	0
5	B78-22	594.5	259.7 ± 4	14.8	0.01	0.000501	0.013926	0
6	B78-25	1302.4	265.3 ± 3.9	12.3	0.01	0.000416	0.014017	0

MEAN AGE(SPOTS 1 - 6)= 260.4 ± 2.8 Ma (2σ UNCERTAINTY,INCLUDING ERROR IN J)

J = .002533 ± .000025 (.9 %)

37/39,36/40 AND 39/40 Ar RATIOS ARE CORRECTED FOR MASS SPECTROMETER DISCRIMINATION,INTERFERING ISOTOPES AND SYSTEM BLANKS

% IIC - INTERFERING ISOTOPES CORRECTION

WAM ARGON SUMMARY

SPOT NO.	CODE NO.	mV 39	AGE (Ma)±2σ	% ATM	37/39	36/40	39/40	% IIC
1	Y79-1-1	88.7	365.4 ± 6.6	1.6	0	0.000057	0.009757	0
2	Y79-3-1	274.8	365.3 ± 4.8	1.4	0	0.00005	0.00978	0
3	Y79-2-1	94.2	367.6 ± 5	3.3	0	0.000114	0.009526	0

MEAN AGE(SPOTS 1 - 3)= 365.8 ± 4.1 Ma (2σ UNCERTAINTY,INCLUDING ERROR IN J)
J = .002229 ± .0000222 (.9 %)
37/39,36/40 AND 39/40 Ar RATIOS ARE CORRECTED FOR MASS SPECTROMETER DISCRIMINATION,INTERFERING ISOTOPES AND SYSTEM BLANKS
% IIC - INTERFERING ISOTOPES CORRECTION

WB MUSCOVITE ARGON SUMMARY

T°C	mV 39	39%	AGE (Ma)±1σ	% ATM	37/39	36/40	39/40	% IIC
650	31.1	1.5	337.4 ± 3.5	16.2	0	0.00055	0.008957	0.01
750	73	3.6	357.4 ± 2.3	13.3	0	0.000453	0.008699	0.01
775	69.8	3.4	365.1 ± 2.1	4.3	0	0.000146	0.009384	0.01
800	105.5	5.2	364 ± 1.8	1.8	0	0.000063	0.00966	0.01
825	146.7	7.3	364.7 ± 1.8	0.8	0	0.000029	0.009737	0.01
850	172.2	8.5	364.2 ± 1.7	0.6	0	0.000021	0.009774	0.01
875	212	10.5	364.8 ± 1.7	0.6	0	0.000021	0.009756	0.01
900	223.7	11.1	368.3 ± 2.4	0.7	0	0.000024	0.009646	0.01
925	213.1	10.6	366.1 ± 1.7	0.6	0	0.000022	0.009718	0.01
950	135.1	6.7	365.8 ± 1.8	0.8	0	0.000027	0.009709	0.01
1000	174.7	8.7	364.6 ± 1.7	0.7	0	0.000026	0.009748	0.01
1025	142	7	364.9 ± 1.7	0.7	0	0.000024	0.009746	0.01
1050	153.7	7.6	365.9 ± 1.9	0.6	0	0.000021	0.009725	0.01
1150	75.9	3.7	361.4 ± 2.1	1.7	0	0.000058	0.009748	0.01
1450	74.4	3.7	345.1 ± 2.4	16.7	0.01	0.000565	0.008693	0.01

MEAN AGE(775°C-1150°C)= 365.3 ± 2.1 Ma (2σ UNCERTAINTY,INCLUDING ERROR IN J)
J = .002202 ± .000012 (.5 %)
37/39,36/40 AND 39/40 Ar RATIOS ARE CORRECTED FOR MASS SPECTROMETER DISCRIMINATION,INTERFERING ISOTOPES AND SYSTEM BLANKS
% IIC - INTERFERING ISOTOPES CORRECTION

WBM MUSCOVITE ARGON SUMMARY

SPOT NO.	CODE NO.	mV 39	AGE (Ma)±2σ	% ATM	37/39	36/40	39/40	% IIC
1	Y75-3-1	25.4	363.3 ± 5.7	2.6	0	0.00009	0.009759	0.01
2	Y75-3-2	52.1	364.7 ± 4.9	1.7	0	0.000057	0.009816	0.01
3	Y75-3-3	89.3	368.5 ± 4.8	2	0	0.000069	0.009673	0.01
4	Y75-4-1	179.1	363.9 ± 5	1.4	0	0.00005	0.009861	0.01
5	Y75-4-2	17.1	363.7 ± 6.5	0.1	0	0.000005	0.009999	0.01
6	Y75-4-3	31.1	365.6 ± 5.5	0.2	0	0.000007	0.009936	0.01
7	Y75-1-1	77.7	366.7 ± 5.3	11	0	0.000372	0.008836	0.01
8	Y75-8-1	189.5	369.4 ± 5.2	2.5	0	0.000087	0.009591	0.01
9	Y75-13-1	154.9	364 ± 4.8	2.1	0.02	0.000072	0.009795	0.01

MEAN AGE(SPOTS 1 - 9)= 366.1 ± 3.6 Ma (2σ UNCERTAINTY,INCLUDING ERROR IN J)

J = .002239 ± .000022 (.9 %)

37/39,36/40 AND 39/40 Ar RATIOS ARE CORRECTED FOR MASS SPECTROMETER DISCRIMINATION,INTERFERING ISOTOPES AND SYSTEM BLANKS

% IIC - INTERFERING ISOTOPES CORRECTION

SC-9-W MUSCOVITE ARGON SUMMARY

SPOT NO.	CODE NO.	mV 39	AGE (Ma)±2σ	% ATM	37/39	36/40	39/40	% IIC
1	A84-4	247.1	365.3 ± 4.7	0.9	0	0.000033	0.010778	0
2	A84-5	247	360.6 ± 4.7	0.9	0	0.000033	0.010934	0
3	A84-6	315.8	365.1 ± 4.7	0.8	0	0.000029	0.010794	0
4	A84-7-3	182.1	367.7 ± 4.8	0.4	0	0.000015	0.01076	0
5	A84-3	141.7	368.7 ± 4.9	0.7	0.01	0.000023	0.010698	0
6	A84-2-1	67.9	357.5 ± 5.6	4.6	0.09	0.000158	0.010628	0.01
7	A84-2-2	416.8	365.8 ± 4.7	0.2	0.01	0.000009	0.010839	0
8	A84-1	306.6	361 ± 4.7	1.1	0.04	0.000038	0.010903	0
9	A84-10	168.2	365.3 ± 4.8	0.6	0.01	0.000023	0.01081	0
10	A84-12	241.6	360 ± 4.7	0.8	0.01	0.000029	0.010966	0
11	A84-13	240.6	361.3 ± 4.7	0.8	0.01	0.000028	0.010925	0
12	A84-14	133.4	358.4 ± 4.9	2.4	0.05	0.000084	0.010838	0
13	A84-8	65.2	327 ± 5.3	3.5	0.18	0.000119	0.011859	0.02
14	A84-9	114.9	349.2 ± 5	1.8	0.08	0.000063	0.011224	0.01
15	A84-10	285.8	359 ± 4.7	1.2	0.03	0.000043	0.010952	0
16	A84-15	50.8	368.7 ± 6	0.5	0	0.000017	0.010719	0

MEAN AGE(SPOTS 1 - 18)= 359.8 ± 3.3 Ma (2σ UNCERTAINTY,INCLUDING ERROR IN J)
J = .002444 ± .0000244 (.9 %)
37/39,36/40 AND 39/40 Ar RATIOS ARE CORRECTED FOR MASS SPECTROMETER DISCRIMINATION,INTERFERING ISOTOPES AND SYSTEM BLANKS
% IIC - INTERFERING ISOTOPES CORRECTION

SC-9-W K-FELDSPAR ARGON SUMMARY

T°C	mV 39	39%	AGE (Ma)±1σ	% ATM	37/39	36/40	39/40	% IIC
550	39.4	1.8	344.7 ± 7.6	15.5	0.02	0.000526	0.008994	0
580	52	2.4	335.8 ± 4.8	4.3	0.01	0.000145	0.010485	0
610	54.9	2.5	345.7 ± 3.9	2.5	0	0.000087	0.010336	0
640	51.6	2.3	348.1 ± 3.9	1.8	0	0.000061	0.010341	0
670	49.9	2.3	344.8 ± 4.9	4.9	0	0.000166	0.010118	0
700	52.6	2.4	352.6 ± 4.4	3.4	0	0.000118	0.010018	0
730	56.1	2.5	350.2 ± 4.3	3.5	0	0.00012	0.010086	0
760	48	2.2	346.9 ± 4.8	4.2	0	0.000143	0.010125	0
790	38.5	1.7	343.8 ± 5.3	3.4	0	0.000118	0.010306	0
820	38.7	1.7	344.1 ± 5.7	3.2	0	0.000109	0.010324	0
850	37.2	1.7	343.7 ± 6.3	4.4	0	0.000151	0.010206	0
880	35.9	1.6	341.7 ± 6.3	6	0.01	0.000203	0.010105	0
910	38.4	1.7	340.7 ± 6.1	5.6	0.01	0.000193	0.010174	0
940	86.1	3.9	344.9 ± 3.3	5	0	0.000171	0.010092	0
970	107.4	4.9	343.7 ± 3	5.2	0	0.000176	0.010115	0
1000	150.6	6.9	342.4 ± 2.4	5.2	0	0.000177	0.010154	0
1025	152.3	7	343.1 ± 2.4	5.1	0	0.000172	0.010144	0
1050	95.7	4.4	343.6 ± 3.1	4.9	0	0.000166	0.010152	0
1075	136.1	6.3	349.4 ± 2.4	2.9	0	0.0001	0.010168	0
1100	114.3	5.2	349.4 ± 2.8	3.9	0	0.000132	0.010068	0
1125	121.1	5.6	349.5 ± 2.6	2.8	0	0.000095	0.01018	0
1150	149.1	6.9	350.4 ± 2.4	2.7	0	0.000094	0.010154	0
1200	325.8	15	354.8 ± 1.8	2.3	0	0.00008	0.010055	0
1250	93.1	4.3	358.6 ± 3.4	6.3	0	0.000215	0.009537	0
1350	14.9	0.6	359.7 ± 20	36	0	0.001222	0.006511	0
1450	16.4	0.7	339.2 ± 22.9	55.7	0	0.00189	0.004799	0
1500	1.6	0	412.4 ± 623	94	0.1	0.003187	0.000523	0.01

TOTAL GAS AGE = 347.9 ± 2.3 Ma

J = .002239 ± 1.1195E-05 (.5 %)

37/39,36/40 AND 39/40 Ar RATIOS ARE CORRECTED FOR MASS SPECTRO-METER DISCRIMINATION,INTERFERING ISOTOPES AND SYSTEM BLANKS

% IIC - INTERFERING ISOTOPES CORRECTION

SC-2-T MUSCOVITE ARGON SUMMARY

SPOT NO.	CODE NO.	mV 39	AGE (Ma)±2σ	% ATM	37/39	36/40	39/40	% IIC
1	A82-21	71.8	376.6 ± 5.3	1.8	0	0.000062	0.009645	0
2	A82-10	54.7	375.9 ± 5.7	3.7	0	0.000127	0.009477	0
3	A82-3-1	53.5	371.1 ± 5.6	2.5	0	0.000085	0.009737	0
4	A82-3-2	42.7	371 ± 5.8	0.2	0	0.000007	0.009969	0
5	A82-3-3	7.5	362.1 ± 25.8	0.1	0.02	0.000005	0.01025	0
6	A82-3-4	64.6	367.1 ± 5.6	0	0	0.000001	0.010104	0
7	A82-5-2	43.9	321.6 ± 5.6	4.1	0.1	0.000139	0.011209	0.01
8	A82-5-3	55.3	349.8 ± 5.7	2.4	0.07	0.000084	0.010395	0.01
9	A82-6	441.8	370.4 ± 4.9	4.2	0.01	0.000143	0.009584	0
10	A82-7	794.3	369.4 ± 4.8	1.7	0.03	0.000059	0.009863	0
11	A82-1	227.4	363.5 ± 4.8	3.5	0.01	0.000119	0.009857	0
12	A82-2	154.1	364.3 ± 4.8	2.2	0.02	0.000076	0.009964	0
13	A82-4	133.3	362.8 ± 4.9	2.1	0.05	0.000071	0.010023	0
14	A82-8	233.1	362.3 ± 4.9	4.1	0.02	0.00014	0.009831	0
15	A82-9	226.4	363.7 ± 4.8	2.5	0.05	0.000085	0.009955	0
16	A82-11	237.2	364.7 ± 4.8	1.9	0.08	0.000066	0.009981	0.01
17	A82-14	294.6	368.3 ± 4.8	1.8	0.07	0.000061	0.009889	0.01
18	A82-17	401.7	374.6 ± 4.8	2.6	0	0.00009	0.009621	0

MEAN AGE(SPOTS 1 - 18)= 366.5 ± 3.5 Ma (2σ UNCERTAINTY,INCLUDING ERROR IN J)
J = .002282 ± .000023 (1 %)
37/39,36/40 AND 39/40 Ar RATIOS ARE CORRECTED FOR MASS SPECTROMETER DISCRIMINATION,INTERFERING ISOTOPES AND SYSTEM BLANKS
% IIC - INTERFERING ISOTOPES CORRECTION

SC-14-T MUSCOVITE ARGON SUMMARY

SPOT NO.	CODE NO.	mV 39	AGE (Ma)±2σ	% ATM	37/39	36/40	39/40	% IIC
1	A81-12	94.3	369.5 ± 5.3	0.1	0	0.000005	0.01016	0
2	A81-9	55.6	369.3 ± 5.8	1.7	0.06	0.00006	0.010001	0
3	A81-1	160	365.4 ± 4.8	0.7	0	0.000024	0.010229	0
4	A81-5	111.5	365.7 ± 5	0.5	0	0.000018	0.010236	0
5	A81-11-1	35.6	352.3 ± 6.3	2.2	0.05	0.000075	0.010488	0
6	A81-6-1	44.4	371.8 ± 6	0.2	0	0.000008	0.010082	0
7	A81-6-3	24.5	362.2 ± 9.1	0.5	0.03	0.000019	0.010346	0
8	A81-8-2	220.7	370 ± 5	0.7	0.02	0.000025	0.010085	0
9	A81-8-2	254.6	370.3 ± 4.8	0.3	0.02	0.00001	0.010119	0
10	A81-14	615.7	374.1 ± 4.8	0.7	0.02	0.000026	0.009958	0
11	A81-13	572.5	371.1 ± 4.8	0.9	0.02	0.00003	0.010036	0
12	A81-7	550.1	369.1 ± 4.7	0.3	0	0.000011	0.010155	0
13	A81-10	37.7	355.2 ± 6.8	2	0.15	0.000068	0.010416	0.02
14	A81-11	114.5	361.4 ± 4.9	0.8	0.06	0.000028	0.01034	0
15	A81-16	661	366.9 ± 4.7	0.4	0.01	0.000014	0.010214	0
16	A81-4	273.5	367.5 ± 4.8	1	0.05	0.000035	0.01013	0

MEAN AGE(SPOTS 1 - 16)= 369 ± 3.5 Ma (2σ UNCERTAINTY,INCLUDING ERROR IN J)
J = .002314 ± .000023 (.9 %)
37/39,36/40 AND 39/40 Ar RATIOS ARE CORRECTED FOR MASS SPECTROMETER DISCRIMINATION,INTERFERING ISOTOPES AND SYSTEM BLANKS
% IIC - INTERFERING ISOTOPES CORRECTION

S1 MUSCOVITE ARGON SUMMARY

SPOT NO.	CODE NO.	mV 39	AGE (Ma)±2σ	% ATM	37/39	36/40	39/40	% IIC
1	C58-7-1	76.7	373.1 ± 4.8	2.8	1.35	0.000097	0.010402	0.19
2	C58-8-1	66.2	373.2 ± 4.8	1.5	0.71	0.000051	0.010541	0.1
3	C58-9-1	91.8	377.4 ± 4.8	1.6	0.48	0.000057	0.010394	0.07
4	C58-10-1	121.3	379.6 ± 4.9	2	0.37	0.000069	0.010288	0.05
5	C58-11-1	79.5	376.3 ± 4.8	2.6	0.57	0.000089	0.010327	0.08
6	C58-12-1	179.8	367.3 ± 4.8	4	1.1	0.000135	0.010459	0.16
7	C58-13-1	58.4	368.9 ± 4.7	1.2	0.82	0.000041	0.01071	0.12
8	C58-16-1	116.9	378.4 ± 4.9	3.8	0.58	0.00013	0.010135	0.08
9	C58-5-1	155	372.5 ± 4.9	2.1	0.54	0.000072	0.010495	0.07
10	C58-3-1	298.1	377.8 ± 4.8	1.1	0.27	0.00004	0.010433	0.03
11	C58-2-1	207.3	361.2 ± 4.7	2.7	1.72	0.000094	0.010787	0.25
12	C58-1-1	85.7	365.6 ± 4.8	4	1.76	0.000135	0.010511	0.25

MEAN AGE(SPOTS 1 - 12)= 372.4 ± 3.6 Ma (2σ UNCERTAINTY,INCLUDING ERROR IN J)
J = .002461 ± .000025 (1 %)
37/39,36/40 AND 39/40 Ar RATIOS ARE CORRECTED FOR MASS SPECTROMETER DISCRIMINATION,INTERFERING ISOTOPES AND SYSTEM BLANKS
% IIC - INTERFERING ISOTOPES CORRECTION

S2 MUSCOVITE ARGON SUMMARY

SPOT NO.	CODE NO.	mV 39	AGE (Ma)±2σ	% ATM	37/39	36/40	39/40	% IIC
1	C59-3-1	87.1	374.3 ± 4.8	0.6	0	0.00002	0.010502	0
2	C59-4-1	69.5	368.9 ± 4.8	3.5	0	0.000121	0.010353	0
3	C59-5-1	168.8	372.7 ± 4.9	3.6	0.73	0.000123	0.010229	0.1
4	C59-6-1	89.4	374.8 ± 4.8	2.1	0.24	0.000071	0.010328	0.03
5	C59-7-1	177.9	375.7 ± 4.8	2.4	0.21	0.000082	0.010264	0.03
6	C59-8-1	81.1	372.4 ± 4.8	1.8	0.46	0.000064	0.010424	0.06
7	C59-9-1	105.3	383.6 ± 4.9	1.8	0.44	0.000061	0.010094	0.06
8	C59-10-1	59.2	375.3 ± 4.9	3.5	0.63	0.000118	0.010164	0.09
9	C59-11-1	105.1	382.3 ± 4.9	2.6	0.34	0.000088	0.010052	0.04
10	C59-12-1	66.7	374.4 ± 4.9	1.7	0.19	0.000058	0.01038	0.02
11	C59-13-1	104.2	387.6 ± 5	0.9	0.32	0.000032	0.010066	0.04
12	C59-14-1	112.2	380 ± 5	2.9	0.25	0.000101	0.010078	0.03
13	C59-15-1	139.2	372.8 ± 4.8	1.6	0	0.000056	0.010436	0
14	C59-16-1	117.4	376.4 ± 4.8	1.7	0.23	0.000058	0.01032	0.03
15	C59-17-1	65.2	379.5 ± 4.9	2	0.51	0.00007	0.010188	0.07

MEAN AGE(SPOTS 1 - 15)= 376.8 ± 3.6 Ma (2σ UNCERTAINTY,INCLUDING ERROR IN J)
J = .002437 ± .000025 (1 %)
37/39,36/40 AND 39/40 Ar RATIOS ARE CORRECTED FOR MASS SPECTROMETER DISCRIMINATION,INTERFERING ISOTOPES AND SYSTEM BLANKS
% IIC - INTERFERING ISOTOPES CORRECTION

DK-MB-99-1 MUSCOVITE ARGON SUMMARY

SPOT NO.	CODE NO.	mV 39	AGE (Ma)±2σ	% ATM	37/39	36/40	39/40	% IIC
1	A83-3	105.8	365.7 ± 5.1	0.7	0	0.000026	0.010819	0
2	A83-2	128	367.7 ± 4.9	0.8	0	0.000027	0.010749	0
3	A83-1	122.2	372.4 ± 5	0.6	0	0.000022	0.010615	0
4	A83-6	35.9	373.6 ± 6.7	1.2	0.03	0.000041	0.010519	0
5	A83-7	38.1	368.9 ± 6.9	1.4	0.03	0.000049	0.01064	0
6	A83-8	48.8	369.2 ± 5.8	0.6	0.02	0.000023	0.010715	0
7	A83-9	36.4	360.5 ± 6.4	0.9	0.04	0.000031	0.010978	0
8	A83-10	24.5	338.9 ± 7.6	2.3	0.1	0.000079	0.011582	0.01
9	A83-4	127.5	363.5 ± 4.9	1.1	0.02	0.000037	0.010856	0
10	A83-13	47	355.2 ± 6.6	1.9	0.09	0.000067	0.011036	0.01

MEAN AGE(SPOTS 1 - 10)= 365.8 ± 3.6 Ma (2σ UNCERTAINTY,INCLUDING ERROR IN J)
J = .002451 ± .0000245 (.9 %)
37/39,36/40 AND 39/40 Ar RATIOS ARE CORRECTED FOR MASS SPECTROMETER DISCRIMINATION,INTERFERING ISOTOPES AND SYSTEM BLANKS
% IIC - INTERFERING ISOTOPES CORRECTION

DK-MB-99-01 K-FELDSPAR ARGON SUMMARY

SPOT NO.	CODE NO.	mV 39	AGE (Ma)±2σ	% ATM	37/39	36/40	39/40	% IIC
1	B82-17	448.5	355.2 ± 4.7	1.7	0	0.00006	0.011513	0
2	B82-26	265.8	354.4 ± 4.8	2.2	0.01	0.000077	0.011481	0
3	B82-25	103.8	358.4 ± 6.2	1	0.01	0.000035	0.011489	0
4	B82-18	168.9	358.7 ± 5.4	2.9	0.01	0.000099	0.011258	0
5	B82-22	242.5	346.5 ± 4.8	1.2	0	0.000043	0.011893	0
6	B82-16	212.1	363.4 ± 5.3	1.3	0.01	0.000045	0.011278	0

MEAN AGE(SPOTS 1 - 6)= 355.4 ± 3.5 Ma (2σ UNCERTAINTY,INCLUDING ERROR IN J)
J = .002552 ± .000025 (.9 %)
37/39,36/40 AND 39/40 Ar RATIOS ARE CORRECTED FOR MASS SPECTROMETER DISCRIMINATION,INTERFERING ISOTOPES AND SYSTEM BLANKS
% IIC - INTERFERING ISOTOPES CORRECTION

DK-MB-99-01 K-FELDSPAR ARGON SUMMARY

T°C	mV 39	39%	AGE (Ma)±1σ	% ATM	37/39	36/40	39/40	% IIC
500	1.5	0	301.4 ± 107	-72.8	0.34	-0.002734	0.023843	0.05
550	18.3	0.6	356.1 ± 7.3	0.4	0.02	0.000016	0.010336	0
600	56.5	1.8	361.3 ± 3.6	2.8	0	0.000097	0.009901	0
625	43.3	1.4	362.6 ± 3.9	0.4	0.01	0.000015	0.010111	0
650	40.2	1.3	362.4 ± 3.8	0.4	0.01	0.000015	0.010119	0
675	45.9	1.5	360.9 ± 4.7	4.1	0.01	0.000141	0.009781	0
700	47.7	1.5	364.8 ± 3	0.2	0.01	0.000009	0.010059	0
725	49.5	1.6	364.8 ± 3.1	0.2	0.01	0.000007	0.010063	0
750	50.4	1.6	362 ± 3.2	0.7	0.01	0.000025	0.010097	0
775	43.5	1.4	363 ± 3.3	0.4	0	0.000014	0.0101	0
800	35.8	1.1	363.6 ± 3.8	0.3	0.01	0.000012	0.010091	0
825	31.3	1	364.8 ± 4.4	0.2	0.01	0.00001	0.010065	0
850	27	0.8	359.6 ± 5.5	1.1	0.01	0.000039	0.01014	0
875	31.8	1	359.8 ± 5.7	2.8	0.01	0.000096	0.009958	0
900	31.1	1	357.3 ± 5.2	2.8	0	0.000096	0.010035	0
925	39.7	1.3	358 ± 3.9	1.5	0.01	0.000053	0.010141	0
950	49.6	1.6	356.2 ± 3.8	1.7	0	0.000059	0.010173	0
975	67.8	2.2	354 ± 3.2	2.3	0	0.000079	0.010178	0
1000	108.9	3.5	354.2 ± 2.5	2.4	0	0.000083	0.010155	0
1025	171	5.6	353.5 ± 2.1	2.2	0	0.000076	0.010194	0
1050	216.2	7	354.4 ± 2	2.3	0	0.00008	0.010154	0
1075	221	7.2	355.2 ± 1.9	2	0.01	0.00007	0.010161	0
1100	205.8	6.7	357.1 ± 1.9	1.8	0.01	0.000062	0.010126	0
1150	410.2	13.4	358.5 ± 1.7	1.5	0	0.000052	0.010109	0
1250	892	29.2	360.4 ± 1.9	2.2	0	0.000076	0.00998	0
1450	111.8	3.6	358.6 ± 4	27.1	0	0.000917	0.007484	0

TOTAL GAS AGE = 358.5 ± 2.2 Ma
J = .002258 ± 1.129E-05 (.5 %)
37/39,36/40 AND 39/40 Ar RATIOS ARE CORRECTED FOR MASS SPECTROMETER DISCRIMINATION,INTERFERING ISOTOPES AND SYSTEM BLANKS
% IIC - INTERFERING ISOTOPES CORRECTION

DK-MB-99-05 K-FELDSPAR ARGON SUMMARY

T°C	mV 39	39%	AGE (Ma)±1σ	% ATM	37/39	36/40	39/40	% IIC
550	30.1	0.9	344.6 ± 4.8	3.8	0.17	0.000129	0.011064	0.02
580	46	1.4	365.6 ± 3.2	1.7	0.06	0.000058	0.010587	0.01
610	57.5	1.8	365.7 ± 3	1.3	0.03	0.000045	0.010623	0
640	59.4	1.8	364.1 ± 2.7	0.7	0.02	0.000026	0.010737	0
670	66.9	2.1	360.3 ± 2.8	4.5	0.02	0.000154	0.010449	0
700	70.5	2.2	366.5 ± 2.8	0.9	0.02	0.000033	0.010636	0
730	68.5	2.1	367.4 ± 2.5	0.3	0.01	0.000011	0.010675	0
760	71.8	2.2	367.1 ± 2.5	0.3	0.01	0.000011	0.010684	0
790	64.4	2	365.8 ± 2.8	1	0.01	0.000037	0.010647	0
820	49.1	1.5	367.8 ± 3.7	0.2	0.02	0.000009	0.010671	0
850	39.1	1.2	366.6 ± 3.9	0.4	0.02	0.000013	0.010698	0
880	39.4	1.2	363.4 ± 4	1	0.02	0.000034	0.010739	0
910	39.6	1.2	364.1 ± 3.9	0.8	0	0.000029	0.01073	0
940	46.8	1.4	360.6 ± 3.4	1.1	0.02	0.00004	0.010809	0
970	65.6	2	363.2 ± 2.6	1.1	0.02	0.000038	0.010727	0
1000	100.4	3.1	359.9 ± 2.2	1.3	0.01	0.000045	0.01081	0
1025	149.7	4.7	359.3 ± 1.9	1.4	0.01	0.000049	0.010814	0
1050	216.2	6.8	359.1 ± 1.8	1.4	0.01	0.00005	0.010818	0
1075	250.9	7.9	359.5 ± 1.8	1.3	0.01	0.000046	0.010816	0
1100	255.1	8.1	361.4 ± 1.7	1.1	0.01	0.000038	0.010781	0
1125	279	8.8	363.2 ± 1.7	0.7	0	0.000025	0.010762	0
1150	361.9	11.4	363.6 ± 1.7	0.5	0	0.000019	0.010769	0
1200	614.8	19.5	365.4 ± 1.6	0.4	0	0.000016	0.010717	0
1250	67.9	2.1	371.8 ± 3.3	2.3	0.01	0.000078	0.010327	0
1350	10.6	0.3	369.6 ± 16.3	26.3	0.08	0.000893	0.007859	0.01
1450	26.7	0.8	358.8 ± 8	32.3	0.03	0.001095	0.007446	0

TOTAL GAS AGE = 363.1 ± 1.9 Ma
J = .002419 ± 1.2095E-05 (.5 %)
37/39,36/40 AND 39/40 Ar RATIOS ARE CORRECTED FOR MASS SPECTROMETER DISCRIMINATION,INTERFERING ISOTOPES AND SYSTEM BLANKS
% IIC - INTERFERING ISOTOPES CORRECTION

SC-3-MB ARGON SUMMARY

SPOT NO.	CODE NO.	mV 39	AGE (Ma)±2σ	% ATM	37/39	36/40	39/40	% IIC
1	A79-4	85	373.8 ± 5.4	0.5	0	0.000018	0.010265	0
2	A79-8	31.1	366.3 ± 7.3	2.1	0.01	0.000072	0.01033	0
3	A79-9	16	358.3 ± 11.2	1.5	0.02	0.000052	0.010649	0
4	A79-10	41.3	371.1 ± 6.4	0.3	0	0.000013	0.010363	0
5	A79-5	16.5	359.7 ± 11.1	1.4	0.02	0.000048	0.010619	0
6	A79-6	87.2	372.9 ± 5.3	0.8	0	0.000029	0.010258	0
7	A79-7	13.4	339 ± 12.5	1.9	0.07	0.000065	0.011277	0.01
8	A79-12	13.7	321.5 ± 12.4	2.7	0.1	0.000094	0.011847	0.01
9	A79-13	21.9	338.6 ± 8.7	3	0.08	0.000101	0.011167	0.01
10	A79-1	230	365.1 ± 4.7	0.3	0	0.000011	0.010559	0
11	A79-2-1	39.3	341.7 ± 6.3	2	0.08	0.000068	0.011164	0.01
12	A79-2-2	27.9	363.6 ± 7.6	0.4	0.02	0.000016	0.010591	0
13	A79-2-3	29.5	366.7 ± 8.4	1.4	0.04	0.000047	0.010398	0
14	A79-3	37.6	371.1 ± 7.6	1	0.03	0.000034	0.010298	0

MEAN AGE(SPOTS 1 - 14)= 364.1 ± 3.6 Ma (2σ UNCERTAINTY,INCLUDING ERROR IN J)
J = .002377 ± .0000238 (1 %)
37/39,36/40 AND 39/40 Ar RATIOS ARE CORRECTED FOR MASS SPECTROMETER DISCRIMINATION,INTERFERING ISOTOPES AND SYSTEM BLANKS
% IIC - INTERFERING ISOTOPES CORRECTION

SC-1-D MUSCOVITE ARGON SUMMARY

SPOT NO.	CODE NO.	mV 39	AGE(Ma)±2σ	%ATM	37/39	36/40	39/40	%IIC
1	A80-4	401.8	353.8 ± 4.9	3.2	0	0.000109	0.010487	0
2	A80-16	167.6	368.1 ± 4.8	0.5	0	0.000018	0.010317	0
3	A80-20	105.8	376 ± 5.8	0.9	0	0.00003	0.010041	0
4	A80-21	108.9	362.3 ± 5	1.1	0.02	0.000037	0.010441	0
5	A80-15	67.7	378.8 ± 5.4	0.4	0	0.000015	0.010004	0
6	A80-18	45.2	378.8 ± 6	0.2	0	0.000007	0.010028	0
7	A80-14	49.3	371.4 ± 6.2	0.9	0.01	0.000033	0.010172	0
8	A80-13-2	56.7	369.7 ± 5.9	0.3	0.01	0.000012	0.010287	0
9	A80-5	381.7	369.4 ± 4.7	1	0	0.000036	0.010222	0
10	A80-8	163.4	374.4 ± 4.9	0.4	0.01	0.000014	0.010136	0
11	A80-1	56	367.2 ± 6.3	1.9	0.06	0.000066	0.010198	0
12	A80-2	66	378.8 ± 6.1	0.8	0	0.000028	0.009965	0
13	A80-3	79.5	375.8 ± 5.4	0.6	0	0.000023	0.01007	0
14	A80-7	102.2	373.3 ± 5.2	0.4	0.01	0.000016	0.010167	0
15	A80-9	108.6	369.7 ± 5	0.3	0	0.000013	0.010284	0
16	A80-8	33.4	368.4 ± 7.6	0.6	0.05	0.000023	0.010295	0
17	A80-10	40.9	367.2 ± 7	0.8	0.05	0.000028	0.010314	0
18	A80-11	30.7	356.4 ± 7.7	1.8	0.09	0.000063	0.010549	0.01
19	A80-12	85	365.6 ± 5.3	1.1	0.04	0.000037	0.010335	0

MEAN AGE(SPOTS 1 - 19)= 367.6 ± 3.5 Ma (2σ UNCERTAINTY, INCLUDING ERROR IN J) J = .002349 ± .0000234 (.9 %)
37/39,36/40 AND 39/40 Ar RATIOS ARE CORRECTED FOR MASS SPECTROMETER DISCRIMINATION,INTERFERING ISOTOPES AND SYSTEM BLANKS
% IIC - INTERFERING ISOTOPES CORRECTION

SC-11-D MUSCOVITE ARGON SUMMARY

SPOT NO.	CODE NO.	mV 39	AGE (Ma)±2σ	% ATM	37/39	36/40	39/40	% IIC
1	C60-1-1	60.6	378.6 ± 4.9	3	0.66	0.000104	0.010116	0.09
2	C60-2-1	35.8	369.4 ± 5.3	2.9	1	0.0001	0.010406	0.14
3	C60-3-1	70.7	379.1 ± 4.9	2.6	0.57	0.000088	0.010149	0.08
4	C60-4-1	48.3	374.7 ± 5	2.4	0.97	0.000082	0.0103	0.14
5	C60-5-1	40.4	372.2 ± 5.3	4.4	1.3	0.000149	0.010165	0.18
6	C60-7-1	34	374.5 ± 4.9	2.5	1.82	0.000087	0.01029	0.26
7	C60-8-1	48.2	369.9 ± 5	1.5	1.15	0.000053	0.010541	0.16

MEAN AGE(SPOTS 1 - 7)= 374.8 ± 3.7 Ma (2σ UNCERTAINTY,INCLUDING ERROR IN J)
J = .002438 ± .000025 (1 %)
37/39,36/40 AND 39/40 Ar RATIOS ARE CORRECTED FOR MASS SPECTROMETER DISCRIMINATION,INTERFERING ISOTOPES AND SYSTEM BLANKS
% IIC - INTERFERING ISOTOPES CORRECTION

DC-DUMP K-FELDSPAR ARGON SUMMARY

T°C	mV 39	39%	AGE (Ma)±1σ	% ATM	37/39	36/40	39/40	% IIC
550	79.7	2.7	276.4 ± 2.2	2.1	0.04	0.000072	0.014307	0
580	140.7	4.8	294.1 ± 1.7	0.9	0.01	0.000032	0.013539	0
610	179.6	6.2	301.8 ± 1.5	0.2	0.01	0.000008	0.013257	0
640	204.2	7	305.1 ± 1.5	0.4	0	0.000014	0.013078	0
670	167.8	5.8	308.4 ± 1.6	1.1	0	0.000039	0.012828	0
700	143.9	4.9	312.3 ± 1.6	0.1	0	0.000006	0.01278	0
730	107.4	3.7	315.1 ± 1.9	1.2	0	0.000043	0.012518	0
760	68.6	2.3	316.9 ± 2.3	0.4	0.01	0.000016	0.012546	0
790	48.3	1.6	320.3 ± 3.3	0.1	0.01	0.000006	0.01244	0
820	39.8	1.3	320.4 ± 3.6	0.9	0.02	0.000032	0.012342	0
850	36.8	1.2	326.4 ± 4.2	1.1	0.01	0.000038	0.012077	0
880	37	1.2	333.6 ± 4	1.3	0.01	0.000046	0.01176	0
910	35.5	1.2	337.8 ± 3.9	0.9	0	0.00003	0.011655	0
940	41.7	1.4	341.9 ± 3.6	0.9	0	0.000031	0.011499	0
970	61.4	2.1	343.4 ± 2.8	1.3	0	0.000044	0.011393	0
1000	95.3	3.3	346.6 ± 2.2	1.1	0	0.000039	0.011291	0
1025	73.6	2.5	350.6 ± 2.5	1.1	0	0.000038	0.011154	0
1050	68.1	2.3	348.7 ± 2.8	1.1	0	0.000039	0.01122	0
1075	89.2	3	348.8 ± 2.2	1.3	0	0.000044	0.011199	0
1100	135.2	4.6	350.5 ± 1.9	1.7	0	0.000059	0.011085	0
1125	150.6	5.2	349.6 ± 1.9	2	0	0.000069	0.011087	0
1150	207.2	7.1	346.3 ± 1.8	3.8	0	0.000131	0.01099	0
1200	200.9	6.9	347.5 ± 1.8	4	0	0.000135	0.010934	0
1250	328	11.3	349.6 ± 1.8	4.2	0	0.000144	0.010829	0
1350	134.7	4.6	348.6 ± 2.2	10.1	0	0.000342	0.010204	0
1450	9.3	0.3	342 ± 28.4	61.5	0.07	0.002087	0.004463	0.01

TOTAL GAS AGE = 330.2 ± 1.7 Ma

J = .00242 ± .0000121 (.5 %)

37/39,36/40 AND 39/40 Ar RATIOS ARE CORRECTED FOR MASS SPECTRO-METER DISCRIMINATION,INTERFERING ISOTOPES AND SYSTEM BLANKS

% IIC - INTERFERING ISOTOPES CORRECTION

DC-86-3-847 K-FELDSPAR ARGON SUMMARY

T°C	mV 39	39%	AGE (Ma)±1σ	% ATM	37/39	36/40	39/40	% IIC
550	40.9	1.1	313.3 ± 4.7	7.7	0.03	0.000264	0.01096	0
600	87.7	2.3	321.9 ± 2.5	2.9	0	0.000098	0.011192	0
640	86.4	2.3	313.8 ± 2.4	0.9	0	0.000031	0.011745	0
680	76.9	2	308.1 ± 2.6	3.4	0	0.000117	0.011676	0
720	66.7	1.7	313.8 ± 2.9	2.2	0	0.000075	0.011593	0
760	50.3	1.3	307.7 ± 3.3	0.7	0	0.000026	0.012026	0
800	38.4	1	303.6 ± 4.3	0.4	0	0.000015	0.012252	0
825	28.7	0.7	302.2 ± 5.8	0.9	0	0.000031	0.012259	0
850	26.7	0.7	297.6 ± 6.1	0.7	0	0.000024	0.012493	0
875	29.9	0.8	304.2 ± 5.5	3	0	0.000104	0.011904	0
900	30.4	0.8	303.9 ± 5.4	1.8	0	0.000062	0.01207	0
920	38.4	1	306.1 ± 4.5	1.8	0	0.000063	0.011969	0
940	50.2	1.3	316.5 ± 3.7	2.2	0.01	0.000075	0.011493	0
960	126.5	3.4	321.3 ± 2.3	3.3	0	0.000113	0.01116	0
1000	274.9	7.4	338 ± 1.7	3.1	0	0.000105	0.01058	0
1000	253.7	6.8	332 ± 1.8	4.6	0	0.000156	0.010624	0
1020	210	5.6	331.7 ± 1.8	4.9	0	0.000166	0.010601	0
1040	318	8.5	323.5 ± 1.7	6.1	0	0.000207	0.010758	0
1060	221.1	5.9	333.9 ± 1.9	8.3	0	0.000283	0.010144	0
1080	357.2	9.6	336.1 ± 1.9	11.8	0	0.000401	0.009684	0
1100	376.3	10.1	342.5 ± 1.8	8.1	0	0.000277	0.009882	0
1102	49.6	1.3	344.4 ± 4.4	7.3	0	0.000247	0.009932	0
1150	68.6	1.8	341.2 ± 2.8	2.1	0	0.000072	0.010589	0
1200	418.8	11.2	343.4 ± 1.6	1.4	0	0.00005	0.010574	0
1300	247.5	6.6	337.3 ± 1.7	2.3	0	0.000079	0.010691	0
1450	133.5	3.6	328.5 ± 2.3	10.3	0	0.000349	0.010108	0

TOTAL GAS AGE = 331.1 ± 1.8 Ma
J = .002251 ± 1.1255E-05 (.4 %)
37/39,36/40 AND 39/40 Ar RATIOS ARE CORRECTED FOR MASS SPECTROMETER DISCRIMINATION,INTERFERING ISOTOPES AND SYSTEM BLANKS
% IIC - INTERFERING ISOTOPES CORRECTION

DC-85-3-217 K-FELDSPAR ARGON SUMMARY

T°C	mV 39	39%	AGE (Ma)±1σ	% ATM	37/39	36/40	39/40	% IIC
550	124.7	3.4	360.8 ± 2.3	3.9	0.02	0.000133	0.010512	0
580	33.5	0.9	363.7 ± 5.1	2.1	0.06	0.000072	0.010631	0
610	51.1	1.4	363.2 ± 3.6	2.1	0.05	0.000073	0.010634	0
640	53.2	1.4	361.6 ± 3.6	1.4	0.06	0.00005	0.01076	0
700	87.8	2.4	356 ± 2.7	5.3	0.07	0.000182	0.010511	0.01
730	43.9	1.2	365.3 ± 4	0.6	0.17	0.000022	0.010734	0.02
760	31.4	0.8	362.3 ± 5.3	0.7	0.19	0.000027	0.010824	0.02
790	28.5	0.7	361 ± 6	2.6	0.16	0.000088	0.010669	0.02
820	26.9	0.7	361.6 ± 5.8	2.1	0.1	0.000073	0.0107	0.01
850	29.3	0.8	359.4 ± 5.7	1.9	0.07	0.000066	0.010793	0.01
880	36	1	357.5 ± 4.6	2.2	0.05	0.000076	0.010821	0
910	48.3	1.3	358.8 ± 4	1.6	0.04	0.000056	0.010836	0
940	64.9	1.8	358.8 ± 2.9	1.9	0.03	0.000065	0.010803	0
970	80.4	2.2	358.2 ± 2.7	1.7	0.04	0.000059	0.010843	0
1000	114.4	3.1	357.1 ± 2.2	1.8	0.03	0.000062	0.010869	0
1025	145.8	4	357.7 ± 2	1.8	0.03	0.000063	0.010841	0
1050	187.6	5.2	359 ± 1.9	1.6	0.03	0.000055	0.010824	0
1075	237.5	6.6	360.7 ± 1.8	1.3	0.02	0.000046	0.010793	0
1100	350.4	9.7	362.7 ± 1.7	1	0.02	0.000036	0.010762	0
1125	538.9	15	364.2 ± 1.7	0.8	0.01	0.000029	0.010736	0
1150	677.5	18.8	365.7 ± 1.6	0.7	0.01	0.000025	0.010698	0
1450	599.5	16.6						

J = .002423 ± 1.2115E-05 (.5 %)

37/39,36/40 AND 39/40 Ar RATIOS ARE CORRECTED FOR MASS SPECTROMETER DISCRIMINATION,INTERFERING ISOTOPES AND SYSTEM BLANKS

% IIC - INTERFERING ISOTOPES CORRECTION

DC-1406 K-FELDSPAR ARGON SUMMARY

T°C	mV 39	39%	AGE (Ma)±1σ	% ATM	37/39	36/40	39/40	% IIC
550	60.8	2	294.4 ± 3.4	3.1	0.01	0.000105	0.012296	0
600	145.3	4.9	314.6 ± 2	2.7	0.01	0.000092	0.011473	0
650	172.8	5.8	325.6 ± 1.8	1.2	0.01	0.000042	0.01122	0
700	163.4	5.5	333.4 ± 2	3.1	0.01	0.000105	0.010727	0
725	119.4	4	341.8 ± 2.1	0	0	0.000003	0.010763	0
750	116.8	3.9	341.8 ± 2.1	0.1	0.01	0.000003	0.010765	0
775	114.2	3.8	341.6 ± 2.1	0.3	0.01	0.000011	0.010748	0
800	118.7	4	342.2 ± 2.1	0.5	0.01	0.000018	0.010701	0
825	121.1	4	342.3 ± 2.1	0.5	0.01	0.000017	0.010705	0
850	127.9	4.3	342.7 ± 2.1	0.6	0.02	0.000021	0.010675	0
875	144.3	4.8	343.2 ± 2	1.1	0.04	0.000037	0.010607	0
900	158	5.3	345 ± 1.9	1.1	0.05	0.000038	0.010542	0
925	151.8	5.1	344.9 ± 2	1.2	0.06	0.000043	0.01053	0
950	136.5	4.6	344.7 ± 2.1	0.9	0.07	0.000031	0.010576	0.01
975	127.1	4.2	343.8 ± 2.1	0.9	0.09	0.000032	0.010604	0.01
1000	91.6	3	342.7 ± 2.5	0.7	0.13	0.000024	0.010667	0.02
1025	68.5	2.3	342.6 ± 2.9	0.5	0.17	0.00002	0.010687	0.02
1040	244.9	8.2	341.5 ± 1.8	4.9	0.18	0.000166	0.01025	0.02
1060	117	3.9	342.3 ± 2.5	8.9	0.22	0.000301	0.009798	0.03
1080	201.5	6.7	341.4 ± 2.4	17.9	0.26	0.000607	0.008851	0.03
1100	86.9	2.9	345.4 ± 4	23.8	0.28	0.000806	0.008116	0.04
1150	18.3	0.6	346.2 ± 9.2	4.2	0.26	0.000145	0.010207	0.03
1200	63.2	2.1	347.1 ± 3.3	4.3	0.18	0.000148	0.010137	0.02
1300	55.3	1.8	351.9 ± 4	9.8	0.3	0.000332	0.00942	0.04
1450	38.5	1.2	345.7 ± 6.2	22.5	0.26	0.000765	0.008247	0.03

TOTAL GAS AGE = 339.3 ± 1.8 Ma

J = .002247 ± 1.1235E-05 (.5 %)

37/39,36/40 AND 39/40 Ar RATIOS ARE CORRECTED FOR MASS SPECTROMETER DISCRIMINATION,INTERFERING ISOTOPES AND SYSTEM BLANKS

% IIC - INTERFERING ISOTOPES CORRECTION

NS-86-3 K-FELDSPAR ARGON SUMMARY

T°C	mV 39	39%	AGE (Ma)±1σ	% ATM	37/39	36/40	39/40	% IIC
550	60.5	1.5	315.5 ± 3	4.9	0.07	0.000168	0.012029	0.01
580	74	1.9	284.5 ± 2.3	2	0.03	0.00007	0.013868	0
610	87	2.2	290.1 ± 2	1.1	0.01	0.000039	0.013703	0
640	120.1	3.1	304.6 ± 1.9	0.9	0	0.000032	0.01302	0
670	71.2	1.8	317.3 ± 2.7	3.3	0.01	0.000114	0.012155	0
700	89.3	2.3	335.6 ± 2.2	1.1	0.01	0.00004	0.011689	0
730	79.9	2	345.4 ± 2.4	0.8	0.01	0.000027	0.011368	0
760	61.3	1.5	345.4 ± 2.8	0.2	0.01	0.000009	0.01143	0
790	64.7	1.6	344.4 ± 2.8	0.3	0.01	0.000012	0.011458	0
820	66.5	1.7	347.3 ± 2.7	0.3	0	0.000013	0.011352	0
850	55.7	1.4	342.5 ± 3	0.4	0	0.000014	0.011524	0
880	57.3	1.4	339.7 ± 2.8	0.9	0	0.000032	0.011565	0
910	61.9	1.6	338.1 ± 2.8	1.2	0	0.000043	0.011586	0
940	91	2.3	338.7 ± 2.3	2	0	0.000069	0.011468	0
970	142.8	3.7	334.5 ± 1.9	3.1	0	0.000106	0.011497	0
1000	136.1	3.5	333.8 ± 2	3.5	0	0.00012	0.011472	0
1025	144.5	3.7	334.9 ± 2	3.5	0	0.00012	0.01143	0
1050	248.3	6.4	341.3 ± 1.7	3.1	0	0.000106	0.011241	0
1075	201.7	5.2	345.7 ± 1.8	2.6	0	0.00009	0.011138	0
1100	242.5	6.3	348.3 ± 1.7	2.1	0	0.000073	0.011107	0
1125	337.9	8.7	351.6 ± 1.7	1.7	0	0.000059	0.011035	0
1150	483.7	12.5	354.2 ± 1.6	1.6	0	0.000055	0.010959	0
1175	498.3	12.9	357.2 ± 1.6	1.7	0	0.000059	0.010846	0
1200	203.6	5.3	354.1 ± 1.8	3.1	0	0.000107	0.010791	0
1250	67.6	1.7	351.5 ± 3.1	5.5	0	0.000188	0.010619	0
1350	80.8	2.1	350.4 ± 2.8	7.9	0	0.00027	0.010382	0
1450	12.6	0.3	350.5 ± 18.4	44.8	0.03	0.00152	0.006235	0

TOTAL GAS AGE = 342.8 ± 1.8 Ma
J = .002418 ± 1.209E-05 (.5 %)
37/39,36/40 AND 39/40 Ar RATIOS ARE CORRECTED FOR MASS SPECTROMETER DISCRIMINATION,INTERFERING ISOTOPES AND SYSTEM BLANKS
% IIC - INTERFERING ISOTOPES CORRECTION

Appendix D: Details from thermometric measurements on fluid inclusions

Abbreviations in the following Table are as follows:

Tf: freezing temperature

Tfm: first melting temperature

Tm(HH): melting temperature of hydrohalite

Tm(ice): melting temperature of ice

Tm(halite): melting temperature of halite

Th: homogenisation temperature

sample #	Chip #	area	inclusion #	Tf	Tfm	Tm (HH)	Tm (ice)	Tm (halite)	Th	Salinity
DK-85-19	1	A	1	-58.4	-40		-5			8
DK-85-19	1	B	1	-73	-35	-25	-16.5			19
DK-85-19	1	B	2	-64	-30		-18			20
DK-85-19	1	B	3	-74			-17.8			19.5
DK-85-19	1	B	4	-77			-17.8			19.5
DK-85-19	1	B	5	-78	-35		-17.5			20.6
DK-85-19	1	B	6	-74	-35		-18.5			21.33
DK-85-19	1	B	7	-62	-35					
DK-85-19	1	B	8	-67			-19			21
DK-85-19	1	B	9	-72	-28		-19			21.68
DK-85-19	1	C	1	-57	-40		-13.8		176	17
DK-85-19	1	C	2	-71	-40		-19.5		160	21
DK-85-19	1	C	3	-53	-40		-11.5		169	15
DK-85-19	1	C	4	-53	-40		-11.1		171	15
DK-85-19	1	D	1	-61	-28		-14.5			18.22
SC-4-R	1	A	1	-43			0		233	0
SC-4-R	1	A	2	-43			0		225	0
SC-4-R	1	A	3	-43			0			0
SC-11-R	1	A	1	-90	-65		-22.4		137	
SC-11-R	1	A	2	-90	-65		-22.4			
SC-11-R	1	A	3	-90	-65		-22.4			
SC-11-R	1	A	4	-90	-65		-22.4			
SC-11-R	1	A	1	-50	-25		-2.4		184	4.03
SC-11-R	1	A	2	-50	-25		-2.4		191	4.03
SC-11-R	1	A	3	-49	-25		-2		177	3.39
SC-11-R	1	A	4	-49	-25		-2		187	3.39
SC-11-R	1	A	5	-92	-45		-23.5		136	
U2	1	A	1	-42	-20		-3		241	4.96
U2	1	A	2	-37	-20		-3.8		253	6.16
U2	1	A	3	-43	-20		-3		218	4.96
U2	1	A	4	-43			-2.9			4.8
U2	1	A	5	-43			-2.5			4.18
U2	1	A	6	-43			-2.5			4.18
U2	1	B	1	-42			-2.8		207	4.65
U2	1	B	2	-42			-2.8		195	4.65
U2	1	B	3	-42			-2.8		229	4.65
U2	1	B	4	-43			-2.8		251	4.65
U2	1	B	5	-43			-2.8		235	4.65
U2	1	B	6	-42			-2.8		248	4.65
U2	1	B	7	-41			-3		235	4.96
U2	1	B	8	-39			-2.5		192	4.18
U2	1	C	1	-40	-20		-2.5		292	4.18
U2	1	C	2	-40	-20		-2.5		292	4.18
U2	1	C	3	-40	-20		-2.5		292	4.18
U2	1	D	1	-40			-3			4.96
U2	1	D	2	-40			-3		214	4.96
U2	1	D	3	-40			-3		292	4.96
U2	1	D	4	-40			-3		240	4.96
U2	2	A	1	-55		11	-23		154	23 to 26
U2	2	B	1			11	-24			23 to 26

sample #	Chip #	area	inclusion #	Tf	Tfm	Tm (HH)	Tm (ice)	Tm (halite)	Th	Salinity
U2	2	B	2			11	-24		144	23 to 26
U2	3	A	1	-40			-2.5		194	4.18
U2	3	A	2	-40			-3		196	4.96
U2	3	A	3	-40			-3		196	4.96
U2	3	A	4							
U2	3	A	5	-39			-2		191	3.39
U2	3	A	6	-41			-2.6		191	4.34
U2	3	A	7	-41			-2.6		176	4.34
U2	3	A	8	-40			-2.2		176	3.71
U2	3	A	9	-42			-2.1		181	3.55
U2	3	A	10	-42			-2.7		181	4.49
U2	3	B	1	-40			-2.7		225	4.49
U2	3	C	1					253		
U2	3	C	3					246		
U2	3	D	1	-42			-2		313	3.39
U2	3	D	2	-42			-2		319	3.39
U2	3	D	3	-42			-2		264	3.39
U2	3	D	4	-42			-2		307	3.39
U2	3	D	5	-42			-2		304	3.39
U2	3	E	1	-68	-65	-26	-23.9			23
U2	3	E	2		-65	-26	-20			22
U2	3	E	3		-58	-28	-23			23
U2	3	E	4	-80	-65	-24.5	-20			21
U2	3	F	1	-72	-60	-25	-22.6		240	23
U2	3	F	2		-60	-25	-23.8		268	23
U2	3	F	3						292	
U2	3	F	4						358	
U2	3	F	5		-70		-26.7		360	
U2	3	F	6		-60	-25	-23		256	23
U2	3	G	1	-42	-15		-3.2		303	5.26
U2	3	G	2	-42	-15		-3.2		303	5.26
U2	3	H	1	-42	-17		-2.8		240	4.65
U2	3	H	2		-60	-25	-2.4	>360	226	
U2	3	H	3		-60	-25	-20		220	21
U2	3	H	4		-60	-25	-20		206	21
U2	4	A	1					158.8	134.5	31.89
U2	4	B	1					303	125	30.92
U2	4	B	2						130	
U2	4	B	3							
U2	4	B	4						141	
U2	4	B	5						135	

sample #	Chip #	area #	inclusion #	Tf	Tfm	Tm (HH)	Tm(ice)	Tm(halite)	Th	Salinity
DK-85-36	1	1A	1	-65	in -60		-20.2			
DK-85-36	1	1A	2							
DK-85-36	1	1B	1		-66	-35	-26.4		127	23.7
DK-85-36	1	1B	2				-25.4		138	
DK-85-36	1	1B	3				-24.4			
DK-85-36	1	1C	1	-67	-65		-10.1			
DK-85-36	1	1D	1				-29			
DK-85-36	1	1D	2		-67		-3.5			
DK-85-36	1	1E	1							
DK-85-36	1	1E	2	-70	in -50	in -30	-21.6			22
DK-85-36	1	1E	3			in -30	-8			12.1
DK-85-36	1	1F	1	-68	in -60		-19.8		290	21
DK-85-36	1	2A	1						259	
DK-85-36	1	2A	2						259	
DK-85-36	1	2A	3							
DK-85-36	1	2A	4							
DK-85-36	1	2B	1				-15			
DK-85-36	1	2C	1		-50		-19			20.5
DK-85-36	1	2C	2		-50		-19			20.5
DK-85-36	1	2D	1		-48		-22.5			22
DK-85-36	1	2D	2		-48		-13.4			16.8
DK-85-36	1	2E	1	-65	-55		-21.5			22
DK-85-36	1	2F	1	-67	-55		-21.5			22
DK-85-36	1	2G	1	-62	in -50		-17			19.4
DK-85-36	1	2G	2	-61			-17.4			19.5
DK-85-36	1	2G	3	-61			-17.4			19.5
DK-85-36	1	2G	4	-61			-17.4			19.5
DK-85-36	1	3A	1						130	
DK-85-36	1	3B	1	-77	-60	-27	-21.7		133	22
DK-85-36	1	3B	2	-77	-60				132	
DK-85-36	1	3B	3	-77	-60				148	
DK-85-36	1	3B	4	-77	-60				133	
DK-85-36	1	3C	1	-77	-60		-22		103	22.5
DK-85-36	1	3C	2	-77	-60		-22		120.5	22.5
DK-85-36	1	3C	3	0	-65		-21.6			22
DK-85-36	1	3D	1	-70	-60		-19.4		125	21.5
DK-85-36	1	3D	2	-70	-60		-19.4		125	21.5
DK-85-36	1	3D	3	-70	-60		-19.4		130	21.5
DK-85-36	1	3D	4	-71	-60		-19.3		135	21.5
DK-85-36	1	3D	5	-70			-20		140	21.5
DK-85-36	1	3D	6	-70			-19.6		115.4	21.5
DK-85-36	1	3D	7	-70			-19.6		120	21.5
DK-85-36	1	3E	1	-70			-19		143.7	21
DK-85-36	1	3E	2	-70			-18.5		140.6	21
DK-85-36	1	3E	3	-70			-18.7		150	21
DK-85-36	1	3F	1	-70	-57		-19.5		140	21.5
DK-85-36	1	3F	2	-70	-57		-19.5		139	21.5
DK-85-36	1	3F	3	-70	-57		-19.5		138	21.5
DK-85-36	1	3F	4	-68	-57		-18.9		135	21

sample #	Chip #	area #	inclusion #	Tf	Tfm	Tm (HH)	Tm(ice)	Tm(halite)	Th	Salinity
DK-85-36b	1	1	1	-43			-3		177	4.96
DK-85-36b	1	1	2	-43			-3		178	4.96
DK-85-36b	1	1	3	-44			-3			4.96
DK-85-36b	1	1	4	-44			-3			4.96
DK-85-36b	1	1	5	-44			-3		176	4.96
DK-85-36b	1	1	6	-44			-3			4.96
DK-85-36b	1	1	7	-43			-2.5			4.18
DK-85-36b	1	1	8							
DK-85-36b	1	1	9	-44			-3.2		165	5.26
DK-85-36b	1	1	10	-44			-3.2		165	5.26
DK-85-36b	1	2	1	-38			-3.5		180\185	5.71
DK-85-36b	1	2	2	-38			-3.4		180\185	5.56
DK-85-36b	1	2	3	-38			-3.4		180\185	5.56
DK-85-36b	1	2	4	-36			-4.4		180\185	7.02
DK-85-36b	1	2	5	-38			-3.3		180\185	5.41
DK-85-36b	1	2	6	-36			-3.6		180\185	5.86
DK-85-36b	1	2	7	-36			-3.6		180\185	5.86
DK-85-36b	1	2	8	-36					180\185	
DK-85-36b	1	3	1	-60	in -50		-16.3			19
DK-85-36b	1	3	2	-60	in -50					
DK-85-36b	1	3	3	-60	in -50		-17			19
DK-85-36b	1	3	4	-60	in -50					
DK-85-36b	1	4	1	-65	-48	-20	-14.8		139	18
DK-85-36b	1	4	2	-65	-45	-23	-14.5			18
DK-85-36b	1	4	3	-64			-14		139.8	18
DK-85-36b	1	4	4	-64	-50	-21	-17.2		106.4	20
DK-85-36b	1	4	5	-68	-53	-23	-9.5			13
DK-85-36b	1	4	6	-68	-60	-23	-9.5			13
DK-85-36b	1	4	7	-66	-44		-16.9			20
DK-85-36b	1	4	8	-61	-53		-13			17
DK-85-36b	1	4	9	-63	-55		-12			16
DK-85-36b	1	4	10	-65	-50		-16			19
DK-85-36b	1	4	11	-58	-48		-13			17
DK-85-36b	1	4	12						161	
DK-85-36b	1	4	13						162	
DK-85-36b	1	4	14						140	
DK-85-36b	1	4	15						140	
DK-85-36b	1	4	16						108	
DK-85-36b	1	5	1	-45			-3.5		203	5.71
DK-85-36b	1	5	2				-4.1		208	6.59
DK-85-36b	1	5	3				-4.3		203	6.88

sample #	Chip #	area #	inclusion #	Tf	Tfm	Tm (HH)	Tm (ice)	Tm (halite)	Th	Salinity
DK-85-34b	1	1A	1	-41			-1.5		214.5	2.57
DK-85-34b	1	1A	2						285	
DK-85-34b	1	1B	1	-40			-1.7			2.9
DK-85-34b	1	1B	2				-0.5			0.88
DK-85-34b	1	1B	3				-0.5			0.88
DK-85-34b	1	1C	1	-40			-0.5			0.88
DK-85-34b	1	1C	2	-40			-0.5			0.88
DK-85-34b	1	1D	1						247	
DK-85-34b	1	1D	2							
DK-85-34b	1	1E	1						195	
DK-85-34b	1	1F	1						266	
DK-85-34b	1	1F	2						290	
DK-85-34b	1	1F	3						350	
DK-85-34b	1	1F	4						350	
DK-85-34b	1	2A	1	-65	-63	-24	-23.4		246	23
DK-85-34b	1	2B	1			-26	-24			23
DK-85-34b	1	2B	2							
DK-85-34b	1	2B	3							
DK-85-34b	1	2B	4			-28	-22.6		213	22.5
DK-85-34b	1	2C	1				-14.6			
DK-85-34b	1	2C	2				-0.7			1.23
DK-85-34b	1	2D	1				-1.2			2.07
DK-85-34b	1	2E	1						223	
DK-85-34b	2	1	1						318	
DK-85-34b	2	1	2						318	
DK-85-34b	2	1	3						318	
DK-85-34b	2	1	4						230	
DK-85-34b	2	1	5						230	
DK-85-34b	2	2	1						250	
DK-85-34b	2	3	1						223	
DK-85-34	1	1A	1	-43			-2.1			3.55
DK-85-34	1	1A	2	-43			-2.1			3.55
DK-85-34	1	1A	3	-43			-2.1			3.55
DK-85-34	1	1B	1				-2		181.8	3.39
DK-85-34	1	1C	1							
DK-85-34	1	1C	2						165.5	
DK-85-34	1	1C	3							
DK-85-34	1	1D	1						177	
DK-85-34	1	1E	1	-80	-65		-22.2			
DK-85-34	1	1F	1						176	
DK-85-34	1	1F	2						216.5	
DK-85-34	1	1F	3						193	
DK-85-34	1	1F	4						255.2	
DK-85-34	1	1F	5	-45			-2.1		176	3.55
DK-85-34	1	1G	1						214	
DK-85-34	1	1G	2						197	
DK-85-34	1	1G	3				-1.6		222.6	2.74
DK-85-34	1	1H	1						194	
DK-85-34	1	1H	2						195	

sample #	Chip #	area #	inclusion #	Tf	Tfm	Tm (HH)	Tm (ice)	Tm (halite)	Th	Salinity
DK-85-34	1	1H	3						192.2	
DK-85-34	1	1H	4						194.5	
DK-85-34	1	2A	1	-60			-16.2		131	19.5
DK-85-34	1	2A	2	-45			-1.7		191	2.9
DK-85-34	1	2A	3	-60			-16.5		160	19.5
DK-85-34	1	2B	1	-70			-16.9		160	20
DK-85-34	1	2B	2	-75			-18		246	20.5
DK-85-34	1	2C	1	-64			-15.8			19
DK-85-34	1	2C	2	-66						
DK-85-34	1	2C	3	-66			-16.2		130	19.5
DK-85-34	1	2C	4	-66			-16		143.5	19
DK-85-34	2	1	1	-65	-57	-24	-17.6		98.6	20
DK-85-34	2	1	2	-65	-57	-24	-17.6		119	20
DK-85-34	2	1	3	-65	-57	-24	-17.6		86	20
DK-85-34	2	1	4	-65	-57	-24	-17.6			20
DK-85-34	2	1	5	-69	-55				113.6	
DK-85-34	2	1	6		-70	-40				
DK-85-34	2	1	7	-69	-45		-17.3		125.8	
DK-85-34	2	2	1						175	
DK-85-34	2	2	2						170	
DK-85-34	2	2	3							
DK-85-34	2	2	4						167	
DK-85-34	2	2	5						170	
DK-85-34	2	2	6							
DK-85-34	2	2	7					185	180	37.83
DK-85-34	2	2	8						155	
DK-85-34	2	2	9						155	
DK-85-34	2	3	1		-75	-50	-40	167	148	33.32
DK-85-34	2	3	2		-75	-45	-36		164.2	26.8
DK-85-34	2	3	3							
DK-85-34	2	3	4						122	
DK-85-34	2	3	5		-75		-40	177	114	29.99
DK-85-34	2	3	6	-67	-35	-50	-15.5		107	19.05
DK-85-34	2	3	7	-42			-3			4.96
DK-85-34	2	3	8					188	170	36.26
SC-2-L	1	A	1	-50	-26		-1			1.74
SC-2-L	1	A	2	-50	-26		-1			1.74
DK-85-32	1	1A	1							
DK-85-32	1	1B	1		late -60					
DK-85-32	1	1C	1		-59					
DK-85-32	1	1C	2							
DK-85-32	1	1D	1							
DK-85-32	1	1E	1	-42			-4			6.45
DK-85-32	1	1F	1				-5			7.86
DK-85-32	1	1G	1	-50						
DK-85-32	1	1H	1	-57			-11.6			
DK-85-32	1	1H	2				-1.5			2.57
DK-85-32	1	1I	1						241	
DK-85-32	1	1I	2						207	

sample #	Chip #	area #	inclusion #	Tf	Tfm	Tm (HH)	Tm (ice)	Tm (halite)	Th	Salinity
DK-85-32	1	1I	3						241	
DK-85-32	1	1I	4			-44.3	-44.3		226	29
DK-85-32	1	1I	5			-43.7	-43.7		246	29
DK-85-32	1	1I	6		-70	-44	-44		247	29
DK-85-32	1	2A	1						>350	
DK-85-32	1	2B	1						decr	
DK-85-32	1	2B	2						decr	
DK-85-32	1	2B	3						331	
DK-85-32	1	2B	4						307	
DK-85-32	1	2C	1						300	

sample #	Chip #	area #	inclus #	Tf	Tfm	Tm (HH)	Tm (ice)	Tm (halite)	Th	Salinity
DK-85-11-4	1	1	1						262.8	
DK-85-11-4	1	1	2							
DK-85-11-4	1	1	3							
DK-85-11-4	1	1	4							
DK-85-11-4	1	1	5						353	
DK-85-11-4	1	2	1	-77			-41		251	28.2
DK-85-11-4	1	2	2	-77			-41		290	28.2
DK-85-11-4	1	2	3	-77			-41			28.2
DK-85-11-4	1	2	4	-77			-40		240	28.2
DK-85-11-4	1	2	5	-68		-21	-17.5		258	20
DK-85-11-4	1	3	1	-48			-20			22.38
DK-85-11-4	1	3	2	-48			-19.3			21.89
DK-85-11-4	1	3	3	-67			-15.8			18
DK-85-11-4	1	3	4	-47			-16			19.45
DK-85-11-4	1	3	5						233	
DK-85-11-4	1	3	6	-68			-19		285	21.8
DK-85-11-4	1	3	7	-68			-20			22
DK-85-11-4	1	3	8	-40						
DK-85-11-4	1	4	1	-68			-20		193	22
DK-85-11-4	1	4	2	-69			-20			22
DK-85-11-4	1	4	3							
DK-85-11-4	1	4	4	-43			-2			3.39
DK-85-11-4	1	4	5	-43			-2.5			4.18
DK-85-11-4	1	4	6				-20			
DK-85-11-4	1	4	7	-40			-2			3.39
DK-85-11-4	1	4	8			-38	-36			27
DK-85-11-4	1	4	9	-45			-15			18.63
DK-85-11-4	1	4	10	-42			-7			10.49
DK-85-11-4	3	1	1	-34			-2.6			4.34
DK-85-11-4	3	1	2							
DK-85-11-4	3	1	3	-53			-20			
DK-85-11-4	3	1	4						195	
DK-85-11-4	3	1	5	-45			-37		162	27
DK-85-11-4	3	1	6	-57			-20			
DK-85-11-4	3	1	7	-56			-20			
DK-85-11-4	3	1	8	-56			-20			
DK-85-11-4	3	1	9							
DK-85-11-4	3	1	10							
DK-85-11-4	3	1	11	-52						
DK-85-11-4	3	1	12				-32.6			25.5
DK-85-11-4	3	1	13			-38	-36			26.78
DK-85-11-4	3	1	14			-43	-36.5			26.78
DK-85-11-4	4	1	1	-32			-2			3.39
DK-85-11-4	4	2	1							
DK-85-11-4	4	2	2							
DK-85-11-4	4	2	3	-37			-2.2			3.71
DK-85-11-4	4	2	4	-30			-0.5			0.88
DK-85-11-4	4	2	5	-39			-0.5			0.88
DK-85-11-4	4	2	6	-36			-1.5			2.57

sample #	Chip #	area #	inclus #	Tf	Tfm	Tm (HH)	Tm (ice)	Tm (halite)	Th	Salinity
DK-85-11-4	4	3	1	-45					273	
DK-85-11-4	4	3	2	-37			0		169	0
DK-85-11-4	4	3	3	-37			0		169	0
DK-85-11-4	4	4	1	-48			-5		194	7.86
DK-85-11-4	4	4	2	-48			-5		215	7.86
DK-85-11-4	4	4	3	-48			-5		175	7.86
DK-85-11-4	4	4	4	-48			-5			7.86
DK-85-11-2	1	A	1	-39.4			-2		225	3.39
DK-85-11-2	1	A	2	-39.4			-2		215	3.39
DK-85-11-2	1	A	3	-40.3			-1.8		225	3.06
DK-85-11-2	1	A	4	-38.9			-1.4		160	2.41
DK-85-11-2	1	B	1	-75		-26	-24		147	23
DK-85-11-2	1	B	2	-67		-30	-23.7		134	23
DK-85-11-2	1	B	3	-75		-30	-23.3			23
DK-85-11-2	2	A	1	-72	-60	-30	-21.5			22
DK-85-11-2	2	B	1	-67	-50		-22			23
DK-85-11-2	2	B	2	-68	-50		-22		123	23
DK-85-11-2	2	B	3	-68	-50		-22		128.9	23
DK-85-11-2	2	B	4	-67	-50		-18.4		126.8	20
DK-85-11-2	2	C	1	-74		-25	-18.3		138.4	20
DK-85-11-2	2	C	2	-52	-68	-25	-18.6		122.8	20
DK-85-11-2	2	C	3	-72	-45	-25	-18		132	20
DK-85-11-2	2	C	4	-72	-44		-21.7		136.4	22
DK-85-11-2	2	C	5	-72	-45	-25	-18.5		140	20
DK-85-11-2	2	D	1	-75	-40	-25	-21.9			22
DK-85-11-2	2	D	2	-75	-40	-25	-21.9			22
DK-85-11-2	2	D	3	-75	-40	-25	-21.9			22
DK-85-11-2	2	D	4	-75	-40	-25	-21.9			22
DK-85-11-2	3	A	1	-75	-40	-25	-21.8		168	22
DK-85-11-2	3	A	2	-75	-40	-25	-21.8		145	22
DK-85-11-2	3	A	3	-75	-40	-25	-21.8		172	22
DK-85-11-2	3	A	4	-75	-40	-25	-21.8		181	22
DK-85-11-2	3	A	5	-75	-40	-25	-21.8			22
DK-85-11-2	3	A	6	-75	-40	-25	-21.8		170	22
DK-85-11-2	3	A	7	-75	-40	-25	-21.8			22
DK-85-11-2	3	A	8	-75	-40	-25	-21.8		169	22
DK-85-11-2	3	A	9	-75	-40	-25	-21.8			22
DK-85-11-2	3	A	10	-62	-48	-26	-21			22
DK-85-11-2	3	A	11	-75	-40	-25	-21.8		162	22
DK-85-11-2	3	B	1	-72	-50	-25	-21.3		120	22
DK-85-11-2	3	B	2	-72	-50	-25	-20.8		132	22
DK-85-11-2	3	B	3	-70	-50		-21.9		113	22
DK-85-11-2	4	A	1	-53	-50	-18.8			140	
DK-85-11-2	4	A	2	-30	-40				267	
DK-85-11-2	4	A	3						147	
DK-85-11-2	4	A	4						147	
SC-14-W	1	A	1					175	154	34.06
SC-14-W	1	A	2					175	140	32.41
SC-14-W	1	A	3					175	140	32.41

sample #	Chip #	area #	inclus #	Tf	Tfm	Tm (HH)	Tm (ice)	Tm (halite)	Th	Salinity
SC-14-W	1	A	4					175	140	32.41
SC-14-W	1	B	1	-39	-25		-1		199	1.74
SC-14-W	1	B	2	-39	-25		-1		210	1.74
SC-14-W	1	B	3	-39	-25		-1		220	1.74
SC-14-W	1	B	4	-39	-25		-1		196	1.74
SC-14-W	1	C	1	-49	-18		-3			4.96
SC-14-W	1	C	2	-49	-18		-3			4.96
SC-14-W	1	C	3	-49	-18		-3			4.96
SC-14-W	1	C	4	-49	-18		-3			4.96
SC-14-W	1	C	5	-49	-18		-3			4.96
SC-14-W	1	C	6	-49	-18		-3			4.96
SC-14-W	1	C	7	-49	-18		-3			4.96
SC-14-W	2	A	1		-67	-24	-22			233
SC-14-W	2	A	2	-78	-67	-24	-22			23
SC-14-W	2	A	3	-78	-67	-24	-22			23
SC-14-W	2	A	4	-76	-67	-25	-21.6			22
SC-14-W	2	B	1	-45	-18		-3.5		183	5.71
SC-14-W	2	B	2	-45	-18		-3.5			5.71
SC-14-W	2	B	3	-45	-18		-3.5		197	5.71
SC-14-W	2	B	4	-45	-18		-3.5		197	5.71
SC-14-W	2	B	5	-45	-18		-3.5		197	5.71
SC-14-W	2	B	6	-45	-18		-3.5		197	5.71
SC-14-W	2	B	7	-45	-18		-3.5		211	5.71
SC-14-W	2	B	8	-45	-18		-3.5		183	5.71
SC-9-W	1	A	1					<200	145	32.97
SC-9-W	1	A	2					<200	115	30.15
SC-9-W	1	A	3					<200	116	30.07
SC-9-W	1	A	4					<200	116	30.15
SC-9-W	1	B	1	-52	-40	-21.2	-10.9		153	14.87
SC-9-W	1	B	2	-52	-40	-21.2	-10.9			14.87
SC-9-W	1	B	3	-52	-40	-21.2	-10.9		118	14.87
SC-9-W	1	B	4	-52	-40	-21.2	-10.9			14.87
SC-9-W	1	B	5	-56	-40	-21.2	-10.9			14.87
SC-9-W	1	B	6	-56	-40	-21.2	-10.9			14.87
SC-9-W	1	C	1	-44	-20		-2.3		207	3.87
SC-9-W	1	C	2	-44	-20		-2.3		202	3.87
SC-9-W	1	C	3	-44	-20		-2.3		228	3.87
SC-9-W	1	D	1		-40		-2		208	
SC-9-W	1	D	2		-40		-2.5		203	
SC-9-W	2	A	1					156	156	34.32
SC-9-W	2	B	1					>250	129	31.29
SC-9-W	2	B	2					>250	114	29.99
SC-9-W	2	B	3						156	
SC-9-W	2	B	4						141	
SC-9-W	2	B	5						141	
SC-9-W	2	C	1						180	
SC-9-W	2	C	2						180	
SC-15-W	1	A	1	-73	-70	-25	-22		122	23
SC-15-W	1	A	2	-75	-70	-25	-22		118.6	23

sample #	Chip #	area #	inclus #	Tf	Tfm	Tm (HH)	Tm (ice)	Tm (halite)	Th	Salinity
SC-15-W	1	A	3	-70	-66		-18			21
SC-15-W	1	A	1	-74	-69	-26	-22		96	22
SC-15-W	1	A	2	-74	-69	-26	-22		81.5	22
SC-15-W	1	A	3	-76	-69		-22.2		90	22.5
SC-15-W	1	A	1	-44			-1			1.74
SC-15-W	1	A	2	-44			-5			7.86
SC-15-W	1	A	3	-44			-5			7.86
SC-10-W	1	A	1	-46	-25		-1		172	1.74
SC-10-W	1	A	2	-46	-25		-1		191	1.74
SC-13-W	1	A	1					250	212	43.92
SC-13-W	1	A	2					212		
SC-13-W	1	A	1	-40			0		244	0
SC-13-W	1	A	2	-40			0		236	0
SC-13-W	1	A	3	-40			0		248	0

sample#	Chip #	area #	inclusion #	Tf	Tfm	Tm (HH)	Tm (ice)	Tm (halite)	Th	Salinity
SC-8-K	2	A	1	-46	-20		-4		182	6.45
SC-8-K	2	A	2						180	
SC-8-K	2	A	3						223	
SC-8-K	2	A	4	-46	-20		-4		240	6.45
SC-8-K	2	B	1	-49					219	
SC-8-K	2	B	2	-38	-20		0		141	0
SC-8-K	2	B	3	-45	-15		-2.2		161	3.71
SC-8-K	2	B	4	-48			-4.2		190	6.74
SC-8-K	2	B	5	-48			-4		170	6.45
SC-8-K	2	C	1				0		160	0
SC-8-K	2	C	2				0		177	0
SC-8-K	2	C	3				0		185	0
SC-8-K	3	A	1	-49			-2		232	3.39
SC-8-K	3	A	2	-48			-1		196	1.74
SC-8-K	3	A	3	-47			-1			1.74
SC-8-K	4	A	1	-49			-5			7.86
SC-8-K	4	A	2	-46			-5			7.86
SC-8-K	4	B	1						172	
SC-4-K	1	A	1						223	
SC-4-K	1	A	2	-46			-8		162	11.7
SC-4-K	1	A	3	-40			-9		233	12.85
SC-4-K	1	A	4	-42			-6		173	9.21
SC-4-K	1	A	5						187	
SC-4-K	1	B	1						226	
SC-4-K	1	B	2						223	
SC-4-K	1	B	3						252	
SC-4-K	1	B	4						204	
SC-4-K	1	C	1	-47			-5.5			8.55
SC-4-K	1	C	2	-49						
SC-4-K	1	C	3	-48						
SC-4-K	1	C	4	-48			-4.5			7.17
SC-4-K	2	A	1	-39			-8			11.7
SC-4-K	2	B	1	-44			-7		246	10.49
SC-4-K	2	B	2	-43			-5		238	7.86
SC-4-K	2	B	3	-43			-7		243	10.49
SC-4-K	3	A	1	-48			-4		265	6.45
SC-4-K	3	A	2	-44			-5		225	7.86
SC-4-K	3	A	3	-44			-5		183	7.86
SC-4-K	3	A	4	-45			-6		195	9.21
SC-4-K	4	A	1	-45			-4		231	6.45
SC-4-K	4	A	2	-45			-4		230	6.45
SC-4-K	4	A	3	-45			-4		228	6.45
SC-3-K	1	A	1	-48			-4.5		139.5	7.17
SC-3-K	1	A	2	-48			-4.5		193	7.17
SC-3-K	1	A	3	-48			-4.5		183	7.17
SC-3-K	1	A	4	-48			-4.5		157	7.17
SC-3-K	1	B	1	-46			-4.7		170	7.45
SC-3-K	1	B	2	-46			-4.7		179	7.45
SC-3-K	1	B	3	-43			0.5		171	0.88

sample#	Chip #	area #	inclusion #	Tf	Tfm	Tm (HH)	Tm (ice)	Tm (halite)	Th	Salinity
SC-3-K	1	C	1	-43			-5		151	7.86
SC-3-K	1	C	2	-43			-5		169	7.86
SC-3-K	1	C	3	-43			-5		186	7.86
SC-3-K	1	C	4	-43			-5		187	7.86
SC-3-K	1	C	5	-43			-5		172	7.86
SC-2-K	1	A	1					210	135	31.89
SC-2-K	1	A	2					160	130	31.39
SC-2-K	1	A	3					180	140	32.41
SC-2-K	1	B	1	-49	-25		-3		166	4.96
SC-2-K	1	B	2	-48	-25		-2.5		170	4.18
SC-2-K	1	B	3	-48	-25		-2.5		170	4.18
SC-2-K	1	B	4	-48	-25		-2.5		170	4.18
SC-2-K	1	B	5	-48	-25		-2.5		170	4.18
SC-2-K	1	B	6	-45	-25		-2.5			4.18
SC-2-K	1	B	7							
SC-2-K	1	B	8	-49	-25		-3			4.96
SC-2-K	1	B	9	-45	-25		-2.5		180	4.18
SC-2-K	2	A	1	-48			-2		185	3.39
SC-2-K	2	A	2	-48			-2		185	3.39
SC-2-K	2	A	3	-48			-2		185	3.39
SC-2-K	2	A	4	-48			-2		185	3.39
SC-2-K	2	A	5	-48			-2		185	3.39
SC-2-K	2	A	6	-48			-2		185	3.39

sample #	Chip #	area #	inclusion #	Tf	Tfm	Tm (HH)	Tm (ice)	Tm (halite)	Th	salinity
A16 G332	1	1	1	-36			-0.4			0.71
A16 G332	1	1	2	-36			-0.4			0.71
A16 G332	1	1	3						293	
A16 G332	1	2	1	-37			-0.4			0.71
A16 G332	1	2	2	-37			-0.4		273.7	0.71
A16 G332	1	2	3	-37			-0.4		287	0.71
A16 G332	1	3	1	-36			-0.2		282	0.35
A16 G332	1	3	2	-36			-0.3			0.53
A16 G332	1	3	3	-33			-0.2			0.35
A16 G332	1	3	4	-39			-0.8			1.4
A16 G332	1	3	5	-36			-0.7			1.23
A16 G332	1	3	6	-38.5			-0.6			1.05
A16 G332	1	3	7						293.5	
A16 G332	1	4	1	-38			-0.6			1.05
A16 G332	1	4	2	-38			-0.6			1.05
A16 G332	1	4	3	-38			-0.6			1.05
A16 G332	2	1	1				-0.5		282	0.88
A16 G332	2	1	2				-0.2		275	0.35
A16 G332	2	1	3						299	
A16 G332	2	2	1				-0.5		284	0.88
A16 G332	2	2	2				-0.6		305	1.05
A16 G332	2	2	3				-0.6		270	1.05
A16 G332	2	3	1						309.4	
A16 G332	2	3	2				-0.3		308.8	0.53
A16 G332	2	3	3				-0.3		315	0.53
A16 G332	2	3	4	-36			-0.6		314.2	1.05
A16 G332	2	3	5						323	
SC-5-D	1	A	1	-50	-20		-1.5		170	2.57
SC-5-D	1	A	2	-50	-20		-1.5		238	2.57
SC-5-D	1	A	3	-50	-20		-1.5			2.57
SC-5-D	1	A	1	-42			-0.1		144	0.18
SC-5-D	1	B	1	-49	-30		-1.8		152	3.06
SC-5-D	1	B	2	-49	-30		-1.8			3.06
SC-5-D	1	B	3	-46	-30		-2.9		161	4.8
SC-5-D	1	B	4	-46	-30		-2.9		161	4.8
SC-6-D	1	A	1	-60			-3.5		269	5.71
SC-6-D	1	A	2						180	
SC-6-D	2	A	1	-48			0		190	0
SC-6-D	2	A	2						>250	
SC-6-D	2	B	1	-47			-0.6			1.05
SC-6-D	2	B	2	-47			-0.6			1.05
SC-6-D	2	B	2	-47			-0.6			1.05
SC-6-D	2	C	3	-63			-16.5			
SC-7-D	1	A	1						239	
SC-7-D	1	A	2						225	
SC-7-D	1	B	1	-49	-35	-15	-2.6		264	4.34
SC-7-D	1	B	2	-48	-35	-15	-2.6		255	4.34
SC-7-D	1	B	3	-50	-35	-15	-2.6		259	4.34
SC-7-D	1	B	4							

sample #	Chip #	area #	inclusion #	Tf	Tfm	Tm (HH)	Tm (ice)	Tm (halite)	Th	salinity
SC-7-D	1	B	5	-49	-38	-15	-2.3		256	3.87
SC-7-D	1	B	6	-49	-38	-15	-2.3		257	3.87
SC-7-D	1	B	7	-49	-38	-15	-2.3		254	3.87
SC-7-D	1	B	8	-49	-38	-15	-2.3			3.87
SC-7-D	1	B	9	-49	-38	-15	-2.7			4.49
SC-7-D	1	B	10	-49	-38	-15	-2			3.39
SC-7-D	1	B	11	-49	-38	-15	-2.7			4.49
SC-7-D	1	C	1	-48	-27		-2		240	3.39
SC-7-D	1	C	2	-48	-27		-2		240	3.39
SC-7-D	2	A	1	-50			-2			3.39
SC-7-D	2	A	2	-50			-2			3.39
SC-7-D	2	A	3	-50			-2			3.39
SC-7-D	2	A	4	-50			-2			3.39
SC-7-D	2	A	5	-50			-2			3.39

sample #	Chip #	area #	inclusion #	Tf	Tfm	Tm (HH)	Tm (ice)	Tm (halite)	Th	Salinity
SC-1-MB	1	A	1	-40			-4		240	6.45
SC-1-MB	1	A	2	-40			-4		235	6.45
SC-1-MB	1	A	3	-40			-4			6.45
SC-1-MB	1	B	1	-53			-10		239	14
SC-1-MB	1	B	2	-53			-10		235	14
SC-1-MB	1	B	3	-53			-10		244	14
SC-1-MB	2	A	1					300		
SC-1-MB	2	A	2					300	228	
SC-1-MB	2	A	3	-65			-6		230	9
SC-1-MB	2	A	4	-65			-6		230	9
SC-1-MB	2	A	5				-6	300	233	
SC-1-MB	2	A	6	-55	-40		-6			9
SC-1-MB	2	A	7	-55	-40		-6			9
SC-1-MB	2	B	1	-65	-60					
SC-1-MB	2	B	2	-65	-60					
SC-1-MB	2	C	1	-55	-48		-1.5		200	3
SC-1-MB	2	C	2	-55	-48		-1.5		200	3
SC-1-MB	2	C	3	-55	-48		-1.5		200	3
SC-1-MB	2	C	4	-54			-1.5		200	3
SC-1-MB	2	C	5	-54			-1.5		200	3
SC-1-MB	2	C	6	-54			-1.5		200	3
SC-1-MB	2	C	7	-54			-1.5		200	3
SC-1-MB	2	C	8	-54			-1.5		243	3
SC-1-MB	2	C	9	-54			-1.5		222	3
SC-1-MB	2	C	10	-54			-1.5		225	3
SC-1-MB	2	C	11							
SC-1-MB	2	C	12	-52			-1.5		225	3
SC-1-MB	2	D	1	-52	-45		-2		259	4
SC-1-MB	2	D	2	-52	-45		-2		240	4
SC-1-MB	2	D	3	-52	-45		-2		231	4
SC-1-MB	3	A	1	-52	-45	-27	-13			17
SC-1-MB	3	A	2	-52	-45	-27	-13			17
SC-1-MB	3	A	3	-52	-45	-27	-13			17
SC-1-MB	3	B	1				-2.7		210	
SC-1-MB	3	B	2				-2.7		238	
SC-1-MB	3	C	1	-46			0			0
SC-1-MB	3	C	2	-46			0			0
SC-1-MB	3	C	3	-46			0			0
SC-1-MB	3	D	1	-54			-1.8		237	3
SC-1-MB	3	D	2	-54			-1.8		237	3
SC-1-MB	3	D	3	-54			-1.8			3
SC-1-MB	3	D	4	-54			-1.8			3
SC-1-MB	3	E	1	-43			-1.5		293	2.57
SC-1-MB	3	E	2	-54	-30		-2		232	3.39
SC-1-MB	3	E	3						254	
SC-1-MB	3	E	4						307	
SC-1-MB	3	E	5	-43			-1.5		320	2.57
SC-1-MB	3	E	6	-43			-1.5		322	2.57
SC-1-MB	3	E	7	-45			-0.8		228	1.4

sample #	Chip #	area #	inclusion #	Tf	Tfm	Tm (HH)	Tm (ice)	Tm (halite)	Th	Salinity
SC-1-MB	3	E	8	-45			-0.8		307	1.4
SC-1-MB	3	E	9	-40			-0.7			1.23
SC-2-MB	1	A	1	-48						
SC-2-MB	1	A	2	-48						
SC-2-MB	1	A	3	-48						
SC-2-MB	1	B	1	-55						
SC-2-MB	1	B	2				-2.5			4
SC-2-MB	1	C	1	-50			-2.5			4
SC-2-MB	1	C	2	-50			-2.5			4
SC-2-MB	1	D	1	-50			-1.5		240	3
SC-2-MB	1	D	2	-50			-1.5		220	3
SC-2-MB	1	D	3	-50			-1.5		223	3
SC-2-MB	1	D	4	-50			-1.5		196	3
SC-2-MB	1	D	5	-45			-1.5		217	2.57
SC-2-MB	1	D	6	-45			-1.5		206	2.57
SC-2-MB	1	E	1		-40		-1.8		294	3
SC-2-MB	1	E	2		-40		-1.8		285	3
SC-2-MB	1	E	3		-40		-1.8		320	3
SC-2-MB	1	E	4		-40		-1.7		312	3
SC-5-MB	1	A	1		-40		-4		353	7
SC-5-MB	1	A	2		-40		-4		328	7
SC-5-MB	1	A	3		-40		-4		369	7
SC-5-MB	1	C	1						214	
SC-5-MB	1	C	2	-80	-60	-23	-21.2		192	22
SC-5-MB	1	C	3	-84			-20.9		220	22
SC-5-MB	1	E	1				1		263	
SC-5-MB	1	E	2						286	
SC-5-MB	1	E	3				1			
SC-5-MB	1	E	4						232	
SC-5-MB	2	B	1	-48	-35		-1.5			2.57
SC-5-MB	2	B	2	-48	-35		-1.5			2.57
SC-5-MB	2	B	3	-48	-35		-1.5			2.57
SC-5-MB	2	C	4	-48	-35		-2.6			4.34
SC-5-MB	2	D	5	-48	-35		-2.6			4.34
SC-5-MB	2	C	1						244	
SC-5-MB	2	C	2	-59	-35		-1.5		360	2.57
SC-5-MB	2	C	3						335	
SC-5-MB	2	C	4	-59	-35		-1.5		339	2.57
SC-5-MB	2	D	1	-60	-25	-20	-10		304	13.94
SC-5-MB	2	D	2	-60	-25	-20	-10		304	13.94
SC-5-MB	2	D	3	-60	-25	-20	-10			13.94
SC-5-MB	3	A	1	-43		-16	-2.9			4.8
SC-5-MB	3	A	2	-43		-16	-3.1			5.11
SC-5-MB	3	B	1	-46			-2		173	3.39
SC-5-MB	3	B	2	-46			-2		207	3.39
SC-5-MB	3	B	3	-46			-2		164	3.39
SC-5-MB	3	B	4	-46			-2		169	3.39
SC-5-MB	3	B	5	-46			-2		176	3.39
SC-3-MB	1	B	1	-45			-5		182	7.86

sample #	Chip #	area #	inclusion #	Tf	Tfm	Tm (HH)	Tm (ice)	Tm (halite)	Th	Salinity
SC-3-MB	1	B	2	-45			-5		188	7.86
SC-3-MB	1	B	3	-45			-5		185	7.86
SC-9-MB	1	A	1	-58					347	
SC-9-MB	1	A	2	-58					343	
SC-9-MB	1	A	3	-58					360	
SC-9-MB	1	B	1				-10		318	
SC-9-MB	1	B	2				-2.9		318	
SC-9-MB	2	A	1	-42	-33		-1			1.74
SC-9-MB	2	A	2	-38	-33		-1			1.74
SC-9-MB	3	A	1	-48			-1.9			3.23
SC-9-MB	3	A	2	-48			-1.9			3.23
SC-8-MB	1	A	1	-62	-30		-2			3.39
SC-8-MB	1	A	2	-62	-30		-1.5			2.57
SC-8-MB	1	A	3	-55	-30		-5			7.86
SC-8-MB	1	B	1	-48			-4.4			7.02
SC-8-MB	1	B	2	-48			-4.4			7.02
SC-7-MB	1	A	1	-50			0			0
SC-7-MB	1	A	2	-50			0			0
SC-7-MB	1	B	1	-47			-1.8			3.06
SC-7-MB	1	B	2	-47			-1.8			3.06
SC-7-MB	1	B	3	-47			-1.8			3.06
SC-7-MB	1	B	4	-48			-2			3.39
SC-7-MB	1	C	1	-46			-3			3.39
SC-7-MB	1	C	2	-46			-3			3.39
SC-7-MB	2	A	1	-50		-20	-1.5			2.57
SC-7-MB	3	A	1	-55			-5		160	8.5
SC-7-MB	3	A	2	-55			-5			8.5
SC-7-MB	3	A	3	-55			-5		154	8.5
SC-7-MB	3	A	4	-55			-5		192	8.5
SC-6-MB	1	A	1	-50			-4		207	6.45
SC-6-MB	1	A	2	-50			-4		202	6.45
SC-6-MB	1	B	1	-50			-6			9.21
SC-6-MB	1	B	2	-50			-6			9.21
SC-6-MB	2	A	1	-54			-0.5			0
SC-6-MB	2	A	2	-52		-18	0			0
SC-6-MB	2	A	3	-52		-18	-1.7			3
SC-6-MB	2	A	4	-48	-40		-0.5			0
SC-6-MB	2	A	5	-48	-40		-3.3			6
SC-6-MB	2	A	6	-54			2			

sample #	Chip #	area #	inclus #	Tf	Tfm	Tm (HH)	Tm (ice)	Tm (halite)	Th	salinity
DK-85-26A	A	1	1	-63	-58		-23.5		172	23
DK-85-26A	A	1	2	-63	-58		-23.5		172	23
DK-85-26A	A	1	3							
DK-85-26A	A	1	4	-83			-23		175	23
DK-85-26A	A	1	5	-80			-21		173	22
DK-85-26A	A	2	1	-74	-55	-27	-21.6			22
DK-85-26A	A	2	2	-75	-55	-27	-20.4			22
DK-85-26A	A	2	3	-75		-27	-20.6			22
DK-85-26A	A	3	1						173	
DK-85-26A	A	3	2						176	
DK-85-26A	A	3	3						173	
DK-85-26A	A	3	4						148	
DK-85-26A	A	3	5						179	
DK-85-26A	A	4	1	-78	-52		-23.6		148	23
DK-85-26A	A	4	2	-84	-52		-23		162	23
DK-85-26A	A	4	3	-82			-24		165	23
DK-85-26A	A	4	4	-83					165	
DK-85-26A	A	4	5				-30		153	
DK-85-26A	A	5	1	-68	-55	-29	-20.9		132	21
DK-85-26A	A	5	2	-68	-40		-14.8		240	17.5
DK-85-26A	A	5	3	-74	-63	-29	-21.3		166	21
DK-85-26A	A	5	4	-72	-63	-29	-21.3		172	21
DK-85-26A	C	1	1	-75	-57		-21.2			21
DK-85-26A	C	1	2	-70	-57		-21.6			22
DK-85-26A	C	2	1	-72	-55		-20.3			21.5
DK-85-26A	C	2	2	-71	-55		-20.3			21.5
DK-85-26A	C	3	1	-64	-60	-26.9	-18			20
DK-85-26A	C	3	2	-70	-56		-18.5			20
DK-85-26A	C	3	3	-71	-57	-29	-19.3			20.5
DK-85-26A	C	3	4	-70	-56		-19			20
DK-85-26A	B	1	1	-78	-50		-23		177	23
DK-85-26A	B	1	2	-74	-50		-22		174	22.5
DK-85-26A	B	1	3	-73	-50		-21.5			22
DK-85-26A	B	1	4	-74	-56		-22.7		168	23
DK-85-26A	B	2	1						145	
DK-85-26A	B	2	2						152	
DK-85-26A	B	2	3						170	
DK-85-26A	B	2	4						170	
DK-85-26A	B	2	5						154	
DK-85-29b-1	1B	1	1	-28			-3			4.96
DK-85-29b-1	1B	1	2	-83	-50		-23.4		145.4	23
DK-85-29b-1	1B	1	3	-28			-2.9		200	4.8
DK-85-29b-1	1B	1	4	-83	-50		-23.4		155	23
DK-85-29b-1	1B	1	5							
DK-85-29b-1	1B	1	6						169	
DK-85-29b-1	1B	1	7						157	
DK-85-29b-1	1B	2	1	-64	-40		-22			22
DK-85-29b-1	1B	2	2	-68	-45		-16.5			18
DK-85-29b-1	1B	3	1	-61	-58		-16.1			18

sample #	Chip #	area #	inclus #	Tf	Tfm	Tm (HH)	Tm (ice)	Tm (halite)	Th	salinity
DK-85-29b-1	1B	3	2	-61	-58		-21			22
DK-85-29b-1	1B	3	3		-58		-21		150.1	22
DK-85-29b-1	1B	3	4		-58		-20.5		149.9	22
DK-85-29b-1	1B	3	5		-58		-20.5		159.3	22
DK-85-29b-1	1B	3	6	-72	-55		-20		144.3	21.5
DK-85-29b-1	1B	3	7	-72	-55		-18.2		150.7	20
DK-85-29b-1	1B	4	1	-34			-3			4.96
DK-85-29b-1	1B	4	2	-39			-2.5			4.18
DK-85-29b-1	1B	5	1	-36			-3.4			5.56
DK-85-29b-1	1B	5	2	-36			-3.4			5.56
DK-85-29-2	1	A	1	-79	-50	-30	-21.8		115	22
DK-85-29-2	1	A	2	-79	-50	-30	-21.8		120	22
DK-85-29-2	1	A	3	-59	-60		-21.8		113	
DK-85-29-2	1	B	1	-42	-60		-10		261	
DK-85-29-2	1	B	2	-43	-55		-8		250	
DK-85-29-2	1	B	3	-43	-55		-8		260	
DK-85-29-2	1	B	4	-42	-60		-11		246	
DK-85-29-2	1	B	5	-44			-2		243	3.39
DK-85-29-2	1	B	6	-48			-3			4.96
DK-85-29-2	1	C	1						230	
DK-85-29-2	1	C	2						229	
DK-85-29-2	1	C	3						233	
DK-85-29-2	1	D	1	-51		-20	-10			13.94
DK-85-29-2	1	E	1	-45			-4			6.45
DK-85-29-2	1	E	2	-45			-4			6.45
DK-85-29-2	1	F	1						229	
DK-85-29-2	1	F	2							
DK-85-29-2	1	F	3							
DK-85-29-2	1	F	4						198	
DK-85-29-2	1	F	5	-52			-2.5		295	4.18
DK-85-29-2	1	F	6	-50			-2		220	3.39
DK-85-29-2	1	F	7	-50			-2		212	3.39
DK-85-29-2	1	F	8	-42	-12		-1.5		220	2.57
DK-85-29-2	1	F	9	-41	-12.8		-1.8		194	3.06
DK-85-29-2	1	F	10	-40			-1		250	1.74
DK-85-29-2	1	F	11	-45			-2.5		247	4.18
DK-85-29-2	1	F	12							
DK-85-29-2	1	F	13						228	
DK-85-29-2	2	A	1	-46			-3.8		229	6.16
DK-85-29-2	2	A	2	-47			-3		165	4.96
DK-85-29-2	2	A	3	-47			-3		269	4.96
DK-85-29-2	2	A	4	-41			-3			4.96
DK-85-29-2	2	A	5	-41			-3			4.96
DK-85-29-2	2	A	6	-45			-2.5			4.18
DK-85-29-2	2	A	7	-45			-2.5			4.18
DK-85-29-2	3	A	1	-44			-2.5			4.18
DK-85-29-2	3	A	2	-44			-2.5			4.18
DK-85-29-2	3	A	3	-44			-3.8			6.16
DK-85-29-2	3	A	4	-44			-3.5			5.71

sample #	Chip #	area #	inclus #	Tf	Tfm	Tm (HH)	Tm (ice)	Tm (halite)	Th	salinity
DK-85-29-2	3	A	5	-44			-3.5			5.71
DK-85-29-2	3	A	6	-44			-4			6.45
DK-85-27	1	A	1	-79	-55		-26		175	24.5
DK-85-27	1	A	2	-79	-60		-25.2		188	24
DK-85-27	1	A	3	-80	-60		-25.3		190	24
DK-85-27	1	A	1	-80			-25.7			24
DK-85-27	1	A	2	-80			-24.2			24
DK-85-27	1	A	3	-80			-24.2			24
DK-85-27	1	A	4	-68	-40		-17.5			19.5
DK-85-27	1	A	5	-74			-21.2			21.5
DK-85-27	1	A	6	-77	-62		-24.2			24

Appendix E: Geochemical data for the New Ross pluton from Ham et al. (1991)

Majors	SiO2	Al2O3	Fe2O3	CaO	MgO	Na2O	K2O	TiO2	P2O5	MnO	H2O	A/CNK
Biotite granodiorite	66.87	14.96	5.07	1.83	1.77	3.25	3.8	0.75	0.21	0.1	0.48	1.68
Biotite granodiorite	68.94	14.62	3.94	1.75	1.82	3.35	3.52	0.61	0.19	0.07	0.8	1.70
Biotite granodiorite	71.08	14.51	2.78	1.42	1.31	3.3	4.03	0.4	0.16	0.06	0.8	1.66
Biotite monzogranite	69.04	14.42	4.1	1.4	1.51	3.45	3.95	0.59	0.22	0.09	0.7	1.64
Biotite monzogranite	68.75	14.74	4.31	1.56	1.52	2.83	4.19	0.61	0.21	0.09	0.49	1.72
Biotite monzogranite	68.52	14.67	4.72	1.79	1.66	3.17	3.44	0.68	0.24	0.1	0.7	1.75
Biotite monzogranite	68.93	14.92	3.97	1.75	1.55	2.97	4.09	0.56	0.19	0.08	0.24	1.69
Muscovite-biotite monzogranite	72.47	14.51	2.26	0.71	1.08	3.58	4.67	0.31	0.28	0.05	0.6	1.62
Coarse-grained leucomonzogranite	73.84	13.88	1.7	0.7	0.92	2.98	4.73	0.19	0.27	0.03	0.4	1.65
Coarse-grained leucomonzogranite	74.46	13.82	1.47	0.38	0.76	3.45	4.32	0.11	0.33	0.03	0.7	1.70
Coarse-grained leucomonzogranite	71.44	14.43	2.65	0.69	1.31	3.26	4.68	0.31	0.23	0.06	1	1.67
Coarse-grained leucomonzogranite	72.09	14.95	1.6	0.52	1.04	3.32	4.76	0.21	0.3	0.04	0.6	1.74
Coarse-grained leucomonzogranite	73.65	14.02	1.92	0.75	1.07	3.13	4.75	0.21	0.18	0.05	0.4	1.62
Coarse-grained leucomonzogranite	72.3	14.66	2.05	1.21	1.14	3.93	3.92	0.24	0.22	0.05	0.4	1.62
Coarse-grained leucomonzogranite	74.79	13.99	1.38	0.37	0.82	3.21	4.65	0.14	0.23	0.04	0.4	1.70
Coarse-grained leucomonzogranite	74.52	13.99	1.68	0.29	0.92	3.91	4.27	0.16	0.27	0.04	0.74	1.65
Coarse-grained leucomonzogranite	73.01	14.13	2.31	0.57	1.03	3.43	4.68	0.3	0.27	0.05	0.57	1.63
Coarse-grained leucomonzogranite	74.09	13.79	1.87	0.5	0.92	3.65	4.9	0.16	0.17	0.07	0.39	1.52
Coarse-grained leucomonzogranite	72.68	13.76	2.56	0.91	1.13	3.38	4.7	0.34	0.24	0.05	0.21	1.53
Coarse-grained leucomonzogranite	74.14	13.65	2.11	0.67	1.02	3.04	4.62	0.22	0.17	0.06	0.2	1.64
Coarse-grained leucomonzogranite	74.93	13.38	1.83	0.52	0.89	3.16	4.59	0.14	0.15	0.06	0.1	1.62
Coarse-grained leucomonzogranite	73.44	14.2	1.76	0.83	0.96	2.87	5.1	0.22	0.23	0.03	0.24	1.61
Coarse-grained leucomonzogranite	75.25	13.47	1.2	0.46	0.86	3.25	4.82	0.14	0.12	0.04	0.48	1.58
Coarse-grained leucomonzogranite	74.25	13.32	1.85	0.51	0.9	3.44	4.39	0.2	0.29	0.04	0.5	1.60
Coarse-grained leucomonzogranite	74.11	14.11	1.27	0.31	0.8	2.98	4.91	0.11	0.28	0.02	0.73	1.72
Coarse-grained leucomonzogranite	73.12	14.33	1.78	0.36	0.87	3.46	4.53	0.19	0.27	0.04	0.63	1.72
Coarse-grained leucomonzogranite	72.31	14.72	1.96	0.85	1.17	3.43	4.46	0.25	0.22	0.06	0.54	1.68

Majors	SiO2	Al2O3	Fe2O3	CaO	MgO	Na2O	K2O	TiO2	P2O5	MnO	H2O	A/CNK
Coarse-grained leucomonzogranite	72.95	13.7	2.54	0.61	1.12	2.8	4.76	0.33	0.22	0.05	0.47	1.68
Coarse-grained leucomonzogranite	74.38	14.2	1.61	0.48	0.84	3.62	4.52	0.12	0.23	0.05	0.6	1.65
Coarse-grained leucomonzogranite	72.98	14.58	2.16	0.62	0.9	3.83	4.58	0.18	0.18	0.06	0.5	1.61
Coarse-grained leucomonzogranite	74.8	13	1.96	0.34	0.82	3.48	4.81	0.15	0.19	0.05	0.5	1.51
Coarse-grained leucomonzogranite	73.49	14.54	1.4	0.38	0.77	3.49	4.93	0.11	0.3	0.03	0.4	1.65
Coarse-grained leucomonzogranite	73.7	14.33	1.32	0.36	0.73	4.39	4.18	0.09	0.38	0.04	0.89	1.60
Coarse-grained leucomonzogranite	73.5	14.33	1.66	0.43	0.86	3.23	4.63	0.18	0.31	0.03	0.6	1.73
Coarse-grained leucomonzogranite	72.09	14.08	2	0.71	1	3.47	5.01	0.21	0.17	0.05	0.4	1.53
Fine-grained leucomonzogranite	73.44	14.7	1.24	0.36	0.88	3.83	4.57	0.13	0.3	0.04	0.53	1.68
Fine-grained leucomonzogranite	75.1	14.07	0.99	0.31	0.74	3.4	4.27	0.07	0.36	0.02	0.49	1.76
Fine-grained leucomonzogranite	73.8	14.02	1.72	0.41	0.77	2.97	4.84	0.15	0.31	0.04	0.67	1.71
Fine-grained leucomonzogranite	73.97	13.33	0.79	1.31	0.78	3.57	4.7	0.14	0.21	0.02	1.3	1.39
Fine-grained leucomonzogranite	75.87	13.09	1.58	0.31	0.81	3.01	4.27	0.12	0.27	0.03	0.62	1.72
Fine-grained leucomonzogranite	74.12	14.21	1.41	0.35	0.84	4.56	4.33	0.11	0.36	0.03	0.4	1.54
Fine-grained leucomonzogranite	74.64	13.98	0.93	0.25	0.8	3.41	4.36	0.04	0.24	0.05	0.49	1.74
Fine-grained leucomonzogranite	74.56	14.14	1.13	0.35	0.76	3.35	4.6	0.07	0.24	0.07	0.58	1.70
Fine-grained leucomonzogranite	74.09	14.06	1.65	0.46	0.82	3.43	4.81	0.18	0.31	0.03	0.54	1.62
Fine-grained leucomonzogranite	74.81	13.91	1.24	0.24	0.77	3.62	4.22	0.06	0.22	0.07	0.77	1.72
Fine-grained leucomonzogranite	73.35	14.36	1.73	0.39	0.97	3.32	4.63	0.15	0.19	0.06	0.63	1.72
Fine-grained leucomonzogranite	73.01	14.97	1.3	0.37	0.89	3.38	4.8	0.17	0.32	0.03	0.8	1.75
Fine-grained leucomonzogranite	73.51	14.67	1.34	0.34	2.16	3.49	4.67	0.14	0.3	0.04	0.4	1.73
Fine-grained leucomonzogranite	74.98	14.24	1.32	0.28	0.81	3.53	4.38	0.06	0.24	0.04	0.3	1.74
Fine-grained leucomonzogranite	74.21	14.08	1.03	0.43	0.83	4.75	4.46	0.1	0.36	0.03	0.6	1.46
Fine-grained leucomonzogranite	75.22	13.69	1.55	0.31	0.83	3.82	4.49	0.12	0.24	0.04	0.2	1.59
Fine-grained leucomonzogranite	73.18	14.17	1.81	0.68	0.97	3.61	4.58	0.19	0.21	0.05	0.4	1.60
Fine-grained leucomonzogranite	74.65	13.81	1.67	0.35	0.87	3.32	4.43	0.14	0.22	0.04	0.4	1.70
Fine-grained leucomonzogranite	75.42	13.71	0.73	0.3	0.8	2.91	5.3	0.06	0.15	0.03	0.48	1.61

Majors	SiO2	Al2O3	Fe2O3	CaO	MgO	Na2O	K2O	TiO2	P2O5	MnO	H2O	A/CNK
Fine-grained leucomonzogranite	75.24	14	1.16	0.3	0.8	3.8	4.48	0.07	0.28	0.04	0.51	1.63
Fine-grained leucomonzogranite	74.78	14.27	1.22	0.3	0.72	3.93	4.06	0.06	0.32	0.04	0.6	1.72
Fine-grained leucomonzogranite	75.37	14.26	0.6	0.24	0.67	3.76	4.29	0.04	0.17	0.03	0.59	1.72
Fine-grained leucomonzogranite	74.38	13.71	1.57	0.38	0.96	3.13	4.46	0.11	0.18	0.09	0.7	1.72
Fine-grained leucomonzogranite	74.32	14.52	0.83	0.24	0.75	4.28	4.37	0.03	0.21	0.04	0.33	1.63
Fine-grained leucomonzogranite	74.84	14.42	0.7	0.31	0.68	3.75	3.92	0.05	0.29	0.05	0.54	1.81
Fine-grained leucomonzogranite	75.24	14.35	0.54	0.32	0.76	3.75	3.94	0.05	0.26	0.05	0.41	1.79
Fine-grained leucomonzogranite	74.51	13.96	1.42	0.33	0.74	2.95	4.14	0.1	0.34	0.03	0.7	1.88
Fine-grained leucomonzogranite	74.69	13.86	1.48	0.3	0.8	3.54	4.64	0.11	0.26	0.04	0.6	1.63
Fine-grained leucomonzogranite	74.82	13.87	1.35	0.27	0.68	3.46	4.45	0.08	0.28	0.03	0.63	1.70
Fine-grained leucomonzogranite	74	14.52	1.1	0.4	0.81	3.67	4.39	0.09	0.3	0.04	0.4	1.72
Fine-grained leucomonzogranite	74.33	14.2	1.15	0.32	0.74	3.74	4.16	0.06	0.34	0.03	0.6	1.73
Fine-grained leucomonzogranite	72.71	14.59	0.9	0.43	0.73	4.08	3.38	0.05	0.5	0.03	0.8	1.85
Fine-grained leucomonzogranite	73.9	14.97	0.86	0.34	0.8	3.83	3.64	0.06	0.46	0.02	0.8	1.92
Fine-grained leucomonzogranite	73.91	13.74	1.46	0.31	0.78	4.11	4.41	0.11	0.28	0.05	0.45	1.56
Fine-grained leucomonzogranite	73.19	14.11	2.11	0.32	1.24	3.03	5.2	0.22	0.18	0.05	0.6	1.65
Fine-grained leucomonzogranite	73	14.61	1.44	0.36	0.9	3.82	4.62	0.12	0.34	0.04	0.6	1.66
Fine-grained leucomonzogranite	73.58	14.88	1.75	0.83	0.99	3.33	4.97	0.28	0.19	0.03	0.3	1.63
Fine-grained leucomonzogranite	71.88	14.44	2.16	0.6	0.97	3.69	4.97	0.25	0.27	0.05	0.5	1.56
Fine-grained leucomonzogranite	73.68	13.92	1.77	0.37	0.8	3.65	4.75	0.16	0.24	0.04	0.7	1.59
Fine-grained leucomonzogranite	73	14.46	1.89	0.66	1.14	3.65	4.52	0.19	0.19	0.07	0.8	1.64
Fine-grained leucomonzogranite	74.56	13.5	0.87	0.34	0.9	3.98	4.17	0.04	0.19	0.03	0.5	1.59
Fine-grained leucomonzogranite	71.96	14.7	1.78	0.48	1.31	3.55	4.82	0.25	0.29	0.03	0.9	1.66
Fine-grained leucomonzogranite	72.34	14.22	2.52	0.94	1.14	2.92	4.6	0.34	0.26	0.05	0.3	1.68
Fine-grained leucomonzogranite	72.42	14.23	2.38	0.71	1.12	3.75	4.66	0.31	0.27	0.05	0.4	1.56
Fine-grained leucomonzogranite	72.17	14.47	2.14	0.67	1.25	4.21	4.69	0.28	0.27	0.05	0.56	1.51
Muscovite leucogranite	74.77	14.22	1.38	0.21	0.69	3.72	4.37	0.08	0.29	0.03	0.71	1.71

Majors	SiO2	Al2O3	Fe2O3	CaO	MgO	Na2O	K2O	TiO2	P2O5	MnO	H2O	A/CNK
Muscovite leucogranite	74.9	14.16	1.33	0.26	0.66	3.49	4.23	0.08	0.34	0.03	0.82	1.77
Muscovite leucogranite	74.27	13.88	1.79	0.31	0.84	3.21	4.38	0.13	0.33	0.04	0.7	1.76
Muscovite leucogranite	73.82	14.46	1.18	0.31	0.7	3.55	4.3	0.06	0.41	0.04	0.6	1.77
Muscovite leucogranite	73.81	14.72	1.13	0.32	0.71	3.97	4.09	0.06	0.48	0.03	0.2	1.76
Muscovite leucogranite	72.05	15.38	0.95	0.4	0.72	4.86	3.5	0.04	0.54	0.03	0.67	1.76
Muscovite leucogranite	72.74	14.66	1.19	0.22	0.7	3.57	4.17	0.06	0.41	0.03	0.7	1.84

Traces	Ba	Rb	Sr	Zr	Nb	V	Y	Ga	Cu	Zn	Hf	Ta	Sc	La	Th	U	Li	F	As	Sn	W
Biotite granodiorite	610	160	147	211	12	58	40	18	11	79	6	1.4	13	37	14	3.8	72	690	2.3	4	0
Biotite granodiorite	525	143	127	182	15	53	30	21	1	88	7	1.2	8.9	34	12	2.2	74	660	4.7	2	1
Biotite granodiorite	504	142	122	128	10	31	24	19	3	51	4	0.9	6.1	24	8.8	1.9	65	400	5.6	7	2
Biotite monzogranite	511	157	138	197	13	41	32	20	6	72	6	12	9.4	32	12	3	88	620	4.2	11	1
Biotite monzogranite	547	164	127	185	11	16	35	16	8	60	6	1.5	11	32	12	4.7	79	575	10	5	1
Biotite monzogranite	496	154	132	216	13	54	34	26	0	77	7	0.8	10	33	12	3.6	94	700	2.9	6	1
Biotite monzogranite	552	158	126	165	11	42	34	16	8	58	6	1	10	30	11	3.7	40	535	8.4	1	0
Muscovite-biotite monzogranite	292	310	57	140	14	11	20	20	0	56	3	2.1	3.7	26	20	3.2	104	1300	3.4	13	2
Coarse-grained leucomonzogranite	271	294	52	94	14	11	20	22	0	53	3	2	2.3	18	12	2.9	97	1250	4.7	12	2
Coarse-grained leucomonzogranite	52	676	17	58	24	3	26	25	11	114	1	4.6	2.2	7	8.1	24.8	431	4500	1.3	41	11
Coarse-grained leucomonzogranite	410	216	64	112	11	22	23	17	0	32	4	1.9	5	17	9.1	4.3	68	450	1.2	10	2
Coarse-grained leucomonzogranite	311	236	51	77	12	11	14	20	0	47	3	1.1	2.9	14	9	2.9	99	510	1.8	16	3
Coarse-grained leucomonzogranite	224	260	53	84	10	11	27	16	0	40	3	1.4	4.2	18	1	3.5	86	615	1.9	6	0
Coarse-grained leucomonzogranite	412	280	135	113	11	13	26	16	0	53	5	2	3.8	26	12	3.2	162	1165	0.9	11	5
Coarse-grained leucomonzogranite	140	348	31	52	10	0	22	18	0	39	2	2.1	3.1	11	7.3	8.3	109	770	1.5	10	3
Coarse-grained leucomonzogranite	151	240	37	69	10	6	18	18	0	19	3	2	3.5	7	6.1	8.4	21	420	1.6	13	3
Coarse-grained leucomonzogranite	275	289	52	118	13	13	30	17	0	55	4	2	5	26	18	5.1	61	1165	2.4	5	2
Coarse-grained leucomonzogranite	161	308	37	77	10	9	38	17	0	44	3	1.8	3.8	13	9	3.3	47	875	12	16	2
Coarse-grained leucomonzogranite	292	296	63	134	12	19	33	18	0	55	5	1.9	5.1	30	20.6	4.1	39	1220	2.1	7	0
Coarse-grained leucomonzogranite	136	278	45	91	10	11	37	18	0	51	3	1.7	4.5	16	11	3.9	126	1020	5.9	10	1
Coarse-grained leucomonzogranite	101	304	32	73	10	5	35	15	0	59	3	2.2	3.6	11	9	5.2	192	1495	1.6	9	2
Coarse-grained leucomonzogranite	392	245	70	112	11	7	27	20	0	40	4	1.1	2.2	27	18	3	55	620	1.7	9	1
Coarse-grained leucomonzogranite	249	194	54	60	6	7	21	15	5	36	2	1.3	3	8	4.8	5.4	47	150	1.6	5	2
Coarse-grained leucomonzogranite	144	336	34	84	15	10	20	24	0	61	3	2	2.7	17	12	3.3	135	1100	1.5	14	3
Coarse-grained leucomonzogranite	140	353	29	54	10	0	20	20	0	44	2	2.2	2.2	9	6.1	3.5	35	1030	1.7	13	3
Coarse-grained leucomonzogranite	173	303	43	73	12	8	24	18	0	49	3	2.3	3.5	11	6.3	4.3	36	900	4.1	22	8
Coarse-grained leucomonzogranite	254	210	76	86	9	12	22	17	0	49	2	1.4	4.5	15	7.7	3	48	540	2	10	0
Coarse-grained leucomonzogranite	249	261	61	121	11	16	26	19	0	57	4	1.8	4.8	20	12	2.9	39	990	1.9	11	1
Coarse-grained leucomonzogranite	83	275	22	55	11	2	17	23	0	40	1	1.7	2	9	6.2	3.6	74	660	1.8	12	3
Coarse-grained leucomonzogranite	230	275	53	84	11	11	26	20	0	49	3	1.4	3.8	16	8.8	3.8	99	720	0.8	13	1
Coarse-grained leucomonzogranite	120	274	33	77	10	6	25	22	0	60	3	1.3	2.5	11	7.5	3.8	67	590	3.7	16	4
Coarse-grained leucomonzogranite	86	374	25	62	14	4	20	19	0	71	2	0.9	1.7	8	5.5	7.1	209	1800	0.6	24	3

Traces	Ba	Rb	Sr	Zr	Nb	V	Y	Ga	Cu	Zn	Hf	Ta	Sc	La	Th	U	Li	F	As	Sn	W
Coarse-grained leucomonzogranite	48	692	32	55	24	10	35	26	0	67	1	5.6	2.5	6	5.7	5.8	312	3875	1.1	40	13
Coarse-grained leucomonzogranite	164	347	30	79	16	6	19	25	0	48	3	6.8	2.5	13	11	16	123	1650	2.9	16	5
Coarse-grained leucomonzogranite	277	233	66	92	11	10	25	20	0	42	3	1.2	3.7	19	10	3.3	75	570	1.5	17	1
Fine-grained leucomonzogranite	210	277	43	53	12	0	19	17	0	32	2	2	2.9	7	4	2.1	90	620	3.3	16	4
Fine-grained leucomonzogranite	19	521	10	32	15	0	26	23	0	48	1	3.6	2.2	3	3.4	14	182	1825	1.5	16	6
Fine-grained leucomonzogranite	150	487	28	78	14	5	32	22	0	59	3	3.1	2.5	14	12	13	129	1825	1.3	12	6
Fine-grained leucomonzogranite	591	246	63	73	7	0	32	15	8	12	3	1.6	2.1	40	8.4	6.2	12	7680	5.3	5	3
Fine-grained leucomonzogranite	44	499	10	69	17	0	32	21	0	60	3	3.6	2.1	9	11	28.6	96	2535	1.6	22	5
Fine-grained leucomonzogranite	29	572	15	53	21	3	20	25	0	59	1	5.1	3.7	6	6.3	24.1	342	3200	19	34	14
Fine-grained leucomonzogranite	32	321	9	29	7	0	22	17	0	13	1	2.7	2.7	2	2.7	10	16	385	65.5	7	4
Fine-grained leucomonzogranite	66	314	18	36	8	0	21	19	0	30	2	2.9	3.2	5	3.2	3.1	46	495	4.5	11	2
Fine-grained leucomonzogranite	139	416	31	81	14	0	29	23	0	63	3	3.1	2.8	14	11	15	73	2350	2.7	21	6
Fine-grained leucomonzogranite	34	390	8	41	10	0	29	18	0	36	2	3.2	3.5	4	4.8	7.6	88	855	7	23	7
Fine-grained leucomonzogranite	155	288	34	63	8	0	28	18	0	28	3	1.8	3.6	10	6.7	4.6	68	495	1.3	12	3
Fine-grained leucomonzogranite	292	356	37	66	9	5	17	21	0	49	1	1.6	1.9	11	8.7	5.1	221	1400	4.9	20	3
Fine-grained leucomonzogranite	212	321	31	59	14	2	17	20	0	46	1	2.6	2.9	10	6.6	4.4	156	1150	1.6	14	2
Fine-grained leucomonzogranite	15	290	0	26	8	0	20	18	5	32	0	1.7	2.3	2	3.1	13	70	605	2.3	14	41
Fine-grained leucomonzogranite	155	296	30	50	9	0	22	18	0	17	1	2.2	3.1	6	4.6	6.9	52	580	3.9	17	4
Fine-grained leucomonzogranite	72	319	23	57	10	0	26	20	0	42	3	2.5	2.9	10	7.1	7.4	90	755	1.6	13	5
Fine-grained leucomonzogranite	158	273	48	81	10	8	26	18	0	44	3	1.6	3.7	15	8.2	7.8	76	760	2.5	10	2
Fine-grained leucomonzogranite	78	296	26	67	10	0	27	19	0	33	3	1.7	3.2	10	7.2	5.9	73	645	2.3	13	2
Fine-grained leucomonzogranite	100	235	26	24	6	6	22	17	10	41	0	1	1.9	4	2.2	6	6	155	15	9	2
Fine-grained leucomonzogranite	14	409	9	26	11	0	24	22	0	51	1	2.8	2.2	2	3	16	18	675	8.4	18	5
Fine-grained leucomonzogranite	12	547	0	34	13	0	32	22	0	42	1	3.7	2.4	3	3.7	4.9	59	1845	2	35	6
Fine-grained leucomonzogranite	23	234	8	35	10	0	20	16	37	20	2	2.7	3.9	2	3.8	15	23	350	17	21	35
Fine-grained leucomonzogranite	72	332	22	55	8	0	31	17	5	49	3	2.6	3.3	7	6.3	5.3	124	815	11	21	4
Fine-grained leucomonzogranite	17	401	6	35	10	0	25	21	0	58	2	2.7	3.3	2	4.1	22.1	67	600	22	25	6
Fine-grained leucomonzogranite	33	457	6	26	13	0	21	21	0	24	2	3.8	3.9	0	1.8	14	83	850	1.6	33	9
Fine-grained leucomonzogranite	28	442	8	23	10	0	26	19	0	27	2	3.1	3.3	0	1.6	7.1	127	825	3.3	30	6
Fine-grained leucomonzogranite	20	504	5	46	19	1	20	25	0	46	1	4.5	2.5	5	5	13	190	1900	3.7	22	7
Fine-grained leucomonzogranite	67	347	17	61	12	4	17	20	0	43	1	1.2	2.5	8	5.6	11	162	1275	8.9	21	4
Fine-grained leucomonzogranite	30	386	8	47	11	0	23	22	57	66	2	2.5	2.3	4	4.2	7.6	87	990	7.7	22	6

Traces	Ba	Rb	Sr	Zr	Nb	V	Y	Ga	Cu	Zn	Hf	Ta	Sc	La	Th	U	Li	F	As	Sn	W
Fine-grained leucomonzogranite	207	187	54	40	10	5	14	19	0	78	1	2.4	4.5	5	1.2	1.5	34	210	4.1	12	5
Fine-grained leucomonzogranite	26	4.9	6	33	13	2	16	23	0	56	1	2.2	1.4	2	2.2	10	143	1175	2.5	19	5
Fine-grained leucomonzogranite	14	485	15	28	25	0	16	29	0	58	1	0.8	4.2	2	1.3	21.4	89	1150	2.6	20	8
Fine-grained leucomonzogranite	17	550	6	20	34	0	17	34	0	69	1	1.2	7.6	2	1	8.8	109	1150	3.4	31	10
Fine-grained leucomonzogranite	63	364	17	56	12	0	23	19	13	49	2	2.7	3	7	4.8	5	132	1005	6	22	5
Fine-grained leucomonzogranite	312	248	53	101	11	10	26	23	0	30	3	1.6	4.1	19	10	3.2	60	570	9.3	15	2
Fine-grained leucomonzogranite	183	248	37	54	11	6	15	20	0	29	2	2.4	3.8	7	2.9	2.6	46	490	2.3	22	5
Fine-grained leucomonzogranite	396	250	74	132	9	15	18	25	0	46	4	1.1	3.4	32	17	4	68	690	0.5	10	1
Fine-grained leucomonzogranite	222	334	48	112	17	9	23	25	0	59	4	2.5	3.8	25	15	5.4	114	1000	1.5	20	2
Fine-grained leucomonzogranite	139	298	31	73	12	3	20	24	0	46	2	1.9	2.8	12	7.7	4	80	820	2.2	16	1
Fine-grained leucomonzogranite	230	262	62	77	11	9	23	20	0	44	2	1.6	4	14	7.3	2.8	95	660	3	12	1
Fine-grained leucomonzogranite	89	168	27	24	5	0	10	19	4	2	1	1	0.6	3	1.2	5.1	28	245	7.2	9	3
Fine-grained leucomonzogranite	254	331	56	99	15	16	17	21	0	78	1	1.6	2.9	9	15	5.4	182	2150	352	20	26
Fine-grained leucomonzogranite	288	272	65	146	15	20	27	20	0	56	5	1.6	4	25	17	3	128	1175	0.8	10	1
Fine-grained leucomonzogranite	240	299	56	116	13	19	28	21	0	58	4	2.1	4.9	25	17	3.3	41	1145	1.6	5	1
Fine-grained leucomonzogranite	291	347	56	127	13	13	29	20	0	60	4	2.3	4.2	25	20.6	4.1	71	1705	1.5	8	3
Muscovite leucogranite	27	754	11	44	27	0	38	28	0	69	2	7	2.2	5	6.2	4	324	4200	0.9	39	11
Muscovite leucogranite	34	677	16	42	22	0	37	24	0	55	2	6.6	2.4	6	6.9	3.6	375	4240	0.9	26	9
Muscovite leucogranite	80	691	23	76	22	5	41	24	0	69	3	5.7	2.7	12	13	4.4	419	3965	2.5	30	7
Muscovite leucogranite	19	765	14	39	28	3	26	30	0	77	1	1.1	1.7	3	4.5	5.2	417	3300	1.9	38	19
Muscovite leucogranite	15	896	16	39	28	4	25	32	0	87	1	1.1	1.8	2	5	4.6	502	3650	2.1	41	8
Muscovite leucogranite	77	845	28	26	34	0	39	30	0	64	2	14	2.2	0	2	4.3	336	4135	0.7	31	8
Muscovite leucogranite	23	866	20	43	29	1	27	26	0	74	1	8.7	1.7	3	5.5	5.7	497	3700	1.4	36	9